AD_____
(Leave blank)

Award Number: **DAMD17-01-1-0689**

TITLE: BESCT (Biology, Education, Screening, Chemoprevention and Treatment) Program

PRINCIPAL INVESTIGATOR:
Waun Ki Hong, M.D.

CONTRACTING ORGANIZATION:
University of Texas M.D. Anderson Cancer Center
Houston, TX 77030

REPORT DATE: October 2010

TYPE OF REPORT: Addendum to Final

PREPARED FOR: U.S. Army Medical Research and Materiel Command
Fort Detrick, Maryland 21702-5012

DISTRIBUTION STATEMENT: (Check one)

X Approved for public release; distribution unlimited

☐ Distribution limited to U.S. Government agencies only; report contains proprietary information

The views, opinions and/or findings contained in this report are those of the author(s) and should not be construed as an official Department of the Army position, policy or decision unless so designated by other documentation.

REPORT DOCUMENTATION PAGE

Form Approved
OMB No. 0704-0188

Public reporting burden for this collection of information is estimated to average 1 hour per response, including the time for reviewing instructions, searching existing data sources, gathering and maintaining the data needed, and completing and reviewing this collection of information. Send comments regarding this burden estimate or any other aspect of this collection of information, including suggestions for reducing this burden to Department of Defense, Washington Headquarters Services, Directorate for Information Operations and Reports (0704-0188), 1215 Jefferson Davis Highway, Suite 1204, Arlington, VA 22202-4302. Respondents should be aware that notwithstanding any other provision of law, no person shall be subject to any penalty for failing to comply with a collection of information if it does not display a currently valid OMB control number. **PLEASE DO NOT RETURN YOUR FORM TO THE ABOVE ADDRESS.**

1. REPORT DATE *(DD-MM-YYYY)*	**2. REPORT TYPE**	**3. DATES COVERED** *(From - To)*
14-10-2010	Addendum to Final	15 FEB 2010 - 14 SEP 2010

4. TITLE AND SUBTITLE
BESCT (Biology, Education, Screening, Chemoprevention and Treatment) Program

5a. CONTRACT NUMBER

5b. GRANT NUMBER
DAMD17-01-1-0689

5c. PROGRAM ELEMENT NUMBER

6. AUTHOR(S)
Waun Ki Hong, M.D.
Email: whong@mdanderson.org

5d. PROJECT NUMBER

5e. TASK NUMBER

5f. WORK UNIT NUMBER

7. PERFORMING ORGANIZATION NAME(S) AND ADDRESS(ES)
University of Texas M.D. Anderson Cancer Center
Houston, TX 77030

8. PERFORMING ORGANIZATION REPORT NUMBER

9. SPONSORING / MONITORING AGENCY NAME(S) AND ADDRESS(ES)
U.S. Army Medical Research and Materiel Command
Fort Detrick, Maryland 21702-5012

10. SPONSOR/MONITOR'S ACRONYM(S)

11. SPONSOR/MONITOR'S REPORT NUMBER(S)

12. DISTRIBUTION / AVAILABILITY STATEMENT
Approved for public release; distribution unlimited

13. SUPPLEMENTARY NOTES

14. ABSTRACT
The BESCT program aims to define molecular abnormalities contributing to lung cancer initiation and progression and to develop innovative therapeutic approaches for this cancer. Our specific aims are 1) to understand molecular alterations in lung cancer, 2) to develop chemoprevention strategies for lung cancer, and 3) to implement experimental molecular therapeutic approaches for lung cancer treatment.

15. SUBJECT TERMS
Lung cancer, genetic alterations, chemoprevention, molecular therapy

16. SECURITY CLASSIFICATION OF:			**17. LIMITATION OF ABSTRACT**	**18. NUMBER OF PAGES**	**19a. NAME OF RESPONSIBLE PERSON**
a. REPORT	**b. ABSTRACT**	**c. THIS PAGE**			**19b. TELEPHONE NUMBER** *(include area code)*
U	U	U	UU	309	USAMRMC

Standard Form 298 (Rev. 8-98)
Prescribed by ANSI Std. Z39.18

TABLE OF CONTENTS

INTRODUCTION.....4

PROGRESS REPORT (BODY).....4

Project 1.....4
Project 2.....7
Project 3.....11
Developmental Research Project 13

KEY RESEARCH ACCOMPLISHMENTS.....15

REPORTABLE OUTCOMES.....17

APPENDIX

Publications
Personnel Report

INTRODUCTION

The BESCT program, developed in 2001, aimed to define molecular abnormalities contributing to lung cancer initiation and progression and to develop innovative therapeutic approaches for this cancer. The specific aims were as follows:

- To understand molecular alterations in lung cancer
- To develop chemoprevention strategies for lung cancer
- To implement experimental molecular therapeutic approaches for lung cancer treatment

This report also details the latest results of a major change to one of the aims of Project 2 (PI: Fadlo Khuri, MD). As described in Aim 2, difficulties resulting from the purchase of Ligand Pharmaceuticals by Eisai in 2006 led to the conclusion that the clinical trial planned and agreed upon in the original grant proposal would not be able to be completed. Thus, building upon the preclinical work in BESCT and in BATTLE, a revised Specific Aim 2.1, which we believed would be synergistic with both studies and accomplish the original intent of the BESCT program, was submitted to and approved by the DoD (on 7/14/08), to be undertaken through a no-cost extension of the grant period. The accomplishment of these revised aims is described below in Specific Aim 2 of Project 2.

This final report summarizes work conducted over the entire research period, highlights key research accomplishments and reportable outcomes with the bibliography of all publications and meeting abstracts derived from **BESCT**, and includes a list of personnel receiving pay from the research effort.

PROGRESS REPORT

Project 1: Study Mechanisms of Molecular Alterations in Lung Cancer
(PI: Li Mao, M.D.)

Specific Aim 1 **To determine the mRNA complex responsible for C-CAM1 splicing and identify factor(s) regulating exon 7 splicing.**

We hypothesized that the fidelity of splicing machinery is defective in majority of the lung cancers due to impaired factors in the splicing complexes. To test our hypothesis, we utilized *C-CAM1* as a model system for the following reasons. (1) *C-CAM1* expression is significantly altered in the form of alternative splicing in lung cancers. (2) Model cell lines consistently expressing either a predominant L-form *C-CAM1* or predominant S-form *C-CAM1* are readily available to our investigators. (3) Introns and exons flanking the splicing exon are relatively small, which may facilitate the identification of critical regions for the splicing regulation.

Findings: We analyzed nuclear proteins from four cancer cell lines (H1944, A549, H460, and 17B) and found two patterns of expression. We have shown differential patterns of hnRNP proteins between cells with distinct *CEACAM1* splicing patterns. In light of this finding, we developed Specific Aim 5 to determine hnRNP variants in these tumor cells and their role in regulating *CEACAM1* splicing.

Specific Aim 2 **To determine function of identified splicing factor(s) in regulation of CEACAM1 and its potential alterations in lung cancer.**

Candidate factors identified in Specific Aim 1 must be validated, and a better understanding of how these factors play a role in splicing control may further the understanding of biological processes altered in tumorigenesis. If the loss or gain function of these factors could be also demonstrated in human lung cancer cells, they might be further studied as potential diagnostic and therapeutic targets.

Findings: We found that the consensus-alternative splicing sequence of *CEACAM1* locates within exon 7 of CEACAM1. This site binds two major proteins,hnRNP-A1 and polypyrimidine tract-binding protein (PTB), both known to be important in splicing regulation. The data further suggested that PTB can function as an exonic splicing enhancer to exclude the *CEACAM1* exon 7, which is a novel PTB function. We also demonstrated that PTB expression was increased in most of primary lung tumors that exhibited predominant short-form *CEACAM1* when compared with matched normal lung tissues.

Specific Aim 3 **To determine function of DNA methyltransferases and their role in controlling methylation and expression of critical tumor suppressor genes and tumor antigen genes.**

Tissue- and gene-specific patterns of cytosine-DNA methylation are characteristic features of vertebrate genomes and DNA methylation has been considered an important mechanism in tumorigenesis. We have shown that *DNMT3B* expression level is higher in primary NSCLC tissues than in the corresponding normal lung tissue, and *DNMT3B* produces various alternative-splicing forms (or a form derives from different promoter), which share a common enzyme catalyst structure at the C-terminal, but have distinct N-terminal structures in its prototype protein structure. We hypothesize that different *DNMT3B* isoforms may have distinct roles in targeting different genomic structures and therefore, are important in tissue- or gene-specific DNA methylation regulation.

Findings: To determine the expression profile of the new transcript, we analyzed a panel of different tissues including peripheral lymphocytes, normal lung tissues, paired lung cancer tissues, lung cancer cell lines, and head and neck cancer cell lines, and found that DNMT3B6 is the predominant expressing form of DNMT3B in these tissues. We demonstrated that the core promoter of DNMT3B6 is in a 477-bp fragment containing one repressor element and three cis-acting elements. We noticed a stronger promoter activity of the T form than the C form (18-fold vs. 12-fold compared to the control, respectively). We analyzed the mRNA expression profiles of DNMT3B6s in the normal lung cDNA library and lung cancer cell lines, and found that the transcripts initiated from this novel promoter may generate at least 7 isoforms of DNMT3B6 through inclusion or exclusion of different combinations of exons. Detected by RT-PCR, these DNMT3B6 transcripts showed variable expression levels and patterns in different cancer cell lines and primary tumors. A comparative analysis of putative amino acid sequences shows that all variables are within the PWWP motif, which has recently been shown to have direct DNA binding capability.

We proved that promoter hypermethylation in *p16*^{INK4a} and in *RASSF1A* tumor suppressor genes is frequently and strongly associated with clinical outcomes in patients with resectable non-small cell lung cancer. We also demonstrated that hypermethylation of the death-associated protein kinase promoter attenuates the sensitivity of human NSCLC cells to TRAIL-induced apoptosis.

Specific Aim 4 **To determine expression and abnormalities of DNMT3B isoforms in lung tumorigenesis and their association with de novo DNA methylation patterns, and clinical applications.**

DNA hypermethylation and hypomethylation profiles are significantly altered in tumor cells. We hypothesized that abnormal expression of *DNMT3B* isoforms is associated with hypermethylation or hypomethylation status in critical genes in lung tumors. If such an association can be established, novel strategies may be developed to target these molecules for lung cancer detection, prevention, and therapy.

Findings: We determined expression of seven splicing variants of DNMT3B in 119 primary non-small cell lung cancer (NSCLC) specimens and their corresponding non-malignant lung tissues using specific primer sets. We analyzed the association between the expression and patients' clinical parameters including survivals, and further analyzed an association between expression patterns of the variants and the promoter methylation status of the *p16*^{INK4a} and *RASSF1A* in these tumors. We observed strong association between expression of DNMT3B variants and promoter methylation of p16^{INK4a} and *RASSF1A*, particularly between *DNMT3B4* expression and *RASSF1A* ($P<0.0001$). The expression of any of the low frequent *DNMT3B* variants (*DNMT3B5-7*) was strongly associated with poor survival in patients with stage I/II or stage IIIa disease (P values between 0.002 and 0.0003). In patients with stage IIIa disease, the expression of *DNMT3B4* was found to be strongly associated with poor overall, disease-free, and disease-specific survivals ($P<0.0001$, $P=0.0007$, and $P<0.0001$, respectively). These data suggest that *DNMT3B* variants are involved in differential regulation of promoter methylation in lung tumorigenesis and may serve as biomarkers in lung cancer early detection and molecular classification.

Specific Aim 5 To determine expression of hnRNP-A1 variants in lung cancer cells and their role in the regulation of pre-mRNA splicing.

Limited progress was made for this task due to our inability to isolate the protein complex responsible for the splicing abnormality. Thus, this task was terminated and our emphasis was shifted to the extended task, Specific Aim 6.

Specific Aim 6 To determine the role of hepatoma-derived growth factor (HDGF) in lung cancer.

Findings: We knocked down HDGF with *HDGF*-specific small interfering RNA (siRNA) in four NSCLC cell lines and we found that down-regulation of HDGF did not affect cell proliferation and cell cycle, but cells transfected with *HDGF*-siRNA grew more slowly and formed significantly fewer colonies in soft agar than with Lipofectamine alone or with negative control siRNA. The results suggest that HDGF is involved in anchorage-independent growth, cell invasion, and formation of neovasculature in NSCLC.

Based on the *in vitro* and *in vivo* data, we used recombinant HDGF to develop a panel of monoclonal antibodies that specifically bind to HDGF, two of which (C1 and H3) exhibited significant antitumor activity in A549 lung cancer xenografts. No toxicity was observed in the living mice and major organs of antibody-treated mice. Consistent with known biologic functions of HDGF, our morphologic and biomarker analyses suggest that H3 may neutralize HDGF released from tumor cells, resulting in disruption of tumor stroma and extracellular matrix structures. Thus, we conclude that HDGF is a novel therapeutic target for multiple human cancers and a neutralized monoclonal antibody targeting HDGF may be effective in treating lung and pancreatic cancers.

Project 2: Develop Novel Strategies for Lung Cancer Chemoprevention
(Project Leader: Fadlo Khuri, M.D.)

Specific Aim 2.1 To evaluate the effects of oral bexarotene delivered to former smokers by inhalation alone or in combination with celecoxib.

(PI: Fadlo Khuri, M.D)

As reported in 2004, we were unable to conduct the clinical trial proposed in the original Specific Aim, "To evaluate the effects of aerosolized 13cRA delivered to former smokers by inhalation alone or in combination with Celecoxib," due to unexpected excessive toxicity with aerosolized delivery. Initial clinical studies have indicated that retinoids decrease the incidence of second primary tumors in patients who have previously undergone resection for NSCLC or head and neck cancer. However, subsequent large-scale chemoprevention trials have demonstrated that retinoids induce substantial toxicity and are of minimal benefit to individuals at high risk for lung cancer, illustrating the need for more effective lung cancer chemoprevention strategies.

We thus proposed the clinical trial "A Phase I Biologic Study of Bexarotene (Targretin®) and Celecoxib in Patients With Solid Tumors Previously Treated With Standard Chemotherapy." The objective of this project was to evaluate the chemopreventive potential of bexarotene (Targretin®) and non-steroidal anti-inflammatory agents (NSAIDs; e.g., celecoxib) in high-risk lung cancer patients.

Findings: The protocol was reviewed and approved by Emory Institutional Review Board (IRB) on January 5, 2007. Negotiations with Eisai Pharmaceuticals to provide Targretin fell through due to several issues:

1) Emory requested the ability to terminate the study if needed to protect the health and safety of study subjects.

2) Emory required indemnification from any claims that may come out of the use of results if Eisai wanted the right to use study results for their respective purposes.

3) Eisai asked for outright ownership to inventions from the study but Emory did not feel this was possible given federal funding is being utilized for the study.

These issues remained unresolved after Eisai bought Ligand Pharmaceuticals, with whom we had negotiated the original agreement for this trial.

We thus explored a similar proposal with AstraZeneca for a clinical trial with celecoxib and ZD1839 (gefitinib), but were also unable to secure an agreement. As a result, we agreed not to further pursue an agreement and trial with Eisai and, given the litigious environment and press surrounding celecoxib, it was also agreed that we would not further pursue the trial with AstraZeneca for this program. Consequently, the strategy to best accomplish our aims in a timely manner under these circumstances was to synergize our program with the DoD-funded Biomarker-integrated Approaches of Targeted Therapy for Lung Cancer Elimination (BATTLE) program, with specific correlative research directed towards a revised Aim 2.1 and Aim 3.2.

Through these aims, we proposed to build on our initial work showing that combining an mTOR inhibitor with PI3 kinase inhibitors leads to accelerated cell growth inhibition. The development of PI3 kinase inhibitors in lung cancer has had an uncertain course; however, inhibition of IGFR by

either a monoclonal antibody or tyrosine kinase inhibitors (TKIs) is undergoing accelerated development in the lung cancer arena. With a strong track record of developing agents both in prevention [1-3] and therapy [4-16], we proposed mechanistic work in vitro to understand the basis of the enhanced pharmacologic dependence on the Akt/mTOR axis in lung cancer cell lines treated with rapamycin or its analogs, such as RAD001. We subsequently studied the biology behind the accelerated cell growth inhibition kinetics when we introduced an IGFR inhibitor after initial treatment with rapamycin. Importantly, we studied the optimal treatment sequence for these agents to see whether the maximum effect is obtained when Akt is first paradoxically upregulated by rapamycin blockade, followed by treatment with IGFR inhibitors. We then took this combination into a biomarker-driven phase I clinical trial incorporating serial biopsies of accessible tumors during defined treatment intervals, and using sequential PET scans to assess metabolic changes induced by the combination. We believe that understanding the correlations between downregulation of tissue biomarkers and quenching of the metabolic signal, as assayed by PET, can help us develop a new paradigm to establish the range of biologically effective doses of novel agents. This new approach is particularly important as assessment of targeted therapies is likely to differ substantially from the development of cytotoxic agents. Downregulation of key signaling pathways (assessed in serial tumor biopsies and correlated with PET imaging) will allow us to see if Akt is upregulated after initial treatment with the mTOR inhibitor, and then quenched in human subjects after subsequent treatment with an IGFR TKI. It is not only important to assay these biological and pharmacological parameters for therapy of established advanced disease, it is also critical that we determine tolerable doses of IGFR/mTOR inhibitor combinations for long-term chemoprevention of individuals at high risk for the development of lung cancer.

By developing this potentially potent combination of mTOR and IGFR inhibitors in parallel, we believe we can make important inroads into developing clinically meaningful data to potentially benefit populations at risk in the long term, while deriving relevant biological data about targeting important pathways that have, to date, been resistant to therapeutic intervention.

***Revised* Specific Aim 2.1** **To determine whether treatment of lung cancer cells with mTOR inhibitors enhances dependence of these cells on survival signaling via IGFR**

mTOR inhibition-induced Akt activation appears to depend on IGF-1R in certain types of cancer cells. Thus, inhibition of IGF-1R signaling augments mTOR inhibitors' anticancer activity in these cell lines. However, the synergy effect and the effective application sequence of mTOR and IGF-1R inhibitors in human lung cancer have not been documented. We will test how IGF-1R is involved in mediating Akt activation induced by mTOR inhibition in human lung cancer cells (Aim 1a) and whether co-inhibition of mTOR and IGF-1R signaling augments efficacy against lung cancer (Aim 1b). It has been documented that IGFR/EGFR heterodimerization counteracts the antitumor action of TKIs, whereas high levels of IGF-1R levels are associated with EGFR overexpression in human lung cancers. Moreover, IGF-1R signaling can activate the Raf/ERK MAPK pathway through EGFR. EGFR mutations impact lung cancer response to EGFR TKIs; however, the impact of the EGFR mutations on the co-targeting of mTOR and IGF-1R signaling remains unclear. Therefore, we will determine whether EGFR mutations impact cell sensitivivity to the combination of mTOR and IGF-1R inhibitions (Aim 1c).

Sub-Aim 1a. Determine whether IGF-1R is involved in mediating Akt activation by mTOR inhibition in human lung cancer cells.

Sub-Aim 1b. Determine whether co-inhibition of mTOR and IGF-1R signaling augments efficacy against lung cancer.

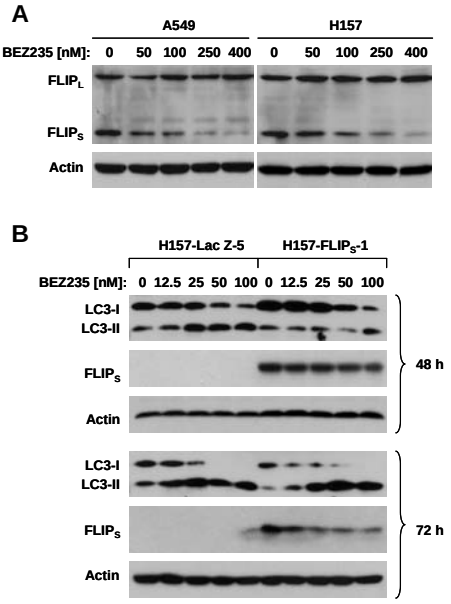


Figure 1. BEZ235 downregulates $FLIP_S$ expression *(A)* and overexpression of $FLIP_S$ transiently abrogates the ability of BEZ235 to increase type II of LC3 (LC3-II) *(B)*.

Sub-Aim 1c. Determine whether EGFR mutations impact cell sensitivity to co-targeting of mTOR and IGF-1R.

Findings: We revised our research aims to concentrate on the treatment of lung cancer cells with mTOR inhibitors to enhance the dependence of these cells on PI3K survival signaling. Thus, we specifically analyzed the anticancer effects of the sequential treatment with an mTOR inhibitor followed by a PI3K inhibitor (e.g., RAD001 followed by BEZ235) *in vitro* and *in vivo*, and we found that the concurrent combination of rapamycin with LY294002 was far more potent than both sequential treatments—rapamycin followed by LY294002, and LY294002 followed by rapamycin—in inhibiting the growth of cancer cells in a 12-day colony formation assay. These data clearly indicate that the concurrent combination of an mTOR inhibitor and a PI3K inhibitor is an effective and potential cancer therapeutic regimen. Further research discovered that the combination of RAD001 and BEZ235 exhibits enhanced growth-inhibitory effects without inhibition of Akt activation.

We revealed that DNA-PK is involved in rapamycin-induced Akt phosphorylation because rapamycin-induced Akt phosphorylation could be abolished by the DNA-PK inhibitor, Nu7441. This finding suggests not only a novel mechanism by which mTOR1 inhibition induces Akt activation, but also a new strategy to enhance mTOR-targeted cancer therapy by co-targeting the mTOR and DNA-PK.

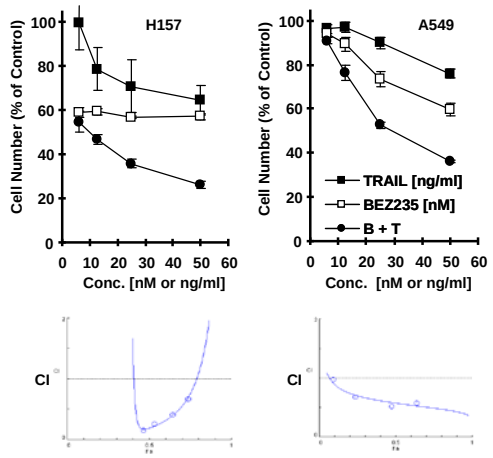


Figure 2. Synergistic effects on decreasing the survival cancer cells by combination of BEZ235 and TRAIL. Combination index (CI) was calculated (bottom panels) to show the synergy.

We found that BEZ235 inhibited c-FLIP in human lung cancer cells by downregulating c-FLIP ($FLIP_S$) expression (Figure 1). Overexpression of $FLIP_S$ transiently abrogated the ability of BEZ235 to increase the conversion of LC3-I to LC3-II (Figure 1, 48 h), indicating that $FLIP_S$ partially protects cells from undergoing autophagy. Collectively, we suggest that $FLIP_S$ downregulation may contribute to BEZ235-induced autophagy.

In addition to induction of autophagy, the downregulation of $FLIP_S$ also suggests that BEZ235 may enhance TRAIL/death receptor-induced apoptosis. We found that the combination of BEZ235 and TRAIL was much more effective than each single agent in decreasing the survival of lung cancer cells (Figure 2). We therefore speculated that $FLIP_S$ downregulation may also mediate enhancement of TRAIL-induced apoptosis by BEZ235. Our ongoing work is trying to approve this hypothesis outside the scope of this grant.

We examined the effects of BEZ235 on the growth of a panel of human lung cancer cells lines (up to 18) with known genetic mutations of alterations to determine whether certain genetic alterations impact cell response to BEZ235. We found that all cell lines with wild-type p53 (e.g., H292, H460, A549 and H1944) are among the most sensitive cell lines to BEZ235 (Fig. 4). We will continue to investigate whether presence of p53 indeed affects cell sensitivity to BEZ235 in studies outside the scope of this grant.

Specific Aim 2.2 To evaluate effects of NSAIDs and 4HPR (replace 13cRA) as single agents and in combinations on growth, apoptosis, and carcinogenesis using an in vitro cell system and an animal model.

(PI: Reuben Lotan, Ph.D.)

Because the retinoid 13cRA shows enhancement of lung cancer among smokers in a clinical trial but has side effects, whereas the synthetic retinoid fenretinide [*N*-(4-hydroxyphenyl) retinamide, 4HPR] is more potent with fewer side effects and has additive effects with celecoxib, we replaced 13cRA with 4HPR for subsequent *in vitro* and animal experiments.

Findings: We explored the mechanisms by which 4HPR induces apoptosis in NSCLC cells and possible nodes for convergence of mechanisms of action of NSAIDs (e.g., celelcoxib) and 4HPR that might explain their additive/synergistic effects. Using the bronchioalveolar cancer cell line H522, we found that 4HPR activates the NADPH oxidase regulatory subunit Rac and that this activation is involved in ROS increase and subsequent apoptosis induction. The Rac1 inhibitor NSC-23766 suppressed the increase in ROS in 4HPR-treated cells indicating that Rac1 is upstream of ROS production. Targeting Rac1 expression using small interfering RNA (siRNA), which has been shown to down-regulate Rac1, suppressed the induction of ROS generation by 4HPR in H522 cells by about 50%. These results indicate that NADPH oxidase may be the source of about 50% of the enhanced ROS production induced by 4HPR with the rest coming presumably from the mitochondria.

Our *in vivo* chemoprevention studies have shown previously that 4HPR used as a single agent was able to suppress lung carcinogenesis induced in Gprc5a knockout mice at a borderline significant rate, whereas celecoxib alone failed to suppress carcinogenesis. We examined the effects of the combination of 4HPR and celecoxib and found that the combination of agents had a greater effect than each agent alone.

Specific Aim 2.3. To investigate whether genetic approaches to inhibit PI3K activity decrease lung tumor size and number in k-ras mutant mice.

(PI: Ho-Young Lee, Ph.D.)

This Aim was discontinued as reported in the 2004 Annual Report due to the variability in the delivery system.

Specific Aim 2.4. To analyze differential gene expression between untreated NSCLC cells and celecoxib-treated NSCLC cells using affymetrix oligonucleotide microarrays and characterize genes that may be implicated in mediating apoptosis induction.

(PI: Reuben Lotan, Ph.D.)

This Aim was discontinued as reported in the 2008 Annual Report due to the challenges that persisted with celecoxib use in the clinic.

Project 3: Implement Experimental Molecular Therapeutic Approaches for Lung Cancer
(Project Leader: Fadlo Khuri, M.D.)

Specific Aim 3.1 **To develop a relatively faithful murine model of lung cancer by crossing the k-ras mutant mouse (T. Jacks) with p53 mutant missense mouse (G. Lozano) and study the evolution of non-small cell lung cancer in primary lung tumor model with metastatic potential and the effectiveness of targeted agents in the model.**
(PI: Guillermina Lozano, Ph.D.)

Findings: We have developed a mouse lung cancer model that develops lung carcinomas due to an inherited mutation in the p53 tumor suppressor ($p53^{R172H\Delta g/+}$) and somatic inactivation of the *ras* oncogene ($K\text{-}Ras^{LA1/+}$). This model recapitulates lung adenocarcinoma and more faithfully demonstrates highly aggressive adenocarcinomas that metastasize to multiple intrathoracic and extrathoracic sites in a pattern similar to that found in humans. Gender differences were also observed. Thus, this model is thought to be invaluable for future studies relating to metastasis of human lung cancer.

Specific Aim 3.2 **To evaluate novel signal transduction inhibitors alone, in combination with one another, or with cytotoxic agents in the treatment of the mouse lung cancer and, ultimately, in the treatment of human lung cancers.**
(PI: Fadlo Khuri, M.D.)

Findings: We studied farnesyltransferase inhibitors (FTIs) including lonafarnib, and found that lonafarnib increased microtubule acetylation and synergy with taxanes in anti-proliferation activity. We designed a Phase Ib combination trial of lonafarnib and docetaxel in biopsy-accessible solid tumor patients to combine lonafarnib with low doses of docetaxel weekly as an extended study.
The trial was supported by our NIH/NCI P01 (CA116676-01A1) Program Project grant and Sanofi-Aventis pharmaceuticals, and lonafarnib is provided by Schering Plough.

We found that ERK phosphorylation was decreased in all cell lines tested regardless of TRAIL-induced apoptosis. Consequently, we have concluded that for lung cancer, ERK inhibition is unlikely to be critical for the apoptosis response observed with perifosine. We determined that perifosine, at clinically achievable concentrations, induces apoptosis by inhibiting Akt phosphorylation, reducing total Akt levels. In addition, perifosine induced expression of TRAIL.

Specific Aim 3.3 **To produce and test a liposomal gene-therapeutic strategy targeted to a novel tumor suppressor gene located on chromosome 3p, both in the mouse model and in human patients with advanced non-small cell lung cancer.**
(PI: Charlie Lu, M.D)

Findings: We discovered that systemically delivered FUS1-lipoplex suppressed tumor growth in experimental lung metastasis mouse model and demonstrated the feasibility of the DOTAP:cholesterol-DNA vector for systemic therapy. Further, we tested its toxicity in mice and

monkeys and found a well-tolerated non-lethal dose. These preclinical data were used to develop the phase I trial of DOTAP:cholesterol-FUS1 liposome complex (Human Gene Transfer Protocol #0201-513) that was supported by a different funding mechanism outside of this grant.

Specific Aim 3.4 To develop specific vascularly targeted strategies to the vascular endothelium of lung cancer cells to decrease the toxicity to normal cells and enhance the therapeutic index.

(PI: Ho-Young Lee, Ph.D)

Findings: We showed that the farnesyl transferase inhibitor (FTI), SCH66336, has antiangiogenic activity in aerodigestive tract cancer, including lung and head /neck cancers, by suppressing the expression of HIF-1α and VEGF. We also demonstrated that the insulin growth factor 1(IGF)-mediated pathway plays an important role in angiogenesis by stimulating the synthesis of HIF-1α and VEGF, and their down-stream signaling mediators, including phosphatidylinositol 3-kinase (PI3K)/Akt and mitogen-activated protein kinase (MAPK), cooperate to promote cell proliferation. Thus, we have tested whether inhibition of PI3K/Akt and MAPK pathways effectively inhibits NSCLC tumor growth and angiogenesis. Results indicate that PI3K/Akt and MKK4/JNK pathways cooperate to stimulate cell proliferation and angiogenesis, suggesting that simultaneously targeting the two pathways might be an effective therapeutic strategy against NSCLC.

We investigated the mechanisms of resistance to SCH66336 in aerodigestive tract cancer using lung and head/neck cancer cell lines. We found that IGF-1R and Akt were activated in the HNSCC cell lines insensitive to apoptotic activities of SCH66336 after the treatment with SCH66336. Moreover, combined treatment with SCH66336 and IGF-1R tyrosine kinase inhibitor AG1024 induced marked decreases in the levels of pIGF-1R and concomitant cleavage of caspase-3.

Knock-down of survivin expression abolished resistance to SCH66336 and induced apoptosis in the TR146 and UMSCC 38 cells as determined by FACS and Western blot analysis on survivin and caspase-3. Overexpression of survivin by the use of adenoviral vector protected SCH66336-sensitive HNSCC cells from the apoptotic activities of SCH66336. Thus, our results suggest that expression of pIGF-1R, pAkt, pmTOR, and survivin may serve as predictive markers for SCH66336 responsiveness in HNSCC.

Specific Aim 3.5 To study in vivo and in vitro effects of farnesyl transferase inhibitors and tyrosine kinase inhibitors in mouse models and, ultimately, in humans with lung cancer.

(PI: Guillermina Lozano, Ph.D.)

Findings: We used erlotinib in our mouse model of lung cancer created in Aim 3.1. The mean number of lesions on the lung surface was significantly reduced in mice given erlotinib (p=0.0072). Treatment with erlotinib reduced the size or stabilized the growth of many but not all tumors. Resistance to erlotinib suggested that these tumors acquired additional genetic changes. Since erlotinib targets the epidermal growth factor receptor (EGFR), we examined adenocarcinomas for its expression. EGFR was expressed in all 15 lung adenocarcinomas examined and was present in both cytoplasmic and nuclear compartments. Thus, we show that erlotinib significantly reduces the mean number of lesions on the lung surface. Micro-CT monitoring demonstrates that erlotinib reduces or stabilizes the growth of many, but not all lung tumors, similar to clinical scenarios in lung cancer patients treated with erlotinib.

Specific Aim 3.6 To measure differences in gene expression between lung tumors that do or do not show metastasis, and in metastatic lesions themselves using the Affymetrix gene chip system.

(PI: Guillermina Lozano, Ph.D.)

Findings: The quality of the mRNA was measured and the cRNA generated and hybridized to Affymetrix chips. Analysis of the array data indicate that the primary tumors and metastases segregate separately. A total of 79 genes were differentially expressed between the data sets with a p value less than 0.001. We verified by the Western blot analysis that several of the genes in tumors, e.g., vimentin and Bub1b, were overexpressed and that C-cam1 was down modulated in metastases.

Specific Aim 3.7 To perform array CGH experiments to determine if other genomic changes have occurred.

Specific Aim 3.8 To perform LOH studies at specific loci (if warranted from the data obtained in Specific Aim 3.7).

(Leader: Guillermina Lozano, Ph.D.)

These studies were dropped from the project due to lack of funds, as reported in 2008.

Specific Aim 3.9 To evaluate GFE-1 peptide effects on blocking lung metastases in a rat model.

(PI: Yun W Oh, M.D)

Findings: Our studies with GFE peptide and lung vasculature suggest that MDP mediates cancer cell adhesion to lung vasculature and development of lung metastases, but that MDP is not present in vasculature of lung metastases. MDP appears to occupy a vascular distribution similar to the pulmonary artery circulation. These results demonstrate the promise of defining critical functional and anatomic characteristics of endothelial cells in lung and other organs by *in vivo* phage display.

Dr. Yun Oh discontinued participation in the BESCT program as noted in an official letter to Dr. Julie Wilberding in 2005.

Developmental Research Project: A Genetic/Combinatorial Algorithmic Strategy for Anticancer Therapy Development

(PI: Ralph Zinner, M.D)

Targeted therapeutic agents are highly promising in combination because they are both well-tolerated and interact with the targets that cause cancer. However, with new drugs added to the list, the number of possible combinations rises exponentially beyond the capacity of any foreseeable technology to fully screen. In addition, molecular insight often fails to predict clinical performance of single agents, a difficulty that will likely remain as these drugs are combined. We thus proposed a direct functional screen of combinations as a complement to the molecular insight-based approach, MACS (Medicinal Algorithmic Combinatorial Screen), to identify promising combinations that would be otherwise impossible to be found through a simple screen alone. The foundation of MACS is a genetic algorithm. The study adopts a preclinical screen that assesses anticancer efficacies of combinations with cell proliferation assays.

Specific Aim 1 To determine feasibility of screening process (robots, cell death assays, combining drugs).

Findings: We screened 19 different drugs using the Medicinal Algorithmic Combinatorial Screen (MACS). Two different algorithms have been used and identified 4HPR, SAHA, and bortezomib to be the "fittest" combinations of all drugs screened.

Specific Aim 2 **To determine the range of outcomes and patterns of cellular response from an initial screening of drug combinations.**

Findings: Analyses of several power sets of 6 drugs in A549 cells showed that 67% of the variance could be explained by linear combinations. More than 500 combinations were studied through the process and were analyzed for linearity.

Specific Aim 3 **To develop genetic algorithm to guide selection and identification of promising combinations of drugs.**

Findings: We screened combinations from 19 drugs (524,288 possible cocktails) for inhibition of the lung cancer cell line, A549, guided by MACS. We applied a hybrid nonlinear optimization algorithm (MACS) to search for effective cocktails composed of up to 19 different drugs each with a fixed single agent IC_{10} dose. The fittest combination of drugs identified was SAHA, bortezomib, and 4HPR (4SB) after the local search was conducted. Our research supports the premise that a functional screen that composes the MACS can serve as a useful complement to molecular insight based therapy development.

KEY RESEARCH ACCOMPLISHMENTS

Project 1: Study Mechanisms of Molecular Alterations in Lung Cancer

- Analyzed nuclear proteins from four cancer cell lines (H1944, A549, H460, and 17B) and found two patterns of expression.
- Discovered the consensus-alternative splicing sequence of *CEACAM1* is located within exon 7 of CEACAM1, and this site binds two major proteinsboth known to be important in splicing regulation.
- Demonstrated that PTB expression was increased in most of primary lung tumors that exhibited predominant short form *CEACAM1* when compared with matched normal lung tissues.
- Proved that promoter hypermethylation in $p16^{INK4a}$ and in *RASSF1A* tumor suppressor genes is frequently and strongly associated with clinical outcomes in patients with resectable non-small cell lung cancer.
- Demonstrated that hypermethylation of the death-associated protein kinase promoter attenuates the sensitivity of human NSCLC cells to TRAIL-induced apoptosis.
- Determined expression of seven splicing variants of DNMT3B in 119 primary non-small cell lung cancer (NSCLC) specimens and their corresponding non-malignant lung tissues.
- Illustrated that *DNMT3B* variants are involved in differential regulation of promoter methylation in lung tumorigenesis and may serve as biomarkers in lung cancer early detection and molecular classification.
- Concluded that HDGF is a novel therapeutic target for multiple human cancers and that a neutralized monoclonal antibody targeting HDGF will be effective in treating lung and pancreatic cancers.

Project 2: Develop Novel Strategies for Lung Cancer Chemoprevention

- Illustrated enhanced effects on decreasing the levels of p-4EBP1 and cyclin D1 and on increasing PARP cleavage *in vivo* from the combination of RAD001 and BEZ235.
- Induced autophagy involving downregulation of $FLIP_S$ with the use of BEZ235.
- Enhanced TRAIL-induced apoptosis with BEZ.
- Explored the mechanisms by which 4HPR induces apoptosis in NSCLC cells.
- Demonstrated that 4HPR activates the NADPH oxidase regulatory subunit Rac and that this activation is involved in ROS increase and subsequent apoptosis induction.

Project 3: Implement Experimental Molecular Therapeutic Approaches for Lung Cancer

- Developed a mouse lung cancer model that develops lung carcinomas due to an inherited mutation in the p53 tumor suppressor ($p53^{R172H\Delta g/+}$) and somatic inactivation of the *ras* oncogene ($K\text{-}Ras^{LA1/+}$).
- Discovered that lonafarnib increased microtubule acetylation and synergy with taxanes in anti-proliferation activity.
- Designed a Phase Ib combination trial of lonafarnib and docetaxel in biopsy-accessible solid tumor patients supported by a NIH/NCI P01 (CA116676-01A1) Program Project grant and pharmaceutical funds.
- Determined that determined perifosine induces apoptosis and the expression of TRAIL by inhibiting Akt phosphorylation, and reducing total Akt levels.
- Discovered that systemically delivered FUS1-lipoplex suppressed tumor growth *in vivo* and demonstrated the feasibility of the DOTAP:cholesterol-DNA vector for systemic therapy.

- Developed a phase I trial of DOTAP:cholesterol-FUS1 liposome complex (Human Gene Transfer Protocol #0201-513) that was supported by a different funding mechanism outside of this grant.
- Illustrated that the farnesyl transferase inhibitor (FTI), SCH66336, has antiangiogenic activity in aerodigestive tract cancer by suppressing the expression of HIF-1α and VEGF.
- Indicated that simultaneously targeting the PI3K/Akt and MKK4/JNK pathways might be an effective therapeutic strategy against NSCLC.
- Used mouse models to demonstrate that erlotinib significantly reduces the mean number of lesions on the lung surface.
- Analyzed array data using Affymetrix chips and indicated that the primary tumors and metastases segregate separately.
- Suggested that MDP mediates cancer cell adhesion to lung vasculature and development of lung metastases.

DRP: A Genetic/Combinatorial Algorithmic Strategy for Anticancer Therapy Development

- Screened 19 different drugs using the Medicinal Algorithmic Combinatorial Screen (MACS).
- Studied more than 500 drug combinations and analyzed for linearity**.**
- Demonstrated that research supports the premise that a functional screen that composes the MACS can serve as a useful complement to molecular insight based therapy development.

REPORTABLE OUTCOMES

Publications

Carboni GL, Gao B, Nishizaki M, Xu K, Minna JD, Roth JA, Ji L. CACNA2D2 mediated apoptosis in NSCLC cells is associated with alterations of the intracellular calcium signaling and disruption of mitochondria membrane integrity. *Oncogene* 2003 Jan 30;22(4):615-26. PMID: 12555074.

Chang YS, Wu W, Walsh G, Hong WK, Mao L. Enolase-α is Frequently Down-Regulated in Non-Small Cell Lung Cancer and Produces Aggressive Biological Behavior. *Clinical Cancer Research* 2003 Sep 1;9(10 Pt 1):3641-4. PMID: 14506152.

Elrod HA, Lin Y-D, Yue P, Wang X, Lonial S, Khuri FR, Sun S-Y. The alkylphospholipid perifosine induces apoptosis of human lung cancer cells requiring inhibition of Akt and activation of the extrinsic apoptotic pathway. *Molecular Cancer Therapeutics* 2007 Jul;6(7):2029-38. PMID: 17604333.

Han JY, Oh SH, Morgillo F, Myers JN, Kim E, Hong WK, Lee HY. Hypoxia-inducible factor 1alpha and antiangiogenic activity of farnesyltransferase inhibitor SCH66336 in human aerodigestive tract cancer. *Journal of National the Cancer Institute* 2005 Sep 7;97(17):1272-86. PMID: 16145048.

Ito I, Saeki T, Mohuiddin I, Saito Y, Branch CD, Vaporciyan A, Roth JA, Ramesh R. Persistent transgene expression following intravenous administration of a liposomal complex: role of interleukin-10-mediated immune suppression. *Molecular Therapy* 2004 Mar;9(3):318-27. PMID: 15006598.

Ji L, Nishizaki M, Gao B. Burbee D, Kondo M, Kamibayashi G, Xu K, Yen N, Atkinson EN, Fang B, Lerman MI, Roth JA, and Minna JD. Expression of Several Genes in the Human Chromosome 3p21.3 Homozygous Deletion Region by an Adenovirus Vector Results in Tumor Suppressor Activities *in Vitro* and *in Vivo*. *Cancer Research* 2002 May 1;62(9):2715-20. PMID: 11980673.

Kadara H, Schroeder CP, Lotan D, Pisano C, Lotan R. Induction of GDF-15/NAG-1/MIC-1 in human lung carcinoma cells by retinoid-related molecules and assessment of its role in apoptosis. *Cancer Biology & Therapy.* 2006 May;5(5):518-22. PMID: 16582595.

Kadara H, Tahara E, Kim HJ, Lotan D, Myers J, Lotan R. Involvement of Rac in 4HPR induced apoptosis. *Cancer Research* 2008 Jun 1;68(11):4416-23. PMID: 18519704.

Khuri FR, Glisson BS, Kim ES, Statkevich P, Thall PF, Meyers ML, Herbst RS, Munden RF, Zaknoen S, Tendler C, Zhu Y, Bangert S, Thompson E, Lu C, Wang X-M, Shin DM, Kies MS, Papadimitrakopoulou V, Fossella FV, Kirschmeier P, Bishop WR, Hong WK. Phase I study of farnesyl transferase inhibitor (FTI) lonafarnib with paclitaxel in solid tumors. *Clinical Cancer Research* 2004 May 1;10(9):2968-76. PMID: 15131032.

Lee HY, Oh SH, Suh YA, Baek JH, Papadimitrakopoulou V, Huang S, Hong WK. Response of non-small cell lung cancer cells to the inhibitors of phosphatidylinositol 3-kinase/Akt- and MAPK kinase 4/c-Jun NH2-terminal kinase pathways: an effective therapeutic strategy for lung cancer. *Clinical Cancer Research* 2005 Aug 15;11(16):6065-74.

Lee HY, Srinivas H, Xia D, Lu Y, Superty R, LaPushin R, Gomez-Manzano C, Gal AM, Walsh GL, Force T, Ueki K, Mills GB, Kurie JM. Evidence that phosphatidylinositol 3-kinase-and mitogen-

activated protein kinase kinase-4 / cJun N-terminal kinase-dependent pathways cooperate to maintain lung cancer cell survival. *Journal of Biological Chemistry* 2003 Jun 27;278(26):23630-8. PMID: 12714585.

Lu C, Soria JC, Tang X, Xu XC, Wang L, Mao L, Lotan R, Kemp B, Bekele BN, Feng L, Hong WK, Khuri FR. Prognostic Factors in Resected Stage I Non-Small Cell Lung Cancer (NSCLC): A Multivariate A nalysis of S ix M olecular Markers. *Journal of Clinical Oncology* 2004 N ov 15;22(22):4575-83. PMID: 15542809.

Marcus AI, Zhou J , O'Brate A , Hamel E, Wong J, Nivens M, El-Naggar A , Yao T P, Khuri FR, Giannakakou P . The sy nergistic combination o f t he farnesyl t ransferase i nhibitor l onafarnib an d paclitaxel enhance s tubulin ace tylation and r equires a functional t ubulin deace tylase. *Cancer Research* 2005 May 1;65(9):3883-93. PMCID: PMC1861827.

Morgillo F, Lee H-Y. Lonafarnib in Cancer Therapy: A Review. *Expert Opinion on Investigational Drugs* 2006 Jun;15(6):709-19. PMID: 16732721.

Oh Y, Mohiuddin I, Sun C, Putnam JB Jr., Hong WK, Arap W, Pasqualini R. Phenotypic Diversity of the Lung Vasculature in Experimental Models of Metastases. *Chest.* 2005 Dec;128(6 Suppl):596S-600S. PMID: 16373855.

Ramesh R, Saeki T, Templeton NS, Ji L, Stephens LC, Ito I, Wilson DR, Wu Z, Branch CD, Minna JD, Roth JA. Successful treatment of primary and disseminated human lung cancers by systemic delivery of tumor suppressor genes using an improved liposome vector. *Molecular Therapy* 2001 Mar;3(3):337-50. PMID: 11273776.

Ren H, Tang X, Lee JJ, Feng L, Everett AD, Hong WK, Khuri FR, Mao L. Expression of Hepatoma-Derived G rowth Fact or I s a S trong P rognostic Predictor for P atients with E arly-Stage N on-Small Cell Lung Cancer. *Journal of Clinical Oncology* 2004 Aug 15;22(16):3230-7. PMID: 15310766.

Schroeder C P, K adara H , Lot an D , Woo JK, Lee H Y, H ong WK, Lotan R . I nvolvement of Mitochondria and A kt-Signaling P athway i n Augmented A poptosis Induced by a C ombination of Low Doses of C elecoxib and 4H PR i n Premalignant H uman B ronchial E pithelial Cells. *Cancer Research* 2006 Oct 1;66(19):9762-70. PMID: 17018636.

Schroeder C P, Y ang P, N ewman R A, Lot an R . E icosanoid M etabolism i n S quamous Cell Carcinoma C ell Li nes Derived f rom P rimary and M etastatic Head a nd N eck Cancer and i ts Modulation by Celecoxib. *Cancer Biology & Therapy* 2004 Sep;3(9):847-52. PMID: 15254428.

Schroeder CP, Yang P , N ewman R A, Lot an R . S imultaneous inhibition of C OX-2 and 5 -LOX activities augments growth arrest and dea th of premalignant and malignant human lung cell lines. *Journal of Experimental Therapeutics & Oncology* 2007;6(3):183-92. PMID: 17552358.

Soria JC, Lee HY, Lee JI, Wang L, Issa JP, Kemp BL, Liu DD, Kurie JM, Mao L, Khuri FR. Lack of PTEN expression in non-small cell lung cancer could be r elated to promoter methylation. *Clinical Cancer Research* 2002 May;8(5):1178-84. PMID: 12006535.

Soria JC , M oon C , K emp B L, Li u D D, Fen g L, Tang X, C hang Y S, M ao L, K huri FR . Lack o f Interleukin-10 Expression Predicts Poor Outcome in Patients with State I Non-Small Cell Lung Cancer. *Clinical Cancer Research* 2003 May;9(5):1785-91. PMID: 12738735.

Sun SY, Schroeder CP, Yue P, Lotan D, Hong WK, Lotan R. Enhanced Growth Inhibition and Apoptosis Induction in NSCLC Cell Lines by Combination of Celecoxib and 4HPR at Clinically Relevant Concentrations. *Cancer Biology & Therapy* 2005 Apr;4(4):407-13. PMID: 15846100.

Tang X, Wu W, Sun SY, Wistuba II, Hong WK, Mao L. Hypermethylation of the Death-Associated Protein-Kinase Promoter Attenuates the Sensitivity to Tumor Necrosis Factor-Related Apoptosis-Inducing Ligand-Induced Apoptosis in Human Non-Small-Cell Lung Cancer Cells. *Molecular Cancer Research* 2004 Dec;2(12):685-91. PMID: 15634757.

Uno F, Sasaki J, Nishizaki M, Carboni G, Xu K, Gao B, Kondo M, Atkinson EN, Lerman MI, Minna JD, Roth JA, Ji L. Myristoylation of Fus1 protein is required for tumor suppression in lung cancer. *Cancer Research* 2004 May 1;64(9):2969-76. PMID: 15126327.

Wang J, Bhutani M, Pathak AK, Lang W, Ren H, Jelinek J, He R, Shen L, Issa J-P, Mao L. ΔDNMT3B variants regulate DNA methylation in a promoter-specific manner. *Cancer Research* 2007 Nov 15;67(22):10647-52. PMID: 18006804.

Wang J, Lee JJ, Wang L, Liu D D, Lu C, Fan Y H, Hong WK, Mao L. Value of *p16*^{INK4a} and *RASSF1A* promoter hypermethylation in prognosis of patients with resectable non-small cell lung cancer. *Clinical Cancer Research* 2004 Sep 15;10(18 Pt 1):6119-25. PMID: 15447998.

Wang L, Soria JC, Chang Y S, Lee H Y, Wei Q, Mao L. Association of a Functional Tandem Repeats in Downstream of Human Telomerase Gene and Lung Cancer. *Oncogene* 2003 Oct 16;22(46):7123-9. PMID: 14562040.

Wang L, Soria JC, Kemp BL, Liu DD, Mao L, Khuri FR. hTERT expression is a prognostic factor of survival in patients with stage I non-small cell lung cancer. *Clinical Cancer Research* 2002 Sep;8(9):2883-9. PMID: 12231532.

Wang J, Walsh G, Liu D, Lee JJ, Mao L. Expression of *ΔDNMT3B* Variants and its association with promoter methylation of *p16* and *RASSF1A* in primary non-small cell lung cancer. *Cancer Research* 2006 Sep 1;66(17):8361-6. PMID: 16951144.

Wang L, Wang J, Sun SY, Rodriguez M, Yue P, Jang SJ, Mao L. A Novel DNMT3B Subfamily, ΔDNMT3B, is the Predominant Form of DNMT3B in Non-Small Cell Lung Cancer. *International Journal of Oncology* 2006 Jul;29(1):201-7. PMID: 16773201.

Wei Q, Wang L E, Sturgis EM, Mao L. Expression of nucleotide excision repair proteins in lymphocytes as a marker of susceptibility to squamous cell carcinomas of the head and neck. *Cancer Epidemiology Biomarkers and Prevention* 2005 Aug;14(8):1961-6.. PMID: 16103444.

Zhang J, Ren H, Yuan P, Lang W, Zhang L, Mao L. Down-Regulation of Hepatoma-Derived Growth Factor Inhibits Anchorage-Independent Growth and Invasion of Non-Small Cell Lung Cancer Cells. *Cancer Research* 2006 Jan 1;66(1):18-23. PMID: 16397209.

Zheng S, El-Naggar AK, Kim ES, Kurie JM, Lozano G. A Genetic Mouse Model for Metastatic Lung Cancer with Gender Differences in Survival. *Oncogene* 2007 Oct 18;26(48):6896-904. PMID: 17486075.

Zinner RG, Barrett BL, Popova E, Damien P, Volgin AY, Gelovani JG, Lotan R, Tran HT, Pisano C, Mills G B, Mao L, Hong W K, Lippman S M, Miller JH. Algorithmic guided screening of drug

combinations of arbitrary size for activity against cancer cells. *Molecular Cancer Therapeutics* 2009 Mar;8(3):521-32. PMID: 19276160. PMID: 19276160.

Abstracts and Presentations

Began G, Ji L, Ito I, Saito Y, Branch C, Xu K, Stephens C, Minna JD, Roth JA, Ramesh R. The anti-inflammatory drug naproxen protects mice from lipoplex-mediated toxicity. National Cancer Institute, Winter Lung Cancer SPORE Meeting, Santa Monica, California, February 15-16, 2003, pp. # 41.

Chang YS, Khuri FR, Hassan KA, Wiehle SA, Ji L, Lotan R. Chun K. Hong WK, Cristiano R, Lee H. IGFBP-3 and the farnesyl transferase inhibitor SCH66336 act synergistically to induce apoptosis in non-small cell lung cancer (NSCLC) cells. American Association for Cancer Research (AACR), 94th Annual Meeting, Washington, District of Columbia, July 11-14, 2003. Proc. Am. Assoc. Cancer Res., 44:1234, 2003.

Carboni GL, Shao J, Xu K, Gao B, Nishizaki M, Schmid RA, Minna JD, Roth JA, Ji L. Synergistic inhibition of tumor cell growth by CACNA2D2 and p53 via activation of DAPK pathway in lung cancer. American Association for Cancer Research (AACR), 94th Annual Meeting, Toronto, Ontario, Canada, April 5-9, 2003. Proc. Am. Assoc. Cancer Res., 44:241-242, 2003.

Gopalan B, Ji L, Ito I. Saito Y, Branch CD. Xu K, Stephens C, Minna JD, Roth JA, Ramesh R. Protection of mice from liposome-DNA complex induced toxicity by anti-inflammatory drugs. Annual Trainee Recognition Day, M. D. Anderson Cancer Center, Houston, TX April 25, 2003

Gopalan B, Ji L. Ito I. Saito Y, Branch CD, Xu K, Stephens C, Minna JD, Roth JA, Ramesh R. The anti-inflammatory drug naproxen protects mice from lipoplex-mediated toxicity. American Association for Cancer Research (AACR), 94th Annual Meeting, Washington, District of Columbia, July 11-14, 2003. Proc. Am. Assoc Cancer Res., 44:923, 2003.

Ji L, Xu K, Sasaki J, Nishizaki M, Carboni G, Girard L, Garner H, Minna JD, Roth JA. Discovery of specific cellular regulatory pathway mediated by the tumor gene FHIT in NSCLC cells by mRNA microarray and protein chip expression profiling. National Cancer Institute Winter Lung SPORE Meeting, Santa Monica, California, February 15-16, 2003, pp. #10.

Ji L, Xu K, Nishizaki M, Sasaki J. Uno F, Girard L. Garner H, Minna JD, Roth JA. Discovery of specific cellular regulatory pathway medicated by the tumor suppressor gene FHIT in NSCLC cells by gene and protein expression profiling. American Association for Cancer Research (AACR), 94th Annual Meeting, Washington, District of Columbia, July 11-14, 2003. Proc. Am. Assoc. Cancer Res., 44:243, 2003. (presentation)

Khuri F. The treatment of lung cancer as an emerging paradigm for translational research. 2004 Cancer Research Conference, Braselton, GA, May 2004.

Khuri F. Update of retinoid studies in NSCLC, Fifth International Lung Cancer Congress, Kauai, HI, July 2004.

Khuri F. Non-small cell lung cancer therapeutics as a model for translational research, Future Directions in Hematology and Oncology, Sea Island, GA, July 2004.

Khuri F. From Prevention to Proteomics and Beyond, Lung Cancer Symposium, Mayo Clinic, Rochester, MN, August 2004.

Khuri F. Molecularly Targeted Approaches to the Chemoprevention of Lung Cancer, 10th World Conference on Lung Cancer, Lisbon, Portugal, September 2004.

Khuri F. Update of retinoid studies in NSCLC, The Future of Lung Cancer: A Translational Focus, Las Vegas, NV, September 2004.

Khuri F. Molecularly Targeted Approaches to Lung Cancer, Grand Rounds at the University of Maryland, Baltimore, MD, January 2005.

Mao L, Ren H, Chu Z, Yuan P. Therapeutic activity of neutralizing monoclonal antibodies targeting hepatoma-derived growth factor in cancer xenograft models. *ASCO Annual Meeting Proceedings* 42, Abstract #: 2517, 2006.

Lu C, Sepulveda CA, Ji L, Ramesh R, O'Connor S, Jayachandran G, Hicks ME, Munden RF, Lee JJ, Templeton NS, McMannis JD, Roth JA. Systemic therapy with tumor suppressor FUS1-nanoparticles for stage IV lung cancer. AACR Annual Meeting, 2007, Abstract #LB-348.

Marcus A, Hamel E, Nivens MD, Iaconelli J, Khuri FR, Giannakakou P. Farnesyl transferase inhibitors affect microtubule stability and function. *American Association for Cancer Research,* 2004.

Nishizaki M, Sasaki J. Carboni G, Roth JA, Ji L. Overexpression of FHIT inhibits tumor cell invasion and metastases via inactivation of the Rho-PKC-Ezrin signaling pathway in human pancreatic cancer. American Association for Cancer Research (AACR) 94th Annual Meeting, Washington, District of Columbia, July 11-14, 2003. Proc. Am. Assoc. Cancer Res., 44: 1178, 2003.

Ren H, Tang X, Feng L, Lee JJ, Everett AD, Mao L. Frequent overexpression of hepatoma-derived growth factor in early stage non-small cell lung cancer. *Proc AACR* 44: #371, 2003.

Uno F, Sasaki J, Nishizaki M. Carboni G, Xu K, Minna JD. Roth JA, Ji L. Myristoylation of Fus1 protein is required for Fus1-mediated tumor suppressing activities in human lung cancer. American Association for Cancer Research (AACR), 94th Annual Meeting, Washington, District of Columbia, July 11-14, 2003. Proc. Am. Assoc. Cancer Res., 44:75, 2003.

Zhang J, Mao L. SiRNA targeting hepatoma-derived growth factor (HDGF) inhibits growth of non-small cell lung cancer in xenograft models. The proceeding of AACR meeting abstract #: 5135, 2006.

Zinner R. MACS, Medicinal Algorithmic Combinatorial Screen. Lawrence Berkeley National Laboratory Fall 2005 Seminar Series Berkeley, CA, October 2005.

Zinner R. MACS Medicinal Algorithmic Combinatorial Screen. Biostatistics Seminar, MD Anderson Cancer Center. June 2005.

Zinner R. MACS, Medicinal Algorithmic Combinatorial Screen. Keystone Symposia: Molecular Targets for Cancer Prevention. Lake Tahoe, CA, March 9, 2006.

Patents

Ji L, Roth JA, Minna JD, Lerman MI. Chromosome 3p21.3 genes as tumor suppressors. U.S. Patent pending N0. 60/217, 112; International Patent Application No. PCT/US01/2178; European Patent Application Based on PCT/US01/21781.

Mao L, Wang J, and Wang L. A method of treating a cancer. Reference number: UTXC:875USP1.

Mao L et al. Patent application No.: 60/753,600; Title: Cancer Therapies Targeting HDGF. 2005.

Mao L et al. Anti-Hyperproliferative Therapies Targeting HDGF. Patent application No. 11611554; International Patent Application No. PCT/US2006/062176, filed December 15, 2006.

Project Generated Resources

NIH U01 (Mouse Models of Human Cancers Consortium) 4/1/2004-3/31/2009
(Baylor College of Medicine and U.T. M.D. Anderson Cancer Center)
Modeling Airway Lung Cancer and the Role of Inflammation
Role: Project (2, and 5) Leader (Lin Ji)

IRG (Institutional Research Grant) 9/30/2006-6/30/2007
This funding is to characterize the toxicity and efficacy of the triplet we identified through MACS, 4SB (4HPR plus SAHA plus bortezomib) in a nude mouse model. In addition, we are acquiring tumor and mouse host tissues to do molecular-pathological analyses
Role: Principal Investigator: Ralph Zinner, M.D.

UT Biomedical Engineering Seed Grant: 1/15/2007- 12/14/2007
Data Mining Combinations Derived from the Medicinal Algorithmic Combinatorial Screen (MACS). Through this grant, we will be using data from more than 500 cocktails screened through the MACS to analyze patterns of efficacy and the composition of the combinations. Baysean techniques will be used to generate novel candidate combinations which will then be tested using clonigenic *in vitro* assays.
Role:

R01 CA135536 Mao (PI) 05/01/2009–04/30/2014
NIH/NCI
Role of DNA Methylation Transferase 3B in Lung Tumorigenesis
The goal of the project is to determine the role of DNMT3B/deltaDNMT3B and their splicing variants in lung cancer development and progression.
Role: PI

APPENDIX A

Publications

APPENDIX B

Personnel Report

Oncogene (2003) 22, 615–626
© 2003 Nature Publishing Group All rights reserved 0950-9232/03 $25.00
www.nature.com/onc

CACNA2D2-mediated apoptosis in NSCLC cells is associated with alterations of the intracellular calcium signaling and disruption of mitochondria membrane integrity

Giovanni L Carboni[1,3], Boning Gao[2], Masahiko Nishizaki[1], Kai Xu[1], John D Minna[2], Jack A Roth[1] and Lin Ji[1]

[1]Section of Thoracic Molecular Oncology, Department of Thoracic and Cardiovascular Surgery, The University of Texas MD Anderson Cancer Center, Houston, TX 77030, USA; [2]Department of Internal Medicine and Pharmacology, Hamon Center for Therapeutic Oncology Research, University of Texas Southwestern Medical Center, Dallas, TX 75390, USA; [3]Division of General Thoracic Surgery, University Hospital Bern, Switzerland

The CACNA2D2 gene, a new subunit of the Ca^{2+}-channel complex, was identified in the homozygous deletion region of chromosome 3p21.3 in human lung and breast cancers. Expression deficiency of the CACNA2D2 in cancer cells suggests a possible link of it to Ca^{2+} signaling in the pathogenesis of lung cancer and other cancers. We investigated the effects of overexpression of CACNA2D2 on intracellular Ca^{2+} contents, mitochondria homeostasis, cell proliferation, and apoptosis by adenoviral vector-mediated wild-type CACNA2D2 gene transfer in 3p21.3-deficient nonsmall cell lung cancer cell lines. Exogenous expression of CACNA2D2 significantly inhibited tumor cell growth compared with the controls. Overexpression of CACNA2D2 induced apoptosis in H1299 (12.5%), H358 (13.7%), H460 (22.3%), and A549 (50.1%) cell lines. Levels of intracellular free Ca^{2+} were elevated in AdCACNA2D2-transduced cells compared with the controls. Mitochondria membrane depolarization was observed prior to apoptosis in Ad-CACNA2D2 and Adp53-transduced H460 and A549 cells. Release of cyt *c* into the cytosol, caspase 3 activation, and PARP cleavage were also detected in these cells. Together, these results suggest that one of the pathways in CACNA2D2-induced apoptosis is mediated through disruption of mitochondria membrane integrity, the release of cyt *c*, and the activation of caspases, a process that is associated with regulation of cytosolic free Ca^{2+} contents.
Oncogene (2003) **22,** 615–626. doi:10.1038/sj.onc.1206134

Keywords: tumor suppressor genes; apoptosis; calcium channel proteins; human chromosome 3p21.3; lung cancer

Introduction

The novel gene CACNA2D2 has recently been identified in the homozygous deletion region of chromosome 3p21.3 in human lung and breast cancers (Gao *et al*., 2000, Lerman and Minna, 2000). It is characterized structurally as a new $\alpha 2\delta 2$ auxiliary subunit of the voltage-activated calcium channel (VACC) protein complex. The CACNA2D2 gene spans an $\sim$140 kb genomic locus in the 3p21.3 region, consists of at least 40 exons, and is expressed as a 5.5–5.7 kb mRNA. The CACNA2D2 protein consists of 1146 amino acids with a predicted molecular mass of 130 kDa (Gao *et al*., 2000). Three splicing variants of CACNA2D2 mRNA have been detected, which result in two protein isoforms with different N-terminals (Angeloni *et al*., 2000). The CACNA2D2 protein shows a 56% amino-acid sequence homology to that of the $\alpha 2\delta 1$ subunit of the VACC complexes and shares a similar secondary and tertiary structure with the CACNA2D1, as suggested by the analysis of hydrophobicity, potential glycosylation sites, and bridge-forming cysteines of the primary sequence (Angeloni *et al*., 2000). The CACNA2D2 protein is highly expressed in normal lung tissue, but either absent or underexpressed in more than 50% of lung cancers (Gao *et al*., 2000). Since cancer cells are deficient in CACNA2D2, it has been suggested that CACNA2D2 could be a tumor suppressor gene linking Ca^{2+} signaling with the pathogenesis of lung cancer and other cancers (Gao *et al*., 2000).

Growing evidence has demonstrated that Ca^{2+} signaling regulates and controls diverse cellular processes such as cell fertilization, development, proliferation, learning and memory, contraction and secretion, and cell death (Berridge *et al*., 1998, 2000). The universality of calcium as an intracellular messenger depends on the enormous range of timing, spatial, and temporal signals it can create in the complicated cellular processes (Berridge *et al*., 1998, 2000). Alteration of the spatial and temporal balances of intracellular calcium by either environmental stimuli or calcium effectors can result in cell death by both necrosis and apoptosis (Lemasters *et al*., 1998; Berridge *et al*., 2000; Zhu *et al*., 2000).

Early loss of CACNA2D2 expression in the pathogenesis of lung cancer (Angeloni *et al*., 2000), inactivation of expression of other calcium channel-related

*Correspondence: L Ji, Department of Thoracic and Cardiovascular Surgery, Box 445, The University of Texas MD Anderson Cancer Center, 1515 Holcombe Blvd, Houston, TX 77030, USA;
E-mail: lji@mail.mdanderson.org
Received 7 July 2002; revised 4 October 2002; accepted 8 October 2002

proteins such as calcium/calmodulin-dependent death-associated protein kinase (DAPK) (Raveh and Kimchi, 2001) and CACNA1G by promoter hypermethylation in various human cancers (Toyota *et al*., 1999; Ueki *et al*., 2000; Zochbauer-Muller *et al*., 2001), and the growing role of Ca^{2+} signaling in cell regulation (Berridge *et al*., 2000), and especially its involvement in the mitochondria-mediated apoptotic pathway (Rutter and Rizzuto, 2000; Zhu *et al*., 2000), motivated us to further investigate the function of the calcium channel protein CACNA2D2 in the regulation of cell proliferation and cell death and in the pathogenesis of human cancers. This study encompasses the effect of the ectopic expression of CACNA2D2 on mitochondria homeostasis, cell proliferation, apoptosis, and intracellular Ca^{2+} contents by adenoviral vector-mediated wild-type (wt)-CACNA2D2 gene transfer in various 3p21.3-deficient NSCLC cell lines. We demonstrated that CACNA2D2-induced apoptosis was mediated through a cellular process involved in the regulation of the intracellular Ca^{2+} contents, the disruption of mitochondria membrane integrity, the release of cyt *c*, and the activation of downstream caspases.

Results

Exogenous expression of CACNA2D2 inhibits tumor cell growth

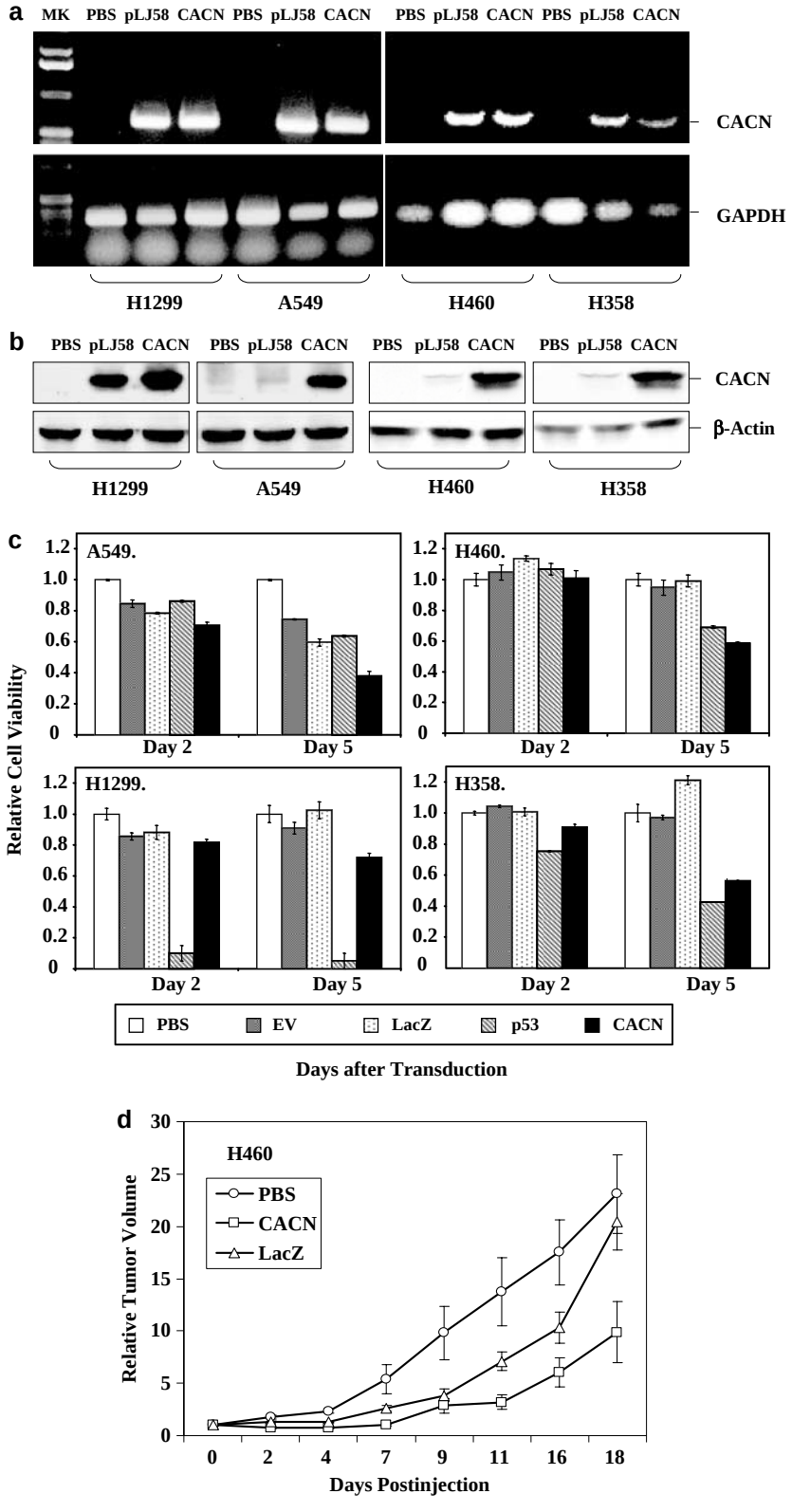
To evaluate whether the CACNA2D2 could function as a tumor suppressor or a cell death mediator by inhibition of tumor cell growth in lung cancer, we performed a series of experiments to study the effect of ectopic expression of the CACNA2D2 gene on cell proliferation in various Ad-CACNA2D2-transduced human NSCLC cell lines NCI-H1299, NCI-H460, NCI-H358, and A549, with varying status of 3p21.3 markers (Figure 1). Cells from each line were transduced *in vitro* by the Ad-CACNA2D2 vector administered at various MOIs, and cells treated with PBS, the empty vector Ad-EV, Ad-LacZ, or Ad-GFP were used as controls. The transduction efficiency was determined by examining the GFP-expressing cells in the Ad-GFP transduced cell population under a fluorescence microscope. The transduction efficiency of the adenoviral vectors was greater than 80% at the highest MOI applied for each cell line. Expression of CACNA2D2 was verified by RT-PCR analysis (Figure 1a) and Western blot analysis (Figure 1b), respectively, in Ad-CACNA2D2-transduced NSCLC cells. The transfection by plasmid DNA and the transduction by adenoviral vector are less efficient in A549, H460, and H358 cells than those in H1299 cells. Although the transcription of CACNA2D2 could be detected by RT-PCR (Figure 1a), the protein expression could only be detected at a trace amount by Western blot analysis (Figure 1b) in the CACNA2D2-containing plasmid DNA-transfected A459, H460, and H358 cells. A significantly elevated expression of CACNA2D2 proteins could be detected in all cell lines transduced by the Ad-CACN vector (Figure 1b).

We analysed cell proliferation by determining the viability of cells at 2 and 5 days post-transduction, respectively. Tumor cell growth was significantly inhibited in all the cell lines transduced by the Ad-CACNA2D2 vector 5 days after transduction, compared with what we observed with untreated cells (PBS) or those treated with Ad-EV and Ad-LacZ controls (Figure 1c). The A549 cell line appeared to be the most sensitive to the ectopic expression of CACNA2D2 and showed a more than 60% reduction in cell viability at day 5 (Figure 1c, A549), while moderate reduction of cell viability was observed in Ad-CACNA2D2-transduced H358 (44%), H460 (42%), and H1299 (28%) cells (Figure 1c). Adp53 was used as a positive control and was less effective than Ad-CACNA2D2 in A549 and H460, which contain wt-p53. No significant effect on cell viability was observed in controls treated with PBS, AdEV, and Ad-LacZ.

The effect of enforced expression of the wt-CACNA2D2 gene on tumor growth was further evaluated *in vivo* by direct intratumoral injection of Ad-CACNA2D2 vector, along with PBS and Ad-LacZ vector as controls, into human NSCLC H460 tumor xenografts in *nu*/*nu* mice (Figure 1d). The growth of tumors was recorded from the first injection until about 20 days after the last injection. Tumor volumes were normalized by calculat-

Figure 1 Adenoviral vector-mediated ectopic expression of CACNA2D2 gene inhibited NSCLC cell growth *in vitro*. (**a**) Expression of the CACNA2D2 gene in Ad-CACNA2D2 (CACN)-transduced NSCLC cells by RT–PCR analysis. Total RNAs were prepared from H1299, A549, H460, and H358 cells transduced by the Ad-CACNA2D2 vector for 48 h at MOIs of 1000 and 2500 vp/c, respectively, and the RNA prepared from cells transfected with a CACNA2D2-expressing plasmid DNA (pLJ58) was used as a positive control. The RNA samples were treated with DNAse prior to the RT reaction. (**b**) Western blot analysis of expression of CACNA2D2 protein. The crude protein lysates were prepared from NSCLC cells treated in the same way as described for RNA sample preparation in **a**. The rabbit anti-CACNA2D2 polyclonal antibodies were used for blotting. (**c**) XTT assay shows the effect of ectopic expression of CACNA2D2 on tumor cell viability. Cells from NSCLC cell lines A549, H460, H1299, and H358 were tranduced with Ad-CACNA2D2 vectors (CACN) at varied MOIs: 2500 for A549, 4000 for H460, 1000 for H1299, and 2000 vp/c for H358 cells. Untreated (PBS), Ad-EV (EV) treated, and Ad-LacZ(LacZ)-treated cells were used as negative controls and Adp53(p53)-treated cells as a positive control, at the same MOIs as CACN-treated cells for each cell line. Cell viability was calculated relative to that of untreated (PBS) controls. Differences were significant in the CACN-transduced cells compared to the untreated (PBS) control cells ($P=0.021$ in H1299, $P<0.0001$ in H358, H460, and A549 cells) and to the Ad-LacZ-transduced cells ($P<0.0001$ in H358, H460, and A549 cells) after 5 days of transduction. Differences between CACN-treated cells and controls were not significant in the H1299 cell line. (**d**) Effects of intratumoral administration of CACN on growth of human lung cancer H460 subcutaneous tumors in *nu*/*nu* mice. Results were reported as the mean $\pm$ s.d. in five to 10 mice for each treatment group. Tumor volumes were normalized by the percentage increase of tumor sizes after treatment relative to those at the beginning of the treatment in each group. Mean tumor volumes $\pm$ s.e. from these experiments are shown. The differences of the tumor volumes in the CACN-treated mice versus the PBS- and Ad-LacZ-treated controls were significant ($P<0.0001$ and 0.015, respectively)

ing the percentage increase in tumor volume after treatment relative to volume at the beginning of treatment in each group. A significant suppression of tumor growth was observed in H460 tumors treated with Ad-CACNA2D2 vector compared with those control groups treated with PBS ($P<0.0001$) and with Ad-LacZ ($P=0.015$) (Figure 1d). These results obtained *in vivo* are consistent with those observed *in vitro* for effects on inhibition of tumor cell growth and induction of apoptosis in the same cell line.



Induction of apoptosis by exogenous expression of CACNA2D2

One of the physiological functions associated with calcium channel proteins is their ability to induce apoptosis by regulating intracellular Ca^{+2} signaling and several downstream pathways (Lam *et al*., 1994; Walker and De Waard, 1998; Felix, 1999; Wang *et al*., 1999a; Zhu *et al*., 1999, 2000). To test whether the growth inhibition by the ectopic expression of CACNA2D2 was caused by induction of apoptosis, we performed FACS analysis with TUNEL reaction and PI staining to examine DNA fragmentation and cell cycle kinetics in Ad-CACNA2D2-transduced cells (Figure 2). Significant induction of apoptosis was observed in Ad-CACNA2D2-transduced A549 (50.1%) (Figure 2a), H460 (22.3%) (Figure 2b), and H358 (18.7%) (Figure 2d) cells at 5 days after transduction compared with cells treated with what was seen with the Ad-EV or Ad-LacZ (from 2 to 10%) control vectors at the same time (Figure 2). However, no significant induction of apoptosis was detected in Ad-CACNA2D2-transduced H1299 cells (Figure 2c) at the same MOIs. The magnitude of and trend toward the induction of apoptosis in these Ad-CACNA2D2-treated cells paralleled the degree and trend towards growth inhibition (Figure 1c). The correlation coefficients between the relative cell viability and the relative apoptotic cell populations in Ad-CACNA2D2-treated cells versus PBS-treated controls/PBS are significant ($P<0.05$) in all four NSCLC cell lines A549, H1299, H460, and H358 cells ($r=-0.96198$, -0.79416, -0.99436, and -0.95744, respectively), but with a less degree of correlation in H1299 cells which are less sensitive to exogenous expression of CACNA2D2, suggesting that the growth inhibition by the ectopic expression of CACNA2D2 might be mediated by the induction of apoptosis. We saw no significant alteration in cell cycle kinetics, such as G1 arrest or G2/M arrest, in these Ad-CACNA2D2-transduced cells (data not shown).

Upregulation of intracellular free cytosolic Ca^{2+}

CACNA2D2 is structurally related to the $\alpha 2\delta 2$ subunit of the VACC protein complex, which has been suggested to regulate Ca^{+2} trafficking through the channel and the retention of VACC at the plasma membrane without significant change in such properties as channel gating or permeation (Wang *et al*., 1999b; Marais *et al*., 2001). To examine whether the ectopic overexpression of this CACNA2D2 subunit would increase free cytosolic Ca^{2+} influx, we measured changes in the levels of intracellular Ca^{2+} in Ad-CACNA2D2-transduced cells by a sensitive FACS and fluorescence image analysis with fluorescent Fluo3-AM staining (Kao *et al*., 1989). Fluo3-AM dye binds specifically to free Ca^{2+} and shows an increase of emission fluorescence at 530 nm upon excitation at 488 nm. The fluorescence intensity depends on how much free Ca^{2+} is bound. We detected a significant increase of fluorescence emission in Ad-CACNA2D2-transduced H460 ($P=0.015$ and 0.03) (Figure 3a (panel c) and b) and A549 ($P=0.001$ and 0.002) (Figure 3a (panel g) and b)

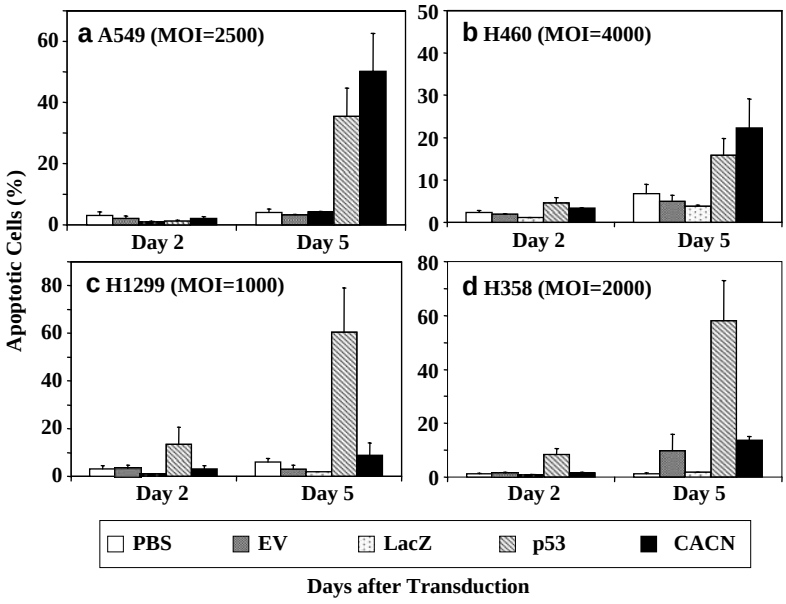


Figure 2 Apoptosis is induced by adenoviral vector-mediated expression of CACNA2D2 *in vitro*. NSCLC cell lines A549 (**a**), H460 (**b**), H1299 (**c**), and H358 (**d**) were tranduced with Ad-CACNA2D2 vectors (CACN) at varied MOIs for each line as shown in Figure 1. Untreated (PBS), Ad-EV (EV)-treated, and Ad-LacZ (LacZ)-treated cells were used as negative controls and Ad-p53(p53)-treated as a positive control. The percentage of apoptosis (TUNEL-positive) in cells transduced for 2 or 5 days, respectively, was determined by FACS analysis. Induction of apoptosis was significant in CACN-treated A549, H460, and H358 cells compared to those in PBS-treated ($P=0.0004$, 0.0321, and 0.0003, respectively) and to those in Ad-LacZ-treated ($P=0.021$, 0.048, and 0.027, respectively) controls 5 days after transduction. Differences in induction of apoptosis were not significant ($P>0.05$) between CACN-treated cells and controls in A549, H460, and H358 cell lines at 48 h post-transduction and in H1299 at both 48 and 120 h post-transduction

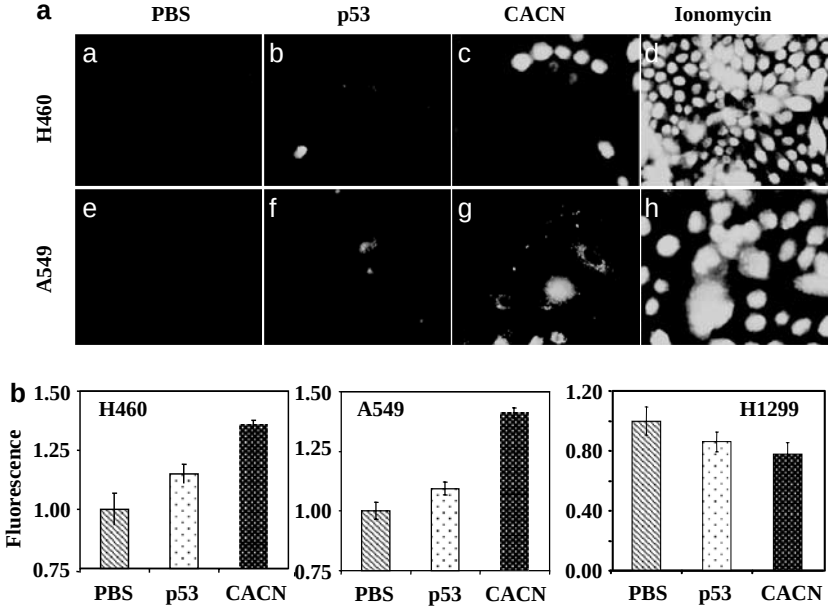


Figure 3 Ectopic expression of CACNA2D2 increased the level of the intracellular free calcium. (**a**) Fluorescence image analysis of free cytosolic Ca^{2+} in Ad-CACNA2D2 (CACN)-transduced H460 and A549 cells by Fluo 3-AM staining. Images of the CACN-treated H460 cells at an MOI of 4000 vp/c (c) and A549 cells (g) at an MOI of 2500 vp/c, untreated (PBS) (a and e) and Adp53 (p53)-treated cells (b and f), and ionomycin-treated control cells (d and h) at 48 h post-treatment are shown. (**b**) Free Ca^{2+}-specific fluorescence emission was quantified by FACS analysis with Fluo 3-AM staining. Cells were treated as described in panel. (**a**) The differences of free intracellular Ca^{2+} are expressed semiquantitatively through the differences in relative fluorescence . The increase in free cytosolic Ca^{2+} was significant in the CACN-treated H460 ($P=0.015$ and 0.032) and A549 cells ($P=0.001$ and 0.002), but not significant in H1299 cells ($P=0.785$ and 0.865) compared with the increase seen with untreated (PBS) and p53-treated controls

48 h after treatment, but this was not seen in the untreated cells and the p53-transduced cells (Figures 2a (panels a and e) and 3b), but not a significant increase in Ad-CACNA2D2-transduced H1299 cells (Figure 3b). An increase in the level of fluorescence emission in Adp53-treated cells (Figure 3a (panels b and f) and b) was also detected, but exhibited a lower magnitude and a slower manifestation (the peak emission was registered 72–96 h post-treatment) than that in Ad-CACNA2D2-transduced cells (the peak emission was registered 48 h post-treatment). The increase of free cytosolic Ca^{2+} occurred shortly prior to apoptosis in these Ad-CACNA2D2-treated cells, suggesting a possible association of the induction of apoptosis by CACNA2D2 activity and the regulation of intracellular Ca^{2+} signaling, homeostasis, or both. However, this experimental setting does not allow to link mechanistically the Ca^{2+} increase to the apoptotic induction. The Fluo3-AM loading and staining conditions were optimized and confirmed by treating cell samples with 2 μg of ionomycin (a ionophore) (Kochegarov *et al*., 2001) as a positive control, which showed uniform fluorescence emission increase in all treated cells (Figure 3a, panels d and e).

Interruption of mitochondria membrane potential

Depolarization of mitochondria and loss of mitochondria membrane potential can be a rate-limiting step in apoptosis as well as in necrotic cell death (Kroemer and Reed, 2000; Vieira *et al*., 2000). The emerging evidence suggests that an excessive influx of Ca^{2+} represents a prototypical example of a cell death stimulus where mitochondria membrane depolarization precedes cyt *c* release (Reed and Kroemer, 2000; Vieira *et al*., 2000). To investigate further the impact of the observed increase in intracellular free Ca^{2+} influx by ectopic expression of CACNA2D2 on mitochondria membrane integrity, we analysed the changes of mitochondria membrane potential in Ad-CACNA2D2-transduced NSCLC cells by FACS with mitochondria membrane potential-specific fluorescent JC-1 staining (Figure 4). Mitochondria depolarization, as demonstrated by a significant fluorescent shift with an increase in green (540 nm) emission (Figure 4a), was observed in Ad-CACNA2D2-transduced H460 and A549, cells between 24 and 48 h after transduction (Figure 4b), but not in untreated or Ad-LacZ-transduced cells. After 72 h of transduction by the Ad-CACNA2D2 vector, more than 84% of the A549 cells (Figure 4b, A549) and 80% of H460 (Figure 4b, H460) cells revealed mitochondria membrane depolarization; however, no significant changes were observed in the H1299 cells (Figure 4b, H1299). Adp53 induced similar changes in H460, A549 and H1299 cells (Figure 4). Mitochondria membrane depolarization preceding induction of apoptosis in cells transduced by Ad-CACNA2D2 at the same MOIs (Figure 2) suggests that the mitochondria depolarization mediated by an elevated level of Ca^{2+} influx is an earlier event in CACNA2D2-induced apoptosis.

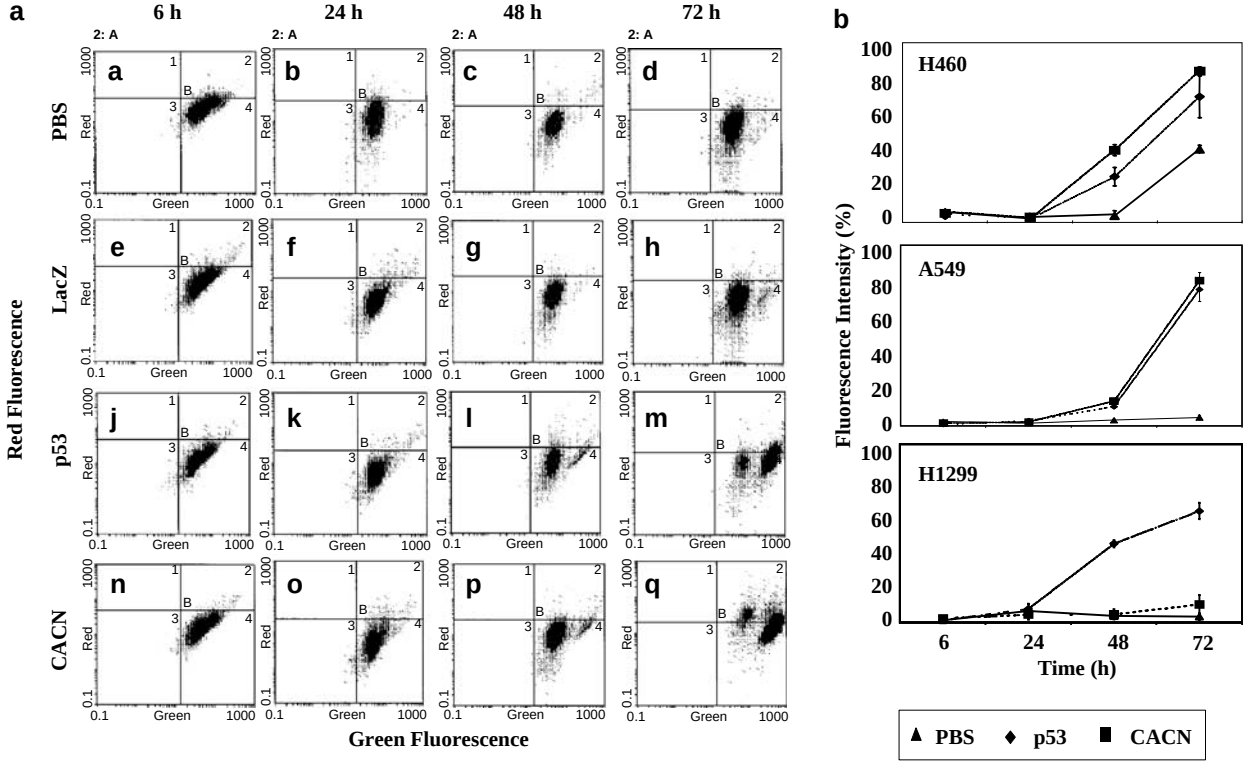


Figure 4 Ectopic expression of CACNA2D2 reduced the mitochondria membrane potential. (**a**) Changes in the mitochondria membrane potential in Ad-CACNA2D2-transduced A549 cells are revealed by FACS analysis with JC-1 staining. A549 cells were transduced with adenoviral vectors for 6, 24, 48, and 72 h at an MOI of 2500 vp/c. Fluorescence emission of red at 590 nm (indicating high membrane potential and aggregation of JC-1 dye) and green at 530 nm (indicating the collapse of membrane potential and the monomer of JC-1 dye) were measured by FACS. CACN (n, o, p, q)- and p53 (j, k, l, m)-transduced cells showed mitochondria membrane depolarization as evidenced by the fluorescence emission shift to the longer wavelength of green. PBS (a, b, c, d)- and LacZ (e, f, g, h)-transduced cells did not show a marked shift to the right. (**b**) Relative green fluorescence was higher in CACN-transduced A549, H460, and H1299 cells than in untreated (PBS) control cell. The decrease of the mitochondria membrane potential or depolarization is significant in the CACN-transduced A549 cells ($P = 0.002$) and H460 ($P = 0.005$) but not in H1299 cells after 48 h of transduction or in the untreated (PBS) control cells

Cyt c *release from mitochondria*

Release of cyt *c* from the mitochondria plays an integral role in apoptosis. To evaluate whether cyt *c* release might be an integral part of CACNA2D2-mediated apoptosis in a process involving regulation of Ca^{2+} influx and interruption of the mitochondria membrane integrity, we performed Western blot analysis of cyt *c* in the fractionated mitochondria and cytosolic lysates in Ad-CACNA2D2-treated A549 cells (Figure 5). The release of cyt *c* from mitochondria to cytosol was detected in both the Ad-CACNA2D2-transduced A549 cells at an MOI of 2500 (viral particles/cell) vp/c (Figure 5a, lanes 3 and 9) and H460 cells at an MOI of 4000 vp/c (Figure 5a, lanes 6 and 12), but no significant changes in cyt *c* in the cytosol fraction were detected in untreated (PBS) (Figure 5a, lanes 1, 4, 7, and 10) and Ad-LacZ-transduced (Figure 5a, lanes 2, 5, 8, and 11) cells. No significant change in levels of the cyt *c* in both the mitochondria and cytosol fractions was observed in Ad-CACNA2D2-transduced H1299 cells (data not shown). Cyt *c* release began at 48 h after transduction and increased over time as demonstrated in Ad-CACNA2D2-transduced A549 cells (Figure 5b). The changes in cell morphology and subcellular localization of cyt *c* (probed with an anti-human cyt *c* monoclonal antibody) were demonstrated in fluorescence images of A549 cells transduced with Ad-CACNA2D2 (Figure 5c). The characteristic pattern of the mitochondria distribution of cyt *c* still remained 24 h after transduction (Figure 5c, panel a) but was lost 48 h after transduction at this MOI (Figure 5c, panel b). The release of cyt *c* from mitochondria into the cytosol and the typical nuclear changes because of apoptosis were evident 48 h after (Figure 5c, panel b) and 72 h after (Figure 5c, panel c) transduction. The accumulation of apoptotic cell populations was also detected 48 h after transduction and increased in time as shown by FACS with PI staining (Figure 5d). The timing of the CACNA2D2-induced cyt *c* release was sequential and matched the timing of CACNA2D2-induced changes in intracellular Ca^{2+} influx (Figure 3) and mitochondria membrane potential (Figures 4 and 5d).

Activation of caspase 3 and PARP

Activation of caspases and PARP by translocation of cyt *c* from mitochondria to the cytosol is one of the

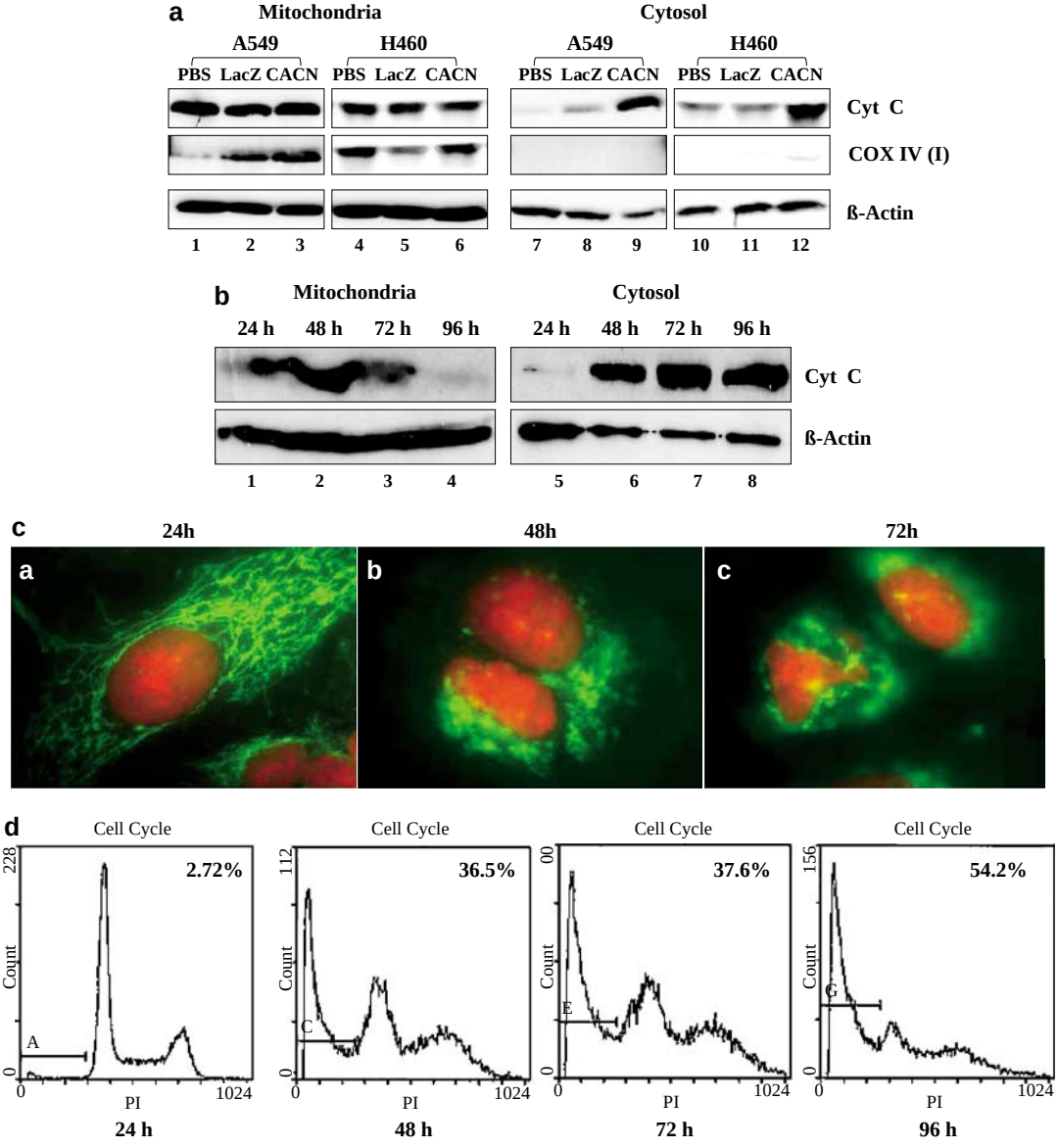


Figure 5 Western blotting was used to analyse cyt *c* release from mitochondria to cytosol in Ad-CACNA2D2-transduced cells. (**a**) Western blot of cyt *c* in CACN-transduced A549 and H460 cells. Cells were transduced with adenoviral vectors at an MOI of 2500 vp/c for A549 and MOI of 4000 vp/c for H460 for 48 h, and untreated (PBS) (lanes 1 and 4) and Ad-LacZ (LacZ)-transduced (lanes 2 and 5) cells were used as controls. Immunoblotting for cyt *c* was performed in fractionated lysates of mitochondria (lanes 1–6) and cytosol (lanes 7–12). Immunoblots of COX IV (I) were used as a mitochondria enzyme marker and *β*-actin as an internal loading control. (**b**) Time course of cyt *c* release in Ad-CACNA2D2-transduced A549 cells. (**c**) Immunofluorescence image analysis of the subcellular rearrangement of mitochondria and translocation of cyt *c* in Ad-CACNA2D2-transduced A549 cells. Mitochondria were probed with an FITC-labeled cyt *c* antibody (green) and the nucleus was counterstained with PI (red). (**d**) Timetable of induction of apoptosis in Ad-CACNA2D2-transduced A459 cells by FACS analysis with PI staining for DNA content. The percentage of induction of apoptosis was indicated by the increase of the $SubG_0$-G_1 cell populations (shown by a bar in each plot)

events that establishes the mitochondrion as an important regulator of cell life and death (von Ahsen *et al*., 2000; Martinou and Green, 2001). Western blot analysis was performed to evaluate the activation of caspase 3 and PARP downstream of the mitochondria-mediated apoptotic pathway (Figure 6). The activation of both apoptotic executioners, caspase 3 (Figure 6a) and PARP (Figure 6b), was detected in Ad-CACNA2D2-transduced H460 and A549 cells, as demonstrated by the cleaved fragments of the procaspase3 and pro-PARP on the Western blot (Figure 6). These results provide further evidence that CACNA2D2-mediated apoptosis occurs via the mitochondrion.

Discussion

The protein product of the recently cloned CACNA2D2 gene is structurally related to the $\alpha 2\delta 2$ auxiliary subunit of the voltage-activated calcium channel (VACC)

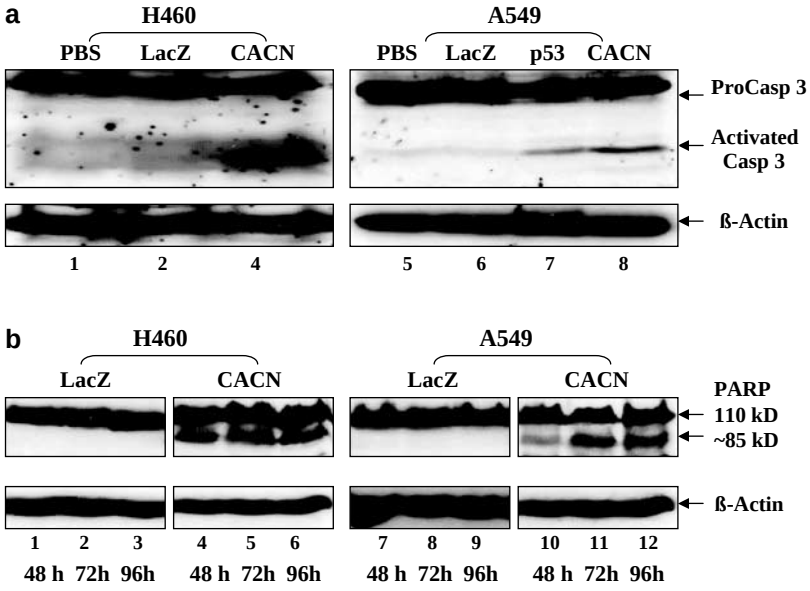


Figure 6 Downstream caspase 3 and PARP are activated by ectopic expression of the CACNA2D2 gene. (**a**) Western blot analysis of caspase 3. The whole cell lysate was prepared from Ad-CACNA2D2 (CACN)-transduced H460 cells (lanes 1–3) at an MOI of 4000 vp/c and A549 (lanes 5 and 6) cells at an MOI of 2500 vp/c after 72 h of transduction, and untreated (PBS) and Ad-LacZ (LacZ)- or Ad-p53 (p53)-transduced cells were used as controls. The cleaved procaspase 3 was indicated by an arrow. (**b**) Western blot analysis of PARP. Cells were transduced by Ad-CACNA2D2 (CACN) at the same MOI as described in **a** for each cell line. The cleaved PARP is indicated by the immunoblotting complexes of about 85 kDa. β-actin was used as an internal loading control

protein complex (Angeloni *et al*., 2000; Gao *et al*., 2000). Various VACC protein subunits such as the pore-forming $\alpha 1$ unit and the auxiliary β, γ, and $\alpha 2\delta$ subunits have been identified and partially characterized (Singer *et al*., 1991; Castellano *et al*., 1993; Brown and Gee, 1998; Burgess *et al*., 1999; Felix, 1999, Hofmann *et al*., 1999; Varadi *et al*., 1999; Catterall, 2000; Lacinova *et al*., 2000). The $\alpha 2\delta 2$ subunit (CACNA2D2) of VACC is a regulatory subunit (Gao *et al*., 2000). Mutation of this gene has been found to lead to a phenotype characterized by epilepsy, ataxia, and alterations of calcium currents in cerebellar cells in mice, which is ultimately fatal (Barclay *et al*., 2001). Although the exact physiological function of CACNA2D2 in nonexcitable cells remains unknown, functional studies of CACNA2D2 have revealed that the activity of CACNA2D2 protein may alter the conductance properties of the pore-forming $\alpha 1$ unit as well as their membrane trafficking and, therefore dynamically regulates Ca^{2+} current through the VACC (Gao *et al*., 2000; Hobom *et al*., 2000; Hurley *et al*., 2000; Klugbauer *et al*., 1999). The very frequent and early loss of expression of CACNA2D2 together with a subset of genes in the 3p21.3 homozygous deletion region of human chromosome 3 in human lung and breast cancers suggest a link between the CACNA2D2 and the regulation of proliferation and cell death in lung cancer pathogenesis, possibly through the regulation of the VACC-mediated Ca^{2+} influx (Angeloni *et al*., 2000; Gao *et al*., 2000; Lerman and Minna, 2000). However, no direct evidence has been presented for this link. In this study, we focused on CACNA2D2-mediated apoptosis by adenoviral vector-mediated ectopic expression of the wt-CACNA2D2 gene in the CACNA2D2-deficient NSCLC cells. We presented indirect evidence to link the CACNA2D2-mediated apoptosis with the regulation of the intracellular calcium content, interruption of mitochondria membrane integrity, and activation of downstream caspases.

Inhibition of tumor cell growth by ectopic expression of CACNA2D2 is concomitant with induction of apoptosis in these Ad-CACNA2D2-transduced NSCLC cells. A significant induction of apoptosis was observed 48 h after transduction. The cell lines most sensitive to CACNA2D2-induced apoptosis were A549 and H460, which contain a wt-p53 gene and are generally resistant to either the transduction of adenoviral vectors or to wt-p53-mediated cell death. Ad-CACNA2D2-transduced H358 cells, which carry a mutated p53 gene, showed remarkable inhibition of cell growth but no significant induction of apoptosis. H1299 cells, which are p53-null, were the most resistant to CACNA2D2-induced growth inhibition and apoptosis *in vitro* and *in vivo*. These results suggest a possible association of the CACNA2D2-mediated apoptosis with the activities of wt-p53, which is very interesting and needs to be explored further.

Based on the evidence that the activity of CACNA2D2 dynamically regulates Ca^{2+} currents in L- and T-type calcium channels (Klugbauer *et al*., 1999; Gao *et al*., 2000; Hobom *et al*., 2000; Hurley *et al*., 2000), we expected that overexpression of CACNA2D2 might result in an increase in the level of cytosolic Ca^{2+} influx. A significant increase in the basal level of the intracellular free Ca^{2+} was indeed detected in Ad-CACNA2D2-transduced H460 and A549 cells using

sensitive free-Ca^{2+}-specific Fluo3-AM staining in a semiquantitative manner. Several factors, however, hinder the accurate determination of the kinetic events of the modulation of Ca^{2+} influx influenced by the adenoviral vector-mediated transient expression of CACNA2D2 protein. Gradual expression of the CACNA2D2 subunit after 24 h of transduction would cause the modulation of intracellular Ca^{2+} influx with time. Since Ca^{2+} is a multivalent messenger, several cytosolic Ca^{2+} binding proteins, such as calmodulin, can bind to the free Ca^{2+} to execute downstream effects on cellular processes, which would significantly reduce the availability of free Ca^{2+}; other Ca^{2+} effectors or mediators, such as calbindin-D, parvalbumin, and calretinin, can buffer the cytosolic increases of Ca^{2+} (Berridge *et al*., 1998, 2000). Furthermore, Ca^{2+} signals have a wide range of spatial and temporal distribution and so are capable of conveying signals in a very complex way (Lemasters *et al*., 1998; Berridge *et al*., 2000; Zhu *et al*., 2000). Together, these factors make it difficult to detect even the global Ca^{2+} oscillations in our experimental setting; therefore, our data may not represent the accurate dynamic changes of intracellular Ca^{2+} contents and influx.

Mitochondria play a major role in apoptosis triggered by many stimuli. Disruption and permeation of the mitochondria membrane are general phenomena associated with the processes of apoptosis and necrotic cell death (Kroemer and Reed, 2000, Vieira *et al*., 2000). An excessive mitochondria Ca^{2+} influx has been suggested to be a potent cell death stimulus leading to mitochondria membrane depolarization and cyt *c* release (Reed and Kroemer, 2000; Vieira *et al*., 2000). Activation of caspases by translocation of cyt *c* from mitochondria to the cytosol is a downstream event through which the mitochondrion's role as a regulator of cell life and death has become unquestioned (Chen *et al*., 2000; von Ahsen *et al*., 2000; Martinou and Green, 2001). We demonstrated that ectopic expression of CACNA2D2 was associated with the accumulation of intracellular free Ca^{2+} and the collapse of the mitochondria membrane potential prior to cyt *c* release and nuclear apoptotic changes, suggesting a physiological effect of CACNA2D2 activity in regulating cell survival by indirectly altering the mitochondria membrane integrity in concomitance with cytosolic Ca^{2+} increase. Rupture of the outer membrane results in the release of many proteins such as cyt *c* and some caspases (Desagher and Martinou, 2000). However, whether this is the result of a direct effect of the CACNA2D2-mediated Ca^{2+} oscillations on mitochondria permeability needs to be further investigated. It would also be interesting to explore the CACNA2D2-mediated Ca^{2+}-signaling pathways involved in activation of the proapoptotic mediators such as Bad and Bax and inactivation of the antiapoptotic factors such as Bcl-2 and Bclx that convey the apoptotic signal to the mitochondrion (Gross *et al*., 1999; Vieira *et al*., 2000; von Ahsen *et al*., 2000).

Together, our results suggest that ectopic expression of CACNA2D2 is capable of inducing apoptosis in several NSCLC cell lines. The induction of apoptosis by CACNA2D2 activity is associated with the regulation of cytosolic Ca^{2+} contents and the activation of the mitochondria pathway. Further identification of the physiological functions of CACNA2D2 in unexcitable cells such as normal bronchial epithelial cells, the evaluation of the cellular modulation of endogenous and exogenous expression of CACNA2D2 in response to environmental stimuli such as DNA-damaging agents and oncogene activities in normal and tumor cells, and the characterization of the effects of CACNA2D2 activity on both L- and T-type calcium channels in the presence and absence of selective inhibitors of the various VACC subtypes will provide us insight into the molecular mechanisms in the CACNA2D2-mediated regulation of cell proliferation and cell death in the pathogenesis of lung cancers and other human cancers.

Materials and methods

Cell lines and cell culture

Four human NSCLC cell lines, A549 (homozygous for multiple 3p21.3 markers and wt-*p53*), NCI-H1299 (homozygous for multiple 3p21.3 markers and homozygous deletion of *p53*), NCI-H358 (retained heterozygosity of multiple 3p21.3 markers and homozygous deletion of *p53*), and NCI-H460 (homozygous for multiple 3p21.3 markers and wt-*p53*), with varied 3p21.3 and *p53* gene status, and a normal human bronchial epithelial cell line (HBEC) or fibroblast cells were used for *in vitro* experiments. The multiple 3p21.3 markers located in the 630 kb region used for this analysis were described previously (Fondon *et al*., 1998). The A549 line was maintained in Ham's F12 medium supplemented with 10% fetal calf serum. The H1299, H358, and H460 lines were maintained in RPMI-1640 medium supplemented with 10% fetal calf serum and 5% glutamine.

Recombinant adenoviral vectors

The recombinant Ad-CACNA2D2 was constructed using our recently developed ligation-mediated plasmid adenovirus vector construction system, named herein pAd-RAP and pAd-RAP-Shuttle. The CACNA2D2 was assembled as a mammalian gene expression cassette that is driven by a CMV promoter and tailed with a bovine growth hormone (BGH) poly (A) signal sequence. Sequences of the CACNA2D2 gene in the viral vectors were confirmed by automated DNA sequencing. A vector expressing the GFP (green fluorescence protein) gene (Ad-GFP) and a vector carrying the β-galactosidase gene *Lac*Z (Ad-LacZ) were used to monitor the efficiency of transduction by the viral vectors and as nonspecific transgene expression controls. Ad-EV, an empty E1-deleted vector, was used as a negative control; Ad-p53, a vector containing the wt-*p53* gene, was used as a positive control for tumor suppression. Viral titers were determined by both optical density measurement (i.e. vp/ml) and plaque assay (i.e. plaque-forming units (PFU)/ml).

Animal experiments

All animals were maintained and animal experiments were performed under NIH and institutional guidelines established for the Animal Core Facility at the University of Texas MD Anderson Cancer Center. Procedures for H460 subcutaneous tumor inoculations in *nu*/*nu* mice were described previously

(Ji *et al*., 1999). When the average tumor size reaches about 0.5 cm in diameter, mice were injected intratumorally three times within a week with Ad-CACNA2D2 and control vectors at a dose of 3×10^{10} PFU (3×10^{12} vp)/tumor in a volume of 0.2 ml. Differences in tumor volumes between treatment groups were analysed with a mixed model ANOVA using the Statistica software (StatSoft Inc., Tulsa, OK, USA). A difference was considered to be statistically significant when $P = 0.05$.

Analysis of CACNA2D2 gene Expression by RT–PCR

Total RNA samples were isolated from Ad-CACNA2D2-transduced tumor cells using TRIZOL reagent (Life Technologies, Grand Island, NY, USA) as instructed by the manufacturer. The RT reaction was performed using a reverse transcription kit with the oligo-d$(T)_{16}$ as a primer under the conditions recommended by the manufacturer (Perkin-Elmer Applied Biosystems, Foster City, CA, USA). The RT–PCR products amplified with human total RNA as a template and glyceraldehyde-3-phosphate dehydrogenase (GAPDH) primers were used as an internal control. The primers for CACNA2D2 were 5′GACTGACCAACACCACTCTTCTC (sense, within CACNA2D2 cDNA) and 5′CTCATCGTACCTCAGCTCCTTCC (antisense, within the BGH poly (A) signaling region). The PCR was performed using an AmpliTaq PCR Kit and a 9600 PCR instrument according to the manufacturer's instructions (Perkin-Elmer Applied Biosystems).

Cell viability assay

Inhibition of tumor cell growth by treatment with Ad-CACNA2D2 and control vectors was analysed by quantitatively determining cell viability using an improved XTT assay (Roche Molecular Biochemicals, Indianapolis, IN, USA). Briefly, cells were plated in 96-well microtiter plates at 1×10^3 cells/well in 100 μl of medium. One day after the cells were plated, a 100-μl aliquot of medium containing individual adenoviral vectors at various multiplicities of infection MOI in units of vp/cell (vp/c) was placed into each sample well, and phosphate-buffered saline (PBS), Ad-EV, Ad-LacZ, and Adp53 were added as controls. On designated sampling days after transduction, cell growth and viability were quantified by XTT assay as described previously (Nishizaki *et al*., 2001). The percentage of cell viability was calculated in terms of the absorbency of treated cells relative to the absorbency of untreated control cells. Experiments were repeated at least three times with quadruplicate samples for each treatment in each individual experiment.

Analysis of apoptosis and cell cycle kinetics

Induction of apoptosis in tumor cells treated with various adenoviral vectors was analysed by flow cytometry (FACS) using terminal deoxynucleotidyl transferase-mediated dUTP nickend labeling (TUNEL) reaction with fluorescein (FITC)-labeled dUTP (Roche Molecular Biochemicals, Mannheim, Germany). Briefly, cells were plated in six-well plates (1×10^6 cells/well) and treated by various Ad-CACNA2D2 vectors; PBS, Ad-EV, Ad-LacZ, and Adp53 were used as controls. At designated times after transduction, cells were harvested and washed in PBS. Cells were processed for FACS analysis to determine apoptosis and cell cycle kinetics as described previously (Ji *et al*., 1999).

Measurement of cytosolic free calcium

The intracellular free Ca^{2+} was measured by FACS and fluorescence image analysis with free-Ca^{2+}-sensitive Fluo3-AM green fluorescent staining (Molecular Probes, Eugene, OR, USA) in Ad-CACNA2D2-transduced A549 and H460 cells. Cells were cultured in 100 mm dishes at about 5 x 10^6 cells/dish and transduced with adenoviral vectors at varied MOIs. After 24 and 48 h of transduction, cells were collected and washed once with 1 × HBSS supplemented with 1 mM Ca^{2+}, 1 mM Mg^{2+}, and 1% fetal bovine serum (FBS). The Fluo3-AM stock solution was prepared by first dissolving 50 μg of Fluo3-AM dye in 20 μl of DMSO containing 20% of the detergent Fluronic F-127 (Molecular Probes) and then mixing it with 117 μl of FBS. The cells were resuspended in 1 ml of HBSS containing the Fluo3-AM dye in a final concentration of 2.5–5.0 μg/ml, depending on the cell type. The anion carrier inhibitor probenecid was added at a final concentration of 4 mM to minimize the dye leakage. The cells were incubated for 45 min at room temperature on an orbital shaker in the dark. Cells were spun down by centrifugation for 5 min at 1500 r.p.m. and washed once with HBSS. Cells were gently resuspended in HBSS containing 4 mM of probenecid and then incubated for 20 min in the dark to allow cellular esterases to cleave the acetoxymethyl group of Fluo3-AM. Fluorescence intensity in the stained cells was measured by FACS analysis at an excitation wavelength of 488 nm and an emission wavelength of 530 nm. Experiments were performed three times independently. To evaluate the conditions of dye loading, 2 μg of ionomycin, an ionophoric antibiotic synthesized by *Streptomyces conglobatus* sp. (Calbiochem, Fremont, CA, USA), was added to each of the cell samples in a separate tube, and the dynamic fluorescence emission was measured by FACS after baseline fluorescence was assessed. For fluorescence imaging analysis of Fluo3-AM stained cells, the cells were cultured in chamber slides (Falcon), and then treated and stained with Fluo3-AM with the same procedure as was described for FACS analysis. The stained cells were examined under a microscope (Nikon Labophot 2) equipped with a digital camera (Nikon DMX1200, Tokyo, Japan) and the analysis software (Nikon ACT-1 V2.0).

Analysis of mitochondria membrane potential by FACS with JC-1 staining

Changes in mitochondria membrane potential in adenoviral vector-transduced cells were measured by flow cytometry with JC-1 (5,5′,6,6′-tetrachloro-1,1′3,3′-tetraethylbenzimidazolylcarbocyanine iodide) staining (Molecular Probes, Eugene, OR, USA). JC-1 exists as a monomer at low concentrations or at low membrane potential and emits green fluorescence at 527 nm. However, at higher concentrations or higher membrane potentials, JC-1 forms J-aggregates and emits maximum red fluorescence at ~590 nm. The measurement of the ratio of the red to green JC-1 fluorescence in cells by flow cytometry is a sensitive and specific method for monitoring changes in mitochondria potential in living cells during induction of apoptosis by various agents (Ankarcrona *et al*., 1995; Cossarizza *et al*., 1995). Cells were cultured in six-well plates and, after reaching ~70% confluence, transduced with various adenoviral vectors at varied MOIs. Cells were collected by centrifugation for 5 min at 2000 r.p.m. at 4°C and resuspended in complete medium containing 10 mg/ml JC-1 at a density of 5×10^5 cells/ml. The cells were incubated for 10 min at room temperature in the dark, washed twice with cold PBS, resuspended in 400 ml of PBS, and analysed immediately by flow cytometry.

For *in situ* fluorescent staining with JC-1, cells were cultured in chamber slides. At designated time points, the medium was removed and the cells incubated in reduced serum Opti-MEM-I medium (GIBCO BRL, Grand Island, NY, USA) containing 10 μg/ml of JC-1 for 10 min in the dark. After washing and air-drying, stained cells were immediately examined by fluorescence microscopy.

Western blot analysis

Western blot analysis was performed to evaluate the expression of CACNA2D2 protein, the release of cyt *c*, activation of caspase 3 and PARP, and other protein expression in Ad-CACNA2D2 and control vector-transduced cells. For the preparation of crude cell lysates, cells were suspended in SDS–PAGE running buffer containing a complete set of proteinase inhibitors (Roche Molecular Biochemials, Mannheim, Germany) and lysed for 20 min at 4°C. Cell lysates were passed through a 25-gauge needle and briefly sonicated twice for 30 s. For cyt *c* analysis, cell fractionation was performed to separate mitochondria-enriched fractions from cytosol fractions using an Apo-Alert Cell Fractionation Kit (ClonTech, Palo Alto, CA, USA) according to the manufacturer's instructions. Fractionated cell lysates were kept in equal volume in 2 × lysis buffer supplemented with 62.5 mM urea. Protein concentrations were assayed using the Bio-Rad protein assay reagent (Bio-Rad Laboratories, Hercules, CA, USA). The crude cell lysates (about 50 μg) were used in standard SDS–PAGE and Western blot analysis.

Immunofluorescence staining

Immunofluorescence staining was performed in cells cultured in chamber slides. At designated time points, the cells were washed twice with cold PBS fixed in 4% paraformaldehyde for 15 min at 4°C and made permeable by incubation for 5 min in a solution containing 0.1% Triton X-100 and 0.1% sodium citrate. The cells were incubated with the primary monoclonal mouse anti-cyt C antibody for 60 min at 37°C, and after washing were incubated with the FITC-labeled secondary rabbit anti-mouse IgG antibodies for 60 min. After three washing steps in 0.1% Tween 20–PBS solution and air-drying, the slides were mounted with aqueous mounting medium containing 50 μg/ml of PI for nuclear staining and immediately examined under a fluorescence microscope.

Statistics

All the experiments were repeated at least two times with duplicates or triplicates of samples. The results were expressed as mean $\pm$ s.d. Student's two-sided *t*-test was used to compare the values of the test and control samples. A value of $P<0.05$ was taken as significant.

Abbreviation:
ADP, adenosinediphosphate; CACNA2D2, calcium-channel alfa-2-delta-2 subunit; COX IV (I), cytochrome oxidase IV subunit I; cyt C, cytochrome C; DAPK, death-associated protein kinase; DMSO, dimethylsulfoxide; FBS, fetal bovine serum; HBSS, Hanks balanced saline solution; MOI, multiplicity of infection; NSCLC, non-small cell lung cancer; PARP, poly ADP-ribose polymerase; PI, propidiumiodide; TUNEL, terminal deoxynucleotidyl transferase-mediated dUTP nick-end labeling; VACC, voltage-activated calcium channel; XTT, sodium 3,3′-{1-[(phenylamino)carbonyl]-3,4-tetrazolium}-bis(4-methoxy-6-nitro)-benzene sulfonic acid hydrate; wt, wild-type.

Acknowledgments
The authors would like to thank Karen Ramirez and Wendy Schober-Ditmore for their assistance in FACS analysis, and David McConkey, Leta Nutt, and Abujiang Pataer for discussions on the methodology. This work was partially supported by grants from the National Cancer Institute, the National Institutes of Health SPORE (2P50-CA70907-04); (P01 CA78778-01A1) (JAR); (CA71618) (JDM), a WM Keck Gene Therapy Career Development Grant (LJ), by a grant from the Department of the Army BESCT Lung Cancer Program (DAMD17011068902); by the Swiss National Science Foundation (GLC) and Bernische Krebsliga (GLC); by gifts to the Division of Surgery MD Anderson Cancer Center, from Tenneco and Exxon for the Core Laboratory Facility; by the M. D. Anderson Cancer Center Support Core Grant (CA16672); by a grant from the Tobacco Settlement Funds as appropriated by the Texas State Legislature (Project 8), and by a sponsored research agreement with Introgen Therapeutics, Inc. (SR93-004-1).

References

Angeloni D, Wei MH, Duh FM, Johnson BE and Lerman MI. (2000). *Mol. Cell Probes*, **14,** 53–54.

Ankarcrona M, Dypbukt JM, Bonfoco E, Zhivotovsky B, Orrenius S, Lipton SA and Nicotera P. (1995). *Neuron.*, **15,** 961–973.

Barclay J, Balaguero N, Mione M, Ackerman SL, Letts VA, Brodbeck J, Canti C, Meir A, Page KM, Kusumi K, Perez-Reyes E, Lander ES, Frankel WN, Gardiner RM, Dolphin AC and Rees M. (2001). *J. Neurosci.*, **21,** 6095–6104.

Berridge MJ, Bootman MD and Lipp P. (1998). *Nature*, **395,** 645–648.

Berridge MJ, Lipp P and Bootman MD. (2000). *Nat. Rev. Mol. Cell. Biol.*, **1,** 11–21.

Brown JP and Gee NS. (1998). *J. Biol. Chem.*, **273,** 25458–25465.

Burgess DL, Davis CF, Gefrides LA and Noebels JL. (1999). *Genome Res.*, **9,** 1204–1213.

Castellano A, Wei X, Birnbaumer L and Perez-Reyes E. (1993). *J. Biol. Chem.*, **268,** 3450–3455.

Catterall WA. (2000). *Annu. Rev. Cell Dev. Biol.*, **16,** 521–555.

Chen Q, Gong B and Almasan A. (2000). *Cell Death Differ.*, **7,** 227–233.

Cossarizza A, Cooper EL, Quaglino D, Salvioli S, Kalachnikova G and Franceschi C. (1995). *Biochem. Biophys. Res. Commun.*, **214,** 503–510.

Desagher S and Martinou JC. (2000). *Trends Cell Biol.*, **10,** 369–377.

Felix R. (1999). *Receptors Channels*, **6,** 351–362.

Fondon JW, Mele GM, Brezinschek RI, Cummings D, Pande A, Wren J, O'Brien KM, Kupfer KC, Wei MH, Lerman M, Minna JD and Garner HR. (1998). *Proc. Natl. Acad. Sci. USA*, **95,** 7514–7519.

Gao B, Sekido Y, Maximov A, Saad M, Forgacs E, Latif F, Wei MH, Lerman M, Lee JH, Perez-Reyes E, Bezprozvanny I and Minna JD. (2000). *J. Biol. Chem.*, **275,** 12237–12242.

Gross A, McDonnell JM and Korsmeyer SJ. (1999). *Genes Dev.*, **13,** 1899–1911.
Hobom M, Dai S, Marais E, Lacinova L, Hofmann F and Klugbauer N. (2000). *Eur. J. Neurosci.*, **12,** 1217–1226.
Hofmann F, Lacinova L and Klugbauer N. (1999). *Rev. Physiol. Biochem. Pharmacol.*, **139,** 33–87.
Hurley JH, Cahill AL, Currie KP and Fox AP. (2000). *Proc. Natl. Acad. Sci. USA*, **97,** 9293–9298.
Ji L, Fang B, Yen N, Fong K, Minna JD and Roth JA. (1999). *Cancer Res.*, **59,** 3333–3339.
Kao JP, Harootunian AT and Tsien RY. (1989). *J. Biol. Chem.*, **264,** 8179–8184.
Klugbauer N, Lacinova L, Marais E, Hobom M and Hofmann F. (1999). *J. Neurosci.*, **19,** 684–691.
Kochegarov AA, Beylina SI, Matveeva NB, Leontieva GA and Zinchenko VP. (2001). *Comparative Biochem. Physiol.* **128**(Part A), 279–288.
Kroemer G and Reed JC. (2000). *Nat. Med.*, **6,** 513–519.
Lacinova L, Klugbauer N and Hofmann F. (2000). *Gen. Physiol. Biophys.*, **19,** 121–136.
Lam M, Dubyak G, Chen L, Nunez G, Miesfeld RL and Distelhorst CW. (1994). *Proc. Natl. Acad. Sci. USA*, **91,** 6569–6573.
Lemasters JJ, Nieminen AL, Qian T, Trost LC, Elmore SP, Nishimura Y, Crowe RA, Cascio WE, Bradham CA, Brenner DA and Herman B. (1998). *Biochim. Biophys. Acta.*, **1366,** 177–196.
Lerman MI and Minna JD. (2000). *Cancer Res.*, **60,** 6116–6133.
Marais E, Klugbauer N and Hofmann F. (2001). *Mol. Pharmacol.*, **59,** 1243–1248.
Martinou JC and Green DR. (2001). *Nat. Rev. Mol. Cell Biol.*, **2,** 63–67.
Nishizaki M, Meyn RE, Levy LB, Atkinson EN, White RA, Roth JA and Ji L. (2001). *Clin. Cancer Res.*, **7,** 2887–2897.
Raveh T and Kimchi A. (2001). *Exp. Cell Res.*, **264,** 185–192.
Reed JC and Kroemer G. (2000). *Cell Death Differ.*, **7,** 1145.
Rutter GA and Rizzuto R. (2000). *Trends Biochem. Sci.*, **25,** 215–221.
Singer D, Biel M, Lotan I, Flockerzi V, Hofmann F and Dascal N. (1991). *Science*, **253,** 1553–1557.
Toyota M, Ho C, Ohe-Toyota M, Baylin SB and Issa JP. (1999). *Cancer Res.*, **59,** 4535–4541.
Ueki T, Toyota M, Sohn T, Yeo CJ, Issa JP, Hruban RH and Goggins M. (2000). *Cancer Res.*, **60,** 1835–1839.
Varadi G, Strobeck M, Koch S, Caglioti L, Zucchi C and Palyi G. (1999). *Crit. Rev. Biochem. Mol. Biol.*, **34,** 181–214.
Vieira HL, Haouzi D, El Hamel C, Jacotot E, Belzacq AS, Brenner C and Kroemer G. (2000). *Cell Death Differ.*, **7,** 1146–1154.
von Ahsen O, Waterhouse NJ, Kuwana T, Newmeyer DD and Green DR. (2000). *Cell Death Differ.*, **7,** 1192–1199.
Walker D and De Waard M. (1998). *Trends Neurosci.*, **21,** 148–154.
Wang HG, Pathan N, Ethell IM, Krajewski S, Yamaguchi Y, Shibasaki F, McKeon F, Bobo T, Franke TF and Reed JC. (1999a). *Science*, **284,** 339–343.
Wang M, Offord J, Oxender DL and Su TZ. (1999b). *Biochem. J.*, **342,** 313–320.
Zhu L, Ling S, Yu XD, Venkatesh LK, Subramanian T, Chinnadurai G and Kuo TH. (1999). *J. Biol. Chem.*, **274,** 33267–33273.
Zhu LP, Yu XD, Ling S, Brown RA and Kuo TH. (2000). *Cell Calcium*, **28,** 107–117.
Zochbauer-Muller S, Fong KM, Virmani AK, Geradts J, Gazdar AF and Minna JD. (2001). *Cancer Res.*, **61,** 249–255.

Enolase-α Is Frequently Down-Regulated in Non-Small Cell Lung Cancer and Predicts Aggressive Biological Behavior[1]

Yoon Soo Chang, Weiguo Wu, Garrett Walsh, Waun Ki Hong, and Li Mao[2]

Molecular Biology Laboratory, Department of Thoracic/Head and Neck Medical Oncology [Y. S. C., W. W., W. K. H., L. M.] and Department of Thoracic and Cardiovascular Surgery [G. W.], The University of Texas M. D. Anderson Cancer Center, Houston, Texas, 77030

ABSTRACT

Purpose: **Enolase-α is a cytoplasmic glycolytic enzyme important in the formation of phosphoenolpyruvate. Enolase-α and *c-myc* binding protein (MBP-1) originate from a single gene through alternative use of translational starting sites. Both enolase-α and MBP-1 can bind to the P2 element in the *c-myc* promoter and compete with TATA-box binding protein (TBP) to suppress transcription of *c-myc*.**

Experimental Design: **To determine a potential role of enolase-α *in vivo*, we analyzed enolase-α expression in non-small cell lung cancer (NSCLC) tissues from 46 patients by Western blotting and immunohistochemical analysis.**

Results: **Twelve (26%) of the 46 tumors showed a significantly reduced enolase-α expression. Although no statistically significant association was observed between the down-regulation of enolase-α and pathological stage, tumor histology, or differentiation, the patients whose tumors showed reduced enolase-α expression had a significantly poorer overall survival compared with those without down-regulation of this molecule ($P = 0.0398$).**

Conclusions: **Our results indicate down-regulation of enolase-α is common in NSCLC and may play an important role in lung tumorigenesis.**

INTRODUCTION

Lung cancer is the leading cause of cancer-related death in the United States. More than 157,000 patients will die of the disease this year alone. Development of lung cancer is the result of an accumulation of molecular abnormalities that activate oncogenes and inactive tumor suppressor genes. Understanding the biology of the disease is critical to developing novel strategies for early detection, prevention, classification, and treatment. The *c-myc* proto-oncogene is a critical factor in controlling both cell proliferation and apoptosis (1–4). The *c-myc* oncogene is important in tumor progression in multiple tumor types, including NSCLC[3] (2, 3). Several distinct mechanisms have been suggested as regulating *c-myc* expression (5). Because *c-myc* has multiple promoters, termed P0, P1, P2, and P3, regulation of its gene expression is complicated. Yet in normal and transformed cells, the majority of *c-myc* transcripts are initiated through the P2 promoter (3, 4).

MBP-1 is a M_r 37,000–38,000 protein that can bind just 5′ to the P2 TATA motif and decrease *c-myc* promoter activity in both human and mouse models (6–8). Both MBP-1 and TBP can bind to the minor groove of the *c-myc* P2 promoter, suggesting that MBP-1 may negatively regulate *c-myc* transcription by preventing transformation of a transcriptional initiation complex (8, 9). MBP-1 mRNA is identical to enolase-α mRNA, which encodes a polypeptide of about M_r 48,000 using an alternative translation site (GenBank accession nos.: M14328 and M55914). *In vitro* transcription and translation experiments show that the enolase-α transcript encodes 2 proteins, M_r 48,000 and 37,000, both of which have the ability to down-regulate *c-myc* expression (10, 11). To determine a role of enolase-α in lung tumorigenesis, we analyzed enolase-α protein expression in 46 primary NSCLC. We found that enolase-α was down-regulated in 26% of the primary NSCLC and that such down-regulation was associated with a poor clinical outcome, suggesting that enolase-α plays an important role in NSCLC.

MATERIALS AND METHODS

Study Population. Surgically resected primary tumors and corresponding normal lung tissues were obtained from the Department of Pathology at The University of Texas M. D. Anderson Cancer Center after patients' consent. These specimens were collected between 1995 and 1998, and follow-up information was obtained from the Tumor Registry at the M. D. Anderson Cancer Center. All of the patients were treated by surgery at the time of diagnosis. The primary tumor specimens consisted of 20 adenocarcinomas, 19 squamous cell carcinomas, and 7 samples of other cell types. The study population consisted of 24 males and 22 females, with a mean age of 64.1 ± 10.83 years. Other clinical characteristics are shown in Table 1.

Protein Extraction. The samples consisted of 46 paired normal/tumor tissues from patients with lung cancer. Briefly, samples were weighed and diced into small pieces with a clean

Received 12/5/02; revised 4/14/03; accepted 4/17/03.

The costs of publication of this article were defrayed in part by the payment of page charges. This article must therefore be hereby marked *advertisement* in accordance with 18 U.S.C. Section 1734 solely to indicate this fact.

[1] Supported in part by National Cancer Institute Grants CA 16620, CA 68437, CA86390, and CA91844; Tobacco Research Fund from the State of Texas; and Department of Defense Grant DAMD17-01-1-01689-1. W. K. H. is an American Cancer Society Clinical Research Professor.

[2] To whom requests for reprints should be addressed, at Molecular Biology Laboratory, Department of Thoracic/Head and Neck Medical Oncology, The University of Texas M. D. Anderson Cancer Center, 1515 Holcombe Boulevard, Houston, TX 77030. Phone: (713) 745 6363; Fax: (713) 796 8655: E-mail: lmao@mdanderson.org.

[3] The abbreviations used are: NSCLC, non-small cell lung cancer; MBP-1, *c-myc* binding protein-1; TBP, TATA-box binding protein; IHC, immunohistochemistry; CI, confidence interval.

Table 1 Analysis of the patients with NSCLC according to the expression status of enolase-α

	Normal expression	Down-Regulation	*P*
Age	64.3 ± 10.07	63.6 ± 13.24	0.394
Gender			
Male	18	6	
Female	16	6	1.000
Diameter of tumor	4.83 ± 2.72	8.32 ± 8.58	0.193
Tumor stage			
I, II	21	6	
III, IV	13	6	0.298
Tumor histology			
Adenocarcinoma	13	7	
Squamous carcinoma	15	4	
Large cell carcinoma	2	1	
Others	4	0	0.463
Differentiation			
Well differentiated	4	2	
Moderately differentiated	10	4	
Poorly differentiated	18	6	
Unclassified	2	0	0.911
Smoking status: *n* (%)			
Current; pack-year	17; 40.4 ± 22.98	2; 29.0 ± 25.52	0.183
Ex-smoker	12	7	
Nonsmoker	3	2	
Unknown	2	1	0.130
Median survival, mo (95% CI)			
Overall survival	43 (8.1–77.7)	6 (0–19.9)	0.040

razor blade and then were disrupted with a dunce homogenizer in ice-cold radioimmunoprecipitation buffer containing a protease inhibitor cocktail (Boehringer Mannheim, Indianapolis, IN). Phenylmethanesulfonyl fluoride (Sigma Chemical Co., St. Louis, MO) stock solution was added, and the lysates were incubated on ice for 30 min, followed by centrifugation twice at 10,000 × *g* for 10 min at 4°C. The supernatant was taken and stored for protein analysis.

Western Blot Analysis. Twenty μg of protein extract were loaded into each well and were separated in 10% SDS-PAGE gel under reducing conditions. Separated proteins on the gel were electrotransferred onto Hybond-polyvinylidene difluoride membranes (Amersham Pharmacia Biotechnology, Arlington Heights, IL). Membranes were blocked with 5% nonfat dry milk to reduce background.

The membrane was incubated at 4°C overnight with anti-enolase-α monoclonal antibody (9C12) at a dilution of 1:50. This antibody, donated by Dr. E. F. Plow, does not cross-react with enolase-β and γ. β-actin was detected with a monoclonal anti-β-actin antibody AC-15 (Sigma) at a dilution of 1:1000. Then the blots were incubated with a sheep antimouse secondary antibody conjugated to horseradish peroxidase. Signals were detected by enhanced chemiluminescence on Hyperfilm ECL films (Amersham Pharmacia Biotechnology). Each signal was scanned and measured using the Scion Image program (Scion Corp., Frederick, MD). β-actin was used as an internal control. The level of enolase-α expression was calculated by dividing the signal of normal tissue by that of tumor tissue. Patient tissues were classified into two groups according to the level of enolase-α expression. One group included cases that did not show down-regulation of enolase-α (ratio, <2.0), and the other was composed of cases that did show down-regulation of enolase-α (ratio, ≥2.0).

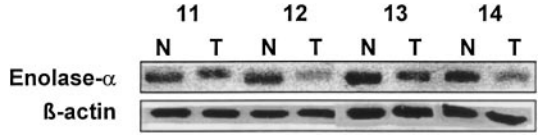


Fig. 1 Western blot of normal (*N*)-tumor (*T*) paired samples revealed that enolase-α is frequently down-regulated in primary NSCLC. β-actin was used as an internal control of protein loading.

Immunohistochemistry. IHC was performed in a conventional manner. Briefly, paraffin sections on slides were deparaffinized and rehydrated in serial graded ethanol. Antigen retrieval was skipped. Endogenous peroxidase activity was blocked in methanol containing 3% hydrogen peroxide. The blocking was performed by incubation in 5% horse serum, followed by overnight incubation with 1:100 anti-enolase-α antibody. After the sections were incubated with secondary antibody, the ABC complex and 3,3′-diaminobenzidine (Vector Laboratories, Inc., Burlingame, CA) solutions were used serially, and the slides were counterstained with hematoxylin.

Statistical Analysis. In univariate analysis, independent sample *t* tests and χ^2 tests were used for continuous and categorical variables, respectively. Kaplan-Meier analysis was performed to estimate a survival function over time for individual covariates. The log-rank test was used to compare patient survival time between groups. All of the statistical tests were two-sided. $P < 0.05$ was considered to be statistically significant.

RESULTS

Enolase-α Is Frequently Down-Regulated in NSCLC. We analyzed the expression level of enolase-α from 46 normal/cancer pairs from patients with NSCLC through Western blotting. Although 42 (91.3%) of 46 of the tumors showed some degree of reduced enolase-α expression, we used a more stringent cutoff (a 2-fold reduction) to offset experimental variations (Fig. 1). Twelve (26.1%) of the tumors were assigned to the down-regulation group according to this criterion. We performed further IHC to determine enolase-α expression status at the cellular level. In normal lung tissues, IHC showed a ubiquitous cytoplasmic and membranous staining, including staining of the bronchial epithelium and alveolar wall (Fig. 2*A*). Nuclear staining also was observed in bronchial epithelial cells, type I and type II alveolar cells, and endothelial cells, consistent with a recent report (10). Endothelial cells showed a strong cytoplasmic and nuclear staining with the anti-enolase-α antibody. Lymphocytes, however, were barely stained with this antibody. In contrast, tumors exhibiting down-regulation of enolase-α exhibited lack of antibody staining, consistent with Western blotting analysis (Fig. 2, *B* and *C*).

Enolase-α Expression and Clinical/Pathological Parameters. We analyzed clinical and pathological parameters according to enolase-α expression status. In univariate analysis, we found no age and gender differences among patients with down-regulation and those without down-regulation. In addition, no significant associations were found between down-

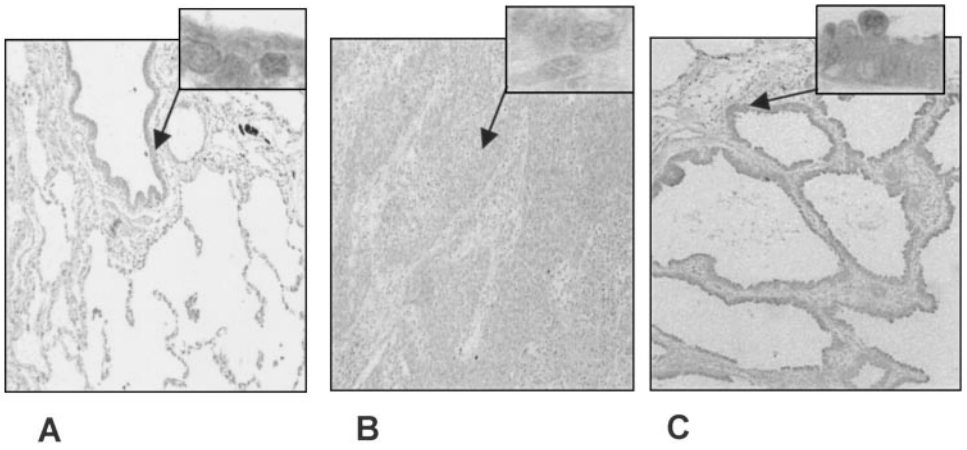


Fig. 2 IHC of normal lung tissue with enolase-α showed ubiquitous staining, including bronchial epithelium and alveolar structure (*A*). IHC of squamous lung cancer showed down-regulation of enolase-α that was consistent with the Western blot (*B*). Bronchioalveolar carcinoma, which generally has an excellent prognosis, showed a staining pattern similar to that of normal bronchial epithelium (*C*).

regulation of enolase-α and pathological stage, tumor histology, or the degree of differentiation. Although the difference was not statistically significant, patients whose tumors showed down-regulation of enolase-α bore larger tumors at the time of surgery (8.3 ± 8.58 cm) than did patients without down-regulation (4.8 ± 2.72 cm; Table 1).

Down-Regulation of Enolase-α and Clinical Outcome. At last follow-up, 29 of the 46 patients had died, and 17 were still alive. Among the living patients, the median follow-up duration was 5.7 years. During the same follow-up period, 9 (75.0%) of the 12 patients whose tumors showed loss of enolase-α expression died, compared with 20 (59%) of the 34 patients whose tumors retained enolase-α expression.

Kaplan-Meier estimates were used to examine the relationship between down-regulation of enolase-α and patients' overall survival. The median survival of patients whose tumors showed down-regulation of enolase-α was only 6 months (95% CI, 0.00–19.9 months), whereas the median survival of those whose tumors showed no down-regulation was 43 months (95% CI, 8.1–77.7 months; $P = 0.0398$ by log-rank test; Fig. 3).

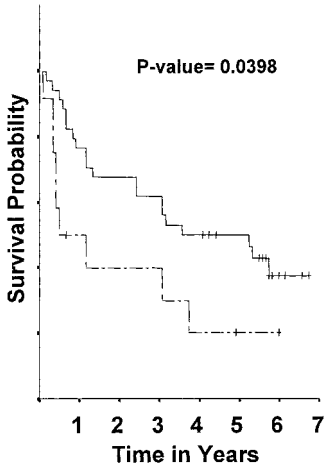


Fig. 3 Survival analysis demonstrated that patients whose tumors showed down-regulation of enolase-α had poorer overall survival compared with those whose tumors had normal expression levels of enolase-α.

DISCUSSION

Enolases have been characterized as highly conserved cytoplasmic glycolytic enzymes that catalyze the formation of phosphenolpyruvate from 2-phosphoglycerate, the second of the two high-energy intermediates that generate ATP in glycolysis (12). Three isoforms of enolase have been identified and named as enolase-α, -β, and -γ. Enolase-α expression has been detected in almost all of adult tissues, whereas enolase-β is expressed predominantly in muscle and enolase-γ is detected only in nerve tissues (13, 14). These three isoforms may exist as either homodimers or heterodimers.

Diverse functions of enolase-α have been reported in the ecosystem. It has been identified as a heat shock protein in yeast (15), an immunodominant antigen in *Candida albicans* (16), and toxin B in *Clostridium difficile* (17). It also known as a component of the centrosome in HeLa cells (18) and as a molecule associated with connective tissue disorders (19). Enolase-α is considered to have potential roles in tumorigenesis. Tumor cells possess higher metabolic rate than surrounding normal tissues, and enolases, the representative glycolytic enzyme, are an important factor in cell metabolism. There is evidence to suggest that enolase-α may involve cancer invasion and metastasis. Enolase-α has a COOH terminus that spans plasma membrane. With this domain, monocytes, neutrophils, and some cancer cell lines, such as U937, are capable of binding with, activating, and stabilizing plasminogen. By doing so, they have the capacity to clear a path for themselves through the macromolecular barriers of basement membrane and other extracellular matrix (20). Additionally the gene encoding enolase-α (*ENO-1*) maps to a region of human chromosome 1(1p35-p36) that is often deleted in several types of human malignancies, including neuroblastoma, melanoma, pheochromocytoma, and carcinoma of the breast and liver (21). Furthermore, as described earlier, the capability of enolase-α to compete with TBP to repress transcription of oncogene *c-myc* suggests a potential mechanism for how enolase-α may be involved in tumorigenesis.

To demonstrate the relevance of this finding in primary

tumors, we used a monoclonal anti-enolase-α antibody to analyze enolase-α expression status in NSCLC and its potential role in molecular classification of the tumors. We found that enolase-α is localized in both the cytoplasm and the nucleus in various cell types of normal lung tissue, including bronchial epithelium, a finding that is consistent with previous reports (8). However, 26% of the primary NSCLC exhibits substantial down-regulation of the molecule, and this down-regulation proportionally reduces staining in both the cytoplasm and the nucleus, supporting the notion that the proteins in the cytoplasm and nucleus are both enolase-α. Interestingly, tumors with enolase-α down-regulation tend to be larger than those without down-regulation, suggesting that the down-regulation is associated with tumor progression. The biological role of the down-regulation in NSCLC needs further investigation.

The association of the down-regulation of enolase-α with a poorer clinical outcome further supports the importance of this molecule in determining tumor aggressiveness in patients with NSCLC. It also indicates the importance of proteomic approaches in identifying potential biomarkers useful in cancer detection and classification. Our results should be validated in larger and independent studies to reach a definitive conclusion. It would also be interesting to determine whether up-regulation of enolase-α might have a therapeutic role in tumors lacking the molecule.

ACKNOWLEDGMENTS

We greatly appreciate the generosity of Dr. E. F. Plow at the Cleveland Clinic Foundation (Cleveland, OH), who provided the enolase-α monoclonal antibody (9G12) that was critical for this study. We also thank Georgia O. Lange in our tumor registry for providing clinical information.

REFERENCES

1. Ginsberg R. J., Vokes, E. E., and Rosenzweig, K. Non-small cell lung cancer. *In*: V. T. DeVita, Jr., S. Hellman, and S. A. Rosenberg (eds.), Cancer: Principles and Practice of Oncology, Ed. 6, pp. 925–983. Philadelphia-New York: Lippincott-Raven, 2001.

2. Weinberg, R. A. Oncogenes, anti-oncogenes, and the molecular basis of multistep carcinogenesis. Cancer Res., *49:* 3713–3721, 1989.

3. Marcu, K. B., Bossone, S. A., and Patel, A. J. *myc* function and regulation. Annu. Rev. Biochem., *61:* 809–860, 1992.

4. Potter, M., and Marcu, K. B. The *c-myc* story: where we've been, where we seem to be going. Curr. Topics. Microbiol. Immunol., *224:* 1–17, 1997.

5. Dalla-Favera, R., and Gaidano, G. Molecular pathogenesis of T-cell non-Hodgkin's lymphomas. *In*: V. T. DeVita, Jr., S. Hellman, and S. A. Rosenberg (eds.), Cancer, Principles and Practice of Oncology, Ed. 6, pp. 2228–2230. Philadelphia-New York: Lippincott-Raven, 2001.

6. Ray, R., and Miller, D. M. Cloning and characterization of a human *c-myc* promoter-binding protein. Mol. Cell. Biol., *11:* 2154–2161, 1991.

7. Ray, R. B. Induction of cell death in murine fibroblasts by a *c-myc* promoter binding protein. Cell Growth Differ., *6:* 1089–1096, 1995.

8. Ghosh, A. K., Steele, R., and Ray, R. B. Functional domain of *c-myc* promoter binding protein-1 involved in transcriptional repression and cell growth regulation. Mol. Cell. Biol., 2880–2886, 1999.

9. Chaudhary, D., and Miller, D. M. The *c-myc* promoter binding protein (MBP-1) and TBP bind simultaneously in the minor groove of the *c-myc* P2 promoter. Biochem., *34:* 3438–3445, 1995.

10. Subramanian, A., and Miller, D. M. Structural analysis of α-enolase: mapping the functional domains involved in down-regulation of the *c-myc* proto-oncogene. J. Biol. Chem., *275:* 5958–5965, 2000.

11. Feo, S., Arcuri, D., Piddini, E., Passotino, R., and Giallonogo, C. ENO-1 gene product binds to the *c-myc* promoter and acts as transcriptional repressor. FEBS Lett., *473:* 47–52, 2000.

12. Harris, R. A. Carbohydrate metabolism 1: major metabolic pathways and their control. *In:* T. M. Devlin (ed.), Textbook of Biochemistry with Clinical Correlations, Ed. 5, pp. 597–664. New York: Wiley-Liss, 2002.

13. Deloulme, J. C., Helies, A., Ledig, M., Lucas, M., and Sensenbrenner, M. A comparative study of the distribution of α- and γ–enolase subunit in cultured rat neural cells and fibroblasts. Int. J. Dev. Neurosci., *15:* 183–194, 1997.

14. Sensenbrenner, M., Lucas, M., and Deloume, J. C. Expression of two neuronal markers, growth-associated protein 43 and neuron-specific enolase, in rat glial cells. J. Mol. Med., *75:* 653–663, 1997.

15. Ida, H., and Yahara, I. Durable synthesis of high molecular weight heat shock proteins in G_0 cells of the yeast and other eucaryotes. J. Cell Biol., *99:* 199–207, 1984.

16. Sundrom, P., and Aliaga, G. R. Molecular cloning of cDNA and analysis of protein secondary structure of *Candida albicans* enolase, an abundant, immunodominant glycolytic enzyme. J. Bacteriol., *174:* 6789–6799, 1992.

17. Bisseret, F., Keith, G., Rihn, B., Amiri, I., Werneburg, B., Girardot, R., Baldacini, O., Green, G., Nguyen, V. K., and Monteil, H. *Clostridium difficile* toxin B: characterization and sequence of three peptides. J. Chromatogr., *490:* 91–100, 1989.

18. Johnstone, S. A., Waisman, D. M., and Rattner, J. B. Enolase is present at the centrosome of HeLa cells. Exp. Cell Res., *202:* 458–463, 1992.

19. Moscato, S., Pratesi, F., Sabbatini, A., Chimenti, D., Scavuzzo, M., Passatino, R., Bombardieri, S., Giallongo, A., and Migliorini, P. Surface expression of a glycolytic enzyme, α-enolase, recognized by autoantibodies in connective tissue disorders. Eur. J. Immunol., *30:* 3575–3584, 2000.

20. Redlitz, A., Fowler, B. J., Plow, E. F., and Miles, L. A. The role of an enolase-related molecule in plasminogen binding to cells. Eur. J. Biochem., *227:* 407–415, 1995.

21. Weith, A., Brodeur, G. M., Bruns, G. A., Matise, T. C., Mischke, D., Nizetic, D., Seldin, M. F., van Roy, N., and Vance, J. Report of the second international workshop on human chromosome 1 mapping 1995. Cytogenet. Cell Genet., *72:* 114–144, 1996.

The alkylphospholipid perifosine induces apoptosis of human lung cancer cells requiring inhibition of Akt and activation of the extrinsic apoptotic pathway

Heath A. Elrod, Yi-Dan Lin, Ping Yue, Xuerong Wang, Sagar Lonial, Fadlo R. Khuri, and Shi-Yong Sun

Department of Hematology and Oncology, Winship Cancer Institute, Emory University School of Medicine, Atlanta, Georgia

Abstract

The Akt inhibitor, perifosine, is an alkylphospholipid exhibiting antitumor properties and is currently in phase II clinical trials for various types of cancer. The mechanisms by which perifosine exerts its antitumor effects, including the induction of apoptosis, are not well understood. The current study focused on the effects of perifosine on the induction of apoptosis and its underlying mechanisms in human non–small cell lung cancer (NSCLC) cells. Perifosine, at clinically achievable concentration ranges of 10 to 15 μmol/L, effectively inhibited the growth and induced apoptosis of NSCLC cells. Perifosine inhibited Akt phosphorylation and reduced the levels of total Akt. Importantly, enforced activation of Akt attenuated perifosine-induced apoptosis. These results indicate that Akt inhibition is necessary for perifosine-induced apoptosis. Despite the activation of both caspase-8 and caspase-9, perifosine strikingly induced the expression of the tumor necrosis factor–related apoptosis-inducing ligand (TRAIL) receptor, death receptor 5, and down-regulated cellular FLICE-inhibitory protein (c-FLIP), an endogenous inhibitor of the extrinsic apoptotic pathway, with limited modulatory effects on the expression of other genes including Bcl-2, Bcl-X_L, PUMA, and survivin. Silencing of either caspase-8 or death receptor 5 attenuated perifosine-induced apoptosis. Consistently, further down-regulation of c-FLIP expression with c-FLIP small interfering RNA sensitized cells to perifosine-induced apoptosis, whereas enforced overexpression of ectopic c-FLIP conferred resistance to perifosine. Collectively, these data indicate that activation of the extrinsic apoptotic pathway plays a critical role in perifosine-induced apoptosis. Moreover, perifosine cooperates with TRAIL to enhance the induction of apoptosis in human NSCLC cells, thus warranting future *in vivo* and clinical evaluation of perifosine in combination with TRAIL in the treatment of NSCLC. [Mol Cancer Ther 2007;6(7):2029–38]

Introduction

Alkylphospholipids are a class of antitumor agents which target the cell membrane and induce apoptosis (1, 2). Perifosine, the first orally bioavailable alkylphospholipid, has shown antitumor activity in preclinical models and is currently in phase II clinical trials (1, 3). The mechanisms by which perifosine exerts its antitumor effect remain unclear, although it seems to inhibit Akt (2, 4) and mitogen-activated protein kinase activation (5), whereas inducing c-Jun-NH_2-kinase (JNK) activation (5). Perifosine has also been shown to induce p21 expression leading to cell cycle arrest (6). In addition, perifosine, in combination with other antitumor agents such as the PDK1 inhibitor, UCN-01 (7), histone deacetylase inhibitors (8), and the chemotherapeutic agent etoposide (9), show synergistic antitumor effects.

It is well known that there are two major apoptotic pathways used by mammalian cells to undergo apoptosis. One pathway involves signals transduced through death receptors known as the extrinsic apoptotic pathway; the second pathway relies on signals from the mitochondria called the intrinsic apoptotic pathway. Both pathways involve the activation of a set of caspases, which in turn, cleave cellular substrates and result in the characteristic morphologic and biochemical changes constituting the process of apoptosis (10, 11). The extrinsic pathway is characterized by the oligomerization of cell surface death receptors and activation of caspase-8, whereas the intrinsic pathway involves in the disruption of mitochondrial membranes, the release of cytochrome *c*, and the activation of caspase-9. Through caspase-8–mediated cleavage or truncation of Bid, the extrinsic death receptor apoptotic pathway is linked to the intrinsic mitochondrial apoptotic pathway (10, 11).

Molecules that can block the extrinsic apoptotic pathway include cellular FLICE-inhibitory protein (c-FLIP). c-FLIP prevents caspase-8 activation by death receptors. There are two major isoforms of c-FLIP: $FLIP_L$ consists of two

Received 1/4/07; revised 5/2/07; accepted 5/25/07.

Grant support: The Georgia Cancer Coalition Distinguished Cancer Scholar award (S-Y. Sun), Department of Defense grants W81XWH-04-1-0142-VITAL (S-Y. Sun for Project 4), DAMD17-01-1-0689-BESCT (F.R. Khuri), and an American Cancer Society Fellowship award (H.A. Elrod).

The costs of publication of this article were defrayed in part by the payment of page charges. This article must therefore be hereby marked *advertisement* in accordance with 18 U.S.C. Section 1734 solely to indicate this fact.

Note: H.A. Elrod and Y-D. Lin contributed equally to this work and share equal first authorship. F.R. Khuri and S-Y. Sun are Georgia Cancer Coalition Distinguished Cancer Scholars. H.A. Elrod is a recipient of an American Cancer Society Fellowship.

Requests for reprints: Shi-Yong Sun, Winship Cancer Institute, Emory University School of Medicine, 1365-C Clifton Road Northeast, C3088, Atlanta, GA 30322. Phone: 404-778-2170; Fax: 404-778-5520. E-mail: shi-yong.sun@emoryhealthcare.org

Copyright © 2007 American Association for Cancer Research.

doi:10.1158/1535-7163.MCT-07-0004

NH_2-terminal death effector domains and a COOH-terminal caspase homology domain devoid of enzymatic activity, whereas $FLIP_S$ is only composed of the NH_2-terminal death effector domains and a short COOH-terminal stretch of amino acids not found in $FLIP_L$. It has been shown that c-FLIP expression correlates with resistance against death receptor–induced apoptosis in a variety of cancer cells, and c-FLIP–transfected tumor cell lines develop more aggressive tumors *in vivo* (12, 13). In addition, many studies have shown that down-regulation of c-FLIP is sufficient to confer sensitivity against death receptor–induced apoptosis, whereas c-FLIP expression is associated with chemoresistance and down-regulation of c-FLIP using antisense oligonucleotides or small interfering RNAs (siRNA) sensitizes cells to chemotherapeutic agent–induced apoptosis (12–14).

Akt is known to be critical for tumor cell survival. One of the ways that Akt promotes cell survival is to inhibit apoptosis through its ability to phosphorylate several proapoptotic proteins such as Bad, which are involved in the regulation of the intrinsic apoptotic pathway (15). Moreover, Akt also inhibits the extrinsic death receptor–mediated apoptotic pathway through up-regulation of c-FLIP expression (16, 17). Thus, Akt negatively regulates apoptosis by suppressing both the mitochondria- and death receptor–mediated pathways.

The induction of apoptosis by perifosine has been observed in several cancer cell lines (3, 8, 9, 18). However, this effect has not been determined in non–small cell lung cancer (NSCLC) cells. Moreover, the mechanisms by which perifosine induces apoptosis is generally unknown. In this study, we examined the effects of perifosine on apoptosis in human NSCLC cells and its modulation on different apoptotic molecules in an attempt to understand its mechanisms of action. Our data show that perifosine induces apoptosis, inhibits Akt activation, up-regulates death receptor 5 (DR5) expression, and reduces c-FLIP levels in NSCLC cells. In addition, perifosine in combination with tumor necrosis factor–related apoptosis-inducing ligand (TRAIL) augments the induction of apoptosis.

Materials and Methods

Reagents

Perifosine was supplied by Keryx Biopharmaceuticals, Inc. This agent was dissolved in PBS and stored at −20°C. Stock solution was diluted to the appropriate concentrations with growth medium immediately before use. Human recombinant TRAIL was purchased from PeproTech, Inc.

Cell Lines and Cell Culture

The human NSCLC cell lines used in this study were described previously (19). H157 cell lines that stably express ectopic Lac Z (Lac Z-5) and $FLIP_L$ ($FLIP_L$-6), respectively, and A549 cell lines that stably express ectopic Lac Z (Lac Z-9) and $FLIP_L$ ($FLIP_L$-2), respectively, were described previously (20, 21). These cell lines were grown in a monolayer culture in RPMI 1640 supplemented with glutamine and 5% fetal bovine serum at 37°C in a humidified atmosphere consisting of 5% CO_2 and 95% air.

Cell Growth Assay

Cells were cultured in 96-well cell culture plates and treated the next day with the agents indicated. Viable cell number was estimated using the sulforhodamine B assay, as previously described (19).

Western Blot Analysis

Preparation of whole cell protein lysates and Western blot analysis were described previously (22, 23). Mouse anti–caspase-3 monoclonal antibody was purchased from Imgenex. Rabbit polyclonal antibodies against PTEN, Akt, phospho (p)-Akt (Ser^{473}), phospho (p)-FKHR (Ser^{256}), phospho (p)-GSK3β (Ser^{9}), c-Jun, phospho (p)-c-Jun (Ser^{63}), p44/42, phospho (p)-p44/42 (Thr^{202}/Tyr^{204}), survivin, caspase-8, caspase-9, poly(ADP-ribose) polymerase (PARP) were purchased from Cell Signaling Technology. Rabbit polyclonal anti-DR5 antibody was purchased from ProSci, Inc. Mouse monoclonal anti-FLIP antibody (NF6) was purchased from Alexis Biochemicals. Rabbit anti-G3PDH polyclonal antibody and mouse anti-Bax monoclonal antibody were purchased from Trevigen. Rabbit anti-Puma polyclonal antibody was purchased from EMD Biosciences, Inc. Mouse anti–Bcl-2 and rabbit anti–Bcl-X_L antibodies were purchased from Santa Cruz Biotechnology, Inc. Rabbit anti–β-actin polyclonal antibody was purchased from Sigma Chemicals. Secondary antibodies, goat anti-mouse and goat anti-rabbit horseradish peroxidase conjugates, were purchased from Bio-Rad.

Adenoviral Infection

Adenovirus harboring an empty vector (Ad-CMV) or a constitutively activated form of Akt (myristoylated Akt; Ad-myr-Akt) were provided by Lily Yang (Department of Surgery, Emory University School of Medicine, Atlanta, GA). The procedure for adenoviral infection of cancer cells was described previously (24).

Gene Silencing Using siRNA

Silencing of caspase-8, DR5, c-FLIP, and PTEN were achieved by transfecting siRNA using RNAifect transfection reagent (Qiagen) following the instructions of the manufacturer. Control, caspase-8, and DR5 siRNAs were described previously (22). These siRNAs and c-FLIP siRNA targeting the sequence 5′-AATTCTCCGAACGTGTCACGT-3′ (14) were all synthesized from Qiagen. PTEN siRNA was purchased from Cell Signaling. Cells were plated in 6- or 24-well cell culture plates and transfected with the given siRNAs the next day. After 24 h, the cells were trypsinized and replated in new plates, and on the second day, treated with perifosine as indicated. Gene silencing effects were evaluated by Western blot as described above after the indicated times of treatment.

Apoptosis Assays

Apoptosis was detected either by analysis of caspase activation using Western blot analysis as described above or by Annexin V staining using Annexin V-PE apoptosis detection kit (BD Bioscience) following the instructions of the manufacturer, and analyzed by flow cytometry using FACScan (Becton Dickinson). In addition, we measured

the amounts of cytoplasmic histone-associated DNA fragments (mononucleosome and oligonucleosomes) formed during apoptosis using a Cell Death Detection ELISA^{Plus} kit (Roche Molecular Biochemicals) according to the instructions of the manufacturer.

Results

Effects of Perifosine on Cell Survival and Apoptosis in NSCLC Cells

The effects of perifosine on cell survival were examined in a panel of NSCLC cell lines (Fig. 1A). For the majority of the cell lines tested, there was a dose-dependent decrease in cell survival. The H460 cell line was the most sensitive to perifosine, showing an IC_{50} value of ~1 μmol/L. The H226 cell line was the most resistant to perifosine, in which perifosine at 20 μmol/L decreased cell survival by <20%. Most of the tested cell lines exhibited moderate response to perifosine with IC_{50}s ranging from 8 to 15 μmol/L (Fig. 1A), which are within the clinically achievable and safe peak plasma concentrations of 12 to 15 μmol/L (25, 26). The *p53* and *PTEN* mutation status in the NSCLC cell lines tested did not correlate with sensitivity to perifosine, suggesting that perifosine inhibits cell growth independently of *p53* and *PTEN* mutation status (Fig. 1A). In addition, we examined the protein expression levels of PTEN, total Akt, and p-Akt in the cell lines tested. It seemed that those cell lines (e.g., H460 and H358) with low levels of p-Akt and high levels of PTEN were the most sensitive to perifosine (Fig. 1B).

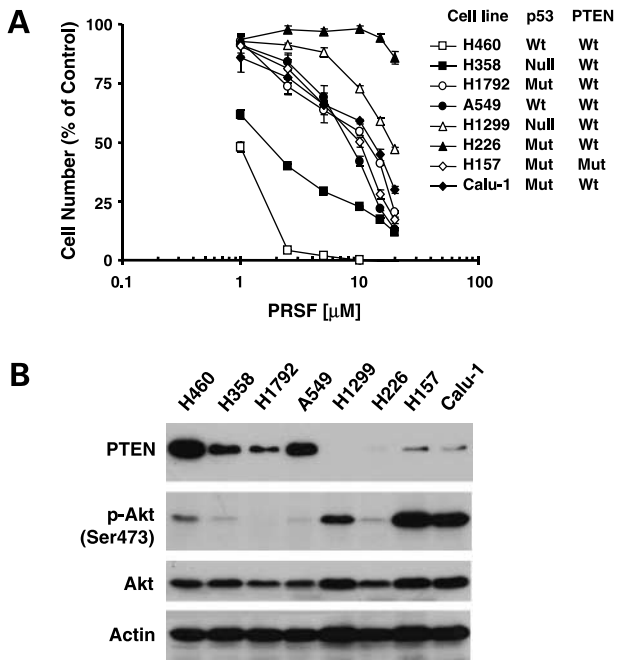


Figure 1. Effects of perifosine on the survival of NSCLC cells (**A**) and their association with basal levels of p-Akt (**B**). **A,** cell lines treated with different concentrations of perifosine (*PRFS*) ranging from 1 to 20 μmol/L. After 3 d, the cells were subjected to sulforhodamine B assay for estimating the viable cells. In addition, the *p53* status and *PTEN* status of the cell lines were also indicated. *Points,* means of four replicate determinations; *bars,* SD. **B,** cell lines with similar cell densities were harvested for the preparation of whole cell protein lysates. The indicated proteins were analyzed by Western blot analysis.

We further examined the effects of perifosine on apoptosis in NSCLC cell lines. As shown in Fig. 2A, perifosine induced apoptosis in H460 and A459 cells as indicated by Annexin V–positive staining. At concentrations of 10 μmol/L, perifosine induced cell death in ~50% of H460 cells, whereas apoptosis was induced in 23% and 33% of the A549 cells after treatment with 10 and 15 μmol/L of perifosine, respectively, suggesting that the H460 cells were more sensitive to perifosine-induced apoptosis. The H157 cells were the least sensitive to perifosine-induced apoptosis with only 10% of H157 cells undergoing apoptosis after treatment with 15 μmol/L of perifosine. We found that perifosine at concentrations ranging from 2.5 to 10 μmol/L induced cleavage of caspase-8, caspase-9, caspase-3, and PARP in H460 cells, whereas it induced partial cleavage of the caspases and PARP only at 10 μmol/L in A549 cells (Fig. 2B). In H157 cells treated with perifosine (up to 10 μmol/L), we failed to detect cleaved bands of the caspases and PARP (Fig. 2B). Because perifosine is effective in decreasing cell number in H157 cells (Fig. 1), we further examined cell cycle alteration in H157 cells after exposure to perifosine and detected 17.9%, 35.8%, and 42.4% G_2-M cells in cells treated with PBS, 10 μmol/L of perifosine, and 15 μmol/L of perifosine, respectively, after a 48 h treatment, indicating that perifosine primarily decreases cell numbers in H157 cells via induction of cell cycle arrest. In the following studies, we focused on revealing the mechanisms underlying perifosine-induced apoptosis.

Effects of Perifosine on the Phosphorylation of Akt, JNK, and ERK

Perifosine has been shown to modulate Akt as well as other signaling pathways (6, 18, 27). We therefore examined whether perifosine modulated similar signal transduction pathways in human NSCLC cells. In examining Akt phosphorylation, we observed that both H460 and A549 cells have very low basal levels of p-Akt, whereas H157 cells have much higher basal levels of p-Akt. When comparing the apoptosis results presented in Fig. 2A, it seems that low basal levels of p-Akt correlated with high sensitivity to perifosine-induced apoptosis. These cell lines exhibited a concentration-dependent decrease in p-Akt levels when exposed to perifosine (p-Akt levels were only detectable in H460 cells after a very long exposure). Interestingly, perifosine also decreased the levels of total Akt in the tested cell lines (Fig. 3A) and the degree of Akt down-regulation also seemed to correlate with cell sensitivity to perifosine-induced apoptosis. In H460 cells, decreases in both Akt and p-Akt levels occurred at 3 h after treatment with perifosine (Fig. 3B), indicating that Akt down-regulation is an early event. In H157 cells, Akt levels were only slightly decreased, whereas p-Akt levels were substantially (by 2.5 μmol/L of perifosine) and rapidly (3 h posttreatment) reduced upon perifosine treatment

(Fig. 3A and B). These results suggest that the perifosine-mediated decrease in p-Akt levels could be due to either Akt protein down-regulation or upstream signaling suppression, depending on the cell lines used. To our knowledge, this is the first demonstration that perifosine down-regulates the levels of total Akt in human cancer cells. We also detected a decrease in the levels of p-FKHR and p-GSK3β, two well-known substrates of Akt (Fig. 3B), furthering the notion that perifosine inhibits Akt signaling in NSCLC cells.

In examining other signal transduction pathways, we observed the basal levels of p-c-Jun were very low in the tested NSCLC cells and were only slightly increased by perifosine in H157 cells, indicating that perifosine-induced JNK activation was a cell line–dependent event. Perifosine did not alter the levels of p42/44, but did decrease the levels of p-p42/44 in all three cell lines tested (Fig. 3A). These data indicate that perifosine down-regulates the ERK (or p42/44) signaling pathway in NSCLC cells.

Enforced Akt Activation Attenuates Perifosine-Induced Apoptosis

To decipher the role of Akt inhibition in perifosine-induced apoptosis, we artificially activated Akt in H460 cells by infecting the cells with adenoviruses carrying a *myr-Akt* gene that codes a constitutively activated form of Akt, and then examined the response of these cells to perifosine treatment. Using Western blot analysis, we detected high levels of myr-Akt, p-Akt, and p-GSK3β in cells infected with Ad-myr-Akt (Fig. 3C). In addition, infection of cells with Ad-myr-Akt also elevated the levels of c-FLIP, which has been shown to be regulated by Akt. (refs. 16, 17; Fig. 3C). In Ad-CMV–infected control cells, treatment with perifosine caused 37% apoptotic cell death (9% in PBS-treated cells) plus 15.2% necrotic cell death. However, we detected only 16% apoptosis (~12% in PBS-treated cells) and <2% necrosis in cells infected with Ad-myr-Akt after treatment with perifosine (Fig. 3D). These results clearly show that enforced Akt activation restores cell resistance to perifosine-induced apoptosis, thus indicating that Akt inhibition is necessary in mediating perifosine-induced apoptosis.

Given that there is an inverse relationship between PTEN expression and p-Akt levels (Fig. 1B), we further determined whether down-regulation of PTEN affects p-Akt levels and cell sensitivity to perifosine. Knockdown of PTEN using PTEN siRNA in H460 cells, which is the most sensitive cell line to perifosine and have the highest levels of PTEN (Fig. 1), increased basal levels of p-Akt. However,

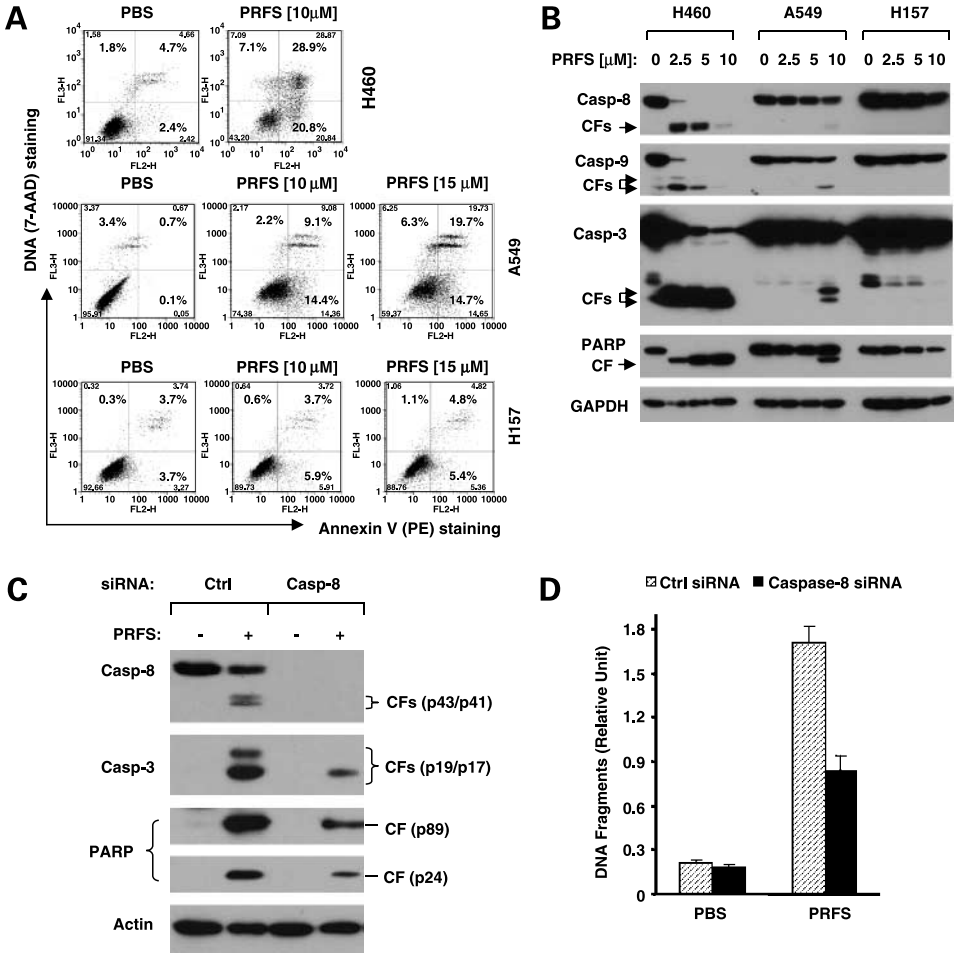


Figure 2. Effects of perifosine on apoptosis induction (**A**) and caspase activation (**B**), and involvement of caspase-8 activation in perifosine-induced apoptosis (**C** and **D**) in NSCLC cells. **A,** cell lines treated with the given concentrations of perifosine (*PRFS*) for 24 h and harvested for the estimation of apoptosis by Annexin V staining. Early apoptotic (*bottom right*), late apoptotic (*top right*), and necrotic (*top left*) cells. **B,** the indicated cell lines were treated with the given concentrations of perifosine for 16 h and harvested for the detection of caspase cleavage by Western analysis. **C** and **D,** H460 cells were seeded in 24-well plates and transfected with control (*Ctrl*) or caspase-8 siRNA the next day. After ~24 h, the cells were trypsinized and replated in new 6-well (**C**) or 96-well (**D**) plates. On the second day, the cells were treated with PBS or 5 μmol/L of perifosine. After 16 h, the cells were subjected to Western blot analysis for the indicated proteins (**C**) or ELISA for measurement of DNA fragments (**D**). *CF,* cleaved form. *Columns,* means of triplicate determinations; *bars,* SD.

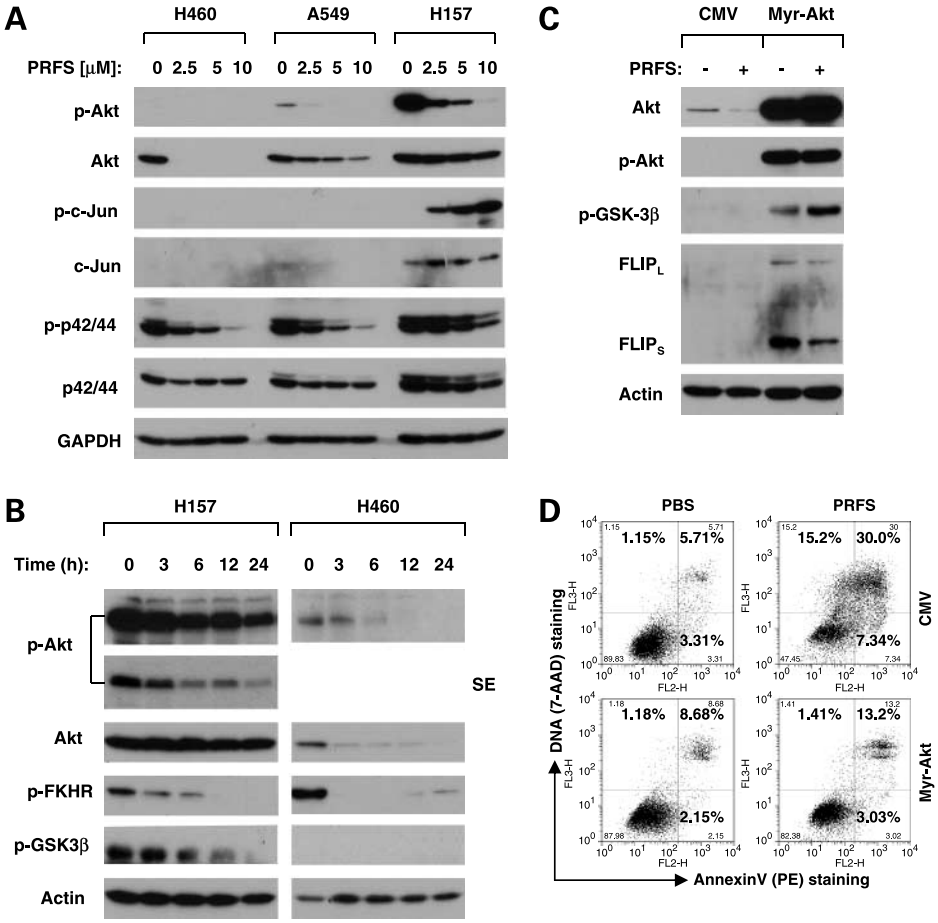


Figure 3. Modulation of Akt, JNK, and ERK signaling pathways by perifosine (**A** and **B**), and involvement of Akt inhibition in perifosine-induced apoptosis (**C** and **D**) in human NSCLC cells. **A** and **B,** NSCLC cell lines treated with the given concentrations of perifosine (*PRFS*) for 16 h (**A**) or with 10 μmol/L (H157) or 5 μmol/L (H460) of perifosine for the indicated times (**B**). The cells were then subjected to a preparation of whole cell protein lysates and subsequent detection of the indicated proteins using Western blot analysis. **C** and **D,** H460 cells were infected with a multiplicity of infection of 200 Ad-CMV or Ad-myr-Akt. Twenty-four hours later, the cells were exposed to 10 μmol/L of perifosine. After 24 h, the cells were harvested for analysis of the given proteins by Western blotting (**C**) and for the detection of apoptosis by Annexin V staining (**D**). *SE,* short exposure.

the p-Akt increase caused by PTEN knockdown could be abrogated by perifosine treatment. Surprisingly, perifosine decreased PTEN levels, which itself did not result in an increase of p-Akt levels, probably because perifosine also inhibits Akt phosphorylation (see Supplemental Fig. S1A).[1] As a result, down-regulation of PTEN by siRNA did not alter cell sensitivity to perifosine as shown by measuring cell number change (Supplemental Fig. S1B),[1] caspase activation (Supplemental Fig. S1A),[1] and apoptotic cells (Supplemental Fig. S1C).[1]

Effects of Perifosine on the Expression of Key Molecules Involved in the Regulation of Apoptosis

To further explore how perifosine induces apoptosis, we next examined the effects of perifosine on the expression of several key genes involved in either the extrinsic apoptotic pathway (e.g., DR5 and c-FLIP) or the intrinsic apoptotic pathway (e.g., Bax, Bcl-2, Bcl-X_L, PUMA, and survivin). Perifosine increased the levels of DR5, particularly in H460 cells (Fig. 4). It seems that DR5 induction is associated with increased sensitivity of cell lines to perifosine. c-FLIP is another key protein that inhibits the extrinsic apoptotic pathway by blocking caspase-8 activation (12). The H460 cells, which are the most sensitive to perifosine, had very low basal levels of c-FLIP, particularly $FLIP_L$, which were further down-regulated by perifosine, whereas the less sensitive A549 and H157 cells have high basal levels of c-FLIP, particularly $FLIP_L$, which were only weakly decreased by perifosine. Perifosine also decreased $FLIP_S$ levels in these cell lines (Fig. 4). It seems that low levels of c-FLIP and their further down-regulation by perifosine were associated with high sensitivity to perifosine-induced apoptosis. Collectively, these results suggest that activation of the DR5-mediated extrinsic apoptotic pathway is important in perifosine-induced apoptosis.

In examining the signaling molecules involved in the intrinsic apoptotic pathway, we found that perifosine did not significantly alter the levels of Bcl-2 in NSCLC cells (Fig. 4). Surprisingly, perifosine decreased Bax levels in all the tested NSCLC cell lines. Perifosine decreased Bcl-X_L levels in H460 cells that were very sensitive to perifosine, but not in A549 and H157 cells that were less sensitive to perifosine (Fig. 4). These data suggest that Bcl-X_L down-regulation may affect cell sensitivity to undergo perifosine-induced apoptosis. H460 cells had low basal levels of survivin, which were further decreased by perifosine,

[1] Supplementary material for this article is available at Molecular Cancer Therapeutics Online (http://mct.aacrjournals.org/).

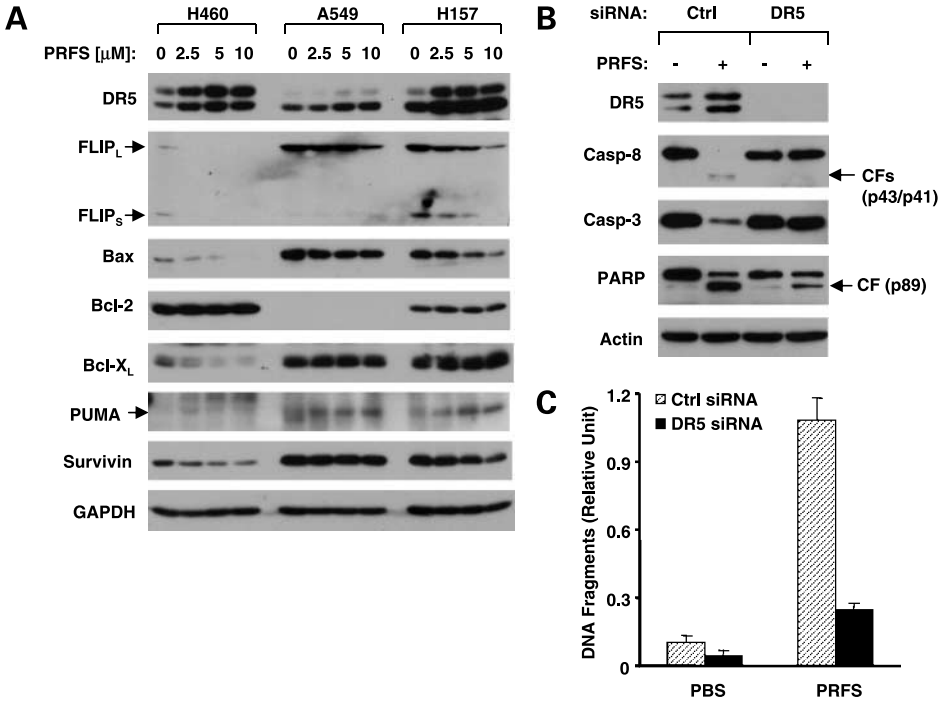


Figure 4. Modulation of apoptosis-related gene expression by perifosine (**A**) and demonstration of the role of DR5 induction in perifosine-induced apoptosis (**B** and **C**) in human NSCLC cells. **A,** NSCLC cell lines treated with the given concentrations of perifosine (*PRFS*) for 16 h. The cells were then subjected to a preparation of whole cell protein lysates and subsequent detection of the indicated proteins using Western blot analysis. **B** and **C,** H460 cells were seeded in six-well plates and transfected with control (*Ctrl*) or DR5 siRNA the next day. After ~20 h, the cells were trypsinized and replated in new 6-well (**B**) or 96-well (**C**) plates. On the second day, the cells were treated with PBS or 7.5 μmol/L of perifosine. After 16 h, the cells were subjected to Western blot analysis for the detection of the indicated proteins (**B**) or ELISA for the measurement of DNA fragments (**C**). *Columns,* means of triplicate determinations; *bars,* SD; *CF,* cleaved form.

whereas H157 and A549 cells had high levels of survivin, which were apparently not altered by perifosine (Fig. 4). Thus, it seems that low basal levels of survivin and its further down-regulation with perifosine are also associated with increased cell sensitivity to perifosine-induced apoptosis. PUMA was slightly increased in A549 and H157 cells, but not in H460 cells, suggesting that PUMA was not important in perifosine-induced apoptosis.

Perifosine Cooperates with TRAIL to Enhance the Induction of Apoptosis

Because perifosine induces DR5 expression and down-regulates c-FLIP levels, we hypothesized that perifosine would cooperate with TRAIL, a DR5 ligand, to enhance the induction of apoptosis. Thus, we examined the effects of perifosine in combination with TRAIL on apoptosis induction in NSCLC cells. As shown in Fig. 5A, perifosine in combination with TRAIL induced higher levels of DNA fragments than did each single agent alone. Moreover, increased amounts of cleaved caspase-8, caspase-9, caspase-3, and PARP were detected in cells treated with the perifosine and TRAIL combination, but were only minimally detected in cells treated with either perifosine or TRAIL alone (Fig. 5B). Thus, we conclude that perifosine cooperates with TRAIL to enhance the induction of apoptosis.

Perifosine Induces Apoptosis Requiring Caspase-8 Activation and DR5 Up-regulation

The data presented above strongly suggest a role for the activation of the extrinsic apoptotic pathway in perifosine-induced apoptosis. Thus, we determined whether perifosine induces apoptosis requiring activation of caspase-8 and up-regulation of DR5. To this end, we silenced the expression of caspase-8 and DR5 using caspase-8 and DR5 siRNAs, respectively, and then examined cell sensitivity to perifosine. By Western blotting, we detected substantially reduced levels of caspase-8 levels including cleaved forms in H460 cells transfected with caspase-8 siRNA compared with those in control siRNA-transfected cells (Fig. 2C), indicating successful caspase-8 knockdown or inhibition of caspase-8 activation. Accordingly, cleavage of caspase-3 and PARP and an increase in DNA fragmentation were also attenuated in caspase-8 siRNA-transfected cells in comparison with control siRNA–transfected cells (Fig. 2C and D). These results indicate that perifosine induces a caspase-8–dependent apoptosis. Similarly, silencing of DR5 expression using DR5 siRNA abrogated DR5 induction (Fig. 4B) and impaired the ability of perifosine to induce cleavage of caspase-8, caspase-3, and PARP (Fig. 4B). In addition, an increase in DNA fragmentation in DR5 siRNA-transfected cells was also reduced compared with control siRNA-transfected cells (Fig. 4C). These data show that DR5 up-regulation is also involved in perifosine-induced apoptosis.

Manipulation of c-FLIP Levels Regulates Cell Sensitivity to Perifosine-Induced Apoptosis and Enhancement of TRAIL-Induced Apoptosis

To further show that the activation of the extrinsic apoptotic pathway participates in perifosine-induced apoptosis, we examined the sensitivity of cell lines that express ectopic FLIP$_L$ to perifosine-induced apoptosis. As presented in Fig. 6A, perifosine increased DNA fragmentation in a dose-dependent fashion in H157-Lac Z-5 cells, but only minimally in H157-FLIP$_L$-6 cells. As a positive control treatment, TRAIL-induced increase in DNA fragmentation

was abolished in H157-$FLIP_L$-6 cells. Similarly, perifosine-induced increase in DNA fragmentation was also abrogated in A549-$FLIP_L$-2 cells in comparison with A549-Lac Z-9 cells (Fig. 6B). Together, these results clearly show that overexpression of ectopic c-FLIP protects cells from perifosine-induced apoptosis.

Because c-FLIP down-regulation was often associated with the enhancement of TRAIL-induced apoptosis (20, 21, 28), we further compared apoptosis induction by the combination of perifosine and TRAIL between A549-Lac Z-9 and A549-$FLIP_L$-2 cell lines. In agreement with the results presented in Fig. 5, the combination of perifosine and TRAIL was much more potent than either perifosine or TRAIL alone in increasing DNA fragmentation in A549-Lac Z-9 cells. However, not only perifosine and TRAIL alone but also their combination exhibited minimal effects on increasing DNA fragmentation in A549-$FLIP_L$-2 cells (Fig. 6B). These results clearly show that overexpression of ectopic c-FLIP confers cell resistance to the combination of perifosine and TRAIL, indicating that c-FLIP down-regulation contributes to perifosine-mediated enhancement of TRAIL-induced apoptosis.

Because the cell lines, A549 and H157, with high basal levels of c-FLIP were relatively less sensitive than H460 cells which have low basal levels of c-FLIP to perifosine-induced apoptosis, we wanted to determine whether down-regulation of c-FLIP sensitized cells to perifosine-induced apoptosis. To this end, we silenced the expression of c-FLIP (both $FLIP_L$ and $FLIP_S$) using siRNA in A549 cells, and then examined their response to perifosine-induced apoptosis. As presented in Fig. 6C, transfection of c-FLIP siRNA reduced the levels of both $FLIP_L$ and $FLIP_S$, which were further reduced after treatment with perifosine. Those cells whose expression of c-FLIP had been reduced with siRNA were more sensitive to caspase-8, caspase-3, and PARP cleavage after perifosine treatment compared with control cells, indicating that c-FLIP levels indeed affect cell sensitivity to perifosine-induced apoptosis.

Discussion

In this study, we have shown that perifosine exerts its growth-inhibitory effects in a panel of NSCLC cell lines, primarily through the induction of apoptosis and/or cell cycle arrest. Importantly, perifosine inhibited the growth of most of the tested NSCLC cell lines with IC_{50}s ranging between 8 and 15 μmol/L (Fig. 1A), which are within the

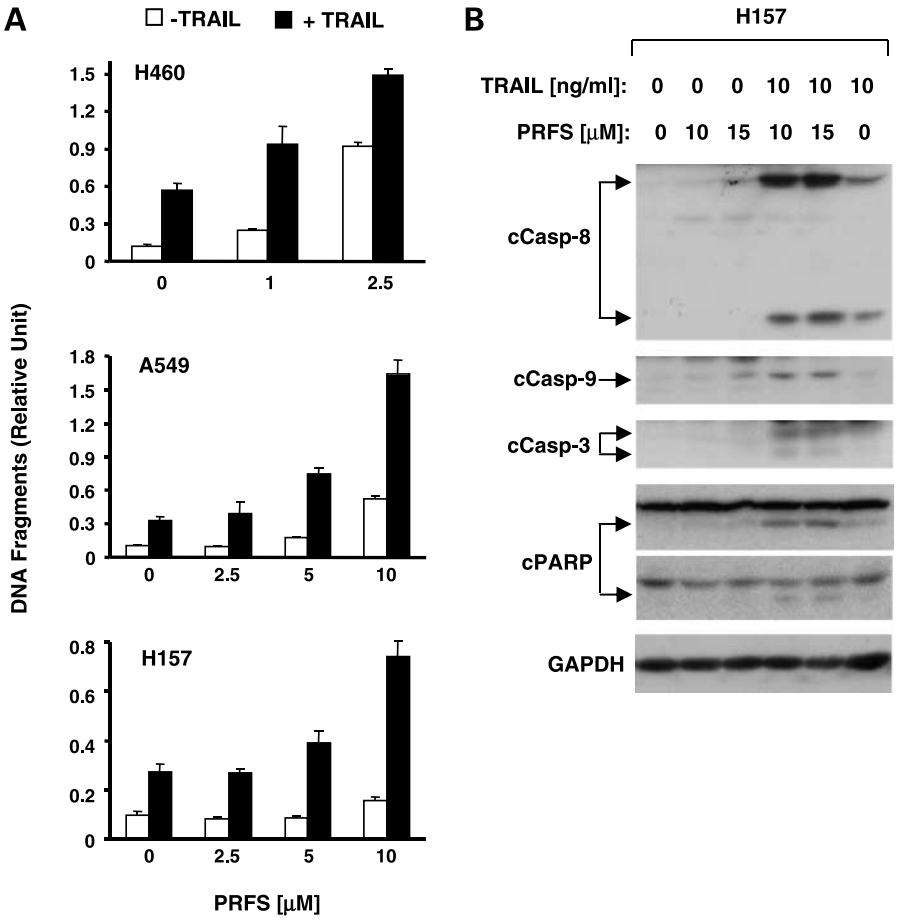


Figure 5. Perifosine cooperates with TRAIL to enhance DNA fragmentation (**A**) and caspase activation (**B**) in human NSCLC cells. **A,** cell lines plated in 96-well plates and treated with the given doses of perifosine (*PRFS*) alone, 20 ng/mL TRAIL alone, or TRAIL plus perifosine on the second day. After 24 h, the cells were subjected to DNA fragmentation using the Cell Death Detection ELISA kit. *Columns,* means of triplicate determinations; *bars,* SD. **B,** H157 cells were treated with perifosine alone, TRAIL alone, and their combinations. After 16 h, the cells were subjected to a preparation of whole cell protein lysates and subsequent detection of the indicated proteins by Western blot analysis. *c,* cleaved.

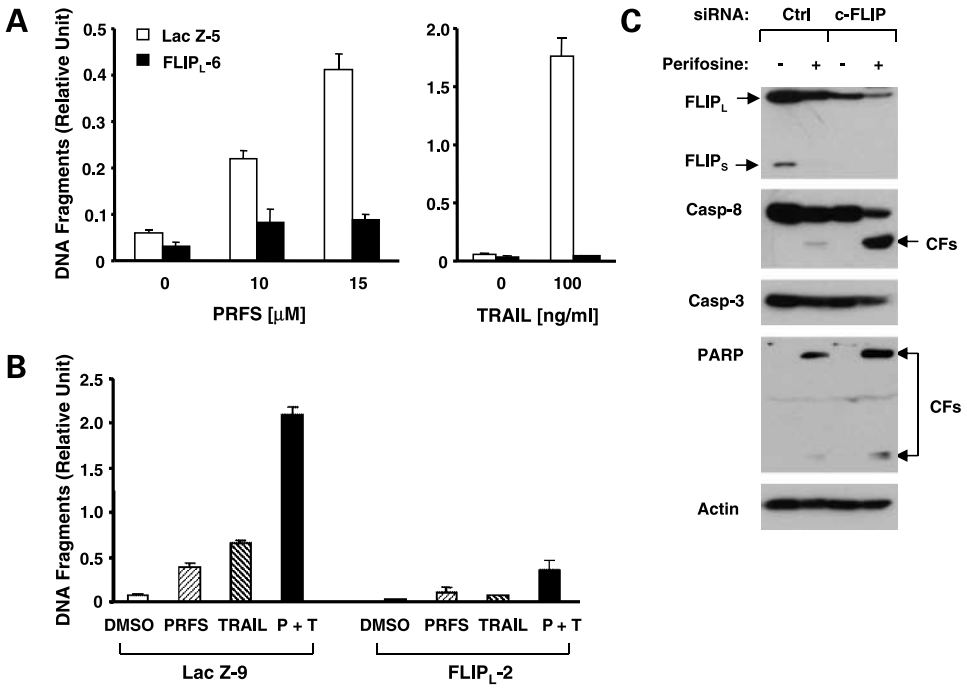


Figure 6. Overexpression of ectopic c-FLIP (**A** and **B**) and silencing of c-FLIP expression (**C**) modulate cell sensitivity to perifosine-induced apoptosis. **A,** H157 cell lines that stably express Lac Z and FLIP$_L$, respectively, were treated with the indicated concentrations of perifosine (*PRFS*) or TRAIL. **B,** A549 cell lines that stably express Lac Z and FLIP$_L$, respectively, were exposed to 10 μmol/L of perifosine, 20 ng/mL of TRAIL, and the combination of perifosine and TRAIL (*P + T*). Twenty-four hours later, after the aforementioned treatment, the cells were subjected to estimation of DNA fragmentation using the Cell Death Detection ELISA kit. *Columns,* mean of triplicate determinations; *bars,* SD. **C,** A549 cells plated in 24-well plates were transfected with control (*Ctrl*) or c-FLIP siRNA. Twenty-four hours later, the cells were exposed to 10 μmol/L of perifosine (*PRFS*). After 24 h, the cells were subjected to a preparation of whole cell protein lysates and subsequent detection of the indicated proteins using Western blot analysis. *CFs,* cleaved fragments.

clinically achievable and safe peak plasma concentration ranges (i.e., 10–15 μmol/L; refs. 25, 26), suggesting the potential of perifosine in the treatment of NSCLCs.

Modulation of Akt, JNK, and ERK signaling pathways and their involvement in perifosine-induced apoptosis has been studied in other types of cancer cells (4, 18, 27). Despite the proapoptotic role of JNK activation in perifosine-induced apoptosis in multiple myeloma (18), we found that perifosine increased p-c-Jun only in one (i.e., H157 cells) of three cell lines tested (Fig. 3A). Given that H157 cells were relatively insensitive to perifosine-induced apoptosis (Fig. 2), we suggest that JNK activation is unlikely to account for the perifosine-induced apoptosis in human NSCLC cells. Perifosine was reported to either decrease or increase ERK phosphorylation depending on cancer cell type (5, 18, 27). In our study, perifosine decreased ERK phosphorylation in all of the three tested cell lines tested, regardless of cell sensitivity to TRAIL-induced apoptosis. Thus, we suggest that ERK inhibition is also unlikely to be critical for perifosine-induced apoptosis in human NSCLC cells.

Although perifosine inhibits Akt activation in different types of cancer cells including the NSCLC cells shown in the current study, enforced activation of Akt through overexpression of the constitutively activated form of Akt, myr-Akt, protects cells from perifosine-induced cell death in one type of cancer cell line (e.g., PC-3 prostate cancer cells; ref. 4) but not in another type of cancer cell (e.g., MM.1S multiple myeloma cells; ref. 18). In our study, we found that the low basal levels of p-Akt (e.g., H460 < A549 < H157) and its further down-regulation were associated with high sensitivity to perifosine-induced apoptosis (H460 > A549 > H157; Figs. 1 and 2). Moreover, overexpression of myr-Akt in H460 cells led to increased levels of p-Akt and resistance to perifosine-induced apoptosis (Fig. 3). Collectively, we conclude that Akt inhibition plays an important role in mediating perifosine-induced apoptosis in human lung cancer cells. We noted that perifosine decreased the levels of total Akt in some NSCLC cells (e.g., H460 and A549), the potency of which is associated with cell sensitivity to perifosine-induced apoptosis, in addition to decreasing Akt phosphorylation. To the best of our knowledge, this is the first demonstration that perifosine decreases the total levels of Akt. Given that Akt reduction is an early event, which occurred at 3 h post–perifosine treatment (Fig. 3B), it is unlikely that Akt reduction occurs secondary to perifosine-induced apoptosis (e.g., cleavage by caspase activation). Nevertheless, ongoing studies are attempting to reveal how perifosine decreases the levels of total Akt.

Perifosine activated both caspase-8 and caspase-9 in human NSCLC cells (Fig. 2B), suggesting that perifosine can induce apoptosis through the extrinsic and/or intrinsic apoptotic pathways. In examining several key proteins involved in the regulation of the extrinsic or intrinsic apoptotic pathways, we found that perifosine strikingly induced DR5 expression and decreased the levels of c-FLIP in all the cells lines tested, whereas having limited or no modulatory effects on the levels of Bcl-2, Bcl-X$_L$, PUMA, and survivin (Fig. 4A). Importantly, the low basal levels of c-FLIP (e.g., FLIP$_L$) and its further down-regulation are associated with increased sensitivity to undergo perifosine-induced apoptosis (e.g., H460 cells). We noted that Bax

levels were lower and Bcl-2 levels were higher in the sensitive H460 cells than in less sensitive A549 and H157 cells (Fig. 4A). Moreover, we found that Bax levels were actually decreased in cells treated with perifosine, although the underlying mechanisms and its effects on perifosine-induced apoptosis are unclear. In fact, our preliminary data show that Bax or PUMA deficiency does not alter cell sensitivity to perifosine-induced apoptosis.[2] Together, we suggest that the activation of the extrinsic apoptotic pathway is important in mediating perifosine-induced apoptosis. This observation is supported by our findings that silencing of caspase-8 or DR5, or overexpression of ectopic c-FLIP protects cells from perifosine-induced apoptosis (Figs. 2, 4, and 6), whereas down-regulation of endogenous c-FLIP using c-FLIP siRNA sensitizes cells to perifosine-induced apoptosis (Fig. 6). In agreement with our findings, a recent study has shown that perifosine induces apoptosis through activation of the Fas-mediated extrinsic apoptotic pathway in human leukemia cells (29). To the best of our knowledge, this is the first study showing that perifosine modulates the expression of DR5 and c-FLIP in human cancer cells.

Some studies have shown that Akt also inhibits the extrinsic apoptotic pathway through the up-regulation of c-FLIP expression (16, 17). In this study, we have shown that perifosine inhibits Akt and reduces c-FLIP levels, both of which are involved in perifosine-induced apoptosis. Indeed, we detected increased levels of c-FLIP in cells infected with Ad-myr-Akt (Fig. 3C), suggesting that Akt activation indeed increases c-FLIP levels in the tested cells. Thus, it is possible that Akt exerts its inhibitory effect on perifosine-induced apoptosis through the up-regulation of c-FLIP. On other hand, perifosine may down-regulate c-FLIP levels through inhibition of Akt; this needs to be investigated in detail in the future.

It is known that TRAIL functions as the DR5 ligand and rapidly induces apoptosis in a wide variety of transformed cells but is not cytotoxic in normal cells *in vitro* and *in vivo* (10, 16, 17). Therefore, TRAIL is considered to be a tumor-selective, apoptosis-inducing cytokine with promising potential for cancer treatment and is currently being tested in phase I clinical trials. In our study, we showed that the combination of perifosine and TRAIL exhibited augmented induction of apoptosis in human NSCLC cells (Fig. 5), which is likely due to the ability of perifosine to induce DR5 expression and down-regulate c-FLIP levels. This finding warrants future *in vivo* animal studies and clinical evaluation of the efficacy of perifosine in combination with TRAIL for the treatment of NSCLC.

Acknowledgments

We are grateful to Zhongmei Zhou for her excellent technical assistance, Dr. Xiangguo Liu for establishment of stable cell lines that overexpress c-FLIP, and Dr. Lily Yang for providing us with Ad-CMV and Ad-myr-Akt.

[2] Unpublished data.

References

1. Hilgard P, Klenner T, Stekar J, et al. D-21266, a new heterocyclic alkylphospholipid with antitumour activity. Eur J Cancer 1997;33:442 – 6.

2. Ruiter GA, Verheij M, Zerp SF, van Blitterswijk WJ. Alkyl-lysophospholipids as anticancer agents and enhancers of radiation-induced apoptosis. Int J Radiat Oncol Biol Phys 2001;49:415 – 9.

3. Vink SR, Schellens JH, van Blitterswijk WJ, Verheij M. Tumor and normal tissue pharmacokinetics of perifosine, an oral anti-cancer alkylphospholipid. Invest New Drugs 2005;23:279 – 86.

4. Kondapaka SB, Singh SS, Dasmahapatra GP, Sausville EA, Roy KK. Perifosine, a novel alkylphospholipid, inhibits protein kinase B activation. Mol Cancer Ther 2003;2:1093 – 103.

5. Li X, Luwor R, Lu Y, Liang K, Fan Z. Enhancement of antitumor activity of the anti-EGF receptor monoclonal antibody cetuximab/C225 by perifosine in PTEN-deficient cancer cells. Oncogene 2006;25:525 – 35.

6. Patel V, Lahusen T, Sy T, et al. Perifosine, a novel alkylphospholipid, induces p21(WAF1) expression in squamous carcinoma cells through a p53-independent pathway, leading to loss in cyclin-dependent kinase activity and cell cycle arrest. Cancer Res 2002;62:1401 – 9.

7. Dasmahapatra GP, Didolkar P, Alley MC, et al. *In vitro* combination treatment with perifosine and UCN-01 demonstrates synergism against prostate (PC-3) and lung (A549) epithelial adenocarcinoma cell lines. Clin Cancer Res 2004;10:5242 – 52.

8. Rahmani M, Reese E, Dai Y, et al. Coadministration of histone deacetylase inhibitors and perifosine synergistically induces apoptosis in human leukemia cells through Akt and ERK1/2 inactivation and the generation of ceramide and reactive oxygen species. Cancer Res 2005;65:2422 – 32.

9. Nyakern M, Cappellini A, Mantovani I, Martelli AM. Synergistic induction of apoptosis in human leukemia T cells by the Akt inhibitor perifosine and etoposide through activation of intrinsic and Fas-mediated extrinsic cell death pathways. Mol Cancer Ther 2006;5:1559 – 70.

10. Ashkenazi A, Dixit VM. Death receptors: signaling and modulation. Science 1998;281:1305 – 8.

11. Hengartner MO. The biochemistry of apoptosis. Nature 2000;407:770 – 6.

12. Kataoka T. The caspase-8 modulator c-FLIP. Crit Rev Immunol 2005;25:31 – 58.

13. Wajant H. Targeting the FLICE inhibitory protein (FLIP) in cancer therapy. Mol Interv 2003;3:124 – 7.

14. Longley DB, Wilson TR, McEwan M, et al. c-FLIP inhibits chemotherapy-induced colorectal cancer cell death. Oncogene 2006;25:838 – 48.

15. Cheng JQ, Lindsley CW, Cheng GZ, Yang H, Nicosia SV. The Akt/PKB pathway: molecular target for cancer drug discovery. Oncogene 2005;24:7482 – 92.

16. Panka DJ, Mano T, Suhara T, Walsh K, Mier JW. Phosphatidylinositol 3-kinase/Akt activity regulates c-FLIP expression in tumor cells. J Biol Chem 2001;276:6893 – 6.

17. Nam SY, Jung GA, Hur GC, et al. Upregulation of FLIP(S) by Akt, a possible inhibition mechanism of TRAIL-induced apoptosis in human gastric cancers. Cancer Sci 2003;94:1066 – 73.

18. Richardson PG, Mitsiades C, Hideshima T, Anderson KC. Bortezomib: proteasome inhibition as an effective anticancer therapy. Annu Rev Med 2006;57:33 – 47.

19. Sun SY, Yue P, Dawson MI, et al. Differential effects of synthetic nuclear retinoid receptor-selective retinoids on the growth of human non-small cell lung carcinoma cells. Cancer Res 1997;57:4931 – 9.

20. Liu X, Yue P, Schonthal AH, Khuri FR, Sun SY. Cellular FLICE-inhibitory protein down-regulation contributes to celecoxib-induced apoptosis in human lung cancer cells. Cancer Res 2006;66:11115 – 9.

21. Zou W, Liu X, Yue P, Khuri FR, Sun SY. PPARγ ligands enhance TRAIL-induced apoptosis through DR5 upregulation and c-FLIP down-regulation in human lung cancer cells. Cancer Biol Ther 2007;6:99 – 106.

22. Liu X, Yue P, Zhou Z, Khuri FR, Sun SY. Death receptor regulation and celecoxib-induced apoptosis in human lung cancer cells. J Natl Cancer Inst 2004;96:1769 – 80.

23. Sun SY, Yue P, Wu GS, et al. Mechanisms of apoptosis induced by the synthetic retinoid CD437 in human non-small cell lung carcinoma cells. Oncogene 1999;18:2357 – 65.

24. Jin F, Liu X, Zhou Z, et al. Activation of nuclear factor-κB contributes to induction of death receptors and apoptosis by the synthetic retinoid CD437 in DU145 human prostate cancer cells. Cancer Res 2005;65: 6354 – 63.

25. Crul M, Rosing H, de Klerk GJ, et al. Phase I and pharmacological study of daily oral administration of perifosine (D-21266) in patients with advanced solid tumours. Eur J Cancer 2002;38:1615 – 21.

26. Van Ummersen L, Binger K, Volkman J, et al. A phase I trial of perifosine (NSC 639966) on a loading dose/maintenance dose schedule in patients with advanced cancer. Clin Cancer Res 2004;10:7450 – 6.

27. Momota H, Nerio E, Holland EC. Perifosine inhibits multiple signaling pathways in glial progenitors and cooperates with temozolomide to arrest cell proliferation in gliomas *in vivo*. Cancer Res 2005;65: 7429 – 35.

28. Zhang S, Shen HM, Ong CN. Down-regulation of c-FLIP contributes to the sensitization effect of 3,3′-diindolylmethane on TRAIL-induced apoptosis in cancer cells. Mol Cancer Ther 2005;4:1972 – 81.

29. Gajate C, Mollinedo F. Edelfosine and perifosine induce selective apoptosis in multiple myeloma by recruitment of death receptors and downstream signaling molecules into lipid rafts. Blood 2007;109:711 – 9.

Hypoxia-inducible Factor 1α and Antiangiogenic Activity of Farnesyltransferase Inhibitor SCH66336 in Human Aerodigestive Tract Cancer

Ji-Youn Han, Seung Hyun Oh, Floriana Morgillo, Jeffrey N. Myers, Edward Kim, Waun Ki Hong, Ho-Young Lee

Background: **The farnesyltransferase inhibitor SCH66336, in combination with other receptor tyrosine kinase inhibitors, inhibits the growth of non–small-cell lung cancer (NSCLC) cells. We examined whether SCH66336 inhibits angiogenesis of aerodigestive tract cancer cells.** ***Methods:*** **Antiangiogenic activities of SCH66336 against NSCLC, head and neck squamous cell carcinoma (HNSCC), and endothelial cells were examined with cell proliferation, capillary tube formation, and chick aorta (under hypoxic, normoxic, insulin-like growth factor I (IGF)–stimulated, and unstimulated conditions); reverse transcription–polymerase chain reaction; and western blot analyses. The specific roles of the ubiquitin-mediated proteasome machinery, mitogen-activated protein kinase (MAPK) and Akt pathways, and heat shock protein 90 (Hsp90) in the SCH66336-mediated degradation of hypoxia-inducible factor 1α (HIF-1α) were assessed with ubiquitin inhibitors and adenoviral vectors that express constitutively active MAP kinase kinase (MEK)1, constitutively active Akt, or Hsp90.** ***Results:*** **SCH66336 showed antiangiogenic activities and decreased the expression of vascular endothelial cell growth factor (VEGF) and HIF-1α in hypoxic, IGF-stimulated, and unstimulated aerodigestive tract cancer and endothelial cells. SCH66336 reduced the half-life of the HIF-1α protein, and ubiquitin inhibitors protected the hypoxia- or IGF-stimulated HIF-1α protein from SCH66336-mediated degradation. SCH66336 inhibited the interaction between HIF-1α and Hsp90. The overexpression of Hsp90, but not constitutive Akt or constitutive MEK, restored HIF-1α expression in IGF-stimulated or hypoxic cells but not in unstimulated cells.** ***Conclusions:*** **SCH66336 appears to inhibit angiogenic activities of NSCLC and HNSCC cells by decreasing hypoxia- or IGF-stimulated HIF-1α expression and to inhibit VEGF production by inhibiting the interaction between HIF-1α and Hsp90, resulting in the proteasomal degradation of HIF-1α.** **[J Natl Cancer Inst 2005;97:1272–86]**

Despite recent therapeutic advances, the survival rate of patients with aerodigestive tract cancer has not improved substantially *(1)*, and most patients with aerodigestive tract cancer die of metastatic disease *(2)*. Generation of blood vessels (i.e., angiogenesis) plays a critical role in malignant solid tumor growth and subsequent metastasis to other organs *(3)*, suggesting that targeting the mechanisms that stimulate tumor angiogenesis should be explored as a therapeutic approach for solid tumors of the aerodigestive tract.

Among various proteins that have been identified as potential targets of antiangiogenesis therapy is vascular endothelial cell growth factor (VEGF). VEGF is expressed by activated endothelial cells and promotes the proliferation, survival, and migration of endothelial cells, and thus it is essential for blood vessel formation *(4)*. In addition, the expression and secretion of VEGF by tumor cells are stimulated by activation of Ras *(5)* and the phosphatidylinositol 3-kinase (PI3K)–Akt pathway *(6,7)*. The major physiologic stimulus for VEGF expression is hypoxia, which induces transcription of the VEGF gene by hypoxia-inducible factor 1 (HIF-1). HIF-1 is a heterodimer composed of HIF-1α and HIF-1β subunits *(1,8)*. A nuclear localization signal at the carboxyl-terminal end of HIF-1α allows its transport from the cytoplasm to the nucleus, where it forms an active transcription complex by binding to HIF-1β. HIF-1β is constitutively expressed, whereas the expression and activity of HIF-1α protein are regulated by O_2-dependent and -independent mechanisms [for review, see Harris *(9)*]. Under normoxic conditions, HIF-1α is subject to O_2-dependent prolyl hydroxylation, which triggers binding of von Hippel–Lindau tumor suppressor protein (VHL) and ubiquitin-mediated protein degradation by proteasome *(10,11)*. Under the hypoxic condition, O_2 becomes limiting for prolyl hydroxylase activity, HIF-1α ubiquitination is inhibited, and active HIF-1 transcription complexes can be formed. However, the level of HIF-1α also increases via an O_2-independent mechanism *(6,7)*. Growth factors, such as epidermal growth factor, heregulin, insulin-like growth factors (IGFs) I and -II, and insulin, induce expression of HIF-1α protein under nonhypoxic conditions *(7,12,13)*. They bind to cognate receptor tyrosine kinases and activate the PI3K or mitogen-activated protein kinase (MAPK) pathway, which in turn increases the rate of HIF-1α protein synthesis. PI3K–Akt and MAPK have also been implicated in the stabilization of HIF-1α induced by oncogenes, hypoxia, and growth factors [for review, see Semenza *(14)*]. HIF-1 associates with the molecular chaperone heat shock protein 90 (Hsp90); pharmacologic disruption of this association promotes the ubiquitination and proteasome-mediated degradation of HIF-1 in an oxygen- and VHL-independent manner *(15)*, suggesting that inhibitors of the interaction between HIF-1α and Hsp90 could be used to regulate the expression of hypoxia- or IGF-I–induced HIF-1α protein.

Affiliation of authors: Department of Thoracic/Head and Neck Medical Oncology (J-YH, SHO, FM, EK, WKH, H-OL), Department of Head and Neck Surgery (JNM), The University of Texas M. D. Anderson Cancer Center, Houston, TX.

Correspondence to: Ho-Young Lee, PhD, Unit 432, Department of Thoracic/Head and Neck Medical Oncology, The University of Texas M. D. Anderson Cancer Center, 1515 Holcombe Blvd., Houston, TX 77030 (e-mail: hlee@mdanderson.org).

See "Notes" following "References."

DOI: 10.1093/jnci/dji251

© The Author 2005. Published by Oxford University Press. All rights reserved. For Permissions, please e-mail: journals.permissions@oupjournals.org.

Downloaded from jnci.oxfordjournals.org at M D Anderson Hospital on October 8, 2010

We have shown that SCH66336, a nonpeptide tricyclic farnesyltransferase inhibitor (FTI) that inhibits the farnesylation of various components, in combination with other inhibitors of the receptor tyrosine kinase signaling pathway, inhibits the growth of non–small-cell lung cancer (NSCLC) cells *(16)*. In addition, in this study, we found that treatment with SCH66336 alone led to regression of orthotopic tongue tumors of human head and neck squamous cell carcinoma (HNSCC) in mice. Because angiogenesis is an essential step in the transition of a tumor from a small cluster of mutated cells to a large, malignant growth *(17)*, we investigated the activity of SCH66336 on VEGF and HIF-1α expression and the mechanisms of its antiangiogenic action in aerodigestive tract cancers.

Materials and Methods

Cells, Animals, and Materials

UMSCC38 HNSCC cells established originally by Dr. Thomas Carey (University of Michigan, Ann Arbor) were obtained from Dr. Reuben Lotan *(18)*. We purchased the human NSCLC cell line H1299 from American Type Culture Collection (Manassas, VA). These cells were cultured in RPMI 1640 medium supplemented with 10% fetal bovine serum and antibiotics. Human umbilical vein endothelial cells (HUVECs; Cambrex BioScience, Walkersville, MD) were maintained in a gelatin-coated dish in endothelial growth medium (Cambrex BioScience) at 37 °C in a humidified atmosphere of 5% CO_2–95% air. HUVECs used in this study were from passages 2–7. Tissue culture reagents and plasticware were from Nunc (Roskilde, Denmark). Transwell chambers were from Corning-Costar (Corning, NY). Amicon Ultra-4 centrifugal filter was obtained from Millipore Co. (Bedford, MA). Cell culture inserts incorporating polyester transwell membranes (6.4-mm diameter with a 8-μm pore size) and 24-well plates were from Costar (Cambridge, MA). We used the following adenoviral (Ad) vectors for experiments in this article: a vector expressing constitutively active MAP kinase kinase (MEK) 1 (in which both serine residues at positions 217 and 221 were changed to a glutamine residue), referred to as Ad-MEK1 *(19)*; a vector expressing constitutively active Akt (MyrAkt), referred to as Ad-HA-MyrAkt *(20)*; a vector expressing hemagglutinin (HA)-tagged Hsp90, referred to as Ad-HA-Hsp90 *(21)*; and an empty vector, referred to as EV. These vectors were amplified as described previously *(16)*. Female nude mice, 6 weeks old, were purchased from Harlan-Sprague Dawley (Indianapolis, IN). SCH66336, i.e., [+]4-(2-[4-(8-chloro-3,0-dibromo-6,11-dihydro-5-benzocyclohepa(1,2-β) pyridin-11-yl)-1-piperidinyl]-2-oxoethyl)-1-piperidinecarboxamide, was obtained from Schering-Plough (Kenilworth, NJ). We confirmed that SCH66336 can inhibit farnesylation *(22)* by assessing the level of unfarnesylated H-Ras in NSCLC cell lines after treatment with SCH66336 (data not shown). FTI-277, another farnesyltransferase inhibitor, was purchased from Calbiochem (San Diego, CA). SCH66336 and FTI-277 were dissolved in dimethyl sulfoxide at various concentrations to establish dose–response relationships. Bovine serum albumin, gelatin, the ubiquitin inhibitors MG132 and ALLN, cycloheximide, and 3-(4,5-dimethylthiazol-2-yl)-2,5-diphenyltetrazolium bromide (MTT) were obtained from Sigma-Aldrich (St. Louis, MO). Inhibitors were prepared as 20 m*M* stock solutions in dimethyl sulfoxide and stored at −20 °C. Synthetic small interfering RNAs (siRNAs) targeting H-ras, VHL, or HIF-1α were purchased from Ambion (Austin, TX).

Hypoxic Treatment

Tissue culture dishes were transferred to a modular incubator chamber (Billups-Rothenberg, Del Mar, CA), the chamber was sealed, and the temperature was set at 37 °C. For hypoxic exposures, cells were placed in an airtight chamber (Biospherix, Redfield, NY), the chamber was flushed with a mixture of 1% O_2, 5% CO_2, and 94% N_2 to maintain O_2 concentration at 1% with Pro-Ox model 110 O_2 regulators (BioSpherix), and cells were incubated at 37 °C.

Conditioned Medium

To obtain conditioned medium from SCH66336-treated H1299 NSCLC cells, we plated 10^6 H1299 cells in a 10-cm-diameter plate containing RPMI 1640 medium with 10% fetal bovine serum. After 24 hours, the medium on these cells was replaced with fresh growth medium containing SCH66336 (0 or 5 μ*M*). The plates were then incubated under normoxic or hypoxic conditions for 1 day, and cells were washed with phosphate-buffered saline, and then serum-free medium containing the same concentration of SCH66336 was added. After 2 days of incubation, conditioned medium was removed and centrifuged at 4000*g* for 20 minutes at 4 °C through an Amicon Ultra-4 centrifugal filter (Millipore) to remove any trace of SCH66336. The molecular mass cutoff of the filters was 5 kDa, and the molecular mass of SCH66336 (M_r = 638.6) is 0.56 kDa. The flowthrough containing excess SCH66336 was discarded, and the retentate was collected. Because SCH66336 itself may have an inhibitory effect on this assay, we confirmed that this approach efficiently removed SCH66336 from the conditioned medium by treating UMSCC38 HNSCC cells with the conditioned medium and measuring farnesylated H-ras levels in the cells by western blot analysis. We found that inhibition of H-ras farnesylation required more than 0.5 μ*M* SCH66336 (data not shown), which was insufficient to induce antiangiogenic effects in H1299 cells. By comparing supernatants from filtration spins with that from control cells treated with known concentrations of SCH66336, we determined that the amount of SCH66336 remaining after two successive filtration spin supernatants was not sufficient to inhibit H-Ras farnesylation when the starting concentration did not exceed 10 μ*M*. The final filter retentate was concentrated 40-fold for use in the angiogenesis assay. This conditioned medium was used for several analyses, including Matrigel plug, chick aortic arch, HUVEC proliferation, and tube formation assays.

Cell Treatments

To assess the effects of SCH66336 on the expression of various proteins and mRNAs by western blot and reverse transcription–polymerase chain reaction (RT–PCR) analyses, we treated 10^6 cells per 100-mm^3-diameter dish (H1299 NSCLC cells, UMSCC38 HNSCC cells, or HUVECs) with SCH66336 (0.5, 1, or 5 μ*M*) in complete medium. For H-ras, HIF-1α, VHL, or scrambled (control) siRNA transfection, H1299 cells were plated at a concentration of 10^5 cells per well in six-well plates. The next day, cells were transfected with 60 nmol of the indicated siRNAs by use of Oligofectamine (Invitrogen, Carlsbad, CA) for 6 hours and then cells were placed in fresh medium with or without 5 μ*M* SCH66336. Scrambled siRNA was used as a

Downloaded from jnci.oxfordjournals.org at M D Anderson Hospital on October 8, 2010

negative control. After 2 days of incubation, medium was replaced with complete medium or serum-free medium, and then cells were incubated for another day. Serum-starved cells were stimulated by IGF-I at 100 ng/mL under normoxic (20% O_2) or hypoxic (1% O_2) conditions for 4 hours before harvest. Total protein extracts were collected for western blot analysis as described elsewhere *(16)*. Briefly, cells were washed in phosphate-buffered saline and lysed in a buffer containing 50 m*M* Tris–HCl (pH 8.0), 150 m*M* NaCl, 0.1% sodium dodecyl sulfate (SDS), 1% Nonidet P-40, 1 m*M* phenylmethylsulfonyl fluoride, aprotinin at 5 μg/mL, and leupeptin at 5 μg/mL. After incubation on ice for 30 minutes and centrifugation at 1500g for 20 minutes at 4 °C, the supernatants were collected, and the protein concentration of each was determined with a BCA protein assay kit (Pierce, Rockford, IL).

To test the effects of SCH66336 on HIF-1α half-life, cycloheximide (100 ng/mL) was added to the medium from SCH66336-treated H1299 cells that had been stimulated with hypoxia or IGF-I for 4 hours, and whole-cell extracts were prepared as described above. In some experiments, ubiquitin inhibitors (10 μ*M* MG132 or 10 μ*M* ALLN) were added to growth medium when cells were stimulated with IGF-I or hypoxia.

To assess the contributions of the MAPK and Akt signaling pathways and Hsp90 expression to the SCH66336-mediated regulation of HIF-1α stability, H1299 cells were infected with Ad-HA-Myr-Akt (25 plaque-forming units [PFU] per cell), Ad-MEK (25 PFU per cell), Ad-HA-Hsp90 (50 PFU per cell), or Ad-EV (the parental virus control, 25–50 PFU per cell). For infection, cells and vectors were incubated for 2 hours in the absence of serum, incubated in growth medium containing 0.5–5 μ*M* SCH66336 for 2 days, and then incubated with complete medium or with serum-free medium for another day. Cells were unstimulated or stimulated by IGF-I or hypoxia for 4 hours as described above.

To test the effects of conditioned medium on proliferation of vascular endothelial cells, 3×10^3 HUVECs (in 100 μL of endothelial basal medium [EBM], Cambrex Bioscience) per well of 96-well culture plates were treated with 10 μg of conditioned medium from the hypoxic, normoxic IGF-stimulated, or unstimulated NSCLC or HNSCC cells. To test the direct effects of SCH66336 on proliferation of vascular endothelial cells, we treated 3×10^3 HUVECs per well with 1 or 5 μ*M* SCH66336 in 96-well culture plates. After 72 hours of incubation under hypoxic or normoxic conditions, cell proliferation was assessed by the MTT assay. For each analysis, six replicate wells were used, and at least three independent experiments were performed.

Chick Aortic Arch Assay

The chick aortic arch assay was as described elsewhere *(24)*. In brief, thoracic aortas were obtained from chick eggs after 13–15 days of incubation. Excess perivascular tissue was removed, and transverse sections (1–2 mm) were cut. The resulting aortic rings were washed in medium 199 (Life Technologies) and embedded in 30 μL of Matrigel in 24-well plates (Costar) with the lumen perpendicular to the base of the well. Each ring was covered with 4 μL of Matrigel, which was allowed to gel, and then 300 μL of ECM and 10 μL of conditioned medium were added to each well. These plates were incubated for 24 hours or 48 hours at 37 °C to allow microvessel sprouting from the adventitial layer of the ring. The plates were photographed under a stereomicroscope (Zeiss, Göttingen, Germany), and average sprouting was measured with the imageJ program (National Institutes of Health, Bethesda, MD). Each condition was tested in six wells. The experiment was repeated three times, each with similar results.

In Vitro Capillary Tube Formation Assay

The capillary tube formation assay was as described elsewhere *(23)*. We evenly dispersed 5×10^4 HUVECs on 250-μL Matrigel surfaces that were depleted of growth factors (Matrigel; Becton Dickinson, Bedford, MA); cells were incubated in 250 μL of EBM containing 30 μL of conditioned medium from H1299 cells cultured under hypoxic or normoxic conditions. To determine the direct effects of SCH66336 on HUVECs, cells were incubated in complete medium containing 5 μ*M* SCH66336 under normoxic or hypoxic conditions. After incubation at 37 °C for 1 day, capillary tube formation was assessed as described elsewhere *(23)*. Morphologic changes in the cells were assessed under a microscope and photographed at ×40 magnification. Tube formation was scored; a three-branch-point event was scored as one tube *(25)*. The experiment was repeated three times, each with similar results.

Immunoblot Assays

Whole-cell lysates were prepared in lysis buffer from 10^6 cells as described elsewhere *(16)*. Equivalent amounts of protein (30–80 μg) were resolved by SDS–polyacrylamide electrophoresis in 7.5%–12% gels (80 V for 20 minutes and 100 V for 1 hour) and transferred by electroblotting overnight at 20 V to a nitrocellulose membrane. After nonspecific binding to the blot was blocked in Tris-buffered saline (TBS) containing 0.05% Tween 20 (TBST) and 5% nonfat powdered milk, the blot was incubated with primary antibody at the appropriate dilution in TBS–5% nonfat milk at 4° C for 16 hours. The membrane was then washed multiple times with TBST and incubated with the appropriate horseradish peroxidase–conjugated secondary antibody for 1 hour at room temperature. The protein–antibody complexes were detected by using the enhanced chemiluminescence kit (Amersham, Arlington Heights, IL), according to the manufacturer's recommended protocol. To identify HIF-1α on these blots, 80 μg of protein was analyzed with a monoclonal antibody against HIF-1α (BD-Transduction Laboratories, Lexington, KY; 1 : 500 dilution), as described elsewhere *(24)*. We used 30 μg of protein for other western blot analyses with mouse monoclonal antibodies against phosphorylated p44/42MAPK (pp44/42 MAPK; Thr202/Tyr204; 1 : 500 dilution) or HIF-1β (H1β234; 1 : 1000 dilution) (Novus Biologicals); rabbit polyclonal antibodies against phosphorylated Akt (Ser473; 1 : 1000 dilution), phosphorylated glycogen synthase kinase 3β (GSK-3β; 1 : 1000 dilution), GSK-3β, and VHL antibodies (1 : 1000 dilution) (Cell Signaling Technology, Beverly, MA); goat polyclonal antibodies against p44/42 MAPK (1 : 1000 dilution), rabbit polyclonal anti-Akt, -HA, -MEK1/2, and -β-actin (1 : 4000 dilution) antibodies (Santa Cruz Biotechnology, Santa Cruz, CA); rabbit polyclonal anti-HSP90 (1 : 5000 dilution) (Stressgen, Victoria, British Columbia, Canada); rabbit anti–mouse immunoglobulin G (IgG)–horseradish peroxidase conjugate (1 : 2000 dilution; DAKO, Carpinteria, CA); and donkey anti–rabbit IgG–horseradish peroxidase conjugate (1 : 2000 dilution) and rabbit anti–goat IgG–horseradish peroxidase conjugate (1 : 2000 dilution; both from Amersham Pharmacia Biotech, Arlington Heights, IL).

Downloaded from jnci.oxfordjournals.org at M D Anderson Hospital on October 8, 2010

RT–PCR Assay

Total RNA was isolated from cells by using the Trizol reagent (Invitrogen). cDNA was synthesized from 1 μg of total RNA as a template in a 50-μL reaction mixture by using TaqMan reverse transcription reagents, according to the manufacturer's protocol (Applied Biosystems, Foster City, CA). The reaction was incubated at 25 °C for 10 minutes and at 48 °C for 30 minutes and then inactivated at 95 °C for 5 minutes. After inactivation, the cDNA was stored at −20 °C until use. RT–PCR was performed by coamplification of the genes with a reference gene (18S ribosomal RNA) by use of the cDNA template and corresponding gene-specific primer sets. The primer sequences were as follows: (sense) 5′-GGGAGAAAATCAAGTCGTGC-3′ and (antisense) 5′-AGCAAGGAGGGCCTCTGATG-3′ for HIF-1α; (sense) 5′-CCATGAACTTTCTGCTGTCTT-3′ and (antisense) 5′-ATCGCATCAGGGGCACACAG-3′ for VEGF; (sense) 5′-GGTGAAGGTCGGTGTGAACGGATTT-3′ and (antisense) 5′-AATGCCAAAGTTGTCATGGATGACC-3′ for GAPDH. To avoid amplification of genomic DNA, we chose the primers from different exons. PCR was carried out in a total volume of 25 μL containing 1 μL of cDNA solution, 0.2 μ*M* of sense primers, and 0.2 μ*M* of antisense primers. The RT–PCR exponential phase was determined after 28–33 cycles to allow quantitative comparisons among the cDNAs developed from identical reactions. The thermocycler conditions used for amplification were 94 °C for 6 minutes (hot start) and then cycles of 94 °C for 45 seconds, 56–60 °C for 45 seconds, and 72 °C for 1 minute. The control PCR was performed for 26 or 27 cycles with 0.5 μL of cDNA solution to allow quantitative comparisons among the cDNAs developed from identical reactions with primers for GAPDH. Amplified products (8 μL) were resolved on 2% agarose gels, stained with ethidium bromide, visualized with a transilluminator, and photographed.

Immunoprecipitation

Whole-cell lysates were prepared in lysis buffer (50 m*M* Tris, 150 m*M* NaCl, 5 m*M* EDTA, 0.5% Nonidet P-40, 5% glycerol, 1 m*M* phenylmethylsulfonyl fluoride, and protease inhibitor mixture [Roche diagnostics, Mannheim, Germany], pH 7.5), followed immediately by three 15-second periods of vortex mixing. After centrifugation (15 000*g* for 30 minutes at 4 °C), supernatants were transferred to fresh tubes. Supernatants (1 mg of protein each) were mixed with 1 μg of anti-HIF-1α antibody (Santa Cruz Biotechnology) and incubated at 4 °C overnight. Thereafter, 50 μL of protein A–Sepharose beads (Amersham Pharmacia Biotech AB, Uppsala, Sweden) was added, and the mixture was incubated at 4 °C for 4 hours. Beads were washed three times with the lysis buffer and two times with 1× phosphate-buffered saline, boiled in Laemmli loading buffer, and separated by SDS–polyacrylamide electrophoresis in 8% gels. HIF-1α (BD-Transduction Laboratories, Lexington, KY), Hsp90, and ubiquitin were assessed by immunoblot analysis with corresponding antibodies.

In Vivo Tumor Model and Immunohistochemical Staining

Sublingual injections for implantation of orthotopic tumors were performed as described elsewhere *(26)*. All animal procedures were performed in accordance with a protocol approved by the M. D. Anderson institutional Animal Care and Usage Committee. We injected 2×10^6 UMSCC38 cells into the lateral tongue of anesthetized 6-week-old female nude mice (n = 5 per group). One week after tumor cell injection, when tumors started to develop, drug treatment was started. SCH66336 (40 mg/kg of body weight) or 20% hydroxyl-propyl-betacyclodexatrin control vehicle was given orally twice a day for 3 weeks. Two and 4 weeks after tumor cell injection, tumor size and body weight were measured; thereafter, the mouse food was replaced by commercially available soft food (transgenic mice dough; Bio-serv, Frenchtown, NJ) that the mice could swallow even when the oral cavity was blocked by tumor. Four weeks after tumor cell injection, the mice were humanely killed by exposure to CO_2. Tumor growth was assessed by measuring tumor size in two dimensions and calculating tumor volume as described elsewhere *(27)*. After each mouse was killed, its tongue was removed and divided into two parts.

One part of the tongue was fixed, embedded in paraffin, and sectioned for VEGF and HIF-1α staining. The 5-μm tumor tissue sections were deparaffinized through a series of xylene baths and rehydrated through a series of graded ethanol baths. The sections were then immersed in methanol containing 0.3% hydrogen peroxidase for 20 minutes to block endogenous peroxidase activity and incubated in 2.5% blocking serum to reduce nonspecific binding. Sections were incubated overnight at 4 °C with primary antibody against VEGF (Santa Cruz Biotechnology; 1 : 200 dilution) or HIF-1α (Santa Cruz Biotechnology; 1 : 100 dilution) and then processed for avidin–biotin immunohistochemistry according to the manufacturer's recommendations (Vector Laboratories, Burlingame, CA). Diaminobenzidine was used as a chromogen, and commercial hematoxylin was used for counterstaining. The other part of tongue was frozen for CD31 staining; 20-μm frozen sections of tumor tissues were stained with anti-CD31 antibody (1 : 100 dilution; BD-Pharmingen, San Diego, CA), and then the antibody was detected by Cy3-conjugated secondary antibody as previously described *(28)*.

Statistical Analysis

Data are expressed as the means and 95% confidence intervals (CIs) from triplicate samples, calculated with Microsoft Excel software (version 5.0; Microsoft Corporation, Seattle, WA). The Wilcoxon rank-sum test in the statistical SPSS statistical program (SPSS version 10; SPSS, Chicago, IL) was used to determine the statistical significance of antitumorigenic and antiangiogenic effects of SCH66336. Cell proliferation data were analyzed with a Student's *t* test. The null hypothesis that there was no difference in the cell proliferation between control and treatment groups was rejected at the probability (*P*) of less than .05. All statistical tests were two-sided.

Results

SCH66336 and Angiogenic Activities of Aerodigestive Tract Cancer Cells

We investigated whether the farnesyltransferase inhibitor SCH66336 had antiangiogenic activity on aerodigestive tract cancer cells, including NSCLC and HNSCC cells. The angiogenic process consists of several steps that include degradation of the basement membrane by endothelial cells, migration to

Downloaded from jnci.oxfordjournals.org at M D Anderson Hospital on October 8, 2010

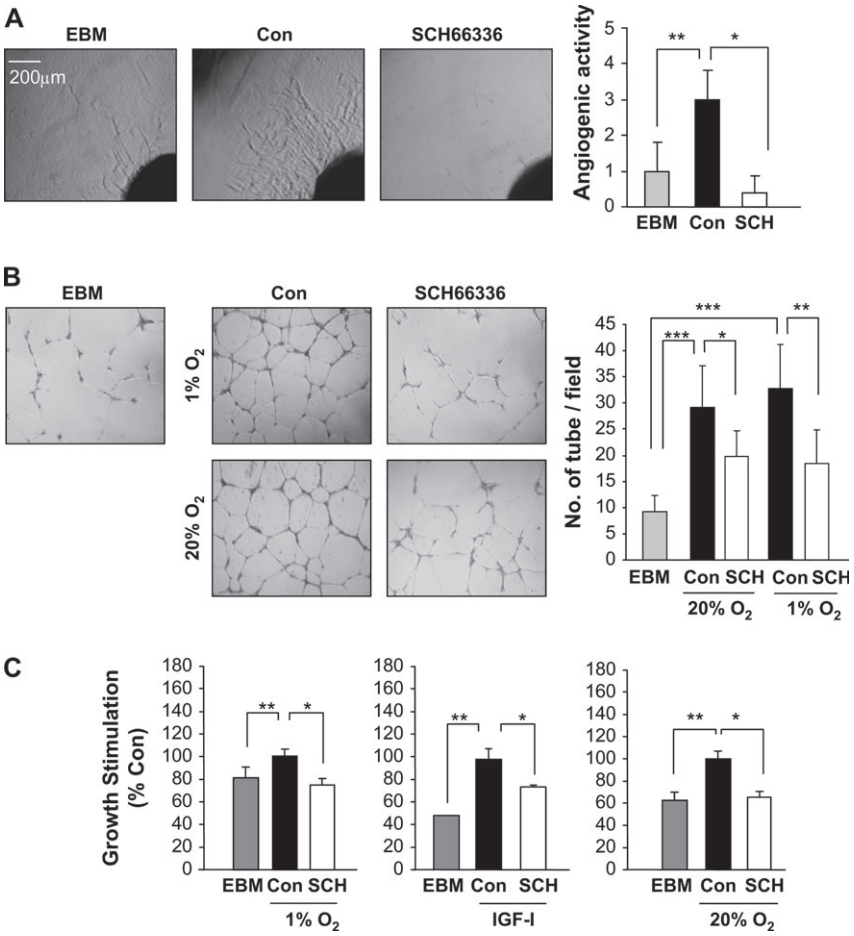


Fig. 1. Antiangiogenic activities of SCH66336 in aerodigestive tract cancer cells and endothelial cells. **A**) Chick aortic ring assay. Endothelial cell sprouting from chick aortic rings, incubated with endothelial basal medium (EBM) alone or with conditioned medium from untreated (Con) or SCH66336-treated (SCH) H1299 non–small-cell lung cancer cells (shown to the left), was evaluated, by scoring angiogenic activity on a scale of 0–4. Results, shown to the right, are expressed as percent endothelial cell sprouting from chick aorta exposed to conditioned medium from untreated or SCH66336-treated H1299 cells relative to the EBM-stimulated endothelial cell sprouting. **Error bars** = upper 95% confidence interval. (EBM alone, mean = 1, 95% CI = 0.2 to 1.8; conditioned medium from untreated control cells, mean = 3, 95% CI = 2.2 to 3.8; conditioned medium from SCH66336-treated, mean = 0.38, 95% CI = −0.1 to 0.8). Scoring results, shown to the right, are expressed as the means from six replicate points. **Error bars** = 95% confidence intervals. *, P = .03, compared with control. **, P = .04, compared with EBM. Con = control. **B**) Tube formation assay. Angiogenic activity in conditioned medium from H1299 cells was tested by plating human umbilical vein endothelial cells (HUVECs) onto Matrigel-coated 12-well plates and treating the cells with conditioned medium from H1299 cells treated with 5 μ*M* SCH66336 under hypoxic or normoxic conditions. After 24 hours, images of capillary tube formation were captured (shown to the left), and tube formation was scored in one ×4 microscopic field, with one tube was designated as a three branch point event. Capillary tube formation results, shown to the right, are the means from three samples. EBM alone, mean = 9.2 tubes per field, 95% CI = 6.8 to 11.6; conditioned medium from untreated control cells under hypoxic (1% O_2) conditions, mean = 32.8 tubes per field, 95% CI = 28.0 to 37.7; conditioned medium from untreated control cells under normoxic (20% O_2) conditions, mean = 29.1 tubes per field, 95% CI = 24.4 to 33.8; conditioned medium from cells treated with 5 μ*M* SCH66336 under hypoxic (1% O_2) conditions, mean = 18.4 tubes per field, 95% CI = 14.8 to 22.0; conditioned medium from cells treated with 5 μ*M* SCH66336 under normoxic (20% O_2) conditions, mean = 19.9 tubes per field, 95% CI = 16.3 to 23.4. Two independent experiments with triplicate samples were performed with similar results. *, P = .04, compared with control; ** P<.001, compared with control; ***, P<.001, compared with EBM. **C**) Cell proliferation. HUVECs were cultured in EBM (a negative control) or EBM containing conditioned medium from H1299 cells that were untreated or treated with 5 μ*M* SCH66336 for 3 days and then were unstimulated or stimulated by hypoxia (1% O_2) or IGF-I (100 ng/mL) for 4 hours. Cell proliferation was measured with the 3-(4,5-dimethylthiazol-2-yl)-2,5-diphenyltetrazolium bromide (MTT) assay. Results are expressed as the mean of eight samples. Independent experiments were repeated three times. **Error bars** = 95% confidence intervals. Conditioned medium from SCH66336-treated cells under hypoxic (1% O_2) conditions, mean = 73.2%, 95% CI = 68.2% to 78.2%; or normoxic (20% O_2) conditions, mean = 67.1%, 95% CI = 63.0% to 71.1%. **Error bars** = 95% confidence intervals. *, P = .004 (hypoxic condition), compared with control; P<.001 (IGF treatment condition), compared with control; P = .002 (normoxic condition), compared with control; **, P = .03 (hypoxic condition) compared with EBM, P<.001 (IGF treatment condition) compared with EBM, or P = .002 (normoxic condition) compared with EBM. All statistical tests were two-sided.

the extravascular space, proliferation, and synthesis of a new basement membrane *(29)*. We first performed the ex vivo chick aortic arch ring assay to determine the effects of SCH66336 on the ability of aerodigestive tract cancer cells to promote growth and migration of endothelial cells in three-dimensional cultures. The cell sprouting was evaluated by scoring angiogenic activity on a scale of 0–4. Conditioned medium from untreated control H1299 cells stimulated statistically significantly more endothelial cell sprouting (mean = 3, 95% CI = 2.2 to 3.8) than EBM (mean = 1, 95% CI = 0.2 to 1.8) (P = .04) (Fig. 1, A). However, conditioned medium from SCH66336-treated cells stimulated less endothelial cell sprouting (mean = 0.5, 95% CI = 0.1 to 0.9) than conditioned medium from untreated control cells (P = .03).

The in vitro capillary tube formation assay uses HUVECs to assess endothelial cell morphogenesis into capillaries on Matrigel-coated plates. Because tumor angiogenesis is also stimulated by hypoxia, we used conditioned medium from untreated control

Downloaded from jnci.oxfordjournals.org at M D Anderson Hospital on October 8, 2010

H1299 cells incubated under hypoxic (1% O_2) or normoxic (20% O_2) conditions. Conditioned medium from untreated control cells cultured under hypoxic (mean = 32.8 tubes per field, 95% CI = 28.0 to 37.7; n = 3 samples) or normoxic (mean = 29.1 tubes per field, 95% CI = 24.4 to 33.8; n = 3 samples) conditions stimulated capillary tube formation of HUVECs on Matrigel-coated culture plates statistically significantly more than EBM alone (Fig. 1, B). However, conditioned medium from cells treated with 5 μ*M* SCH66336 under hypoxic (mean = 18.4 tubes per field, 95% CI = 14.8 to 22.0; $P<.001$) or normoxic (mean = 19.9 tubes per field, 95% CI = 16.3 to 23.4; $P = .04$) conditions stimulated endothelial cell morphogenesis statistically significantly less than conditioned medium from untreated control cells. These findings indicate that SCH66336 inhibited the angiogenic activities of H1299 cells.

Finally, because tumor angiogenesis is induced by angiogenic growth factors that are secreted from hypoxia- or IGF-stimulated cancer cells and then bind to their corresponding receptors expressed on endothelial cells to stimulate endothelial cell proliferation *(30)*, we investigated whether conditioned medium from SCH66336-treated H1299 cells altered HUVEC proliferation. We found that addition of conditioned medium from hypoxic, normoxic IGF-stimulated, or unstimulated normoxic H1299 cells statistically significantly increased proliferation of HUVECs, whereas addition of conditioned medium from SCH66336-treated cells statistically significantly decreased HUVEC proliferation under hypoxic (73.2% of control growth stimulation, 95% CI = 68.2% to 78.2%; $P = .004$) or normoxic (67.1% of control growth stimulation, 95% CI = 63.0% to 71.1%; $P = .002$) conditions (Fig. 1, C). HUVECs incubated with conditioned medium from hypoxic, normoxic IGF–stimulated, or unstimulated normoxic UMSCC38 cells had comparable patterns of decreased cell proliferation (data not shown). Thus, SCH66336 appears to inhibit hypoxia- or growth factor–stimulated and constitutive secretion of angiogenic growth factors from aerodigestive tract cancer cells.

Expression of HIF-1α and VEGF by SCH66336-treated Cells

Because VEGF plays an important role in angiogenesis and because its expression is regulated largely by the transcription factor HIF-1α, we investigated whether SCH66336 treatment alters the expression, and thus the secretion, of HIF-1α and VEGF in aerodigestive tract cancer cells. To determine whether HIF-1α is involved in the regulation of VEGF in H1299 cells, we transfected these cells with an siRNA targeting HIF-1α, to inhibit the expression of HIF-1α, or with a control scrambled siRNA and measured VEGF levels in corresponding conditioned media. The basal level of HIF-1α protein in untransfected H1299 cells was very low but increased markedly after cells were incubated under hypoxic conditions for 4 hours (Fig. 2, A). Levels of HIF-1α and VEGF proteins in H1299 cells transfected with HIF-1α siRNA were lower in normoxic and hypoxic conditions than cells transfected with scrambled siRNA. As expected, HIF-1β protein expression was unchanged in these cells. Thus, the expression of HIF-1α and VEGF appear to be associated in H1299 cells.

Because growth factors and oncogenes can increase the expression of HIF-1α *(14,31,32)*, we investigated whether the level of HIF-1α protein in H1299 cells is regulated by Ras or IGF-I. The role of Ras in HIF-1α expression was tested in H1299 cells transfected with siRNAs targeting H-Ras. H-Ras siRNA-transfected H1299 cells had lower levels of H-Ras mRNA and protein under normoxic (Fig. 2, B, upper panels) and hypoxic (data not shown) conditions than control cells transfected with scrambled siRNA. Levels of GAPDH mRNA and β-actin protein were unchanged in these cells under these conditions (data not shown). In addition, HIF-1α protein levels were not affected by H-Ras siRNA under hypoxic or normoxic conditions (Fig. 2, B, lower panels). To determine whether HIF-1α expression was affected by IGF-I, we cultured H1299 cells in serum-free medium containing IGF-I (50 ng/mL). As previously reported *(14)*, we found that IGF-I had induced the expression of HIF-1α protein after 4 hours of incubation (Fig. 2, C). Thus, the level of HIF-1α protein appears to be regulated by oxygen concentration and growth factors in H1299 cells.

We then investigated whether SCH66336 treatment could alter the level of HIF-1α protein in H1299 cells under hypoxic, normoxic and IGF-stimulated, or normoxic and unstimulated conditions. Hypoxic conditions or IGF treatment increased the expression of HIF-1α protein in H1299 cells, compared with that in cells under normoxic conditions, and this increased expression was reduced by SCH66336 treatment in a time- and dose-dependent manner (Fig. 2, D). In addition, the level of HIF-1α protein in unstimulated H1299 cells was also reduced by SCH66336 treatment, but the level of HIF-1β protein was not altered by SCH66336 treatment under any condition tested. Another farnesyltransferase inhibitor, FTI-277, also decreased the level of HIF-1α protein in hypoxic, normoxic IGF-stimulated, and normoxic unstimulated H1299 cells (Fig. 2, E). In addition, patterns of decreased HIF-1α protein expression, which were similar to those in H1299 cells, were observed in UMSCC38 HNSCC cells treated with SCH66336 or FTI-277 under hypoxic, normoxic IGF-stimulated, and normoxic unstimulated conditions (Fig. 2, F). Thus, inhibition of HIF-1α protein in aerodigestive tract cancer cells appears to be a generic response to farnesyltransferase inhibitors.

We next tested whether the SCH66336-mediated decreased HIF-1α protein expression was associated with VEGF expression in hypoxic, normoxic IGF-stimulated, and normoxic unstimulated H1299 cells. Both VEGF mRNA expression in the SCH66336-treated cells and VEGF protein secreted in the conditioned medium decreased under all conditions tested, whereas GAPDH mRNA expression was not affected (Fig. 2, G). Thus, suppression of HIF-1α expression by SCH66336 appears to contribute to the inhibition of hypoxia- or IGF-stimulated, or constitutive VEGF production.

Because HIF-1α has recently been shown to have an important role in endothelial-cell survival *(33)*, we investigated whether SCH66336 treatment would alter the expression of HIF-1α in HUVECs. Pretreatment of HUVECs with 5 μ*M* SCH66336 inhibited the expression of HIF-1α protein and VEGF mRNA under hypoxic, normoxic IGF-stimulated, and normoxic unstimulated conditions, similar to the patterns previously observed (Fig. 3, A). We also examined whether SCH66336 treatment would alter HUVEC capillary tube formation and cell proliferation. For the capillary tube formation assay, HUVECs were untreated or treated with 5 μ*M* SCH66336 for 24 hours under hypoxic or normoxic conditions, and 5×10^4 untreated or treated cells were cultured on a Trans-well chamber coated with a thin layer of Matrigel. In control medium,

Downloaded from jnci.oxfordjournals.org at M D Anderson Hospital on October 8, 2010

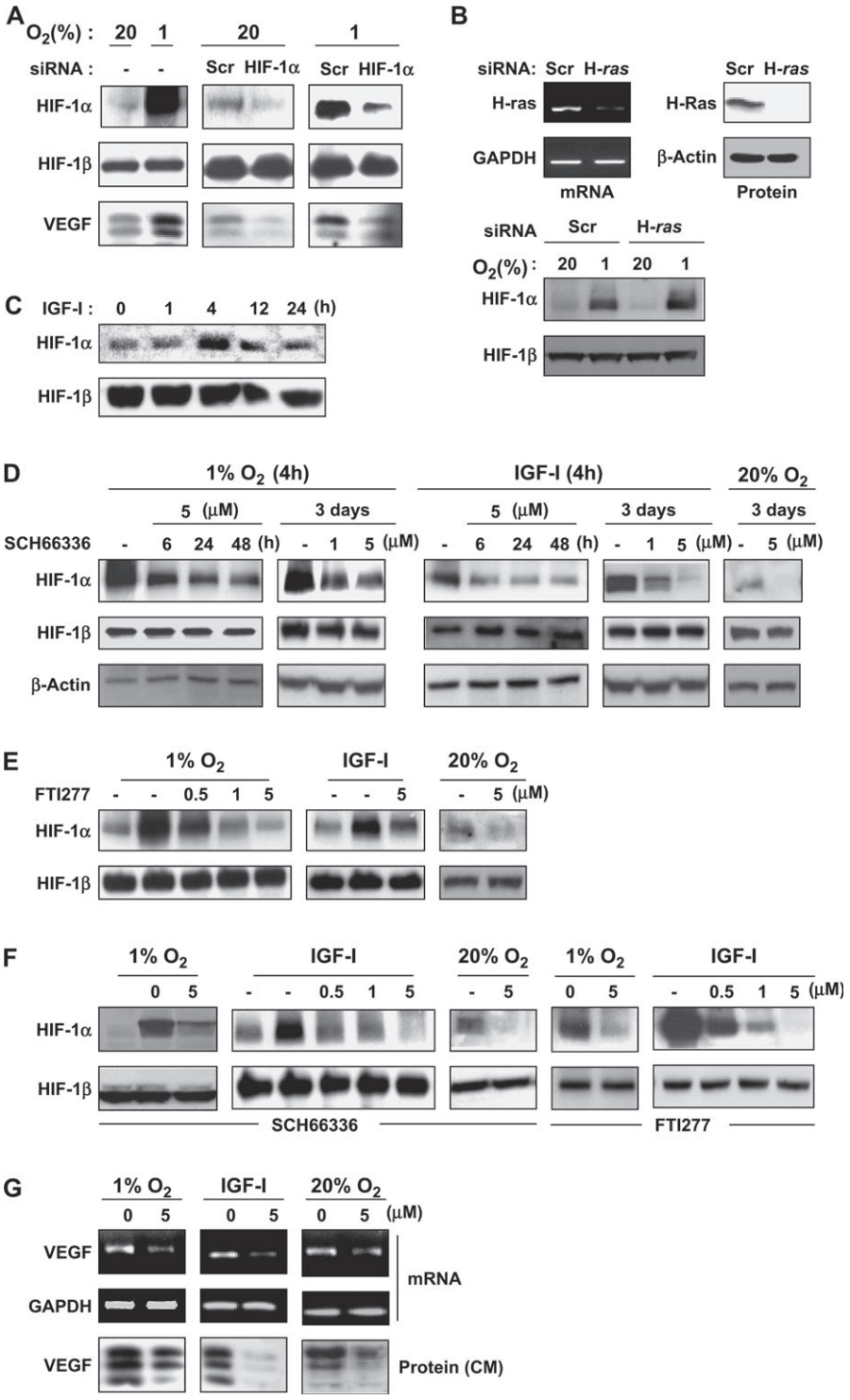


Fig. 2. Hypoxia-inducible factor 1α (HIF-1α) and antiangiogenic activities of farnesyltransferase inhibitors in aerodigestive tract cancer cells. **A**) Expression of HIF-1α in the cell and vascular endothelial cell growth factor (VEGF) in the conditioned medium, as assessed by immunoblot assay. Levels of HIF-1α and HIF-1β, indicated to the left, were measured in total protein extracts of H1299 cells that were untransfected (–), transfected with scrambled (Scr) small interfering RNAs (siRNAs), or transfected with HIF-1α siRNAs and then incubated under normoxic (lanes 20) or hypoxic (lanes 1) conditions for 4 hours. β-Actin protein was used as a loading control for western blot analysis. Levels of VEGF were measured in the conditioned medium from these cells by western blot analysis. Ponceau staining of the blot after the transfer of the protein bands was used to confirm that amounts of protein in each conditioned medium were equal. **B**) H-Ras expression and the induction of HIF-1α expression in H1299 cells. Semiquantitative reverse transcription–polymerase chain reaction (RT–PCR) analysis of H-ras and GAPDH mRNA expression (upper left) and immunoblot assays of H-Ras and β-actin protein (upper right) were performed in H1299 cells that were untransfected or transfected with Scr or H-ras siRNA and incubated under normoxic conditions for 4 hours. Immunoblot assays of HIF-1α and HIF-1β (lower) were performed in H1299 cells that were untransfected or transfected with Scr or H-ras siRNA, and then incubated under normoxic (lanes 20) or hypoxic (lanes 1) conditions for 4 hours. **C**) HIF-1α induction by insulin-like growth factor I (IGF-I) in H1299 cells as a function of time. Cells exposed to IGF-I (100 ng/mL), as indicated, were harvested and subjected to western blot analysis for HIF-1α and HIF-1β. **D**) SCH66336 treatment and the levels of HIF-1α and HIF-1β protein expression under hypoxic and normoxic IGF-stimulated or unstimulated H1299 cells by western blot analysis. H1299 cells were untreated (–) or pretreated with 5 μ*M* SCH66336 as indicated or were treated with 1 or 5 μ*M* SCH66336 for 3 days in complete medium under normoxic conditions. Some cells were incubated for 2 days in complete medium and 1 day in serum-free medium and then exposed to 1% O_2 or IGF-I for 4 hours. Whole-cell extracts were subjected to immunoblot assays with antibodies specific for HIF-1α, HIF-1β, or β-Actin. **E, F**) H1299 cells (panel E) or UMSCC38 cells (panel F) were treated continuously with SCH66336 or FTI-277, as indicated, in complete medium for 3 days under normoxic condition or pretreated with 0.5–5 μ*M* FTI-277, as indicated, for 2 days in complete medium and for 1 day in serum-free medium; serum-starved cells were then exposed to 1% O_2 or IGF-I (100 ng/mL) for 4 hours. Whole-cell extracts were prepared and subjected to immunoblot assays with antibodies specific for HIF-1α or HIF-1β, as indicated to the left. **G**) Semiquantitative RT–PCR analysis of VEGF mRNA expression. H1299 cells were treated continuously with 5 μ*M* SCH66336 in complete medium for 3 days or pretreated with 1 or 5 μ*M* SCH66336 for 2 days in complete medium and 1 day in serum-free medium; serum-starved cells were then exposed to 1% O_2 or IGF-I (100 ng/mL) for 4 hours and VEGF or GAPDH mRNA in whole-cell extracts was measured by RT–PCR. VEGF protein level in conditioned medium (CM) was measured by immunoblot analysis.

capillary tube formation was observed after 6 hours of incubation and was almost completed at 24 hours (Fig. 3, B); however, in medium containing 5 μ*M* SCH66336 under hypoxic (mean = 16.4% of control capillary tube formation, 95% CI = 9.4% to 23.5%, *P*<.001) or normoxic (mean = 6.4% of control capillary tube formation, 95% CI = 3.0% to 9.7%, *P*<.001) conditions, HUVECs were statistically significantly less able to differentiate into capillary tube-like structures. For the cell proliferation assay, HUVECs were treated with 5 μ*M* SCH66336 for 3 days under hypoxic or normoxic conditions, and cell proliferation was assessed. Proliferation of SCH66336-treated cells was statistically significantly lower under hypoxic (1.0 μ*M* SCH66336, 83.2%, 95% CI = 80.3% to 86.1%, *P*<.001; 5 μ*M* SCH66336, 66.3%, 95% CI = 63.5% to 69.1%, *P*<.001) and normoxic (1.0 μ*M* SCH66336, 69.6%, 95% CI = 65.8% to 73.4%, *P*<.001; 5 μ*M* SCH66336, 52.7%, 95% CI = 50.2% to 55.2%, *P*<.001) conditions than that of untreated cells (Fig. 3, C). These data suggest that SCH66336 acts directly on endothelial cells to inhibit the angiogenic-associated processes of tube formation and cell proliferation.

Downloaded from jnci.oxfordjournals.org at M D Anderson Hospital on October 8, 2010

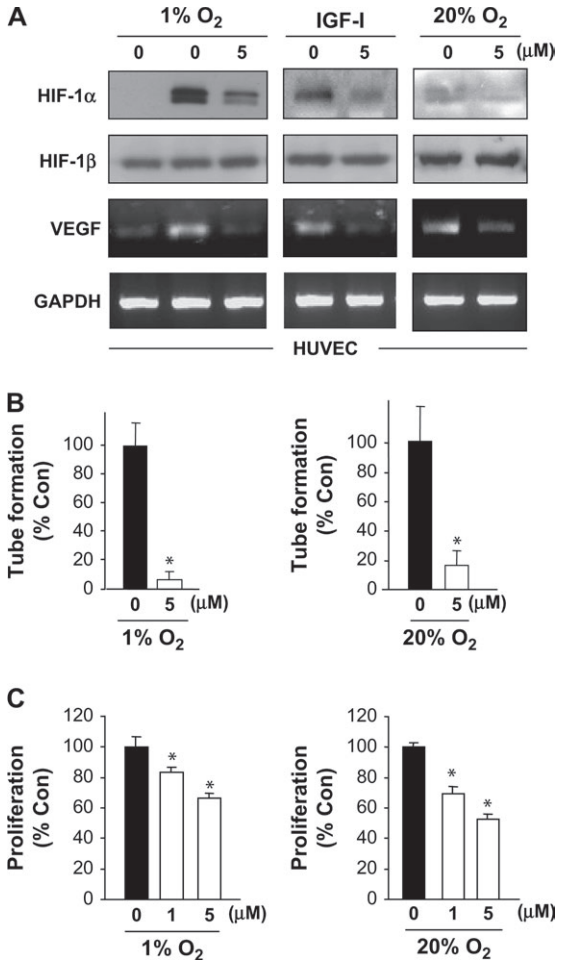


Fig. 3. SCH66336 treatment of human umbilical vein endothelial cells (HUVECs) and hypoxia-inducible factor 1 α (HIF-1α) and vascular endothelial cell growth factor (VEGF) expression, tube formation, and proliferation. **A**) Expression of HIF-1α or HIF-1β. HUVECs were treated continuously with 5 μ*M* SCH66336 in complete medium for 3 days or pretreated with 5 μ*M* SCH66336 for 2 days in complete medium and 1 day in serum-free medium; serum-starved cells were then exposed to 1% O_2 or IGF-I (100 ng/mL) for 4 hours. Whole-cell extracts and total RNA were prepared and subjected to immunoblot assays and RT-RCR, respectively. GAPDH was used as the loading control. **B**) Capillary tube formation. HUVECs (5×10^4 cells) untreated or treated with 5 μ*M* SCH66336 for 1 day under hypoxic (1% O_2) or normoxic (20% O_2) conditions were seeded onto Matrigel-coated 12-well plates. After 6 hours, images of capillary tube formation were captured, and tube formation was scored in one ×4 microscopic field, with one tube designated as a three-branch-point event. Data are the mean percentage 95% confidence interval (CI) of samples in triplicate. Two independent experiments showed similar results. *, *P*<.001, compared with control. **C**) Cell proliferation. HUVECs were cultured in complete medium containing indicated concentrations of SCH66336 in hypoxic conditions (1% O_2) or in normoxic conditions (20% O_2) for 3 days. Cell proliferation was analyzed by the 3-(4,5-dimethylthiazol-2-yl)-2,5-diphenyltetrazolium bromide (MTT) assay. Results are expressed as the mean percentage 95% CI. Independent experiments were repeated three times, and each value is the mean of eight samples. **Error bars** = 95% confidence intervals. *, *P*<.001, compared with negative control. All statistical tests were two-sided.

SCH66336 and Angiogenic Activities in HNSCC cells

To determine whether SCH66336 inhibits HIF-1α protein and VEGF expression in vivo and whether inhibition of these proteins affects tumor angiogenesis and tumor growth in vivo, we established HNSCC orthotopic tongue tumors in nude mice and treated the mice with SCH66336. Three weeks of oral treatment with SCH66336 (40 mg/kg) statistically significantly suppressed tongue tumor growth compared with untreated tumors (*P* = .02). On day 28 of cell injection, the average tumor volume among untreated control mice had increased to 336.4% of the pretreatment volume, whereas that among SCH66336-treated mice was 123.8% of the pretreatment volume (difference in means = 212.6, 95% CI for difference = 150.7% to 274.4%; *P* = .02) (Fig. 4, A, left panel). In contrast, the average body weight of SCH66336-treated mice was not reduced during the treatment (Fig. 4, A, middle panel), indicating that side effects of SCH66336 are minimal.

We next evaluated whether SCH66336 treatment would alter angiogenesis and HIF-1α and VEGF expression in HNSCC tumors in nude mice. SCH66336 treatment statistically significantly decreased tumor vascularization (*P* = .02), as reflected by microvessel densities that was measured with anti-CD31 staining in tongue tumor tissue sections from control and SCH6636-treated nude mice (Fig. 4, A, right panel, and 4, B). Decreased levels of HIF-1α and VEGF were detected in SCH66336-treated tongue tumor tissue, compared with levels in untreated control mice, which did not change over time. Consequently, SCH66336 appears to target HIF-1α and VEGF expression in aerodigestive tract cancer tissue.

SCH66336 and IGF-I–induced HIF-1α Protein Synthesis

We next investigated the mechanism through which SCH66336 reduces the expression of HIF-1α. Because HIF-1α protein expression is very weak in normoxic unstimulated cells, we used hypoxic and normoxic IGF-stimulated H1299 cells for these studies. H1299 cells under hypoxic and normoxic IGF-stimulated conditions were treated with SCH66336, and then total RNA was isolated and subjected to RT–PCR. Untreated cells served as the control group. SCH66336 treatment did not measurably alter HIF-1α mRNA levels in the hypoxic and normoxic IGF-stimulated cells (Fig. 5, A), indicating that SCH66336 affects the level of HIF-1α at the posttranscriptional level, possibly by decreasing the rate of degradation and/or increasing the rate of synthesis *(14)*.

To determine which mechanism is used by SCH66336 to mediate a reduction in the level of HIF-1α protein, H1299 cells were incubated with 5 μ*M* SCH66336 for 3 days. These cells were then exposed to hypoxia or IGF-I at 100 ng/mL for 4 hours to induce HIF-1α expression, and cycloheximide was added to a final concentration of 100 μ*M* to block protein synthesis. HIF-1α protein levels were measured before and at various times during cycloheximide treatment. Half-lives of both hypoxia- and IGF-I–induced HIF-1α proteins in the SCH66336-treated cells were statistically significantly deceased compared with those in untreated cells (half-life of hypoxia-induced HIF-1α protein = 180 minutes in untreated H1299 cells and 115 minutes in SCH66336-treated cells, difference = 65 minutes; half-life of IGF-I–induced HIF-1α protein = more than 30 minutes, difference = 150 minutes) (Fig. 5, B). Thus, SCH66336 appears to decrease the stability of HIF-1α protein in H1299 cells.

Because HIF-1α protein is degraded mainly through the ubiquitin–proteasome pathway, we investigated whether SCH66336-induced reduced HIF-1α protein level is dependent on proteasomal degradation by incubating SCH66336-treated H1299 cells with proteasome inhibitors and measuring the level of HIF-1α protein in such cells. Pretreatment for 8 hours with various proteasome inhibitors, including 10 μ*M* MG132 or 10 μ*M* ALLN, prevented the SCH66336-mediated decrease in the level of HIF-1α protein under hypoxic or IGF-I–stimulated conditions (Fig. 5, C). Because the polyubiquitin chain, which serves as a recognition signal for targeting the proteasome *(34)*, is added

Downloaded from jnci.oxfordjournals.org at M D Anderson Hospital on October 8, 2010

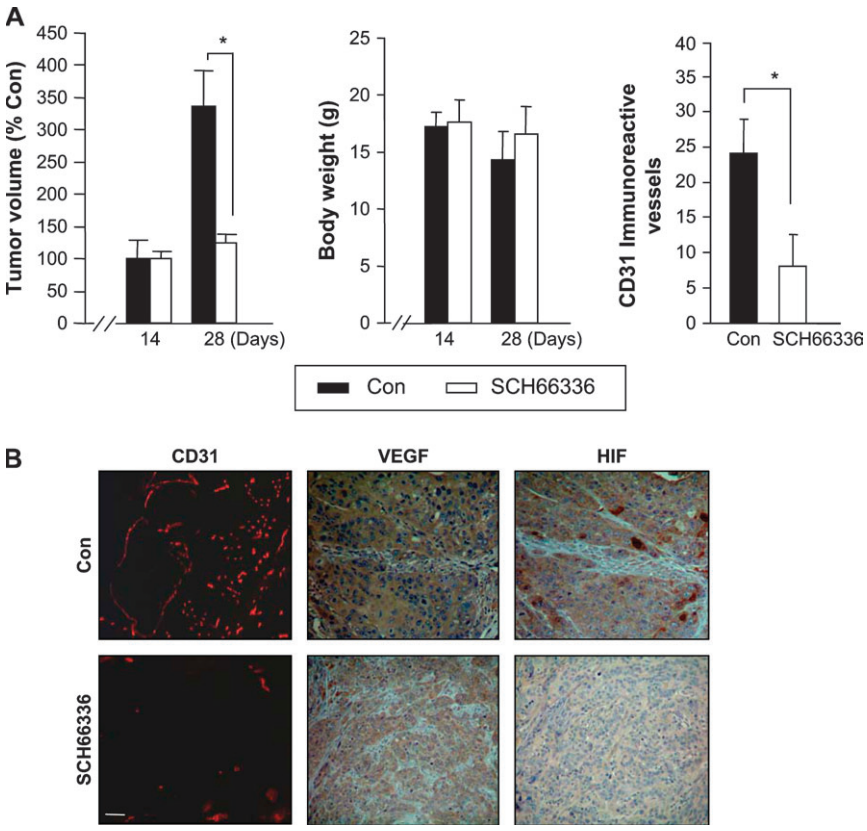


Fig. 4. Inhibition of HNSCC orthotopic tongue tumor growth by SCH66336 treatment. **A**) Effect of SCH66336 on growth of orthotopic tongue tumors. The tongues of nude mice were injected with UMSCC38 cells and then untreated or treated with SCH66336. Changes in mouse tumor volume (left), body weight (middle), and CD31-immunoreactive vessels on day 14 and 28 days (right) are shown. Results are expressed as the mean percent (calculated from five mice) of control at baseline. Tumor volume: control mice, mean = 336.4%, 95% CI = 276.9% to 395.9%; SCH66336-treated mice, mean = 123.8%, 95% CI = 112.1% to 135.6%; *, $P = .02$, compared with control at 28 days. CD31-positive cells: control mice, mean = 23.7 cells, 95% CI = 16.8 to 30.5 cells; SCH66336-treated mice, mean = 8.3 cells, 95% CI = 2.1% to 14.6; *, $P = .03$, compared with control at 28 days. Statistical tests were two-sided. **B**) Immunohistochemical analysis of CD31 (red staining), vascular endothelial cell growth factor (VEGF, brown staining), and HIF-1α (brown staining) was performed in UMSCC38 orthotopic tongue tumor tissues from hydroxyl-propyl-betacyclodexatrin–treated control (Con) and SCH66336-treated nude mice on day 28 after injection of UMSCC38 cells.

to most proteins degraded in the proteasome, we examined polyubiquitination of HIF-1α and found that treatment of cells with a proteasome inhibitor, alone or in combination with SCH66336, resulted in the formation of polyubiquitinated, higher-molecular-weight forms of HIF-1α (Fig. 5, D). Thus, SCH66336 appears to interfere with HIF-1α protein accumulation by modifying a proteasome-dependent degradation pathway under hypoxic and normoxic IGF-stimulated conditions.

Role of VHL in SCH66336-mediated Degradation of HIF-1α

We next investigated the role of VHL in the mechanism of SCH66336-mediated reduced HIF-1α expression in H1299 cells, because HIF-1α is constitutively stabilized in normoxic tumors and in cell lines that are VHL-null or that express a nonfunctional mutant form of VHL *(35)* and because VHL-inactivated tumors are highly vascularized and overproduce VEGF *(36)*. We assessed the levels of VHL in hypoxic or normoxic IGF-stimulated or normoxic unstimulated SCH66336-pretreated H1299 cells and found that the expression of VHL protein in these cells was not changed by treatment with 5 μ*M* SCH66336 (Fig. 6, A). We also examined whether inhibition of VHL expression with a VHL siRNA abrogates the effects of SCH66336 on HIF-1α expression by use of H1299 cells that were untransfected or transfected with a VHL or a control scrambled siRNA. We confirmed that VHL expression decreased in VHL siRNA-transfected H1299 cells (data not shown) and then measured HIF-1α protein levels in cells under various conditions. HIF-1α protein expression was higher in normoxic IGF-stimulated or unstimulated VHL siRNA-transfected H1299 cells than in control scrambled siRNA–transfected cells (Fig. 6, B). However, use of VHL siRNA to inhibit VHL expression did not abrogate the effects of SCH66336 on HIF-1α expression in H1299 cells under any condition tested. Thus, SCH66336 appears to reduce the level of HIF-1α by acting through VHL-independent pathways.

Role of MAPK and PI3K–Akt Pathways in SCH66336-mediated Degradation of HIF-1α

Because PI3K–Akt and p44/42 MAPK pathways have been implicated in synthesis and stabilization of HIF-1α protein [for review, see Semenza *(14)*] and because SCH66336 can inhibit these pathways, we first investigated whether the PI3K–Akt and p44/42 MAPK pathways are involved in SCH66336-mediated decreased HIF-1α expression in H1299 cells. SCH66336 treatment decreased the levels of phosphorylated Akt (Ser-473) and phosphorylated p44/42 MAPK in hypoxic and normoxic IGF-stimulated H1299 cells, whereas the level of phosphorylated Akt was mildly decreased and the level of phosphorylated p44/42

Downloaded from jnci.oxfordjournals.org at M D Anderson Hospital on October 8, 2010

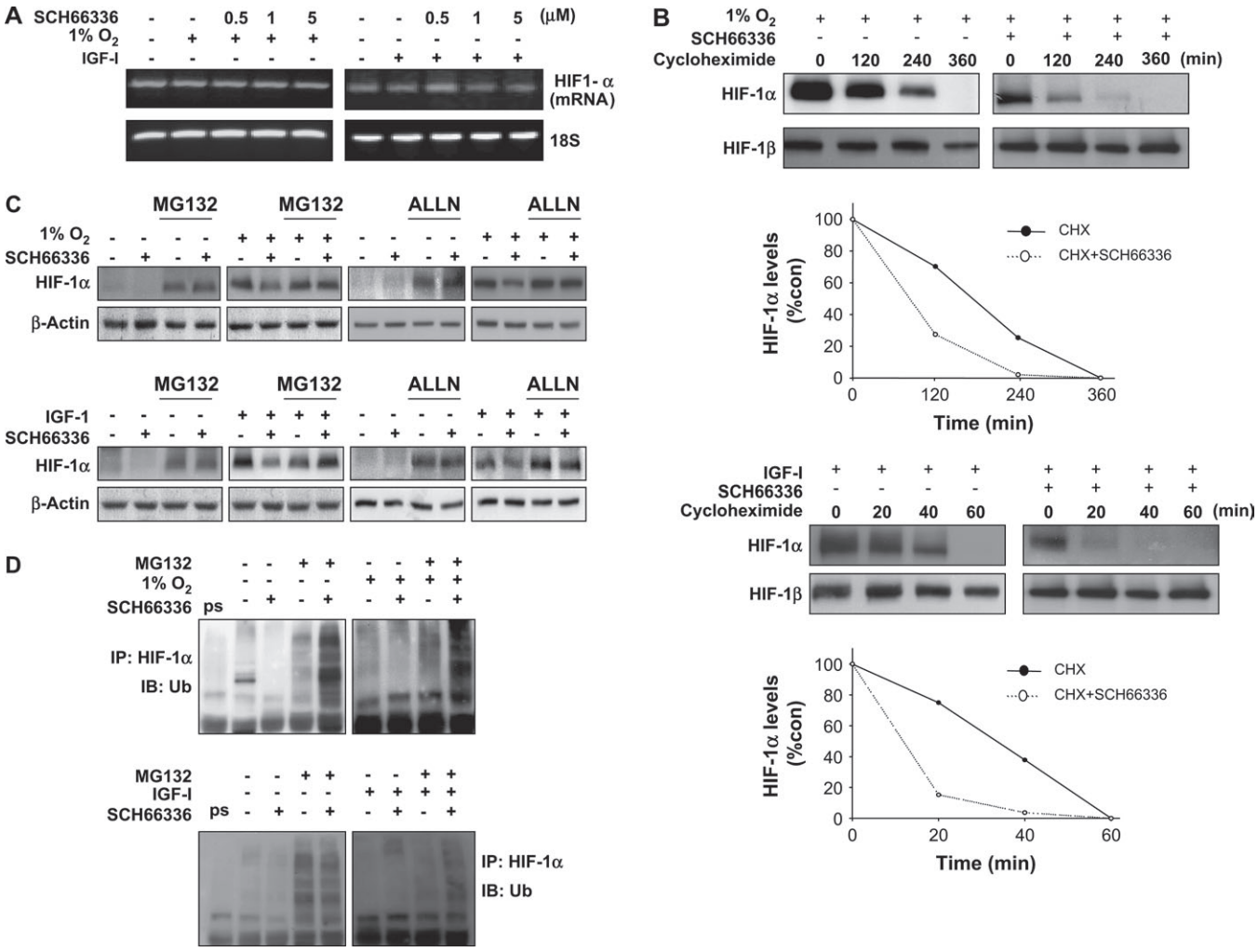


Fig. 5. SCH66336 treatment and the proteasomal degradation of hypoxia- or insulin-like growth factor I (IGF-I)–induced hypoxia-inducible factor 1 α (HIF-1α) protein. **A**) Reverse transcription–polymerase chain reaction of HIF-1α expression. H1299 cells were pretreated with indicated concentrations of SCH66336 in complete medium for 2 days and in serum-free medium for 1 day were exposed to 1% O_2 or IGF-I (100 ng/mL) for 4 hours. Total cellular RNA was isolated, and HIF-1α mRNA expression was analyzed by semiquantitative RT–PCR. 18S ribosomal RNA (rRNA) was used as the loading control. **B**) Half-life of HIF-1α and HIF-1β. H1299 cells that were pretreated with 5 μ*M* SCH66336 in complete medium for 2 days and in serum-free medium for 1 day were exposed to 1% O_2 or IGF-I (100 ng/mL) for 4 hours, and then cycloheximide was added to a final concentration of 100 μ*M*. Cells were harvested as indicated, and whole-cell lysates were subject to immunoblot assay to assess HIF-1α and HIF-1β protein expression. Densitometry was used to measure the autoradiographic HIF-1α signal, and results are shown below blots. Values were normalized to the expression of HIF-1β and expressed as percentages of that at time zero. One representative result from two experiments performed are shown. **C**) HIF-1α expression and inhibition of ubiquitin. H1299 cells were untreated or treated with 5 μ*M* SCH66336 for 3 days and then incubated with or without ubiquitin inhibitors (10 μ*M* MG132 or 50 μ*M* ALLN) for 4 hours in hypoxic (1% O_2) or normoxic (IGF-I at 100 g/mL) conditions. Whole-cell extracts were prepared and subjected to immunoblot assays with antibodies specific for HIF-1α or β-actin. β-Actin was used as the loading control. **D**) HIF-1α ubiquitination. Whole-cell extracts from H1299 cells that were untreated or treated with 5 μ*M* SCH66336 for 3 days and then incubated with or without 10 μ*M* MG132 for 4 hours in hypoxic (1% O_2) or normoxic (IGF-I at 100 ng/mL) conditions. Equal amounts of whole-cell extracts were immunoprecipitated (IP) with an anti-HIF-1α antibody, and immunoprecipitates were washed and subjected to electrophoresis and then to immunoblot (IB) analysis with an anti-ubiquitin (Ub) antibody. Whole-cell extracts from MG132-treated cells in normoxic conditions were immunoprecipitated with preimmune rabbit serum (ps) and included as a negative control.

MAPK was not affected by SCH66336 treatment in normoxic unstimulated H1299 cells (Fig. 6, C). Unphosphorylated Akt and p44/42 MAPK remained unchanged in the cells under every condition examined. Thus, expression of Akt and p44/42 MAPK does not appear to be affected by SCH66336 treatment.

Second, we explored whether the PI3K–Akt and p44/42 MAPK signaling pathways are involved in SCH66336-mediated decreased HIF-1α protein levels. In this experiment, we infected H1299 cells with a control adenoviral vector (EV), an adenovirus expressing HA-MyrAkt (Ad-HA-MyrAkt) to generate constitutively active Akt, or an adenovirus expressing MEK1 (Ad-MEK1) to generate constitutively active MEK1. The induced expression of HA-MyrAkt and MEK1 and the constitutive activity of these proteins were confirmed by western blot analysis with antibodies against HA, MEK1, phosphorylated GSK-3β, an Akt downstream effector, and p44/42MAPK, as previously described *(19)* (Fig. 6, D–G). We next determined whether infection by Ad-HA-MyrAkt or Ad-MEK1 could protect HIF-1α expression from SCH66336-mediated degradation. Basal levels of HIF-1α protein levels were increased by Ad-HA-MyrAkt or Ad-MEK1 infection in hypoxic (Fig. 6, D, F), normoxic IGF-stimulated (Fig. 6, E, G), or normoxic unstimulated (Fig. 6, H) H1299 cells. However, treatment with SCH66336 mediated a decrease in the level of HIF-1α protein in these cells that was not restored when HA-MyrAkt or MEK1 were overexpressed, suggesting that neither the PI3K–Akt pathway nor the MAPK pathway plays a major role in

Downloaded from jnci.oxfordjournals.org at M D Anderson Hospital on October 8, 2010

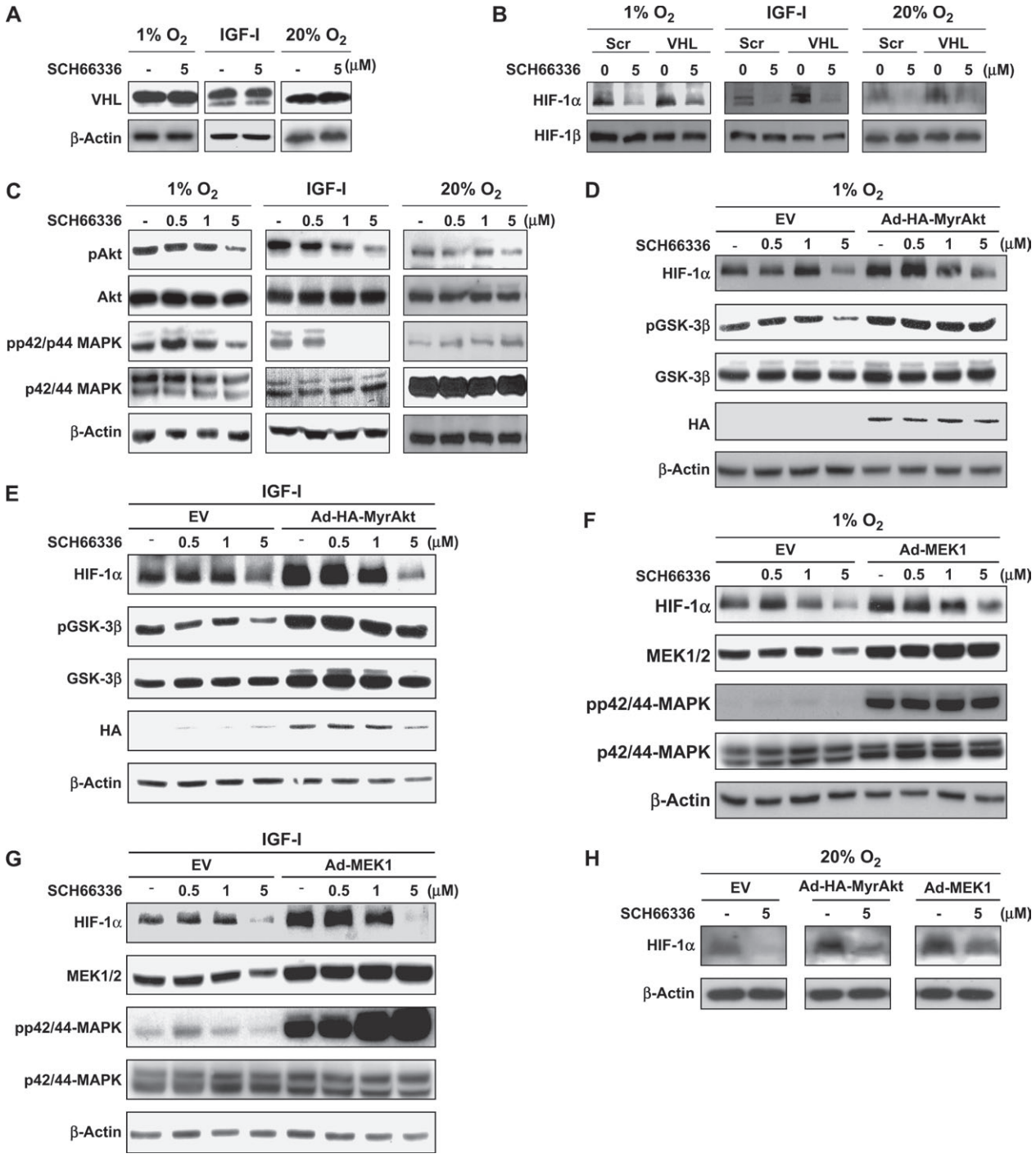


Fig. 6. Association of von Hippel–Lindau tumor suppressor protein (VHL), mitogen-activated protein kinase (MAPK), and phosphatidylinositol 3-kinase (PI3K)–Akt with SCH66336-mediated inhibition of hypoxia-inducible factor 1 α (HIF-1α) protein. **A**) SCH66336 treatment and VHL expression. Whole-cell extracts were prepared from H1299 cells that were untreated or treated with 5 μ*M* SCH66336 for 3 days and then exposed to hypoxia or insulin-like growth factor I (IGF-I) at 100 ng/mL for 4 hours or left unstimulated, as indicated. Whole-cell lysates were collected and subjected to western blot analysis with antibodies against VHL and β-actin. β-Actin was used as the loading control. **B**) VHL-independent regulation of HIF-1α expression by SCH66336. Immunoblot analysis with antibodies against HIF-1α or HIF-1β was performed in H1299 cells that were transfected with Scr or VHL siRNA, incubated with 5 μ*M* SCH66336 in complete medium for 2 days and in serum-free medium for 1 day, and then exposed to 1% O_2 or to IGF-I at 100 ng/mL (normoxic conditions) for 4 hours, or continuously treated after transfection with 5 μ*M* SCH66336 in complete medium for 3 days in normoxic conditions. **C**) Phosphorylation of Akt or p42/44 MAPK and SCH66336 treatment. H1299 cells were incubated alone or with 0.5, 1, or 5 μ*M* SCH66336 in complete medium for 2 days and in serum-free medium for 1 day and then exposed to 1% O_2 or at IGF-I at 100 ng/mL (normoxic conditions) for 4 hours or continuously treated alone or with 0.5, 1, or 5 μ*M* SCH66336 in complete medium for 3 days in normoxic conditions. Whole-cell extracts were subjected to immunoblot assays with antibodies specific for unphosphorylated or phosphorylated p42/p44 MAPK or Akt. **D–H**) MAPK and PI3K–Akt pathways-independent regulation of HIF-1α expression by SCH66336. 1299 cells were infected at 50 plaque-forming units (PFU) per cell with control adenovirus (EV), an adenoviral vector that expresses constitutively active Akt with a hemagglutinin (HA) tag (Ad-HA-MyrAkt) (**D–E**), or with an adenoviral vector that expresses constitutively active MAP kinase kinase (MEK)1 (Ser-217/221 to Glu) (Ad-MEK1) (**F, G**). Infected cells were treated with the indicated concentrations of SCH66336 for 2 days in complete medium and for 1 day in serum-free medium and then exposed to 1% O_2 (**D, F**) or IGF-I at 100 ng/mL (**E, G**) for 4 hours or were incubated in complete medium for 3 days (**H**). Expression of HIF-1α, phosphorylated and unphosphorylated glycogen synthase kinase (pGSK)-3β, HA, MEK1/2, unphosphorylated and phosphorylated p42/p44 MAP kinase, and β-actin were analyzed by immunoblot.

Downloaded from jnci.oxfordjournals.org at M D Anderson Hospital on October 8, 2010

protecting HIF-1α protein from SCH66336-mediated degradation in H1299 cells.

Hsp90 and Destabilization of HIF-1α Induced by SCH66336 Under Normoxic and Hypoxic Conditions

Because the protein chaperone Hsp90 plays a pivotal role in mediating the proper folding and subsequent activation of its many client proteins, including HIF-1α *(37)*, we investigated the role of Hsp90 in HIF-1α protein expression under hypoxic, normoxic IGF-stimulated, or normoxic unstimulated conditions in H1299 cells, by examining whether overexpression of Hsp90 would protect H1299 cells from the SCH66336-induced degradation of HIF-1α. We introduced Hsp90 into H1299 cells by infection with an adenoviral vector containing HA-tagged Hsp90 under the control of the cytomegalovirus promoter (i.e., Ad-HA-Hsp90). Induction of Hsp90 protein expression in the cells infected with Ad-HA-Hsp90 was confirmed by the appearance of the HA band on a western blot probed with an anti-HA antibody (Fig. 7, A). Under hypoxic or normoxic IGF-stimulated conditions, cells infected with Ad-HA-Hsp90 were completely rescued from the HIF-1α–inhibiting effect of SCH66336, unlike cells infected with the control vector (Fig. 7, A). However, the SCH66336-mediated decrease in HIF-1α protein level was not restored by overexpression of Hsp90 in normoxic unstimulated cells. Thus, Hsp90 activity appears to be required for the accumulation of HIF-1α protein induced by hypoxia or IGF-I, but SCH66336 appears to modify the constitutive expression of HIF-1α protein under normoxic conditions through an Hsp90-independent pathway.

We next investigated whether SCH66336 treatment was associated with Hsp90 expression in hypoxic and normoxic IGF-stimulated H1299 cells and found that SCH66336 treatment did not change total Hsp90 protein expression in these cells (Fig. 7, B). Because HIF-1α interacts with Hsp90 *(38)* and because pharmacologic disruption of the association between HIF-1α and Hsp90 promotes ubiquitination and proteasome-mediated degradation of HIF-1α *(15)*, we explored whether SCH66336 affected this interaction in H1299 cells. We carried out coimmunoprecipitation assays with anti–HIF-1α antibody and protein extracts of H1299 cells that had been exposed to hypoxia or IGF-I (100 ng/mL) for 4 hours and treated with 5 μ*M* SCH66336 for various times. Coimmunoprecipitated proteins were resolved on a polyacrylamide gel, and Hsp90 protein was detected by western blotting with an anti-Hsp90 antibody. The interaction between Hsp90 and HIF-1α was detected in cells treated under hypoxic or with IGF-I (Fig. 7, C), but treatment of hypoxic and normoxic IGF-stimulated H1299 cells with SCH66336 resulted in decreased levels of HIF-1α and Hsp90 proteins. Thus, SCH66336 appears to inhibit the function of Hsp90 as a chaperone protein and so inhibit the interaction between Hsp90 and HIF-1α.

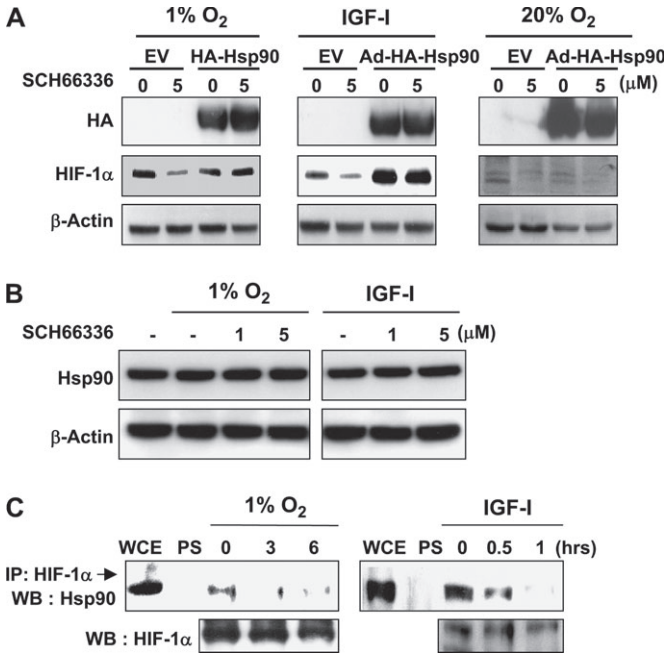


Fig. 7. SCH66336 treatment and heat shock protein 90 (Hsp90)–mediated stabilization of hypoxia-inducible factor 1 α (HIF-1α). **A**) Hsp90 and the level of HIF-1α protein. H1299 cells were infected with an adenovirus carrying the gene for Hsp90 (Ad-Hsp90) or an empty control adenovirus (EV) and the levels of HIF-1α protein were measured. After infection with EV or Ad-Hsp90-HA (50 plaque-forming units per cell), H1299 cells were untreated or treated with 5 μ*M* SCH66336 for 3 days. After exposure to 1% O_2 or insulin-like growth factor I (IGF-I) at 100 ng/mL for 4 hours, the expression levels of hemagglutinin (HA), HIF-1α, and β-actin were assessed by immunoblot analysis. **B**) Effects of SCH66336 on Hsp90 expression. Cells were pretreated for 3 days with 1 or 5 μ*M* SCH66336 and then exposed to 1% O_2 or IGF-I (100 ng/mL) for 4 hours. Whole-cell extracts were prepared and subjected to immunoblot assays with antibodies specific for Hsp90 and β-actin, as a loading control. **C**) SCH66336 and the interaction between HIF-1α and Hsp90 in H1299 cells. H1299 cells were exposed to 1% O_2 or IGF-I (100 ng/mL) for 4 hours and then treated with 5 μ*M* SCH66336 for the indicated periods. Cells were harvested, and whole-cell extracts (WCEs) were prepared and immunoprecipitated (IP) with an anti–HIF-1α antibody. Hsp90 in immunoprecipitates was assessed by western blot (WB) analysis with an anti-Hsp90 antibody. Whole-cell extracts from IGF-I–treated cells under normoxic conditions were immunoprecipitated with preimmune rabbit serum (PS) and included as a negative control. The position of HIF-1α on the western blot was confirmed by use of whole-cell extracts without immunoprecipitation. The same samples were used for western blot analysis of HIF-1α.

Discussion

In this article, we have demonstrated, to our knowledge for the first time, that the farnesyltransferase inhibitor SCH66336 has antiangiogenic activity in aerodigestive tract cancers, including NSCLC and HNSCC, by inhibiting the interaction between HIF-1α and Hsp90, resulting in the proteasomal degradation of HIF-1α and decreased production of VEGF. We have also demonstrated that treatment with the farnesyltransferase inhibitor SCH66336, which inhibits PI3K–Akt *(18)* either alone or in combination with other apoptotic agents, caused tumor regression in mice bearing human NSCLC xenografts *(16)* or HNSCC orthotopic tongue tumors; however, the mechanism of action of SCH66336 is still unresolved. In this study, we showed that 1) SCH66336 reduces HIF-1α protein expression and, consequently, inhibits VEGF expression in hypoxic, normoxic IGF-stimulated, and normoxic unstimulated H1299 cells; 2) SCH66336 inhibits normoxic IGF-induced or hypoxia-stimulated HIF-1α protein expression via ubiquitination and a proteasome-mediated degradation pathway; 3) degradation of HIF-1α protein by SCH66336 is independent of VHL and PI3K–Akt and MAPK pathways both in normoxic and hypoxic conditions; and 4) Hsp90 associates with normoxic IGF-induced or hypoxia-accumulated HIF-1α protein, and SCH66336 inhibits this interaction.

Angiogenesis has a critical role in primary tumor growth and metastasis *(39,40)*. A principal mediator of tumor angiogenesis is VEGF, and a major transcriptional activator of the VEGF gene is

Downloaded from jnci.oxfordjournals.org at M D Anderson Hospital on October 8, 2010

HIF-1α *(9)*. An increasing body of evidence indicates that oncogenes, growth factors, and hypoxia regulate VEGF expression by elevating the HIF-1α translation rate and stability via activation of MAPK or PI3K–Akt pathways *(41,42)*. Moreover, Hsp90 associates with HIF-1α and increases its stability and function *(14,15)*. Consequently, agents that block PI3K–Akt and MAPK signaling pathways and/or Hsp90 function may be candidates to inhibit tumor angiogenesis via decreasing HIF-1α and VEGF expression.

The antiangiogenic actions of SCH66336 in aerodigestive tract cancers could have been the result of blocking farnesylation of RAS or inducing geranylgeranylation of RhoB *(43)*, but H1299 *(16,44,45)* and UMSCC38 cells used in this study have no ras mutations. In addition, antiangiogenic activities of SCH66336 were unchanged when H-Ras or RhoB expression was knocked down by transfection with H-Ras or RhoB siRNA (unpublished data), indicating the presence of other as yet unidentified targeted proteins.

The farnesyltransferase inhibitor SCH66336 decreased the half-life of the HIF-1α protein by inducing ubiquitin-mediated protein degradation, resulting in the decreased expression of HIF-1α and VEGF in NSCLC and HNSCC cell lines and in HUVECs. Given the importance of HIF-1α and VEGF to survival of endothelial cells has recently been demonstrated *(46,47)*, the SCH66336-mediated loss of HIF-1α by in these cells may disrupt HIF-1α–driven VEGF-induced autocrine and paracrine loops, inhibiting endothelial cell proliferation and suppressing tumor angiogenesis.

We further investigated the mechanism of SCH66336-mediated posttranslational degradation of HIF-1α. We first hypothesized that SCH66336-mediated HIF-1α degradation is caused, at least in part, by decreased MAPK and PI3K–Akt activities because 1) MAPK and PI3K–Akt pathways have critical roles in HIF-1α expression, 2) SCH66336 inhibited activation of MAPK and Akt in hypoxic and normoxic IGF-stimulated H1299 cells, and 3) expression of HIF-1α was increased in H1299 cells by constitutive activation of MAPK and Akt under both hypoxic and normoxic conditions. Overexpression of a constitutively active Akt or a constitutively active MEK1 failed, however, to overcome the SCH66336-mediated decrease in the level of HIF-1α protein, indicating that the action of SCH66336 on HIF-1α may be independent of its inhibitory effects on PI3K–Akt and MAPK pathways. We also found that VHL, which has an important role in ubiquitin-mediated degradation of HIF-1α *(35)*, is not implicated in the SCH66336-mediated decrease in HIF-1β protein level. Therefore, SCH66336 appears to affect the level of HIF-1α through mechanisms other than inactivation of MAPK, PI3K–Akt, or VHL.

Because Hsp90 binds to HIF-1α and prevents its ubiquitination and proteasome-mediated degradation, independently of both oxygen concentration and VHL *(15)*, Hsp90 was another candidate target of farnesyltransferase inhibitor function. Geldanomycin, which specifically binds in the amino-terminal ATP-binding site of Hsp90 and inhibits Hsp90-dependent ATPase activity, induces destabilization and degradation of HIF-1α *(15,48)*. We found that overexpression of Hsp90 by infection by an adenoviral vector completely blocked the SCH66336-mediated decrease in HIF-1α protein level in hypoxic and normoxic IGF-stimulated H1299 cells and that SCH66336 induced dissociation of HIF-1α from Hsp90 before HIF-1α protein levels decreased in these cells. Therefore, HIF-1α protein is probably protected by Hsp90 under hypoxic conditions. In addition, under normoxic conditions, most growth factor–induced HIF-1α is changed to a hydroxylated form, binds to VHL, and is degraded by the ubiquitin-mediated proteasome. The HIF-1α that remains bound to Hsp90, and is thus protected, could function as a transcription factor for VEGF (Fig. 8). Thus, Hsp90 appears to be required to chaperone growth factor- and hypoxia-induced HIF-1α protein under normoxic or hypoxic conditions. The role of Hsp90 in maintaining HIF-1α stability has been documented, insofar as Hsp90 inhibitors cause ubiquitination of HIF-1α, targeting the proteasome, and its degradation *(15,49–52)*. Therefore, SCH66336-mediated blockade of the interaction between Hsp90 and HIF-1α may be quite important in decreasing HIF-1α expression and VEGF gene transcription in normoxic IGF-induced and hypoxic cells.

Our results also indicate that novel oxygen-independent E3 ubiquitin ligases, which catalyze the ubiquitination of a variety of protein substrates for targeted degradation via the 26S proteasome *(53)*, may be active under hypoxic conditions. We are currently screening several candidate E3 enzymes, such as mdm2 and Hsp90/Hsp70-binding ubiquitin ligase CHIP (carboxyl terminus of Hsc70-interacting protein) *(54,55)*, to identify the oxygen-independent ubiquitin ligase responsible for SCH66336-induced ubiquitination of HIF-1α. It is of interest

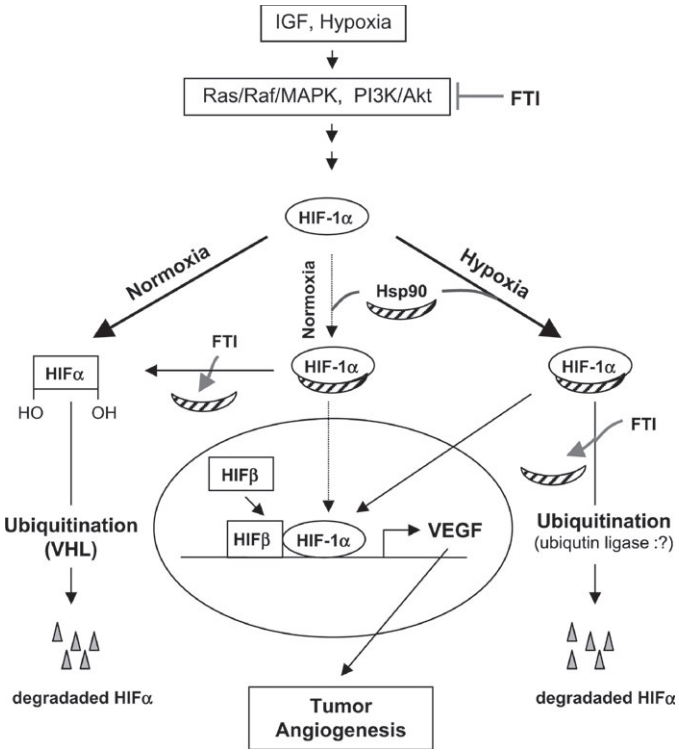


Fig. 8. Schematic representation of the cell signaling events leading to ubiquitin-mediated degradation of hypoxia-inducible factor 1 α (HIF-1α) and inhibition of vascular endothelial cell growth factor (VEGF) protein expression by SCH66336 in aerodigestive tract cancer cells. Under normoxic conditions, a major portion of HIF-1α becomes hydroxylated (–OH) by proline hydroxylase, binds to von Hippel–Lindau tumor suppressor protein (VHL), and then is subjected to ubiquitin-mediated proteasome degradation. A minor portion of HIF-1α, which is stabilized by binding to heat shock protein 90 (Hsp90), still translocalizes to the nucleus and combines with HIF-1β to form an active transcription factor. This heterodimer binds to the VEGF promoter and activates VEGF expression and secretion, indicating that angiogenesis can be stimulated in normoxic conditions. SCH66336 (indicated as farnesyltransferase inhibitor [FTI]) also inhibits the interaction between HIF-1α and Hsp90 in hypoxic conditions and induces ubiquitin-mediated proteasome degradation, which results in the decreased VEGF expression and inhibition of tumor angiogenesis. IGF = insulin-like growth factor; MAPK = mitogen-activated protein kinase; PI3K = phosphatidylinositol 3-kinase.

Downloaded from jnci.oxfordjournals.org at M D Anderson Hospital on October 8, 2010

that SCH66336-induced decreases in expression of the HIF-1α protein in normoxic conditions were not restored by overexpression of Hsp90, which may indicate that the effect of SCH66336 on HIF-1α expression could be mediated through Hsp90-independent pathways rather than a mechanism involving the direct interaction between HIF-1α and Hsp90. Our results, however, support a substantial role for Hsp90 in the regulation of HIF-1α and VEGF expression by SCH66336.

We found that basal HIF-1α expression was stimulated in a cell type–specific manner. Under hypoxic conditions, H1299 cells expressed higher levels of HIF-1α than UMSCC 38 cells, whereas under normoxic, IGF-I–stimulated conditions, UMSCC38 cells expressed higher levels of HIF-1α than H1299 cells, suggesting that differences in genetic background of cells contribute to the variable HIF-1α and VEGF expression. Moreover, levels of HIF-1α were not completely associated with VEGF production by cancer cells, and the level of HIF-1α alone cannot account for VEGF expression. In addition, the association between HIF-1α expression and cancer cells' stimulating effects on HUVEC proliferation was not strong. These collective findings indicated that regulation of HIF-1α may not be sufficient to explain antiangiogenic activities of SCH66336 and that the drug can influence other pathways involved in the angiogenic activities of cancer cells.

Overexpression of HIF-1α protein has been demonstrated in a variety of human cancers including aerodigestive cancers, in which HIF-1α protein overexpression is associated with poor prognosis *(19,56–61)*. Disruption of HIF-1α transcriptional activity has shown therapeutic effects in xenograft models of colon and breast cancers *(8)*. SCH66336 suppressed HIF-1α protein levels at a concentration less than 5 μ*M*, which is considerably below that achievable in vivo (about 8 μ*M*) in mice given a single oral dose of SCH66336 at 25 mg/kg *(62)*. Thus, these results provide an important new rationale for the use of farnesyltransferase inhibitors as an inhibitor of tumor angiogenesis in aerodigestive tract cancers, which depends in part on HIF-1 overexpression for tumor angiogenesis. Because farnesyltransferase inhibitors are not specific for HIF-1α, their inhibition of HIF-1α and reduction in VEGF levels could be circumstantial, and additional inhibitory pathways could be involved. Further investigations into the role of other VEGF-inducing transcription factors in HIF-1α regulation by SCH66336 *(9)* are required.

References

(1) Carmeliet P, Dor Y, Herbert JM, Fukumura D, Brusselmans K, Dewerchin M, et al. Role of HIF-1alpha in hypoxia-mediated apoptosis, cell proliferation and tumour angiogenesis. Nature 1998;394:485–90.

(2) Coello MC, Luketich JD, Litle VR, Godfrey TE. Prognostic significance of micrometastasis in non-small-cell lung cancer. Clin Lung Cancer 2004;5:214–25.

(3) Zetter BR. Angiogenesis and tumor metastasis. Annu Rev Med 1998;49: 407–24.

(4) Ferrara N. VEGF and the quest for tumour angiogenesis factors. Nat Rev Cancer 2002;2:795–803.

(5) Rak J, Yu JL, Klement G, Kerbel RS. Oncogenes and angiogenesis: signaling three-dimensional tumor growth. J Investig Dermatol Symp Proc 2000;5:24–33.

(6) Jiang BH, Jiang G, Zheng JZ, Lu Z, Hunter T, Vogt PK. Phosphatidylinositol 3-kinase signaling controls levels of hypoxia-inducible factor 1. Cell Growth Differ 2001;12:363–9.

(7) Fukuda R, Hirota K, Fan F, Jung YD, Ellis LM, Semenza GL. Insulin-like growth factor 1 induces hypoxia-inducible factor 1-mediated vascular endothelial growth factor expression, which is dependent on MAP kinase and phosphatidylinositol 3-kinase signaling in colon cancer cells. J Biol Chem 2002;277:38205–11.

(8) Jiang BH, Rue E, Wang GL, Roe R, Semenza GL. Dimerization, DNA binding, and transactivation properties of hypoxia-inducible factor 1. J Biol Chem 1996;271:17771–8.

(9) Harris AL. Hypoxia—a key regulatory factor in tumour growth. Nat Rev Cancer 2002;2:38–47.

(10) Jaakkola P, Mole DR, Tian YM, Wilson MI, Gielbert J, Gaskell SJ, et al. Targeting of HIF-alpha to the von Hippel-Lindau ubiquitylation complex by O2-regulated prolyl hydroxylation. Science 2001;292:468–72.

(11) Ivan M, Kondo K, Yang H, Kim W, Valiando J, Ohh M, et al. HIFalpha targeted for VHL-mediated destruction by proline hydroxylation: implications for O2 sensing. Science 2001;292:464–8.

(12) Zhong H, Chiles K, Feldser D, Laughner E, Hanrahan C, Georgescu MM, et al. Modulation of hypoxia-inducible factor 1alpha expression by the epidermal growth factor/phosphatidylinositol 3-kinase/PTEN/AKT/FRAP pathway in human prostate cancer cells: implications for tumor angiogenesis and therapeutics. Cancer Res 2000;60:1541–5.

(13) Treins C, Giorgetti-Peraldi S, Murdaca J, Semenza GL, Van Obberghen E. Insulin stimulates hypoxia-inducible factor 1 through a phosphatidylinositol 3-kinase/target of rapamycin-dependent signaling pathway. J Biol Chem 2002;277:27975–81.

(14) Semenza GL. Targeting HIF-1 for cancer therapy. Nat Rev Cancer 2003;3:721–32.

(15) Isaacs JS, Jung YJ, Mimnaugh EG, Martinez A, Cuttitta F, Neckers LM. Hsp90 regulates a von Hippel Lindau-independent hypoxia-inducible factor-1 alpha-degradative pathway. J Biol Chem 2002;277:29936–44.

(16) Lee HY, Moon H, Chun KH, Chang YS, Hassan K, Ji L, et al. Effects of insulin-like growth factor binding protein-3 and farnesyltransferase inhibitor SCH66336 on Akt expression and apoptosis in non–small-cell lung cancer cells. J Natl Cancer Inst 2004;96:1536–48.

(17) Hanahan D, Weinberg RA. The hallmarks of cancer. Cell 2000;100: 57–70.

(18) Chun KH, Lee HY, Hassan K, Khuri F, Hong WK, Lotan R. Implication of protein kinase B/Akt and Bcl-2/Bcl-XL suppression by the farnesyl transferase inhibitor SCH66336 in apoptosis induction in squamous carcinoma cells. Cancer Res 2003;63:4796–800.

(19) Bueno OF, De Windt LJ, Tymitz KM, Witt SA, Kimball TR, Klevitsky R, et al. The MEK1-ERK1/2 signaling pathway promotes compensated cardiac hypertrophy in transgenic mice. EMBO J 2000;19:6341–50.

(20) Chun KH, Kosmeder JW 2nd, Sun S, Pezzuto JM, Lotan R, Hong WK, et al. Effects of deguelin on the phosphatidylinositol 3-kinase/Akt pathway and apoptosis in premalignant human bronchial epithelial cells. J Natl Cancer Inst 2003;95:291–302.

(21) Fontana J, Fulton D, Chen Y, Fairchild TA, McCabe TJ, Fujita N, et al. Domain mapping studies reveal that the M domain of hsp90 serves as a molecular scaffold to regulate Akt-dependent phosphorylation of endothelial nitric oxide synthase and NO release. Circ Res 2002;90: 866–73.

(22) Gibbs JB, Graham SL, Hartman GD, Koblan KS, Kohl NE, Omer CA, et al. Farnesyltransferase inhibitors versus Ras inhibitors. Curr Opin Chem Biol 1997;1:197–203.

(23) Kim MS, Kwon HJ, Lee YM, Baek JH, Jang JE, Lee SW, et al. Histone deacetylases induce angiogenesis by negative regulation of tumor suppressor genes. Nat Med 2001;7:437–43.

(24) Malinda KM, Nomizu M, Chung M, Delgado M, Kuratomi Y, Yamada Y, et al. Identification of laminin alpha1 and beta1 chain peptides active for endothelial cell adhesion, tube formation, and aortic sprouting. FASEB J 1999;13:53–62.

(25) Reimer CL, Agata N, Tammam JG, Bamberg M, Dickerson WM, Kamphaus GD, et al. Antineoplastic effects of chemotherapeutic agents are potentiated by NM-3, an inhibitor of angiogenesis. Cancer Res 2002;62: 789–95.

(26) Myers JN, Holsinger FC, Jasser SA, Bekele BN, Fidler IJ. An orthotopic nude mouse model of oral tongue squamous cell carcinoma. Clin Cancer Res 2002;8:293–8.

(27) Lee HY, Chun KH, Liu B, Wiehle SA, Cristiano RJ, Hong WK, et al. Insulin-like growth factor binding protein-3 inhibits the growth of non-small cell lung cancer. Cancer Res 2002;62:3530–7.

Downloaded from jnci.oxfordjournals.org at M D Anderson Hospital on October 8, 2010

(28) Wigle JT, Harvey N, Detmar M, Lagutina I, Grosveld G, Gunn MD, et al. An essential role for Prox1 in the induction of the lymphatic endothelial cell phenotype. EMBO J 2002;21:1505–13.
(29) Ponce ML, Nomizu M, Delgado MC, Kuratomi Y, Hoffman MP, Powell S, et al. Identification of endothelial cell binding sites on the laminin gamma 1 chain. Circ Res 1999;84:688–94.
(30) Shepherd FA. Angiogenesis inhibitors in the treatment of lung cancer. Lung Cancer 2001;34(Suppl 3):S81–9.
(31) Rak J, Mitsuhashi Y, Sheehan C, Tamir A, Viloria-Petit A, Filmus J, et al. Oncogenes and tumor angiogenesis: differential modes of vascular endothelial growth factor up-regulation in ras-transformed epithelial cells and fibroblasts. Cancer Res 2000;60:490–8.
(32) Lim JH, Lee ES, You HJ, Lee JW, Park JW, Chun YS. Ras-dependent induction of HIF-1alpha785 via the Raf/MEK/ERK pathway: a novel mechanism of Ras-mediated tumor promotion. Oncogene 2004;23:9427–31.
(33) Tang N, Wang L, Esko J, Giordano FJ, Huang Y, Gerber HP, et al. Loss of HIF-1alpha in endothelial cells disrupts a hypoxia-driven VEGF autocrine loop necessary for tumorigenesis. Cancer Cell 2004;6:485–95.
(34) Ciechanover A. The ubiquitin-proteasome pathway: on protein death and cell life. EMBO J 1998;17:7151–60.
(35) Wiesener MS, Munchenhagen PM, Berger I, Morgan NV, Roigas J, Schwiertz A, et al. Constitutive activation of hypoxia-inducible genes related to overexpression of hypoxia-inducible factor-1alpha in clear cell renal carcinomas. Cancer Res 2001;61:5215–22.
(36) Benjamin LE, Keshet E. Conditional switching of vascular endothelial growth factor (VEGF) expression in tumors: induction of endothelial cell shedding and regression of hemangioblastoma-like vessels by VEGF withdrawal. Proc Natl Acad Sci U S A 1997;94:8761–6.
(37) Caplan AJ. Hsp90's secrets unfold: new insights from structural and functional studies. Trends Cell Biol 1999;9:262–8.
(38) Minet E, Mottet D, Michel G, Roland I, Raes M, Remacle J, et al. Hypoxia-induced activation of HIF-1: role of HIF-1alpha-Hsp90 interaction. FEBS Lett 1999;460:251–6.
(39) Folkman J. Fighting cancer by attacking its blood supply. Sci Am 1996;275:150–4.
(40) Folkman J. Seminars in Medicine of the Beth Israel Hospital, Boston. Clinical applications of research on angiogenesis. N Engl J Med 1995;333:1757–63.
(41) Chan DA, Sutphin PD, Denko NC, Giaccia AJ. Role of prolyl hydroxylation in oncogenically stabilized hypoxia-inducible factor-1alpha. J Biol Chem 2002;277:40112–7.
(42) Laughner E, Taghavi P, Chiles K, Mahon PC, Semenza GL. HER2 (neu) signaling increases the rate of hypoxia-inducible factor 1alpha (HIF-1alpha) synthesis: novel mechanism for HIF-1-mediated vascular endothelial growth factor expression. Mol Cell Biol 2001;21:3995–4004.
(43) Sebti SM, Hamilton AD. Farnesyltransferase and geranylgeranyltransferase I inhibitors and cancer therapy: lessons from mechanism and bench-to-bedside translational studies. Oncogene 2000;19:6584–93.
(44) Chun KH, Lee HY, Hassan K, Khuri F, Hong WK, Lotan R. Implication of protein kinase B/Akt and Bcl-2/Bcl-XL suppression by the farnesyl transferase inhibitor SCH66336 in apoptosis induction in squamous carcinoma cells. Cancer Res 2003;63:4796–800.
(45) Mitsudomi T, Steinberg SM, Oie HK, Mulshine JL, Phelps R, Viallet J, et al. ras gene mutations in non-small cell lung cancers are associated with shortened survival irrespective of treatment intent. Cancer Res 1991;51:4999–5002.
(46) Franklin SL, Ferry RJ Jr, Cohen P. Rapid insulin-like growth factor (IGF)-independent effects of IGF binding protein-3 on endothelial cell survival. J Clin Endocrinol Metab 2003;88:900–7.
(47) Tang N, Wang L, Esko J, Giordano FJ, Huang Y, Gerber HP, et al. Loss of HIF-1alpha in endothelial cells disrupts a hypoxia-driven VEGF autocrine loop necessary for tumorigenesis. Cancer Cell 2004;6:485–95.
(48) Mabjeesh NJ, Post DE, Willard MT, Kaur B, Van Meir EG, Simons JW, et al. Geldanamycin induces degradation of hypoxia-inducible factor 1alpha protein via the proteosome pathway in prostate cancer cells. Cancer Res 2002;62:2478–82.
(49) Suzuki H, Tomida A, Tsuruo T. Dephosphorylated hypoxia-inducible factor 1alpha as a mediator of p53-dependent apoptosis during hypoxia. Oncogene 2001;20:5779–88.
(50) Katschinski DM, Le L, Heinrich D, Wagner KF, Hofer T, Schindler SG, et al. Heat induction of the unphosphorylated form of hypoxia-inducible factor-1alpha is dependent on heat shock protein-90 activity. J Biol Chem 2002;277:9262–7.
(51) Gradin K, McGuire J, Wenger RH, Kvietikova I, Whitelaw ML, Toftgard R, et al. Functional interference between hypoxia and dioxin signal transduction pathways: competition for recruitment of the Arnt transcription factor. Mol Cell Biol 1996;16:5221–31.
(52) Kallio PJ, Okamoto K, O'Brien S, Carrero P, Makino Y, Tanaka H, et al. Signal transduction in hypoxic cells: inducible nuclear translocation and recruitment of the CBP/p300 coactivator by the hypoxia-inducible factor-1alpha. EMBO J 1998;17:6573–86.
(53) Burger AM, Seth AK. The ubiquitin-mediated protein degradation pathway in cancer: therapeutic implications. Eur J Cancer 2004;40:2217–29.
(54) Connell P, Ballinger CA, Jiang J, Wu Y, Thompson LJ, Hohfeld J, et al. The co-chaperone CHIP regulates protein triage decisions mediated by heat-shock proteins. Nat Cell Biol 2001;3:93–6.
(55) Melillo G, Taylor LS, Brooks A, Musso T, Cox GW, Varesio L. Functional requirement of the hypoxia-responsive element in the activation of the inducible nitric oxide synthase promoter by the iron chelator desferrioxamine. J Biol Chem 1997;272:12236–43.
(56) Giatromanolaki A, Koukourakis MI, Sivridis E, Turley H, Talks K, Pezzella F, et al. Relation of hypoxia inducible factor 1 alpha and 2 alpha in operable non-small cell lung cancer to angiogenic/molecular profile of tumours and survival. Br J Cancer 2001;85:881–90.
(57) Schindl M, Schoppmann SF, Samonigg H, Hausmaninger H, Kwasny W, Gnant M, et al. Overexpression of hypoxia-inducible factor 1alpha is associated with an unfavorable prognosis in lymph node-positive breast cancer. Clin Cancer Res 2002;8:1831–7.
(58) Birner P, Schindl M, Obermair A, Plank C, Breitenecker G, Oberhuber G. Overexpression of hypoxia-inducible factor 1alpha is a marker for an unfavorable prognosis in early-stage invasive cervical cancer. Cancer Res 2000;60:4693–6.
(59) Aebersold DM, Burri P, Beer KT, Laissue J, Djonov V, Greiner RH, et al. Expression of hypoxia-inducible factor-1alpha: a novel predictive and prognostic parameter in the radiotherapy of oropharyngeal cancer. Cancer Res 2001;61:2911–6.
(60) Koukourakis MI, Giatromanolaki A, Skarlatos J, Corti L, Blandamura S, Piazza M, et al. Hypoxia inducible factor (HIF-1a and HIF-2a) expression in early esophageal cancer and response to photodynamic therapy and radiotherapy. Cancer Res 2001;61:1830–2.
(61) Kung AL, Wang S, Klco JM, Kaelin WG, Livingston DM. Suppression of tumor growth through disruption of hypoxia-inducible transcription. Nat Med 2000;6:1335–40.
(62) Liu M, Bryant MS, Chen J, Lee S, Yaremko B, Lipari P, et al. Antitumor activity of SCH 66336, an orally bioavailable tricyclic inhibitor of farnesyl protein transferase, in human tumor xenograft models and wap-ras transgenic mice. Cancer Res 1998;58:4947–56.

NOTES

J.-Y. Han and S.H. Oh contributed equally to this work and should be considered joint first authors.

Supported by National Institutes of Health grants R01 CA100816-01 and R01 CA109520-01 (to H.-Y. Lee), American Cancer Society grant RSG-04-082-01-TBE 01 (to H.-Y. Lee), M. D. Anderson Cancer Center Spore Grant in Head and Neck Cancer, P50 CA 97007-01 (to W.K. Hong), U.S. Department of Defense grant DAMD17-01-1-0689 (to W.K. Hong), and NFCR grant LF01-065-1 (to W.K. Hong); W.K. Hong is an American Cancer Society clinical research professor.

Manuscript received October 20, 2004; revised June 28, 2005; accepted July 21, 2005.

Downloaded from jnci.oxfordjournals.org at M D Anderson Hospital on October 8, 2010

ARTICLE

doi:10.1016/j.ymthe.2004.01.007

Persistent Transgene Expression Following Intravenous Administration of a Liposomal Complex: Role of Interleukin-10-Mediated Immune Suppression

Isao Ito,[*] Tomoyuki Saeki,[†] Imran Mohuiddin, Yuji Saito,[†] Cynthia D. Branch, Ara Vaporciyan, Jack A. Roth, and Rajagopal Ramesh[‡]

Department of Thoracic and Cardiovascular Surgery, The University of Texas M. D. Anderson Cancer Center, Houston, TX 77030, USA

[*]*Current address: Department of Surgery, Tokai University School of Medicine, Ooiso Hospital, Kanagawa, Japan.*
[†]*Current address: Department of Surgery, Jikei University School of Medicine, Tokyo, Japan.*

[‡]*To whom correspondence and reprint requests should be addressed at the Department of Thoracic and Cardiovascular Surgery, The University of Texas M. D. Anderson Cancer Center, 1515 Holcombe Boulevard, Box 445, Houston, TX 77030, USA. Fax: (713) 794-4901. E-mail: rramesh@mdanderson.org.*

Studies conducted in non-tumor-bearing, immunocompetent mice have shown that intravenous administration of liposome–DNA complex elicits an inflammatory response that results in a failure to sustain adequate transgene expression. In the present study, however, we investigated the effects of a cationic liposomal DOTAP:cholesterol (DOTAP:Chol)–DNA complex on cytokine production and transgene expression in both experimental lung tumor-bearing (TB) mice and non-tumor-bearing (NTB) syngeneic mice and nude mice. Intravenous injection of DOTAP:Chol–luciferase (*luc*) DNA complex resulted in tumor necrosis factor-α levels that were 50% lower and interleukin-10 levels that were 50–60% higher in TB mice than in NTB mice. Furthermore, a significant increase in luc expression ($P = 0.001$) that persisted for 7 days was observed in TB mice. In contrast, luc expression decreased significantly from day 1 to day 2 in NTB mice. Also, luc expression was two- to threefold higher in TB mice that were given multiple injections of DOTAP:Chol-*luc* complex than in mice who received a single injection. In contrast, luc expression was significantly suppressed following multiple injections in NTB mice ($P = 0.01$). Further analysis revealed IL-10 protein expression by the tumor cells in TB mice. Injection of anti-IL-10 antibody in TB mice resulted in a significant decrease in luc expression ($P = 0.01$) compared with that in mice injected with a control antibody. Based on these findings, we conclude that transgene expression persists in TB mice and is partly mediated by IL-10. Additionally, multiple injections of liposome–DNA complex can increase transgene expression in TB mice. These findings have clinical applications in the treatment of cancer.

Key Words: gene therapy, liposome, IL-10, cancer, cytokines, inflammation, lung, gene expression

INTRODUCTION

The development of efficient nonviral vectors that can deliver therapeutic genes when injected systemically will provide novel therapeutic options for the treatment of disseminated cancers. However, recent studies have demonstrated that liposomal vectors elicit an inflammatory response when injected systemically resulting in toxicity [1–7]. Induction of inflammatory responses due to the presence of immunostimulatory CpG sequences in plasmid DNA has been reported previously [8–12]. Associated with the inflammatory response is the production of proinflammatory cytokines (tumor necrosis factor- (TNF-α), interleukin-1 (IL-1), IL-6), which in turn have been shown to inhibit transgene expression [9,13]. Failure to achieve sustained transgene expression following repeated injections has also been attributed to the production of these proinflammatory cytokines [13]. Furthermore, a 3- to 4-day interval between injections was shown to be necessary to achieve sustained gene expression [14]. This need for injections at intervals has

Copyright © The American Society of Gene Therapy
1525-0016/$30.00

been attributed to the cells' ''refractory'' state [14]. Thus, the inability to increase transgene expression following repeated injections has been a major obstacle in the development of therapeutic applications of liposomes. Likewise, reducing the number of CpG sequences in the plasmid DNA has been shown to reduce the inflammatory response and increase transgene expression [15]. These results, however, were obtained from studies of non-tumor-bearing (NTB), immunocompetent animals.

In contrast to these reports, we recently demonstrated effective gene transfer to experimental lung tumors in mice following intravenous injections of extruded DOTAP:cholesterol (DOTAP:Chol)–DNA:liposome complex [16]. In that study, although animals were treated with repeated injections, the relative effectiveness of multiple treatments was not studied. However, the major difference between the results of our study and those of others is that we conducted experiments in tumor-bearing (TB) animals, while others studied NTB animals. It is therefore possible that the pathophysiological condition of the animal may influence transgene expression following intravenous administration of the liposome:DNA complex.

Several preclinical and clinical studies have demonstrated functional alterations of immune cells (macrophages, neutrophils, and T cells) resulting in immune suppression in lung cancer [17–21]. These alterations have been attributed to several factors, including the production of immunosuppressive factors by tumor cells [22–25] and alterations in the immune cell receptors [26]. On the basis of these reports, we speculated that TB and NTB animals might respond differently to liposome:DNA complexes administered intravenously.

In the present study, we investigated the effects of intravenous administration of DOTAP:Chol–DNA complex on the cytokine profile and transgene expression of lung TB and NTB immunocompetent mice and nude mice.

RESULTS

Cytokine Expression Following Intravenous Injection of DOTAP:Chol–luciferase (*luc*) DNA Complex

Prior to the start of the experiment, we established lung tumors by injecting 1×10^6 UV2237m or A549 cells intravenously via the tail vein into female C3H and nude mice, respectively. Ten to fifteen days after injection of tumor cells, we treated the animals with DOTAP:Chol-*luc* complex. Note that at this time the tumors are well established in the lungs and can be detected histologically (data not shown). Animals receiving no treatment served as controls. In a separate but parallel set of experiments, NTB animals were also untreated or treated with DOTAP:Chol-*luc* complex.

We analyzed serum samples from NTB and lung TB C3H mice injected with DOTAP:Chol-*luc* DNA complex for cytokine levels at regular time intervals. TNF-α, IL-1α, interferon-γ (IFN-γ), and IL-10 were produced by TB and NTB mice, with maximum peak levels observed in both groups at 2 h for TNF-α and at 6 h for IFN-γ (Fig. 1A). We observed maximum levels of IL-10 expression at 12 and 24 h in both groups. However, TNF-α levels were 50% lower in TB mice than in NTB mice. In contrast, IL-10 levels were 50–60% higher in TB mice (Fig. 1A). The expression of cytokines was time dependent over the 24-h postinjection period. IL-1α levels did not differ significantly in animals from the two groups. Cytokine levels except those of IL-1α were not detected in control animals that were not treated, were treated with naked plasmid DNA, or were treated with an empty liposome (data not shown).

To examine whether a similar phenomenon occurred in other tumor models we also determined serum cytokine levels in A549 lung TB nude mice and compared them to NTB nude mice (Fig. 1B). Both TB and NTB nude mice produced TNF-α, IL-1α, IFN-γ, and IL-10. The time courses for production of these cytokines were identical to those observed in C3H mice described above, with maximum production occurring at 2 h for TNF-α and at 6 h for IFN-γ. Similarly, we observed maximum levels of IL-10 expression at 12 and 24 h in TB and NTB mice. However, the levels of the cytokine produced in nude mice differed from the levels produced in C3H mice (Figs. 1A and 1B). Furthermore, TNF-α levels were moderately reduced in TB nude mice compared to NTB mice. The difference in the reduction of TNF-α levels in TB C3H mice and TB nude mice can be attributed to strain difference. However, other possibilities may exist and need additional investigation. In TB C3H mice we observed a significant increase in IL-1α at 12 h compared to NTB mice. This increase in IL-1α levels is not clear and needs additional investigation. These results demonstrate that increased IL-10 is produced in TB mice compared to NTB mice following injection of DOTAP:Chol–DNA complex.

Transgene Expression Persists in Tumor-Bearing Mice Following a Single Intravenous Injection of DOTAP:Chol-*luc* DNA Complex

To determine transgene expression *in vivo*, we injected lung TB and NTB C3H mice intravenously via the tail vein with DOTAP:Chol-*luc* DNA complex and removed their lungs at different times and analyzed them for luc activity. We observed luc expression in both TB and NTB mice, with maximal gene expression occurring 24 h after treatment in both groups (Fig. 2A). However, luc expression in NTB mice had decreased by 48 h after treatment and reached baseline levels by 72 h; luc expression remained at baseline through day 7. In contrast, levels of luc activity remained significantly higher than baseline ($P = 0.01$) in TB animals through

Copyright © The American Society of Gene Therapy

doi:10.1016/j.ymthe.2004.01.007

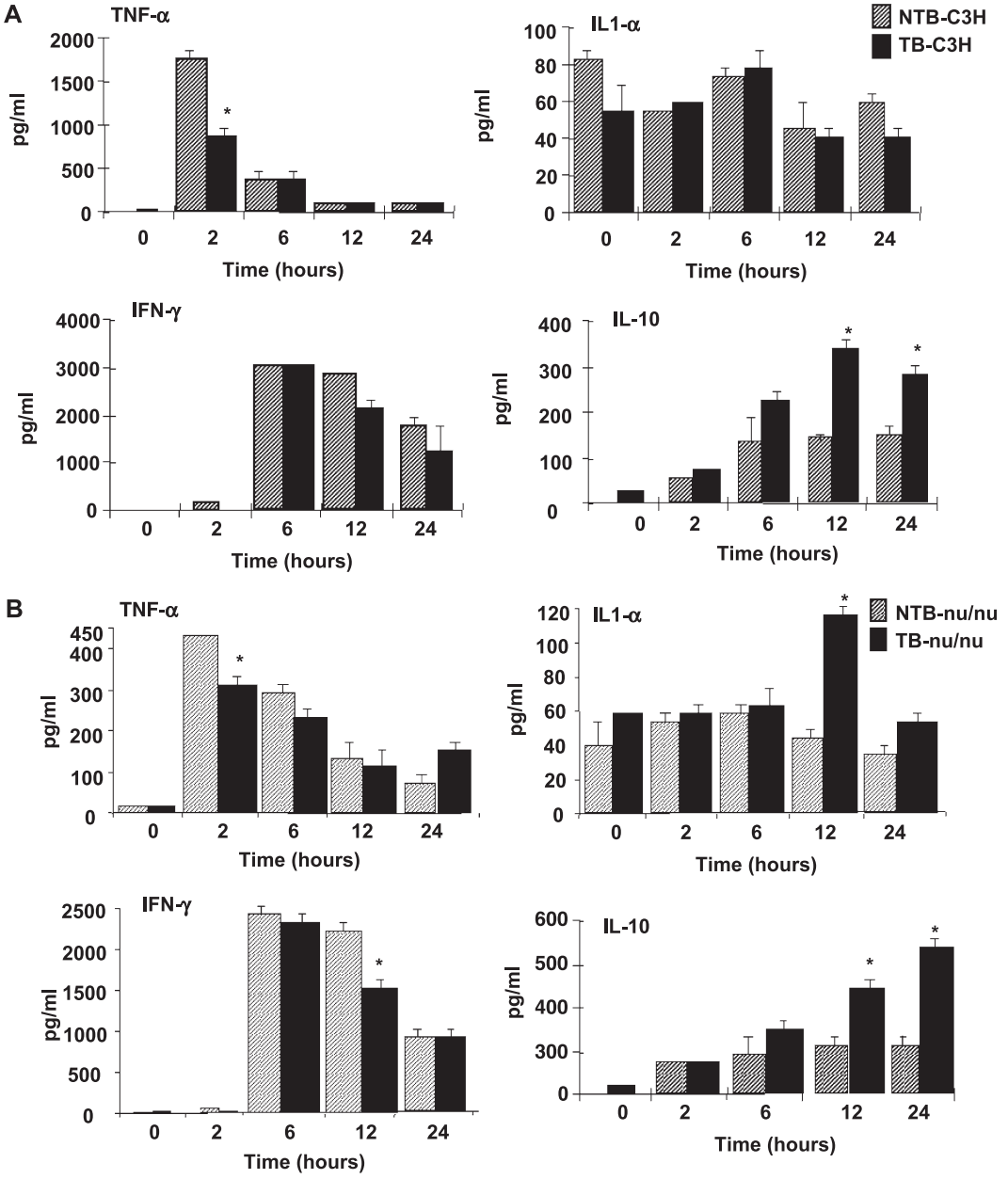


FIG. 1. Cytokine profile following systemic injection of DOTAP:Chol-*luc* DNA complex. Serum was collected from lung TB and NTB mice at 0, 2, 6, 12, and 24 h after injection of DOTAP:Chol-*luc* DNA complex (50 μg) and was assayed for cytokines (TNF-α, IL-1α, IFN-γ, IL-10) using ELISA. Untreated TB and NTB animals served as controls from each group. (A) Cytokine profile in UV2337m TB and NTB mice. (B) Cytokine profile in A549 lung TB and NTB mice. Data represent the average cytokine levels in four animals per group per time point.

day 7. However, a trend in decline (50%) of luc expression was observed on day 7 compared to day 1 in TB animals.

We performed an analysis of transgene expression in A549 lung TB and NTB nude mice. We observed increased luc expression at 24 h in both groups after treatment (Fig. 2B). However, significant levels of luc expression persisted in TB mice until day 7 compared to NTB mice. Although luc expression in NTB mice did not reach baseline levels as observed in C3H mice, luc expression was significantly reduced by day 3 compared to day 1. These results demonstrate that persistent trans-

Copyright © The American Society of Gene Therapy

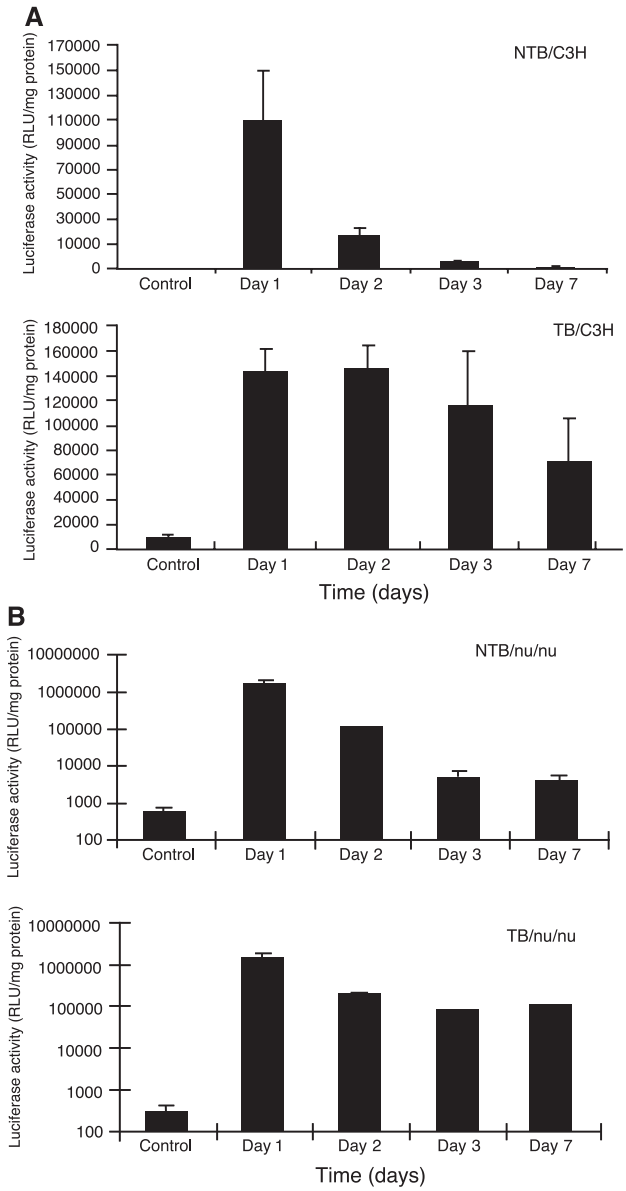


FIG. 2. Persistent transgene expression occurs in TB animals. (A) UV2237M TB and NTB C3H mice and (B) A549 TB and NTB nude mice were injected with DOTAP:Chol-*luc* DNA complex via the tail vein. Their lungs were resected on days 1, 2, 3, and 7 after treatment and analyzed for luc expression. Luc activity is expressed as relative light units (RLU) per milligram of total protein. Each time point represents the average luc activity in four animals. Bars represent standard deviation.

gene expression occurs in TB mice compared to NTB mice.

Repeated Injections of DOTAP:Chol-*luc* DNA Complex Result in Increased Transgene Expression

We next evaluated the effects of repeated injections on transgene expression in both lung TB and NTB C3H mice and nude mice. We injected the animals via the tail vein with the DOTAP:Chol-*luc* DNA complex either one time or daily for 3 consecutive days. We analyzed lungs for luc activity 48 h after injection. In C3H mice luc expression was observed in both TB and NTB mice. In TB C3H mice, however, luc expression was twofold greater ($P = 0.001$) in mice treated three times than in mice treated once (Fig. 3A). In contrast, NTB mice treated three times expressed significantly lower levels of luc than did those treated only once ($P = 0.01$). Similarly, analysis of luc expression in TB nude mice and NTB nude mice demonstrated expression of luc expression (Fig. 3B). TB nude mice that received three treatments demonstrated threefold increase in luc expression compared to mice treated once ($P = 0.001$). In contrast, NTB mice that received three treatments showed decreased luc expression compared to mice receiving a single treatment. Thus, expression of luc in TB mice receiving multiple treatments was higher than in TB mice receiving a single treatment. Furthermore, luc expression in TB mice receiving multiple treatments was higher than in NTB mice that received multiple treatments. These results demonstrate that repeated injections of DOTAP:Chol–DNA complex in TB mice results in increased transgene expression and are in agreement with our previous results [16].

Lung Tumor Cells Express IL-10

To determine whether tumor cells contributed to the production of IL-10, we stained lungs from UV2237m TB and NTB mice for murine IL-10. TB lungs, especially tumor cells, stained intensely for IL-10 (Fig. 4). We also observed staining of infiltrating lymphocytes in the lung tumor sections. In contrast, NTB lung cells showed very little IL-10 expression. We also observed IL-10 protein expression in human lung tumor cell lines and in clinical specimens from patients diagnosed with lung cancer (data not shown). To determine further the levels of IL-10 produced by UV2237m tumor cells, we analyzed cell culture supernatants for IL-10 production by ELISA. The level of IL-10 produced by murine tumor cells was approximately 30 pg/ml (data not shown). These results demonstrate that tumor cells in addition to lymphocytes produce IL-10.

Alveolar Macrophages from Lung TB Mice Are Less Responsive to Stimulation

Since we had observed IL-10 production by lung TB mice, we examined the suppressive effects of IL-10 on alveolar macrophages by macrophage activation assay. We plated alveolar macrophages isolated from lung TB and NTB C3H mice in 96-well plates and stimulated them with phorbol myristic acetate (PMA). We measured stimulation of macrophages by addition of 2′ ,7′ -dicholorofluorescein diacetate. Macrophages from NTB mice showed significantly more activation ($P = 0.001$) than those from TB mice (Fig. 5A). Furthermore, a significant reduction

Copyright © The American Society of Gene Therapy

doi:10.1016/j.ymthe.2004.01.007

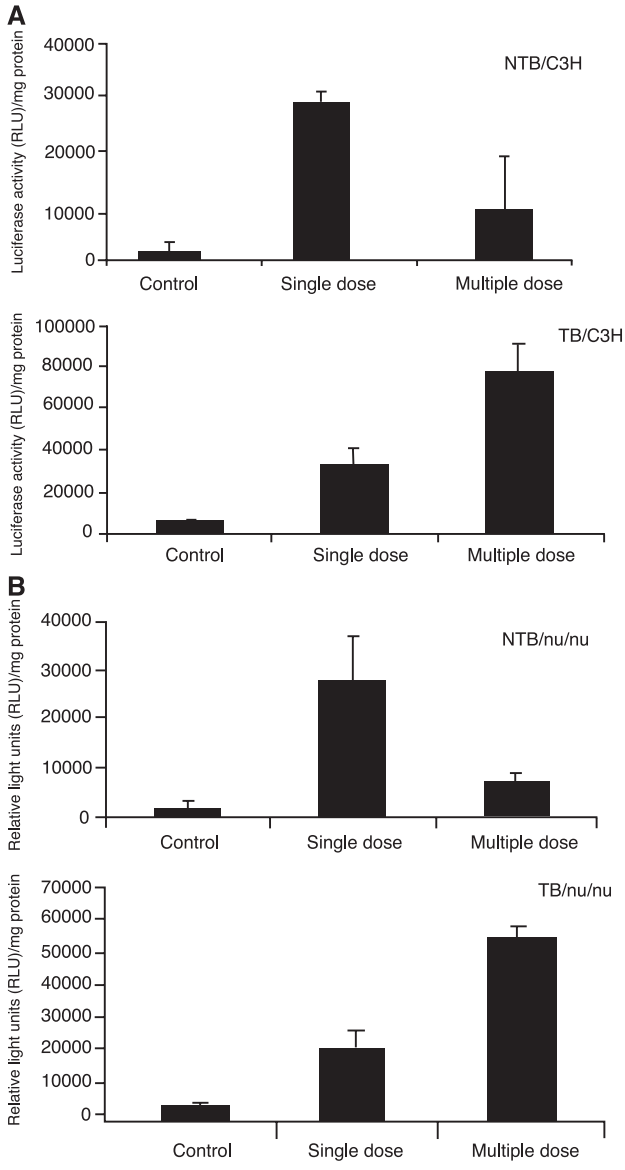


FIG. 3. Multiple treatments resulted in increased transgene expression. TB and NTB C3H or nude mice injected either once or three times with DOTAP:Chol-*luc* DNA complex (50 μg DNA/dose) via a tail vein were assayed for luc activity. (A) A twofold increase in luc activity was observed in TB C3H mice receiving three treatments compared with those receiving one treatment. In contrast, luc activity in NTB C3H mice receiving three treatments was significantly lower that in those receiving one treatment. (B) Luc activity in TB nude mice receiving three treatments showed two- to threefold increase in luc expression compared with those receiving one treatment. In contrast, luc activity in NTB nude mice receiving three treatments was significantly lower than in those receiving one treatment. Luc activity is expressed as RLU per milligram of total protein. Bars represent standard deviation.

($P = 0.01$) in TNF-α production by alveolar macrophages from TB mice was observed when the macrophages were treated with LPS (Fig. 5B). In contrast, macrophages from NTB animals produced higher levels of TNF-α when treated with LPS.

Neutralization of IL-10 in TB Animals Results in Decreased Transgene Expression

To determine the effects of IL-10 on transgene expression *in vivo,* we injected TB animals with a mouse IL-10 neutralizing antibody 24 h prior to injection of DOTAP:-Chol-*luc* DNA complex. Analysis of the lungs 48 h after liposome–DNA complex injection showed a significant reduction in luc expression ($P \leq 0.01$) compared with that in TB animals that were not treated with the neutralizing IL-10 antibody (DOTAP:Chol-*luc* complex

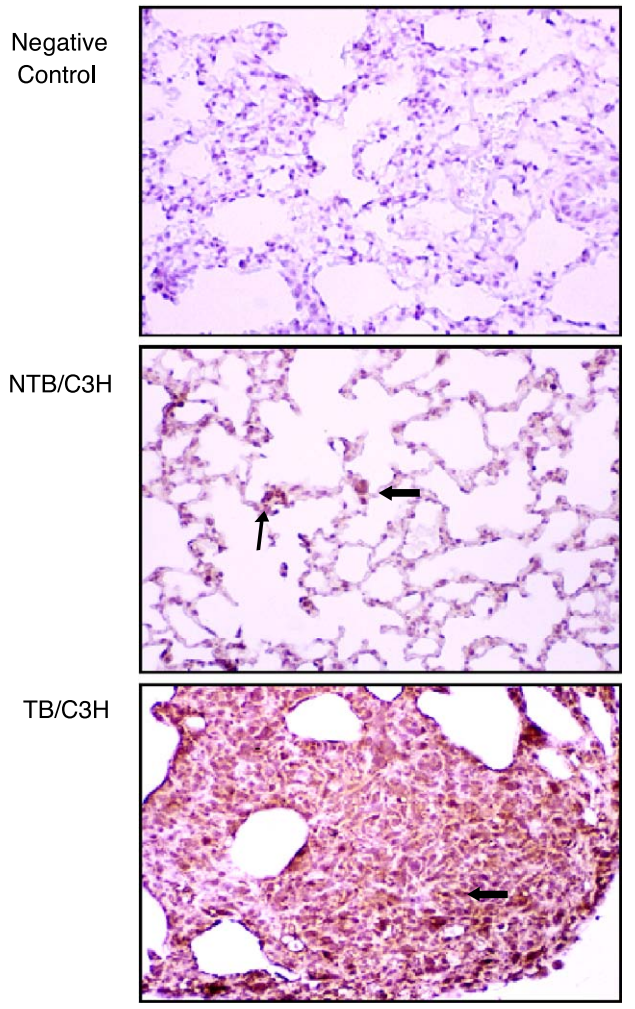


FIG. 4. UV2237M tumor cells produce IL-10. UV2237m TB and NTB lung tissue sections were immunohistochemically stained for mouse IL-10. IL-10 was detected in lung tissue sections as indicated by the intense brown cytoplasmic staining. Staining for IL-10 in NTB lung tissue sections was weak. Tissue sections stained only with secondary antibody served as negative controls. Arrows indicate cells staining positive for IL-10.

Copyright © The American Society of Gene Therapy

only) and in animals that were treated with a control isotypic antibody (Fig. 6). Luc expression was also significantly lower in animals that received the control IgG antibody than in animals that did not receive any antibody treatment, indicating nonspecific inhibition of gene expression.

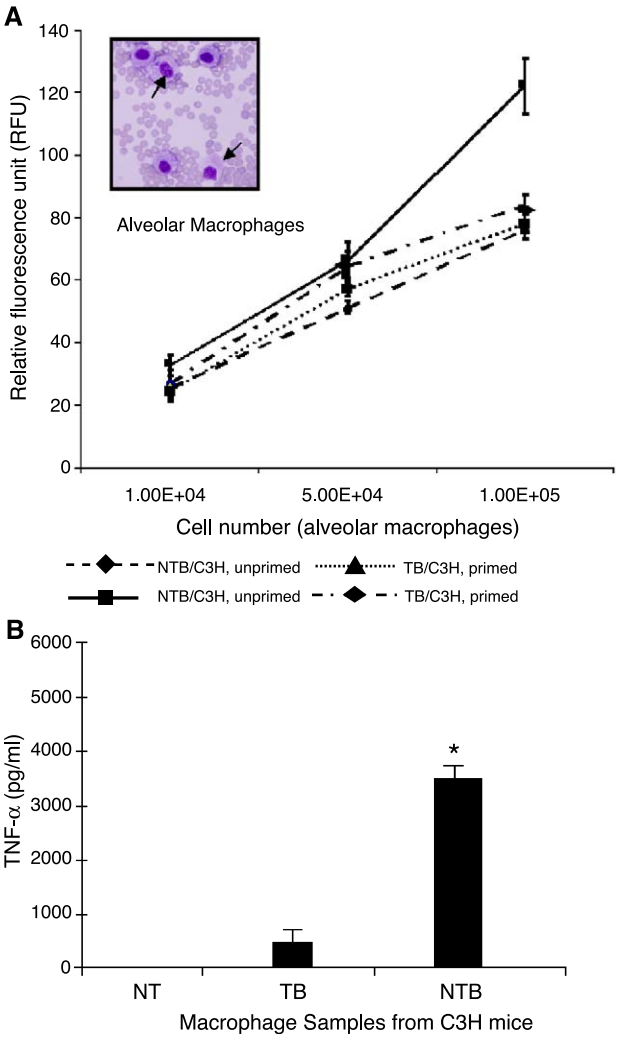


FIG. 5. Alveolar macrophages (AM) from TB mice are less responsive to PMA stimulation. (A) Alveolar macrophages from TB and TNB C3H mice were plated in 96-well plates at various cell densities and incubated overnight at 37°C. Cells were exposed to PMA (1 μg/ml) for 1 h. After 1 h, 2′,7′ dichlorofluorescein diacetate was added and incubated for 30 min. Macrophage stimulation was detected by measuring the fluorescence intensity at 530 nm in a spectrofluorometer. AM from TNB animals responded to PMA stimulation significantly compared to those from TB animals. AM not exposed to PMA served as controls. Values shown are the means of quadruplicate wells. Bars represent standard error. (B) Alveolar macrophages from TB and TNB C3H mice were treated with LPS (1 μg/ml) for 24 h and the culture medium was assayed for murine TNF-α. A significant amount of TNF-α protein was detectable in the medium from AM harvested from NTB mice compared to that from TB mice. AM not exposed to LPS served as negative control (NT). Positive control included was provided in the kit. Data are represented as the means of quadruplicate wells. Bars represent standard error.

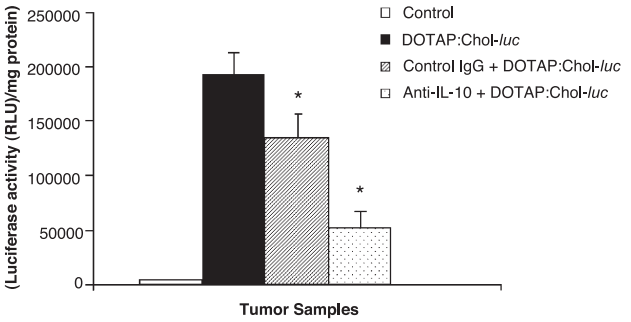


FIG. 6. Neutralization of IL-10 in TB mice results in decreased transgene expression. Lung tumors were established in C3H mice by injecting UV2237m cells (1 × 10^6cells/well) via the tail vein. Three weeks later, animals were divided into three groups and treated as follows: group 1 received no treatment, group 2 received an intraperitoneal (ip) injection of isotypic control IgG antibody (20 μg), and group 3 received an ip injection of neutralizing anti-IL-10 antibody (20 μg). Twenty-four hours later, animals from all three groups were treated with DOTAP:Chol-*luc* DNA complex via the tail vein. Animals that did not receive any treatment served as negative controls. Animals were euthanized 48 h after injection, and their lungs were removed and analyzed for luc activity. Luc expression was significantly less in animals from group 3 than in those from groups 1 and 2. A significant reduction in luc activity was also observed in group 2 compared with group 1, indicating nonspecific inhibition. Luc activity is expressed as RLU per milligram of total protein. Bars represent standard error.

DISCUSSION

The present study demonstrated for the first time that transgene expression persists in TB animals but not in NTB animals. Although persistent transgene expression was demonstrated in TB animals *in vivo*, the cell types that primarily express the transgene were not investigated in the present study. However, we have recently demonstrated that tumor cells primarily express the transgene at higher levels compared to surrounding normal tissues, both *in vitro* and *in vivo* [27]. Based on our previous observation we can speculate that persistent transgene expression primarily occurs in tumor cells. However, expression can also persist in other cell types that are present within the tumor microenvironment.

The underlying mechanism for the prolonged transgene expression was next examined. It is possible that inflammatory cytokines (TNF-α, IL-1α), which have been previously shown to inhibit transgene expression, may be altered in TB animals or that the immune cells (macrophages, neutrophils, T cells) that produce the inflammatory cytokines are functionally altered in TB animals [17–25]. To understand the mechanism involved, we measured cytokine expression levels in TB and NTB animals after intravenous administration of a liposome–DNA complex. TNF-α, IL-1α, IFN-γ, and IL-10 expression was observed in both TB animals and NTB animals.

Copyright © The American Society of Gene Therapy

doi:10.1016/j.ymthe.2004.01.007

However, TNF-α levels were 50% lower in TB animals. The role of TNF-α as a proinflammatory cytokine and its primary source, alveolar macrophages, are well known [26,28]. It appears that the alveolar macrophages may be functionally suppressed by soluble factors released by the *in situ* tumor [29,30]. As a result, production of TNF-α and other cytokines triggered by TNF-α may also be reduced, thereby allowing persistent transgene expression. The observation that IL-10 levels were higher in TB animals supports this hypothesis. The inhibitory effects of IL-10 on macrophages and TNF-α production are well documented [29–34]. Similarly, IL-10 expression by tumor cells has been previously demonstrated [35–39]. Based on these reports we next determined the source of IL-10. Immunohistochemical analysis of TB lung tissue sections demonstrated intense cytoplasmic staining for IL-10 in UV2237m tumor cells. Additionally, *in vitro* assay demonstrated IL-10 production by tumor cells albeit at low levels. The difference in *in vitro* and *in vivo* IL-10 levels can be due to several reasons that include difference in tumor cell number, cell type (tumor cells, epithelial cells, mononuclear cells, etc.), and *in situ* tumor conditions. In support of this are the findings that IL-10 staining was also observed in infiltrating lymphocytes. Additionally, IL-10 expression was also observed in the surrounding normal tissues that comprised fibroblast and epithelial cells. In contrast, IL-10 expression was observed to be minimal in NTB lung tissue sections.

IL-10 is a Th_2-type cytokine that acts as an immunosuppressor under a variety of conditions and is primarily produced by macrophages and T cells [36,37]. Production of IL-10 and its effects on immune cells have been shown in a variety of human cancers [39–43]. In fact, it has been shown that IL-10 production by tumor cells suppresses the immune functions of macrophages and T cells, thereby promoting tumor growth [44–49]. Furthermore, when present in the tumor microenvironment, macrophages can produce IL-10 in an autocrine fashion, resulting in functional inactivation [36,37]. Based on these findings, we examined the effect of exogenous IL-10 on transgene expression in alveolar macrophages from TB and NTB animals, as well as the effect of PMA on macrophage stimulation as a measure of function. Transgene expression was significantly higher in alveolar macrophages from NTB animals compared with those from TB animals. However, in the presence of IL-10, transgene expression was significantly suppressed in macrophages from NTB animals (data not shown). This observation suggests two possibilities: the transgene expression was transcriptionally suppressed or the macrophages were functionally inactivated, resulting in a decreased inflammatory response. We believe that functional inactivation is a more likely mechanism since alveolar macrophages from TB animals, when exposed to PMA, were not stimulated. In contrast, macrophages from NTB animals, when exposed to PMA, were observed to undergo significant stimulation. Furthermore, a reduction in TNF-α production was observed in alveolar macrophages from TB animals compared with those from NTB animals.

The difference in the alveolar macrophage function may partly explain the observed increase in transgene expression in TB mice receiving repeated treatments compared to NTB mice. Although persistent and increased transgene expression has been demonstrated in TB mice it is not clear whether this is a local effect or a systemic effect. Preliminary studies from our laboratory indicate that this is primarily a local effect that is influenced by the tumor microenvironment. Analysis of transgene expression in mice bearing subcutaneous tumors demonstrated an increase in transgene expression over time when the mice were injected with a single dose of DOTAP:Chol-*luc* DNA complex. However, analysis of the normal tumor-free lungs from these subcutaneous tumor-bearing mice demonstrated a decrease in transgene expression over time (data not shown). We are currently conducting additional studies in the laboratory to delineate the local versus systemic effect.

Finally, the effect of IL-10 on transgene expression was demonstrated by *in vivo* neutralization experiments conducted in TB animals. Treating animals with a neutralizing anti-IL-10 antibody prior to injection of the liposome–DNA complex resulted in an approximately 50% reduction in luc expression compared with animals that did not receive the neutralizing antibody and animals that received an isotypic control antibody. These results indicate that blocking IL-10 activity might restore the inflammatory response, thereby resulting in decreased transgene expression levels. Based on these results, we would like to propose the following hypothesis: Tumor cells in addition to infiltrating inflammatory cells produce IL-10, which acts in an autocrine fashion to promote its growth and produce more IL-10 and in paracrine fashion to suppress the functions of immune cells (macrophages, monocytes, T cells) present in the tumor microenvironment or stimulate them to produce more IL-10 (Fig. 7). Intravenous injection of liposome–DNA complex in TB animals thus results in a diminished inflammatory response, resulting in persistent and enhanced transgene expression following repeated multiple treatments and in therapeutic effect. A note of caution in that apart from IL-10 other immunosuppressive factors produced by the tumor cells may also play a role in the observed persistent transgene expression. We are currently investigating these possibilities in the laboratory.

In conclusion, this study demonstrates for the first time that a diminished inflammatory response, partly mediated by IL-10, leads to persistent gene expression in lung TB animals.. This phenomenon allows multiple treatments, resulting in enhanced transgene expression and therapeutic efficacy. Thus, repeated delivery of ther-

Copyright © The American Society of Gene Therapy

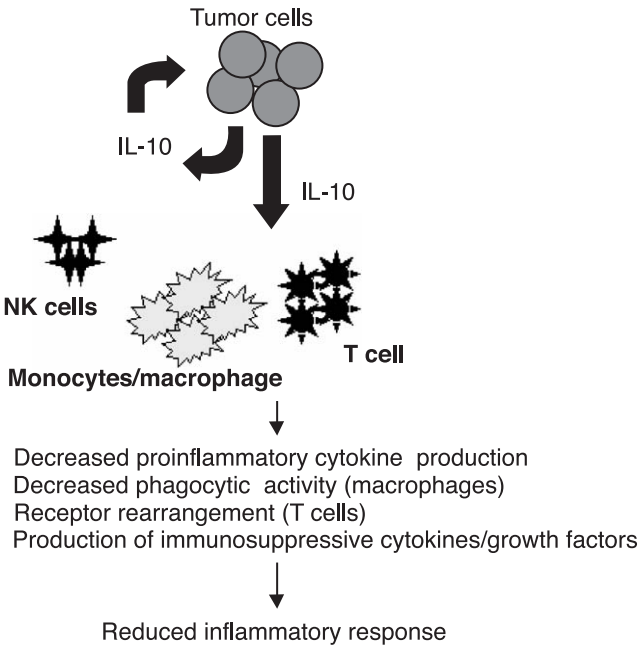


FIG. 7. Schematic representation of IL-10 production by tumor cells and its effects on immune cells and inflammatory response. Tumor cells produce IL-10, which acts in an autocrine manner to promote growth and production of more IL-10 and in a paracrine fashion to suppress the functions of immune cells (macrophages, T cells) present in the tumor milieu by decreasing phagocytic activity and proinflammatory cytokine production (IL-1, TNF-α, IL-6) and rearranging receptors. Intravenous injection of liposome–DNA complex in TB animals thus results in a diminished inflammatory response, resulting in persistent and enhanced transgene expression after repeated treatments and in a therapeutic effect.

apeutic genes encapsulated in a liposome is feasible for lung cancer treatment.

MATERIALS AND METHODS

Materials. All lipids (DOTAP, cholesterol) were purchased from Avanti Polar Lipids (Alabaster, AL, USA). RPMI 1640 medium and fetal bovine serum were purchased from Invitrogen (New York, NY, USA). Polyclonal goat anti-human IL-10 antibody and anti-mouse IL-10 monoclonal antibody were obtained from Pharmingen (San Diego, CA, USA). Anti-IL-10 neutralizing antibody was purchased from Biosource International (Camarillo, CA, USA) and isotypic IgG antibody was purchased from Sigma Chemicals (St. Louis, MO, USA).

Cell lines and animals. Murine fibrosarcoma cells (UV2237) obtained from Dr. Isaiah Fidler, M. D. Anderson Cancer Center, were maintained in RPMI 1640 medium. Human A549 lung cancer cells were obtained from American Tissue Culture Collection (Rockville, MD, USA) and maintained in Hams/F12 medium. Cells were regularly passaged and tested for the presence of mycoplasma. Four- to six-week-old female C3H/Ncr mice (National Cancer Institute, Frederick, MD, USA) and athymic nude mice (Charles River Laboratories, Wilmington, DE, USA) used in the study were maintained in a pathogen-free environment and handled according to institutional guidelines established for animal care and use.

Purification of plasmids. Growth and purification of plasmids used in the study have been described previously [16].

Synthesis, preparation, and particle size analysis of liposome:DNA complexes. The synthesis of 20 mM DOTAP:Chol, the preparation of liposome:DNA complexes, and the determination of mean particle sizes in freshly prepared liposome:DNA complexes have been described previously [16,50].

Cytokine profiles in TB and NTB mice. Experimental lung tumors were established by injecting 1×10^6 UV2237m and A549 tumor cells into C3H/Ncr mice and nude mice, respectively. Tumor cells were injected via the tail vein. Ten to fifteen days after tumor cell injection animals were given a single intravenous injection of DOTAP:Chol-*luc* DNA complex (50 μg DNA) via the tail vein. Cytokine profiles were determined in these lung TB mice and compared with those in NTB mice after treatment. Serum samples were collected from the animals at 0, 2, 6, 12, and 24 h after injection; the samples were stored at −80°C and analyzed for cytokines using murine cytokine ELISA kits (R&D Systems, Inc., Minneapolis, MN, USA). Assays were performed in quadruplicate according to the manufacturer's guidelines.

Luciferase expression in TB and NTB animals. Lung TB and NTB C3H mice and nude mice were injected with a single dose of DOTAP:Chol-*luc* DNA:liposome complex (50 μg DNA) via the tail vein. On days 1, 2, 3, and 7 after injection, the animals were euthanized using CO_2 inhalation, and their lungs were resected. The lungs were snap-frozen in liquid nitrogen and analyzed for luc expression as described previously [50]. Luc was expressed as relative light units (RLU) per milligram of protein. Four animals were analyzed at each of the time points. The experiments were performed twice, and the results reported were the average means of the two experiments.

In vivo luc expression following single and multiple treatments with DOTAP:Chol-luc DNA complex. UV2237m lung TB ($n = 15$) and NTB ($n = 15$) C3H mice and A549 lung TB ($n = 15$) and NTB ($n = 15$) nude mice were divided into three groups each. Five TB and five NTB mice were treated with intravenous injections of DOTAP:Chol-*luc* DNA complex once, and five more from each group were treated daily for 3 days. Five TB mice and five NTB mice did not receive any treatment and served as controls. The mice were euthanized by CO_2 inhalation 48 h after treatment, and their lungs were resected. Total protein was extracted from the lung tissues by homogenizing the tissue in lysis buffer and assaying for luc activity as described above (RLU/mg of protein). Each experiment was performed at least three times and the results reported were the means of the three experiments.

Immunohistochemical analysis. UV2237m lung tumors removed from C3H/Ncr mice were fixed in 10% buffered formalin before being embedded in paraffin and cut into 4-μm sections. Sections were stained for murine IL-10 expression as previously described [16]. Briefly, tissue sections were treated with 0.3% H_2O_2 in methanol for 30 min to block endogenous peroxidase activity and subsequently incubated with normal goat serum for 30 min at room temperature. Following incubation, slides were treated with goat polyclonal anti-IL-10 antibody for 60 min. After 30 min more of incubation with an appropriate secondary antibody (provided with the ABC kit; Vector Laboratories, Burlingame, CA, USA), IL-10 protein was detected in tissues using diaminobenzidine enhanced with the avidin–biotin reaction ABC kit. The slides were then counterstained with hematoxylin and mounted with Aqua-Mount (Lerner Laboratories, Pittsburgh, PA, USA).

Alveolar macrophage activation assay. Alveolar macrophages from TB and NTB C3H mice were acquired as previously described [27,51]. Briefly, the mice were euthanized using CO_2 inhalation, and an incision was made in the region of the trachea. Once the trachea was exposed, a 21-gauge needle was inserted, and 10 ml of sterile Hanks' balanced salt solution (HBSS) was infused into the lungs with a 10-ml syringe. After the lungs were flushed with HBSS, the remaining liquid was aspirated into a sterile Falcon centrifuge tube placed on ice. The procedure was repeated three to four times. Cells were centrifuged at 1000 rpm for 10 min, washed

Copyright © The American Society of Gene Therapy

doi:10.1016/j.ymthe.2004.01.007

thrice, and seeded in six-well plates. An aliquot of the cell preparation was subjected to cytopathological analysis, and more than 90% of the cells were identified as macrophages. Alveolar macrophages thus isolated were used for activation assay. Briefly, alveolar macrophages from TB and NTB C3H mice were plated in 96-well plates at varying cell densities (1×10^4, 5×10^4, and 5×10^5 cells/well) and incubated overnight at 37°C. The next day, PMA was added (1 μg/ml) to the wells and incubated. One hour after incubation with PMA, 2′ ,7′ -dicholorofluorescein diacetate (DCFH-DA; Sigma Chemicals) was added to the wells. DCFH-DA is a substrate that is converted into a fluorescent 2′ ,7′ -dicholorofluorescein product by intracellular oxidants produced by alveolar macrophages [52]. The amount of fluorescence produced is directly proportional to the macrophage response (activation) to PMA. This test is routinely used to measure alveolar macrophage response to various stress inducers [53,54]. Plates were incubated in the dark for 30 min, after which the plates were read in a spectrofluorometer at 485 nm excitation and 530 nm emissions. Values were obtained, and the results reported were the average of quadruplicates for each sample.

In a separate but parallel set of experiments, alveolar macrophages from TB and NTB C3H mice were plated in 96-well plates and incubated overnight. The next day, cells were treated with LPS (1 μg/ml; Sigma Chemicals) and culture supernatants assayed for TNF-α production using a murine TNF-α ELISA kit (R&D Systems). Untreated cells served as negative controls. Positive control was provided in the kit.

In vivo neutralization experiments with anti-IL-10 antibody. UV2237m lung TB C3H mice ($n = 15$) were divided into three groups and treated as follows: group 1 ($n = 5$) received no treatment, group 2 ($n = 5$) received a single intraperitoneal injection of control isotypic IgG antibody (20 μg); and group 3 ($n = 5$) received a single intraperitoneal injection of murine anti-IL-10 neutralizing antibody (20 μg). Twenty-four hours later, mice from all three groups were injected with DOTAP:Chol-*luc* DNA complex (50 μg DNA) via the tail vein. An additional group of animals ($n = 5$) that did not receive any treatment served as negative control for these experiments. The mice were euthanized 48 h after treatment with DOTAP:Chol-*luc*, and their lungs were resected and analyzed for luc activity as described above. Experiments were performed twice and results reported were the averages of two separate experiments.

Statistical analysis. The statistical significance of the experimental results was calculated using ANOVA. A P value <0.05 was considered significant.

ACKNOWLEDGMENTS

The authors thank Dawn Chalaire for editorial assistance and Alma Vega for preparation of the manuscript. This work was supported in part by the Texas Higher Education Coordinating Board, ATP/ARP Grant 003657-0078-2001 (R.R.); by a Career Development Award from The University of Texas M. D. Anderson Cancer Center, SPORE in Lung Cancer P50-CA70907-5 (R.R.); by Public Health Service Grant P01CA78778-01A1 (J.A.R.); by the Texas Tobacco Settlement Fund; by the BESCT Lung Cancer Program, Grant DAMD17-01-1-0689 (Project 3); by TARGET Lung Cancer Grant DAMD17-02-1-0706 (Project 7); by an Institutional Research Grant (R.R.); by a Grant from the W. M. Keck Foundation (R.R.); by Cancer Center Support (CORE) Grant CA16672; and by a sponsored research agreement with Introgen Therapeutics, Inc.

RECEIVED FOR PUBLICATION MAY 26, 2003; ACCEPTED JANUARY 9, 2004.

REFERENCES

1. Whitmore, M., *et al.* (1999). LPD lipopolyplex initiates a potent cytokine response and inhibits tumor growth. *Gene Ther.* **6:** 1867–1875.
2. Huang, L., and Li, S. (1997). Liposomal gene delivery—a complex package. *Nat. Biotechnol.* **15:** 620–621.
3. Li, S., *et al.* (1999). Effect of immune response on gene transfer to the lung via systemic administration of cationic lipidic vectors. *Am. J. Physiol.* **276:** L796–L804.
4. Freimark, B. D., *et al.* (1998). Cationic lipids enhance cytokine and cell influx levels in the lung following administration of plasmid–cationic lipid complexes. *J. Immunol.* **160:** 4580–4586.
5. Whitmore, M., *et al.* (1999). LPD lipopolyplex initiates a potent cytokine response and inhibits tumor growth. *Gene Ther.* **6:** 1867–1875.
6. Dow, S. W., *et al.* (1999). Lipid–DNA complexes induce potent activation of innate immune responses and antitumor activity when administered intravenously. *J. Immunol.* **163:** 1552–1561.
7. Scheule, R. K. J., *et al.* (1997). Basis of pulmonary toxicity associated with cationic lipid-mediated gene transfer to the mammalian lung. *Hum. Gene Ther.* **8:** 689–707.
8. Tousignant, J. D., *et al.* (2003). DNA sequences in cationic lipid:pDNA-mediated systemic toxicities. *Hum. Gene Ther.* **14:** 203–214.
9. Tan, Y., *et al.* (1999). The inhibitory role of CpG immunostimulatory motifs in cationic lipid vector mediated transgene expression in vivo. *Hum. Gene Ther.* **10:** 2153–2161.
10. Yew, N. S., *et al.* (2000). Reduced inflammatory response to plasmid DNA vectors by elimination and inhibition of immunostimulatory CpG motifs. *Mol. Ther.* **1:** 255–262.
11. Schwartz, D. A., *et al.* (1997). Cpg motifs in bacterial DNA cause inflammation in the lower respiratory tract. *J. Clin. Invest.* **100:** 68–73.
12. McLachlan, G., *et al.* (2000). Bacterial DNA is implicated in the inflammatory response to delivery of DNA/DOTAP to mouse lungs. *Gene Ther.* **7:** 384–392.
13. Qin, L., *et al.* (1997). Promoter attenuation in gene therapy: interferon-gamma and tumor necrosis factor alpha inhibit transgene expression. *Hum. Gene Ther.* **8:** 2019–2029.
14. Li, S., *et al.* (1998). Characterization of cationic lipid–protamine–DNA (LPD) complexes for intravenous gene delivery. *Gene Ther.* **5:** 930–997.
15. Yew, N. S., *et al.* (2002). Cpg-depleted plasmid DNA vectors with enhanced safety and long-term gene expression *in vivo*. *Mol. Ther.* **5:** 731–738.
16. Ramesh, R., *et al.* (2001). Successful treatment of primary and disseminated human lung cancers by systemic delivery of tumor suppressor genes using an improved liposome vector. *Mol. Ther.* **3:** 337–350.
17. Kuda, T., Yasumoto, K., Yano, T., Nakahashi, H., Sugimachi, K., and Nomoto, K. (1987). Role of antitumor activity of alveolar macrophages in lung cancer patients. *Cancer Res.* **47:** 2199–2202.
18. Sotomayor, E. M., *et al.* (1993). Impaired activation of tumoricidal function in macrophages from mammary tumor bearers: the role of IFN-γ. *Int. J. Oncol.* **3:** 719–727.
19. Sotomayor, E. M., *et al.* (1995). Decreased macrophage mediated cytotoxicity in mammary tumor bearing mice is related to alterations in nitric oxide production and/or release. *Int. J. Cancer* **60:** 660–667.
20. Mazzoccoli, G., *et al.* (1999). Lymphocyte subpopulations anomalies in lung cancer patients and relationship to the stage of disease. *In Vivo* **13:** 205–209.
21. Koutsami, M. K., Gorgoulis, V. G., Kastrinakis, N. G., Asimacopoulos, P. J., and Kittas, C. (2002). Prognostic factors in non-small cell lung carcinoma. *Anticancer Res.* **22:** 347–374.
22. Sotomayor, E. M., *et al.* (1991). Role of tumor-derived cytokines on the immune system of mice bearing a mammary adenocarcinoma. *J. Immunol.* **147:** 2816–2823.
23. Lopez, D. M., *et al.* (1996). Cytokine production by lymphoreticular cells from mammary tumor bearing mice: the role of tumor-derived factors. *Anticancer Res.* **16:** 3923–3930.
24. Lopez, D. M., *et al.* (1991). Modulation of the immune system by mammary tumor derived factors. *Cancer Invest.* **9:** 643–653.
25. Ghosh, P., *et al.* (1995). Gradual loss of T-helper 1 populations in spleen of mice during progressive tumor growth. *J. Natl. Cancer Inst.* **87:** 1478–1483.
26. Beutler, B., and Cerami, A. (1989). The biology of cachectin/TNF-α as primary mediator of host response. *Annu. Rev. Immunol.* **7:** 625.
27. Ito, I., *et al.* (2003). Increased uptake of liposomal–DNA complexes by lung metastases following intravenous administration. *Mol. Ther.* **7:** 409–418.
28. Vassali, P. (1992). The pathophysiology of tumor necrosis factor. *Annu. Rev. Immunol.* **10:** 411.
29. Fiorentino, D. F., Zlotnik, A., Mossman, T., Howard, M., and O'Garra, A. (1991). IL-10 inhibits cytokine production by activated macrophages. *J. Immunol.* **147:** 3815.
30. Alleva, D. G., Burger, C. J., and Elgert, K. D. (1994). Tumor-induced regulation of suppressor macrophage nitric oxide and TNF-α production: role of tumor-derived IL-10, TGF-β, and prostaglandin E_2. *J. Immunol.* **153:** 1674.
31. Kambayashi, T., Alexander, H. R., Fong, M., and Strassman, G. (1995). Potential involvement of IL-10 in suppressing tumor-associated macrophages. *J. Immunol.* **154:** 3383–3390.
32. Bogdan, C. Y., Vodovotz, Y., and Nathan, C. (1991). Macrophage deactivation by interleukin-10. *J. Exp. Med.* **174:** 1549.
33. de Waal Malefyt, R., Abrams, J., Bennet, B., Figdor, C., and deVries, J. E. (1991). Interleukin-10 inhibits cytokine synthesis by human monocytes: an autoregulatory role for IL-10 production by monocytes. *J. Exp. Med.* **174:** 1209.
34. Strassman, G., Koota, V., Finkelman, F., Fong, M., and Kambayashi, T. (1994). Evidence for the involvement of interleukin 10 in the differential deactivation of murine peritoneal macrophages by prostaglandin E2. *J. Exp. Med.* **180:** 2365.
35. Gastl, G. A., *et al.* (1993). Interleukin 10 production by human carcinoma cell lines and its relation to interleukin 6 expression. *Int. J. Cancer.* **55:** 96.
36. Howard, M., and O'Garra, A. (1992). Biological properties of interleukin 10. *Immunol. Today* **13:** 198.

Copyright © The American Society of Gene Therapy

37. Moore, K. W., *et al.* (1993). Interleukin-10. *Annu. Rev. Immunol* **11:** 165–190.
38. Loercher, A. E., *et al.* (1999). Identification of an IL-10 producing HLA DR negative monocyte subset in the malignant ascites of patients with ovarian carcinoma that inhibits cytokine protein expression and proliferation of autologous T cells. *J. Immunol.* **163:** 6251–6260.
39. Gotlieb, W. H., *et al.* (1992). Presence of interleukin-10 (IL-10) in the ascites of patients with ovarian and other intra-abdominal cancers. *Cytokine* **4:** 385–390.
40. de Waal Malefyt, R., *et al.* (1991). IL-10 and viral IL-10 strongly reduce antigen-specific human T cell proliferation by diminishing the antigen-presenting capacity of monocytes via downregulation of class II MHC expression. *J. Exp. Med.* **174:** 915–924.
41. Fiorentino, D. F., *et al.* (1991). L-10 acts on the antigen-presenting cells to inhibit cytokine production by Th1 cells. *J. Immunol.* **146:** 3444–3451.
42. Ding, L., and Shevach, E. M. (1992). IL-10 inhibits mitogen-induced T cell proliferation by selectively inhibiting macrophage costimulatory function. *J. Immunol.* **148:** 3133–3139.
43. Bogdan, C., Vodovotz, Y., and Nathan, C. (1991). Macrophage deactivation by interleukin-10. *J. Exp. Med.* **174:** 1549–1555.
44. Armstrong, L., Jordan, N., and Miller, A. (1996). Interleukin-10 (IL-10) regulation of tumor necrosis factor alpha (TNF-alpha) from human alveolar macrophages and peripheral blood monocytes. *Thorax* **51:** 143–149.
45. Ralph, P., *et al.* (1992). IL-10, T lymphocyte inhibitor of human blood cell production of IL-1 and tumor necrosis factor. *J. Immunol.* **148:** 808–814.
46. de Waal Malefyt, R., Yssel, H., and de Vries, J. E. (1993). Direct effects of IL-10 on subsets of human $CD4^+$ T cell clones and resting T cells. *J. Immunol.* **150:** 4754–4765.
47. Yue, F. Y., *et al.* (1997). Interleukin-10 is a growth factor for human melanoma cells and downregulates HLA class-I, HLA class-II and ICAM-1 molecules. *Int. J. Cancer* **71:** 630–637.
48. Lu, Z. Y., *et al.* (1995). Interleukin-10 is a proliferation factor but not differentiation factor for human myeloma cells. *Blood* **85:** 2521–2527.
49. Masood, R., *et al.* (1995). Interleukin-10 is an autocrine growth factor for acquired immunodeficiency syndrome-related B-cell lymphoma. *Blood* **85:** 3423–3430.
50. Templeton, N. S., *et al.* (1997). Improved DNA:liposome complexes for increased systemic delivery and gene expression. *Nat. Biotechnol.* **15:** 647–652.
51. Moxley, M. A., Baird, T. L., and Corbett, J. A. (2000). Adoptive transfer of acute lung injury. *Am. J. Physiol. Lung Cell Mol. Physiol.* **279:** 985–993.
52. Wan, X. S., Zhou, Z., and Kennedy, A. R. (2003). Adaptation of the dichlorofluorescein assay for detection of radiation-induced oxidative stress in cultured cells. *Radiat. Res.* **160:** 622–630.
53. Goldsmith, C. A., Imrich, A., Danaee, H., Ning, Y. Y., and Kobzik, L. (1998). Analysis of air pollution particulate-mediated oxidant stress in alveolar macrophages. *J. Toxicol. Environ. Health A* **54:** 529–545.
54. Tsai, J. J., Kao, M. H., and Han, S. H. (1999). The respiratory burst activity of activated eosinophils in atopic asthmatics. *Int. Arch. Allergy Immunol.* **119:** 38–44.

Copyright © The American Society of Gene Therapy

[CANCER RESEARCH 62, 2715–2720, May 1, 2002]

Expression of Several Genes in the Human Chromosome 3p21.3 Homozygous Deletion Region by an Adenovirus Vector Results in Tumor Suppressor Activities *in Vitro* and *in Vivo*[1]

Lin Ji,[2] Masahiko Nishizaki, Boning Gao, David Burbee, Masashi Kondo, Craig Kamibayashi, Kai Xu, Nancy Yen, E. Neely Atkinson, Bingliang Fang, Michael I. Lerman, Jack A. Roth, and John D. Minna

Section of Thoracic Molecular Oncology, Departments of Thoracic and Cardiovascular Surgery [L. J., M. N., K. X., N. Y., B. F., J. A. R.] and Biomathematics [E. N. A.], The University of Texas M. D. Anderson Cancer Center, Houston, Texas 77030; Department of Internal Medicine and Pharmacology, Hamon Center for Therapeutic Oncology Research, University of Texas Southwestern Medical Center, Dallas, Texas 75390 [B. G., D. B., M. K., C. K., J. D. M.]; and Laboratory of Immunobiology, National Cancer Institute, Frederick Cancer Research and Development Center, Frederick, Maryland 21702 [M. I. L.]

ABSTRACT

A group of candidate tumor suppressor genes (designated *CACNA2D2, PL6, 101F6, NPRL2, BLU, RASSF1, FUS1, HYAL2,* and *HYAL1*) has been identified in a 120-kb critical tumor homozygous deletion region (found in lung and breast cancers) of human chromosome 3p21.3. We studied the effects of six of these 3p21.3 genes (*101F6, NPRL2, BLU, FUS1, HYAL2,* and *HYAL1*) on tumor cell proliferation and apoptosis in human lung cancer cells by recombinant adenovirus-mediated gene transfer *in vitro* and *in vivo*. We found that forced expression of wild-type *FUS1, 101F6,* and *NPRL2* genes significantly inhibited tumor cell growth by induction of apoptosis and alteration of cell cycle processes in 3p21.3 120-kb region-deficient (homozygous) H1299 and A549 cells but not in the 3p21.3 120-kb region-heterozygous H358 and the normal human bronchial epithelial cells. Intratumoral injection of Ad-101F6, Ad-FUS1, Ad-NPRL2, and Ad-HYAL2 vectors or systemic administration of protamine-complexed vectors significantly suppressed growth of H1299 and A549 tumor xenografts and inhibited A549 experimental lung metastases in *nu/nu* mice. Together, our results, coupled with other studies demonstrating a tumor suppressor role for the *RASSSF1A* isoform, suggest that multiple contiguous genes in the 3p21.3 120-kb chromosomal region may exhibit tumor suppressor activity *in vitro* and *in vivo*.

INTRODUCTION

Lung cancers develop after a multistage process involving a variety of genetic and epigenetic changes in dominant oncogenes and TSGs[3] (1, 2). Several of these changes can be found in smoking damaged respiratory epithelium in preneoplastic lesions, normal appearing epithelium, and in persons even before lung cancer develops (3–6). In these and related studies, allelic loss of chromosome region 3p (particularly 3p21.3) was found to be a frequent and early event in the development of several cancers, including lung and breast cancers (4–9). Several *3p* genes have been extensively studied and include *FHIT* at 3p14.2, *RARB* at 3p24, and *VHL* at 3p25 (summarize for lung cancer in Ref. 1). These results directed an intensive TSG search of the 3p21.3 region for one or more genes that could function as "gatekeepers" in the molecular pathogenesis of lung cancer, as well as several other human cancers.

Identification of nested 3p21.3 homozygous deletions in small cell lung cancers and a breast cancer line directed positional cloning efforts to a 630-kb region, which was narrowed subsequently to a 120-kb subregion by a breast cancer homozygous deletion (10, 11). This defined 3p21.3 region undergoes allele loss in ~80% of primary lung cancers and ~40% of preneoplastic or normal epithelial samples of smoking-damaged lung, marking it as one of the first sites to be involved (6). In addition, patients whose peripheral blood lymphocytes showed greater damage in this 3p21.3 region after *in vitro* treatment with the carcinogen benzo-a-pyrene diol epoxide had an increased risk of having lung cancer, suggesting the potential for genetic polymorphisms in this region predisposing to lung cancer development (12). The 630-kb region contains ≥25 genes, whereas 9 genes are located in or on the border of the 120-kb 3p21.3 region (10). This group of potential TSGs includes *CACNA2D2* (GenBank no. AF040709), *PL6* (U09584), *101F6* (AF040704), *NPRL2* (AF040707), *FUS1* (AF055479), *BLU* (U70880), *RASSF1* (AF040703, RASSF1C and AF102770, RASSF1A), *HYAL2* (U09577), and *HYAL1* (U03056). The *RASSF1A* isoform of the *RASSF1* gene has been studied extensively for promoter methylation in a variety of tumors, including lung and breast cancer, found to be frequently epigenetically inactivated in these tumors, and shows the ability to suppress lung cancer malignant growth (13, 14). The *FUS1* gene was also found to suppress the growth of NSCLCs *in vitro* (15). However, there have been no detailed tests comparing the activity of several of the genes in this small region or in testing their effect on lung cancer xenografts (local tumors or metastases) *in vivo*. At the start of the search for a 3p21.3 TSG, everyone expected that one gene would be found that frequently suffered mutations. However, from detailed studies of the genes in the region, that was not the case (10). In addition, the possibility of haploinsufficiency needed to be considered. Thus, it was important to further define the tumor suppressing capability of these genes both *in vitro* and *in vivo*. Such identification, which is the focus of the current report, would target the gene(s) for development as new tools for the early detection, monitoring of prevention efforts, prognosis, and therapy of lung and other cancers.

In this study, we used recombinant adenoviruses to introduce WT 3p21.3 genes into NSCLC tumor cell lines or tumor xenografts, where 3p21.3 120-kb region genes are either heterozygous or homozygous to characterize their potential tumor suppressing function *in vitro* and *in vivo*. We demonstrate that introduction of individual WT 3p21.3 genes by recombinant adenoviral vector-mediated transfer into lung cancer cells with loss of heterozygosity at the3p21.3 120-kb region inhibited tumor cell growth and induced apoptosis *in vitro*. Moreover, intratumoral injection of recombinant adenoviral vectors containing WT 3p21.3 genes significantly suppressed growth of human NSCLC xenografts, whereas systemic administration of protamine-complexed

Received 1/4/01; accepted 3/4/02.

The costs of publication of this article were defrayed in part by the payment of page charges. This article must therefore be hereby marked *advertisement* in accordance with 18 U.S.C. Section 1734 solely to indicate this fact.

[1] Supported in part by grants from the National Cancer Institute and the NIH SPORE (2P50-CA70970-04, to J. D. M. and J. A. R.; P01 CA78778–01A1, to J. A. R.; and CA71618, to J. D. M.), gifts to the Division of Surgery from Tenneco and Exxon for the Core Laboratory Facility, the UT M. D. Anderson Cancer Center Support Core Grant (CA 16672), a grant from the Tobacco Settlement Funds as appropriated by the Texas State Legislature (Project 8), a W. M. Keck Gene Therapy Career Development Grant (L. J.), and a sponsored research agreement with Introgen Therapeutics, Inc. (SR93-004-1).

[2] To whom requests for reprints should be addressed, at Department of Thoracic and Cardiovascular Surgery, Box 445, The University of Texas M. D. Anderson Cancer Center, 1515 Holcombe Boulevard, Houston, TX 77030. Phone: (713) 745-4530; Fax: (713) 794-4901; E-mail: lji@mail.mdanderson.org.

[3] The abbreviations used are: TSG, tumor suppressor gene; NSCLC, non-small cell lung cancer; TUNEL, terminal deoxynucleotidyl transferase-mediated nick end labeling; WT, wild type; HBEC, human bronchial epithelial cell; GFP, green fluorescence protein; pfu, plaque-forming unit(s); vp, viral particle; FACS, fluorescence-activated cell sorter; MOI, multiplicities of infection.

adenoviral vectors of 3p21.3 genes efficiently inhibited development of experimental metastases of lung cancer cells in xenograft mouse models. Together, our results strongly suggest that multiple contiguous genes in the 3p21.3 chromosomal region may function as TSGs *in vitro* and *in vivo*.

MATERIALS AND METHODS

Cell Lines and Cell Culture. Four human NSCLC cell lines with varied 3p21.3 and *p53* gene status, A549 (homozygous for multiple 3p21.3 region markers and WT *p53*), NCI-H1299 (homozygous for multiple 3p21.3 region markers and homozygous deletion of *p53*), NCI-H358 (retained heterozygosity of multiple 3p21.3 region markers and homozygous deletion of *p53*), and NCI-H460 (homozygous for multiple 3p21.3 region markers and WT *p53*), and a normal HBEC line, were used for *in vitro* and *in vivo* experiments. The multiple 3p21.3 polymorphic markers that were used for typing the lung cancer lines are located in the 630-kb homozygous deletion region in which the 120-kb region containing the six genes studied in this report reside and have been described previously (16). The homozygosity of multiple markers is consistent with loss of heterozygosity in this region. In this report, lung cancer cell lines with such homozygosity are referred to as "3p21.3-deficient" cells. The A549 line was maintained in Ham's F12 medium supplemented with 10% FCS. The H1299, H358, and H460 lines were maintained in RPMI 1640 supplemented with 10% FCS and 5% glutamine. Normal HBECs were obtained from Clonetics, Inc. (Walkersville, MD) and cultured in the medium supplied by the manufacturer according to the instructions provided.

Construction of Recombinant Ad-3p21.3 Gene Vectors. The recombinant Ad-3ps were constructed using our recently developed ligation-mediated plasmid adenovirus vector construction system, named herein pAd-RAP and pAd-RAP-Shuttle (detailed structures of plasmids will be provided on request). The 3p21.3 genes were assembled as a mammalian expression cassette that is driven by a cytomegalovirus promoter and tailed with Bovine Growth Hormone poly(A) signal sequence. The resulting Ad-3p vectors were named Ad-101F6, Ad-NPRL2, Ad-BLU, Ad-RASSF1C, Ad-FUS1, Ad-HYAL1, and Ad-HYAL2. Sequences of 3p21.3 genes in the viral vectors were confirmed by automated DNA sequencing. A vector expressing GFP gene (Ad-GFP), and a vector carrying the β-galactosidase gene *Lac*Z (Ad-LacZ), were used to monitor efficiency of transduction by the viral vectors and as nonspecific transgene expression controls. Ad-EV, an E1-deleted empty vector, was used as a negative control. Ad-p53, a vector containing the WT *p53* gene, was used as a positive tumor suppressor control. Viral titers were determined by both absorbance measurement (*i.e.*, vp/ml) and plaque assay (*i.e.*, pfu/ml).

Cell Viability Assay. Inhibition of tumor cell growth by treatment with various Ad-3p vectors was analyzed by quantitatively determining cell viability using an improved 2,3-bis[2-methoxy-4-nitro-5-sulfophenyl]-2H-tetrazolium-5-carboxanilide inner salt (XTT) assay (Roche Molecular Biochemicals, Indianapolis, IN; Ref. 17) as described previously (18). Percentage of cell viability was calculated in terms of the absorbency of treated cells relative to the absorbency of untreated control cells. Experiments were repeated at least three times with quadruplicate samples for each treatment in each individual experiment.

Analysis of Apoptosis and Cell Cycle Kinetics. Induction of apoptosis in tumor cells treated by various Ad-3p vectors was analyzed by flow cytometry (FACS) using TUNEL reaction with FITC-labeled dUTP (Roche Molecular Biochemicals, Mannheim, Germany). Cells were processed for FACS analysis for apoptosis and cell cycle kinetics as described previously (19).

Animal Studies. All animals were maintained, and animal experiments were performed under NIH and institutional guidelines established for the Animal Core Facility at the University of Texas M. D. Anderson Cancer Center. Procedures for A549 and H1299 s.c. tumor inoculations in *nu/nu* mice were described previously (19). When average tumor size reaches ~0.5 cm in diameter, mice were injected intratumorally three times within a week with various Ad-3p and control vectors at a dose of 3×10^{10} pfu (3×10^{12} vp)/tumor in a volume of 0.2 ml. Differences in tumor volumes between treatment groups were analyzed with a mixed model ANOVA using the Statistica software (StatSoft, Inc., Tulsa, OK). A difference was considered to be statistically significant when $P < 0.05$.

An experimental A549 lung metastasis model was used to study the effects of 3p21.3 genes on development of metastases. Briefly, *nu/nu* mice were inoculated with A549 cells ($1–2 \times 10^6$) in 200 μl of PBS via tail vein injection. Pulmonary experimental metastatic tumor colonies were formed 7–10 days after inoculation. Then, protamine-complexed Ad-3p (P-Ad3p) vectors or control complexes were administered systemically to animals by i.v. injection for three times within a week at each a dose of $2–5 \times 10^{10}$ vp/200–500 μg of protamine in a total volume of 200 μl/animal. The P-Ad complexes are prepared by mixing an equal volume of the adenoviral vector (1×10^{10} vp) and the protamine sulfate (100 μg; Fujisawa USA, Inc., Deerfield, IL) in room temperature for 15 min and then bringing it to a total volume of 200 μl with PBS. Two weeks after the last injection, the animals were euthanized, and their lung metastatic tumors were stained with India ink. Tumor colonies on lung surfaces were counted under a dissecting microscope without knowledge of the treatment groups, and the lung tissues were sectioned for further pathologic and immunohistochemical analysis.

RESULTS

Effects of Forced Expression of 3p Genes on Tumor Cell Growth. To test the hypothesis that one or more of the 3p genes function as tumor suppressors *in vitro*, we performed a series of experiments to study the effects of expression of the 3p21.3 genes on cell proliferation in several types of Ad-3p-transduced human NSCLC and normal HBEC cells. Cells from each line were transduced *in vitro* by Ad-101F6, Ad-FUS1, Ad-NPRL2, Ad-BLU, Ad-RASSF1C, Ad-HYAL2, and Ad-HYAL1 vectors at various MOIs in units of vp/c; cells were also treated with PBS, Ad-EV, Ad-LacZ, or Ad-p53 as mock, negative, nonspecific, or positive controls, respectively. The ratio of vp/ml:pfu/ml in our adenoviral preparations is ~100:1. The transduction efficiency was determined by examining GFP-expressing cells in the Ad-GFP-transduced cell population under a fluorescence microscope and was found to be >80% at the highest MOI applied for each cell line.

Cell proliferation was analyzed by using the XTT assay to determine the number of viable cells at 1, 2, 3, and 5 days after transduction (only data for day 5 at various MOIs are shown; Fig. 1). In all cases, the viability of transduced cells was compared with that of untransduced (PBS treated) control cells (whose viability was set at 100%). As can be seen in Fig. 1, cell viability was reduced significantly in Ad-101F6-, Ad-Fus1-, and Ad-NPRL2-transduced A549 and H460 cells, which show homozygosity for multiple 3p21.3 markers and contain WT *p53*, and H1299 cells, which exhibit 3p21.3 homozygosity but also have a homozygous deletion of p53. A modest reduction of cell viability was shown in Ad-RASSF1C-transduced H1299 cells (data not shown). However, no significant effect on growth was observed in any of these cells transduced with Ad-HYAL1, Ad-HYAL2, Ad-BLU, Ad-EV, or Ad-LacZ. These results suggest that exogenous expression of some but not all WT 3p21.3 genes can inhibit 3p-deficient tumor cell growth *in vitro*.

To clarify the specificity of the observed inhibitory effects on tumor cell growth and examine the potential cytotoxicity of the exogenously expressed 3p21.3 genes on normal cells, we analyzed the effects of these 3p21.3 genes on cell proliferation in 3p21.3 heterozygous H358 cells and normal HBECs (Fig. 1). As shown in Fig. 1, HBECs transduced with all Ad-3p genes at MOIs that generated >80% transduction efficiency had reductions in cell number after 5 days of transduction of <10%, whereas H358 cells transduced with the same vectors had losses of <20% when compared with the untransduced control cells. Similar levels of losses of cell numbers were observed in H358 and HBEC cells transduced with control vectors Ad-EV and Ad-LacZ. As a positive control, H358 cells, which are homozygously deleted for *p53*, showed reduced cell numbers when transduced with the Ad-p53 vector. These results, coupled with the lack of effect with Ad-LacZ, Ad-HYAL2, Ad-HYAL1, Ad-RASSF1C, and Ad-BLU,

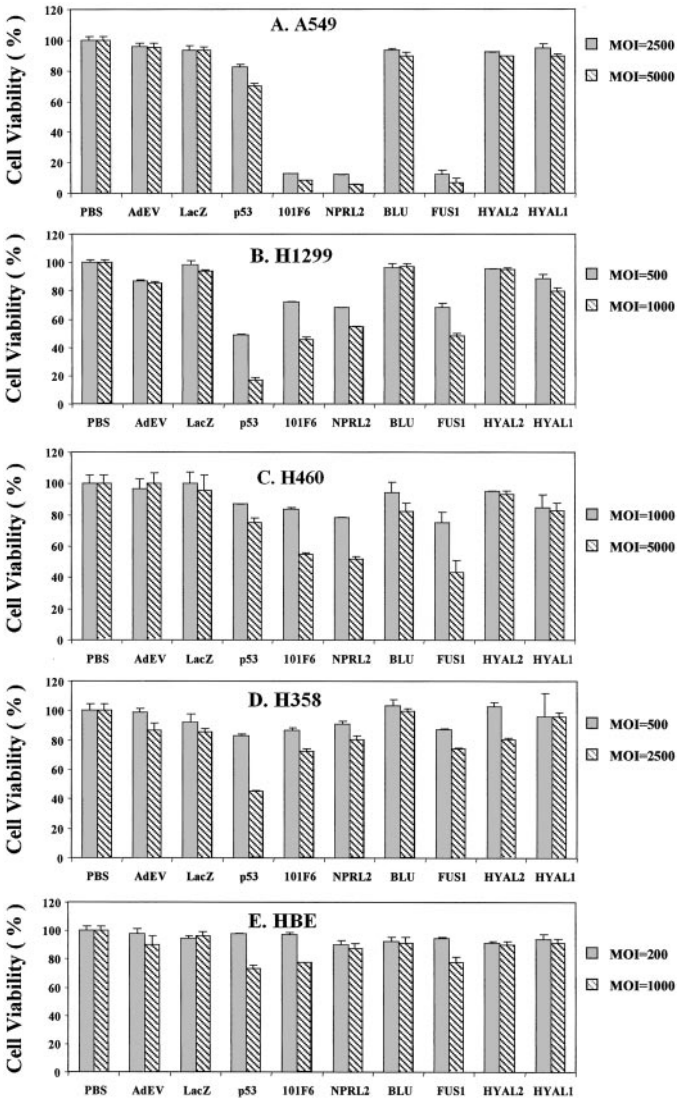


Fig. 1. Effects of exogenous expression of 3p21.3 genes on tumor cell growth in Ad-3p-transduced human lung cancer cells and normal bronchial epithelial cells. Cells were transduced with adenoviral vectors of 3p21.3 genes *101F6, NPRL2, BLU, FUS1, HAYL2,* and *HYAL1,* control genes *LacZ* and *p53,* and empty vector, Ad-EV, at various MOIs (vp/c) as indicated, and PBS alone was used as a mock control. The cell viability was expressed as the percentage of viable adenoviral vector-transduced cells in relation to PBS-treated control cells (100%). *Bars,* SDs of the mean in at least three individual experiments. Treatments were given in quadruplicate for each experiment. The significance of the difference in cell viability between vector-treated cells and the Ad-EV-, Ad-LacZ-, or PBS-treated controls was analyzed by two-sided Student's *t* test. $P < 0.05$ was taken as significant. The differences between the cell viability of the Ad-EV- and Ad-LacZ-transduced cells *versus* PBS-treated controls were not significant ($P = 0.25$–0.95 from different time points and cell lines). The differences between the cell viability of the Ad-101F6-, Ad-Fus1-, and Ad-NPRL2-transduced cells *versus* the Ad-EV- and Ad-LacZ-transduced or PBS-treated controls at the same MOI were significant in A549, H1299, and in H460 at both 3 and 5 days post-transduction ($P \leq 0.0001$–0.005) but not significant in H358 and HBEC cell lines at both 3 and 5 days post-transduction ($P \geq 0.10$–0.95, from different time points and cell lines), respectively. The effects of Ad-BLU, Ad-HYAL2, and Ad-HYAL1 on cell viability were not significant in all cell lines ($P > 0.45$), compared with those of Ad-EV and Ad-LacZ.

demonstrate the specificity of the tumor suppressing function of 3p21.3 genes *FUS1*, *NPRL2*, and *101F6* in 3p-deficient tumor cells and indicate that no generalized cytotoxicity was associated with exogenous expression of these WT 3p21.3 120-kb region genes.

Expression of 3p21.3 genes in Ad-3p-transduced H1299 and normal HBEC cells was verified by quantitative real-time reverse transcription-PCR. Known concentrations of human Raji total RNA and a TaqMan probe for *glyceraldehyde-3-phosphate dehydrogenase* cDNA were used to make a standard curve as an internal control. The increase in levels of transcripts of exogenously expressed 3p21.3 genes relative to those of endogenously expressed mRNAs in HBEC is ~10–15-, 30–50-, and 50–80-fold at an MOI of 100, 500, and 1000 vp/cell, respectively (data not shown). The levels of expression in transduced H1299 cells were similar to those in HBEC (data not shown). In addition, there was an association between increased levels of expression of these 3p21.3 genes and increased MOIs of the corresponding Ad-3p vectors transduced in both H1299 and HBEC cells. The expression of FUS1 and 101F6 proteins after transfection was detected by Western blot analysis using available polyclonal antibodies raised against the oligopeptides derived from their deduced amino acid sequences (data not shown).

Induction of Apoptosis by 3p Genes in Ad-3p-transduced Tumor Cells. The ability of exogenously expressed 3p21.3 genes to induce apoptosis in the Ad-3p-transduced H1299, A549, H460, H358, and HBEC cells was analyzed by FACS using the TUNEL reaction (Fig. 2). Induction of apoptosis was detected in Ad-101F6-, Ad-FUS1-, and Ad-NPRL2-transduced A549 (Fig. 2*A*), H1299 (Fig. 2*B*), and H460 (Fig. 2*C*) cells but not in H358 (Fig. 2*D*) and HBEC (Fig. 2*E*) cells. The apoptotic cell populations increased with increased duration of transduction; >15–20, 40–65, and 75% of cells were apoptotic 5 days after transduction with Ad-101F6, Ad-FUS1, and Ad-NPRL2 in the transduced H1299, A549, and H460 cells, respectively, whereas only ~7 and 10% of cells treated with PBS alone and transduced with Ad-EV vector, respectively, were TUNEL positive after the same time interval. The levels of apoptosis induction by Ad-101F6, Ad-FUS1, and Ad-NPRL2 were quantitatively greater in A549 and H460 cell lines with WT *p53* genes (Fig. 2, *A* and *C*) than that in H1299 cell line deleted for *p53* gene (Fig. 2*B*). Levels of apoptosis in A549 and H460 cells were comparable with those induced by Ad-p53 in *p53*-deficient H1299 and H358 cells (Fig. 2, *B* and *D*). However, no significant induction of apoptosis was observed in any tumor cell line transduced by Ad-BLU, Ad-RASSF1, Ad-HYAL2, and Ad-HYAL1 (Fig. 2). The levels and time of induction of apoptosis in cells transduced by these Ad-3p vectors correlated with those of reduction of cell numbers in cells treated with the same vectors (Fig. 1), suggesting that suppression of tumor cell growth by these 3p21.3 genes is mediated directly or indirectly through a mechanism of apoptosis.

Suppression of Tumor Growth by Intratumoral Injection of Ad-3p Vectors. To determine whether the observed inhibitory effects of these 3p21.3 genes on tumor cell proliferation *in vitro* could be demonstrated on tumor growth *in vivo*, we evaluated the efficacy of 3p21.3 genes in suppressing tumor growth by direct intratumoral injection of Ad-3p21.3 gene vectors, along with PBS and Ad-EV, Ad-LacZ, and Ad-p53 vectors as controls, into A549 or H1299 tumor xenografts in *nu/nu* mice (Fig. 3). The growth of tumors was recorded from the first injection until 23 days after the last injection. Tumor volumes were normalized by calculating the percentage increase in tumor volume after treatment relative to volume at the beginning of treatment in each group. In both A549 (Fig. 3*A*) and H1299 (Fig. 3*B*) tumor models, all of the tumors treated with Ad-101F6, Ad-FUS1, or Ad-NPRL2 showed significantly suppressed growth ($P < 0.001$), compared with mouse groups treated with Ad-LacZ or Ad-EV controls, whereas no significant effect was observed in Ad-HYAL1-, Ad-BLU (data not shown)-, and Ad-HYAL2 (data not shown)-treated tumors. Moreover, a significantly stronger inhibition of tumor growth was shown in A549 tumors treated with Ad-101F6 and Ad-NPRL2 vectors than in tumors treated with the Ad-p53 vector (Fig. 3*A*).

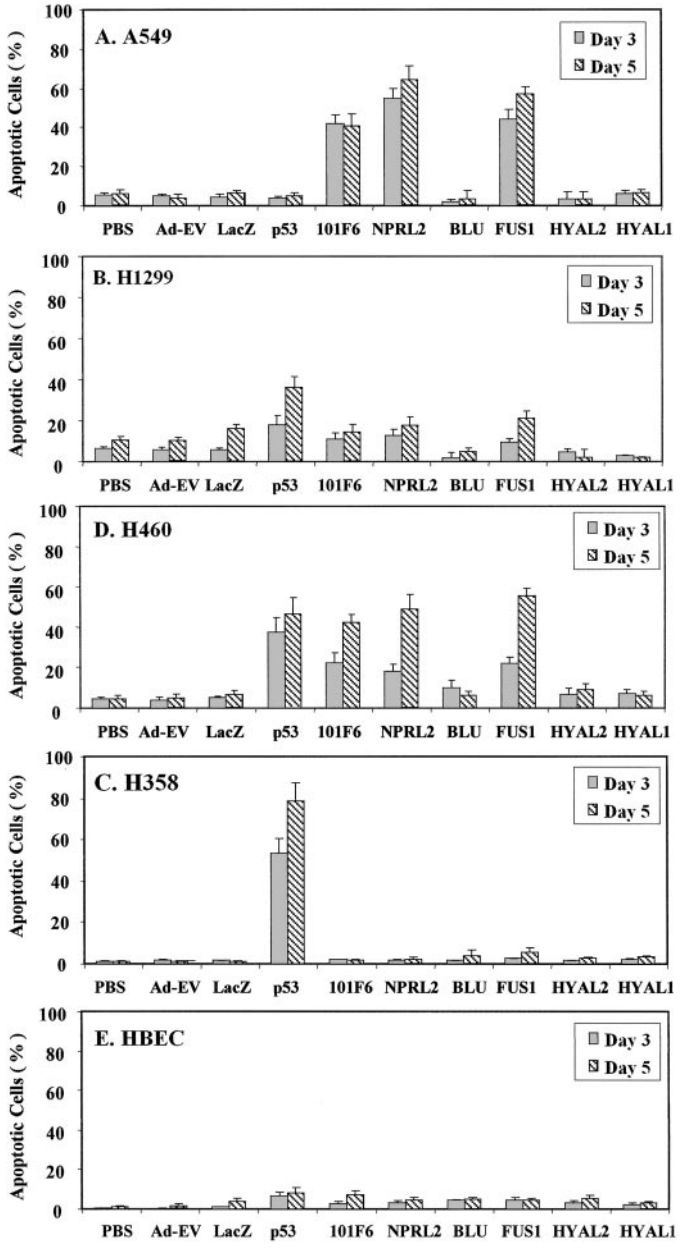


Fig. 2. Induction of apoptosis by exogenous expression of 3p21.3 genes in Ad-3p-transduced human NSCLC cells and normal HBECs. Apoptosis was analyzed by FACS, using TUNEL reaction with FITC-labeled dUTP. Cells were transduced with adenoviral vectors of 3p21.3 genes at an MOI (vp/c) of 5000 for A549 (*A*), 1000 for H1299 (*B*), 5000 for H460 (*C*), 2500 for H358 (*D*), and 1000 for HBEC (*E*), respectively, and PBS, Ad-EV, and p53 were used as controls. Cells were harvested and analyzed for apoptosis at the indicated days post-transduction. The rate of apoptosis is expressed as the percentage of FITC-labeled cells in the total cell population. *Bars*, SDs of the mean in two or three repeated experiments with triplicate treatments and TUNEL reactions for each experiment. The significance of the difference in apoptosis between vector-treated cells and the Ad-EV-, Ad-LacZ-, or PBS-treated controls was analyzed by two-sided Student's *t* test. $P < 0.05$ was considered significant. The differences between the apoptosis induced by the Ad-EV- and Ad-LacZ-transduced cells *versus* PBS-treated controls were not significant ($P = 0.925–0.675$ from different time points and cell lines). The differences between the apoptosis induced in the Ad-101F6-, Ad-FUS1-, and Ad-NPRL2-transduced cells *versus* the Ad-EV-, Ad-LacZ-, or PBS-treated controls were significant in A549 and H460 cells at both 3 and 5 days post-transduction ($P \leq 0.0001–0.005$) and significant *versus* the Ad-EV- and PBS-treated cells in H1299 at 5 days post-transduction ($P \leq 0.02$) but not significant in H358 and HBEC cell lines at both 3 and 5 days post-transduction at all time points ($P \geq 0.85–0.95$), respectively. Induction of apoptosis in Ad-p53-transduced H358 cells was significant at all time points compared with all other treatments ($P < 0.0001$). Induction of apoptosis in cells treated with Ad-BLU, Ad-HYAL2, and Ad-HYAL1 was not significant compared with those treated with PBS, Ad-EV, or Ad-LacZ, in all cell lines at all time points ($P > 0.85$).

Inhibition of Development of Experimental Lung Metastases by Protamine-Adenovirus Complex-mediated 3p21.3 Gene Transfer. A novel formulation using protamine/adenovirus complexes (designated P-Ad) for enhanced systemic delivery of recombinant adenovirus *in vivo* was developed to further explore the potential of 3p21.3 genes in suppressing systemic metastases. An experimental A549 metastatic human lung cancer model (established by i.v. injection of tumor cells) was used to study the effects of 3p21.3 gene transfer on the development of lung metastases in *nu/nu* mice (Fig. 4). The adenoviral 3p21.3 gene vectors were complexed to protamine and delivered via i.v. injection. The development of A549 pulmonary metastases was inhibited significantly, and the numbers of metastatic tumor colonies found on the surfaces of lungs from mice inoculated with A549 cells were reduced by >80% in animals treated with P-Ad-101F6, P-Ad-FUS1, P-Ad-NPRL2, or P-Ad-HYAL2 (70% reduction), compared with those in control treatment groups (Fig. 4). However, no significant reduction of metastatic colony formation was observed in animals treated with P-Ad-HYAL1 and P-Ad-BLU. These data are consistent with results obtained from Ad-3p-treated s.c. tumor xenografts, further supporting the roles of these 3p21.3 genes in suppression of tumor growth and inhibition of tumor progression *in vivo*. Finally, we noted no systemic toxicity to the mice given the systemic injection of PAd-3p complexes.

DISCUSSION

In this study, we used recombinant adenoviral vectors to introduce individual WT 3p21.3 genes into 3p-deficient tumor xenograft or tumor cell lines. The ectopic expression of WT 3p21.3 genes *101F6*, *FUS1*, and *NPRL2* effectively inhibited the growth of 3p-deficient NSCLC A549, H1299, and H460 cells *in vitro* but had no effect on the growth of H358 cells (which remains heterozygous for multiple polymorphic markers in the 3p21.3 650-kb homozygous deletion region) or on the growth of normal HBECs, suggesting the specificity of the exogenous WT 3p21.3 genes in inhibiting tumor cell growth. These findings also indicate the possibility that exogenous expression of 3p21.3 genes will be safe as cancer gene therapy agents because they caused no generalized cytotoxicity to normal cells or in mice treated systemically. The tumor suppressing effects of some TSGs under normal physiological conditions are generally mediated by increased levels of TSG expression in response to the oncogenic and environmental stimuli. These include *p53*, *WAF1*, *BAX*, and *BAK* (20), *e.g.*, expression of both endogenous WT *p53* gene and protein increased 6–8-fold after heat treatment of myeloblastic leukemia cells and DNA-binding activity of p53 increased >17-fold after γ-irradiation of human glioblastoma cells (21, 22). The level of 3p21.3 gene expression by the adenoviral vector-mediated 3p21.3 gene transfer in normal HBEC cells was increased ~10–15-fold (data not shown) and is close to the elevated levels of TSG expression induced by environmental stimuli under physiological conditions shown by that of p53.

In most cases, there is loss of heterozygosity at the 3p21.2 locus with no mutations detected in the remaining allele. However, haploinsufficiency can be associated with abrogation of tumor suppressor activity, *e.g.*, the *p27* gene is haploinsufficient for tumor suppression with tumor suppressor activity critically dependent on the absolute level of p27 protein expression (23). Elevated p27 expression inhibits cell cycle progression and promotes apoptosis in human glioma, colon, NSCLC, and mantle cell lymphoma, suggesting that p27 acts as a rheostat rather than as an on/off switch tumor suppressor in suppressing neoplasia (24). Similar to *p27*, some of the 3p21.3 genes are possibly inactivated by haploinsufficincy (10), and the modulation of protein expression may play an important role for their tumor suppressor activities. Furthermore, the overexpression of these 3p21.3

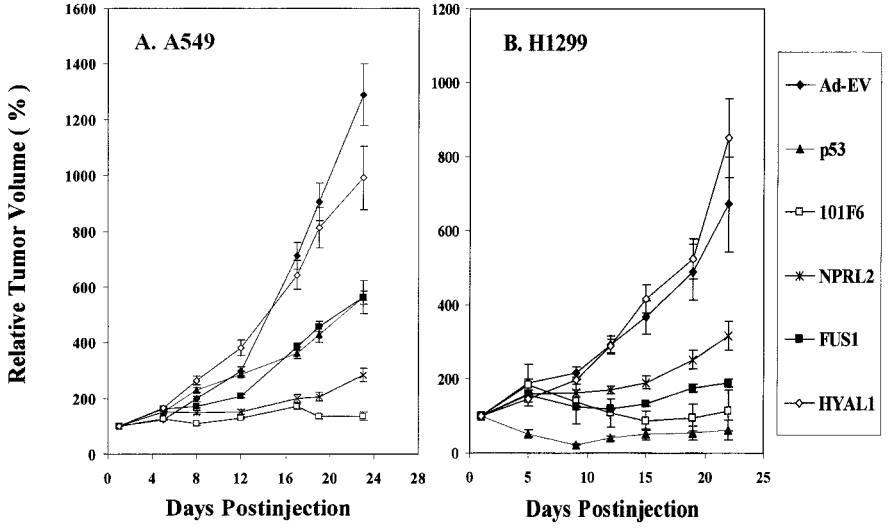


Fig. 3. Effects of intratumoral administration of adenoviral vectors of 3p21.3 genes on growth of human lung cancer A549 (*A*) and H1299 (*B*) s.c. tumors in *nu/nu* mice. When the tumor reached 5–10 mm in diameter at ~2 weeks after tumor inoculation, the tumor was injected with individual adenoviral vectors of 3p21.3 genes *101F6, NPRL2, FUS1,* and *HYAL1* or control vectors Ad-EV and p53, at a dose of 5×10^{10} vp/tumor each in 200 μl of PBS for three times within a week, respectively, and PBS alone was used as a mock control. Results were reported as the mean ± SD in 5–10 mice for each treatment group. Tumor volumes were normalized by the percentage increase of tumor sizes after treatment relative to those at the beginning of the treatment in each group. Mean tumor volumes ±SE from these experiments are shown. ANOVA was performed to determine statistical significance between each treatment group using Statistica software (StatSoft, Inc.), and $P \leq 0.05$ was considered significant. The differences of the tumor volumes in the Ad-101F6-, Ad-FUS1-, and Ad-NPRL2-treated mice *versus* in the Ad-EV-treated mouse controls were statistically significant in both A549 and H1299 tumor models ($P < 0.0001$) after 5 days from the last injection but not significant in Ad-HYAL1 ($P > 0.05$ in both A549 and H1299 tumor models).

genes at higher MOIs may be pharmaceutically appropriate for enhancing their function as cancer therapeutics and may be necessary for proper TSG function to overcome degradation pathways and inactive pathways in the cancer cell. The selectivity of the vectors with respect to growth inhibition and induction of the specific pathway of apoptosis in cancer compared with normal cells further supports their physiological role.

Inhibition of cell proliferation and induction of cell death by activated TSGs, such as *retinoblastoma* (*Rb*) and *p53,* are attributed primarily to these genes' ability to mediate cell cycle arrest and apoptosis (25–27). Because apoptosis is a genetically programmed cellular response to environmental stresses or stimuli, inactivation of TSGs involved in the apoptotic pathways could result in deregulated cell proliferation and tumorigenesis. To elucidate the mechanism governing the inhibition of NSCLC cell growth by 3p21.3 genes, we studied the effects of exogenously expressed 3p21.3 genes on apoptosis mediated by adenoviral vector transduction. Introduction of WT 3p21.3 genes *101F6, FUS1,* and *NPRL2* into the 3p-deficeint A549, H1299, and H460 cells induced apoptosis. However, this was not a generalized feature of 3p21.3 gene overexpression, as the *HYAL2, HYAL1,* and *BLU* genes from this same 120-kb region did not induce a significant increase in apoptosis in the same lung cancer cells. The time and the magnitude of the induction of apoptosis by these 3p21.3 genes were also well correlated with those of the inhibition of growth observed *in vitro*. These observations suggest that the tumor suppressing function mediated by the 3p21.3 genes is through induction of apoptosis.

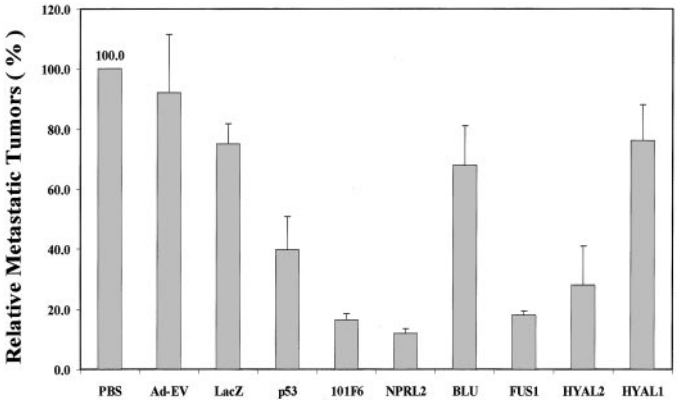


Fig. 4. Effect of systemic administration of protamine-Ad-3p complexes on development of A549 experimental lung metastases in *nu/nu* mice. All animals were i.v. injected with various protamine-adenoviral vector complexes every other 2 days for three times each at a dose of 3×10^{10} vp plus 300 μg of protamine in a total volume of 200 μl/animal, and PBS alone was used as a mock control. Each treatment group consisted of 5–10 animals. Lungs were harvested 2 weeks after the last injection, and metastastic colonies on the surfaces of lung were counted without knowledge of the treatment groups. Development of metastases was represented as the percentages of metastatic colonies formed in protamine-adenovirus complex-treated groups in relation to those in the PBS-treated group (as 100%). *Bars*, SE. Nonparametric *t* test (Wald-Wolfowitz Runs Test) was performed to determine statistical significance between each treatment group using Statistica software (StatSoft, Inc.), and $P \leq 0.05$ was considered significant. A significant inhibition of development of metastases was observed in mice treated with P-Ad-101F6 ($P = 0.002$), P-Ad-NPRL2 ($P = 0.001$), P-Ad-FUS1 ($P = 0.002$), and P-Ad-HYAL2 ($P = 0.014$), respectively, compared with mice treated with PBS, P-Ad-EV, or P-Ad-LacZ but no significant inhibition in mice treated with P-Ad-BLU ($P = 0.818$) or P-Ad-HYAL1 ($P = 0.904$).

To demonstrate whether the observed inhibitory effects of these 3p21.3 genes on tumor cell growth *in vitro* could be reproduced *in vivo,* we evaluated the efficacy of 3p21.3 genes in suppressing tumor growth by directly injecting Ad-3p vectors into A549 or H1299 tumor xenografts in *nu/nu* mice. Growth of both A549 and H1299 tumors was suppressed significantly by treatments with Ad-101F6, Ad-FUS1, and Ad-NPRL2. Furthermore, we explored the tumor suppressing potential of 3p21.3 genes in inhibiting experimental metastases *in vivo* by systemic administration of protamine-Ad-3p complexes. The novel protamine-Ad-3p complexes developed as part of this study allowed us to deliver 3p21.3 genes efficiently to the lung by systemic injection. The development of metastases was inhibited effectively by the protamine-adenovirus complex-mediated transfer of the *101F6, FUS1, HYAL2,* and *NPRL2* genes. These *in vivo* data are consistent with the *in vitro* data, further supporting the roles of 3p21.3 genes as TSGs.

Two of the 3p21.3 genes, *HYAL1* and *RASSF1C,* showed neither tumor suppressor activity *in vitro* nor *in vivo* nor apoptosis-inducing activity *in vitro* in all cell lines tested. Recently, one splicing isoform of one of the genes, *RASSF1A,* has been shown to undergo epigenetic inactivation by promoter region hypermethylation acquired in tumors. This isoform, but not the expressed *RASSF1C* isoform, also exhibits functional tumor suppressing activity. Consistent with these results, we also found no significant effects on growth of NSCLC cells and induction of apoptosis in these NSCLC cells *in vitro* and *in vivo* in our experiments using the Ad-RASSF1C vector (data not shown). The results with *RASSF1A* indicate that it will be important to study all of the genes in the region for loss of expression via tumor-acquired promoter hypermethylation. Alternatively, with 3p allele loss, haploinsufficiency of one or more of these 3p21.3 genes may play a role in tumorigenesis. On the basis of the evidence that multiple contiguous

3p21.3 genes, including *101F6*, *NPRL2*, *RASSF1A*, and *FUS1*, exhibited varied degrees of tumor suppressing activity, we propose that genes in this 3p21.3 120-kb region act together as part of a tumor suppressor region to suppress tumor growth through their functional activation of tumor suppressing pathways. Likewise, their inactivation may contribute directly to the development of cancer because of haploinsufficiency, loss of expression, or rarely mutations. In summary, we have demonstrated here for the first time that introduction of several WT 3p21.3 genes (*101F6*, *NPRL2*, and *FUS1*) contiguously located within a 120-kb region by recombinant adenoviral vector-mediated gene transfer into 3p-deficient tumor xenografts and tumor cell lines efficiently suppressed tumor cell growth and metastases and induced apoptosis *in vitro* and *in vivo*. These results suggest the role of these genes as TSGs. A better understanding of the biological function of genes in this region may result in the development of new strategies for the prevention, early detection, diagnosis, and treatment for lung cancer and other human cancers.

ACKNOWLEDGMENTS

The Minna's Lab thanks Eva Forgacs, Gena Mele, and Adrin Avila for assistance with this work and Dr. Yoshitaka Sekido for his invaluable assistance in identifying and characterizing the genes in this 3p21.3 region.

REFERENCES

1. Zochbauer-Muller, S., Gazdar, A. F., and Minna, J. D. Molecular pathogenesis of lung cancer. Ann. Rev. Physiol., *64:* 681–708, 2002.
2. Fong, K., Sekido, Y., and Minna, J. D. The molecular basis of lung carcinogenesis. *In:* W. B. Coleman and G. Tsongalis (eds.), The Molecular Basis of Human Cancer, pp. 379–405. Totowa, NJ: Humana Press, 2001.
3. Park, I. W., Wistuba, I. I., Maitra, A., Milchgrub, S., Virmani, A. K., Minna, J. D., and Gazdar, A. F. Multiple clonal abnormalities in the bronchial epithelium of patients with lung cancer. J. Natl. Cancer Inst. (Bethesda), *91:* 1863–1868, 1999.
4. Wistuba, I. I., Lam, S., Behrens, C., Virmani, A. K., Fong, K. M., LeRiche, J., Samet, J. M., Srivastava, S., Minna, J. D., and Gazdar, A. F. Molecular damage in the bronchial epithelium of current and former smokers. J. Natl. Cancer Inst. (Bethesda), *89:* 1366–1373, 1997.
5. Wistuba, I. I., Berry, J., Behrens, C., Maitra, A., Shivapurkar, N., Milchgrub, S., Mackay, B., Minna, J. D., and Gazdar, A. F. Molecular changes in the bronchial epithelium of patients with small cell lung cancer. Clin. Cancer Res., *6:* 2604–2610, 2000.
6. Wistuba, I. I., Behrens, C., Virmani, A. K., Mele, G., Milchgrub, S., Girard, L., Fondon, J. W., Garner, H. R., McKay, B., Latif, F., Lerman, M. I., Lam, S., Gazdar, A. F., and Minna, J. D. High resolution chromosome 3p allelotyping of human lung cancer and preneoplastic/preinvasive bronchial epithelium reveals multiple, discontinuous sites of 3p allele loss and three regions of frequent breakpoints. Cancer Res., *60:* 1949–1960, 2000.
7. Girard, L., Zochbauer-Muller, S., Virmani, A. K., Gazdar, A. F., and Minna, J. D. Genome-wide allelotyping of lung cancer identifies new regions of allelic loss, differences between small cell lung cancer and non-small cell lung cancer, and loci clustering. Cancer Res., *60:* 4894–4906, 2000.
8. Maitra, A., Wistuba, I. I., Washington, C., Virmani, A. K., Ashfaq, R., Milchgrub, S., Gazdar, A. F., and Minna, J. D. High-resolution chromosome 3p allelotyping of breast carcinomas and precursor lesions demonstrates frequent loss of heterozygosity and a discontinuous pattern of allele loss. Am. J. Pathol., *159:* 119–130, 2001.
9. Wistuba, I. I., Behrens, C., Milchgrub, S., Bryant, D., Hung, J., Minna, J. D., and Gazdar, A. F. Sequential molecular abnormalities are involved in the multistage development of squamous cell lung carcinoma. Oncogene, *18:* 643–650, 1999.
10. Lerman, M. I., and Minna, J. D. The 630-kb lung cancer homozygous deletion region on human chromosome 3p21.3: identification and evaluation of the resident candidate tumor suppressor genes. Cancer Res., *60:* 6116–6133, 2000.
11. Sekido, Y., Ahmadian, M., Wistuba, I. I., Latif, F., Bader, S., Wei, M. H., Duh, F. M., Gazdar, A. F., Lerman, M. I., and Minna, J. D. Cloning of a breast cancer homozygous deletion junction narrows the region of search for a 3p21.3 tumor suppressor gene. Oncogene, *16:* 3151–3157, 1998.
12. Wu, X., Zhao, Y., Honn, S. E., Tomlinson, G. E., Minna, J. D., Hong, W. K., and Spitz, M. R. Benzo[a]pyrene diol epoxide-induced 3p21.3 aberrations and genetic predisposition to lung cancer. Cancer Res., *58:* 1605–1608, 1998.
13. Burbee, D. G., Forgacs, E., Zochbauer-Muller, S., Shivakumar, L., Fong, K., Gao, B., Randle, D., Kondo, M., Virmani, A., Bader, S., Sekido, Y., Latif, F., Milchgrub, S., Toyooka, S., Gazdar, A. F., Lerman, M. I., Zabarovsky, E., White, M., and Minna, J. D. Epigenetic inactivation of RASSF1A in lung and breast cancers and malignant phenotype suppression. J. Natl. Cancer Inst. (Bethesda), *93:* 691–699, 2001.
14. Dammann, R., Li, C., Yoon, J. H., Chin, P. L., Bates, S., and Pfeifer, G. P. Epigenetic inactivation of a RAS association domain family protein from the lung tumour suppressor locus 3p21.3. Nat. Genet., *25:* 315–319, 2000.
15. Kondo, M., Ji, L., Kamibayashi, C., Tomizawa, Y., Randle, D., Sekido, Y., Yakota, J., Kashuba, V., Zabarovsky, E., Kuzmin, I., Lerman, M., Roth, J. A., and Minna, J. D. Overexpression of candidate tumor suppressor gene FUS1 isolated from the 3p21.3 homozygous deletion region leads to G1 arrest and growth inhibition of lung cancer cells. Oncogene, *20:* 6258–6262, 2001.
16. Fondon, J. W., Mele, G. M., Brezinschek, R. I., Cummings, D., Pande, A., Wren, J., O'Brien, K. M., Kupfer, K. C., Wei, M. H., Lerman, M., Minna, J. D., and Garner, H. R. Computerized polymorphic marker identification: experimental validation and a predicted human polymorphism catalog. Proc. Natl. Acad. Sci. USA, *95:* 7514–7519, 1998.
17. Roehm, N. W., Rodgers, G. H., Hatfield, S. M., and Glasebrook, A. L. An improved colorimetric assay for cell proliferation and viability utilizing the tetrazolium salt XTT. J. Immunol. Methods, *142:* 257–265, 1991.
18. Nishizaki M., Meyn R. E., Atkinson E. N., White R. A., Roth, J. A., and Ji, L. Synergistic inhibition of human lung cancer cell growth by adenovirus-mediated wild-type *p53* gene transfer in combination with docetaxel and radiation therapeutics *in vitro* and *in vivo*. Clin. Cancer Res., *7:* 2683–2689, 2001.
19. Ji, L., Fang, B., Yen, N., Fong, K., Minna, J. D., and Roth, J. A. Induction of apoptosis and inhibition of tumorigenicity and tumor growth by adenovirus vector-mediated fragile histidine triad (FHIT) gene overexpression. Cancer Res., *59:* 3333–3339, 1999.
20. Bishay, K., Ory, K., Lebeau, J., Levalois, C., Olivier, M. F., and Chevillard, S. DNA damage-related gene expression as biomarkers to assess cellular response after γ irradiation of a human lymphoblastoid cell line. Oncogene, *19:* 916–923, 2000.
21. Kastan, M. B., Radin, A. I., Kuerbitz, S. J., Onyekwere, O., Wolkow, C. A., Civin, C. I., Stone, K. D., Woo, T., Ravindranath, Y., and Craig, R. W. Levels of p53 protein increase with maturation in human hematopoietic cells. Cancer Res., *51:* 4279–4286, 1991.
22. Ohnishi, T., Wang, X., Ohnishi, K., Matsumoto, H., and Takahashi, A. p53-dependent induction of WAF1 by heat treatment in human glioblastoma cells. J. Biol. Chem., *271:* 14510–14513, 1996.
23. Fero, M. L., Randel, E., Gurley, K. E., Roberts, J. M., and Kemp, C. J. The murine gene *p27Kip1* is haplo-insufficient for tumour suppression. Nature (Lond.), *396:* 177–180, 1998.
24. Kemp, C. J., Sun, S., and Gurley, K. E. p53 induction and apoptosis in response to radio- and chemotherapy *in vivo* is tumor-type-dependent. Cancer Res., *61:* 327–332, 2001.
25. Evan, G., and Littlewood, T. A matter of life and cell death. Science (Wash. DC), *281:* 1317–1322, 1998.
26. Levine, A. J. p53, the cellular gatekeeper for growth and division. Cell, *88:* 323–331, 1997.
27. Vousden, K. H. p53: death star. Cell, *103:* 691–694, 2000.

[Cancer Biology & Therapy 5:5, 518-522, May 2006]; ©2006 Landes Bioscience

Research Paper

Induction of GDF-15/NAG-1/MIC-1 in Human Lung Carcinoma Cells by Retinoid-Related Molecules and Assessment of Its Role in Apoptosis

Humam Kadara
Claudia P. Schroeder
Dafna Lotan
Claudio Pisano
Reuben Lotan

Department of Thoracic/Head and Neck Medical Oncology; The University of Texas; MD Anderson Cancer Center; Houston, Texas USA

Sigma-Tau; Pomezia, Rome, Italy

*Correspondence to: Reuben Lotan; Department of Thoracic/Head and Neck Medical Oncology; The University of Texas; MD Anderson Cancer Center; Houston, Texas 77030 USA; Tel.: 713.792.8467; Fax: 713.745.5656; Email: rlotan@mdanderson.org

Received 01/25/06; Accepted 02/13/06

Previously published online as a *Cancer Biology & Therapy* E-publication: http://www.landesbioscience.com/journals/cbt/abstract.php?id=2602

KEY WORDS

GDF-15, NAG-1, apoptosis, lung cancer cells, CD437, ST1926, retinoids, p53, DNA damage

ABBREVIATIONS

4HPR	N-(4-hydroxyphenyl)retinamide
ATRA	all-trans retinoic acid
DMSO	dimethyl sulfoxide
DMEM	Dulbecco's Modified Eagle's Minimum Essential Medium
Egr-1	early growth response 1
GDF-15	Growth and differentiation factor 15
PARP	poly(ADP ribose) polymerase
PBS	phosphate buffered-saline
RRMs	retinoid-related molecules
RPA	replication protein A
TGF-β	transforming growth factor β

ACKNOWLEDGEMENTS

Supported in part by grant W81XWH-04-1-0142 (VITAL) from the Department of Defense.

ABSTRACT

Growth and Differentiation Factor-15 (GDF-15, NAG-1, MIC-1) is induced by several apoptosis-inducing agents including the retinoid-related molecule (RRM) 6-[3-(1-adamantyl-4-hydroxyphenyl]-2-naphthalene carboxylic acid (CD437). It has been suggested that GDF-15 may be involved in the induction of apoptosis by CD437 in H460 lung cancer cells. The present study was designed to probe this hypothesis more directly. Several RRMs (CD437, ST1926 and MX3350-1) but not the retinoids all-trans- retinoic acid and 4HPR were able to induce GDF-15 in H460 cells. A similar differential effect of these retinoids was observed for the induction of p53, which has been reported to regulate GDF-15 expression. In H460 cells transfected with a neo vector control (H460-Neo), treatment with RRMs but not ATRA or 4HPR resulted in increases in p53, GDF-15 and apoptosis evidenced by poly(ADP ribose) polymerase (PARP) cleavage. In contrast, RRMs failed to increase p53 or induce apoptosis in H460 cells in which p53 was inactivated by transfection of the human papillomavirus E6-6 (H460-E6-6). The increase in GDF-15 by RRMs was also compromised in the H460-E6-6 cells. Because PARP cleavage was only evident when GDF-15 levels where elevated it appeared that GDF-15 was mediating the pro-apoptotic effects of RRMs. However, silencing of GDF-15 induction by RNA interference failed to decrease the ability of CD437 and ST1926 to induce apoptosis. These results demonstrate that GDF-15 is dispensable for the pro-apoptotic activity of CD437 and ST1926.

INTRODUCTION

Growth and differentiation factor 15 (GDF-15), also known as MIC-1, NAG-1, PTGFβ and PLAB, was first identified as a member of the transforming growth factor β (TGF-β) superfamily of cytokines involved in inhibition of macrophage activation.[1] More recently, GDF-15 has been shown to be induced by several anti-tumorigenic and apoptosis-inducing compounds including nonsteroidal anti-inflammatory drugs (NSAIDs) and cyclo-oxygenase inhibitors,[2-4] resveratrol,[5] genistein,[6] epicatechin gallate,[7] diallyl sulfide,[8] and indole-3-carbinol.[9] These compounds activate GDF-15 expression by means of several transcription factors including Sp-1 and Sp-3,[10] early growth response-1 (Egr-1) gene[11] and p53.[12]

Retinoids are a class of natural and synthetic vitamin A analogues some of which have shown potential and promise for prevention or treatment of certain types of cancer.[13] CD437 is a synthetic retinoid that has been demonstrated previously to induce apoptosis in a variety of cancer cell types including lung cancer cells.[14-18] The molecular mechanisms underlying CD437-mediated apoptosis in human lung cancer have been partially elucidated.[19,20] Recently, the induction of GDF-15 has been associated with CD437-mediated apoptosis.[21] However the role of GDF-15 in apoptosis induced by CD437 and related synthetic retinoids known as retinoid-related molecules (RRMs) has not been fully resolved.[22,23]

Here, we used several RRMs and lung cancer cells with normal and compromised p53 as well as the RNA interference strategy to examine the role of GDF-15 in mediating apoptosis by these agents.

MATERIALS AND METHODS

Reagents. The RRMs CD437, MX3350-1, ST1926, the natural all-trans retinoic acid (ATRA), and the synthetic retinoid *N*-(4-hydroxyphenyl)retinamide (4HPR) were obtained from Dr. B. Shroot (Galderma R+D, Sophia Antipolis, France), Dr. M. Pfahl (Maxia Pharmaceuticals, San Diego, CA), Dr. C. Pisano (Sigma Tau, Pomezia, Rome, Italy), Dr. W. Bollag (F. Hoffmann-La Roche, Basel,

©2006 LANDES BIOSCIENCE. DO NOT DISTRIBUTE

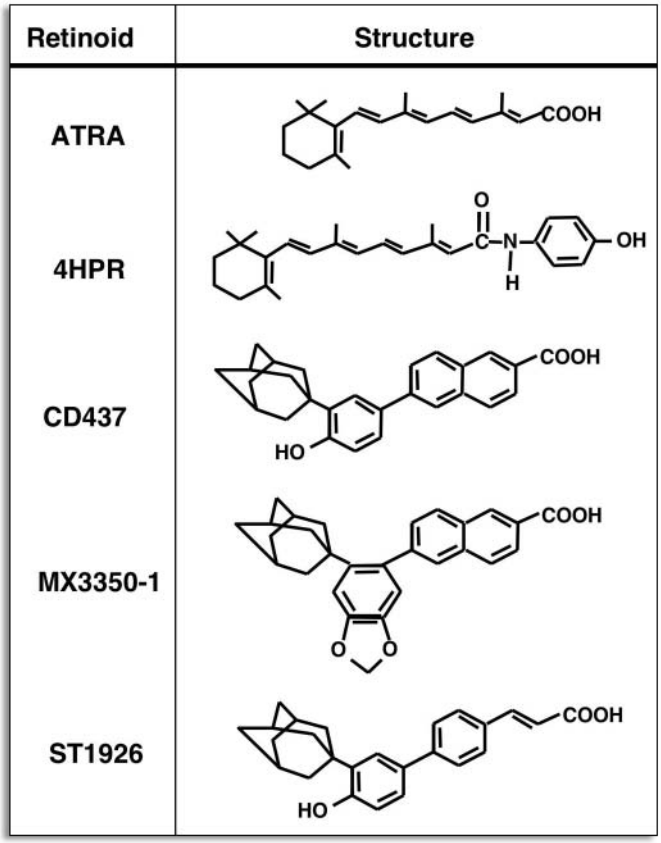


Figure 1. Chemical structures of retinoids used in this study.

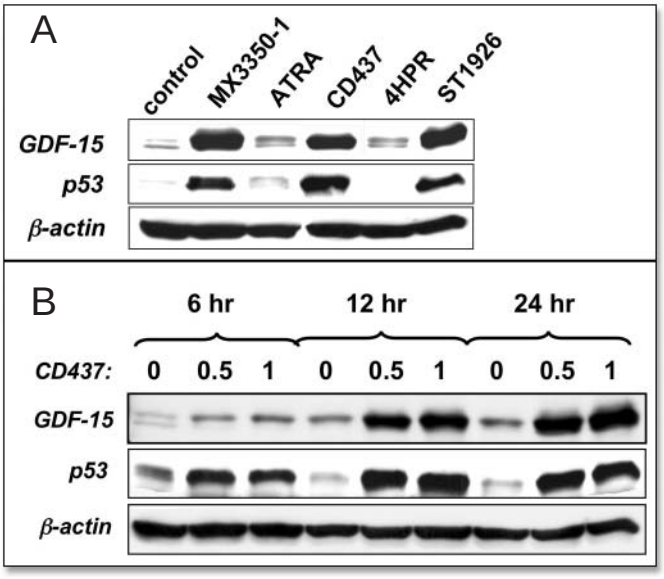


Figure 2. (A) Effect of retinoids on the levels of GDF-15 and p53 in H460 cells. Cells were seeded 24 hours prior to treatment with 0.5 μM of the indicated retinoids for 24 additional hours. The cells were then harvested and lysed to prepare total protein extracts. Samples of the protein extracts were then subjected to western immunoblotting (50 μg/lane). β-Actin was used as a loading control. (B) H460 cells were seeded 24 hours prior to treatment with 0.5 and 1 μM CD437 for 6, 12 and 24 hours after which the cells were harvested and lysed to extract proteins. Samples of total protein extracts were subjected to immunoblotting (50 μg/lane). β-Actin was used as a loading control.

Switzerland), and Dr. J. Zweibel (National Cancer Institute, Bethesda, MD), respectively. All retinoids were dissolved in dimethyl sulfoxide (DMSO) at a concentration of 10 mM and stored in dark containers at -80°C under N_2 atmosphere. Stock solutions were diluted to the final concentration with growth medium just before use. DMSO was from Sigma Chemical Co. (St. Louis, MO). Cell Line Nucleofector® Kit T was purchased from Amaxa Biosystems (Gaithersburg, MD). siGenome™ *SMART*pool® siRNA against GDF-15, and si*CONTROL* NonTargeting siRNA 1 were from Dharmacon RNA Technologies (Lafayette, CO).

Cell lines, cell culture and treatment with retinoids. The human lung cancer cell line H460 (large cell carcinoma) was purchased from the American Type Culture Collection (Rockville, MD). Parental and transfected H460 cells were maintained in monolayer culture in a 1:1 (v/v) mixture of Dulbecco's modified Eagle's medium (DMEM) and Ham's F12 medium. The medium was supplemented with 5% fetal bovine serum and antibiotics and the cells were incubated at 37°C in an atmosphere consisting of humidified air with 5% CO_2. The cells were seeded in 10-cm diameter dishes at a density of approximately 2 x 10^6 cells/dish. After 24 hours, cells were treated with retinoids. The control cells were treated with the same final concentration of DMSO as the retinoid-treated cultures.

Targeting p53 in H460 lung cancer cell line. A H460 cell line in which p53 function is lost after transfecting the cells with an HPV-16 *E6* expression plasmid was utilized.[24] Cells transfected with Neo plasmid were used as a control of cells with wild-type p53. Transfectants were maintained in the presence of 500 μg/ml G418.

Western blot analysis. Cell monolayers were washed twice with ice-cold phosphate buffered-saline (PBS) and harvested and processed for western immunoblotting as described previously.[20] The antibodies used for immunoblotting included: anti-human NAG-1 (GDF-15) (Upstate Cell Signaling Solutions, Lake Placid, NY), p53 (Calbiochem® EMD Biosciences, San Diego, CA), RPA/p34 (Neomarkers, Fremont, CA), EGR-1 (Santa Cruz Biotechnology, Santa Cruz, CA), or PARP (Cell Signaling Technology, Charlottesville, VA). Antibody binding was detected by enhanced chemiluminescence (Amersham Biosciences Corp., Piscataway, NJ). Equality of loading and transfer (internal controls) was confirmed by probing membranes with anti-β-actin antibody (Sigma Chemical Co., St. Louis, MO).

siRNA silencing and transfection. siGenome™ *SMART*pool® siRNA against GDF-15, and si*CONTROL* NonTargeting siRNA 1 were reconstituted in 1x siRNA buffer (20 mM KCl; 6.0 mM HEPES, pH 7.5; and 0.2 mM $MgCl_2$). H460-Neo cells were seeded in six-well plates at a density of 10^6 cells per well. After 24 hours, cells were transfected with 200 pmol per well of either siGenome™ *SMART*pool® siRNA against GDF-15, or the si*CONTROL* Non-Targeting siRNA 1 by electroporation using Nucleofector® Technology (Amaxa Biosystems, Gaithersburg, MD) according to the manufacturer's instructions. After transfection, the cells were maintained for 24 hours in serum-containing medium. Then the cells were washed twice with PBS and incubated for another 24 hours in serum-free DMEM media prior to treatment with retinoids.

RESULTS

The retinoids CD437, ST1926 and MX3350-1 induce both GDF-15 and p53 in H460 human lung cancer cells. CD437 and ST1926 (Fig. 1) induce DNA damage, stabilize p53 and induce apoptosis in lung cancer cells.[19,25] Resveratrol induced GDF-15 in a p53-dependent mechanism involving the DNA damage response.[5] Therefore, we tested whether any of the retinoids and RRMs listed in Figure 1 can induce GDF-15 expression in H460 lung cancer cells. Treating cells with 0.5 μM of CD437, ST1926 or MX3350 for 24 hours led to significant induction of GDF-15 compared to cells treated with either 4HPR or ATRA (Fig. 2A). Moreover, GDF-15 induction was highly associated with p53 induction and both p53 and GDF-15 protein levels increased concurrently in CD437-treated cells (Fig. 2B).

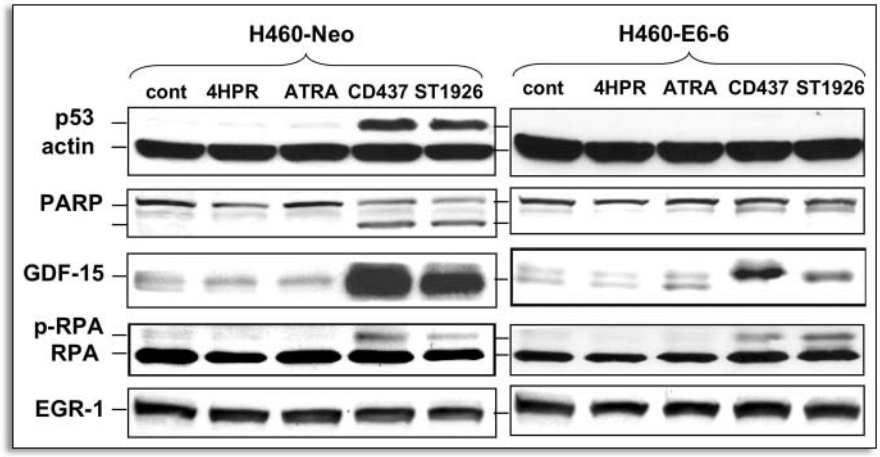


Figure 3. Effects of retinoids on apoptosis (PARP cleavage) and levels of GDF-15, p53, Egr-1 and RPA phosphorylation (p-RPA), in H460-Neo cells and in H460-E6-6 cells. Cells were seeded 24 hours prior to treatment with 0.5 μM of the indicated retinoids for an additional 24 hours. The cells were then lysed to extract proteins and samples of total protein extracts were subjected to immunoblotting (50μg/lane). β-Actin was used as a loading control.

Comparison of the effects of CD437 and ST1926 on H460 cells with wildtype p53 (H460-Neo) and their counterparts with compromised p53 function (H460-E6-6). To assess the importance of p53 for apoptosis and GDF-15 induction by retinoids, we used an isogenic pair of H460 cells that exhibits wild type or compromised p53.[24] Whereas p53 protein level was increased dramatically by both CD437 and ST1926 in H460-Neo cells, no such increase was detected in HPV-E6-6-transfected H460 cells (Fig. 3). Furthermore, apoptosis assayed by PARP cleavage was detected only in the H460-Neo cells after CD437 or ST1926 treatment. CD437 and ST1926 increased GDF-15 substantially in the H460-Neo cells but only minor increases were detected in the H460-E6-6 cells with degraded p53 (Fig. 3). Recently, p53 was shown to play a critical role in the DNA damage response induced by ST1926 in these cells.[25,26] The phosphorylation of replication protein A (RPA), a multifunctional protein complex upstream of p53 involved in DNA replication and repair,[27] is induced in response to ST1926,[26] ionizing radiation and other DNA-damaging agents.[28] Treatment of both H460-E6-6 cells and H460-Neo with CD437 or ST1926 induced RPA phosphorylation indicating the DNA damaging effects of both retinoids and that RPA phosphorylation is upstream of p53 stabilization (Fig. 3). CD437 was shown to induce the transcription factor early growth response 1 (Egr-1) in H460 cells[29] and Egr-1 was reported to regulate GDF-15 in colon cancer cells.[11,30] However, CD437 or ST1926 failed to change the level of Egr-1 after 24 hours (Fig. 3) or at earlier time points (data not shown).

GDF-15 is dispensable for apoptosis mediated by CD437 and ST1926. Transfection of GDF-15 siRNA partially protected ovarian cancer cells from growth suppression by sulindac sulfide.[31] However, the implied role of GDF-15 in apoptosis mediated by CD437[21] was not proven. To determine whether GDF-15 plays a role in the pro-apoptotic effects of RRMs, we transfected H460-Neo cells with GDF-15 siRNA or control siRNA. The interfering siRNA successfully suppressed the induction of GDF-15 by RRMs (Figs. 4A and 4B), however apoptosis evidenced by PARP cleavage was comparable to si*CONTROL* transfectants (Fig. 4A and B). Moreover, quantitative analysis of both uncleaved (116 kD) and cleaved PARP (89 kD) as well as GDF-15 levels clearly shows the close similarity in levels of cleaved PARP and apoptosis between GDF-15 siRNA transfected cells and control transfectants. p53 induction by CD437 and ST1926 was not affected by suppression of GDF-15 (Fig. 4A).

DISCUSSION

CD437 is one of several synthetic retinoids that has been demonstrated to induce apoptosis in a variety of cancer cells including human lung cancer cells but not their normal counterparts.[14-18] CD437's anti-tumorigenic activity was also shown in animal xenograft models.[32] Moreover, CD437 was shown to induce apoptosis in lung cancer cells through a p53-dependent mechanism while sparing wt-p53 containing normal human lung epithelial cells.[33] Although CD437 can selectively bind to and transactivate the retinoic acid receptor γ (RARγ),[34] this retinoid has been shown to induce apoptosis through several unique mechanisms independent of the retinoic acid receptor-mediated pathway that involve p53[19,20] and c-myc.[35] More recently, GDF-15 induction was suggested to be related to the effects of CD437.[21]

The complex process of apoptosis[36] can be induced by CD437 by either retinoid receptor-dependent or independent mechanisms[23] and several molecules, including p53, have been implicated.[19,20] We studied the possible role of GDF-15 in mediating the ability of RRMs and retinoids to induce apoptosis of H460 cells. CD437, ST1926 and MX3350-1 were able to induce p53 in the H460 cells, whereas 4HPR and ATRA failed to do so. All RRMs that increased p53 levels also induced GDF-15, suggesting that both genes may be a part of a single pathway involved in CD437-mediated apoptosis. Indeed, previous reports demonstrated that induction of GDF-15 by resveratrol[5] or genistein[6] was mediated by p53. We tested the importance of p53 and GDF-15 in apoptosis mediated by RRMs in H460 cells by using an isogenic H460 cell pair that exhibits wild type (H460-neo) or p53 compromised by transfection of the human papillomavirus 16 E6 (H460-E6-6). CD437 and ST1926 increased the levels of both p53 and GDF-15 and induced apoptosis in the H460-neo control cells but none of these changes were observed in the H460-E6-6 cells. The ability of CD437 and ST1926 to stabilize p53 has been linked to induction of the DNA damage response.[19,25,26] The DNA damage response involves many proteins that play important roles during DNA replication and repair.[27] One of these, RPA, is a multifunctional trimeric protein, which is phosphorylated in response to ST1926, ionizing radiation, and other DNA-damaging agents and is upstream of p53.[26,28] The induction of RPA phosphorylation after treatment of both H460-E6-6 cells and control transfectants with CD437 or ST1926 indicates that both RRMs induce DNA damage. The finding of this effect in H460-E6-6 demonstrates that RPA phosphorylation is independent of p53, supporting the assertion that it is upstream of p53. At this point it appeared that RRMs induce DNA damage, which resulted in increased RPA phosphorylation followed by p53 stabilization and GDF-15 induction. Our results demonstrate that GDF-15 induction by CD437 and ST1926 requires p53 stabilization such that p53 degradation leads to inhibition of GDF-15 induction by both retinoids.

In addition to the p53 consensus sequence, GDF-15 gene contains response elements for binding of the transcriptional factor Egr-1.[11] We examined the possibility whether Egr-1 is involved in GDF-15 induction in the H460-neo cells because a role for Egr-1 in GDF-15 induction by peroxisome proliferators-activated receptor gamma

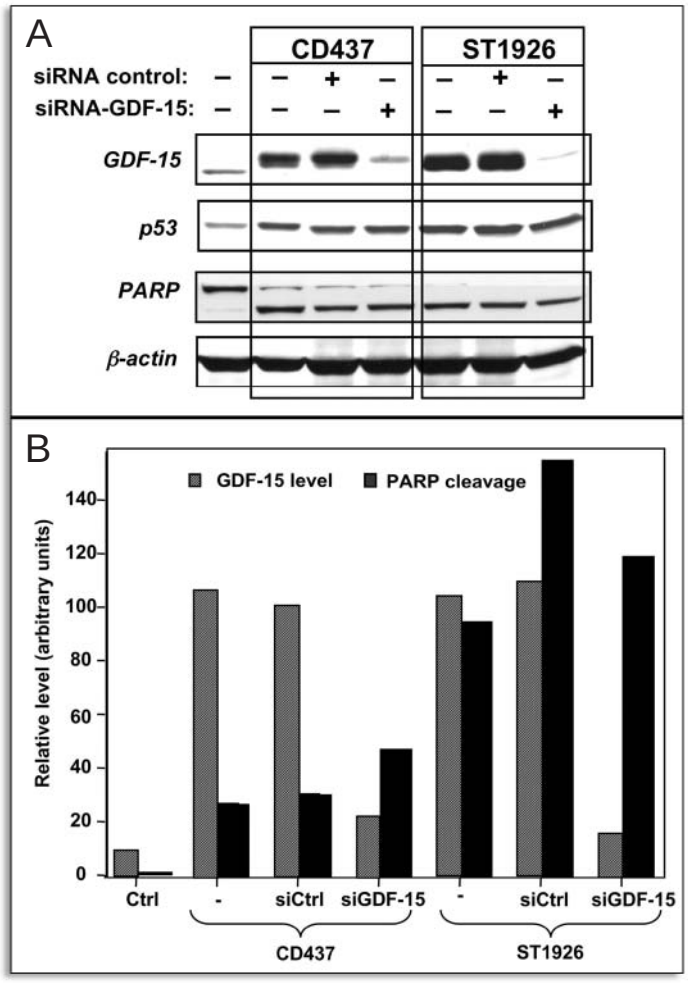


Figure 4. (A) Effect of silencing GDF-15 on CD437- and ST1926-mediated apoptosis of H460-Neo cells. Cells were seeded at 1×10^6 cells/well in six well plates. After 24 hours, cells were transfected with 200 pmol/well of either siRNA against GDF-15, or siCONTROL Non-Targeting siRNA 1. Cells were then incubated in serum-free medium for 24 hours, and were then treated with 0.5 μM of either CD437 or ST1926 for 24 hours, after which they were harvested and lysed for total protein extracts. Samples of the total protein extracts were subjected to immunoblotting (50 μg/lane). β-Actin was used as a loading control. (B) PARP cleavage (89 kD), GDF-15 levels and β-actin band intensities were analyzed and quantified using NIH 1.63 imaging software.

(PPARγ) agonists has been proposed[30,37] and a previous report has shown that CD437 can induce Egr-1 in H460 lung cancer cells.[29] However, our data do not support a role for Egr-1 in GDF-15 induction because both H460-E6-6 and H460-Neo cells expressed Egr-1 constitutively and its levels were not increased after treatment with CD437 or ST1926 for 24 hours or at earlier time points (data not shown).

Because previous studies strongly implicated GDF-15 in apoptosis induction, it was plausible to surmise that it may mediate the pro-apoptotic effects of RRMs. To directly test this hypothesis, we silenced GDF-15 expression (and induction) by transfecting H460-Neo cells with GDF-15 siRNA or si*CONTROL*. This approach resulted in a successful inhibition of GDF-15 induction by the RRMs, however, the expected protection from apoptosis was not achieved as PARP cleavage was very similar in the siRNA transfectants and in the si*CONTROL* transfectants. In addition, p53 induction by CD437 and ST1926 was not affected by GDF-15 siRNA indicating that p53 is upstream of GDF-15 and that apoptosis is mediated by p53 via a GDF-15 independent pathway.

In conclusion, although GDF-15 is highly associated with cell death mediated by CD437 and ST1926 and thus can serve as a surrogate marker for their apoptotic activities, the results of its silencing clearly demonstrate that it is dispensable for the apoptotic effects of these RRMs.

References

1. Bootcov MR, Bauskin AR, Valenzuela SM, Moore AG, Bansal M, He XY, Zhang HP, Donnellan M, Mahler S, Pryor K, Walsh BJ, Nicholson RC, Fairlie WD, Por SB, Robbins JM, Breit SN. MIC-1, a novel macrophage inhibitory cytokine, is a divergent member of the TGF-beta superfamily. Proc Natl Acad Sci USA 1997; 94:11514-9.
2. Baek SJ, Kim KS, Nixon JB, Wilson LC, Eling TE. Cyclooxygenase inhibitors regulate the expression of a TGF-beta superfamily member that has proapoptotic and antitumorigenic activities. Mol Pharmacol 2001; 59:901-8.
3. Baek SJ, Wilson LC, Lee CH, Eling TE. Dual function of nonsteroidal anti-inflammatory drugs (NSAIDs): Inhibition of cyclooxygenase and induction of *NSAID*-activated gene. J Pharmacol Exp Ther 2002; 301:1126-31.
4. Kim KS, Yoon JH, Kim JK, Baek SJ, Eling TE, Lee WJ, Ryu JH, Lee JG, Lee JH, Yoo JB. Cyclooxygenase inhibitors induce apoptosis in oral cavity cancer cells by increased expression of nonsteroidal anti-inflammatory drug-activated gene. Biochem Biophys Res Commun 2004; 325:1298-303.
5. Baek SJ, Wilson LC, Eling TE. Resveratrol enhances the expression of nonsteroidal anti-inflammatory drug-activated gene (*NAG-1*) by increasing the expression of p53. Carcinogenesis 2002; 23:425-34.
6. Wilson LC, Baek SJ, Call A, Eling TE. Nonsteroidal anti-inflammatory drug-activated gene (*NAG-1*) is induced by genistein through the expression of p53 in colorectal cancer cells. Int J Cancer 2003; 105:747-53.
7. Baek SJ, Kim JS, Jackson FR, Eling TE, McEntee MF, Lee SH. Epicatechin gallate-induced expression of NAG-1 is associated with growth inhibition and apoptosis in colon cancer cells. Carcinogenesis 2004; 25:2425-32.
8. Bottone Jr FG, Baek SJ, Nixon JB, Eling TE. Diallyl disulfide (DADS) induces the antitumorigenic *NSAID*-activated gene (*NAG-1*) by a p53-dependent mechanism in human colorectal HCT 116 cells. J Nutr 2002; 132:773-8.
9. Lee SH, Kim JS, Yamaguchi K, Eling TE, Baek SJ. Indole-3-carbinol and 3,3'-diindolylmethane induce expression of NAG-1 in a p53-independent manner. Biochem Biophys Res Commun 2005; 328:63-9.
10. Baek SJ, Horowitz JM, Eling TE. Molecular cloning and characterization of human nonsteroidal anti-inflammatory drug-activated gene promoter. Basal transcription is mediated by Sp1 and Sp3. J Biol Chem 2001; 276:33384-92.
11. Baek SJ, Kim JS, Moore SM, Lee SH, Martinez J, Eling TE. Cyclooxygenase inhibitors induce the expression of the tumor suppressor gene *EGR-1*, which results in the upregulation of NAG-1, an antitumorigenic protein. Mol Pharmacol 2005; 67:356-64.
12. Li PX, Wong J, Ayed A, Ngo D, Brade AM, Arrowsmith C, Austin RC, Klamut HJ. Placental transforming growth factor-beta is a downstream mediator of the growth arrest and apoptotic response of tumor cells to *DNA* damage and *p53* overexpression. J Biol Chem 2000; 275:20127-35.
13. Sun SY, Lotan R. Retinoids and their receptors in cancer development and chemoprevention. Crit Rev Oncol Hematol 2002; 41:41-55.
14. Oridate N, Higuchi M, Suzuki S, Shroot B, Hong WK, Lotan R. Rapid induction of apoptosis in human C33A cervical carcinoma cells by the synthetic retinoid 6-[3-(1-adamantyl)hydroxyphenyl]-2-naphtalene carboxylic acid (CD437). Int J Cancer 1997; 70:484-7.
15. Hail Jr N, Lotan R. Synthetic retinoid CD437 promotes rapid apoptosis in malignant human epidermal keratinocytes and G_1 arrest in their normal counterparts. J Cell Physiol 2001; 186:24-34.
16. Langdon SP, Rabiasz GJ, Ritchie AA, Reichert U, Buchan P, Miller WR, Smyth JF. Growth-inhibitory effects of the synthetic retinoid CD437 against ovarian carcinoma models in vitro and in vivo. Cancer Chemother Pharmacol 1998; 42:429-32.
17. Sun SY, Yue P, Shroot B, Hong WK, Lotan R. Induction of apoptosis in human nonsmall cell lung carcinoma cells by the novel synthetic retinoid CD437. J Cell Physiol 1997; 173:279-84.
18. Adachi H, Preston G, Harvat B, Dawson MI, Jetten AM. Inhibition of cell proliferation and induction of apoptosis by the retinoid AHPN in human lung carcinoma cells. Am J Respir Cell Mol Biol 1998; 18:323-33.
19. Sun SY, Yue P, Wu GS, El-Deiry WS, Shroot B, Hong WK, Lotan R. Implication of p53 in growth arrest and apoptosis induced by the synthetic retinoid CD437 in human lung cancer cells. Cancer Res 1999; 59:2829-33.
20. Sun SY, Yue P, Wu GS, El-Deiry WS, Shroot B, Hong WK, Lotan R. Mechanisms of apoptosis induced by the synthetic retinoid CD437 in human nonsmall cell lung carcinoma cells. Oncogene 1999; 18:2357-65.

21. Newman D, Sakaue M, Koo JS, Kim KS, Baek SJ, Eling T, Jetten AM. Differential regulation of nonsteroidal anti-inflammatory drug-activated gene in normal human tracheobronchial epithelial and lung carcinoma cells by retinoids. Mol Pharmacol 2003; 63:557-64.
22. Lu XP, Fanjul A, Picard N, Pfahl M, Rungta D, Nared-Hood K, Carter B, Piedrafita J, Tang S, Fabbrizio E. Novel retinoid-related molecules as apoptosis inducers and effective inhibitors of human lung cancer cells in vivo. Nat Med 1997; 3:686-90.
23. Lotan R. Receptor-independent induction of apoptosis by synthetic retinoids. J Biol Regul Homeost Agents 2003; 17:13-28.
24. Wu GS, El-Deiry WS. Apoptotic death of tumor cells correlates with chemosensitivity, independent of *p53* or *bcl-2*. Clin Cancer Res 1996; 2:623-33.
25. Zuco V, Zanchi C, Cassinelli G, Lanzi C, Supino R, Pisano C, Zanier R, Giordano V, Garattini E, Zunino F. Induction of apoptosis and stress response in ovarian carcinoma cell lines treated with ST1926, an atypical retinoid. Cell Death Differ 2004; 11:280-9.
26. Zuco V, Zanchi C, Lanzi C, Beretta GL, Supino R, Pisano C, Barbarino M, Zanier R, Bucci F, Aulicino C, Carminati P, Zunino F. Development of resistance to the atypical retinoid, ST1926, in the lung carcinoma cell line H460 is associated with reduced formation of DNA strand breaks and a defective DNA damage response. Neoplasia 2005; 7:667-77.
27. Wold MS. Replication protein A: A heterotrimeric, single-stranded DNA-binding protein required for eukaryotic DNA metabolism. Annu Rev Biochem 1997; 66:61-92.
28. Wang H, Guan J, Perrault AR, Wang Y, Iliakis G. Replication protein A2 phosphorylation after DNA damage by the coordinated action of ataxia telangiectasia-mutated and *DNA*-dependent protein kinase. Cancer Res 2001; 61:8554-63.
29. Sakaue M, Adachi H, Dawson M, Jetten AM. Induction of Egr-1 expression by the retinoid AHPN in human lung carcinoma cells is dependent on activated ERK1/2. Cell Death Differ 2001; 8:411-24.
30. Chintharlapalli S, Papineni S, Baek SJ, Liu S, Safe SH. 1,1-Bis(3'-indolyl)-1-(p-substitutedphenyl)methanes are peroxisome proliferator-activated receptor {gamma} agonists but decrease HCT-116 colon cancer cell survival through receptor-independent activation of early growth response-1 and NAG-1. Mol Pharmacol 2005; 68:1782-92.
31. Kim JS, Baek SJ, Sali T, Eling TE. The conventional nonsteroidal anti-inflammatory drug sulindac sulfide arrests ovarian cancer cell growth via the expression of NAG-1/MIC-1/GDF-15. Mol Cancer Ther 2005; 4:487-93.
32. Schadendorf D, Kern MA, Artuc M, Pahl HL, Rosenbach T, Fichtner I, Nurnberg W, Stuting S, von Stebut E, Worm M, Makki A, Jurgovsky K, Kolde G, Henz BM. Treatment of melanoma cells with the synthetic retinoid CD437 induces apoptosis via activation of AP-1 in vitro, and causes growth inhibition in xenografts in vivo. J Cell Biol 1996; 135:1889-98.
33. Sun SY, Yue P, Chen X, Hong WK, Lotan R. The synthetic retinoid CD437 selectively induces apoptosis in human lung cancer cells while sparing normal human lung epithelial cells. Cancer Res 2002; 62:2430-6.
34. Bernard BA, Bernardon JM, Delescluse C, Martin B, Lenoir MC, Maignan J, Charpentier B, Pilgrim WR, Reichert U, Shroot B. Identification of synthetic retinoids with selectivity for human nuclear retinoic acid receptor gamma. Biochem Biophys Res Commun 1992; 186:977-83.
35. Sun SY, Yue P, Shroot B, Hong WK, Lotan R. Implication of c-Myc in apoptosis induced by the retinoid CD437 in human lung carcinoma cells. Oncogene 1999; 18:3894-901.
36. Vogelstein B, Kinzler KW. Cancer genes and the pathways they control. Nat Med 2004; 10:789-99.
37. Baek SJ, Kim JS, Nixon JB, DiAugustine RP, Eling TE. Expression of NAG-1, a transforming growth factor-beta superfamily member, by troglitazone requires the early growth response gene *EGR-1*. J Biol Chem 2004; 279:6883-92.

Involvement of Rac in Fenretinide-Induced Apoptosis

Humam Kadara,[1] Eiji Tahara,[1] Hyun-Jung Kim,[1] Dafna Lotan,[1] Jeffrey Myers,[2] and Reuben Lotan[1]

Departments of [1]Thoracic/Head and Neck Medical Oncology and [2]Head and Neck Surgery, The University of Texas M. D. Anderson Cancer Center, Houston, Texas

Abstract

The synthetic retinoid *N*-(4-hydroxyphenyl)retinamide (4HPR) has shown potential as a chemopreventive and therapeutic agent. The ability of 4HPR to enhance production of reactive oxygen species (ROS) leading to apoptosis has been suggested as a possible mechanism underlying these effects. We explored the possibility that ROS induction by 4HPR involves the small GTPase Ras-related C3 botulinum toxin substrate (Rac), a regulatory subunit of the NADPH oxidase complex. Rac was activated in human head and neck squamous cell carcinoma (HNSCC) cells as early as 5 minutes following 4HPR exposure. Moreover, inhibition of Rac activity or silencing of its expression by RNA interference decreased ROS generation in human head and neck, lung, and cervical cancer cells and murine melanoma cells. In HNSCC UMSCC-22B cells, this decrease correlated with reduction in apoptosis induction by 4HPR. Expression of a constitutive active mutant Rac increased basal and 4HPR-induced ROS generation and poly(ADP-ribose) polymerase cleavage. In addition, the metastatic DM14 cells exhibited higher Rac activation following 4HPR treatment compared with the primary Tu167-C2 cells. Furthermore, the metastatic cancer cells tested exhibited higher ROS generation and growth inhibition due to 4HPR exposure compared with their primary cancer cell counterparts. These findings show a preferential susceptibility of metastatic cells to the proapoptotic retinoid 4HPR through Rac activation and support the use of ROS-inducing agents such as 4HPR against metastatic cancer cells. [Cancer Res 2008;68(11):4416–23]

Introduction

Programmed cell death or apoptosis is a natural process for elimination of defective cells such as those bearing detrimental mutations or alterations in important cellular processes (1). It is now well appreciated that evasion of apoptosis represents a major mechanism that drives tumor growth and is considered a hallmark of most, if not all, cancers (2). Therefore, induction of apoptosis is increasingly recognized as a desired effect for chemopreventive and therapeutic agents because it results in the elimination of premalignant or malignant cells (3, 4).

One promising anticancer agent, *N*-(4-hydroxyphenyl)retinamide (4HPR), also known as fenretinide, which exhibits a substitution of an amide-linked 4-(hydroxyphenyl) group for the carboxyl group of all-*trans* retinoic acid, was first shown to prevent breast cancer in rats (5). In addition, fenretinide displayed markedly reduced adverse side effects such as liver toxicity compared with the natural retinoid all-*trans* retinoic acid (6). Moreover, 4HPR showed efficacy as a chemopreventive and therapeutic agent in various experimental models and clinical trials (7). In addition, 4HPR was effective in clinical trials aimed at chemoprevention of oral leukoplakias recurrence and new incidence in postsurgical patients (8) as well as patients resistant to natural retinoids (9). 4HPR was also shown to significantly reduce the risk of second breast cancer in premenopausal women, the effect of which persisting for several years after treatment cessation in a 15-year-long randomized phase III trial for breast cancer prevention (10). In addition and more recently, 4HPR was shown to significantly delay onset of ovarian cancer (11).

The proposed mechanism for the above-mentioned 4HPR-induced effects was induction of apoptosis based largely on earlier studies, which have shown that 4HPR can induce apoptosis in a variety of cell lines including head and neck squamous cell carcinoma (HNSCC) cells (12). Apoptosis induction by 4HPR is mediated by various mechanisms including ceramide induction (13), triggering of the mitochondrial pathway and modulating mitochondrial membrane permeability and cytochrome *c* release (14), activation of lipoxygenase 12 (15), nitric oxide production (16), and reactive oxygen species (ROS) generation (12, 17–19). The increase in ROS generation can cause sustained activation of c-Jun NH_2-terminal kinase (JNK) and other mitogen-activated protein kinases (MAPK; refs. 20–22), triggering of the mitochondrial pathway (19), and, more recently, induction of endoplasmic reticulum stress (23), all of which seem to be downstream of ROS and to contribute to cell death induction. Whereas these studies have highlighted the pivotal role of the downstream effects of ROS, many gaps still exist in our knowledge of upstream mechanisms responsible for ROS generation by 4HPR.

ROS are produced from the reactions of unpaired electrons of oxygen molecules from various intracellular sources such as the mitochondrial electron transport chain and the NADPH oxidase complex, a multicomponent electron transfer complex composed of the membrane-bound cytochrome b_{558} (gp91phox and p22phox) and the cytosolic components [p67phox, p47phox, p40phox, and Ras-related C3 botulinum toxin substrate (Rac)-1; ref. 24]. On activation, the cytosolic components of the enzyme complex translocate to the plasma membrane where they associate with cytochrome b_{558}, forming an active NADPH oxidase (25, 26). Because NADPH-mediated generation of ROS is involved in various apoptosis signaling pathways (27–30), we hypothesized that it may be a target through which 4HPR induces ROS generation and apoptosis.

In this study, we found that 4HPR activates the NADPH oxidase regulatory subunit Rac, and that this activation results in excessive ROS levels in cancer cells that lead to apoptosis induction apparently by exceeding the endogenous antioxidant capacity. Moreover, we found that 4HPR caused a higher activation of Rac in metastatic cells compared with their corresponding primary cancer cells, which correlated with increased ROS generation and cell growth inhibition.

Requests for reprints: Reuben Lotan, Department of Thoracic/Head and Neck Medical Oncology, The University of Texas M. D. Anderson Cancer Center, Houston, TX 77030. Phone: 713-792-8467; Fax: 713-745-5656; E-mail: rlotan@mdanderson.org.

©2008 American Association for Cancer Research.

doi:10.1158/0008-5472.CAN-08-0031

Materials and Methods

Retinoid and reagents. The synthetic retinoid 4HPR was obtained from Dr. James A. Zwiebel (Cancer Therapy Evaluation Program, National Cancer Institute, Bethesda, MD) and dissolved in DMSO at a concentration of 10 mmol/L and stored in dark containers at −80°C under N_2 atmosphere. Stock solutions were diluted to the final concentration with growth medium just before use. DMSO, Krebs-Ringer buffer, *tert*-butyl hydroxyl anisole, sulforhodamine B, and crystal violet were purchased from Sigma Chemical Co. The Rac inhibitor NSC-23766 was obtained from Calbiochem. Dichlorofluorescein diacetate (DCFH-DA) was purchased from Molecular Probes. The RacV12 expression vector was obtained from Dr. Kaikobad Irani (University of Pittsburgh Medical Center, Pittsburgh, PA).

Cell culture. The HNSCC cell lines UMSCC-22A and UMSCC-22B, derived from pharyngeal primary tumors and lymph node metastasis, respectively, and isolated originally from the same patient, were obtained from Dr. Thomas Carey (University of Michigan, Ann Harbor, MI). The primary and metastatic isogenic HNSCC cell line pair Tu167-C2 and DM14 was obtained from Dr. Jeffrey Myers (The University of Texas M. D. Anderson Cancer Center, Houston, TX). Murine melanoma B16-F1 and B16-F10 cells were obtained from Dr. Isaiah Fidler (The University of Texas M. D. Anderson Cancer Center, Houston, TX), and bronchioalveolar cancer H522 cells and squamous cervical cancer C33A cells were purchased from the American Type Culture collection. The cells were grown and maintained in monolayer culture in a 1:1 (v/v) mixture of DMEM and Ham's F12 medium. The medium was supplemented with 5% fetal bovine serum and the cells were incubated at 37°C in an atmosphere consisting of humidified air with 5% CO_2.

Treatment with 4HPR and the Rac inhibitor NSC-23766. The Rac inhibitor NSC-23766 was prepared as a 50 mmol/L stock solution in distilled water and stored at −80°C. Cells were seeded in 10-cm-diameter dishes for Rac activation assays and Western blot analysis, and in 24-well plates for assessment of ROS levels. After 24 h, cells were serum starved for 1 d in serum-free medium or medium containing NSC-23766 at different doses before treatment with 5 μmol/L 4HPR for different time points. The control cells were treated with the same final concentration of DMSO as the retinoid-treated cultures.

Measurement of intracellular ROS levels. Intracellular ROS levels were measured with the oxidation-sensitive fluorescent dye DCFH-DA, with the conversion of DCFH-DA to dichlorofluorescein (DCF) assessed as previously described (31). Briefly, cells were electroporated with small interfering RNA (siRNA) or expression vectors and/or seeded at a density of $\sim 8 \times 10^4$ per well in 24-well plates. After 1 d, cells were washed twice with PBS and incubated in either serum-free medium alone or in serum-free medium containing NSC-23766 for Rac inhibition studies. The following day, the cells were washed twice with prewarmed Krebs-Ringer buffer and then incubated in the same buffer containing 10 μg/mL DCFH-DA with DMSO alone, NSC-23766, 4HPR, or both 4HPR and NSC-23766 at 37°C. The fluorescence intensity of DCF was measured at an emission of 530 nm after excitation at 485 nm at 1-h intervals using a CytoFluor 2350 Fluorescence Measurement System (Millipore). An increase in fluorescence intensity as arbitrary units indicated the generation of net intracellular ROS. Each treatment was done in four replicate wells and results were calculated, with error bars representing SE.

Measurement of Annexin V–positive cells. Apoptotic cell death was quantitatively measured by measuring externalized phosphatidylserine with the Annexin V-FLOUS Staining Kit (Roche) according to the manufacturer's instructions. Briefly, cells were harvested at the indicated time points after treatment and were washed twice with PBS before staining with and incubation in 100 μL of prediluted Annexin V-FLOUS labeling agent for 15 min at room temperature in the dark. Cells were then washed once with the manufacturer's incubation buffer and finally resuspended in 400 mL of the same buffer. Propidium iodide solution was added to the Annexin V-FLOUS–labeled cells just before analysis with the BD Flow cytometer for quantification of Annexin V–positive cells.

Cell growth inhibition assay. The cells were seeded at calculated cellular densities that allow them to reach near-confluent states 24 h after seeding, at which time the cells were incubated in serum-free medium containing either DMSO or 4HPR. After 1 or 2 d of treatment, cell number was estimated by the sulforhodamine B assay as previously described (32). Briefly, after treatment of cells for the indicated time points, the media were poured on the cells gently, then cells were fixed by adding 100 μL of cold 10% trichloroacetic acid (from Sigma) and incubated for 60 min at 4°C. Following fixation, the supernatants were discarded and plates were washed five times with deionized water and then air-dried or stored in a warm chamber until use. After drying, 50 μL of 0.4% (w/v) sulforhodamine B solution in 1% acetic acid were added to each well, and the plates were then incubated with the stain for 10 min at room temperature. Following staining, plates were washed five times with 1% acetic acid and air-dried at 37°C, after which 100 μL of 10 mmol/L unbuffered Tris base (pH 10.5) were added to each well to solubilize the dye. Plates were shaken for 5 min on a titer plate shaker and optical densities were read on an automated spectrophotometric plate reader at a wavelength of 510 nm. The error bars represent the SE of four replicate measures.

Colony formation assay. Following transfection with RacV12, cells were seeded in six-well plates at a seeding density of 5,000 per well. Ten days later, the medium was decanted and cells were gently washed with PBS to remove residual medium. Cells were then incubated with Carnoy's fixative (3 parts methanol to 1 part acetic acid) at room temperature for 10 min. The cells were then gently washed with distilled water several times and stained with crystal violet for 10 min. The cells were then washed with distilled water several times, after which excess water was gently shaken off and the plates were left to dry.

Western blot analysis. Cell monolayers were washed twice with ice-cold PBS, harvested, and processed for immunoblotting as previously described (12). The antibodies used for immunoblotting included antihuman Rac1 and anti-myc tag (Upstate); HSP70/HSPA1A (Stressgen Bioreagents); poly(ADP-ribose) polymerase (PARP), p21-activated kinase (PAK)-1, JNK, phospho-JNK, c-Jun, and phospho-Jun (Ser^{63}) (Cell Signaling Technology); and β-actin (Sigma Chemical Co.). Antibody binding was detected by enhanced chemiluminescence (Amersham Biosciences Corp.). Equality of loading and transfer (internal controls) were estimated by probing membranes with β-actin or staining the blots with the protein stain Ponceau S.

Rac activation assay. To test for Rac activation by 4HPR, cells were seeded at $\sim 10^6$ cells in serum-containing medium in 10-cm dishes. The next day, the cells were switched to serum-free medium and serum starved for 48 h before treatment with 4HPR in serum-free medium for the indicated time points. Samples were handled for the Rac activation assay according to the manufacturer's instructions (Cytoskeleton). Briefly, the medium was decanted, dishes were washed with 5 mL of PBS at room temperature, and 0.5 mL of the manufacturer's ice cold lysis buffer was added. Cells were scraped off the plates into lysis buffer and cell lysates were clarified by centrifuging. Samples of the cell lysates were incubated with 20 μg of PAK-p21 binding domain (PBD) beads and 1× of the manufacturer's protease inhibitor cocktail in a total volume of 1 mL and were incubated at 4°C on a rocker for 1 h. The beads were then pelleted by centrifugation and washed thrice with the manufacturer's 1× wash buffer, after which they were resuspended in Laemmli buffer and subjected to SDS-PAGE and Western blotting analysis. Membrane blots were incubated with the manufacturer's antibody raised against Rac and antibody binding was detected as described before.

Transfection of cells with siRNA and plasmids. siRNAs against Rac1 and PAK1 were synthesized by a proprietary design as SMARTpool siRNA, which consists of four pooled SMARTselection-designed siRNAs that are 21 nucleotides forming a 19-bp duplex core with symmetrical two nucleotide 3′-UU overhangs (Dharmacon, Inc.). Cells were electroporated with the siRNAs and plasmids as previously described (23). Briefly, 1.2×10^6 cells were reconstituted in 100 μL of electroporation transfection solution or Nucleofector Solution V from Cell Line Nucleofection Kit V (Amaxa Biosystems). siCONTROL or siGenome SMARTpool siRNA against Rac1 and PAK1 was added to the cells at a final concentration of 200 pmol per sample, and the mixtures were transferred to electroporation cuvettes and subjected to electroporation according to the manufacturer's programs and instructions. The electroporated and transfected cell suspensions were

immediately mixed with 500 μL of prewarmed RPMI medium supplemented with 5% fetal bovine serum (FBS). The cells were then transferred to six-well plates for Western blot analysis or to 24-well plates for measurement of ROS levels containing prewarmed DMEM/F12 medium supplemented with 5% FBS. Cells were incubated for 24 h, after which they were incubated in serum-free medium for another 24 h before treatment with 4HPR. Cells were also electroporated with the expression vector encoding the mutant Rac, RacV12, and were subjected to analysis in the same manner as described above following transfection with siRNAs.

Results

Activation of Rac in HNSCC cells by 4HPR. Treatment of UMSCC-22B HNSCC cells with 4HPR increased the amount of GTP-Rac compared with control cells (Fig. 1*A*). This effect was inhibited by pretreating the cells with NSC-23766, a Rac GTPase inhibitor that targets Rac activation by guanine nucleotide exchange factors (Fig. 1*A*; ref. 33). These results indicate that Rac is activated by 4HPR.

Inhibition of 4HPR-induced apoptosis by suppression of Rac expression or activity. 4HPR induced apoptosis in UMSCC-22B cells as indicated by increased PARP cleavage (Fig. 1*B*) and percentage of Annexin V–positive cells. This effect was suppressed by inhibition of Rac with NSC-23766 (Fig. 1*B*). Because up-regulation and phosphorylation of c-Jun by JNK (21) and up-regulation of HSPA1A/HSP70 (23) were found to be important for apoptosis induction by 4HPR, we examined whether they are affected by inhibition of Rac before exposure to 4HPR. Pretreatment of the cells with NSC-23766 decreased both phosphorylated and total levels of c-Jun, as well as HSPA1A levels, profoundly (Fig. 1*B*), suggesting that Rac is upstream of these changes. Further support for this conclusion has come from targeting Rac1 expression by RNA interference, which diminished the level of Rac1 (Fig. 1*C*) and decreased 4HPR-induced up-regulation of HSPA1A and PARP cleavage (Fig. 1*D*). These results showed that Rac activation contributes to 4HPR-induced apoptosis and Rac is upstream of JNK activation and HSPA1A induction.

Induction of ROS by 4HPR is downstream of Rac activation. Our group has previously shown that 4HPR induces ROS increase, which is abrogated by cotreatment of cells with the antioxidant

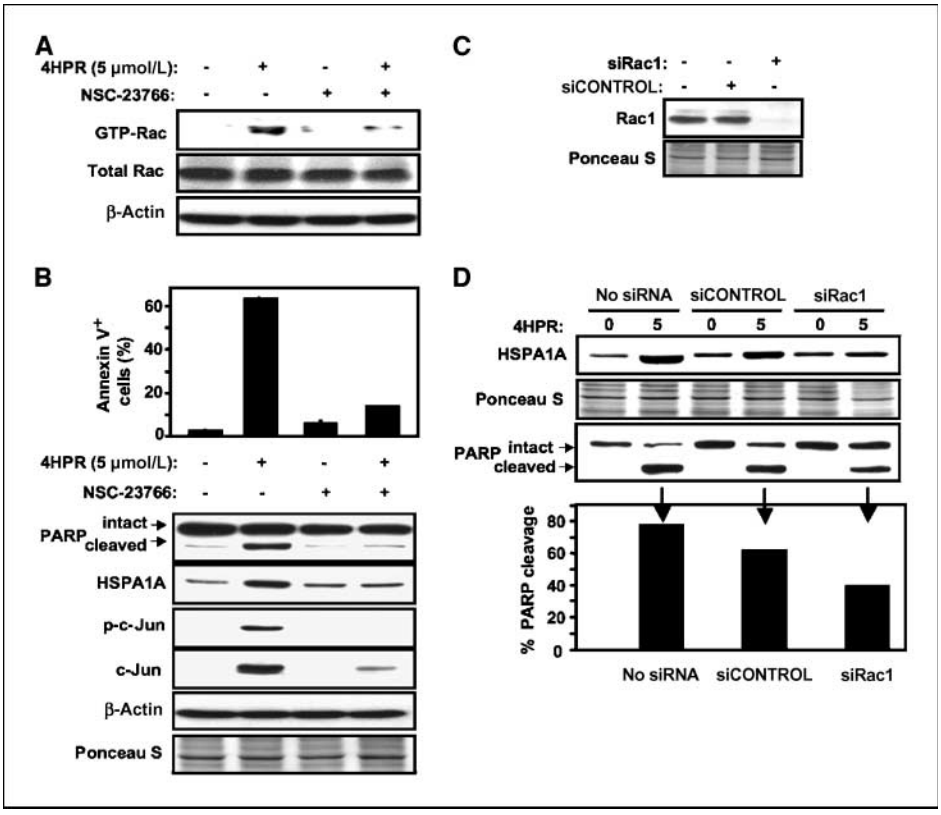


Figure 1. Apoptosis induction by 4HPR in HNSCC cells mediated by Rac activation. *A,* UMSCC-22B cells were seeded at 1×10^6 per dish in a series of 10-cm dishes for 24 h. The cells were then incubated in serum-free medium for another 24 h before overnight pretreatment with the Rac inhibitor NSC-23766 (60 μmol/L). The cells were then incubated for 5 min in medium containing either DMSO (control) or 5 μmol/L 4HPR, harvested, and then scraped into lysis buffer. The cell lysates were processed for assessment of activated Rac (GTP-Rac) levels as described in Materials and Methods. Material adsorbed to PBD beads was analyzed by immunoblotting with anti-GTP-Rac antibodies after SDS-PAGE and samples of the nonadsorbed material were also analyzed by immunoblotting for total Rac levels and β-actin. *B,* cells seeded as in *A* were used for Rac inhibition by pretreating them with 60 μmol/L NSC-23766 overnight before incubation in medium containing DMSO, 60 μmol/L NSC-23766, 5 μmol/L 4HPR alone, or a combination of both NSC-23766 and 4HPR for 24 h. Cells were then harvested and used to extract total protein fraction. Samples of these extracts were subjected to immunoblotting analysis to assess PARP cleavage, HSPA1A levels, and total and phosphorylated levels of c-Jun. Membrane blots were probed with β-actin and stained with the dye Ponceau S to assess for equality of protein loading in the different lanes. Similarly treated cells were also subjected to analysis of Annexin V–positive cells as described in Materials and Methods. *Columns,* mean of two duplicate measurements; *bars,* SE. *C,* Western blot analysis depicting the effect of RNA interference on Rac1 protein levels. UMSCC-22B cells were transfected with siCONTROL or siRNA targeting Rac1 (*siRac1*) as described in Materials and Methods. Two days later, cells were harvested and used to extract total protein fraction. Samples of these extracts were subjected to Western blot analysis with anti-Rac1 antibody. Membrane blots were stained with the dye Ponceau S to compare protein loading in the different lanes. *D,* UMSCC-22B cells were transfected with siCONTROL and siRNA against Rac1, as described in Materials and Methods, and then transferred to six-well plates. After 24 h, cells were maintained in serum-free medium for another 24 h before treatment with 5 μmol/L 4HPR. Total protein lysates of these samples were prepared following 4HPR treatment and subjected to immunoblotting to assess PARP cleavage and HSPA1A levels. Membrane blots were stained with Ponceau S to compare loading in the different lanes.

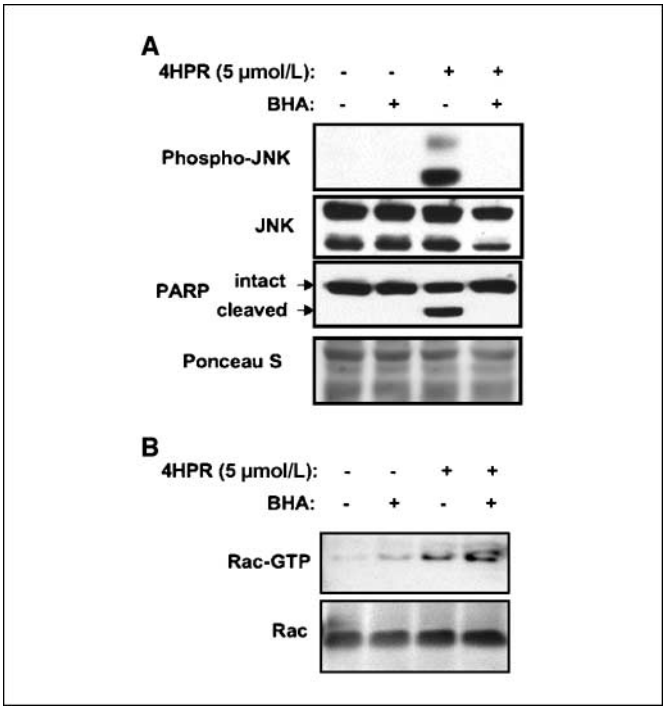


Figure 2. Induction of apoptosis by 4HPR involves sequential activation of Rac, increase in ROS, and JNK activation. *A,* cells were seeded as in Fig.1*A*, and, 24 h after exposure to 4HPR in the presence or absence of *tert*-butyl hydroxyl anisole (*BHA*), were harvested and used to extract total protein fraction. Samples of these extracts were analyzed by immunoblotting for PARP cleavage, as well as total and phosphorylated levels of JNK. Membrane blots were stained with the dye Ponceau S to assess for equality of protein loading in the different lanes. *B,* UMSCC-22B cells were seeded at 1×10^6 per dish in a series of 10-cm dishes for 24 h. The cells were then incubated in serum-free medium for another 24 h. The cells were then incubated in medium containing DMSO (control), 50 μmol/L BHA, 5 μmol/L 4HPR, or both 5 μmol/L 4HPR and 50 μmol/L BHA for 5 min, harvested, and then scraped into lysis buffer. The cell lysates were processed for assessment of activated Rac or GTP-Rac levels as described in Materials and Methods. Protein samples were also resolved on SDS-PAGE before incubation with PBD beads for analysis of total Rac levels.

tert-butyl hydroxyl anisole (13). *tert*-Butyl hydroxyl anisole suppressed 4HPR-induced JNK activation and PARP cleavage, indicating the importance of ROS in 4HPR-induced apoptosis and placing JNK activation downstream of ROS (Fig. 2*A*). In contrast, ROS scavenging by *tert*-butyl hydroxyl anisole failed to inhibit Rac activation by 4HPR (Fig. 2*B*). These results indicate that in 4HPR-treated cells, Rac activation is upstream of ROS generation.

Suppression of ROS induction by 4HPR by the Rac inhibitor NSC-23766. The findings that the Rac inhibitor NSC-23766 compromised the ability of 4HPR to induce apoptosis and that ROS generation was required for 4HPR-induced apoptosis and was downstream of Rac activation prompted us to examine the possibility that Rac activation by 4HPR is important for ROS generation. Pretreatment of cells overnight decreased ROS generation by 4HPR in a Rac inhibitor dose–dependent manner (Fig. 3*A*). A 4-hour pretreatment with NSC-23766 was also effective albeit less than the longer pretreatment (data not shown). In contrast, the Rac inhibitor (overnight pretreatment schedule) did not decrease the high level of ROS measured in cells incubated with 0.1% hydrogen peroxide (Fig. 3*B*), excluding the possibility that NSC-23766 acts as an oxygen scavenger and leading to the conclusion that Rac acts upstream of ROS generation. Similarly to the effects in HNSCC UMSCC-22B cells, pretreatment with the Rac inhibitor suppressed ROS induction by 4HPR in bronchioalveolar cancer H522 cells and cervical cancer C33A cells (Fig. 3*C*).

siRNA-mediated knockdown of either Rac1 or its downstream effector kinase PAK1 decreased 4HPR-induced ROS generation. Targeting Rac1 expression with siRNA, which has been shown to down-regulate Rac1 (Fig. 1*C*), suppressed the induction of ROS generation by 4HPR in HNSCC cells (UMSCC-22B and DM14) and bronchioalveolar cancer cells (H522) by ~50% (Fig. 4*A*). To determine whether the established Rac signaling pathway is involved in ROS generation, we interfered with expression of PAK1, the downstream effector kinase of Rac signaling (34). Transfection of UMSCC-22B cells with siRNA targeting PAK1 reduced PAK1 expression (Fig. 4*B*) and decreased ROS generation by 4HPR in both UMSCC-22B and DM14 HNSCC cells relative to cells transfected with control siRNA (Fig. 4*C*).

Expression of a constitutively active RacV12 increased ROS generation and cell growth inhibition in HNSCC cells. Because we have shown that activation of Rac by 4HPR is important for ROS generation and apoptosis induction, we hypothesized that expression of RacV12, a constitutively active mutant form of Rac, will emulate the effects of 4HPR. The expression of RacV12 was confirmed by the differential detection of the Myc tag by Western blotting (Fig. 5*B*). RacV12 expression has led to a small increase in ROS (Fig. 5*A*) and a modest but reproducible increase in PARP cleavage (Fig. 5*B*). Moreover, RacV12 increased the sensitivity of cells to 4HPR-induced ROS and apoptosis, evident in the increased PARP cleavage in 4HPR-treated RacV12-expressing cells compared with control plasmid–transfected treated cells (Fig. 5*A* and *B*). In addition, expression of RacV12 inhibited colony formation by HNSCC cells compared with cells that were either nontransfected or transfected with a control plasmid (Fig. 5*C* and *D*).

4HPR induced higher levels of Rac activation, ROS, and cell growth inhibition in metastatic cancer cells compared with their primary cancer cell counterparts. Our finding that 4HPR can induce apoptosis by activating Rac and increasing ROS in cancer cells raised the question on whether metastatic cells are partially resistant to 4HPR because they are known to have elevated levels of both Rac and ROS, which are important for their proliferation, growth, and migration (35–37). Therefore, we compared and contrasted the effects of 4HPR on pairs of cell lines derived from primary and metastatic cancers (UMSCC-22A and UMSCC-22B, respectively) or selected *in vivo* for enhanced metastasis from less metastatic cells (DM14/Tu167-C2 and B16 F10/F1). 4HPR induced higher Rac activation in the metastatic DM14 HNSCC cancer cells relative to the primary cancer Tu167-C2 cells, evidenced by the increased Rac-GTP levels in DM14 cells (Fig. 6*A*). Interestingly, 4HPR induced higher levels of ROS in DM14 and B16-F10 cells compared with their primary cancer cell counterparts, Tu167-C2 and B16-F1 (Fig. 6*B*). ROS levels in all of these cell lines were inhibited by cotreatment of cells with the Rac inhibitor. The increase in ROS levels in 4HPR-treated cells correlated with increased cell growth inhibition in the metastatic cancer cells compared with their corresponding primary cancer cells (Fig. 6*C*). The growth inhibitory effect of 4HPR was decreased by cotreatment of cells with the Rac inhibitor NSC-23766 (Fig. 6*D*).

Discussion

Several groups including our own have shown that 4HPR generates ROS and that this effect is important for apoptosis

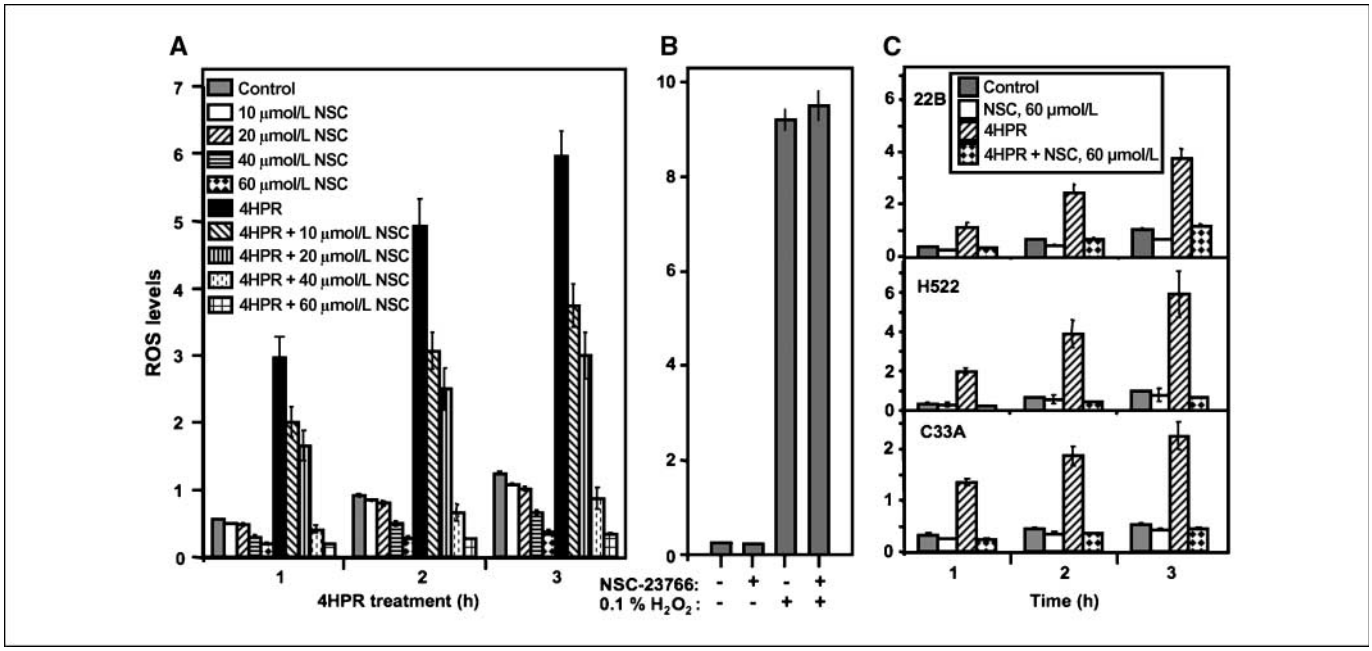


Figure 3. Decrease in 4HPR-induced ROS generation by Rac inhibition. *A,* UMSCC-22B cells were seeded at a density of 8×10^4 per well in 24-well plates for 24 h, after which they were switched to serum-free medium alone or containing the different indicated doses of the Rac inhibitor NSC-23766 and incubated overnight. The next day, ROS levels in the different experimental conditions were then assessed as described in Materials and Methods. Each treatment was done in four replicate wells. *Columns,* mean; *bars,* SE. *B,* UMSCC-22B cells were seeded in 24-well plates at a density of 8×10^4 per well for 24 h, after which they were switched to serum-free medium alone or containing 60 μmol/L NSC-23766 and incubated overnight. The cells were then washed twice with prewarmed Krebs-Ringer buffer and then incubated in the same buffer containing 10 μg/mL DCFH-DA with DMSO (control), 60 μmol/L NSC-23766, 0.1% hydrogen peroxide, or a combination of both NSC-23766 and hydrogen peroxide. ROS levels were then assessed as indicated in *A. C,* HNSCC UMSCC-22B cells, bronchioalveolar cancer H522 cells, and cervical cancer C33A cells were seeded at a density of 8×10^4 per well in 24-well plates for 24 h, after which they were switched to serum-free medium alone or containing 60 μmol/L NSC-23766 and incubated overnight. ROS levels were then assessed as described in Materials and Methods.

induction (12, 13). Various effects of 4HPR leading to apoptosis seem to be downstream of ROS induction, including activation of MAPKs (21). However, little is known about events or mechanisms by which 4HPR increases ROS generation. Although activation of the small GTPase Rac is often associated with cancer progression (36, 37), it also functions as a catalytic subunit of NADPH oxidase leading to ROS generation (24, 38) and has been implicated in apoptosis induction (39). Therefore, we hypothesized that Rac plays a role in 4HPR-induced ROS generation and subsequent apoptosis. Indeed, in this study, we present for the first time evidence that pinpoints to a novel role of Rac activation in 4HPR-induced ROS generation and subsequent apoptosis. Different experimental approaches provided this evidence. Chemical inhibition of the function of Rac or siRNA-mediated silencing of its expression resulted in decreased ROS generation. In addition, siRNA-mediated targeting of the downstream Rac effector kinase PAK1 has led to a decrease in ROS generation by 4HPR. All of these changes in Rac were associated with modulation of 4HPR-induced apoptosis. Furthermore, expression of the constitutively active Rac mutant RacV12 alone inhibited the growth of human head and neck cancer cells and sensitized them to 4HPR-induced ROS generation and apoptosis.

The finding that ROS generated following Rac activation can cause apoptosis, as shown in 4HPR-treated cells, is novel because the previous studies implicating Rac in apoptosis induction by bufalin and capsaicin did not explore the possible involvement of Rac-mediated ROS generation in this effect (39, 40).

The JNK MAPK is involved in c-Jun phosphorylation and activation as well as expression (41). In this study, we showed that inhibition of Rac activation by cotreating cells with 4HPR and a Rac inhibitor abrogated both 4HPR-induced c-Jun phosphorylation and expression, supporting the conclusion that Rac is involved in JNK activation. Interestingly, Rac has previously been shown to selectively activate JNK as well as c-Jun transcriptional activity (41). However, in this study, we also showed that ROS elevation in 4HPR-treated cells leads to sustained JNK activation and apoptosis evidenced by PARP cleavage, both of which were abrogated following scavenging of 4HPR-induced ROS by *tert*-butyl hydroxyl anisole. Moreover, we have shown that this ROS increase by 4HPR is downstream and dependent on Rac activation by 4HPR. These findings indicate that ROS generation induced by Rac activation mediates 4HPR-induced apoptosis and not other signaling mechanisms possibly initiated by Rac activation alone.

In an attempt to elucidate the mechanism of Rac activation by 4HPR, we targeted signaling pathways that have been shown to activate Rac. For example, we inhibited epidermal growth factor signaling with the irreversible tyrosine kinase inhibitor EKB569 (42) and the phosphatidylinositol 3-kinase inhibitor LY129004 (43) and found no change in ROS generation by 4HPR in UMSCC-22B HNSCC cells (data not shown). Further studies are needed to determine how 4HPR activates Rac.

It is has been shown that transformed cells exhibit higher basal ROS levels compared with nontransformed cells. The higher ROS level is thought to be essential for stimulation of cell growth and sustenance of high metabolic rates in transformed cells (44). Furthermore, metastatic cells also exhibit high levels of ROS thought to be important for their growth and progression (37). In addition, elevated ROS levels confer a growth advantage to cells by activation of several mitogenic signaling pathways (45). We thought it plausible that elevated ROS levels, although capable of inducing

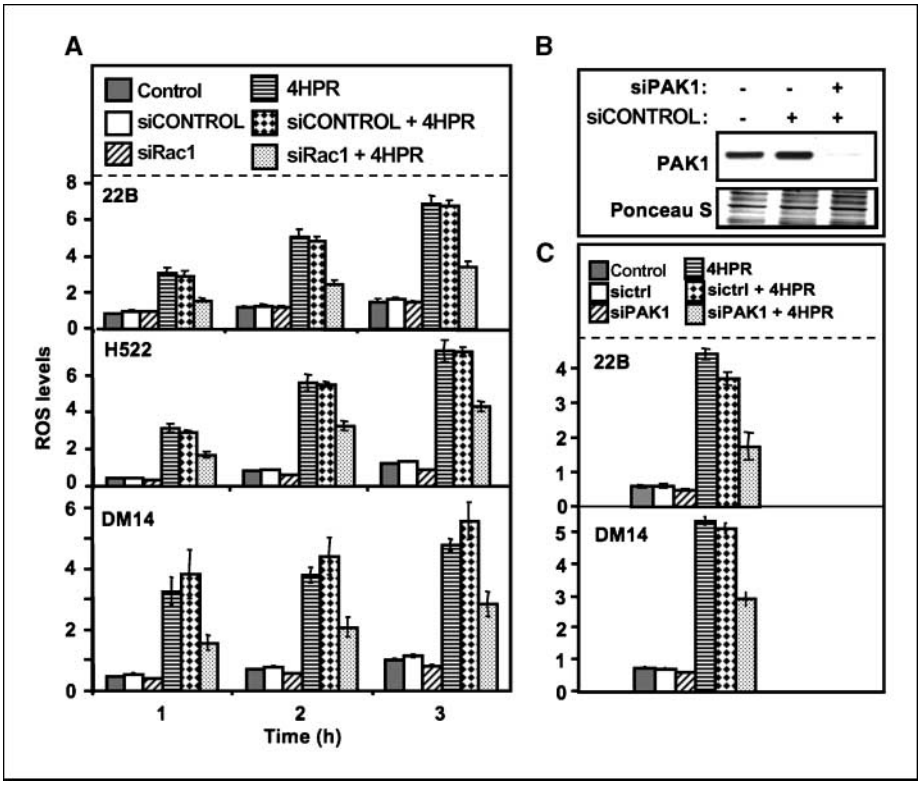


Figure 4. Decrease in 4HPR-induced ROS generation by siRNA-mediated knockdown of Rac1 or of its effector kinase, PAK1. *A,* UMSCC-22B, DM14, and H522 cells were transfected with siCONTROL or Rac1-specific siRNA, as described in Materials and Methods, and then transferred to 24-well plates. The following day, cells were switched to serum-free medium in which they were incubated overnight before assessment of induction of ROS generation by 4HPR as described in Materials and Methods. *B,* Western blot analysis of cells transfected with either siCONTROL siRNA against PAK1 (*siPAK1*) showing efficacy of the siRNA on PAK1 protein levels. *C,* UMSCC-22B cells were transfected with siCONTROL or siRNA targeting PAK1 as described in Materials and Methods. Cells were then transferred to 24-well plates for assessment of ROS generation by 4HPR as previously mentioned.

apoptosis, can still instigate growth-promoting signals in the metastatic UMSCC-22B HNSCC cells we used in this study. We compared levels of ROS generation and cell growth inhibition by 4HPR in isogenic pairs of primary and metastatic cancer cells. Interestingly, 4HPR led to increased ROS generation, which correlated with increased cell growth inhibition in the metastatic cancer cells compared with their corresponding primary cancer cells. Moreover, Rac, which we also found in this report to be important for ROS generation by 4HPR, was activated by 4HPR to higher levels in the DM14 metastatic cancer cells compared with their corresponding Tu167-C2 primary cancer cells. It is worthwhile to note that in one report, β-phenylethyl isothiocyanate was shown to selectively kill oncogenically transformed cells through a ROS-dependent mechanism (46).

Rac plays crucial roles in migration and invasion, which are important steps in the metastasis process of cancer cells to near or

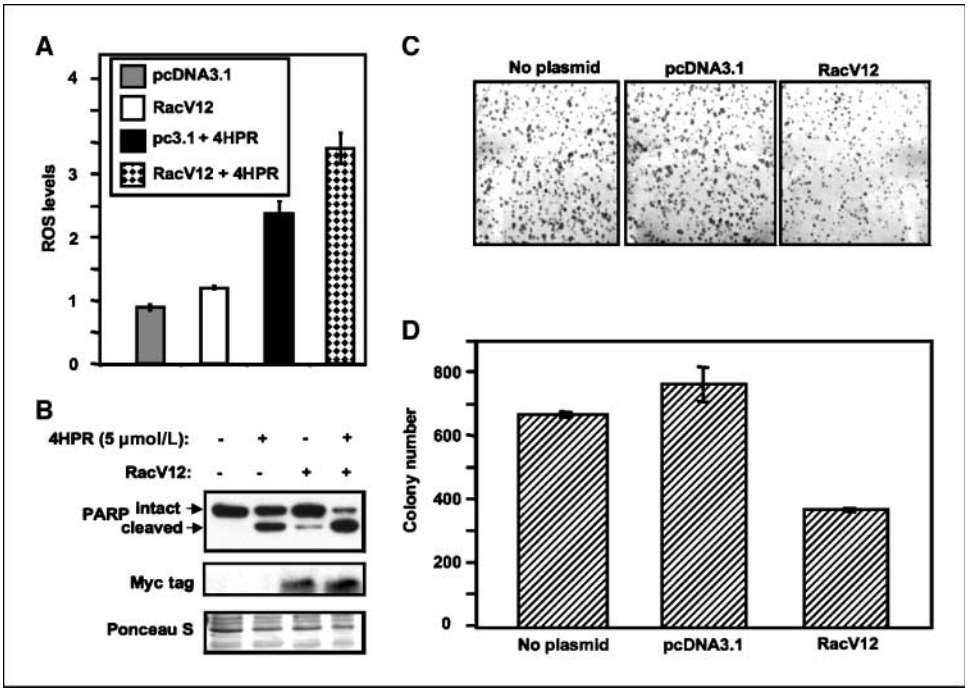


Figure 5. Increased ROS generation, PARP cleavage, and decreased colony growth and formation by expression of the mutant and constitutively active RacV12. UMSCC-22B cells were transfected with an expression vector encoding the constitutive active mutant form of Rac, RacV12, or with pcDNA3.1 (control) as described in Materials and Methods. Cells were then transferred to 24-well plates for assessment of ROS generation by RacV12 and/or 4HPR, as previously described (*A*), or to six-well plates for preparation of protein samples for Western blot analysis of PARP cleavage (*B*). *C,* UMSCC-22B cells were transfected as in *A* and seeded at a cell density of 5×10^3 per well in duplicates in six-well plates for assessment of cell colony formation and growth. Cells were maintained in culture following transfection for 10 d, after which they were washed with PBS, fixed, and stained with crystal violet. *D, columns,* mean number of cell colonies from replicate measurements; *bars,* SE.

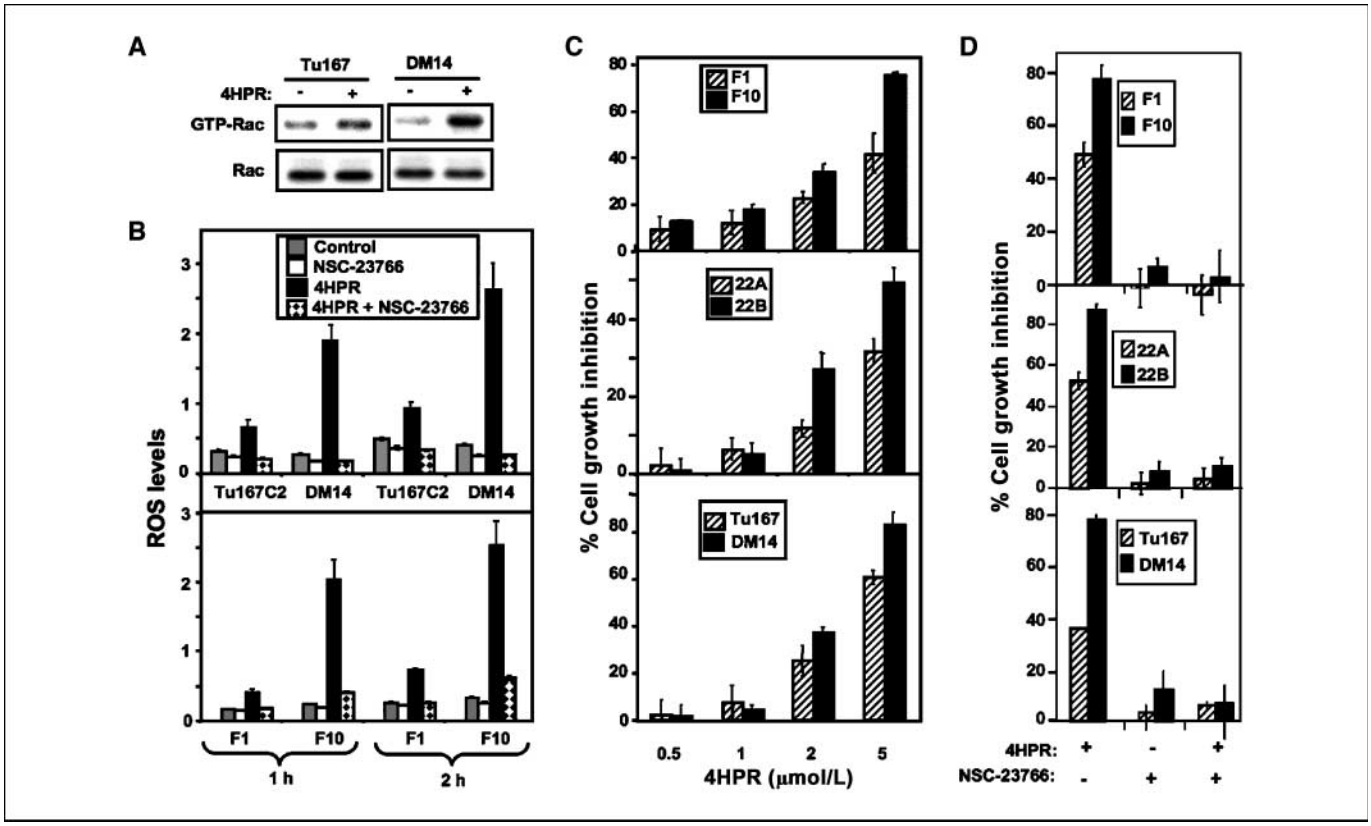


Figure 6. Increased ROS generation, Rac activation, and cell growth inhibition by 4HPR in metastatic cancer cells compared with their corresponding primary cancer cells. *A,* Tu167-C2 and DM14 cells were equally seeded in 10-cm dishes. After 24 h, the cells were incubated in serum-free medium for at least 24 h. At 5 min after incubation of cells in medium containing either DMSO (control) or 5 μmol/L 4HPR, cells were harvested and scraped into lysis buffer and lysates were processed for assessment of activated Rac or GTP-Rac levels as described in Materials and Methods. Protein samples were also resolved on SDS-PAGE before incubation with PBD beads for analysis of total Rac levels. *B,* the metastatic cancer DM14 cells and murine melanoma B16-F10 and their corresponding primary cancer cells, Tu167-C2 and B16-F1, were equally seeded in 24-well plates at the same time. After 24 h, the cells were switched to serum-free medium alone or containing 60 μmol/L NSC-23766 and incubated overnight. ROS levels were then assessed as described in Materials and Methods. The metastatic cancer cells, UMSCC-22B, DM14, and B16-F10, along with their corresponding primary cancer cells, UMSCC-22A, Tu167-C2, and B16-F1, respectively, were seeded in 96-well plates at a seeding density of 10^4 per well for analysis of cell growth inhibition by 4HPR. After 24 h, cells were gently washed with PBS and switched to serum-free medium containing the different indicated doses of 4HPR (*C*) or 5 μmol/L 4HPR in the presence or absence of 60 μmol/L NSC-23766 (*D*). After 48 h, cells were fixed and stained with sulforhodamine B, and absorbance readings quantified. *Columns,* mean of four replicate measurements; *bars,* SE.

distant tissues and organs (35). Interestingly, Ferraro and colleagues (47) have shown that endogenous ROS levels are higher in the B16-F10 metastatic cells compared with the B16-F1 murine melanoma cells due to increased Rac1 activation. Nonetheless, our findings show that the activation of a protein involved in cancer promotion, such as Rac, may still lead to cell death in conjunction with 4HPR treatment because the metastatic cells showed an augmented activation of Rac by 4HPR, which resulted in the generation of higher ROS levels and enhanced apoptosis.

In conclusion, we have shown that Rac activation by 4HPR precedes ROS generation and is required for cell death induction by the proapoptotic 4HPR and that metastatic cancer cells exhibit increased sensitivity to 4HPR because of higher Rac activation in these cells compared with their primary isogenic cancer cell counterparts. Moreover, our findings support the use of the ROS-generating and promising anticancer agent 4HPR against metastatic cancer cells.

Disclosure of Potential Conflicts of Interest

No potential conflicts of interest were disclosed.

Acknowledgments

Received 1/3/2008; revised 2/28/2008; accepted 3/26/2008.

Grant support: NIH Head and Neck Cancer Specialized Program in Research Excellence grant P50 CA907007 (W.K. Hong and R. Lotan) and by the Irving and Nadine Mansfield and Robert David Levitt Cancer Research Chair (R. Lotan).

The costs of publication of this article were defrayed in part by the payment of page charges. This article must therefore be hereby marked *advertisement* in accordance with 18 U.S.C. Section 1734 solely to indicate this fact.

We thank Dr. Kaikobad Irani for the RacV12 expression vector, and Wendy Schober for assistance with flow cytometry analysis.

References

1. Fesik SW. Promoting apoptosis as a strategy for cancer drug discovery. Nat Rev Cancer 2005;5:876–85.
2. Hanahan D, Weinberg RA. The hallmarks of cancer. Cell 2000;100:57–70.
3. Hail N, Jr., Kim HJ, Lotan R. Mechanisms of fenretinide-induced apoptosis. Apoptosis 2006;11:1677–94.
4. Sun SY, Hail N, Jr., Lotan R. Apoptosis as a novel target for cancer chemoprevention. J Natl Cancer Inst 2004;96:662–72.
5. Moon RC, Thompson HJ, Becci PJ, et al. *N*-(4-Hydroxyphenyl)retinamide, a new retinoid for prevention of breast cancer in the rat. Cancer Res 1979;39:1339–46.
6. Sporn MB, Newton DL. Chemoprevention of cancer with retinoids. Fed Proc 1979;38:2528–34.

7. Malone W, Perloff M, Crowell J, Sigman CHigley H. Fenretinide: a prototype cancer prevention drug. Expert Opin Investig Drugs 2003;12:1829–42.
8. Chiesa F, Tradati N, Grigolato R, et al. Randomized trial of fenretinide (4-HPR) to prevent recurrences, new localizations and carcinomas in patients operated on for oral leukoplakia: long-term results. Int J Cancer 2005; 115:625–9.
9. Lippman SM, Lee JJ, Martin JW, et al. Fenretinide activity in retinoid-resistant oral leukoplakia. Clin Cancer Res 2006;12:3109–14.
10. Veronesi U, Mariani L, Decensi A, et al. Fifteen-year results of a randomized phase III trial of fenretinide to prevent second breast cancer. Ann Oncol 2006;17: 1065–71.
11. Bast RC, Jr., Brewer M, Zou C, et al. Prevention and early detection of ovarian cancer: mission impossible? Recent Results Cancer Res 2007;174:91–100.
12. Sun SY, Li W, Yue P, et al. Mediation of *N*-(4-hydoxyphenyl)retinamide-induced apoptosis in human cancer cells by different mechanisms. Cancer Res 1999; 59:2493–8.
13. Maurer BJ, Metelitsa LS, Seeger RC, Cabot MC, Reynolds CP. Increase of ceramide and induction of mixed apoptosis/necrosis by *N*-(4-hydroxyphenyl)-retinamide in neuroblastoma cell lines. J Natl Cancer Inst 1999;91:1138–46.
14. Hail N, Jr., Lotan R. Mitochondrial permeability transition is a central coordinating event in *N*-(4-hydroxyphenyl)retinamide-induced apoptosis. Cancer Epidemiol Biomarkers Prev 2000;9:1293–301.
15. Lovat PE, Oliverio S, Ranalli M, et al. GADD153 and 12-lipoxygenase mediate fenretinide-induced apoptosis of neuroblastoma. Cancer Res 2002;62:5158–67.
16. Simeone AM, Ekmekcioglu S, Broemeling LD, Grimm EA, Tari AM. A novel mechanism by which *N*-(4-hydroxyphenyl)retinamide inhibits breast cancer cell growth: the production of nitric oxide. Mol Cancer Ther 2002;1:1009–17.
17. Asumendi A, Morales MC, Alvarez A, Arechaga J, Perez-Yarza G. Implication of mitochondria-derived ROS and cardiolipin peroxidation in *N*-(4-hydroxyphenyl)retinamide-induced apoptosis. Br J Cancer 2002;86: 1951–6.
18. Delia D, Aiello A, Meroni L, et al. Role of antioxidants and intracellular free radicals in retinamide-induced cell death. Carcinogenesis 1997;18:943–8.
19. Hail N, Jr., Lotan R. Mitochondrial respiration is uniquely associated with the prooxidant and apoptotic effects of *N*-(4-hydroxyphenyl)retinamide. J Biol Chem 2001;276:45614–21.
20. Chen YR, Zhou G, Tan TH. c-Jun N-terminal kinase mediates apoptotic signaling induced by *N*-(4-hydroxyphenyl)retinamide. Mol Pharmacol 1999;56:1271–9.
21. Kim HJ, Chakravarti N, Oridate N, et al. *N*-(4-Hydroxyphenyl)retinamide-induced apoptosis triggered by reactive oxygen species is mediated by activation of MAPKs in head and neck squamous carcinoma cells. Oncogene 2006;25:2785–94.
22. Osone S, Hosoi H, Kuwahara Y, et al. Fenretinide induces sustained-activation of JNK/p38 MAPK and apoptosis in a reactive oxygen species-dependent manner in neuroblastoma cells. Int J Cancer 2004;112: 219–24.
23. Kadara H, Lacroix L, Lotan D, Lotan R. Induction of endoplasmic reticulum stress by the pro-apoptotic retinoid *N*-(4-hydroxyphenyl)retinamide via a reactive oxygen species-dependent mechanism in human head and neck cancer cells. Cancer Biol Ther 2007;6:705–11.
24. Lambeth JD. NOX enzymes and the biology of reactive oxygen. Nat Rev Immunol 2004;4:181–9.
25. Babior BM. NADPH oxidase: an update. Blood 1999; 93:1464–76.
26. De Leo FR, Ulman KV, Davis AR, Jutila KL, Quinn MT. Assembly of the human neutrophil NADPH oxidase involves binding of p67phox and flavocytochrome *b* to a common functional domain in p47phox. J Biol Chem 1996;271:17013–20.
27. Hwang JJ, Choi SY, Koh JY. The role of NADPH oxidase, neuronal nitric oxide synthase and poly(ADP ribose) polymerase in oxidative neuronal death induced in cortical cultures by brain-derived neurotrophic factor and neurotrophin-4/5. J Neurochem 2002;82:894–902.
28. Lee TK, Poon RT, Yuen AP, et al. Rac activation is associated with hepatocellular carcinoma metastasis by up-regulation of vascular endothelial growth factor expression. Clin Cancer Res 2006;12:5082–9.
29. Lee YS, Kang YS, Lee SH, Kim JA. Role of NAD(P)H oxidase in the tamoxifen-induced generation of reactive oxygen species and apoptosis in HepG2 human hepatoblastoma cells. Cell Death Differ 2000;7:925–32.
30. Tammariello SP, Quinn MT, Estus S. NADPH oxidase contributes directly to oxidative stress and apoptosis in nerve growth factor-deprived sympathetic neurons. J Neurosci 2000;20:RC53.
31. Suzuki S, Higuchi M, Proske RJ, et al. Implication of mitochondria-derived reactive oxygen species, cytochrome C and caspase-3 in *N*-(4-hydroxyphenyl)retinamide-induced apoptosis in cervical carcinoma cells. Oncogene 1999;18:6380–7.
32. Sun SY, Yue P, Dawson MI, et al. Differential effects of synthetic nuclear retinoid receptor-selective retinoids on the growth of human non-small cell lung carcinoma cells. Cancer Res 1997;57:4931–9.
33. Gao Y, Dickerson JB, Guo F, Zheng J, Zheng Y. Rational design and characterization of a Rac GTPase-specific small molecule inhibitor. Proc Natl Acad Sci U S A 2004;101:7618–23.
34. Kumar R, Gururaj AE, Barnes CJ. p21-activated kinases in cancer. Nat Rev Cancer 2006;6:459–71.
35. Chan AY, Coniglio SJ, Chuang YY, et al. Roles of the Rac1 and Rac3 GTPases in human tumor cell invasion. Oncogene 2005;24:7821–9.
36. Rassool FV, Gaymes TJ, Omidvar N, et al. Reactive oxygen species, DNA damage, and error-prone repair: a model for genomic instability with progression in myeloid leukemia? Cancer Res 2007;67:8762–71.
37. Wu WS. The signaling mechanism of ROS in tumor progression. Cancer Metastasis Rev 2006;25:695–705.
38. Cheng G, Diebold BA, Hughes Y, Lambeth JD. Nox1-dependent reactive oxygen generation is regulated by Rac1. J Biol Chem 2006;281:17718–26.
39. Kawazoe N, Watabe M, Masuda Y, Nakajo S, Nakaya K. Tiam1 is involved in the regulation of bufalin-induced apoptosis in human leukemia cells. Oncogene 1999;18: 2413–21.
40. Kim S, Moon A. Capsaicin-induced apoptosis of H-ras-transformed human breast epithelial cells is Rac-dependent via ROS generation. Arch Pharm Res 2004;27: 845–9.
41. Minden A, Lin A, Claret FX, Abo A, Karin M. Selective activation of the JNK signaling cascade and c-Jun transcriptional activity by the small GTPases Rac and Cdc42Hs. Cell 1995;81:1147–57.
42. Yoshimura N, Kudoh S, Kimura T, et al. EKB-569, a new irreversible epidermal growth factor receptor tyrosine kinase inhibitor, with clinical activity in patients with non-small cell lung cancer with acquired resistance to gefitinib. Lung Cancer 2006;51:363–8.
43. Vlahos CJ, Matter WF, Hui KY, Brown RF. A specific inhibitor of phosphatidylinositol 3-kinase, 2-(4-morpholinyl)-8-phenyl-4*H*-1-benzopyran-4-one (LY294002). J Biol Chem 1994;269:5241–8.
44. Schimmel M, Bauer G. Proapoptotic and redox state-related signaling of reactive oxygen species generated by transformed fibroblasts. Oncogene 2002;21:5886–96.
45. Benhar M, Engelberg D, Levitzki A. ROS, stress-activated kinases and stress signaling in cancer. EMBO Rep 2002;3:420–5.
46. Trachootham D, Zhou Y, Zhang H, et al. Selective killing of oncogenically transformed cells through a ROS-mediated mechanism by β-phenylethyl isothiocyanate. Cancer Cell 2006;10:241–52.
47. Ferraro D, Corso S, Fasano E, et al. Pro-metastatic signaling by c-Met through RAC-1 and reactive oxygen species (ROS). Oncogene 2006;25:3689–98.

Phase I Study of the Farnesyltransferase Inhibitor Lonafarnib with Paclitaxel in Solid Tumors

Fadlo R. Khuri,[1] Bonnie S. Glisson,[2] Edward S. Kim,[2] Paul Statkevich,[3] Peter F. Thall,[2] Michael L. Meyers,[3] Roy S. Herbst,[2] Reginald F. Munden,[2] Craig Tendler,[3] Yali Zhu,[3] Sandra Bangert,[2] Elizabeth Thompson,[2] Charles Lu,[2] Xue-Mei Wang,[2] Dong M. Shin,[2] Merrill S. Kies,[2] Vali Papadimitrakopoulou,[2] Frank V. Fossella,[2] Paul Kirschmeier,[3] W. Robert Bishop,[3] and Waun Ki Hong[2]

[1]Winship Cancer Institute, Emory University, Atlanta, Georgia; [2]The University of Texas M. D. Anderson Cancer Center, Houston, Texas; and [3]Schering-Plough Research Institute, Kenilworth, New Jersey

ABSTRACT

Purpose: **To establish the maximum tolerated dose of lonafarnib, a novel farnesyltransferase inhibitor, in combination with paclitaxel in patients with solid tumors and to characterize the safety, tolerability, dose-limiting toxicity, and pharmacokinetics of this combination regimen.**

Experimental Design: **In a Phase I trial, lonafarnib was administered p.o., twice daily (b.i.d.) on continuously scheduled doses of 100 mg, 125 mg, and 150 mg in combination with i.v. paclitaxel at doses of 135 mg/m^2 or 175 mg/m^2 administered over 3 h on day 8 of every 21-day cycle. Plasma paclitaxel and lonafarnib concentrations were collected at selected time points from each patient.**

Results: **Twenty-four patients were enrolled; 21 patients were evaluable. The principal grade 3/4 toxicity was diarrhea (5 of 21 patients), which was most likely due to lonafarnib. dose-limiting toxicities included grade 3 hyperbilirubinemia at dose level 3 (100 mg b.i.d. lonafarnib and 175 mg/m^2 paclitaxel); grade 4 diarrhea and grade 3 peripheral neuropathy at dose level 3A (125 mg b.i.d. lonafarnib and 175 mg/m^2 paclitaxel); and grade 4 neutropenia with fever and grade 4 diarrhea at level 4 (150 mg b.i.d. lonafarnib and 175 mg/m^2 paclitaxel). The maximum tolerated dose established by the continual reassessment method was lonafarnib 100 mg b.i.d. and paclitaxel 175 mg/m^2. Paclitaxel appeared to have no effect on the pharmacokinetics of lonafarnib. The median duration of therapy was eight cycles, including seven cycles with paclitaxel. Six of 15 previously treated patients had a durable partial response, including 3 patients who had previous taxane therapy. Notably, two of five patients with taxane-resistant metastatic non-small cell lung cancer had partial responses.**

Conclusions: **When combined with paclitaxel, the recommended dose of lonafarnib for Phase II trials is 100 mg p.o. twice daily with 175 mg/m^2 of paclitaxel i.v. every 3 weeks. Additional studies of lonafarnib in combination regimens appear warranted, particularly in patients with non-small cell lung cancer.**

INTRODUCTION

Mutations of the *ras* family of oncogenes that result in unregulated cell proliferation are common in human cancers (1). The *ras* mutations have been implicated in the development of colorectal cancer and have been associated with shortened survival in several tumor types, including non-small cell lung cancer (NSCLC; Refs. 2–6). *Ras* genes encode a protein, p21, that is located on the inner surface of the plasma membrane (1, 7). The p21 protein has GTPase activity and participates in signal transduction. Activation of the ras oncoprotein requires prenylation, a process that is catalyzed by farnesyltransferase (8–12).

Farnesyltransferase inhibitors (FTIs) are a novel class of compounds that block this critical enzymatic step in the formation of active ras proteins (8–13). Lonafarnib (Sarasar; Schering-Plough Corporation, Kenilworth, NJ) is a tricyclic nonpeptidomimetic compound (Fig. 1) that is active against a variety of tumors *in vitro* and in animal models of cancer (14). The antitumor activity of lonafarnib and other FTIs is related to the inhibition of farnesylation, although controversy currently surrounds the exact farnesylated proteins that are the key targets of FTIs (15, 16). For example, Ashar *et al.* (17) and Crespo *et al.* (18) have shown that FTIs have important effects on cell cycle arrest. The data of Crespo *et al.* suggest a direct effect on spindle formation with resultant prometaphase accumulation of mitotic lung cancer cells. Ashar *et al.* also showed that CENP-E and CENP-F, two centromeric proteins preferentially expressed in mitotic cells, are direct substrates for FTIs, and that their prenylation is completely inhibited by lonafarnib (19).

Compelling data reported by Moasser *et al.* supplied the scientific underpinning for our present study (20). They showed that, in several cell lines initially resistant to paclitaxel, the addition of a FTI enhanced the sensitivity of those cell lines to paclitaxel. Subsequent preclinical studies have demonstrated synergistic effects with lonafarnib plus paclitaxel on a number of human cell lines *in vitro* (21, 22) and enhanced activity *in vivo* (22). In the NCI-H460 lung cancer xenograft model, inhi-

Received 10/15/03; revised 12/16/03; accepted 1/9/04.
Grant support: F. Khuri was supported by Schering-Plough Research Institute and DAMD 17-02-1-0706.
The costs of publication of this article were defrayed in part by the payment of page charges. This article must therefore be hereby marked *advertisement* in accordance with 18 U.S.C. Section 1734 solely to indicate this fact.
Requests for reprints: Fadlo R. Khuri, Winship Cancer Institute, Emory University, 1365 Clifton Road NE, Building C-3094, Atlanta, GA 30322. Phone: (404) 778-4250; Fax: (404) 778-5520; E-mail: fkhuri@emory.edu.

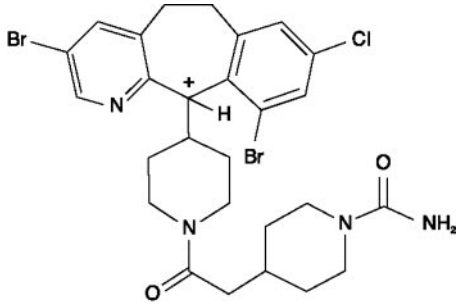


Fig. 1 Structure of lonafarnib {(11*R*)-4-[2-[4-(3,10-dibromo-8-chloro-6,11-digydro-5*H*-benzo[5,6] cyclohepta [1,2b]pyridin-11yl)-1-piperazinyl]-2-oxoethyl]-1-piperidinecarboxamide}.

bition of tumor growth was significantly greater with oral lonafarnib plus i.p. paclitaxel than with either agent alone (86% *versus* 52% and 61%, respectively; $P < 0.05$). Tumor growth inhibition on days 7 and 14 were 56 and 65% greater, respectively, with the combination than with paclitaxel alone. In line 69 wap-*ras*/F transgenic male mice, which develop paclitaxel-resistant mammary tumors at 6–9 weeks of age, oral lonafarnib significantly inhibited tumor growth ($P = 0.05$) and also sensitized the tumors to paclitaxel treatment, so that the combination of lonafarnib plus paclitaxel was more effective than lonafarnib alone ($P = 0.06$ for days 7 to 21; Refs. 22, 23). One proposed explanation for the synergistic activity is that treatment with FTI causes cells to accumulate in the G_2-M phase of the cell cycle in which paclitaxel is most effective (21, 24).

The main objectives of this trial were to establish the maximum tolerated dose (MTD) of lonafarnib, a novel FTI, in combination with paclitaxel in patients with solid tumors and to characterize the safety, tolerability, and dose-limiting toxic effects of this combination in patients with advanced solid malignancies. Furthermore, we particularly wanted to see whether durable responses could be achieved in a variety of taxane-sensitive tumors in patients previously treated with taxanes. Finally, we sought to characterize the pharmacokinetics of multiple-dose lonafarnib after its daily oral administration and of paclitaxel coadministered with daily lonafarnib.

PATIENTS AND METHODS

We sought to establish the MTD and the dose-limiting toxicity (DLT) of the lonafarnib/paclitaxel combination in adult patients with solid tumors. Previously treated patients and untreated patients were allowed to participate in the study. Eligibility criteria included a Karnofsky performance status of at least 70%, a histologically confirmed malignancy for which no curative treatment was available, measurable disease, and adequate hematological parameters [including a WBC count $\geq 3{,}000/mm^3$, an absolute neutrophil count of $1{,}500/\mu l$ ($\geq 1.5 \times 10^9$/liter), a platelet count $\geq 100 \times 10^9$/liter, and a hemoglobin level ≥ 10 g/dl]. Furthermore, patients were required to have adequate renal function, with a serum creatinine level ≤ 1.5 times the upper limit of normal or a measured 12-h creatinine clearance time of ≥ 50 ml/min/1.73 m^2. Also mandatory were normal hepatic function (baseline transaminase levels ≤ 3 times the upper limit of normal, bilirubin ≤ 2.0 mg/dl, and albumin ≥ 3.0 g/dl) and no manifestations of a malabsorption syndrome. All patients had to sign a written informed consent approved by the Institutional Review Board at the University of Texas M. D. Anderson Cancer Center. Patients taking agents that might alter the metabolism of lonafarnib via the CYP3A4 hepatic enzymatic system (such as azoles, macrolides, cyclosporin, systemic corticosteroids, estrogens, antiseizure drugs, rifampin, or isoniazid), or who had metastases to the brain were excluded from the study.

Patients received lonafarnib capsules p.o. twice daily (b.i.d.) with food as 50-mg, 75-mg, and 100-mg formulations in combination with paclitaxel administered i.v. every 3 weeks at 135 mg/m^2 or 175 mg/m^2 over 3 h (Fig. 2). Premedication consisted of 20 mg i.v. dexamethasone and 8 mg of i.v. ondansetron.

Statistical Methods. The dose-finding portion of the trial was conducted in a group of patients with a variety of different head and neck and lung cancers. The principal scientific goal was to determine a MTD, defined as the dose level at which the toxicity rate was closest to 20% and less than 33% with at least 33% of patients experiencing dose-limiting toxicities (DLT) at the next higher level. DLT was defined as the following: absolute neutrophil count $< 500/\mu l$ for longer than 5 days or with fever $\geq 38.3°C$; grade 4 thrombocytopenia (platelets $< 25{,}000/\mu l$) or anemia (Hb < 6.5 g/dl); grade 3–4 nausea/vomiting or grade 3 diarrhea despite optimal antiemetic or antidiarrheal treatment; or any other grade 3 treatment-related nonhematological toxicity; and treatment delay for toxicity lasting >2 weeks.

Associations between pairs of variables were assessed using the Fisher exact test, Kruskal-Wallis test, and Jonkheere-

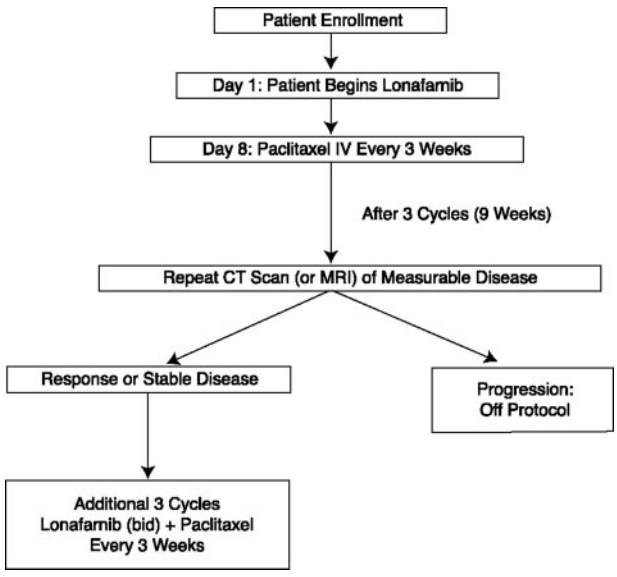


Fig. 2 Study design. Patients begin lonafarnib 1 week before receiving paclitaxel. Reevaluation occurs after every three cycles of treatment. If patients have responsive or stable disease, they proceed on study. If patients have progressive disease, they go off the study protocol. *CT*, computed tomography; *MRI*, magnetic resonance imaging.

Table 1 Number of patients and cycles by dose level of paclitaxel and lonafarnib in Phase I trial

Dose levels	Paclitaxel (mg/m^2)	Lonafarnib (mg b.i.d.)	Cycles	No. of patients
1	135	50	0	0
2	135	100	1–9	3
			10–15	2
			16–32	1
3	175	100	1–3	9
			4–6	6
			7	5
			8	4
			9	2
			10–11	1
3A	175	125	1	5
			2–3	6
			4–6	5
			7–8	4
			9–10	3
			11–17	2
			18–24	1
4	175	150	1–2	4
			3–7	3
			8	2
			9–27	1

Terpstra test (25). Regression models of toxicity on the doses of paclitaxel and lonafarnib, and the indicator of prior chemotherapy, were fit using exact logistic regression (26, 27). Confidence intervals for probabilities of toxicity at particular dose and prior chemotherapy combinations were computed by repeating the exact logistic regression on 1000 bootstrap samples of the data. All of the computations were carried out using StatXact and SAS Proc Logistic.

Pharmacokinetic Methods. Plasma lonafarnib and paclitaxel concentrations were determined using validated liquid chromatography with tandem mass spectrometric detection and the high-performance liquid chromatography method, respectively. The lower limits of quantitation were 5.00 and 10.0 ng/ml plasma for lonafarnib and paclitaxel, respectively, and the linear ranges were 5.00–2500 ng/ml and 10.0–2500 ng/ml, respectively. The assay precision (% coefficient of variation) and accuracy (% Bias) were $<11\%$ and $<10\%$, respectively, for lonafarnib, and $<9\%$ and $<6\%$, respectively, for paclitaxel. Noninterference from the respective coadministered drug was demonstrated for both of the lonafarnib and paclitaxel methods.

Blood samples ($\sim$3 ml) for determination of plasma lonafarnib and paclitaxel concentrations were collected on day 1 of Cycle 1. Plasma was separated by centrifugation (4°C, $\sim$3000 rpm for 15 min), then divided into two aliquots, and was stored frozen at -70°C until shipped to the analytical facility.

Individual plasma lonafarnib and paclitaxel concentrations were used for pharmacokinetic analysis using model-independent methods. The maximum plasma concentration (C_{max}) and time of maximum plasma concentration (T_{max}) were the observed values. The terminal phase rate constant (K) was calculated as the negative of the slope of the log-linear terminal portion of the plasma concentration-*versus*-time curve using linear regression. The terminal phase half-life, $t_{1/2}$, was calculated as $0.693/K$. The area under the plasma concentration-*versus*-time curve from time 0 to the time of final quantifiable sample ($AUC_{(tf)}$) and from time 0 to 12 h ($AUC_{(0-12\ h)}$) was calculated using the linear trapezoidal method. For paclitaxel, the $AUC_{(tf)}$ was extrapolated to infinity when appropriate as follows: $AUC_{(\infty)} = AUC_{(tf)} + C_{(tf)}/K$, where $C_{(tf)}$ is the estimated concentration determined from linear regression at time *tf*. Total body clearance, *CL/F* (lonafarnib) or *CL* (paclitaxel), was calculated by the following equation: $CL/F = \text{Dose}/AUC$. The apparent volume of distribution, *Vd/F* (lonafarnib) or *Vd* (paclitaxel), was calculated as: $Vd/F = (\text{Dose}/AUC)/K$.

For paclitaxel, the volume of distribution at steady state, *Vdss*, was estimated as total body clearance multiplied by mean residence time (*MRT*).

RESULTS

Twenty-four patients with a mean age of 58.3 years were enrolled on this Phase I study at the University of Texas M. D. Anderson Cancer Center, with the enrollment of new patients beginning on June 16, 1999, and continuing through March 30, 2000. Twenty-one patients actually received both paclitaxel and lonafarnib (Table 1). Patients were predominantly male (67%) and Caucasian (92%), with Karnofsky performance status of 90 to 100 (71%; Table 2). Slightly more than one-half of the patients had a primary diagnosis of NSCLC.

Toxicities. Among all of the dose levels, 92% of patients reported at least one toxicity at any grade and 54% of patients reported at least one grade 3/4 treatment-emergent nonhematological adverse event judged to be related to the study drugs. The most common treatment-related treatment-emergent nonhematological adverse events (including all grades) reported were gastrointestinal effects in 92% of patients (diarrhea 92%, nausea 79%, vomiting 50%, constipation 46%, stomatitis 38%, abdominal pain 29%); fatigue (88%), alopecia (83%), peripheral neuropathy (79%), arthralgia (71%), infections and infestations in 50% of patients (folliculitis 38%, oral candidiasis 13%, pneu-

Table 2 Patient demographics and disease characteristics

Subjects (*n*)	24
Age (yr)	
Median	59.5
Range	41–75
Sex	
Men	16 (67%)
Women	8 (33%)
Karnofsky performance status:	
Missing	1 (4%)
70–85	6 (25%)
90–100	17 (71%)
Histology	
NSCLC[a]	14 (58%)
Salivary	6 (25%)
HNSCC	4 (17%)
Prior chemotherapy ($n = 21$)	13
Prior taxane ($n = 21$)	9

[a] NSCLC, non-small cell lung cancer; HNSCC, head and neck squamous cell carcinoma.

Table 3 Number of patients with severe (grade 3) or life-threatening (grade 4) nonhematologic toxicities

	Dose level 2 ($n = 3$)		Dose level 3 ($n = 9$)		Dose level 3A ($n = 5$)		Dose level 4 ($n = 4$)	
Toxic effect	Grade 3	Grade 4	Grade 3	Grade 4	Grade 3	Grade 4	Grade 3	Grade 4
Bronchitis	0	0	0	0	1	0	0	0
Cardiac arrest	0	0	0	0	0	0	0	1
Chest wall pain	0	0	1	0	0	0	0	0
Diarrhea	0	0	2	0	1	1	2	0
Dysphagia	0	0	1	0	0	0	0	0
Dyspnea	0	0	0	0	1	0	0	0
Fatigue/weakness	0	0	0	0	0	0	2	0
Hyperglycemia	0	0	0	0	0	0	1	0
Neuropathy, peripheral	0	0	0	0	1	0	0	0
Fever	0	0	1	0	0	0	0	0
Infections (pneumonia)	0	0	0	0	1	0	0	0
Neoplasms, benign and malignant	0	0	1	0	0	0	0	0
Hyperbilirubinemia	0	0	1	0	0	0	0	0

Table 4 Number of patients with hematological toxicities by dose level during the treatment period

	Dose level 2			Dose level 3			Dose level 3A			Dose level 4		
Toxic effect	All	Gd[a] 3	Gd 4	All	Gd 3	Gd 4	All	Gd 3	Gd 4	All	Gd 3	Gd 4
Neutropenia	0	0	0	2	0	1	2	1	1	0	0	0
Leukopenia	1	1	0	4	1	1	3	1	0	1	1	0
Anemia	1	0	0	2	1	0	3	0	0	2	0	0

[a] Gd, grade.

monia 8%), respiratory system disorders (63%), anorexia (54%), rash (46%), weight decrease (29%); dizziness (25%); fever, blurred vision, liver and biliary system disorders, dehydration, myalgia, dry skin (21% each). All other adverse events occurred in fewer than 20% of patients. Grade 3 and grade 4 nonhematological toxicities by dose level are listed in Table 3.

Hematological toxicities occurred in 54% (13 of 24) of patients overall. Seven patients (29%) had grade 3/4 hematological toxicities. Table 4 shows that any grade and grade 3/4 anemia occurred in 34% (8 of 24) and 4% (1 of 24) of patients, respectively; any and grade 3/4 leukopenia occurred in 38% (9 of 24) and 21% (5 of 24) patients, respectively; and any and grade 3/4 neutropenia occurred in 17% (4 of 24) and 13% (3 of 24) of patients, respectively. Thrombocytopenia at any level was not observed in this study.

Both hematological and nonhematological toxic effects were generally mild and were neither more common nor more severe than those expected with paclitaxel. Patients had a median of one prior treatment with 13 of 22 evaluable patients having had prior chemotherapy including 9 who had a prior taxane (Table 2). Seven of the 9 patients previously treated with a taxane had disease progression on or within 3 months of taxane-based therapy, and 10 of 13 pretreated patients overall had progression of disease on or within 3 months of therapy.

Protocol-Defined DLTs. Overall, seven patients had DLTs as defined by protocol. No DLTs were seen at dose level 2. One patient at dose level 3 had grade 3 bilirubinemia. When the dose was escalated to level 4 (150 mg b.i.d. lonafarnib and 175 mg/m^2 paclitaxel) two of four patients had dose-limiting toxic effects in the first cycle (one grade 4 neutropenic fever, one grade 4 diarrhea). We then introduced dose level 3A (125 mg b.i.d. of lonafarnib, 175 mg/m^2 of paclitaxel) to determine whether an intermediate dose level would be tolerated. At this dose, two patients had grade 4 diarrhea in the first cycle. All of the DLTs were reversible on modification or cessation of treatment. On the basis of analysis of all available safety data, it has been determined that lonafarnib 100 mg b.i.d. and paclitaxel 175 mg/m^2 is appropriate for further evaluation in patients with NSCLC.

Table 5 Mean (percentage coefficient of variation) pharmacokinetic parameters of lonafarnib

Parameter	Dose level 2	Dose level 3	Dose level 3A	Dose level 4
C_{max}[a] (ng/ml)	760 (25)	960 (40)	1394 (35)	1267 (35)
Median T_{max} (h); range	5; 3–8	3; 0–10	8; 4–12	5; 3–6
AUC_{0-12h} (ng·h/ml)	5550 (51)	8789 (32)	12803 (36)	15443 (NA)
CL/F (ml/min)	364 (54)	207 (33)	181 (36)	165 (NA)
C_{min} (ng/ml)	286 (84)	524 (51)	883 (35)	1010 (47)

[a] C_{max}, maximum plasma concentration; T_{max}, time of maximum plasma concentration; AUC_{0-12h}, the area under the plasma concentration − *versus* = time curve from time 0 to 12 h; CL/F, total body clearance (lonafarnib); C_{min}, minimum plasma clearance.

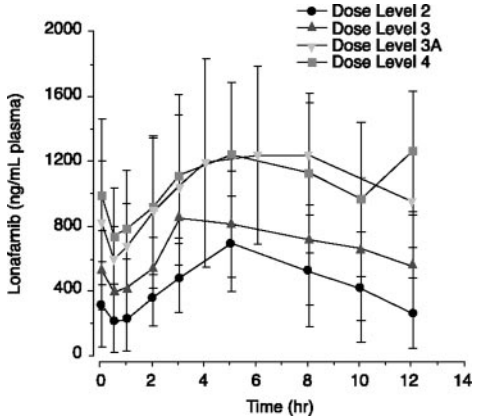


Fig. 3 Mean (±1 SD) plasma lonafarnib concentrations after multiple-dose oral administration of lonafarnib in combination with single-dose 3-h i.v. infusion of paclitaxel to patients with solid tumors.

Pharmacokinetics of Lonafarnib. Nineteen patients had samples collected for pharmacokinetic evaluations. Lonafarnib was slowly absorbed after oral administration with food. Median T_{max} ranged from 3 to 8 h (Table 5; Fig. 3). Half-life ($t_{1/2}$) could not be estimated in this study because of the lack of a definitive terminal phase in the plasma concentration-*versus*-time profiles after b.i.d. oral administration of lonafarnib with food (see Fig. 3). Mean plasma lonafarnib concentrations at 12 h after the dose were ~34–99% of the corresponding mean C_{max} values. The mean total body clearance ranged from 165 to 364 ml/min. The increases in lonafarnib *AUC* values were dose-related after oral administration of 100 mg, 125 mg, and 150 mg in combination with paclitaxel 175 mg/m^2. After administration of lonafarnib 100 mg with paclitaxel 175 mg/m^2, the mean lonafarnib C_{max} and *AUC* values were higher than those with paclitaxel 135 mg/m^2. However, given the variability of the data and sample size, the distribution of individual C_{max} and *AUC* values encompassed the same range, regardless of paclitaxel dose (Fig. 4). The C_{max} and *AUC* values obtained in this trial with lonafarnib 100 mg in combination with paclitaxel were similar to those obtained in previous Phase I trials in which lonafarnib 100 mg was administered alone (Table 6; Refs. 28–30). Thus, these observations suggest that a single dose of either 135 mg/m^2 or 175 mg/m^2 of paclitaxel did not affect the pharmacokinetics of lonafarnib.

Pharmacokinetics of Paclitaxel. Plasma paclitaxel concentrations (C_{max} and *AUC*) were similar among the dose groups for paclitaxel 175 mg/m^2 with lonafarnib 100 mg, 125 mg, and 150 mg (Table 7; Figs. 5 and 6). There appear to be no effects on paclitaxel pharmacokinetics at a dose of 175 mg/m^2 paclitaxel when the lonafarnib dose is increased from 100 mg to 150 mg. The relationships between dose and paclitaxel C_{max} or *AUC* values were disproportionate after the administration of paclitaxel 135 mg/m^2 and 175 mg/m^2 in combination with lonafarnib 100 mg; a 30% increase in paclitaxel dose resulted in an increase of ~74% in C_{max} and ~87% in *AUC*. This finding provided additional evidence for the nonlinear disposition for paclitaxel, as noted previously (31).

Plasma paclitaxel concentrations decreased rapidly immediately after cessation of the 3-h infusion, which was followed by a prolonged terminal phase (see Fig. 5). The mean terminal elimination $t_{1/2}$ of paclitaxel ranged from 12 to 19 h when blood samples were collected up to 48 h postdose for the first 17 patients. The mean $t_{1/2}$ was ~6 h when blood samples were collected up to 24 h postdose for patients 18–24 (see Table 7). The 6-h half-life was similar to that reported in the literature (31). The C_{max} and *AUC* values obtained in this study were similar to those previously reported when paclitaxel was given alone as a 3-h i.v. infusion (Table 8; Ref. 31).

Clinical Activity. The median number of treatment cycles on trial was eight, with a median of seven cycles containing paclitaxel. Activity was seen at the four dose levels studied (2, 3, 3A, and 4). Nine responses were durable, which we defined as a response detected at three or six cycles and confirmed at six or eight cycles, with median response duration of 6 months (range, 4–14 months). Most provocatively, we saw meaningful responses in three patients who had received prior taxane-based therapy, including two of five NSCLC patients who met the standard definition of taxane resistance (progression on or within 3 months

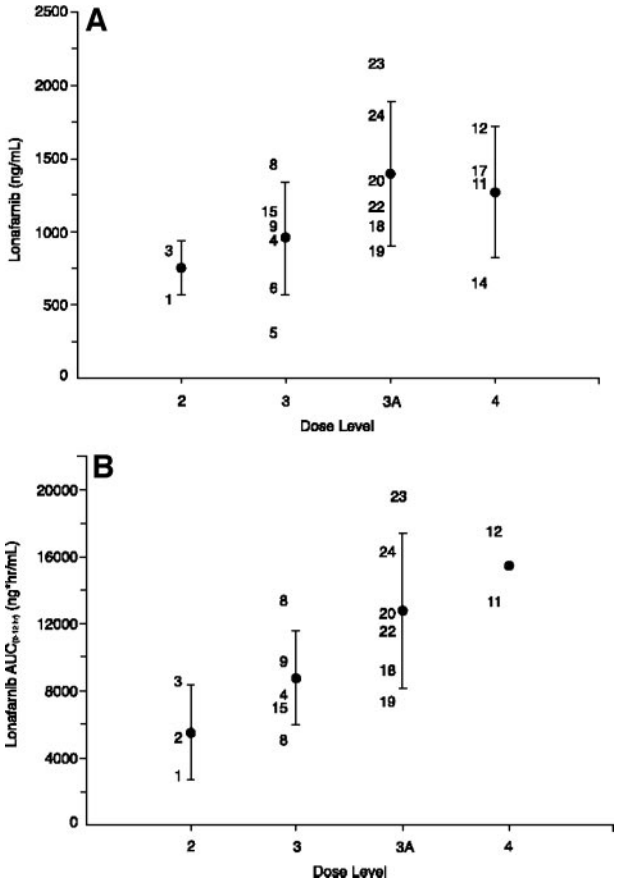


Fig. 4 Individual and mean (±1 SD) C_{max} (*A*) and $AUC_{0-12\ h}$ values (*B*) of lonafarnib after multiple-dose oral administration of lonafarnib in combination with single-dose 3-h i.v. infusion of paclitaxel to patients with solid tumors.

Table 6 Mean (coefficient of variation) pharmacokinetic parameters of lonafarnib after multiple-dose administration of lonafarnib 100 mg alone (previous Phase I studies) or in combination with paclitaxel (this study)

Study	Dose	*n*	C_{max}[a] (ng/ml)	AUC_{0-12} (ng·h/ml)
This study	100 + 135[b]	3	760 (25)	5550 (51)
This study	100 + 175[b]	8	960 (40)	8789[c] (32)
Eskens *et al.*[d]	100[e]	3	942 (58)	7299 (75)
Adjei *et al.*[f]	100	1	1680 (NA)	18295 (NA)
Hurwitz *et al.*[g]	100	2	784 (NA)	6221 (NA)

[a] C_{max}, maximum plasma concentration; AUC_{0-12}, the area under the plasma concentration - *versus* - time curve from time 0 to 12 h; NA, not appropriate (sample size < 3).
[b] Lonafarnib dose (mg) + paclitaxel dose (mg/m^2).
[c] $n = 6$.
[d] Ref. 34.
[e] Lonafarnib alone dose (mg).
[f] Ref. 32.
[g] Ref. 33.

Table 7 Mean (percentage coefficient of variation) pharmacokinetic parameters of paclitaxel

Parameter	Dose level 2	Dose level 3	Dose level 3A	Dose level 4
C_{max}[a] (ng/ml)	1937 (19)	3368 (55)	4258 (43)	3515 (38)
AUC_{∞} (ng·h/ml)	9936 (7)	18563 (40)	17526 (38)	17634 (23)
$t_{1/2}$ (h)	18.6 (12)	13.3 (9)	5.62 (15)	12.1 (24)
CL (ml/min/m^2)	227 (8)	182 (43)	183 (33)	171 (19)
Vd (liter/m^2)	365 (7)	211 (47)	88.1 (35)	174 (9)
Vdss (liter/m^2)	130 (16)	90.6 (54)	40.2 (47)	66.9 (12)

[a] C_{max}, maximum plasma concentration; AUC_{∞}, area under the plasma concentration - *versus* - time curve from time 0 to the final quantifiable sample extrapolated to infinity; $t_{1/2}$, terminal phase half-life; *CL*, total body clearance; *Vd*, volume of distributions; *Vdss*, the volume of distribution at steady state.

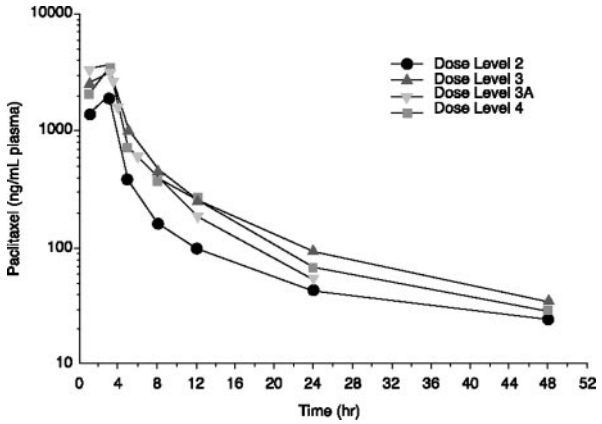


Fig. 5 Mean plasma paclitaxel concentrations after single-dose 3-h i.v. infusion of paclitaxel in combination with multiple-dose oral administration of lonafarnib to patients with solid tumors.

of taxane therapy). Only 4 of 21 patients had progressive disease by cycle 3, although all 21 patients had manifested disease progression within 3 months of study enrollment.

At the cycle-3 assessment interval, 7 patients demonstrated a partial response, 10 had minor responses or stable disease, and 4 had progressive disease (Table 9). Six of 7 responses were confirmed after six cycles. When total responses achieved on study were examined, 6 (50%) of the 12 patients with NSCLC achieved a partial response. In the setting of head and neck squamous cell carcinoma, two of the three patients had a partial response, and the one patient with a salivary gland tumor had prolonged disease stabilization and was treated for 30 cycles before disease progression. No significant associations were noted between response after three cycles or after six cycles and the dose of either lonafarnib ($P = 0.81$, $P = 0.70$, respectively) or paclitaxel ($P = 0.19$, $P = 0.32$, respectively).

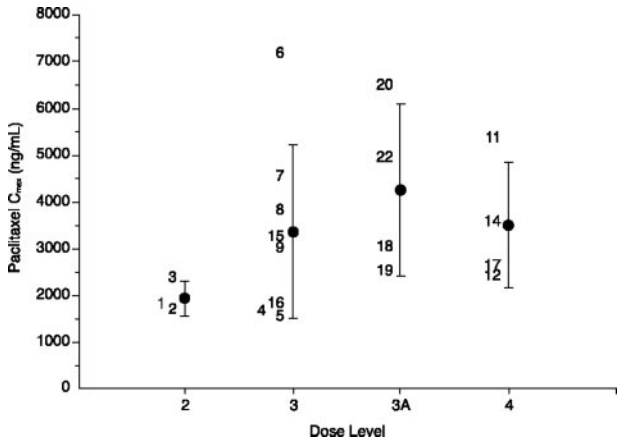


Fig. 6 Individual and mean (±1 SD) C_{max} values of paclitaxel after single-dose 3-h i.v. infusion of paclitaxel in combination with multiple-dose oral administration of lonafarnib to patients with solid tumors.

Table 8 Mean (coefficient of variation) pharmacokinetic parameters of paclitaxel after 3-h i.v. infusion of paclitaxel 135 mg/m^2 or 175 mg/m^2 in combination with multiple-dose lonafarnib 100 mg b.i.d., 125 mg b.i.d., or 150 mg b.i.d. (this study) or alone (previously reported study)

Dose	Study	*n*	C_{max} (ng/ml)	AUC_∞ (ng·h/ml)	*CL* (ml/min/m^2)
135	This study	3	1937 (19)	9936 (7)	227 (8)
	Gianni *et al.*[a]	4	2818 (12)	9308 (10)	247 (9)
175	This study	16	3627 (46)	18309[c] (34)	179[c] (34)
	Gianni *et al.*[a]	3	5038 (15)	15797 (16)	190 (16)

[a] C_{max}, maximum plasma concentration; AUC_∞, area under the plasma concentration - *versus* - time curve from time 0 to the final quantifiable sample extrapolated to infinity; *CL*, total body clearance.
[b] Ref. 35.
[c] $n = 15$.

DISCUSSION

Other than the occasionally dose-limiting side effect of diarrhea, lonafarnib did not seem to contribute any significant side effects to those caused by paclitaxel. Patients with previous chemotherapy had a higher risk of toxicity. The substantial overlap of the eight 90% confidence intervals is due in large part to the small sample size ($n = 21$ evaluable patients). The only discernable trend with dose is an increase in the upper confidence limit with increasing total combined dose. Seven of the eight confidence intervals contain the targeted 30% toxicity rate. More precise estimates of the probability of toxicity would necessitate a larger sample size. The MTDs of lonafarnib and paclitaxel in this trial were lower than the doses recommended for either agent alone. The MTD of lonafarnib alone was determined to be 200 mg b.i.d. DLTs in studies of lonafarnib alone were generally similar to those seen in this trial and included reversible renal insufficiency (elevated creatinine levels), gastrointestinal symptoms (diarrhea, nausea, vomiting, anorexia), and hematological toxicities. Phase I studies of paclitaxel have demonstrated an MTD of 200 mg/m^2 for a single continuous infusion i.v. regimen. Myelosuppression and neurotoxicity are the primary DLTs of paclitaxel. Severe allergic reactions and skin rash associated with the vehicle (cremaphor EL) necessitate pretreatment with dexamethasone, diphenhydramine, and cimetidine or ranitidine.

No pharmacokinetic evidence was observed that either paclitaxel or lonafarnib enhanced the metabolism of the other agent. The pharmacokinetic values suggest that areas under the curve of both drugs were achieved in the active range. The target exposure for lonafarnib in clinical studies was to maintain a predose concentration in the range of 1–1.5 μM based on the concentration required to inhibit anchorage-independent growth of a series of human tumor cell lines.

We saw encouraging clinical activity in this Phase I study of combined paclitaxel and lonafarnib, confirming the preclinical activity previously reported for this combination (14, 20, 22, 32–34). Several Phase I studies of farnesyltransferase inhibitors have now been published (28–30, 35–39). Before this study, a total of two responses have been documented (one each with tipifarnib and lonafarnib) in previously treated patients with NSCLC (29, 36). The activity manifested with this protocol using fairly moderate doses of lonafarnib and paclitaxel is more

Table 9 Clinical activity of lonafarnib in combination with paclitaxel

After 3 Cycles	
Partial response	7 patients (3 previously treated with taxanes)
Minor response	3 patients
Stable disease	7 (4 previously treated with taxanes)
Progressive disease	4 (2 previously treated with taxanes)
Not assessed	3 (1 did not tolerate lonafarnib at 125 mg b.i.d.)
Median no. of total cycles on study:	8 (range, 2–30)
Median no. of paclitaxel courses on study:	7 (range, 2–30)
After 6 to 9 Cycles	
Partial response	8 patients (3 previously treated with taxanes)
Minor response	2 patients
Stable disease	6 (4 previously treated with taxanes)
Progressive disease	2 (2 previously treated with taxanes)
Not assessed	3
Median no. of total cycles on study:	8 (range, 2–30)
Median no. of paclitaxel courses on study:	7 (range, 2–30)
Any response by histology	
NSCLC[a]	12 patients (6 PR, 3 MR or StD, 3 PD)[b]
HNSCC	3 patients (2 PR, 1 StD)
Salivary	6 patients (1 PR, 4 StD, 1 PD)

[a] NSCLC, non-small cell lung cancer; PR, partial response; MR, minor response; StD, stable disease; PD, progressive disease; HNSCC, head and neck squamous cell carcinoma.
[b] Five patients (all NSCLC) were considered taxane-refractory/resistant. PRs were seen in 2 of 5 taxane-refractory/resistant NSCLC patients.

substantial. It is particularly heartening because little if any evidence exists to support the efficacy of paclitaxel as a second-line agent when administered as a 3-h infusion on a 3-week cycle (40–44).

The extent of disease stabilization that our trial revealed with this regimen was dramatic in an extensively pretreated heterogeneous patient population with progressive disease at the time of study enrollment. Recent evidence suggests that the stabilization of NSCLC may lead to clinically meaningful survival benefits.

In conclusion, this is the first reported clinical study of the combination of a taxane with a farnesyltransferase inhibitor in human solid tumors. Phase II trials of the combination as first-line and second-line therapy of stage III and IV NSCLC are ongoing to confirm or refute our data-driven hypothesis, namely, that lonafarnib may enhance taxane sensitivity and possibly overcome clinical taxane resistance in solid tumors.

ACKNOWLEDGMENTS

We thank Judie Wells for transcription and editing of the manuscript, Julie Starr for her expert editorial assistance, and Delores Curtis and Stephen Maxwell for bioanalytical support.

REFERENCES

1. Bos JL. ras oncogenes in human cancer: a review. Cancer Res 1989;49:4682–9. Erratum in: Cancer Res 1990;50:1352.

2. Slebos RJ, Kibbelaar RE, Dalesio O, et al. K-ras oncogene activation as a prognostic marker in adenocarcinoma of the lung. N Engl J Med 1990;323:561–5.

3. Rosell R, Li S, Skacel Z, et al. Prognostic impact of mutated K-ras in surgically resected non-small cell lung cancer patients. Oncogene 1993;8:2407–12.

4. Malats N, Porta M, Corominas JM, et al. Ki-ras mutations in exocrine pancreatic cancer: association with clinico-pathological characteristics and with tobacco and alcohol consumption. PANK-ras I Project Investigators. Int J Cancer 1997;70:661–7.

5. Sugio K, Molberg K, Albores-Saavedra J, et al. K-ras mutations and allelic loss at 5q and 18q in the development of human pancreatic cancers. Int J Pancreatol 1997;21:205–17.

6. Rall CJ, Yan YX, Graeme-Cook F, et al. Ki-ras and p53 mutations in pancreatic ductal adenocarcinoma. Pancreas 1996;12:10–7.

7. Bollag G, McCormick F. Regulators and effectors of ras proteins. Ann Rev Cell Dev Biol 1991;7:601–32.

8. Gibbs JB. Lipid modifications of proteins in the ras superfamily. In: Birnbaumer L, Dickey B, editors. GTPases in biology. New York: Springer-Verlag; 1993. p. 335–44.

9. Hancock JF, Magee AI, Childs JE, Marshall CJ. All ras proteins are polyisoprenylated but only some are palmitoylated. Cell 1989;57: 1167–77.

10. Hancock JF, Paterson H, Marshall CJ. A polybasic domain or palmitoylation is required in addition to the CAAX motif to localize p21ras to the plasma membrane. Cell 1990;63:133–9.

11. Jackson JH, Cochrane CG, Bourne JR, et al. Farnesol modification of Kirsten-ras exon 4B protein is essential for transformation. Proc Natl Acad Sci USA 1990;87:3042–6.

12. Kato K, Cox AD, Hisaka MM, et al. Isoprenoid addition of Ras protein is the critical modification for its membrane association and transforming activity. Proc Natl Acad Sci USA 1992;89:6403–7.

13. Rowinsky EK, Windle JJ, Von Hoff DD. Ras protein farnesyltransferase: a strategic target for anticancer therapeutic development. J Clin Oncol 1999;17:3631–52.

14. Liu M, Bryant MS, Chen J, et al. Antitumor activity of SCH 66336, an orally bioavailable tricyclic inhibitor of farnesyl protein transferase, in human tumor xenograft models and wap-ras transgeneic mice. Cancer Res 1998;58:4947–56.

15. Cox AD, Der CJ. Farnesyltransferase inhibitors and cancer treatment: targeting simply ras? Biochim Biophys Acta 1997;1333:F51–71.

16. Du W, Prendergast GC. Activation of the PI3′K-AKT pathway masks the proapoptotic effects of farnesyltransferase inhibitors. Cancer Res 1999;59:4208–12.

17. Ashar HR, James L, Gray K, et al. The farnesyl transferase inhibitor SCH 66336 induces a G(2) → M or G(1) pause in sensitive human tumor cell lines. Exp Cell Res 2001;262:17–27.

18. Crespo NC, Ohkanda J, Yen TJ, Hamilton AD, Sebti SM. The farnesyltransferase inhibitor, FTI-2153, blocks bipolar spindle formation and chromosome alignment and causes prometaphase accumulation during mitosis of human lung cancer cells. J Biol Chem 2001;276: 16161–7.

19. Ashar HR, James L, Gray K, et al. Farnesyl transferase inhibitors block the farnesylation of CENP-E and CENP-F and alter the association of CENP-E with the microtubules. J Biol Chem 2000;275:30451–7.

20. Moasser MM, Sepp-Lorenzino L, Kohl NE, et al. Farnesyl transferase inhibitors cause enhanced mitotic sensitivity to Taxol and epothilones. Proc Natl Acad Sci USA 1998;95:1369–74.

21. Nielsen LL, Shi B, Hajian G, et al. Combination therapy with the farnesyl protein transferase inhibitor SCH66336 and SCH58500 (p53 adenovirus) in preclinical cancer models. Cancer Res 1999;59:5896–901.

22. Shi B, Yaremko B, Hajian G, et al. The farnesyl protein transferase inhibitor SCH66336 synergizes with taxanes in vitro and enhances their antitumor activity in vivo. Cancer Chemother Pharmacol 2000;46: 387–93.

23. Porter GM, Armstrong L, Nielsen LL. Strategy for developing transgenic assays for screening antineoplastic drugs that affect tubulin polymerization. Lab Anim Sci 1995;45:145–50.

24. Donaldson KL, Goolsby GL, Wahl AF. Cytotoxicity of the anticancer agents cisplatin and Taxol during cell proliferation and the cell cycle. Int J Cancer 1994;57:847–55.

25. Hirji, KF. Exact distributions for polytomous data. J Am Stat Assoc 1992;87:487–92.

26. Mehta CR, Patel NR, Jajoo B. Exact logistic regression: theory, methods and software. Technical report. Cambridge, MA: Cytel Software Corporation; 1993.

27. Mehta CR, Patel NR, Senchaudhuri, P. Efficient Monte Carlo methods for conditional logistic regression. J Am Stat Assoc 2000;95: 99–108.

28. Adjei AA, Erlichman C, Davis JN, et al. A Phase I trial of the farnesyl transferase inhibitor SCH66336: evidence for biological and clinical activity. Cancer Res 2000;60:1871–7.

29. Hurwitz HI, Colvin OM, Petros WP, et al. Phase I and pharmacokinetic study of SCH66336, a novel FPTI, using a 2-week on, 2-week off schedule [abstract[. Proc Am Soc Clin Oncol 1999;18:599.

30. Eskens F, Awada A, Cutler D, et al. Phase I and pharmacokinetic study of the oral farnesyl transferase inhibitor SCH 66336 given twice daily to patients with advanced solid tumors. J Clin Oncol 2001;19: 1167–75.

31. Gianni L, Kearns CM, Giani A, et al. Nonlinear pharmacokinetics and metabolism of paclitaxel and its pharmacokinetic/pharmacodynamic relationships in humans. J Clin Oncol 1995;13:180–90.

32. Kohl NE, Omer CA, Conner MW, et al. Inhibition of farnesyltransferase induces regression of mammary and salivary carcinomas in ras transgenic mice. Nat Med 1995;1:792–97.

33. Sun J, Qian Y, Hamilton AD, Sebti SM. Ras CAAX peptidomimetic FTI276 selectively blocks tumor growth in nude mice of a human lung carcinoma with K-Ras mutation and p53 deletion. Cancer Res 1995;55:4243–7.

34. Prendergast GC, Davide JP, deSolms SJ, et al. Farnesyltransferase inhibition causes morphological reversion of ras-transformed cells by a complex mechanism that involves regulation of the actin cytoskeleton. Mol Cell Biol 1994;14:4193–202.

35. Zujewski J, Horak ID, Bol CJ, et al. Phase I and pharmacokinetic study of farnesyl protein transferase inhibitor R115777 in advanced cancer. J Clin Oncol 2000;18:927–41.

36. Schellens JHM, de Klerk G, Swart M, et al. Phase I and pharmacologic study with the novel farnesyltransferase inhibitor (FTI) R115777 [abstract]. Proc Am Assoc Cancer Res 1999;40:4780.

37. Soignet S, Yao S-L, Britten C, et al. Pharmacokinetics and pharmacodynamics of the farnesyl protein transferase inhibitor (L-778, 123) in solid tumors [abstract]. Proc Am Assoc Cancer Res 1999;40:3413.

38. Britten CD, Rowinsky E, Yao S-L, et al. The farnesyl protein transferase (FPTase) inhibitor L-78,123 in patients with solid cancers [abstract]. Proc Am Soc Clin Oncol 1999;18:597.

39. Hudes GR, Schol J, Baab J, et al. Phase I clinical and pharmacokinetic trial of the farnesyltransferase inhibitor R115777 on a 21-day dosing schedule [abstract]. Proc Am Soc Clin Oncol 1999;18:601.

40. Huisman C, Smit EF, Giaccone G, Postmus PE. Second-line chemotherapy in relapsing or refractory non-small cell lung cancer: a review. J Clin Oncol 2000;18:3722–30.

41. Fossella FV, Lee JS, Shin DM, et al. Phase II study of docetaxel for advanced or metastatic platinum-refractory non-small cell lung cancer. J Clin Oncol 1995;13:645–51.

42. Gatzemeier U, von Pawel J, Gottfried M, et al. Phase III comparative study of high-dose cisplatin versus a combination of paclitaxel and cisplatin in patients with advanced non-small cell lung cancer. J Clin Oncol 2000;18:3390–9.

43. Socinski MA, Steagall A, Gillenwater H. Second-line chemotherapy with 96-hour infusional paclitaxel in refractory non-small cell lung cancer: report of a Phase II trial. Cancer Investig 1999;17:181–8.

44. Stewart DJ, Tomiak EM, Goss G, et al. Paclitaxel plus hydroxyurea as second-line therapy for non-small cell lung cancer. Lung Cancer 1996;15:115–23.

Response of Non–Small Cell Lung Cancer Cells to the Inhibitors of Phosphatidylinositol 3-Kinase/Akt- and MAPK Kinase 4/c-*Jun* NH_2-Terminal Kinase Pathways: An Effective Therapeutic Strategy for Lung Cancer

Ho-Young Lee,[1] Seung-Hyun Oh,[1] Young-Ah Suh,[2] Jin Hyen Baek,[4] Vali Papadimitrakopoulou,[1] Suyun Huang,[3] and Waun Ki Hong[1]

Abstract

Purpose: We previously showed that phosphatidylinositol 3-kinase (PI3K)/Akt and mitogen-activated protein kinase (MAPK) pathways cooperate to promote non–small cell lung cancer (NSCLC) cell proliferation *in vitro*. This study was designed to explore whether inhibition of these pathways effectively inhibits NSCLC tumor growth *in vivo*.

Experimental Design: The effects of PI3K/Akt inhibitors {LY294002, adenoviruses expressing dominant-negative mutant of the p85α adaptor subunit of PI3K (Ad-dnp85α), dominant-negative Akt [Ad-HA-Akt(KM)], or PTEN (Ad-PTEN)}, MKK4/c-*jun* NH_2-terminal kinase (JNK) inhibitor [SP600215, adenovirus expressing dominant-negative MKK4, Ad-MKK4(KR)], and their combinations on proliferation and apoptosis in NSCLC cells were tested *in vitro* and *in vivo* using the 3-(4,5-dimethylthiazol-2-yl)-2,5-diphenyltetrazolium bromide assay, a flow cytometry-based terminal deoxynucleotidyl transferase–mediated nick-end labeling assay, Western blot and immunohistochemical analyses, and an NSCLC xenograft tumor model.

Results: Ad-dnp85α significantly inhibited proliferation of a subset of NSCLC cell lines used in our study. Intratumoral injection of Ad-dnp85α induced a significant decrease in the growth of H1299 NSCLC xenograft tumors. Concurrent inhibition of the PI3K/Akt and MKK4/JNK pathways showed enhanced antiproliferative effects on H1299 cells *in vitro* and *in vivo* by increasing apoptosis.

Conclusions: PI3K/Akt and MKK4/JNK pathways cooperate to stimulate NSCLC cell proliferation by maintaining cell survival, suggesting that simultaneously targeting these two pathways might be an effective therapeutic strategy against NSCLC.

Lung cancer is the leading cause of cancer death in the United States and worldwide, a fact that underscores the need for more effective treatment strategies. Because tumorigenic transformation results from the deregulation of cell cycle control and provides tumor cells with constitutive mitogenic and survival signals, selectively inhibiting growth factor signaling pathways could be an efficient strategy to inhibit tumor progression (1). The phosphatidylinositol 3-kinase (PI3K)/Akt signal transduction pathway is an attractive target because it is important in the transformation, proliferation, survival, and metastatic potential of a variety of cancer cells, including lung cancer cells (2–6).

Class I PI3K consists of a family of heterodimeric complexes, each composed of a p110 catalytic subunit and an adaptor subunit that exists predominately as a p85 form (7, 8). PI3K phosphorylates the D3 position of phosphatidylinositol on PI(4)P and PI(4,5)P to produce PI(3,4)P2 and PI(3,4,5)P3 (9), which recruit the pleckstrin homology domains of specific intracellular proteins, such as PDK-1 and Akt/PKB (7), to the cytoplasmic membrane. This mechanism is regulated by the phosphatase and tensin homologue deleted on chromosome 10 (*PTEN*) tumor suppressor gene (10). Akt phosphorylates and inactivates several proapoptotic proteins, including the Bcl-2 family member BAD and caspase-9 (11–13). Akt also phosphorylates proteins that indirectly inhibit apoptosis, such as forkhead transcription factors, IκB kinase, and mdm-2 (14–16). In addition, Akt affects cell proliferation by regulating the cell cycle machinery; Akt induces the accumulation of cyclin D1 via inactivation of glycogen synthase kinase-3 and expression of the cyclin-dependent kinase inhibitors p27 and $p21^{WAF1}$ (17–20).

Authors' Affiliations: Departments of [1]Thoracic/Head and Neck Medical Oncology, [2]Molecular Genetics, and [3]Neurosurgery-Research, University of Texas M.D. Anderson Cancer Center, Houston, Texas and [4]Institute for Cell Engineering, Department of Medicine, Johns Hopkins University School of Medicine, Baltimore, Maryland

Received 1/3/05; revised 5/9/05; accepted 5/17/05.

Grant support: NIH grants R01 CA109520 (H-Y. Lee) and CA100816 (H-Y. Lee), American Cancer Society grant RSG-04-082-01-TBE (H-Y. Lee), U.S. Department of Defense grant DAMD17-01-1-0689 (W. K. Hong), and American Cancer Society Clinical Research professorship (W.K. Hong).

The costs of publication of this article were defrayed in part by the payment of page charges. This article must therefore be hereby marked *advertisement* in accordance with 18 U.S.C. Section 1734 solely to indicate this fact.

Requests for reprints: Ho-Young Lee, Department of Thoracic/Head and Neck Medical Oncology, University of Texas M.D. Anderson Cancer Center, Unit 432, 1515 Holcombe Boulevard, Houston, TX 77030. Phone: 713-792-6363; Fax: 713-796-8655; E-mail: hlee@mdanderson.org.

©2005 American Association for Cancer Research.

doi: 10.1158/1078-0432.CCR-05-0009

We and others have suggested that the PI3K/Akt signaling pathway is involved in the early stage of lung cancer progression; increases in gene copy number of the PI3K catalytic subunit α and phosphorylated Akt expression have been observed in premalignant and malignant human bronchial epithelial cells and non–small cell lung cancer (NSCLC) cells (21–26). In addition, inhibition of PI3K/Akt through pharmacologic and genetic approaches induces antiproliferative effects on certain NSCLC cell lines (21–25). We found that inhibition of the PI3K/Akt pathway by overexpression of the dominant-negative mutant form of the p85α adaptor subunit induced NSCLC cells to undergo apoptosis *in vitro*, whereas cell cycle arrest in NSCLC cells was induced by overexpression of PTEN. Because the dominant-negative mutant form of p85α inhibits both Akt and c-*jun* NH_2-terminal kinase (JNK) activation in NSCLC cells and treatment with the PI3K inhibitor LY294002 induced apoptosis in mitogen-activated protein kinase (MAPK) kinase 4 (MKK4)-null cells (23), we hypothesized that the PI3K/Akt- and MKK4/JNK-dependent pathways cooperate to maintain the survival of NSCLC cells. In this study, we undertook a systematic approach to determine whether a dominant-negative mutant form of p85α inhibits tumor growth and whether inhibition of both PI3K/Akt and MKK4/JNK pathways exhibits enhanced antitumor activities *in vivo* in mouse xenograft models.

Materials and Methods

Animals, cell lines, and reagents. Female nude mice, 4 weeks old, were purchased from Harlan-Sprague-Dawley (Indianapolis, IN). H1299 NSCLC cells and 293 cells were maintained in RPMI 1640 and DMEM supplemented with 10% FCS (Life Technologies, Inc., Gaithersburg, MD), respectively, in a humidified environment with 5% CO_2. We purchased insulin-like growth factor (IGF)-I (R&D Systems, Minneapolis, MN), the class I PI3K inhibitor LY294002, JNK inhibitor SP600215 and its companion [(−)SP600215)], MAPK kinase (MEK) inhibitor PD98059, and p38 MAPK inhibitor SB202190 (Calbiochem, La Jolla, CA), recombinant GST-c-Jun and H2B (Santa Cruz Biotechnology, Santa Cruz, CA), and basic protein A-G agarose beads (Santa Cruz Biotechnology). We also purchased rabbit polyclonal antibodies against human phosphorylated Akt (Ser^{473}) and Akt (Cell Signaling Technology, Beverly, MA), rabbit polyclonal anti-Bax and anti-caspase-3 antibodies (PharMingen, San Diego, CA), and rabbit polyclonal anti-Bcl-xL and rabbit polyclonal anti-poly(ADP-ribose) polymerase antibodies (VIC 5, Roche Molecular Biochemicals, Indianapolis, IN). Murine monoclonal anti-PTEN and anti-β-actin antibodies (Santa Cruz Biotechnology) were used for Western blot analyses. Adenoviral vectors that express the dominant-negative 85α (Ad-dnp85α) or PTEN (Ad-PTEN) were previously described (23, 24, 27). Adenoviral vectors expressing full-length human Akt-KM, a kinase-dead, dominant-negative Akt, with a hemagglutinin (HA) tag, in which the lysine (Lys^{179}) in the ATP binding site has been mutated to methionine [Ad-HA-Akt(KM)], or expressing dominant-negative MKK4 in which the lysine (Lys^{129}) in the ATP binding site has been mutated to arginine [Ad-MKK4(KR)] were generated and amplified as previously described (24, 28). The presence of human Akt-KM or MKK4(KR) was confirmed by dideoxy-DNA sequencing and Western blot analysis. Viral titers were determined by plaque assays and spectrophotometric analysis.

Cell proliferation analysis. For cell proliferation assays, NSCLC cell lines were seeded at 1 to 2×10^3 cells per well in 96-well plates. After 24 hours, cells were uninfected or infected in serum-free media with different doses of Ad-dnp85α, Ad-MKK4(KR), Ad-HA-Akt-KM, Ad-PTEN, or their combinations. Empty virus was used to adjust the total doses of adenoviruses in each infection. After 2 hours, cells were changed to RPMI 1640 supplemented with 10% FCS containing different concentrations of LY294002, SP600215 or its companion [(−)SP600215)], SB202190, PD98059, or their combinations. After 3 days of incubation, cell number was measured in a 3-(4,5-dimethylthiazol-2-yl)-2,5-diphenyltetrazolium bromide assay as previously described (24). Six replicate wells were used for each analysis, and data from replicate wells are presented as mean values with 95% confidence intervals. At least three independent experiments were done to obtain each result, and the mean was calculated.

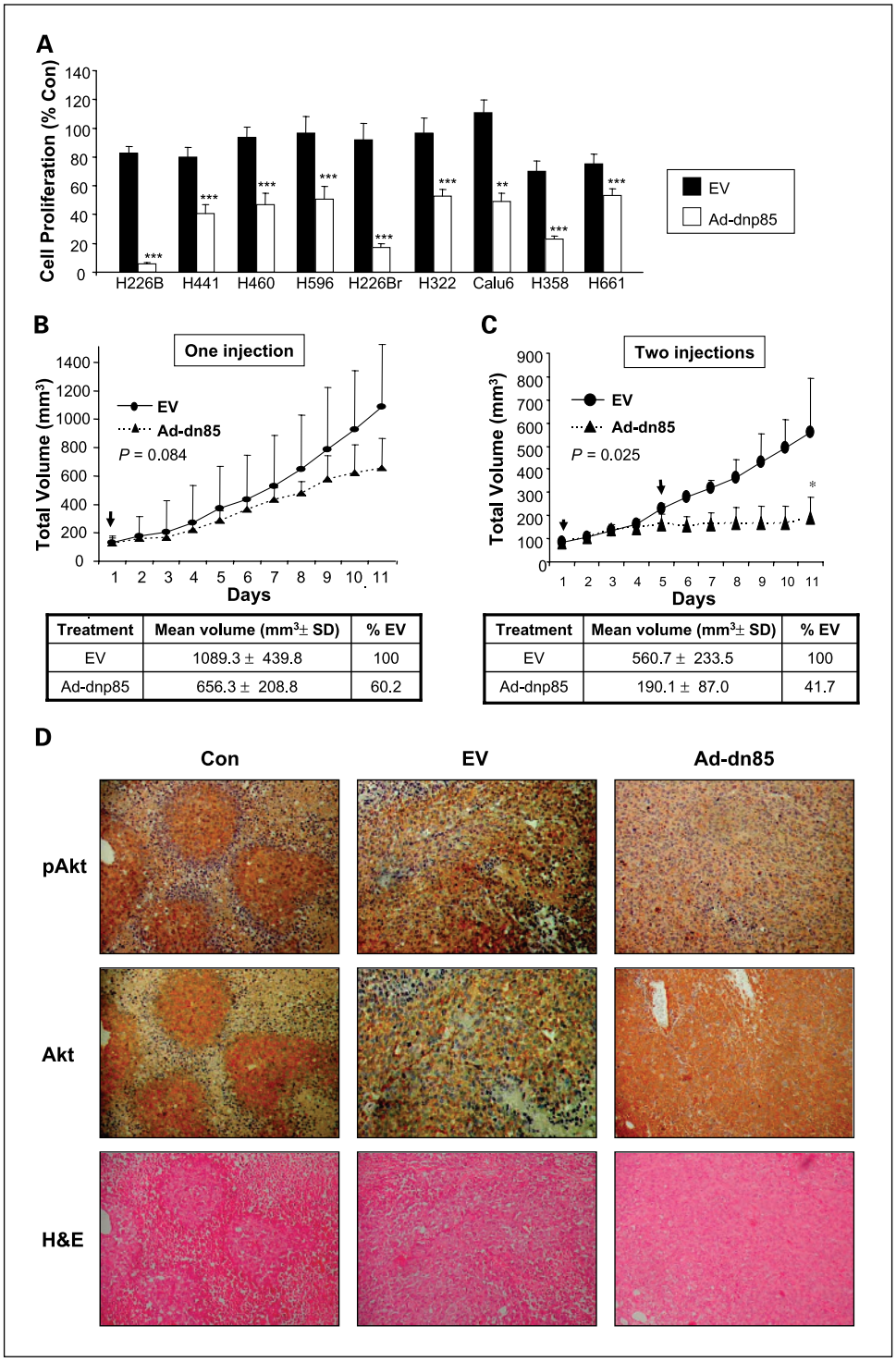
***Inhibition of tumor growth* in vivo.** The effects of Ad-dnp85α, Ad-MKK4(KR), and Ad-HA-Akt(KM) on growth of established s.c. tumor nodules were determined in athymic nude mice in a defined pathogen-free environment as described elsewhere (28). Briefly, 1 day after irradiation with 350 Gy (^{137}Cs source), mice were s.c. injected with H1299 cells (5×10^6) in 100 μL of PBS at a single dorsal site. After tumor volume reached about 100 mm^3, 12 groups of five mice were randomized. The six groups were given intratumoral injections of 100 μL of 1× PBS containing 1×10^{10} viral particles of empty virus, Ad-dnp85α, Ad-MKK4(KR), Ad-HA-Akt(KM), or a combination of Ad-MKK4(KR) and Ad-HA-Akt(KM). The other six groups of five mice were injected with the indicated viruses twice, days 0 and 5 (for Ad-dnp85α or empty virus) or days 0 and 7 [for empty virus, Ad-MKK4(KR), Ad-HA-Akt(KM), or combined injection of Ad-MKK4(KR) and Ad-HA-Akt(KM)]. Tumor size was measured everyday for 11 days (mice injected with empty virus or Ad-dnp85α) or 14 days [mice injected with single or combination of empty virus, Ad-MKK4(KR), or Ad-HA-Akt(KM)], when all mice were sacrificed. Tumor volumes were calculated by $0.5 \times a \times b^2$, where a and b are the long and short diameters, respectively. Mice with necrotic tumors or tumors of >1.5 cm in diameter were euthanized. Results were expressed as the mean (±SD) tumor volumes (calculated in each group of five mice) relative to the volume of tumors injected with control adenovirus. Immunohistochemical staining for phosphorylated Akt and Akt and Western blot analysis on caspase-3 and β-actin were done on tumors collected from mice at the end of measurement of tumors injected with indicated viruses twice.

Immunoblotting. For immunoblotting, whole cell lysates were prepared in lysis buffer, as described previously (21). Equivalent amounts of protein were resolved using SDS-PAGE (7.5-12%) and transferred to nitrocellulose membranes. After being blocked in TBS containing 0.05% Tween 20 (TBST) and 5% w/v nonfat powdered milk, the membranes were incubated with primary antibody at the appropriate dilution in TBS with 5% nonfat milk at 4°C for 16 hours. The membranes were then washed several times with TBST and incubated with the appropriate horseradish peroxidase–conjugated secondary antibody for 1 hour at room temperature. The protein-antibody complexes were detected using enhanced chemiluminescence (ECL kit; Amersham, Arlington Heights, IL) according to the manufacturer's recommended protocol.

Immune complex kinase assays. H1299 cells untreated, treated with various concentrations of LY294002 and SP600215, or infected with several doses of empty virus, Ad-PTEN, Ad-Akt(KM), and Ad-MKK4(KR) were incubated in RPMI supplemented with 10% FCS for 1 day. The cells were serum starved for 24 hours, treated with insulin-like growth factor-I (50 ng/mL) for 15 minutes, lysed, and then subjected to the Western blot analysis and immune complex kinase reactions. Total cell extracts (100 μg) were subjected to immunoprecipitation with a JNK1 antibody or Akt antibodies by rotation at 4°C overnight. Protein A-G agarose beads (20 μL) were added, and the solution was incubated at 4°C for 1 hour. The beads were washed thrice with lysis buffer and once with kinase buffer [20 mmol/L HEPES (pH 7.5), 20 mmol/L β-glycerol phosphate, 10 mmol/L $MgCl_2$, 1 mmol/L DTT, and 50 mmol/L sodium orthovanadate]. Kinase assays were done by incubating the beads with 30 μL kinase buffer to which 20 μmol/L cold ATP, 5 μCi [$\gamma^{32}P$]ATP (2,000 cpm/pmol), and 2 μg of GST-c-Jun or H2B as a substrate were added, as previously described (21). The kinase reaction was done at 30°C for 20 minutes. The samples were suspended in 1× Laemmli

buffer and boiled for 5 minutes, and the samples were analyzed by 12% SDS-PAGE. The gel was dried and autoradiographed.

Apoptosis assays. H1299 cells were plated at a concentration of 5×10^5 cells on 60-mm plates. H1299 cells were untreated, treated with LY294002 (10 μmol/L), Ad-PTEN [10 plaque-forming units (pfu) per cell], Ad-Akt(KM) (20 pfu per cell), Ad-MKK4(KR) (20 pfu per cell), or their combinations, incubated in RPMI supplemented with 10% FCS for 3 days, and then used for Western and fluorescence-activated cell sorting (FACS) assays to analyze apoptosis. For FACS analysis, all cells (i.e., nonadherent and adherent) were harvested, fixed with 1% paraformaldehyde and 70% ethanol, processed using the APO-bromodeoxyuridine staining kit (Phoenix Flow Systems, San Diego, CA), and subjected to a flow cytometry-based, modified terminal deoxynucleotidyl transferase–mediated nick-end labeling (TUNEL) assay as described previously (21). The number of apoptotic cells is represented by the number of FITC-positive cells of the total 10,000 gated cells. The percentage of dead cells was determined using a FACScan flow cytometer (Becton Dickinson, San Jose, CA). Cells treated with empty virus were used as a control for nonapoptotic populations and as a reference for cells treated with Ad-MKK4(KR) or Ad-HA-Akt(KM).



Treatment	Mean volume (mm^3 ± SD)	% EV
EV	1089.3 ± 439.8	100
Ad-dnp85	656.3 ± 208.8	60.2

Treatment	Mean volume (mm^3 ± SD)	% EV
EV	560.7 ± 233.5	100
Ad-dnp85	190.1 ± 87.0	41.7

Fig. 1. Ad-dnp85α inhibits the growth of NSCLC cells. *A*, effects of Ad-dnp85α on the growth of NSCLC cell lines were measured. NSCLC cell lines were uninfected or infected with 20 pfu per cell of Ad-dnp85α or empty virus (*EV*) and incubated in a growth medium for 3 days. Cell proliferation was measured using 3-(4,5-dimethylthiazol-2-yl)-2, 5-diphenyltetrazolium bromide assays, and the results are expressed relative to the number of uninfected control cells incubated in the same medium. Column, mean from six identical wells; bars, ±SD. **, $P < 0.01$; ***, $P < 0.001$ compared with control cells. *B-C*, effects of Ad-dnp85α on the growth of H1299 NSCLC xenograft tumors were tested. H1299 cells were injected into the dorsal flank of athymic nude mice. Once tumor volume reached about ~100 mm^3, 1×10^{10} viral particles of Ad-dnp85α were intratumorally injected. These viruses were injected (*B*) once (day 0) or (*C*) twice (days 0 and 5). The growth of H1299 NSCLC xenograft tumors were measured every day. Point, mean tumor volume (calculated from five mice) relative to the volume of tumors injected with empty virus; bars, ±SD. *, $P < 0.05$ compared with control tumors. *D*, immunohistochemical analysis for phosphorylated Akt (*pAkt*) and Akt expression was done on the xenograft tumor tissues that were injected with empty virus or Ad-dnp85α twice (days 0 and 5) and then collected at 11 days, when mice were sacrificed.

As an internal control, HL-60 cells provided in the apoptosis detection kit were treated with camptothecin to induce apoptosis to ensure that the TUNEL reaction was occurring during the staining procedure. Representative results from two independent experiments were presented.

Statistical analysis. All data are expressed as means ± SD. Cell proliferation among groups was compared using Student's *t* tests. Synergistic indexes of combination treatment was calculated by growth inhibition rate, as previously described (29). *P*s < 0.05 were considered statistically significant.

Results

***Effects of dominant-negative p85α on non–small cell lung cancer cell growth* in vitro *and* in vivo.** We previously showed that inhibition of the PI3K/Akt pathway by Ad-dnp85α efficiently induced expression of dominant-negative p85α in the H1299 NSCLC cell line and markedly inhibited cell proliferation (23). In the present study, we further tested the antiproliferative effects of Ad-dnp85α on a number of NSCLC cell lines. Relative to the control, Ad-dnp85α infection inhibited the growth of NSCLC cells (Fig. 1A). To determine the effects of Ad-dnp85α on the growth of NSCLC cells *in vivo*, H1299 xenograft tumor nodules established in athymic nude mice were injected with Ad-dnp85α. After a single injection of Ad-dnp85α, tumor growth was decreased, although statistically not significant (Fig. 1B); the mean volume of tumors injected with Ad-dnp85α (mean volume, 656.3 ± 208.8 mm^3) reduced by 39.8% compared with tumors injected with empty virus (mean volume, 1,089.3 ± 439.8 mm^3) at day 11(P = 0.084). Compared with a single injection, however, double injections of Ad-dnp85α significantly reduced tumor volume by 58.3% (mean volume, 190.1 ± 87.0 mm^3) compared with tumors injected with empty virus twice (mean volume, 560.7 ± 233.5 mm^3; P = 0.025; Fig. 1C). According to the immunohistochemical analysis, the level of phosphorylated Akt was reduced dramatically in the tumors injected with Ad-dnp85α and not in the tumors injected with empty virus or 1× PBS alone (*Con*; Fig. 1D), showing the specific *in vivo* activity of Ad-dnp85α on Akt activity.

Response of non–small cell lung cancer cells to the inhibition of both phosphatidylinositol 3-kinase/Akt and mitogen-activated protein kinase kinase 4/c-jun NH_2-terminal kinase pathways. Our previous work showed that PI3K/Akt- and MKK4/JNK-dependent pathways interact to maintain cell survival (23); the PI3K inhibitor LY294002 induced apoptosis in MKK4-null (−/−) cells but not in wild-type (+/+) MEF cells. We also observed that overexpression of dominant-negative p85α inhibited activation of Akt and JNK, whereas PTEN suppressed activation of Akt but not JNK (23). Therefore, we hypothesized that PI3K/Akt and MKK4/JNK pathways cooperate to maintain NSCLC cell survival and the antitumor activities of Ad-dnp85α on NSCLC cells are due to its inhibitory effects on these two pathways.

To test our hypothesis, we tested the effects of PI3K inhibitors (i.e., LY294002, Ad-PTEN, and Ad-Akt(KM)], JNK inhibitors [i.e., SP600215 and Ad-MKK4(KR)], and their combinations on the proliferation of NSCLC cells *in vitro* and *in vivo*. We previously found that these inhibitors regulate JNK or PI3K/Akt pathways in NSCLC cells incubated in complete medium (data not shown). We then tested the activities of these inhibitors on growth factor–stimulated JNK and PI3K/Akt activities in

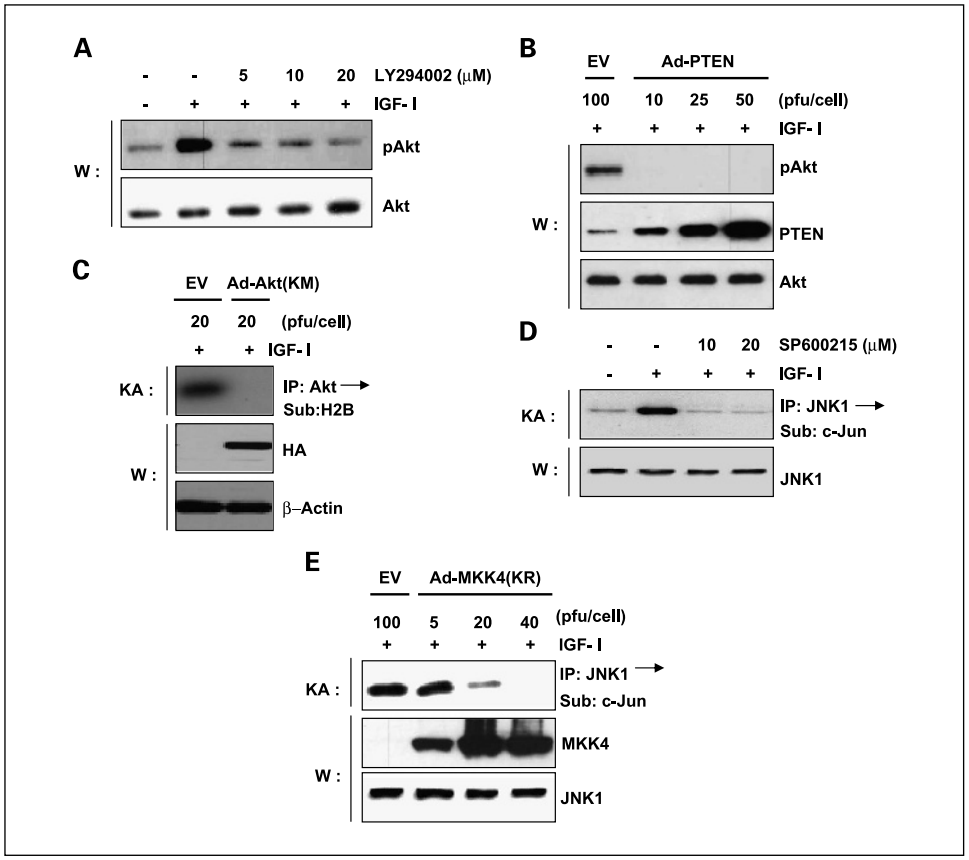


Fig. 2. Effect of inhibitors of PI3K/Akt and MKK4/JNK pathways on Akt and JNK activity. *A-B*, H1299 cells were untreated, treated with the indicated concentrations of LY294002 (*A*), or infected with the indicated doses of empty virus (*EV*) or Ad-PTEN (*B*). One day after incubation in complete medium, cells were serum-starved for on day and unstimulated or stimulated with IGF-I (100 ng/mL) for 15 minutes. Expression of phosphorylated Akt (*pAkt*), Akt, and PTEN was analyzed by Western blot analysis (*W*). *C-E*, H1299 cells were untreated, infected with the indicated dose of empty virus, Ad-Akt(KM) (*C*), or Ad-MKK4(KR) (*D*), or treated with 10 or 20 μmol/L of SP600215 (*E*). One day after incubation in complete medium, cells were serum-starved and then stimulated with IGF-I (100 ng/mL) for 15 minutes as described above. Akt or JNK activity was determined by immune complex kinase assays using H2B or GST-c-Jun, respectively, as a substrate. HA, MKK4, and JNK1 expression was examined by Western blot analysis.

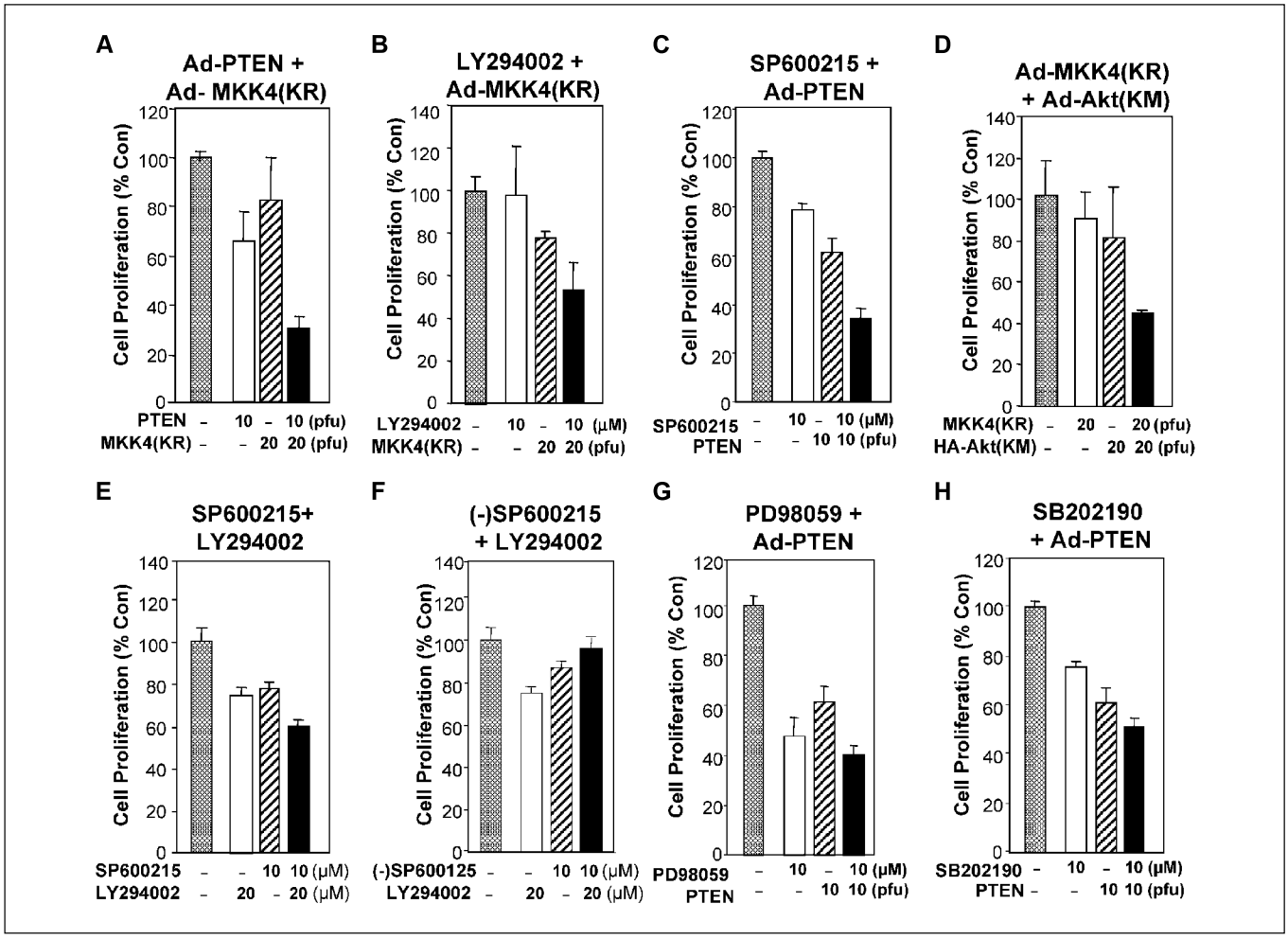


Fig. 3. Effects of the PI3K/Akt inhibitor, MKK4/JNK inhibitors, or their combination on the proliferation of NSCLC cells; 1-2 × 10^3 H1299 cells per well in 96-well plate were uninfected (*E*, *F*) or infected (*A-D*, *G*, *H*) with indicated doses of Ad-MKK4(KR), Ad-PTEN, Ad-HA-Akt(KM), or their combination in serum-free condition for 2 hours. Empty virus (*EV*) was used to adjust the total doses of adenoviruses same in each infection. Then, cells were changed to RPMI 1640 supplemented with 10% FCS containing LY294002 (10 or 20 μmol/L), SP600215 (10 μmol/L), (−)SP600215 (10 μmol/L), PD98059(10 μmol/L), SB202190(10 μmol/L), or their combinations. Cells treated with same doses of empty virus (*A-D, G, H*) or 0.1% DMSO (*E, F*) were used as a control. After 3 days, cell number was measured by the 3-(4,5-dimethylthiazol-2-yl)-2,5-diphenyltetrazolium bromide assay. % Cell proliferation relative to the proliferation of control cells (−). Column, mean value of six identical wells from a representative single experiment ($n = 3$); bars, upper 95% confidence intervals. At least three independent experiments were done to obtain each result, and the mean was calculated.

H1299 cells 2 days after the drug treatment. According to the Western blot analysis (Fig. 2A-B) and *in vitro* immune complex kinase assay (Fig. 2C), IGF-I increased phosphorylation and activation of AKt, which were suppressed by the treatment with LY294002 (Fig. 2A), Ad-PTEN (Fig. 2B), or Ad-Akt(KM) (Fig. 2C). IGF-I also induced JNK activities, which were suppressed by SP600215 (Fig. 2D) or Ad-MKK4(KR) (Fig. 2E). Western blot analysis of PTEN, HA, and MKK4 revealed that Ad-PTEN, Ad-HA-Akt(KM), and Ad-MKK4(KR) increased the expression of the adenoviral gene products. Equal amounts of protein loading for Akt and JNK1 were confirmed by Western blot analysis. These results indicate that the pharmacologic and genetic approaches used in our study effectively blocked the PI3K/Akt or MKK4/JNK signaling pathways.

We then tested the effects of single or combined treatment of these inhibitors on the proliferation and apoptosis of NSCLC cells. To avoid nonspecific effects of these inhibitors on other signaling pathways, we used 10 or 20 μmol/L of LY294002, 10 pfu per cell of Ad-PTEN, 20 pfu per cell of Ad-Akt(KM), 20 pfu per cell of Ad-MKK4(KR), 10 μmol/L of SP600215 or its companion [(−)SP600215] that lacks the ability to inhibit JNK (30, 31); the minimum doses that were enough to inhibit the respective kinases after 3 days of treatment (data not shown). H1299 cells infected with Ad-PTEN, Ad-MKK4(KR), or Ad-Akt(KM), or treated with LY294002 or SP600215 showed mild but significant anti-proliferative effects compared with control (Fig. 3; Table 1). Ad-PTEN/Ad-MKK4(KR) (Fig. 3A), LY294002/Ad-MKK4(KR) (Fig. 3B), SP600215/Ad-PTEN (Fig. 3C), and Ad-MKK4(KR)/Ad-Akt(KM) (Fig. 3D) showed synergistically enhanced anti-proliferative effects on H1299 cells compared with single-agent treatment (Table 1). Similar results of significantly decreased H1299 cell proliferation were observed after the combined treatment of chemical inhibitors, LY294002 (20 μmol/L) and SP600215 (10 μmol/L), compared with the effects of single-agent treatment (Fig. 3E). In contrast, (−)SP600215 did not enhance the effects of LY294002 on proliferation of NSCLC cells (Fig. 3F). MEK inhibitor (PD98059, 10 μmol/L) alone

Table 1. Synergistic indexes of combination treatment calculated by growth inhibition rate

Treatment A				Treatment B				Combination treatment			Index*
Drug	Concentration	MGI†	P‡	Drug	Concentration	MGI†	P‡	Expected§	Observed	P‡	
Ad-PTEN	10 pfu	0.662	9.937e−05	Ad-MKK4(KR)	20 pfu	0.829	0.047	0.505	0.293	1.101e−10	1.723
LY294002	10 μmol/L	0.973	0.857	Ad-MKK4(KR)	20 pfu	0.774	0.007	0.753	0.528	0.002	1.427
SP600215	10 μmol/L	0.784	9.979e−05	Ad-PTEN	10 pfu	0.617	2.991e−05	0.484	0.349	2.537e−07	1.387
Ad-MKK4 (KR)	20 pfu	0.905	0.430	Ad-HA-Akt(KM)	20 pfu	0.819	0.314	0.741	0.446	0.005	1.663
LY294002	20 μmol/L	0.757	0.001	SP600215	10 μmol/L	0.781	0.002	0.591	0.589	4.134e−05	1.004
LY294002	20 μmol/L	0.751	0.001	(−)SP600215	10 μmol/L	0.888	0.056	0.672	0.957	0.29	0.703
SB202190	10 μmol/L	0.765	9.979e−05	Ad-PTEN	10 pfu	0.617	2.991e−05	0.472	0.519	2.537e−07	0.909
PD98059	10 μmol/L	0.47	2.481e−05	Ad-PTEN	10 pfu	0.617	2.991e−05	0.29	0.402	2.393e−07	0.721
LY294002	20 μmol/L	0.746	9.187e−05	PD98059	10 μmol/L	0.795	7.846e−03	0.593	0.816	0.001	0.727
LY294002	20 μmol/L	0.746	9.187e−05	SB202190	10 μmol/L	0.758	0.004	0.565	0.743	6.658e−05	0.761

Abbreviation: MGI, mean growth inhibition.

*Calculated by dividing the expected growth inhibition rate by the observed growth inhibition rate. An index of >1 indicates synergistic effect and an index of <1 indicates less than additive effect.

†MGI = growth rate of treated group/growth rate of untreated group.

‡*P* (two sided) was calculated by *t* test compared to control cells.

§Growth inhibition rate of treatment A × growth inhibition rate of treatment B.

decreased H1299 cell proliferation (Fig. 3G) to the similar degree as the combination of JNK and Akt inhibitors (compared with the Fig. 3B, D, and E). Moreover, PD98059 and p38 MAPK inhibitor (SB202190) mildly enhanced the antiproliferative effects of Ad-PTEN (Fig. 3G and H). However, the cooperativity between Ad-PTEN with PD98059 or SB202190 in inhibiting NSCLC cell proliferation was less than additive (Table 1). Similarly, combinations of chemical inhibitors of PI3K/Akt and MEK (LY294002/PD98059) or PI3K/Akt and p38 MAPK (LY294002/SB202190) did not show enhanced antiproliferative effects on NSCLC cells (Table 1). Because PD98059 inhibits more than MEK depending on cellular context, we also tested the effects of combined treatment with U0126, another MEK inhibitor, and PI3K/Akt inhibitors. Similar to PD98059, U0126 showed antiproliferative effects on NSCLC cells at <10 μmol/L, however, it did not enhance the antiproliferative effects of PI3K/Akt inhibitors on NSCLC cells (data not shown). These findings suggest that the specific MAPK pathway MKK4/JNK and PI3K/Akt cooperate to stimulate NSCLC cell proliferation.

We then studied whether inhibition of PI3K/Akt- and MKK4/JNK-dependent pathways enhanced apoptosis in H1299 cells that were simultaneously treated with Ad-Akt(KM)/Ad-MKK4(KR), Ad-MKK4(KR)/Ad-PTEN, or Ad-MKK4(KR)/LY294002. The cells simultaneously treated with these inhibitors showed typical morphologic changes of apoptosis, including membrane blebbing, increased refractoriness, and chromatin condensation (data not shown). To measure apoptotic cell population, we did terminal deoxynucleotidyl transferase–mediated nick-end labeling staining of H1299 cells. One representative data out of two separate experiments with similar results are shown in Fig. 4. Compared with 0.5% of H1299 cells infected with empty virus, 15.3% of H1299 cells infected with Ad-Akt(KM), and 5.3% of H1299 cells infected with Ad-MKK4(KR), 62.4% of H1299 cells treated with Ad-Akt(KM)/Ad-MKK4(KR) underwent apoptosis (Fig. 4A, *top*). Similarly, cells treated with Ad-MKK4(KR)/Ad-PTEN or Ad-MKK4(KR)/LY294002 showed a marked increase in apoptotic populations compared with those treated with a single agent (Fig. 4A, *bottom*). Western blot analysis revealed that the combined treatment of Ad-MKK4(KR) and Ad-Akt(KM) induced decreased levels of procaspase-3 (M_r = 32 kDa) and antiapoptotic Bcl-xL protein expression and increased levels of poly(ADP-ribose) polymerase cleavage (113-kDa to the 89-kDa fragment) and proapoptotic Bax protein expression (Fig. 4B), suggesting that a change in the ratio of antiapoptotic protein (i.e., Bcl-xL) to proapoptotic protein (i.e., Bax) might have contributed to the apoptotic activities of Ad-Akt(KM)/Ad-MKK4(KR) in NSCLC cells. All of these results support our hypothesis that the PI3K/Akt and MKK4/JNK pathways cooperate to maintain NSCLC cell survival.

Effect of the phosphatidylinositol 3-kinase/Akt and mitogen-activated protein kinase kinase 4/c-jun NH_2-terminal kinase pathways on tumor growth. The cooperative growth and regulatory effects of PI3K/Akt- and MKK4/JNK-dependent pathways were further explored *in vivo* using s.c. H1299 tumor nodules established in athymic nude mice. Ad-MKK4(KR) and Ad-Akt(KM), either individually or in a combination, were injected into the tumors once (day 0) or twice (days 0 and 7). Mean volumes of tumors injected with empty virus were used as a control. A single treatment with Ad-MKK4(KR) or Ad-Akt(KM) reduced tumor volume by 29.70% (mean volume, 1,131.22 ± 561.14 mm^3; P = 0.3506) or 16.50% (mean volume, 1,344.09 ± 559.56 mm^3; P = 0.5922), respectively, compared with the empty virus-injected tumor (mean volume, 1,609.65 ± 638.25 mm^3). Suppression of tumor growth was significantly enhanced by the concurrent injection of Ad-MKK4(KR) and Ad-Akt(KM) (58.86%; mean volume, 662.21 ± 322.69 mm^3; P = 0.0381) compared with the volume of tumors injected with Ad-MKK4(KR) or Ad-Akt(KM) alone (Fig. 5A). Compared with a single injection, double injections significantly enhanced the inhibitory effects on tumor growth. Double injections of Ad-MKK4(KR) or Ad-Akt(KM) significantly reduced the tumor

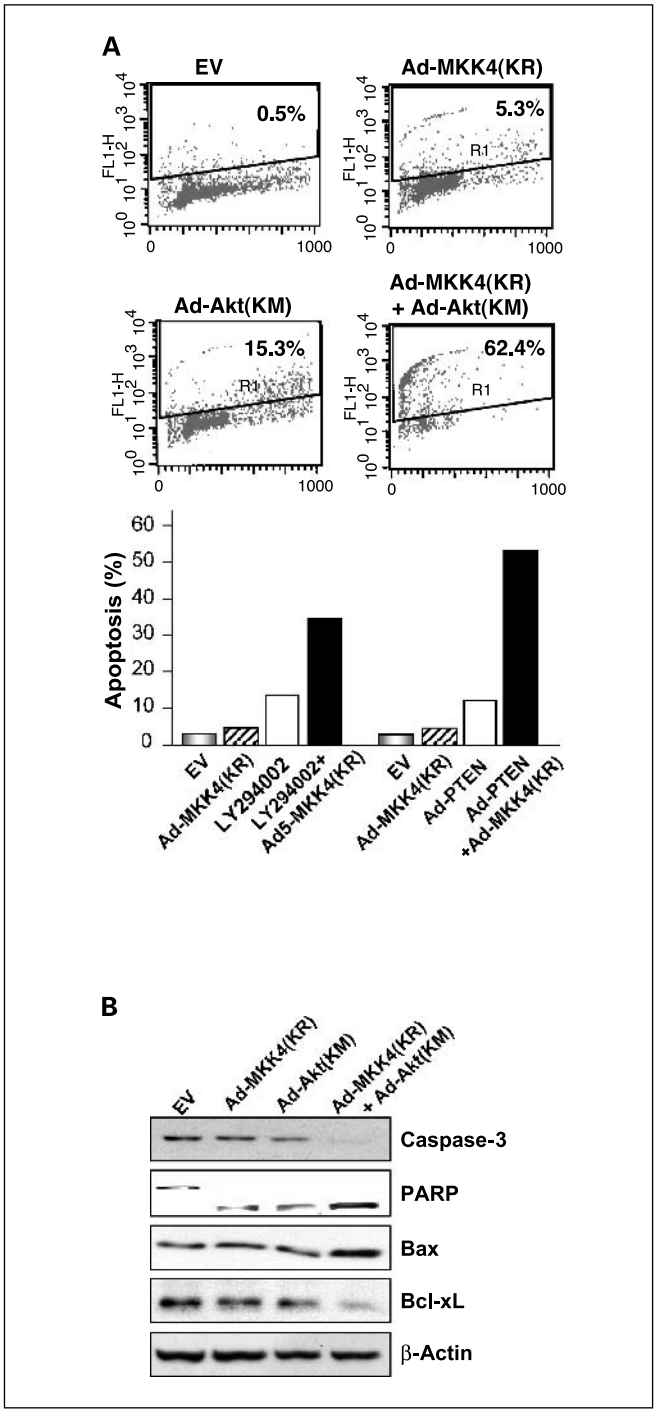


Fig. 4. Effects of the PI3K/Akt inhibitor, MKK4/JNK inhibitors, or their combination on the apoptosis of NSCLC cells. *A*, H1299 cells were treated with empty virus (*EV*), Ad-MKK4(KR) (20 pfu per cell), Ad-HA-Akt(KM) (20 pfu per cell), LY294002 (10 μmol/L), Ad-PTEN (10 pfu per cell), or their combinations. Flow cytometry was done using APO-BRDU staining. Living gating of the forward and orthogonal scatter channels was used to exclude debris and to selectively acquire cell events. All values reflect the percentage of cells as determined by light scatter. The percentage of dead cells was determined by fluorescence-activated cell sorting analysis of propidium iodide – stained nuclei. Top, representative cytogram from the cells infected with empty virus, Ad-MKK4(KR), Ad-Akt(KM), or Ad-MKK4(KR)/Ad-Akt(KM). The number of apoptotic cells is represented by the number of FITC-positive cells of the total 10,000 gated cells. Two separate experiments were done with similar results. *B*, H1299 cells infected with empty virus, Ad-Akt(KM), Ad-MKK4(KR), or Ad-Akt(KM)/Ad-MKK4(KR) were subjected to Western blot analysis for the expression of caspase-3, poly(ADP-ribose) polymerase (*PARP*), Bax, and BcL-xL. β-Actin was included as an indicator of equal protein loading.

volume by 53.46% (mean volume, 389.26 ± 90.03 mm^3; P = 0.0297) or 80.80% (mean volume, 160.56 ± 91.29 mm^3; P = 0.0074), respectively, compared with the volume of tumors injected with empty virus (mean volume, 829.60 ± 225.27 mm^3) twice (Fig. 5B). Concurrent double injections of Ad-MKK4(KR) and Ad-Akt(KM) resulted in significantly enhanced inhibitory effects on NSCLC tumor growth (95.25%; mean volume, 39.69 ± 7.22 mm^3; P = 0.0031) compared with the tumors injected with Ad-MKK4(KR) or Ad-Akt(KM) alone. Representative tumors injected with empty virus, Ad-MKK4(KR), Ad-Akt(KM), or combination of Ad-MKK4(KR) and Ad-Akt(KM) twice are shown in Fig. 5C. Enhanced apoptosis by concurrent injection of Ad-MKK4(KR) and Ad-Akt(KM) was evident by Western blot analysis on caspase-3 using the H1299 xenograft tumor tissues injected with indicated viruses twice and then collected at 14 days, when mice were cleaved sacrificed. Densitometric analysis of the levels of cleaved active caspase-3 (Ac-caspase3/uncleaved pro-caspase-3 [pro-caspase3]) revealed that injection of both Ad-MKK4(KR) and Ad-Akt(KM) induced activation of caspase-3 compared with the levels induced by empty virus, Ad-MKK4(KR), or Ad-Akt(KM) alone (Fig. 5D). These findings indicate that inhibition of both the PI3K/Akt and MKK4/JNK signaling pathways markedly enhance antitumor activities *in vivo*.

Discussion

The studies reported herein show that intratumoral injection of the dominant-negative mutant form of p85α inhibited NSCLC xenograft tumor growth. Simultaneous inhibition of the PI3K/Akt and MKK4/JNK pathways also efficiently inhibited NSCLC cell proliferation *in vitro* and *in vivo* by inducing apoptosis. These findings indicate cooperative activities of the PI3K/Akt and MKK4/JNK pathways in promoting the growth of NSCLC.

Tumor cells have devised several mechanisms to inhibit apoptosis and prolong their survival. Clear evidence exists for the involvement of the PI3K/Akt signaling pathway in lung carcinogenesis. Akt is constitutively active in premalignant and malignant human bronchial epithelial cells (21, 32) as well as in NSCLCs (23, 25, 26), probably owing to the activating mutations of *ras* (33, 34), overexpression of the epidermal growth factor receptor family and one of its ligands, transforming growth factor α (35, 36), increased copy number of PI3K catalytic subunit α (26), elevated levels of the subunits of PI3K (37), and reduced level of PTEN expression (38). Activation of Akt has been suggested an early biochemical effect of tobacco constituents on normal human bronchial epithelial cells (39). These findings indicated that Akt activation is an early event in lung tumorigenesis and, as a corollary, that the PI3K/Akt signaling pathway is a potential target for chemoprevention and treatment of lung cancer. In fact, our recent attempts to interfere with the PI3K/Akt pathway have shown some promise in lung cancer prevention (21). Moreover, inhibition of the PI3K/Akt signaling pathway by treatment with PI3K inhibitor LY294002 or by overexpression of dominant-negative *p85α* or *PTEN* lipid phosphatase effectively inhibited H1299 NSCLC cell lines (23). Based on our previous findings that (a) overexpression of a dnp85α regulatory subunit of PI3K induced apoptosis, whereas LY294002 or overexpression of the *PTEN* induced proliferative arrest in H1299 NSCLC

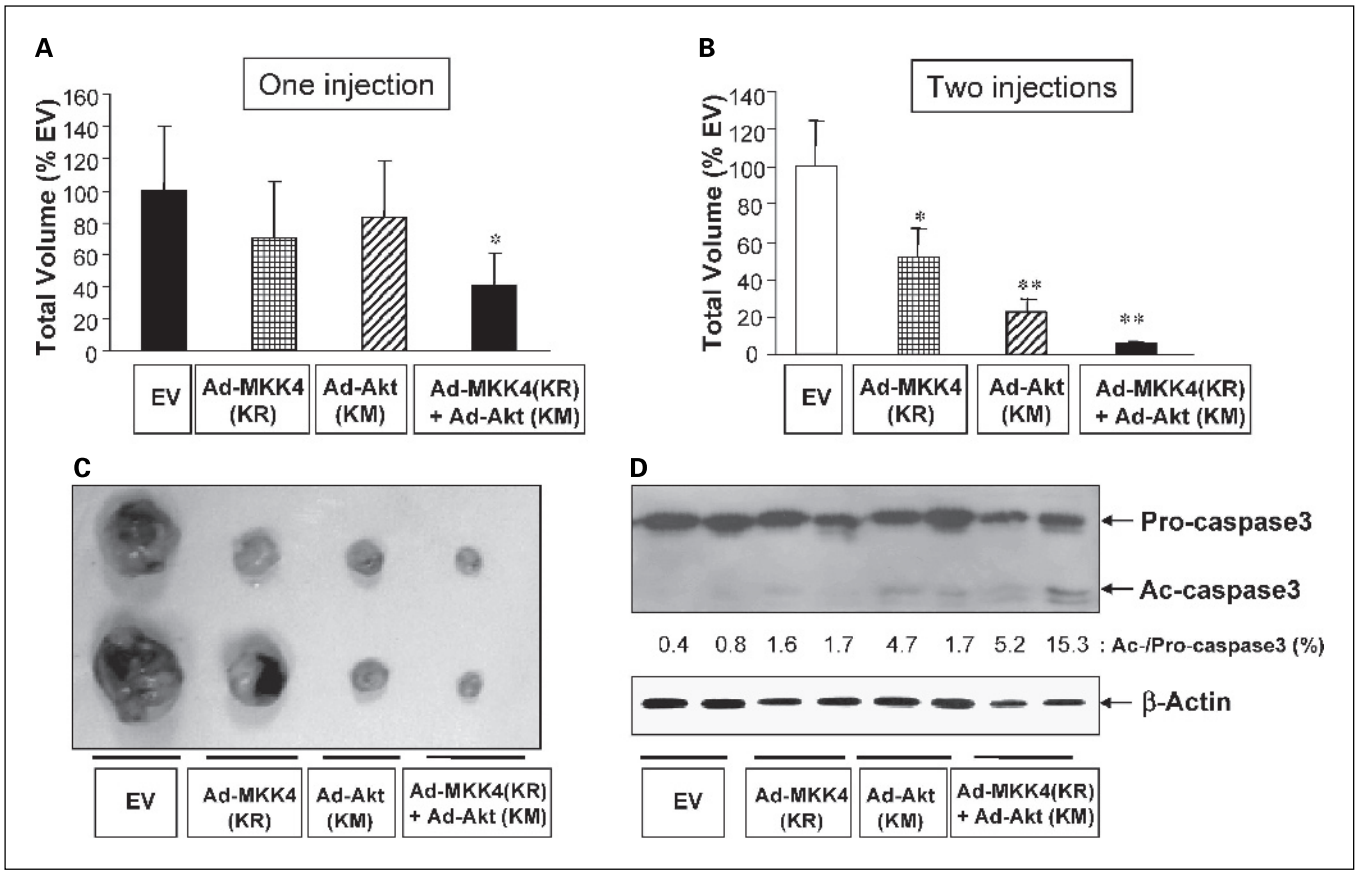


Fig. 5. Effect of simultaneous treatment with Ad-Akt(KM) and Ad-MKK4(KR) on the growth of NSCLC xenografts. H1299 cells were injected into the dorsal flank of athymic nude mice. Once tumor volume reached ~100 mm^3, 1 $\times 10^{10}$ viral particles of single or combination of the indicated adenovirus were intratumorally injected. These viruses were injected (*A*) once (day 0) or (*B* and *C*) twice (days 0 and 7). Tumors were measured everyday. Column, mean tumor volume (calculated from five mice) relative to the volume of tumors injected with empty virus; bars, ±SD (*A*, *B*). *, $P < 0.05$; **, $P < 0.01$ compared with control tumors. *D*, Western blot analysis was done on the tissues from H1299 xenograft tumor nodules injected with indicated viruses twice and then collected at 14 days, when mice were sacrificed. β-Actin was included as a loading control.

cells; (b) dnp85α inhibited JNK activity and Akt activities, whereas LY294002 or overexpression of the *PTEN* inhibited Akt activity with no effect on JNK activity in H1299 cells; (c) constitutively active *Rac-1* (Val^{12}) blocked dnp85α-induced apoptosis in these cells; and (d) LY294002 treatment induced apoptosis in *MKK4*-null MEF cells but not in wild-type MEF cells, we hypothesized that the PI3K/Akt signaling pathway cooperates with other mitogen-activated signaling pathways to maintain cell survival and that dnp85α induces apoptosis through the combined inhibition of MKK4/JNK- and PI3K/Akt-dependent pathways. This hypothesis is further supported by the previous finding that MAPK family members play distinct biological roles in tumor cells (40, 41). Therefore, we set out the current study to evaluate the antitumor activities of dnp85α as well as that of combined inhibition of PI3K/Akt and MKK4/JNK pathways in NSCLC *in vitro* as well as *in vivo*.

Overexpression of dominant-negative p85α inhibited proliferation of most of the NSCLC cell lines used in this study and was shown to reduce tumor growth in the H1299 NSCLC xenograft tumor model. We previously found that the introduction of wild-type p85α did not recapitulate the effects of dnp85α on JNK and Akt, suggesting that dnp85α functions through mechanisms other than increasing intracellular levels of p85α, which inactivates PI3K lipid kinase activity through changes in the stoichiometry of p85/p110 (42). In this study, we also found that wile-type p85 PI3K adenovirus had no effects on the induction of cell death and adenovirus expressing wild-type p85 did not enhance apoptotic activities in NSCLC cells, when simultaneously treated with MKK4/JNK inhibitors (data not shown). Moreover, supporting our hypothesis, enhanced regression of tumor volume was also observed in the H1299 xenograft tumors injected with Ad-Akt(KM) and Ad-MKK(KR) compared with tumors injected with each virus alone, providing an *in vivo* evidence of the cooperative activities between these two pathways in maintaining survival of NSCLC cells. These findings also suggest that the *MKK4* gene is a potential tumor promoter in NSCLC. Evidence relating to the role of *MKK4* as a tumor promoter or suppressor is contradictory. Deletion or mutation of the *MKK4* gene has been observed in several types of carcinomas, and reintroduction of *MKK4* inhibits the metastatic ability of certain tumor cells, indicating the activity of MKK4 as a tumor suppressor (43–45). In contrast, MKK4 has been shown to play a role in cellular transformation by mediating the effects of Rac-1 that contribute to Ras-induced cellular transformation (46). Similarly, the role of JNK in apoptosis has been in debate. JNK is involved in the apoptotic response of cells exposed to stress, but in some studies in tumor cells, the JNK signal transduction pathway has been implicated in cell survival. The possibility that JNK might mediate a survival signal in tumor cells is

further supported by the finding that it is activated in response to some oncoprotein, such as *BCR-ABL* (47). In addition, JNK has been implicated in the phosphorylation of Bcl-2, which may be required for Bcl-2 to achieve its full potent anti-apoptotic activity (48). Therefore, it is plausible that the MKK4/JNK pathway can act as both a promoter and a suppressor of human carcinogenesis, depending on the presence of cell type-specific factors that induce or inhibit specific functions of the pathway.

We found that induction of apoptosis by Ad-MKK4(KR) and Ad-Akt(KM) has been associated with an abrogation of caspase-3 activity and changes in the expression of Bcl-2 family members, including Bax and Bcl-xL. The balance between antiapoptotic and proapoptotic proteins has been shown to determine whether a cell survives or undergoes apoptosis (49). These findings suggest that the enhanced antiapoptotic activities of Ad-MKK4(KR) and Ad-Akt(KM) resulted, in part, from changes in the regulation of the antiapoptotic to proapoptotic protein ratio. Because Bcl-xL also functions independently in regulating cell death (50), the reduction in Bcl-xL protein expression could, in part, account for the increased apoptosis in NSCLC cells treated with these adenoviral vectors.

In conclusion, the findings presented here indicate for the first time that the PI3K/Akt and MKK4/JNK pathways cooperate to promote the survival of NSCLC cells *in vitro* and *in vivo*. Our findings illustrate the importance of understanding the role of interactions between different signaling pathways, especially PI3K/Akt and MKK4/JNK, in the growth of NSCLC cells, providing a rationale for designing effective therapeutic strategies for lung cancer. Whereas we showed the cooperativity between the Akt and JNK pathways in NSCLC cell proliferation and tumor growth, this effect could be specific to the H1299 cell line. Therefore, intensive studies using several NSCLC cell types with the multiple individual pathway inhibitors are required to investigate how variations in PI3K and Akt signaling can predetermine the efficacy of this treatment strategy. In addition, further studies are warranted to determine the optimal sequence of the administration of PI3K/Akt and MKK4/JNK pathway inhibitors, which would affect the degree of synergism and thus the therapeutic efficacy of these treatments (51).

References

1. Gibbs JB. Anticancer drug targets: growth factors and growth factor signaling. J Clin Invest 2000;105:9–13.
2. Kennedy SG, Kandel ES, Cross TK, Hay N. Akt/Protein kinase B inhibits cell death by preventing the release of cytochrome *c* from mitochondria. Mol Cell Biol 1999;19:5800–10.
3. Hausler P, Papoff G, Eramo A, Reif K, Cantrell DA, Ruberti G. Protection of CD95-mediated apoptosis by activation of phosphatidylinositide 3-kinase and protein kinase B. Eur J Immunol 1998;28:57–69.
4. Brodt P, Samani A, Navab R. Inhibition of the type I insulin-like growth factor receptor expression and signaling: novel strategies for antimetastatic therapy. Biochem Pharmacol 2000;60:1101–7.
5. Vivanco I, Sawyers CL. The phosphatidylinositol 3-kinase AKT pathway in human cancer. Nat Rev Cancer 2002;2:489–501.
6. Brazil DP, Hemmings BA. Ten years of protein kinase B signalling: a hard Akt to follow. Trends Biochem Sci 2001;26:657–64.
7. Toker A, Newton AC. Cellular signaling: pivoting around PDK-1. Cell 2000;103:185–8.
8. Wymann MP, Pirola L. Structure and function of phosphoinositide 3-kinases. Biochim Biophys Acta 1998;1436:127–50.
9. Toker A, Cantley LC. Signalling through the lipid products of phosphoinositide-3-OH kinase. Nature 1997;387:673–6.
10. Li J, Yen C, Liaw D, Podsypanina K, Bose S, Wang SI, et al. PTEN, a putative protein tyrosine phosphatase gene mutated in human brain, breast, and prostate cancer. Science 1997;275:1943–7.
11. Di Cristofano A, Pandolfi PP. The multiple roles of PTEN in tumor suppression. Cell 2000;100:387–90.
12. Datta SR, Dudek H, Tao X, et al. Akt phosphorylation of BAD couples survival signals to the cell-intrinsic death machinery. Cell 1997;91:231–41.
13. Cardone MH, Roy N, Stennicke HR, et al. Regulation of cell death protease caspase-9 by phosphorylation. Science 1998;282:1318–21.
14. Kops GJ, Burgering BM. Forkhead transcription factors: new insights into protein kinase B (c-akt) signaling. J Mol Med 1999;77:656–65.
15. Romashkova JA, Makarov SS. NF-κB is a target of AKT in anti-apoptotic PDGF signalling. Nature 1999;401:86–90.
16. Mayo LD, Donner DB. A phosphatidylinositol 3-kinase/Akt pathway promotes translocation of Mdm2 from the cytoplasm to the nucleus. Proc Natl Acad Sci U S A 2001;98:11598–603. Epub 2001 Aug 14.
17. Zhou BP, Liao Y, Xia W, Spohn B, Lee MH, Hung MC. Cytoplasmic localization of p21Cip1/WAF1 by Akt-induced phosphorylation in HER-2/*neu*-overexpressing cells. Nat Cell Biol 2001;3:245–52.
18. Collado M, Medema RH, Garcia-Cao I, et al. Inhibition of the phosphoinositide 3-kinase pathway induces a senescence-like arrest mediated by p27Kip1. J Biol Chem 2000;275:21960–8.
19. Cross DA, Alessi DR, Cohen P, Andjelkovich M, Hemmings BA. Inhibition of glycogen synthase kinase-3 by insulin mediated by protein kinase B. Nature 1995;378:785–9.
20. Diehl JA, Cheng M, Roussel MF, Sherr CJ. Glycogen synthase kinase-3β regulates cyclin D1 proteolysis and subcellular localization. Genes Dev 1998;12:3499–511.
21. Chun KH, Kosmeder JW II, Sun S, et al. Effects of deguelin on the phosphatidylinositol 3-kinase/Akt pathway and apoptosis in premalignant human bronchial epithelial cells. J Natl Cancer Inst 2003;95:291–302.
22. Lee HY. Molecular mechanisms of deguelin-induced apoptosis in transformed human bronchial epithelial cells. Biochem Pharmacol 2004;68:1119–24.
23. Lee HY, Srinivas H, Xia D, et al. Evidence that phosphatidylinositol 3-kinase- and mitogen-activated protein kinase kinase-4/c-Jun NH_2-terminal kinase-dependent pathways cooperate to maintain lung cancer cell survival. J Biol Chem 2003;278:23630–8. Epub 2003 Apr 24.
24. Lee HY, Moon H, Chun KH, et al. Effects of insulin-like growth factor binding protein-3 and farnesyltransferase inhibitor SCH66336 on Akt expression and apoptosis in non-small-cell lung cancer cells. J Natl Cancer Inst 2004;96:1536–48.
25. Brognard J, Clark AS, Ni Y, Dennis PA. Akt/protein kinase B is constitutively active in non-small cell lung cancer cells and promotes cellular survival and resistance to chemotherapy and radiation. Cancer Res 2001;61:3986–97.
26. Massion PP, Taflan PM, Shyr Y, et al. Early involvement of the phosphatidylinositol 3-kinase/Akt pathway in lung cancer progression. Am J Respir Crit Care Med 2004;170:1088–94.
27. Hara K, Yonezawa K, Sakaue H, et al. 1-Phosphatidylinositol 3-kinase activity is required for insulin-stimulated glucose transport but not for RAS activation in CHO cells. Proc Natl Acad Sci U S A 1994;91:7415–9.
28. Lee HY, Chun KH, Liu B, et al. Insulin-like growth factor binding protein-3 inhibits the growth of non-small cell lung cancer. Cancer Res 2002;62:3530–7.
29. Dings RP, Yokoyama Y, Ramakrishnan S, Griffioen AW, Mayo KH. The designed angiostatic peptide anginex synergistically improves chemotherapy and anti-angiogenesis therapy with angiostatin. Cancer Res 2003;63:382–5.
30. Bennett BL, Sasaki DT, Murray BW, et al. SP600125, an anthrapyrazolone inhibitor of Jun N-terminal kinase. Proc Natl Acad Sci U S A 2001;98:13681–6.
31. Shin M, Yan C, Boyd D. An inhibitor of c-*jun* amino-terminal kinase (SP600125) represses c-Jun activation, DNA-binding and PMA-inducible 92-kDa type IV collagenase expression. Biochimica et Biophysica Acta 2002;1589:311–6.
32. Tsao AS, McDonnell T, Lam S, et al. Increased phospho-AKT (Ser(473)) expression in bronchial dysplasia: implications for lung cancer prevention studies. Cancer Epidemiol Biomarkers Prev 2003;12:660–4.
33. Mitsudomi T, Steinberg SM, Oie HK, et al. ras gene mutations in non-small cell lung cancers are associated with shortened survival irrespective of treatment intent. Cancer Res 1991;51:4999–5002.
34. Mills NE, Fishman CL, Rom WN, Dubin N, Jacobson DR. Increased prevalence of K-*ras* oncogene mutations in lung adenocarcinoma. Cancer Res 1995;55:1444–7.
35. Rusch V, Klimstra D, Venkatraman E, Pisters PW, Langenfeld J, Dmitrovsky E. Overexpression of the epidermal growth factor receptor and its ligand transforming growth factor α is frequent in resectable non-small cell lung cancer but does not predict tumor progression. Clin Cancer Res 1997;3:515–22.
36. Fontanini G, De Laurentiis M, Vignati S, et al. Evaluation of epidermal growth factor-related growth factors and receptors and of neoangiogenesis in completely resected stage I-IIIA non-small-cell lung cancer: amphiregulin and microvessel count are independent prognostic indicators of survival. Clin Cancer Res 1998;4:241–9.
37. Lin X, Bohle AS, Dohrmann P, et al. Overexpression of phosphatidylinositol 3-kinase in human lung cancer. Langenbecks Arch Surg 2001;386:293–301.

38. Soria JC, Lee HY, Lee JI, et al. Lack of PTEN expression in non-small cell lung cancer could be related to promoter methylation. Clin Cancer Res 2002;8:1178–84.

39. West KA, Brognard J, Clark AS, et al. Rapid Akt activation by nicotine and a tobacco carcinogen modulates the phenotype of normal human airway epithelial cells. J Clin Invest 2003;111:81–90.

40. Gupta S, Plattner R, Der CJ, Stanbridge EJ. Dissection of Ras-dependent signaling pathways controlling aggressive tumor growth of human fibrosarcoma cells: evidence for a potential novel pathway. Mol Cell Biol 2000;20:9294–306.

41. Shields JM, Mehta H, Pruitt K, Der CJ. Opposing roles of the extracellular signal-regulated kinase and p38 mitogen-activated protein kinase cascades in Ras-mediated downregulation of tropomyosin. Mol Cell Biol 2002;22:2304–17.

42. Cuevas BD, Lu Y, Mao M, et al. Tyrosine phosphorylation of p85 relieves its inhibitory activity on phosphatidylinositol 3-kinase. J Biol Chem 2001;276:27455–61.

43. Su GH, Hilgers W, Shekher MC, et al. Alterations in pancreatic, biliary, and breast carcinomas support MKK4 as a genetically targeted tumor suppressor gene. Cancer Res 1998;58:2339–42.

44. Yoshida BA, Dubauskas Z, Chekmareva MA, Christiano TR, Stadler WM, Rinker-Schaeffer CW. Mitogen-activated protein kinase kinase 4/stress-activated protein/Erk kinase 1 (MKK4/SEK1), a prostate cancer metastasis suppressor gene encoded by human chromosome 17. Cancer Res 1999;59:5483–7.

45. Teng DH, Perry WL III, Hogan JK, et al. Human mitogen-activated protein kinase kinase 4 as a candidate tumor suppressor. Cancer Res 1997;57:4177–82.

46. Qiu RG, Chen J, Kirn D, McCormick F, Symons M. An essential role for Rac in Ras transformation. Nature 1995;374:457–9.

47. Hess P, Pihan G, Sawyers CL, Flavell RA, Davis RJ. Survival signaling mediated by c-Jun NH(2)-terminal kinase in transformed B lymphoblasts. Nat Genet 2002;32:201–5.

48. Deng X, Xiao L, Lang W, Gao F, Ruvolo P, May WS Jr. Novel role for JNK as a stress-activated Bcl2 kinase. J Biol Chem 2001;276:23681–8. Epub 2001 Apr 25.

49. Oltvai ZN, Milliman CL, Korsmeyer SJ. Bcl-2 heterodimerizes *in vivo* with a conserved homolog, Bax, that accelerates programmed cell death. Cell 1993;74:609–19.

50. Coll ML, Rosen K, Ladeda V, Filmus J. Increased Bcl-xL expression mediates v-Src-induced resistance to anoikis in intestinal epithelial cells. Oncogene 2002;21:2908–13.

51. Chou TC, Talalay P. Quantitative analysis of dose-effect relationships: the combined effects of multiple drugs or enzyme inhibitors. Adv Enzyme Regul 1984;22:27–55.

THE JOURNAL OF BIOLOGICAL CHEMISTRY
Vol. 278, No. 26, Issue of June 27, pp. 23630–23638, 2003
© 2003 by The American Society for Biochemistry and Molecular Biology, Inc.
Printed in U.S.A.

Evidence That Phosphatidylinositol 3-Kinase- and Mitogen-activated Protein Kinase Kinase-4/c-Jun NH_2-terminal Kinase-dependent Pathways Cooperate to Maintain Lung Cancer Cell Survival*

Received for publication, January 29, 2003, and in revised form, April 17, 2003
Published, JBC Papers in Press, April 24, 2003, DOI 10.1074/jbc.M300997200

Ho-Young Lee‡, Harish Srinivas‡, Dianren Xia‡, Yiling Lu§, Robert Superty‡, Ruth LaPushin§, Candelaria Gomez-Manzano‡, Anna Maria Gal‡, Garrett L. Walsh¶, Thomas Force‖, Kohjiro Ueki, Gordon B. Mills§, and Jonathan M. Kurie‡ ‡‡**

*From the Departments of ‡Thoracic/Head and Neck Medical Oncology, §Molecular Therapeutics, and ¶Thoracic and Cardiovascular Surgery, The University of Texas M. D. Anderson Cancer Center, Houston, Texas 77030, the ‖Molecular Cardiology Research Institute, New England Medical Center, Boston, Massachusetts 02111, and the **Research Division, Joslin Diabetes Center and Departments of Medicine and Cell Biology, Harvard Medical School, Boston, Massachusetts 02215*

Cancer cells in which the *PTEN* lipid phosphatase gene is deleted have constitutively activated phosphatidylinositol 3-kinase (PI3K)-dependent signaling and require activation of this pathway for survival. In non-small cell lung cancer (NSCLC) cells, PI3K-dependent signaling is typically activated through mechanisms other than *PTEN* gene loss. The role of PI3K in the survival of cancer cells that express wild-type *PTEN* has not been defined. Here we provide evidence that H1299 NSCLC cells, which express wild-type *PTEN*, underwent proliferative arrest following treatment with an inhibitor of all isoforms of class I PI3K catalytic activity (LY294002) or overexpression of the *PTEN* lipid phosphatase. In contrast, overexpression of a dominant-negative mutant of the p85α regulatory subunit of PI3K (Δp85) induced apoptosis. Whereas PTEN and Δ85 both inhibited activation of AKT/protein kinase B, only Δp85 inhibited c-Jun NH_2-terminal kinase (JNK) activity. Co-transfection of the constitutively active mutant *Rac-1* (Val^{12}), an upstream activator of JNK, abrogated Δp85-induced lung cancer cell death, whereas constitutively active mutant mitogen-activated protein kinase kinase (*MKK*)-1 (R4F) did not. Furthermore, LY294002 induced apoptosis of *MKK4*-null but not wild-type mouse embryo fibroblasts. Therefore, we propose that, in the setting of wild-type *PTEN*, PI3K- and MKK4/JNK-dependent pathways cooperate to maintain cell survival.

Class I phosphatidylinositol 3-kinase (PI3K)[1] consists of a family of heterodimeric complexes composed of a p110 catalytic subunit and a regulatory subunit that exists predominantly in a p85 form (1–3). The known gene family members for *p85* (α, β, and γ) and *p110* (α, β, δ, and γ) are expressed in a tissue-specific fashion. p85α and -β can also exist in smaller forms (p50 and p55). PI3K phosphorylates the D3 position of PI on PI(4)P and PI(4,5)P to produce $PI(3,4)P_2$ and $PI(3,4,5)P_3$. The 3′ sites of $PI(3,4)P_2$ and $PI(3,4,5)P_3$ are dephosphorylated by the PTEN tumor suppressor, whereas the 5′ site of $PI(3,4,5)P_3$ is dephosphorylated by SHIP to produce $PI(3,4)P_2$ (1). These mechanisms tightly regulate the levels of 3-phosphorylated PI in the cell. $PI(3,4,5)P_3$ and $PI(3,4)P_2$ recruit the pleckstrin homology domains of specific intracellular proteins to the plasma membrane, an essential event in the activation of PI3K-dependent kinases such as phosphoinositide-dependent kinase-1 and AKT, also known as protein kinase B. In addition, AKT phosphorylation at Thr^{308} by phosphoinositide-dependent kinase-1 and Ser^{473} by integrin-linked kinase (and possibly other kinases) constitutes an essential event in AKT activation (4, 5).

The PI3K pathway clearly has a key role in cellular survival and transformation. AKT phosphorylates several pro- and anti-apoptotic proteins, including the Bcl-2 family member BAD, caspase-9, cyclic AMP response element-binding protein, the inhibitor of NF-κB kinase IKKα, and forkhead transcription factor-1 (6). Tumor cells feature genetic and epigenetic alterations of *p85α*, *p110α/β*, *AKT2*, *AKT3*, and *PTEN* that activate PI3K-dependent signaling (7–13). *In vitro* studies have confirmed the oncogenic effects of PI3K and its downstream mediators as well as the tumor-suppressive properties of PTEN (14–19).

PI3K mediates its oncogenic effects, in part, through the GTP-binding protein Rac-1, which plays a key role in the reorganization of the actin cytoskeleton induced by growth factors or oncogenic Ras (20). p85α interacts directly with Rac-1 (21). Ras activates Rac-1 indirectly as a consequence of PI3K-mediated phosphorylation of membrane PIs (22). $PI(3,4,5)P_3$ binds to the guanosine nucleotide-exchange factor SOS, stimulating SOS to load Rac-1 with GTP, an essential event in Rac-1 activation. Rac-1, in turn, activates downstream signaling through PAK-1 and its mediators, which include mitogen-acti-

* This work was supported by National Institutes of Health Grants P50 CA70907, CA80686, CA82716, CA83639, DAMD17-01-1-0689, and CA64602. The costs of publication of this article were defrayed in part by the payment of page charges. This article must therefore be hereby marked "*advertisement*" in accordance with 18 U.S.C. Section 1734 solely to indicate this fact.

‡‡ To whom correspondence should be addressed: Unit 432, The University of Texas M. D. Anderson Cancer Center, 1515 Holcombe Blvd., Houston, TX 77030-4009. Tel.: 713-792-6363; Fax: 713-796-8655; E-mail: jkurie@mdanderson.org.

[1] The abbreviations used are: PI3K, phosphatidylinositol 3-kinase; $PI(3,4)P_2$, phosphatidylinositol 3,4-bisphosphate; $PI(3,4,5)P_3$, phosphatidylinositol 3,4,5-bisphosphate; PI(4,5)P, phosphatidylinositol 4,5-phosphate; PI(4)P, phosphatidylinositol 4-phosphate; MKK, mitogen-activated protein kinase kinase; JNK, c-Jun NH_2-terminal kinase; NSCLC, non-small cell lung cancer; MEF, mouse embryo fibroblast; EGF, epidermal growth factor; IGF-1, insulin-like growth factor-1; MAP, mitogen-activated protein kinase; SH2, Src homology domain 2; HA, hemagglutinin; PBD, p21 binding domain; CMV, cytomegalovirus; GST, glutathione *S*-transferase; MBP, myelin basic protein; GSK3, glycogen synthase kinase 3; CDK2, cyclin-dependent kinase 2; ERK1/2, extracellular signal-regulated kinase 1/2; BrdUrd, bromodeoxyuridine; PTEN, phosphatase and tensin homolog deleted from chromosome 10.

This paper is available on line at http://www.jbc.org

Downloaded from www.jbc.org at M D ANDERSON HOSP, on October 7, 2010

vated protein kinase kinase-4 (MKK4) and its substrates c-Jun NH_2-terminal kinase (JNK) and p38/HOG1 (23).

Certain cancer cell types with *PTEN* gene loss have constitutively active PI3K and undergo apoptosis in response to pharmacologic or genetic inhibition of PI3K (24). Most non-small cell lung cancer (NSCLC) cell lines demonstrate hallmarks of PI3K pathway activation, such as phosphorylation of AKT and its downstream mediators, but have a wild-type *PTEN* gene (25–30). Despite having wild-type *PTEN*, NSCLC cells undergo apoptosis in response to PI3K pathway inhibition (25). The apoptosis reported by Brognard *et al.* (25) may depend in part on the absence of serum, which rescues cells from apoptosis induced by PI3K inhibition (18, 19, 31, 32). Thus, serum-induced activation of other peptide growth factor-induced signaling pathways can overcome the pro-apoptotic effect of PI3K inhibition. In this study, we investigated the signaling pathways that interact with PI3K to control NSCLC cell survival. Using pharmacologic and genetic approaches, we found that inhibition of PI3K-dependent signaling alone induced proliferative arrest, whereas inhibition of both PI3K and MKK4/JNK-dependent pathways induced apoptosis. These findings indicate that, in the setting of wild-type *PTEN*, PI3K- and MKK4/JNK-dependent pathways cooperate to maintain cell survival.

EXPERIMENTAL PROCEDURES

Reagents—H358, H661, Calu-6, H460, H226B, H226Br, H441, and H1299 NSCLC cells were maintained in RPMI 1640 supplemented with 10% fetal calf serum (complete medium). COS-7 cells and *MKK4*-null and wild-type mouse embryo fibroblast (MEF) cells (33) were maintained in Dulbecco's modified Eagle's medium supplemented with 10% fetal calf serum. We purchased epidermal growth factor (EGF) (Invitrogen), insulin-like growth factor-1 (IGF-1) (R&D Systems, Minneapolis, MN), the class I PI3K inhibitor LY294002 (Calbiochem, La Jolla, CA), tumor necrosis factor-α (Sigma), recombinant GST-c-Jun (Santa Cruz Biotechnology, Santa Cruz, CA), myelin basic protein (MBP) (New England Biolabs, Beverly, MA), GST-GSK3β (Santa Cruz), and protein A-G-agarose beads (Santa Cruz). We also purchased rabbit polyclonal antibodies against human phospho-AKT (pAKT1; Ser^{473}) and AKT1 (New England Biolabs), phospho-JNK (Thr^{183}/Tyr^{185}; Cell Signaling Technologies), p85α, cyclin-dependent kinase (CDK) 2, and p27 (Santa Cruz), and murine monoclonal antibodies against human PTEN (Santa Cruz), phosphoextracellular signal-regulated kinase (ERK) (Thr^{202}/Tyr^{204}; Cell Signaling), caspase-3 and -9 (BD Pharmingen), poly(ADP-ribose) polymerase (VIC5) (Roche Diagnostics), and goat polyclonal antibodies against human ERK1/2, JNK-1, and β-actin (Santa Cruz). The adenoviral vector expressing wild-type p85α (Adex1CAp85α-HA) has been described elsewhere (34). A recombinant adenovirus expressing human PTEN under the control of a cytomegalovirus (CMV) promoter was a gift from Dr. W. K. A. Yung (M. D. Anderson Cancer Center). Plasmid expression vectors containing *Rac-1* (Val^{12}) and *MKK1* (R4F) were gifts from Dr. Melanie Cobb (The University of Texas Southwestern Medical Center, Dallas, TX).

Generation of Ad5-Δp85—Δ*p85* is a bovine p85α mutant lacking 35 amino acids (residues Met^{479} to Lys^{513}) in the inter-SH2 region that are necessary for binding to the p110 catalytic subunit (35). The Δ*p85* cDNA was inserted into the 5′ end of the bovine growth hormone polyadenylation signal at the *Hin*dIII site of the pAd-shuttle vector, which was a gift from Dr. Jack Roth (M. D. Anderson Cancer Center). The Δ*p85*-containing shuttle vector was digested with *Bst*I/*Cla*I and inserted into the pAd-speed vector (36). 293 cells were transfected with the resulting plasmid and then maintained until the onset of the cytopathic effect. Viral titers were determined by plaque assays and spectrophotometric analysis. The presence of Δ*p85* in viral particles was confirmed by dideoxy-DNA sequencing and Western blot analysis.

Cell Growth Assays—NSCLC cell lines were seeded at 1–2 $\times$ 10^3 cells/well in 96-well plates. After 24 h, cells were incubated in serum-free conditions with 5 $\times$ 10^2, 1 $\times$ 10^3, 5 $\times$ 10^3, or 1 $\times$ 10^4 p/cell of Ad5-Δp85, Ad5-PTEN, or Ad5-CMV (control virus). After 2 h, cells were changed to complete medium. In the case of LY294002 treatment, cells were treated with 0.2, 2, 20, 40, 60, or 80 μM LY294002 in complete medium, which was changed every 48 h. After 5 days, cell growth was measured by 3-(4,5-dimethylthiazol-2-yl)-2,5-diphenyltetrazolium bromide assay.

Western Blot Analysis—Whole cell lysates were prepared by incubating cell pellets in lysis buffer (50 mM HEPES (pH 7.5), 150 mM NaCl, 1.5 mM $MgCl_2$, 1 mM EDTA, 0.2 mM EGTA, 1% Nonidet P-40, 10% glycerol, 1 mM dithiothreitol, 1 mM phenylmethylsulfonyl fluoride, 20 mM sodium fluoride, 5 mM sodium orthovanadate, 10 μg/ml aprotinin, 10 μg/ml leupeptin, 2 μg/ml pepstatin, and 1 mM benzamidine) for 20 min on ice. After clarification by centrifugation at 13,000 $\times$ *g* for 20 min, the supernatants were collected, and the protein concentration was determined with a BCA protein assay kit (Pierce). Cell lysates (30 μg) were subjected to SDS-PAGE and transferred onto a polyvinylidene fluoride nitrocellulose membrane (Bio-Rad). Membranes were immunoblotted overnight at 4 °C with primary antibodies in Tris-buffered saline containing 5% nonfat dry milk. Antibody binding was detected with an electrochemiluminescence kit (Amersham Biosciences) according to the manufacturer's directions.

Cell Cycle and Apoptosis Assays—For these experiments, 1 $\times$ 10^6 H1299 cells were transferred onto 100-mm plates. Twenty-four hours later, the cells were incubated with 1 $\times$ 10^3, 5 $\times$ 10^3, or 1 $\times$ 10^4 particles of Ad5-Δp85 or Ad5-PTEN per cell. For combination treatments, H1299 cells were transiently transfected with 5 μg of plasmids containing *Rac-1* (Val^{12}), *MKK1* (R4F), or empty vector using FuGENE (Roche Diagnostics). After 6 h, the cells were incubated for 2 h in serum-free conditions with Ad5-Δp85 or Ad5-CMV at 1 $\times$ 10^3 or 5 $\times$ 10^3 particles/cell. Cells were allowed to grow in complete medium for 48 h before being subjected to apoptosis assays.

Apoptosis and cell cycle progression were measured by TUNEL with the APO-BRDU staining kit (Phoenix Flow Systems, San Diego, CA). Floating cells and attached cells were dispersed with trypsin-EDTA, pelleted, washed, and fixed in 1% paraformaldehyde for 15 min on ice and then fixed in 70% ethanol. The fixed cells were washed and incubated with DNA labeling solution containing terminal deoxynucleotidyltransferase reaction buffer, deoxynucleotidyltransferase enzyme, and bromodeoxyuridine triphosphate (BrdUrd-dUTP). The cells were rinsed before being resuspended with fluorescein-PRB-1 antibody solution and analyzed by flow cytometry in the presence of propidium iodide/RNase solution. Analyses of 3,000 to 10,000 events were done with a FACScan flow cytometer (BD Pharmingen) equipped with a 488-nm argon ion laser and two software packages: CellQuest 3.1 (BD Pharmingen) and ModFit LT 2.0 (Verity Software House, Topsham, ME). Live gating of the forward and orthogonal scatter channels was used to exclude debris and to selectively acquire cell events. A dual display of DNA area (linear red fluorescence) and BrdUrd-dUTP incorporation (FITC-PRB-1) was used to determine the percentage of propidium iodine-stained cells that were apoptotic.

Apoptosis was also determined by the detection of nucleosomal DNA fragmentation by using the TACS apoptotic DNA laddering kit (Trevigen, Inc., Gaithersburg, MD) according to the manufacturer's protocol. Briefly, DNA was isolated from cells after adenovirus transfection or LY294002 treatment by incubating them in lysis buffer. DNA samples were subjected to electrophoresis on a 1.5% agarose gel and visualized by ethidium bromide staining.

Immune Complex Kinase Assay—H1299 cells were incubated for 2 h with Ad5-CMV, Ad5-Δp85, or Ad5-PTEN at 1 $\times$ 10^3, 5 $\times$ 10^3, or 1 $\times$ 10^4 p/cell in serum-free conditions, changed to complete medium, and incubated for 48 h. Cells were then washed twice in 1$\times$ phosphate-buffered saline, serum-starved for 24 h, treated with 50 ng/ml EGF for 15 min, and lysed in lysis buffer. Extracts were subjected to immunoprecipitation (100 μg) with antibodies to JNK1, AKT1/2, or ERK1/2 by rotation at 4 °C overnight. Protein A-G-agarose beads (20 μl) were added, and the solution was incubated at 4 °C for 1 h. The beads were washed three times with lysis buffer and once with kinase buffer (20 mM Hepes (pH 7.5), 20 mM β-glycerol phosphate, 10 mM $MgCl_2$, 1 mM dithiothreitol, and 50 mM sodium orthovanadate). Kinase assays were performed by incubating the beads with 30 μl of kinase buffer, to which 20 μM cold ATP, 5 μCi of [γ-^{32}P]ATP (2,000 cpm/pmol), and 2 μg of GST-c-Jun, GST-GSK3β, or MBP as substrates were added. The kinase reaction was performed at 30 °C for 20 min. The samples were then suspended in 1$\times$ Laemmli buffer and boiled for 5 min, and the samples were analyzed by 12% SDS-PAGE. The gel was dried and autoradiographed.

Immune complex assays were also performed with COS-7 cells, which were transiently transfected for 6 h with 5 μg of plasmids containing *Rac-1* (Val^{12}), *MKK1* (R4F), or empty vector using FuGENE. The cells were then transfected with Ad5-Δp85 or Ad5-CMV (1 $\times$ 10^3 or 5 $\times$ 10^3 particles/cell) and incubated in complete medium for 24 h. The cells were then changed to serum-free medium for 24 h, treated with IGF-1 (50 ng/ml) for 15 min, and lysed. JNK and ERK were immunoprecipitated from 100 μg of total cell lysates and subjected to kinase assays using GST-c-Jun and MBP, respectively, as substrates.

Downloaded from www.jbc.org at M D ANDERSON HOSP, on October 7, 2010

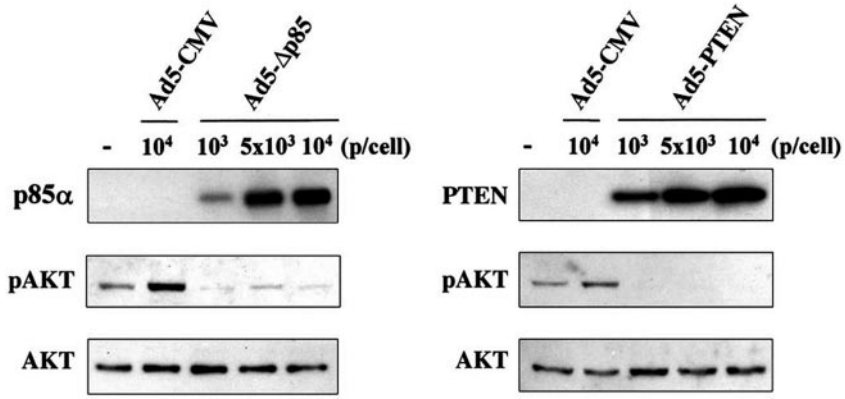


FIG. 1. **Expression of adenoviral gene products and pAKT (Ser^{473}) in H1299 NSCLC cells after transfection with Ad5-CMV, Ad5-Δp85, or Ad5-PTEN.** H1299 cells were treated with medium alone (−) or incubated with the indicated viral particles (particles/cell). Three days later, the cells were lysed, and 30 μg of whole cell lysates were subjected to Western blot analysis of PTEN, p85α, pAKT (Ser^{473}), and, as a control, total AKT1 (AKT1).

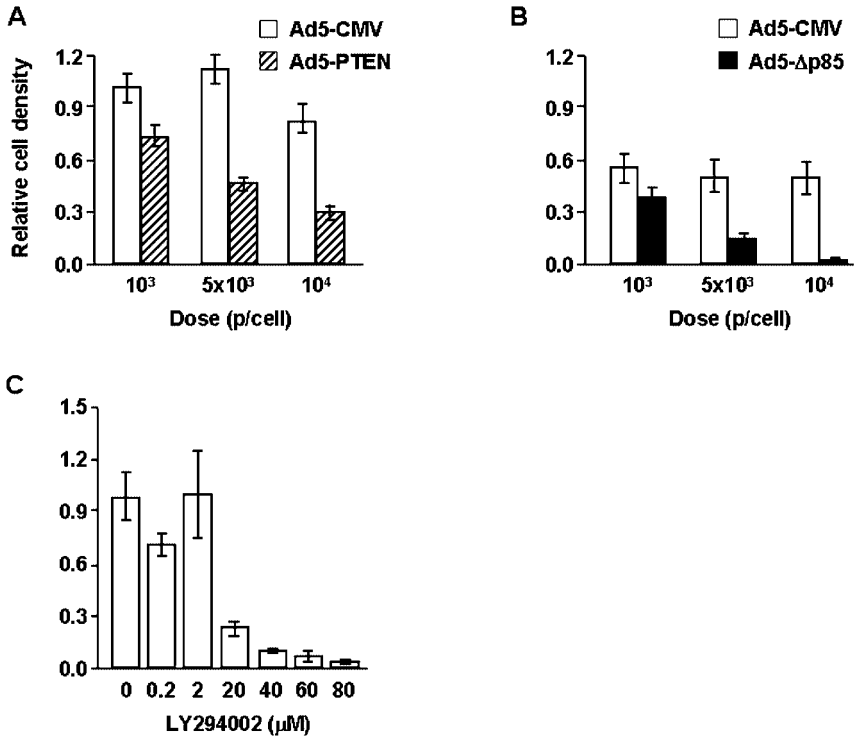


FIG. 2. **Effect of PI3K inhibition on H1299 cell numbers.** H1299 cells were (*A*) incubated with the indicated titers of Ad5-PTEN or Ad5-CMV, (*B*) incubated with the indicated titers of Ad5-Δp85 or Ad5-CMV, or (*C*) treated with medium alone (0) or the indicated doses of LY294002. The cells were incubated for 5 days, at which time they were subjected to 3-(4,5-dimethylthiazol-2-yl)-2,5-diphenyltetrazolium bromide assays. Results are expressed relative to the density of cells treated with medium alone. Each value is the mean (± S.D.) of five identical wells.

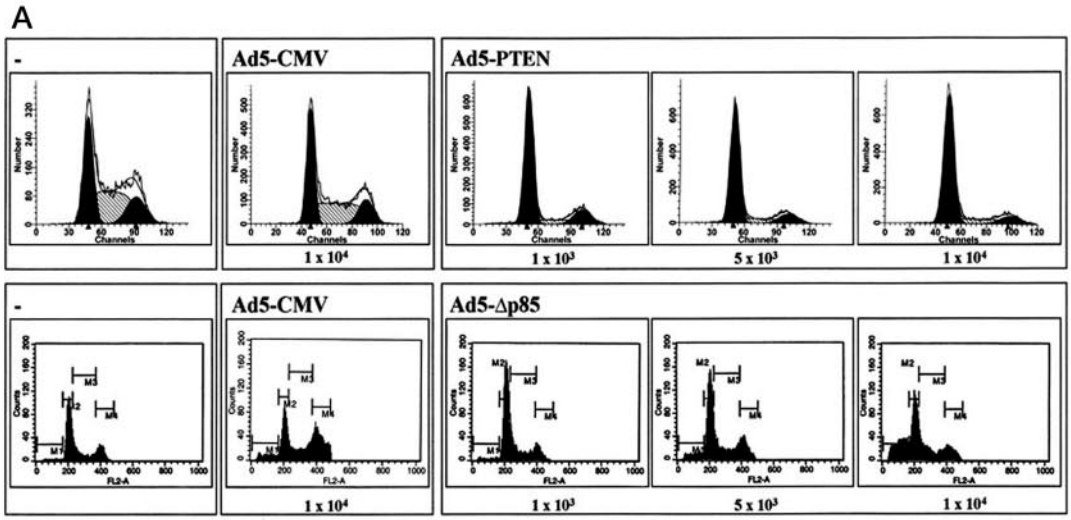
Rac-1 Activity Assays—Pull-down assays with GST-tagged p21 binding domain (PBD) of PAK-1 were performed as follows. COS-7 cells were co-transfected with 2 μg of HA-tagged *p85α*, HA-tagged *p110α*, and *Δp85* (2, 4, or 6 μg) using LipofectAMINE (Invitrogen). Total amount of DNA transfected per plate was equalized with empty vector. After 6 h, transfectants were washed and changed to normal growth medium. After 24 h, transfectants were serum-starved for 16 h, treated with 50 ng/ml EGF or IGF-1 for 15 min, and lysed. PAK-1 PBD-agarose (5 μg in a 50% slurry) was added to the lysates and the mixture was incubated for 1 h at 4 °C. The bead pellet was collected by centrifugation (5 s at 14,000 × *g*) and the supernatant was drained off. The beads were then washed and suspended in 20 μl of 1× Laemmli sample buffer. Proteins were separated by 12% SDS-PAGE, transferred to nitrocellulose membrane, and blotted against Rac-1 and CDC42 polyclonal antibodies.

RESULTS

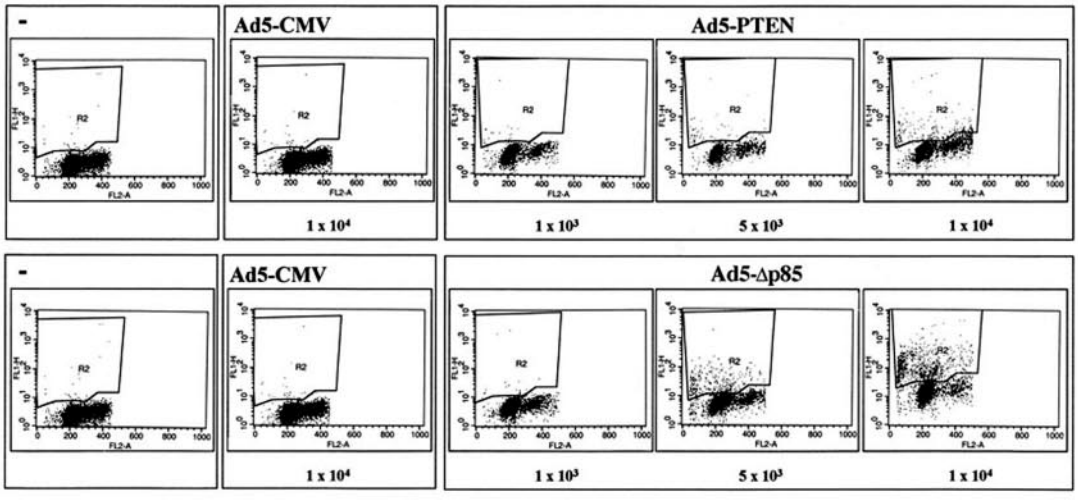
PI3K-dependent Pathway Contributes to NSCLC Cell Proliferation and Survival—We investigated the effects of PI3K inhibition on the proliferation and viability of H1299 NSCLC cells, which have a wild-type *PTEN* gene (27). H1299 cells were transfected with recombinant adenoviruses that express *PTEN* (Ad5-PTEN) or *Δp85* (Ad5-Δp85), a p85α dominant-negative mutant lacking the inter-SH2 residues required for binding to the p110 catalytic domain (35). Transfection of H1299 cells with Ad5-PTEN or Ad5-Δp85 increased the expression of the adenoviral gene products and suppressed pAKT levels (Fig. 1), providing evidence that these adenoviral vectors effectively blocked PI3K-dependent signaling. When H1299 cells were incubated with Ad5-PTEN or Ad5-Δp85, cell number decreased in a dose-dependent fashion (Fig. 2, *A* and *B*). H1299 cell number also decreased in a dose-dependent manner after treatment with LY294002, a competitive inhibitor of ATP binding to all isoforms of class I PI3K (Fig. 2*C*). Other NSCLC cell lines with wild-type *PTEN* (H358, Calu-6, H460, H661, H226B, H441, H1299, and H226Br) underwent a similar decrease in cell number following treatment with LY294002 or transfection with Ad5-Δp85 or Ad5-PTEN (data not shown).

We next investigated whether PI3K inhibition induced proliferative arrest or apoptosis of NSCLC cells by performing flow cytometric analysis of H1299 cells transfected with Ad5-PTEN or Ad5-Δp85 and then stained with propidium iodide (Fig. 3*A*). Ad5-PTEN transfection induced proliferative arrest in the G_0/G_1 phase of the cell cycle, with minimal evidence of programmed cell death, as shown by the lack of a hypodiploid peak. Although Ad5-Δp85 transfection also caused an accumulation of cells in G_1, its most striking effect was apoptosis, as indicated by the appearance of a hypodiploid peak. We examined this finding further by using terminal deoxynucleotidetransferase nick-end labeling (TUNEL), a more sensitive assay

Downloaded from www.jbc.org at M D ANDERSON HOSP, on October 7, 2010



Virus	Dose (p/cell)	Pre-G1(%)	G1(%)	S (%)	G2-M (%)
-	0	2.12	53.16	27.33	18.12
Ad5-CMV	1 x 10^4	0	40.41	42.62	16.97
Ad5-PTEN	1 x 10^3	0	72.43	11.97	15.60
Ad5-PTEN	5 x 10^3	0	75.17	12.99	11.83
Ad5-PTEN	1 x 10^4	0	77.17	13.48	9.35
Ad5-CMV	1 x 10^4	7.24	27.34	28.23	38.05
Ad5-Δp85	1 x 10^3	2.69	53.63	29.92	9.89
Ad5-Δp85	5 x 10^3	7.73	49.06	27.47	15.76
Ad5-Δp85	1 x 10^4	28.25	35.38	24.65	11.55



Virus	Dose(p/cell)	TUNEL(%)
-	0	0.22
Ad5-CMV	1 x 10^4	0.33
Ad5-PTEN	1 x 10^3	0.41
	5 x 10^3	2.17
	1 x 10^4	5.23
Ad5-Δp85	1 x 10^3	0.58
	5 x 10^3	8.22
	1 x 10^4	24.82

FIG. 3. **Evidence of proliferative arrest and apoptosis in cells incubated with Ad5-PTEN or Ad5-Δp85.** H1299 cells were incubated for 3 days with the indicated titers of Ad5-PTEN, Ad5-Δp85, or Ad5-CMV. Floating and adherent cells were isolated, fixed with 1% paraformaldehyde and 70% ethanol, stained with propidium iodide, and subjected to flow cytometric analysis to determine (*A*) the percentages of cells in specific phases of the cell cycle (pre-G_1, G_1, S, and G_2/M) and (*B*) percentages that were apoptotic (TUNEL analysis). Results are summarized in the adjoining tables.

Downloaded from www.jbc.org at M D ANDERSON HOSP, on October 7, 2010

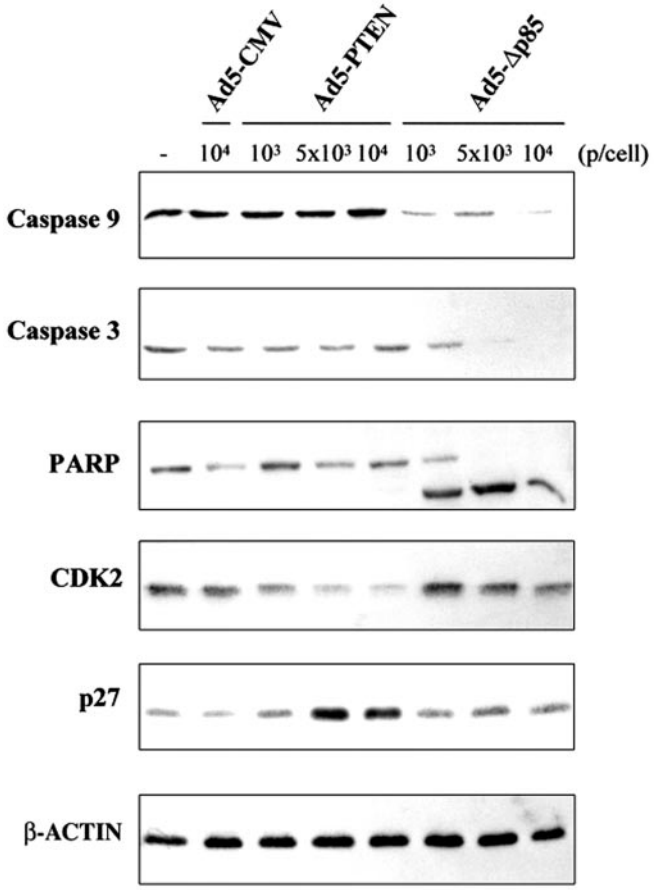


FIG. 4. **Effects of Ad5-PTEN or Ad5-Δp85 transfection on the expression of CDK2, p27, caspase-9 and -3, and poly(ADP-ribose) polymerase.** H1299 cells were treated with medium alone (−) or incubated for 72 h with the indicated titers (particles/cell) of Ad5-PTEN, Ad5-Δp85, or Ad5-CMV and lysed. Lysates (30 μg/sample) were subjected to Western blot analysis. Western blot analysis for β-actin was performed to determine the relative amounts of protein loaded per well.

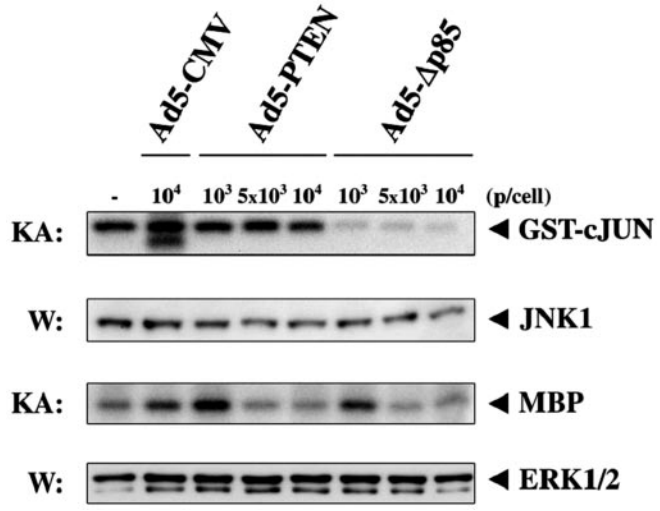


FIG. 5. **Effects of Ad5-PTEN or Ad5-Δp85 transfection on EGF-induced JNK and ERK activity.** H1299 cells were incubated for 48 h with the indicated titers (particles/cell) of Ad5-Δp85, Ad5-PTEN, or Ad5-CMV or treated with medium alone (−). The cells were then serum-starved for 24 h, treated with EGF (50 ng/ml) for 15 min, and lysed. JNK and ERK were immunoprecipitated from 100-μg aliquots of the cell lysate and subjected to immune complex kinase assays (*KA*) using GST-c-Jun and MBP as substrates to examine the activities of JNK and ERK, respectively. As a control, JNK1 and ERK1/2 expression were examined by Western blot analysis (*W*) of whole cell lysates.

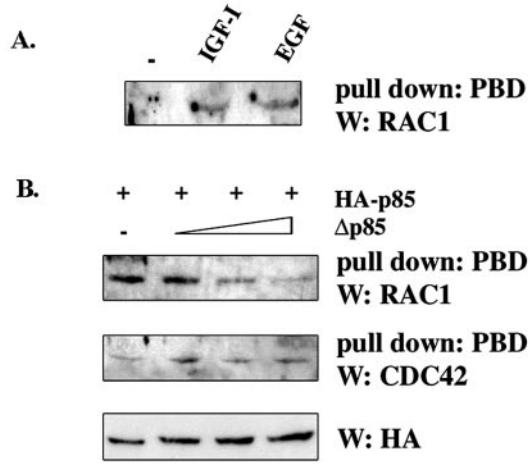


FIG. 6. **Effect of Δp85 on Rac-1 activation by peptide growth factors.** *A*, COS-7 cells were treated for 15 min with 50 ng/ml IGF-1, EGF, or medium alone. *B*, COS-7 cells were co-transfected overnight with plasmids containing HA-p85 and increasing doses of Δ*p85*, serum-starved for 16 h, and treated with IGF-1 for 15 min. Cells were lysed, and Rac-1 activity was analyzed by performing a pull-down assay on cell extracts using a GST-tagged PBD of PAK-1, followed by Western analysis (*W*) to quantitate PAK-1-associated Rac-1 or CDC42. To examine relative transfection efficiencies in each sample, Western analysis of HA expression was performed on total cell extracts.

for apoptosis, and found low levels of DNA fragmentation in cells transfected with Ad5-PTEN (Fig. 3*B*). In contrast, transfection with Ad5-Δp85 produced much more DNA fragmentation, which is compatible with the induction of high levels of apoptosis (Fig. 3*B*).

We investigated the effect of Ad5-PTEN and Ad5-Δp85 on signaling events known to contribute to apoptosis, proliferative arrest, or both (Fig. 4). Ad5-Δp85 transfection reduced the levels of procaspase-9, procaspase-3, and poly(ADP-ribose) polymerase, demonstrating evidence of caspase activation and proteolysis of a caspase-3 substrate. In contrast, Ad5-PTEN transfection decreased CDK2 levels and increased p27 CDK inhibitor levels without evidence of caspase activation or poly-(ADP-ribose) polymerase cleavage. Together, these findings support a role for PI3K in the proliferation of NSCLC cells and demonstrate a pro-apoptotic effect of Δp85.

Δ*p85 Inhibits the Activity of MAP Kinases*—Δp85 induced apoptosis of NSCLC cells whereas PTEN did not. Therefore, we hypothesized that inhibition of the PI3K/AKT pathway was required but not sufficient to induce apoptosis. We sought to identify additional survival signals typically activated by peptide growth factors that are inhibited by Δp85. Receptor tyrosine kinases maintain NSCLC cell survival, in part, by activating MAP kinases (37). We investigated the role of MAP kinases in Δp85-induced cell death. H1299 NSCLC cells were incubated with Ad5-PTEN or Ad5-Δp85, treated with EGF, and subjected to *in vitro* kinase assays of JNK and ERK activity (Fig. 5). ERK activity increased in cells incubated with Ad5-CMV. Ad5-PTEN and Ad5-Δp85 had similar, dose-dependent effects on ERK activity. Relative to the effect of Ad5CMV, ERK activity increased with low dose (10^3 particles/cell) and decreased with high dose (5×10^3 or 10^4 particles/cell) Ad5-PTEN or Ad5-Δp85. JNK activity decreased minimally after Ad5-PTEN and, to a much greater extent, after Ad5-Δp85 incubation. Thus, Δp85 was unique in its ability to inhibit JNK activity.

We investigated the mechanism by which Δp85 inhibited JNK. p85α associates with Rac-1, an upstream activator of JNK, and activates Rac-1 through association with a multiprotein complex that binds to p85 SH2 domains (38). We investi-

Downloaded from www.jbc.org at M D ANDERSON HOSP, on October 7, 2010

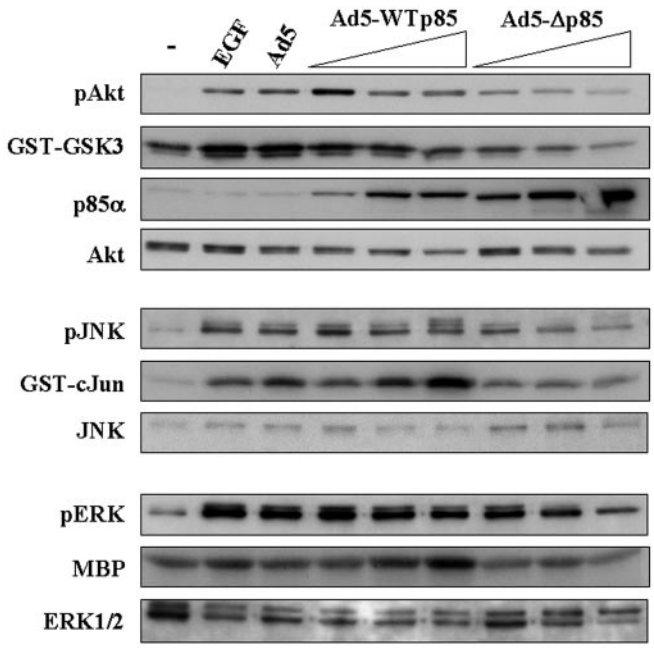


FIG. 7. **Effect of wild-type p85α and Δp85 on AKT, JNK, and ERK.** H1299 cells were incubated with no virus (lanes designated − and *EGF*), empty vector (Ad5) at 10^4 particles/cell, Adex1CAp85α-HA (*Ad-WTp85*), which expresses wild-type *p85*α, or Ad5-Δp85 at 10^3, 5×10^3, or 10^4 particles/cell. After transfection, the cells were grown in complete medium at 37 °C for 48 h. The cells were then subjected to serum-free conditions for 12 h (−), treated for 15 min with EGF (50 ng/ml), and lysed. Lysates were subjected to either Western blot analysis (20 μg/sample) using antibodies to the indicated proteins or immunoprecipitation (100 μg/sample) to isolate AKT, JNK, and ERK for *in vitro* kinase assays using GST-GSK3, GST-c-Jun, and MBP, respectively, as substrates.

gated whether wild-type p85α and Δp85 differ in their ability to activate Rac-1. We quantitated Rac-1 activity in cell extracts using a pull-down assay with a GST-tagged PBD of PAK-1, which associates selectively with GTP-bound (activated) Rac-1 or CDC42. PBD-associated proteins are subjected to Western analysis to quantitate Rac-1 and CDC42. We performed this experiment in COS-7 cells, in which peptide growth factors activate Rac-1 through a PI3K-dependent mechanism (21, 22). Using this assay we showed that Rac-1 is activated by treatment with EGF or IGF-1 (Fig. 6*A*). COS cells were co-transfected with wild-type *p85* and increasing amounts of Δ*p85* and treated with EGF to activate Rac-1. Relative to the effect of wild-type *p85*, Δ*p85* inhibited peptide growth factor-induced activation of Rac-1 but not CDC42 (Fig. 6*B*). Thus, in contrast to the stimulatory effect of *p85*α, Δ*p85* inhibited Rac-1.

p85α serves both to stabilize p85 protein and to inactivate PI3K lipid kinase activity (39). Therefore, we tested the hypothesis that Ad5-Δp85 inhibits intracellular signaling activity by increasing intracellular p85 protein levels. We incubated H1299 NSCLC cells with various doses of Ad5-Δp85 or an adenoviral vector expressing full-length *p85*α (Adex1CAp85α-HA) and examined their relative effects on EGF-induced phosphorylation and activation of AKT, JNK, and ERK by Western blotting and *in vitro* kinase assays (Fig. 7). We measured the intensity of pAKT, GST-GSK3, total AKT, and p85 bands by densitometric scanning and corrected for differences in total p85 and AKT protein levels at each virus dose. pAKT levels in cells transfected with 10^3, 5×10^3, and 10^4 particles/cell of Ad5-Δp85 were 20.6, 74.6, and 56.7%, respectively, of pAKT levels in cells transfected with the same doses of Adex1CAp85α-HA (Fig. 7, *top*). *In vitro* kinase assays using GST-GSK3 as substrate demonstrated that Ad5-Δp85 inhibited AKT kinase activity to a greater extent than Adex1CAp85α-HA (Fig. 7, *top*). In contrast to Ad5-Δp85, Adex1CAp85α-HA increased the phosphorylation and activity of JNK and minimally increased ERK activity (Fig. 7, *middle* and *bottom*). Treatment with LY294002 did not block the effects of Adex1CAp85α-HA on JNK and ERK (data not shown), providing evidence that PI3K activity was not required. These findings indicate that increasing the levels of wild-type p85α was not sufficient to recapitulate the effects of Δp85 on AKT, JNK, and ERK.

MAP Kinase Signaling Contributes to NSCLC Cell Survival—We investigated the importance of JNK and ERK inhibition in Δp85-induced cell death by examining whether co-transfection of upstream activators of these kinases would block Δp85-induced cell death. In COS-7 cells, a constitutively active mutant *Rac-1* (Val^{12}) blocked Δp85-induced inhibition of JNK and ERK, whereas a constitutively active mutant MAPK/ERK kinase (*MKK1*) (R4F) blocked Δp85-induced inhibition of ERK but not JNK (Fig. 8*A*). In H1299 NSCLC cells, Ad5-Δp85-induced cell death was abrogated by *Rac-1* (Val^{12}) but not by *MKK1* (R4F) (Fig. 8, *B* and *C*). Together, these findings indicate that Δp85-induced cell death requires inhibition of JNK but not ERK.

On the basis of these findings, we hypothesized that Rac-1 and its downstream mediators (PAK-1/MKK4/JNK) cooperate with PI3K-dependent signaling to maintain cell survival. To test this hypothesis, we examined whether PI3K inhibition would be sufficient to induce apoptosis of *MKK4*-null MEF cells. These cells did not activate JNK in response to EGF (Fig. 9*A*). We treated *MKK4*-null and wild-type MEF cells with LY294002 and examined them for evidence of apoptosis. LY294002 treatment induced apoptosis in *MKK4*-null MEF cells, but wild-type MEF cells demonstrated minimal evidence of cell death (Fig. 9, *B* and *C*). Together, these findings support the hypothesis that PI3K- and MKK4-dependent pathways cooperate to maintain cell survival.

DISCUSSION

Cancer cells with *PTEN* gene loss require activation of the PI3K-dependent pathway for survival. However, PI3K-dependent signaling is activated in cancer cells through mechanisms other than *PTEN* gene loss, as demonstrated in NSCLC cells, which typically have evidence of PI3K pathway activation and express wild-type *PTEN* (25–30). Here we investigated the role of PI3K in the survival of a NSCLC cell line that expresses wild-type *PTEN*. We found that LY294002 treatment and *PTEN* overexpression arrested cells in the G_0/G_1 phase of the cell cycle with minimal evidence of apoptosis. Unexpectedly, we found that Δp85 induced marked apoptosis.

Several lines of evidence presented here support the hypothesis that Δp85 induced apoptosis through the combined inhibition of MAP kinase- and PI3K-dependent pathways. First, in addition to inhibiting AKT, Δp85 inhibited JNK activity. Second, constitutively active *Rac-1* (Val^{12}) blocked Δp85-induced apoptosis of H1299 cells. Third, LY294002 treatment induced apoptosis in *MKK4*-null MEF cells but not wild-type MEF cells. The cooperative effect between PI3K and MAP kinase pathways was specific to JNK-dependent signaling, as introduction of constitutively active mutant *MKK1* did not block apoptosis of H1299 cells induced by Δp85. This finding is consistent with previous reports that MAP kinase family members play distinct biological roles in tumor cells (40, 41). Together, these findings indicate that, in the setting of wild-type *PTEN*, PI3K- and MKK4/JNK-dependent pathways cooperate to maintain cell survival.

Mechanisms by which Δp85 inhibited JNK activity have not been fully defined. Introduction of wild-type p85α did not recapitulate the effects of Δp85 on JNK and AKT, suggesting that

Downloaded from www.jbc.org at M D ANDERSON HOSP, on October 7, 2010

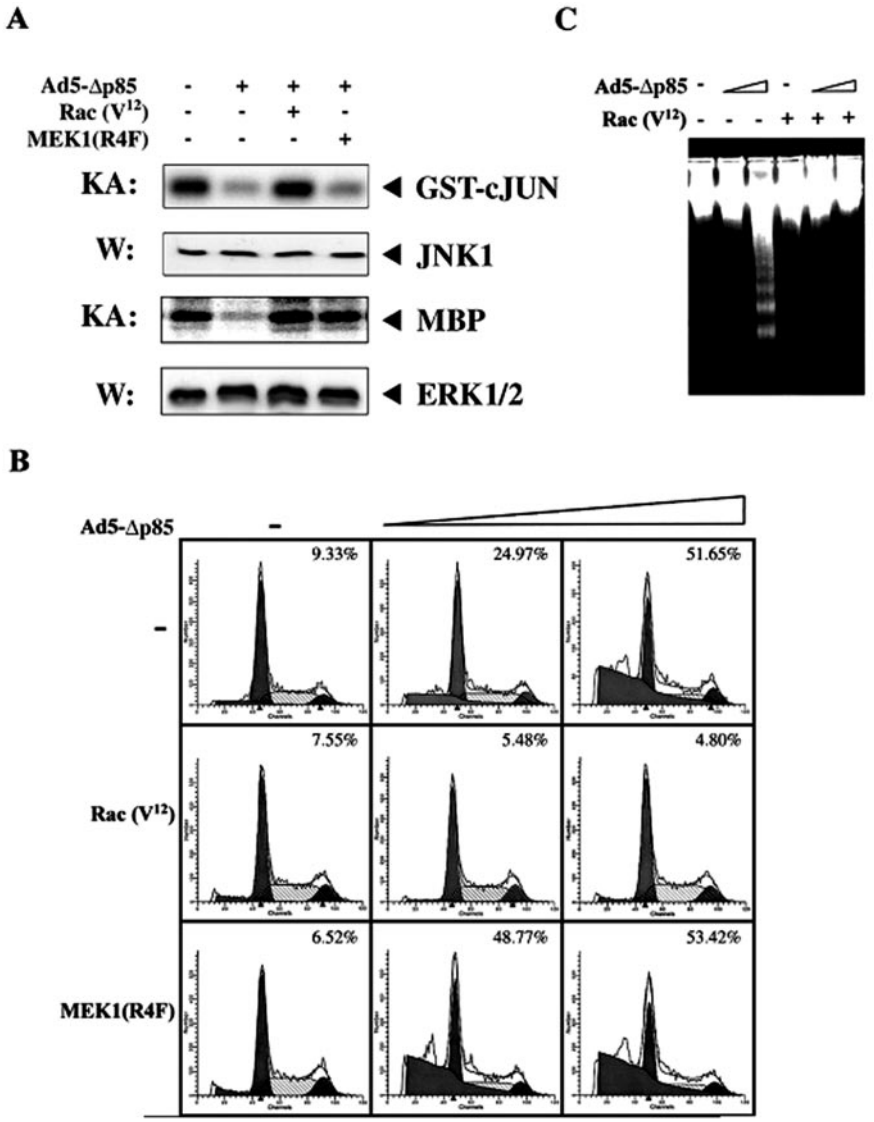


FIG. 8. **Effects of constitutively active mutants of *MKK1* (R4F) and *Rac-1* (Val^{12}) on Ad5-Δp85-induced MAP kinase inhibition and apoptosis.** *A*, COS-7 cells were transiently transfected for 6 h with 5-μg plasmids containing *Rac-1* (Val^{12}), *MKK1* (R4F), or empty vector using FuGENE. The cells were then transfected with Ad5-Δp85 or Ad5-CMV (1×10^3 or 5×10^3 particles/cell) and incubated for 24 h in complete medium. The cells were then changed to serum-free medium for 24 h, treated with IGF-1 (50 ng/ml) for 15 min, and lysed. JNK and ERK were immunoprecipitated from 100-μg aliquots of total cell lysates and subjected to kinase assays (*KA*) using GST-c-Jun and MBP, respectively, as substrates. As a control, JNK1 and ERK1/2 levels were examined by Western blot analysis (*W*). *B*, H1299 cells were transfected with 5 μg of plasmids containing *Rac-1* (Val^{12}), *MKK1* (R4F), or empty vector (−). The next day, the cells were incubated with Ad5-CMV at 5×10^3 particles/cell (−) or Ad5-Δp85 at 1×10^3 or 5×10^3 particles/cell. Two days later, floating and adherent cells were isolated, fixed in 1% paraformaldehyde and 70% ethanol, stained with propidium iodide and APO-BrdUrd, and subjected to flow cytometric analysis. The percentage of dead cells was determined by quantification of the pre-G_1 cell population and is indicated in the *upper right corner* of each flow diagram. *C*, H1299 cells were transfected with *Rac-1* (Val^{12}) and then incubated with increasing amounts of Ad5-Δp85, as described in *panel b*. Genomic DNA was isolated from floating and adherent cells and subjected to 1.5% gel electrophoresis for DNA fragmentation analysis.

Δp85 functions through mechanisms other than increasing intracellular levels of p85α, which inactivates PI3K lipid kinase activity through changes in the stoichiometry of p85:p110 (39). Alternatively, Δp85 may inhibit recruitment of p85-associated proteins required for activation of MAP kinase pathways by receptor tyrosine kinases. Supporting this possibility, we found that Δp85 inhibited Rac-1 activation by peptide growth factors. The inhibitory effect of Δp85 on peptide growth factor-induced Rac-1 activation in lung cancer cells is not consistent with previous reports that overexpression of Δp85 stimulates Rac-1 activity in T lymphocytes (42). Although we have yet to identify the mechanism by which Δp85 inhibits Rac-1, cell type-specific factors may be important. Recent findings indicate that p85 activates Rac-1 by associating with a multiprotein complex (including Eps8, Abi1, and SOS-1) that binds to p85 SH2 domains (38). We hypothesize that, in certain cell types, the p85 inter-SH2 domain is also required for Rac-1 activation. Recent findings have shown that this region of p85 contains several motifs that, in addition to binding to the p110 catalytic subunit, interact with other factors regulated by GTPase- and tyrosine kinase-dependent pathways (43), supporting the possibility that another multiprotein complex associates with this region. Additional studies will be needed to identify these proteins and to examine their role in Rac-1 activation.

Although adenoviral vectors expressing *PTEN* and Δ*p85* shared the ability to inhibit AKT activity, they differed in other downstream signaling events. Ad5-PTEN increased p27 levels and decreased CDK2 levels, which has been described previously in cells transfected with adenoviral vectors expressing *PTEN* (18, 44) and is consistent with the G_0/G_1 proliferative arrest we observed. In contrast to Ad5-PTEN, Ad5-Δp85 did not increase p27 or decrease CDK2 levels. This finding was somewhat surprising, given the ability of Δp85 to inhibit PI3K-dependent signaling. Analysis of the dose-dependent effects of Ad5-PTEN and Ad5-Δp85 demonstrated that Ad5-PTEN was a more potent inhibitor of pAKT levels than was Ad5-Δp85, which could account for their differences in downstream signaling. The adenoviral dose-dependent changes in ERK activity we observed in NSCLC cells transfected with Ad5-PTEN differs from observations in glioblastoma and prostate cancer cells transfected with Ad-PTEN and in PTEN-null embryonic stem cells, in which ERK activity did not change (19, 45–47). This difference could be the result of cell type-specific factors or nonspecific effects of exogenous PTEN in H1299 cells.

Previous studies have shown that MKK4 expression and activity are altered in human tumor cells and that MKK4 can act as both a promoter and a suppressor of human tumorigenesis. The *MKK4* gene is deleted or mutated in a subgroup of pancreatic, biliary, and breast carcinomas, and reintroduction of *MKK4* inhibits the metastatic ability of certain tumor cells,

Downloaded from www.jbc.org at M D ANDERSON HOSP, on October 7, 2010

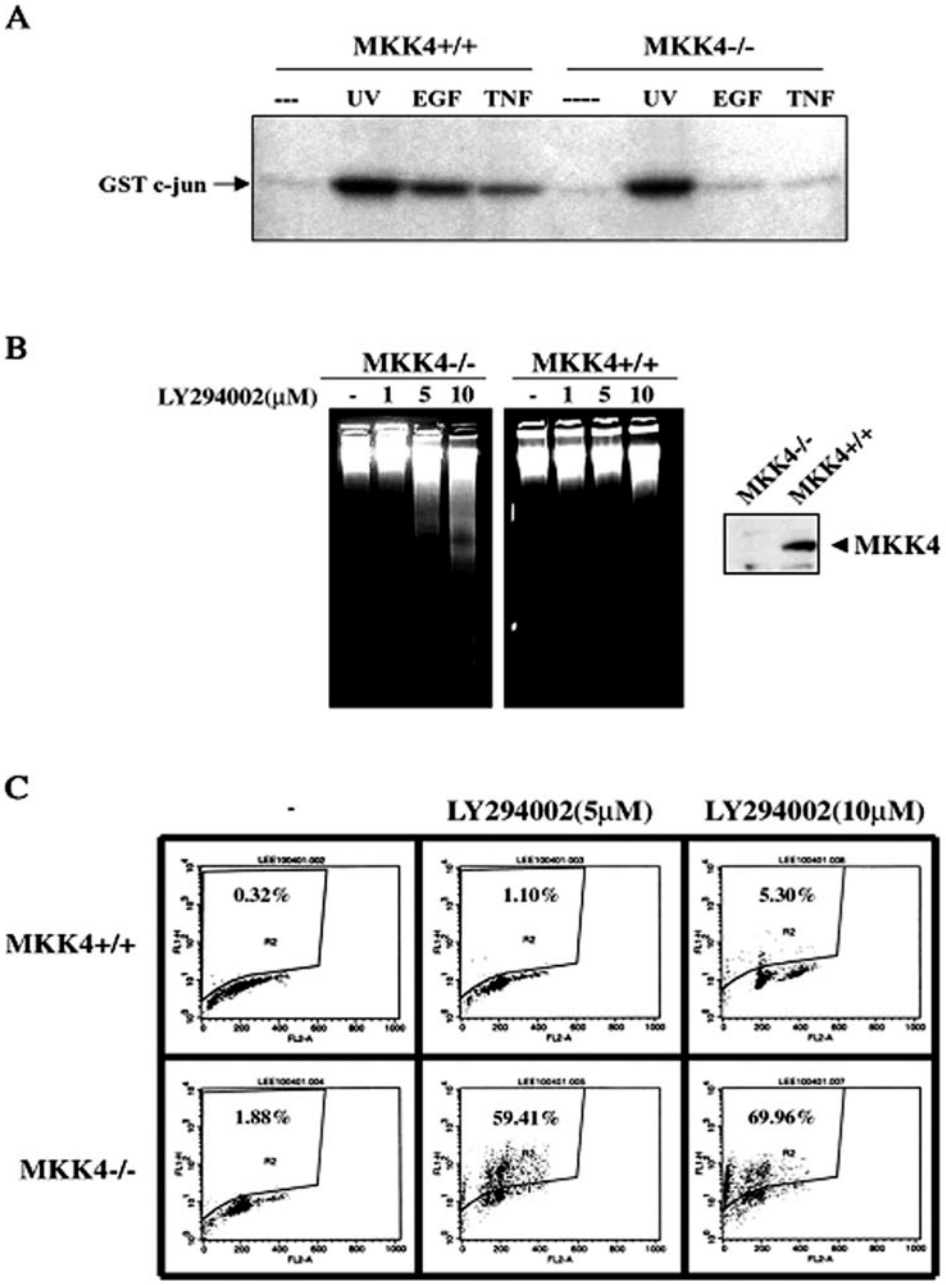


FIG. 9. **Relative to wild-type (+/+) MEF cells, *MKK4*-null (−/−) cells exhibit defects in JNK activation in response to specific stress activators and enhanced apoptosis in response to LY294002.** *A*, MEF cells were serum-starved overnight and then subjected to no treatment (−) or treatment with UV light (60 J/m^2 for 30 min), tumor necrosis factor-α (*TNF*) (30 ng/ml for 30 min), or EGF (50 ng/ml for 30 min). JNK was immunopurified and subjected to kinase assays using GST-c-Jun as substrate. *B* and *C*, MEF cells were treated for 3 days with the indicated doses of LY294002 or medium alone (−) and subjected to (*B*) DNA fragmentation assay and (*C*) TUNEL analysis as described under "Experimental Procedures." The relative MKK4 expression levels in *MKK4*-null and wild-type MEF cells were examined by Western blot analysis. The percentages of apoptotic cells as determined by TUNEL analysis are indicated in the *upper left corner* of each flow diagram.

demonstrating that MKK4 has tumor suppressor activity (48–50). Potentially mediating this effect, Ras pathway activation increases the expression of p53 and p16^{INK4a}, which induces premature cellular senescence; conversely, inactivation of p53 or p16 prevents Ras-induced growth arrest (51). In contrast to these studies, MKK4 is known to be a downstream mediator of Rac-1, and Rac-1 activation contributes to Ras-induced cellular transformation (20), indicating that MKK4 plays a role in cellular transformation. Supporting the latter hypothesis, we found that Rac-1 activation rescued lung cancer cells from Δp85-induced apoptosis, and MKK4 cooperated with PI3K to maintain MEF cell survival. This finding supports *in vitro* studies of lung cancer cells demonstrating that MKK4-dependent pathways play a dominant role in mutant Ras-induced colony formation (52, 53). Thus, MKK4 and its downstream mediators play apparently contradictory roles in the regulation of cellular growth and transformation that may depend on the presence of cell type-specific factors or the activity of tumor suppressor pathways that inhibit the mitogenic and transforming effects of MKK4.

Findings presented here have implications for the design of effective therapeutic approaches for lung cancer. Signal transduction inhibitors are being assessed in clinical trials as therapeutic agents for several types of cancer. The enthusiasm for these agents has been fueled by the efficacy of ABL kinase inhibitors in the treatment of chronic myelogenous leukemia,

Downloaded from www.jbc.org at M D ANDERSON HOSP, on October 7, 2010

which arises from a reciprocal chromosomal translocation involving the *Bcr* and *Abl* genes (54). However, unlike chronic myelogenous leukemia, in which constitutively active Abl is sufficient to induce the disease (55), lung tumorigenesis is a multistep process leading to aberrant activity of a variety of oncogenic and tumor suppressive pathways. These pathways act in combination to induce malignant transformation of NHBE cells and to maintain the survival of lung cancer cells (56). Thus, in patients with lung cancer, inhibition of multiple pathways may be necessary to induce tumor regression. The findings presented here support the hypothesis that PI3K- and MKK4/JNK-dependent pathways cooperate in lung cancer cells to maintain their survival, and combination therapy targeting these pathways should be considered in future clinical trials.

REFERENCES

1. Toker, A., and Cantley, L. C. (1997) *Nature* **387,** 673–676
2. Vanhaesbrock, B., Leevers, S. J., Panayotou, G., and Waterfield, M. D. (1997) *Trends Biochem. Sci.* **22,** 267–272
3. Wymann, M. P., and Pirola, L. (1998) *Biochim. Biophys. Acta* **1436,** 127–150
4. Alessi, D. R., James, S. R., Downes, C. P., Holmes, A. B., Gaffney, P. R. J., Reese, C. B., and Cohen, P. (1997) *Curr. Biol.* **7,** 261–269
5. Persad, S., Attwell, S., Gray, V., Delcommenne, M., Troussard, A., Sanghera, J., and Dedhar, S. (2000) *Proc. Natl. Acad. Sci. U. S. A.* **97,** 3207–3212
6. Di Cristofano, A., and Pandolfi, P. P. (2000) *Cell* **100,** 387–390
7. Bellacosa, A., de Feo, D., Godwin, A. K., Bell, D. W., Cheng, J. Q., Altomare, D. A., Wan, M., Dubeau, L., Scambia, G., and Godwin, A. K. (1995) *Int. J. Cancer* **64,** 280–285
8. Cheng, J. Q., Ruggeri, B., Klein, W. M., Sonoda, G., Altomore, D. A., Watson, D. K., and Testa, J. R. (1996) *Proc. Natl. Acad. Sci. U. S. A.,* **93,** 3636–3641
9. Janssen, J. W. G., Schleithoff, L., Bartram, C. R., and Schultz, A. S. (1998) *Oncogene,* **16,** 1767–1772
10. Li, J., Yen, C., Liaw, D., Podsypanina, K., Bose, S., Wang, S. I., Puc, J., Miliaresis, C., Rodgers, L., McCombie, R., Bigner, S. H., Giovanella, B. C., Ittmann, M., Tycko, B., Hibshoosh, H., Wigler, M. H., and Parsons, R. (1997) *Science* **275,** 1943–1947
11. Shayesteh, L. M., Lu, Y., Kuo, W. L., Baldocchi, R., Godfrey, T., Collins, C., Pinkel, D., Powell, B., Mills, G. B., and Gray, J. W. (1999) *Nat. Genet.* **21,** 99–102
12. Steck, P. A., Pershouse, M. A., Jasser, S. A., Yung, W. K. A., Lin, H., Ligon, A. H., Langford, L. A., Baumgard, M. L., Hattier, T., Davis, T., Frye, C., Hu, R., Swedlund, B., David, H. F., Tavtigian T., and Tavtigian, S. V. (1997) *Nat. Genet.* **15,** 356–362
13. Teng, D. H., Hu, R., Lin, H., Davis, T., Iliev, D., Frye, C., Swedlund, B., Hansen, K. L., Vinson, V. L., Gumpper, K. L., Ellis, L., El-Naggar, A., Frazier, M., Jasser, S., Langford, L. A., Lee, J., Mills, G. B., Pershouse, M. A., Pollack, R. E., Tornos, C., Troncoso, P., Yung, W. K., Fujii, G., Berson, A., and Steck, P. A. (1997) *Cancer Res.* **57,** 5221–5225
14. Bellacosa, A., Testa, J. R., Staal, S. P., and Tsichlis, P. N. (1991) *Science* **254,** 274–277
15. Chang, H. W., Aoki, M., Fruman, D., Auger, K. R., Bellacosa, A., Tsichlis, P. N., Cantley, L. C., Roberts, T. M., and Vogt, P. K. (1997) *Science* **276,** 1848–1850
16. Furnari, F. B., Lin, H., Huang, H.-J., and Cavenee, W. K. (1997) *Proc. Natl. Acad. Sci. U. S. A.* **94,** 12479–12484
17. Klippel, A., Escobedo, M. A., Wachowicz, M. S., Apell, G., Brown, T. W., Giedlin, M. A., Kavanaugh, W. M., and Williams, L. T. (1998) *Mol. Cell. Biol.* **98,** 5699–5711
18. Li, D. M., and Sun, H. (1998) *Proc. Natl. Acad. Sci. U. S. A.* **95,** 15406–15406
19. Lu, Y., Lin Y. Z., LaPushin, R., Cuevas, B., Fang, X., Yu, S. X., Davies, M. A., Khan, H., Furui, T., Mao, M., Zinner, R., Hung, M. C., Steck, P., Siminovitch, K., and Mills, G. B. (1999) *Oncogene* **18,** 7034–7045
20. Qiu, R. G., Chen, J., Kirn, D., McCormick, F., and Symons, F. (1995) *Nature* **374,** 457–459
21. Tolias, K. F., Cantley, L. C., and Carpenter, C. L. (1995) *J. Biol. Chem.* **270,** 17656–17659
22. Nimnual, A. S., Yatsula, B. A., and Bar-Sagi, D. (1998) *Science* **279,** 560–563
23. Davis, R. J. (2000) *Cell* **103,** 239–252
24. Neshat, M. S., Mellinghoff, I. K., Tran, C., Stiles, B., Thomas, G., Petersen, R., Frost, P., Gibbons, J. J., Wu, H., and Sawyers, C. L. (2001) *Proc. Natl. Acad. Sci. U. S. A.* **98,** 10314–10319
25. Brognard, J., Clark, A. S., Ni, Y., and Dennis, P. A. (2001) *Cancer Res.* **61,** 3986–3997
26. Massion, P., Kuo, W. L., Stokoe, D., Olshen, A. B., Treseler, P. A., Chin, K., Chen, C., Polikoff, D., Jain, A. N., Pinkel, D., Albertson, D. G., Jablons, D. M., and Gray, J. W. (2002) *Cancer Res.* **62,** 3636–3640
27. Forgacs, E., Biesterveld, E. J., Sekido, Y., Fong, K., Muneer, S., Wistuba, I. I., Milchgrub, S., Brezinschek, R., Virmani, A., Gazdar, A. F., and Minna, J. D. (1998) *Oncogene* **17,** 1557–1565
28. Moore, S. M., Rintoul, R. C., Walker, T. R., Chilvers, E. R., Haslett, C., and Sethi, T. (1998) *Cancer Res.* **58,** 5239–5247
29. Yokomizo, A., Tindall, D. J., Drabkin, H., Gemmill, H., Franklin, W. A., Yang, P., Sugio, K., Smith, D. I., and Liu, D. (1998) *Oncogene* **17,** 475-479
30. Soria, J. C., Lee, H. Y., Lee, J. I., Wang, L., Issa, J. P., Kemp, B. L., Liu, D. D., Kurie, J. M., and Khuri, F. R. (2002) *Clin. Cancer Res.* **8,** 1178–1184
31. Lin, J., Adam, R. M., Santiestevan, E., and Freeman, M. R. (1999) *Cancer Res.* **59,** 2891–2897
32. Furnari, F. B., Huang, H. J., and Cavenee, W. K. (1998) *Cancer Res.* **58,** 5002–5008
33. Nishina, H., Fischer, K. D., Radvani, L., Shahinian, A., Hakem, R., Rubie, E. A., Bernstrin, A., Mak, T. W., Woodgett, J. R., and Penninger, J. M. (1997) *Nature* **385,** 350–353
34. Ueki, K., Algenstaedt, P., Mauvais-Jarvis, F., and Kahn, C. R. (2000) *Mol. Cell. Biol.* **20,** 8035–8046
35. Hara, K., Yonezawa, K., Sakaue, H., Ando, A., Kotani, K., Kitamura, T., Kitamura, Y., Ueda, H., Stephens, L., Jackson, T. R., Waterfield, M. D., and Kasuga, M. (1994) *Proc. Natl. Acad. Sci. U. S. A.* **91,** 7415–7419
36. Ji, L., Nishizaki, M., Gao, B., Burbee, D., Toyooka, S., Kamibayashi, C., Xu, K., Yen, N., Atkinson, E. N., Fang, B., Lerman, M. I., Roth, J. A., and Minna, J. D. (2002) *Cancer Res.* **62,** 2715–2720
37. Schlessinger, J. (2000) *Cell* **103,** 211–225
38. Innocenti, M., Fritolli, E., Ponzanelli, I., Falck, J. R., Brachman, S. M., Di Fiore, P. P., and Scita, G. (2003) *J. Cell Biol.* **160,** 17–23
39. Cuevas, B. D., Lu, Y., Mao, M., Zhang, J., LaPushin, R., Siminovitch, K., and Mills, G. B. (2001) *J. Biol. Chem.* **276,** 27455–27461
40. Gupta, S., Plattner, R., Der, C. J., and Stanbridge, E. J. (2000) *Mol. Cell. Biol.* **20,** 9294–9306
41. Shields, J. M., Mehta, H., Pruitt, K., and Der, C. J. (2002) *Mol. Cell. Biol.* **22,** 2304–2317
42. Kang, H., Schneider, H., and Rudd, C. E. (2002) *J. Biol. Chem.* **277,** 912–921
43. Tung, T. O., Rodeck, U., Chan, A. M., Kimmelman, A. C., Rittenhouse, S. E., Panayotou, G., and Tsichlis, P. N. (2002) *Cancer Cell* **1,** 181–191
44. Gottschalk, A. R., Basila, D., Wong, M., Dean, N. M., Brandts, C. H., Stokoe, D., and Haas-Kogan, D. A. (2001) *Cancer Res.* **61,** 2105–2111
45. Davies, M. A., Koul, D., Dhesi, H., Berman, R., McDonnell, T. J., McConkey, D., Yung, W. K. A., and Steck, P. (1999) *Cancer Res.* **59,** 2551–2556
46. Sun, H., Lesche, R., Li, D. M., Liliental, J., Zhang, H., Gao, J., Gavrilova, N., Mueller, B., Liu, X., and Wu, H. (1999) *Proc. Natl. Acad. Sci. U. S. A.* **96,** 6199–6204
47. Wu, X., Senechal, K., Neshat, M. S., Whang, Y. E., and Sawyers, C. L. (1998) *Proc. Natl. Acad. Sci. U. S. A.* **95,** 15587–15591
48. Teng, D. H. F., Perry, W. L., 3rd, Hogan, J. K., Baumgard, M., Bell, R., Berry, S., Davis, T., Frank, D., Frye, C., Hattier, T., Hu, R., Jammulapati, S., Janecki, T., Leavitt, A., Mitchell, J. T., Pero, R., Sexton, D., Schroeder, M., Su, P. H., Swedlund, B., Kyriakis, J. M., Avruch, J., Bartel, J., Wong, A. K., and Tavtigian, S. V. (1997) *Cancer Res.* **57,** 4177–4182
49. Yoshida, B. A., Dubauskas, Z., Chekmareva, M. A., Christiano, T. R., Stadler, W. M., and Rinker-Schaeffer, C. W. (1999) *Cancer Res.* **59,** 5483–5487
50. Su, G., Hilgers, W., Shekher, M. C., Tang, D. J., Yeo, C. J., Hruban, R. H., and Kern, S. E. (1998) *Cancer Res.* **58,** 2339–2342
51. Serrano, M., Lin, A. W., McCurrach, M. E., Beach, D., and Lowe, S. W. (1997) *Cell* **88,** 593–602
52. Bost, F., McKay, R., Bost, M., Potapova, O., Dean, N. M., and Mercola, D. (1999) *Mol. Cell. Biol.* **99,** 1938–1949
53. Xiao, L., and Lang, W. (2000) *Cancer Res.* **60,** 400–408
54. Druker, B., Talpaz, J., Resta, M., Peng, D. J., Buchdunger, B., Ford, E., Lydon, J. M., Kantarjian, N. B., Capdeville, H., Ohno-Jones, R., and Sawyers, C. L. (2001) *N. Engl. J. Med.* **344,** 1031–1037
55. Honda, H., Oda, H., Suzuki, T., Takahashi, T., Witte, O., Ozawa, K., Ishikawa, T., Yazaki, Y., and Harai, H. (1998) *Blood* **91,** 2067–2075
56. Fong, K. M., Sekido, Y., and Minna, J. D. (1999) *J. Thorac. Cardiovasc. Surg.* **118,** 1136–1152

Downloaded from www.jbc.org at M D ANDERSON HOSP, on October 7, 2010

VOLUME 22 · NUMBER 22 · NOVEMBER 15 2004

JOURNAL OF CLINICAL ONCOLOGY ORIGINAL REPORT

Prognostic Factors in Resected Stage I Non–Small-Cell Lung Cancer: A Multivariate Analysis of Six Molecular Markers

Charles Lu, Jean-Charles Soria, Ximing Tang, Xiao-Chun Xu, Luo Wang, Li Mao, Reuben Lotan, Bonnie Kemp, B. Nebiyou Bekele, Lei Feng, Waun K. Hong, and Fadlo R. Khuri

From the Departments of Thoracic/Head and Neck Medical Oncology, Clinical Cancer Prevention, Pathology, and Biostatistics, The University of Texas M.D. Anderson Cancer Center, Houston, TX; Institut Gustave Roussy, Villejuif, France; and Winship Cancer Institute, Emory University, Atlanta, GA.

Submitted January 13, 2004; accepted August 26, 2004.

Supported in part by National Cancer Institute grant No. K12 CA088084 and the Department of Defense, Biology, Education, Screening, Chemoprevention, and Treatment of Lung Cancer grant No. DAMD17-01-1-0689 and Translational Approaches for the Reversal, Genetic, Evaluation and Treatment of Lung Cancer grant No. DAMD17-02-1-0706.

Presented in part at the 93rd Annual Meeting of the American Association for Cancer Research, San Francisco, CA, April 6-10, 2002.

Authors' disclosures of potential conflicts of interest are found at the end of this article.

Address reprint requests to Charles Lu, MD, SM, The University of Texas M.D. Anderson Cancer Center, 1515 Holcombe Boulevard, Box 432, Houston, TX 77030-4009; e-mail: clu@mdanderson.org.

© 2004 by American Society of Clinical Oncology

0732-183X/04/2222-4575/$20.00

DOI: 10.1200/JCO.2004.01.091

ABSTRACT

Purpose

To analyze the prognostic significance of six molecular biomarkers (death-associated protein kinase [*DAPK*] promoter methylation, interleukin-10 [IL-10] protein expression, cyclooxygenase-2 [COX-2] mRNA expression, human telomerase reverse transcriptase catalytic subunit [hTERT] mRNA expression, retinoic acid receptor-beta [RAR-β] mRNA expression, and K-*ras* mutational status) in stage I non–small-cell lung cancer (NSCLC) patients.

Patients and Methods

Biomarker analyses were performed on tumors from 94 patients with stage I NSCLC who underwent surgical resection at our institution. A minimum follow-up period of 5 years was required. *DAPK* methylation was assessed by methylation-specific polymerase chain reaction (PCR). RAR-β, COX-2, and hTERT mRNA levels were determined by in situ hybridization with digoxigenin-labeled antisense riboprobes. K-*ras* mutation status was determined by the PCR–primer introduced restriction with enrichment for mutant alleles method. IL-10 protein expression was analyzed by immunohistochemistry using a polyclonal antihuman IL-10 antibody. Cancer-specific survival was analyzed with a Cox proportional hazards model. To identify independent prognostic factors, a stepwise selection method was used.

Results

DAPK methylation, IL-10 lack of expression, COX-2 expression, hTERT expression, RAR-β expression, and K-*ras* mutations were observed in 46.8%, 29.8%, 59.6%, 34.0%, 23.4%, and 34.0% of patients, respectively. In the final model, *DAPK* methylation and IL-10 lack of expression were significant negative prognostic factors for cancer-specific survival, whereas COX-2 expression was of borderline significance.

Conclusion

In this cohort of resected stage I NSCLC patients, molecular markers that independently predict cancer-specific survival have been identified. The prognostic roles of *DAPK* methylation, IL-10, and other biomarkers in NSCLC merit further investigation.

J Clin Oncol 22:4575-4583. © 2004 by American Society of Clinical Oncology

INTRODUCTION

Lung cancer remains a worldwide public health issue of immense proportions. In the year 2003, cancers of the lung and bronchus are expected to continue to account for the most cancer deaths in the United States (157,200 deaths or 28.2%), more than the estimated total number of deaths as a result of cancers of the breast, prostate, colon, and rectum combined.[1] Approximately 80% of lung cancers will have non–small-cell carcinoma histology.[2]

Approximately 25% of patients present with early-stage disease.[3] The standard treatment is surgical resection with appropriate lymph node sampling or dissection. Although early-stage non–small-cell lung

Information downloaded from jco.ascopubs.org and provided by at M D ANDERSON HOSP on October 7, 2010 from
Copyright © 2004 American Society of Clinical Oncology. All rights reserved.

cancer (NSCLC) patients have a relatively favorable prognosis, the risk of disease recurrence and death remains substantial. Five-year survival rates for pathologic stages I and II disease are 57% to 67% and 38% to 55%, respectively.[4] Identification of reliable prognostic factors for disease recurrence and death could have significant clinical import. Patients in a high-risk group, for example, would be appropriate candidates for novel adjuvant or chemoprevention strategies.

Both our group[5-12] and others[13-16] have focused on identifying molecular prognostic factors in early-stage NSCLC. We have established a retrospective cohort of stage I NSCLC patients who underwent surgical resection at our institution. Over the past few years, investigators in our group have analyzed a number of tumor biomarkers within this valuable clinical research database.

Given the roles that retinoids play in the regulation of cell growth, differentiation, and apoptosis, Khuri et al[8] investigated the prognostic significance of retinoic acid receptor-beta (RAR-β) mRNA expression in 156 patients. Because RAR-β expression seems to be suppressed during carcinogenesis, these investigators hypothesized that lower RAR-β levels would predict a poor clinical outcome. Surprisingly, overall survival was significantly worse in patients with strongly positive RAR-β expression. Because one RAR-β isoform, RAR-β4, may promote hyperplasia and neoplasia,[17] the authors hypothesized that differential expression of RAR-β isoforms may be a possible explanation for their unexpected findings.

Khuri et al[9] subsequently evaluated cyclooxygenase-2 (COX-2) mRNA expression and correlated it with the expression of RAR-β in this cohort of stage I NSCLC patients. COX-2 overexpression had previously been demonstrated in lung, head and neck, and other tumors,[18-20] and cell line data indicated that retinoic acid could suppress COX-2.[21] These investigators found that COX-2 expression was associated with worse overall and disease-free survival and that COX-2 and RAR-β mRNA levels were correlated. These findings were in conflict with the prior cell line data, which would have predicted that RAR-β upregulation should downregulate COX-2.

Telomerase is a ribonucleoprotein that lengthens and maintains the ends of chromosomes that are shortened with successive cell divisions.[22] Telomerase is expressed in up to 85% of NSCLC tumors and plays a critical role in sustaining cellular immortality and carcinogenesis.[23,24] Wang et al[11] examined mRNA expression of the human telomerase reverse transcriptase catalytic subunit (hTERT) in 153 patients from our database. Positive hTERT expression was significantly associated with worse overall and disease-specific survival.

Tang et al[7] examined hypermethylation of the death-associated protein kinase (*DAPK*) promoter in 135 patients from this cohort. Epigenetic inactivation of tumor suppressor genes by promoter hypermethylation frequently occurs in NSCLC.[25,26] *DAPK* is a putative tumor-suppressor gene that encodes for a calmodulin-dependent kinase that possesses a death domain at its C terminus.[27] *DAPK* is required for interferon-gamma–induced apoptosis and seems to suppress the metastatic ability of lung cancer cells.[28] In the study by Tang et al,[7] *DAPK* hypermethylation was significantly associated with poorer overall and disease-specific survival.

Soria et al[12] examined the role of interleukin-10 (IL-10) protein expression among 135 patients. The immunomodulatory effects of IL-10 have demonstrated conflicting results in various tumor systems. Some reports support the role of IL-10 in helping tumors evade immunosurveillance because IL-10 can inhibit macrophage, T-cell, and antigen-presenting cell functions.[29,30] Others have demonstrated that IL-10 may function as a potent inhibitor of tumor growth and metastasis.[31,32] In this study, IL-10 lack of expression was significantly associated with poorer overall and disease-specific survival.

The aforementioned hypothesis-driven studies each focused on one or a few biomarkers. To simultaneously examine multiple potential molecular prognostic factors in this clinical research database, we identified 94 patients who had complete information for a panel of six biomarkers (RAR-β, COX-2, hTERT, *DAPK* promoter methylation, IL-10, and K-*ras*). Multivariate Cox regression analysis was used to identify independent predictors of cancer-specific survival in this population of resected stage I NSCLC patients.

PATIENTS AND METHODS

Study Population

Five hundred ninety-five consecutive patients with stage I NSCLC underwent definitive surgical resection, defined as a lobectomy or a pneumonectomy, from 1975 to 1990 at The University of Texas M.D. Anderson Cancer Center (Houston, TX). Patients did not receive preoperative or postoperative chemotherapy or radiotherapy. We retrospectively identified 185 patients for whom both tissue samples and a median follow-up period of more than 5 years were available. All available tissue blocks were reviewed by a thoracic pathologist (B.K.), and 163 cases had adequate tumor present in the surgical specimen. The patient population was identified through a search of the Tumor Registry database maintained by the Department of Medical Informatics at The University of M.D. Anderson Cancer Center. Survival status was verified and updated from Tumor Registry records as of December 1, 2000. This study was reviewed and approved by the institutional review board and conducted in accordance with its policies.

Five published studies[7-9,11,12] had previously examined different molecular prognostic factors among the 163 patients with sufficient tumor specimens and more than 5 years of follow-up data. The sample sizes ranged from 135 to 160 patients. A total of

Information downloaded from jco.ascopubs.org and provided by at M D ANDERSON HOSP on October 7, 2010 from
Copyright © 2004 American Society of Clinical Oncology. All rights reserved.

94 patients had complete information for a panel of six biomarkers, and these patients were included in our analysis.

Methylation-Specific Polymerase Chain Reaction (PCR)

These methods have been previously described.[7] Briefly, 8-μm sections from paraffin-embedded tissue blocks were obtained, and regions with tumor cells were dissected under a stereomicroscope. In the initial chemical modification step, 200 ng of DNA from each tumor was denatured by NaOH and treated with sodium bisulfite (Sigma Chemical Co, St Louis, MO). DNA was recovered in water and was ready to add to a PCR with the use of specific primers for either the methylated or the unmethylated *DAPK* promoter, as described previously.[33] DNA was amplified for 35 cycles, and PCR products were separated on 2% agarose gels and visualized. For each DNA sample, primer sets for methylated DNA and unmethylated DNA were used for analysis. The hypermethylation status was determined by visualizing a 98-base pair (bp) PCR product with the methylation-specific primer set. All PCRs were repeated twice, and the results were reproducible.

Immunohistochemical Staining for IL-10 Protein

Paraffin-embedded, 4-μm–thick tissue sections were stained for IL-10 protein using a primary goat polyclonal antihuman IL-10 antibody (AF-217-NA; R&D Systems, Minneapolis, MN) as previously described.[12] Routinely processed tissue sections of normal lymph nodes and tonsils were used as positive staining controls and were also stained with the primary antibody omitted to confirm staining specificity. Normal bronchial epithelial cells that constitutively produce IL-10 were also used as internal positive controls.[34]

The IL-10 labeling index was defined as the percentage of tumor cells displaying cytoplasmic immunoreactivity and was calculated by counting IL-10–stained tumor cells among at least 1,000 tumor cells for each section as previously described.[12] On the basis of previous reports, if 10% or more of the tumor cells were positive for IL-10, the case was considered to be IL-10 positive.[35] All slides were scored concomitantly by a pathologist (X.T.) and another investigator (J.-C.S.) in a blinded manner.

hTERT In Situ Hybridization (ISH)

These methods have been previously described.[11] The riboprobes were a 430-bp EcoRV-BamH1 fragment of the hTERT cDNA that has been used in other studies[36,37] as well as part of exon 1 from the heterogeneous nuclear ribonucleoprotein A1 as a control to verify sample quality. The single-strand–specific, digoxigenin-labeled riboprobes were generated by in vitro transcription. ISH was performed as previously described.[37] Slides displaying a diffuse but clear cytoplasmic signal were considered to be positive, as reported by Falchetti et al.[38] More specifically, our slides were rated as positive if a definite and clear signal was present in more than two large areas on the slide. Slides with faint signal, the absence of signal, or only focal positivity were considered to be negative. We did not grade the intensity of the hybridization signals.

COX-2 and RAR-β ISH

COX-2 and RAR-β mRNA were detected in 4-μm–thick sections from paraffin-embedded tissue using nonradioactive ISH with digoxigenin-labeled antisense riboprobes as previously described.[8,9,39] Retinoid X receptor-alpha (RXR-α), which is present in greater than 90% of NSCLCs,[40] was used as a control to detect RNA degradation. The rationale for using RXR-α as a control for intact RNA was the observation that all 70 cases of NSCLC and normal lung tissue expressed RXR-α mRNA in a previous study.[40] Stained sections were reviewed by three independent researchers, including two pathologists, in a blinded fashion. Only cytoplasmic staining was considered positive. Because normal bronchial epithelium expresses RAR-β, positive and aberrant RAR-β expression was defined as $\geq$ 10% and less than 10% intratumoral staining, respectively.[8] The RAR-β probe that was used identified all RAR-β isoforms. COX-2 expression was defined as either positive (present) or negative (absent).[9]

K-ras Mutation Analysis With PCR–Primer Introduced Restriction With Enrichment for Mutation Alleles (PCR-PIREMA)

A modified PCR-PIREMA method was used to detect K-*ras* codon 12 mutations.[41] Briefly, 8-μm sections from paraffin-embedded tissue blocks were obtained, and regions with tumor cells were dissected under a stereomicroscope. Dissected tissues were digested in 200 μL of digestion buffer containing 50 mmol/L Tris-HCl (pH 8.0), 1% sodium dodecyl sulfate, and proteinase K (0.5 mg/mL) at 42°C for 36 hours. The digested products were purified by extracting with phenol-chloroform twice. DNA was then precipitated by the ethanol precipitation method in the presence of glycogen (Roche Biochemicals, Indianapolis, IN), recovered in distilled water, and then stored at −20°C until used for PCR.

Briefly, PCR around K-*ras* codon 12 was performed using a mismatched primer (forward primer: 5′-TGAATATAAACTTGTGGTAGTTGGACCT-3′; reverse primer: 5′-CTGTATCAAAGAATGGTCC TGCACC-3′) that introduced an *Mva*I restriction site into the PCR products derived from normal alleles. *Mva*I digestion of the PCR products left only the PCR products derived from mutant alleles intact, after which further PCR selectively amplified the mutant PCR products. The first PCR reaction was performed with mixtures containing 0.5 μL of DNA recovery solution, 10 ng of each nucleotide, and the mismatched primer to introduce an *Mva* I restriction site flanking the K-*ras* exon 1, with 15 cycles at an annealing temperature of 55°C. The first PCR products were digested with *Mva*I and diluted 1:100. One microliter of the diluted product was amplified by 20 cycles of PCR with the same primers at an annealing temperature of 40°C, and the products were digested with *Mva*I a second time. The second PCR products were diluted 1:100, amplified by 35 cycles with the previous forward primer and a new reverse primer (5′-CTCTATTGTTGGATCATATTCGTCCAC-3′) at an annealing temperature of 65°C, and digested with *Mva*I a third time. The final digested products were then electrophoresed on 2.5% agarose gels and stained with ethidium bromide. A digestion-resistant 106-bp band indicated the presence of a K-*ras* codon 12 mutation. Extensive measures were taken to prevent cross-contamination of samples. A normal control sample and a known mutation sample were included in all of the experiments.

Statistical Analyses

Overall survival, disease-specific survival, and disease-free survival were analyzed in this study. Survival curves were estimated by the Kaplan-Meier method. The log-rank test was used to compare survival time between groups. Fisher's exact test was used to analyze the association between categoric variables. Using a stepwise selection method, a Cox proportional hazards model was created to identify independent predictors of survival, with adjustment for relevant clinical covariates (tumor stage, histology,

Information downloaded from jco.ascopubs.org and provided by at M D ANDERSON HOSP on October 7, 2010 from
Copyright © 2004 American Society of Clinical Oncology. All rights reserved.

smoking status, and sex). All statistical tests were two-sided, and $P < .05$ was considered statistically significant.

All survival curves were calculated from the date of surgery. Overall survival took all deaths (cancer related or not) into account. Disease-specific survival time was calculated from the date of surgery to death from cancer-related causes. Disease-free survival time was calculated from the date of surgery to relapse or death from cancer-related causes.

RESULTS

Data for a panel of six molecular markers (RAR-β, COX-2, hTERT, *DAPK* promoter methylation, IL-10, and K-*ras*) were available for 94 patients in our retrospective cohort. These patients were the study population for our analysis. Patient characteristics are listed in Table 1. Median follow-up time for alive patients and those lost to follow-up was 10.9 years. Sixty-nine patients have died. Twenty-nine deaths were cancer related.

The frequency of each molecular marker, displayed as a negative prognostic factor, is listed in Table 2. Univariate analyses of each molecular marker and its association with disease-specific survival and overall survival were performed (Table 3). Similar univariate survival analyses of clinical variables (age, sex, and smoking status) were performed. A highly significant association was demonstrated between age ($<$ 60 years $v \geq$ 60 years) and overall survival ($P = .003$). Sex and smoking status were not associated with overall or disease-specific survival. Age $\geq$ 60 years was associated with a significant increased risk of noncancer-related death ($P < .001$) and was not associated with disease-specific survival ($P = .577$). This phenomenon is likely explained by the relatively long follow-up of these subjects and by the fact that that the majority of deaths (40 of 69 deaths) were unrelated to cancer. In light of these findings, we reasoned that disease-specific survival would serve as a more clinically relevant end point for this cohort, although we continued to include overall survival in our analyses. Disease-specific survival stratified by each molecular marker is shown in Figure 1.

Table 1. Patient Characteristics

Characteristic	No. of Patients	%
Age, years		
Median	63.5	
Range	41-82	
Sex		
Male	72	77
Female	22	23
Race		
White	83	88
Other	11	12
Smoker		
Yes	82	87
No	5	5
Unknown	7	7
Histology		
Adenocarcinoma	39	41
Squamous cell carcinoma	39	41
Other	16	17
TNM stage		
T1N0M0	44	47
T2N0M0	50	53

Abbreviation: TNM, tumor-node-metastasis.

Table 2. Frequency of Molecular Markers in Stage I NSCLC

Molecular Marker	Frequency (%)
COX-2 expression	60
DAPK methylation	47
K-*ras* mutation	34
hTERT expression	34
IL-10 lack of expression	30
RAR-β expression	23

Abbreviations: NSCLC, non–small-cell lung cancer; COX-2, cyclooxygenase; *DAPK*, death-associated protein kinase; hTERT, human telomerase reverse transcriptase catalytic subunit; IL-10, interleukin-10; RAR-β, retinoic acid receptor-beta.

A multivariate Cox proportional hazards model was created to identify predictors of disease-specific survival (Table 4). *DAPK* promoter methylation and IL-10 lack of expression were significant negative prognostic factors for disease-specific survival, whereas COX-2 expression was of borderline significance. The same variables were selected when tumor stage, histology, smoking status, and sex were included in the model. The poorer disease-specific and overall survival of patients with both *DAPK* methylation and IL-10 lack of expression are illustrated in Figure 2. We defined these patients as a high-risk group, and the remaining patients were defined as a low-risk group. A log-rank test assessing the difference in survival between these groups was statistically significant for both disease-specific survival ($P < .0001$) and overall survival ($P < .0001$). We note that the definitions of the high- and low-risk groups are data dependent. That is, the definition of high risk was not determined a priori. A similar model for overall survival yielded three significant negative prognostic factors (age $\geq$ 60 years, $P = .0017$; COX-2 expression, $P = .021$; and *DAPK* methylation, $P = .044$), whereas IL-10 lack of expression was of borderline significance ($P = .069$).

Exploratory analyses of the relationships between the various molecular markers were performed. Significant associations were found between hTERT and COX-2 expression (odds ratio [OR], 6.14; 95% CI, 2.09 to 18.04; $P = .0004$) and K-*ras* mutations and *DAPK* methylation (OR, 2.64; 95% CI, 1.10 to 6.36; $P = .032$). Associations between IL-10 lack of expression and hTERT expression (OR, 2.63; 95% CI, 1.06 to 6.67; $P = .056$), IL-10 lack of

Information downloaded from jco.ascopubs.org and provided by at M D ANDERSON HOSP on October 7, 2010 from
Copyright © 2004 American Society of Clinical Oncology. All rights reserved.

Table 3. Univariate Analysis of Molecular Markers With Disease-Specific and Overall Survival

Molecular Marker	Disease-Specific Survival			Overall Survival		
	Hazard Ratio	95% CI	*P*	Hazard Ratio	95% CI	*P*
IL-10 lack of expression	3.17	1.53 to 6.62	.002	1.98	1.21 to 3.25	.007
DAPK methylation	3.00	1.39 to 6.47	.005	1.69	1.05 to 2.72	.030
hTERT expression	2.39	1.15 to 4.97	.020	1.48	0.91 to 2.42	.116
COX-2 expression	2.44	1.08 to 5.54	.032	1.80	1.09 to 2.96	.022
RAR-β expression	1.47	0.66 to 3.25	.345	1.23	0.72 to 2.09	.446
K-*ras* mutation	1.00	0.45 to 2.20	.998	1.18	0.71 to 1.95	.517

Abbreviations: IL-10, interleukin-10; *DAPK*, death-associated protein kinase; hTERT, human telomerase reverse transcriptase catalytic subunit; COX-2, cyclooxygenase-2; RAR-β, retinoic acid receptor-beta.

expression and COX-2 expression (OR, 2.63; 95% CI, 0.99 to 7.14; $P = .066$), and COX-2 expression and RAR-β expression (OR, 2.88; 95% CI, 0.96 to 8.64; $P = .08$) were of borderline significance.

We also investigated other models by performing all two-variable, three-variable, and four-variable multivariate models. On the basis of these analyses, only *DAPK* methylation and IL-10 lack of expression were statistically significant ($P < .05$) for all models. Furthermore, the three-variable model, including *DAPK* methylation, IL-10 lack of expression, and COX-2 expression, had the lowest Akaike Information Criterion (AIC) value of 224.029 (although the two-variable model that excluded COX-2 expression had an AIC of similar value). We noted that there was some evidence of association between IL-10 lack of expression and hTERT expression (OR, 2.63; $P = .056$) and IL-10 lack of expression and COX-2 expression (OR, 2.63; $P = .066$). Moreover, hTERT and COX-2 expression were highly

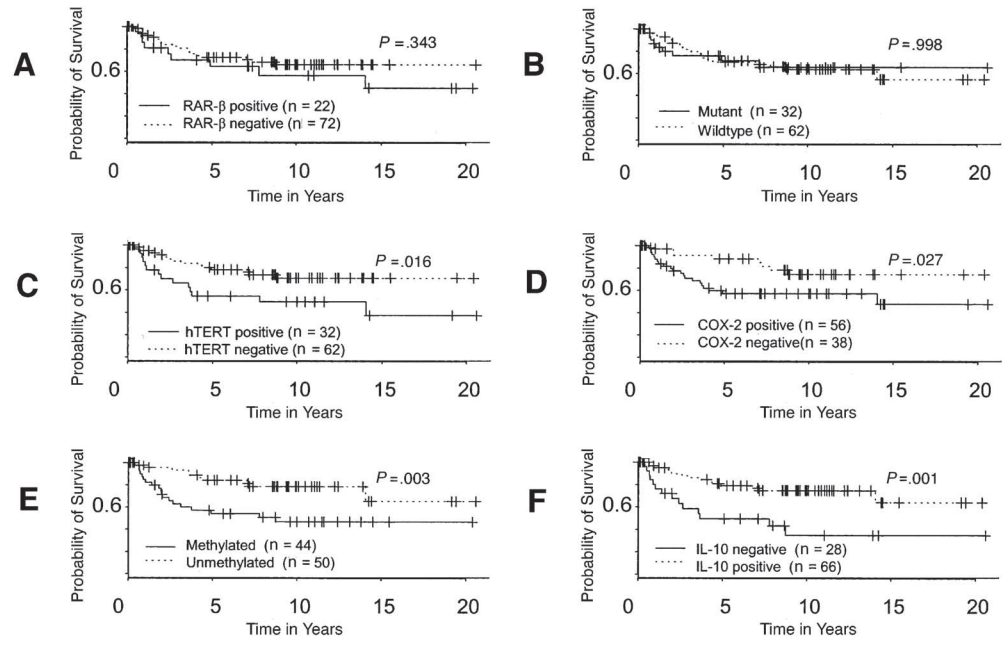


Fig 1. Disease-specific survival stratified by (A) retinoic acid receptor-beta (RAR-β) mRNA expression, (B) K-*ras* mutation status, (C) human telomerase reverse transcriptase catalytic subunit (hTERT) mRNA expression, (D) cyclooxygenase-2 (COX-2) mRNA expression, (E) death-associated protein kinase (*DAPK*) methylation, and (F) interleukin-10 (IL-10) protein expression.

Information downloaded from jco.ascopubs.org and provided by at M D ANDERSON HOSP on October 7, 2010 from
Copyright © 2004 American Society of Clinical Oncology. All rights reserved.

Table 4. Multivariate Cox Regression Model for Disease-Specific Survival

Molecular Marker	Hazard Ratio	95% CI	*P*
DAPK methylation	3.11	1.42 to 6.79	.004
IL-10 lack of expression	2.62	1.24 to 5.56	.012
COX-2 expression	2.13	0.92 to 4.95	.077

Abbreviations: *DAPK*, death-associated protein kinase; IL-10, interleukin-10; COX-2, cyclooxygenase-2.

associated (OR, 6.14; $P = .0004$). We ensured that the effect of these variables was not masked by colinearity by modeling them separately. Specifically, we modeled COX-2 expression with *DAPK* methylation (AIC = 228.135) and hTERT expression with *DAPK* methylation (AIC = 228.654). Neither of these models provided better fit than the model chosen.

DISCUSSION

Our findings further characterize and extend our group's previous research efforts to identify novel molecular prognostic factors in patients with early-stage NSCLC. We identified 94 patients with complete information for a panel of six molecular markers. Each biomarker had been previously studied as a prognostic factor based on its role in carcinogenesis. When analyzed individually, five of these biomarkers (RAR-β, COX-2, hTERT, *DAPK* promoter methylation, and IL-10) were demonstrated in prior studies[7-9,11,12] by our group to be significant predictors of survival. One available marker (K-*ras*) was included in the current analysis based on published data demonstrating that it had prognostic significance in early-stage NSCLC,[14,42] even though it did not have prognostic significance in univariate analysis in our patients. Our multivariable analysis indicates that two biomarkers (*DAPK* promoter methylation and IL-10) function as independent predictors of disease-specific survival, and a third biomarker (COX-2) is of borderline significance in this cohort. These findings should be confirmed in other NSCLC patient populations.

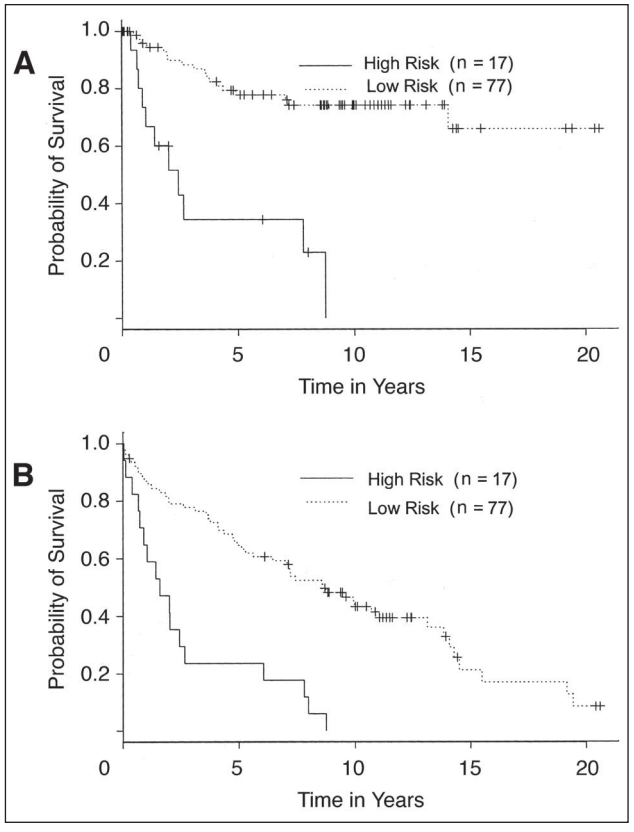


Fig 2. Disease-specific survival (A) and overall survival (B) of patients with both death-associated protein kinase methylation and interleukin-10 lack of expression (high risk) versus other patients (low risk).

Our results further support the importance of epigenetic gene regulation in lung carcinogenesis. Others have demonstrated that aberrant promoter methylation of *DAPK* and other genes frequently occurs in NSCLC tumors,[25,26] suggesting that methylation may be a common mechanism of inactivation of cancer-related genes. *DAPK* promoter methylation was the most statistically significant predictor of survival in our study. Kim et al[43] investigated the role of *DAPK* methylation in 185 NSCLC patients who underwent surgical resection, including 102 patients with stage I disease. *DAPK* methylation was significantly correlated with advanced stage, suggesting that *DAPK* may be important in the progression of NSCLC. Stage I patients with *DAPK* methylation had worse overall survival, although this association was not statistically significant. The authors noted that patient follow-up data was limited, and this factor may have contributed to their findings. Harden et al[44] examined promoter methylation of a panel of five genes in tumors and lymph nodes of 90 stage I NSCLC patients. Interestingly, patients with both *DAPK* and *adenomatous polyposis coli* gene methylation had poorer overall survival that did not reach statistical significance, although the methylation of either gene alone was not a predictor of survival. Possible explanations for these results include the relatively low frequency of *DAPK* methylation (17%) compared with our findings (47%). The smaller number of patients with *DAPK* methylation (n = 15) would result in the study having less power to detect significant associations with survival.

The role of IL-10 in carcinogenesis remains controversial. Our findings indicate that loss of IL-10 expression predicts poor disease-specific survival in early-stage NSCLC. Human bronchial epithelial cells constitutively produce IL-10, which may regulate the local immune response in normal lungs.[34] IL-10 also seems to have

Information downloaded from jco.ascopubs.org and provided by at M D ANDERSON HOSP on October 7, 2010 from
Copyright © 2004 American Society of Clinical Oncology. All rights reserved.

significant inhibitory effects on tumor growth and metastasis in multiple animal models and tumor types, including melanoma, breast cancer, prostate cancer, and Burkitt's lymphoma.[31,32,45-47] Evidence suggests that IL-10 exerts its antitumor and antimetastatic activity by inhibiting angiogenesis, and this activity is, in part, mediated by the downregulation of angiogenic molecules, such as vascular endothelial growth factor, IL-1β, tumor necrosis factor-α, IL-6, and matrix metalloproteinase-9 (MMP-9), in tumor-associated macrophages.[31] In addition, IL-10 may also directly affect the secretion of angiogenic molecules from the tumor. Stearns et al[46] demonstrated that IL-10 induces tissue inhibitor of metalloproteinase-1 production and inhibits MMP-2 and MMP-9 secretion by human prostate cancer cell lines orthotopically implanted into mice, resulting in decreased tumor microvessel formation and increased mice survival. In a murine mammary tumor model, the antitumor and antimetastatic effects of IL-10 gene transfection were associated with elevated nitric oxide levels in tumors.[48] Others have shown that IL-10 can directly inhibit the proliferation of endothelial cells stimulated with vascular endothelial growth factor or fibroblast growth factor-2 in vitro.[47] An intriguing molecular epidemiologic case-control study demonstrated that IL-10 promoter polymorphisms that resulted in lower IL-10 expression were associated with an increased risk of developing melanoma.[49] Furthermore, some authors have suggested that lung cancer cells can modulate IL-10 expression by stromal components. In the present study, only nine of 94 samples displayed tumor-infiltrating lymphocytes or tumor-associated macrophages, therefore hindering any relevant analysis of IL-10 production by infiltrating immune cells.

The data supporting the antitumor and antimetastatic activity of IL-10 are compelling, but most preclinical models using IL-10 to mediate such effects do so at concentrations that far exceed the levels demonstrated in lung cancer patients. Other authors have demonstrated that IL-10 is a potent immunosuppressive molecule that may promote lung cancer growth by suppressing T-cell and macrophage function and enabling tumors to escape immune detection.[50-52] Elevated baseline serum IL-10 levels were found to be independent predictors of poorer survival in 60 advanced-stage NSCLC patients receiving platinum-based chemotherapy.[53] Hatanaka et al[54] measured IL-10 mRNA levels by reverse transcriptase PCR in the tumors of 82 NSCLC patients who underwent surgical resection. Their assay demonstrated IL-10 expression in 83% of the surgical specimens. In contrast to our results, IL-10 expression was significantly associated with worse survival. The reasons for these discrepant findings remain unclear. These investigators included patients with stages I to IIIb disease in their study and used a different IL-10 assay (mRNA *v* protein) than the assay we used in our study. These factors may have contributed to these divergent results.

Our exploratory analyses demonstrate a highly significant association between hTERT expression and COX-2 expression ($P = .0004$). A precise explanation for this correlation is lacking, although various COX-2 inhibitors have been reported to inhibit both tumor growth and telomerase activity in mice.[55,56] We also observed a significant association between K-*ras* mutations and *DAPK* methylation ($P = .032$). Reports suggesting that DNA methylation may be regulated by the ras signaling pathway[57,58] are consistent with these findings. However, others have not found correlations between ras mutations and promoter hypermethylation in NSCLC tumors.[43,59] Clearly, a better understanding of the significance of these associations will require future studies. Our analyses also demonstrate a borderline significant association between IL-10 lack of expression and COX-2 expression ($P = .066$).[60,61] This finding is consistent with data suggesting that IL-10 has the capacity to potently downregulate COX-2. Therefore, in the absence of IL-10, COX-2 and its derived products would be more abundant and could further promote tumor progression.

This study is limited by its retrospective nature and the inclusion only of patients with complete information for all six biomarkers. It is difficult to speculate on potential biases affecting our results. It is possible, for example, that small tumors with limited tissue availability were underrepresented in this cohort. These results should be validated in a separate population of NSCLC patients.

In conclusion, our analysis of six molecular markers in patients with resected stage I NSCLC yielded two independent predictors of poorer disease-specific survival: *DAPK* methylation and IL-10 lack of expression. Future studies are warranted to further define their roles in tumor proliferation and metastasis. However, these and other potential molecular prognostic factors have yet to be validated, and thus, the integration of molecular marker assessments into the routine clinical management of NSCLC has remained an elusive goal. As the number of potential molecular markers increases, it has become more difficult to assess which prognostic factors are likely to be clinically relevant. A comprehensive multivariable analysis is not feasible because the majority of studies analyze only a single or a few biomarkers at a time. In this regard, the development of high-throughput technologies to determine gene-expression profiles and proteomic patterns of tissue specimens represents a significant methodologic advance. Several recent reports have demonstrated that mRNA and protein patterns of NSCLC tumors may be predictive of survival.[62,63] Hopefully, these technologies will eventually provide the clinician with a reliable, validated molecular staging system that will improve therapeutic strategies for NSCLC.

Authors' Disclosures of Potential Conflicts of Interest

The authors indicated no potential conflicts of interest.

Information downloaded from jco.ascopubs.org and provided by at M D ANDERSON HOSP on October 7, 2010 from
Copyright © 2004 American Society of Clinical Oncology. All rights reserved.

REFERENCES

1. Jemal A, Murray T, Samuels A, et al: Cancer statistics, 2003. CA Cancer J Clin 53:5-26, 2003

2. Travis W, Travis LB, Devesa SS: Lung cancer incidence and survival by histologic type. Cancer 75:191-202, 1995 (suppl 1)

3. Fry W, Phillips JL, Menck HR: Ten-year survey of lung cancer treatment and survival in hospitals in the United States. Cancer 86:1867-1876, 1999

4. Mountain CF: Revisions in the International System for Staging Lung Cancer. Chest 111:1710-1717, 1997

5. Tseng JE, Kemp BL, Khuri FR, et al: Loss of Fhit is frequent in stage I non-small cell lung cancer and in the lungs of chronic smokers. Cancer Res 59:4798-4803, 1999

6. Herbst RS, Yano S, Kuniyasu H, et al: Differential expression of E-cadherin and type IV collagenase genes predicts outcome in patients with stage I non-small cell lung carcinoma. Clin Cancer Res 6:790-797, 2000

7. Tang X, Khuri FR, Lee JJ, et al: Hypermethylation of the death-associated protein (DAP) kinase promoter and aggressiveness in stage I non-small-cell lung cancer. J Natl Cancer Inst 92:1511-1516, 2000

8. Khuri FR, Lotan R, Kemp BL, et al: Retinoic acid receptor-beta as a prognostic indicator in stage I non–small-cell lung cancer. J Clin Oncol 18:2798-2804, 2000

9. Khuri FR, Wu H, Lee JJ, et al: Cyclooxygenase-2 overexpression is a marker of poor prognosis in stage I non-small cell lung cancer. Clin Cancer Res 7:861-867, 2001

10. Zhou X, Kemp BL, Khuri FR, et al: Prognostic implication of microsatellite alteration profiles in early-stage non-small cell lung cancer. Clin Cancer Res 6:559-565, 2000

11. Wang L, Soria JC, Kemp BL, et al: HTERT expression is a prognostic factor of survival in patients with stage I non-small cell lung cancer. Clin Cancer Res 8:2883-2889, 2002

12. Soria JC, Moon C, Kemp BL, et al: Lack of interleukin-10 expression could predict poor outcome in patients with stage I non-small cell lung cancer. Clin Cancer Res 9:1785-1791, 2003

13. Pastorino U, Andreola S, Tagliabue E, et al: Immunocytochemical markers in stage I lung cancer: Relevance to prognosis. J Clin Oncol 15:2858-2865, 1997

14. Kwiatkowski DJ, Harpole DH Jr, Godleski J, et al: Molecular pathologic substaging in 244 stage I non-small-cell lung cancer patients: Clinical implications. J Clin Oncol 16:2468-2477, 1998

15. D'Amico TA, Massey M, Herndon JE II, et al: A biologic risk model for stage I lung cancer: Immunohistochemical analysis of 408 patients with the use of ten molecular markers. J Thorac Cardiovasc Surg 117:736-743, 1999

16. Ahrendt SA, Hu Y, Buta M, et al: p53 mutations and survival in stage I non-small-cell lung cancer: Results of a prospective study. J Natl Cancer Inst 95:961-970, 2003

17. Berard J, Gaboury L, Landers M, et al: Hyperplasia and tumours in lung, breast and other tissues in mice carrying a RAR beta 4-like transgene. EMBO J 13:5570-5580, 1994

18. Taketo MM: Cyclooxygenase-2 inhibitors in tumorigenesis (Part II). J Natl Cancer Inst 90:1609-1620, 1998

19. Hida T, Yatabe Y, Achiwa H, et al: Increased expression of cyclooxygenase 2 occurs frequently in human lung cancers, specifically in adenocarcinomas. Cancer Res 58:3761-3764, 1998

20. Wolff H, Saukkonen K, Anttila S, et al: Expression of cyclooxygenase-2 in human lung carcinoma. Cancer Res 58:4997-5001, 1998

21. Li M, Song S, Lippman SM, et al: Induction of retinoic acid receptor-beta suppresses cyclooxygenase-2 expression in esophageal cancer cells. Oncogene 21:411-418, 2002

22. Hahn WC: Role of telomeres and telomerase in the pathogenesis of human cancer. J Clin Oncol 21:2034-2043, 2003

23. Hiyama K, Hiyama E, Ishioka S, et al: Telomerase activity in small-cell and non-small-cell lung cancers. J Natl Cancer Inst 87:895-902, 1995

24. Kim NW, Piatyszek MA, Prowse KR, et al: Specific association of human telomerase activity with immortal cells and cancer. Science 266: 2011-2015, 1994

25. Zochbauer-Muller S, Fong KM, Maitra A, et al: 5′ CpG island methylation of the FHIT gene is correlated with loss of gene expression in lung and breast cancer. Cancer Res 61:3581-3585, 2001

26. Esteller M, Corn PG, Baylin SB, et al: A gene hypermethylation profile of human cancer. Cancer Res 61:3225-3229, 2001

27. Deiss LP, Feinstein E, Berissi H, et al: Identification of a novel serine/threonine kinase and a novel 15-kD protein as potential mediators of the gamma interferon-induced cell death. Genes Dev 9:15-30, 1995

28. Inbal B, Cohen O, Polak-Charcon S, et al: DAP kinase links the control of apoptosis to metastasis. Nature 390:180-184, 1997

29. Beissert S, Hosoi J, Grabbe S, et al: IL-10 inhibits tumor antigen presentation by epidermal antigen-presenting cells. J Immunol 154:1280-1286, 1995

30. Rohrer JW, Coggin JH Jr: CD8 T cell clones inhibit antitumor T cell function by secreting IL-10. J Immunol 155:5719-5727, 1995

31. Huang S, Ullrich SE, Bar-Eli M: Regulation of tumor growth and metastasis by interleukin-10: the melanoma experience. J Interferon Cytokine Res 19:697-703, 1999

32. Kundu N, Beaty TL, Jackson MJ, et al: Antimetastatic and antitumor activities of interleukin 10 in a murine model of breast cancer. J Natl Cancer Inst 88:536-541, 1996

33. Esteller M, Sanchez-Cespedes M, Rosell R, et al: Detection of aberrant promoter hypermethylation of tumor suppressor genes in serum DNA from non-small cell lung cancer patients. Cancer Res 59:67-70, 1999

34. Bonfield TL, Konstan MW, Burfeind P, et al: Normal bronchial epithelial cells constitutively produce the anti-inflammatory cytokine interleukin-10, which is downregulated in cystic fibrosis. Am J Respir Cell Mol Biol 13:257-261, 1995

35. Fujieda S, Lee K, Sunaga H, et al: Staining of interleukin-10 predicts clinical outcome in patients with nasopharyngeal carcinoma. Cancer 85:1439-1445, 1999

36. Kolquist KA, Ellisen LW, Counter CM, et al: Expression of TERT in early premalignant lesions and a subset of cells in normal tissues. Nat Genet 19:182-186, 1998

37. Soria JC, Moon C, Wang L, et al: Effects of N-(4-hydroxyphenyl)retinamide on hTERT expression in the bronchial epithelium of cigarette smokers. J Natl Cancer Inst 93:1257-1263, 2001

38. Falchetti ML, Pallini R, D'Ambrosio E, et al: In situ detection of telomerase catalytic subunit mRNA in glioblastoma multiforme. Int J Cancer 88:895-901, 2000

39. Xu XC, Ro JY, Lee JS, et al: Differential expression of nuclear retinoid receptors in normal, premalignant, and malignant head and neck tissues. Cancer Res 54:3580-3587, 1994

40. Xu XC, Sozzi G, Lee JS, et al: Suppression of retinoic acid receptor beta in non-small-cell lung cancer in vivo: Implications for lung cancer development. J Natl Cancer Inst 89:624-629, 1997

41. Jacobson DR, Mills NE: A highly sensitive assay for mutant ras genes and its application to the study of presentation and relapse genotypes in acute leukemia. Oncogene 9:553-563, 1994

42. Slebos RJ, Kibbelaar RE, Dalesio O, et al: K-ras oncogene activation as a prognostic marker in adenocarcinoma of the lung. N Engl J Med 323:561-565, 1990

43. Kim DH, Nelson HH, Wiencke JK, et al: Promoter methylation of DAP-kinase: Association with advanced stage in non-small cell lung cancer. Oncogene 20:1765-1770, 2001

44. Harden SV, Tokumaru Y, Westra WH, et al: Gene promoter hypermethylation in tumors and lymph nodes of stage I lung cancer patients. Clin Cancer Res 9:1370-1375, 2003

45. Gerard CM, Bruyns C, Delvaux A, et al: Loss of tumorigenicity and increased immunogenicity induced by interleukin-10 gene transfer in B16 melanoma cells. Hum Gene Ther 7:23-31, 1996

46. Stearns ME, Garcia FU, Fudge K, et al: Role of interleukin 10 and transforming growth factor beta1 in the angiogenesis and metastasis of human prostate primary tumor lines from orthotopic implants in severe combined immunodeficiency mice. Clin Cancer Res 5:711-720, 1999

47. Cervenak L, Morbidelli L, Donati D, et al: Abolished angiogenicity and tumorigenicity of Burkitt lymphoma by interleukin-10. Blood 96: 2568-2573, 2000

48. Kundu N, Dorsey R, Jackson MJ, et al: Interleukin-10 gene transfer inhibits murine mammary tumors and elevates nitric oxide. Int J Cancer 76:713-719, 1998

49. Howell WM, Turner SJ, Bateman AC, et al: IL-10 promoter polymorphisms influence tumour development in cutaneous malignant melanoma. Genes Immun 2:25-31, 2001

50. Sharma S, Stolina M, Lin Y, et al: T cell-derived IL-10 promotes lung cancer growth by suppressing both T cell and APC function. J Immunol 163:5020-5028, 1999

51. Spagnoli GC, Juretic A, Schultz-Thater E, et al: On the relative roles of interleukin-2 and interleukin-10 in the generation of lymphokine-

Information downloaded from jco.ascopubs.org and provided by at M D ANDERSON HOSP on October 7, 2010 from
Copyright © 2004 American Society of Clinical Oncology. All rights reserved.

activated killer cell activity. Cell Immunol 146: 391-405, 1993

52. Huang M, Sharma S, Mao JT, et al: Non-small cell lung cancer-derived soluble mediators and prostaglandin E2 enhance peripheral blood lymphocyte IL-10 transcription and protein production. J Immunol 157:5512-5520, 1996

53. De Vita F, Orditura M, Galizia G, et al: Serum interleukin-10 levels as a prognostic factor in advanced non-small cell lung cancer patients. Chest 117:365-373, 2000

54. Hatanaka H, Abe Y, Kamiya T, et al: Clinical implications of interleukin (IL)-10 induced by non-small-cell lung cancer. Ann Oncol 11:815-819, 2000

55. Nishimura G, Yanoma S, Mizuno H, et al: A selective cyclooxygenase-2 inhibitor suppresses tumor growth in nude mouse xenografted with human head and neck squamous carcinoma cells. Jpn J Cancer Res 90:1152-1162, 1999

56. Lonnroth C, Andersson M, Lundholm K: Indomethacin and telomerase activity in tumor growth retardation. Int J Oncol 18:929-937, 2001

57. Rouleau J, MacLeod AR, Szyf M: Regulation of the DNA methyltransferase by the Ras-AP-1 signaling pathway. J Biol Chem 270: 1595-1601, 1995

58. Bigey P, Ramchandani S, Theberge J, et al: Transcriptional regulation of the human DNA methyltransferase (dnmt1) gene. Gene 242:407-418, 2000

59. Pulling LC, Divine KK, Klinge DM, et al: Promoter hypermethylation of the O6-methylguanine-DNA methyltransferase gene: More common in lung adenocarcinomas from never-smokers than smokers and associated with tumor progression. Cancer Res 63:4842-4848, 2003

60. Moore KW, de Waal Malefyt R, Coffman RL, et al: Interleukin-10 and the interleukin-10 receptor. Annu Rev Immunol 19:683-765, 2001

61. Molina-Holgado E, Arevalo-Martin A, Ortiz S, et al: Theiler's virus infection induces the expression of cyclooxygenase-2 in murine astrocytes: Inhibition by the anti-inflammatory cytokines interleukin-4 and interleukin-10. Neurosci Lett 324:237-241, 2002

62. Beer DG, Kardia SL, Huang CC, et al: Gene-expression profiles predict survival of patients with lung adenocarcinoma. Nat Med 8:816-824, 2002

63. Yanagisawa K, Shyr Y, Xu BJ, et al: Proteomic patterns of tumour subsets in non-small-cell lung cancer. Lancet 362:433-439, 2003

Attention Authors: You Asked For It - You Got It!

Online Manuscript System Launched November 1st

On November 1st, *JCO* formally introduced its online Manuscript Processing System that will improve all aspects of the submission and peer-review process. Authors should notice a quicker turnaround time from submission to decision through this new system.

Based on the well known Bench>Press system by HighWire Press, the *JCO* Manuscript Processing System promises to further *JCO's* reputation of providing excellent author service, which includes an already fast turnaround time of 7 weeks from submission to decision, no submission fees, no page charges, and allowing authors to freely use their work that has appeared in the journal.

JCO's Manuscript Processing System will benefit authors by

- eliminating the time and expense of copying and sending papers through the mail
- allowing authors to complete required submission forms quickly and easily online
- receiving nearly immediate acknowledgement of receipt of manuscripts
- tracking the status of manuscripts at any time online and
- accessing all reviews and decisions online.

Authors are encouraged to register at http://submit.jco.org.

For more details on *JCO's* new online Manuscript Processing System, go online to http://www.jco.org/misc/announcements.shtml. Also, watch upcoming issues of *JCO* for updates like this one.

Information downloaded from jco.ascopubs.org and provided by at M D ANDERSON HOSP on October 7, 2010 from
Copyright © 2004 American Society of Clinical Oncology. All rights reserved.

Expert Opinion

1. Introduction
2. Preclinical activity
3. Chemistry, pharmacokinetics and metabolism
4. Clinical efficacy and toxicity spectrum of lonafarnib
5. Other FTIs
6. Expert opinion

informa
healthcare

Expert Opin. Investig. Drugs Downloaded from informahealthcare.com by UTMD Anderson Cancer Center on 10/08/10
For personal use only.

Lonafarnib in cancer therapy

Floriana Morgillo & Ho-Young Lee†
†*M. D. Anderson Cancer Center, Department of Thoracic/Head & Neck Medical Oncology, Houston, TX, USA*

Farnesyl transferase inhibitors (FTIs) are anticancer agents that were designed to block the post-translational attachment of the prenyl moiety to C-terminal cysteine residue of Ras and thus inactivate it. Because Ras plays an important role in tumour progression and the *ras* mutation is one of the most frequent aberrations in cancer, FTIs have been expected to exert excellent therapeutic activities. Phase I and II clinical trials confirmed relevant antitumour activity and low toxicity; however, no improvement in overall survival has been reported in Phase III trials. The exact mechanism of action of this class of agents is currently unknown. Increasing lines of evidence indicate that the cytotoxic actions of FTIs are not due to the inhibition of Ras proteins exclusively, but to the modulation of other targets, including RhoB, the centromere-binding proteins and other proteins that have not yet been identified. This review describes the pharmacological and clinical data as well as mechanisms of action of FTIs, especially lonafarnib (SCH-66336), a non-peptidomimetic inhibitor that has shown anticancer activity.

Keywords: farnesyl transferase inhibitor, lonafarnib, Ras, SCH-66336, targeted therapy

Expert Opin. Investig. Drugs (2006) ***15****(6):709-719*

1. Introduction

Recent advances in the understanding of cell biology and cancer genetics have permitted identification of novel therapeutic targets and led to the development of rational mechanism-based drugs. Farnesyl transferase inhibitors (FTIs) are among the first and most-studied oncogene-targeted agents. They were designed to prevent the function of Ras proteins by blocking the post-translational attachment of the prenyl moiety to its C-terminal cysteine, thereby inhibiting its membrane localisation and function (**Figure 1**). Protein prenylation is a post-translational modification in which either a farnesyl or geranylgeranyl isoprenoid is linked to specific cysteine residues of proteins via a thioether bond. These proteins belong to a group termed 'CAAX proteins', which is defined by a specific C-terminal motif that directs their modification. The CAAX group of prenylated proteins includes Ras and a multitude of guanosine triphosphate (GTP)-binding proteins and several protein kinases and phosphatases.

Ras proteins are 21-kDa membrane-associated guanine nucleotide-binding proteins [1] that alternate between an inactive form bound to guanosine diphosphate (GDP) and an active form bound to GTP (**Figure 2**) [2,3].

Mutations in *ras* is one of the most frequent aberrations in cancer and has been observed in ~ 30% of human cancers [2], with ~ 90% in pancreatic cancer [4], and in 10 – 65% of haematological malignancies [2,5]. Because farnesylation is the most important step in Ras activation [6], agents that block FTase have been developed to affect cancer cell survival and proliferation.

On activation, Ras stimulates the Raf/MEK/MAPK pathway, which induces an increase in the levels of cyclin D1 that promote the progression of cells through the G1 checkpoint and into S phase, leading to proliferation [7]. Activated Ras also stimulates PI3K/Akt and their downstream signalling pathways that stimulate cell

RIGHTSLINK

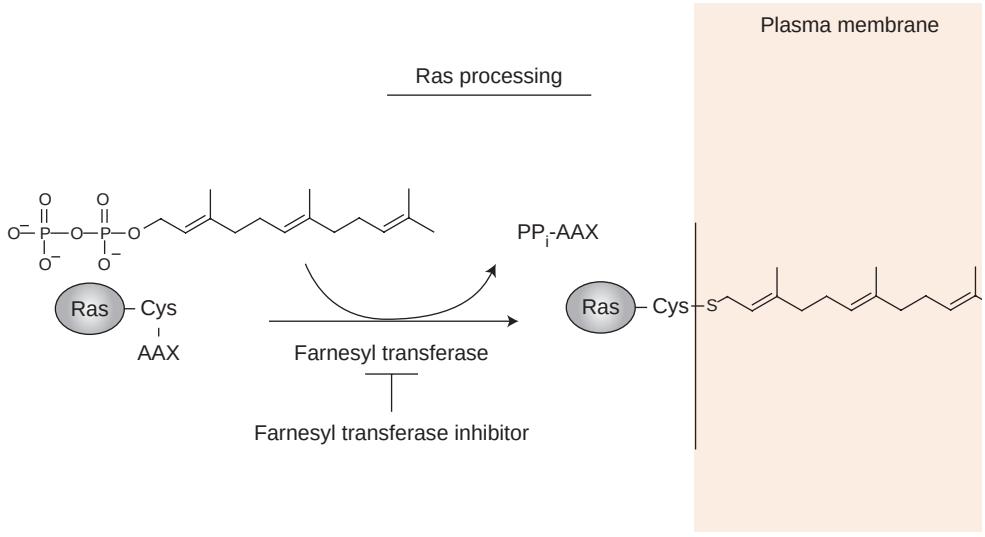


Figure 1. Mechanism of action of farnesyltransferase inhibitors. To become activated, Ras proteins must be localised to the inner side of the plasma membrane through a process called prenylation, which is the covalent addition of an isoprenoid moiety, farnesyl or geranylgeranyl issued from the cholesterol biosynthetic pathway to the C-terminal cysteine of substrate proteins. This process is catalysed by farnesyl- or geranylgeranyltransferase and occurs on the cysteine in a CAAX consensus sequence. In the CAAX sequence, the 'C' represents the cysteine, 'A' is an aliphatic amino acid and 'X' any amino acid. Once the prenyl group attaches to the CAAX moiety, the AAX part is cleaved. The C-terminal farnesyl-cysteine moiety is then carboxymethylated and a fatty acid palmitate residue is attached. This makes the Ras protein hydrophobic and facilitates its transfer to the cell membrane, where it becomes phosphorylated when activated by upstream tyrosine kinase signalling.
PP_i: Pyrophosphate group.

Expert Opin. Investig. Drugs Downloaded from informahealthcare.com by UTMD Anderson Cancer Center on 10/08/10
For personal use only.

proliferation and survival [8]. In addition, Ras regulates Ral-GDS (Ras-related GTPase guanine nucleotide dissociation stimulator) proteins, guanine nucleotide exchange factors (GEFs) for Ral and phospholipase Cε (PLCε) that catalyse the hydrolysis of phosphatidylinositol-4,5-bisphosphate to diacylglycerol and inositol trisphosphate. Therefore, once in its active GTP-bound state, Ras can stimulate gene expression, cell-cycle progression and survival, cytoskeleton rearrangement, vesicle transport and Ca^{2+} signalling [7,8]. In addition, Ras interacts with specific integrin-α cytoplasmic domains and small GTP-binding protein, such as Rac and the Rho proteins, which may lead to an increase in the invasive capacity of neoplastic cells [7].

Substantial knowledge about the molecular biology of Ras and its downstream pathways has been obtained during the past decades. A series of recent studies has suggested that inhibition of the farnesylation of not-yet-identified protein/s other than Ras might be responsible for FTI effects. In this respect, RhoB, an important downstream effector of Ras, which affects various cellular processes – such as proliferation, apoptosis, actin formation, adhesion and motility – is also farnesylated as well as geranylgeranylated. This implies that FTI will also affect the function of this protein [9,10].

Moreover, Jiang *et al.* [11] found that the administration of a FTI to human cancer cells induces apoptosis through an inhibition of the PI3K/Akt2 cascade, but neither Ras nor RhoB (instead, an as-yet-unknown short-lived farnesylated protein) mediates this inhibition.

There is evidence that FTI might affect the activation of the centromere-binding proteins (CENP)-E and -F, which play an important role during mitosis by interfering with their prenylation [12].

Thus, although the Ras pathways have been investigated intensively, the complex biology and contribution of other main proteins to the cellular pharmacology of FTIs have probably not been sufficiently elucidated during the preclinical and clinical development of these anticancer drugs.

FTIs have demonstrated anticancer activity as single agents or in combination with standard radiation or cytotoxic chemotherapy [13-15]. In addition, FTIs have shown potential as a lung cancer chemopreventive agent [16]. Following the encouraging preclinical results, FTIs are now in clinical development.

On the basis of an understanding of the FTase reaction and the substrate specificity of the various enzymes, FTIs can be grouped into four main classes: farnesyl pyrophosphate analogues; CAAX peptidomimetics; bisubstrate inhibitors; and non-peptidomimetic inhibitors. FTIs compete with the CAAX-containing peptides for FTase binding sites. A total of three major nonpeptide FTIs have been developed and tested in clinical trials. Lonafarnib (SCH-66336) is an orally bioavailable tricyclic inhibitor of CAAX binding [17].

RIGHTSLINK

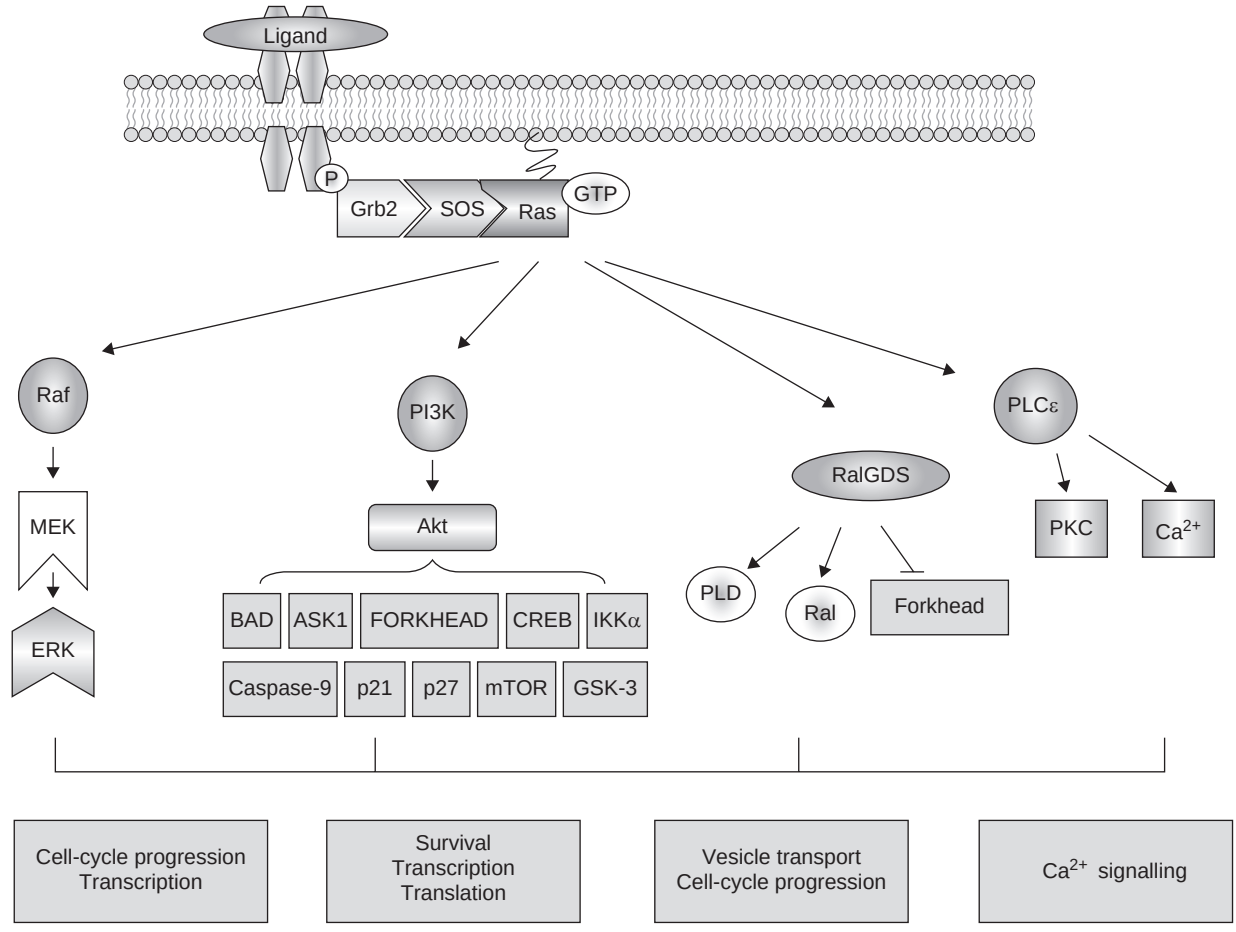


Figure 2. A simplified scheme of Ras-mediated signaling pathway. Once stimulated by extracellular signals (i.e. growth factor), tyrosine kinase receptors dimerise and autophosphotylate Src-homology-2 domains on the intracellular surface of the protein. This leads to binding of Grb-2, an adapter protein, and the SOS that interacts with Ras. The activated GTP-Ras is subsequently able to stimulate cell-proliferative and -survival processes through the activation of multiple pathways, such as Raf/MEK/Erk, PI3K/Akt/PKB, RalGDS (guanine nucleotide exchange factors for Ral) and PLCε, which activates PKC and mobilises Ca^{2+} from intracellular stores.
ERK: Extracellular-regulated kinase; Grb2: Growth factor receptor-bound protein 2; GSK3: Glycogen synthase kinase 3; MEK: Mitogen-activated kinase/ERK kinase; PKC: Protein kinase C; PL: Phospholipase; Ral: Ras-related GTPase; RalGD: Ral guanine nucleotide dissociation stimulator; SOS: Son of sevenless.

Lonafarnib has demonstrated activity against human tumour cell lines and xenografts. Tipifarnib (R-115777) is an orally active heterocyclic agent with an imidazole pharmacophore [18]. A third nonpeptide FTI in clinical trials is BMS-214662, an intravenously administered agent that induced apoptosis *in vitro* in several solid tumour cell types [19]. This review focuses on the pharmacological profile, preclinical and clinical activities, and toxicity spectrum of lonafarnib.

2. Preclinical activity

Lonafarnib has been known to inhibit anchorage-independent growth of K-*ras*-transformed rodent fibroblasts and of various mutated K-*ras*-containing human tumour cell lines with a median inhibitory concentration (IC_{50}) of 0.4 – 0.5 µmol/l [17,20]. Lonafarnib altered the cell-cycle distribution of several human tumour cell lines in two distinct ways. Most sensitive human tumour cell lines – such as HCT 116 (colon cancer cell line), NCI-H460 (lung cancer), McF7 (breast cancer) and MIA PaCa-2 (pancreatic cancer) – accumulated in the G2 – M phase after FTI treatment, but those with an activated H-*ras* (such as T 24 cell [bladder carcinoma]) accumulated in the G1 phase, suggesting that the biological effects induced by FTIs in cells with an activated H-*ras* are distinct from those in other sensitive cells [21]. Moreover, the cell-cycle blockade is often correlated with a p53-dependent p21 ($p21^{waf}$ or $p21^{Cip1}$) induction in many cell types [21].

Another important effect of lonafarnib is the induction of apoptosis notably at low serum concentrations [22]. Likewise, simultaneous treatment of H-*ras*-transformed fibroblasts with a MEK1 or -2 inhibitor markedly enhanced caspase-3

Expert Opin. Investig. Drugs Downloaded from informahealthcare.com by UTMD Anderson Cancer Center on 10/08/10
For personal use only.

RIGHTSLINK

activity and the apoptotic response to lonafarnib [23]. Earlier reports [24,25] have shown the antileukaemic activity of lonafarnib in cell culture models of BCR-ABL transformation and in mouse models of BCR-ABL-positive leukaemia.

Lonafarnib has demonstrated excellent oral bioavailability and pharmacokinetic properties in *in vivo* studies, including mouse, rat and monkey systems [17]. Lonafarnib has shown growth-inhibitory effects on several human tumour xenografts, including DLD-1 and HCT16 colon carcinoma, A549 and HTB177 lung carcinoma, AsPc-1, HPAF-II, HS700T and MIA PaCa-2 pancreatic carcinoma, DU145 prostatic carcinoma and a H-*ras* transgenic mouse model [17]. In this study [17], the tumour regression that was observed after lonafarnib treatment in transgenic mice correlated with an increase in apoptosis in the tumour cells [17]. Enhanced efficacy was also observed when lonafarnib was combined with various cytotoxic agents (cyclophosphamide, 5-fluorouracil and vincristine). These collective findings indicate effective antitumour activity of lonafarnib.

Although FTIs were originally shown to inhibit farnesylation and activation of Ras, accumulating evidence suggests that lonafarnib suppresses anchorage-dependent and -independent growth of many human cancer cell lines, irrespective of whether they express wild-type or mutated Ras [17,26]. It has been suggested that RhoB (a protein that is prenylated) mediates the response to treatment with FTIs; RhoB can be farnesylated or geranylgeranylated and the antitumour effects of FTIs probably depend on the accumulation of geranylgeranylated forms of RhoB [9,10]. Lonafarnib also inhibits the PI3K/Akt-mediated growth and adhesion-dependent survival pathways and induces apoptosis via a Ras-independent mechanism [11]. In addition, lonafarnib has been demonstrated to block the prenylation of Rheb (a Ras homologue enriched in the brain), which is a small farnesylated GTPase that positively regulates mammalian target of rapamycin signalling and is generally higher in tumour cell lines than in normal cells [27]. Moreover, lonafarnib induces phosphorylation in head and neck squamous cell cancer (HNSCC) cell lines and, therefore, the inactivation of the eukaryotic translation elongation factor 2 (eEF2), which results in the suppression of protein synthesis [28]. Therefore, the lonafarnib-induced apoptotic activities that were shown in several human HNSCC cell lines could be due to the effects of the drug on protein synthesis. Indeed, several human cancer HNSCC cell lines treated with lonafarnib showed a reduction in the protein expression of antiapoptotic Bcl-2 and Bcl-XL and prosurivival Akt [29]. Recently, Takada *et al.* [30] have shown that lonafarnib inhibits activation of NF-κB and NF-κB-regulated gene expression induced by carcinogens and inflammatory stimuli identifying a new molecular basis for the suppression of proliferation and angiogenesis by SCH-66336.

Of interest, lonafarnib was shown to inhibit microtubule cytoskeleton, resulting in microtubule stabilisation and suppression of microtubule dynamics [31]. The microtubule-stabilising action of lonafarnib could be due to its effects on histone deacetylase 6 (HDAC6), the known tubulin deacetylase [31], or on CENPs [12]. These studies provided preclinical support for the following clinical studies [14,32] of the lonafarnib–paclitaxel combination that evidenced clinical activity with a good tolerability.

A recent study [33] has shown that lonafarnib has potential as an antiangiogenic therapeutic agent for aerodigestive tract tumours, a new role for this class of drugs. Lonafarnib appears to inhibit angiogenic activities of non-small cell lung cancer (NSCLC) and HNSCC cells by decreasing hypoxia- or IGF-stimulated HIF-1α expression by inhibiting the interaction between HIF-1α and heat-shock protein (Hsp)-90, thus causing the proteasomal degradation of HIF-1α and a decrease in vascular endothelial growth factor (VEGF) production from cancer and vascular endothelial cells. The action of lonafarnib seems to be mediated via an inhibition of tumour angiogenesis [33], leading to regression of orthotopic HNSCC on the tongue in mice. Tumour angiogenesis and metastases have been proposed to be associated with oncogenic *ras* mutations that mediate the increased expression of angiogenic growth factor and key metalloprotease, such as VEGF, gelatinase and stromelysin [34-36]. However, the antiangiogenic activities of lonafarnib in this study have also been documented as being Ras independent.

Despite diverse therapeutic actions of lonafarnib *in vitro*, ranging from antiangiogenic to antiproliferative and apoptotic effects on different types of cancer cells, it has shown therapeutic effects on a limited number of tumour types. Except for haematological malignancies, it appears to have only modest and variable antineoplastic effects on several types of tumours, probably because it stimulates alternative survival and antiapoptotic pathways. Therefore, it has been hypothesised that combination of lonafarnib with other targeted therapies that can block the alternative survival pathway could be a better therapeutic strategy to treat various malignancies. Indeed, the combination of lonafarnib and SCH58500 (a replication-deficient recombinant adenovirus that expresses the human p53 tumour suppressor) has shown synergistic or additive antiproliferative effects on a panel of tumour cell lines *in vitro* [37], and greater combined efficacy was observed *in vivo* in the DU145 human prostatic cancer and the *wap-ras/F* transgenic mouse cancer models [37]. Moreover, when the three-drug combination of lonafarnib, SCH58500 and paclitaxel was tested, each two-drug interaction displayed such marked synergy that the addition of a third drug to the statistical model only produced additivity [37]. Investigators have also looked at combinations of lonafarnib and IGFBP-3, a major serum IGF-binding protein that regulates IGF-mediated cancer cell survival and growth. Ras-mediated signalling has been suggested as interfering with antiproliferative effects of IGFBP-3 [38] and the enhancement of antitumour activity by the combination could have resulted from the blockade of Ras-mediated signalling by lonafarnib; however, the *ras* mutation does not seem to account for the increased apoptotic response of NSCLC cells

Expert Opin. Investig. Drugs Downloaded from informahealthcare.com by UTMD Anderson Cancer Center on 10/08/10
For personal use only.

RIGHTSLINK

Expert Opin. Investig. Drugs Downloaded from informahealthcare.com by UTMD Anderson Cancer Center on 10/08/10
For personal use only.

to combined treatment of IGFBP-3 and lonafarnib. Lonafarnib has also shown enhanced antitumour activities in several cancer cells *in vitro* and *in vivo* when combined with PI3K inhibitors, including LY-294002 and wortmannin [39]. Importantly, these PI3K inhibitors unmask the proapoptotic effects of FTIs in malignantly transformed cells, but not in normal cells. Lonafarnib has also shown enhanced antitumour activity when combined with cisplatin, taxanes and gemcitabine [7,40,41]; for example, lonafarnib sensitised tumour cells to paclitaxel-induced mitotic arrest [31], probably through its effects on HDAC6 [31] and CENPs [12]. Combined treatment with lonafarnib and the proteasome inhibitor bortezomib has also been tested in multiple myeloma cell lines whose growth depends on the Ras/Raf/MAPK pathway signalling [42]. This combination induced synergistic tumour cell death and an increase in the cleavage of caspase-3, -8 and -9 with concomitant downregulation of pAkt [42]. Recently, Nakajima *et al.* [43] showed that lonafarnib enhances the antiproliferative effects of imanitib against Bcr-Abl-expressing cells, which was consistent with the report of Hoover *et al.* [44]. Both groups have shown that treatment of the imanitib-resistant Bcr-Abl-expressing cells with imanitib plus lonafarnib leads to enhanced antiproliferative or proapoptotic effects.

3. Chemistry, pharmacokinetics and metabolism

Lonafarnib ([+]4-(2-[4-(8-chloro-3,*O*-dibromo-6,11-dihydro-5-benzocyclohepa[1,2-f]pyridin-11-yl)-1-piperidinyl]-2-oxoethyl)-1-piperidinecarboxamide is a tricyclic nonpeptidyl, nonsulfhydryl FTI (**Figure 3**). *In vitro*, it blocks farnesylation of H-*ras* with a IC_{50} of 1.9 nmol/l and inhibits the farnesylation of K-*ras*4B with a IC_{50} of 5.2 nmol/l. It does not inhibit geranylgeranyl protein transferase-1 in concentrations of ≤ 50 µmol/l [45]. The drug is absorbed relatively slowly and peak concentrations are generally reached at 2.7 – 8 h after drug administration. Peak plasma concentrations and area under the curve (AUC) values increase in a dose-proportional manner. An increase in dose from 25 to 400 mg was associated with an increase in mean peak plasma concentration by a factor of ~ 56 and in the AUC by a factor of ~ 200. The apparent clearance of lonafarnib decreases exponentially from 1190 ± 462 ml/min at a dose of 25 mg to 101 ± 27.3 ml/min at 400 mg and the volume of distribution ($V_{d,ss}$/F) decreases from 331 ± 27 l to 90.4 ± 22.4 l with the same doses. A trend of increasing plasma half-life with increasing dose that was statistically significant for lonafarnib 300 and 400 mg b.i.d. ($p < 0.007$; Kruskal–Wallis test) has been described [46]. The peak plasma concentrations and $AUC_{0\text{-}12}$ increase by a factor of ~ 2 – 5 on repeated dosing in a dose-independent manner ($p = 0.103$; Kruskal–Wallis test), which is more than expected when only based on accumulation effects ($p = 0.0016$; paired student's t test). In contrast, the terminal disposition half-life is comparable between days 1 and 15 although the mean difference reached borderline significance ($p = 0.04$; Wilcoxon test for matched pairs of 10 patients). This suggests that the dose dependence in the apparent clearance does not arise primarily from factors associated with saturation of excretory routes. Steady-state concentrations of lonafarnib are attained by days 7 – 14 and there is only minor intrapatient variability in these levels [46]. The cumulative urinary excretion of unchanged lonafarnib was dose independent and accounted for < 0.02% of the administered dose. The mean renal clearance (the product of the dose fraction excreted unchanged in urine and the apparent total body clearance) is estimated as 0.117 ± 0.0105 ml/min, thus suggesting that lonafarnib is not cleared by renal processes [46].

4. Clinical efficacy and toxicity spectrum of lonafarnib

4.1 Phase I clinical trial

Several Phase I trials (**Table 1**) were performed with lonafarnib in patients who had advanced cancer. Adjei *et al.* [47] evaluated its effects in 20 patients by administering it orally twice daily for 7 days in a 21-day cycle. The most common haematological toxic effect was leucopoenia, which was usually associated with neutropoenia and was generally brief, mild and noncumulative. Diarrhoea was the principal non-haematological toxic effect; it was severe and dose limiting with lonafarnib 400 mg b.i.d. In a preliminary evaluation of drug activity, 1 patient who had metastatic NSCLC that had been refractory to other treatments presented a partial response after 2 courses of treatment and remained in the study for 14 months. Disease in another 8 patients was stable over 5 – 10 treatment cycles.

Lonafarnib has shown some toxicity in patients. The first clinical trial with lonafarnib in haematological malignancies was a Phase I study in 18 patients who had high-risk malignancies, including chronic myeloid leukaemia in the blastic phase (CML-BP), chronic myelomonocytic leukaemia (CMML), myelodysplastic syndrome (MDS), acute myelogenous leukaemia (AML) and acute lymphoblastic leukaemia (ALL) [48]. A starting dose of lonafarnib 100 mg b.i.d. p.o. was administered on a continuous schedule and the dose was increased until the maximum-tolerated dose (MTD) of 200 mg b.i.d. was reached. A total of 6 of 16 evaluable patients had a clinical response. Gastrointestinal toxicity, particularly diarrhoea (grade I/II), occurred in two-thirds of the patients. Farnesylation of the protein DNAJ was consistently inhibited.

A Phase Ib monotherapy study was undertaken in patients who had HNSCC. They were randomised to receive lonafarnib 100 – 300 mg b.i.d. or best supportive care for ≤ 14 days before surgery. Gastrointestinal side effects were observed but no dose-limiting toxicity (DLT) was reported. Partial responses were observed in 3 of 17 patients treated. Analysis of the surrogate marker DNAJ (Hdj-2), a

RIGHTSLINK

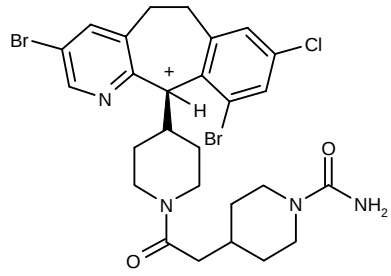


Figure 3. Chemical structure of lonafarnib.

farnesylated chaperone protein, in surgical samples revealed an increase in unfarnesylated protein in patients treated with lonafarnib [49].

A Phase I study [32] was conducted to establish the MTD of lonafarnib in combination with paclitaxel in patients who had solid tumours and to characterise the safety, tolerance, DLT and pharmacokinetics of the combination. Uninterrupted scheduled doses of lonafarnib 100, 125 and 150 mg b.i.d. p.o. were administered in combination with paclitaxel 135 or 175 mg/m^2 i.v. over 3 h on day 8 of every 21-day cycle. DLT consisted of grade 3 hyperbilirubinaemia, grade 4 diarrhoea, grade 3 peripheral neuropathy and grade 4 neutropoenia with fever. The MTDs established with the continual-reassessment method were lonafarnib 100 mg b.i.d. and paclitaxel 175 mg/m^2. A total of 21 patients were evaluable. Of 15 previously treated patients, 6 had durable partial responses, which included 2 of the 5 patients who had taxane-resistant metastatic NSCLC. A Phase I combination study [50] of continuous oral administration of lonafarnib with gemcitabine administered on days 1, 8 and 15 every 28 days has been reported in abstract form. The recommended doses for Phase II testing were either lonafarnib 150 mg in the morning and 100 mg in the evening with gemcitabine 1000 mg/m^2, or lonafarnib 200 mg b.i.d. with gemcitabine 600 mg/m^2. A total of two partial responses were documented in pancreatic cancer and one minor response each was documented in pancreatic cancer and pleural mesothelioma.

Hurwitz *et al.* [51] have also shown that 14 consecutive days of treatment with lonafarnib 200 mg b.i.d. p.o. (a recommended Phase II dose) induced nausea, diarrhoea and malaise as DLTs. Eskens *et al.* [46] used continuous oral administration of lonafarnib for 28 days and reported DLTs of grade 4 vomiting, grade 4 neutropoenia and thrombocytopenia, and grade 3 anorexia and diarrhoea; reversible grade 3 plasma creatinine increase occurred with lonafarnib 400 mg b.i.d. p.o. When the dose was reduced to 300 mg b.i.d., DLTs consisted of grade 4 neutropoenia, grade 3 neurocortical toxicity and grade 3 fatigue with grade 2 nausea and diarrhoea. No partial or complete responses were observed; 1 patient with pseudomyxoma peritonei had stable disease for > 9 months and 1 patient with metastatic follicular thyroid carcinoma had stable disease for 7 months with ongoing treatment. There were no partial or complete responses with the administration of lonafarnib 300 mg q.d. to 12 evaluable patients [52]. Haematological toxicity was not observed with lonafarnib 300 mg but became pronounced with 400 mg.

Lonafarnib has been investigated in eight and four patients with CML in chronic or accelerated phase, respectively, in whom imatinib therapy had been unsuccessful [53]. The patients received lonafarnib 200 mg b.i.d. continuously. A total of two patients had a haematological response. Diarrhoea was the most common adverse event, with grade 3 or 4 diarrhoea occurring in 4 patients.

4.2 Phase II/III clinical trial

Sharma *et al.* [54] conducted a Phase II trial in patients who had metastatic colorectal cancer that was considered to be refractory to first- and second-line therapy with 5-fluorouracil and irinotecan. The starting dose was lonafarnib 200 mg b.i.d. for 28 consecutive days. The major side effects were fatigue (grade 1 in 42% of the patients, grade 2 in 42% and grade 3 in 14%), diarrhoea (grade 1 in 23% and grade 3 in 42%) and nausea (grade 2 in 16%). In 19% of patients, grade 2 or 3 increases in serum creatinine concentration were observed and appeared to be related to dehydration induced by diarrhoea. Significant haematological toxicity was not observed. Pharmacological studies revealed adequate mean predose plasma concentrations in this group of patients on day 15 of therapy. In 21 evaluable patients, no objective responses were observed, although stable disease was seen in 3 patients for several months. Administration of lonafarnib was accompanied by gastrointestinal toxicity.

A recent Phase II study was conducted [55] to evaluate the antitumour activity of lonafarnib in patients who had urothelial cancer that was refractory to first-line cytotoxic treatment. Lonafarnib 200 mg b.i.d. p.o. was administered continuously in a 28-day cycle. In 19 eligible patients, drug-related grade 3 toxic effects included fatigue, anorexia, nausea, confusion, dehydration, muscle weakness, depression, headache and dyspnoea. A total of five patients discontinued the study protocol because of toxicity. No responses were observed in 10 evaluable patients. Of nine patients who were not evaluable, five had symptomatic progression and thus the study met multinomial criteria for stopping the study after the first stage.

An open-label Phase II, single-centre study [56] was conducted to determine the rate of objective responses to lonafarnib 200 mg b.i.d. to 15 patients with HNSCC that was refractory to chemotherapy, all of whom had received ≥ 1 platinum regimen but not > 3 courses of therapy. No objective response was observed; 7 patients maintained stable disease through ≥ 3 courses of therapy and 1 maintained stable disease for 8 courses (220 days). No treatment-related deaths were reported. Grade 4 hyperuricaemia occurred in 1 patient. Grade 3 adverse effects included anorexia, infection without

Expert Opin. Investig. Drugs Downloaded from informahealthcare.com by UTMD Anderson Cancer Center on 10/08/10
For personal use only.

RIGHTSLINK

Table 1. Phase I and II trials of lonafarnib.

Study type	Tumour type	Schedule	Toxicity	Response	Ref.
Phase I					
Monotherapy	Solid tumour	25 – 400 mg b.i.d. on day 7 of every 21-day cycle	Leucopoenia with neutropoenia, diarrhoea, nausea and fatigue	1/20 PR in NSCLC; 8/20 SD	[47]
Monotherapy	CML-BP, CMML, MDS, AML and ALL	100 – 200 mg b.i.d. continuously	Nausea, diarrhoea and anorexia	6/16 clinical response (response rate: 38%)	[48]
Combination with paclitaxel	Solid tumours	100 – 150 mg b.i.d. continuously with paclitaxel 135 – 175 mg/m^2	Peripheral neuropathy, hyperbilirubinaemia, neutropoenia with fever, and diarrhoea	8/21 PR in NSCLC, salivary gland tumour; 7/21 SD	[32]
Combination with gemcitabine	Solid tumours	100 – 200 mg b.i.d. continuously with gemcitabine 600 – 1000 mg on days 1, 8 and 15 of every 28-day cycle	Nausea, vomiting, diarrhoea and myelosuppression	2/25 PR pancreatic cancer; 11/25 SD	[50]
Phase II					
Monotherapy	HNSCC	200 mg b.i.d.	Hyperuricaemia, anorexia, neutropoenia, QT elongation and diarrhoea	0/15 PR or CR, 7/15 SD	[56]
Monotherapy	MDS, CMML	200 – 300 mg b.i.d.	Diarrhoea and nausea	12/42 response (2CR and 10HI)	[57]
Combination with paclitaxel	NSCLC	100 mg b.i.d. with paclitaxel 175 mg/m^2 on days 1 and 8 of every 28-day cycle	Fatigue, diarrhoea, neutropoenia, dyspnoea and respiratory insufficiency	3/20 PR; 11/29 SD	[14]
Combination with gemcitabine	TCC	150 and 100 mg with gemcitabine 1000 mg on days 1, 8 and 15 of every 28-day cycle	Vomiting and diarrhoea	9/31PR and 1/31 CR	[59]

ALL: Acute lymphoblastic leukaemia; AML: Acute myelogenous leukaemia; CML-BP: Chronic myeloid leukaemia blast phase; CMML: Chronic myelomonocytic leukaemia; CR: Complete response; HI: Hazard index; HNSCC: head and neck squamous cell carcinoma; MDS: Myelodisplastic syndrome; NSCLC: Non-small cell lung cancer; PR: Partial response; SD: Standard deviation; TCC: Transitional cell cancer.

Expert Opin. Investig. Drugs Downloaded from informahealthcare.com by UTMD Anderson Cancer Center on 10/08/10
For personal use only.

neutropoenia, cardiac toxicity (QTc interval elongation) and syncope in 1 patient each, respectively. No grade 3 or 4 haematological toxicity was reported, but grade 2 anaemia was noted in 2 patients. The most common toxic effects were grade 1 or 2 and were diarrhoea, nausea and fatigue in 10, 9 and 7 patients.

Results of a Phase II study in patients who had MDS (n = 32) or CMML (n = 35) were recently reported [57]. Patients received lonafarnib 200 – 300 mg b.i.d. p.o. Of 42 evaluable patients, 12 responded (4 MDS patients and 8 CMML patients), 2 of whom had complete response and 10 had a haematological improvement. In addition, 16 of 37 patients who had bone marrow (BM) blasts of 45% at baseline showed a reduction of ≥ 50% in BM blasts. Gastrointestinal toxicity, including diarrhoea and nausea, of grade 3 or 4 was observed in 17 patients (26%) who discontinued therapy.

The Phase I study [32] of combined therapy with lonafarnib and paclitaxel revealed manageable toxicity with evidence of clinical activity in heavily pretreated patients, some of whom had been resistant to each cytotoxic agent given alone. On the basis of the results of the Phase I study, a Phase II study of lonafarnib in combination with paclitaxel was conducted in patients who had metastatic (stage IIIB/V), or taxane-refractory or -resistant NSCLC to evaluate safety, tolerance and efficacy [14]. Patients received continuous lonafarnib 100 mg b.i.d. p.o. beginning on day 1 and paclitaxel 175 mg/m^2 i.v. over 3 h on day 8 of each 21-day cycle, and the MTD of this drug combination was as determined in the Phase I study. Of the 33 patients enrolled, 29 were evaluable for response. Partial response and stable disease were observed in 3 and 11 patients, respectively. Thus 14 patients experienced some clinical benefit. The updated and final median overall survival time was 39 weeks and the median progression-free survival time was 16 weeks. The combination of lonafarnib and paclitaxel was well tolerated with minimal toxicity and the results were not very different from those of single treatment; grade 3 toxicity included fatigue (9%), diarrhoea (6%) and dyspnoea (6%). Grade 3 neutropoenia occurred in only 1 patient. Grade 4 adverse events included respiratory insufficiency and acute respiratory failure in 2 and 1 patients, respectively.

RIGHTSLINK

The addition of lonafarnib to the combination of paclitaxel and carboplatin in patients with previously untreated advanced NSCLC did not produce a survival benefit in a recent Phase III study. In an interim analysis of 616 patients (of a total of 675 patients involved in this study), the overall survival was 144 days for patients treated with lonafarnib and 168 for patients who received placebo [58].

A Phase II study [59] of lonafarnib and gemcitabine combination therapy was conducted in patients who had been treated for advanced urothelial carcinoma. Patients were given a combination of lonafarnib 150 mg in the morning and 100 mg in the evening and gemcitabine 1000 mg/m^2 on days 1, 8 and 15 of each 28-day cycle. The 9 partial responses and 1 complete response in 31 assessable patients corresponded to an overall response rate of 32.3% (95% confidence interval [CI]: 17 – 51%). Lonafarnib had no effect on the pharmacokinetics of gemcitabine. In the combined treatment with gemcitabine, no patients had severe haematological toxicity, which was defined as grade 4 thrombocytopoenia or febrile neutropoenia. In another Phase II study [60], patients who had metastatic pancreatic cancer were randomised to lonafarnib 200 mg b.i.d. or gemcitabine 1000 mg/m^2/week for 7 weeks in an 8-week cycle. Drug activity was observed in both groups. A larger fraction of cases of stable or responsive disease was seen in the gemcitabine-treated group (40 versus 24%).

4.3 Safety and tolerance

The most frequent forms of non-haematological toxicity that have been reported for lonafarnib 200 mg b.i.d. were grade 1 or 2 fatigue (in ~ 47% of the patients), grade 1 or 2 diarrhoea (60 – 70%) and grade 1 – 2 nausea (2 – 16%). All of these were generally brief and reversible on discontinuation of the drug. Increased serum creatinine (grade 2 or 3) has been observed and appears to correlate with drug dosage; it is probably due to dehydration induced by diarrhoea. At higher dosages of lonafarnib, such as 400 mg b.i.d., grade 3 neurocortical toxicity has been described. Significant haematological toxicity with lonafarnib 200 mg b.i.d. has not been observed (only grade 1 thrombocytopoenia in ~ 20% of the patients and grade 2 or 3 anaemia in 20 – 30%).

Hyperleukocytosis complicating lonafarnib treatment has been reported in a recent clinical trial of lonafarnib in patients who had CMML [61]. Of 35 patients enrolled in the study, 15 experienced a rise in total leukocyte count to > 5000/µl/week. Of those patients, three developed rapid and progressive increases in white blood cells with lonafarnib treatment, associated with respiratory distress in two cases that resolved promptly after treatment with dexamethasone or withdrawal of lonafarnib. In two patients who presented with pulmonary infiltrates, infectious aetiology was excluded; cytological examination of the bronchoalveolar lavage fluid confirmed alveolar infiltration by mature monocytes. Patients with proliferative CMML in particular appear to be at significant risk for this complication.

5. Other FTIs

Among several inhibitors of the target enzyme (FTase) that have been developed, tipifarnib and lonafarnib have both entered Phase III clinical studies and are considered to be the two most promising oral FTIs. Tipifarnib was the first FTI tested in a clinical trial. In a Phase II trial in patients with advanced breast cancer, tipifarnib showed a significant activity with 9 partial responses and nine cases of stable disease (for ≥ 24 weeks) in 76 patients [13]. To date, the most promising activity of tipifarnib was reported in patients with untreated poor-risk acute myeloid leukaemia or MDS, in which a 33% response rate (8 complete and 2 partial responses) was seen [62]. Treatment with tipifarnib has been compared with placebo or standard therapies in at least two Phase III studies [18,63] and no significant antitumour effect was evidenced in both studies.

6. Expert opinion

Although contrasting results of clinical trials have moderated the initial enthusiasm for FTIs, they (and particularly lonafarnib) remain a promising class of novel antineoplastic agents. Lonafarnib monotherapy has important significant activity in haematological malignancies, even overcoming resistance to imanitib. In solid tumours, its activity seems to be modest and it should probably be studied in combination with cytotoxic agents, ionising radiation and other novel targeted drugs, such as antiangiogenic agents and IGFBP-3. FTIs were designed as Ras-blocking agents, but increasing lines of evidence indicate that other farnesylated targets are involved in their cytotoxic effects. The critical target proteins of FTIs and their mechanisms of action, particularly of their downstream effectors, are subjects of active investigation. Understanding those mechanisms will provide relevant biological markers that can help in the selection of patients who can benefit from FTI treatment.

Many clinical studies of combinations of FTIs and standard cytotoxic agents are underway. The toxic effects of the combinations appear to be manageable, and evidence of clinical activity in heavily pretreated patients, some of whom had been resistant to the cytotoxic agents when they were administered alone, has led to the consideration of FTIs as modulators of genotoxic agents, such as those that are used in standard chemotherapy and radiotherapy.

Acknowledgments

This work was supported by NIH grants RO1 CA100816 and R01 CA109520, American Cancer Society grant RSG-04-082-01-TBE and Department of Defense grant DAMD17-01-1-0689.

Expert Opin. Investig. Drugs Downloaded from informahealthcare.com by UTMD Anderson Cancer Center on 10/08/10
For personal use only.

RIGHTSLINK

Expert Opin. Investig. Drugs Downloaded from informahealthcare.com by UTMD Anderson Cancer Center on 10/08/10
For personal use only.

Bibliography

Papers of special note have been highlighted as either of interest (•) or of considerable interest (••) to readers.

1. BARBACID M: *Ras* genes. *Ann. Rev. Biochem.* (1987) **56**:779-827.

• **A comprehensive review.**

2. BEAUPRE DM, KURZROCK R: Ras and leukemia: from basic mechanisms to gene-directed therapy. *J. Clin. Oncol.* (1999) **17**(3):1071-1079.

3. McCORMICK F: Activators and effectors of ras p21 proteins. *Curr. Opin. Genet. Dev.* (1994) **4**(1):71-76.

4. ALMOGUERA C, SHIBATA D, FORRESTER K *et al.*: Most human carcinomas of the exocrine pancreas contain mutant c-K-*ras* genes. *Cell* (1988) **53**(4):549-554.

5. BOS JL: Ras oncogenes in human cancer: a review. *Cancer Res.* (1989) **49**(17):4682-4689.

6. KHOSRAVI-FAR R, COX AD, KATO K, DER CJ: Protein prenylation: key to ras function and cancer intervention? *Cell Growth Differ.* (1992) **3**(7):461-469.

7. ADJEI AA, DAVIS JN, BRUZEK LM, ERLICHMAN C, KAUFMANN SH: Synergy of the protein farnesyltransferase inhibitor SCH66336 and cisplatin in human cancer cell lines. *Clin. Cancer Res.* (2001) 7(5):1438-1445.

8. GILLE H, DOWNWARD J: Multiple ras effector pathways contribute to G_1 cell cycle progression. *J. Biol. Chem.* (1999) **274**(31):22033-22040.

•• **Identification of Ras effectors in regulating the cell-cycle machinery.**

9. LIU A, PRENDERGAST GC: Geranylgeranylated RhoB is sufficient to mediate tissue-specific suppression of Akt kinase activity by farnesyltransferase inhibitors. *FEBS Lett.* (2000) **481**(3):205-208.

10. LIU A, DU W, LIU JP, JESSELL TM, PRENDERGAST GC: RhoB alteration is necessary for apoptotic and antineoplastic responses to farnesyltransferase inhibitors. *Mol. Cell. Biol.* (2000) **20**(16):6105-6113.

11. JIANG K, COPPOLA D, CRESPO NC *et al.*: The phosphoinositide 3-OH kinase/AKT2 pathway as a critical target for farnesyltransferase inhibitor-induced apoptosis. *Mol. Cell. Biol.* (2000) **20**(1):139-148.

12. ASHAR HR, JAMES L, GRAY K *et al.*: Farnesyl transferase inhibitors block the farnesylation of CENP-E and CENP-F and alter the association of CENP-E with the microtubules. *J. Biol. Chem.* (2000) **275**(39):30451-30457.

13. JOHNSTON SR, HICKISH T, ELLIS P *et al.*: Phase II study of the efficacy and tolerability of two dosing regimens of the farnesyl transferase inhibitor, R115777, in advanced breast cancer. *J. Clin. Oncol.* (2003) **21**(13):2492-2499.

14. KIM ES, KIES MS, FOSSELLA FV *et al.*: Phase II study of the farnesyltransferase inhibitor lonafarnib with paclitaxel in patients with taxane-refractory/resistant nonsmall cell lung carcinoma. *Cancer* (2005) **104**(3):561-569.

•• **The first Phase II study showing objective response in NSCLC patients by combined treatment of lonafarnib and palitaxel.**

15. BERNHARD EJ, McKENNA WG, HAMILTON AD *et al.*: Inhibiting Ras prenylation increases the radiosensitivity of human tumor cell lines with activating mutations of *ras* oncogenes. *Cancer Res.* (1998) **58**(8):1754-1761.

16. ZHANG Z, WANG Y, LANTRY LE *et al.*: Farnesyltransferase inhibitors are potent lung cancer chemopreventive agents in A/J mice with a dominant-negative p53 and/or heterozygous deletion of Ink4a/Arf. *Oncogene* (2003) **22**(40):6257-6265.

17. LIU M, BRYANT MS, CHEN J *et al.*: Antitumor activity of SCH 66336, an orally bioavailable tricyclic inhibitor of farnesyl protein transferase, in human tumor xenograft models and *wap-ras* transgenic mice. *Cancer Res.* (1998) **58**(21):4947-4956.

18. VAN CUTSEM E, VAN DE VELDE H, KARASEK P *et al.*: Phase III trial of gemcitabine plus tipifarnib compared with gemcitabine plus placebo in advanced pancreatic cancer. *J. Clin. Oncol.* (2004) **22**(8):1430-1438.

19. TABERNERO J, ROJO F, MARIMON I *et al.*: Phase I pharmacokinetic and pharmacodynamic study of weekly 1-hour and 24-hour infusion BMS-214662, a farnesyltransferase inhibitor, in patients with advanced solid tumors. *J. Clin. Oncol.* (2005) **23**(11):2521-2533.

20. IZBICKA E, LAWRENCE R, DAVIDSON K *et al.*: Activity of a farnesyl transferase inhibitor (SCH66336) against a broad range of tumors taken directly from patients. *Proc. Am. Assoc. Cancer Res.* (1999) **40**:524 (Abstract 3454).

21. ASHAR HR, JAMES L, GRAY K *et al.*: The farnesyl transferase inhibitor SCH 66336 induces a $G_2 - > M$ or G_1 pause in sensitive human tumor cell lines. *Exp. Cell Res.* (2001) **262**(1):17-27.

22. SUN SY, ZHOU Z, WANG R, FU H, KHURI FR: The farnesyltransferase inhibitor lonafarnib induces growth arrest or apoptosis of human lung cancer cells without downregulation of Akt. *Cancer Biol. Ther.* (2004) **3**(11):1092-1098 (Discussion 1099-1101).

23. BRASSARD DL, ENGLISH JM, MALKOWSKI M *et al.*: Inhibitors of farnesyl protein transferase and MEK1,2 induce apoptosis in fibroblasts transformed with farnesylated but not geranylgeranylated H-*Ras*. *Exp. Cell Res.* (2002) **273**(2):138-146.

24. REICHERT A, HEISTERKAMP N, DALEY GQ, GROFFEN J: Treatment of Bcr/Abl-positive acute lymphoblastic leukemia in P190 transgenic mice with the farnesyl transferase inhibitor SCH66336. *Blood* (2001) **97**(5):1399-1403.

• **One of the first *in vivo* studies demonstrating the antileukaemic activity of lonafarnib.**

25. PETERS DG, HOOVER RR, GERLACH MJ *et al.*: Activity of the farnesyl protein transferase inhibitor SCH66336 against BCR/ABL-induced murine leukemia and primary cells from patients with chronic myeloid leukemia. *Blood* (2001) **97**(5):1404-1412.

26. FELDKAMP MM, LAU N, RONCARI L, GUHA A: Isotype-specific Ras. GTP-levels predict the efficacy of farnesyl transferase inhibitors against human astrocytomas regardless of *Ras* mutational status. *Cancer Res.* (2001) **61**(11):4425-4431.

• **The absence of *Ras* mutations does not preclude the chemotherapeutic efficacy of FTIs.**

27. BASSO AD, MIRZA A, LIU G *et al.*: The farnesyl transferase inhibitor (FTI) SCH66336 (lonafarnib) inhibits Rheb farnesylation and mTOR signaling. Role in FTI enhancement of taxane and tamoxifen anti-tumor activity. *J. Biol. Chem.* (2005) **280**(35):31101-31108.

28. REN H, TAI SK, KHURI F, CHU Z, MAO L: Farnesyltransferase inhibitor SCH66336 induces rapid phosphorylation of eukaryotic translation elongation factor 2 in head and neck squamous cell carcinoma cells. *Cancer Res.* (2005) **65**(13):5841-5847.

RIGHTSLINK

Expert Opin. Investig. Drugs Downloaded from informahealthcare.com by UTMD Anderson Cancer Center on 10/08/10
For personal use only.

29. CHUN KH, LEE HY, HASSAN K *et al.*: Implication of protein kinase B/Akt and Bcl-2/Bcl-XL suppression by the farnesyl transferase inhibitor SCH66336 in apoptosis induction in squamous carcinoma cells. *Cancer Res.* (2003) **63**(16):4796-4800.

30. TAKADA Y, KHURI FR, AGGARWAL BB: Protein farnesyltransferase inhibitor (SCH 66336) abolishes NF-kappaB activation induced by various carcinogens and inflammatory stimuli leading to suppression of NF-κB-regulated gene expression and up-regulation of apoptosis. *J. Biol. Chem.* (2004) **279**(25):26287-26299.

31. MARCUS AI, ZHOU J, O'BRATE A *et al.*: The synergistic combination of the farnesyl transferase inhibitor lonafarnib and paclitaxel enhances tubulin acetylation and requires a functional tubulin deacetylase. *Cancer Res.* (2005) **65**(9):3883-3893.

32. KHURI FR, GLISSON BS, KIM ES *et al.*: Phase I study of the farnesyltransferase inhibitor lonafarnib with paclitaxel in solid tumors. *Clin. Cancer Res.* (2004) **10**(9):2968-2976.

• **Evidence of clinical activity of lonafarnib and paclitaxel in NSCLC patients with taxane-resistant disease.**

33. HAN JY, OH SH, MORGILLO F *et al.*: Hypoxia-inducible factor 1α and antiangiogenic activity of farnesyltransferase inhibitor SCH66336 in human aerodigestive tract cancer. *J. Natl. Cancer Inst.* (2005) **97**(17):1272-1286.

• ***In vitro* study showing the antiangiogenic effects of lonafarnib.**

34. SU ZZ, AUSTIN VN, ZIMMER SG, FISHER PB: Defining the critical gene expression changes associated with expression and suppression of the tumorigenic and metastatic phenotype in Ha-*ras*-transformed cloned rat embryo fibroblast cells. *Oncogene* (1993) **8**(5):1211-1219.

35. ZABRENETZKY V, HARRIS CC, STEEG PS, ROBERTS DD: Expression of the extracellular matrix molecule thrombospondin inversely correlates with malignant progression in melanoma, lung and breast carcinoma cell lines. *Int. J. Cancer.* (1994) **59**(2):191-195.

36. RAK J, MITSUHASHI Y, BAYKO L *et al.*: Mutant ras oncogenes upregulate VEGF/VPF expression: implications for induction and inhibition of tumor angiogenesis. *Cancer Res.* (1995) **55**(20):4575-4580.

37. NIELSEN LL, SHI B, HAJIAN G *et al.*: Combination therapy with the farnesyl protein transferase inhibitor SCH66336 and SCH58500 (p53 adenovirus) in preclinical cancer models. *Cancer Res.* (1999) **59**(23):5896-5901.

• **Study showing the synergistic combination of FTIs with p53 adenovirus.**

38. MARTIN JL, BAXTER RC: Oncogenic ras causes resistance to the growth inhibitor insulin-like growth factor binding protein-3 (IGFBP-3) in breast cancer cells. *J. Biol. Chem.* (1999) **274**(23):16407-16411.

• **Implication of Ras-mediated signaling as a resistance mechanism to IGFBP-3 treatment.**

39. EDAMATSU H, GAU CL, NEMOTO T, GUO L, TAMANOI F: Cdk inhibitors, roscovitine and olomoucine, synergize with farnesyltransferase inhibitor (FTI) to induce efficient apoptosis of human cancer cell lines. *Oncogene* (2000) **19**(27):3059-3068.

40. SUN J, BLASKOVICH MA, KNOWLES D *et al.*: Antitumor efficacy of a novel class of non-thiol-containing peptidomimetic inhibitors of farnesyltransferase and geranylgeranyltransferase I: combination therapy with the cytotoxic agents cisplatin, Taxol, and gemcitabine. *Cancer Res.* (1999) **59**(19):4919-4926.

•• ***In vitro* study of the combination of lonfarnib and cytotoxic agents.**

41. LOPREVITE M, FAVONI RE, DE CUPIS A *et al.*: *In vitro* study of farnesyltransferase inhibitor SCH 66336, in combination with chemotherapy and radiation, in non-small cell lung cancer cell lines. *Oncol. Rep.* (2004) **11**(2):407-414.

42. DAVID E, SUN SY, WALLER EK *et al.*: The combination of the Farnesyl transferase inhibitor (lonafarnib) and the proteasome inhibitor (bortezomib) induces synergistic apoptosis in human myeloma cells that is associated with down-regulation of p-AKT. *Blood* (2005) **106**(13):4322-9.

• ***In vitro* study of the combined treatment of lonafarnib and the proteasome inhibitor bortezomib.**

43. NAKAJIMA A, TAUCHI T, SUMI M, BISHOP WR, OHYASHIKI K: Efficacy of SCH66336, a farnesyl transferase inhibitor, in conjunction with imatinib against BCR-ABL-positive cells. *Mol. Cancer Ther.* (2003) **2**(3):219-224.

• **Role of lonafarnib in enhancing the antiproliferative effects of imatinib.**

44. HOOVER RR, MAHON FX, MELO JV, DALEY GQ: Overcoming STI571 resistance with the farnesyl transferase inhibitor SCH66336. *Blood* (2002) **100**(3):1068-1071.

45. BISHOP WR, BOND R, PETRIN J *et al.*: Novel tricyclic inhibitors of farnesyl protein transferase. Biochemical characterization and inhibition of Ras modification in transfected Cos cells. *J. Biol. Chem.* (1995) **270**(51):30611-30618.

46. ESKENS FA, AWADA A, CUTLER DL *et al.*: Phase I and pharmacokinetic study of the oral farnesyl transferase inhibitor SCH 66336 given twice daily to patients with advanced solid tumors. *J. Clin. Oncol.* (2001) **19**(4):1167-1175.

47. ADJEI AA, ERLICHMAN C, DAVIS JN *et al.*: A Phase I trial of the farnesyl transferase inhibitor SCH66336: evidence for biological and clinical activity. *Cancer Res.* (2000) **60**(7):1871-1877.

48. LIST AF, DEANGELO D, O'BRIEN S *et al.*: Phase I study of continuous oral administration of lonafarnib (Sarasar) in patients with advanced hematologic malignancies. *Blood* (2002) **100**:789a.

• **The first Phase I clinical study in haematological malignancies.**

49. KIES MS, CLAYMAN GL, El-NAGGAR AK *et al.*: Induction therapy with SCH 66336, a farnesyltransferase inhibitor, in squamous cell carcinoma (SCC) of the head and neck. *Proc. Ann. Meet. Am. Soc. Clin. Oncol.* (2001) **20**:896 (Abstract).

• **Phase I study in HNSCC.**

50. HURWITZ H, AMADO R, PRAGER D *et al.*: Phase I and clinical pharmacokinetic trial of the farnesyl transferase inhibitor SCH66336 plus gemcitabine in advanced cancer. *Proc. Am. Soc. Clin. Oncol.* (2000):185a (Abstract 717).

• **Evidence of clinical activity of lonafarnib–gemcitabine in pancreatic cancer.**

51. HURWITZ H, COLVIN OM, PETROS WP *et al.*: Phase I and pharmacokinetic study of SCH66336, a novel FPTI, using a 2-week on, 2-week off schedule. *Proc. Am. Soc. Clin. Oncol.* (1999) **18**:156a.

52. AWADA A, ESKENS FA, PICCART M *et al.*: Phase I and pharmacological study of the oral farnesyltransferase inhibitor SCH 66336 given once daily to patients with advanced solid tumours. *Eur. J. Cancer* (2002) **38**(17):2272-2278.

RIGHTSLINK

53. CORTES J, DALEY GQ, TALPAZ M *et al.*: Pilot study of SCH66336 a farnesyl transferase inhibitor in patients with chronic or accelerator phase resistant or refractory to imanitib. *Blood* (2002) **100**:164a.

54. SHARMA S, KEMENY N, KELSEN DP *et al.*: A Phase II trial of farnesyl protein transferase inhibitor SCH 66336, given by twice-daily oral administration, in patients with metastatic colorectal cancer refractory to 5-fluorouracil and irinotecan. *Ann. Oncol.* (2002) **13**(7):1067-1071.

•• **Phase II study of single-agent lonafarnib in colorectal cancer patients; no objective responses were observed.**

55. WINQUIST E, MOORE MJ, CHI KN *et al.*: A multinomial Phase II study of lonafarnib (SCH 66336) in patients with refractory urothelial cancer. *Urol. Oncol.* (2005) **23**(3):143-149.

56. YANG H, KIES MS, GLISSON B *et al.*: A Phase II study of Lonafarnib (SCH66336) in patients with chemo-refractory advanced head and neck squamous cell carcinoma (HNSCC). *Proc. Am. Soc. Clin. Oncol.* (2000) (Abstract 5565 C).

• **Phase II study of single-agent lonafarnib in HNSCC patients; no objective responses were observed.**

57. FELDMAN E, CORTES J, HOLYOAK T *et al.*: Continuous oral lonafarnib (Sarasar) for the treatment of patients with myelodysplastic syndrome. *Blood* (2003) **102**:421a.

58. BLUMENSCHEIN G, LUDWIG C, THOMAS G *et al.*: A randomized Phase III trial comparing lonafarnib/carboplatin/paclitaxel versus carboplatin/paclitaxel (CP) in chemotherapy-naive patients with advanced or metastatic non-small cell lung cancer (NSCLC). *Proceedings from the 11th World Conference on Lung Cancer*, Barcelona, Spain (2005) (Abstract O-082).

59. THEODORE C, GEOFFROIS L, VERMORKEN JB *et al.*: Multicentre EORTC study 16997: feasibility and Phase II trial of farnesyl transferase inhibitor and gemcitabine combination in salvage treatment of advanced urothelial tract cancers. *Eur. J. Cancer* (2005) **41**(8):1150-1157.

• **Phase II study evidencing objective responses by combined treatment of lonafarnib and gemcitabine in patients with advanced urothelial carcinoma.**

60. LERSCH C, VAN CUSTEM E, AMADO R *et al.*: Randomized Phase II study of SCH 66336 and gemcitabine in the treatment of metastatic adenocarcinoma of the pancreas. *Proc. Ann. Meet. Am. Soc. Clin. Oncol.* (2001) **20**:608.

• **Phase II study evidencing objective responses with the combined treatment of lonafarnib and gemcitabine in patients with metastatic pancreatic cancer.**

61. BURESH A, PERENTESIS J, RIMSZA L *et al.*: Hyperleukocytosis complicating lonafarnib treatment in patients with chronic myelomonocytic leukemia. *Leukemia* (2005) **19**(2):308-310.

62. LANCET JE, KARP JE, GOTLIB L *et al.*: Zarnestra™ (R115777) in previously untreated poor-risk AML and MDS: preliminary results of a Phase II trial. *Blood* (2002) **100**:560a.

63. RAO S, CUNNINGHAM D, DE GRAMONT A *et al.*: Phase III double-blind placebo-controlled study of farnesyl transferase inhibitor R115777 in patients with refractory advanced colorectal cancer. *J. Clin. Oncol.* (2004) **22**:3950-3957.

Affiliation

Floriana Morgillo MD & Ho-Young Lee† PhD
†Author for correspondence
M. D. Anderson Cancer Center, Department of Thoracic/Head & Neck Medical Oncology, Houston, TX, USA
Tel: +1 713 792 6363; Fax: +1 713 796 8655;
E-mail: hlee@mdanderson.org

Expert Opin. Investig. Drugs Downloaded from informahealthcare.com by UTMD Anderson Cancer Center on 10/08/10
For personal use only.

RIGHTSLINK

CHEST®

Official publication of the American College of Chest Physicians



Phenotypic Diversity of the Lung Vasculature in Experimental Models of Metastases*

Yun Oh, Imran Mohiuddin, Yan Sun, Joseph B. Putnam, Jr, Waun Ki Hong, Wadih Arap and Renata Pasqualini

Chest 2005;128;596S-600S
DOI 10.1378/chest.128.6_suppl.596S

The online version of this article, along with updated information and services can be found online on the World Wide Web at:
http://chestjournal.chestpubs.org/content/128/6_suppl/596S.full.html

Chest is the official journal of the American College of Chest Physicians. It has been published monthly since 1935. Copyright2005by the American College of Chest Physicians, 3300 Dundee Road, Northbrook, IL 60062. All rights reserved. No part of this article or PDF may be reproduced or distributed without the prior written permission of the copyright holder.
(**http://chestjournal.chestpubs.org/site/misc/reprints.xhtml**)
ISSN:0012-3692



Downloaded from chestjournal.chestpubs.org at M D Anderson Hospital on October 8, 2010
© 2005 American College of Chest Physicians

administration of a superoxide scavenger, Cu/Zn superoxide dismutase (SOD) (150 U/mL) [decrease in maximal isometric tension from 5.43 ± 0.35 to 3.74 ± 0.44 mN; n = 5; $p < 0.05$]. The CH-enhanced PA constrictor response to ET-1 was completely blocked in PAs isolated from gp91^{phox} KO mice (wt + CH mice, 5.43 ± 0.35 mN; gp91^{phox} KO + CH mice, 3.33 ± 0.19 mN; n = 7; $p < 0.01$).

CH increased PA superoxide production (increase in mean chemiluminescence from 12.0 ± 0.40 to 24.8 ± 1.74 relative light units [RLU]/s; n = 6; $p < 0.05$) [Fig 1, *bottom*, *B*] in wt mice that was further increased in the presence of 10 nmol/L ET-1 (37.5 ± 1.8 RLU/s; n = 6; $p < 0.01$). However, this CH-increased PA chemiluminescence was significantly reduced either by treatment with Cu/Zn SOD (150 U/mL; 18.7 ± 1.17 RLU/s; n = 6; $p < 0.01$) or in PA isolated from gp91^{phox} KO mice (14.4 ± 0.66 RLU/s; n = 6; $p < 0.01$).

Discussion

This study supports a model of CH-enhanced superoxide formation via a gp91^{phox}-dependent NADPH oxidase pathway. Activation of this pathway leads to enhanced PA vasoconstrictor responses. Enhanced vasoconstrictor response to ET-1, via ETA or ETB receptors, has been documented in various models of CH-associated PH.[9] Prior studies have established that CH-induced PH is associated with increased PA vasoconstrictor activity, but the mechanisms by which these PA constrictor responses are modulated remain unclear. In CH-induced PH in rats, ETA or ETB receptor-mediated PA vasoconstriction was increased.[9] We show that the exogenous addition of SOD can significantly reduce CH-enhanced vasoconstrictor responses to ET-1 (Fig 1, *top*, *A*). This strongly suggests that CH-enhanced vasoconstrictor responses are mediated, at least in part, by an overproduction of superoxide radicals. In PA isolated from gp91^{phox} KO mice, the CH-enhanced vasoconstrictor responses to ET-1 were completely blocked, and the CH-induced superoxide overproduction was markedly reduced (Fig 1, *bottom*, *B*), demonstrating that NADPH oxidase (gp91^{phox}) is the major superoxide generator in this model. In conclusion, our studies demonstrate that superoxide overproduction, via NADPH oxidase (gp91^{phox}) following CH, plays a central role in enhancing ET-1-mediated PA vasoconstriction.

References

1 Adnot S, Raffestin B, Eddahibi S, et al. Loss of endothelium-dependent relaxant activity in the pulmonary circulation of rats exposed to chronic hypoxia. J Clin Invest 1991; 87:155–162

2 Brandes RP, Barton M, Philippens KM, et al. Endothelial-derived superoxide anions in pig coronary arteries: evidence from lucigenin chemiluminescence and histochemical techniques. J Physiol 1997; 500:331–342

3 Griendling KK, Sorescu D, Ushio-Fukai M. NAD(P)H oxidase: role in cardiovascular biology and disease. Circ Res 2000; 86:494–501

4 Griffith SL, Rhoades RA, Packer CS. Pulmonary arterial smooth muscle contractility in hypoxia-induced pulmonary hypertension. J Appl Physiol 1994; 77:406–414

5 Herget J, Wilhelm J, Novotna J, et al. A possible role of the oxidant tissue injury in the development of hypoxic pulmonary hypertension. Physiol Res 2000; 49:493–501

6 Kennedy TP, Michael JR, Summer W. Calcium channel blockers in hypoxic pulmonary hypertension. Am J Med 1985; 78:18–26

7 Liu JQ, Folz RJ. Extracellular superoxide enhances 5-HT-induced murine pulmonary artery vasoconstriction. Am J Physiol Lung Cell Mol Physiol 2004; 287:L111–L118

8 Liu JQ, Zelko IN, Folz RJ. Reoxygenation-induced constriction in murine coronary arteries: the role of endothelial NADPH oxidase (gp91phox) and intracellular superoxide. J Biol Chem 2004; 279:24493–24497

9 MacLean MR, McCulloch KM, Baird M. Effects of pulmonary hypertension on vasoconstrictor responses to endothelin-1 and sarafotoxin S6C and on inherent tone in rat pulmonary arteries. J Cardiovasc Pharmacol 1995; 26:822–830

10 Morrell NW, Atochina EN, Morris KG, et al. Angiotensin converting enzyme expression is increased in small pulmonary arteries of rats with hypoxia-induced pulmonary hypertension. J Clin Invest 1995; 96:1823–1833

11 Weissmann N, Tadic A, Hanze J, et al. Hypoxic vasoconstriction in intact lungs: a role for NADPH oxidase-derived H(2)O(2)? Am J Physiol Lung Cell Mol Physiol 2000; 279: L683–L690

Phenotypic Diversity of the Lung Vasculature in Experimental Models of Metastases*

Yun Oh; Imran Mohiuddin; Yan Sun; Joseph B. Putnam, Jr; Waun Ki Hong; Wadih Arap, MD, PhD; and Renata Pasqualini, PhD

***In vivo* phage display is a screening method in which peptides homing to specific vascular beds are selected after IV administration of a random peptide library. This strategy has revealed a vascular address system that allows tissue-specific targeting of normal blood vessels and angiogenesis-related targeting of tumor blood vessels by selected peptides. Many vascular receptors or "addresses" targeted by homing peptides have been identified. One such vascular**

*From the Departments of Thoracic/Head & Neck Medical Oncology (Drs. Oh and Hong), Thoracic Surgery (Drs. Mohiuddin and Putnam), and Genitourinary Medical Oncology (Drs. Sun, Arap, and Pasqualini), The University of Texas M.D. Anderson Cancer Center, Houston, TX.

This work was funded in part by an award from the Gillson-Longenbaugh Foundation (Drs. Arap and Pasqualini) and the Biology, Education, Screening, Chemoprevention and Treatment (BESCT) Lung Cancer Program (contract No. DAMD17–01-1–0689; Dr. Oh).

Reproduction of this article is prohibited without written permission from the American College of Chest Physicians (www.chestjournal.org/misc/reprints.shtml).

Correspondence to: Wadih Arap, MD, PhD, or Renata Pasqualini, PhD, M.D. Anderson Cancer Center, 1515 Holcombe Blvd, Houston, TX 77030; e-mail: warap@mdanderson.org or rpasqual@mdanderson.org

Downloaded from chestjournal.chestpubs.org at M D Anderson Hospital on October 8, 2010
© 2005 American College of Chest Physicians

receptor of normal lung endothelium is membrane dipeptidase (MDP), which was found by *in vivo* phage display to bind the tripeptide motif gly-phe-glu (GFE). Our studies with GFE peptide and lung vasculature suggest that MDP mediates cancer cell adhesion to lung vasculature and the development of lung metastases, but that MDP is not present in the vasculature of lung metastases. MDP appears to occupy a vascular distribution that is similar to the pulmonary artery circulation. These results demonstrate the promise of defining critical functional and anatomic characteristics of endothelial cells in lung and other organs by *in vivo* phage display.

(CHEST 2005; 128:596S–600S)

Key words: lung endothelium; membrane dipeptidase; metastasis; phage display; random peptide library; vascular targeting

Abbreviations: GFE = gly-phe-glu; MDP = membrane dipeptidase

Efforts to target therapeutics and imaging agents to blood vessels in an organ- specific or disease-specific manner has led to the development of a technique by which small peptides that target receptors on endothelial cells can be identified.[1–3] This approach, using large, random peptide libraries displayed on the surface of the bacteriophage, has been termed *in vivo phage display*. A random peptide phage library is injected IV, and peptides that home selectively to specific organs or tumors are then recovered. Putative human homologs have been identified from ligands and receptors isolated by this approach in mouse models, suggesting that at least some ligand peptide motifs and their corresponding receptors may be evolutionarily conserved and pertinent in humans.[4] *In vivo* phage display is uncovering a vascular address system that can be used for organ-specific targeting of normal blood vessels and angiogenesis-related targeting of blood vessels in tumors.[5–11] Methods are also being developed for determining the *in vivo* distribution of probes targeted to the vasculature,[2,3] and their organ-specificity, vessel-specificity, and cellular targets. As the complexity of vascular diversity is further revealed, *in vivo* phage display will target particular regions of organs, such as pancreatic islets or the glomeruli of the kidney,[12] and eventually will identify receptor ligand pairs for functionally distinct vessels within these regions.

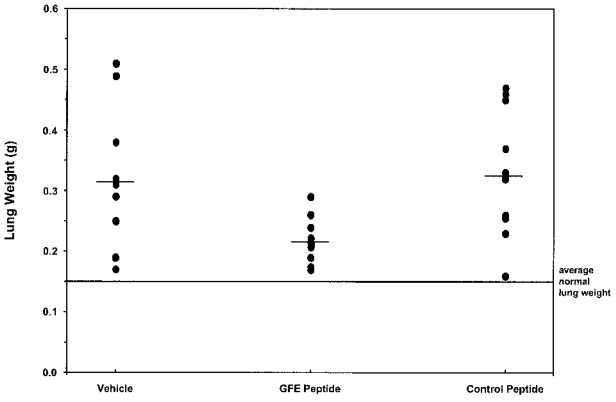


FIGURE 1. The GFE lung homing peptide inhibits the experimental metastasis of IV administered C8161 melanoma. Tumor cells were preincubated for 10 min with GFE or a control peptide, as indicated, and then were injected into the tail vein (10^6 cells per mouse, 10 mice per group). Lung weights are shown for the three experimental groups. The average normal lung weight (0.175 g) is marked with a line. Relative to the vehicle (DMEM) and control peptide groups, p values were < 0.01. Shown is one of five experiments in which similar results were obtained.

MEMBRANE DIPEPTIDASE AND ITS LIGAND GLY-PHE-GLU IN LUNG VASCULATURE

Membrane dipeptidase (MDP) was biochemically identified as a vascular receptor for lung-homing peptides containing the tripeptide motif gly-phe-glu (GFE) selected by *in vivo* phage display,[2,13] and appears to be a vascular receptor that binds to and mediates GFE homing to normal lung endothelium. MDP is a member of the zinc-metalloprotease family and a GP-anchored cell sur-

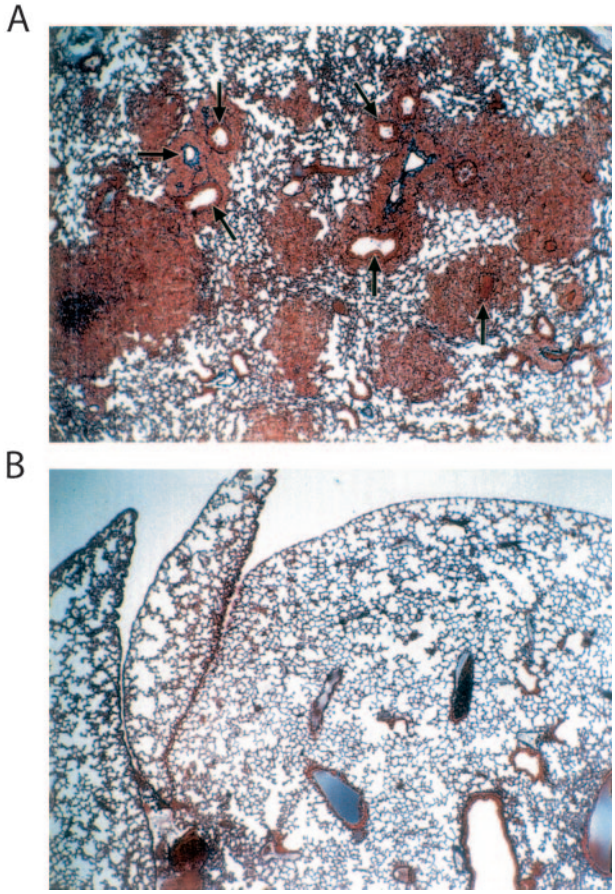


FIGURE 2. Lung tumor foci develop preferentially around the bronchia. *Top*, *A*: trichrome-stained sections of mouse lungs with C8161 metastases demonstrate that early tumors are found centered around bronchioles (arrows indicate lumens with blue-green borders, indicating collagen within the bronchial walls). Tumors secondarily also envelop pulmonary arteries that accompany the bronchioles. *Bottom*, *B*: normal lung is shown for comparison (trichrome, magnification).

Downloaded from chestjournal.chestpubs.org at M D Anderson Hospital on October 8, 2010
© 2005 American College of Chest Physicians

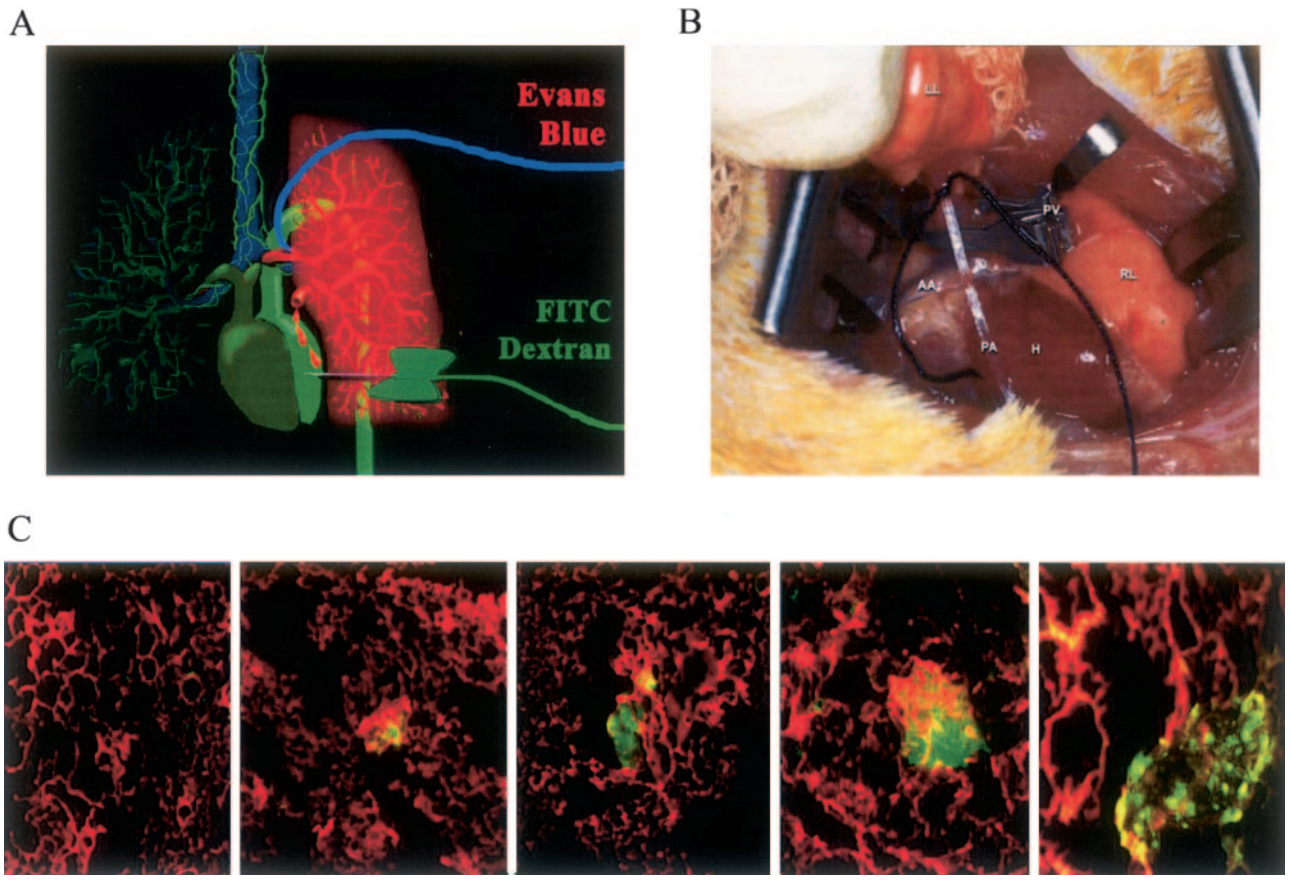


FIGURE 3. Tumor vasculature is preferentially recruited from the bronchial circulation. *Top left*, *A*: fluorescein isothiocyanate (FITC)-dextran was perfused into the left ventricle and Evans blue into the isolated left pulmonary artery of anesthetized rats. *Top right*, *B*: a photograph of the operative field demonstrates left lung (LL), right lung (RL), pulmonary artery catheter (PA), clamps placed on both pulmonary veins (PV), the left ventricle of the heart (H), and the ascending aorta (AA). *Bottom*, *C*: high-power views of the earliest detectable microscopic tumor nodules, the largest of which at far right, appears to have central necrosis with only punctate peripheral perfusion.

face protein expressed primarily in the lung and kidney.[14] In the rat and mouse, levels of MDP activity are highest in the lung.[14,15] MDP is involved in the metabolism of glutathione and cysteinyl leukotrienes,[14,16] and it is the only known mammalian enzyme that is capable of degrading β-lactam antibiotics.[14] The work presented here describes the expression and functional role of MDP in the dual circulation of the lung in the context of the vasculature of pulmonary metastases.

Role of MDP in Experimental Melanoma Lung Metastases

To determine whether the lung vascular receptor MDP mediates the homing of tumor cells and the subsequent development of experimental pulmonary metastases in mice, we used the C8161 human melanoma cell model of experimental lung metastases.[17,18] C8161 cells were coadministered IV with either the GFE-containing peptide (a ligand targeting MDP[2,13]) or a negative control peptide (Fig 1). The median weight of lungs from mice that received GFE peptide was only 12% greater than that of normal lungs, whereas the median weight of lungs from mice that received control peptide or no peptide (vehicle alone) was 88% greater than that of normal lungs ($p < 0.01$ [t test]). Consistent with these findings, histologic examination showed many fewer and smaller metastatic foci in mice treated with GFE. Moreover, GFE did not affect cell viability, as demonstrated by Trypan Blue exclusion and MTT assays on aliquots of melanoma cells prepared for injection into mice; cell viability was > 95% (results not shown). These results suggest that the tripeptide GFE binds to MDP and blocks the vascular homing of metastatic melanoma cells via this receptor.

Bronchial vs Pulmonary Artery Perfusion of Metastases

Photomicroscopy of lung metastases in the C8161 model demonstrated that the earliest visible lung metastases grew preferentially in close proximity to bronchioles (Fig 2). These observations led to the hypothesis that these

Downloaded from chestjournal.chestpubs.org at M D Anderson Hospital on October 8, 2010
© 2005 American College of Chest Physicians

metastatic tumors were preferentially recruiting angiogenic blood vessels from the bronchial vs pulmonary artery circulations. To test this hypothesis, we used a rat fibrosarcoma lung metastasis model[19] and isolated rat lung perfusion model.[20] After surgically isolating the left pulmonary artery circulation of rats under general anesthesia, Evans blue (with red fluorescence) was perfused; the remaining systemic circulation was perfused with fluorescein isothiocyanate-dextran via left ventricular injection. Rats were sacrificed after a 2-min circulation time, and lung tissue was processed according to the method of Li et al.[21] Indeed, we found that microscopic lung metastases of rat fibrosarcoma cells recruited tumor blood vessels preferentially from the bronchial vasculature, at least in early stages of growth (Fig 3). This was a surprising result since IV inoculated cancer cells pass through the pulmonary artery circulation first and would have a greater chance to deposit in the lung near pulmonary arteriolar capillaries than around the bronchial circulation.

Distribution of MDP in C8161 Metastases to the Lung

Finally, we analyzed the distribution of GFE binding to lung vasculature to evaluate whether MDP is expressed in the angiogenic vasculature of lung metastases because the expression of MDP in the lung endothelium closely recapitulates the distribution of a GFE-displaying phage.[2,13] Either a GFE-displaying phage or a control insertless phage were injected IV into mice bearing C8161 lung metastases and were examined for their ability to home to tumor vasculature. Strong phage immunoreactivity was observed in normal lung tissue, but the lung metastases were clearly negative (Fig 4). The failure of GFE-displaying phage to accumulate in tumor blood vessels indicates that its homing receptor, MDP, is not expressed in these blood vessels.

Conclusions

The molecular differences based on the heterogeneous expression of MDP in the lung and lung tumors could be explained by tumors differentially recruiting the dual blood circulations of the lung. Based on our perfusion experiments, we concluded that early lung metastases derive their blood supply primarily from the bronchial artery circulation. In contrast, based on the pattern of GFE-displaying phage binding in alveolar capillaries and pulmonary arterioles, it appears that MDP is selectively expressed in the pulmonary artery vasculature.

The patterns and function of MDP based on the results presented here imply that normal organ vascular receptors are still not necessarily valid targets for imaging or treating tumors in those organs. Previous studies have identified vascular receptors that can be used to deliver therapeutic agents to cancers originating in host organs[5–11] or to cancers originating in normal organs.[22–24] MDP likely cannot be utilized in this manner since it appears to be

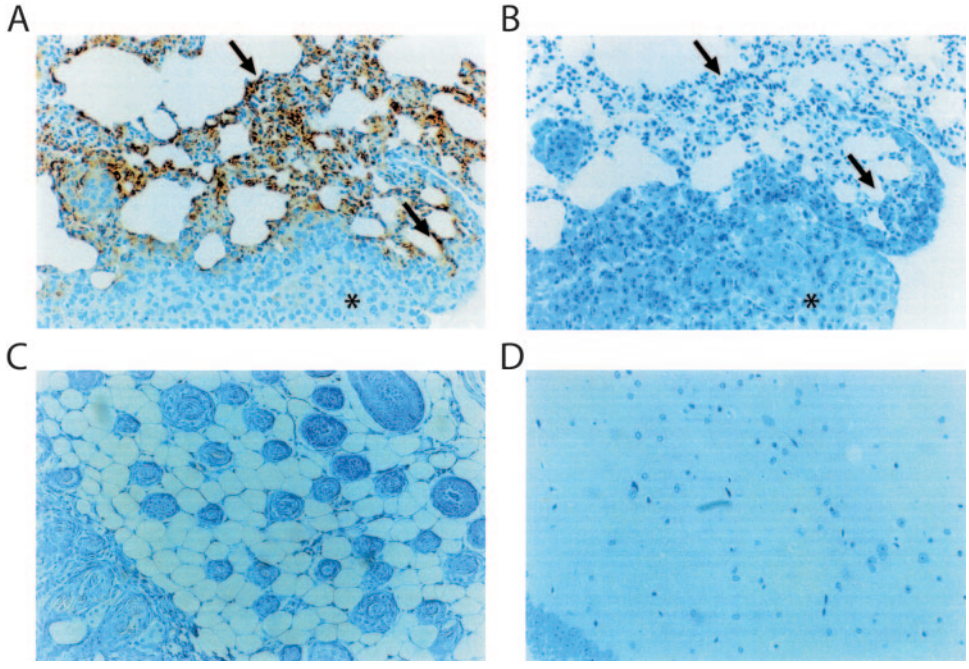


Figure 4. GFE does not bind to the vasculature within lung tumors. Lungs were harvested from mice bearing C8161 metastases after the animals had been injected with phage displaying the GFE peptide. Tissue sections were immunostained with an anti-M13 antibody to detect phage particles. *Top left*, *A*: brown peroxidase staining indicates phages are distributed throughout the lung vasculature (arrows). Phage staining, however, is absent in tumor (T) vasculature. As a negative control for the staining, a serial tissue section obtained from the GFE-injected mouse lung was processed with the secondary antibody alone (*top right*, *B*), and control tissues are shown for skin (*bottom left*, *C*) and brain (*bottom right*, *D*).

Downloaded from chestjournal.chestpubs.org at M D Anderson Hospital on October 8, 2010
© 2005 American College of Chest Physicians

absent in the vasculature of lung metastases. Even if MDP were present in lung tumor vasculature, it would not be an optimal target for delivering drugs to lung tumors. Unlike the prostate and breast, the lung is an essential organ for survival, and the risk of collateral damage to normal lung vasculature may be unacceptable. On the other hand, the delivery of radioprotective agents to the lungs would remain an open possibility.

Taken together, these data illustrate the diversity and functional relevance of a vascular receptor in the lung vasculature. Novel antimetastatic strategies may emerge from interfering with tumor cell attachment to MDP and/or mechanisms underlying angiogenesis in lung cancer.

ACKNOWLEDGMENT: We thank Dr. Wolfgang Kuschinsky for references and advice on vascular imaging techniques.

References

1 Kolonin MG, Arap W, Pasqualini R. Molecular addresses in blood vessels as targets for therapy. Curr Opin Chem Biol 2001; 5:308–313
2 Rajotte D, Arap W, Hagedorn M, et al. Molecular heterogeneity of the vascular endothelium revealed by in vivo phage display. J Clin Invest 1998; 102:430–437
3 Pasqualini R, Ruoslahti E. Organ-targeting *in vivo* using phage display peptide libraries. Nature 1996; 380:364–366
4 Ellerby HM, Arap W, Ellerby LM, et al. Anti-cancer activity of targeted pro-apoptotic peptides. Nat Med 1999; 5:1032–1038
5 Koivunen E, Arap W, Valtanen H, et al. Tumor targeting with a selective gelatinase inhibitor. Nat Biotechnol 1999; 17:768–774
6 Burg MA, Pasqualini R, Arap W, et al. NG2 proteoglycan-binding peptides target tumor neovasculature. Cancer Res 1999; 59:2869–2874
7 Arap W, Pasqualini R, Ruoslahti E. Cancer treatment by targeted drug delivery to tumor vasculature in a mouse model. Science 1998; 279:377–380
8 Pasqualini R, Koivunen E, Ruoslahti E. α_v integrins as receptors for tumor targeting by circulating ligands. Nat Biotechnol 1997; 15:542–546
9 Zurita AJ, Troncoso P, Cardo-Vila M, et al. Combinatorial screenings in patients: the interleukin-11 receptor alpha as a candidate target in the progression of human prostate cancer. Cancer Res 2004; 64:435–439
10 Marchio S, Lahdenranta J, Schlingemann RO, et al. Aminopeptidase A is a functional target in angiogenic blood vessels. Cancer Cell 2004; 5:151–162
11 Rajotte D, Ruoslahti E. Membrane dipeptidase is the receptor for a lung-targeting peptide identified by *in vivo* phage display. J Biol Chem 1999; 274:11593–11598
12 Arap W, Kolonin MG, Trepel M, et al. Steps toward mapping the human vasculature by phage display. Nat Med 2002; 8:121–127
13 Yao VJ, Ozawa MG, Trepel M, et al. Targeting pancreatic islets with phage display assisted by laser pressure catapult microdissection. Am J Pathol 2005; 166:625–636
14 Keynan S, Hooper NM, Turner A. Zinc metalloproteases in health and disease. London, UK: Taylor & Francis Ltd, 1995; 285–309
15 Hirota T, Nishikawa Y, Tanaka M, et al. Characterization of dehydropeptidase I in the rat lung. Eur J Biochem 1986; 160:521–525
16 Habib GM, Shi ZZ, Cuevas AA, et al. Leukotriene D4 and cystinyl-bis-glycine metabolism in membrane-bound dipeptidase-deficient mice. Proc Natl Acad Sci U S A 1998; 95:4859–4863
17 Welch DR, Bisi JE, Miller BE, et al. Characterization of a highly invasive and spontaneously metastatic human malignant melanoma cell line. Int J Cancer 1991; 47:227–237
18 Pasqualini R, Bourdoulous S, Koivunen E, et al. A polymeric form of fibronectin has antimetastatic effects against multiple tumor types. Nat Med 1996; 2:1197–1203
19 Tsunenari I, Yamate J, Iwaki M, et al. Angioarchitecture of tumors induced by two different cloned cell lines established from a transplantable rat malignant fibrous histiocytoma. Microsc Microanal 2003; 9:532–541
20 Wang HY, Port JL, Hochwald SN, et al. Revised technique of isolated lung perfusion in the rat. Ann Thorac Surg 1995; 60:211–212
21 Li P-A, Vogel J, He Q-P, et al. Preischemic hyperglycemia leads to rapidly developing brain damage with no change in capillary patency. Brain Res 1998; 782:175–183
22 Kolonin MG, Saha PK, Chan L, et al. Reversal of obesity by targeted ablation of adipose tissue. Nat Med 2004; 10:625–632
23 Trepel M, Arap W, Pasqualini R. *In vivo* phage display and vascular heterogeneity: implications for targeted medicine. Curr Opin Chem Biol 2002; 6:399–404
24 Pasqualini R, Arap W. Translation of vascular proteomics into individualized therapeutics. In: Licinio J, Wong ML, eds. Pharmacogenomics: the search for individualized therapies. New York, NY: Wiley-VCH Verlag GmbH, 2002; 525–530

Hypoxia Amplifies the Proliferative Capacity of Distal Human Pulmonary Artery Smooth-Muscle Cells*

Ellena J. Growcott, MD; Kathy H. Banner, MD; and John Wharton, MD

(CHEST 2005; 128:600S–601S)

Abbreviations: cAMP = cyclic adenosine monophosphate; PASMC = pulmonary artery smooth-muscle cell

Hypoxia is an important factor in pulmonary hypertension and vascular remodeling. We sought to determine whether the growth capabilities of human pulmonary artery smooth-muscle cells (PASMCs) differ when isolated and grown under normoxic (95% ambient air, 5% CO_2) and hypoxic conditions (2% O_2, 93% N_2, 5% CO_2). Cells from explants of the same distal (< 1 mm external diameter) pulmonary artery segments (n = 6 patients) were

*From Imperial College London (Drs. Growcott and Wharton), Hammersmith Campus, London; and Pfizer Global Research & Development (Dr. Banner), Sandwich, Kent, UK.
Funded by a BBSRC-CASE Award and BHF.
Reproduction of this article is prohibited without written permission from the American College of Chest Physicians (www.chestjournal.org/misc/reprints.shtml).
Correspondence to: Ellena J. Growcott, MD, Experimental Medicine and Toxicology, Imperial College London, Hammersmith Campus, London W12 0NN, UK

Downloaded from chestjournal.chestpubs.org at M D Anderson Hospital on October 8, 2010
© 2005 American College of Chest Physicians

Phenotypic Diversity of the Lung Vasculature in Experimental Models of Metastases *

Yun Oh, Imran Mohiuddin, Yan Sun, Joseph B. Putnam, Jr, Waun Ki Hong, Wadih Arap and Renata Pasqualini

Chest 2005;128; 596S-600S
DOI 10.1378/chest.128.6_suppl.596S

This information is current as of October 8, 2010

Updated Information & Services
Updated Information and services can be found at:
http://chestjournal.chestpubs.org/content/128/6_suppl/596S.full.html

References
This article cites 22 articles, 7 of which can be accessed free at:
http://chestjournal.chestpubs.org/content/128/6_suppl/596S.full.html#ref-list-1

Permissions & Licensing
Information about reproducing this article in parts (figures, tables) or in its entirety can be found online at:
http://www.chestpubs.org/site/misc/reprints.xhtml

Reprints
Information about ordering reprints can be found online:
http://www.chestpubs.org/site/misc/reprints.xhtml

Citation Alerts
Receive free e-mail alerts when new articles cite this article. To sign up, select the "Services" link to the right of the online article.

Images in PowerPoint format
Figures that appear in *CHEST* articles can be downloaded for teaching purposes in PowerPoint slide format. See any online figure for directions.

AMERICAN COLLEGE OF CHEST PHYSICIANS®

Downloaded from chestjournal.chestpubs.org at M D Anderson Hospital on October 8, 2010
© 2005 American College of Chest Physicians

doi:10.1006/mthe.2001.0266, available online at http://www.idealibrary.com on IDEAL

ARTICLE

Successful Treatment of Primary and Disseminated Human Lung Cancers by Systemic Delivery of Tumor Suppressor Genes Using an Improved Liposome Vector

Rajagopal Ramesh,*,[1] Tomoyuki Saeki,* Nancy Smyth Templeton,[†] Lin Ji,* L. Clifton Stephens,[‡] Isao Ito,* Deborah R. Wilson,[§] Zheng Wu,[§] Cynthia D. Branch,* John D. Minna,[¶] and Jack A. Roth*

*Section of Thoracic Molecular Oncology, Department of Thoracic and Cardiovascular Surgery, and [‡]Department of Veterinary Medicine and Surgery, The University of Texas M. D. Anderson Cancer Center, Houston, Texas 77030
[†]Center for Cell and Gene Therapy, Baylor College of Medicine, Houston, Texas 77030
[§]Introgen Therapeutics Inc., Houston, Texas 77030
[¶]Department of Pathology, The University of Texas Southwestern Medical Center, Dallas, Texas 75390

Received for publication November 8, 2000; accepted in revised form January 10, 2001; published online March 9, 2001.

Delivery of therapeutic genes to disseminated tumor sites has been a major challenge in the field of cancer gene therapy due to lack of an efficient vector delivery system. Among the various vectors currently available, liposomes have shown promise for the systemic delivery of genes to distant sites with minimal toxicity. In this report, we describe an improved extruded DOTAP:cholesterol (DOTAP:Chol) cationic liposome that efficiently delivers therapeutic tumor suppressor genes *p53* and *FHIT,* which are frequently altered in lung cancer, to localized human primary lung cancers and to experimental disseminated metastases. Transgene expression was observed in 25% of tumor cells per tumor in primary tumors and 10% in disseminated tumors. When treated with DOTAP:Chol–*p53* and –*FHIT* complex, significant suppression was observed in both primary ($P < 0.02$) and metastatic lung tumor growth ($P < 0.007$). Furthermore, repeated multiple treatments revealed a 2.5-fold increase in gene expression and increased therapeutic efficacy compared to single treatment. Finally, animal survival experiments revealed prolonged survival (median survival time: 76 days, $P < 0.001$ for H1299; and 96 days, $P = 0.04$ for A549) when treated with liposome–*p53* DNA complex. Our findings may be of importance in the development of treatments for primary and disseminated human lung cancers.

Key Words: lung cancer; *p53; FHIT;* liposome; gene therapy; tumor suppressor; intratumoral; intravenous.

INTRODUCTION

Cancer of the lung is one of the leading causes of death worldwide (1). Patients often present with locally advanced or disseminated disease, and long-term survival rates have not improved appreciably over the past 20 years. Current treatments for lung cancer have shown little success, because they cannot eradicate disseminated tumors with an acceptable toxicity. One alternative strategy that has shown promise in the treatment of cancer is gene therapy. However, so far this approach has been shown in patients to mediate tumor regression only when delivered directly to solid tumors via intralesional or intraperitoneal injection (2–6). A gene therapy has yet to be developed that is effective for disseminated cancer. One reason for this has been the lack of a vector that is nontoxic and that can efficiently deliver genes when injected intravenously. However, Templeton *et al.* (7) recently reported development of extruded DOTAP:cholesterol (DOTAP:Chol) cationic liposomes that efficiently delivered the chloramphenicol acetyl transferase (*CAT*) gene to various organs and tissues with maximal gene delivery to the lung following intravenous administration. Indeed, in the same study DOTAP:Chol proved superior to previously reported liposome preparations, and it was the extrusion of the liposomes during synthesis that was impor-

[1] To whom correspondence and reprint requests should be addressed at Department of Thoracic and Cardiovascular Surgery, Box 109, The University of Texas M. D. Anderson Cancer Center, 1515 Holcombe Boulevard, Houston, TX 77030. Fax: (713) 794-4669. E-mail: rramesh@mdanderson.org.

Copyright © The American Society of Gene Therapy
1525-0016/01 $35.00

tant for mediating very high gene transfer to the lung. Although, effective gene delivery to the lung was previously demonstrated using DOTAP:Chol, the ability of these cationic liposomes to efficiently deliver and express therapeutic genes in primary or disseminated lung tumors has not been previously reported.

In this study, we therefore tested the ability of improved extruded DOTAP:Chol cationic liposomes to deliver the therapeutic tumor suppressor genes *p53* and fragile histidine triad (*FHIT*) to primary and disseminated experimental metastatic murine and human lung tumors and compared with conventional liposomes. We chose the *p53* gene because it is the most commonly mutated gene identified to date in human cancers (8) and the *FHIT* gene because its aberrant transcripts as well as the lack of detectable *Fhit* protein have been frequently observed in a variety of primary tumors and their derived cell lines, including cancers of the lung, stomach, breast, colon, cervix, and the head and neck (9, 10). The overall frequencies of *p53* and *FHIT* gene alterations in small cell lung cancer are 90 and 80%, respectively, and in non-small-cell lung cancer, approximately 55 and 40% (9–11). Furthermore, reintroduction and overexpression of the wild-type p53 or *Fhit* protein have demonstrated ability to suppress tumor cell growth *in vitro* and *in vivo* (12–15). As part of this study, we developed xenograft models of experimental metastases with human lung cancer cells that did not produce wild-type p53 or Fhit protein. We observed that extruded DOTAP:Chol cationic liposome-mediated gene delivery effectively transfected both primary and disseminated murine tumors and human lung tumor xenografts, and this was associated with suppressed tumor growth and prolonged animal survival with minimal toxicity.

METHODS

Materials. All lipids (DOTAP, DOPE, cholesterol) were purchased from Avanti Polar Lipids (Albaster, AL). Lipofectamine (DOSPA:DOPE), RPMI 1640 medium, Ham's/F12 medium, and fetal bovine serum (FBS) were purchased from GIBCO-BRL-Life Technologies (New York, NY). DOTAP transfection reagent was purchased from Roche Molecular Biochemicals (Indianapolis, IN). Polyclonal rabbit antihuman FHIT antibody and mouse antihuman p53 monoclonal antibody (BP53.12) were obtained from Zymed Laboratories (San Francisco, CA) and Santa Cruz Biotechnology, Inc. (Palo Alto, CA), respectively.

Cell lines and animals. Human non-small cell lung carcinoma cell lines H1299 ($p53^{null}$/*FHIT*−) and A549 ($p53^{+}$/*FHIT*−) were obtained from American Type Culture Collection and maintained in RPMI 1640 and Ham's/F12 media supplemented with 10% FBS, 1% glutamate, and antibiotics. Murine fibrosarcoma cell line UV2337m, which has a mutant *p53* (16), was obtained from Dr. Isaiah J. Fidler, The University of Texas M. D. Anderson Cancer Center, and maintained in Dulbecco's modified Eagle's medium supplemented with 10% FBS. Cells were regularly passaged and tested for presence of mycoplasma. Four- to 6-week-old female immunocompetent C3H/HeNcr mice (National Cancer Institute, Frederick, MD), BALB/c nude (*nu/nu*) mice (Harlan–Sprague–Dawley Inc., Indianapolis, IN), and SCID/Beige mice (Charles River Laboratories, Wilmington, MA) used in the study were maintained in a pathogen-free environment and handled according to institutional guidelines established for animal care and use.

Purification of plasmids. The plasmids used in the study were either purchased (β-*gal*, Clontech Inc., Palo Alto, CA; *Luc*, Promega, Madison, WI) or cloned in an adenoviral shuttle vector (*p53, FHIT,* and *CAT*) and purified as described previously (7, 17). Briefly, plasmids carrying the bacterial β-galactosidase (*Lac-Z*), firefly luciferase (*Luc*), or *CAT* genes, or human *p53* or *FHIT* cDNA, under the control of cytomegalovirus (CMV) promotor, were grown under ampicillin or kanamycin selection in the *Escherichia coli* host strain DH5α. Endotoxin levels of purified plasmids were determined using the chromogenic limulus amebocyte lysate kinetic assay kit (Kinetic-QCL, Biowhittaker, Walkersville, MD). The concentration and purity of the purified plasmid DNAs were determined by $OD_{260/280}$ ratios.

Synthesis of liposomes and preparation of DNA:liposome mixtures. Liposomes (DOTAP:Chol and DOTAP:DOPE) were synthesized and extruded through Whatman filters (Kent, UK) of decreasing size (1.0, 0.45, 0.2, and 0.1 μm) as described previously (7). DNA:liposome complexes were prepared fresh 2 to 3 h before tail vein injection in mice. Briefly, DOTAP:Chol (20 mM) or DOTAP:DOPE (20 mM) stock solution and stock DNA solution diluted in 5% dextrose in water (D5W) were mixed in equal volumes to give a final concentration of 4 mM DOTAP:Chol–150 μg DNA in 300 μl final volume (ratio 1:2.6). All reagents were diluted and mixed at room temperature. Reagents were gently mixed in a 1.5-ml Eppendorf tube by pipetting. The DNA solution was added at the surface of the liposome and mixed rapidly up and down twice with the pipet tip. The DNA:liposome mixture thus prepared was precipitate free and used for all *in-vivo* experiments. The DOTAP–DNA liposome complex and lipofectamine–DNA liposome complex were prepared according to manufacturer's guidelines.

Particle size analysis. Freshly prepared DNA:liposome complexes were analyzed for mean particle size using the N4 particle size analyzer (Coulter, Miami, FL). The average mean particle size of the DNA:liposome complexes ranged between 300–325 nm.

In vivo transfection efficiency in normal lung, subcutaneous tumors, and tumor-bearing lungs. Before the start of the experiment, *nu/nu* mice were subjected to 3.5 Gy of total body irradiation to increase tumor uptake using a cesium source according to institutional guidelines. Mice were then injected with *p53* gene-null H1299 tumor cells [5×10^6/100 μl of phosphate-buffered saline (PBS)] subcutaneously on the right flank. When the tumors reached 4–5 mm^2 in size, a single dose of DOTAP:Chol–DNA complex (100 μg of *Lac-Z* DNA) was injected intratumorally. Forty-eight hours after injection, mice were euthanized by CO_2 inhalation, and tumors were removed and analyzed histochemically for β-galactosidase expression (18). Tumors were cut into 4-μm sections, stained for β-galactosidase, and evaluated by light microscopy.

Expression of the p53 and Fhit proteins in tumors was determined by Western blot analysis. Briefly, subcutaneous H1299 tumors injected intratumorally with DOTAP:Chol–DNA complex (100 μg of *Lac-Z, CAT, p53,* or *FHIT* DNA) were harvested 48 h after treatment and homogenized in Laemmli buffer. Protein concentrations were determined by using Bio-Rad protein assay reagent (Bio-Rad, Fremont, CA), and 50 μg of total protein was analyzed by sodium dodecyl sulfate (SDS)–polyacrylamide gel electrophoresis (PAGE). p53 and Fhit proteins were detected using mouse antihuman *p53* antibody (BP53.12) and rabbit antihuman *FHIT* antibody as described previously (15, 19, 20).

To determine the transfection efficiency of the liposome:DNA complexes in normal lungs, C3H mice were injected with DOTAP:Chol–*Lac-Z* or DOTAP:Chol–*p53* via tail vein. Forty-eight hours after injection, animals were euthanized by CO_2 inhalation; their lungs were harvested and either snap frozen for β-galactosidase analysis or formalin fixed for p53 analysis. Tissue sections were cut and analyzed histochemically (β-gal) or immunohistochemically (p53) as described previously (18, 19). To determine the transfection efficiency of the complexes in lung tumors *in vivo,* nude mice were injected with 1×10^6 A549 tumor cells suspended in 200 μl of PBS via tail vein. Two to 3 weeks later, a single dose of DOTAP:Chol–*Lac-Z* or DOTAP:Chol–*FHIT* complex (50 μg DNA) or naked plasmid DNA (50 μg) was injected via tail vein. Lungs were harvested 48 h later and analyzed for protein expression by histochemical (β-gal) or immunohistochemical (Fhit) analysis (18, 20).

Tumor growth and treatments in vivo. Before the start of all experiments involving subcutaneous tumor growth and treatments, *nu/nu* mice were irradiated (3.5 Gy) using a cesium source to enhance tumor uptake. In all the experiments, 5×10^6 tumor cells (H1299, A549) suspended in 100 μl sterile PBS were injected into the right dorsal flank. When the tumor had reached a size of 4–5 mm^2, the animals were randomized into groups and

Copyright © The American Society of Gene Therapy

treatment was initiated. Intratumoral injections were performed under anesthesia using methoxyflurane (Schering-Plough, Kenilworth, NJ) per institutional guidelines. Tumor measurements were recorded every other day without knowledge of the treatment groups, and tumor volumes were calculated by using the formula $V\,(mm^3) = a \times b^2/2$, where a is the largest dimension and b is the perpendicular diameter (21). Antitumor efficacy data are presented as cumulative tumor volumes for all animals in each group to account for both size and number of tumors.

For p53 experiments, subcutaneous H1299 tumor-bearing animals were divided into three groups of eight animals. Group 1 received no treatment, Group 2 received naked *p53* plasmid DNA (100 μg/dose), and Group 3 received extruded DOTAP:Chol–*p53* complex (100 μg/dose); treatments were given daily for a total of six doses. In a separate but parallel experiment, an additional control group was included that received a complex of extruded DOTAP:Chol with an irrelevant DNA plasmid (pAd). All other experimental conditions and treatment schedules were identical.

For FHIT experiments, H1299 and A549 subcutaneous tumors were established in nude mice. For each tumor type, four treatment groups were established comprising seven animals per group. Group 1 received no treatment, Group 2 received *FHIT* plasmid DNA (100 μg/dose), Group 3 received extruded DOTAP:Chol–*CAT* complex (100 μg/dose), and Group 4 received extruded DOTAP:Chol–*FHIT* complex (100 μg/dose). Animals were treated daily for a total of six doses. In all experiments, the statistical significance of changes in tumor size was determined by using the Student's t test.

Establishment of lung metastases and their treatments in vivo. To establish lung metastases, female SCID/Beige mice were injected via tail vein with 10^6 H1299 tumor cells suspended in 200 μl of sterile PBS. Three days later, the mice were divided into nine groups and treated as follows: no treatment (Group 1), naked *p53* plasmid DNA (Group 2), DOTAP–DOPE–*p53* complex (Group 3), extruded DOTAP:Chol–*CAT* complex (Group 4), nonextruded DOTAP:Chol–*p53* complex (Group 5), extruded DOTAP:Chol–*p53* complex (Group 6), empty liposome (Group 7), lipofectamine–*p53* complex (Group 8), and DOTAP:*p53* complex (Group 9). There were eight mice in each group. All treatments comprised 50 μg of plasmid DNA or 50 μg DNA:liposome complex and were administered via tail vein using a 27-gauge needle daily for a total of six doses. Two weeks following the last dose, animals were euthanized by CO_2 inhalation. Lungs from each of the mice from the nine groups were injected intratracheally with India ink and fixed in Feketes solution (22). The therapeutic effect of systemic *p53* gene treatment was determined by counting the number of metastatic tumors in each lung under a dissecting microscope without knowledge of the treatment groups. The data were analyzed, and differences among groups were interpreted as statistically significant if the P value was <0.05 by the Mann–Whitney rank-sum test.

To determine the therapeutic effect of the *p53* and *FHIT* tumor suppressor genes on lung tumor cells expressing wild-type p53, mice (*nu/nu*) were injected with A549 tumor cells (1×10^6) via tail vein. On day 6 after injection, mice were divided into groups ($n = 6$ or 8 animals per group) for treatment. Group 1 received no treatment; Group 2 received *p53* or *FHIT* plasmid DNA; Group 3 received extruded DOTAP:Chol–*CAT* complex; Group 4 received extruded DOTAP:Chol–*p53* complex or DOTAP:Chol–*FHIT* DNA:liposome complex; Group 5 received lipofectamine–*p53* DNA:liposome complex; Group 6 received empty liposome. Animals were treated daily for a total of six doses (50 μg/dose). Following the last dose, mice were euthanized, and the therapeutic effects of the *p53* and *FHIT* DNA:liposome complexes were determined as described above for the H1299/SCID/Beige model.

As a syngeneic lung tumor model, C3H mice were injected with murine UV2237m fibrosarcoma cells (1×10^6) and divided into nine groups (n = 5/group). Six days after injection, animals were treated as follows: no treatment, empty liposome, *p53* plasmid DNA, DOTAP–*p53* complex, lipofectamine–*p53* complex, DOTAP:DOPE–*p53* complex, nonextruded DOTAP:Chol–*p53* complex, extruded DOTAP:Chol–*CAT* complex, or extruded DOTAP:Chol–*p53* complex. Treatment schedule and analyses of therapeutic effect were the same as described above for the H1299 and A549 models.

Gene expression and therapeutic efficacy of single and multiple treatments in lung tumor-bearing animals. For evaluation of gene expression, UV2237m lung tumor-bearing C3H mice were divided into three groups. One group was not treated; the others were treated with one dose of extruded DOTAP:Chol–*Luc* complex or three daily doses of the same complex (50 μg DNA/dose). Lungs were harvested 48 h after injection, and the protein was extracted and analyzed for luciferase activity using the luciferase assay kit (Promega, Madison, WI). Luciferase activity was expressed as relative light units (RLU) per milligram of protein.

To determine the therapeutic efficacy of repeated treatments, UV2237m tumor-bearing animals were divided into groups (n = 7/group). Treatments comprised no treatment, one dose of extruded DOTAP:Chol–*p53* complex, or six daily doses of the same complex (50 μg DNA/dose). Lungs were harvested 2 weeks after the last treatment, and the number of tumor nodules counted as described earlier.

p53 effects on tumor cells. After subcutaneous H1299 tumors established in *nu/nu* mice, the mice were separated into groups; one group was not treated; a second was treated with *p53* plasmid DNA, and a third with *p53* DNA:liposome complex. The tumors were then harvested and fixed in 4% buffered formalin, paraffin embedded, and cut in 4-μm sections. Tissue sections were stained for *p53* gene expression as previously described (13, 23). The tumor cells staining positive for *p53* were analyzed under bright field microscopy and quantitated without knowledge of the treatment groups. At least five fields per specimen were analyzed. To determine the fate of tumor cells following treatment, sections of subcutaneous tumors and tumor-bearing lungs were stained for apoptotic cell death with terminal deoxynucleotide transferase (Tdt) (Boehringer Mannheim) and counterstained with methylene blue or methyl green as described previously (13, 23). In all the staining procedures, appropriate negative controls were included.

Tumor characteristics after treatment. To determine the therapeutic effect of the *p53* gene on metastatic lung tumors, tumor-bearing lungs were harvested from *nu/nu* mice 21 days after treatment and evaluated histopathologically for tumor size, viability, and mitotic index. Analysis was done by a pathologist without knowledge of the treatment groups.

Animal survival after treatment. To determine the efficacy of systemic treatment, survival experiments were performed using the two metastatic lung tumor (H1299, A549) models. Briefly, female SCID/Beige mice were injected with 10^6 H1299 tumor cells via the tail vein. Six days later, mice were divided into four groups of six mice. Group 1 received no treatment, Group 2 received naked *p53* plasmid DNA, Group 3 received extruded DOTAP:Chol–*CAT* complex, and Group 4 received DOTAP:Chol–*p53* complex. In a separate set of experiments, two additional groups were tested, which received treatment with DOTAP:DOPE–*p53* complex or nonextruded DOTAP:Chol–*p53* complex. The treatment schedule consisted of six daily injections of naked plasmid DNA or DNA:liposome complex in 100 μl volumes (50 μg DNA/dose). Mice were monitored daily following the last injection. Moribund animals were euthanized by CO_2 inhalation. The lungs, heart, liver, spleen, brain, kidney, colon, ovaries, pancreas, and bone were removed from each animal and analyzed histopathologically for the presence of disseminated tumors and treatment-associated toxic effects. Statistical differences in actuarial survival curves were analyzed by using the Kaplan–Meier survival estimation and Wilcoxon signed-rank tests.

The A549 lung metastatic tumor model was used to evaluate the effect of the DOTAP:Chol–*p53* complex on tumors that have the wild-type *p53* gene. Briefly, *nu/nu* mice were injected with 10^6 A549 tumor cells via the tail vein. Six days later, mice were divided into four groups of seven mice each. The experimental conditions and treatment schedule were identical to those used for the H1299-SCID/Beige lung tumor model. The effect of DOTAP:Chol–*p53* DNA:liposome complex on survival was calculated by using the Kaplan–Meier survival estimation and the Wilcoxon signed-rank tests.

Statistical analysis. The statistical significance of the experimental results was calculated using Student's t test for tumor measurements, the Mann–Whitney rank-sum test for lung metastases, and the Wilcoxon log-rank test and Kaplan–Meier survival test for animal survival.

Copyright © The American Society of Gene Therapy

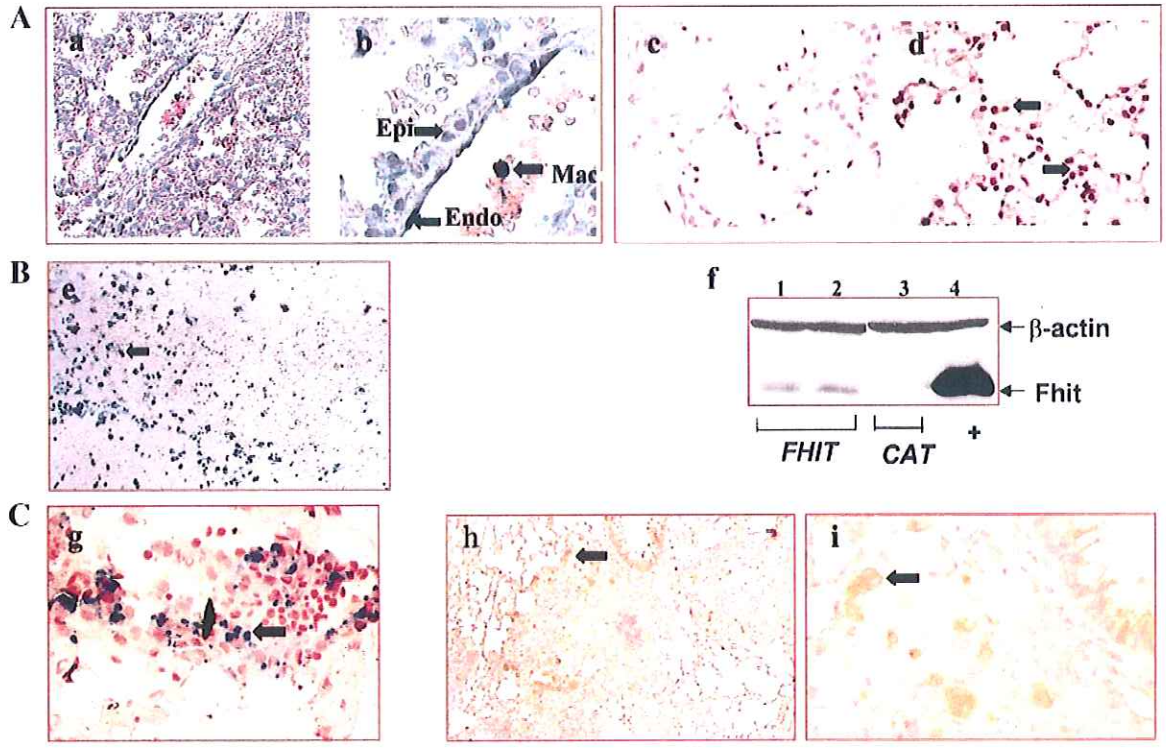


FIG. 1. *In vivo* transfection efficiency in normal lung, subcutaneous tumor, and metastatic lung tumors. (A) Female C3H mice were injected via the tail vein with either 50 μg of naked plasmid DNA (*Lac-Z* or *p53*) or 50 μg of plasmid DNA (*Lac-Z* or *p53*) complexed to liposomal DOTAP:Chol. Forty-eight hours after injection, lungs were harvested and analyzed for protein expression using histochemical (*Lac-Z*) and immunohistochemical (*p53*) methods. Alveolar epithelial (Epi) cells, endothelial (End) cells, and macrophages (Mac) of the lung from animals injected with DOTAP:Chol–DNA complexes showed gene expression, while those from animals injected with plasmid DNA showed no gene expression. This figure shows the production of β-galactosidase in lung tissue from an animal treated with DOTAP:Chol–*Lac-Z* complex at low (a) and high (b) magnification. Lung from a control animal treated with *p53* plasmid DNA is shown in c. Lung from an animal treated with DOTAP:Chol–*p53* produced p53 protein (d). (B) Subcutaneous H1299 tumors established in *nu/nu* mice given a single intratumoral injection of DOTAP:Chol liposome complexed to *Lac-Z, CAT,* or *FHIT* plasmid DNA (50 μg). Forty-eight hours later, tumors were removed and underwent either X-gal staining for β-galactosidase expression or Western blot analysis for Fhit protein production. A total of 25% of tumor cells treated with *Lac-Z* produced β-galactosidase (e). Fhit protein (f, lanes 1 and 2) production was demonstrated in tumors treated with *FHIT*. Lane 3 (f) represents tumors from animals treated with DOTAP:Chol–*CAT*. Lane 4 (f) represents the positive control for Fhit protein. (C) A549 lung tumor-bearing nude mice were injected with DOTAP:Chol liposome complexed to *Lac-Z* or *FHIT* DNA (50 μg) via the tail vein, and the lung tumors were analyzed for protein expression 48 h later. β-Galactosidase production (g) and Fhit production in lung tumors are shown at low (h) and high magnification (i). Arrows denote cells expressing transgene.

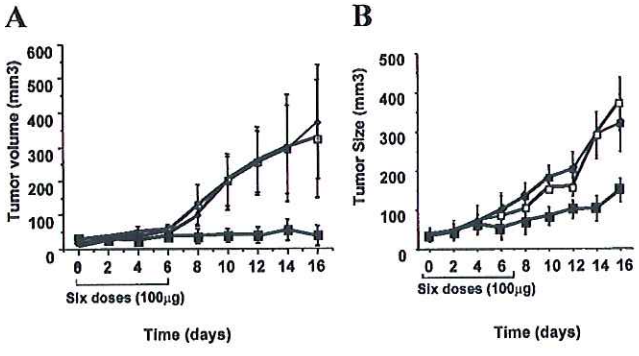


FIG. 2. DOTAP:Chol–*p53* complex suppress growth of subcutaneous human lung cancer xenografts. Subcutaneous H1299 tumor-bearing mice were divided into three groups (8 animals/group) and treated daily for a total of six doses (100 μg/dose), as follows: no treatment (●), *p53* plasmid DNA (□) and DOTAP:Chol–*p53* DNA:liposome complex (■) (A); no treatment (●), DOTAP:Chol–*pAd* complex (□) and DOTAP:Chol–*p53* complex (■) (B). Tumors were measured by using calipers, and the statistical significance of size changes was calculated using Student's *t* test. Each time point represents the mean tumor volume for each group. Bars represent standard errors.

RESULTS

In Vivo Transfection in Normal Lung, Primary Lung Tumor Xenografts, and Experimental Metastatic Lung Tumors

We determined the ability of extruded DOTAP:Chol liposomes to effectively transfect and deliver plasmid DNA into normal lung, subcutaneous lung tumor xenografts, and experimental metastatic lung tumors by using expression plasmids encoding the bacterial β-galactosidase (*Lac-Z* gene) or the human p53 or Fhit protein. Forty-eight hours following a single tail vein injection of DOTAP:Chol liposomes complexed with *Lac-Z* plasmid DNA or human *p53* plasmid DNA, alveolar epithelial cells (type II pneumocytes) and endothelial cells in the lung were observed to produce β-galactosidase (Figs. 1a and 1b) or p53 protein (Fig. 1d). Few alveolar macrophages expressed the transgene. In contrast, no gene expression was ob-

Copyright © The American Society of Gene Therapy

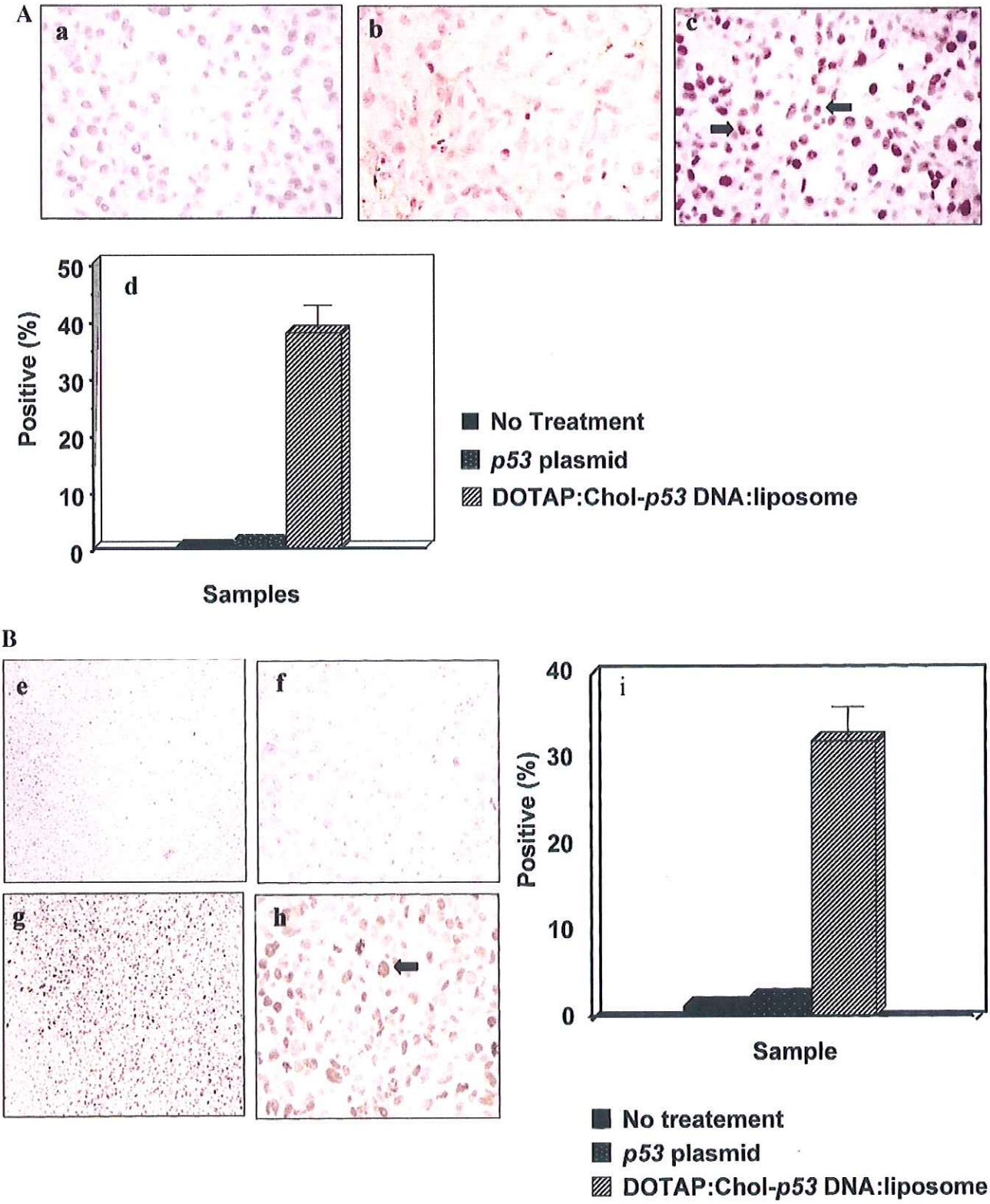


FIG. 3. *p53* gene expression and apoptotic cell death following treatment with the DOTAP:Chol–*p53* complex. Subcutaneous H1299 tumors from animals receiving no treatment (a), *p53* plasmid (b, e, f), or the DOTAP:Chol–*p53* complex (c, g, h) were harvested 48 h after treatment. p53 protein production was analyzed by (A) immunohistochemistry (a, b, c) and (B) apoptotic cell death by TUNEL staining (e, f, g, h). The percentages of cells producing the p53 protein (39%) (d) and undergoing apoptotic cell death (32%) (i) in tumors receiving the DOTAP:Chol–*p53* complex were significantly ($P = 0.001$) higher than the percentages of cells in the no treatment and p53 plasmid treatment groups.

Copyright © The American Society of Gene Therapy

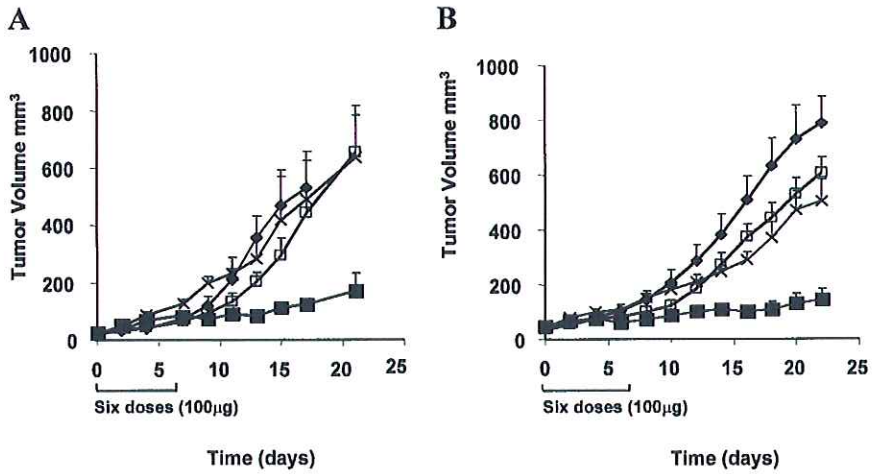


FIG. 4. Therapeutic effect of the DOTAP:Chol–*FHIT* complex on lung tumor xenografts. Subcutaneous H1299 and A549 tumor-bearing nude mice were divided into four groups (7 animals/group) and treated daily for a total of six doses (100 μg/dose), as follows: no treatment (◆), *FHIT* plasmid DNA, (□) DOTAP:Chol–*CAT* complex (X), and DOTAP:Chol–*FHIT* complex (■). The effects in H1299 tumors are shown in (A) and those in A549 tumors in (B). Tumor growth was significantly inhibited in both H1299 ($P = 0.02$) and A549 ($P = 0.001$) tumor-bearing animals treated with the DOTAP:Chol–*FHIT* complex. Bars denote standard errors.

served in animals injected with naked *p53* plasmid DNA (Fig. 1c).

To determine whether gene expression could also be achieved in solid primary tumors, human H1299 lung tumors were established subcutaneously in nude mice. Forty-eight hours following a single intratumoral injection of DOTAP:Chol–*LacZ* complex, 25% of the tumor cells produced β-galactosidase, as shown by histochemical staining (Fig. 1e). In contrast, no β-galactosidase production was observed in the untreated control tumors. Intratumoral injection of DOTAP:Chol–*FHIT* resulted in production of Fhit protein, as determined by Western blot analysis (Fig. 1f). Tumor-bearing animals injected with DOTAP:Chol -CAT (Fig. 1f) served as controls. Similarly, p53 protein expression was observed by Western blot analysis (data not shown).

The ability to transfect experimental human A549 lung metastatic tumors established in nude mice was also evaluated. A single tail vein injection of DOTAP:Chol–*Lac-Z* or DOTAP:Chol–*FHIT* into lung tumor-bearing mice resulted in 10% of the tumor cells producing β-galactosidase (Fig. 1g) or Fhit protein (Figs. 1h and 1i) at 48 h.

In Vivo Local Tumor Growth Suppression by p53 and FHIT

We assessed the ability of the DOTAP:Chol–*p53* complex to suppress the growth of *p53* gene-null H1299 human lung subcutaneous tumors in *nu/nu* mice. Treatment of tumor-bearing mice with the DOTAP:Chol–*p53* complex inhibited tumor growth significantly ($P = 0.001$) (Fig. 2A) compared with tumor growth in the control groups.

To further demonstrate the specific tumor-suppressive effects of the *p53* gene delivered by DOTAP:Chol liposomes, we performed a separate set of experiments in which subcutaneous H1299 tumor-bearing animals were divided into three groups, one receiving no treatment, one treatment with DOTAP:Chol liposome complexed to irrelevant plasmid DNA (*pAd*), and one treatment with the DOTAP:Chol–*p53* complex. No significant inhibition of tumor growth was observed in animals that were either not treated or treated with the DOTAP:Chol–pAd complex (Fig. 2B). In contrast, animals treated with the DOTAP:Chol–*p53* complex showed significant tumor growth inhibition ($P = 0.01$).

Further evidence that the observed therapeutic effect was due to *p53* gene expression was obtained by removing subcutaneous tumors 48 h after injection and analyzing them for *p53* gene expression by immunohistochemistry. *p53* gene expression was seen in 39% of tumor cells in animals receiving the DOTAP:Chol–*p53* complex (Figs. 3c and 3d) ($P = 0.001$), a significantly higher number than in the animals that were either not treated (Fig. 3a) or treated with *p53* plasmid DNA (Fig. 3b). Analysis of apoptotic tumor cell death by TUNEL studies showed that 32% of the tumor cells in mice receiving the DOTAP:Chol–*p53* complex were positive ($P = 0.001$) (Figs. 3g–3i), whereas tumors from control mice showed minimal apoptotic cell death (Figs. 3e, 3f, and 3i).

The therapeutic effects of the *FHIT* tumor suppressor gene on H1299 and A549 subcutaneous tumors in nude mice were similarly evaluated. Mice bearing tumors of each cell type were divided into four groups, one receiving no treatment, a second treatment with naked *FHIT* plasmid DNA, a third treatment with the DOTAP:Chol–*CAT* complex, and a fourth treatment with the DOTAP:Chol–*FHIT* complex. A significant growth inhibition of both H1299 tumors ($P = 0.02$; Fig. 4A) and A549 tumors ($P = 0.001$; Fig. 4B) was observed in mice treated with the DOTAP:Chol–*FHIT* complex when compared with the tumor growth in the three control groups for each tumor type.

Copyright © The American Society of Gene Therapy

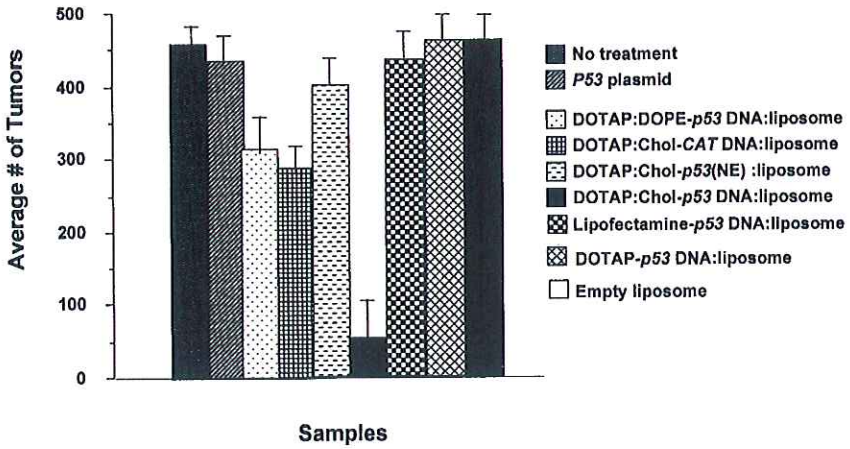


FIG. 5. Inhibition of H1299 lung metastases following treatment with the extruded DOTAP:Chol–*p53* complex. H1299 lung tumor-bearing SCID/Beige mice were either not treated or treated daily for a total of six doses (50 μg/dose) with *p53* plasmid DNA, empty liposome, lipofectamine–*p53* complex, DOTAP–*p53* complex, DOTAP:DOPE–*p53* DNA:liposome complex, nonextruded DOTAP:Chol–*p53* complex, extruded DOTAP:Chol–*CAT* complex, or extruded DOTAP:Chol–*p53* complex. Each group comprised eight animals. Metastatic tumor growth (P = 0.001) was significantly inhibited in mice treated with extruded DOTAP:Chol–*p53* complex when compared with growth in the other groups.

In Vivo Efficacy of p53 and FHIT Liposome:DNA Complexes for Treatment of Experimental Lung Metastases

The effectiveness of extruded DOTAP:Chol liposomes was compared to those of nonextruded DOTAP:Chol liposomes and other conventional liposome formulations [DOTAP, lipofectamine (DOSPA:DOPE), and DOTAP:DOPE] in a therapeutic xenograft model of human lung metastases using H1299 *p53*-null human lung cancer cells in SCID/Beige mice. There was a significantly ($P < 0.001$) lower number of lung metastases in mice receiving the extruded DOTAP:Chol–*p53* complex (Fig. 5) than in mice receiving no treatment, *p53* plasmid DNA, empty DOTAP:Chol liposome, DOTAP–*p53* complex, lipofectamine–*p53* complex, extruded DOTAP:Chol–*CAT* complex, DOTAP:DOPE–*p53* complex, or nonextruded DOTAP:Chol–*p53* complex. Metastatic tumor growth was also significantly (P = 0.02) inhibited in animals treated with the extruded DOTAP:Chol–*CAT* complex when compared with tumor growth in mice receiving no treatment, *p53* plasmid DNA, empty liposome, lipofectamine–*p53* DNA:liposome complex, or the DOTAP:*p53* complex.

To determine if the observed *p53* gene-mediated tumor inhibitory effects were restricted to *p53* gene-mutated or -null tumors, we studied the effects of the DOTAP:Chol–*p53* complex in A549 tumor cells, which are homozygous for the wild-type *p53* gene and form lung metastases following tail vein injection in *nu/nu* mice. A significantly lower (P = 0.001) number of metastases was observed in mice treated with the extruded DOTAP:Chol–*p53* complex (Fig. 6) than in control mice that were either not treated or were treated with *p53* plasmid DNA, empty DOTAP:Chol liposome, lipofectamine–*p53* complex, or DOTAP:Chol–*CAT* complex, thus eliminating the possibility that the *p53* gene-mediated inhibition was limited to *p53* gene-mutated or null tumors. No significant differences were observed in the number of metastases among the control groups.

The ability of the *FHIT* tumor suppressor gene to inhibit lung metastases formed by A549 tumor cells in nude mice was also evaluated. A significantly lower (P = 0.007) number of tumor metastases was observed in animals treated with the DOTAP:Chol–*FHIT* complex (Fig. 7) than in control animals that were not treated or were treated with *FHIT* plasmid DNA, empty DOTAP:Chol liposome, lipofectamine–*FHIT* complex or DOTAP:Chol–*CAT* complex. None of the control groups showed significant reductions in the number of tumor metastases.

Repeated Intravenous Injections of DOTAP:Chol–DNA Complex Increase Gene Expression and Therapeutic Efficacy

To determine whether repeated intravenous injections of DOTAP:Chol complex yield greater gene expression and thus therapeutic efficacy than single injections, UV2237m lung tumor-bearing immunocompetent C3H mice were divided into three groups; one group was not treated, another was treated with one dose of DOTAP:Chol–*luc* complex and the third was treated daily for a total of three doses of DOTAP:Chol–*luc* complex. Analysis of the animal's lungs 48 h after the last injection demonstrated a 2.5-fold greater (P = 0.0004) luciferase activity in the animals treated with three doses than in those treated with a single dose (Fig. 8). In addition, UV2237m lung tumor-bearing C3H mice that received repeated daily treatment with DOTAP:Chol–*p53* complex for a total of six doses demonstrated a significantly lower (P = 0.0006) number of tumors than those treated with only a single dose of DOTAP:Chol–*p53* complex or no treatment (Fig. 9).

Copyright © The American Society of Gene Therapy

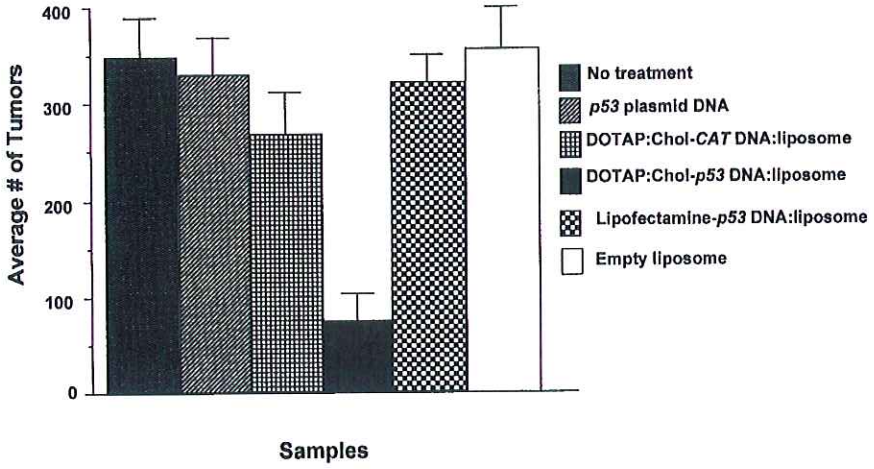


FIG. 6. Inhibition of A549 lung metastases following treatment with the extruded DOTAP:Chol–*p53* complex. A549 lung tumor-bearing *nu/nu* mice were either not treated or treated daily for a total of six doses (50 μg/dose) with *p53* plasmid DNA, empty liposome, lipofectamine–*p53* complex, extruded DOTAP:Chol–*CAT* complex, or extruded DOTAP:Chol–*p53* complex. Each group comprised eight animals. Metastatic tumor growth ($P = 0.001$) was significantly inhibited in mice treated with extruded DOTAP:Chol–*p53* complex compared with growth in the two control groups.

Apoptotic Cell Death in Lung Tumors Treated with DOTAP:Chol–p53 Complex

To determine the fate of tumor cells after treatment with the DOTAP:Chol–*p53* complex, A549 lung tumors from *nu/nu* mice were analyzed histologically, and apoptotic cell death was assessed by TUNEL staining. Histopathologic examination of lung sections from mice treated with the DOTAP:Chol–*p53* complex showed the presence of very few metastases; those that were present were small and contained only a few viable tumor cells (Figs. 10C and 10D). In addition, the number of tumor metastases in the lungs of these animals was significantly less than in control animals (data not shown). Furthermore, apoptotic cell death had occurred in these tumors (Fig. 11B). In contrast, lungs from control mice that received no treatment showed several large tumors with numerous mitoses (Figs. 10A and 10B) and no evidence of apoptotic cell death (Fig. 11A).

Inhibition of Murine UV2237m Lung Metastases in C3H Immunocompetent Mice Following Treatment with DOTAP:Chol–p53 Complex

To evaluate the efficacy of repeated treatments with DOTAP:Chol–p53 complex in an immunocompetent host, groups of UV2237m lung tumor-bearing C3H mice were either not treated or treated with *p53* plasmid DNA, empty DOTAP:Chol liposome, lipofectamine–*p53* com-

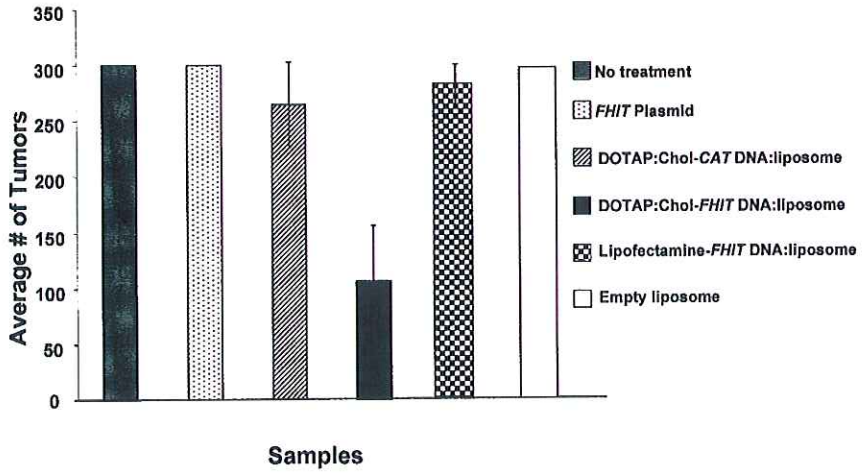


FIG. 7. Inhibition of A549 lung metastases following treatment with DOTAP:Chol–*FHIT* complex. A549 lung tumor-bearing *nu/nu* mice were divided into six groups and treated as follows: no treatment or treatment with *FHIT* plasmid DNA, empty liposome, lipofectamine–*FHIT* complex, extruded DOTAP:Chol–*CAT* complex, or extruded DOTAP:Chol–*FHIT* complex. Treatments were given daily for a total of six doses (50 μg/dose). Each group comprised six animals. There were significantly fewer lung tumors ($P = 0.007$) in mice treated with DOTAP:Chol–*FHIT* complex. In all the experiments, lungs were harvested 2 weeks after the last treatment, and metastases were counted without knowledge of the treatment group. Bars denote standard errors.

Copyright © The American Society of Gene Therapy

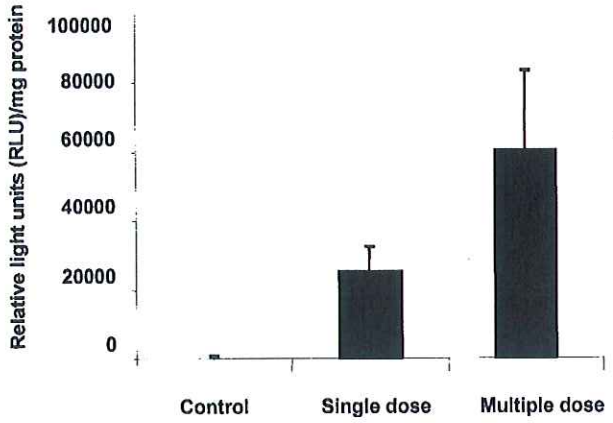


FIG. 8. Repeated intravenous injections of DOTAP:Chol–DNA complex increases gene expression. UV2237m lung tumor-bearing C3H animals were divided into three groups; one group was not treated, one was treated, with one dose of DOTAP:Chol–*luc* complex (50 μg DNA), and one was treated with three doses of DOTAP:Chol–*luc* complex (50 μg DNA/dose). Lungs were harvested 48 h after the last treatment and analyzed for luciferase activity. A 2.5-fold greater level of gene expression ($P = 0.0004$) was observed in animals treated with three doses than in animals treated with a single dose. Luciferase activity is expressed as relative light units (RLU) per milligram of protein.

plex, DOTAP–*p53* complex, the DOTAP:DOPE–*p53* complex, nonextruded DOTAP:Chol–*p53* complex, extruded DOTAP:Chol–*CAT* complex, or extruded DOTAP:Chol–*p53* complex. Each group comprised five animals. Analysis of the number of tumor nodules in each mouse 2 weeks after the last treatment demonstrated statistically significant tumor inhibition ($P = 0.01$) in mice treated with six doses of extruded DOTAP:Chol–*p53* complex when compared with any of the other groups (Fig. 12). Significant inhibition ($P = 0.03$) was also observed in animals treated with nonextruded DOTAP:Chol–*p53* complex when compared with animals receiving no treatment, empty liposome, or lipofectamine–*p53* complex. However, tumor inhibition was significantly less in the group treated with the nonextruded liposome:DNA complex than in the group treated with the extruded DNA:liposome complex.

DOTAP:Chol–p53 Prolongs Survival in a Mouse Model of Disseminated Human Lung Cancer

To determine the efficacy of the systemically administered extruded liposomal tumor suppressor gene complex, survival experiments were performed in the H1299 and A549 lung metastasis tumor models. H1299 lung tumor-bearing SCID/Beige mice were divided into four groups of six mice, as follows: no treatment (Group 1), *p53 plasmid DNA* (Group 2), DOTAP:Chol–*CAT* complex (Group 3), or DOTAP:Chol–*p53* complex (Group 4). Animals were monitored daily following the last treatment to assess morbidity and mortality. Mice from Groups 1, 2, and 3 died from the tumor burden between 30 and 60 days after tumor cell injection (median survival times: 38 days in Group 1, 40 days in Group 2, and 41 days in Group 3). In contrast, mice treated with the DOTAP:Chol–*p53* complex (Group 4) survived for a significantly longer period (median survival time: 76 days; $P = 0.001$). Moreover, 33% of mice from Group 4 were still alive on day 150 at the end of the experiment (Fig. 13A). In a separate set of experiments, additional control groups were tested that included DOTAP:DOPE–*p53* complex and nonextruded DOTAP:Chol–*p53* complex, but neither of these treatments significantly ($P = 0.35$) prolonged survival (median survival times: 44.8 days and 43.7 days, respectively, when compared with animals that were either not treated or treated with plasmid DNA. Again, in these experiments, treatment with extruded DOTAP:Chol–*p53* complex significantly prolonged ($P = 0.0002$) animal survival (median survival time: 81.3 days) (Fig. 13B). Histopathologic analysis of organs from animals in all the groups tested that died during the experiment showed no treatment-related toxic effects. However, all had dissemination of lung tumors to multiple organs and sites that included cervical lymph nodes, intestine, mesenteric lymph nodes, liver, kidney, spleen, pancreas, adrenal glands, ovaries, uterus, peritoneal cavity with ascites, and in all cases this was the cause of death (Figs. 13C–13F).

Survival in A549 lung tumor-bearing *nu/nu* mice was also evaluated. Following tumor cell injection, animals were divided into four groups, as follows: no treatment (Group 1), *p53* plasmid DNA (Group 2), DOTAP:Chol–*CAT* complex (Group 3), or DOTAP:Chol–*p53* complex (Group 4). The treatment schedule was identical to that followed in the H1299/SCID/Beige model. Mice in Group 4 had significantly longer survival (median survival time:, 96 days; $P = 0.04$) than mice in the three control groups (median survival times: 50 days in Group 1, 49 days in Group 2, and 52 days in Group 3) (Fig. 14). Histopathologic analysis of various organs revealed extensive tumor spread in the lungs of all four groups of animals, but

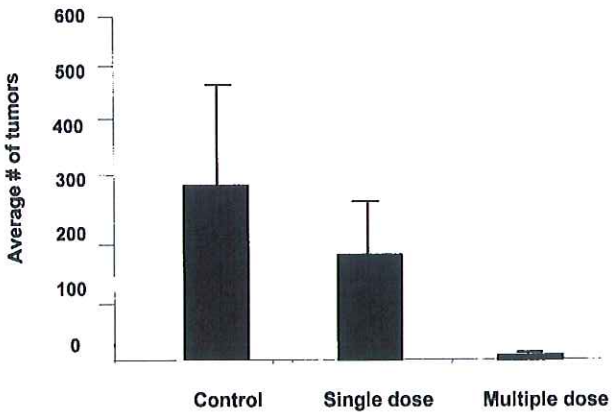
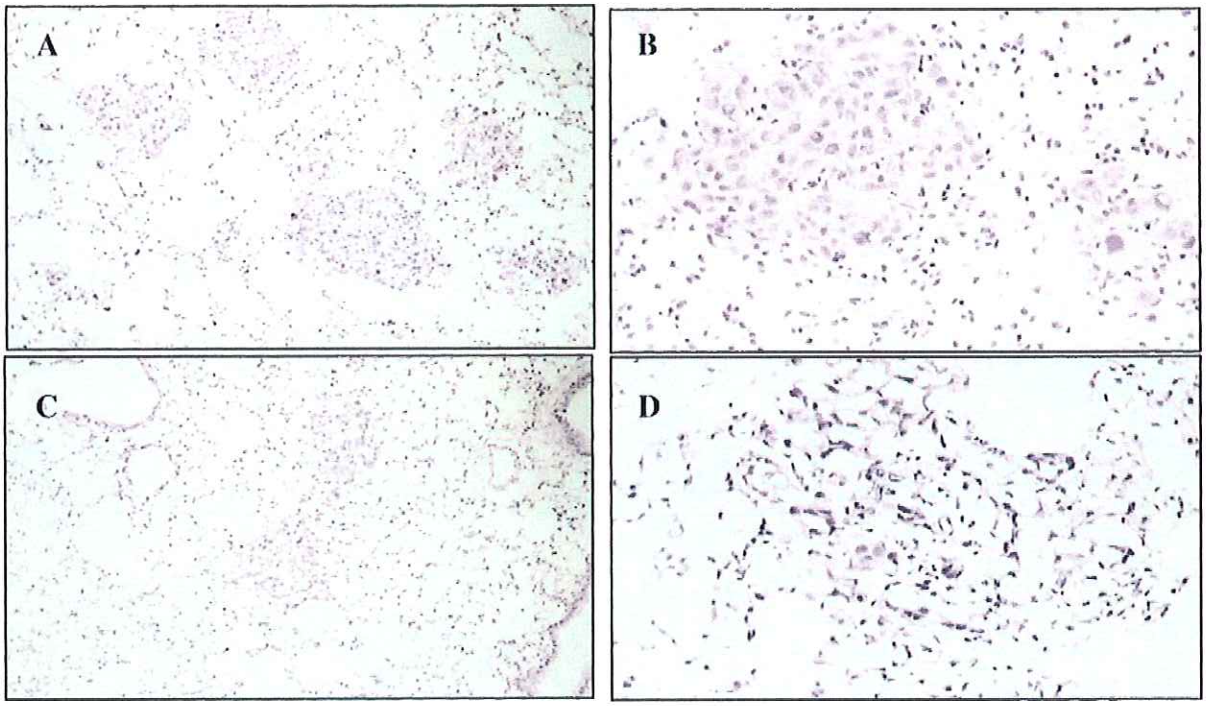
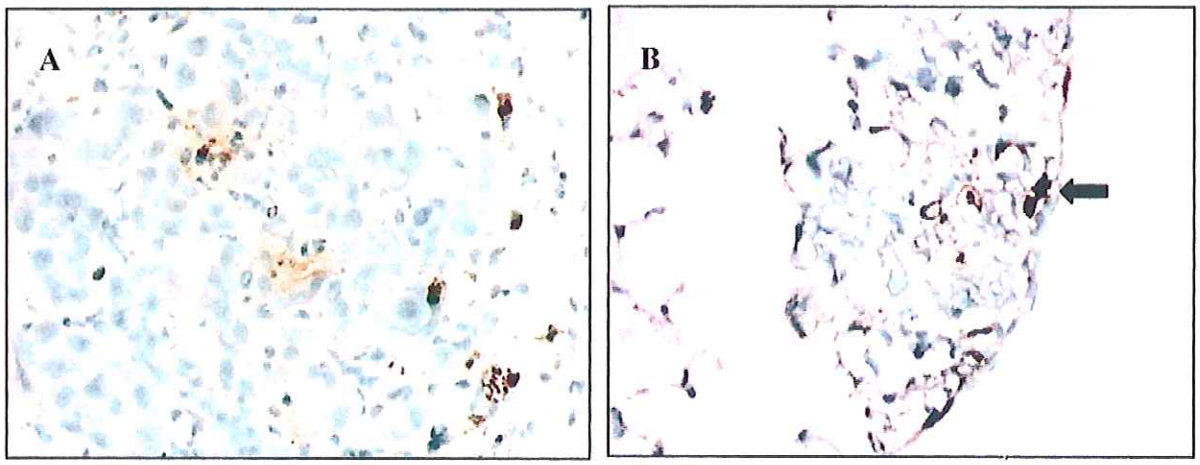


FIG. 9. Repeated intravenous injections of DOTAP:Chol–DNA complex increases therapeutic efficacy. UV2237m lung tumor-bearing C3H mice were divided into three groups ($n = 7$/group); one group was not treated, one received one dose of DOTAP:Chol–*p53* complex (50 μg DNA), and the third group received six daily doses of DOTAP:Chol–*p53* complex (50 μg DNA/dose). Lungs were harvested 2 weeks after the last treatment, and the tumor nodules were counted. Significantly ($P = 0.0006$) fewer tumors were observed in animals treated with six doses than in animals that were not treated or treated with one dose.

Copyright © The American Society of Gene Therapy



10



11

FIG. 10. Histopathologic analysis of A549 lung metastases treated with DOTAP:Chol–*p53* complex. Tumor viability, the mitotic index, and the number of tumors were analyzed histologically in tumor-bearing lungs from untreated control mice and from mice treated with DOTAP:Chol–*p53* complex. Many viable tumors with high mitotic indices were observed in untreated control mice (A, B), while few tumors with pyknotic nuclei were observed in animals treated with the DOTAP:Chol–*p53* complex (C, D) [magnification = ×100 (A, C) and ×250 (B, D)].

FIG. 11. Systemic treatment of A549 lung metastases with DOTAP:Chol–*p53* complex induces apoptosis. Apoptotic cell death in A549 lung tumors from mice untreated (A) or treated with the DOTAP:Chol–*p53* complex (B), as determined by TUNEL staining. Arrows indicate tumor cells undergoing apoptotic cell death (magnification ×250).

dissemination to other organs was not observed in animals in any of the four groups. In addition, treatment-associated toxic effects were not observed in animals in any of the four groups.

DISCUSSION

Local-regional treatment of cancers by viral vector-mediated replacement with the *p53* tumor suppressor gene has shown success (2–4). However, the use of this strategy for the systemic treatment of disseminated diseases, such as cancers of the lung, breast, and colon, has been limited by the potential for vector-associated toxicity and the inability to efficiently deliver genes to the target. Recent studies demonstrated the ability of extruded DOTAP:Chol cationic liposomes to deliver genes efficiently to systemic sites with minimal vector-associated toxicity (7). In this study, we evaluated the ability of the extruded DOTAP:Chol liposome to deliver two tumor suppressor genes, *p53* and *FHIT*, and the efficacy of this treatment in primary

Copyright © The American Society of Gene Therapy

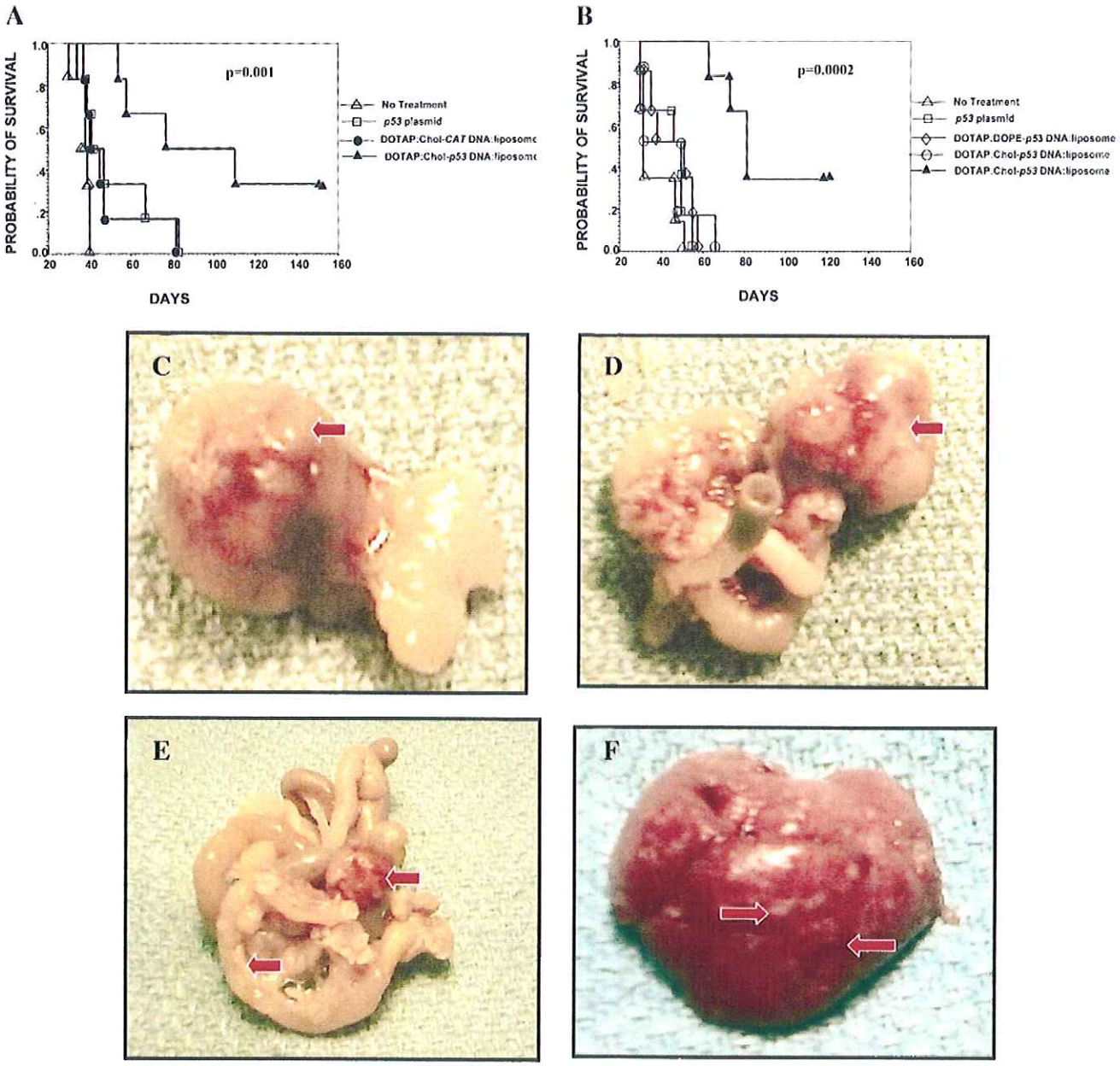


FIG. 13. Prolonged survival in H1299 lung tumor bearing mice treated with DOTAP:Chol–*p53* complex. Female SCID/Beige mice were injected with 10^6 H1299 tumor cells (six animals/group) via the tail vein. Groups were treated daily, as follows: no treatment (△), *p53* plasmid DNA (□), treatment with the DOTAP:Chol–*CAT* complex (●), DOTAP:DOPE–*p53* complex (◇), nonextruded DOTAP:Chol–*p53* complex (○), or DOTAP:Chol–*p53* complex (▲). Animals in each group received a total of six daily doses (50 μg/dose) and were monitored daily thereafter to assess morbidity and mortality. Animal survival was estimated by using the Kaplan–Meier and Wilcoxon signed-rank tests. Survival was significantly longer in H1299 lung tumor-bearing animals treated with the DOTAP:Chol–*p53* complex ($P = 0.001$) than in control animals that received either no treatment or treatment with *p53* plasmid DNA or DOTAP:Chol–*CAT* complex (A). It was also significantly longer ($P = 0.0002$) than in control animals treated with DOTAP:DOPE–*p53* complex or nonextruded DOTAP:Chol–*p53* complex (B). H1299 tumor-bearing animals receiving no treatment showed tumor dissemination to various organs and tissues, including the cervical lymph nodes (C), colon (D), mesentery (E), and liver (F). Arrows denote tumors.

and disseminated lung tumors of murine and human origin.

Before testing the therapeutic effect we determined the toxicity and transfection efficiency of the DOTAP:Chol–DNA complexes in subcutaneous tumors, normal lung, and experimental lung metastases. Liver enzyme profile and histopathologic analysis demonstrated no significant liposome–DNA complex mediated toxicity. A single intratumoral injection resulted in 25% of tumor cells expressing the transgene. The ability to deliver and mediate high levels of gene expression throughout solid tumors, albeit at lower levels than adenoviral vectors, following a single injection has not been previously demonstrated. Similarly the type of cells expressing the transgene in the lung has not been previously determined (7). Our study showed that the transgene was expressed primarily in the alveolar

Copyright © The American Society of Gene Therapy

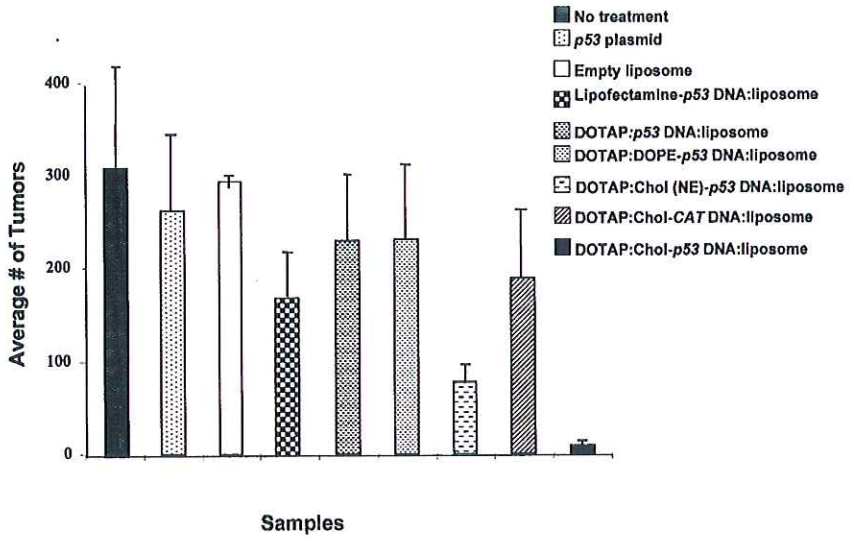


FIG. 12. Inhibition of murine UV2237m lung metastases following treatment with DOTAP:Chol–*p53* complex. UV2237m lung tumor-bearing C3H mice were either not treated or treated daily for a total of six doses (50 μg/dose) with *p53* plasmid DNA, empty liposome, lipofectamine–*p53* complex, DOTAP–*p53* complex, DOTAP:DOPE–*p53* complex, nonextruded DOTAP:Chol–*p53* complex, extruded DOTAP:Chol–*CAT* complex, or extruded DOTAP:Chol–*p53* complex. Each group comprised five animals. The number of tumor nodules was significantly lower ($P = 0.01$) in mice treated with six doses of extruded DOTAP:Chol–*p53* DNA:liposome complex than in the other groups. Bars denote standard errors.

epithelia of type II pneumocyte origin and endothelial cells. Few alveolar macrophages also expressed the transgene.

The ability of the injected DNA:liposome complexes to escape the reticuloendothelial system (RES) and be expressed in epithelial cells was surprising, since previous studies using a variety of formulations have demonstrated RES to be a major target for liposomes (24, 25). Therefore, we further assessed gene expression in alveolar macrophages of Balb/c mice (data not shown). The plasmid used in these experiments contained only a macrophage-specific promoter and enhancer to regulate *Lac-Z* expression. Intravenous tail vein injection of DOTAP:Chol–*Lac-Z* complex showed little or no *LacZ* expression in the lungs; low-level expression was detected infrequently and only at high doses (100 μg of DNA). Therefore, this formulation does not efficiently transfect macrophages in the lung (data not shown). The mechanism by which these DNA:liposome complexes escape the RES system is not well understood, and elucidation of the mechanism was beyond the scope of the present study.

Similarly, a single intravenous injection of a DNA:liposome complex into tumor bearing animals resulted in 10% of tumor cells per tumor expressing the transgene.

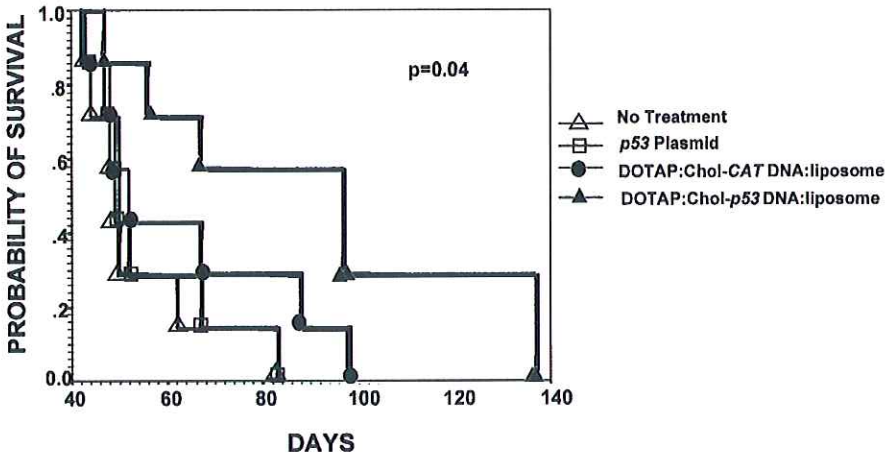


FIG. 14. Prolonged survival in A549 lung tumor bearing mice treated with DOTAP:Chol–*p53* complex. Female BALB/c *nu/nu* mice were injected with 10^6 A549 tumor cells (seven animals/group) via the tail vein. Groups were treated daily, as follows: no treatment (△), *p53* plasmid DNA (□), treatment with the DOTAP:Chol–*CAT* complex (●), or DOTAP:Chol–*p53* complex (▲). Animals in each group received a total of six daily doses (50 μg/dose) and were monitored daily thereafter to assess morbidity and mortality. Animal survival was estimated by using the Kaplan–Meier and Wilcoxon signed-rank tests. Survival was significantly longer ($P = 0.04$) in A549 lung tumor-bearing animals treated with the DOTAP:Chol–*p53* complex than in animals from control groups.

Copyright © The American Society of Gene Therapy

The reason for the discrepancy observed between the percent of tumor cells in the lung and in subcutaneous tumors expressing the transgene is not clear. It is possible that intratumoral injection leads to DNA uptake directly by the tumor cells while systemic delivery leads to DNA uptake through another mechanism, possibly leaky tumor vasculature. Whatever the underlying mechanism(s), the ability of the DNA:liposome complexes to escape the RES, extravasate through endothelial cell junctions, and be expressed in tumor cells is of clinical importance in the treatment of metastatic cancer.

We also determined the ability of these complexes to effectively deliver therapeutic genes and mediate tumoricidal effects in *vivo*. Treatment of subcutaneous tumors with DOTAP:Chol–*p53* or –*FHIT* DNA complexes resulted in tumor shrinkage and, in some cases, complete cures. The possibility that the observed tumoricidal effect was due simply to mechanical disruption or liposomal toxicity was eliminated by demonstrating transgene expression and induction of apoptosis in distinct regions of the tumors. Furthermore, treatment with empty liposomes and other conventional liposome:DNA complexes demonstrated no significant tumor inhibition (data not shown).

Although treatment of subcutaneous tumors with DOTAP:Chol–*FHIT* complex inhibited tumor growth in most cases, tumors in a few treated animals grew slowly but progressively. When treated with a second cycle of six doses, 3 weeks after the first cycle, however, tumors in 33% of these animals demonstrated complete regression, and have been tumor free for more than 9 months (data not shown). Despite the small sample number, these results indicate the feasibility of administering multiple treatments with no treatment resistance.

The ability of the extruded DOTAP:Chol DNA:liposome complexes to eliminate lung tumors when given intravenously was then compared with that of the nonextruded complexes. Repeated treatments with extruded DOTAP:Chol–*p53* complex significantly reduced the number of metastases, compared to nonextruded DOTAP:Chol–*p53*, suggesting that extrusion of DOTAP:Chol liposome is an important component for its function. The lack of resistance to repeated treatments observed in the present study was surprising, since resistance to repeated treatments and suppression of transgene expression has been documented previously (26, 27). One possibility is that experiments in the present study were primarily performed in immunodeficient animals. To further understand this, experiments were performed in syngeneic lung tumor-bearing C3H mice. Repeated multiple treatments resulted in a significantly greater gene expression than a single treatment. Furthermore, multiple treatments with DOTAP:Chol–*p53* yielded a significantly higher therapeutic efficacy in tumor-bearing animals than single treatment. The difference between the results observed in our study and those observed in other studies reflects the type of liposome used and its use in lung tumor bearing animal models. It is possible, as demonstrated by Lopez *et al.* (28), that the inflammatory response is suppressed in these tumor-bearing animals by tumor-derived factors that are not present in tumor-nonbearing animals, thereby allowing greater gene expression.

The ability of DOTAP:Chol–*CAT* complex and the conventional liposome: DNA complex (DOTAP:DOPE–*p53*) to show some tumor-inhibitory effects is not surprising and can be attributed to nonspecific antitumor activity as observed previously with the use of other cationic liposome:DNA complexes (29–31). To further differentiate the observed nonspecific antitumor activity from transgene-mediated specific antitumor activity, *in vivo* experiments were performed. Treatment of UV2237m lung tumors with DOTAP:Chol–*p53* complex resulted in a very significant tumor inhibition when compared to treatments with other cationic liposomes or nonextruded DOTAP:Chol liposomes. These results indicate that the observed tumor-inhibitory activity is mediated only in part by the transgene (*p53, FHIT*) and may be enhanced by the liposome: DNA mixture. Furthermore, histopathologic analysis revealed that DOTAP:Chol–*p53*-treated A549 tumors had been eliminated by apoptotic cell death in the few small tumors that had developed; this contrasts markedly with the relative lack of apoptotic cell death in the several large tumors showing numerous mitoses that developed in the lungs of control mice. Similar to previous observations (32, 33) the ability to eliminate A549 tumors *in vivo* demonstrates the efficiency of using exogenous wild-type *p*53 to suppress tumors with endogenous wild type *p*53. Similar reduction in the number of tumors when treated with DOTAP:Chol–*FHIT* complex, indicates that this effect is not restricted to a single tumor suppressor gene.

To further evaluate the effects of extruded liposomes on disseminated cancer, animal survival experiments were performed. Repeated treatments with DOTAP:Chol–*p53* complex significantly prolonged survival in H1299 or A549 lung tumor bearing mice. In particular 33% of the H1299 tumor-bearing animals were alive at the end of the experiment (150 days), suggesting that tumor cells at multiple metastatic sites were totally eliminated, since mice that died in these experiments all had widely disseminated metastases.

It is interesting that the degree of inhibition of tumor growth appeared to exceed the inhibition expected from the greater transfection efficiency of the improved liposomal vector. This effect has been attributed to p53 mediated bystander effects, and several mechanisms acting in concert are most likely responsible for the bystander effect (2, 3, 12, 34–40). The mechanism by which *FHIT* exerts its tumor suppressive effect is currently not known. Reintroduction of *FHIT* demonstrated upregulation of *p*53 and *p*27 in A549 cells and inhibition of tumor angiogenesis in both, 1299 and A549 lung tumors (unpublished observations). On the basis of these observations, we hypothesize that a bystander effect similar to that observed with *p53* might exist.

The most important observation from the study presented here is that extruded DOTAP:Chol liposome-mediated *p53* and *FHIT* gene delivery can suppress tumor

Copyright © The American Society of Gene Therapy

growth *in vivo* when administered locally and systemically and that this activity is associated with no toxic effects. Our studies further indicated that this extruded liposomal delivery system is restricted by neither gene nor tumor type. Of the greatest consequence are our data indicating that extruded DOTAP:Chol cationic liposome-based tumor gene therapy may be useful either alone or in combination with other therapeutic strategies in the treatment of human cancers *in vivo.*

ACKNOWLEDGMENTS

The authors thank Dr. Neely Atkinson (Department of Biomathematics, The University of Texas M. D. Anderson Cancer Center) and Kelly Willis Merriman for statistical analysis, Stacey Mott and Willie Virgil for technical assistance, and Monica Contreras for preparation of the manuscript. This work was supported in part by Public Health Service Grant P01CA78778-01A1 (J. A. Roth), by the Specialized Program of Research Excellence (SPORE) in Lung Cancer (P50-CA70907) (J. A. Roth), by the Texas Tobacco Settlement Fund, by The M. D. Anderson Cancer Center W. M. Keck Center for Cancer Gene Therapy, by Cancer Center Support (CORE) Grant CA 16672, and by a sponsored research agreement with Introgen Therapeutics, Inc.

REFERENCES

[1] Parker, S. L., Tong, T., Bolden, S., and Wingo, P. A. (1997) Cancer statistics, 1997. *CA Cancer J. Clin.* **47:** 5–27.

[2] Swisher, S. G., *et al.* (1999). Adenoviral-mediated *p53* gene transfer in advanced non-small cell lung cancer. *J. Natl. Cancer Inst.* **91:** 763–771.

[3] Roth, J. A., *et al.* (1996). Retrovirus-mediated wild-type *p53* gene transfer to tumors of patients with lung cancer. *Nat. Med.* **2:** 985–991.

[4] Clayman, G. L., *et al.* (1998). Adenovirus-mediated *p53* gene transfer in patients with advanced recurrent head and neck squamous cell carcinoma. *J. Clin. Oncol.* **16:** 2221–2232.

[5] Nabel, G. J., *et al.* (1993). Direct gene transfer with DNA–liposome complexes in melanoma—Expression, biologic activity, and lack of toxicity in humans. *Proc. Natl. Acad. Sci. USA* **90:** 11307–11311.

[6] Hung, M. C., Wang, S. C., and Hortobagyi, G. (1999). Targeting *HER-2/neu*-overexpressing cancer cells with transcriptional repressor genes delivered by cationic liposome. In *Non Viral Vectors for Gene Therapy* (L. Huang, M. C. Hung, and E. Wagner, Eds.), pp. 357–377. Academic Press, San Diego.

[7] Templeton, N. S., *et al.* (1997). Improved DNA:liposome complexes for increased systemic delivery and gene expression. *Nat. Biotechnol.* **15:** 647–652.

[8] Levine, A. J., Momand, J., and Finlay, C. A. (1991). The *p53* tumour suppressor gene. *Nature* **351:** 453–456.

[9] Mao, L. (1998). Tumor suppressor genes: Does *FHIT* fit? (Editorial Comment). *J. Natl. Cancer Inst.* **90:** 412–414.

[10] Lebeau, M. M., *et al.* (1998). A *FHIT* tumor suppressor gene. *Genes Chromosomes Cancer* **21:** 281–289.

[11] Minna, J. D., and Gazdar, A. F. (1996). Translational research comes of age [comment]. *Nat. Med.* **2:** 974–975.

[12] Cai, D. W., Mukhopadhyay, T., Liu, Y., Fujiwara, T., and Roth, J. A. (1993). Stable expression of the wild-type *p53* gene in human lung cancer cells after retrovirus-mediated gene transfer. *Hum. Gene Ther.* **4:** 617–624.

[13] Fujiwara, T., *et al.* (1993). A retroviral wild-type *p53* expression vector penetrates human lung cancer spheroids and inhibits growth by inducing apoptosis. *Cancer Res.* **53:** 4129–4133.

[14] Sard, L., *et al.* (1999). The tumor-suppressor gene *FHIT* is involved in the regulation of apoptosis and in cell cycle control. *Proc. Natl. Acad. Sci. USA* **96:** 8489–8492.

[15] Ji, L., *et al.* (1999). Induction of apoptosis and inhibition of tumorigenicity and tumor growth by adenovirus vector-mediated *FHIT* gene overexpression. *Cancer Res.* **59:** 3333–3339.

[16] Kanjilal, S., *et al.* (1993). High frequency of *p53* mutations in ultraviolet radiation-induced murine skin tumors: Evidence for strand bias and tumor heterogeneity. *Cancer Res.* **53:** 2961–2964.

[17] Gaensler, K. M. L., *et al.* (1999). Fetal gene transfer by transuterine injection of cationic liposome–DNA complexes. *Nat. Biotechnol.* **17:** 1188–1192.

[18] Couffinhal, T., *et al.* (1997). Histochemical staining following *LacZ* gene transfer underestimates transfection efficiency. *Hum. Gene Ther.* **8:** 929–934.

[19] Hamada, K., *et al.* (1996). Adenovirus-mediated transfer of a wild-type *p53* gene and induction of apoptosis in cervical cancer. *Cancer Res.* **56:** 3047–3054.

[20] Sozzi, G., *et al.* (1997). Absence of Fhit protein in primary lung tumors and cell lines with *FHIT* gene abnormalities. *Cancer Res.* **57:** 5207–5212.

[21] Georges, R. N., Mukhopadhyay, T., Zhang, Y., Yen, N., and Roth, J. A. (1993). Prevention of orthotopic human lung cancer growth by intratracheal instillation of a retroviral antisense K-*ras* construct. *Cancer Res.* **53:** 1743–1746.

[22] Kataoka, M., *et al.* (1998). An agent that increases tumor suppressor transgene product coupled with systemic transgene delivery inhibits growth of metastatic lung cancer *in vivo*. *Cancer Res.* **58:** 4761–4765.

[23] Fujiwara, T., *et al.* (1994) Induction of chemosensitivity in human lung cancer cells *in vivo* by adenoviral-mediated transfer of the wild-type *p53* gene. *Cancer Res.* **54:** 2287–2291.

[24] Liu, Y., *et al.* (1997). Factors influencing the efficiency of cationic liposome-mediated intravenous gene delivery. *Nat. Biotechnol.* **15:** 167–173.

[25] McLean, J. W., Thurston, G., and McDonald, D. M. (1999). Sites of uptake and expression of cationic liposome/DNA complexes injected intravenously. In *Non Viral Vectors for Gene Therapy* (L. Huang, M. C. Hung, and E. Wagner, Eds.), pp. 119–135. Academic Press, San Diego.

[26] Li, S., *et al.* (1999). Effect of immune response on gene transfer to the lung via systemic administration of cationic lipidic vectors. *Am. J. Physiol.* **276:** L796–L804.

[27] Song, Y. K., *et al.* (1997). Characterization of cationic liposome-mediated gene transfer *in vivo* by intravenous administration. *Hum. Gene Ther.* **8:** 1585–1594.

[28] Lopez, D. M., *et al.* (1996). Cytokine production by lymphoreticular cells from mammary tumor bearing mice: The role of tumor-derived factors. *Anticancer Res.* **16:** 3923–3930.

[29] Lesoonwood, L. A., Kim, W. H., Kleinman, H. K., Weintraub, B. D., and Mixson, A. J. (1995). Systemic gene therapy with *p53* reduces growth and metastases of a malignant human breast cancer in nude mice. *Hum. Gene Ther.* **6:** 395–405.

[30] Dow, S. W., *et al.* (1999). Lipid–DNA complexes induce potent activation of innate immune responses and antitumor activity when administered intravenously. *J. Immunol.* **163:** 1552–1561.

[31] Whitmore, M., *et al.* (1999). LPD lipopolyplex initiates a potent cytokine response and inhibits tumor growth. *Gene Ther.* **6:** 1867–1875.

[32] Cajot, J. F., *et al.* (1992). Growth suppression mediated by transfection of p53 in Hut292DM human lung cancer cells expressing endogenous wild-type *p53* protein. *Cancer Res.* **52:** 6956–6960.

[33] Hsiao, M., *et al.* (1997). Intracavitary liposome-mediated *p53* gene transfer into glioblastoma with endogenous wild-type *p53 in vivo* results in tumor suppression and long-term survival. *Biochem. Biophys. Res. Commun.* **233:** 359–364.

[34] Munshi, A., Ramesh, R., Marrogi, A., and Freeman, S. (1997). Evaluation of adenovirus *p53* mediated bystander effect *in vivo*. *Proc. Am. Assoc. Cancer Res.* **38:** 343. [abstract]

[35] Rizk, N., *et al.* (1996). Evaluation of the bystander effect in adeno virus mediated *p53* gene therapy. *Cancer Gene Ther.* **3:** 536. [abstract]

[36] Nishizaki, M., *et al.* (1999). Recombinant adenovirus expressing wild-type *p53* is antiangiogenic: A proposed mechanism for bystander effects. *Clin. Cancer Res.* **5:** 1015–1023.

[37] Dameron, K. M., Volpert, O. V., Tainsky, M. A., and Bouck, N. (1994). Control of angiogenesis in fibroblasts by p53 regulation of thrombospondin-1. *Science* **265:** 1582–1584.

[38] Bouvet, M., *et al.* (1998). Adenovirus-mediated wild-type *p53* gene transfer down-regulates vascular endothelial growth factor expression and inhibits angiogenesis in human colon cancer. *Cancer Res.* **58:** 2288–2292.

[39] Owen-Schaub, L. B., *et al.* (1995). Wild-type human *p53* and a temperature-sensitive mutant induce Fas/APO-1 expression. *Mol. Cell. Biol.* **15:** 3032–3040.

[40] Owen-Schaub, L. B., Cusack, J. C., Kruzel, E., Bucana, C. D., and Roth, J. A. (1998). Induction of Fas expression and sensitivity by adenoviral-mediated p53 gene transfer in a non-small cell lung carcinoma: Implications for gene therapy for lung cancer. *Proc. Am. Assoc. Cancer Res.* **39:** 78. [abstract]

Copyright © The American Society of Gene Therapy

VOLUME 22 · NUMBER 16 · AUGUST 15 2004

JOURNAL OF CLINICAL ONCOLOGY ORIGINAL REPORT

Expression of Hepatoma-Derived Growth Factor Is a Strong Prognostic Predictor for Patients With Early-Stage Non–Small-Cell Lung Cancer

Hening Ren, Ximing Tang, J. Jack Lee, Lei Feng, Allen D. Everett, Waun Ki Hong, Fadlo R. Khuri, and Li Mao

From the Department of Thoracic/Head and Neck Medical Oncology, Departments of Biostatistics, Department of Pathology, The University of Texas M.D. Anderson Cancer Center, Houston, TX; Department of Pediatrics, The Johns Hopkins University, School of Medicine, Baltimore, MD.

Submitted February 10, 2004; accepted May 20, 2004.

Supported in part by Department of Defense Grant DAMD17-01-1-0689-1; and National Cancer Institute Grants PO1 CA91844, UO1 CA86390, and P30 CA 16620.

Authors' disclosures of potential conflicts of interest are found at the end of this article.

Address reprint requests to Li Mao, MD, Department of Thoracic/Head and Neck Medical Oncology, Unit 432, The University of Texas M.D. Anderson Cancer Center, 1515 Holcombe Blvd, Houston, TX 77030; e-mail: lmao@mdanderson.org.

© 2004 by American Society of Clinical Oncology

0732-183X/04/2216-3230/$20.00

DOI: 10.1200/JCO.2004.02.080

ABSTRACT

Purpose
Hepatoma-derived growth factor (HDGF), which is unrelated to hepatocyte growth factor, can stimulate DNA synthesis and cell proliferation on entering the nucleus. We hypothesize that HDGF plays an important role in biologic behavior of early-stage non–small-cell lung cancer (NSCLC).

Patients and Methods
Ninety-eight patients with pathologic stage I NSCLC who underwent curative surgery were studied. Immunohistochemistry was used to determine the expression level of HDGF in the tumor specimens. The intensity of the protein staining and percentage of stained tumor cells were used to determine a labeling index. Statistical analyses, all two-sided, were performed to determine the prognostic effect of HDGF expression levels on clinical parameters and outcomes.

Results
The mean ± standard deviation HDGF labeling index in the 98 tumors was 185 ± 41. Patients whose tumors had higher HDGF indexes (≥ 185) had a significantly poorer probability of overall survival at 5 years after surgery than did those with lower HDGF indexes (0.26 *v* 0.82; $P < .0001$). Similarly, the 5-year disease-specific and disease-free survival probabilities were lower in those with higher HDGF indexes (0.42 *v* 0.92, and 0.34 *v* 0.71; $P < .0001$ and $P = .0008$; respectively). Multivariate analysis indicated that HDGF level was an independent predictor of overall, disease-specific, and disease-free survivals.

Conclusion
Overexpression of HDGF is common in early-stage NSCLC. The expression level in tumor cells is strongly correlated with poor overall, disease-specific, and disease-free survivals, suggesting HDGF may be a powerful prognostic marker for patients with early-stage NSCLC.

J Clin Oncol 22:3230-3237. © 2004 by American Society of Clinical Oncology

INTRODUCTION

Lung cancer is the most common cause of cancer-related death in the United States, accounting for more deaths than those caused by prostate, breast, and colorectal cancers combined.[1] The prognosis for patients with lung cancer is correlated with disease stage at the time of diagnosis. Patients with stage I non–small-cell lung cancer (NSCLC), the earliest stage in current staging system, have a 5-year survival rate of approximately 60%, whereas patients with stage II to IV disease have 5-year survival rates ranging from 40% to less than 5%.[2,3] Unfortunately, even among patients with stage I NSCLC, 40% will die of the disease within 5 years after potentially curative surgery. Recent studies have shown that patients with early stage NSCLC may benefit from adjuvant chemotherapy following curative surgical attempt.[4,5] These findings may lead the adjuvant chemotherapy to become standard care for those patients. However, only 4% of the patients may actually benefit from such therapy, while most of the patients will suffer undesired and potentially fatal side effects.[5] Therefore, the identification of novel strategies to further stratify such patients

Information downloaded from jco.ascopubs.org and provided by at M D ANDERSON HOSP on October 7, 2010 from
Copyright © 2004 American Society of Clinical Oncology. All rights reserved.

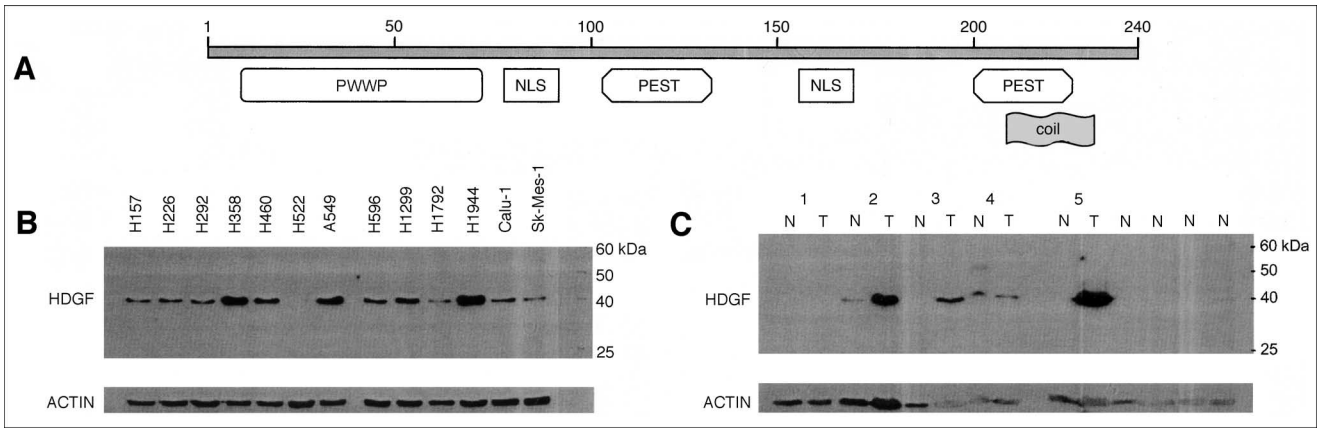


Fig 1. (A) Putative domains of hepatoma-derived growth factor (HDGF). (B) HDGF expression in non–small-cell lung cancer (NSCLC) cell lines and paired normal lung tissue specimens and primary NSCLC specimens, as well as (C) normal lung tissue specimens from patients without primary lung cancer (patients with metastatic lung tumors). Actin is used as a loading control. N, normal lung tissue specimens; T, primary NSCLC specimens.

based on their likelihood to benefit from an adjuvant therapy is an unmet need.

Hepatoma-derived growth factor (HDGF), which is unrelated to hepatocyte growth factor, is a heparin-binding growth factor originally purified from media conditioned with the human hepatoma cell line HuH-7, and can stimulate proliferation of Swiss 3T3 cells.[6] The amino acid sequence, as deduced from a cDNA clone of HDGF, contains 240 residues with a motif homologous to the consensus sequences of bipartite nuclear localization sequence and a DNA-binding PWWP motif (Fig 1A). The precise function of HDGF is unknown. Recent studies indicate that HDGF is highly expressed during early development of many tissues, including cardiovascular,[7] kidney,[8] and liver[9] tissues. Although lacking the typical secretory sequence present in most secretory proteins,[10] HDGF has been shown to act as a potent exogenous mitogen for HuH-7,[11] COS-7,[11] aortic vascular smooth muscle cells,[12] and endothelia cells.[8]

We found that HDGF is overexpressed in NSCLC cell lines and primary tumors compared to normal lung tissues. To determine the importance of HDGF in the biologic behavior of NSCLC, we further studied HDGF expression in tumor specimens from 98 patients with pathologic stage I NSCLC. The patients were treated with potentially curative surgery with a median follow-up of 10 years. Expression levels of HDGF in the primary tumors were compared to clinical parameters and outcomes.

PATIENTS AND METHODS

Study Population

Patients were included in the study if they were diagnosed with pathologic stage I NSCLC; had undergone lobectomy or pneumonectomy for complete resection of their primary tumors at The University of Texas M.D. Anderson Cancer Center (Houston, TX) from 1975 through 1990; had not received adjuvant chemotherapy or radiation therapy before or after surgery; had at least 5 years of follow-up data; and had adequate paraffin-embedded tissue sections available in the institution's tumor archive. During the period between 1975 and 1990, a total of 588 patients were diagnosed as having pathologic stage I NSCLC and treated surgically at M.D. Anderson. Tissue sections were available for 105 of these 588 patients, and sections from 98 patients contained adequate tumor cells for evaluation. The follow-up information was based on chart review and from reports from the M.D. Anderson tumor registry service. The study was reviewed and approved by the institution's Surveillance Committee to allow us to study the tissues and pertinent follow-up information. Tissue sections were from each tissue block, stained with hematoxylin-eosin, and reviewed to confirm the diagnosis and the presence or absence of tumor cells. NSCLC cell lines (H157, H226, H292, H358, H460, H522, A549, H596, H1299, H1792, H1944, Calu-1, and SK-Mes-1) used in the study were obtained from American type Culture Collection (Manassas, VA) and were grown in RPMI-1640 median with 10% fetal bovine serum (Life Technologies Inc, Rockville, MD).

Immunohistochemical Analysis

Tissue sections (4 μm thick) from formalin-fixed and paraffin-embedded tissue blocks were mounted on positively charged glass slides. Slides were baked at 60°C for 1 hour and then deparaffinized through a series of xylene baths. Rehydration was performed with graded concentrations of alcohol. To retrieve antigenicity, tissue sections were treated with microwaves in 10 mmol/L citrate buffer (pH 6.0) for 10 minutes. The sections were then immersed in methanol containing 0.3% hydrogen peroxidase for 20 minutes to block the endogenous peroxidase activity, and incubated in 2.5% blocking serum for 30 minutes to reduce nonspecific binding. Sections were incubated overnight at 4°C with an affinity-purified rabbit polyclonal antibody produced against the COOH-terminal amino acids (222-237) of the mouse HDGF sequence at a dilution of 1:4000 rabbit anti-HDGF polyclonal antibody,[12] followed by incubation for 30 minutes with biotinylated antirabbit immunoglobulin G (Vector Laboratories, Burlingame, CA). The sections were then processed using standard avidin-biotin immunohistochemistry according to the manufacturer's recommendations. Diaminobenzidine was used as a chromogen, and commercial hematoxylin was used for counterstaining.

Information downloaded from jco.ascopubs.org and provided by at M D ANDERSON HOSP on October 7, 2010 from
Copyright © 2004 American Society of Clinical Oncology. All rights reserved.

The HDGF labeling index was defined as the weighted mean of percentage of tumor cells displaying nuclear immunoreactivity (calculated by counting the number of HDGF positive tumor cells among at least 1,000 tumor cells for each tissue section manually) multiplied by the degree of the staining intensity (1, 2, or 3, defined as weak staining, moderate staining, or strong staining, respectively). The final index of each tumor was the average of indices generated by two observers (H.R. and X.T.). The differences between the two observers were less than 20% in almost all cases. The weak staining in the smooth muscle cells of blood vessels was used as an internal control and the basis for the intensity score. Almost all tumor cells showed some degree of staining.

Western Blot Analysis

Tissues or cells were either homogenized or harvested in lysis buffer 50 mmol/L HEPES, 1% Triton X-100, 10 mmol/L NaF, 30 mmol/L Na3P04, 150 mmol/L NaCl, and 1 mmol/L EDTA and freshly added 10 mmol/L glycerophosphate, 1 mmol/L Na3VO4, 20 μg/mL pepstatin A, 10 μg/mL aprotinin, 20 μg/mL leupeptin, and 40 μmol/L microcystin-LR. Twenty micrograms of total proteins from each sample was separated in sodium dodecyl sulfate-polyacrylamide gel electrophoresis using a Bio-Rad Mini-Protean II apparatus (Schleicher & Schuell BioScience, Keene, NH), and separated proteins in the gels were transfered to nitrocellulose membrane. The membranes were then blocked with 5% nonfat milk for 2 hours at room temperature followed by incubation with the rabbit anti-HDGF antibody (1:10,000 dilution) at 4° C overnight. The immune reactive band was detected using a goat-antirabbit immunoglobulin G horseradish peroxidase conjugate (1:10,000; Jackson ImmunoResearch Lab, West Grove, PA,) as the secondary antibody and SuperSignal West Pico Substrate (Pierce Biotechnology, Rockford, IL) as the detection agent. A mouse antiactin monoclonal antibody AC-15 (Sigma, St. Louis, MO) was used to normalize protein loading.

Statistical Analysis

Survival probability as a function of time was computed by the Kaplan-Meier estimator. The variance of the Kaplan-Meier estimator was computed by the Greenwood formula. The 5-year survival probabilities were estimated and compared by the asymptotic z between the high expression and low expression groups. The log-rank test was used to compare patients' survival time between groups. Overall, disease-specific (ie, those who died of lung cancer-related causes specifically), and disease-free (ie, those who developed recurrence and/or metastasis) survivals were analyzed. HDGF-labeling index was analyzed as a continuous variable as well as a categoric variable. The mean labeling index and quartiles of the labeling index were used as cutoff points for HDGF in the survival analysis. The χ^2 test was used to test equal proportion between groups in two-way contingency tables. Cox regression was used to model the risks of HDGF expression level on survival time, with adjustment for clinical and histopathologic parameters (age, sex, race, smoking status, and histologic subgroup). Martingale residual analysis was used to determine the functional form for HDGF (untransformed data on the continuous scale) to best explain its effect on survival through a Cox regression model. The Martingale residual plots using the Martingale residuals, from a Cox model that includes only baseline hazard function but no covariate, on the vertical axis and HDGF on the horizontal axis were provided. By applying a nonparametric smoother to create a line, the plots allow one to examine visually the nature of the relationship between the residuals and the HDGF scores. Appropriate transformation and/or cutoff points can be chosen accordingly. All statistical tests are two-sided and a P value of .05 or lower was considered statistically significant.

RESULTS

Of the 98 patients included in this study, 71 patients died, and 27 patients were still alive at the time of last follow-up. Among the 71 patients who died, 29 died of lung cancer, and 42 died of other causes including heart diseases, respiratory diseases, and other organ failures. The median follow-up time was 10.1 years among the patients who remained alive. Patient ages at the time of diagnosis ranged from 37 to 82 years, with a median age of 62.5 years; this is similar to the age distribution in a large database of NSCLC at M.D. Anderson (data not shown). Twenty-four (24%) of the patients were women, and 74 (76%) were men, which is comparable to the sex distribution of the disease in the 1970s and 1980s.[2] Ninety-six percent of the patients were smokers or former smokers. The histology types of squamous, adenocarcinoma, and others were found in 40%, 45%, and 15% of the patients, respectively. The 5-year overall survival rate was 55%, and the 5-year disease-specific survival rate was 71% in our patient population; these rates are similar to the rates reported in a previous study with a large number of cases from our institution.[13] The general clinical characteristics of the patients are shown in Table 1.

The high expression of HDGF in NSCLC was observed by Western blot analysis in NSCLC cell lines and primary tumors (Fig 1B and C). A single band of molecular weight about 40 kDa was detected in all 13 NSCLC cell lines using the anti-HDGF antibody (Fig 1B). Overexpression of HDGF was observed in three of five primary NSCLC tumors compared to corresponding normal lung tissues, as well as in four normal lung tissues from patients with lung metastasis of other organ origins (Fig 1C).

We analyzed the expression status of HDGF protein in the 98 primary tumor samples from patients with pathologic stage I NSCLC by immunohistochemistry using a polyclonal anti-HDGF antibody. HDGF staining was observed in all tumor sections but at various intensities (Fig 2). Strong nuclear staining with minimal cytoplasmic staining was observed in many lung adenocarcinomas (Fig 2A through C). The staining intensity was in general weaker and more variable in squamous cell type (Fig 2D and E). The mean labeling index was 185[14] in the overall tumor population with range from 100 to 291. The quartiles of the HDGF labeling index were 158, 182.5, and 211, respectively (25th, 50th, and 75th percentiles). Thirty-four percent of the adenocarcinomas exhibited an HDGF labeling index more than 211 (highest quartile) while only 15% of the squamous cell carcinomas did so; however, this difference was not statistically significant ($P = .09$). Weak cytoplasmic

Information downloaded from jco.ascopubs.org and provided by at M D ANDERSON HOSP on October 7, 2010 from
Copyright © 2004 American Society of Clinical Oncology. All rights reserved.

Table 1. Demographic Characteristics of the Patient Population by HDGF Expression

Characteristic	HDGF < 185 No. of Patients	HDGF < 185 %	HDGF ≥ 185 No. of Patients	HDGF ≥ 185 %	Total No. of Patients	Total %
	(n = 51; 52%)		(n = 47; 48%)		(N = 98)	
Sex						
Male	39	53	35	47	74	76
Female	12	50	12	50	24	24
Age, years						
Mean	62.7		63.0		62.8	
SD	10.4		8.7		9.6	
Smoking status						
Smoker	48	53	42	47	90	96
Nonsmoker	1	25	3	75	4	4
Histology						
Squamous	24	62	15	38	39	40
Adeno	21	48	23	52	44	45
Other*	6	40	9	60	15	15
Five-year survival probability						
Overall	.82		.26		.55	
95% CI	.72 to .93		.16 to .43		.46 to .66	
Disease-specific	.92		.42		.71	
95% CI	.84 to 1.0		.28 to .62		.61 to .81	
Disease-free	.71		.34		.55	
95% CI	.60 to .85		.22 to .53		.46 to .66	

NOTE. Percentages are the row percentage of HDGF groups in each category of the variables (first two columns) and the percentage of each category for each variable (last column).
Abbreviations: HDGF, hepatoma-derived growth factor; SD, standard deviation.
*Other histology types: bronchioalveoli (seven patients), large cell (three patients), and mixed (five patients).

staining was observed in some HDGF-positive squamous carcinoma cells. In normal lung tissues, vascular smooth muscle cells might show weak staining and were used as an internal control (intensity level 1). In normal lung tissues, the HDGF expression level was low (Fig 2F). The HDGF expression level was not associated with age, sex, or race. In 40 tumors, HDGF expression and the expression of the proliferation marker Ki-67[14] were compared. We failed to observe an association between the two markers (Spearman's correlation coefficient = 0.1; $P = .52$).

In our analysis of potential associations between the level of HDGF in the primary tumors and survival, we found that patients whose primary tumors exhibited a high level of HDGF (when the mean labeling index of 185 was used as a cut-off point) had a significantly poorer overall survival probability ($P < .0001$, log-rank test). The probability of overall survival at 5 years after surgery was 0.82 (95% CI, 0.72 to 0.93) for patients whose tumors showed a low HDGF labeling index (< 185) compared with 0.26 (95% CI, 0.16 to 0.43) for patients whose tumors showed a high HDGF labeling index (≥ 185; Fig 3A). The probability of overall survival at 10 years after surgery was also lower for patients whose tumors had a high HDGF labeling index, but the difference was smaller compared to that at 5 years, probably as a result of an increase in non–cancer-related deaths over time in this patient population (median age of 62.5 years and 96% smokers; Fig 3A). The striking difference in disease-specific survival at 5 years remained at 10 years after surgery and beyond between the high HDGF group and the low HDGF group (Fig 3B). The probability of 5-year disease-specific survival was 0.92 (95% CI, 0.84 to 1.00) for patients with a lower HDGF labeling index compared with only 0.42 (95% CI, 0.28 to 0.62) for the group with a high HDGF labeling index. The disease-specific survival probability was highly significantly different between the two groups ($P < .0001$, log-rank test). Consistent with a role of HDGF in development of recurrence or metastasis, patients whose tumors expressed a higher level of HDGF had significantly poorer disease-free survivals ($P = .0008$, log-rank test; Fig 3C). The probability of 5-year disease-free survival was 0.71 (95% CI, 0.60 to 0.85) for patients with a high HDGF labeling index compared with 0.34 (95% CI, 0.22 to 0.53) for the group with a high HDGF labeling index.

To evaluate the robustness of the prognostic value of HDGF labeling index, we further divided the patients into four groups based on quartiles of HDGF labeling indexes and compared the survival probabilities of the groups. As the HDGF labeling index increases, overall survival (Fig 3D;

Information downloaded from jco.ascopubs.org and provided by at M D ANDERSON HOSP on October 7, 2010 from
Copyright © 2004 American Society of Clinical Oncology. All rights reserved.
DOI: 10.1200/JCO.2004.11.026

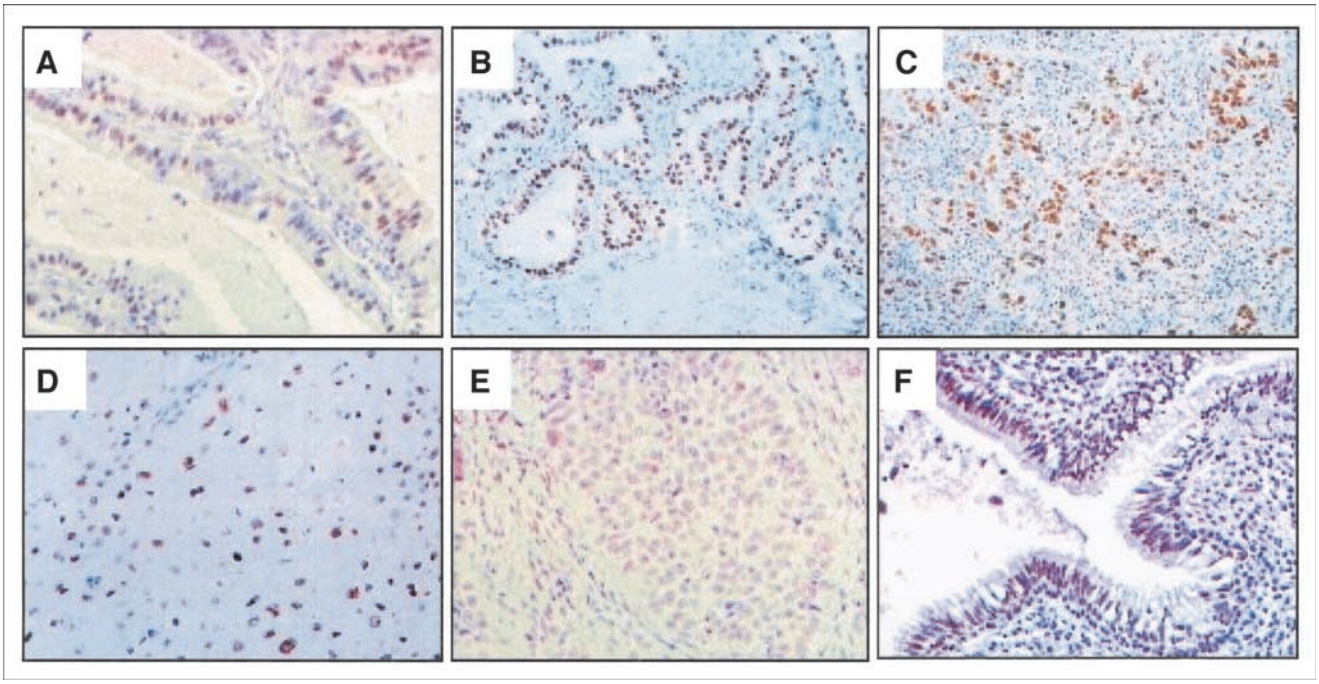


Fig 2. Hepatoma-derived growth factor expression detected by immunohistochemistry in lung adenocarcinomas (A, B, and C), lung squamous cell carcinomas (D and E) and bronchial epithelium in adjacent normal lung tissue (F).

$P < .0001$), disease-specific survival (Fig 3E; $P < .0001$), and disease-free survival (Fig 3F; $P = .0002$) decreased. When we compared patients whose tumors exhibited a labeling index less than 158 (the lowest quartile) with those whose tumors exhibited a labeling index ≥ 211 (the highest quartile), the difference in the survival probabilities was striking. At 5 years, none of the patients in the lowest quartile had died, while 84% of the patients in the highest quartile had died of any cause (95% CI, 0.07 to 0.40) and 76% died of lung cancer (95% CI, 0.11 to 0.54). Consistently, only 12% of the patients at the lowest quartile developed recurrence or metastasis at 5 years compared to 80% of the patients at the highest quartile.

To determine whether HDGF expression level is an independent factor in predicting survival probability for patients with pathologic stage I NSCLC, we performed multicovariable analysis using the Cox model. We found that HDGF expression level was the only independent predictor of disease-specific and disease-free survival probabilities ($P < .0001$) among the parameters tested, including age, sex, race, smoking status, and tumor histology. When overall survival was analyzed, HDGF expression level remained the most significant independent predictor ($P < .0001$); not surprisingly, age was also an independent predictor for overall survival ($P = .0002$). Martingale residual analysis showed that the Cox model fit the data well. It was confirmed that there was a linear relationship of higher HDGF and poorer overall, disease-specific, and disease-free survivals, suggesting that the higher the HDGF expression, the worse the clinical outcome observed in early stage NSCLC patients (Fig 4).

DISCUSSION

The capability of exogenous HDGF to stimulate the growth of fibroblasts and HuH-7 cells, aortic endothelial cells, and vascular smooth muscle cells[15] supports its role as a growth factor. Structurally, HDGF has a significant homology with the high-mobility group-1 DNA-binding protein,[11] but lacks the high-mobility box responsible for DNA binding. However, HDGF contains a PWWP domain at its *N*-terminal. The PWWP domain is a weakly conserved sequence motif found in over 50 eukaryotic proteins, including the mammalian DNA methyltransferases Dnmt3a and Dnmt3b, the transcription coactivator PC4, and the DNA mismatch repair protein MSH6,[16] all important in tumorigenesis. The precise function of the PWWP domain is not clear, but in the case of Dnmt3b, this domain has been shown to have a direct DNA-binding capability.[17] HDGF also contains two nuclear localization cassettes, two PEST (proline, glutamic/aspartic, serine, and threonine rich) domains, and a putative coiled-coil structure (Fig 1A). Recent studies have shown that nuclear localization is required for HDGF-mediated DNA synthesis and growth stimulation,[15,18] suggesting a role of HDGF as a transcription factor.

The finding that the expression level of HDGF in NSCLC strongly correlates with patients' clinical outcomes

Information downloaded from jco.ascopubs.org and provided by at M D ANDERSON HOSP on October 7, 2010 from
Copyright © 2004 American Society of Clinical Oncology. All rights reserved.

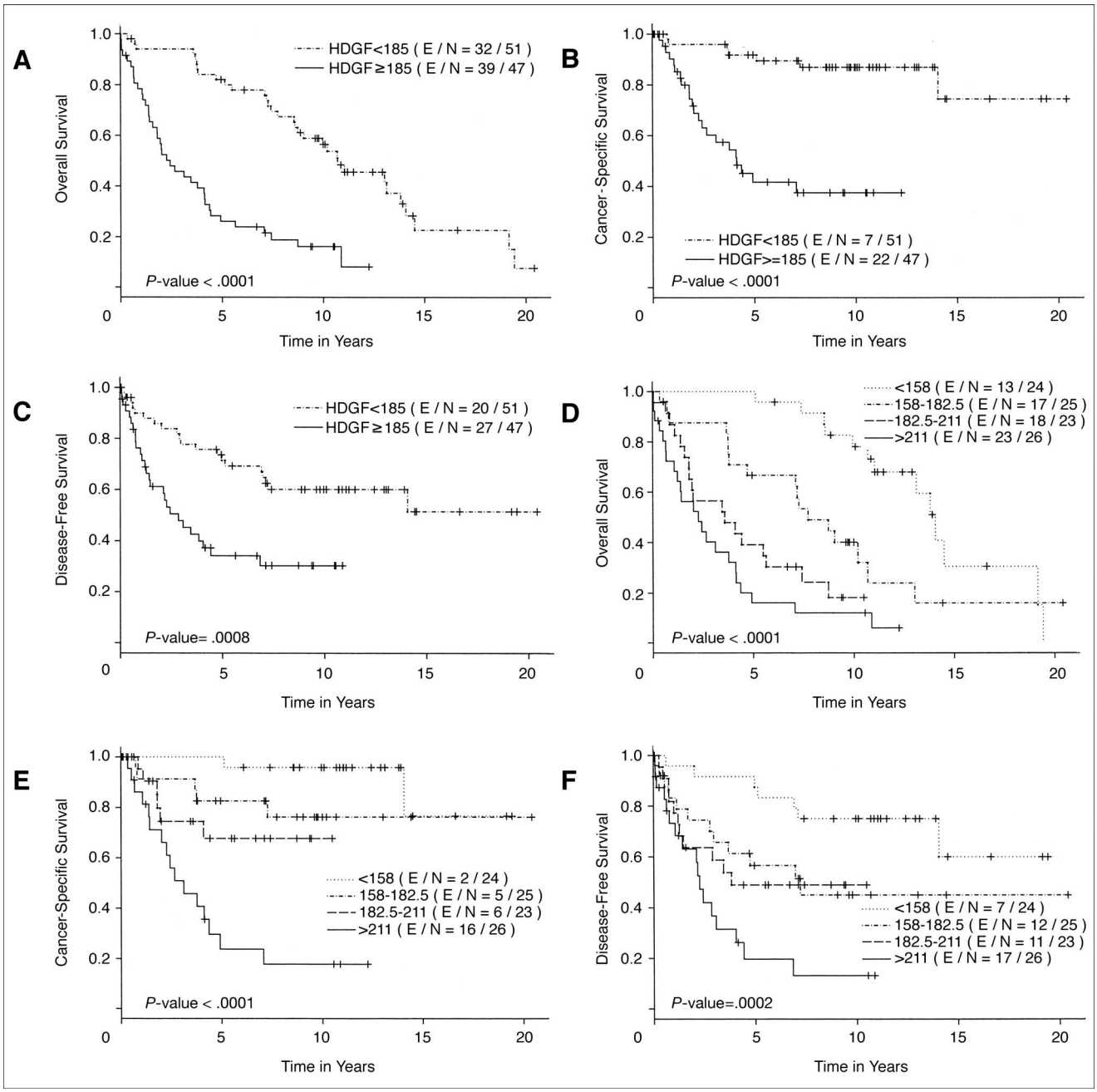


Fig 3. Probability of (A, D) overall survival; (B, E) cancer-specific survival; and (C, F) disease-free survival by levels of hepatoma-derived growth factor (HDGF) expression in primary non–small-cell lung cancer (NSCLC). The Kaplan-Meier method was used to determine the survival probability, and the log-rank test was used to compare the survival curves between groups.

suggests that HDGF plays an important role in lung tumorigenesis and in the determination of the biologic behavior of NSCLC. The analysis of HDGF labeling index by quartiles indicated a dose-dependent relationship between HDGF expression and survivals (Figs 3D through F). The striking differences between the patients in the lowest quartile and those in the highest quartile are consistent with the fact that the scoring method used for immunohistochemistry is more objective for cells expressing a very high level of proteins or a very low level of proteins while more subjective for cells expressing a medium level of proteins. A linear relationship between the HDGF expression level and patients' clinical outcome was further confirmed by using Martingale residual analysis (Fig 4). In the multivariate analysis, HDGF expression was an independent predictor of overall, disease-specific, and disease-free survivals. The consistency of

Information downloaded from jco.ascopubs.org and provided by at M D ANDERSON HOSP on October 7, 2010 from
Copyright © 2004 American Society of Clinical Oncology. All rights reserved.

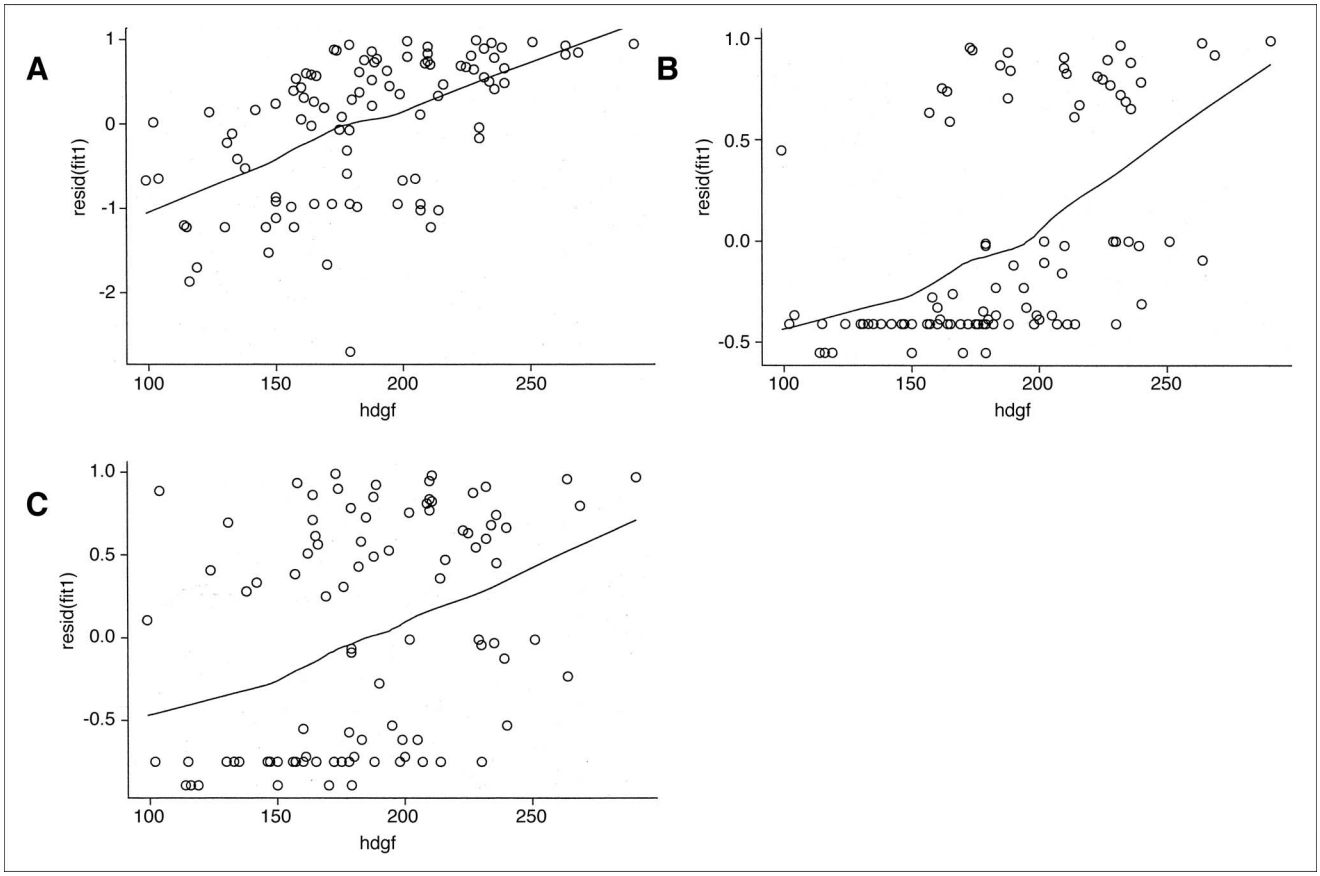


Fig 4. Martingale residual analysis shown as scatter plots of null Martingale residuals versus hepatoma-derived growth factor expressions. A linear trend was revealed in each subpanel by fitting the nonparametric, lowess-smoothing regression lines through the data points. (A) overall survival; (B) cancer-specific survival; and (C) disease-free survival.

the results from different statistical analyses may allow us to conclude that HDGF has an important role in determining the behavior of NSCLC and is a promising biomarker for classifying patients with early-stage NSCLC. Given the advances in adjuvant therapy,[5] it must now be considered to offer adjuvant chemotherapy to patients whose primary tumors have been surgically resected in a curative attempt because 4% of these patients may benefit from such additional treatment. If it becomes standard care, however, most of the patients will suffer unwanted toxicity, which can be fatal to some patients, without gaining benefit in survival and quality of life. Therefore, the identification of patients with the highest risk of dying of lung cancer after potentially curative surgical treatment is a critical step in selecting patients for subsequent treatment with adjuvant therapy.

Although this study was not designed to provide direct evidence demonstrating that HDGF promotes tumorigenesis or facilitates metastasis, our findings together with data from previous reports provide a strong rationale to suggest such possibilities. In an in vitro study, Kishima et al[19] showed that downregulation of HDGF by antisense oligonucleotides can inhibit proliferation of hepatoma cell lines. Besides being mitogenic, HDGF has been shown to play a role in renal vascular development and in vascular lesion formation.[8] Mori et al[20] recently reported that HDGF can stimulate proliferation of lung epithelial cells in both in vitro and in vivo models. Therefore, HDGF may promote proliferation of tumor cells, as well as serve as a paracrine factor to facilitate neovascular formation, which is important for invasion and metastasis. Interestingly, we did not observe a correlation between HDGF and Ki-67 expression in the present study, suggesting that HDGF contributes to the aggressive biologic behavior through its paracrine activity rather than by stimulating tumor cell proliferation. We have, in fact, noticed that tumor cells at the invading front and metastases in lymph nodes exhibited stronger HDGF staining compared with the noninvading cells and the primary tumor sites (Tang and Mao, unpublished data). Interestingly, there were nine patients who developed brain metastasis after surgery in this study population. Eight of the nine patients were in the high HDGF group. The only patient whose primary tumor had a low HDGF labeling index developed brain metas-

Information downloaded from jco.ascopubs.org and provided by at M D ANDERSON HOSP on October 7, 2010 from
Copyright © 2004 American Society of Clinical Oncology. All rights reserved.

tasis 6 months after surgery but survived for more than 6 years (data not shown).

In summary, our data demonstrated that HDGF expression is quantitatively associated with poor prognosis in all three types of clinical outcomes (disease-free survival, disease-specific survival, and overall survival) and strongly suggests that HDGF is involved in the disease aggressiveness, progression, and lethality. HDGF is a promising prognostic marker, not only to identify individuals with poor prognostic potential for more aggressive treatment, but also point to a new direction for searching effective molecular targeted therapies.

Note: The anti-HDGF antibody used in this study and/or monoclonal antibodies we are developing currently will be made available upon request.

Authors' Disclosures of Potential Conflicts of Interest

The authors indicated no potential conflicts of interest.

REFERENCES

1. Parkin DM, Pisani P, Ferlay J: Global cancer statistics. CA Cancer J Clin 49:33-64, 1999

2. Jemal A, Thomas A, Murray T, et al: Cancer statistics, 2002. CA Cancer J Clin 52:23-47, 2002

3. Willians DE, Pariolero PC, Davis CS, et al: Survival of patients surgically treated for stage I lung cancer. J Thorac Cardiovasc Surg 82:70-76, 1981

4. Chemotherapy in non-small cell lung cancer: A meta-analysis using updated data on individual patients from 52 randomised clinical trials. Non-small Cell Lung Cancer Collaborative Group. BMJ 311:899-909, 1995

5. Le Chevalier T, for the IALT Investigators: Results of the randomized international adjuvant lung cancer trial (IALT): Cisplatin-based chemotherapy (CT) vs no CT in 1,867 patients with resected non–small-cell lung cancer. Proc Am Soc Clin Oncol 22:2, 2003 (abstr 6)

6. Nakamura H, Kambe H, Egawa T, et al: Partial purification and characterization of human hepatoma-derived growth factor. Clin Chim Acta 183:273-284, 1989

7. Everett AD: Identification, cloning, and developmental expression of hepatoma-derived growth factor in the developing rat heart. Dev Dyn 222:450-458, 2001

8. Oliver JA, Al-Awqati Q: An endothelial growth factor involved in rat renal development. J Clin Invest 102:1208-1219, 1998

9. Enomoto H, Yoshida K, Kishima Y, et al: Hepatoma-derived growth factor is highly expressed in developing liver and promotes fetal hepatocyte proliferation. Hepatology 36:1519-1527, 2002

10. von Heijne G: A new method for predicting signal sequence cleavage sites. Nucleic Acids Res 14:4683-4690, 1986

11. Nakamura H, Izumoto Y, Kambe H, et al: Molecular cloning of complementary DNA for a novel human hepatoma-derived growth factor. Its homology with high mobility group-1 protein. J Biol Chem 269:25143-25149, 1994

12. Everett AD, Lobe DR, Matsumura ME, et al: Hepatoma-derived growth factor stimulates smooth muscle cell growth and is expressed in vascular development. J Clin Invest 105:567-575, 2000

13. Mountain CF: Value of the new TNM system staging system for lung cancer. Chest 96: 47S-49S, 1989

14. Soria JC, Jang SJ, Khuri FR, et al: Overexpression of cyclin B1 in early-stage non–small-cell lung cancer and its clinical implication. Cancer Res 60:4000-4004, 2000

15. Everett AD, Stoops T, McNamara CA: Nuclear targeting is required for hepatoma-derived growth factor-stimulated mitogenesis in vascular smooth muscle cells. J Biol Chem 276:37564-37568, 2001

16. Stec I, Nagl SB, van Ommen GJ, et al: The PWWP domain: A potential protein–protein interaction domain in nuclear proteins influencing differentiation? FEBS Lett 473:1-5, 2000

17. Qiu C, Sawada K, Zhang X, et al: The PWWP domain of mammalian DNA methyltransferase Dnmt3b defines a new family of DNA-binding folds. Nat Struct Biol 9:217-224, 2002

18. Kishima Y, Yamamoto H, Izumoto Y, et al: Hepatoma-derived growth factor stimulates cell growth after translocation to the nucleus by nuclear localization signals. J Biol Chem 277: 10315-10322, 2002

19. Kishima Y, Yoshida K, Enomoto H, et al: Antisense oligonucleotides of hepatoma-derived growth factor (HDGF) suppress the proliferation of hepatoma cells. Hepatogastroenterology 49: 1639-1644, 2002

20. Mori M, Morishita H, Nakamura H, et al: Hepatoma-derived growth factor is involved in lung remodeling by stimulating epithelial growth. Am J Respir Cell Mol Biol 30:459-469, 2004

Information downloaded from jco.ascopubs.org and provided by at M D ANDERSON HOSP on October 7, 2010 from
Copyright © 2004 American Society of Clinical Oncology. All rights reserved.

Involvement of Mitochondrial and Akt Signaling Pathways in Augmented Apoptosis Induced by a Combination of Low Doses of Celecoxib and *N*-(4-Hydroxyphenyl) Retinamide in Premalignant Human Bronchial Epithelial Cells

Claudia P. Schroeder, Humam Kadara, Dafna Lotan, Jong K. Woo, Ho-Young Lee, Waun Ki Hong, and Reuben Lotan

Department of Thoracic, Head and Neck Medical Oncology, The University of Texas M.D. Anderson Cancer Center, Houston, Texas

Abstract

Celecoxib is being evaluated as a chemopreventive agent. However, its mechanism of action is not clear because high doses were used for *in vitro* studies to obtain antitumor effects. We found that celecoxib inhibited the growth of premalignant and malignant human bronchial epithelial cells with IC_{50} values between 8.9 and 32.7 μmol/L, irrespective of cyclooxygenase-2 (COX-2) expression. Normal human bronchial epithelial cells were less sensitive to celecoxib. Because these concentrations were higher than those attainable *in vivo* (≤5.6 μmol/L), we surmised that combining celecoxib with the synthetic retinoid *N*-(4-hydroxyphenyl) retinamide (4HPR) might improve its efficacy. Treatment of premalignant lung cell lines with combinations of clinically relevant concentrations of celecoxib (≤5 μmol/L) and 4HPR (≤0.25 μmol/L) resulted in greater growth inhibition, apoptosis induction, and suppression of colony formation than did either agent alone. This combination also decreased the levels of Bcl-2, induced the release of mitochondrial cytochrome *c*, activated caspase-9 and caspase-3, and induced cleavage of poly(ADP-ribose)polymerase at concentrations at which each agent alone showed no or minimal effects. Furthermore, combinations of celecoxib and 4HPR suppressed the phosphorylation levels of serine/threonine kinase Akt and its substrate glycogen synthase kinase-3β more effectively than the single agents did. Accordingly, overexpression of constitutively active Akt protected bronchial epithelial cells from undergoing apoptosis after incubation with both celecoxib and 4HPR. These findings indicate that activation of the mitochondrial apoptosis pathway and suppression of the Akt survival pathway mediate the augmented apoptosis and suggest that this combination may be useful for lung cancer chemoprevention. (Cancer Res 2006; 66(19): 9762-70)

Introduction

Lung cancer is the leading cause of cancer-related death worldwide (1). The overall survival rate is poor and has not changed appreciably for several decades despite the introduction of novel agents and combined treatment modalities using surgery, radiotherapy, and chemotherapy. Therefore, new strategies are needed for intervention at early stages of lung carcinogenesis before malignant tumors become clinically evident. One of the promising approaches to accomplishing this goal is cancer chemoprevention (2, 3). In fact, high-risk populations for developing lung cancer, including former and current smokers, represent suitable candidates for chemoprevention trials (4). However, randomized controlled trials using dietary supplementation to prevent lung cancer in smokers have shown rather disappointing results (5) and have highlighted the necessity to find novel agents and combination strategies.

Nonsteroidal, anti-inflammatory drugs have been observed to reduce the relative risk for tobacco-induced lung carcinogenesis in both preclinical and clinical studies (4, 6). The anti-inflammatory action of these drugs is mediated through their inhibitory effect on cyclooxygenases (COX), which are essential enzymes for the synthesis of prostaglandins generated from arachidonic acid (7). In fact, COX-2 isoenzyme is frequently up-regulated in neoplastic tissue of the lung and seems to be associated with a poor prognosis among patients with non–small cell lung cancer, implicating a role in carcinogenesis (8, 9). Celecoxib, the first selective COX-2 inhibitor approved for chemoprevention of colon cancer in patients with familial adenomatous polyposis (10), has also been found to decrease the incidence of esophageal cancer in humans (11), and colon (12), gastric (13), lung (14, 15), mammary (16), oral (17), prostate (18), urinary bladder (19), and skin (20) cancer in various animal models with no associated toxicity. Moreover, a number of studies have shown that celecoxib at clinically feasible concentrations (≤5.6 μmol/L) markedly suppresses the biosynthesis of PGE_2 in COX-2–expressing lung cancer cells (21, 22). However, the fact that much higher doses of celecoxib (≥25 μmol/L) are required for growth inhibition and apoptosis induction in cell culture systems suggests a mode of action independent of COX-2–inhibitory activity and raises questions about the clinical relevance of *in vitro* findings (23). Additionally, data have shown that celecoxib was similarly effective in distinct types of cancer cells that were negative for COX-2 expression (24, 25). In short, the precise molecular mechanisms underlying the antitumor effects of celecoxib is not fully understood.

A strong rationale exists for the use of combinations of agents that act in an additive or synergistic manner by increasing treatment efficacy and/or decreasing drug toxicity (5). We previously showed that *N*-(4-hydroxyphenyl) retinamide (4HPR; fenretinide), a synthetic derivative of retinoic acid, exerts potent proapoptotic effects on a variety of cancer cells (26, 27). Moreover, 4HPR

Note: W.K. Hong is an American Cancer Society Clinical Research Professor. R. Lotan is the incumbent of the Irving and Nadine Mansfield and Robert David Levitt Cancer Research Chair.

Requests for reprints: Reuben Lotan, Department of Thoracic, Head and Neck Medical Oncology, The University of Texas M.D. Anderson Cancer Center; 1515 Holcombe Boulevard, P.O. Box 432, Houston, TX 77030. Phone: 713-792-8467; Fax: 713-745-5656; E-mail: rlotan@mdanderson.org.

©2006 American Association for Cancer Research.

doi:10.1158/0008-5472.CAN-05-4124

combined with celecoxib inhibited growth and induced apoptosis of non–small cell lung cancer cell lines more efficiently than either agent alone did (25), suggesting further investigations for the treatment of human lung cancer. Supported by findings of preclinical and clinical cancer chemoprevention trials, which have indicated great promise for 4HPR and celecoxib administered as single agents (28, 29), we asked whether the combination of both would enhance their individual effects in an *in vitro* model of tobacco-induced human lung carcinogenesis. We found that celecoxib combined with 4HPR at clinically attainable concentrations inhibited growth and induced apoptosis of premalignant and tumorigenic bronchial epithelial cell lines by activating the mitochondrial apoptosis pathway as well as suppressing the Akt survival pathway.

Materials and Methods

Reagents. Celecoxib (4-[5-(4-methylphenyl)-3-(trifluoromethyl)-1*H*-pyrazol-1-] benzene-sulfonamide) was obtained from GD Searle & Co (Chicago, IL), and 4HPR was kindly provided by Dr. James Zweibel. The stock solutions of celecoxib (0.05 mol/L) and 4HPR (0.01 mol/L), both in DMSO, were stored at −80°C and diluted to the desired concentrations with culture medium before use. Bovine serum albumin, DMSO, EDTA, and SDS were purchased from Sigma Chemical Co. (St. Louis, MO). PBS and trypsin were from Life Technologies Invitrogen Corporation (Carlsbad, CA). All culture plasticwares were obtained from BD Bioscience Labware (Bedford, MA).

***In vitro* model of human lung carcinogenesis.** The cell lines used in this study represent an *in vitro* model of human lung carcinogenesis. BEAS-2B is a human bronchial epithelial cell line immortalized using an adenovirus 12-SV40 hybrid virus. The transformed 1198 and the tumorigenic 1170-I cell lines were derived from BEAS-2B by exposure to cigarette smoke condensate *in vivo* after transplantation into nude mice (30). The immortalized 1799 cell line was derived from BEAS-2B cells by *in vivo* transplantation without exposure to cigarette smoke condensate (31). These cell lines were obtained from Dr. Klein-Szanto (Fox Chase Cancer Center, Philadelphia, PA). Normal human bronchial epithelial (NHBE) cells were purchased from Clonetics (San Diego, CA) and used at the second passage only. The non–small cell lung cancer cell line A549 (American Type Cell Culture Collection, Rockville, MD) was included as a positive control for COX-2 expression (25). BEAS-2B and 1799 cells were grown in keratinocyte serum-free medium (K-SFM) containing human recombinant epidermal growth factor (2.5 μg) and bovine pituitary extract (25 mg; Life Technologies Invitrogen Corporation) at 37°C in a humidified atmosphere of 95% air and 5% CO_2. The cell lines 1198 and 1170-I were maintained in K-SFM supplemented with 3% fetal bovine serum (FBS) from HyClone Laboratories, Inc. (Logan, UT).

Cell growth studies. The cell lines cultured in the medium described above were seeded into 96-well culture plates (6×10^3 or 2×10^4 per well for confluent NHBE culture) in K-SFM with and without 3% FBS, allowed to adhere overnight at 37°C, followed by treatment with celecoxib, 4HPR, and their combinations for 3 days. Control cultures were incubated with DMSO alone. An automated plate reader (model MR5000, Dynatech Laboratories Inc., Chantilly, VA) was used to estimate cell numbers using the sulforhodamine B assay (32). The inhibition of cell growth was calculated as $(1 - A_t / A_c) \times 100\%$, where A_t and A_c represent absorbencies of treated and control cultures, respectively. Concentration response curves were plotted, and IC_{50} concentrations of celecoxib were calculated by interpolation after 3 days in the presence or absence of 3% FBS.

Colony formation studies. Exponentially growing cells were seeded into six-well culture plates (0.8×10^5/well) overnight before treatment with celecoxib, 4HPR, and their combinations. The medium was removed and replaced with fresh medium containing these agents every 3 days. After 14 days of incubation, the cells were fixed with methanol/acetic acid (3:1, v/v) and stained with crystal violet in methanol (0.5%, v/v) to visualize the colonies. For quantification, each well was divided into eight fields, and the number of colonies ≥1 mm was estimated with a colony counter (Fisher Scientific, Pittsburgh, PA).

Terminal deoxynucleotidyl transferase-mediated dUTP nick end labeling (TUNEL) assay. Fragmentation of intranucleosomal DNA was evaluated using an apoptosis *in situ* detection kit (Apo-Direct, Phoenix Flow Systems, Inc., San Diego, CA) based on the terminal deoxynucleotidyl transferase-mediated dUTP nick end labeling (TUNEL) technique (33). After treatment, both adherent and nonadherent cells were harvested by trypsinization, pelleted by centrifugation, fixed with ice-cold ethanol (70%, v/v), and stained according to the protocol of the manufacturer. Fluorimetric measurement and data analysis were done on a Coulter XL flow cytometer (Miami, FL). The percentage of cells that were apoptotic was determined from the proportion of fluorescein-isothiocyanate–positive cells within 10,000 cells analyzed. Two independent experiments were done.

Western blot analysis. Samples containing 50 μg of total cellular protein mixed in sample buffer [0.5 mol/L Tris (pH 6.8), 0.3% glycerol, 0.03% β-mercaptoethanol, 10% SDS, and 0.001% bromphenol blue] were electrophoretically separated through 8% to 12% SDS-polyacrylamide slab gels, followed by transfer onto nitrocellulose membranes (Bio-Rad Laboratories, Hercules, CA). Briefly, cell monolayers were washed twice with ice-cold PBS and collected in lysis buffer containing 150 mmol/L NaCl, 0.02% NaN_3, 2% Igepal CA-630, 0.5% sodium deoxycholate, 0.2% SDS, and 50 mmol/L Tris-HCl (pH 8.0) supplemented with the protease inhibitors leupeptin (1 μg/mL), aprotinin (1 μg/mL), pepstatin (0.5 μg/mL), and phenylmethylsulfonyl fluoride (100 μg/mL). Protein concentrations were measured using the Bio-Rad protein assay (Bio-Rad Laboratories). After blocking with 3% nonfat dry milk solution in 0.1% (w/v) Tween 20 in PBS, the membranes were probed with antihuman antibodies at appropriate dilutions against COX-2 (Oxford Biomedical Research, Inc., Oxford, MI); caspase-3 (clone 31A1067, Imgenex, San Diego, CA); caspase-8, Bcl-2, Bcl-x_L, Bcl-x_S, and Bax (all from Santa Cruz Biotechnology, Santa Cruz, CA); poly(ADP-ribose) polymerase (PARP); caspase-9; hemagglutinin tag for the recombinant protein (HA-tag 262K); and antibodies included in the phosphorylated Akt pathway sampler kit (all from Cell Signaling Technology, Inc., Charlottesville, VA). Antibody binding was detected with horseradish peroxidase–linked secondary antibody and enhanced chemiluminescence (Amersham Biosciences Corp., Piscataway, NJ). Loading and transferring control was confirmed by probing the membranes with anti-β-actin antibody or staining with Ponceau S solution (Sigma Chemical). Mitochondria and cytosol fractionation was done according to a cytochrome *c* releasing apoptosis assay kit (BioVision, Inc., Mountain View, CA).

Adenoviral vector generation. An adenoviral vector expressing constitutively active Akt (MyrAkt), referred to here as Ad-MyrAkt, and an adenoviral vector expressing empty vector, referred to here as Ad-EV, were amplified as described previously (34). Briefly, 1799 transformed cells were infected at 5×10^3 multiplicity of infection (MOI) with Ad-MyrAkt and Ad-EV, respectively. After 2 hours, the medium was replaced with fresh medium containing celecoxib and 4HPR followed by 2 days of incubation. The adenoviral vector expressing a full-length human Akt1 with the Src myristoylation signal fused in-frame to the c-Akt coding sequence with HA under the control of the cytomegalovirus promoter (Ad5CMV-MyrAkt-HA) was constructed using the pAd-shuttle vector system (35, 36). The presence of MyrAkt-HA was confirmed by Western blot analysis of Akt and HA expression. The activity of Ad5CMV-MyrAkt-HA was assessed by detection of cleavage of PARP (Cell Signaling Technology), activation of caspase-3 (Imgenex), and expression of Bcl-2 (Cell Signaling Technology) using immunoblotting.

Statistical analysis. Growth studies and the number of colonies were analyzed for statistical significance using Student's two-tailed *t* test with $P \leq 0.05$ and $P \leq 0.005$, respectively. The results represent mean values ± SD of three independent experiments, each done in quadruplicate.

Results

Celecoxib inhibits growth of human premalignant and malignant lung cell lines independent of COX-2. To determine whether the growth-inhibitory effects of celecoxib in an *in vitro*

model of human lung carcinogenesis were associated with the expression of the presumed target enzyme, we analyzed the constitutive COX-2 levels of cells. COX-2 was expressed at a very low level in NHBE cells; was not detected in BEAS-2B, 1799, 1198, or 1170-I cells; and was not induced in 1198 or 1170-I cell lines whether they were cultured in the presence or absence of 3% FBS (Fig. 1*A*). However, the robust expression of COX-2 in A549 lung cancer cells, which were included as a positive control for COX-2, increased by ~20% when grown in the absence of FBS. Furthermore, the constitutive levels of PGE_2 in BEAS-2B, 1198, and A549 cells were 0.2, 0.04, and 2.7 ng/10^6 cells, respectively, as determined by electrospray ionization liquid chromatography tandem mass spectrometry (24), correlated with their differential COX-2 expression. As shown in Fig. 1*B*, celecoxib inhibited the growth of premalignant (BEAS-2B, 1799, and 1198) and tumorigenic 1170-I cell lines with IC_{50} values ranging from 8.9 to 10.1 μmol/L in K-SFM and from 15.9 to 18.7 μmol/L in 3% FBS-containing K-SFM. A549 lung cancer cells were ~2-fold less sensitive to celecoxib than premalignant cell lines irrespective of the presence or absence of serum. NHBE cells, which were seeded at subconfluent density to allow them to proliferate, exhibited a lower sensitivity to celecoxib characterized by IC_{50} values of 23.2 and 62 μmol/L in the absence and presence of 3% FBS, respectively. Confluent cultures of NHBE cells, which better mimic the nonproliferative state *in vivo*, were less sensitive to celecoxib with IC_{50} values of 29.2 and 80 μmol/L in serum-free and serum-containing medium, respectively. Thus, the growth-inhibitory activity of celecoxib seemed to be independent of COX-2 expression and activity. In addition, COX-2 was not modulated in 1198 cells cultured in standard medium or medium supplemented with celecoxib (2.5 and 5 μmol/L), 4HPR (0.25 μmol/L), or both, as shown by immunoblotting (Fig. 1*C*).

Celecoxib plus 4HPR is more potent than either agent alone in inhibiting growth of premalignant and tumorigenic lung cell lines. The effects of low doses of celecoxib in combination with the proapoptotic retinoid 4HPR on cell growth were studied because the IC_{50} values determined in the previous experiment were at least 3-fold higher than peak plasma levels obtained in patients treated with celecoxib (23) and because our recent studies on various non–small cell lung cancer cell lines showed that simultaneous treatment of celecoxib with 4HPR resulted in additive growth suppression (25). As shown in Fig. 2, combinations of 5 μmol/L celecoxib with 0.2 μmol/L 4HPR inhibited cell growth of premalignant and tumorigenic cell lines more effectively than treatment with either agent alone ($P \leq 0.05$ and $P \leq 0.005$ compared with untreated cultures). Furthermore, combinations of 2.5 μmol/L celecoxib and 0.2 μmol/L 4HPR showed greater growth suppression in 1799, 1198, and 1170-I than in BEAS cells. In contrast, NHBE cells grown *in vitro* under either subconfluent or confluent condition seemed to be sensitive to the growth-inhibitory effects of 4HPR (0.2 μmol/L), whereas celecoxib showed no significant activity at concentrations up to 5 μmol/L. Interestingly, combinations of the two agents were less or similarly effective than treatment of NHBE cells with each agent alone.

Celecoxib plus 4HPR suppresses colony formation of premalignant and tumorigenic lung cell lines more effectively than either agent alone. Because the growth-inhibitory effects induced by celecoxib, 4HPR, or both in monolayer cultures were modest, we asked whether treatment with either or both agents could exert greater activity on the formation of colonies, which allows an investigation over a longer period of time. As single

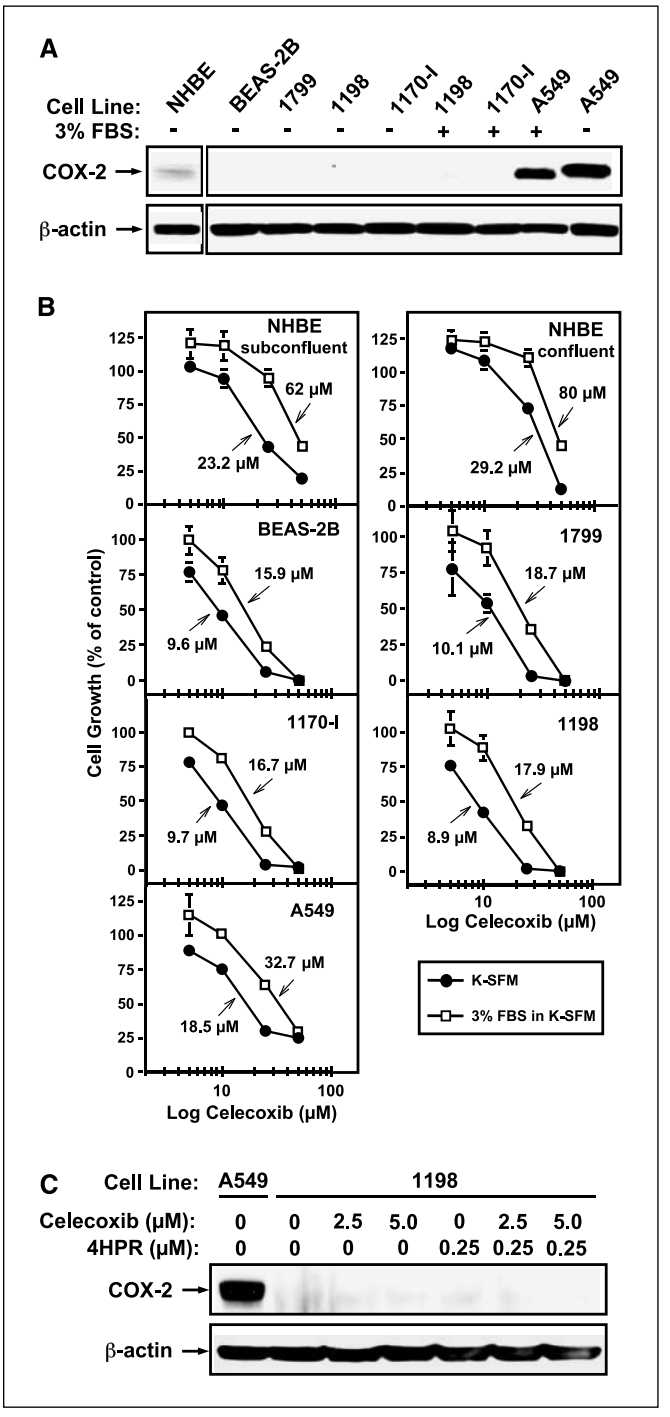


Figure 1. Expression of COX-2 in various premalignant, normal, and malignant human lung cell lines and their growth inhibition by celecoxib. *A,* human normal (NHBE), immortalized (BEAS-2B and 1799), transformed (1198), and tumorigenic (1170-I and A549) epithelial cells were grown in K-SFM supplemented with epidermal growth factor (2.5 μg) and bovine pituitary extract (25 mg) in the presence or absence of FBS (3%). The cells were harvested after 5 days, lysed, and subjected to Western blot analysis (50 μg/lane) using anti-human COX-2 and anti-β-actin (loading control) antibodies. *B,* cells were cultured in K-SFM in the presence or absence of 3% FBS for 3 days. Cell numbers were estimated by the sulforhodamine B assay. *Points,* means from three independent experiments done in quadruplicate; *bars*, SD. The concentrations of celecoxib shown are IC_{50} values calculated from the concentration-response curves of each cell line using DMSO as a control. *C,* expression of COX-2 in 1198 cells treated with celecoxib (2.5 and 5 μmol/L), 4HPR (0.25 μmol/L), and their combinations for 3 days. A549 cells were included as a positive control for COX-2. β-Actin served as the loading control.

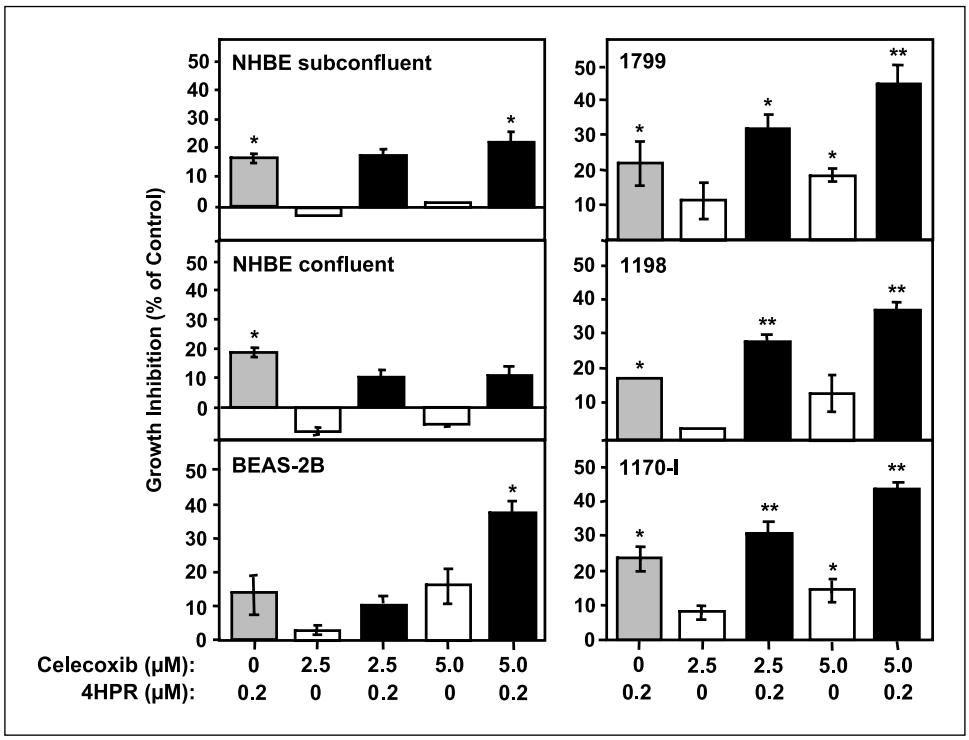


Figure 2. Comparison of the effects of celecoxib, 4HPR, and their combinations on the growth of human bronchial epithelial cell lines representing an *in vitro* model of lung carcinogenesis. Cells were seeded into 96-well culture plates and incubated overnight before treatment with celecoxib (2.5 and 5 μmol/L), 4HPR (0.2 μmol/L), or both agents for 3 days. Cultures incubated with DMSO alone served as a control. Cell numbers were estimated by the sulforhodamine B assay and analyzed for statistical significance using Student's paired *t* test with $P \leq 0.05$ (*) and $P \leq 0.005$ (**) related to control cultures in DMSO, respectively. *Columns*, means from three independent experiments done in quadruplicate; *bars*, SD.

agents, both 4HPR and celecoxib exerted some inhibitory effects on colony formation in all cell lines (Fig. 3). For example, 5 μmol/L celecoxib reduced the mean size of colonies in BEAS-2B cells as well as the size and number of colonies in the other cell lines. The colony-forming ability of 1799, 1198, and 1170-I cells was inhibited by 61%, 45%, and 27%, respectively ($P < 0.05$ for all comparisons), after treatment with 5 μmol/L celecoxib. 4HPR (0.2 μmol/L) was also effective by itself in reducing the size of colonies in BEAS-2B cells, however, without altering their number. On the contrary, 0.2 μmol/L 4HPR suppressed colony formation of 1799, 1198, and 1170-I cells by 36%, 15%, and 57%, respectively ($P < 0.05$, P = NS, and $P < 0.005$). 4HPR at the lower concentration of 0.1 μmol/L significantly inhibited the number of colonies in only 1198 and 1170-I cells by 24% and 38% ($P < 0.05$ and $P < 0.005$), respectively. Combining celecoxib and 4HPR substantially augmented the modest effect of treatment with the single agents. In particular, 5 μmol/L celecoxib plus 0.2 μmol/L 4HPR markedly suppressed colony formation in all cell lines by 86% (BEAS-2B) to 99% (1799, 1198, and 1170-I; $P < 0.005$ for all comparisons). Even 0.1 μmol/L 4HPR plus 5 μmol/L celecoxib significantly reduced the number of colonies in 1799, 1198, and 1170-I cells by 92%, 79%, and 63% ($P < 0.005$ for all comparisons), respectively, while decreasing the size of colonies in BEAS-2B cells without altering their number (Fig. 3).

Celecoxib plus 4HPR induces apoptosis in BEAS-2B and 1198 cells more efficiently than either agent alone. Treatment of BEAS-2B and 1198 cells with up to 5 μmol/L celecoxib had negligible effects on the induction of apoptosis as determined by the TUNEL assay (Fig. 4*A* and *B*). On the other hand, treatment with 0.25 μmol/L 4HPR increased the amount of apoptotic BEAS-2B and 1198 cells to 10 ± 2.4% and 18 ± 1.7%, respectively. However, combinations of 0.25 μmol/L 4HPR and celecoxib (≤5 μmol/L) significantly augmented apoptosis compared with treatment with either agent alone ($P \leq 0.05$ and $P \leq 0.005$ compared with untreated culture). For example, incubation with 5 μmol/L celecoxib plus 0.25 μmol/L 4HPR caused ~60% apoptotic BEAS-2B and 1198 cells, respectively.

Effects of celecoxib plus 4HPR on apoptosis-related proteins in BEAS and 1198 cells. The expression of proteins related to apoptosis was applied to confirm apoptotic events induced by the combination of celecoxib and 4HPR in BEAS-2B and 1198 cells. As a result, we obtained a decrease in the expression levels of procaspase-3 and procaspase-9, indicating caspase activation concomitant with an increase in cleavage of the 113 kDa PARP to the 89 kDa fragment (Fig. 4*C* and *D*). These effects were most profound in cells treated with a combination of 5 μmol/L celecoxib and 0.25 μmol/L 4HPR. Notably, in BEAS-2B cells, 4HPR alone diminished the level of procaspase-3 and increased the cleavage of PARP. No changes were detected in the expression levels of caspase-8 in either cell line. The level of the antiapoptotic protein Bcl-2 decreased and that of the proapoptotic molecule Bcl-X_S increased in both cell lines in response to combined treatment, whereas the expression of the proapoptotic protein Bax and the antiapoptotic protein Bcl-X_L was unaltered regardless of treatment. We further examined the effects of celecoxib and 4HPR on the mitochondrial pathway by analysis of cytochrome *c* release, which contributes to caspase-3 and caspase-9 activation, resulting in the degradation of PARP and subsequent cleavage of internucleosomal DNA. Treatment of 1198 cells with 5 μmol/L celecoxib plus 0.25 μmol/L 4HPR markedly induced cytochrome *c* release from the mitochondria into the cytosol (Fig. 4*D, bottom*). Altogether, these TUNEL and Western blot data confirm the apoptosis-inducing effects of combined celecoxib and 4HPR treatment.

Celecoxib plus 4HPR induces apoptosis partly by suppressing the Akt signaling pathway in 1799 cells. To determine whether combinations of celecoxib and 4HPR can alter the Akt signaling pathway in 1799 transformed human bronchial epithelial cells, we investigated the effects of these agents alone and in combination on the activation of Akt and its downstream molecule

glycogen synthase kinase-3β (GSK-3β). The constitutively high levels of phosphorylated Akt and phosphorylated GSK-3β were marginally decreased in response to 5 μmol/L celecoxib or 0.25 μmol/L 4HPR alone, but greatly decreased by the combination of these two agents. Likewise, the expression of the antiapoptotic protein Bcl-2 only declined after incubation with celecoxib in combination with 4HPR. No alterations appeared in the expression of Akt and GSK-3α/β after treatment with celecoxib and/or 4HPR compared with DMSO control cultures (Fig. 5*A* and *B*).

To further examine whether expression of constitutively active Akt can protect cells from undergoing apoptosis, we infected 1799 cells with adenoviral vector containing MyrAkt tagged with hemagglutinin for the recombinant protein (MyrAkt-HA) before treatment with celecoxib and 4HPR and compared the levels of apoptosis-related proteins in those cells with cells infected with adenoviral vector control (Ad5CMV). Successful infection is illustrated by the appearance of a single protein band by an antibody against HA-tag and a second band by an anti-Akt antibody (Fig. 5*C, top two panels*). As expected, these bands were not detected in cells infected with at Ad5CMV only. The 1799 cells expressing MyrAkt-HA were less sensitive than the cells infected with control vector to the apoptosis-inducing effects of celecoxib plus 4HPR as indicated by unaltered expressions of procaspase-3, Bcl-2, and decreased levels of PARP cleavage (Fig. 5*C*).

Discussion

Celecoxib has been shown to regress colorectal adenomas in patients with familial adenomatous polyposis relative to placebo, which resulted in the Food and Drug Administration approving celecoxib for adjunctive management of this disease (10). The presumed mechanism of action of celecoxib is selective inhibition of COX-2, an enzyme responsible for the metabolic conversion of arachidonic acid to prostaglandins, which play important roles in inflammation, cell proliferation, cell survival, and carcinogenesis (7). Moreover, the induction of COX-2 represents an early event in cancer development, and its expression seems to be associated with a poor prognosis in various types of cancer, including lung

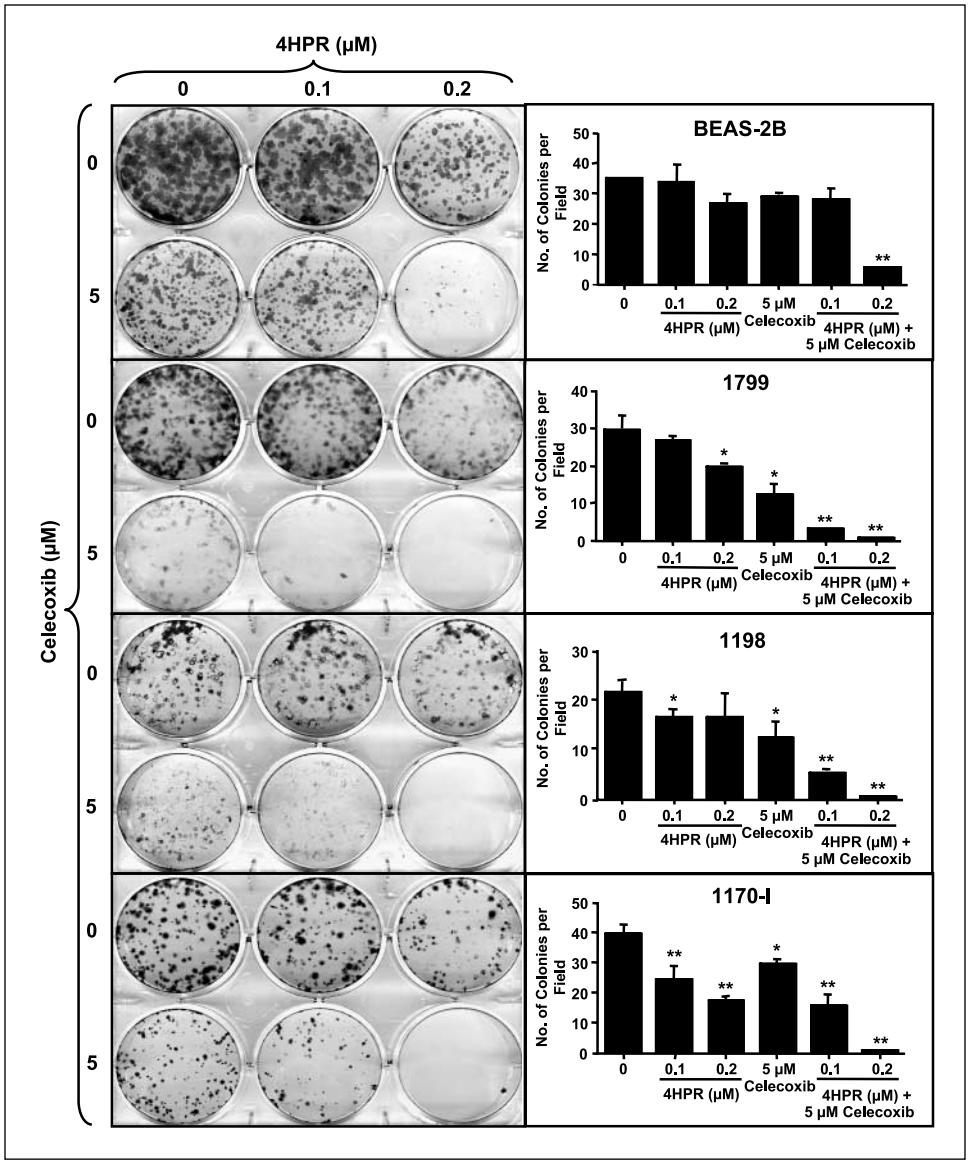


Figure 3. Effects of celecoxib, 4HPR, and their combinations on the colony-forming ability of human bronchial epithelial cell lines representing an *in vitro* model of lung carcinogenesis. Exponentially growing cells were seeded into six-well culture plates and treated with celecoxib (5 μmol/L), 4HPR (0.1 and 0.2 μmol/L), and their combinations for 14 days. *Columns,* number of colonies for each cell line calculated from quadruplicate determinations; *bars*, SD. $P \leq 0.05$ (*) and $P \leq 0.005$ (**) compared with cultures in DMSO (*leftmost column*) by Student's paired *t* test.

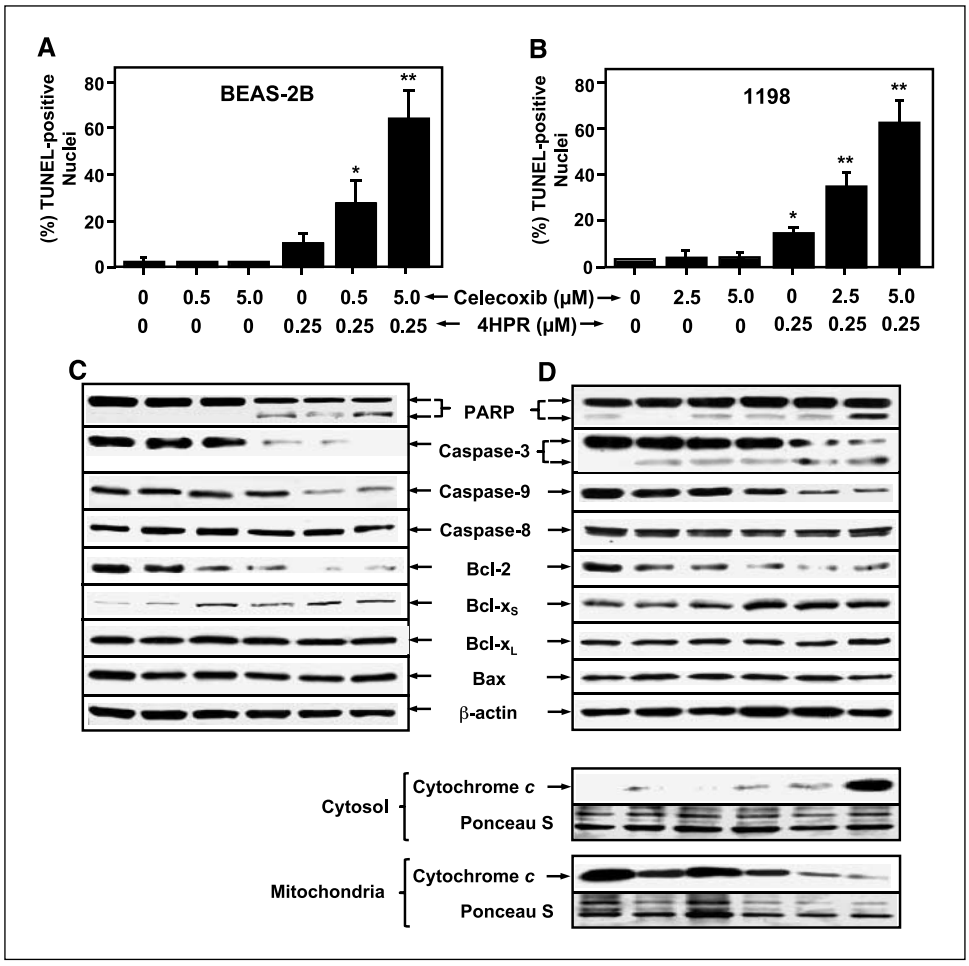


Figure 4. Effects of celecoxib, 4HPR, and their combinations on the induction of apoptosis and expression of apoptosis-related proteins in BEAS-2B and 1198 bronchial epithelial cell lines. *A* and *B,* the cells were treated with celecoxib (≤5 μmol/L), 4HPR (0.25 μmol/L), or both for 3 days before being harvested and analyzed by TUNEL assay. *Columns,* percentage of TUNEL-positive nuclei representative of two independent experiments and calculated for statistical significance using Student's two-tailed *t* test with $P \leq 0.05$ (*) and $P \leq 0.005$ (**), respectively. *C* and *D,* cells treated as above were harvested, lysed, and subjected to Western blot analysis using antibodies against the indicated proteins. The release of cytochrome *c* into the cytosol of 1198 cells was determined by Western blotting after fractionation of mitochondria and cytosol. β-Actin and Ponceau S staining were used as loading controls.

cancer (8, 9, 18). The fact that celecoxib at clinically achievable concentrations markedly decreased the PGE_2 production in COX-2–expressing cells supports its use as a cancer therapeutic and chemopreventive agent (17, 18, 20–24).

However, recent studies have suggested that the activity of celecoxib *in vivo* may not be exclusively mediated by a COX-2–dependent pathway (23, 24). For example, Sinicrope et al. (37) reported that celecoxib administered at 400 mg twice daily over 6 months induced polyp regression in patients with familial adenomatous polyposis by modulating *in vivo* rates of cell proliferation and apoptosis without evidences for suppression of PGE_2 in either normal tissue or adenomas. Furthermore, the concentrations of celecoxib needed to exert antitumor activity (e.g., apoptosis) *in vitro* are at least 10-fold higher than those required to inhibit COX-2 activity *in vivo*, raising the question whether the mechanisms identified *in vitro* are applicable to tumor responses *in vivo* (23–25). In addition, experimental studies have consistently shown that the sensitivity of various cancer cells to celecoxib is not related to their COX-2 expression status (24, 25).

We have used an *in vitro* model of human lung carcinogenesis to investigate the effects of clinically relevant concentrations of celecoxib in combination with the synthetic retinoid 4HPR. This model consists of distinct bronchial epithelial cell lines derived from SV40 large T-antigen immortalized BEAS-2B cells after exposure to cigarette smoke condensate and has proven useful in studying the process of carcinogenic transformation and the efficacy of cancer chemopreventive agents (30, 31). Our results indicate that cell lines constituting this model showed no detectable COX-2 expression, had corresponding low levels of PGE_2, and were nonetheless sensitive to the growth-inhibitory activity of celecoxib, such as A549 cancer cells, which constitutively expressed COX-2. Because the IC_{50} values for celecoxib were higher than those achievable in clinical trials (23), we decided to combine celecoxib with the proapoptotic retinoid 4HPR. Our data show that treatment of premalignant and tumorigenic cell lines with celecoxib or 4HPR at clinically relevant concentrations exhibited only modest inhibitory effects (<20%) on cell growth. However, incubation of these cell lines with 5 μmol/L celecoxib plus 0.2 μmol/L 4HPR revealed additive effects on growth suppression in monolayer cultures determined after 3 days of incubation.

The preclinical evaluation of therapeutic and chemopreventive drugs typically involves the comparison of the effects on premalignant and normal cells to determine whether a "therapeutic window" exists. Clearly, chemopreventive agents are required to have a better safety profile than therapeutic drugs because they may be administered over a prolonged period of time. Both celecoxib (10, 37) and 4HPR (29, 38) have been found to have low or no side effects in humans at doses that lead to plasma levels comparable with concentrations we used in this study and even considerably higher in the case of 4HPR (38). Therefore, we anticipated finding low or no effects of these agents on NHBE cells. However, celecoxib inhibited the growth, especially of subconfluent

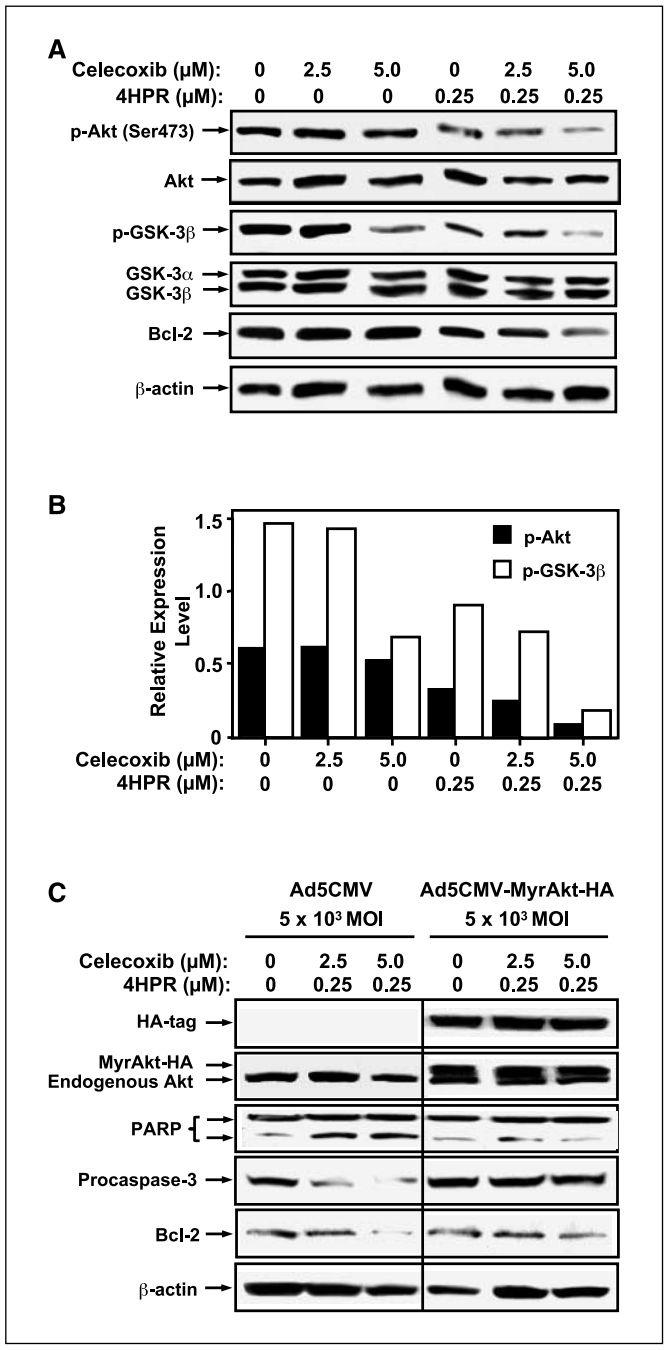


Figure 5. Effects of celecoxib, 4HPR, and their combinations on the Akt survival pathway in 1799 human transformed bronchial epithelial cells. *A,* after 2 days of treatment with celecoxib and 4HPR, protein extracts (50 μg/lane) prepared from the cells were subjected to Western blot analysis to determine the expression of phosphorylated Akt (Ser^{473}), phosphorylated GSK-3β, Akt, GSK-3α/β, and Bcl-2. *B,* the blots were scanned using SF Launcher v2.0.5, and the densities of p-Akt (Ser^{473}) and p-GSK-3β were quantified in relation to the corresponding total protein expression and normalized to β-actin by NIH image 1.58 software. *C,* effects of constitutively active Akt on the response of 1799 bronchial epithelial cells to apoptosis induced by celecoxib and 4HPR. The cells were infected at 5×10^3 MOI of adenoviral vector control (Ad5CMV) or adenoviral vector containing myristoylated Akt (Ad5CMV-MyrAkt-HA) in keratinocyte SFM for 1 day before incubation with celecoxib/4HPR for an additional 2 days. Successful infection is illustrated by the appearance of a single protein band by an antibody against HA-tag and a second band by an anti-Akt antibody (*top two panels*). As expected, these bands were not detected in cells infected with at Ad5CMV. Apoptosis-inducing activity was determined by the expression of procaspase-3, Bcl-2, and cleavage of PARP. β-Actin served as a control for protein loading.

proliferating NHBE cultures, albeit with lower potency than it did inhibit premalignant and tumorigenic cell proliferation. Interestingly, at low concentrations (2.5 and 5 μmol/L), celecoxib failed to inhibit NHBE cell growth, whereas it suppressed the growth of their premalignant and tumorigenic counterparts. 4HPR (0.2 μmol/L) showed significant but low inhibition compared with untreated cultures; however, combinations with celecoxib did not augment this effect. Thus, these agents appear to exert a selective effect on premalignant and tumorigenic cells compared with NHBE cells. Notably, the use of NHBE cells as a control is not straightforward because these cells are cultured under conditions where they are stimulated to proliferate, i.e., K-SFM supplemented with epidermal growth factor and bovine pituitary extract, hence emulate hyperplasia rather than normal bronchial epithelium. In fact, the proliferative index of histologically normal lung epithelium from nonsmokers *in vivo* is 0.16 ± 0.15% and 1.26 ± 1.17% in biopsies obtained from smokers (39) as opposed to 4.8% to 36% in premalignant lesions such as dysplasia (39, 40). Therefore, we investigated the effects of the agents on both subconfluent (proliferating) and confluent (quiescent) NHBE cells. Indeed, we found that confluent NHBE cells were less inhibited by high concentrations of celecoxib or low concentrations of celecoxib combined with 4HPR than premalignant and tumorigenic cells.

Combinations of low doses of both celecoxib and 4HPR resulted in a more dramatic inhibitory activity on the formation of colonies, where cells were seeded at low density and treated for 14 days, compared with growth inhibition in cultures at higher density measured after 3 days of incubation. We observed that BEAS-2B cells exhibited lower sensitivity to combinations of celecoxib and 4HPR than 1799, 1198, and 1170-I cells did (Figs. 2 and 3). The reason for such difference is unclear. However, it is noteworthy that the three more sensitive cell lines were derived from BEAS-2B cells after growing as xenotransplants in nude mice for 6 months (30). This *in vivo* passage may have been accompanied by selective pressure that resulted in some distinction from the parental cell line, which was immortalized with SV40 large T-antigen. Recently, we found that various human bronchial epithelial cell lines immortalized with hTERT and CDK4 (41) also lack COX-2 expression yet exhibit higher sensitivity to the combination of celecoxib and 4HPR than to either agent alone (data not shown). Thus, we conclude that the sensitivity of premalignant bronchial epithelial cell lines to this combination is not restricted to SV40 large T-antigen immortalized cells.

To gain insight into the mechanisms by which celecoxib in combination with 4HPR enhanced the apoptosis of human bronchial epithelial cell lines, as observed with the TUNEL assay, we examined the expression levels of several apoptosis-related proteins. Our data indicate that celecoxib plus 4HPR activates the mitochondrial apoptosis pathway as evidenced by suppression of the antiapoptotic protein Bcl-2, increase in the proapoptotic protein Bcl-x_S, release of apoptogenic cytochrome *c* into the cytosol, activation of caspase-9 and caspase-3, and cleavage of PARP. However, no changes were detected in the expression levels of Bcl-x_L, Bax, or caspase-8. On the basis of our initial findings that none of these cell lines expressed COX-2, we concluded that the growth-inhibitory and apoptosis-inducing effects of celecoxib in combination with 4HPR are mediated by COX-2–independent mechanisms. Numerous studies have shown that celecoxib induces apoptosis in a variety of cell types, but only at concentrations between 50 and 100 μmol/L (23, 25, 42–44). The mechanism ascribed to these effects was based on activation of the

mitochondrial signaling pathway, as indicated by breakdown of the mitochondrial membrane potential, release of cytochrome *c*, activation of caspase-9 and caspase-3, and cleavage of PARP via a Bcl-2/Bcl-x_L–independent pathway in rat cholangiocarcinoma (42), human lymphoma (43), and prostate carcinoma (44) cell lines. Correspondingly, various reports have delineated the proapoptotic effects of 4HPR at concentrations above 3 μmol/L by a mechanism that includes augmented generation of reactive oxygen species from the mitochondria with subsequent release of cytochrome *c*, activation of caspase-9 and caspase-3, and cleavage of PARP without altering Bcl-2 and Bax (25–27). However, ectopic overexpression of Bcl-2 did not protect T-cell acute lymphoblastic leukemia cells from apoptosis induced by 4HPR but markedly delayed its onset (45). Nonetheless, in those cells, 4HPR induced apoptosis via a mitochondrial (reactive oxygen species mediated) pathway that involves the obligatory contributions of the proapopotic Bcl-2 family members Bax and/or Bak (46).

It is well established that alterations to the Akt signaling pathway are frequent in human malignancies that result in enhanced resistance to apoptosis through multiple mechanisms (47). In fact, previous studies on rat cholangiocarcinoma (42), human prostate (44), hepatocellular (48), and colon cancer (49) cells have shown that celecoxib inhibits Akt phosphorylation in association with induction of apoptosis via the mitochondrial pathway. However, these effects required high concentrations of celecoxib that are not attainable *in vivo*. In contrast, our data indicate that incubation of premalignant bronchial epithelial cells with clinically relevant concentrations of celecoxib combined with 4HPR augments apoptosis by reducing phosphorylation levels of Akt and its direct downstream substrate GSK-3β. This conclusion was supported by further experiments showing that overexpression of constitutive active Akt protects, at least partly, premalignant cells from undergoing apoptosis induced by celecoxib plus 4HPR. Taken together, our findings strongly warrant additional evaluation of the efficacy of this combination in chemoprevention and therapy of lung cancer in animal models and eventually in clinical trials.

Acknowledgments

Received 11/17/2005; revised 7/24/2006; accepted 8/7/2006.

Grant support: National Cancer Institute grant PO1 CA98144; Department of Defense Biology, Education, Screening, Chemoprevention, and Treatment Lung Cancer Program grant DAMD17-01-1-0689-2; Cancer Center Support grant P30 CA 16672; and the David Workman Memorial Endowment Award from the Samuel Waxman Cancer Research Foundation.

The costs of publication of this article were defrayed in part by the payment of page charges. This article must therefore be hereby marked *advertisement* in accordance with 18 U.S.C. Section 1734 solely to indicate this fact.

We thank Dr. James Zweibel (National Cancer Institute, Bethesda, MD) for providing 4HPR, Wendy Schober (Department of Blood and Marrow Transplantation, University of Texas M.D. Anderson Cancer, Houston, TX) for her assistance in the acquisition of flow cytometry data, and Peiying Yang and Robert A. Newman (Department of Experimental Therapeutics, University of Texas M.D. Anderson Cancer) for the PGE_2 analysis.

References

1. Jemal A, Murray T, Ward E, et al. Cancer statistics, 2005. CA Cancer J Clin 2005;55:10–30.
2. Cohen V, Khuri FR. Chemoprevention of lung cancer: concepts and strategies. Expert Rev Anticancer Ther 2005;5:549–65.
3. Hong WK, Sporn MB. Recent advances in chemoprevention of cancer. Science 1997;278:1073–7.
4. Muscat JE, Chen SQ, Richie JP, Jr., et al. Risk of lung carcinoma among users of nonsteroidal antiinflammatory drugs. Cancer 2003;97:1732–6.
5. Hirsch FR, Lippman SM. Advances in the biology of lung cancer chemoprevention. J Clin Oncol 2005;23:3186–97.
6. Rao CV, Reddy BS. NSAIDs and chemoprevention. Curr Cancer Drug Targets 2004;4:29–42.
7. Williams CS, Mann M, DuBois RN. The role of cyclooxygenases in inflammation, cancer, and development. Oncogene 1999;18:7908–16.
8. Khuri FR, Wu H, Lee JJ, et al. Cyclooxygenase-2 overexpression is a marker of poor prognosis in stage I non-small cell lung cancer. Clin Cancer Res 2001;7:861–7.
9. Hida T, Yatabe Y, Achiwa H, et al. Increased expression of cyclooxygenase 2 occurs frequently in human lung cancers, specifically in adenocarcinomas. Cancer Res 1998;58:3761–4.
10. Steinbach G, Lynch PM, Phillips RK, et al. The effect of celecoxib, a cyclooxygenase-2 inhibitor, in familial adenomatous polyposis. N Engl J Med 2000;342:1946–52.
11. Bardou M, Barkun AN, Ghosn J, Hudson M, Rahme E. Effect of chronic intake of NSAIDs and cyclooxygenase 2-selective inhibitors on esophageal cancer incidence. Clin Gastroenterol Hepatol 2004;2:880–7.
12. Reddy BS, Hirose Y, Lubet RA, Steele VE, Kelloff GJ, Rao CV. Chemoprevention of colon cancer by specific cyclooxygenase-2 inhibitor, celecoxib, administered during different stages of carcinogenesis. Cancer Res 2000;60:293–7.
13. Hu PJ, Yu J, Zeng ZR, et al. Chemoprevention of gastric cancer by celecoxib in rats. Gut 2004;53:195–200.
14. Diperna CA, Bart RD, Sievers EM, Ma Y, Starnes VA, Bremner RM. Cyclooxygenase-2 inhibition decreases primary and metastatic tumor burden in a murine model of orthotopic lung adenocarcinoma. J Thorac Cardiovasc Surg 2003;126:1129–33.
15. Klenke FM, Gebhard MM, Ewerbeck V, Abdollahi A, Huber PE, Sckell A. The selective Cox-2 inhibitor Celecoxib suppresses angiogenesis and growth of secondary bone tumors: an intravital microscopy study in mice. BMC Cancer 2006;12:6–9.
16. Harris RE, Alshafie GA, Abou-Issa H, Seibert K. Chemoprevention of breast cancer in rats by celecoxib, a cyclooxygenase-2 inhibitor. Cancer Res 2000;60:2101–3.
17. Li N, Sood S, Wang S, et al. Overexpression of 5-lipoxygenase and cyclooxygenase 2 in hamster and human oral cancer and chemopreventive effects of zileuton and celecoxib. Clin Cancer Res 2005;11:2089–96.
18. Gupta S, Adhami VM, Subbarayan M, et al. Suppression of prostate carcinogenesis by dietary supplementation of celecoxib in transgenic adenocarcinoma of the mouse prostate model. Cancer Res 2004;64:3334–43.
19. Grubbs CJ, Lubet RA, Koki AT, et al. Celecoxib inhibits *N*-butyl-*N*-(4-hydroxybutyl)-nitrosamine-induced urinary bladder cancers in male B6D2F1 mice and female Fischer-344 rats. Cancer Res 2000;60:5599–602.
20. Fischer SM, Lo HH, Gordon GB, et al. Chemopreventive activity of celecoxib, a specific cyclooxygenase-2 inhibitor, and indomethacin against ultraviolet light-induced skin carcinogenesis. Mol Carcinog 1999;25:231–40.
21. Mao JT, Cui X, Reckamp K, et al. Chemoprevention strategies with cyclooxygenase-2 inhibitors for lung cancer. Clin Lung Cancer 2005;7:30–9.
22. Abou-Issa H, Alshafie G. Celecoxib: a novel treatment for lung cancer. Expert Rev Anticancer Ther 2004;4:725–34.
23. Niederberger E, Tegeder I, Vetter G, et al. Celecoxib loses its anti-inflammatory efficacy at high doses through activation of NF-κB. FASEB J 2001;15:1622–4.
24. Schroeder CP, Yang P, Newman RA, Lotan R. Eicosanoid metabolism in squamous cell carcinoma cell lines derived from primary and metastatic head and neck cancer and its modulation by celecoxib. Cancer Biol Ther 2004;3:847–52.
25. Sun SY, Schroeder CP, Yue P, Lotan D, Hong WK, Lotan R. Enhanced growth inhibition and apoptosis induction in NSCLC cell lines by combination of celecoxib and 4HPR at clinically relevant concentrations. Cancer Biol Ther 2005;4:407–13.
26. Suzuki S, Higuchi M, Proske RJ, Oridate N, Hong WK, Lotan R. Implication of mitochondria-derived reactive oxygen species, cytochrome *c* and caspase-3 in *N*-(4 hydroxyphenyl)retinamide-induced apoptosis in cervical carcinoma cells. Oncogene 1999;18:6380–7.
27. Zou CP, Kurie JM, Lotan D, Zou CC, Hong WK, Lotan R. Higher potency of *N*-(4-hydroxyphenyl)retinamide than all-*trans*-retinoic acid in induction of apoptosis in non-small cell lung cancer cell lines. Clin Cancer Res 1998;4:1345–55.
28. Sun SY, Hail N, Jr., Lotan R. Apoptosis as a novel target for cancer chemoprevention. J Natl Cancer Inst 2004;96:662–72.
29. Guerrieri-Gonzaga A, Robertson C, Bonanni B, et al. Preliminary results on safety and activity of a randomized, double-blind, 2 × 2 trial of low-dose tamoxifen and fenretinide for breast cancer prevention in premenopausal women. J Clin Oncol 2006;24:129–35.
30. Klein-Szanto AJ, Iizasa T, Momiki S, et al. A tobacco-specific *N*-nitrosamine or cigarette smoke condensate causes neoplastic transformation of xenotransplanted human bronchial epithelial cells. Proc Natl Acad Sci U S A 1992;89:6693–7.
31. Reddel RR, Ke Y, Gerwin BI, et al. Transformation of human bronchial epithelial cells by infection with SV40 or adenovirus-12 SV40 hybrid virus, or transfection via strontium phosphate coprecipitation with a plasmid containing SV40 early region genes. Cancer Res 1988;48:1904–9.
32. Skehan P, Storeng R, Scudiero D, et al. New colorimetric cytotoxicity assay for anticancer-drug screening. J Natl Cancer Inst 1990;82:1107–12.
33. Li X, Traganos F, Melamed MR, Darzynkiewicz Z. Single-step procedure for labeling DNA strand breaks with fluorescein-or BODIPY-conjugated deoxynucleotides: detection of apoptosis and bromodeoxyuridine incorporation. Cytometry 1995;20:172–80.
34. Chun KH, Kosmeder JW, Sun S, et al. Chemopreventive effects of deguelin, a naturally occurring PI3K/Akt inhibitor, during the malignant transformation of human bronchial epithelial cells. J Natl Cancer Inst 2003;95:291–302.

35. Ji L, Nishizaki M, Gao B, Burbee D, et al. Expression of several genes in the human chromosome 3p21.3 homozygous deletion region by an adenovirus vector results in tumor suppressor activities *in vitro* and *in vivo*. Cancer Res 2002; 62:2715–20.
36. Franke TF, Yang SI, Chan TO, et al. The protein kinase encoded by the Akt protooncogene is a target of the PDGF-activated phosphatidylinositol 3-kinase. Cell 1995;81:727–36.
37. Sinicrope FA, Half E, Morris JS, et al. Cell proliferation and apoptotic indices predict adenoma regression in a placebo-controlled trial of celecoxib in familial adenomatous polyposis patients. Cancer Epidemiol Biomarkers Prev 2004;13:920–7.
38. Garaventa A, Luksch R, Lo Piccolo MS, et al. Phase I trial and pharmacokinetics of fenretinide in children with neuroblastoma. Clin Cancer Res 2003;9: 2032–9.
39. Hiroshima K, Iyoda A, Shibuya K, et al. Evidence of neoangiogenesis and an increase in the number of proliferating cells within the bronchial epithelium of smokers. Cancer 2002;95:1539–45.
40. Lantuejoul S, Soria JC, Morat L, et al. Telomere shortening and telomerase reverse transcriptase expression in preinvasive bronchial lesions. Clin Cancer Res 2005;11:2074–82.
41. Ramirez RD, Sheridan S, Girard L, et al. Immortalization of human bronchial epithelial cells in the absence of viral oncoproteins. Cancer Res 2004;64:9027–34.
42. Zhang Z, Lai GH, Sirica AE. Celecoxib-induced apoptosis in rat cholangiocarcinoma cells mediated by Akt inactivation and Bax translocation. Hepatology 2004;39:1028–37.
43. Jendrossek V, Handrick R, Belka C. Celecoxib activates a novel mitochondrial apoptosis signaling pathway. FASEB J 2003;17:1547–9.
44. Hsu AL, Ching TT, Wang DS, Song X, Rangnekar VM, Chen CS. The cyclooxygenase-2 inhibitor celecoxib induces apoptosis by blocking Akt activation in human prostate cancer cells independently of Bcl-2. J Biol Chem 2000;275:11397–403.
45. Delia D, Aiello A, Formelli F, et al. Regulation of apoptosis induced by the retinoid *N*-(4-hydroxyphenyl) retinamide and effect of deregulated bcl-2. Blood 1995; 85:359–67.
46. Boya P, Morales MC, Gonzalez-Polo RA, et al. The chemopreventive agent *N*-(4-hydroxyphenyl) retinamide induces apoptosis through a mitochondrial pathway regulated by proteins from the Bcl-2 family. Oncogene 2003;22:6220–30.
47. Thompson JE, Thompson CB. Putting the rap on Akt. J Clin Oncol 2004;22:4217–26.
48. Leng J, Han C, Demetris AJ, Michalopoulos GK, Wu T. Cyclooxygenase-2 promotes hepatocellular carcinoma cell growth through Akt activation: evidence for Akt inhibition in celecoxib-induced apoptosis. Hepatology 2003;38:756–68.
49. Arico S, Pattingre S, Bauvy C, et al. Celecoxib induces apoptosis by inhibiting 3-phosphoinositide-dependent protein kinase-1 activity in the human colon cancer HT-29 cell line. J Biol Chem 2002;277: 27613–21.

[Cancer Biology & Therapy 3:9, 847-852, September 2004]; ©2004 Landes Bioscience

Research Paper

Eicosanoid Metabolism in Squamous Cell Carcinoma Cell Lines Derived from Primary and Metastatic Head and Neck Cancer and its Modulation by Celecoxib

Claudia P. Schroeder[1]
Peiying Yang[2]
Robert A. Newman[2]
Reuben Lotan[1,*]

[1]Department of Thoracic, Head and Neck Medical Oncology; [2]Department of Experimental Therapeutics; The University of Texas M. D. Anderson Cancer Center; Houston, Texas USA

*Correspondence to: Reuben Lotan, The University of Texas M. D. Anderson Cancer Center; 1515 Holcombe Blvd.; Houston, Texas 77030 USA; Tel.: 713.792.8467; Fax: 713.745.5656; Email: rlotan@mdanderson.org

Received 05/19/04; Accepted 06/18/04

Previously published online as a *Cancer Biology & Therapy* E-publication: http://www.landesbioscience.com/journals/cbt/abstract.php?id=1037

KEY WORDS

celecoxib, COX-2 inhibitors, cyclooxygenases, eicosanoid metabolism, HNSCC cell lines, leukotrienes, lipoxygenases, prostaglandins

ABBREVIATIONS

BHT	butylated hydroxytoluene
COX	cyclooxygenase
DMEM	Dulbecco's Modified Eagle's Minimal Essential Medium
DMSO	dimethyl sulfoxide
FBS	fetal bovine serum
HETE	hydroxyeicosatetraenoic acid
HNSCC	head and neck squamous cell carcinoma
HODE	hydroxyoctadecadienoic acid
ESI-LC/MS/MS	electrospray ionization liquid chromatography tandem mass spectrometry
LOX	lipoxygenase
MTT	[3-(4,5-dimethylthiazol-2-yl)2,5-diphenyl-2H-tetrazolium-bromide]
NSAIDs	nonsteroidal anti-inflammatory drugs
PBS	phosphate-buffered saline
PG	prostaglandin

ACKNOWLEDGEMENTS

This work was supported by a fellowship from the Deutsche Forschungsgemeinschaft (DFG, Germany); PO1 CA98144 from the National Cancer Institute, and BESCT Lung Cancer Program from the Department of Defense (grant DAMD17-01-1-0689-2).

ABSTRACT

Eicosanoid metabolism through cyclooxygenases (COXs) and lipoxygenases (LOXs) generates various lipids that play a role in squamous cell carcinogenesis. We used pairs of head and neck squamous cell carcinoma (HNSCC) cell lines derived from primary and metastatic tumors of the same patient to analyze eicosanoid metabolites by ESI-LC/MS/MS and COX/LOX expression by western immunoblotting. The effects of celecoxib on eicosanoid synthesis and HNSCC cell growth were examined. Prostaglandin E_2 (PGE_2) was the major metabolite in three of six cell lines. COX-2 was detected in three cell lines, which produced PGE_2 (two from metastases). We found low expression of COX-1 at similar intensities for each pair of cell lines. 5-LOX was detected in all cells. Some expressed 12-LOX, 15-LOX-1, and 15-LOX-2, but there was no correlation between enzyme expression and endogenous product content in cells. Exogenous arachidonic acid did not change the profile of eicosanoid biosynthesis. Low doses of celecoxib inhibited formation of PGE_2 in UMSCC-14A cells by 84% as early as 6 hours. In contrast, 5-HETE, 12-HETE, and 15-HETE levels were increased by approximately 40-, 5- and 3-fold, respectively, with a decline to baseline levels within 24 hours. High dose celecoxib increased the 12-HETE level 2.3-fold after 3 days of incubation. Celecoxib inhibited growth of all HNSCC cell lines in a concentration-dependent manner regardless of their COX expression (IC_{50} values after 3 days; 33 to 62 μM). Our findings provide new informations about individual eicosanoids produced by HNSCC cells and their differential regulation by the selective COX-2 inhibitor celecoxib.

INTRODUCTION

Squamous cell carcinomas (SCC) of the head and neck (HN) are potentially aggressive tumors characterized by considerable morbidity and mortality due to a high incidence of local recurrence and lymph node metastasis.[1] The long-term survival of patients could be improved by prevention of carcinogenesis and secondary lesions that are associated with invasive behavior of the primary tumor. Therefore, understanding mechanisms that affect growth, survival, and invasiveness of tumor cells may benefit future rational design for treatment and prevention of cancer. A body of evidence suggests that the metabolism of polyunsaturated fatty acids (e.g., arachidonic acid) is critically involved in the development of HNSCC.[2-4] In particular, altered expression and activity of cyclooxygenases (COXs) and lipoxygenases (LOXs) including their metabolites referred to as eicosanoids have been implicated in squamous cell carcinogenesis.[5-8]

Arachidonic acid, derived from membrane phospholipids through the action of phospholipase, is metabolized by COXs to prostaglandins (PGs) and thromboxanes, and by LOXs to leukotrienes, lipoxins and a variety of mono-hydroxylated fatty acids such as HETEs.[9] The oxidative pathway of linoleic acid leads to hydroxyoctadecadienoic acids (HODEs) predominantly formed by 15-LOX-1.[10] Although, multiple enzymes related to eicosanoid metabolism are similar in terms of structure, substrate preference and mechanisms of action, a variety of biological effects have been demonstrated for their products in various experimental models.[11-14] In fact, elevated PG levels have been detected in HNSCC cell lines and neoplastic tissues resected from patients.[15-17] Furthermore, there is evidence for a strong correlation between PGE_2 synthesis and prognostic significance as well as metastatic ability of tumor cells in vivo,[18,19] Accordingly, COX-2 isoenzyme is frequently upregulated in HN cancers that have been reported to be associated with tumor growth, resistance to apoptosis, metastasis, and angiogenesis.[7,20-22] The function and molecular mechanisms of LOX products in cancer, however, remain less clear although recent studies have suggested that LOX activation may be involved in both pro- and

anti-tumorigenic effects.[11,13,14] Analysis of human saliva and primary tumor tissue samples from patients with SCC showed significantly elevated levels of 12-HETE, 5-HETE, and 15-HETE.[5,23] In addition, data on SCC cell lines have postulated a close relationship between growth control and LOX pathways.[11] Recent studies have shown that nonsteroidal anti-inflammatory drugs (NSAIDs) can increase the expression of 15-LOX-1 and 15-LOX-2 isoenzymes, which were downregulated in HN cancer cells. These effects were accompanied by inhibition of cell proliferation and induction of apoptosis.[13,14] Nonetheless, modulation of the eicosanoid metabolism by COX-inhibitors such as aspirin and other NSAIDs exerts chemopreventive activity on the development of SCC.[24-26] Celecoxib, a selective COX-2 inhibitor, was found to suppress oral cancer growth and angiogenesis in a nude mouse model.[27] Although the most likely antitumoral effects of NSAIDs are based on the blockade of PG synthesis, accumulating evidence suggests that mechanisms of action may not be exclusively mediated by inhibition of COX activity.[11,13,28-31]

In this study we analyzed eicosanoid metabolites and related enzymes in pairs of HNSCC cell lines derived from primary and recurrent or metastatic tumor samples of the same patient. We found a correlation between PGE_2 production and COX-2 expression, which appeared to be higher in HNSCC cell lines derived from metastasis. We therefore investigated the effects of the selective COX-2 inhibitor, celecoxib, on eicosanoid production and HNSCC cell growth.

MATERIALS AND METHODS

Reagents. Dulbecco's Modified Eagle's Minimal Essential Medium (DMEM)/Ham's F12, penicillin, streptomycin, phosphate-buffered saline (PBS) and trypsin were purchased from Gibco™ Invitrogen Corporation (Carlsbad, CA). Fetal bovine serum (FBS) was from HyClone Laboratories, Inc. (Logan, UT) and celecoxib (Celebrex®) was obtained from GD Searle & Co (Chicago, IL). Arachidonic acid, bovine serum albumin, butylated hydroxytoluene (BHT), citric acid, dimethyl sulfoxide (DMSO), ethylene diamine tetra-acetic acid (EDTA), [3-(4,5-dimethylthiazol-2-yl)2,5-diphenyl-2H-tetrazolium bromide] (MTT) and sodium dodecyl sulfate (SDS) were from Sigma Chemical Co. (St. Louis, MO). Mouse monoclonal antibody against human prostaglandin H synthase-1 peptide (PGHS-1, COX-1), and rabbit polyclonal antibodies against PGHS-2 (COX-2), 12-LOX and 15-LOX-2 were from Oxford Biomedical Research Inc. (Oxford, MI). Anti-actin was obtained from Santa Cruz Biotechnology Inc. (Santa Cruz, CA) and anti-human 5-LOX antiserum was from BD Bioscience Pharmingen (San Diego, CA). Rabbit polyclonal antiserum to human 15-LOX-1 was kindly provided by Dr. I. Shureiqi (Shureiqi et al., 2001). Secondary antibody to IgG conjugated to horseradish peroxidase was from Amersham Biosciences Corp. (Piscataway, NJ). The deuterium-labeled eicosanoids PGE_2, 5-HETE, 12-HETE, 15-HETE, and 13-HODE used as internal standard for ESI-LC/MS/MS analyses were purchased from Cayman Chemical Co. (Ann Arbor, MI).

Human Squamous Carcinoma Cell Lines of the Head and Neck. The continuous human squamous carcinoma cell lines UMSCC-11A/-11B, UMSCC-14A/-14B, UMSCC-17A/-17B, and UMSCC-22A/-22B were kindly provided by Dr. T. Carey (University of Michigan, Ann Arbor, MI) and have been characterized elsewhere.[32] The cell lines derived from the primary tumor *suffix A* and the corresponding recurrent or metastatic lesion *suffix B* of the same patient are shown in Table 1. Cells were routinely maintained in DMEM/Ham's F12 (1:1, v/v) supplemented with 5% FBS, penicillin (100 units/ml) and streptomycin (100 µg/ml) defined as standard medium at 37°C in a humidified atmosphere of 95% air and 5% CO_2. Cultures were passaged twice a week using 0.25% trypsin containing 0.02% EDTA. The desired concentrations of celecoxib were made by diluting the stock solution (0.05 M/DMSO) directly into the culture medium keeping the final concentration of DMSO less than 0.1%. All experiments were carried out in the presence of 5% FBS.

Table 1 **SOURCE OF HNSCC CELL LINES** [a]

Cell line	Location of tumor
UMSCC-11A	Hypopharynx
UMSCC-11B	Recurrence from 11A tumor specimen
UMSCC-14A	Floor of the mouth
UMSCC-14B	Recurrence from 14A tumor specimen
UMSCC-17A	Larynx (supraglottis)
UMSCC-17B	Neck soft tissue metastasis from 17A tumor
UMSCC-22A	Hypopharynx
UMSCC-22B	Lymph node metastasis from 22A tumor

[a]Carey TE. Head and neck tumor cell lines. In: Hay RJ, Park JG, Gazdar A (eds.) Atlas of human tumor cell lines 1994. New York Academic Press:p79.

Cell Growth Studies. The effect of celecoxib on growth of various HNSCC cell lines was determined by MTT colorimetric assay.[33] Briefly, the cells were harvested, centrifuged, and resuspended in standard medium before seeding 2 x 10^4 cells/well in 96-well culture plates (BD Bioscience Labware, Bedford, MA) and incubated overnight at 37°C. Cells were then treated with celecoxib at different concentrations or equal amounts of medium containing DMSO for control cultures. After 72 hours of incubation, MTT (2 mg/ml) was added and the generated formazan crystals were solubilized in 25% SDS/0.075 N NaOH before reading the absorbance at 550/690 nm in a microtiter plate reader MR5000 (Dynatech Laboratories Inc., Chantilly, VA). The percentage of growth inhibition was calculated from the equation, % of control = (OD_t/OD_c) x 100% whereas OD_t and OD_c are optical densities of treated and control cultures, respectively. Concentration-response curves were plotted and levels of celecoxib resulting in 50% inhibition of cell growth (IC_{50} values) were calculated. The data represent mean ± standard deviations (SD) of three independent experiments performed in quadruplicate.

Western Blot Analysis. Immunoblot analyses were performed on cell lysates using 8% SDS-polyacrylamide gel electrophoresis. Cell layers at approximately 80% confluence were washed twice with ice-cold PBS and collected in lysis buffer containing 150 mM NaCl, 0.02% NaN_3, 2% Igepal CA-630, 0.5% sodium deoxycholate, 0.2% SDS, and 50 mM Tris-HCl, pH 8.0) supplemented with protease inhibitors leupeptin (1 µg/ml), aprotinin (1 µg/ml), pepstatin (0.5 µg/ml), and phenylmethylsulfonyl fluoride (100 µg/ml). Protein concentrations were measured using Bio-Rad Protein Assay (Bio-Rad Laboratories, Hercules, CA) with bovine serum albumin used as standard protein. A total of 50 µg of protein was mixed with sample buffer (0.5 M Tris, pH 6.8; 0.3% glycerol; 0.03% β-mercaptoethanol; 10% SDS; 0.001% bromphenolblue), and electrophoretically separated and transferred onto Trans-Blot®nitrocellulose membranes (Bio-Rad Laboratories, Hercules, CA) prior blocking overnight at 4°C in 5% nonfat dry milk solution in 0.1% (w/v) Tween 20 in PBS. The membranes were probed with anti-human antibodies against COX-1 (1:1000), COX-2 (1:1000), 5-LOX (1:500), 12-LOX (1:100), 15-LOX-1 (1:2000) and 15-LOX-2 (1:3000) and incubated with peroxidase conjugated secondary antibody (1:5000). Bands were visualized by either ECL™ Western Blotting Detection Kit from Amersham Biosciences Corp. (Piscataway, NJ) or SuperSignal® West Femto Maximum Kit from Pierce (Rockford, IL) before exposure to Kodak X-Omat film (Eastman Kodak Co., Rochester, NY). Loading and transferring control was confirmed by probing the membranes with anti-β-actin antibody (1:1000).

Determination of Eicosanoid Levels by ESI-LC/MS/MS. Electrospray ionization liquid chromatography tandem mass spectrometry (ESI-LC/MS/MS) was performed to quantify eicosanoids as described previously.[34] For determination of intracellular eicosanoid levels, cells were harvested by

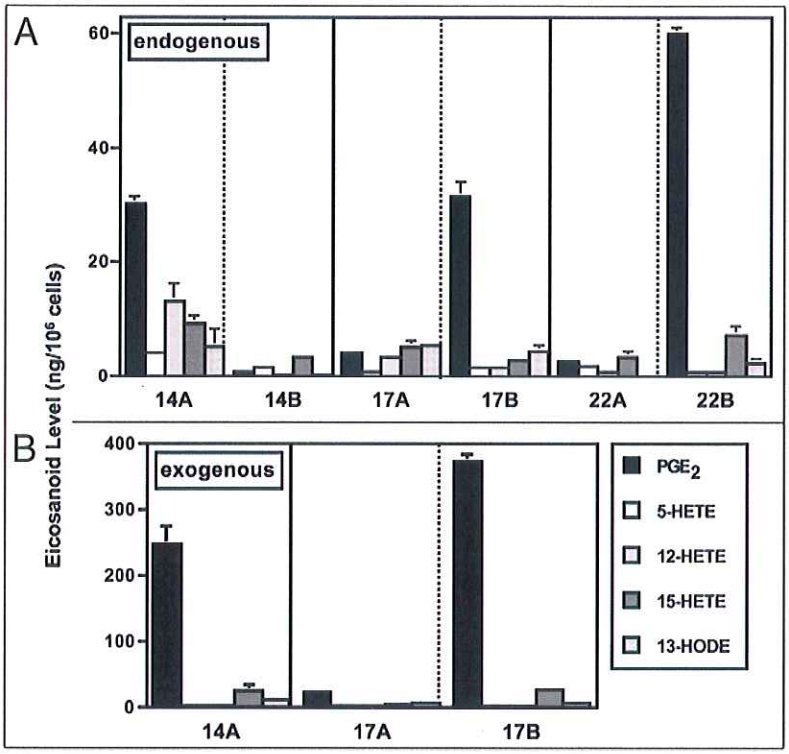


Figure 1 (Left). (A) Endogenous and (B) exogenous production of PGE_2, 5-HETE, 12-HETE, 15-HETE, and 13-HODE in pairs of UMSCC cell lines derived from primary (*suffix A*) and recurrent or metastatic (*suffix B*) tumors of the same patient. Cells were seeded and grown in 5% FBS-containing DMEM/Ham's F12 for 3 days prior to extraction with hexane: ethyl acetate (1:1) and analysis by ESI-LC/MS/MS. For exogenous eicosanoid levels, culture medium of three representative cell lines (UMSCC-14A, UMSCC-17A/-17B) were incubated with arachidonic acid (10 μM, 30 min) prior to collection, extraction, and analysis by ESI-LC/MS/MS as described under Materials and Methods.

trypsinization and resuspended in 500 μl PBS followed by addition of 20 μl of 1 N citric acid and 2.5 μl of 10% BHT to prevent free radical peroxidation. Samples were spiked with a mixture of deuterium-labeled eicosanoids of interest that served as internal standards (PGE_2-d_4, 5-HETE-d_8, 12-HETE-d_8, 15-HETE-d_8, and 13-HODE-d_4). Eicosanoids were extracted with 2 ml of hexane:ethyl acetate (v/v, 1:1) and vortex mixed prior to centrifugation at 1800 x *g* for 10 min. All extraction steps were performed under conditions of minimal light and 4°C. Samples were reconstituted in 200 μl methanol:10 mM ammonium acetate buffer (v/v, 70:30, pH 8.5) prior to analysis by ESI-LC/MS/MS. Eicosanoids secreted into cell culture medium were extracted using a solid phase method. Specifically, an aliquot of 10 μl of 10% BHT and 10 μl of a mixture of internal standards (PGE_2-d_4, 5-HETE-d_8, 12-HETE-d_8, 15-HETE-d_8, and 13-HODE-d_4) was added to 1 ml of culture medium. The solution was applied to a Sep-Pak C18 cartridge (Waters Corp., Milford, MA) that had been preconditioned with methanol and water. Eicosanoids were eluted with 1 ml of methanol and evaporated under a stream of nitrogen. Samples were then reconstituted in 100 μl methanol:10 mM ammonium acetate buffer (v/v, 70:30, pH 8.5) prior to analysis. For determination of exogenous eicosanoid levels, 10 μM arachidonic acid was added prior to collection of media and cells for 30 min.

ESI-LC/MS/MS was performed using a Quattro Ultima tandem mass spectrometer (Micromass, Beverly, MA) equipped with an Agilent HP1100 binary pump HPLC inlet. Metabolites were separated using a Luna 3 μm phenyl hexyl 2 x 150 mm analytical column (Phenomenex, Torrance, CA). The mobile phase consisted of 10 mM ammonium acetate (pH 8.5) and methanol. The flow rate was 250 μl/min with a column temperature maintained at 50°C and an injection volume of 25 μl. Fragmentation for all compounds was performed using argon as the collision gas at a collision cell pressure of 2.10×10^{-3} Torr. The results were expressed as nanograms of each eicosanoid per 10^6 cells. To normalize data, the cell number was measured with an electronic particle counter (Coulter, Hialeah, FL). Results shown represent mean values of at least two independent experiments.

RESULTS

Endogenous and Exogenous Level of Eicosanoids in HNSCC Cell Lines Derived from Primary and Recurrent or Metastatic Tumors. To determine whether progression of HNSCC from primary to metastatic lesion was associated with alterations in their eicosanoid metabolism, we analyzed a series of HNSCC cell lines (Table 1) for their endogenous level of various arachidonic acid and linoleic acid metabolites using ESI-LC/MS/MS. As shown in Figure 1A, three of the six cell lines produced relatively high levels of PGE_2 while 12-HETE was the second most abundant metabolite in UMSCC-14A cells. In two of three pairs, the cell lines which were derived from metastasis maintained considerably higher levels of PGE_2 than cells established from the corresponding primary tumor. The production of eicosanoids other than PGE_2 was found to be low in all HNSCC cell lines. Next, we provided the culture medium of three representative cell lines with exogenous arachidonic acid (10 μM, 30 min) in order to estimate the activity of COXs and LOXs under conditions of substrate abundance. Figure 1B demonstrates that PGE_2 was the major metabolite in UMSCC-14A and UMSCC-17B cells reaching levels of 246 and 372 ng/10^6 cells, respectively. That indicates an approximately 8- and 12-fold increase

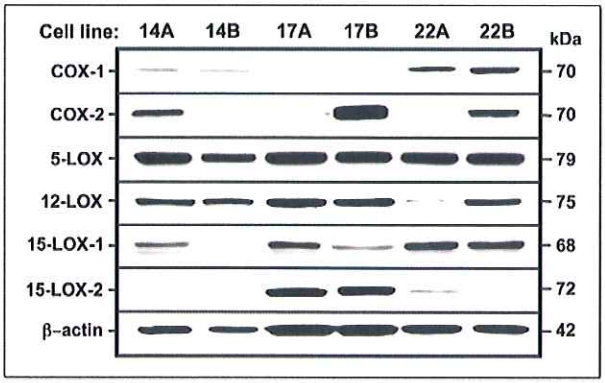


Figure 2. Expression of arachidonic acid and linoleic acid metabolizing enzymes in HNSCC cell lines established from primary (*suffix A*) and recurrent or metastatic (*suffix B*) tumors of the same patient. A total of 50 μg of protein per sample was separated using 8% SDS-polyacrylamid gel electrophoresis and transferred onto nitrocellulose membranes. The immunoblot was probed with antibodies specific for COX-1, COX-2, 5-LOX, 12-LOX, 15-LOX-1, and 15-LOX-2. β-actin was used as loading control. COX-2 protein was overexpressed in two of three HNSCC cell lines derived from metastatic than from primary tumor tissue, whereas COX-1 revealed low levels with similar intensities for each pair of cell lines. 5-LOX was universally detected in all UMSCC cell lines. Likewise for 12-LOX but one of the cell lines, UMSCC-22A, exhibited less protein. For 15-LOX-1 staining, HNSCC cell lines established from primary lesions expressed the protein more profoundly (UMSCC-14A, UMSCC-17A) or similarly (UMSCC-22A/22B) than those derived from metastatic or recurrent tumor. 15-LOX-2 expression was high in UMSCC-17A/-17B cells, low in UMSCC-22A, and absent in UMSCC-14A/- 14B cells.

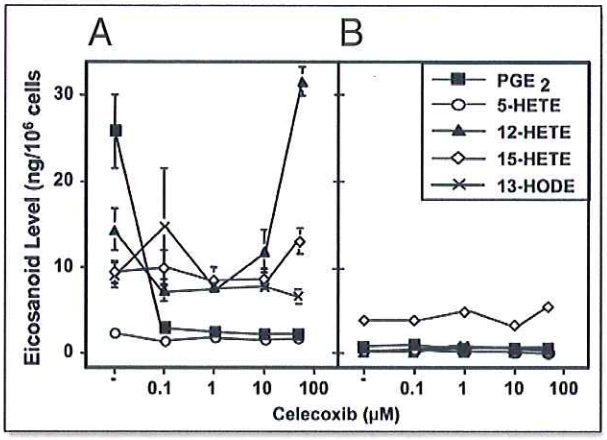


Figure 3. Concentration-dependent effect of celecoxib on endogenous production of PGE_2, 5-HETE, 12-HETE, 15-HETE, and 13-HODE in UMSCC-14A (A) and UMSCC-14B cells (B). Cell cultures were treated with different concentrations of celecoxib for 72 hours before extraction of eicosanoids with hexane:ethyl acetate (1:1) and analysis by ESI-LC/MS/MS. Data presented are the mean ± SD of two separate experiments.

compared with their endogenous production of 30 and 32 ng/10^6 cells, respectively. However, the biosynthesis of other metabolites remained at low levels in spite of exogenous availability of arachidonic acid. UMSCC-17A cells failed to generate detectable levels of any eicosanoids examined.

Expression of Arachidonic Acid- and Linoleic Acid-Metabolizing Enzymes in HNSCC Cell Lines. Next we asked, whether the predominance of PGE_2 among other metabolites resulted in the preferential expression of COXs in HNSCC cells. To address this question, we investigated the constitutive levels of COX-1 and COX-2 including other eicosanoid-generating enzymes such as 5-LOX, 12-LOX, 15-LOX-1, and 15-LOX-2 by western immunoblotting. As shown in Figure 2, COX-1 was weakly expressed in UMSCC-14A/-14B and UMSCC-17A/-17B cells but had a higher level of expression in UMSCC-22A/-22B cells. Immunoreactive bands for COX-1 revealed similar intensities for each pair of cell line. In contrast, COX-2 was differentially regulated in HNSCC cell lines derived from primary or metastatic tumor with a higher expression in two of three pairs in the latter. We found that 5-LOX protein was expressed in all cell lines as well as 12-LOX except for UMSCC-22A cells, which exhibited less protein. Incubation of the same membrane with anti-15-LOX-1 demonstrated that HNSCC cell lines established from primary lesions expressed bands with higher and in case of UMSCC-22A/22B cells, similar intensities than those derived from metastases. 15-LOX-2 expression was high in UMSCC-17A/-17B, low in UMSCC-22A, and absent in UMSCC-14A/14B or UMSCC-22B cells.

Effect of Celecoxib on Eicosanoid Levels in UMSCC-14A and -14B Cells. Because PGE_2 levels correlated with COX-2 protein expression in HNSCC cells, we examined the effect of the selective COX-2 inhibitor, celecoxib, on endogenous production of eicosanoids in UMSCC-14A/ and -14B cells by ESI-LC/MS/MS. Data in Figure 3A indicate that the production of PGE_2, the major metabolite generated by COX-2, was markedly inhibited by 89% (from 25.9 to 2.9 ng/10^6 cells) with as little as 0.1 μM celecoxib after a 3-day treatment of UMSCC-14A cells. No further reduction was observed after treatment with higher doses of celecoxib. The results further demonstrate that celecoxib at concentrations up to 50 μM exerted only minor effects on the production of 5-HETE, 15-HETE, and 13-HODE in UMSCC-14A cells. However, the synthesis of 12-HETE increased from 14.3 to 31.6 ng/10^6 cells after treatment with 50 μM celecoxib. No effects on PGE_2 production and other eicosanoid metabolites were detected in celecoxib treated UMSCC-14B cells (Fig. 3B). These cells produced relatively little PGE_2 (0.9 ng/10^6 cells) and lacked COX-2 expression. However, the cells displayed a considerable amount of 5-LOX and 12-LOX enzymes estimated by immunoblotting (Fig. 2).

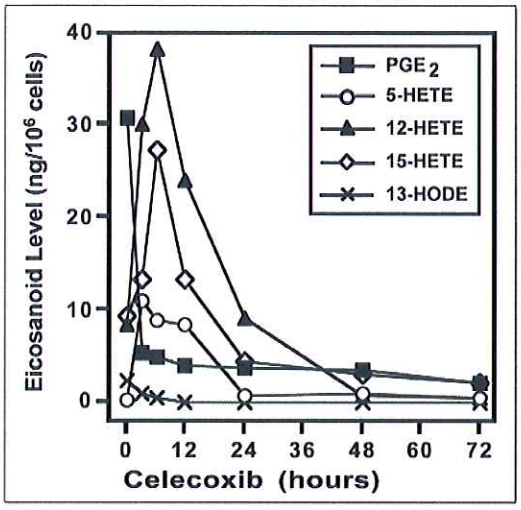


Figure 4. Time-dependent effect of celecoxib (1 μM) on endogenous eicosanoid level in UMSCC-14A cells. Cells were seeded and grown in 5% FBS-containing DMEM/Ham's F12 medium prior to extraction with hexane: ethyl acetate (1:1) and analysis by ESI-LC/MS/MS described under Materials and Methods.

The suppression of PGE_2 in UMSCC-14A cells was observed as early as 3 hours after exposure to 1 μM celecoxib (Fig. 4). In contrast, the production of LOX-derived metabolites 5-HETE, 12-HETE, and 15-HETE increased from 0.23, 8.5, and 9.3 to 8.9, 38.2, and 27.3 ng/10^6 cells, respectively. These effects occurred within 6 hours followed by a subsequent decline to baseline levels after 24 hours of celecoxib treatment. The low synthesis of 13-HODE (2.22 ng/10^6 cells) in UMSCC-14A cells did not change. Rather, it decreased to undetectable levels after 12 hours of incubation with celecoxib.

Effect of Celecoxib on Growth of Various HNSCC Cell Lines. The ability of celecoxib to suppress PGE_2 raised the question whether these effects were associated with growth inhibition in HNSCC cell lines. We examined celecoxib concentrations causing 50% growth inhibition (IC_{50} values) obtained from concentration-response curves after 72 hours of incubation and compared those with constitutive COX expression. Celecoxib inhibited growth of HNSCC cell lines in a concentration-dependent manner between 25 and 75 μM (Fig. 5A). The IC_{50} values ranged from 33 to 62 μM celecoxib (Fig. 5B). The level of COX-2 expression revealed no correlation with the relative sensitivity of HNSCC cell lines to celecoxib (Fig. 5C). In fact, cell lines that expressed COX-2 (UMSCC-11A/11B, UMSCC-14A, UMSCC-17B, UMSCC-22B) were as sensitive as cell lines with low or undetectable COX-2 protein levels (UMSCC-14B, UMSCC-17A, UMSCC-22A). Likewise, no direct correlation between COX-1 and the growth-inhibitory effects of celecoxib in HNSCC cell lines was observed (Fig. 5C).

DISCUSSION

Eicosanoid metabolism leads to generation of bioactive lipids known to promote cancer.[2,9] Metabolites of both, COX and LOX pathways, have been found to be elevated in tumor tissues, plasma and saliva obtained from patients with HN cancer.[5,15,19,23] In addition, altered expression of various enzymes and genes related to arachidonic acid metabolism are known to contribute to squamous cell carcinogenesis.[4,7,8]

In this study, we used an in vitro model consisting of paired SCC cell lines derived from primary and recurrent or metastatic HN tumors to investigate the production of various metabolites of arachidonic acid and linoleic acid pathways by ESI-LC/MS/MS. We found that PGE_2 was the most abundant metabolite in three of six

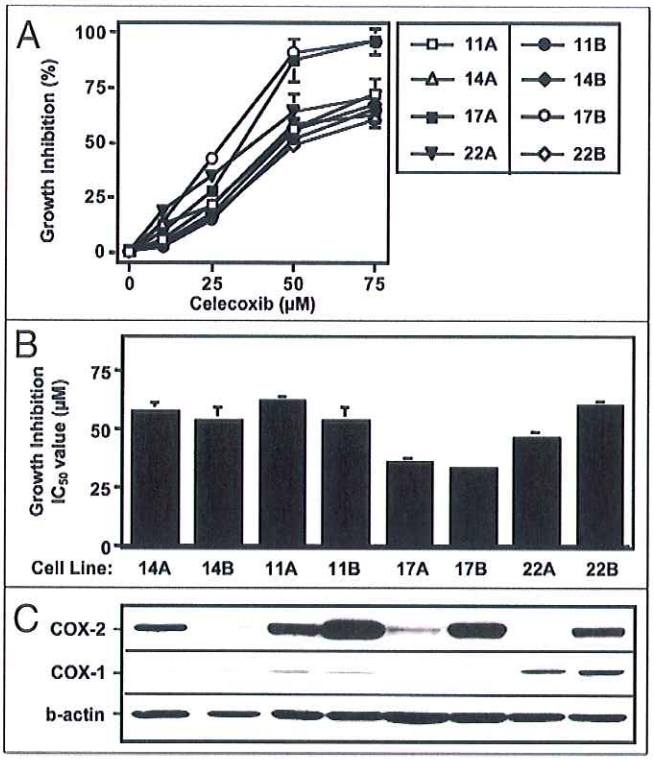


Figure 5. Effect of the selective COX-2 inhibitor celecoxib on growth inhibition of HNSCC cell lines derived from primary (*suffix A*) and recurrent or metastatic (*suffix B*) tumors of the same patient. Cells were seeded into 96-well culture plates and allowed to adhere overnight before treated with celecoxib at different concentrations. Changes in cell survival as a function of the dose of celecoxib was determined by MTT assay after 72 hours of incubation (A). Concentrations required for the determination of IC_{50} values of celecoxib were obtained by interpolation of dose-response curves (B). Results represent mean ± SD of quadruplicate measurements of three independent experiments. Inhibitory effects of celecoxib on cell growth were independent of neither constitutive COX-2 nor COX-1 expression in different HNSCC cell lines analyzed by western blotting. β-actin served as loading control (C).

HNSCC cell lines. Interestingly, two of the three were established from metastases. Other eicosanoid metabolites (e.g., 12-HETE, 15-HETE) were identified in UMSCC-14A cells but were produced at very low levels in all HNSCC cell lines examined. Subsequent western blot analysis of a battery of arachidonic acid- and linoleic acid-metabolizing enzymes has indicated that multiple proteins in addition to COX-1 and COX-2 were expressed. However, with the exception of PGE_2, that correlated with COX-2 levels, other metabolites produced by HNSCC cells showed no correlation with the expression of their corresponding enzymes. The obtained lack of correlation was not due to a limited amount of endogenous arachidonic acid as indicated by the findings that addition of arachidonic acid to the culture medium resulted in an approximately 10-fold increase of PGE_2 only in COX-2 positive HNSCC cell lines but failed to enhance the production of other eicosanoids despite the presence of their metabolizing enzymes. Thus, the activities of eicosanoid-generating enzymes, with the exception of COXs, were impaired in HNSCC cell lines examined for unknown reason(s). Plausible explanations are that particular enzymes might be mutated or localized in intracellular sites that are distinct from the site of their specific substrates. For example, the activities of 15-LOX-1 and 5-LOX have been found to be dependent on the localization of these enzymes in the cytoplasm, nucleoplasm, and intracellular biomembranes, respectively.[35,36] Moreover, COX-2 enzyme was detected in HT-29 colorectal cancer cells by western blotting yet these cells were unable to convert arachidonic acid to prostaglandins.[37] Interestingly, the COX-2 cloned from HT-29 cells was catalytically active when transfected into HCT-116 cancer cells. The authors suggested that a putative endogenous inhibitor of COX-2 may be present or conversely, a cofactor is missing that is necessary for COX-2 activity in HT-29 cells. However, our data on paired HNSCC cell lines revealed a good correlation between COX-2 expression and COX-2 activity measured as PGE_2 production. Here, we show a discrepancy between protein levels and enzymatic activities of a large number of eicosanoid-generating enzymes other than COXs.

The fact that PGE_2 synthesis correlated with the expression levels of COX-2 has led us to investigate the effects of the selective COX-2 inhibitor, celecoxib, on eicosanoid metabolism and growth of HNSCC cells. Here, we demonstrate for the first time, that inhibition of the COX pathway by celecoxib resulted in a time-dependent activation of the LOX pathway. Specifically, the production of multiple LOX-metabolites, e.g., 5-HETE, 12-HETE, and 15-HETE, increased as the PGE_2 level declined in UMSCC-14A cells treated with celecoxib at 1 μM, a concentration that is easily achieved in patients. The increase of various LOX metabolites may be considered as a cellular response to the profound decline of PGE_2 levels. Our results further indicate that inhibition of HNSCC cell growth by celecoxib was not closely related to the expression of COX-2. Comparable IC_{50} values were observed in all HNSCC cell lines regardless of their COX-2 status. Furthermore, celecoxib was effective in decreasing PGE_2 levels at concentrations that showed no effect on cell growth. This suggests that the growth inhibitory activity of celecoxib was at least partially independent of the suppression of PGE_2 synthesis. PGs are important regulators of cellular proliferation known to promote tumorigenesis and suppress immune response in vivo.[9] The prognostic significance of elevated PGE_2 levels in SCC is not entirely known. While increased levels have been detected in carcinomas, the cellular origin of PGE_2 in fresh tumor biopsies is difficult to determine due to the fact that the majority of PGE_2 derives from inflammatory cells participating in tumor-directed immune response.[15,16] The functional relevance of COX-2 derived PGE_2 on HNSCC cell growth has been supported by observations that exogenous PGE_2 was able to abrogate the antiproliferative effects of selective COX-2 inhibitors.[17,30,38] In addition, PGE_2 levels were significantly higher in COX-2 expressing compared to nonexpressing oral cancer cell lines associated with inhibition of proliferation and induction of apoptosis after treatment with selective COX-2 inhibitors.[21] However, a controversy has been raised by reports that COX-2 inhibitors may act independently of inhibition of PG synthesis.[11,13,14,30,31] Our data show that much higher concentrations of celecoxib are needed to suppress cell growth in vitro than those achievable in humans. On the other hand, concentrations required for the inhibition of PGE_2 synthesis in vitro are clinically attainable. The precise mechanisms by which celecoxib suppresses tumor growth has not been fully defined. It is more likely to be related to suppression of PGE_2 synthesis than to direct inhibition of tumor cell growth. For example, suppression of COX-2 derived PGE_2 decreased microvessel density and inhibited mammary tumor progression.[39] Besides, a study using a mouse model of oral cancer has shown that celecoxib significantly delayed cell growth, reduced tumor volume and exerted antiangiogenic activity.[27] Nonetheless, accumulating evidence suggest that COX-2 independent molecular targets may

contribute to the antitumoral effects of NSAIDs including 15-LOX-1,[13] 15-LOX-2,[14] arachidonic acid,[40] NF-κB,[28] and PPARγ.[29] The expression of COX-2, classified as immediate-early response gene, is well known to be upregulated in response to pathological processes such as inflammation and cancer.[2,9] In contrast, COX-1 has been found in both normal and malignant cells. Recently, it has been reported that COX-1 can also be induced in human esophageal SCC by a variety of proinflammatory stimuli and its expression under neoplastic conditions seems related to cellular differentiation.[8] We included the expression levels of COX-1 in our study due to the fact that PGE_2 is synthesized from arachidonic acid by both isoenzymes. Similarly, we found no correlation between COX-1 status and the antiproliferative activity of celecoxib. The levels of LOX products, namely 5-HETE, 12-HETE, and 15-HETE have been reported to be elevated in HN cancer patients.[5,23] Moreover, inhibition of arachidonic acid metabolism, particularly the LOX pathway, exerted antitumor effects postulating a role for LOX metabolites in HN tumorigenesis.[11] Our data indicate an increase of 12-HETE after 3 days of incubation with celecoxib at a concentration above the estimated IC_{50} value. 12-HETE is the only metabolite of the arachidonic acid-metabolizing enzyme 12-LOX suggested to act as regulator of tumor growth and motility.[2] However, the role of 12-HETE in SCC of the HN has not been adequately investigated.

In conclusion, our study demonstrates that western blot analysis of enzymes related to the arachidonic acid and linoleic acid cascade is insufficient for assessment of the eicosanoid metabolism. Therefore, ESI-LC/MS/MS analysis or comparable analytical methods are warranted for a more reliable evaluation. In addition, we have shown that suppressing PGE_2 levels by celecoxib leads to an enhanced activity of 5-LOX, 12-LOX and 15-LOX-2 as indicated by the increases of their products 5-HETE, 12-HETE and 15-HETE. Whereas suppression of PGE_2 was persistent, the increase in LOX metabolites appeared to be transient. Nevertheless, the dynamic transition between COX and LOX pathways may play a role in the cellular response to celecoxib in vivo and raises the need to consider targeting both enzymatic pathways by using COX in combination with LOX inhibitors.

References

1. Greenlee RT, Hill-Harmon MB, Murray T, Thun M. Cancer statistics, 2001. CA Cancer J Clin 2001; 51:15-36.
2. Marnett LJ, Honn KV. Overview of articles on eicosanoids and cancer. Cancer Metastasis Rev 1994; 13:237-9.
3. Long JD, Orlando RC. Eicosanoids and the esophagus. Prostaglandins Other Lipid Mediat 2000; 61:91-104.
4. Zhi H, Zhang J, Hu G, Lu J, Wang X, Zhou C, et al. The deregulation of arachidonic acid metabolism-related genes in human esophageal squamous cell carcinoma. Int J Cancer 2003; 106:327-33.
5. Metzger K, Angres G, Maier H, Lehmann WD. Lipoxygenase products in human saliva: Patients with oral cancer compared to controls. Free Radical Biol Med 1995; 18:185-94.
6. Morgan G. Deleterious effects of prostaglandin E2 in oesophageal carcinogenesis. Med Hypotheses 1997; 48:177-81.
7. Maaser K, Däubler P, Barthel B, Heine B, von Lampe B, Stein H, et al. Oesophageal squamous cell neoplasia in head and neck cancer patients: Upregulation of COX-2 during carcinogenesis. Brit J Cancer 2003; 88:1217-22.
8. Kase S, Osaki M, Honjo S, Hashimoto K, Adachi H, Tsujitani S, et al. Expression of cyclooxygenase-1 and cyclooxygenase-2 in human esophageal mucosa, dysplasia and carcinoma. Pathobiology 2004; 71:84-92.
9. Funk CD. Prostaglandins and leukotrienes: Advances in eicosanoid biology. Science 2001; 294:1871-5.
10. Brash AR, Boeglin WE, Chang MS. Discovery of a second 15S-lipoxygenase in humans. Proc Natl Acad Sci USA 1997; 94:6148-52.
11. Ondrey FG, Juhn SK, Adams GL. Inhibition of head and neck tumor cell growth with arachidonic acid metabolism inhibition. Laryngoscope 1996; 106:129-34.
12. Scioscia KA, Snyderman CH, D'Amico F, Comsa S, Rueger R, Light B. Effects of arachidonic acid metabolites in a murine model of squamous cell carcinoma. Head Neck 2000; 22:149-55.
13. Shureiqi I, Xu X, Chen D, Lotan R, Morris JS, Fischer SM, et al. Nonsteroidal anti-inflammatory drugs induce apoptosis in esophageal cancer cells by restoring 15-lipoxygenase-1 expression. Cancer Res 2001; 61:4879-84.
14. Xu XC, Shappell SB, Liang Z, Song S, Menter D, Subbarayan V, et al. Reduced 15S-lipoxygenase-2 expression in esophageal cancer specimens and cells and upregulation in vitro by the cyclooxygenase-2 inhibitor, NS398. Neoplasia 2003; 5:121-7.
15. Jung TTK, Berlinger NT, Juhn SK. Prostaglandins in squamous cell carcinoma of the head and neck: A preliminary study. Laryngoscope 1985; 95:307-12.
16. Snyderman CH, Milanovich M, Wagner RL, Johnson JT. Prognostic significance of prostaglandin E_2 production in fresh tissues of head and neck cancer patients. Head Neck 1995; 17:108-13.
17. Sumitani K, Kamijo R, Toyoshima T, Nakanishi Y, Takizawa K, Hatori M, et al. Specific inhibition of cyclooxygenase-2 results in inhibition of proliferation of oral cancer cell lines via suppression of prostaglandin E2 production. J Oral Pathol Med 2001; 30:41-7.
18. Botha JH, Robinson KM, Ramchurren N, Reddi K, Norman RJ. Human esophageal carcinoma cell lines: Prostaglandin production, biological properties, and behavior in nude mice. J Nat Cancer Inst 1986; 76:1053-6.
19. Klapan I, Katic V, Culo F, Cuk V. Prognostic significance of plasma prostaglandin E concentration in patients with head and neck cancer. J Cancer Res Clin Oncol 1992; 118:308-13.
20. Mestre JR, Chan G, Zhang F, Yang EK, Sacks PG, Boyle JO, et al. Inhibition of cyclooxygenase-2 expression. An approach to preventing head and neck cancer. Ann NY Acad Sci 1999; 899:62-71.
21. Zimmermann KC, Sarbia M, Weber AA, Borchard F, Gabbert HE, Schrör K. Cyclooxygenase-2 expression in human esophageal carcinoma. Cancer Res 1999; 59:198-204.
22. Gallo O, Franchi A, Magnelli L, Sardi I, Vannacci A, Boddi V, et al. Cyclooxygenase-2 pathway correlates with VEGF expression in head and neck cancer. Implications for tumor angiogenesis and metastasis. Neoplasia 2001; 3:53-61.
23. El Attar TMA, Lin HS, Vanderhoeck JY. Biosynthesis of prostaglandins and hydroxy fatty acids in primary squamous carcinomas of head and neck in humans. Cancer Lett 1985; 27:255-9.
24. Funkhouser EM, Sharp GB. Aspirin and reduced risk of esophageal carcinoma. Cancer 1995; 76:1116-9.
25. Farrow DC, Vaughan TL, Hansten PD, Stanford JL, Risch HA, Gammon MD, et al. Use of aspirin and other nonsteroidal anti-inflammatory drugs and risk of esophageal and gastric cancer. Cancer Epidemiol Biomarkers Prev 1998; 7:97-102.
26. Langman MJS, Cheng KK, Gilman EA, Lancashire RJ. Effect of anti-inflammatory drugs on overall risk of common cancer: Case-control study in general practice research database. Brit Med J 2000; 320:1642-46.
27. Wang Z, Fuentes CF, Shapshay SM. Antiangiogenic and chemopreventive activities of celecoxib in oral carcinoma cell. The Laryngoscope 2002; 112:839-43.
28. Niederberger E, Tegeder I, Vetter G, Schmidtko A, Schmidt H, Euchenhofer C, et al. Celecoxib loses its anti-inflammatory efficacy at high doses through activation of NF-κB. FASEB J 2001; 15:1622-4.
29. Nikitakis NG, Hebert C, Lopes MA, Reynolds MA, Sauk JJ. PPARgamma-mediated antineoplastic effect of NSAID sulindac on human oral squamous carcinoma cells. Int J Cancer 2002; 98:817-23.
30. Minter HA, Eveson JW, Huntley S, Elder DJE, Hague A. The cyclooxygenase 2-selective inhibitor NS398 inhibits proliferation of oral carcinoma cell lines by mechanisms dependent and independent of reduced prostaglandin E_2 synthesis. Clin Cancer Res 2003; 9:1885-97.
31. Fife RS, Stott B, Carr RE. Effects of a selective cyclooxygenase-2 inhibitor on cancer cells in vitro. Cancer Biol Ther 2004; 3:228-32.
32. Carey TE. Head and neck tumor cell lines. In: Hay RJ, Park JG, Gazdar A, eds. Atlas of human tumor cell lines. New York Academic Press, 1994:79.
33. Mosmann T. Rapid colorimetric assay for cellular growth and survival: Application to proliferation and cytotoxicity assays. J Immunol Methods 1983; 65:55-63.
34. Kempen EC, Yang P, Felix E, Madden T, Newman RA. Simultaneous quantification of arachidonic acid metabolites in cultured tumor cells using high performance liquid chromatography/electrospray ionization tandem mass spectrometry. Anal Biochem 2001; 297:183-90.
35. Walther M, Wiesner R, Kuhn H. Investigations into calcium-dependent membrane association of 15-lipoxygenase-1. Mechanistic roles of surface-exposed hydrophobic amino acids and calcium. J Biol Chem 2004; 279:3717-25.
36. Luo M, Jones SM, Peters-Golden M, Brock TG. Nuclear localization of 5-lipoxygenase as a determinant of leukotriene B4 synthetic capacity. Proc Natl Acad Sci USA 2003; 100:12165-70.
37. Hsi LC, Baek SJ, Eling TE. Lack of cyclooxygenase-2 activity in HT-29 human colorectal carcinoma cells. Exp Cell Res 2000; 256:563-70.
38. Zweifel BS, Davis TW, Ornberg RL, Masferrer JL. Direct evidence for a role of cyclooxygenase 2-derived prostaglandin E_2 in human head and neck xenograft tumors. Cancer Res 2002; 62:6706-11.
39. Chang SH, Liu CH, Conway R, Han DK, Nithipatikom K, Trifan OC, et al. Role of prostaglandin E2-dependent angiogenic switch in cyclooxygenase 2-induced breast cancer progression. Proc Natl Acad Sci USA 2004; 101:591-6.
40. Levine L. Does the release of arachidonic acid from cells play a role in cancer chemoprevention? FASEB J 2003; 17:800-2.

Journal of Experimental Therapeutics and Oncology, Vol. 6, pp. 183-192
Reprints available directly from the publisher
Photocopying permitted by license only

© 2007 Old City Publishing, Inc.
Published by license under the OCP Science imprint,
a member of the Old City Publishing Group.

Simultaneous inhibition of COX-2 and 5-LOX activities augments growth arrest and death of premalignant and malignant human lung cell lines

Claudia P. Schroeder[1], Peiying Yang[2], Robert A. Newman[2], Reuben Lotan[1]

[1] Department of Thoracic, Head and Neck Medical Oncology

[2] Department of Experimental Therapeutics; The University of Texas M. D. Anderson Cancer Center
Houston, TX 77030, USA

Correspondence to: Reuben Lotan, Ph.D., MDACC, 1515 Holcombe Boulevard Box 432, Houston, TX 77030 USA
Telephone: +1.713.792.8467. Fax: +1.713.745.5656. E-mail: rlotan@mdanderson.org

(Received November 3, 2006; accepted November 6, 2006; Sponsored by Robert A. Newman)

The arachidonic acid-metabolizing enzymes cyclooxygenase-2 (COX-2) or 5-lipoxygenase (5-LOX) are overexpressed during lung carcinogenesis and their end products (e.g.; PGE_2, 5-HETE, and LTB_4) have been implicated in tumor development. Recently, COX-2 inhibitors (e.g.; celecoxib) and 5-LOX inhibitors (e.g.; MK886 and REV5901) used as single agents have shown promising activities in the treatment and chemoprevention of cancer. However, little is known about the effects of combinations of these inhibitors. We found that simultaneous treatment of premalignant and malignant human lung cell lines with celecoxib, MK886, and REV5901 is more potent in growth suppression and induction of cell death than single or dual combination of these agents. However, their sensitivity to the inhibitors was not directly associated with the expression of COX-2, 5-LOX, or 5-LOX-activating protein (FLAP), but correlated with the production of corresponding metabolites. Furthermore, partial protection of cell death was observed when PGE_2 and/or 5-HETE was added to cell cultures treated with celecoxib, MK886, and REV5901 simultaneously. Our data indicate that a triple drug combination of distinct inhibitors of the eicosanoid metabolism at clinically feasible concentrations were more effective than each agent alone suggesting further investigations.

Key words: COX-2, 5-LOX, MK886, REV5901, celecoxib, human lung cell lines

INTRODUCTION

Lung cancer is the leading cause of cancer-related death in the United States with a less than 15% five-year survival rate, which is only a small improvement over the past several decades[1]. Therefore, the discovery of new strategies and potential agents in order to control the development and progression of human lung cancer is urgently needed.

It has been known that a higher rate of the eicosanoid metabolism, involving the breakdown of arachidonic acid (AA) to multiple endproducts by cyclooxygenases (COXs) and lipoxygenases (LOXs), plays a role in most human epithelial cancers including lung cancer[2-4]. For instance, inducible COX-2 is a known indicator for pathological conditions such as inflammation and cancer, especially those of non-small cell lung cancer histology, which has also been linked to a poorer prognosis[5-7]. Moreover, COX-2 is frequently upregulated in preneoplastic lesions or atypical bronchiolar metaplasia compared with normal lung[8]. As a result, the excessive production of COX-2-derived metabolites, mainly prostaglandin E_2 (PGE_2), stimulates proliferation, reduces apoptosis, and promotes angiogenesis[9,10]. Likewise, abnormalities in the 5-LOX pathway occur frequently during neoplastic transformation of lung tissue involving over-expression of 5-LOX and increased levels of its products, 5-hydroxyeicosatetraenoic acid (5-HETE) and leukotriene B_4 ($LT)B_4$, that have been associated

with proliferative, anti-apoptotic, and angiogenic properties[9,11,12]. Consequently, inhibition of COX-2 and 5-LOX activities suppressed growth and induced apoptosis in a variety of cancer cell lines and preclinical models[13-21]. Moreover, celecoxib and various 5-LOX inhibitors (e.g.; MK886) prevented lung tumorigenesis in carcinogen-induced mouse models[2,15,16]. Interestingly, it has been reported that celecoxib at clinically feasible concentrations not only inhibits the synthesis of PGE_2 but is also capable of modulating various metabolites generated from the LOX pathway, especially 5-HETE and LTB_4 metabolites which derive from the 5-LOX cascade[18,22,23]. Because a dynamic transition between the COX and LOX pathway may play a role in tumor development and progression, it is plausible to target both enzymatic pathways by using COX in combination with LOX inhibitors[20,23,24].

The present study examines the effects of the selective COX-2 inhibitor celecoxib in combination with the selective 5-LOX inhibitor REV5901, and the 5-LOX-activating protein (FLAP) inhibitor MK886 on suppression of cell growth of premalignant and malignant human lung cell lines.

MATERIAL AND METHODS

Reagents and materials

Dulbecco's modified eagle's minimal essential medium (DMEM), keratinocyte serum-free medium (SFM), phosphate-buffered saline (PBS), and trypsin were purchased from Gibco™ Invitrogen Corporation (Carlsbad, CA). Fetal bovine serum (FBS) was from HyClone Laboratories, Inc. (Logan, UT). The COX-2-inhibitor celecoxib (4-[5-(4-methylphenyl)-3-(trifluoromethyl)-1H-pyrazol-1-yl] benzenesulfonamide) was obtained from GD Searle & Co (Chicago, IL), the FLAP-inhibitor MK866 (1-[(4-chlorophenzyl)methyl]-3-[(1,1-dimethylethyl)thio]-α,α-dimethyl-5-(1-methylethyl-1H-indole-2-propanoic acid, sodium salt) was from Biomol Research Laboratories (Plymouth Meeting, PA) and the 5-LOX-inhibitor REV5901 (α-pentyl-3-(2-quinolinylmethoxy)-benzenemethanol) was purchased from Cayman Chemicals Co (Ann Arbor, MI). Bovine serum albumin, dimethyl sulfoxide (DMSO), ethylene diamine tetra acetic acid, and sodium dodecyl sulfate (SDS) were from Sigma Chemical Co. (St. Louis, MO). All culture plastic ware was purchased from BD Bioscience Labware (Bedford, MA). The deuterium-labeled eicosanoids PGE_2, LTB_4, and 5-HETE used as internal standard for ESI-LC/MS/MS analyses were purchased from Cayman Chemical Co. (Ann Arbor, MI).

Cell culture

The cell lines used in this study represent an in vitro model of human lung carcinogenesis including BEAS-2B, bronchial epithelial cells immortalized using SV40/adenovirus-12 hybrid T-antigen, and transformed (1198) or tumorigenic (1170-I) cells derived from BEAS-2B by exposure to cigarette smoke condensate (CSC) in vivo after transplantation into nude mice[25]. Immortalized 1799 cells were derived from BEAS-2B by a similar in vivo transplantation without exposure to CSC[26]. These cell lines were obtained from Dr. Klein-Szanto (Fox Chase Cancer Center, Philadelphia, PA). The non-small cell lung cancer cell lines A549 was purchased from the American Type Cell Culture Collection (ATCC; Rockville, MD). BEAS-2B and 1799 cells were grown in keratinocyte-SFM supplemented with EGF (2.5 µg) and bovine pituitary extract (25 µg) at 37°C in a humidified atmosphere of 95% air and 5% CO_2. The cell lines 1198 and 1170-I were maintained in keratinocyte-SFM containing 3% FBS and bovine pituitary extract (25 µg). A549 cells were cultured in a mixture of DMEM/Ham's F12 medium (1:1, v/v) supplemented with 5% FBS.

Cell growth studies, apoptosis

After trypsinization, 6 x 10^3 cells/well were seeded into 96-well culture plates, allowed to adhere overnight prior to treatment with celecoxib, MK886, REV5901, and their combinations at different concentrations for 72 hrs. Control cultures were grown in medium containing DMSO (0.02%, v/v). Cell number was determined by the sulforhodamine B (SRB) assay using an automated plate reader MR5000 (Dynatech Laboratories Inc., Chantilly, VA)[27]. The inhibition of cell growth was calculated from the equation, % inhibition = (1-OD*t*/OD*c*) x 100%, whereas OD*t* and OD*c* represent optical densities of treated and control cultures, respectively. Concentration response curves were plotted and concentrations of the agents used in this study resulting in 50% growth inhibition (IC_{50}) were calculated by interpolation. The extent of apoptotic and necrotic cells was determined by double staining with Annexin V-FITC and propidium iodide using Annexin-V-FLUOS staining kit from Roche Applied Science (Indianapolis, IN). The cells were seeded into 100 x 20 mm tissue culture dish and allowed to adhere overnight before incubation with the COX and LOX inhibitors. Control cultures were treated with medium containing solvent vehicle only (0.02%, v/v DMSO). After 72 hrs, detached and adherent cells were collected, washed, and stained according to the manufacturer's instructions. Data analysis was performed on a FACSCalibur cytometer utilizing the CellQuest™ software (Becton Dickinson,

San Jose, CA). Three independent experiments were conducted.

Western blot analysis

Samples containing 50 µg of total cellular protein mixed in sample buffer (0.5 M Tris, pH 6.8; 0.3% glycerol; 0.03% β-mercaptoethanol; 10% SDS; 0.001% bromphenolblue) were electrophoretically separated through 10% SDS-polyacrylamide slab gels followed by transfer onto Trans-Blot" nitrocellulose membranes (Bio-Rad Laboratories, Hercules, CA). Briefly, cell monolayers were washed twice with ice-cold PBS and collected in lysis buffer containing 150 mM NaCl; 0.02% NaN_3; 2% Igepal CA-630; 0.5% sodium deoxycholate; 0.2% SDS, and 50 mM Tris-HCl, pH 8.0 supplemented with protease inhibitors leupeptin (1 µg/ml), aprotinin (1 µg/ml), pepstatin (0.5 µg/ml), and phenylmethylsulfonyl fluoride (100 µg/ml). Protein concentrations were measured using Bio-Rad protein assay (Bio-Rad Laboratories, Hercules, CA). After blocking with 3% nonfat dry milk solution in 0.1% (w/v) Tween 20 in PBS, the membranes were probed with anti-human antibodies at appropriate dilutions against COX-2 (Oxford Biomedical Research Inc., Oxford, MI), 5-LOX (BD Transduction Lab, Lexington, KY), and FLAP (Santa Cruz Biotechnology Inc., CA). Antibody binding was detected with horseradish peroxidase-linked second antibody and enhanced chemiluminescence (Amersham Biosciences Corp., Piscataway, NJ). Loading and transferring control was confirmed by probing the membranes with anti-β-actin antibody (Sigma Chemical Co, St. Louis, MO).

Measurement of PGE2, 5-HETE, and LTB4

Electrospray ionization liquid chromatography tandem mass spectrometry (ESI-LC/MS/MS) was performed to quantify eicosanoid metabolites as described elsewhere[28,29]. Briefly, an aliquot of 10 µl of 10% BHT and 10 µl of a mixture of internal standards (PGE_2-d_4, 5-HETE-d_8, LTB_4) was added to 1 ml of culture medium. Eicosanoids were eluted with 1 ml of methanol and evaporated under a stream of nitrogen. Samples were reconstituted in 100 µl methanol: 10 mM ammonium acetate buffer (v/v, 70:30, pH 8.5) prior to analysis. ESI-LC/MS/MS was performed using a Quattro Ultima tandem mass spectrometer (Micromass, Beverly, MA) equipped with an Agilent HP1100 binary pump HPLC inlet. Metabolites were separated using a Luna 3 µm phenyl hexyl 2 x 150 mm analytical column (Phenomenex, Torrance, CA). The mobile phase consisted of 10 mM ammonium acetate (pH 8.5) and methanol. The flow rate was 250 µl/min with a column temperature maintained at 50°C and an injection volume of 25 µl. Fragmentation of all compounds was performed using argon as the collision gas at a collision cell pressure of 2.1 x 10^{-3} Torr. The results were expressed as nanograms of each eicosanoid per 10^6 cells. To normalize data, the cell number was measured with an electronic particle counter (Coulter, Hialeah, FL). Results shown represent mean values of at least two independent experiments.

Statistics

The results on growth inhibition induced by combinations of COX-2 and 5-LOX inhibitors represent mean values ± standard deviation (SD) of three independent experiments each performed in quadruplicates. Significance of difference between samples related to control cultures was determined using Student's paired *t*-test with probability (*P*) values less than 0.05 regarded as significant.

RESULTS

Production of PGE2, 5-HETE, and LTB4 and expression of the corresponding AA-metabolizing enzymes in premalignant and malignant human lung cell lines

To determine whether the AA metabolism is altered in cell lines representing an in vitro model of human lung carcinogenesis, we analyzed their production of PGE_2, 5-HETE, and LTB_4 using ESI-LC/MS/MS[28,29]. The endogenous PGE_2 levels in BEAS-2B and 1198 cell lines were very low (0.2 and 0.04 ng/10^6 cells, respectively), whereas A549 cancer cells produced 2.7 ng PGE_2/10^6 cells (Figure 1A). The synthesis of the 5-LOX metabolites 5-HETE and LTB_4 was low in BEAS-2B cells but higher and to a comparable amount in 1198 and A549 cell lines. We then determined the expression levels of COX-2, FLAP, and 5-LOX using immunoblotting. Figure 1B indicates that the enzyme expression showed a correlation with the production of the corresponding COX-2 and 5-LOX metabolites. For example, COX-2 was undetectable in premalignant bronchial epithelial cell lines, however, was strongly expressed in A549 cancer cells. FLAP was detected in all premalignant cell lines with a lower expression in BEAS-2B and a higher level in A549 cells. 5-LOX was expressed in 1198 and A549 cells compared to a faint detection in BEAS-2B, 1799, and 1170-I cell lines.

Effect of celecoxib, MK886, and REV5901 on growth arrest of premalignant and malignant human lung cell lines

Because the production of PGE_2, 5-HETE, and LTB_4 correlated with the expression levels of the

corresponding enzymes, we asked whether the cell lines used in this study exhibit differential sensitivities to the selective COX-2 inhibitor celecoxib, the selective 5-LOX-inhibitor REV5901 and the FLAP-inhibitor MK886 (chemical structures, Figure 2). We found a dose-dependent growth inhibition after 72 hrs of incubation with IC_{50} values ranging from 15.9 to 30.4 μM for celecoxib, 0.3 to 1.7 μM for MK886, and 6.6 to 14.4 μM for REV5901 (Figure 3). Premalignant bronchial epithelial cell lines were more sensitive to the growth-inhibitory effects of celecoxib, MK886, or REV590 than A549 cancer cells as indicative as 1.5 to 2-fold lower IC_{50} values. Furthermore, MK886 that indirectly inhibits 5-LOX activity by blocking FLAP, was approximately 10-fold more potent on a molar basis compared to the selective enzyme inhibitors celecoxib or REV5901.

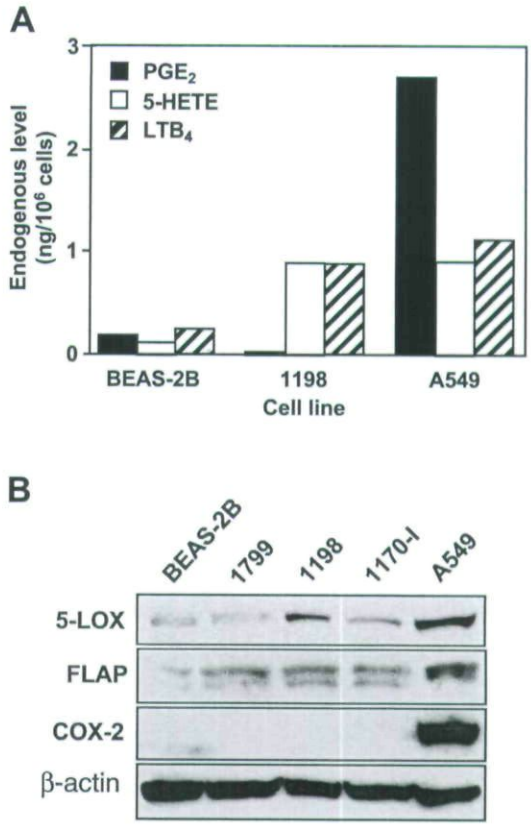


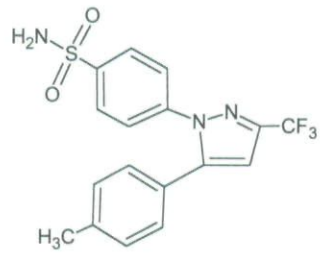
Figure 1. (A) Production of PGE_2, 5-HETE and LTB_4, and (B) expression of 5-LOX, FLAP, and COX-2 in various cell lines representing an in vitro model of human lung carcinogenesis. Cells were treated in standard medium for 72 hrs prior to analysis by ESI-LC/MS/MS or separation of a total of 50 μg of protein per sample using 10% SDS-polyacrylamid gel electrophoresis as described under materials and methods. For the measurement of eicosanoid metabolites, culture medium of three representative cell lines (BEAS-2B, 1198, and A549) was processed. The immunoblot was probed with antibodies specific for COX-2, 5-LOX, and FLAP. β-actin served as loading control.

Simultaneous treatment with celecoxib, MK886, and REV5901 augments growth inhibition compared to treatment with one or two agents

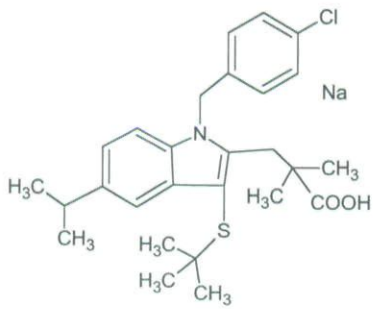
Based on previous studies, which suggest a fine balance between the COX and LOX pathway in tumor cells, we hypothesized that simultaneous inhibition of the AA metabolism by using COX-2 in combination with 5-LOX inhibitors is more effective in suppression of cell growth than each of the inhibitors alone. Therefore, we treated 1198 premalignant and A549 malignant lung cell lines with pharmacologically achievable concentrations of celecoxib (5 μM), MK886 (1 μM), and REV5901 (5 μM) used as single agents and in combinations for 72 hrs before determination of cell numbers by the SRB method. Figure 4 shows that simultaneous treatment of the cells with all three inhibitors was more effective than incubation of the compounds alone or in dual combination. For example, incubation of 1198 and A549 cells with a combination of celecoxib, MK886, and REV5901 suppressed their growth by 58% and 43%, respectively compared to untreated cultures ($P<0.05$). Besides, dual inhibition of COX-2 and 5-LOX enzymes through celecoxib and REV5901 induced a significant growth arrest by 29% and 37% in 1198 and A549 cell lines, respectively ($P<0.05$).

Cell death is increased by combinations of COX-2 and 5-LOX inhibitors and is partially prevented by PGE2 and 5-HETE

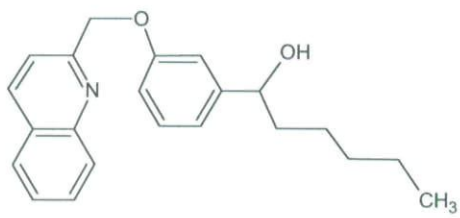
To determine whether induction of apoptosis contributes to the growth-inhibitory activity of COX-2 and 5-LOX inhibitors, we performed double staining of the cells with Annexin V-FITC and propidium iodide followed by flow cytometric analysis. Figure 5 indicates that incubation of 1198 premalignant and A549 malignant cell lines with a triple drug combination of celecoxib (5 μM), MK886 (1 μM), and REV5901 (5 and 7.5 μM, respectively) induced 74.4% and 23.7% cell death, including apoptotic and necrotic cellular fraction, respectively. Addition of exogenous PGE_2 (0.5 μg/ml) and/or 5-HETE (100 nM) to cultures treated with the triple drug combination partially reduced the number of dead cells. For example, 1198



Celecoxib
4-[5-(4-Methylphenyl)-3-(trifluoromethyl)-1H-pyrazol-1-yl] benzenesulfonamide



MK886
1-[(4-Chlorophenzyl)methyl]-3-[(1,1-dimethylethyl)thio]-α,α-dimethyl-5-(1-methylethyl-1H-indole-2-propanoic acid, sodium salt



REV5901
α-Pentyl-3-(2-quinolinylmethoxy)-benzenemethanol

Figure 2. Chemical structure of the selective COX-2 inhibitor celecoxib (4-[5-(4-methylphenyl)-3-(trifluoromethyl)-1H-pyrazol-1-yl]benzenesulfonamide, the FLAP inhibitor **MK886** (1[(4-Chlorophenzyl)methyl]-3-[(1,1-dimethyl)thio]-α,α-dimethyl)-5-(1-methylethyl)-1H-indole-2-propanoic acid, sodium salt), and the selective 5-LOX inhibitor **REV5901** (α-Pentyl-3-(2-quinolinylmethoxy)-benzenemethanol).

cell death induced by a combination of 5 μM celecoxib, 1 μM MK886, and 5 μM REV5901 was partially protected by 56% in the presence of 100 nM 5-HETE (Figure 5A). Moreover, A549 growth arrest was protected by 33% (from 23.7% to 7.9%) when both, PGE_2 and 5-HETE, were added to a combination of 5 μM celecoxib, 1 μM MK886, and 7.5 μM REV5901 (Figure 5B).

DISCUSSION

The deregulation of the AA metabolism in epithelial cancers including lung tumors represents an early sign of malignant transformation[3,9,10]. Hence, its metabolizing enzymes and end products provide promising targets for lung cancer chemoprevention and/or therapy. Indeed, inhibitors of the COX and LOX

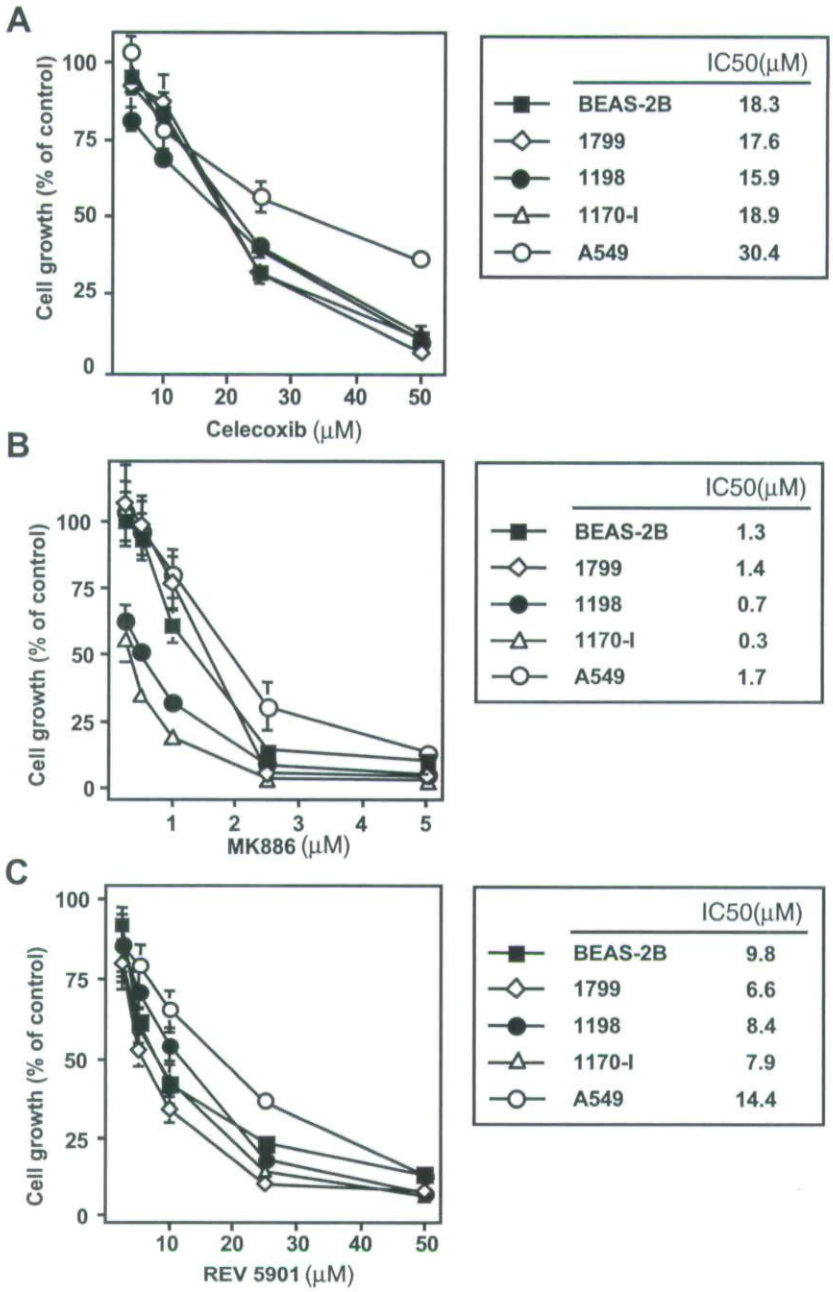


Figure 3. Effects of (A) celecoxib, (B) MK886, or (C) REV5901 on growth suppression of various cell lines representing an in vitro model of human lung carcinogenesis. Cell lines were treated with the inhibitors for 72 hrs before determination of cell number using the SRB assay as described in materials and methods. Concentrations required for the determination of IC50 (μM) values (right panels) were obtained by interpolation of concentration response curves. Results represent mean ± SD of three independent experiments with no drug added serving as control and expressed as 100% cell growth.

pathway have demonstrated anti-tumor and chemopreventive activity in lung cancer cells[13-16,21,22]. However, preclinical and clinical studies that have targeted just one metabolic pathway by using for instance only a COX-2 inhibitor (e.g.; celecoxib) showed modest impact[2,18,30]. It has also been suggested that blocking one metabolic cascade can lead to an enhancement of products generated from another

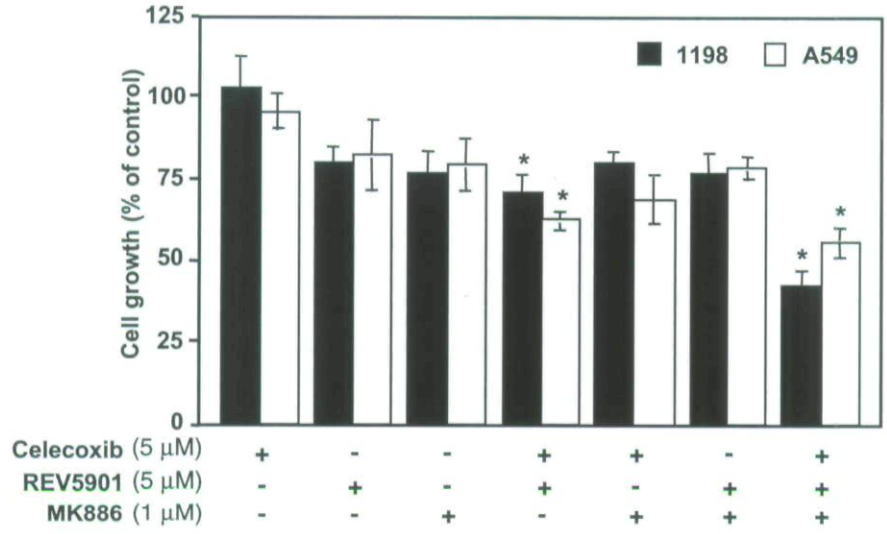


Figure 4. Effects of celecoxib (5 μM), MK886 (1 μM), REV5901 (5 μM), and their combinations on growth of 1198 premalignant (full bars) and A549 malignant (open bars) lung cell lines. The cells were seeded in 96-well culture plates and allowed to adhere overnight before treatment with the inhibitors. Changes in cell growth was determined by the SRB assay after 72 hrs of incubation. Results are expressed as mean ± SD (n=3) with no inhibitor added serving as control and expressed as 100% growth. **P*<0.05, vs untreated cells determined using Student's paired *t*-test.

cascade by re-directing the breakdown of the substrate AA. Specifically, others and we have demonstrated that suppression of PGE_2 by celecoxib at clinically relevant concentrations was accompanied by an increase of multiple 5-LOX metabolites, most significantly 5-HETE or LTB_4[18,22-24]. Therefore, it was of considerable interest to investigate whether a combination of inhibitors of the COX-2 and 5-LOX pathway can suppress growth of human lung cell lines more efficiently than inhibition of either pathway alone.

In this study, we show that a combination of clinically relevant concentrations of the COX-2 inhibitor celecoxib with the 5-LOX inhibitors REV5901, and MK886 was more effective in suppression of growth and induction of death than each of the agents alone or in dual combination. Furthermore, dual inhibition of COX-2 and 5-LOX activities by celecoxib and REV5901 produced a significant greater response than treatment with the individual inhibitors alone. We observed approximately 10-fold greater growth-inhibitory effects on a molar basis with the FLAP inhibitor MK886 than what was achieved with the selective enzyme inhibitors celecoxib or REV5901. MK886 inhibits the translocation of 5-LOX by binding to the active site of FLAP, which is required for the enzymatic activity of 5-LOX[31]. It has also been reported to induce apoptosis independently of both 5-LOX and FLAP[32]. In agreement with previous studies on various type of cancer cell lines, we obtained no direct correlation between the expression status of COX-2, FLAP or 5-LOX and the growth-inhibitory activity of celecoxib, MK886 or REV5901, respectively in premalignant and malignant lung cell lines[17,18,21]. However, the expression levels of COX-2, 5-LOX and FLAP in these cells correlated with the production of their major metabolites PGE_2, 5-HETE, and LTB_4, which increased with the degree of malignancy implicating a role in lung cancer development. Numerous studies have demonstrated that PGE_2 is markedly suppressed by celecoxib at concentrations below 5 μM in cell lines expressing the target enzyme COX-2[18,20,23,24,28]. Likewise, inhibition of 5-LOX activity by MK886 completely blocked the production of 5-HETE in human prostate cancer cells and addition of exogenous 5-HETE protected cells from undergoing apoptosis[14]. On the other hand, COX-2 or 5-LOX inhibitors induce apoptosis in cell lines, which lack the target enzymes, suggesting mechanism(s) unrelated to the suppression of the enzyme activity[18,19,21]. However, our data implicate that suppression of the 5-LOX activity is important for induction of cell death in 1198 and A549 cell lines based on partial protection by exogenous addition of 5-HETE to a triple drug combination of COX-2 and 5-LOX inhibitors compared to cells treated identically

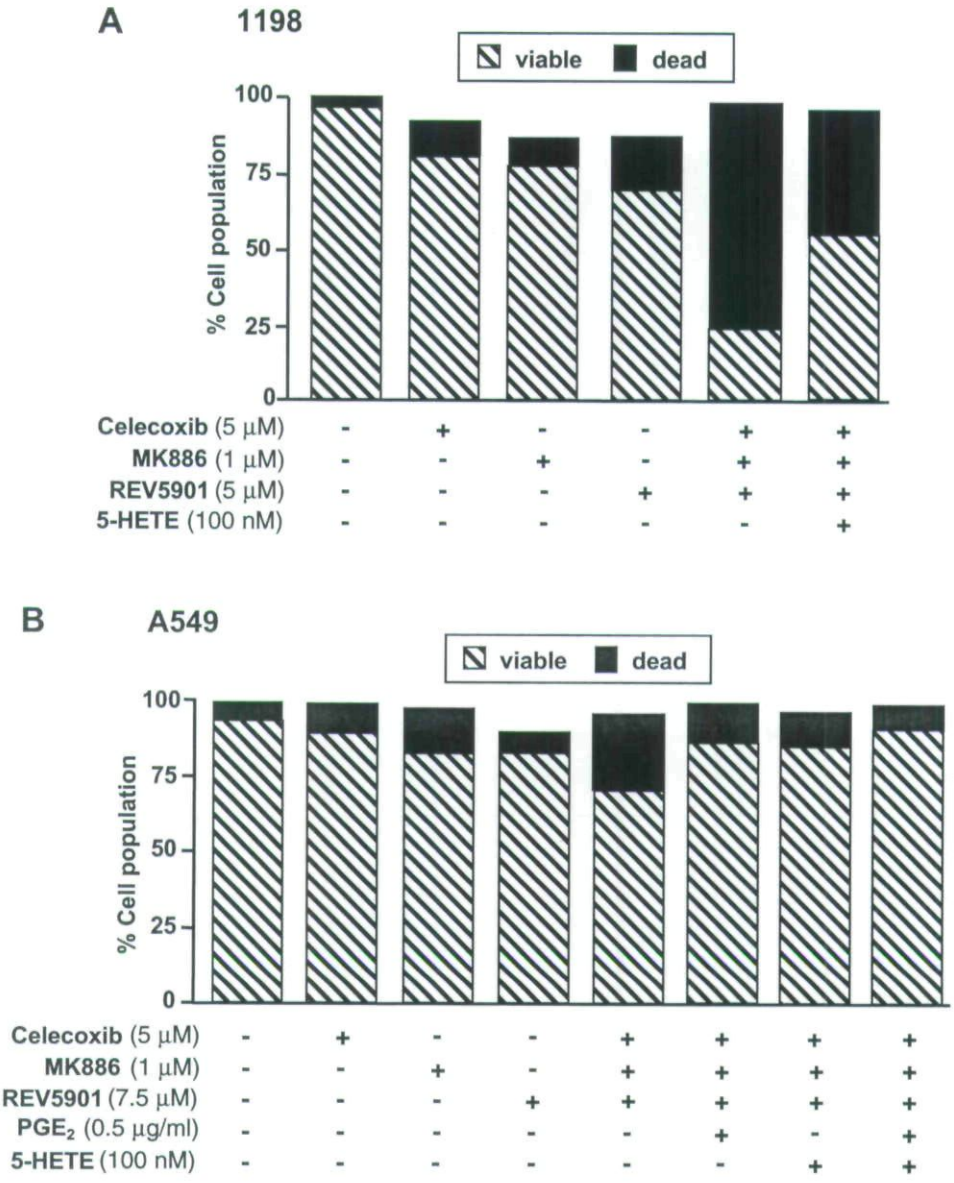


Figure 5. Induction of cell death by celecoxib (5 μM), MK886 (1 μM), REV5901 (5, and 7.5 μM, respectively) alone or in combination and the effects of PGE_2 (0.5 μg/ml), and/or 5-HETE (100 nM) in (A) 1198 and (B) A549 cell lines. The cells were treated with the inhibitors, and/or PGE_2, and 5-HETE for 72 hrs before collection of detached and adherent cells and studied for cell surface Annexin V binding to phosphatidylserin by flow cytometry. Control cultures were treated with medium containing solvent vehicle only (0.02% v/v DMSO). Data shown are representative of three independent experiments.

but without the 5-LOX metabolite. In A549 cells, which express both enzymes COX-2 and 5-LOX, exogenous PGE_2 was also able to rescue some of the cells from death similarly to the effect of 5-HETE while the combination of PGE_2 and 5-HETE in addition to the triple drug treatment was even more effective in preventing cell death than each of the AA metabolites alone. These findings indicate that the COX-2 and 5-LOX inhibitors induced cell death at least in part through suppression of the production of 5-HETE, PGE_2, or both. Moreover, we found that 1198 premalignant cells were more sensitive than A549 malignant cells suggesting that inhibitors of the AA metabolism might be more effective in lung cancer

prevention than in therapy. In fact, Rioux et al. have reported that a combination of the 5-LOX inhibitor A-79175 with the COX inhibitor acetylsalicylic acid reduced tumor multiplicity by 87%, which was the most effective preventive intervention compared to the inhibition of either pathway alone using a mice model of lung carcinogenesis[16].

In conclusion, combinations of low doses of biochemical inhibitors targeting related AA-metabolizing pathways support a rational approach in lung cancer prevention and therapy that warrant further investigations.

ACKNOWLEDGEMENTS

This work was supported by a grant from the National Cancer Institute (PO1 CA98144), and the BESCT Lung Cancer Program from the Department of Defense (DAMD17-01-1-0689-2).

REFERENCES

1. Jemal A, Murray T, Ward E, Samuels A, Tiwari RC, Ghafoor A, et al. Cancer statistics, 2005. *CA Cancer J Clin* 55:10-30, 2005.
2. Bunn PA Jr, Keith RL. The future of cyclooxygenase-2 inhibitors and other inhibitors of the eicosanoid signal pathway in the prevention and therapy of lung cancer. *Clin Lung Cancer* 3:271-277, 2002.
3. Laskin JJ, Sandler AB. The importance of the eicosanoid pathway in lung cancer. *Lung Cancer* 41 Suppl. 1:S73-79, 2003.
4. Sharma S, Yang SC, Zhu L, Reckamp K, Gardner B, Baratelli F, et al. Tumor cyclooxygenase-2/prostaglandin E2-dependent promotion of FOXP3 expression and CD4+ CD25+ T regulatory cell activities in lung cancer. *Cancer Res* 65(12):5211-5220, 2005.
5. Hida T, Yatabe Y, Achiwa H, Muramatsu H, Kozaki K, Nakamura S, et al. Increased expression of cyclooxygenase 2 occurs frequently in human lung cancers, specifically in adenocarcinomas. *Cancer Res* 58:3761-3764, 1998.
6. Wolff H, Saukkonen K, Anttila S, Karjalainen A, Vainio H, Ristimaki A. Expression of cyclooxygenase-2 in human lung carcinoma. *Cancer Res* 58:4997-5001, 1998.
7. Khuri FR, Wu H, Lee JJ, Kemp BL, Lotan R, Lippman SM, et al. Cyclooxygenase-2 overexpression is a marker of poor prognosis in stage I non-small cell lung cancer. *Clin Cancer Res* 7:861-867, 2001.
8. Hosomi Y, Yokose T, Hirose Y, Nakajima R, Nagai K, Nishiwaki Y, et al. Increased cyclooxygenase 2 (COX-2) expression occurs frequently in precursor lesions of human adenocarcinoma of the lung. *Lung Cancer* 30:73-81, 2000.
9. Funk CD. Prostaglandins and leukotriens: advances in eicosanoid biology. *Science* 294:1871-1875, 2001.
10. Wang D, Dubois RN. Prostaglandins and cancer. *Gut* 55:115-122, 2006.
11. Tang DG, Chen YQ, Honn KV. Arachidonate lipoxygenase as essential regulators of cell survival and apoptosis. *Proc Natl Acad Sci USA* 93:5241-5246, 1996.
12. Romano M, Claria J. Cyclooxygenase-2 and 5-lipoxygenase converging functions on cell proliferation and tumor angiogenesis: implications for cancer therapy. *FASEB J* 17:1986-1995, 2003.
13. Avis IM, Jett M, Boyle T, Vos MD, Moody T, Treston AM, et al. Growth control of lung cancer by interruption of 5-lipoxygenase-mediated growth factor signaling. *J Clin Invest* 97:806-813, 1996.
14. Ghosh J, Myers CE. Inhibition of arachidonate 5-lipoxygenase triggers massive apoptosis in human prostate cancer cells. *Proc Natl Acad Sci USA* 95:13182-13187, 1998.
15. Moody TW, Leyton J, Martinez A, Hong S, Malkinson A, Mulshine JL. Lipoxygenase inhibitors prevent lung carcinogenesis and inhibit non-small cell lung cancer growth. *Exp Lung Res* 24:617-628, 1998.
16. Rioux N, Castonguay A. Inhibitors of lipoxygenase: a new class of cancer chemopreventive agents. *Carcinogenesis* 19:1393-1400, 1998.
17. Hong SH, Avis I, Vos MD, Martinez A, Treston AM, Mulshine JL. Relationship of arachidonic acid metabolizing enzyme expression in epithelial cell lines to the growth effects of selective biochemical inhibitors. *Cancer Res* 59:2223-2228, 1999.
18. Schroeder CP, Yang P, Newman RA, Lotan R. Eicosanoid metabolism in squamous cell carcinoma cell lines derived from primary and metastatic head and neck cancer and its modulation by celecoxib. *Cancer Biol Ther* 9:29-34, 2004.
19. Stika J, Vondrácek J, Hofmanová J, Simek V, Kozubík A. MK-886 enhances tumor necrosis factor-α-induced differentiation and apoptosis. *Cancer Lett* 215:129-140, 2004.
20. Gregor JI, Kilian M, Heukamp I, Kiewert C, Kristiansen G, Schimke I, et al. Effects of selective COX-2 and 5-LOX inhibition on prostaglandin and leukotriene synthesis in ductal pancreatic cancer in syrian hamster. *Prostaglandins Leuk Essent Fatty Acids* 73:89-97, 2005.
21. Sun SY, Schroeder CP, Yue P, Lotan D, Hong WK, Lotan R. Enhanced growth inhibition and apoptosis induction in NSCLC cell lines by combination of celecoxib and 4HPR at clinically relevant concentrations. *Cancer Biol Ther* 4:407-413, 2005.
22. Mao JT, Tsu IH, Dubinett SM, Adams B, Sarafian T, Baratelli F, et al. Modulation of pulmonary leukotriene B4 production by cyclooxygenase-2 inhibitors and lipopolysaccharide. *Clin Cancer Res* 10:6872-6878, 2004.
23. Ye YN, Wu WK, Shin VY, Bruce IC, Wong BC, Cho CH. Dual inhibition of 5-LOX and COX-2 suppresses colon cancer formation promoted by cigarette smoke. *Carcinogenesis* 26:827-834, 2005.
24. Li N, Sood S, Wang S, Fang M, Wang P, Sun Z, et al. Overexpression of 5-lipoxygenase and cyclooxygenase 2 in hamster and human oral cancer and chemopreventive effects of zileuton and celecoxib. *Clin Cancer Res* 11:2089-2096, 2005.
25. Klein-Szanto AJ, Iizasa T, Momiki S, Garcia-Palazzo I, Caamano J, Metcalf R, et al. A tobacco-specific N-nitrosamine or cigarette smoke condensate causes neoplastic transformation of xenotransplanted human bronchial epithelial cells. *Proc Natl Acad Sci* USA 89:6693-6697, 1992.
26. Reddel RR, Ke Y, Gerwin BI, McMenamin MG, Lechner JF, Su RT, et al. Transformation of human bronchial epithelial cells by infection with SV40 or adenovirus-12 SV40 hybrid virus, or transfection via strontium phosphate coprecipitation with a plasmid containing SV40 early region genes. *Cancer Res* 48:1904-1909, 1988.

27. Skehan P, Storeng R, Scudiero D, Monks A, McMahon J, Vistica D, et al. New colorimetric cytotoxicity assay for anticancer-drug screening. *J. Natl Cancer Inst* 82: 1107-1112, 1990.

28. Kempen EC, Yang P, Felix E, Madden T, Newman RA. Simultaneous quantification of arachidonic acid metabolites in cultured tumor cells using high performance liquid: chromatography/electrospray ionization tandem mass spectrometry. *Anal Biochem* 297:183-190, 2001.

29. Yang P, Chan D, Felix E, Cartwright C, Menter DG, Madden T, Klein RD, Fischer SM, Newman RA. Formation and antiproliferative effect of prostaglandin E(3) from eicosapentaenoic acid in human lung cancer cells. *J Lipid Res* 45(6):1030-1039, 2004.

30. Lu S, Zhang X, Badawi AF, El-Sohemy A, Archer MC. Cyclooxygenase-2 inhibitor celecoxib inhibits promotion of mammary tumorigenesis in rats fed a high fat diet rich in n-6 polyunsaturated fatty acids. *Cancer Lett* 184:7-12, 2002.

31. Rouzer CA, Ford-Hutchinson AW, Morton HE, Gillard JW. MK886, a potent and specific leukotriene biosynthesis inhibitor blocks and reverses the membrane association of 5-lipoxygenase in ionophore-challenged leukocytes. *J Biol Chem* 265:1436-1442, 1990.

32. Datta K, Biswal SS, Kehrer JP. The 5-lipoxygenase-activating protein (FLAP) inhibitor, MK886, induces apoptosis independently of FLAP. *Biochem J* 340:371-375, 1999.

Copyright of Journal of Experimental Therapeutics & Oncology is the property of Old City Publishing, Inc. and its content may not be copied or emailed to multiple sites or posted to a listserv without the copyright holder's express written permission. However, users may print, download, or email articles for individual use.

Lack of PTEN Expression in Non-Small Cell Lung Cancer Could Be Related to Promoter Methylation[1]

Jean-Charles Soria,[2] Ho-Young Lee,[2] Janet I. Lee,[2] Luo Wang, Jean-Pierre Issa, Bonnie L. Kemp, Diane D. Liu, Jonathan M. Kurie, Li Mao, and Fadlo R. Khuri[3]

Departments of Thoracic/Head and Neck Medical Oncology [J-C. S., H-Y. L., J. I. L., L. W., J. M. K., L. M., F. R. K.], Leukemia [J-P. I.], Pathology [B. L. K.], and Biostatistics [D. D. L.], The University of Texas M. D. Anderson Cancer Center, Houston, Texas 77030

ABSTRACT

Purpose: **The *PTEN* gene at chromosome 10q23.3 is a tumor-suppressor gene that is inactivated in several types of human tumors. Although mutation and homozygous deletion are the most common mechanisms of *PTEN* inactivation, promoter methylation and translational modification can also account for *PTEN* silencing. The aim of this study was to investigate the expression of PTEN protein in primary non-small cell lung cancer (NSCLC) samples and to investigate the promoter methylation status of the gene in a panel of NSCLC cell lines as well as primary tumors.**

Experimental Design: **We analyzed PTEN expression by immunohistochemistry in tissue samples from 125 patients with early-stage NSCLC. We also evaluated *PTEN* promoter methylation status by methylation-specific PCR in 20 microdissected PTEN-negative primary tumors from among the last specimens as well as in a panel of 16 NSCLC cell lines. Western and Northern blotting were performed in the same panel of NSCLC cell lines.**

Results: **Thirty (24%) of the 125 specimens showed a lack of staining for PTEN. *PTEN* methylation was detected in 7 (35%) of the 20 PTEN-negative NSCLC samples and in none of the 10 PTEN-positive NSCLC samples that were microdissected. Furthermore, *PTEN* methylation was observed in 11 (69%) of the 16 NSCLC cell lines tested. *PTEN* mRNA expression was increased in the NCI-H1299 cell line by *in vitro* treatment with the demethylating agent 5-aza-2′-deoxycytidine. *PTEN* methylation was well correlated with PTEN expression in NSCLC cell lines by Western and Northern blot ($P = 0.025$).**

Conclusions: **Although genetic alterations of the *PTEN* gene are rare in NSCLC, loss of PTEN protein is not an uncommon event in early-stage NSCLC. Lack of PTEN expression may be partially explained by promoter methylation.**

INTRODUCTION

Lung cancer is the most common cause of cancer death worldwide, accounting for more deaths than those caused by prostate, breast, and colorectal cancers combined (1). The prognosis for patients with lung cancer is strongly correlated with disease stage at the time of diagnosis: patients with clinical stage I disease have a 5-year survival rate of about 60%, whereas in patients with clinical stage II-IV disease the 5-year survival rate ranges from 40% to less than 5% (2). Improving the survival rate of patients with this disease requires a better understanding of tumor biology and the subsequent development of novel therapeutic strategies.

PTEN/MMAC1/TEP1, located at 10q23.3, is a tumor-suppressor gene that encodes a cytoplasmic protein that has a protein tyrosine phosphatase domain and a domain extensively homologous to the cytoskeletal proteins tensin and auxilin (3). Germ-line mutations of *PTEN* are found in patients with Cowden syndrome, a familial syndrome associated with a predisposition for multiple benign hamartomas and malignant breast, skin, and thyroid neoplasms (3). Somatic mutation or deletion of *PTEN* has been reported in a variety of tumor types, including glioblastoma, melanoma, breast, prostate, renal, and endometrial carcinomas (4–9). Genetic analysis of *PTEN* in NSCLC[4] cancers has demonstrated alterations in *PTEN* in 8–16% of the examined NSCLC cell lines suggesting that *PTEN* is infrequently targeted in NSCLC tumorigenesis (10–13). Because alternative mechanisms such as promoter hypermethylation, alternative splicing of pre-mRNA, and posttranslational modification, may also inactivate gene function, the actual frequency of PTEN abnormalities in NSCLC may be underestimated. To date, few analyses of PTEN protein expression in NSCLC have been performed, and little is known about epigenetic or posttranslational mechanisms that could participate in *PTEN* inactivation.

Received 10/15/01; revised 2/25/02; accepted 2/26/02.

The costs of publication of this article were defrayed in part by the payment of page charges. This article must therefore be hereby marked *advertisement* in accordance with 18 U.S.C. Section 1734 solely to indicate this fact.

[1] Supported in part by Biology, Education, Screening, Chemoprevention, and Treatment (BESCT) Lung Cancer Program, Department of Defense Grant DAMD17-01-1-0689-1 [to F. R. K. (P. I.-Project 3) L. M. (P. I.-Project 1) and W. K. H., P. I.], Cancer Center Grant P30 CA 16620 (to M. D. Anderson Cancer Center), Tobacco Research Fund from State of Texas (to M. D. Anderson Cancer Center), Fondation de France, AP-HP, and Lilly Fondation Grant (to J-C. S).

[2] J-C. S., H-Y. L., and J. I. L. contributed equally to this work.

[3] To whom requests for reprints should be addressed, at Department of Thoracic/Head and Neck Medical Oncology, The University of Texas M. D. Anderson Cancer Center, 1515 Holcombe Boulevard, Houston, TX 77030. Phone: (713) 745-6363; Fax: (713) 796-8655; E-mail: fkhuri@mdanderson.org.

[4] The abbreviations used are: NSCLC, non-small cell lung cancer; PTEN, phosphatase and tensin homologue deleted on chromosome ten; TSA, trichostatin A; MSP, methylation-specific PCR; PIP-3, phosphatidylinositol-3,4,5-triphosphate; HBE, human bronchial epithelial (cells); GAPDH, glyceraldehyde-3-phosphate dehydrogenase; PI3K, phosphoinositol-3-kinase; PKB, protein kinase B.



Fig. 1 Map of the PTEN promoter area. *Vertical bars on top*, CpG sites. *Gray box on the bottom*, exon 1; *arrow*, putative transcription start site. *Horizontal lines*, the areas of homology to the *PTEN* pseudogene, the location of the primers used in Salveson *et al.* (*MSP-old*; Ref. 28), and the location of the primers used in the current study (*MSP*). The area shown is 3454 bases long.

To determine PTEN expression in patients with NSCLC and to ascertain whether promoter methylation accounted in part for the loss of PTEN, we examined immunohistochemically the expression pattern of PTEN in 125 patients with early-stage NSCLC and evaluated promoter methylation status in 20 microdissected tumor samples as well as in a panel of 16 NSCLC cell lines.

MATERIALS AND METHODS

Clinical Samples and Immunohistochemical Staining for PTEN Protein. Surgical specimens were obtained from a total of 125 patients with early stages of lung cancer who underwent a surgical resection at the Department of Thoracic and Cardiovascular Surgery at The University of Texas M. D. Anderson Cancer Center. Paraffin-embedded, 4-μm-thick tissue sections from 125 primary tumors were stained for the PTEN protein using a primary rabbit polyclonal anti-PTEN antibody (Zymed Laboratories, San Francisco, CA), as reported previously (14). All of the sections were deparaffinized by using a series of xylene baths and then rehydrated using a graded alcohol series. To retrieve the antigenicity, the tissue sections were microwaved in 10 mM citrate buffer (pH 6.0) once for 2 min. The sections were then immersed in methanol containing 0.3% hydrogen peroxidase for 20 min to block endogenous peroxidase activity and then incubated in 2.5% blocking serum to reduce nonspecific binding. Sections were incubated overnight at 4°C with primary anti-PTEN antiserum (1:50). The sections were then processed using standard avidin-biotin immunohistochemical techniques according to the manufacturer's recommendations (Vector Laboratories, Burlingame, CA). Diaminobenzidine was used as a chromogen, and commercial hematoxylin was used for counterstaining. Adjacent normal-appearing epithelium within the tissue sections served as a positive internal control.

Representative areas of each tissue section were selected, and cells were counted in at least four fields (at ×200). On the basis of the results of the immunohistochemical staining, specimens were classified into three groups, as reported previously (6): increased or equal staining intensity compared with the corresponding normal tissue (++), decreased staining intensity (+), and absence of staining (−). All of the slides were evaluated and scored independently by two investigators (J. I. L. and J-C. S.) who were blinded to the clinical information pertaining to the subjects.

Cell Lines and Culture Conditions. Normal HBE cells were grown from bronchial epithelium that was harvested from fresh surgical specimens obtained from patients undergoing lobectomy procedures. The mucosal layer was sterilely stripped from bronchial specimens, cut into small pieces, and placed on a plastic tissue culture plate containing a thin layer of medium. For each experiment, normal HBE cells from a single patient were used. Normal HBE cells were grown in keratinocyte serum-free medium (Life Technologies, Inc. Grand Island, NY) on standard plastic ware (Falcon; Becton-Dickinson, Bedford, MA) at 37°C in a 5% CO_2 atmosphere. The NSCLC cell lines NCI-H1792, -H1299, -H661, -H596, -H591, -H460, -H441, -H358, -H322, -H292, -H226, and -H157, A549, Calu-6, Calu-1, and SK-MES-1 were routinely maintained in RPMI 1640 supplemented with 10% FCS. The NSCLC cell lines were obtained from the American Type Culture Collection (Manassas, VA). 5-Aza-2′deoxycytidine was added to the RPMI 1640 containing 2% serum.

Tissue Microdissection and Genomic DNA Extraction. Sections (4 μm thick) from formalin-fixed and paraffin-embedded tissue blocks were obtained. Tissue microdissection was performed manually under a stereomicroscope using a 25-gauge needle. Dissected tissues were digested in 200 μl of digestion buffer containing 50 mM Tris–HCl (pH 8.0), 1% SDS, and proteinase K (0.5 mg/ml) at 42°C for 36 h. The digested products were purified by extraction with phenol-chloroform twice. DNA was then precipitated by the ethanol precipitation method in the presence of glycogen (Roche Molecular Biochemicals, Indianapolis, IN) and recovered in distilled water.

MSP. Sample DNA (at least 100 ng) from the microdissected tumor specimens and from NSCLC cell lines, mixed with 1 μg of salmon sperm (Life Technologies, Inc., Gaithersburg, MD), were submitted to chemical modification following the protocol by Herman *et al.* (15). Briefly, DNA was denatured with 2 M NaOH, followed by treatment with 10 mM hydroquinone and 3 M sodium bisulfite (Sigma Chemical Co., St. Louis, MO). After purification in a Wizard SV Plus kit column (Promega, Madison, WI), the DNA was treated with 3 M NaOH and precipitated with three volumes of 100% ethanol, a one-third volume of 10 M NH_4OAc, and 2 μl of glycogen at −20°C. The precipitated DNA was washed with 70% ethanol and dissolved in distilled water. PCR was conducted with primers that were specific for either the methylated or the unmethylated versions of the *PTEN* gene: PTENM forward, 5′-gtttggggatttttttttcgc-3′, and PTENM reverse, 5′-AACCCTTCCTACGCCGCG-3′, for the methylated sequence; PTENU forward, 5′-TATTAGTTTGGGGATTTTTTTTTTGT-3′, and PTENU reverse, 5′-CCCAACCCTTCCTACACCACA-3′, for the unmethylated sequence. Primers location is shown in Fig. 1. The 12.5-μl total reaction volume contained 25 ng of modified DNA, 3% DMSO, all four deoxynucleoside triphosphates (each at 200 μM), 1.5 mM MgCl2, 0.4 μM PCR primers, and 0.625 units of HotStar Taq DNA polymerase (Qiagen, Valencia, CA). Water was substituted for DNA as a negative control, and NCI-H460 cell line

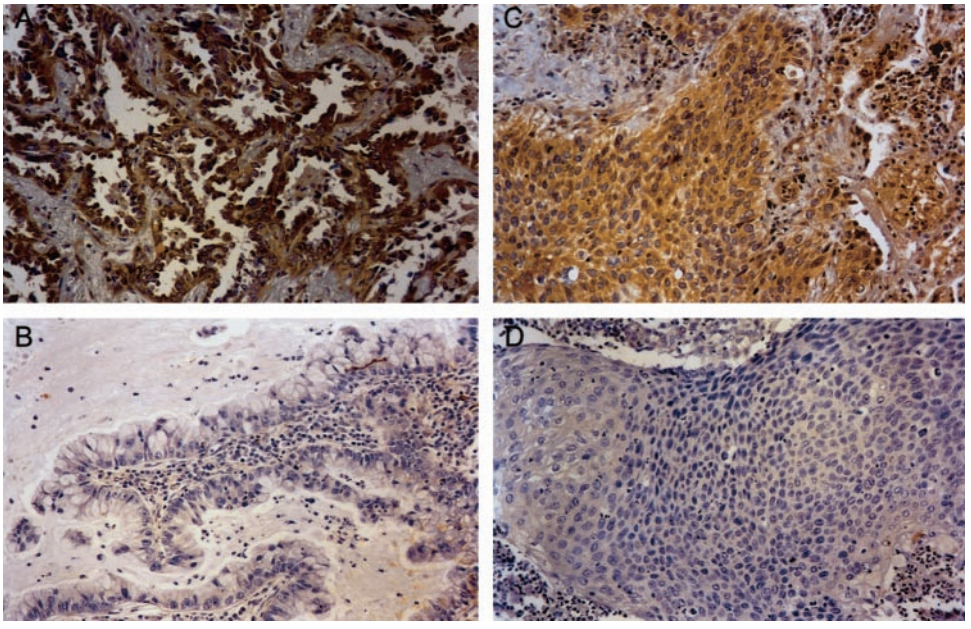


Fig. 2 Immunohistochemical staining patterns of PTEN in early-stage NSCLC. *A*, an adenocarcinoma with most cancer cells expressing PTEN in the cytoplasm. *B*, an adenocarcinoma tumor negative for PTEN expression. *C*, a squamous cell carcinoma tumor with diffuse and strong PTEN expression. *D*, a squamous cell carcinoma tumor with diffusely weak staining. The staining is prominent in the well-differentiated areas. (All panels, ×400).

DNA, treated with SssI Methylase (New England Biolabs, Beverly, MA), was used as a positive control. DNA was amplified by an initial cycle at 95°C for 15 min as required for enzyme activation, followed by 40 cycles of 94°C for 30 s, 60°C for 1 min, and 72°C for 1 min, and ending with a 5-min extension at 72°C in a thermocycler (Applied Biosystems, Foster City, CA). PCR products were separated on 2% agarose gels and visualized after staining with ethidium bromide.

Western Blot Analysis. Whole-cell lysates were prepared in lysis buffer [50 mM HEPES (pH 7.5), 150 mM NaCl, 1.5 mM $MgCl_2$, 1 mM EDTA, 0.2 mM EGTA, 1% NP40, 10% glycerol, 1 mM dithiothreitol, 1 mM phenylmethylsulfonyl fluoride, 20 mM sodium fluoride, 5 mM sodium orthovanadate, 10 mg/ml aprotinin, 10 mg/ml leupeptin, 2 mg/ml pepstatin, and 1 mM benzamidine]. Lysates were incubated for 20 min on ice and centrifugated at 13,000 × *g* for 20 min. The supernatants were collected, and the protein concentration was determined with a protein assay kit (Bio-Rad, Hercules, CA). Cell lysates were electrophoresed using SDS-PAGE and then transferred onto a BA-S-83-reinforced nitrocellulose membrane (Schleicher and Schuell, Inc., Keene, NH). Membranes were immunoblotted overnight at 4°C with a rabbit polyclonal antibody against human PTEN and a goat antibody against β-actin (Santa Cruz Biotechnology, Inc., Santa Cruz, CA) in Tris-buffered saline containing 5% nonfat dry milk. Antibody binding was detected using the ECL kit (Amersham, Inc., Arlington Heights, IL) according to the manufacturer's directions.

5-Aza-2′-deoxycytidine Treatment and Northern Blot Analysis. NCI-H1299 cells were transferred onto a 100-mm^3 dish and, 1 day later, 0.001, 0.01, 0.1, 1, or 5 μM 5-aza-2′-deoxycytidine or 0.001, 0.01, 0.1, 1, or 5 μM TSA were added in RPMI 1640 containing 2% FCS. Cells were changed to a new medium containing 5-aza-2′-deoxycytidine or TSA every day. After 6 days of treatment, the cells were lysed in 4.0 M guanidinium isothiocyanate, and total cellular RNA was extracted. RNA was subjected to electrophoresis (20 μg/lane) on a 1% agarose gel containing 2% formaldehyde, transferred to a Zeta-Probe membrane (Bio-Rad Laboratories), and hybridized to a [γ-^{32}P]dCTP-labeled PTEN or GAPDH probe as a control.

Statistical Analysis. Fisher's exact test or the χ^2 test was used to analyze the association between two categorical variables. All of the tests were two-sided. $P < 0.05$ was considered to be statistically significant.

RESULTS

The usual pattern of positive staining for PTEN in NSCLC was cytoplasmic and not nuclear (Fig. 2). Even when tumor cells were negative for PTEN staining, normal bronchial epithelial cells in the section were positive and were used as an internal positive control of the staining for PTEN. PTEN staining among the tumor specimens was either negative, diffusely weak, strong, or of a heterogeneous pattern of variable intensity. Among the heterogeneously stained specimens, staining was prominent in the well-differentiated areas (Fig. 2*D*). According to our scoring criteria, loss of PTEN expression (−) was noted in 30 (24%) of the 125 NSCLC specimens. Weak expression (+) was seen in 57 (46%) of the tumors, and strongly positive expression (++) was seen in 38 (30%) of the tumors. The frequency of PTEN expression did not differ significantly by tumor-node-metastasis stage, sex, smoking status, age, race, and histological subtype between the group with PTEN positive staining (+ or ++) and the group with PTEN negative staining (−; Table 1). Survival times were similar for patients with PTEN-negative tumors and with PTEN-positive tumors ($P = 0.88$, log rank test; data not shown).

To understand the mechanism explaining loss of PTEN expression in 24% of 125 NSCLC patients, we manually microdissected 20 randomly selected PTEN-negative slides along with 10 PTEN-positive slides. MSP was performed on genomic

Table 1 PTEN status in early-stage NSCLC tumor specimens from 125 patients according to clinicopathological features

Variable	No. of patients (n = 125)	PTEN expression		P
		Positive (n = 95)	Negative (n = 30)	
Age (yr) median (range)	63 (39–83)	64.5 (41–82)	64 (39–83)	0.73
Sex				
Male	93	70	23	0.81
Female	32	25	7	
Race				
White	110	84	26	0.75
Other	15	11	4	
Smoker				
Yes	107	87	20	0.5[a]
No	8	6	2	
Unknown	10	2	8	
Histology of tumors				
Squamous cell carcinoma	50	38	12	1
Adenocarcinoma and others	75	57	18	
TNM stage				
$T_1N_0M_0$	64	45	19	0.14
$T_2N_0M_0$	61	50	11	
5-yr overall survival rate	52.3%	53%	50%	
(95% CI)	(44.2–61.9%)	(43.8–64.2%)	(35–71.5%)	

[a] P was calculated comparing smoking *versus* nonsmoking patients.

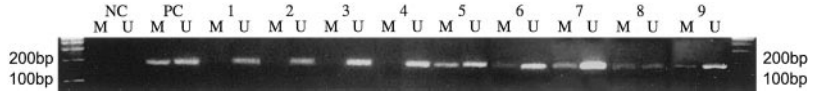


Fig. 3 PTEN promoter methylation status in PTEN-positive (*Lanes 1-4*) and PTEN-negative primary lung cancers (*Lanes 5–9*). *NC*, negative control; *PC*, positive control; *M*, amplified product with primers recognizing methylated sequence; *U*, amplified product with primers recognizing unmethylated sequence.

DNA extracted from those samples (Fig. 3). No methylation was found in the 10 PTEN-positive samples, whereas a methylated band was observed in 7 (35%) of the PTEN-negative samples. To further explore *PTEN* promoter methylation status, we evaluated a panel of 16 NSCLC cell lines. Overall, 11 (69%) of the 16 NSCLC cell lines displayed a methylated band (NCI-H1792, -H1299, -H661, -H441, -H358, -H322, -H292, -H157, Calu-6, Calu-1, and SK-MES-1). The following cell lines only displayed an unmethylated band: NCI-H226, -H460, -H591, -H596, and A549. The NSCLC cell line NCI-H1299 displayed a clear methylated band and had very low levels of *PTEN* mRNA, making it a suitable candidate for treatment with the demethylating agent 5-aza-2′-deoxycytidine. A net increase of *PTEN* mRNA was seen after treatment of NCI-H1299 cells with 5-aza-2′-deoxycytidine (Fig. 4) but not with TSA (data not shown), confirming the role of the 5′ region CpG methylation in regulating *PTEN* expression.

We further evaluated the correlation between *PTEN* promoter methylation status and PTEN expression by Western blot analysis in the same panel of 16 NSCLC cell lines. PTEN expression by Western blot in the NSCLC cell lines was either absent, weak, or strong (Fig. 5). Eleven cell lines displayed a methylated band: of these 11, 5 had a weak PTEN band, and 5 had no PTEN band detectable by Western blotting. Among the five cell lines without a methylated band by MSP, four had a strong PTEN band by Western blotting. The presence of a methylated band by MSP was statistically correlated with weak or absent PTEN expression by Western blotting (P = 0.025, Fisher's exact test; Fig. 6). Northern blotting further confirmed a low mRNA message in the NSCLC cell lines that had a methylated band and a weak or absent PTEN band by Western blot (Fig. 6).

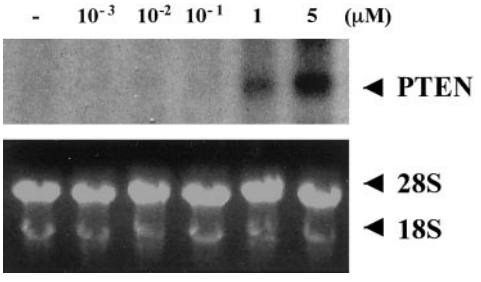


Fig. 4 Effect of 5-aza-2′deoxycytidine on PTEN expression. NCI-H1299 cells cultured *in vitro* were treated with 5-aza-2′deoxycytidine at concentrations of 0.001, 0.01, 0.1, 1, and 5 μM. Expression of PTEN was detected by Northern blot. A GAPDH probe was used as control for the integrity of RNA in all samples.

DISCUSSION

The *PTEN* gene product dephosphorylates tyrosine and serine/threonine residues and exhibits phosphatase activities with both protein and lipid substrates (16, 17). The major

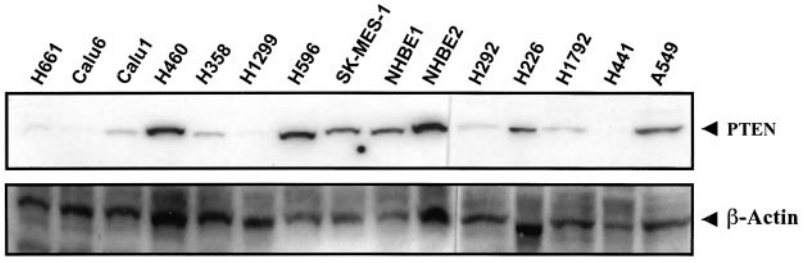


Fig. 5 PTEN expression evaluated by Western blot in a panel of NSCLC cell lines and in two normal HBE cells. A rabbit polyclonal antibody against human PTEN and a goat antibody against β-actin were used to probe the whole-cell extracts.

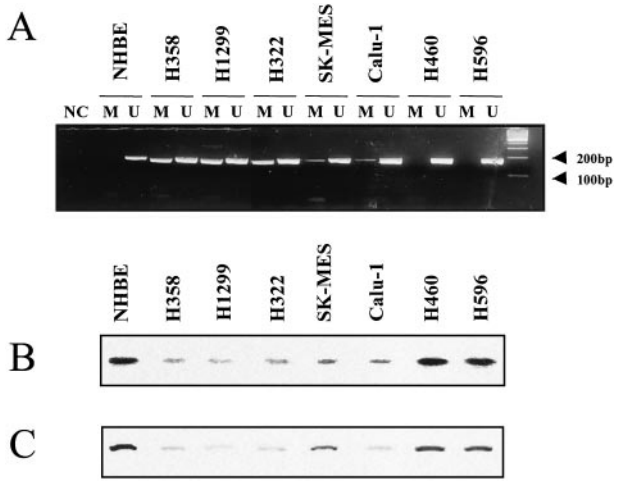


Fig. 6 PTEN promoter methylation was evaluated by MSP (*A*). NSCLC cell lines with a methylated band usually had a weak or absent PTEN band as shown by Western blot analysis (*B*). These same cell lines also displayed low levels of mRNA in Northern blots (*C*).

substrate of PTEN is PIP-3, a product of PI3K (18). The loss of PTEN function increases the concentration of PIP-3, which in turn leads to Akt hyperactivation, which suggests that the tumor-suppressor function of PTEN is exerted through the negative regulation of the PI3K/Akt cell survival pathway (3, 19, 20). The loss of PTEN expression results in increased Akt activity and continued cell survival and cell proliferation. In studied glioma, breast, and prostate cancer cell lines, *PTEN* has been shown to mediate G_1 cell cycle arrest and/or apoptosis through the suppression of the PI3K/Akt pathway (21). PTEN, therefore, seems to play an important role in modulating cell cycle progression and/or apoptosis. Although the protein phosphatase activity of PTEN is not considered to be as important as its lipid phosphatase activity for tumor suppression, the PTEN function as protein phosphatase has been implicated in the inhibition of cell migration and invasion via dephosphorylation of focal adhesion kinase (FAK), a molecule critical in the regulation of integrin signaling (22–24) and also in the inhibition of cell cycle progression (24).

Recently, frequent genetic alterations and loss of expression of the *PTEN* gene have been found in several malignant neoplasms (4–9). The studies of *PTEN* in NSCLC have focused exclusively on searching for mutations or deletions of the gene, with little emphasis on abnormalities at the protein level (10–13). In one study of NSCLC cell lines, homozygous deletions of *PTEN* were reported in 2 (8%) of 25 cell lines tested (10). Two subsequent studies, however, failed to demonstrate mutation of *PTEN* in the NSCLC samples studied, neither in cell lines nor in primary tumors (11, 13). Nevertheless, Forgacs *et al.* (12) described point mutations in 3 (16.7%) of 18 NSCLC cell lines analyzed (12). Using immunohistochemical analysis of 125 NSCLC patients, we showed that the rate of PTEN inactivation at the protein level is more frequent (24%) than that identified at the genetic level (0–16.7%). Interestingly, one previous study (25) that screened a wide variety of human neoplastic tissues, also reported PTEN protein loss in 25% of the NSCLC samples tested. We did not find any significant correlation between the loss of PTEN and clinicopathological characteristics in our NSCLC patients. Furthermore, no association was found between PTEN expression and survival. This is in contrast to the results of a recent report in which patients with breast cancer who lacked PTEN expression in their tumor had a shorter survival time (26). Tissue specificity or technical differences (*e.g.,* different antibody used for immunohistochemical evaluation) may account for these different results.

The loss of PTEN expression in 24% of 125 patients with early-stage NSCLC suggests that abrogation of PTEN function may occur through multiple mechanisms. Loss of PTEN expression may be explained by decreased protein synthesis, elevated protein degradation or turnover, or other posttranslational modifications. Another possible mechanism is the epigenetic inactivation of the gene through hypermethylation of the promoter region (27, 28). Indeed, inactivation of other tumor-suppressor genes by methylation has been previously reported in patients with NSCLC (29, 30). We found promoter methylation in 7 (35%) of 20 PTEN-negative microdissected tumors, whereas none of the 10 PTEN-positive microdissected tumors displayed a methylated band. In the 16 NSCLC cell lines, we found methylation in 69% of the cell lines tested. The higher percentage of methylation found in the lung cancer cell lines compared with primary tumors might be explained by additional changes acquired in culture or by the fact that the tumor cell lines were derived from more aggressive and more advanced tumors (stage III and IV). Furthermore DNA, quality and preservation in the sections from formalin-fixed and paraffin-embedded tissue blocks might not always be optimal. This could partially explain why only 35% of the PTEN-negative sections displayed a methylated band. Additional mechanisms (*e.g.,* posttranslational modifications) could also account for the lack of PTEN expression in some of the primary tumor samples

tested. It is noteworthy that our primer design for *PTEN* MSP differed from the one previously reported by Salvesen *et al.* (28). Indeed, through BLAST search, we have found extensive homology between the *PTEN* DNA region explored by Salvesen *et al.* (28) and the chromosome 9 duplication of the T-cell receptor β gene (AF029308), as well as with the highly conserved processed *PTEN* pseudogene (31). Therefore, we have designed primers to explore a CpG island, with no homology, located ~1.9 kb upstream from the region evaluated by Salvesen *et al.* (28). Fig. 1 represents the PTEN promoter area with the different CpG islands. It is not clear to date, which CpG island in the very large *PTEN* upstream regulatory region is best related to the gene expression. An additional fact that supports the importance of *PTEN* methylation in inactivating this gene is the efficacy of the demethylating agent 5-aza-2′-deoxycytidine in increasing *PTEN* mRNA in NCI-H1299 cell line. It is noteworthy that TSA treatment had no effect on *PTEN* expression, thus highlighting the specificity of the demethylating effect of 5-aza-2′-deoxycytidine. Taken together, these findings suggest that the methylation of *PTEN* may be an important mechanism for silencing this gene in NSCLC.

Our findings are in line with similar findings reported in endometrial cancer (28) and suspected in ovarian carcinomas and melanoma (16, 32). In fact, the loss of *PTEN* function in endometrial, breast, prostate, ovarian, and melanocytic tumors is more frequent than can be adequately explained by structural genomic changes alone (33). We believe that reports on *PTEN* methylation are few because proving an epigenetic mechanism of *PTEN* silencing is technically challenging. Indeed, one has to take into account the large size (>250 kb) of the *PTEN* upstream regulatory region, the existence of a highly conserved processed pseudogene with homology maintained up to 1 kb upstream from the translational start site, and technical challenges in linking epigenetic events with expression level (31, 33).

The elucidation of the mechanism that mediates the loss of PTEN expression has important clinical implications. The role of PI3K/Akt/PKB in apoptosis and survival, as well as the effects of dysregulation of the PI3K/Akt/PKB pathway in the pathogenesis of a large fraction of human cancer, has been identified (34–37). Because demethylating agents are under clinical evaluation, our finding may provide an advantage in therapeutic strategies, especially in the treatment of NSCLC, in which constitutive activation of Akt/PKB occurs at a high frequency (34).

In summary, we have demonstrated that the loss of PTEN is not a rare event in NSCLC, although genetic alterations of the *PTEN* gene are rare in this setting. The lack of PTEN expression may be partially explained by promoter methylation. We found methylation of *PTEN* in 35% of the primary tumors and in 69% of the NSCLC cell lines tested. Moreover, we were able to show that methylation of this gene is reversible with 5-aza-2′-deoxycytidine. Our findings of a frequent acquired tumor-related epigenetic alteration favor the candidacy of *PTEN* as a tumor suppressor gene also subject to methylation in addition to point mutations and homozygous deletions.

REFERENCES

1. Greenlee, R. T., Hill-Harmon, B. B., Murray, T., and Thun, M. Cancer statistics, 2001. CA Cancer J. Clin., *51:* 16–36, 2001.

2. Mountain, C. T. Revision in the international system for staging of lung cancer. Chest, *111:* 1710–1717, 1997.

3. Di Cristofano, A. D., and Pandolfi, P. P. The multiple roles of PTEN in tumor suppression. Cell, *100:* 387–390, 2000.

4. Duerr, E. M., Rollbrocker, B., Hayashi, Y., Peters, N., Meyer-Puttlitz, B., Louis, D. N., Schramm, J., Wiestler, O. D., Parsons, R., Eng, C., and von Deimling, A. PTEN mutations in gliomas and glioneuronal tumors. Oncogene, *16:* 2259–2264, 1998.

5. Tsao, H. S., Zhang, X., Benoit, E., and Haluska, F. G. Identification of PTEN/MMAC 1 alterations in uncultured melanomas and melanoma cell lines. Oncogene, *16:* 3397–3402, 1998.

6. Perren, A., Weng, L-P., Boag, A. H., Ziebold, U., Thakore, K., Dahia, P. L., Komminoth, P., Lees, J. A., Mulligan, L. M., Mutter, G. L., and Eng, C. Immunohistochemical evidence of loss of PTEN expression in primary ductal adenocarcinomas of the breast. Am. J. Pathol., *155:* 1254–1260, 1999.

7. Cairns, P., Okami, K., Halachmi, S., Halachmi, N., Esteller, M., Herman, J. G., Jen, J., Isaacs, W. B., Bova, G. S., and Sidransky, D. Frequent inactivation of PTEN/MMAC1 in primary prostate cancer. Cancer Res., *57:* 4997–5000, 1997.

8. Mutter, G. L., Lin, M-C., Fitzgerald, J. T., Kum, J. B., Baak, J. P., Lees, J. A., Weng, L. P., and Eng, C. Altered PTEN expression as a diagnostic marker for the earliest endometrial precancers. J. Natl. Cancer Inst. (Bethesda), *92:* 924–930, 2000.

9. Kondo, K., Yao, M., Kobayashi, K., Ota, S., Yoshida, M., Kaneko, S., Baba, M., Sakai, N., Kishida, T., Kawakami, S., Uemura, H., Nagashima, Y., Nakatani, Y., and Hosaka, M. PTEN/MMAC1/TEP1 mutations in human primary renal-cell carcinomas and renal carcinoma cell lines. Int. J. Cancer, *91:* 219–224, 2001.

10. Kohno, T., Takahashi, M., Manda, R., and Yokota, J. Inactivation of the *PTEN/MMAC1/TEP1* gene in human lung cancers. Genes Chromosomes Cancer, *22:* 152–156, 1998.

11. Yokomizo, A., Tindall, D. J., Drabkin, H., Gemmill, R., Franklin, W., Yang, P., Sugio, K., Smith, D. I., and Liu, W. PTEN/MMAC1 mutations identified in small cell, but not in non-small cell lung cancers. Oncogene, *17:* 475–479, 1998.

12. Forgacs, E., Biesterveld, E. J., Sekido, Y., Fong, K., Muneer, S., Wistuba, I. I., Milchgrub, S., Brezinschek, R., Virmani, A., Gazdar, A. F., and Minna, J. D. Mutation analysis of the *PTEN/MMAC1* gene in lung cancer. Oncogene, *17:* 1557–1565, 1998.

13. Hosoya, Y., Gemma, A., Seike, M., Kurimoto, F., Uematsu, K., Hibino, S., Yoshimura, A., Shibuya, M., and Kudoh S. Alteration of the *PTEN/MMAC1* gene locus in primary lung cancer with distant metastasis. Lung Cancer, *25:* 87–93, 1999.

14. Lee, J. I., Soria, J. C., Hassan, K. A., El-Naggar, A. K., Tang, X., Liu, D. D., Hong, W. K., and Mao, L. Loss of PTEN expression as a prognostic marker for tongue cancer. Arch. Otolaryngol. Head Neck Surg., *127:* 144–145, 2001.

15. Herman, J. G., Graff, J. R., Myohanen, S., Hamilton, S. R., Nelkin, B. D., and Baylin, S. B. Methylation-specific PCR. A novel PCR assay for methylation status of CpG islands. Proc. Natl. Acad. Sci. USA, *93:* 9821–9826, 1996.

16. Ali, I. U., Schriml, L. M., and Dean, M. Mutational spectra of PTEN/MMAC1: a tumor suppressor with lipid phosphatase activity. J. Natl. Cancer Inst. (Bethesda), *91:* 1922–1932, 1999.

17. Li, D. M., and Sun, H. TEP1, encoded by a candidate tumor suppressor locus, is a novel protein tyrosine phosphatase regulated by transforming growth factor β. Cancer Res., *57:* 2124–2129, 1997.

18. Myers, M. P., Pass, I., Batty, I. H., Van der Kaay, J., Stolarov, J. P., Hemmings, B. A., Wigler, M. H., Downes, C. P., and Tonks, N. K. The lipid phosphatase activity of PTEN is critical for its tumor suppressor function. Proc. Natl. Acad. Sci. USA, *95:* 13513–13518, 1998.

19. Furnari, F. B., Huang, H. J., and Cavenee, W. K. The phosphoinositol phosphatase activity of PTEN mediates a serum-sensitive G_1 growth arrest in glioma cells. Cancer Res., *58:* 5002–5008, 1998.

20. Stambolic, V., Suzuki, A., de la Pompa, J. L., Brothers, G. M., Mirtsos, C., Sasaki, T., Ruland, J., Penninger, J. M., Siderovski, D. P., and Mak, T. W. Negative regulation of PKB/Akt-dependent cell survival by the tumor suppressor PTEN. Cell, *95:* 29–39, 1998.

21. Lu, Y., Lin, Y. Z., LaPushin, R., Cuevas, B., Fang, X., Yu, S. X., Davies, M. A., Khan, H., Furui, T., Mao, M., Zinner, R., Hung, M. C., Steck, P., Siminovitch, K., and Mills, G. B. The *PTEN/MMAC1/TEP* tumor suppressor gene decreases cell growth and induces apoptosis and anoikis in breast cancer cells. Oncogene, *18:* 7034–7035, 1999.

22. Tamura, M., Gu, J., Matsumoto, K., Aota, S., Parsons, R., and Yamada, K. M. Inhibition of cell migration, spreading, and focal adhesions by tumor suppressor PTEN. Science (Wash. DC), *280:* 1614–1617, 1998.

23. Tamura, M., Gu, J., Takino, T., and Yamada, K. M. Tumor suppressor PTEN inhibition of cell invasion, migration, and growth: differential involvement of focal adhesion kinase and p130Cas. Cancer Res., *59:* 442–449, 1999.

24. Tamura, M., Gu, J., Danen, E. H., Takino, T., Miyamoto, S., and Yamada, K. M. PTEN interactions with focal adhesion kinase and suppression of the extracellular matrix-dependent phosphatidylinositol 3-kinase/Akt cell survival pathway. J. Biol. Chem., *274:* 20693–20703, 1999.

25. Torres, J., Navarro, S., Rogla, I., Ripoll, F., Lluch, A., Garcia-Conde, J., Llombart-Bosch, A., Cervera, J., and Pulido, R. Heterogeneous lack of expression of the tumour suppressor PTEN protein in human neoplastic tissues. Eur. J. Cancer, *37:* 114–121, 2001.

26. Depowski, P. L., Rosenthal, S. I., and Ross, J. S. Loss of expression of the *pten* gene protein product is associated with poor outcome in breast cancer. Mod. Pathol., *14:* 672–676, 2001.

27. Whang, Y. E., Wu, X., Suzuki, H., Reiter, R. E., Tran, C., Vessella, R. L., Said, J. W., Isaacs, W. B., and Sawyers, C. L. Inactivation of the tumor suppressor PTEN/MMAC1 in advanced human prostate cancer through loss of expression. Proc. Natl. Acad. Sci. USA, *95:* 5246–5250, 1998.

28. Salvesen, H. B., MacDonald, N., Ryan, A., Jacobs, I. J., Lynch, E. D., Akslen, L. A., and Das, S. PTEN methylation is associated with advanced stage and microsatellite instability in endometrial carcinoma. Int. J. Cancer, *91:* 22–26, 2001.

29. Belinsky, S. A., Nikula, K. J., Palmisano, W. A., Michels, R., Saccomano, G., Gabrielson, E., Baylin, S. B., and Herman, J. G. Aberrant methylation of $p16^{ink4a}$ is an early event in lung cancer and a potential biomarker for early diagnosis. Proc. Natl. Acad. Sci. USA, *95:* 11891–11896, 1998.

30. Zochbauer-Muller, S., Fong, K. M., Virmani, A. K., Geradts, J., Gazdar, A. F., and Minna, J. D. Aberrant promoter methylation of multiple genes in non-small cell lung cancers. Cancer Res., *61:* 249–255, 2001.

31. Dahia, P. L., FitzGerald, M. G., Zhang, X., Marsh, D. J., Zheng, Z., Pietsch, T., von Deimling, A., Haluska, F. G., Haber, D. A., and Eng, C. A highly conserved processed *PTEN* pseudogene is located on chromosome band 9p21. Oncogene, *16:* 2403–2406, 1998.

32. Kurose, K., Zhou, X. P., Araki, T., Cannistra, S. A., Maher, E. R., and Eng, C. Frequent loss of PTEN expression is linked to elevated phosphorylated Akt levels, but not associated with p27 and cyclin D1 expression, in primary epithelial ovarian carcinomas. Am. J. Pathol., *158:* 2097–2106, 2001.

33. Mutter, G. L. PTEN, a protean tumor suppressor. Am. J. Pathol., *158:* 1895–1898, 2001.

34. Brognard, J., Clark, A. S., Ni, Y., and Dennis P. A. Akt/protein kinase B is constitutively active in non-small cell lung cancer cells and promotes cellular survival and resistance to chemotherapy and radiation. Cancer Res., *61:* 3986–3997, 2001.

35. Kauffmann-Zeh, A., Rodriguez-Viciana, P., Ulrich, E., Gilbert, C., Coffer, P., Downward, J., and Evan, G. Suppression of c-Myc-induced apoptosis by Ras signaling through PI(3)K and PKB. Nature (Lond.), *385:* 544–548, 1997.

36. Khwaja, A., Rodriguez-Viciana, P., Wennstrom, S., Warne, P., and Downward, J. Matrix adhesion and ras transformation both activate a phosphoinositide 3-OH kinase and protein kinase B/Akt cellular survival pathway. EMBO J., *16:* 2783–2793, 1997.

37. Chen, R. H., Su, Y. H., Chuang, R. L., and Chang. T. Y. Suppression of transforming growth factor-β-induced apoptosis through a phosphatidylinositol 3-kinase/Akt-dependent pathway. Oncogene, *17:* 1959–1968, 1998.

Lack of Interleukin-10 Expression Could Predict Poor Outcome in Patients with Stage I Non-Small Cell Lung Cancer[1]

Jean-Charles Soria, Chulso Moon, Bonnie L. Kemp, Diane D. Liu, Lei Feng, Ximing Tang, Yoon-Soo Chang, Li Mao, and Fadlo R. Khuri[2]

Departments of Thoracic/Head and Neck Medical Oncology [J-C. S., C. M., X. T., Y-S. C., L. M.], Pathology [B. L. K.], and Biostatistics [D. D. L., L. F.], The University of Texas M. D. Anderson Cancer Center, Houston, Texas 77030, and Winship Cancer Institute, Emory University, Atlanta, Georgia 30322 [F. R. K.]

ABSTRACT

Purpose: **Interleukin-10 (IL-10) may play an important role in controlling tumor growth and metastasis. Some reports have shown that IL-10 can be a potent inhibitor of tumor growth, but others suggest that IL-10 expression by the tumor is an adverse prognostic factor. Because normal bronchial epithelial cells constitutively produce IL-10, we decided to test the prognostic value of IL-10 in a well-defined population of patients with stage I non-small cell lung cancer (NSCLC) treated in a single institution.**

Patients and Methods: **Using immunohistochemical analysis, we retrospectively analyzed IL-10 expression in specimens from 138 patients with completely resected clinical/radiographic stage I NSCLC for whom clinical follow-up data were available.**

Results: **IL-10 expression was retained (IL-10 labeling index $\geq$ 10%) in 94 patients (68.1%) and lost in 44 patients (31.9%). The duration of overall, disease-specific, and disease-free survival in the 44 patients lacking IL-10 expression was worse than in the 94 patients with IL-10 expression ($P = 0.08$, 0.02, and 0.05, respectively; Log-rank test). Interestingly, IL-10 expression was observed more frequently in tumors with squamous cell histology than in tumors of other histological subtypes ($P = 0.04$; χ^2 test). Multivariate analysis confirmed the independent prognostic value of IL-10 expression for disease-specific survival ($P = 0.04$).**

Conclusion: **Lack of IL-10 expression by the tumor was associated with a significantly worse outcome of early stage NSCLC. The mechanisms underlying this clinically and biologically important finding need to be further explored.**

INTRODUCTION

Lung cancer is a major cause of mortality worldwide. Last year, in the United States alone, an estimated 169,400 new cases of lung cancer were diagnosed, and an estimated 154,900 deaths from lung cancer occurred (1). Improving the survival rate of patients with this disease requires a better understanding of tumor biology and the subsequent development of novel therapeutic strategies. One area of intense lung cancer research has been in assessing the prognostic factors of NSCLC,[3] focusing on stage I disease and molecular factors (2–5). This avenue of investigation may lead to the identification of patients with the highest risk stage I NSCLC or of those who are most likely to benefit from adjuvant or chemopreventive approaches.

IL-10 is thought to play a potential pathogenic or therapeutic role in a number of human conditions, such as inflammation, autoimmunity, and cancer (6). The immunomodulatory effects of IL-10 have yielded mixed results in various tumor systems. On one hand, because many tumor types express IL-10, its role in helping tumors evade immunosurveillance has been suggested (7, 8). IL-10 inhibits the tumoricidal capacity of macrophages and the cytotoxicity and cytokine production of tumor-specific T cells and blocks the presentation of tumor antigens by antigen-presenting cells (9, 10). On the other hand, *in vivo* studies in different animal models have demonstrated that IL-10 is a potent inhibitor of tumor growth and metastasis (11–14). Additionally, systemic administration of IL-10 has inhibited tumor metastasis and stimulated antitumor immune responses in murine models (15). Nevertheless, recent data generated by analyzing human lung tissue samples suggest that IL-10 produced by NSCLC is a predictor of poor outcome (16).

Because IL-10 is constitutively expressed in normal bronchial epithelial cells, we hypothesized that loss of IL-10 expression by lung tumors might be a prognostic factor for survival. Therefore, we decided to analyze the prognostic value of IL-10 expression in a homogeneous population of 138 patients with stage I NSCLC.

PATIENTS AND METHODS

Study Population. A total of 595 consecutive patients with stage I NSCLC underwent definitive surgical resection, defined as a lobectomy or a pneumonectomy, from 1975 to 1990

Received 8/12/02; revised 1/22/02; accepted 1/28/03.
The costs of publication of this article were defrayed in part by the payment of page charges. This article must therefore be hereby marked *advertisement* in accordance with 18 U.S.C. Section 1734 solely to indicate this fact.
[1] Supported by Biology, Education, Screening, Chemoprevention, and Treatment Lung Cancer Program, Department of Defense Grant DAMD17-01-1-0689-1 (to F. R. K. and L. M.), Cancer Center Grant P30 CA 16620 (to M. D. Anderson Cancer Center), Tobacco Research Fund from the State of Texas (to M. D. Anderson Cancer Center), American Cancer Society Grant RPG-98-054 (to L. M.), and Fondation de France, AP-HP, and Lilly Foundation Grant (to J-C. S.).
[2] To whom requests for reprints should be addressed, at Winship Cancer Institute, 1365 Clifton Road, Suite B4100, Atlanta, GA 30322. Phone: (404) 778-4250; Fax: (404) 778-5016; E-mail: fkhuri@emory.edu.

[3] The abbreviations used are: NSCLC, non-small cell lung cancer; SCC, squamous cell carcinoma; TNM, Tumor-Node-Metastasis; CI, confidence interval; IL, interleukin; TIMP, tissue inhibitor of metalloprotease; NK, natural killer; MMP, matrix metalloprotease.

Table 1 IL-10 status in stage I NSCLC tumors according to clinicopathological features of patients

		IL-10 expression		
	No. of patients (n = 138)	Positive (n = 94)	Negative (n = 44)	P
Age: median (range)	64 (37–82)	64 (37–82)	65 (45–76)	0.28
Sex				
Male	106	68	38	0.07
Female	32	26	6	
Race				
Caucasian	120	84	36	0.22
Other	18	10	8	
Smoker				
Yes	119	79	40	0.27[a]
No	9	8	1	
Unknown	10	7	3	
Histology of tumors				
SCC	58	45	13	0.04
Adenocarcinoma and others	80	49	31	
TNM stage				
$T_1N_0M_0$	65	44	21	0.92
$T_2N_0M_0$	73	50	23	
5-year overall survival rate	51.5%	56.6%	40.9%	
(95% CI)	(43.8%, 60.6%)	(47.3%, 67.7%)	(28.7%, 58.4%)	

[a] P calculated comparing smoking *vs.* nonsmoking patients.

at The University of Texas M. D. Anderson Cancer Center. We retrospectively examined 138 cases for which both tissue samples and a median follow-up period of >5 years were available at the time of this study. The patient population was identified through a search of the Tumor Registry database maintained by the Department of Medical Informatics at The University of Texas M. D. Anderson Cancer Center. Survival status was verified and updated from Tumor Registry records as of December 1, 2000.

The study population consisted of 106 men and 32 women; 120 patients were Caucasian, and 18 patients were of other ethnicities (Table 1). The mean age of patients at surgery was 63 years. Histological subtypes included 58 cases of SCC, 60 cases of adenocarcinoma, 10 cases of bronchioalveolar carcinoma, 5 cases of large cell carcinoma, 3 cases of adenosquamous carcinoma, and 2 cases unclassified.

Immunohistochemical Staining for IL-10 Protein. All available tissue blocks from each patient were reviewed for the presence of tumor by a thoracic pathologist (B. L. K.). Paraffin-embedded, 4-μm-thick tissue sections from all 154 primary tumors were stained for IL-10 protein using a primary goat polyclonal antihuman IL-10 antibody (AF-217-NA; R&D Systems, Minneapolis, MN). Slides were deparaffinized through a series of xylene baths. Rehydration was performed using graded alcohol. The sections were then immersed in methanol containing 0.3% hydrogen peroxidase for 20 min to block the endogenous peroxidase activity and incubated in 2.5% blocking serum to reduce nonspecific binding. Sections were incubated overnight at 4°C with primary anti-IL-10 antibody at a dilution of 1:75 (1.33 μg/ml). The sections were then processed using a standard avidin-biotin immunohistochemical assay according to the manufacturer's recommendations (Vector Laboratories, Burlingame, CA). Diaminobenzidine was used as a chromogen, and commercial hematoxylin was used for counterstaining. Routinely processed tissue sections of normal lymph nodes and tonsils were used as positive staining controls and also stained with the primary antibody omitted to confirm staining specificity. Normal bronchial epithelial cells that constitutively produce IL-10 were also used as internal positive controls (17).

The IL-10 labeling index was defined as the percentage of tumor cells displaying cytoplasmic immunoreactivity and calculated by counting IL-10-stained tumor cells among ≥1000 tumor cells for each section. Representative areas of each tissue section were selected, and cells were counted in at least four fields (magnified 400 times) in these areas. On the basis of previous reports, if ≥10% of the tumor cells were positive for IL-10, the case was considered to be IL-10 positive (18, 19). Tumors with <10% of the cells stained were counted as negative. All slides were scored concomitantly by a pathologist (X. T.) and another investigator (J-C. S.). Immunohistochemical analysis was performed in a blinded manner with respect to clinical information about the subjects.

Statistical Analysis. Overall, disease-specific, and disease-free survival were analyzed in this study. Survival curves were estimated by the Kaplan-Meier method. The Log-rank test was used to compare patient's survival time between groups. The Fisher exact and χ^2 tests were used to analyze the association between two categorical variables. The Wilcoxon rank-sum test was used for differences in median of age. The Cox proportional hazards model was used for univariate analysis to evaluate the association between survival time and risk factors and for multivariate analysis to model the risks of IL-10 expression on survival time, with adjustment for clinical and histopathological parameters (age, sex, race, tumor histology,

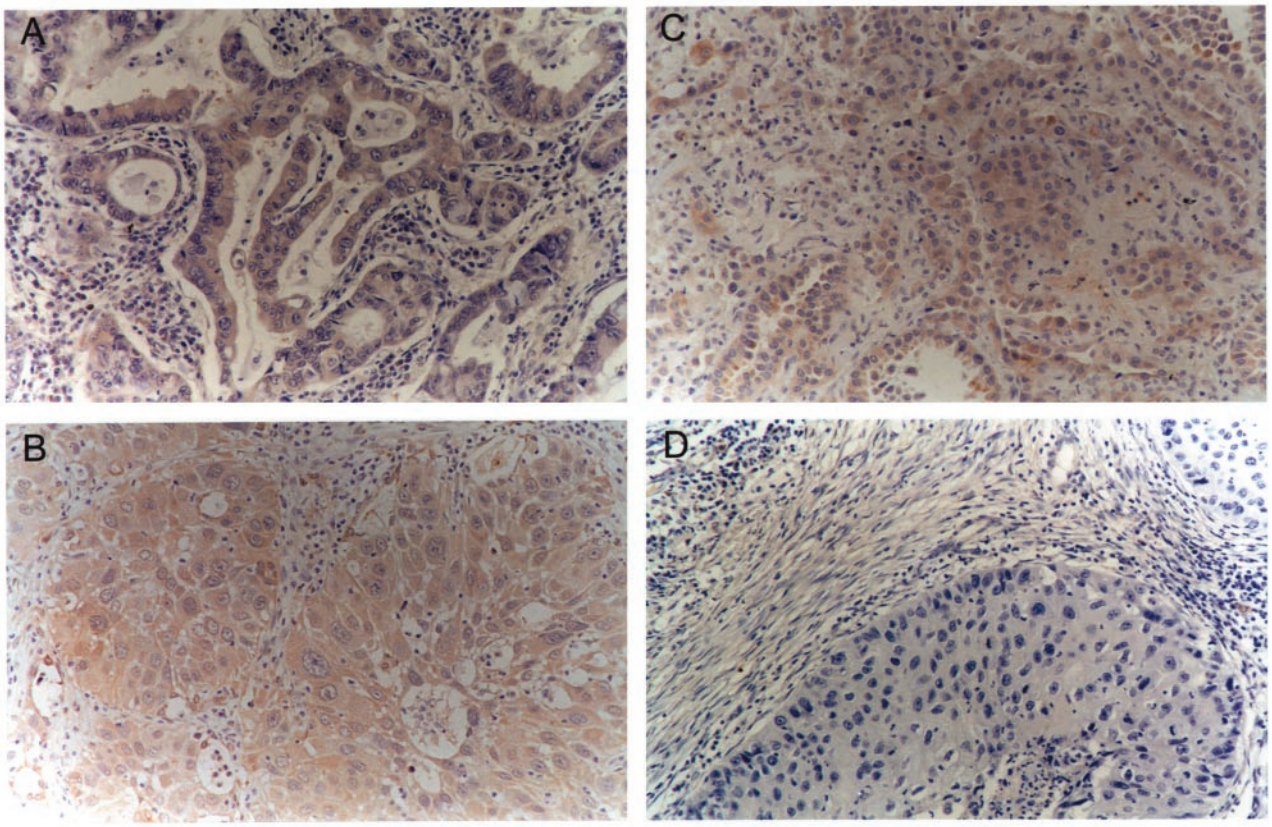


Fig. 1 Immunohistochemical staining patterns of IL-10 in stage I NSCLC. *A*, a well-differentiated adenocarcinoma with most cancer cells expressing IL-10 in the cytoplasm. *B*, a SCC with most carcinoma cells positive for IL-10. *C*, a bronchioalveolar carcinoma tumor with IL-10 expression. *D*, a SCC tumor negative for IL-10 expression (original magnification, ×400).

and tumor size). All statistical tests are two sided, and a $P < 0.05$ was considered to be statistically significant.

All survival curves were calculated from the date of surgery. Overall survival took all deaths (cancer related or not) into account. Disease-specific survival time was calculated from the date of surgery to death from cancer-related causes. Disease-free survival time was calculated from the date of surgery to relapse or death from cancer-related causes.

RESULTS

A total of 138 formalin-fixed, paraffin-embedded NSCLC tumor specimens was stained using a standard immunohistochemical technique reported previously for the identification of IL-10 expression (18, 19). The usual pattern of positive staining for IL-10 in NSCLC was cytoplasmic and not nuclear (Fig. 1, *A–C*). Even if tumors cells were negative for IL-10 staining, normal bronchial epithelial cells in the section were positive and used as an internal positive control of the staining for IL-10. In peribronchial gland cells or alveolar pneumocytes, IL-10 expression was not detectable. Lymphoid cells of tumor areas were occasionally immunostained. Only 20 of 138 samples displayed tumor-infiltrating lymphocytes, therefore hindering any relevant analysis of IL-10 production by infiltrating immune cells. In the positive control tissues (tonsil), the normal stratified squamous epithelium displayed IL-10-positive cells. In the adjacent lymph nodes, IL-10-positive cells were localized predominantly in the germinal centers (data not shown). IL-10 immunohistochemical staining showed a wide heterogeneity from rare scattered cells to a homogeneous pattern for the vast majority of cells examined, suggesting that phenotypic heterogeneity is a major feature in NSCLC (Fig. 1).

IL-10 expression was observed in 94 (68.1%) of the 138 stage I NSCLC specimens. Lack of staining was observed in 44 tumors (31.9%). Table 1 shows the relationships between the expression of IL-10 and clinicopathological factors. There were no statistically significant differences in TNM stage, sex, smoking status, age, and race between the groups with IL-10-positive and -negative staining. Interestingly, IL-10 expression was more prevalent in the SCC subtype than it was in other histological subtypes. Forty-five (77.6%) of the 58 cases of SCC exhibited IL-10 expression, whereas 49 (61.3%) of 80 patients with non-SCC tumors (mainly adenocarcinoma) showed IL-10 expression ($P = 0.04$; χ^2 test).

We subsequently analyzed the relationship between IL-10 expression and length of survival. The median follow-up time for the patient population was 10.6 years. Fig. 2*A* shows the Kaplan-Meier overall survival curves for patients whose tumors were IL-10 positive and negative. Patients with tumors that were

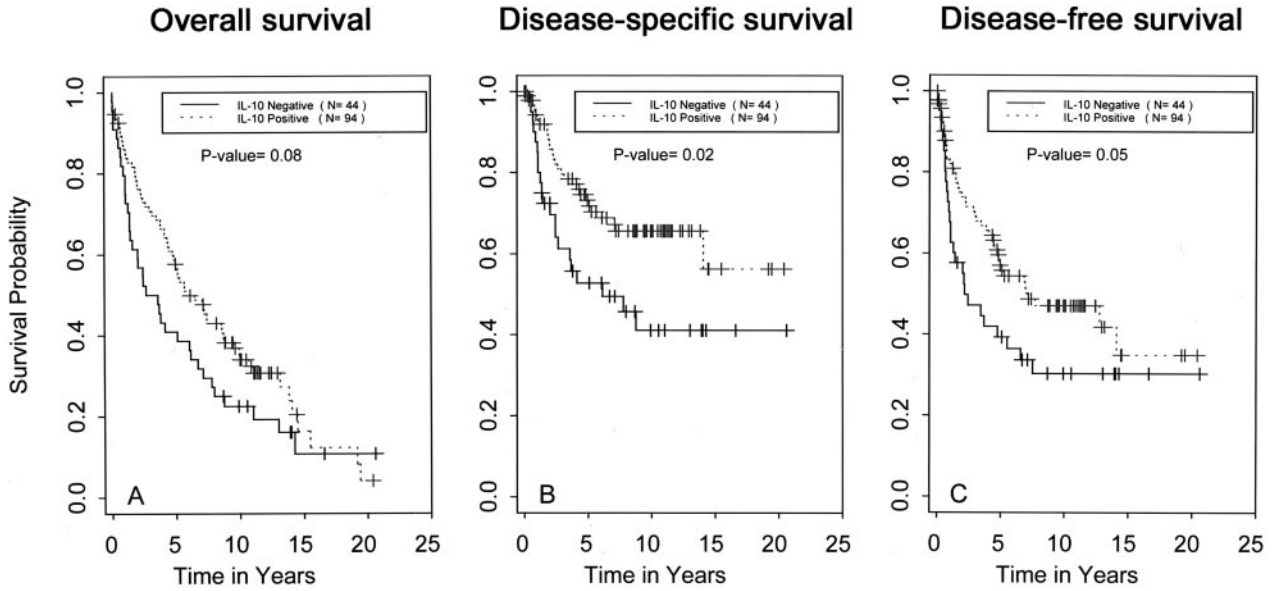


Fig. 2 Survival curves of patients with IL-10-positive and -negative NSCLC. The patients lacking IL-10 expression (*solid line, n* = 44) had worst outcomes than the patients with IL-10 expression (*broken line, n* = 94) for overall (*A*), disease-specific (*B*), and disease-free survival (*C*).

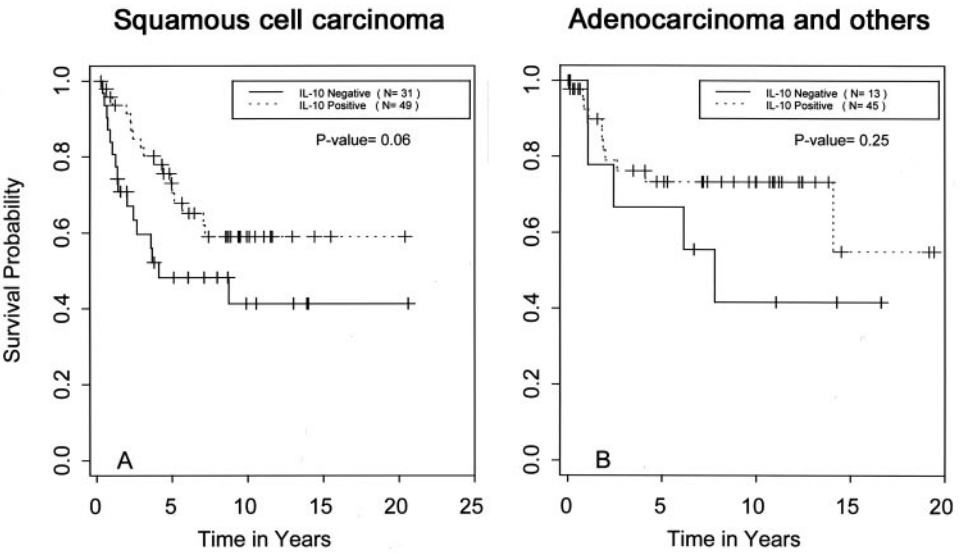


Fig. 3 *A,* disease-specific survival curve of patients with stage I SCC according to IL-10 expression; *B,* disease-specific survival curve of patients with adenocarcinoma or other histological subtypes according to IL-10 expression.

IL-10 negative had a shorter survival time than did patients with tumors that were IL-10 positive ($P = 0.08$; Log-rank test). Five-year overall survival rate for patients whose tumors were IL-10 positive was 56.6% (95% CI = 47.3–67.7%) and 40.9% (95% CI = 28.7–58.4%) for patients whose tumors were IL-10 negative (Table 1). Fig. 2*B* shows that patients with negative IL-10 expression had significantly shorter disease-specific survival times than did patients with positive IL-10 expression ($P = 0.02$; Log-rank test). A comparison of disease-free survival curves in IL-10-negative and -positive patients yielded similar results ($P = 0.05$; Log-rank test; Fig. 2*C*). The prognostic significance of IL-10 expression on disease-specific survival was further explored in each major histological subtype. IL-10 negativity was a borderline significant adverse prognostic factor among patients with non-SCC tumors ($P = 0.06$; Log-rank test; Fig. 3*A*). A similar trend was observed for patients with SCC of the lung, but this trend was not significant ($P = 0.25$; Log-rank test; Fig. 3*B*). Univariate Cox proportional hazards model was used to evaluate the association between IL-10, clinicopathological variables (age, sex, race, histological subtype, and TNM), and survival time. Table 2 shows the results on disease-specific survival. In multivariate Cox proportional hazards model, among all clinicopathological variables, IL-10 expression was the only significant independent prognostic indicator

Table 2 Univariate and multivariate Cox proportional hazards model on disease-specific survival

	Univariate			Multivariate		
	Hazard ratio	95% CI	*P*	Hazard ratio	95% CI	*P*
Age	1.0	0.97–1.03	0.92			
Sex (Male or female)	0.88	0.48–1.64	0.69			
Race (Caucasian or other)	0.49	0.25–0.99	0.047	0.58	0.28–1.2	0.13
Histological subtype (SCC or other)	0.72	0.39–1.30	0.27			
Tumor size (T1 or T2)	0.73	0.42–1.28	0.28			
IL-10 (+ or −)[a]	0.51	0.29–0.89	0.02	0.55	0.31–0.98	0.04

[a] +, IL-10 labeling index ≥ 10%; −, IL-10 labeling index < 10%.

for disease-specific survival. The hazard of cancer death for patients whose tumor was IL-10 positive was only 55% of the hazard for patients whose tumor was IL-10 negative ($P = 0.04$, Cox model).

DISCUSSION

Human lung cancer displays an extremely aggressive clinical course and represents the leading cause of malignancy-related mortality in the United States (1). This behavior may reflect an increased capacity to evade detection and containment by host immune response. Because IL-10 demonstrates *in vitro* immunosuppressive activities (9, 10), some groups have hypothesized that IL-10 production by cancer cells may help the tumor evade immunosurveillance (7, 8). Nevertheless, IL-10 is also able to inhibit tumor growth and metastasis in various tumor models (11–14). These conflicting results imply that it is all about "fine tuning" in case of IL-10-mediated immunosuppression or immunostimulation. Because normal bronchial epithelial cells constitutively express IL-10 (17), loss of IL-10 expression by lung cancer cells would represent a specific change in the tumor as compared with its normal epithelial counterpart. In the present study, we explored the prognostic value of IL-10 expression by lung cancer cells in a large and homogeneous population of 138 completely resected clinical/radiographic stage I NSCLC for whom a median follow-up of 10.6 years was available. We have demonstrated that IL-10 is retained in a significant percentage of stage I NSCLCs. Overall, 94 (68.1%) of 138 tumors expressed IL-10 in ≥10% tumor cells, whereas loss of IL-10 expression was observed in 44 patients (31.9%). Our data show that lack of IL-10 expression is a poor prognostic factor in patients with stage I NSCLC. The poor prognostic value of lack of IL-10 expression was observed for disease-specific and -free survival, with a trend for overall survival. Furthermore, multivariate analysis confirmed the independent prognostic value of lack of IL-10 expression. The prognostic value of IL-10 was retained even when we changed the cutoff level of positivity from 10% (18) to 5 or 15%. Our results are in contrast to a previous report by Hatanaka *et al.* (16), who suggested that IL-10 expression by the tumor was an indicator of poor prognosis. We have analyzed IL-10's prognostic value in a large and homogeneous population of patients with early stage lung cancer ($n = 138$), whereas Hatanaka *et al.* performed their analysis using a smaller and more heterogeneous population that included 82 patients with stage I–IIIb disease. Furthermore, the fact that all of the patients in our study were treated at a single institution and received lengthy follow-up care after surgery helps to increase the credibility of our survival analysis. Finally, Hatanake *et al.* (16) evaluated IL-10 expression by RT-PCR as opposed to immunohistochemistry in this study. Thus, our different results may be related in part to differences in patient population and the technique used to evaluate IL-10 expression. Indeed, we evaluated IL-10 expression at the protein level as compared with the mRNA level for Hatanake *et al.* Furthermore, both studies were retrospectively conducted and therefore potentially subject to some degree of selection bias.

We have analyzed IL-10 expression by performing immunohistochemical analysis with a polyclonal antihuman IL-10 antibody reported previously (18, 19). Other anti-IL-10 antibodies have also been used to evaluate IL-10 expression in paraffin-embedded tissue sections (17, 20). A good concordance between reverse transcription-PCR analysis and immunohistochemical analysis for IL-10 has been suggested in different reports (7, 17). We have used internal and external positive controls to assess the specificity of the staining. We found that even if tumor cells were negative for IL-10 staining, normal bronchial epithelial cells in the section (when present) were positive (17), thus ruling out a false negative result.

Although the mechanisms underlying the current data are not clear, there are several potential explanations for the poor outcome of patients with IL-10-negative tumors. Several laboratories have demonstrated that IL-10 is a potent inhibitor of tumor growth and metastasis in multiple animal models and tumor types, including melanoma, breast and prostate cancers, and Burkitt's lymphoma (11, 13, 20, 21). *In vivo*, the effects of IL-10 may be multifold. They can be related to direct inhibition of IL-10 on the angiogenic process *per se* or indirectly by affecting the angiogenic capacity or signals from tumor and/or tumor-infiltrating cells. Compelling evidence indicates that the antiangiogenic effect of IL-10 results from the inhibition of angiogenic factor release and production by the tumor and/or stromal cells. IL-10 induces production of TIMP-1, an inhibitor of angiogenesis, and inhibits MMP-2 and MMP-9 secretion by cancer cell lines, blocking the induction of microvessel formation *in vitro* (20, 22). It has also been suggested that IL-10 can directly inhibit endothelial cell response to angiogenic factors (21). Moreover, in murine mammary tumors, the antimetastatic and antitumor activity resulting from IL-10 gene transfer is related to enhanced production of nitric oxide (23).

One of the major roles of IL-10 in the regulation of immune responses involves its deactivating effect on macrophages (6). From the many cells and cell products within a tumor that serve as inducers or modulators of angiogenesis, macrophages

have emerged as a major component. IL-10 secreted by the tumor cells may prevent the migration of macrophages from the periphery into the tumor tissue, thus preventing macrophage infiltration (24). IL-10 also inhibits the expression of angiogenic factors (vascular endothelial growth factor, IL-1β, tumor necrosis factor-α, IL-6, and MMP-9) in tumor-associated macrophages (25). These changes correlate with decreased neovascularization of the tumors. Alternatively, the inhibitory effect of IL-10 on tumor metastasis has been suggested to be mediated through a NK cell-dependent mechanism (6, 12). IL-10 is able to affect the activities of NK cells, and NK cells were recently shown to contribute to the antiangiogenic effects of IL-12 through the killing of endothelial cells (26).

The observation that IL-10 expression differs among histological subtypes highlights the biological differences among different subtypes of NSCLC. Different abnormalities in oncogenes and tumor suppressor genes among histological subtypes of NSCLC are well known. Indeed, K-*ras* mutations are much more common in adenocarcinomas than in SCCs, whereas cyclin B1 overexpression or the *p53* mutant immunophenotype is more frequent in SCCs than in adenocarcinoma (2, 27, 28).

In conclusion, we found that a lack of IL-10 expression is a prognostic factor of poor outcome in stage I NSCLC. This result may be explained by the antitumor effects of IL-10, which contrast with the immunomodulatory effects that this cytokine displays *in vitro*. The mechanisms behind IL-10 antitumor effects might include inhibition of angiogenesis, stimulation of TIMPs, inhibition of MMP secretion, and inhibition of macrophage activity (20–25). Nevertheless, this result needs to be interpreted with caution because of potential limitations in the present study: (*a*) IL-10 production by tumor-infiltrating lymphocytes was not addressed because only a small fraction of our tissue samples displayed immune infiltrating cells; and (*b*) the role of IL-10 in cancer progression or regression might be very different according to the level of cytokine produced by the tumor and infiltrating immune cells. Additional studies are clearly required to confirm the present data and resolve the role of IL-10 in tumor growth and metastasis. We plan to conduct additional studies that will help in assessing the clinical importance of the present IL-10 findings and in understanding their possible mechanisms. These studies will be conducted using resected tissue from patients with stage I NSCLC, analyze the expression of MMPs and TIMPs, microvessel density, and the presence of tumor-infiltrating lymphocytes and their phenotype, and relate these factors to IL-10 expression by the tumor and to overall prognosis.

ACKNOWLEDGMENTS

We thank Christophe Borg for helpful discussions, as well as Susan Cweren and Lakshmi Kakarala for technical assistance with immunohistochemistry. We also thank Dawn Chalaire for editing this manuscript and Sandra Ideker for the artwork.

REFERENCES

1. Jemal, A., Thomas, A., Murray, T., and Thun, M. Cancer statistics, 2002. CA Cancer J. Clin., *52:* 23–47, 2002.

2. Soria, J. C., Jang, S. J., Khuri, F. R., Hassan, K., Liu, D., Hong, W. K., and Mao, L. Overexpression of cyclin B1 in early-stage non-small cell lung cancer and its clinical implication. Cancer Res., *60:* 4000–4004, 2000.

3. Zhou, X., Kemp, B. L., Khuri, F. R., Liu, D., Lee, J. J., Wu, W., Hong, W. K., and Mao, L. Prognostic implication of microsatellite alteration profiles in early-stage non-small cell lung cancer. Clin. Cancer Res., *6:* 559–565, 2000.

4. Khuri, F. R., Lotan, R., Kemp, B. L., Lippman, S. M., Wu, H., Feng, L., Lee, J. J., Cooksley, C. S., Parr, B., Chang, E., Walsh, G. L., Lee, J. S., Hong, W. K., and Xu, X. C. Retinoic acid receptor-beta as a prognostic indicator in stage I non-small cell lung cancer. J. Clin. Oncol., *18:* 2798–2804, 2000.

5. Khuri, F. R., Wu, H., Lee, J. J., Kemp, B. L., Lotan, R., Lippman, S. M., Feng, L., Hong, W. K., and Xu, X. C. Cyclooxygenase-2 overexpression is a marker of poor prognosis in stage I non-small cell lung cancer. Clin. Cancer Res., *7:* 861–867, 2001.

6. Howard, M., and O'Garra, A. Biological properties of interleukin 10. Immunol. Today, *13:* 198–200, 1992.

7. Smith, D. R., Kunkel, S. L., Burdick, M. D., Wilke, C. A., Orringer, M. B., Whyte, R. I., and Strieter, R. M. Production of interleukin-10 by human bronchogenic carcinoma. Am. J. Pathol., *145:* 18–25, 1994.

8. Young, M. R., Wright, M. A., Lozano, Y., Matthews, J. P., Benefield, J., and Prechel, M. M. Mechanisms of immune suppression in patients with head and neck cancer: influence on the immune infiltrate of the cancer. Int. J. Cancer, *67:* 333–338, 1996.

9. Rohrer, J. W., and Coggin, J. H. CD81 T cell clones inhibit antitumor T cell function by secreting IL-10. J. Immunol., *155:* 5719–5727, 1995.

10. Beissert, S., Hosoi, J., Grabbe, S., Asahina, A., and Granstein, R. D. IL-10 inhibits tumor antigen presentation by epidermal antigen presenting cells. J. Immunol., *154:* 1280–1286, 1995.

11. Kundu, N., Beaty, T. L., Jackson, M. J., and Fulton, A. M. Antimetastasic and antitumor activities of interleukin10 in a murine model of breast cancer. J. Natl. Cancer Inst. (Bethesda), *88:* 536–541, 1996.

12. Zheng, L. M., Ojcius, D. M., Garaud, F., Roth, C., Maxwell, E., Li, Z., Rong, H., Chen, J., Wang, X. Y., Catino, J. J., and King I. Interleukin-10 inhibits tumor metastasis through an NK cell-dependent mechanism. J. Exp. Med., *184:* 579–584, 1996.

13. Huang, S., Xie, K., Bucana, C. D., Ullrich, S. E., and Bar-Eli, M. Interleukin 10 suppresses tumor growth and metastasis of human melanoma cells: potential inhibition of angiogenesis. Clin. Cancer Res., *2:* 1969–1979, 1996.

14. Giovarelli, M., Musiani, P., Modesti, A., Dellabona, P., Casorati, G., Allione, A., Consalvo, M., Cavallo, F., di Pierro, F., De Giovanni, C., Musso, T., and Forni, G. Local release of IL-10 by transfected mouse mammary adenocarcinoma cells does not suppress but enhances antitumor reaction and elicits a strong cytotoxic lymphocyte and antibody-dependent immune memory. J. Immunol., *155:* 3112–3123, 1995.

15. Berman, R. M., Susuki, T., Tahara, H., Robbins, P. D., Narula, S. K., and Lotze, M. T. Systemic administration of cellular IL-10 induces an effective, specific, and long-lived immune response against established tumors in mice. J. Immunol., *157:* 231–238, 1996.

16. Hatanaka, H., Abe, Y., Kamiya, T., Morino, F., Nagata, J., Tokunaga, T., Oshika, Y., Suemizu, H., Kijima, H., Tsuchida, T., Yamazaki, H., Inoue, H., Nakamura, M., and Ueyama, Y. Clinical implications of interleukin (IL)-10 induced by non-small cell lung cancer. Ann. Oncol., *11:* 815–819, 2000.

17. Bonfield, T. L., Konstan, M. W., Burfeind, P., Panuska, J. R., Hilliard, J. B., and Berger, M. Normal bronchial epithelial cells constitutively produce the anti-inflammatory cytokine interleukin-10, which is downregulated in cystic fibrosis. Am. J. Respir. Cell Mol. Biol., *13:* 257–261, 1995.

18. Huang, M., Wang, J., Lee, P., Sharma, S., Mao, J. T., Meissner, H., Uyemura, K., Modlin, R., Wollman, J., and Dubinett, S. M. Human non-small cell lung cancer cells express a type 2 cytokine pattern. Cancer Res., *55:* 3847–3853, 1995.

19. Fujieda, S., Lee, K., Sunaga, H., Tsuzuki, H., Ikawa, H., Fan, G. K., Imanaka, M., Takenaka, H., and Saito, H. Staining of interleukin-10 predicts clinical outcome in patients with nasopharyngeal carcinoma. Cancer, *85:* 1439–1445, 1999.

20. Stearns, M. E., Garcia, F. U., Fudge, K., Rhim, J., and Wang, M. Role of interleukin 10 and transforming growth factor β 1 in the angiogenesis and metastasis of prostate primary tumor lines from orthotopic implants in severe combined immunodeficiency mice. Clin. Cancer Res., *5:* 711–720, 1999.

21. Cervenak, L., Morbidelli, L., Donati, D., Donnini, S., Kambayashi, T., Wilson, J. L., Axelson, H., Castanos-Velez, E., Ljunggren, H. G., Malefyt, R. D., Granger, H. J., Ziche, M., and Bejarano, M. T. Abolished angiogenicity and tumorigenicity of Burkitt lymphoma by interleukin-10. Blood, *96:* 2568–2573, 2000.

22. Stearns, M. E., Fudge, K., Garcia, F., and Wang, M. IL-10 inhibition of human prostate PC-3 ML cell metastases in SCID mice: IL-10 stimulation of TIMP-1 and inhibition of MMP-2/MMP-9 expression. Invasion Metastasis, *17:* 62–74, 1997.

23. Kundu, N., Dorsey, R., Jackson, M. J., Guiterrez, P., Wilson, K., Fu, S., Ramanujam, K., Thomas, E., and Fulton, A. M. Interleukin-10 gene transfer inhibits murine mammary tumors and elevates nitric oxide. Int. J. Cancer, *76:* 713–719, 1998.

24. Richter, G., Kruger-Kasagakes, S., Hein, G., Huls, C., Schmitt, E., Diamantstein, T., and Blankenstein, T. Interleukin-10 transfected into Chinese hamster ovary cells prevents tumor growth and macrophage infiltration. Cancer Res., *53:* 4134–4137, 1993.

25. Di Carlo, E., Coletti, A., Modesti, A., Giovarelli, M., Forni, G., and Musiani, P. Local release of interleukin-10 by transfected mouse adenocarcinoma cells exhibit pro- and anti-inflammatory activity and results in a delayed tumor rejection. Eur. Cytokine Netw., *9:* 61–68, 1998.

26. Yao, L., Sagadari, C., Furuke, K., Bloom, E. T., Teruya-Feldstein, J., and Tosato, G. Contribution of natural killer cells to inhibition of angiogenesis by IL-12. Blood, *93:* 1612–1621, 1999.

27. Rossell, R., Li, S., Skacel, Z., Mate, J. L., Maestre, J., Canela, M., Tolosa, M., Tolosa, E., Armengol, P., Barnadas, A., and Ariza, A. Prognostic impact of mutated K-ras gene in surgically resected non-small cell lung cancer patients. Oncogene, *8:* 2407–2412, 1993

28. Kishimoto, Y., Murakami, Y., Shiraishi, M., Hayashi, K., and Sekiya, T. Aberrations of the p53 tumor suppressor gene in human non-small cell carcinomas of the lung. Cancer Res., *52:* 4799–4804, 1992.

[Cancer Biology & Therapy 4:4, 407-413, April 2005]; ©2005 Landes Bioscience

Research Paper

Enhanced Growth Inhibition and Apoptosis Induction in NSCLC Cell Lines by Combination of Celecoxib and 4HPR at Clinically Relevant Concentrations

Shi-Yong Sun†
Claudia P. Schroeder
Ping Yue
Dafna Lotan
Waun K. Hong
Reuben Lotan*

Department of Thoracic, Head and Neck Medical Oncology; The University of Texas M.D. Anderson Cancer Center; Houston, Texas USA

†Present Address: Winship Cancer Institute; Emory University School of Medicine; 1365-C Clifton Road; Clinical Building C3088; Atlanta, Georgia 30322 USA

*Correspondence to: Reuben Lotan; Department of Thoracic, Head and Neck Medical Oncology; The University of Texas M.D. Anderson Cancer Center; 1515 Holcombe Blvd., Box 432; Houston, Texas 77030 USA; Tel: 713.792.8467; Fax: 713.745.5656; Email: rlotan@mdanderson.org

Received 12/28/04; Accepted 02/21/05

Previously published online as a *Cancer Biology & Therapy* E-publication: http://www.landesbioscience.com/journals/cbt/abstract.php?id=1618

KEY WORDS

Celecoxib, COX-2, fenretinide, 4HPR, growth inhibition, lung cancer cell lines

ACKNOWLEDGEMENTS

This study was supported by United States Public Health Service Grant PO1 CA98144 and Cancer center Core grant P30 CA16772-30 from the National Cancer Institute, by grant DAMD17-01-1-0689 from the Department of Defense, and by the David Workman Memorial Endowment Award from the Samuel Waxman Cancer Research Foundation (SWCRF). C.P. Schroeder was supported in part by a fellowship from the Deutsche Forschungsgemeinschaft (DFG, Germany). W.K. Hong is an American Cancer Society Clinical Research Professor. R. Lotan is the incumbent of the Irving and Nadine Mansfield and Robert David Levitt Cancer Research Chair.

ABSTRACT

Celecoxib exhibits cancer preventive and therapeutic effects in animal models and clinical trials. It presumably acts through selective inhibition of cyclooxygenase-2 (COX-2) and subsequent reduction of prostaglandin (PG) synthesis. However, the concentrations of celecoxib required for growth inhibition and apoptosis induction in vitro are higher than those needed for suppression of PGs. Moreover, those concentrations are not achievable in humans raising a controversy regarding the clinical relevance of in vitro data. We investigated the activity of celecoxib alone and in combination with the pro-apoptotic retinoid *N*-(4-hydroxyphenyl)retinamide (4HPR) on growth and apoptosis of human non-small cell lung cancer (NSCLC) cell lines. Celecoxib inhibited growth of thirteen NSCLC cell lines with IC_{50} values ranging from 19 to 33 μM regardless of their COX-2 expression. Apoptosis was induced in cells with high (A549) as well as low (H1792) COX-2 levels but only at a concentration of 75 μM celecoxib. However, treatment with pharmacologically feasible concentrations of celecoxib (≤ 10 μM) in combination with 4HPR (≤ 2 μM) resulted in a marked suppression of NSCLC cell growth and colony formation. Apoptosis mediated by activation of caspase-3, cleavage of PARP and lamin A was suppressed by addition of antioxidants, suggesting that the generation of reactive oxygen species was partially involved. This study indicates, that celecoxib combined with 4HPR is more effective than treatment with either agent alone in inhibition of growth and induction of apoptosis in NSCLC cells. It suggests further investigations of this combination for lung cancer treatment.

INTRODUCTION

Lung cancer remains the leading cause of cancer mortality among both men and women in the United States. It has been estimated that 173,770 new cases and 160,440 deaths in 2004 will be attributed to lung cancer.[1] Unfortunately, the severe morbidity of lung cancer and the poor 5-year survival rate of approximately 15% have not been improved substantially by current treatment protocols during the last decade. Therefore, intense efforts are being mounted to find new agents and combinations for treatment and prevention of human lung cancer that may lead to the improvement in patients outcome. Non-steroidal anti-inflammatory drugs (NSAIDs), such as the selective COX-2 inhibitor celecoxib, have gained much attention for their potential use as anticancer agents.[2,3]

The cyclooxygenase (COX) enzymes are responsible for the metabolic conversion of arachidonic acid to prostaglandins (PGs), which play a key role in diverse biological functions involving inflammation, immunological response and development.[4] Several isoforms of COXs have been identified, which differ in their expression pattern and functions.[5] COX-1 is constitutively expressed in most human tissues and important for the maintenance of homeostatic functions. In contrast, COX-2 is inducible during pathological conditions such as inflammation and cancer in response to growth factors, mutagens, and cytokines. In fact, the upregulation of COX-2 has been shown to promote cell growth, inhibit apoptosis, and enhance cell motility and angiogenesis in tumor tissues.[6-8] Lines of evidence have demonstrated that COX-2 is induced at almost all stages of non-small cell human lung cancer (NSCLC) progression relative to adjacent normal bronchial epithelial tissue.[9-11] Interestingly, among patients with stage I NSCLC, COX-2 overexpression was associated with a poor prognosis and a positive expression of RAR-β in their tumors as well.[12]

The selective COX-2 inhibitor celecoxib (Celebrex®) has been approved by the FDA for treatment of rheumatoid arthritis and osteoarthritis in adults and for adjuvant treatment of patients with familial adenomatous polyposis.[13] It has been demonstrated, that celecoxib dose-dependently suppressed tumor growth, lung metastasis and angiogenesis in mice.[7,14-16]

©2005 LANDES BIOSCIENCE. DO NOT DISTRIBUTE

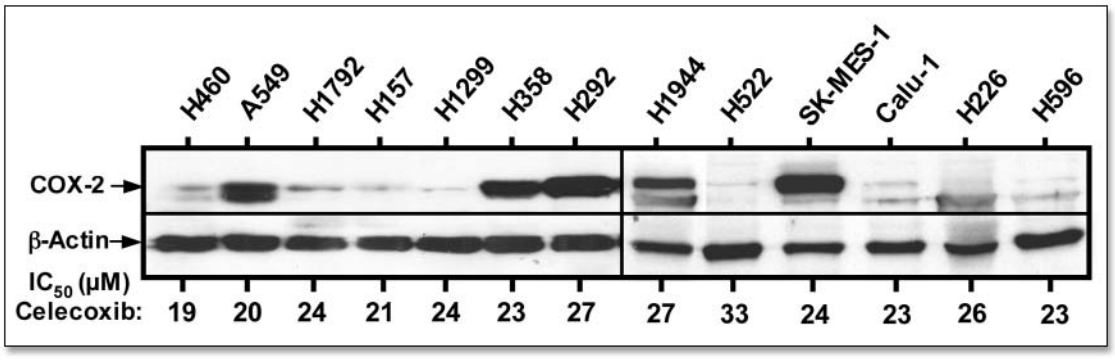


Figure 1. Expression of COX-2 in human NSCLC cell lines and its relation to growth inhibition by celecoxib indicated as IC_{50} values (μM) presented under each lane. Cultures of thirteen cell lines were grown to approximately 80% confluence before they were harvested and separated through 10% SDS-PAGE gel electrophoresis followed by Western immunoblotting as described under Materials and Methods. The effects of celecoxib on NSCLC cell growth were determined using SRB assay[35] after three days of incubation.

The ability of celecoxib to induce apoptosis has been confirmed in various types of cancer cells including lung but only at concentrations that exceeded maximum plasma level in humans ranging from 3.2 to 5.6 μM after administration of a single daily dose of 800 mg celecoxib.[15,17-19] Thus, a controversy has been raised concerning its presumed anti-tumor mechanisms.[14,20] Specifically, the concentrations of celecoxib needed to inhibit cell cycle progression and induce apoptosis in cancer cells are typically 10 to 100-fold higher than those required for suppression of PG synthesis.[15,21] Furthermore, significant anti-tumor effects have been observed in cancer cells irrespective of their COX-2 expression, suggesting that celecoxib may exert in part and/or cell type-specific therapeutic activity via pathways that are independent of selective inhibition of COX-2.[14,15,17-22] As a matter of fact, this assumption is not solely related to celecoxib as such discrepancy between high concentrations needed for anti-proliferative and pro-apoptotic effects compared to plasma levels which can be achieved in vivo, have been reported for other NSAIDs.[15,22,23]

Interestingly, several reports have indicated that celecoxib interacts in additive and synergistic manners with conventional therapeutic regimens in patients with NSCLC.[3,24,25] In addition, various NSAIDs produced synergistic activity in combination with 13-cis-retinoic acid in NSCLC cell lines regardless of drug-resistance

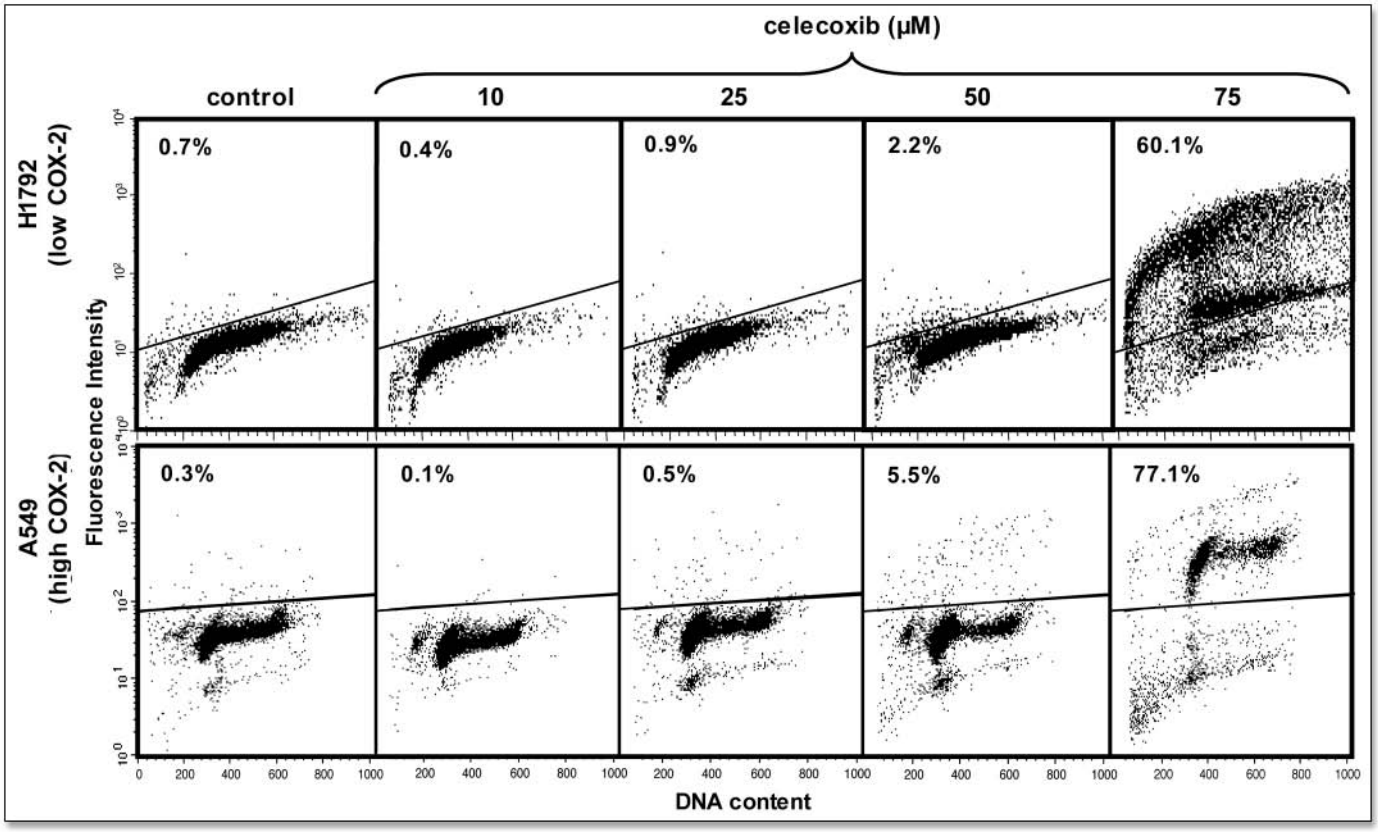


Figure 2. Effects of celecoxib on induction of apoptosis in NSCLC cell lines. H1792 (low COX-2 level) and A549 (high COX-2 level) cell lines were treated with different concentrations of celecoxib for 24 hours before they were harvested and subjected to apoptosis detection using TUNEL assay.[36] The percentages of TUNEL-positive cells are presented inside each histogram.

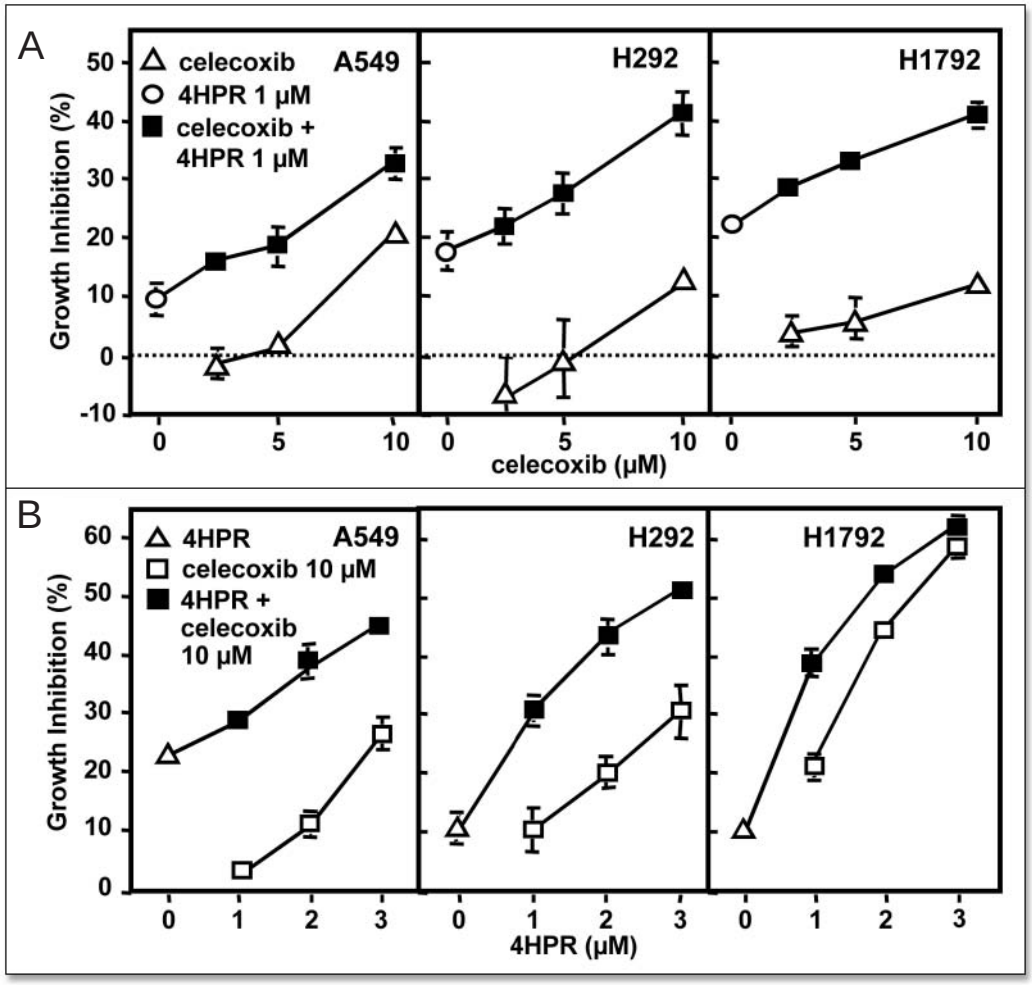


Figure 3. Effects of different concentrations of celecoxib, 4HPR and their combinations on growth of human A549, H292, and H1792 lung cancer cell lines. NSCLC cells were treated with 4HPR (1 μM) or celecoxib (2.5, 5 or 10 μM) and their combinations for three days (A). NSCLC cells were incubated with celecoxib (10 μM), or 4HPR (1, 2 or 3 μM) and their combinations for three days (B). Cell numbers were estimated by SRB assay.[35] The data represent mean values (bars, SE) of four replicate wells of one of two independent experiments, which yielded similar results.

phenotype.[26] For the present study, we chose to evaluate the synthetic retinoid *N*-(4-hydroxyphenyl)retinamide (4HPR, fenretinide) in combination with celecoxib because it has been well established to exert potent pro-apoptotic effects on a variety of cancer cells[27-30] and exhibits lower side effects compared to other retinoids in therapeutic and chemopreventive clinical trials including studies on NSCLC.[31-34]

Our results indicate, that celecoxib in combination with 4HPR exerted enhanced growth inhibitory and apoptosis-inducing effects in NSCLC cells at concentrations that are clinically relevant in humans. Thus, it may be useful in designing novel combination-therapeutic strategies for human lung cancer.

MATERIALS AND METHODS

Reagents. Dulbecco's Modified Eagle's Minimal Essential Medium (DMEM), penicillin, streptomycin, phosphate-buffered saline (PBS) and trypsin were purchased from Gibco™ Invitrogen Corporation (Carlsbad, CA). Fetal bovine serum (FBS) was from HyClone Laboratories, Inc. (Logan, UT) and celecoxib (celebrex®, 4-[5-(4-methylphenyl)-3-(trifluoromethyl)-1H-pyrazol-1-] benzene-sulfonamide) was obtained from GD Searle & Co (Chicago, IL). Dimethyl sulfoxide (DMSO), ethylene diamine tetra-acetic acid (EDTA), N-acetyl cystein (NAC), butylated hydroxyanisol (BHA), and sodium dodecyl sulfate (SDS) were purchased from Sigma Chemical Co. (St. Louis, MO).

Human NSCLC cell lines. The NSCLC cell lines H460, H292, A549, H157, H1299, H358 and H1792 were either obtained from Dr. A. Gadzar (The University of Texas Southwestern Medical Center, Dallas, TX) or purchased from the American Type Culture Collection (ATCC; Rockville, MD). These cells were grown in monolayer cultures in a mixture of DMEM/Ham's F12 medium (1:1, v/v) supplemented with 5% FBS at 37°C in a humidified atmosphere consisting of 5% CO_2 and 95% air. Celecoxib was dissolved in DMSO at a concentration of 0.05 M and stored at -80°C. 4HPR obtained from Dr. R. Lubet (National Cancer Institute, Bethesda, MD) was dissolved in DMSO at a concentration of 0.01 M and stored in the dark at -80°C. Stock solutions were diluted to desired concentrations with culture medium prior to use keeping the final concentration of DMSO less than 0.1%.

Growth inhibition assay. NSCLC cells were seeded in 96-well culture plates (BD Bioscience Labware, Bedford, MA), allowed to adhere overnight and treated with either celecoxib, 4HPR and their combinations in 5% FBS-containing medium for 3 days before estimation of cell number by sulforhodamine B (SRB) assay.[35] The absorbance was measured using an automated plate reader MR5000 (Dynatech Laboratories Inc., Chantilly, VA). The inhibition of cell growth was calculated from the equation, % inhibition = (1 - A*t*/A*c*) x 100%, where A*t* and A*c* represent absorbencies of treated and control cultures, respectively. Concentration response curves were plotted and levels of celecoxib resulting in 50% growth inhibition (IC_{50}) were estimated. The results represent mean ± standard deviation (SD) of three independent experiments.

Colony formation. Exponentially growing H292 cells were seeded in 6-well culture plates (Greiner Bio-One, Inc., Longwood, FL) and allowed to grow overnight before treatment with either celecoxib, 4HPR and their combinations. The culture medium was replaced with fresh medium containing the compounds every 3 days. After 14 days of incubation, the colonies were stained with crystal violet (0.5%) and examined under a microscope.

TUNEL apoptosis assay. Intranucleosomal DNA fragmentation was evaluated using an apoptosis detection kit (Phoenix Flow Systems, Inc., San Diego, CA) based on the TUNEL technique.[36] The reaction labels the 3'hydroxyl termini of DNA fragmented during apoptosis with fluorescein-isothiocyanate-conjugated dUTP. After treatment, the cells were harvested by trypsinization, pelleted by centrifugation, fixed with ice-cold ethanol (70%, v/v) and stained according to the protocol provided by the manufacturer. Cytofluorometric determinations and data analysis were performed on a Coulter XL flow cytometer (Coulter Corp., Miami, FL). Approximately 10,000 cells were evaluated for each sample.

Western blot analysis. Samples containing 50 μg of total cellular protein were electrophoretically separated through 10% sodium dodecyl sulfate (SDS)-polyacrylamide gels followed by transfer onto Hybond-ECL membranes (Amersham, Arlington Heights, IL) as described previously.[20] After blocking with PBS containing 0.1% Tween 20 and 5% low-fat milk, the membranes were incubated with primary antibodies for COX-2 (Oxford Biomedical Research Inc., Oxford, MI), caspase-3 (clone 31A1067, Imgenex, San Diego, CA), PARP and lamin A (Cell Signaling Technology Inc., Beverly, MA), or β-actin (Sigma Chemical Co., St. Louis, MO) at appropriate dilutions. Antibody binding was detected with horseradish peroxidase-linked second antibody and enhanced chemiluminescence (Amersham Biosciences Corp., Piscataway, NJ).

RESULTS

Celecoxib inhibits growth of human NSCLC cells independent of COX-2. To investigate, whether the sensitivity of several human NSCLC cell lines to celecoxib was associated with the target enzyme expression, we analyzed their constitutive COX-2 levels by Western immunoblotting. Figure 1 indicates, that A549, H358, and H292, H1944, and SK-MES-1 cells expressed COX-2 protein, whereas low or undetectable levels were found in other NSCLC cell lines examined. Apparently, some of the cell extracts exhibit a doublet of protein bands as a result of changes in the extent of COX-2 glycosylation. We then determined the concentration of celecoxib causing 50% growth inhibition (IC_{50}) from the dose-response curves of each cell line after 3 days of incubation. The IC_{50} values were in a range between 19 and 33 μM celecoxib (Fig. 1). However, NSCLC cell lines that expressed COX-2 exhibited similar sensitivity as cell lines with low or undetectable COX-2 levels.

Celecoxib induces apoptosis of human NSCLC cells independent of COX-2. To study whether growth inhibition of NSCLC cells by celecoxib resulted from induction of apoptosis, we examined apoptotic events by the TUNEL method after treatment of H1792 (low COX-2 level), and A549 (high COX-2 level) cells with various concentrations of celecoxib. We observed no substantial induction of apoptosis with concentrations up to 50 μM celecoxib in both, COX-2 positive and COX-2 negative, NSCLC cell lines (Fig. 2). However, treatment with 75 μM celecoxib markedly increased the percentage of TUNEL-positive cells from less than 1% in control cultures to 60% in H1792 and 77% in A549 cells, respectively. Similarly to our findings on growth inhibition, the effects of celecoxib on induction of apoptosis appeared independent of COX-2 expression.

Celecoxib in combination with 4HPR is more potent in growth inhibition than treatment with either agent alone. Because the plasma levels of celecoxib feasible in humans are considerably lower than the concentrations found to be effective in vitro, we hypothesized that combinations of low doses of celecoxib with the pro-apoptotic retinoid 4HPR will be more potent in growth inhibition than each agent alone. To test this hypothesis, we treated A549, H1792, and H292 cell lines with celecoxib and 4HPR for 3 days. As shown in Figure 3, simultaneous treatment of celecoxib with 4HPR resulted in additive suppression of cell growth in a dose-dependent manner (Fig. 3A and B). However, the effects of various concentrations of 4HPR in addition to 10 μM celecoxib were less profound in H1792 cells than in the other two NSCLC cell lines (Fig. 3B).

The Celecoxib/4HPR combination reduces colony formation. Due to the modest effects of the celecoxib/4HPR combination on cell growth in monolayer culture, we asked whether colony formation, which allows a relatively longer treatment of tumor cells, would show greater activity. Thus, we estimated the effects of celecoxib and/or 4HPR on the ability of H292 cells to form colonies after 14 days of incubation. Celecoxib at 5 or 10 μM showed no discernible changes, while 4HPR was able to reduce the formation of H292 colonies in a dose-dependent manner (Fig. 4A and B). However, simultaneous treatment suppressed colony formation to a larger extent than 4HPR alone as illustrated in the photomicrographs (Fig. 4A).

Celecoxib in combination with 4HPR is more potent in apoptosis induction than treatment with either agent alone. To determine whether

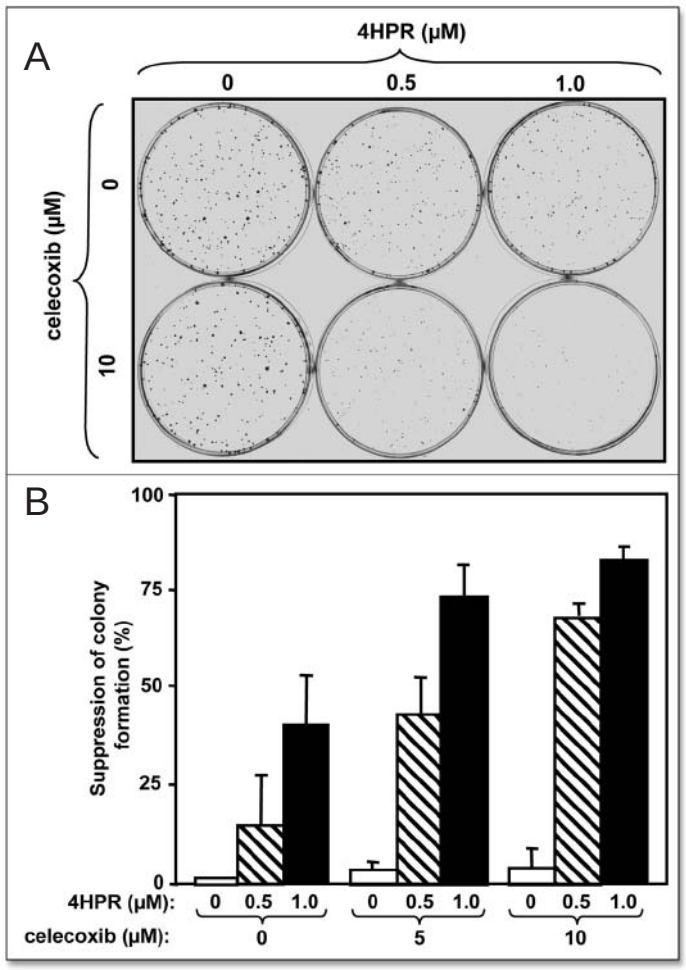


Figure 4. Effects of celecoxib and/or 4HPR on colony formation of H292 lung cancer cells. H292 cells were treated with celecoxib (5 or 10 μM) and/or 4HPR (0.5 or 1.0 μM) for 14 days before staining and examination under the microscope as described under Materials and Methods. Colony-forming ability of H292 lung cancer cells was markedly suppressed by combined treatment of celecoxib and 4HPR as compared with each of the single agents or cultures treated with DMSO alone.

enhanced growth inhibition by celecoxib/4HPR combination resulted from induction of apoptosis, we compared apoptosis in NSCLC cells incubated with either combinations or single treatment of the two agents. Celecoxib alone had no effect on induction of apoptosis up to a tested concentration of 20 μM, whereas treatment with 2 μM 4HPR resulted in 26% apoptosis. In contrast, the combination of both agents exhibited more than 50% apoptotic cells (Fig. 5A and B).

Apoptosis induced by Celecoxib/4HPR is mediated by Caspase-3 cascade and suppressed by antioxidants. To begin to understand the mechanism of the induction of apoptosis, we analyzed the effects of celecoxib and/or 4HPR on caspase-3 cascade. Western blot analysis revealed that combinations of 5 and 10 μM celecoxib, respectively with 2 μM 4HPR resulted in a greater activation of caspase-3 and cleavage of its substrates PARP and lamin A compared to each of the agents alone. In fact, celecoxib alone was inactive whereas 4HPR partially activated caspase-3 and cleavage of PARP and lamin A (Fig. 6A). According to studies, which have demonstrated that apoptosis induced by 4HPR can be suppressed by addition of antioxidants, we examined the effects of butylated hydroxyanisole (BHA) and N-acetyl cysteine (NAC) on apoptosis as well as cleavage of PARP and lamin A in NSCLC cells. Incubation of H1792 cells with 5 μM celecoxib in addition to 50 μM BHA or 5 mM NAC had no effect on apoptosis induction. However, treatment with 2 μM 4HPR alone compared to simultaneous

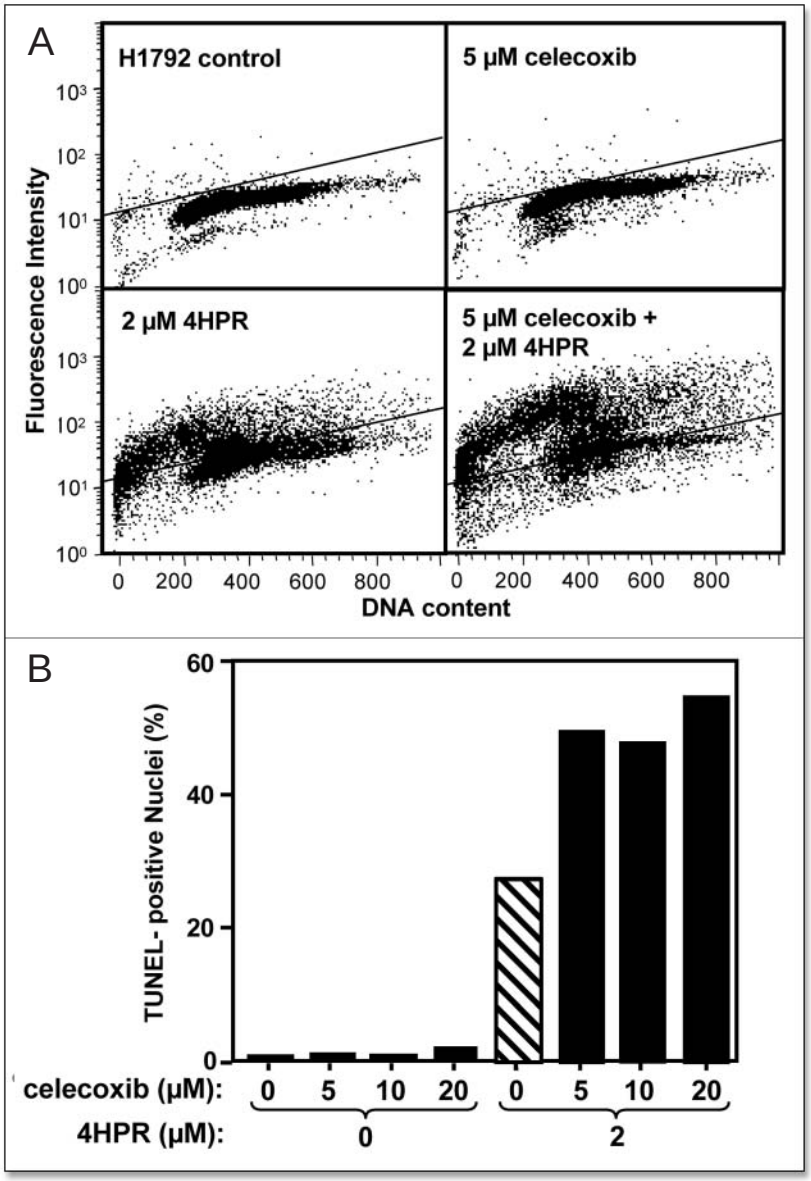


Figure 5. Enhanced induction of apoptosis in H1792 lung cancer cells by combinations of celecoxib and 4HPR. The apoptotic events were examined after 48 hours in the presence or absence of the two drugs as single or combination using TUNEL technique.[36] Dual parameter flow cytometric analysis measuring FITC-labeled DNA fragments (*ordinate*) and cellular DNA content (*abscissa*) in H1792 cells (A). Effects of celecoxib in combination with 4HPR on induction of apoptosis represented as percentage TUNEL-positive nuclei (B).

incubation with 5 μM celecoxib increased the percentage of TUNEL-positive cells from 23% to 52%. Likewise, cleavage of the caspase-3 substrates PARP and lamin A was obtained after simultaneous incubation with celecoxib and 4HPR but partially prevented by cotreatment with the antioxidants BHA and NAC (Fig. 6B).

DISCUSSION

This in vitro study highlights the enhanced growth-inhibitory and apoptosis-inducing effects of celecoxib in combination with 4HPR at clinically relevant concentrations compared to single agent treatment alone in NSCLC cell lines. We have demonstrated that all NSCLC cell lines used in this study were susceptible to the growth-inhibitory activity of celecoxib with comparable IC_{50} values ranging from 19 to 33 μM. However, these effects appeared to be independent of COX-2 expression based on the fact that NSCLC cell lines exhibited variable levels of COX-2 protein ranging from high to very low. Moreover, the celecoxib concentrations required for growth inhibition were considerably higher than those required for suppression of COX-2 activity because we and others have shown that as little as 0.1 μM celecoxib was able to reduce PGE_2 levels in various tumor cell lines including lung cells.[3,17,21] In addition, our data indicate that induction of apoptosis by celecoxib only occured at a concentration of 75 μM regardless of the COX-2 level in NSCLC cells. These findings are in agreement with studies reported by other investigators, which have demonstrated COX-2-independent responses to high doses of celecoxib in various types of cancer cell lines.[15,18,21] Noticeably, in vivo studies revealed significant suppression in tumor growth of COX-2-deficient colorectal cancer xenografts after treatment with celecoxib.[14,15] Recent reports highlighted several COX-2-independent mechanisms including activation of phosphatidylinositol 3-kinase (PI3K)/Akt,[8,19] modulation of NF-κB-dependent gene transcription[17] and peroxisome proliferator-activated receptors (PPARs),[37] alterations of cell-cycle regulatory proteins,[15] and induction of death receptor expression.[22] However, the discrepancy between using high concentrations of celecoxib to obtain apoptosis-inducing effects in cell culture (25 to 100 μM) and those pharmacologically achievable in humans raises questions regarding the clinical relevance of most of the in vitro data.[14,16,17] In fact, pharmacokinetic studies performed in humans revealed that plasma levels did not exceed 5.6 μM in individuals receiving up to 800 mg celecoxib per day.[17,38] At this low concentration, celecoxib neither inhibited cell growth nor induced apoptosis in any cancer cell line tested in vitro.[14,15,17,22] Consequently, we postulated that celecoxib's anti-cancer activity can be potentiated by combination with other pro-apoptotic agents.

We have selected the synthetic retinoid 4HPR as a partner for combination with celecoxib because this retinoid has been shown to induce apoptosis in several types of malignant cells including lung cancer cell lines.[27-30] In addition, it has been tested in several clinical trials for cancer chemoprevention and therapy with a favorable toxicity profile as compared with other retinoids.[31-34] For example, a very recent phase II study has demonstrated that the mean plasma concentration of 4HPR was 3.1 ± 0.7 μM in adults with recurrent gliomas given 900 mg/m^2 4HPR orally twice daily. This regimen was well tolerated.[34] In comparison, the clinical use of all-trans-retinoic acid is associated with the development of a potentially lethal syndrome when reaching peak plasma levels of 1 μM.[31] Moreover, combining celecoxib with retinoids has been previously suggested as protocol for preventing cancers of the upper aerodigestive tract.[2]

Here, we demonstrate that combinations of clinically achievable plasma levels but suboptimal in vitro-concentrations of celecoxib (2.5 to 10 μM) with 4HPR (0.5 to 3.0 μM) resulted in additive

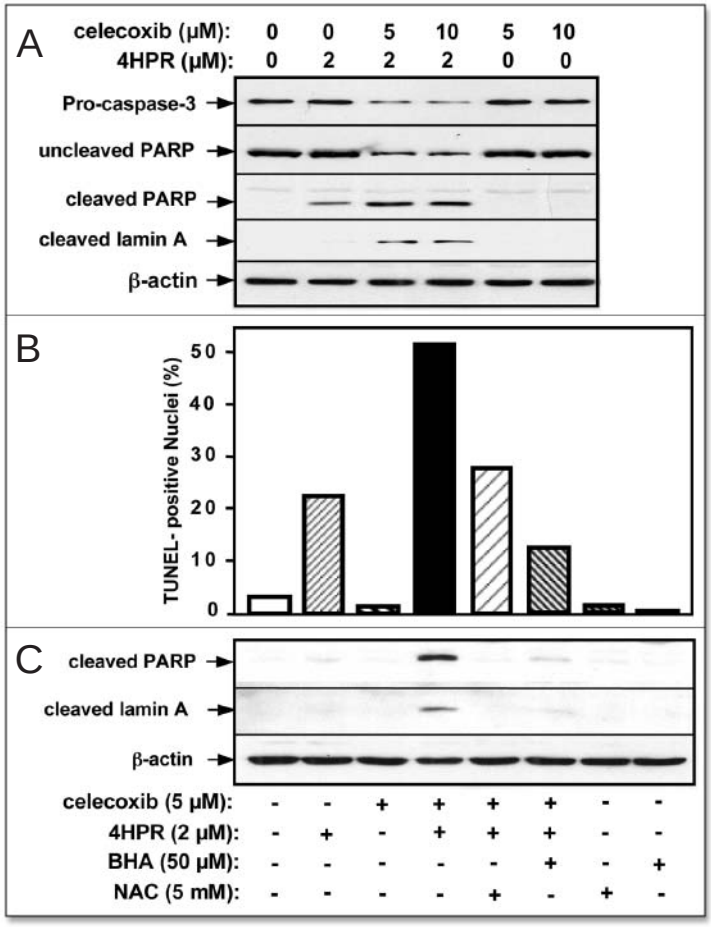


Figure 6. Suppression of apoptosis induced by celecoxib in combination with 4HPR by antioxidants in H1792 cells. Regulation of apoptosis-related proteins by celecoxib and/or 4HPR using Western immunoblot analysis. β-Actin served as loading control (A). Partial suppression of the induction of apoptosis after simultaneous treatment of celecoxib (5 μM) and 4HPR (2 μM) preincubated with 50 μM butylated hydroxyanisole (BHA) or 5 mM N-acetyl cysteine (NAC) for 30 min. The cells were harvested after 24 hours and processed for analysis by TUNEL technique (B) or Western immunoblotting as described under Materials and Methods (C).

growth inhibition, induction of apoptosis and a more than additive suppression of colony formation in NSCLC cell lines. The mechanism of the interaction between celecoxib and 4HPR that results in potentiation of their effects on apoptosis remains to be elucidated fully. In this study, we have begun to understand some aspects of this mechanism. We found that the induction of apoptosis by the celecoxib/4HPR combination was mediated by activation of caspase-3 and cleavage of its substrates PARP and lamin A. Because as a single agent, 4HPR has been shown to induce apoptosis by increasing endogenous ceramide levels and mitochondrial reactive oxygen species (ROS)[27-30] we asked whether ROS generation may also be important in the action of the celecoxib/4HPR combination. Indeed, we found that antioxidants blocked the celecoxib/4HPR-induced apoptosis implicating ROS in their effect. Clearly, additional investigations are needed to fully elucidate the molecular mechanisms underlying the increased efficacy of the combination of these agents. Nonetheless, our demonstration of the more than additive effects of the celecoxib/4HPR combination at pharmacologically achievable concentrations warrants further testing of this regimen in in vivo models and potentially also in clinical trials.

References

1. Surveillance Research. Lung and bronchus. In: Cancer Facts & Figures 2004. Atlanta, GA, USA: American Cancer Society, 2004:5008-04.
2. Mestre JR, Chan G, Zhang F, Yang EK, Sacks PG, Boyle JO, Shah JP, Edelstein D, Subbaramaiah K, Dannenberg AJ. Inhibition of cyclooxygenase-2 expression. An approach to preventing head and neck cancer. Ann NY Acad Sci 1999; 889:62-71.
3. Sandler AB, Dubinett SM. COX-2 inhibition and lung cancer. Semin Oncol 2004; 31:45-52.
4. Williams CS, Mann M, Du Bois RN. The role of cyclooxygenases in inflammation, cancer, and development. Oncogene 1999; 18:7908-916.
5. Cao Y, Prescott SM. Many actions of cyclooxygenase-2 in cellular dynamics and in cancer. J Cell Physiol 2002; 190:279-86.
6. Tsujii M, Du Bois RN. Alterations in cellular adhesion and apoptosis in epithelial cells overexpressing prostaglandin endoperoxide synthase-2. Cell 1995; 83:493-501.
7. Masferrer JL, Leahy KM, Koki AT, Zweifel BS, Settle SL, Woerner BM, Edwards DA, Flickinger AG, Moore RJ, Seibert K. Antiangiogenic and antitumor activities of cyclooxygenase-2 inhibitors. Cancer Res 2000; 60:1306-11.
8. Lin MT, Lee RC, Yang PC, Ho FM, Kuo ML. Cyclooxygenase-2 inducing mcl-1 dependent survival mechanism in human lung adenocarcinoma cells. J Biol Chem 2001; 276:48997-9002.
9. Hida T, Yatabe Y, Achiwa H, Muramatsu H, Kozaki K, Nakamura S, Ogawa M, Mitsudomi T, Sugiura T, Takahashi T. Increased expression of cyclooxygenase 2 occurs frequently in human lung cancers, specifically in adenocarcinomas. Cancer Res 1998; 58:3761-4.
10. Hosomi Y, Yokose T, Hirose Y, Nakajima R, Nagai K, Nishiwaki Y, Ochiai A. Increased cyclooxygenase 2 (COX-2) expression occurs frequently in precursor lesions of human adenocarcinoma of the lung. Lung Cancer 2000; 30:73-81.
11. Riedl K, Krysan K, Pold M, Dalwadi H, Heuze-Vourc'h N, Dohadwala M, Liu M, Cui X, Figlin R, Mao JT, Strieter R, Sharma S, Dubinett SM. Multifaceted roles of cyclooxygenase-2 in lung cancer. Drug Resist Updat 2004; 7:169-84.
12. Khuri FR, Wu H, Lee JJ, Kemp BL, Lotan R, Lippman SM, Feng L, Hong WK, Xu XC. Cyclooxygenase-2 overexpression is a marker of poor prognosis in stage I nonsmall cell lung cancer. Clin Cancer Res 2001; 7:861-7.
13. Steinbach G, Lynch PM, Phillips RK, Wallace MH, Hawk E, Gordon GB, Wakabayashi N, Saunders B, Shen Y, Fujimura T, Su LK, Levin B. The effect of celecoxib, a cyclooxygenase-2 inhibitor, in familial adenomatous polyposis. N Engl J Med 2000; 342:1946-52.
14. Williams CS, Watson AJ, Sheng H, Helou R, Shao J, DuBois RN. Celecoxib prevents tumor growth in vivo without toxicity to normal gut: Lack of correlation between in vitro and in vivo models. Cancer Res 2000; 60:6045-51.
15. Groesch S, Tegeder I, Niederberger E, Brautigam L, Geisslinger G. COX-2 independent induction of cell cycle arrest and apoptosis in colon cancer cells by the selective COX-2 inhibitor celecoxib. FASEB J 2001; 15:2742-4.
16. Zhang S, Lawson KA, Simmons-Menchaca M, Sun LZ, Sanders BG, Kline K. Vitamin E analog α-TEA and celecoxib alone and together reduce human MDA-MB-435-FL-GFP breast cancer burden and metastasis in nude mice. Breast Cancer Res Treat 2004; 87:111-21.
17. Niederberger E, Tegeder I, Vetter G, Schmidtko A, Schmidt H, Euchenhofer C, Brautigam L, Grosch S, Geisslinger G. Celecoxib loses its anti-inflammatory efficacy at high doses through activation of NF-κB. FASEB J 2001; 15:1622-4.
18. Waskewich C, Blumenthal RD, Li H, Stein R, Goldenberg DM, Burton J. Celecoxib exhibits the greatest potency amongst cyclooxygenase (COX) inhibitors for growth inhibition of COX-2-negative hematopoietic and epithelial cell lines. Cancer Res 2002; 62:2029-33.
19. Zhang Z, Lai GH, Sirica AE. Celecoxib-induced apoptosis in rat cholangiocarcinoma cells mediated by akt inactivation and bax translocation. Hepatology 2004; 39:1028-37.
20. Raz A. Is inhibition of cyclooxygenase required for the anti-tumorigenic effects of nonsteroidal, anti-inflammatory drugs (NSAIDs)? In vitro versus in vivo results and the relevance for the prevention and treatment of cancer. Biochem Pharmacol 2002; 63:343-7.
21. Schroeder CP, Yang P, Newman RA, Lotan R. Eicosanoid metabolism in squamous cell carcinoma cell lines derived from primary and metastatic head and neck cancer and its modulation by celecoxib. Cancer Biol & Ther 2004; 9:29-34.
22. Liu X, Yue P, Zhou Z, Khuri FR, Sun SY. Death receptor regulation and celecoxib-induced apoptosis in human lung cancer cells. J Natl Cancer Inst 2004; 96:1769-80.
23. Aggarwal S, Taneja N, Lin L, Orringer MB, Rehemtulla A, Beer DG. Indomethacin-induced apoptosis in esophageal adenocarcinoma cells involves upregulation of bax and translocation of mitochondrial cytochrome c independent of COX-2 expression. Neoplasia 2000; 2:346-56.
24. Carbone D, Choy H, Csiki I, Dang T, Campbell N, Garcia B, Morrow J, Saha D, Johnson DH, Sandler A. Serum/plasma VEGF level changes with cyclooxygenase-2 (COX-2) inhibition in combined modality therapy in state III nonsmall cell lung cancer (NSCLC): Preliminary results of a phase II trial (THO-0059). Proc Am Soc Clin Oncol 2002; 21:1270.
25. Altorki NK, Keresztes RS, Port JL, Libby DM, Korst RJ, Flieder DB, Ferrara CA, Yankelevitz DF, Subbaramaiah K, Pasmantier MW, Dannenberg AJ. Celecoxib, a selective cyclooxygenase-2 inhibitor, enhances the response to preoperative paclitaxel and carboplatin in early-stage nonsmall-cell lung cancer. J Clin Oncol 2003; 21:2645-50.
26. Soriano AF, Helfrich B, Chan DC, Heasley LE, Bunn Jr PA, Chou TC. Synergistic effects of new chemopreventive agents and conventional cytotoxic agents against human lung cancer cell lines. Cancer Res 1999; 59:6178-84.
27. Oridate N, Suzuki S, Higuchi M, Mitchell MF, Hong WK, Lotan R. Involvement of reactive oxygen species in N-(4-hydroxyphenyl)retinamide-induced apoptosis in cervical carcinoma cells. J Natl Cancer Inst 1997; 89:1191-8.

28. Sun SY, Li W, Yue P, Lippman SM, Hong WK, Lotan R. Mediation of N-(4-hydroxyphenyl)retinamide-induced apoptosis in human cancer cells by different mechanisms. Cancer Res 1999; 59:2493-8.
29. Suzuki S, Higuchi M, Proske RJ, Oridate N, Hong WK, Lotan R. Implication of mitochondria-derived reactive oxygen species, cytochrome C and caspase-3 in N-(4-hydroxyphenyl)retinamide-induced apoptosis in cervical carcinoma cells. Oncogene 1999; 18:6380-7.
30. Hail Jr sN, Lotan R. Mitochondrial respiration is uniquely associated with the pro-oxidant and apoptotic effects of N-(4-hydroxyphenyl)retinamide. J Biol Chem 2001; 276:45614-21.
31. Frankel SR, Eardley A, Lauwers G, Weiss M, Warrell R. The 'retinoic acid syndrome' in acute promyelocytic leukemia. Ann Intern Med 1992; 117:292-6.
32. Lotan R. Retinoids and apoptosis: Implications for cancer chemoprevention and therapy. J Natl Cancer Inst 1995; 87:1655-7.
33. Ulukaya E, Wood EJ. Fenretinide and its relation to cancer. Cancer Treat Rev 1999; 25:229-35.
34. Puduvalli VK, Yung WK, Hess KR, Kuhn JG, Groves MD, Levin VA, Zwiebel J, Chang SM, Cloughesy TF, Junck L, Wen P, Lieberman F, Conrad CA, Gilbert MR, Meyers CA, Liu V, Mehta MP, Nicholas MK, Prados M. North American Brain Tumor Consortium. Phase II study of fenretinide (NSC 374551) in adults with recurrent malignant gliomas: A north American brain tumor consortium study. J Clin Oncol 2004; 22:4282-9.
35. Skehan P, Storeng R, Scudiero D, Monks A, McMahon J, Vistica D, Warren JT, Bokesch H, Kenney S, Boyd MR. New colorimetric cytotoxicity assay for anticancer-drug screening. J Natl Cancer Inst 1990; 82:1107-12.
36. Li X, Traganos F, Melamed MR, Darzynkiewicz Z. Single-step procedure for labeling DNA strand breaks with fluorescein-or BODIPY-conjugated deoxynucleotides: Detection of apoptosis and bromodeoxyuridine incorporation. Cytometry 1995; 20:172-80.
37. Levine L. Stimulated release of arachidonic acid by agonists of the peroxisome proliferator-activated receptor and retinoic acid receptors. Prostaglandins Leukot Essent Fatty Acids 2001; 65:229-32.
38. Chow SHH, Anavy N, Salazar D, Frank DH, Alberts DS. Determination of celecoxib in human plasma using solid-phase extraction and high-performance liquid chromatography. J Pharm Biomed Anal 2004; 34:167-74.

Hypermethylation of the Death-Associated Protein Kinase Promoter Attenuates the Sensitivity to TRAIL-Induced Apoptosis in Human Non–Small Cell Lung Cancer Cells

Ximing Tang, Weiguo Wu, Shi-yong Sun, Ignacio I. Wistuba, Waun Ki Hong, and Li Mao

Department of Thoracic/Head and Neck Medical Oncology, University of Texas M.D. Anderson Cancer Center, Houston, Texas

Abstract

Death-associated protein (DAP) kinase plays an important role in IFN-γ, tumor necrosis factor (TNF)-α, or Fas ligand–induced apoptosis. TNF-related apoptosis-inducing ligand (TRAIL) is a member of the TNF ligand family and can induce caspase-dependent apoptosis in cancer cells while sparing most of the normal cells. However, some of the cancer cell lines are insensitive to TRAIL, and such resistance cannot be explained by the dysfunction of TRAIL receptors or their known downstream targets. We reported previously that *DAP kinase* promoter is frequently methylated in non–small cell lung cancer (NSCLC), and such methylation is associated with a poor clinical outcome. To determine whether *DAP kinase* promoter methylation contributes to TRAIL resistance in NSCLC cells, we measured *DAP kinase* promoter methylation and its gene expression status in 11 NSCLC cell lines and correlated the methylation/expression status with the sensitivity of cells to TRAIL. Of the 11 cell lines, 1 had a completely methylated *DAP kinase* promoter and no detectable DAP kinase expression, 4 exhibited partial promoter methylation and substantially decreased gene expression, and the other 6 cell lines showed no methylation in the promoter and normal DAP kinase expression. Therefore, the amount of DAP kinase expression amount was negatively correlated to its promoter methylation ($r = -0.77$; $P = 0.003$). Interestingly, the cell lines without the DAP kinase promoter methylation underwent substantial apoptosis even in the low doses of TRAIL, whereas those with DAP kinase promoter methylation were resistant to the treatment. The resistance to TRAIL was reciprocally correlated to DAP kinase expression in 10 of the 11 cell lines at 10 ng/mL concentration ($r = 0.91$; $P = 0.001$). We treated cells resistant to TRAIL with 5-aza-2′-deoxycytidine, a demethylating reagent, and found that these cells expressed DAP kinase and became sensitive to TRAIL. These results suggest that DAP kinase is involved in TRAIL-mediated cell apoptosis and that a demethylating agent may have a role in enhancing TRAIL-mediated apoptosis in some NSCLC cells by reactivation of DAP kinase. (Mol Cancer Res 2004;2(12):685–91)

Introduction

Death-associated protein (DAP) kinase is a Ca^{2+}/calmodulin-regulated, 160-kDa serine/threonine, microfilament-bound kinase shown recently to be involved in IFN-γ, tumor necrosis factor-α, or Fas ligand–induced apoptosis (1-3). Aggressiveness of malignant tumors has been associated with methylation of the promoter region of the *DAP kinase* gene (4-8) and loss of DAP kinase expression (9).

Tumor necrosis factor–related apoptosis-inducing ligand (TRAIL, also known as Apo-2L), a member of the tumor necrosis factor ligand family, is a cytokine that can induce a rapid caspase-dependent and tumor-specific apoptosis (10-16) through its specific death receptors DR4 and DR5 (17). The activation of DR4 and DR5, like that of Fas/Apo, leads to the activation of the initiator caspase, caspase-8, and its downstream targets (18). TRAIL seems to exert selective toxicity toward neoplastic cells, whereas most normal cells are resistant to TRAIL (19). Multiple factors have been proposed for such resistance, including the presence of the decoy receptors DcR1 and DcR2, the downexpression of DR4 and DR5, the silencing of caspase-8, the inactivity of Akt, and the overexpression of cFLIP and cyclooxygenase-2 (20-27).

In this study, we investigated whether DAP kinase plays a role in determining the sensitivity of cells to TRAIL using non–small cell lung cancer (NSCLC) as a model. Our data suggest that the DAP kinase may be involved in TRAIL-induced apoptosis, and restoration of DAP kinase expression may overcome TRAIL resistance in certain NSCLCs.

Results

Establishment of a Multiplex Methylation-Specific PCR

Methylation-specific PCR (MSP; ref. 28) is the most extensively used method for detecting the methylation status

Received 3/2/04; revised 10/21/04; accepted 11/22/04.
Grant support: American Cancer Society grant RPG-98-054; Tobacco Research Fund from the State of Texas; National Cancer Institute grants CA 16620, CA 68437, CA86390, and CA91844 (L. Mao); and Department of Defense grant DAMD17-01-1-01689-1.
The costs of publication of this article were defrayed in part by the payment of page charges. This article must therefore be hereby marked advertisement in accordance with 18 U.S.C. Section 1734 solely to indicate this fact.
Notes: W.K. Hong is an American Cancer Society clinical research professor.
Requests for reprints: Li Mao, Molecular Biology Laboratory, Department of Thoracic/Head and Neck Medical Oncology, University of Texas M.D. Anderson Cancer Center, Unit 432, 1515 Holcombe Boulevard, Houston, TX 77030. Phone: 713-792-6363; Fax: 713-796-8655. E-mail: lmao@mdanderson.org.
Copyright © 2004 American Association for Cancer Research.

of CpG islands in the promoter regions of genes. Combined bisulfite restriction analysis is more quantitative (29) but requires more strict experimental condition. In this study, we combined multiplex PCR and MSP to create multiplex MSP (MMSP). In this method, unmethylated and methylated DNA are amplified simultaneously with two primer sets specific for methylated and unmethylated CpG islands in the DAP kinase promoter. The intensities of PCR products between methylated and unmethylated DNA were used to determine their relative ratios. Our results indicate that MMSP is robust in quantifying methylated DAP kinase promoter (Fig. 1).

DAP Kinase Promoter Methylation in NSCLC Cell Lines

Using MMSP, we established the methylation status of the *DAP kinase* promoter in the 11 NSCLC cell lines. In 5 of the 11 (46%) cell lines, the CpG island in the promoter region was methylated (Fig. 2A). This percentage is close to the 44% that we found in early-stage NSCLC tissues in an earlier study (8). In the 5 promoter-methylated cell lines, the promoter in Calu-1 was completely methylated, whereas in H157, H460, H1792, and SK-MES-1 the promoter was partially methylated to different degrees.

To further determine the nature of mixed methylation status in some NSCLC cell lines, we isolated 98 individual clones of H460 cells and analyzed their methylation status. We found 77 clones that carried both methylated and unmethylated promoter alleles, 6 clones that contained a completely methylated promoter, and 15 clones that contained a completely unmethylated promoter. It suggests that H460 parental cell line is heterogeneous with respect to DAP kinase promoter methylation and its gene expression. It also suggests that the status of DAP kinase promoter methylation is also unstable in some of the subclones.

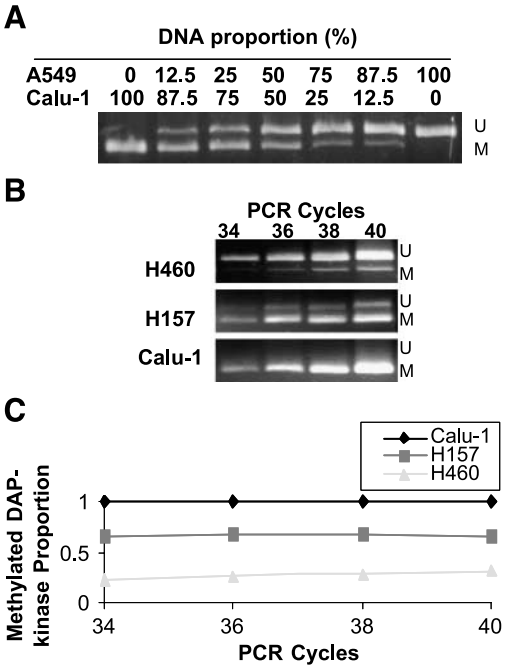


FIGURE 1. MMSP consistency for *DAP kinase* promoter methylation. **A.** MMSP was done using bisulfite-modified DNA from A549 cells (with unmethylated *DAP kinase* promoter) and Calu-1 cells (with methylated *DAP kinase* promoter), with ratios on *top of each lane*. **B.** MMSP using bisulfite-modified DNA isolated from NSCLC cell lines (H460, H157, and Calu-1). *U,* 279-bp unmethylated fragments; *M,* 218-bp methylated fragments. **C.** Scanning densitometry was used to measure and analyze the intensity of the fragment signal of **B**. Relative quantity of the methylation promoter was then calculated.

Expression of DAP Kinase in the NSCLC Cells Negatively Correlates with Its Promoter Methylation Status

Using multiplex reverse transcription-PCR, we examined DAP kinase expression in the 11 lung cancer cell lines. DAP kinase expression was completely or partially silenced in Calu-1, H1792, H157, H460, and SK-MES-1 cells (Fig. 2B), which have methylated CpG islands in their promoters, but not in A549, H226, H292, H522, H596, and H1944 cells, which have an unmethylated promoter. The extent of methylation detected in the *DAP kinase* promoter was negatively correlated with the DAP kinase mRNA level in the 11 cell lines ($r = -0.77$; $P = 0.003$ by linear correlation and regression analysis; Fig. 2C). Of the H460 subclones tested, H460-12 and H460-126, which were completely methylated, had no detectable *DAP kinase* gene and protein expression (example in Fig. 3C and D) but H460-14, H460-120, and H460 -124, which were unmethylated, had detectable DAP kinase expression (example in Fig. 3C and D).

TRAIL-Induced Apoptosis of NSCLC Cells Correlates with DAP Kinase Promoter Methylation and Its Gene Expression

The 11 NSCLC cell lines with different *DAP kinase* promoter methylation status were treated with TRAIL at different doses (10, 40, and 160 ng/mL) to determine their response to TRAIL. The results (Table 1) show that cell deaths induced by TRAIL correlated with DAP kinase expression. When analyzed as a whole, the degree of cell death (% of cells dying) induced by TRAIL at low doses (10 and 40 ng/mL) were positively correlated with DAP kinase mRNA expression (10 ng/mL, $r = 0.91$, $P < 0.001$; 40 ng/mL, $r = 0,80$; $P = 0.008$ by linear correlation and regression analysis) but not at 160 ng/mL ($r = 0.46$; $P = 0.187$; Table 1). Immunochemical double staining with DAP kinase antibody and terminal deoxynucleotidyl transferase–mediated dUTP nick end labeling (TUNEL) showed that only the DAP kinase–expressing H460 cells underwent apoptosis after 12-hour incubation with TRAIL (10 ng/mL; Fig. 3A). To address the relationship of DAP kinase expression to TRAIL-induced apoptosis, we compared two H460 subclones (H460-12 and H460-124) in which the *DAP kinase* promoter was either completely methylated or unmethylated (Fig. 3B-D). 3-(4,5-Dimethylthiazol-2-yl)-2, 5-diphenyltetrazolium bromide (MTT; Fig. 3E) and DNA fragmentation (Fig. 3F) analyses showed that the H460-124 cells were sensitive, whereas the H460-12 cells were resistant to TRAIL-induced cell death.

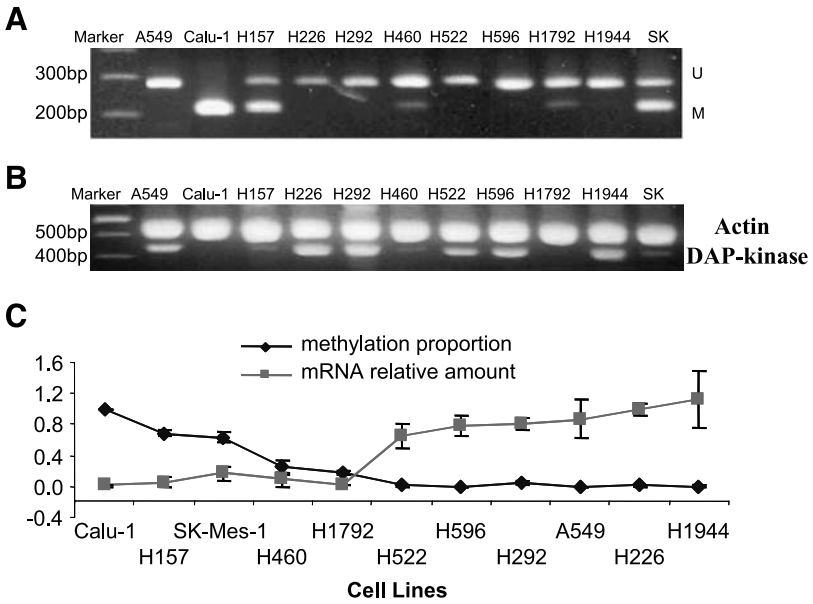


FIGURE 2. Correlation of *DAP kinase* promoter methylation status and expression of the gene in NSCLC cells. **A.** Methylation status of the *DAP kinase* promoter of the 11 NSCLC cell lines. *U,* 279-bp unmethylated PCR fragment; *M,* 218-bp methylated PCR fragment. **B.** DAP kinase mRNA expression in the 11 NSCLC cell lines. *Lane 1,* DNA size marker. **C.** Correlation of *DAP kinase* promoter methylation and expression of the gene based on data from **A** and **B**. *Points,* mean proportions of methylated *DAP kinase* promoter or relative gene expression level of three independent replicates; bars, unbiased SD.

The Restoration of DAP Kinase Expression and TRAIL Sensitivity by Promoter DNA Demethylation

To further establish that DAP kinase is involved in TRAIL-induced apoptosis in NSCLC cells, we pretreated Calu-1 and H460-12 cells, which contain a methylated *DAP kinase* promoter and lack *DAP kinase* gene expression, with 5-aza-2′-deoxycytidine (5ADC), a commonly used demethylation reagent, before TRAIL treatment. After pretreatment for 48 hours at 1 or 2 μmol/L, expression of DAP kinase was restored in both cell lines (Fig. 4A). The treatment substantially enhanced the levels of TRAIL-induced cell death/apoptosis in these cells as measured by MTT and DNA fragmentation assays (Fig. 4B and C).

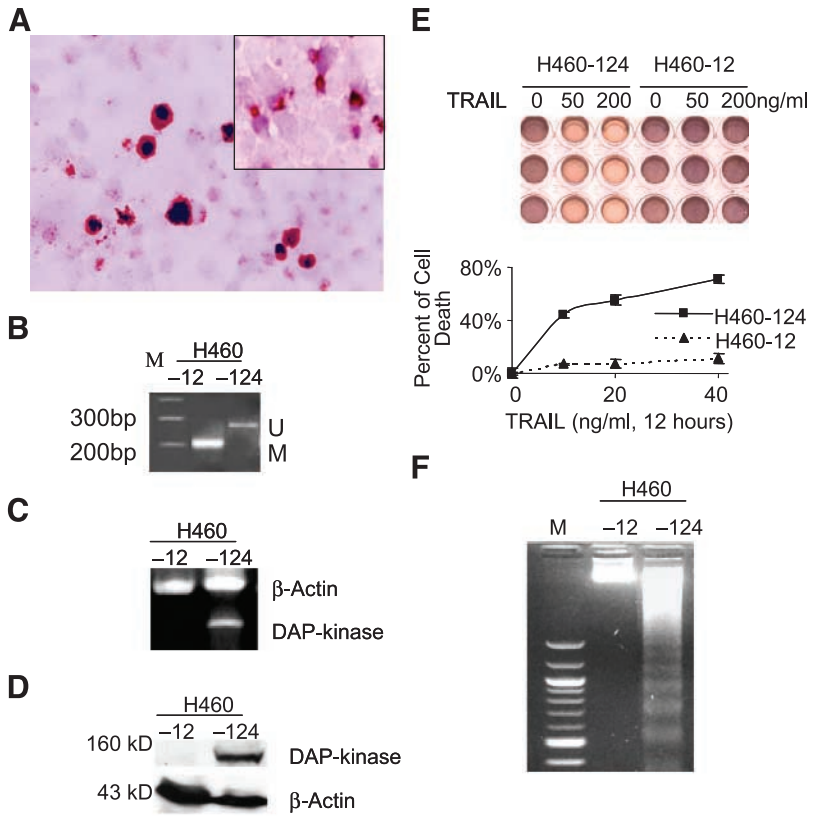


FIGURE 3. Correlation of DAP kinase expression with TRAIL-induced apoptosis in H460 cells. **A.** Double immunohistochemistry staining of H460 cells. *Black nuclear staining,* apoptosis; *red cytoplasmic staining,* expression of DAP kinase. *Top right box,* control panel without TRAIL treatment. **B.** Methylation status of two H460 subclones measured by MMSP. *U,* unmethylated fragment; *M,* methylated fragment. **C.** *DAP kinase* gene expression in H460-12 and H460-124. **D.** DAP kinase protein expression in H460-12 and H460-124. β-actin level was used as a loading control. **E.** TRAIL-induced cell death measured by MTT assay. *Top,* scanned image of the MTT results; *bottom,* measured rates of cell death. *Points,* mean cell death rates of three independent replicates; bars, SD. **F.** TRAIL-induced DNA fragmentation in the two subclones after TRAIL treatment (80 ng/mL for 12 hours). *M,* DNA size marker.

Discussion

In this study, we showed that *DAP kinase* promoter methylation and its gene expression correlate with TRAIL-induced apoptosis in NSCLC cells. We also showed that a demethylation agent activates *DAP kinase* gene expression and sensitizes the cells to TRAIL. We have shown previously that the promoter of the *DAP kinase* gene is methylated in 44% of primary NSCLC tumors (8) similar to the 46% rate we observed in NSCLC cell lines in present study. Methylation of the DAP kinase promoter in the primary tumors is associated with poor survival in patients with early-stage NSCLC (8). The methylation and lack of gene expression in hepatoma also correlated with a poor clinical outcome in patients (30). The inactivation of *DAP kinase* through its promoter methylation has been frequently detected in aggressive tumors of the brain (31), lymphoma (32), and colorectal cancer (33).

Of the 11 NSCLC cell lines studied, 5 contained a methylated *DAP kinase* promoter, including 4 that contained both methylated and unmethylated *DAP kinase* promoter, indicating that they are heterogeneous either due to differential methylation in one of the two *DAP kinase* alleles or the presence of subclones.

A highly negative correlation between *DAP kinase* methylation and gene expression was verified in the 11 NSCLC cell lines ($r = -0.77$; $P = 0.003$) and in the H460 subclones ($r = -0.97$; $P = 0.001$; data not shown). The fact that the promoter methylation status was consistent with *DAP kinase* gene expression indicates that the promoter methylation is the major mechanism to inactivate *DAP kinase*. Measurement of DAP kinase expression either by immunohistochemistry or *in situ* MSP would be helpful for predicting the functional status of the gene.

Previous studies have shown that *DAP kinase* is an important death messenger in IFN-γ, tumor necrosis factor-α, and Fas ligand–mediated apoptosis (3, 9), but *DAP kinase* involvement with TRAIL-induced cell apoptosis has not been reported. Consistent with this involvement is the observation that cells lacking DAP kinase expression were less sensitive to TRAIL-induced apoptosis than cells expressing DAP kinase. The fact that only cells expressing DAP kinase protein underwent apoptosis (Fig. 3) further supports the involvement of DAP kinase in TRAIL-induced apoptosis.

The expression of TRAIL decoy receptors DcR1 and DcR2 and death receptors DR4 and DR5 as messenger receivers directly influences TRAIL-induced apoptosis. In our previous study, we have shown DR5 was expressed, whereas decor receptors were not expressed in H157 cells (34), yet these cells were resistant to TRAIL (Table 1), suggesting the involvement of other mechanisms for this resistance. We have not observed a strong correlation between the expression of TRAIL receptors and their sensitivity to TRAIL in the 11 cell lines we studied.[2] It has been shown that the binding of death ligands to receptors might result in recruitment of the cofactor Fas-associated death domain–containing protein with formation of a death-inducing signaling complex, which results in activation of caspase-8 (18, 35). Recent studies reported that the gene for *caspase-8* is silenced preferentially by aberrant promoter methylation in

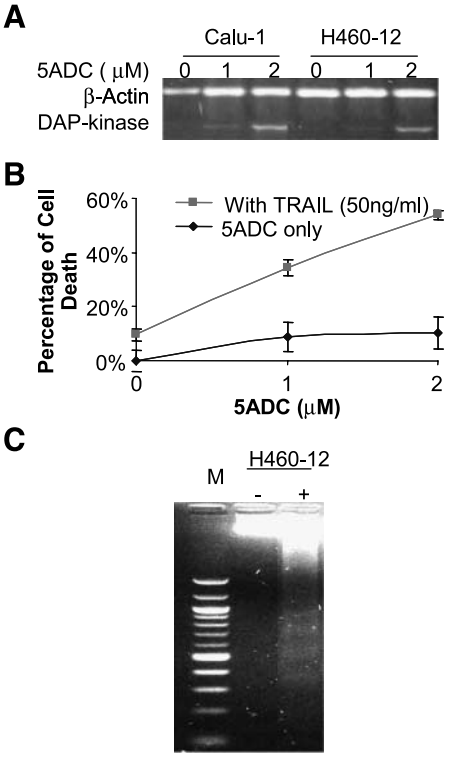


FIGURE 4. Restoration of DAP kinase expression and sensitivity to TRAIL treatment by promoter demethylation. **A.** DAP kinase expression was restored after treatment with 5ADC at the concentration of 1 or 2 μmol/L. **B.** MTT assay measuring cell death induced by TRAIL with or without 5ADC in H460-12 cells. Bars, unbiased SD of the triplicates. **C.** TRAIL-induced DNA fragmentation in H460-12 cells treated with TRAIL with (+) or without (–) 5ADC.

Table 1. Expression of DAP Kinase and TRAIL-Induced Cell Death in NSCLC Cell Lines

Cell Lines	DAP Kinase Expression*	TRAIL-Induced Cell Death (% of Control)		
		10 ng/mL†	40 ng/mL	160 ng/mL
Calu-1	0.000	0.00	6.79	7.22
H1792	0.022	0.00	10.79	24.87
H157	0.059	0.00	0.00	23.97
SK-MES-1	0.176	0.87	13.47	62.26
H522	0.644	9.48	17.95	35.81
H596	0.783	11.20	31.24	59.26
H292	0.812	12.47	13.97	43.22
A549	0.874	8.55	20.31	45.39
H226	0.999	12.61	19.13	29.22
H1944	1.120	25.85	30.05	45.70
r‡ (DAP Kinase Expression: TRAIL-Induced Cell Death)		0.91	0.80	0.46
P		0.001	0.008	0.187

*mRNA relative amount to β-actin detected with multiplex reverse transcription-PCR.
†TRAIL, incubated for 12 hours, MTT analysis.
‡Linear correlation and regression analysis.

[2] Unpublished data.

neuroblastomas, bronchial carcinoids, and small cell lung cancer but not in NSCLC (36, 37). Nevertheless, a potential relationship between TRAIL receptors and DAP kinase warrants further investigation.

When NSCLC cells containing a methylated DAP kinase promoter were treated with 5ADC (a demethylation agent), the cells restored expression of DAP kinase and TRAIL sensitivity (Fig. 4). These results support the involvement of DAP kinase in TRAIL-induced apoptosis and provide justification for combination of demethylation agent(s) with death ligand(s) to improve the therapeutic effects.

Although different cancer cell lines carry distinct patterns of methylated promoters and 5ADC treatment sensitized TRAIL response in multiple cell lines (Fig. 4),[3] it is still possible that activation of other genes by 5ADC treatment contributes to the sensitization. Additional experiments to specifically activate *DAP kinase* or specifically inhibit *DAP kinase* may provide more direct evidence to support the role of DAP kinase in rescuing TRAIL-induced apoptosis in NSCLC.

Materials and Methods

Cell Lines, Cell Culture, and Cell Subcloning

Human NSCLC cell lines A549, Calu-1, H157, H226, H292, H460, H522, H596, H1792, H1944, and SK-MES-1 were obtained from the American Type Cell Culture (Rockville, MD) and grown in DMEM (Life Technologies, Rockville, MD) containing 10% fetal bovine serum and antibiotics. The cells were maintained at 37°C in a humidified atmosphere consisting of 5% CO_2 and 95% air in monolayers.

For each subcloning experiment, 30 to 50 H460 parental cells were seeded into a 100-mm dish and incubated for 4 hours; attached single cells were then identified by marking the back of the dish. After being cultured for 7 days, the individual clones originating from the marked single cells were transferred to 24-well plates for further culture before being transferred to 100-mm dishes for further expansion. All the subclones were harvested once on the same day to avoid biological variation in different generations.

cDNA Preparation and Multiplex Reverse Transcription-PCR

Total RNA was extracted and purified from cultured cells using RNeasy mini kit (Qiagen, Valencia, CA) following the manufacturer's instructions. Total RNA (1 μg) was used to synthesize cDNA with SuperScript II reverse transcriptase (Life Technologies) in 20 μL, and the final product was diluted to 100 μL. The cDNA was then used for the quantitative assay of DAP kinase expression by multiplex PCR. The multiplex reverse transcription-PCR was carried out under optimal conditions after which a linear correlation between cycle numbers and product amount of PCR was obtained (data not shown). PCR reaction mixture (10 μL) contained 1 μL diluted cDNA sample, 1 unit Hotstart polymerase (Qiagen), 0.1 mmol/L deoxynucleotide triphosphates (dATP + dTTP + dCTP + dGTP), 1 μL DMSO, and 50 ng DAP kinase primers (forward 5′-GACACCGGCGAGGAACTTGGC-3′ and reverse 5′-AAAGTCAATGATCTTGATCCGA-3′). The reaction was done according to the following program: at 94°C for 15 minutes for activating the polymerase; for 34 cycles at 94°C for 30 seconds, at 60°C for 1 minute, and at 72°C for 1 minute; and at 72°C for 7 minutes. At the 6th cycle of the 2nd step, β-actin primers (forward 5′-GTTGCTATCCAGG CTGTGC-3′ and reverse 5′-GCATCCTGTCGGCAATGC-3′) were added into the reaction mixture as an internal control. The PCR products were electrophoresed on 2.5% agarose gel. Then, the gel was stained with ethidium bromide and photographed under UV light. The absorbance of the DAP kinase–specific fragments was measured by scanning densitometry using the absorbance of the internal control (β-actin) as the standard. The relative amount of the DAP kinase mRNA was calculated as absorbance of *DAP kinase*/*actin*.

DNA Isolation and MMSP

DNA was extracted and purified from cultured cells. The cells were collected and digested in 200 μL of digestion buffer containing 50 mmol/L Tris-HCl (pH 8.0), 1% SDS, and 0.5 mg/mL proteinase K and incubated at 42°C for 36 hours. The digested products were purified with phenol-chloroform twice. DNA was then precipitated using the ethanol precipitation method and recovered in distilled DNase-free water. Bisulfite modification of DNA was done as described by Herman et al. (28). Briefly, 1 μg of the DNA from each sample was denatured using NaOH and then treated with sodium bisulfite (Sigma, St. Louis, MO) for 16 hours. After purification using the Wizard DNA purification kit (Promega, Madison, WI), the purified DNA was treated again with NaOH, precipitated with ethanol, and recovered in distilled water. The relative quantity of methylated and unmethylated DAP kinase promoters was determined by the MMSP. The primers specific for unmethylated CpG islands were (forward) 5′-TTGTGAGTTGTTGATTTTTTTTTGT-3′ and (reverse) 5′-ATACACAATAAAACACACCAACAAA-3′, which cover a 279-bp fragment; the primers specific for methylated CpG islands were (forward) 5′-CGAGTTGTC-GAGTTTTTTTCGC-3′ and (reverse) 5′-CCGCGC-AAAACCCGCAACG-3′, which cover a 218-bp fragment. The PCR products were separated in 2.5% of agarose gel, stained with ethidium bromide, and then photographed under UV light. The absorbances of the unmethylated fragments (U) at 279 bp and methylated fragments (M) at 218 bp were determined by scanning densitometry of the photographs. The proportion of methylation alleles was calculated as $M / U + M$.

Protein Extraction and Western Blot Analysis

Cellular proteins were collected in lysis buffer containing 150 mmol/L NaCl, 1% Triton X-100, 1% sodium deoxycholate, 0.1% SDS, 10 μg/mL phenylmethylsulfonyl fluoride, 30 μg/mL aprotinin, and 50 mmol/L Tris-HCl (pH 8.0). The samples were then placed on ice for 60 minutes and then centrifuged at 14,000 × g at 4°C for 30 minutes. The protein concentration was measured using a protein assay kit (Bio-Rad, Hercules, CA). Each protein sample (30 μg) was subjected to SDS-PAGE

[3] Unpublished data.

using 8% denaturing polyacrylamide gel. The proteins were then transferred to Hybond-C nitrocellulose membranes (Amersham Pharmacia Biotech, Inc., Piscataway, NJ). The nitrocellulose membranes were incubated in a blocking solution containing 5% bovine skim milk in 10 mmol/L PBS containing 0.1% Tween 20 for 1 hour followed by incubation for 3 hours with monoclonal anti-DAP kinase antiserum (DAPK-55, Sigma) at a concentration of 1:1,000 or monoclonal anti-β-actin (AC15, Sigma) antibody at a concentration of 1:5,000. The membranes were washed with PBS and then incubated with the secondary anti-mouse antibody supplied in the enhanced chemiluminescence kit (Amersham Pharmacia Biotech) for 1 hour. After this incubation, the membranes were washed thrice in PBS, developed in enhanced chemiluminescence solution for 1 to 2 minutes, and exposed to X-ray film for chemiluminescence detection of the positive protein bands.

TUNEL and DAP Kinase Protein Detection by Immunohistochemistry Double Staining

H460 cells were seeded on two glass slides, incubated for 24 hours, and then treated with or without TRAIL (10 ng/mL, Calbiochem, San Diego, CA) for 12 hours. The slides were then fixed in 10% paraformalin [prepared with PBS (pH 7.4)] for 20 minutes and washed in PBS for 5 minutes. The TUNEL assay was done with TUNEL kit (Intergen, Burlington, MA) according to instructions provided by the manufacturer. 3,3′-Diaminobenzidine-conjugated nickel was used as a chromogen to stain the apoptotic cells. The slides were then subjected to double staining with immunohistochemistry to detect the expression of DAP kinase protein by the following procedures: the slides were treated thrice for 5 minutes in a microwave oven with 10 mmol/L citrate buffer (pH 6.0) to retrieve the antigenicity, immersed in methanol containing 0.3% hydrogen peroxidase for 20 minutes to block the endogenous peroxidase, and incubated in 2.5% blocking serum to reduce nonspecific binding. The slides were incubated overnight at 4°C with primary anti-DAP kinase monoclonal antiserum (DAPK-55, Sigma) at a dilution 1:160 and then processed using standard avidin-biotin immunohistochemistry according to the manufacturer's recommendations (Vector Laboratories, Burlingame, CA). Vector NevaRed (Vector Laboratories) was used as a chromogen to detect DAP kinase expression as red in the cytoplasm. Methyl green was used for nuclear counterstaining.

DNA Fragmentation Assay

After treatment with TRAIL, both floating and attached cells were collected, pelleted, and resuspended in Tris-EDTA buffer (pH 8.0). The plasma membrane of the cell was lysed on ice in a mixture of 10 mmol/L Tris-HCl (pH 8.0), 10 mmol/L EDTA, and 0.5% Triton X-100 for 15 minutes. The lysate was centrifuged at 12,000 × *g* for 15 minutes to separate the soluble (fragmented) from pellet (intact genomic) DNA. The soluble DNA was treated with RNase A (50 μg/mL) at 37°C for 1 hour and proteinase K (100 μg/mL) in 0.5% SDS at 50°C for 2 hours, extracted with phenol-chloroform, precipitated in ethanol, electrophoresed on a 1.8% agarose gel, and stained with ethidium bromide. The gels were then photographed under UV illumination.

Demethylation

Cells were treated with 5ADC (Sigma) at 1 or 2 μmol/L concentrations for 48 hours before further treatment with TRAIL.

MTT Assay

About 30,000 cells of each line were seeded in 96-well plates in 0.1 mL DMEM in triplicate and incubated for 24 hours. The medium was then replaced with medium containing a designated concentration of TRAIL and incubated for another 12 hours. At the end of treatment, 10 μL (5 mg/mL) MTT (Sigma) were added and incubated for 3 hours. The medium containing MTT was absorbed off and washed with PBS carefully, and 0.1 mL DMSO was added to each well. Absorbances of controls (A_c) and experimental samples (A_t) at a wavelength of 540 nm with background subtraction at 620 nm were measured using the E_{max} precision microplate reader (Molecular Devices, Sunnyvale CA). Cell death (%) is calculated as $100 \times (1 - A_t / A_c)$.

References

1. Deiss LP, Feinstein E, Berissi H, Cohen O, Kimchi A. Identification of a novel serine/threonine kinase and a novel 15-kD protein as potential mediators of the γ interferon-induced cell death. Genes Dev 1995;9:15–30.

2. Cohen O, Feinstein E, Kimchi A. DAP-kinase is a Ca^{2+}/calmodulin-dependent, cytoskeletal-associated protein kinase, with cell death-inducing functions that depend on its catalytic activity. EMBO J 1997;16:998–1008.

3. Cohen O, Inbal B, Kissil JL, et al. DAP-kinase participates in TNF-α- and Fas-induced apoptosis and its function requires the death domain. J Cell Biol 1999;146:141–8.

4. Shiramizu B, Mick P. Epigenetic changes in the DAP-kinase CpG island in pediatric lymphoma. Med Pediatr Oncol 2003;41:527–31.

5. Ueki T, Toyota M, Sohn T, et al. Hypermethylation of multiple genes in pancreatic adenocarcinoma. Cancer Res 2000;60:1835–9.

6. Katzenellenbogen RA, Baylin SB, Herman JG. Hypermethylation of the DAP-kinase CpG island is a common alteration in B-cell malignancies. Blood 1999;93:4347–53.

7. Sanchez-Cespedes M, Esteller M, Wu L. Gene promoter hypermethylation in tumors and serum of head and neck cancer patients. Cancer Res 2000;60:892–5.

8. Tang X, Khuri FR, Lee JJ, et al. Hypermethylation of the death-associated protein (DAP) kinase promoter and aggressiveness in stage I non-small-cell lung cancer. J Natl Cancer Inst 2000;92:1511–6.

9. Inbal B, Cohen O, Polak-Charcon S, et al. DAP kinase links the control of apoptosis to metastasis. Nature 1997;390:180–4.

10. Pan G, O'Rourke K, Chinnaiyan AM, et al. The receptor for the cytotoxic ligand TRAIL. Science 1998;276:111.

11. Sedger LM, Shows DM, Blamton RA, et al. IFN-γ mediates a novel antiviral activity through dynamic modulation of TRAIL and TRAIL receptor expression. J Immunol 1999;163:920.

12. Yu R, Mandlekar S, Ruben S, Ni J, Kong AN. Tumor necrosis factor-related apoptosis-inducing ligand-mediated apoptosis in androgen-independent prostate cancer cells. Cancer Res 2000;60:2384–9.

13. Thomas WD, Hersy P. TNF-related apoptosis-inducing ligand (TRAIL) induces apoptosis in Fas ligand-resistant melanoma cells and mediates in CD4 T cell killing of target cells. J Immunol 1998;161:2195–200.

14. Walczak H, Miller RE, Ariail K, et al. Tumoricidal activity of tumor necrosis factor-related apoptosis-inducing ligand *in vivo*. Nat Med 1999;5:157–63.

15. Mitsiades N, Poulaki V, Tseleni-Balafouta S, Koutras DA, Stamenkovic I. Thyroid carcinoma cells are resistant to FAS-mediated apoptosis but sensitive to tumor necrosis factor-related apoptosis-inducing ligand. Cancer Res 2000;60:4122–9.

16. Wu M, Das A, Tan Y, Zhu C, Cui T, Wong MC. Induction of apoptosis in glioma cell lines by TRAIL/Apo-2L. J Neurosci Res 2000;61:464–70.

17. Ashkenazi A. Targeting death and decoy receptors of the tumour-necrosis factor superfamily. Nat Rev Cancer 2002;2:420–30.

18. Kischkel FC, Lawrence DA, Chuntharapai A, Schow P, Kim KJ, Ashkenazi A. Apo2L/TRAIL-dependent recruitment of endogenous FADD and caspase-8 to death receptors 4 and 5. Immunity 2000;12:611–20.

19. Pan G, Ni J, Wei YF, Yu G, Gentz R, Dixit VM. An antagonist decoy receptor and a death domain-containing receptor for TRAIL. Science 1997;277:815–8.

20. Kim K, Fisher MJ, Xu S-Q, El-Deiry WS. Molecular determinants of response to TRAIL in killing of normal and cancer cells. Clin Cancer Res 2000;6:335–46.

21. Pitti RM, Marsters SA, Ruppert S, Donahue CJ, Moore A, Ashkenazi A. Induction of apoptosis by Apo-2 ligand, a new member of the tumor necrosis factor cytokine family. J Biol Chem 1996;271:12687–90.

22. Fanger NA, Maliszewski CR, Schooley K, Griffith TS. Human dendritic cells mediate cellular apoptosis via tumor necrosis factor-related apoptosis-inducing ligand (TRAIL). J Exp Med 1999;190:1155–64.

23. Zhang XD, Nguyen T, Thomas WD, Sanders JE, Hersey P. Mechanisms of resistance of normal cells to TRAIL induced apoptosis vary between different cell types. FEBS Lett 2000;482:193–9.

24. Hopkins-Donaldson S, Ziegler A, Kurtz S, et al. Silencing of death receptor and caspase-8 expression in small cell lung carcinoma cell lines and tumors by DNA methylation. Cell Death Differ 2003;10:356–64.

25. Chen X, Thakkar H, Tyan F, et al. Constitutively active Akt is an important regulator of TRAIL sensitivity in prostate cancer. Oncogene 2001;20:6073–83.

26. Jonsson G, Paulie S, Grandien A. High level of cFLIP correlates with resistance to death receptor-induced apoptosis in bladder carcinoma cells. Anticancer Res 2003;23:1213–8.

27. Tang X, Sun YJ, Half E, Kuo MT, Sinicrope F. Cyclooxygenase-2 overexpression inhibits death receptor 5 expression and confers resistance to tumor necrosis factor-related apoptosis-inducing ligand-induced apoptosis in human colon cancer cells. Cancer Res 2002;62:4903–8.

28. Herman JG, Graff JR, Myohanen S, Nelkin BD, Baylin SB. Methylation-specific PCR: a novel PCR assay for methylation status of CpG islands. Proc Natl Acad Sci U S A 1996;93:9821–6.

29. Xiong Z, Laird PW. COBRA: a sensitive and quantitative DNA methylation assay. Nucleic Acids Res 1997;25:2532–4.

30. Matsumoto H, Nagao M, Ogawa S, et al. Prognostic significance of death-associated protein-kinase expression in hepatocellular carcinomas. Anticancer Res 2003;23:1333–41.

31. Gonzalez-Gomez P, Bello MJ, Alonso ME, et al. Frequent death-associated protein-kinase promoter hypermethylation in brain metastases of solid tumors. Oncol Rep 2003;10:1031–3.

32. Nakatsuka S, Takakuwa T, Tomita Y, et al. Hypermethylation of death-associated protein (DAP) kinase CpG island is frequent not only in B-cell but also in T- and natural killer (NK)/T-cell malignancies. Cancer Sci 2003;94:87–91.

33. Yamaguchi S, Asao T, Nakamura J, Ide M, Kuwano H. High frequency of DAP-kinase gene promoter methylation in colorectal cancer specimens and its identification in serum. Cancer Lett 2003;194:99–105.

34. Wu W, Soria J, Wang L, Kemp BL, Mao L. TRAIL-R2 is not correlated with p53 status and is rarely mutated in non-small cell lung cancer. Anticancer Res 2000;20:4525–30.

35. Bodmer JL, Holler N, Reynard S, et al. TRAIL receptor-2 signals apoptosis through FADD and caspase-8. Nat Cell Biol 2000;2:241–3.

36. Shivapurkar N, Toyooka S, Eby MT, et al. Differential inactivation of caspase-8 in lung cancers. Cancer Biol Ther 2002;1:65–9.

37. Teitz T, Wei T, Valentine MB, et al. Caspase-8 is deleted or silenced preferentially in childhood neuroblastomas with amplification of MYCN. Nat Med 2000;6:529–35.

[CANCER RESEARCH 64, 2969–2976, May 1, 2004]

Advances in Brief

Myristoylation of the Fus1 Protein Is Required for Tumor Suppression in Human Lung Cancer Cells

Futoshi Uno,[1] Jiichiro Sasaki,[1] Masahiko Nishizaki,[1] Giovanni Carboni,[1] Kai Xu,[1] Edward N. Atkinson,[2] Masashi Kondo,[3] John D. Minna,[3] Jack A. Roth,[1] and Lin Ji[1]

[1]Section of Thoracic Molecular Oncology, Department of Thoracic and Cardiovascular Surgery, and [2]Department of Biomathematics, The University of Texas M. D. Anderson Cancer Center, Houston, Texas; [3]Department of Internal Medicine and Pharmacology, Hamon Center for Therapeutic Oncology Research, The University of Texas Southwestern Medical Center, Dallas, Texas

Abstract

***FUS1* is a novel tumor suppressor gene identified in the human chromosome 3p21.3 region that is deleted in many cancers. Using surface-enhanced laser desorption/ionization mass spectrometric analysis on an anti-Fus1-antibody-capture ProteinChip array, we identified wild-type Fus1 as an N-myristoylated protein. N-myristoylation is a protein modification process in which a 14-carbon myristoyl group is cotranslationally and covalently added to the NH_2-terminal glycine residue of the nascent polypeptide. Loss of expression or a defect of myristoylation of the Fus1 protein was observed in human primary lung cancer and cancer cell lines. A myristoylation-deficient mutant of the Fus1 protein abrogated its ability to inhibit tumor cell-induced clonogenicity *in vitro*, to induce apoptosis in lung tumor cells, and to suppress the growth of tumor xenografts and lung metastases *in vivo* and rendered it susceptible to rapid proteasome-dependent degradation. Our results show that myristoylation is required for Fus1-mediated tumor-suppressing activity and suggest a novel mechanism for the inactivation of tumor suppressors in lung cancer and a role for deficient posttranslational modification in tumor suppressor-gene-mediated carcinogenesis.**

Introduction

Tumor suppressor genes (TSGs) play a major role in the pathogenesis of human lung and other cancers. Lung cancer cells harbor mutations and deletions in multiple known oncogenes and TSGs; however, genetic alterations and allelic losses on the short arm of chromosome 3 are among the most frequent and earliest cancer abnormalities detected in the pathogenesis of lung cancers and have been shown to occur in 96% of non-small cell lung cancers (NSCLCs) and in 78% of preneoplastic lung lesions (1). The frequent and early loss of heterozygosity and the overlapping homozygous deletions observed in the 3p21.3 region in lung and breast cancers suggest a critical role of one or more 3p21.3 genes as "gatekeepers" in the molecular pathogenesis of these cancers (2, 3).

The novel *FUS1* TSG is one of the candidate TSGs that have been identified in a 120-kb homozygous deletion region in human chromosome 3p21.3 (2, 4, 5). The cloned cDNA of *FUS1* (GenBank accession no. AF055479) is 333 bp in length and encodes a protein of 110 amino acid residues (Fig. 1*A*). However, the *FUS1* gene does not show homology with any known genes and proteins in databases. We have previously demonstrated that exogenous expression of the wild-type (wt) *FUS1* by plasmid- or adenoviral vector-mediated gene transfer significantly inhibits tumor cell growth, induces apoptosis, and alters cell cycle kinetics in 3p21.3-deficient NSCLC cells *in vitro* and efficiently suppresses tumor growth and inhibits tumor progression and metastases in various human lung cancer xenograft mouse models (4–6). However, the mechanisms involved in the inactivation of the *FUS1* gene in primary human cancers and in *FUS1*-mediated tumor suppression remain unknown. On the basis of our findings reported here, we hypothesize that loss of expression, haploinsufficiency, and deficiency of posttranslational modification of Fus1 protein may lead to loss of its tumor-suppression function and play an important role in lung cancer development.

Materials and Methods

Cell Lines and Cell Culture. The human NSCLC cell lines A549, NCI-H1299, NCI-H358, NCI-H226, NCI-H322, and NCI-H460, with various 3p21.3 and *p53* gene status as described previously (7, 8), and a normal human lung fibroblast cell line, WI-38, were used for *in vitro* and *in vivo* experiments. The A549 line was maintained in Ham's F12 medium supplemented with 10% FCS. The H1299, H358, H226, H322, and H460 lines were maintained in RPMI 1640 supplemented with 10% FCS and 5% glutamine. Normal fibroblast WI-38 cells were cultured in MEM supplemented with 10% FCS and 5% glutamine.

Tumor Cell-Induced Clonogenicity Assay. To analyze the effect of myristoylation of Fus1 protein on tumor cell-derived clonogenicity *in vitro*, we transfected H1299 cells (1×10^5) with various *FUS1*-expressing and control plasmid vector DNAs, using FUGEN 6 *in vitro* transfection reagent (Roche Molecular Biochemicals, Indianapolis, IN). Four μg of each test plasmid DNA were cotransfected with 1 μg of the neomycin-resistant gene-containing pcDNA3.1 vector (Invitrogen, Carlsbad, CA); the pcDNA3.1 (1 μg) vector alone and the pcDNA3.1 plus wt-p53 plasmid were used as negative and positive controls, respectively. Twenty-four h after transfection, cells were harvested, stained with trypan blue, and counted. Five thousand cells were replated on a 100-mm tissue culture dish in triplicate and grown in 5% fetal-bovine-serum-supplemented RPMI 1640 containing 400 μg/ml G418 for 2–3 weeks. The numbers of G418-resistant colonies were counted after staining with Crystal Violet.

Immunohistochemical Analysis. Samples of human lung tumor and parallel normal tissues were obtained from patients with informed consent through the Lung SPORE program at the University of Texas Southwestern Medical Center and at the M. D. Anderson Cancer Center. Expression of the Fus1 protein in tissue samples was analyzed by immunohistochemical staining with anti-Fus1 peptide polyclonal antibodies and a VECTASTAIN Elite ABC kit (Vector Laboratories Inc., Burlingame, CA). Briefly, the rabbit anti-Fus1 polyclonal antibodies used for immunohistochemical staining, raised against a synthetic oligopeptide derived from NH_2-terminal amino acid sequence of Fus1 protein, were affinity-purified by use of custom immunochemistry ser-

Received 11/26/03; revised 2/23/04; accepted 3/3/04.

Grant support: Partially supported by grants from the National Cancer Institute, the NIH (Grants SPORE CA70970 and CA71618); a W. M. Keck Gene Therapy Career Development grant (L. Ji); grants from the Department of Defense BESCT (Grant DAMD17-01-1-0689) and TARGET (Grant DAMD17-02-1-0706) Lung Cancer Programs; gifts to the M. D. Anderson Cancer Center Division of Surgery Core Laboratory Facility from Tenneco and Exxon; the M. D. Anderson Cancer Center Support Core Grant (CA16672); a grant from the Tobacco Settlement Funds as appropriated by the Texas State Legislature; and a sponsored research agreement with Introgen Therapeutics, Inc. (SR93-004-1).

The costs of publication of this article were defrayed in part by the payment of page charges. This article must therefore be hereby marked *advertisement* in accordance with 18 U.S.C. Section 1734 solely to indicate this fact.

Note: F. Uno, J. Saski, and M. Nishizaki contributed equally to this work.

Requests for reprints: Lin Ji, Department of Thoracic and Cardiovascular Surgery, Box 445, The University of Texas M. D. Anderson Cancer Center, 1515 Holcombe Boulevard, Houston, TX 77030. Phone: (713) 745-4530; Fax: (713) 794-4901; E-mail: lji@mdanderson.org.

vices provided by Bethyl Laboratories, Inc. (Montgomery, TX). The formalin-fixed, paraffin-embedded tissue sections were incubated with horseradish peroxidase-conjugated rabbit anti-Fus1 antibodies (0.1–2.0 μg/ml in PBS-BSA), and immunostaining was performed with the VECTASTAIN Elite ABC kit according to manufacturer's instruction. Subsequently, the sections were counterstained with Harries hematoxylin. Samples were examined under a microscope, and immunohistochemical images were recorded with an equipped digital camera.

Laser-Capture Microdissection (LCM) and Protein Preparation for Surface-Enhanced Laser Desorption/Ionization Mass Spectrometry (SELDI-MS) Analysis. Frozen tissue sections were rapidly removed from −80°C storage and immersed in or flooded with 70% alcohol for ~1 min, followed by H&E staining. The tumor cells and adjacent normal cells were precisely identified by microscopic examination. LCM was performed with the PixCell LCM microscope (Arcturus Engineering, Mountain View, CA). Approximately 500-1000 microdissected cells were then transferred to a thermoplastic film mounted on optically transparent LCM caps and incubated with 50 μl of protein lysis buffer containing 1% NP40, 0.5% sodium deoxycholate, 0.1% SDS, 1% DTT, and 1× complete protease inhibitors (Roche Biochemicals) in PBS on ice for 15 min. Cell samples were sonicated in a Transsonic 700/H sonication water bath (Lab-Line Instruments, Melrose Park, IL) at 4°C for 3 min, and protein lysate was cleared by centrifugation for 5 min at 13,000 rpm at 4°C. The protein lysates were either used immediately or stored at −80°C.

Antibody-Capture ProteinChip Array (ACPA) with SELDI-MS. The endogenous or exogenous wt-Fus1 or mutant Fus1 proteins were captured with affinity-purified rabbit Fus1 polyclonal antibodies from cultured cells or LCM-separated and enriched human primary lung tumor and noninvolved normal cells. Five μl (~10 μg) of protein lysate were spotted on a Fus1 antibody-coated preactivated surface (PS20) ProteinChip array and analyzed by SELDI-MS in the presence of CHCA matrix solution; both internal and external standards were used for mass/charge (*m/z*) calibration (Ciphergen Biosystems, Fremont CA). ACPA and SELDI-time-of-flight (TOF)-MS analysis were performed according to the manufacturer's instructions and procedures described in detail elsewhere (9–11).

Animal Studies. All animals were maintained and animal experiments were performed under NIH and institutional guidelines established for the Animal Core Facility at the University of Texas M. D. Anderson Cancer Center. Procedures for H1299 s.c. tumor inoculations in *nu/nu* mice have been described previously (8). When tumors reached an average of ~0.5 cm in diameter (~2 weeks after tumor inoculation), *N*-[1-(2,3-dioleoyloxyl)propyl]-*N*,*N*,*N*-trimethylammoniummethyl sulfate–cholesterol-complexed wt-*FUS1* or myristoylation-mutant (myr-mt)-*FUS1* plasmid vectors (*FUS1* lipoplex) were injected into the tumors three times within a week at a dose of 25 μg of plasmid DNA and 10 nmol liposome/tumor in 100 μl of 5% dextrose in water. PBS and *LacZ* were used as mock and negative controls, respectively. Tumor sizes were measured twice a week, and tumor volume was calculated using the equation $V\ (mm^3) = a \times b^2/2$, where a is the largest diameter and b is the smallest dimension.

To evaluate the effect of systemic administration of *FUS1* lipoplex on development of A549 experimental lung metastases in nude mice, we injected various lipoplexes every 2 days (three times/day) i.v. into all animals at a dose of 25 μg of plasmid DNA and 10 nmol of liposome each in 100 μl of 5% dextrose in water per animal. Each treatment group consisted of 10 animals. Lungs were harvested 2 weeks after the last injection, and metastatic colonies on the surfaces of lung were stained with Indian ink. Tumor colonies on lung surfaces were counted under a dissecting microscope without knowledge of the treatment groups, and the lung tissues were sectioned for further pathological and immunohistochemical analysis and for *in situ* apoptosis analysis with terminal deoxynucleotidyl transferase (Tdt)-mediated nick end labeling (TUNEL) staining (Roche Biochemical.)

Results

Loss of Expression of Fus1 Protein in Primary Lung Cancer and Cancer Cell Lines. In a previous study, we examined 40 primary lung cancers and found that mutation of the *FUS1* gene was infrequent and that there were only a few nonsense mutations and a COOH-terminal deletion mutation that arose from aberrant mRNA splicing (Fig. 1*A*; Ref. 5). In addition, we found no evidence for *FUS1* promoter region methylation (data not shown). *FUS1* expression has been detected in various normal human tissues, including brain, heart, pancreas, prostate, kidney, and lung, based on quantification of expressed sequence tags in Unigene clusters, as summarized in GeneCards[4] by the Crown Human Genomics Center and Yeda Research and Development Co. Ltd. (Rehovot, Israel). Although endogenous Fus1 protein expression could be detected in normal human bronchial epithelial cells and fibroblast cells (WI-38) by immunoblot analysis and *FUS1* mRNA transcription could be seen on Northern blots of RNAs prepared from lung cancer cell lines, we could not detect endogenous Fus1 protein in these lung cancer cell lines on immunoblots using the affinity-purified, anti-Fus1 peptide antibodies we developed (Fig. 1*B*). In addition, we performed immunohistochemical staining on a set of paired normal lung and lung cancer tissue sections (Fig. 1, *C–J*). We found that normal lung epithelial cells express Fus1 (Fig. 1, *D–F*) but that many lung cancers (15 of 20; >70%; Fig. 1, *H–J*) did not. We also found that even in those tumor samples with Fus1-positive staining, the staining was not uniformly detectable in all tumor cells (Fig. 1*G*). On the basis of both the lung-cancer-growth-suppressing properties of the Fus1 protein *in vitro* and in animal models and the observed loss of protein expression in primary tumors and tumor-derived cell lines, we hypothesized that *FUS1* would have to act as a TSG in a haploinsufficient manner (because most primary lung cancers experienced allelic loss in this 3p21.3 region; Ref. 12) and that both loss of expression and deficient posttranslational modification of Fus1 protein might lead to loss of its tumor suppression function and to lung cancer development.

Identification of Myristoyl Modification of Fus1 Protein. To test this hypothesis, we first performed computer-based homologous structure modeling and functional domain prediction of Fus1 protein to assess its biochemical and biophysical properties and to obtain possible leads to its biological function (Fig. 1*A*). The secondary protein structure prediction indicated that the wt-Fus1 protein is a highly hydrophobic protein with extensive helix-coil domain structures lacking transmembrane elements (Fig. 1*A*). The functional domains of Fus1 protein were predicted by use of a motif-based profile scanning program (13) and showed a potential myristoylation site at the NH_2 terminus, a protein kinase A interaction site, an A kinase-anchoring protein interaction (protein/protein) site, and a PDZ class II domain (Fig. 1*A*). From these analytical comparisons of Fus1 protein structure and function, we predict that Fus1 is a myristoylated member of the novel cAMP-dependent protein kinase A and A kinase-anchoring protein families, which are associated with many cellular processes, including transcription, signal transduction, metabolism, ion channel regulation, cell cycle progression, and apoptosis (14, 15).

To verify myristoylation of the Fus1 protein, we constructed a plasmid vector expressing either the wt-*FUS1* or a myristoylation-site-deficient mutant (myr-mt-*FUS1*) in which the predicted myristoylation site of glycine (G_2) was replaced with an alanine (A_2; Fig. 1*A*) by site-directed mutagenesis. A double-mutant (dmt-*FUS1*) in the COOH-terminal region, in which two highly hydrophobic isoleucine residues (I_{87} and I_{91}) were replaced with two neutral and rigid-conformation-promoting proline residues (P_{87} and P_{91}; Fig. 1*A*), was also constructed as another control to confirm the biological significance and specificity of the myristoylation-deficient mutation of Fus1 protein. The wt-Fus1- and mutant-Fus1-expressing plasmid vectors were used to transfect Fus1-deficient human NSCLC NCI-H1299 cells. The expression and posttranslational modification status of these wt and mutant Fus1 proteins were analyzed by SELDI-TOF-MS on an

[4] http://bioinfo.weizmann.ac.il/cards-bin/carddisp?FUS1.

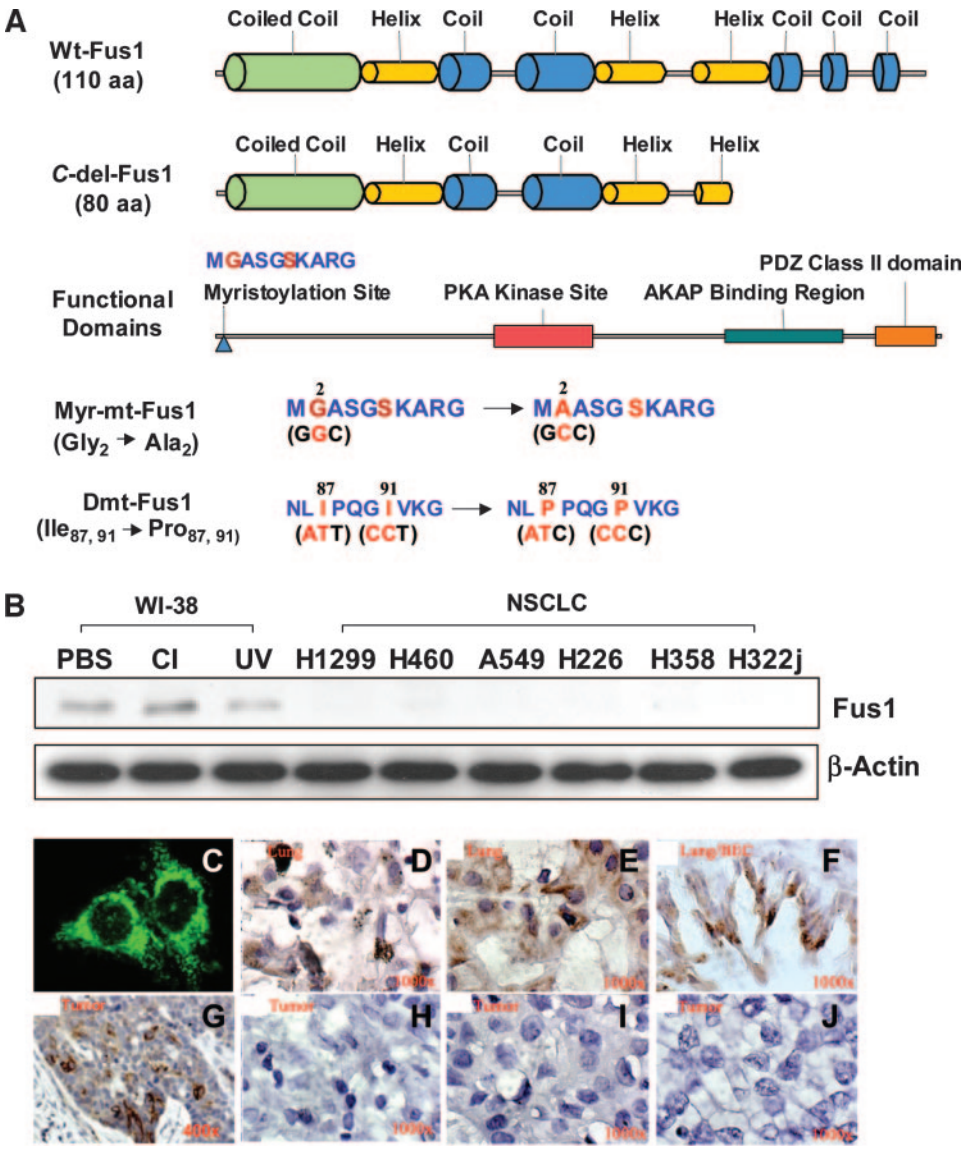


Fig. 1. Predicted secondary structure and functional domains of Fus1 protein and its expression in normal lung and primary lung tumors and tumor-derived cell lines. *A*, predicted secondary structure and functional domains of wild-type (*wt*)-Fus1 and C-del-Fus1. The predicted functional elements and domains, including a potential myristoylation site, protein kinase A (*PKA*) targeting site, A kinase-anchoring protein (*AKAP*) interface, and a PDZ class II domain are indicated. Mutant *myr-mt-Fus1*, in which the codon GGC for Gly_2 was changed to GCC for Ala_2, and double-mutant *Dmt-Fus1*, in which codon ATT for Ile_{87} and ATC for Ile_{91} were changed to CCT for Pro_{87} and CCC for Pro_{91}, respectively, were constructed by site-directed mutagenesis. *C-del-Fus1* is a tumor-related COOH-terminal deletion mutant derived by abnormal mRNA splicing. *B*, immunoblot analysis of endogenous Fus1 protein expression in normal lung fibroblast WI-38 cells grown in PBS under conditions of contact inhibition (*CI*) or after exposure of the cells to UV irradiation (100 joules for 5 min) and in non-small cell lung cancer (*NSCLC*) cells. The same blots were also probed for β-actin to ensure equal loading. *C–J*, immunofluorescence image analysis in wt-*FUS1*-transfected H1299 cells with FITC-conjugated rabbit anti-Fus1 antibodies (*C*) and immunohistochemical analysis of Fus1 protein expression in normal lung cells (*D* and *E*), bronchial epithelial cells (*F*), and primary lung tumor cells (*G–J*) in formalin-fixed, paraffin-embedded tissue samples. wt-Fus1 has a typical mitochondria/endoplasmic reticulum membrane localization in cytoplasm (*C*). Expression of Fus1 was detected in cytoplasm in normal lung (*D* and *E*) and bronchial epithelia (*F*); Fus1 expression was also detected in some tumor cells in one primary NSCLC (*G*) but was undetectable in other primary NSCLC cell lines (*H–J*) when we used rabbit anti-Fus1 polyclonal antibodies at a 1:2000 dilution. Magnifications: ×400 (*G*); ×1000 (*D–F*, *H–J*).

anti-Fus1 ACPA (Ciphergen Biosystems, Fremont, CA; Fig. 2*A*). The expressed Fus1 proteins in transfected H1299 cells were specifically captured on the protein chip and detected in the SELDI-TOF-MS spectra (Fig. 2*A*), but no protein peaks at corresponding mass positions were detected in the spectra with an anti-101F6 (a protein with encoding gene colocated in 3p21.3 region with *FUS1*) antibody-coated chip as a nonspecific control (Fig. 2*B*). The wt-Fus1 protein was identified as a myristoylated protein based on the detected mass of the captured wt-Fus1 protein (Fig. 2*A*), which showed a protein peak with a *m/z* ratio of 12,174 ± 6.25 Da compared with the predicted mass of 12,072.98 Da for the nonmyristoylated wt-Fus1 or 12,174.2 Da for the myristoyl-Fus1 protein. The myristoylation-deficient mutant (12,024.6 Da) and the COOH-terminal deletion mutant (8,783.5 Da) of Fus1 protein were also captured and detected on the protein array by SELDI-MS by comparing them with their calculated masses (Fig. 2*A*). No captured Fus1 proteins were detected in either the untransfected or p*LacZ*-transduced cells (Fig. 2*A*). On the basis of the 232-Da mass shift between the detected myristoylated Fus1 (12,174 Da) and the predicted nonmyristoylated Fus1 protein (11,942 Da; without the first methionine residue because the methionine residue is removed during myristoylation), we predict that the Fus1 protein is acylated at the G_2 with a 14-carbon myristate ($C_{14}H_{28}O_2$; 228.4 Da). The myristoylation of Fus1 protein was also confirmed by immunoblot analysis and immunoprecipitation analysis of the ^{14}C-myristate-labeled and acylated Fus1 protein in the p*FUS1*-transfected cells (Fig. 2*S*).

Defect of Myristoylation of Fus1 Protein in Primary Lung Cancer. Because mutation of *FUS1* is infrequent and no evidence has been found for methylation or mutation of the *FUS1* promoter region in lung cancers, other factors, such as haploinsufficiency, low expression, abnormal products arising from aberrant mRNA splicing, and posttranslational modification of Fus1, may play important roles in lung tumorigenesis (2, 3). We used ACPA analysis with SELDI-TOF-MS to evaluate the protein expression and myristoylation status in primary lung tumor and uninvolved normal lung tissue samples. Molecular analysis of tumors and their precursor lesions requires the isolation of specific cell subpopulations (normal, preneoplastic, and tumors) from a composite background of multiple cell types in tumor tissue biopsies. This was accomplished with LCM technology (16). To evaluate Fus1 protein expression and posttranslational modifications in human lung tumors and noninvolved tissues, we used LCM combined with appropriate tissue preparation methods to separate and enrich tumor or noninvolved normal cells, and the resulting separated cell populations (~500–1000 cells) were used for the Fus1-specific

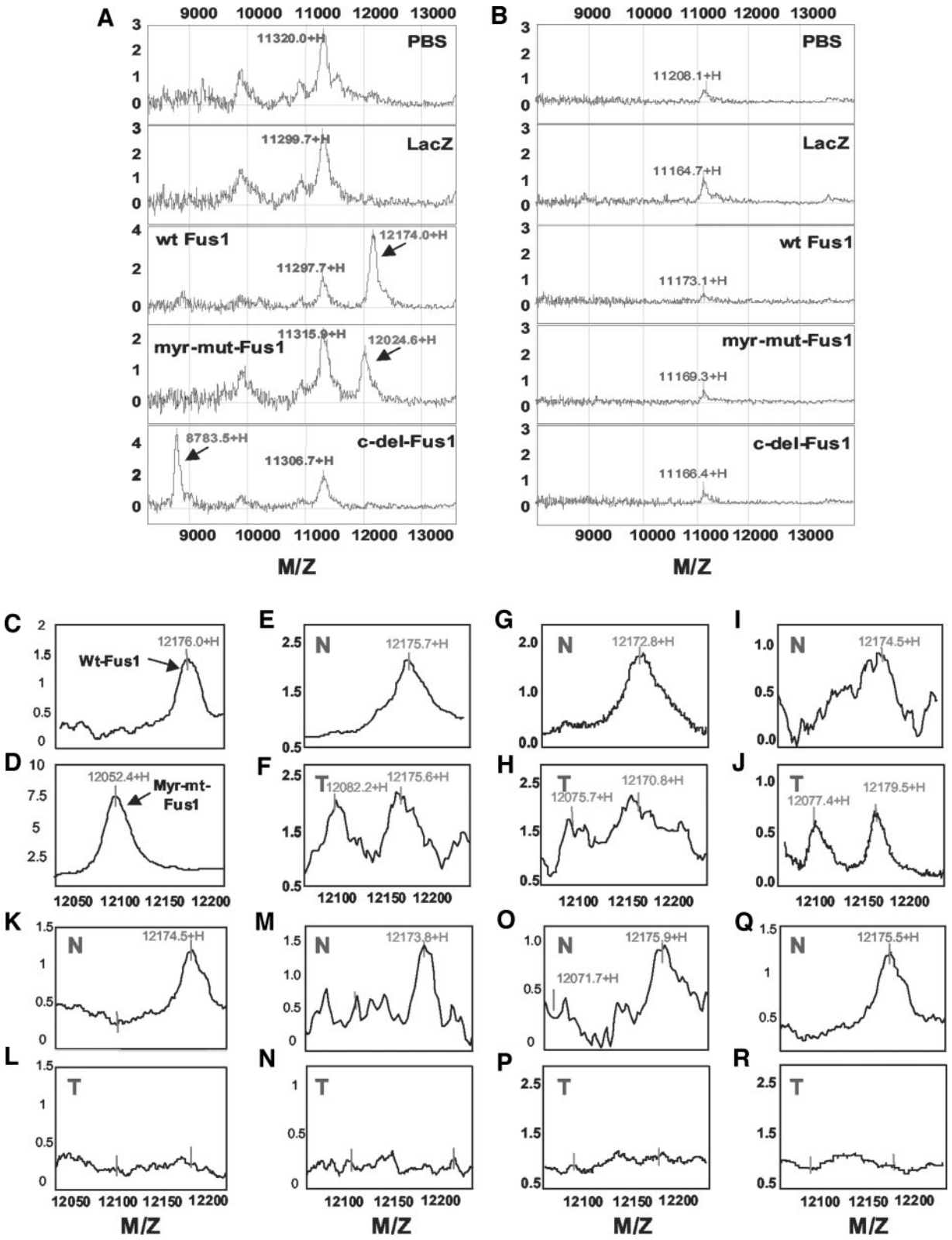


Fig. 2. Detection of myristoylation of Fus1 protein by surface-enhanced laser desorption/ionization time-of-flight mass spectrometric analysis on an anti-Fus1 antibody-capture ProteinChip array (ACPA). *A*, detection of Fus1 proteins captured on the anti-Fus1 antibody-coated preactivated surface (PS20) chip in wild-type (*wt FUS1*) or myristoylated mutant-*FUS1* (*myr-mut-Fus1*)-containing plasmid-transfected H1299 cells. The myristoylated Fus1 proteins are detected as a peak with a mass of 12,174 Da, and the nonmyristoylated Fus1 (*myr-mut-Fus1*) is detected with a mass of 12,024 Da compared with the calculated masses of 12,174 Da for the myristoylated wt-Fus1 and 12,025 Da for the myr-mut-Fus1, respectively. No corresponding proteins were detected in either PBS mock or *LacZ* control cells. B, ACPA assay with PS20 chips coated with nonspecific antibodies (anti-101F6). No Fus1 proteins were detected in these mass spectra when the same protein lysates as in *A* were applied. *C–R*, detection of status of Fus1 protein expression and posttranslational modification in laser-capture microdissection-enriched human primary lung tumor (*T*) and adjacent noninvolved normal (*N*) cells, shown as representative pairs (pair *E* and *F* through pair *Q* and *R*) from 15 tissue samples tested by ACPA assay as described in *B*. The protein lysates prepared from wild-type *FUS1* (*Wt-FUS1)*- (*C*) or myristoylated mutant-*FUS1* (*Myr-mt-FUS1*)-transfected (*D*) H1299 cells were used as positive controls. A single peak of myristoylated wt-Fus1 protein with a mass of 12,174 ± 5.2 Da was detected in normal cells, whereas two peaks, one with a mass of 12,174 Da, corresponding to the mass expected for the myristoylated wt-Fus1 protein, and another with a mass of 12,075 ± 8.5 Da, corresponding to the mass of the nonmyristoylated wt-Fus1 protein, were detected in tumor cells. In some tumors, these peaks were not detected. *S*, Western blot (*WB*) and

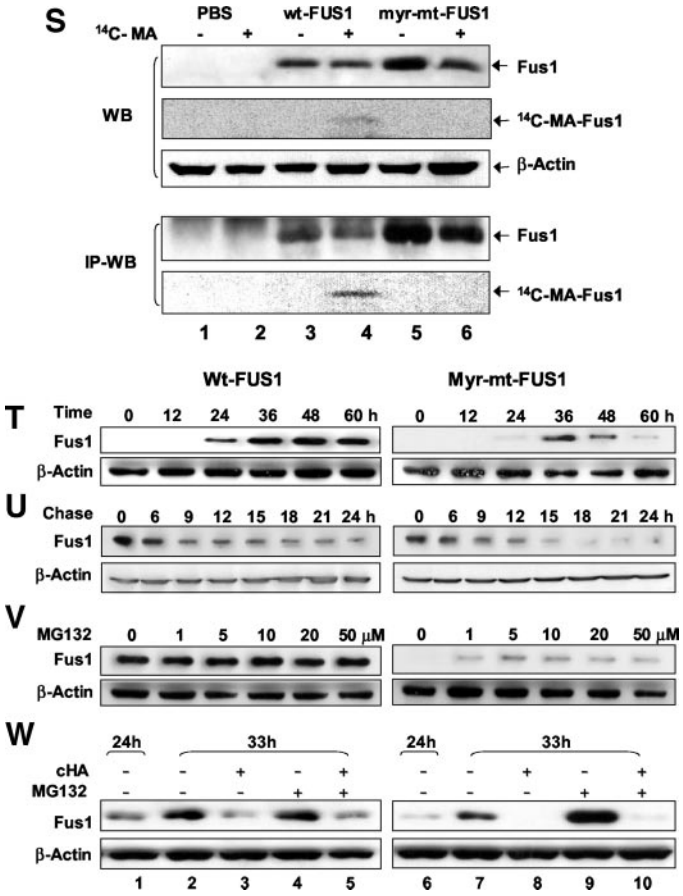


Fig. 2 Continued

ACPA analysis by SELDI-TOF-MS. We found that only myristoylated protein species could be detected in normal cells (13 of 15; $P = 0.0003$, nonparametric 2×2 contingency table; McNemar's χ^2 test) but that both the nonmyristoylated and myristoylated Fus1 protein were detected in tumor cells (5 of 15 samples; $P = 0.0442$) as indicated by detection of a peak corresponding to the Fus1 protein mass on the mass spectra (Fig. 2, *C–R*). In some tumor samples (7 of 15 samples; $P = 0.0030$), neither form of the Fus1 proteins could be captured (Fig. 2, *I*, *N*, *P*, and *R*), consistent with the results of the immunohistochemical analyses for these tumor and normal tissue samples. The remaining three samples tested were unresolvable because of the ambiguous spectra (spectra not shown). The difference in the observed Fus1 protein myristoylation status between the normal and the tumor cell populations was significant as indicated by a nonparametric McNemar marginal homogeneity test for the equality of categorical responses from two paired and dependent populations ($P < 0.001$).

Proteasome-Dependent Degradation of Nonmyristoylated Fus1 Protein. To explore the possible mechanism(s) for the involvement of the nonmyristoylated (or demyristoylated) Fus1 protein and the loss of its expression in primary lung cancer, we evaluated the stability of the exogenously expressed wt-Fus1 and myr-mt-Fus1 proteins in H1299 cells. We found that the duration of transient expression of myr-mt-Fus1 protein was much shorter than that of wt-Fus1. Myr-mt-Fus1 protein expression peaked at 36 h posttransfection and was almost undetectable after 60 h, whereas the wt-Fus1 protein was expressed at high levels beyond 60 h posttransfection (Fig. 2*T*). The half-life of the myr-mt-Fus1 protein was shorter than that of wt-Fus1 (~6 h for the former and 12 h for the later), as shown by pulse-chase of protein synthesis after treatment with the protein synthesis inhibitor cycloheximide (Fig. 2*U*). These results suggest that nonmyristoylated Fus1 protein may be degraded more rapidly than the myristoylated form. We therefore investigated the effect of the proteasome inhibitor (17) MG132 on degradation of Fus1 proteins. We found that the nonmyristoylated Fus1 protein levels increased in myr-mt-*FUS1*-transfected H1299 cells treated with various concentrations of MG132 (Fig. 2*V*). The MG132-induced recovery of the myr-mt-Fus1 protein could be detected at a very low level (1 μM; Fig. 2*V*) and was independent of protein synthesis, as demonstrated by significant protein accumulation on treatment with 10 μM of MG132 in the presence or absence of the protein synthesis inhibitor cycloheximide (Fig. 2*W*), with no effect shown on wt-Fus1 protein under the same experimental conditions (Fig. 2*W*). These results suggest that myristoylation may stabilize Fus1 protein and that demyristoylation may lead to rapid degradation of Fus1 protein through a proteasome-dependent pathway.

Disrupted Subcellular Localization of Myristoylation-Deficient Mutant of Fus1 Protein. One potential function of protein myristoylation is the facilitation of efficient interactions with cell membranes necessary for correct subcellular localization (18–20). We therefore analyzed the subcellular localization of myristoylation-positive wt-Fus1 and the myristoylation-deficient mt-Fus1 proteins in plasmid-transfected H1299 cells by immunofluorescence image analysis using FITC-conjugated anti-Fus1 antibodies (Fig. 33, *A–D*). The myr-mt-Fus1 protein lost its characteristic intracellular membrane localization (Fig. 3, *C* and *D*), suggesting a critical role for myristoylation in the cellular localization of Fus1 protein.

Myristoylation Is Required for Fus1-Mediated Tumor-Suppressing Activities *in Vitro* and *in Vivo*. To evaluate the biological role of myristoylation in Fus1 protein-mediated tumor suppression, we compared the clonogenicity of the wt-Fus1- and myr-mt-Fus1-expressing H1299 cells *in vitro* (Fig. 3, *G* and *H*). The exogenous expression of both the *FUS1* genes and proteins in these H1299 transfectants was confirmed by reverse transcription-PCR (Fig. 3*E*) and by Western blot (Fig. 3*F*) analysis, respectively. Significant inhibition of clonogenicity was observed in myristoylated wt-Fus1-expressing H1299 cells, but no significant growth inhibition was observed in myr-mt-Fus1-expressing cells compared with the Fus1-nonexpressing controls (Fig. 3, *G* and *H*). The COOH-terminal double mutation of Fus1 (dmt-Fus1), which was theoretically expected to severely alter the hydrophobic and conformational properties in this region of Fus1 protein, was still able to significantly inhibit clonogenicity, similar to the effect of wt-Fus1 (Fig. 3, *G* and *H*).

We evaluated the effects of wt-Fus1 and myr-mt-Fus1 protein expression on tumor growth in H1299 s.c. tumor xenografts in *nu/nu*

immunoprecipitation Western blot (*IP-WB*) analyses for verification of myristoylation of Fus1 proteins in H1299 transfectants. H1299 cells were transfected with either wild-type FUS1 (*wt-FUS1*) or myristoylation-deficient mutant-FUS1 (*myr-mt-FUS1*) plasmid vectors for 48 h and then incubated with ^{14}C-labeled myristic acid (*MA*; American Radiolabeled Chemicals, St. Louis, MO) in a final concentration of 5 μCi/ml for 90 min. Crude protein lysate (80 μg) was loaded in each lane for WB, and 1–2 mg of protein lysate with 1–2 μg of anti-Fus1 antibodies were used for IP. *T* and *U*, effect of myristoylation on Fus1 protein synthesis and stability by WB analysis during a 60-h time course posttransfection (*T*) and with a 3-h-interval pulse chase after treatment with 50 μM of protein synthesis inhibitor cycloheximide (*cHA*; *U*) in wild-type-*FUS1* (*Wt-FUS1*) (*left panels*) or myristoylation-deficient mutant-*FUS1* (*Myr-mt-FUS1*)-transfected (*right panels*) H1299 cells. *V* and *W*, effect of proteasome inhibitor MG132 on demyristoylation-induced degradation of Fus1 proteins. H1299 cells were transfected with wt-*FUS1* or myr-mt-*FUS1* plasmid DNAs for 24 h and then treated with DMSO (*Lane 0*) and various concentrations (1–50 μM) of MG132 (*V*), or were treated with 10 μM MG132 in the presence (+) or absence (−) of 50 μM cycloheximide (*W*). Expression of Fus1 proteins was analyzed by WB with anti-Fus1 antibodies. These experiments were carried at least twice with duplicates for each.

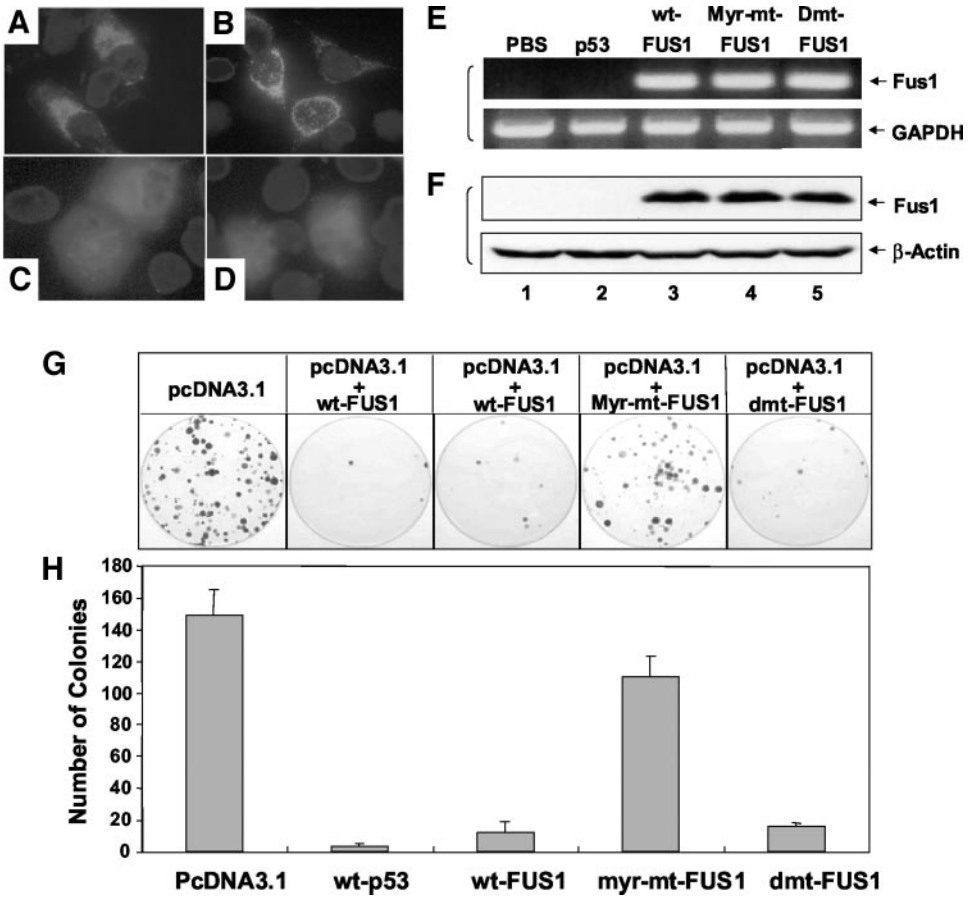


Fig. 3. Effects of myristoylation on Fus1 protein subcellular localization and Fus1-mediated tumor-suppressing activity *in vitro*. *A–D*, immunofluorescence image analysis of Fus1 protein expression and subcellular localization. H1299 cells were transfected with either wild-type Fus1-expressing (*A* and *B*) or myristoylation-deficient mutant-Fus1-expressing (*C* and *D*) plasmid vectors. Fus1 proteins were probed with FITC-conjugated anti-Fus1 antibody (*green*), and the nucleus was stained with Hoechst dye (*blue*; Sigma Chemical Co., St. Louis, MO). *E* and *F*, expression of *Fus1* genes and proteins in H1299 transfectants were verified by reverse transcription-PCR (*E*) and by Western blot analysis (*F*). *wt-FUS1*, wild-type Fus1; *Myr-mt-FUS1*, myristoylation-deficient mutant-Fus1; *Dmt-FUS1*, double-mutant Fus1; *GAPDH*, glyceraldehyde-3-phosphate dehydrogenase. *G* and *H*, effect of myristoylation of Fus1 protein on tumor cell-derived clonogenicity *in vitro*. H1299 cells (1×10^5) were transfected with plasmid DNAs *in vitro*. The wild-type (*wt-FUS1*), myristoylation-deficient mutant (*Myr-mt-FUS1*), or hydrophilic double mutant (*dmt-FUS1*) of Fus1-expressing plasmids were cotransfected with the neomycin-resistant gene-containing pcDNA3.1 vector; the pcDNA3.1 vector alone and the pcDNA3.1 plus wt-p53 plasmid were used as negative and positive controls, respectively. The numbers of G418-resistant colonies were counted after staining with Crystal Violet (*G*), and the quantitative analysis is shown in *H*. The experiments were repeated at least three times. The *bars* represent the SD, and the differences between the pcDNA3.1 vector alone and each testing construct was analyzed statistically by two-tailed Student's *t* test. $P \leq 0.05$ is considered significant.

mice by intratumoral injection of *N*-[1-(2,3-dioleoyloxyl)propyl]-*N*,*N*,*N*-trimethylammoniummethyl sulfate–cholesterol complexed with either wt-*FUS1* or myr-mt-*FUS1*-expressing plasmid DNAs (*FUS1* lipoplexes; Ref. 21) along with PBS as a mock control and *LacZ* plasmid vector as a negative control (Fig. 4*A*). The human NSCLC xenograft model, DNA lipoplex preparation, and treatment procedures were as described previously (4, 6, 21). Tumor growth was recorded from the first injection until 31 days after the last injection. Tumor volumes were normalized by calculating the percentage increase in tumor volume after treatment relative to volume at the beginning of treatment in each group. All of the tumors treated with wt-*FUS1* showed significantly suppressed growth ($P < 0.001$) compared with mouse groups treated with PBS or p*LacZ* controls (Fig. 4*A*). However, the tumor-suppressing activity of the myristoylation-deficient mutant (myr-mt-*FUS1*) of Fus1 protein was significantly reduced compared with wt-Fus1 ($P < 0.001$), although it retained a small inhibitory effect compared with the PBS and p*LacZ* controls (Fig. 4*A*).

We also evaluated the effect of the myristoylation of Fus1 protein on development of lung metastases, using the human NSCLC A549 xenograft metastasis mouse model by systemic (i.v.) administration of the wt-*FUS1* or myr-mt-*FUS1* lipoplexes compared with PBS, p*LacZ*, and the lung cancer-originated COOH-terminal deletion mutant of wt-*FUS1* and dmt-*FUS1* plasmid vector controls (4, 6). The development of A549 pulmonary metastases was significantly inhibited ($P < 0.001$), and the numbers of metastatic tumor colonies found on the surfaces of lungs from mice inoculated with A549 cells were reduced >85% in animals treated with wt-*FUS1* compared with those in control treatment groups (Fig. 4*B*). However, no significant reduction ($P < 0.003$) of metastasis formation was observed in animals treated with myr-mt-*FUS1*. The formation of metastases was significantly reduced ($P < 0.001$) in animals treated with dmt-*FUS1* compared with those controls treated with either PBS or *LacZ*, but the inhibitory effect was weaker than that observed in the wt-*FUS1*-treated group (Fig. 4*B*). The size of any remaining metastatic tumor nodules, as shown in H&E-stained sections of mouse lung tissues (Fig. 4*C*), was reduced in animals treated with wt-*FUS1* but not in those treated with myr-mt-*FUS1*, compared with either PBS or *LacZ*-treated controls. We analyzed the induction of apoptosis in these Fus1-expressing tumor cells by *in situ* apoptosis analysis with FITC-dUTP-labeled TUNEL staining (Roche Biochemicals; Fig. 4, *D–J*). Induction of apoptosis was detected in the wt-Fus1-expressing tumors (Fig. 4*E*) but not in myr-mt-Fus1-expressing (Fig. 4*F*) or PBS-treated (Fig. 4*D*) tumors, providing direct evidence for the need for both Fus1 expression and myristoylation in Fus1-mediated tumor suppression and apoptosis *in vivo*.

Discussion

Our studies present the first evidence supporting the biological importance of myristoyl modification of a TSG product and warrant further study of the role of the expression and posttranslational modification of Fus1 protein in the pathogenesis of lung and other human cancers. The N-myristoyl modification of proteins is achieved by a cotranslational linkage of myristic acid via an amide bond to the NH_2-terminal glycine residues of a variety of cellular and viral proteins in eukaryotic cells (22). Covalent modification of proteins by fatty acids such as myristate and palmitate is now a widely recognized form of protein modification, and ~100 proteins are known to be myristoylated (18, 20). N-Myristoyl proteins play essential roles in

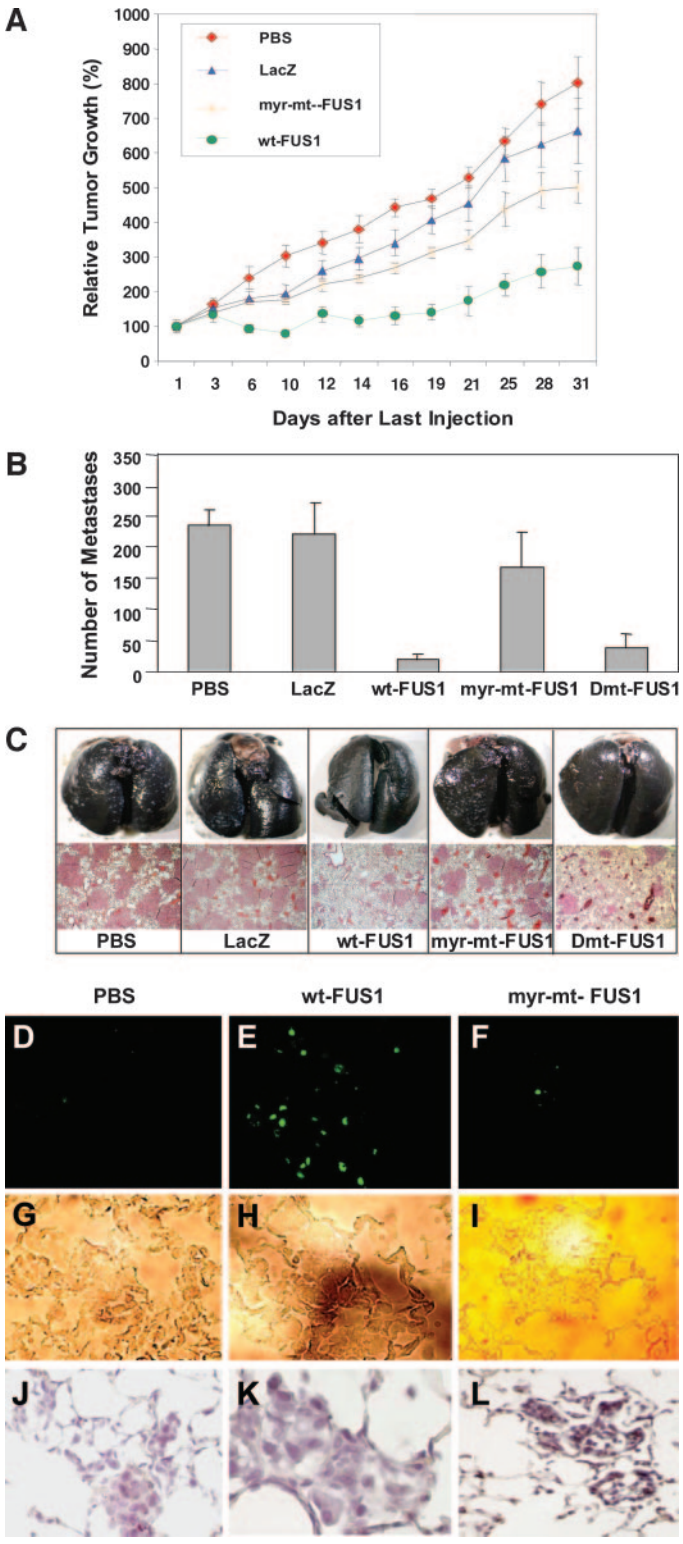


Fig. 4. Effect of myristoylation of Fus1 protein on Fus1-mediated tumor-suppressing activity *in vivo*. *A*, effect on H1299 human tumor xenograft growth in nude mice. Human non-small cell lung cancer H1299 cells were inoculated s.c. in nude mice. When the tumor reached 5–10 mm in diameter (2 weeks after tumor inoculation), *N*-[1-(2,3-dioleoyloxyl)propyl]-*N*,*N*,*N*-trimethylammoniummethyl sulfate-cholesterol-complexed wild-type *FUS1* (*wt-FUS1*) or myristoylation-deficient *FUS1* (*myr-mt-FUS1*) plasmid vectors (*FUS1* lipoplex) was injected into the tumors three times within 1 week. PBS and *LacZ* were used as mock and negative controls, respectively. Results are reported as the mean ± SD for 5–10 mice in each treatment group. Tumor volumes were normalized by the percentage increase of tumor sizes after treatment relative to those at the beginning of the treatment in each group. The mean tumor volumes ± SE (*bars*) from these experiments are shown. ANOVA was performed to determine statistical significance between each treatment group, using Statistica software (StatSoft Inc., Tulsa, OK), and $P \leq 0.05$ was considered significant. *B*, effect of systemic administration of *FUS1* lipoplex on development of A549 experimental lung metastases in nude mice. All animals received i.v. injections of various lipoplexes every 2 days (three times) at a dose of 25 μg of plasmid DNA and 10 nmol of liposome each in 100 μl of 5% dextrose in water per animal; PBS alone was used as a mock control and *LacZ* as a negative control. Each treatment group consisted of 10 animals. Lungs were harvested 2 weeks after the last injection, and metastatic colonies on the surfaces of lung were counted without knowledge of the treatment groups. *Bars* represent SE. A nonparametric *t* test (Wald–Wolfowitz runs test) was performed to determine the statistical significance between each treatment group, using Statistica software (StatSoft Inc.), and $P \leq 0.05$ was considered significant. Significant inhibition of metastasis development was observed in mice treated with wild-type *FUS1* (*wt-FUS1*; $P < 0.001$) and double-mutant-*FUS1* (*Dmt-FUS1*; $P < 0.001$) compared with mice treated with PBS or *LacZ*, but there was no significant inhibition in mice treated with myristoylation-deficient *FUS1* (*myr-mt-FUS1*; $P = 0.892$). The representative India ink-stained lungs and H&E-stained formalin-fixed, paraffin-embedded tissue sections in each treatment group are shown in *C*. The *white spots* on the lung surfaces indicate the metastatic tumor colonies. *D–I*, induction of apoptosis by wt-Fus1 expression *in vivo*. The A549 experimental metastasis tumor-bearing mice were treated with Fus1 lipoplexes three times within 1 week at the same dose as in *B*. Forty-eight h after the last treatment, animals were killed, and the lungs were harvested and freshly frozen. Induction of apoptosis was analyzed using an *in situ* apoptosis detection kit with FITC-dUTP-labeled terminal deoxynucleotidyl transferase (Tdt)-mediated nick end labeling reaction (Roche Biochemicals), and florescence images were examined under a fluorescence microscope and recorded with an equipped digital camera (*D–F*). Tumor morphology is shown in photographs *G–I*, taken at the same positions as above *D–F* under a regular optical light source. The hematoxylin-stained tissues from the same samples but in different sections were shown in photographs *J–L*.

diverse biological functions, such as regulating cellular structure, directing protein intracellular localization, mediating protein-protein and protein-substrate interactions, and regulating calcium and ion channel activities 18–20, 22). The requirement for myristoylation of the viral p60src protein to mediate its transforming and oncogenic properties demonstrated the biological importance of this hydrophobic myristoyl moiety (23). Recent genetic, biochemical, and cell-biological studies have provided insight into the molecular mechanisms of the regulation of protein myristoylation and explored strategies for modulating this process *in vivo* for therapeutic applications (18–20, 22). Our present evidence that primary lung cancers are deficient for myristoylation of Fus1 protein and that myristoylation is required for Fus1-mediated tumor suppressor activity *in vitro* and *in vivo* also indicates the cancer-preventive and therapeutic potential of positively regulating or reactivating myristoylation for Fus1.

Although the mechanism of demyristoylation is not known, demyristoylation of the myristoylated alanine-rich C-kinase substrate, as shown by electrospray mass spectrometry analyses of the myristoylated and demyristoylated forms of myristoylated alanine-rich C-kinase substrate proteins, has been found in brain (24), and the reduced expression of myristoylated alanine-rich C-kinase substrate has been reported in various cell lines after oncogenic or chemical transformation and in melanoma cells compared with normal choroidal melanocytes (25). The existence of a nonmyristoylated pool of a G protein α subunit (Gpa1p) in yeast has also been reported, and myristoylated Gpa1p is required for specific targeting of the protein to the plasma membrane; however, it is not clear how the nonmyristoylated proteins are generated and maintained (20, 26). Because point mutations of *FUS1* are infrequent, no mutation has been identified in its myristoylation site, and no evidence of epigenetic DNA methylation has been found in the *FUS1* promoter region in lung cancers, the observed reduced or lost expression and the deficient myristoylation of the Fus1 proteins in primary lung tumor cells and tumor-derived cell lines probably results from a deregulated myristoylation process or the accelerated proteasome-dependent degradation of demyristoylated Fus1 proteins.

Because most lung cancers experience allelic loss in this 3p21.3 region, haploinsufficiency may play a critical role in inactivation of Fus1 protein in lung cancer (3). In a diploid organism, each gene exists in two copies, in contrast to haploids, in which each cell contains a single copy of the genome. When one of the alleles is mutated or deleted, there is an ~50% reduction in the level of proteins

synthesized. Generally, the haploinsufficiency occurs when the level of proteins synthesized falls below a threshold level and is insufficient for the onset of some desired biological activity, leading to specific types of diseases or pathological changes. In our case, the haplotype in the 3p21.3 region where the *FUS1* gene is located may lead to a reduction or loss of FUS1 protein synthesis and deficiency of myristoylation, thus inactivating FUS1 and leading to the development of lung cancer. The importance of TSG haploinsufficiency in tumor cell biology has recently drawn increasing attention, and it may have profound effects on gene transcription, protein expression, posttranslational modification, stability, and does-dependent activity of TSGs because of the resulting decreased genomic stability, unbalanced chromosomal spatial symmetry, increased susceptibility to stochastic delays of gene initiation, altered transcriptional and translational stoichiometry, and interrupted gene expression (27–33). Although point mutations are rarely found in 3p21.3 genes in lung and other cancers, the accumulating evidence strongly argues that the extensive genomic changes (gains or losses of genetic material) collectively known as aneuploidy, which occurs frequently in lung cancer, particularly in adenocarcinoma, may collaborate with intragenic mutations during tumorigenesis and that changes in gene dosage may be modulated by the presence of adjacent genes with antagonistic activities, such as growth promotion and inhibition, a condition referred to as classic linkage disequilibrium (34). These observations raise the possibility that aneuploidy in chromosome 3; mutations of some critical checkpoint genes, such as *p53*, *Rb*, or *Ras*; and inactivation of the adjacent gatekeeper genes, such as *PTPRG*, *FHIT*, or *VHL* in the 3p region may influence the transcription, translation, and posttranslational processing of loss of heterozygosity-associated 3p21.3 genes such as *FUS1* to permit emergence of protumorigenic gene dosage changes or gene product inactivation that may facilitate early tumor development, inhibit cell proliferation, and induce apoptosis.

Our findings point to an essential role for protein myristoylation in human cancer pathogenesis and warrant further studies of alternative mechanisms involved in the inactivation of novel TSGs. Our results also suggest that it may be possible to prevent and delay tumorigenesis by neutralizing the effects of 3p haploinsufficiency before progression of premalignant lesions to invasive cancer and to suppress tumor growth by inducing apoptosis and altering cell cycle processes after tumor onset through wt-*FUS1* gene transfer.

Acknowledgments

We thank Dr. Sandra Hofmann at the University of Texas Southwestern Medical Center, Dallas for critical review of the manuscript; Drs. Nebiyou Bekele and Michael Gilcrease at M. D. Anderson Cancer Center for performing McNemar statistical analyses and for pathological evaluation of immunohistochemically stained human tissue sections, respectively; and Dr. Charlotte Clarke from Ciphergen Biosystems, Inc., for technical assistance with the SELDI-TOF-MS technology.

References

1. Lerman MI, Glenn GM, Daniel L, et al. A new polymorphic probe on chromosome 3p: lambda LIB28-77 (D3S169E). Nucleic Acids Res 1990;18:205.
2. Lerman MI, Minna JD. The 630-kb lung cancer homozygous deletion region on human chromosome 3p21.3: identification and evaluation of the resident candidate tumor suppressor genes. The International Lung Cancer Chromosome 3p21.3 Tumor Suppressor Gene Consortium. Cancer Res 2000;60:6116–33.
3. Zabarovsky ER, Lerman MI, Minna JD. Tumor suppressor genes on chromosome 3p involved in the pathogenesis of lung and other cancers. Oncogene 2002;21:6915–35.
4. Ji L, Nishizaki M, Gao B, et al. Expression of several genes in the human chromosome 3p21.3 homozygous deletion region by an adenovirus vector results in tumor suppressor activities in vitro and in vivo. Cancer Res 2002;62:2715–20.
5. Kondo M, Ji L, Kamibayashi C, et al. Overexpression of candidate tumor suppressor gene FUS1 isolated from the 3p21.3 homozygous deletion region leads to G_1 arrest and growth inhibition of lung cancer cells. Oncogene 2001;20:6258–62.
6. Ramesh R, Saeki T, Templeton NS, et al. Successful treatment of primary and disseminated human lung cancers by systemic delivery of tumor suppressor genes using an improved liposome vector. Mol Ther 2001;3:337–50.
7. Fondon JW, Mele GM, Brezinschek RI, et al. Computerized polymorphic marker identification: experimental validation and a predicted human polymorphism catalog. Proc Natl Acad Sci USA 1998;95:7514–9.
8. Ji L, Fang B, Yen N, Fong K, Minna JD, Roth JA. Induction of apoptosis and inhibition of tumorigenicity and tumor growth by adenovirus vector-mediated fragile histidine triad (FHIT) gene overexpression. Cancer Res 1999;59:3333–9.
9. Cai H, Wang Y, McCarthy D, et al. BACE1 is the major beta-secretase for generation of Aβ peptides by neurons. Nat Neurosci 2001;4:233–4.
10. Davies H, Lomas L, Austen BM. Profiling of amyloid β peptide variants using SELDI ProteinChip arrays. Biotechniques 1999;27:1258–61.
11. von Eggeling E, Davies H, Lomas L, et al. Tissue-specific microdissection coupled with ProteinChip array technologies: Applications in cancer research. Biotechniques 2000;29:1066–70.
12. Wistuba II, Behrens C, Virmani AK, et al. High resolution chromosome 3p allelotyping of human lung cancer and preneoplastic/preinvasive bronchial epithelium reveals multiple, discontinuous sites of 3p allele loss and three regions of frequent breakpoints. Cancer Res 2000;60:1949–60.
13. Yaffe MB, Leparc GG, Lai J, Obata T, Volinia S, Cantley LC. A motif-based profile scanning approach for genome-wide prediction of signaling pathways. Nat Biotechnol 2001;19:348–53.
14. Feliciello A, Gottesman ME, Avvedimento EV. The biological functions of A-kinase anchor proteins. J Mol Biol 2001;308:99–114.
15. Herberg FW, Maleszka A, Eide T, Vossebein L, Tasken K. Analysis of A-kinase anchoring protein (AKAP) interaction with protein kinase A (PKA) regulatory subunits: PKA isoform specificity in AKAP binding. J Mol Biol 2000;298:329–39.
16. Maitra A, Wistuba II, Virmani AK, et al. Enrichment of epithelial cells for molecular studies. Nat Med 1999;5:459–63.
17. Baumeister W, Walz J, Zuhl F, Seemuller E. The proteasome: paradigm of a self-compartmentalizing protease. Cell 1998;92:367–80.
18. Ames JB, Tanaka T, Stryer L, Ikura M. Portrait of a myristoyl switch protein. Curr Opin Struct Biol 1996;6:432–8.
19. Ames JB, Ishima R, Tanaka T, Gordon JI, Stryer L, Ikura M. Molecular mechanics of calcium-myristoyl switches. Nature (Lond) 1997;389:198–202.
20. Resh MD. Fatty acylation of proteins: new insights into membrane targeting of myristoylated and palmitoylated proteins. Biochim Biophys Acta 1999;1451:1–16.
21. Templeton NS, Lasic DD, Frederik PM, Strey HH, Roberts DD, Pavlakis GN. Improved DNA: liposome complexes for increased systemic delivery and gene expression. Nat Biotechnol 1997;15:647–52.
22. Bhatnagar RS, Futterer K, Farazi TA, et al. Structure of N-myristoyltransferase with bound myristoylCoA and peptide substrate analogs. Nat Struct Biol 1998;5:1091–7.
23. Kamps MP, Buss JE, Sefton BM. Mutation of NH2-terminal glycine of p60src prevents both myristoylation and morphological transformation. Proc Natl Acad Sci USA 1985;82:4625–8.
24. Manenti S, Sorokine O, Van Dorsselaer A, Taniguchi H. Demyristoylation of myristoylated alanine-rich C kinase substrate. Biochem Soc Transact 1995;23:561–4.
25. Manenti S, Malecaze F, Chap H, Darbon JM. Overexpression of the myristoylated alanine-rich C kinase substrate in human choroidal melanoma cells affects cell proliferation. Cancer Res 1998;58:1429–34.
26. Song J, Hirschman J, Gunn K, Dohlman HG. Regulation of membrane and subunit interactions by N-myristoylation of a G protein alpha subunit in yeast. J Biol Chem 1996;271:20273–83.
27. Celeste A, Petersen S, Romanienko PJ, et al. Genomic instability in mice lacking histone H2AX. Science (Wash DC) 2002;296:922–7.
28. Cook DL, Gerber AN, Tapscott SJ. Modeling stochastic gene expression: Implications for haploinsufficiency. Proc Natl Acad Sci USA 1998;95:15641–6.
29. Dworkin J, Losick R. Differential gene expression governed by chromosomal spatial asymmetry. Cell 2001;107:339–46.
30. McLaughlin MEJ. Thinking beyond the tumor cell: Nf1 haploinsufficiency in the tumor environment. Cancer Cell 2002;1:408–10.
31. Seidman JG, Seidman C. Transcription factor haploinsufficiency: when half a loaf is not enough. J Clin Investig 2002;109:451–5.
32. Veitia RA. Exploring the etiology of haploinsufficiency. Bioessays 2002;24:175–84.
33. Zhu Y, Ghosh P, Charnay P, Burns DK, Parada LF. Neurofibromas in NF1: Schwann cell origin and role of tumor environment. Science (Wash DC) 2002;296:920–2.
34. Pihan GDS. Mutations and aneuploidy: co-conspirators in cancer? Cancer Cell 2003;4:89–94.

ΔDNMT3B Variants Regulate DNA Methylation in a Promoter-Specific Manner

Jie Wang,[1,3] Manisha Bhutani,[1] Ashutosh K. Pathak,[1] Wenhua Lang,[1] Hening Ren,[1] Jaroslav Jelinek,[2] Rong He,[2] Lanlan Shen,[2] Jean-Pierre Issa,[2] and Li Mao[1]

Departments of [1]Thoracic/Head and Neck Medical Oncology and [2]Leukemia, The University of Texas M. D. Anderson Cancer Center, Houston, Texas and [3]Department of Oncology, Beijing Cancer Hospital, Beijing University School of Oncology, Beijing, China

Abstract

DNA methyltransferase 3B (DNMT3B) is critical in *de novo* DNA methylation during development and tumorigenesis. We recently reported the identification of a DNMT3B subfamily, ΔDNMT3B, which contains at least seven variants, resulting from alternative pre-mRNA splicing. *ΔDNMT3B*s are the predominant expression forms of *DNMT3B* in human lung cancer. A strong correlation was observed between the promoter methylation of *RASSF1A* gene but not *p16* gene (both frequently inactivated by promoter methylation in lung cancer) and expression of *ΔDNMT3B4* in primary lung cancer, suggesting a role of ΔDNMT3B in regulating promoter-specific methylation of common tumor suppressor genes in tumorigenesis. In this report, we provide first experimental evidence showing a direct involvement of ΔDNMT3B4 in regulating *RASSF1A* promoter methylation in human lung cancer cells. Knockdown of *ΔDNMT3B4* expression by small interfering RNA resulted in a rapid demethylation of *RASSF1A* promoter and reexpression of *RASSF1A* mRNA but had no effect on p16 promoter in the lung cancer cells. Conversely, normal bronchial epithelial cells with stably transfected *ΔDNMT3B4* gained an increased DNA methylation in *RASSF1A* promoter but not *p16* promoter. We conclude that promoter DNA methylation can be differentially regulated and ΔDNMT3Bs are involved in regulation of such promoter-specific *de novo* DNA methylation. [Cancer Res 2007;67(22): 10647–52]

Introduction

DNA methylation plays an essential role in the normal development of the mammalian embryo by regulating gene transcription through genomic imprinting, X chromosome inactivation, and genomic stability (1). It is believed that DNA methylation patterns in somatic cells are established during gametogenesis and early embryonic development via consecutive waves of demethylation and *de novo* methylation (2). The *DNA methyltransferase 3* (*DNMT3*) gene consists of *DNMT3A* and *DNMT3B* and is the major *de novo* DNA methyltransferase that preferentially methylates cytosine in CpG sites (3). Methylation in CpG-rich promoter regions may result in transcriptional silencing of the corresponding genes, which is a major mechanism by which tumor suppressor genes are inactivated in tumorigenesis (4).

DNMT3B contains 24 exons spanning ~47 kb of genomic DNA. Two alternative 5′ exons are used, but the same full-length DNMT3B protein (DNMT3B1 and DNMT3B2) is expected from both transcripts (5). Four additional transcriptional variants (*DNMT3B3, DNMT3B4, DNMT3B5*, and *DNMT3B6*) resulting from alternative pre-mRNA splicing have also been reported (5–7). Some of the variants may compete with each other, thereby resulting in even DNA hypomethylation (7). This possibility suggests a complex biological role of the *DNMT3B* variants. Increased expression of *DNMT3B* has been frequently observed in human cancer cell lines and primary tumors (3). However, an association between the expression level of *DNMT3B* and the promoter methylation status of tumor suppressor genes has not been established (8, 9). These data suggest that the regulation of DNA methylation of these promoters is complex.

ΔDNMT3B, a subfamily of *DNMT3B*, consists of at least seven transcriptional variants by alternative pre-mRNA splicing (10). In non–small cell lung cancer (NSCLC), *ΔDNMT3B* variants are the predominant forms of *DNMT3B* expression (10). We previously observed a strong and independent correlation between *ΔDNMT3B4* expression and DNA methylation of the *RASSF1A* promoter but not the *p16* promoter (11). This finding suggested that *ΔDNMT3B* variants are involved in the regulation of promoter methylation, possibly in a promoter-specific manner.

Materials and Methods

Cell lines. Human NSCLC lines H1299 and H358 were purchased from the American Type Culture Collection. The HBE1 cell line was a gift from Dr. John Minna (The University of Texas Southwest Medical Center, Dallas, TX).

RNA extraction and reverse transcription-PCR. We isolated total RNA from cells by using Tri-Reagent (Molecular Research Center) according to the manufacturer's instruction. The primers used for reverse transcription-PCR (RT-PCR) were described previously (10).

Methylation-specific PCR. One microgram of genomic DNA was used for bisulfite treatment to modify unmethylated cytosine residues, and the modified DNA was used for methylation-specific PCR (MSP) using methylation-specific and unmethylation-specific primers as described previously (10, 11). Unmodified DNA was used to test all the primer sets and we failed to observe any amplified DNA fragment in our experimental conditions.

Small interfering RNA and antisense RNA transfection. Small interfering RNA (siRNA) specifically targeted to the junction of exons 5 and 7 of *ΔDNMT3B* was designed and synthesized chemically (Ambion). Both annealed siRNA and corresponding oligonucleotides of single strands were used. The sequences were 5′-CACGCAACCAGAGAACAAGUU-3′ (sense) and 5′-CUUGUUCUCUGGUUGCGUGUU-3′ (antisense) for the target sequence 5′-AACACGCAACCAGAGAACAAG-3′. siRNA specifically targeting glyceraldehyde-3-phosphate dehydrogenase (*GAPDH*) or scramble siRNA was also obtained from Ambion to serve as controls.

Note: Supplementary data for this article are available at Cancer Research Online (http://cancerres.aacrjournals.org/).

J. Wang, M. Bhutani, and A.K. Pathak contributed equally to this work.

Requests for reprints: Li Mao, Department of Thoracic/Head and Neck Medical Oncology, The University of Texas M. D. Anderson Cancer Center, Box 437, Unit 432, Room FC9.3065, 1515 Holcombe Boulevard, Houston, TX 77030. Phone: 713-792-6363; Fax: 713-792-1220; E-mail: lmao@mdanderson.org.

©2007 American Association for Cancer Research.

doi:10.1158/0008-5472.CAN-07-1337

Bisulfite sequencing of the *RASSF1A* promoter. MSP products were derived from H1299 cells treated with 40 nmol/L siRNA targeting *ΔDNMT3B4/2* or *GAPDH* for 24 h and were recovered by gel purification. The DNA fragments were cloned into a TA cloning vector (Invitrogen) according to the manufacturer's protocol. Plasmid DNA from each clone was then extracted, and inserts in individual clones were sequenced (T3 or T7 primer) using an ABI PRISM 377 DNA sequencer (Perkin-Elmer).

Western blot analysis. Cell lysates were obtained and equal amounts of protein from each sample were diluted with loading buffer, boiled, and loaded onto 7.5% SDS-polyacrylamide gel to be separated by electrophoresis followed by protein transfer to polyvinylidene fluoride membranes (Amersham). Proteins were detected by incubation with corresponding antibodies specific to either DNMT1 or V5 tag (Sigma) followed by blotting with horseradish peroxidase–conjugated secondary antibody (Sigma). The blots were then exposed to chemiluminescent substrate (Amersham) for detection.

Cell growth and cell cycle analyses. The ACEA RT-CES microelectronic cell sensor system (ACEA Biosciences) was used to confirm the number of living cells. The electronic sensors provided a continuous and quantitative measurement of the cell index (which depends on the number of attached

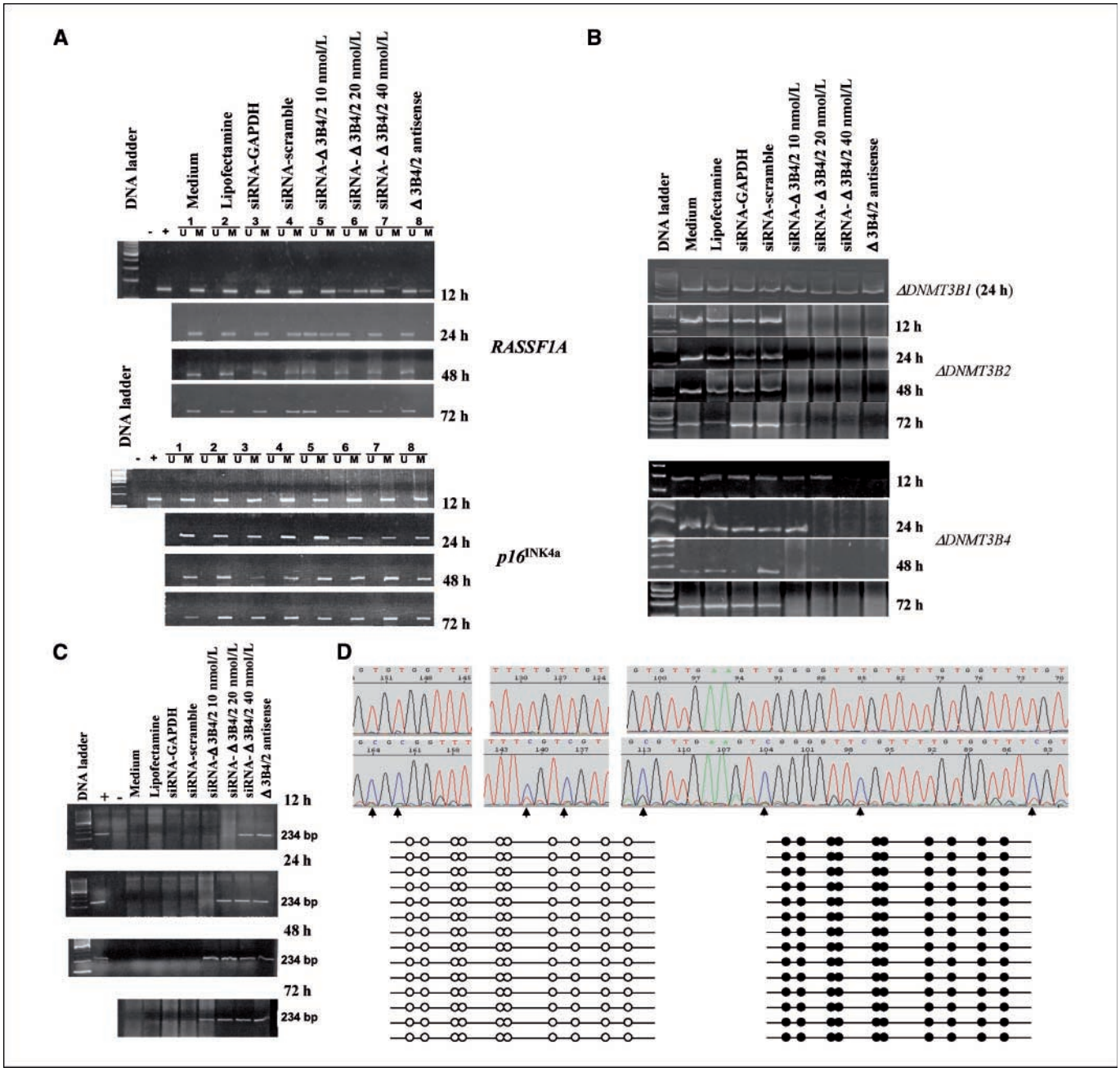


Figure 1. Down-regulation of *ΔDNMT3B4/2* expression and demethylation of *RASSF1A* promoter. *A,* promoter methylation status of *p16* and *RASSF1A* at different time points following treatment as measured by MSP. −, negative control; +, positive control. *U,* unmethylated DNA; *M,* methylated DNA. *B,* expression of *ΔDNMT3Bs* in H1299 cells treated with siRNAs at various time points using RT-PCR. *C,* expression of *RASSF1A* mRNA (234 bp) of the corresponding samples measured by RT-PCR. *D,* methylation status in the *RASS1A* promoter according to bisulfate sequencing analysis. *Arrowheads,* cytosines not converted to thymidines in the CpG sites (*bottom panel of the sequences*) because of the resistance of the methylated cytosines to bisulfate treatment. Line in the figure below the sequences represents a clone. *Open dot,* a CpG site not methylated; *solid dot,* a methylated CpG site. The left set of lines represents clones from cells treated with control, and the right set of lines represents clones from cells treated with siRNA targeting *ΔDNMT3B4/2*.

cells and the shape of the cells) in each well. The cell cycle distribution of the cells was determined using a BD FACSCalibur flow cytometer and CellQuest software (Becton Dickinson).

Stable transfection. pcDNA6/V5-His (Invitrogen) was used to construct plasmids containing full-length *ΔDNMT3B2* or *ΔDNMT3B4*. Empty vector or plasmids containing *ΔDNMT3B2* or *ΔDNMT3B4* were used to transfect HBE1 cells and establish clones with stable expression of the corresponding proteins. Several clones were selected from each transfectant, and passages 5 and 10 were subsequently used for promoter methylation analysis.

Bisulfite pyrosequencing. Pyrosequencing was used to quantitatively measure the levels of cytosine methylation of CpG sites of promoters as described previously (12). The primers used in this study are listed in Supplementary Table S1 and their locations in the CpG islands are presented in Supplementary Fig. S1. Assays were repeated thrice and the means of all experimental results were used with SEs. The quantification of cytosine methylation was performed using Pyro Q-CpG software (Biotage).

Results and Discussion

To test the role of *ΔDNMT3B4* in the promoter-specific methylation of *RASSF1A*, we designed a siRNA that specifically targeted the junction of exons 5 and 7 of *ΔDNMT3B*. Because both *ΔDNMT3B4* and *ΔDNMT3B2* lack exon 6, this siRNA is expected to trigger the degradation of both these transcripts. We used NSCLC cell line H1299 because it carries promoter methylation of both *p16* and *RASSF1A* and expresses a high level of *ΔDNMT3B4* but no detectable *DNMT3B* (10).

We found that down-regulation of *ΔDNMT3B4/2* resulted in *RASSF1A* promoter demethylation in H1299 cells (Fig. 1). In the cells treated with 20 nmol/L or a higher concentration of the siRNA targeting *ΔDNMT3B4/2*, a near complete *RASSF1A* promoter demethylation was observed as early as 12 h after treatment (Fig. 1*A*). This effect was maintained up to 72 h after treatment. The results are consistent with the dose-dependent reduction of *ΔDNMT3B4* expression by the siRNA or antisense treatment (Fig. 1*B*). In contrast, the promoter methylation status of *p16* was not affected (Fig. 1*A*). These results provide the first direct evidence of a causal relationship between ΔDNMT3B4 and the promoter methylation of *RASSF1A* in lung cancer cells.

Consistent with the *RASSF1A* promoter demethylation, *RASSF1A* mRNA expression was restored in the cells also in a dose-dependent manner (Fig. 1*C*). Because MSP is a qualitative assay and cannot reveal the methylation status of each CpG site, we performed bisulfite sequencing of the MSP products from cells with or without *ΔDNMT3B4/2* knockdown. The MSP fragment is a part of the *RASSF1A* promoter and contains 10 CpG sites, excluding the primer sequences. None of the cytosine residues at the 10 CpG sites of the *RASSF1A* promoter fragment were converted to thymidine by bisulfite treatment (an indication of a methylated status) in the 14 individual clones derived from cells without *ΔDNMT3B4/2* knockdown, whereas the cytosine residues at all the 10 CpG sites were converted to thymidine (an indication of an unmethylated status) in all 14 clones derived from cells with *ΔDNMT3B4/2* knockdown (Fig. 1*D*).

In a separate experiment, we used pyrosequencing method to analyze DNA from H1299 cells treated with either 20 nmol/L scramble siRNA control or 20 nmol/L siRNA targeting *ΔDNMT3B4/2* 24 h after treatment. The primers used in this experiment were designed to avoid amplification bias (Supplementary Table S1). We observed that that promoter methylation of *RASSF1A* was decreased from 94% in the control-treated to 33% in the siRNA-treated DNA, whereas no difference was observed in the *p16* promoter between control-treated and the siRNA-treated DNA

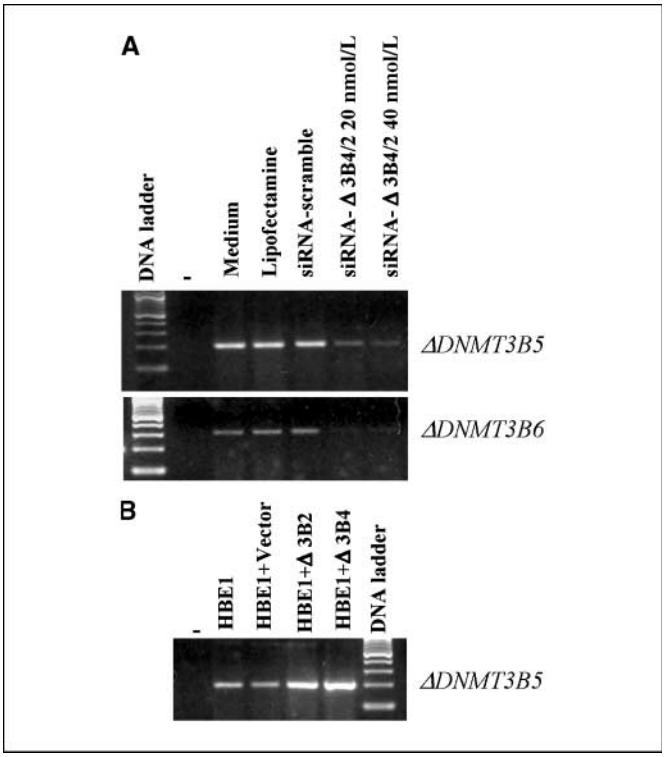


Figure 2. Expression of *ΔDNMT3B5* and *ΔDNMT3B6* following change of *ΔDNMT3B4/2* expression levels. *A,* expression of *ΔDNMT3B5* and *ΔDNMT3B6* in H1299 cells treated with siRNAs measured by RT-PCR. *B,* expression of *ΔDNMT3B5* and *ΔDNMT3B6* in HBE1 cells transfected with *ΔDNMT3B2* or *ΔDNMT3B4*.

(Supplementary Fig. S2). These results indicate that knockdown of *ΔDNMT3B4/2* can reverse the methylated CpG sites in the *RASSF1A* promoter region. Our finding is unlikely due to the inhibition of DNMT1 because the protein expression level was not reduced in the H1299 cells treated with the siRNA (data not shown). To determine whether the *RASSF1A* promoter demethylation due to knockdown of *ΔDNMT3B4/2* is limited to H1299 cells, we performed the same experiments with NSCLC cell line H358. Similar to our results with the H1299 cells, the *RASSF1A* promoter became unmethylated after the siRNA treatment but no effect was observed on the methylated *p16* promoter (data not shown).

To address the issue whether some of the observed results are due to a shift in balance between *ΔDNMT3B4* and other *ΔDNMT3B* isoforms, we also analyzed mRNA expression of *ΔDNMT3B5* and *ΔDNMT3B6* that are expressed in the H1299 cells beside *ΔDNMT3B1* that did not show change in expression levels after siRNA treatment (Fig. 1*A*). Interestingly, the expression of *ΔDNMT3B5* and *ΔDNMT3B6* was reduced in the siRNA-treated samples compared with the controls (Fig. 2*A*). To ensure that the result was not due to nonspecific knockdown by the siRNA, we analyzed the expression of *ΔDNMT3B5* (*ΔDNMT3B6* was not expressed in the cell line) in HBE1 cells transfected with either *ΔDNMT3B2* or *ΔDNMT3B4*. The expression of *ΔDNMT3B5* was increased in the cells transfected with either *ΔDNMT3B2* or *ΔDNMT3B4* compared with controls (Fig. 2*B*). The result indicates that the expression of either *ΔDNMT3B2* or *ΔDNMT3B4* may affect expression levels of *ΔDNMT3B5* and *ΔDNMT3B6*.

We used RT-CES System to determine the dynamic change in cell growth affected by the *ΔDNMT3B4/2* knockout (measured every

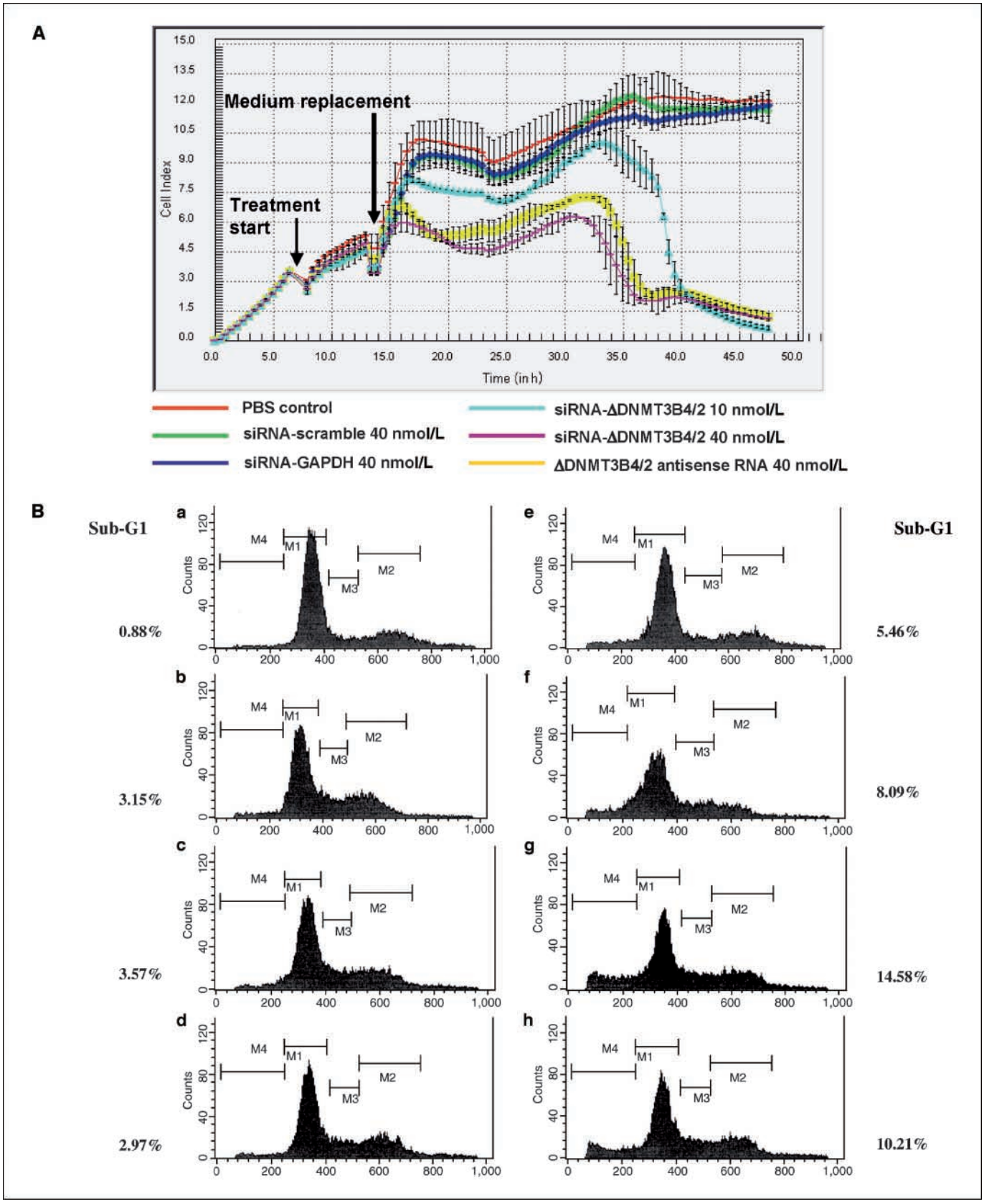
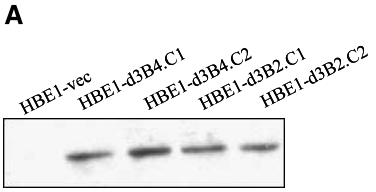


Figure 3. Biological effects of *ΔDNMT3B4/2* down-regulation. *A,* growth of H1299 cells transfected with siRNAs as measured using a microelectronic cell sensor system every 30 min. The representation of individual color lines is indicated and described in the figure. *B,* cell cycle distributions of H1299 cells 24 h after treatment with siRNAs as measured with a flow cytometer (*a*, cells treated with culture medium; *b*, Lipofectamine only; *c*, siRNA targeting *GAPDH; d*, scramble siRNA; *e–g*, 10, 20, and 40 siRNA, respectively; *h*, 40 nmol/L antisense RNA targeting *ΔDNMT3B4/2*). Percentages of sub-G_1 cells were labeled inside each panel.



B

Cell Line	Plasmid	Passage	*MGMT*	*GSTP1*	*p16*	*RASSF1A*	*CDH13*	*PR* A	*PR* B	*Line*
HBE1-vec	vector only	5	4	1	4	15	2	8	30	74
HBE1-vec	vector only	10	3	1	4	15	2	9	29	73
HBE1-d3B4.C1	*ΔDNMT3B4*	10	3	1	8	50	2	8	33	64
HBE1-d3B4.C2	*ΔDNMT3B4*	5	4	1	3	45	1	9	33	70
HBE1-d3B4.C3	*ΔDNMT3B4*	5	4	1	3	46	2	8	31	74
HBE1-d3B4.C4	*ΔDNMT3B4*	5	3	1	3	43	2	8	35	64
HBE1-d3B2.C1	*ΔDNMT3B2*	10	5	1	4	16	3	8	33	76
HBE1-d3B2.C2	*ΔDNMT3B2*	5	5	1	2	19	3	8	34	76
HBE1-d3B2.C3	*ΔDNMT3B2*	5	4	1	3	19	2	8	34	74
Normal DNA	NA		2	1	7	9	6	12	10	84
methylated DNA	NA		93	96	94	89	91	91	89	78

Figure 4. Overexpression of *ΔDNMT3B4* resulted in *RASSF1A* promoter hypermethylation. *A,* expression of recombinant ΔDNMT3B4 and ΔDNMT3B2 in HBE1 clones recognized on Western blots using antibody against V5 tag. *HBE1-vec,* vector only–transfected HBE1 cells. *B,* CpG methylation in promoter regions of six genes and in line sequences. Clones d3B4.C1, d3B4.C2, d3B4.C3, and d3B4.C4 expressed ΔDNMT3B4, and clones d3B2.C1, d3B2.C2, and d3B2.C3 expressed ΔDNMT3B2. The values for the genes represent the approximate percentages of the CpG sites that were methylated as measured by pyrosequencing analysis.

30 min). In the H1299 cells, growth was inhibited at ~10 h after treatment with the siRNA-*ΔDNMT3B4/2* in a dose-dependent manner or with the antisense RNA (Fig. 3*A*). Because the RT-CES System works by measuring the electronic impedance of sensor electrodes integrated on the bottom of microtiter E-plates, factors besides cell numbers, such as morphology and tightness of the cells attached to the culture surface, can affect the reading. The major drop observed 36 h after treatment with the siRNA might reflect to a reduced ability of the cells detaching to the plastic surface. To determine the mechanism by which the growth of the *ΔDNMT3B4/2* knockout is inhibited, we used flow cytometry to examine the cell cycle distribution of the H1299 cells 24 h after treatment. We observed an increase in the sub-G_1 fraction of cells treated with the siRNA-*ΔDNMT3B4/2* in a dose-dependent manner or with the antisense RNA (Fig. 3*B*). These results suggest that treatment with siRNA-*ΔDNMT3B4/2* increased apoptosis.

To provide direct evidence to support the possibility that *ΔDNMT3B4* but not *ΔDNMT3B2* contributed to the differential regulation of *RASSF1A* promoter methylation, we constructed mammalian expression plasmids containing *ΔDNMT3B2* or *ΔDNMT3B4* and used HBE1 cells (immortalized, normal-appearing bronchial epithelial cells from a patient with NSCLC; ref. 13). Stable clones expressing *ΔDNMT3B2* or *ΔDNMT3B4* were established (Fig. 4*A*). At passages 5 and 10, we used the quantitative pyrosequencing method to analyze the promoter methylation status of the genes *MGMT, GSTP1, p16, RASSF1A, CDH13*, and *PR* (two regions) in the HBE1 cells transfected with empty vector only, *ΔDNMT3B2*, or *ΔDNMT3B4*. Consistent with our hypothesis that *ΔDNMT3B4* but not *ΔDNMT3B2* contributed to the differential regulation of *RASSF1A* promoter methylation, cells transfected with *ΔDNMT3B4*, but not cells transfected with the empty vector or *ΔDNMT3B2*, showed substantially increased DNA methylation in the *RASSF1A* promoter compared with vector control ($P < 0.001$, Kruskal-Wallis test; Fig. 4*B*). No change in methylation status was observed in any of the other promoters for any of the transfectants (Fig. 4*B*).

Our findings suggest a mechanism for the development of "tissue-specific DNA methylation." This term refers to different promoters being methylated in different cell types or organs during development and tumorigenesis (14). In somatic cells, most of the CpG sites in genomic DNA are methylated except in CpG-enriched promoter regions (CpG islands) of the transcriptionally active genes. The maintenance of established DNA methylation patterns is largely performed by DNMT1, which is constitutively expressed in somatic tissues. The expression of DNMT3B is low or absent in somatic tissues but significantly increased in transformed cancer cells and is thought to be critical to *de novo* promoter methylation (15). During tumorigenesis, *de novo* DNA methylation occurs in the promoters of selected genes and contributes to their functional inactivation by suppressing the expression of those genes. Global analysis of promoter methylation has revealed several abnormally methylated promoters found in tumors but not in normal tissue counterparts (16). However, each tumor exhibits a unique pattern of methylated promoters, although some promoters are commonly methylated in certain tumor types. These observations indicate the presence of cellular mechanisms, which result in differential promoter methylation that is maintainable during tumor development and progression.

In a previous study, we found a statistically significant correlation between *RASSF1A* promoter methylation and *ΔDNMT3B4* expression in a large number of primary NSCLC tumors (11). That result provided *in vivo* evidence of a role for *ΔDNMT3B4* in regulating the methylation of CpG islands in a promoter-specific manner. The results presented in the current report provide enough direct evidence to establish the causal relationship between *ΔDNMT3B4* and *RASSF1A* promoter methylation but not between several other commonly methylated promoters we examined. In the siRNA-based experiment, the down-regulation of *ΔDNMT3B4* resulted in demethylation of the *RASSF1A* promoter but not the *p16* promoter in two NSCLC cell lines. Because the siRNA used also knocked down *ΔDNMT3B2* (because of the shared exon-exon junction between *ΔDNMT3B2* and *ΔDNMT3B4*), a role for *ΔDNMT3B2* in that process cannot be excluded. The experiments using HBE1 cells that express specific *ΔDNMT3B* variants (*ΔDNMT3B2* or *ΔDNMT3B4*) provided conclusive evidence that *ΔDNMT3B4* but not *ΔDNMT3B2* contributes to *RASSF1A*-specific promoter methylation. Although expression levels of *ΔDNMT3B4* may affect expression levels of *ΔDNMT3B5* and *ΔDNMT3B6*, the expression of the later isoforms is unlikely contributed to *RASSF1A* promoter methylation because overexpressing *ΔDNMT3B2* also caused an increased expression of *ΔDNMT3B5* (Fig. 3*B*) but did not affect the methylation status of *RASSF1A* promoter (Fig. 4*B*).

Although our study results firmly establish the importance of ΔDNMT3Bs in promoter-specific methylation, the detailed mechanisms are unknown. DNMT1 is the predominant cellular DNA methyltransferase, but it requires the participation of DNMT3B to achieve promoter methylation (17, 18). Because DNMT3Bs contain a PWWP domain, which has direct DNA-binding capability (19), the fact that there are ΔDNMT3Bs with structural differences at and around the PWWP domain suggests that the ΔDNMT3B variants interact with a class of promoters with a similar consensus sequence and are responsible for the methylation of the promoters. The recent finding that tumor-specific methylated genes have common sequence motifs in their promoters (20) supports this notion. It should be noted that, in our study, overexpression of ΔDNMT3B4 in the HBE1 cells resulted in only partial methylation of the *RASSF1A* promoter; this observation indicates that an additional component or components are needed for the stable and complete methylation of the promoter. Alternatively, the peptide tags fused with ΔDNMT3B4 may cause changes in protein folding and result in reduced efficiency of the protein.

Our findings place ΔDNMT3Bs at the center of *de novo* promoter methylation, particularly in lung tumorigenesis. The promoter-specific demethylation we observed is particularly interesting for cancer therapy because it raises the possibility of inhibiting specific variants of ΔDNMT3B to selectively activate critical tumor suppressor genes whose expression is down-regulated due to promoter methylation. Such an approach may lead to the development of novel therapeutic strategies tailored to individual tumors with particular epigenetic abnormalities. These strategies would cause limited adverse effects because normal tissue would be spared most of the effects of less targeted treatment on the promoters methylated.

Acknowledgments

Received 4/11/2007; revised 8/30/2007; accepted 10/5/2007.

Grant support: Department of Defense grants DAMD17-01-1-01689-1 and W81XWH-05-2-0027.

The costs of publication of this article were defrayed in part by the payment of page charges. This article must therefore be hereby marked *advertisement* in accordance with 18 U.S.C. Section 1734 solely to indicate this fact.

We thank Elizabeth L. Hess for scientific editing of the manuscript.

References

1. Surani MA. Imprinting and the initiation of gene silencing in the germline. Cell 1998;93:309–12.
2. Monk M, Boubelik M, Lehnert S. Temporal and regional changes in DNA methylation in the embryonic, extra-embryonic, and germ cell lineages during mouse embryo development. Development 1987;99:371–82.
3. Okano M, Xie S, Li E. Cloning and characterization of a family of novel mammalian DNA (cytosine-5) methyltransferases. Nat Genet 1998;19:219–20.
4. Jones PA, Baylin SB. The fundamental role of epigenetic events in cancer. Nat Rev Genet 2002;3:415–28.
5. Okano M, Bell DW, Haber DA, Li E. DNA methyltransferases Dnmt3a and Dnmt3b are essential for *de novo* methylation and mammalian development. Cell 1999;99:247–57.
6. Robertson KD, Uzvolgyi E, Liang G, et al. The human DNA methyltransferases (DNMTs) 1, 3a and 3b: coordinate mRNA expression in normal tissues and overexpression in tumors. Nucleic Acids Res 1999;27:2291–8.
7. Saito Y, Kanai Y, Sakamoto M, Saito H, Ishii H, Hirohashi S. Overexpression of a splice variant of DNA methyltransferase 3b, DNMT3b4, associated with DNA hypomethylation on pericentromeric satellite regions during human hepatocarcinogenesis. Proc Natl Acad Sci U S A 2002;99:10060–5.
8. Yakushiji T, Uzawa K, Shibahara T, Noma H, Tanzawa H. Over-expression of DNA methyltransferases and CDKN2A gene methylation status in squamous cell carcinoma of the oral cavity. Int J Oncol 2003;22:1201–7.
9. Sato M, Horio Y, Sekido Y, Minna JD, Shimokata K, Hasegawa Y. The expression of DNA methyltransferases and methyl-CpG-binding proteins is not associated with the methylation status of p14(ARF), p16(INK4a) and RASSF1A in human lung cancer cell lines. Oncogene 2002;21:4822–9.
10. Wang L, Wang J, Sun S, et al. A novel DNMT3B subfamily, ΔDNMT3B, is the predominant form of DNMT3B in non-small cell lung cancer. Int J Oncol 2006;29:201–7.
11. Wang J, Walsh G, Liu DD, Lee JJ, Mao L. Expression of ΔDNMT3B variants and its association with promoter methylation of p16 and RASSF1A in primary non-small cell lung cancer. Cancer Res 2006;66:8361–6.
12. Issa JP, Gharibyan V, Cortes J, et al. Phase II study of low-dose decitabine in patients with chronic myelogenous leukemia resistant to imatinib mesylate. J Clin Oncol 2005;23:3948–56.
13. Ramirez RD, Sheridan S, Girard L, et al. Immortalization of human bronchial epithelial cells in the absence of viral oncoproteins. Cancer Res 2004;64:9027–34.
14. Kitamura E, Igarashi J, Morohashi A, et al. Analysis of tissue-specific differentially methylated regions (TDMs) in humans. Genomics 2006;89:326–37.
15. Liu K, Wang YF, Cantemir C, Muller MT. Endogenous assays of DNA methyltransferases: evidence for differential activities of DNMT1, DNMT2, and DNMT3 in mammalian cells *in vivo*. Mol Cell Biol 2003;23:2709–19.
16. Hatada I, Fukasawa M, Kimura M, et al. Genome-wide profiling of promoter methylation in human. Oncogene 2006;25:3059–64.
17. Rhee I, Bachman KE, Park BH, et al. DNMT1 and DNMT3b cooperate to silence genes in human cancer cells. Nature 2002;416:552–6.
18. Kim GD, Ni J, Kelesoghu N, Roberts RJ, Prodham S. Co-operation and communication between the human maintenance and *de novo* DNA methyltransferases. EMBO J 2002;21:4183–95.
19. Qiu C, Sawada K, Zhang X, Cheng X. The PWWP domain of mammalian DNA methyltransferase Dnmt3b defines a new family of DNA-binding folds. Nat Struct Biol 2002;9:217–24.
20. Keshet I, Schlesinger Y, Farkash S, et al. Evidence for an instructive mechanism of *de novo* methylation in cancer cells. Nat Genet 2006;38:149–53.

Value of *p16*^{INK4a} and *RASSF1A* Promoter Hypermethylation in Prognosis of Patients with Resectable Non–Small Cell Lung Cancer

Jie Wang,[1,3] J. Jack Lee,[2] Luo Wang,[1] Diane D. Liu,[2] Charles Lu,[1] You-Hong Fan,[1] Waun Ki Hong,[1] and Li Mao[1]

[1]Department of Thoracic/Head and Neck Medical Oncology, and the [2]Department of Biostatistics, The University of Texas M. D. Anderson Cancer Center, Houston, Texas; and [3]Department of Oncology, Beijing University School of Oncology, Beijing Cancer Hospital, Beijing Institution of Cancer Research, Beijing, China

ABSTRACT

The *p16*^{INK4a} and *RASSF1A* are tumor suppressor genes frequently inactivated by *de novo* promoter hypermethylation in non-small cell lung cancer. We studied 119 patients with non-small cell lung cancer (70 stage I/II and 49 stage IIIA) who had undergone surgery with curative intent. The *p16*^{INK4a} and *RASSF1A* promoter methylation statuses were determined by methylation-specific PCR. Statistical analyses, all two-sided, were performed to determine the prognostic effect of hypermethylation on various clinical parameters. Hypermethylation of the *p16*^{INK4a} and *RASSF1A* promoters was found in 58 (49%) and 46 (39%) tumors, respectively, and 30 tumors (25%) exhibited hypermethylation of both gene promoters. In patients with stage I/II tumors, only *p16*^{INK4a} promoter hypermethylation was associated with a poor 5-year overall survival rate ($P = 0.002$). In patients with stage IIIA disease, however, *RASSF1A* promoter hypermethylation was a stronger predictor of a poor 5-year overall survival rate ($P < 0.0001$) than *p16*^{INK4a} promoter hypermethylation. Among the 49 patients with stage IIIA tumors, 16 (89%) of the 18 patients whose tumors showed *RASSF1A* promoter hypermethylation died within 3 years after surgery, as compared with only 12 (39%) of the 31 patients whose tumors had no *RASSF1A* promoter hypermethylation ($P < 0.0001$). Multivariate analysis indicated that *RASSF1A* promoter hypermethylation was the stronger independent predictor for survival in patients with locally advanced non-small cell lung cancer. Our results indicate that *p16*^{INK4a} promoter hypermethylation predicts a poor 5-year survival rates for patients with resectable non-small cell lung cancer, particularly for those with early stage tumors, whereas *RASSF1A* promoter hypermethylation is a profound prognostic predictor for patients with locally advanced non-small cell lung cancer, suggesting an important role of *RASSF1A* in non-small cell lung cancer progression.

INTRODUCTION

Non–small cell lung cancer constitutes 80% of all primary lung cancers, which are the leading cause of cancer-related death in both men and women in the United States (1). Despite advances in the treatment of the disease over the past two decades, the prognosis of patients with non-small cell lung cancer has improved only modestly, with the 5-year overall survival rate increasing from 11% in the 1970s to 15% in the late 1990s (2). Patients with early stage non-small cell lung cancer generally have a better survival than those with advanced-stage tumors. For example, patients with stage I non-small cell lung cancer are expected to have an approximate 60% 5-year overall survival rate after surgical resection of their primary tumors, whereas those with stage IIIA disease have an estimated 25% 5-year overall survival rate after surgery followed by radiation with or without chemotherapy.

Biological features of non-small cell lung cancer are determined by underlying molecular alterations of the tumors, including inactivation of the tumor suppressor genes (3–5). Besides mutations and deletions of genes, it is now clear that *de novo* promoter hypermethylation is a common mechanism to inactivate tumor suppressor genes (6–8). The *p16*^{INK4a} tumor suppressor gene located on 9p21 encodes a cyclin-dependent kinase inhibitor important for G_1 cell cycle arrest (9, 10). Promoter hypermethylation of the gene has been observed frequently early in lung carcinogenesis, including in individuals exposed to tobacco carcinogens but without evidence of cancer (11–13). The *RASSF1A* tumor suppressor gene is located at 3p21, a region frequently deleted in non-small cell lung cancer (14). Another common mechanism to inactivate *RASSF1A* is promoter hypermethylation of the gene (15–17). RASSF1A has been shown to bind to the Ras-GTP binding protein Nore1, consistent with its role as a negative effector of Ras oncoprotein (18). In contrast to *p16*^{INK4a}, which is inactivated early in lung carcinogenesis (13, 19), hypermethylation of the *RASSF1A* promoter occurs relatively late (20), suggesting *RASSF1A* might be important in non-small cell lung cancer progression.

Because of the difference in timing between methylation of the *p16*^{INK4a} and *RASSF1A* promoters in lung carcinogenesis, we wanted to determine the clinical impact of these abnormal-

Received 4/4/04; revised 5/28/04; accepted 6/15/04.
Grant support: Department of Defense Grant DAMD17-01-1-0689-1 and National Cancer Institute Grants PO1 CA91844, UO1 CA86390, and P30 CA 16672. J. Wang is a recipient of the Oncology Research Faculty Development Award, National Cancer Institute (USA).
The costs of publication of this article were defrayed in part by the payment of page charges. This article must therefore be hereby marked *advertisement* in accordance with 18 U.S.C. Section 1734 solely to indicate this fact.
Requests for reprints: Li Mao, Department of Thoracic/Head and Neck Medical Oncology, Unit 432, The University of Texas M. D. Anderson Cancer Center, 1515 Holcombe Boulevard, Houston, TX 77030. Phone: (713) 745-6363; Fax: (713) 796-8655; E-mail: lmao@mdanderson.org.
©2004 American Association for Cancer Research.

ities alone or in combination on patients with non-small cell lung cancer. We studied the primary tumors from 119 patients with surgically respectable, stage I-IIIA non-small cell lung cancer for their *p16*^{INK4a} and *RASSF1A* promoter methylation status for associations between the methylation status and clinical parameters.

MATERIALS AND METHODS

Study Population. One hundred nineteen patients who were diagnosed with pathological stage I to IIIA non-small cell lung cancer and had undergone lobectomy or pneumonectomy for complete resection of their primary tumors at The University of Texas M. D. Anderson Cancer Center between 1994 and 2001 were included in the study. The selection of these patients was based on available fresh tumor tissues and corresponding normal lung tissues. The clinical information and follow-up data were based on chart review and on reports from our Tumor Registry Medical Informatics. Informed consent for the use of residual resected tissues for research was obtained from all of the patients in the study. The study was reviewed and approved by the Surveillance Committee of the institution. None of the patients with stage I or stage II disease received adjuvant chemotherapy or radiotherapy before or after surgery. Among 49 patients with stage IIIA disease, 5 received preoperative chemotherapy or chemoradiotherapy, 20 received postoperative concurrent chemoradiotherapy, 17 received postoperative radiotherapy alone, 2 received postoperative chemotherapy alone, and 5 received no additional treatment.

DNA Extraction and Methylation-Specific PCR. Frozen tissues were homogenized, and genomic DNA was extracted by digestion of the homogenized tissues in a buffer containing 50 mmol/L Tris-HCl (pH 8.0), 1% SDS, and 0.5 mg/ml proteinase K at 42°C for 36 hours. The digested products were purified with phenyl-chloroform twice. DNA was then precipitated using the EtOH precipitation method and recovered in distilled DNase-free water.

For the methylation-specific PCR, 1 μg of genomic DNA from each tissue sample was used in the initial step of chemical modification. Briefly, DNA was denatured by NaOH and treated with sodium bisulfite (Sigma Chemical Co., St. Louis, MO). After purification with Wizard DNA purification resin (Promega Corp., Madison, WI), the DNA was treated again with NaOH. After precipitation, DNA was recovered in water and prepared for PCR using specific primers for either the methylated or the unmethylated *p16*^{INK4a} or *RASSF1A* promoter: p16-MAS (5′-ACCCGAC-CCCGAACCGCGACCGTAA-3′) and p16-MS (5′-TTATTAGAGGGTGGGGCGGATCG-CGTGC-3′) for the methylated *p16*^{INK4a} promoter; p16-UAS (5′-CAAC-CCCAAACCACAA-CCATAA-3′) and p16-US (5′-TTATTA-GAGGGTGGGGTGGATTGT-3′) for the unmethylated *p16*^{INK4a} promoter; RASSF1A-MAS (5′-GCTAACAAACGCGAACCG-3′) and RASSF1A-MS (5′-GGGTTTTGCGAGAGCGCG-3′) for the methylated *RASSF1A* promoter; and RASSF1A-UAS (5′-CACTAACAAACACAAACC-3′) and RASSF1A-US (5′-GGTTTTTGTGAGAGTGTGTT-TAG-3′) for the unmethylated *RASSF1A* promoter. PCR was carried out in 25 μL containing about 100 ng of modified DNA, 3% dimethyl sulfoxide, all four deoxynucleoside triphosphates (each at 200 μM), 1.5 mmol/L $MgCl_2$, 0.4 μM PCR primers, and 1.25 units of HotStar Taq DNA polymerase (Qiagen, Inc., Valencia, CA). DNA was amplified in 500-μl plastic tubes for 35 cycles at 94°C for 30 seconds, 56 to 64°C for 45 seconds, and 72°C for 60 seconds followed by a 5-minute extension at 72°C in a temperature cycler (Hybaid, Omnigene, Woodbridge, NJ). PCR products were separated on 2.5% agarose gels and visualized after staining with ethidium bromide. For each DNA sample, primer sets for methylated DNA and unmethylated DNA were used for analysis. CpGenomeTM universal methylated DNA (Chemicon International, Temecula, CA) was used as a positive control, and water replacing for DNA was used as blank controls. The hypermethylation status was determined by visualizing a 150-bp PCR product for the *p16*^{INK4a} promoter and a 169-bp PCR product for the *RASSF1A* promoter with the respective methylation-specific primer sets. All PCRs were repeated twice, and the results were reproducible.

Statistical Analysis. The χ^2 test or Fisher's exact test were used to test the association between categorical variables. The Cochran-Armitage trend test was used to test the trend of methylation among differentiation levels. Overall survival, disease-specific survival (*i.e.,* survival rates among people who died of lung cancer-related causes specifically), and disease-free survival (*i.e.,* recurrence, metastasis, or cancer death was considered an event) were analyzed. Survival probability was estimated using the Kaplan-Meier method. The log-rank test was used to compare survival times among groups. Cox regression was used to model the risks of *p16*^{INK4a} and/or *RASSF1A* promoter hypermethylation on survival time, with adjustment for clinical and histopathologic parameters (age, sex, tumor histology, tumor size, smoking status, and adjuvant treatment). All statistical tests were two-sided, and $P < 0.05$ was considered statistically significant.

RESULTS

Clinical characteristics of all patients enrolled in the study are summarized in Table 1. At the censor date of November 14, 2003, the median follow-up period was 51 months (range, 16 to 130 months). Of the 70 patients with stage I or stage II disease, 29 (41%) were still alive, 35 (50%) died of lung cancer, and 6 (9%) died of unrelated causes. No significant difference in 5-year overall, disease-specific, and disease-free survival rates were observed by tumor stage, gender, smoking status, differentiation status, and histologic subtype in this patient group. Among the 49 patients with stage IIIA disease, 18 (37%) were still alive, 29 (59%) died of lung cancer, and 2 (4%) died of unrelated causes. In this group of patients, smokers had significantly poorer 5-year survival rates than the nonsmokers did ($P = 0.047$, $P = 0.03$, and $P = 0.03$ for 5-year overall, disease-specific, and disease-free survival rates, respectively). Thirty-five (71%) of the 49 patients received postoperative radiotherapy with (26 patients, including 5 with preoperative chemotherapy) or without (9 patients) concomitant chemotherapy, whereas 14 patients received no adjuvant therapy after surgery.

Promoter methylation was detected in 58 (49%) and 46 (39%) of the tumor tissue for the *p16*^{INK4a} and *RASSF1A* promoters, respectively, compared with 13 (11%, including 4

Table 1 Characteristics of patients and tumors

	$p16^{INK4a}$ promoter methylation		*RASSF1A* promoter methylation		
	Absent	Present	Absent	Present	Total
Patients	58 (49%)	61 (51%)	73 (61%)	46 (39%)	119 (100%)
Gender*					
Female	23 (49%)	24 (51%)	33 (70%)	14 (30%)	47 (39%)
Male	38 (53%)	34 (47%)	40 (56%)	32 (44%)	72 (61%)
Mean age (±SD) (y)	65.0 ± 10.9	63.5 ± 9.1	65.1 ± 10.2	63.0 ± 9.9	64.3 ± 10.1
Smoking status					
Nonsmoker	22 (58%)	16 (42%)	25 (66%)	13 (34%)	38 (32%)
Smoker	39 (48%)	42 (52%)	48 (59%)	33 (41%)	81 (68%)
Histologic type					
Adenocarcinoma	34 (57%)	26 (43%)	40 (67%)	20 (33%)	60 (50%)
Squamous cell carcinoma	23 (47%)	26 (53%)	27 (55%)	22 (45%)	49 (41%)
Large cell carcinoma	2 (29%)	5 (71%)	6 (86%)	1 (14%)	7 (6%)
Other	2 (67%)	1 (33%)	0 (0%)	3 (100%)	3 (3%)
Differentiation†					
Well	5 (45%)	6 (55%)	9 (82%)	2 (18%)	11 (9%)
Moderate	25 (50%)	25 (50%)	32 (64%)	18 (36%)	50 (42%)
Poor	31 (53%)	27 (47%)	32 (55%)	26 (45%)	58 (49%)
Stage					
I and II	37 (53%)	33 (47%)	42 (60%)	28 (40%)	70 (59%)
IIIA	24 (49%)	25 (51%)	31 (63%)	18 (37%)	49 (41%)
Stage I and II, 5-y overall survival	61.7%	28.3%	50.6%	41.1%	46.5%
Stage III, 5-y overall survival	53.5%	10.8%	45.6%	0%	30.8%

* Subset analysis indicated that male patients had a higher rate of *RASSF1A* promoter methylation than females in stage IIIa group ($P = 0.03$).

† Subset analysis indicated that poorly differentiated tumors had a higher rate of *RASSF1A* promoter methylation than well or moderately differentiated tumors in stage IIIa group ($P = 0.04$).

samples whose corresponding tumors lacked methylation of the $p16^{INK4a}$ promoter) and 4 (3%) in the corresponding normal-appearing lung tissues ($P < 0.0001$). Unmethylated promoters of $p16^{INK4a}$ and *RASSF1A* were detected in all of the normal-appearing lung tissues and in 60% of tumor tissues, most likely because of the presence of normal cells in the tumor samples. Examples of methylation-specific PCR results are shown in Fig. 1. The undetectable unmethylated promoter in some of the tumors might be because of highly enriched tumor cells in the tissues or the relatively low sensitivity of our assay to pick up small quantities of unmethylated molecules. In patients with stage I or stage II non-small cell lung cancer, tumors with methylation of the $p16^{INK4a}$ promoter had a higher frequency of *RASSF1A* promoter methylation than those without $p16^{INK4a}$ promoter methylation, 58% *versus* 24% ($P = 0.005$), suggesting that *RASSF1A* promoter methylation tends to occur in tumors with $p16^{INK4a}$ promoter methylation because *RASSF1A* promoter methylation occurs late in lung carcinogenesis (20).[4] However, this association was not significant in tumors from patients with stage IIIA disease (44% *versus* 29%; $P = 0.28$). Altogether, 30 tumors (25%; 19 stage I/II stage IIIA) showed concomitant methylation of both $p16^{INK4a}$ and *RASSF1A* promoters.

We analyzed the potential association between the methylation status of $p16^{INK4a}$ and *RASSF1A* promoters and sex, age, smoking history, histology, differentiation, and tumor stage. *RASSF1A* promoter methylation was more frequently observed in poorly differentiated tumors (50%) than in moderately differentiated (26%) or in well-differentiated tumors (0%; $P = 0.04$) from patients with stage IIIA non-small cell lung cancer, but there was no such association in tumors from patients with

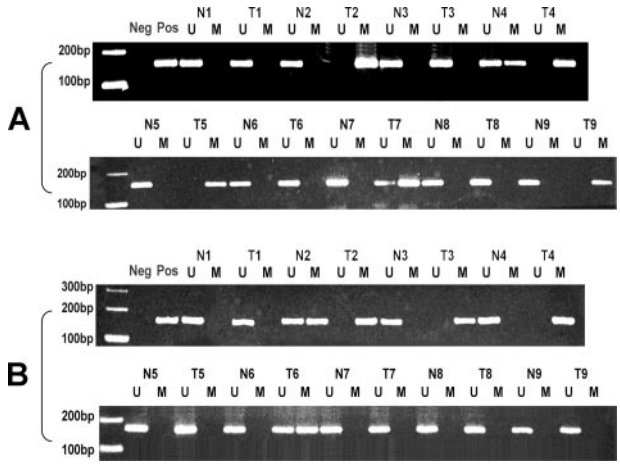


Fig. 1 Examples of promoter methylation status measured using methylation-specific PCR. *A*, PCR products of methylated or unmethylated $p16^{INK4a}$ promoter from primary non-small cell lung cancer and corresponding normal lung tissues. *B*, PCR products of methylated or unmethylated *RASSF1A* promoter from primary non–small cell lung cancer and corresponding normal lung tissues. Molecular weight markers are listed on left side. (*Neg*, negative controls using ummethylated DNA; *Pos*, positive controls using methylated DNA and methylation-specific primer sets; *T*, primary tumors; *N*, corresponding normal lung tissues; *U*, unmethylated promoter; *M*, methylated promoter.)

[4] L. Mao, unpublished data.

stage I/II disease ($P = 0.48$). Additionally, tumors from male patients with stage IIIA non-small cell lung cancer exhibited a significantly higher frequency of *RASSF1A* promoter methylation (47%) than did those from female patients (13%; $P = 0.03$).

We then analyzed the effect of $p16^{INK4a}$ and *RASSF1A* promoter methylation on the survival of the patient. Because stage IIIA patients often received adjuvant treatment after surgery, whereas stage I/II patients received only surgery, we analyzed the two groups separately. In the stage I/II group, patients whose tumors contained $p16^{INK4a}$ promoter methylation had significantly poorer 5-year overall, disease-specific, and disease-free survival rates ($P = 0.002$, $P = 0.0005$, and $P = 0.0006$, respectively) than did patients whose tumors had no $p16^{INK4a}$ promoter methylation (Fig. 2, *A–C*). However, the association between the *RASSF1A* promoter methylation status and 5-year survival rates was not statistically significant ($P = 0.09$, $P = 0.07$, and $P = 0.07$, respectively; Fig. 2, *D–F*). Multivariate analysis, including clinical parameters and promoter methylation status, indicated that $p16^{INK4a}$ promoter methylation was the only independent predictor of 5-year overall, disease-specific, and disease-free survivals. In patients with stage IIIA disease, in contrast to those with stage I/II tumors, the *RASSF1A* promoter methylation status was strongly associated with 5-year overall, disease-free, and disease-specific survivals ($P < 0.0001$, $P < 0.0001$, and $P = 0.0006$, respectively; Fig. 3, *A–C*), as was the $p16^{INK4a}$ promoter methylation status ($P = 0.003$, $P = 0.002$, and $P = 0.01$, respectively; Fig. 3, *D–F*). Although both *RASSF1A* and $p16^{INK4a}$ promoter methylation status were independent predictors of survival, *RASSF1A* was a stronger predictor for 5-year overall, disease-specific, and disease-free survival (hazard ratio = 4.76, $P < 0.0001$; hazard ratio = 6.29, $P < 0.0001$; and hazard ratio = 3.41, $P = 0.0007$ *versus* hazard ratio = 2.89, $P = 0.007$; hazard ratio = 3.16, $P = 0.005$, and hazard ratio = 2.36, $P = 0.02$, respectively).

To determine whether *RASSF1A* inactivation might have an added biological value in patients whose tumors also carried $p16^{INK4a}$ promoter methylation, we analyzed the 5-year survival rates of the group whose tumors had methylation of both gene promoters. In patients with stage I/II disease, the 5-year survival rates of patients whose tumors had methylation of both promot-

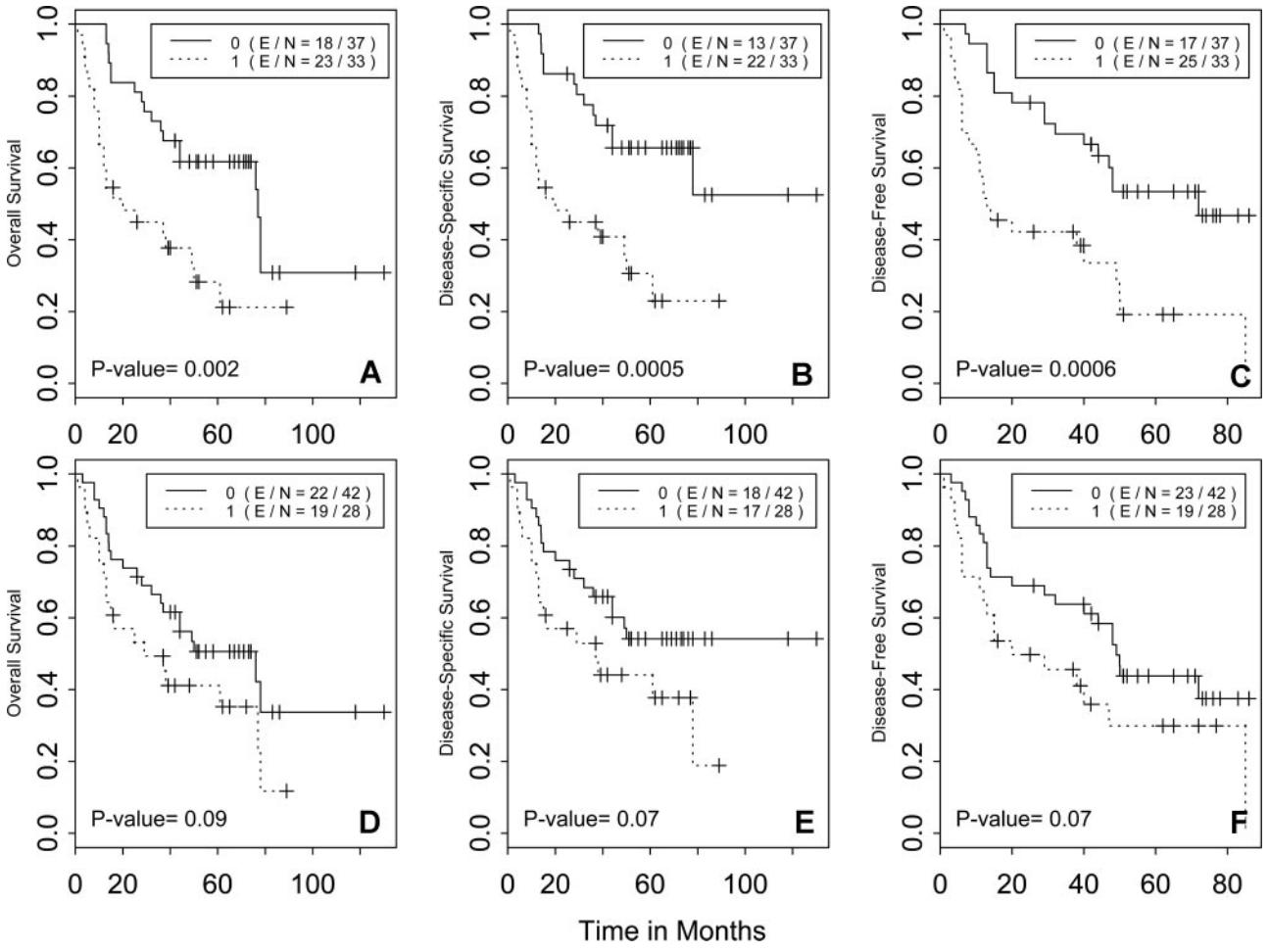


Fig. 2 Association between the $p16^{INK4a}$ promoter methylation status (*A–C*) or *RASSFIA* promoter methylation status (*D–F*) and overall, disease-specific, and disease-free survival in patients with stage I/II non–small cell lung cancer. (*0*, groups without methylation of promoter; *1*, groups with methylation of promoter; *E/N*, number of events/total number in each group.)

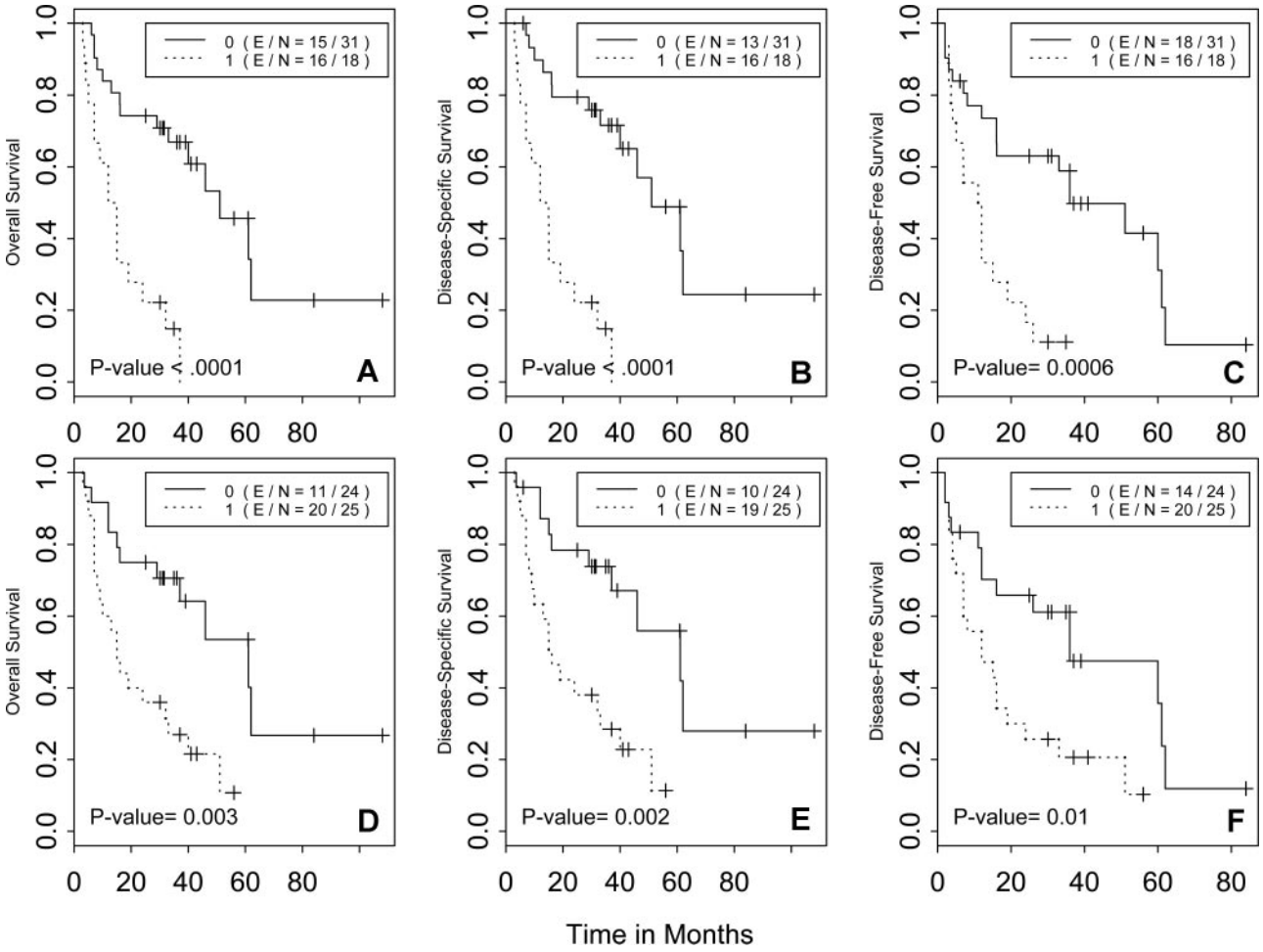


Fig. 3 Association between the *RASSFIA* promoter methylation status (*A–C*) or *p16*^{INK4a} promoter methylation status (*D–F*) and overall, disease-specific, and disease-free survival in patients with stage IIIA non–small cell lung cancer. (*0*, groups without methylation of promoter; *1*, groups with methylation of promoter; *E/N*, number of events/total number in each group.)

ers were significantly worse than in patients whose tumors had no promoter methylation or methylation of only one promoter ($P = 0.01$, $P = 0.005$, and $P = 0.005$, respectively, for 5-year overall, disease-specific, and disease-free survival rates; Fig. 4, *A–C*). Although the number of patients was small in the stage IIIA group, the association between patients whose tumors had methylation of both promoters and poor survivals was striking (Fig. 4, *D–F*). All 11 patients (100%) in this category died of lung cancer within 3 years after surgery, whereas 13 (62%) of the 21 stage IIIA patients whose tumors had methylation of only one promoter died of lung cancer in 5 years, and only 5 (29%) of the 17 patients whose tumors had no promoter methylation died of lung cancer in 6.5 years ($P < 0.0001$ by log-rank test; Fig. 4*F*).

Because 35 (71%) of the 49 patients with stage IIIA tumors received postoperative radiotherapy and 26 (53%) of the patients received adjuvant chemotherapy, we wanted to determine whether these treatments had affected the predictive value of the methylation markers. Despite the small sample size, *RASSF1A* promoter methylation status remained a predictor of overall survival in radiotherapy and nonradiotherapy groups ($P = 0.0004$ and $P = 0.008$, respectively, for overall survival) as well as in chemotherapy and nonchemotherapy groups ($P = 0.001$ and $P = 0.01$, respectively, for overall survival).

DISCUSSION

The *p16*^{INK4a} is frequently inactivated in non-small cell lung cancer through various mechanisms, including promoter hypermethylation (8, 11, 12, 21), but not in small cell lung cancers, which often have an inactivated retinoblastoma tumor suppressor gene. The reported frequencies of *p16*^{INK4a} promoter hypermethylation in primary non-small cell lung cancer have been 25 to 63% (12, 22–24). The *p16*^{INK4a} promoter hypermethylation is an early event in lung carcinogenesis even in bronchial epithelial cells chronically exposed to tobacco carcinogens (13). RASSF1A contains an RAS-associated domain, which interacts with the RAS oncoprotein to promote cellular apoptosis as well as to inhibit cyclin D1 accumulation (25, 26), and a putative ataxia telangiectasia, mutated kinase phosphoryl-

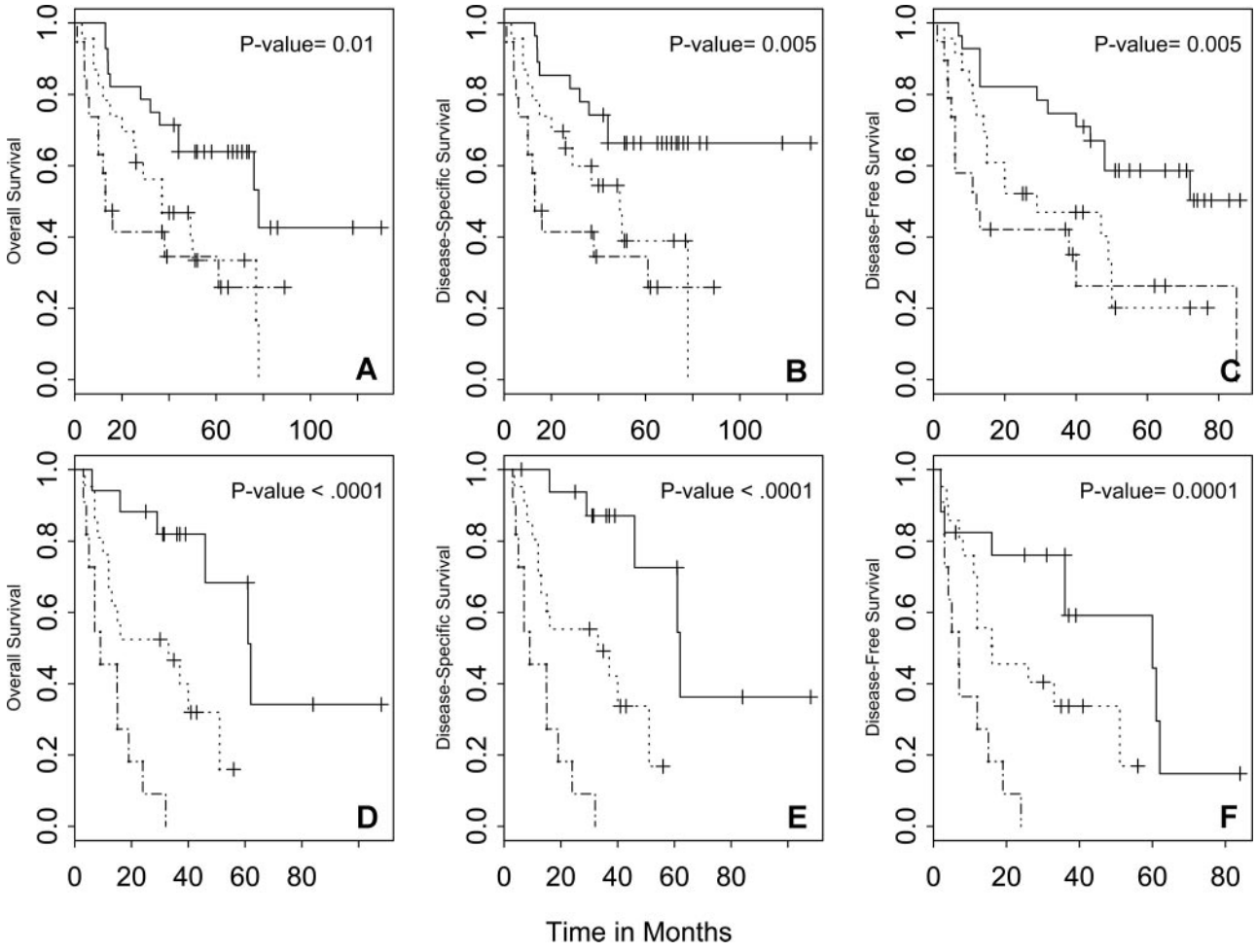


Fig. 4 Association between the *p16*^{INK4a} promoter methylation status and/or *RASSFIA* promoter methylation status and overall survival in patients with stage I/II (*A–C*) or stage IIIA (*D–F*) non–small cell lung cancer. *Solid line* indicates groups without promoter methylation [number of events/total in group (*E/N*): 12 of 28 for *A*; 9 of 28 for *B*; 12 of 28 for *C*; 6 of 17 for *D*; 5of 17 for *E*; and 9 of 17 for *F*]; *dotted line* indicates groups with methylation of the *p16*^{INK4a} or the *RASSF1A* promoter (*E/N*: 16 of 23 for *A*; 13 of 23 for *B*; 16 of 23 for *C*; 14 of 21 for *D*; 13 of 21 for *E*; and 14 of 21 for *F*); *dashed line* indicates groups with methylation of both promoters (*E/N*: 13 of 19 for *A*; 13 of 19 for *B*; 14 of 19 for *C*; and 11 of 11 for *D–F*).

ation consensus site, which links RASSF1A to DNA-damage response (27). RASSF1A has been found to directly bind and stabilize microtubule structures, suggesting a role of the protein in maintaining genome stability (28). It was shown in a recent study that RASSF1A regulates mitosis by inhibiting the APC-cdc20 complex (29). Although mutation of *RASSF1A* is rarely found in non-small cell lung cancer, the gene is located at 3p21, a region frequently deleted in non-small cell lung cancer, and its promoter is frequently (30 to 38%) hypermethylated in primary non-small cell lung cancer (17, 30, 31). In contrast with *p16*^{INK4a}, hypermethylation of the *RASSF1A* promoter is rarely detected in bronchial epithelial cells chronically exposed to tobacco carcinogens (18), suggesting this is a late event in carcinogenesis. In this study, the much lower frequency (3% *versus* 11%) of *RASSF1A* promoter hypermethylation compared with *p16*^{INK4a} promoter hypermethylation detected in the adjacent normal-appearing lung tissues from patients with non-small cell lung cancer supports this notion.

In patients with early stage non-small cell lung cancer, *p16*^{INK4a} promoter methylation was a predictor of the clinical outcome of the patient (Fig. 2, *A–C*), which is consistent with earlier reports analyzing either *p16*^{INK4a} promoter methylation or p16^{INK4a} protein expression and clinical outcome in patients with early stage non-small cell lung cancer (11, 32, 33). Two previous reports showed that patients with stage I/II non-small cell lung cancer that contained *RASSF1A* promoter methylation associated with adverse survival (31, 34). Although the association was not statistically significant in this study, patients whose stage I/II tumors carried *RASSF1A* promoter methylation had poorer 5-year survival rates (Fig. 2, *D–F*).

One of the interesting findings in our study was that patients with stage IIIA disease whose tumors carried *RASSF1A* promoter methylation had extremely poor 5-year survival rates compared with those without the abnormality. This was in contrast to the findings in patients with stage I/II disease (Figs. 2 and 3). Interestingly, in the locally advanced tumors, *p16*^{INK4a}

promoter methylation and *RASSF1A* promoter methylation were not associated ($P = 0.28$; Table 1), again in contrast with data for stage I/II tumors. These results suggest that inactivation of *RASSF1A* together with additional molecular alterations that occur between the early stage and locally advanced stage of non-small cell lung cancer renders the tumors extremely aggressive. It should be noted that *RASSF1A* methylation was not associated with survival in patients with stage III non-small cell lung cancer in a previous report (34). But that study had a smaller sample size and lower rate of methylation frequency compared with stage I/II tumors (34% *versus* 54%) in the same study (34). Additional studies are therefore needed to validate our findings.

The finding that patients with methylation of both gene promoters had a poorer 5-year overall, disease-specific, and disease-free survival rate than did those with only $p16^{INK4a}$ or *RASSF1A* promoter methylation (Fig. 4, *A–C*) suggests that the inactivation of *RASSF1A* might make the tumor cells more aggressive. This dose-dependent correlation between the methylation status and survivals among patients with no methylation in any of the two promoters, with methylation in only one promoter, and with methylation of both promoters was even more profound (Fig. 4, *D–F*). If validated, these epigenetic abnormalities may be useful biomarkers for molecular classification of patients with stage IIIA non-small cell lung cancer as well as reasonable therapeutic targets.

ACKNOWLEDGMENTS

We thank Sarah Taylor in Tumor Registry Medical Informatics for providing follow-up information and Rachel Williams in Scientific Publication for editing.

REFERENCES

1. Greenlee RT, Hill-Harmon MB, Muray T. Cancer statistics, 2001. CA - Cancer J Clin 2001;51:15–36.

2. Greenlee RT, Murray T, Bolden S, Wingo PA. Cancer statistics, 2000. CA - Cancer J Clin 2000;50:7–33.

3. Niklinski J, Niklinska W, Laudanski J. Prognostic molecular markers in non-small cell lung cancer. Lung Cancer 2001;34:S53–8.

4. Fong KM, Sekido Y, Gazdar AF. Lung cancer Molecular biology of lung cancer: clinical implications. Thorax 2003;58:892–900.

5. Hirsch FR, Franklin WA, Gazdar AF, Bunn PA Jr. Early detection of lung cancer: clinical perspectives of recent advances in biology and radiology. Clin Cancer Res 2001;7:5–22.

6. Zochbauer-Muller S, Gazdar AF, Minna JD. Molecular pathogenesis of Lung cancer. Annu Rev Physiol 2002;64:681–708.

7. Forgacs E, Zochbauer-Muller S, Olah E, Minna JD. Molecular genetic abnormalities in the pathogenesis of human lung. Pathol Oncol Res 2001;7:6–13.

8. Merlo A, Herman JG, Mao L, et al. 5′ CpG island methylation is associated with transcriptional silencing of the tumor suppressor p16/CDKN2/ MTS1 in human cancers. Nat Med 1995;1:686–92.

9. Zhang HS, Postigo AA, Dean DC. Active transcriptional repression by the Rb-E2F complex mediates G1 arrest triggered by p16INK4a, TGFbeta, and contact inhibition. Cell 1999;97:53–61.

10. Koh J, Enders GH, Dynlacht BD, Harlow E. Tumour-derived p16 alleles encoding proteins defective in cell-cycle inhibition. Nature (Lond) 1995;375:506–10.

11. Kim DH, Nelson HH, Wiencke JK, et al. p16(INK4a) and histology-specific methylation of CpG islands by exposure to tobacco smoke in non-small cell lung cancer. Cancer Res 2001;61:3419–24.

12. Toyooka S, Toyooka KO, Maruyama R, et al. DNA methylation profiles of lung tumors. Mol Cancer Ther 2001;1:61–7.

13. Soria JC, Rodriguez M, Liu DD, et al. Aberrant promoter methylation of multiple genes in bronchial brush samples from former cigarette smokers. Cancer Res 2002;62:351–5.

14. Brauch H, Johnson B, Hovis J, et al. Molecular analysis of the short arm of chromosome 3 in small-cell and non-small-cell carcinoma of the lung. N Engl J Med 1987;317:1109–13.

15. Dammann R, Li C, Yoon JH, et al. Epigenetic inactivation of a Ras association domain family protein from the lung tumour suppressor locus 3p21.3h. Nat Genet 2000;25:315–9.

16. Pfeifer GP, Yoon JH, Liu L, et al. Methylation of the RASSF1A gene in human cancers. Biol Chem 2002;383:907–14.

17. Burbee DG, Forgacs E, Zochbauer-Muller S, et al. Epigenetic inactivation of RASSF1A in lung and breast cancers and malignant phenotype suppression. J Natl Cancer Inst (Bethesda) 2001;93:691–9.

18. Ortiz-Vega S, Khokhlatchev A, Nedwidek M, et al. The putative tumor suppressor RASSF1A homodimerizes and heterodimerizes with the Ras-GTP binding protein Nore1. Oncogene 2002;21:1381–90.

19. Belinsky SA, Nikula KJ, Palmisano WA, et al. Aberrant methylation of $p16^{ink4a}$ is an early event in lung cancer and a potential biomarker for early diagnosis. Proc Natl Acad Sci USA 1998;95:11891–6.

20. Belinsky SA, Palmisano WA, Gilliland FD, et al. Aberrant promoter methylation in bronchial epithelium and sputum from current and former smokers. Cancer Res 2002;62:2370–7.

21. Cairns P, Mao L, Merlo A, et al. Rates of p16 (MTS1) mutations in primary tumors with 9p loss. Science (Wash DC) 1994;265:415–7.

22. Esteller S, Corn PG, Baylin SB, Herman JG. A gene hypermethylation profile of human cancer. Cancer Res 2001;61:3225–9.

23. Kaye FJ. RB and cyclin dependent kinase pathways defining a distinction between RB and P16 loss in lung cancer. Oncogene 2002;21:6908–14.

24. Zochbauer-Muller S, Fong KM, Virmani AK, et al. Aberrant promoter methylation of multiple genes in non-small cell lung cancers. Cancer Res 2001;61:249–55.

25. Khokhlatchev A, Rablzadeh S, Xavler R, et al. Identification of a novel RAS regulated proapoptotic pathway. Curr Biol 2002;12:253–65.

26. Shivakumar L, Minna J, Sakamaki T, Restell R, White MA. The RASSF1A tumor suppressor blocks cell cycle progression and inhibits cyclin D1 accumulation. Mol Cell Biol 2002;22:4309–18.

27. Kim ST, Lim DS, Camman CE, Kastan MB. Substrate specificities and identification of putative substrates of ATM kinases family members. J Biol Chem 1999;274:37538–43.

28. Liu L, Tommasi S, Lee DH, Dammann R, Pfeifer GP. Control of microtubule stability by the RASSF1A tumor suppressor. Oncogene 2003;22:8125–36.

29. Song MS, Song SJ, Ayad NG, et al. The tumour suppressor RASSF1A regulates mitosis by inhibiting the APC-Cdc20 complex. Nat Cell Biol 2004;6:129–37.

30. Agathanggelou A, Honorio S, Macartney DP, et al. Methylation associated inactivation of RASSF1A from region 3p21.3 in lung, breast and ovarian tumor. Oncogene 2001;20:1509–18.

31. Tomizawa Y, Kohno T, Kondo H, et al. Clinicopathological significance of epigenetic inactivation of RASSF1A at 3p21.3 in stage I lung adenocarcinoma. Clin Cancer Res 2002;8:2362–8.

32. Gonzalez-Quevedo R, Iniesta P, Moran A, et al. Cooperative role of telomerase activity and p16 expression in the prognosis of non-small-cell lung cancer. J Clin Oncol 2002;20:254–62.

33. Jin M, Inoue S, Umemura T, et al. Cyclin D1, p16 and retinoblastoma gene product expression as a predictor for prognosis in non-small cell lung cancer at stages I and II. Lung Cancer 2001;34:207–18.

34. Endoh H, Yatabe Y, Shimizu S, et al. RASSF1A gene inactivation in non-small cell lung cancer and its clinical implication. Int J Cancer 2003;106:45–51.

Oncogene (2003) 22, 7123–7129
© 2003 Nature Publishing Group All rights reserved 0950-9232/03 $25.00
www.nature.com/onc

Association of a functional tandem repeats in the downstream of human telomerase gene and lung cancer

Luo Wang[1], Jean-Charles Soria[1], Yoon-Soo Chang[1], Ho-Young Lee[1], Qingyi Wei[2] and Li Mao*[,1]

[1]*Department of Thoracic/Head and Neck Medical Oncology, The University of Texas MD Anderson Cancer Center, Houston, TX 77030, USA;* [2]*Department of Epidemiology, The University of Texas MD Anderson Cancer Center, Houston, TX 77030, USA*

Chemoprevention has been widely explored as a promising strategy for controlling the incidence of lung cancer, the leading cause of cancer-related death. To maximize the benefit of lung cancer chemoprevention, it is important to identify individuals at high risk for the disease. The genetic background has been shown to play an important role in one's risk of developing lung cancer. We report here the identification of a polymorphic tandem repeats minisatellite (termed MNS16A) in the downstream region of the human telomerase gene. This minisatellite is located upstream of an antisense transcript from the human telomerase gene locus and was demonstrated to have promoter activity. The promoter activity was significantly lower in the construct containing the shorter repeats, suggesting that the MNS16A variant may have a relevance of functionality. To explore the role of this novel polymorphism in lung cancer, we conducted a pilot hospital-based case–control study by identifying the MNS16A genotype with genomic DNA from 53 lung cancer patients and 72 cancer-free controls. We found four different alleles and classified them as shorter (S) or longer (L) on the functional basis of the length of the repeats in the controls. The MNS16A genotype distributions of the SS, SL, and LL genotypes were 11, 32, and 57%, respectively, in the cases, and 14, 40, and 46%, respectively, in the controls. Compared with the SS + SL genotype, the LL genotype was associated with greater than twofold increased risk of lung cancer (odds ratio = 2.18; 95% confidence interval = 0.92, 5.20) after adjustment for age, sex, ethnicity, and smoking status, suggesting a potential role of MNS16A in lung cancer susceptibility. Larger studies are needed to verify our findings.
Oncogene (2003) **22,** 7123–7129. doi:10.1038/sj.onc.1206852

Keywords: minisatellite; tandem repeats; VNTR; hTERT; lung cancer

*Correspondence: L Mao, Department of Thoracic/Head and Neck Medical Oncology, The University of Texas MD Anderson Cancer Center, Box 432, 1515 Holcombe Boulevard, Houston, TX 77030, USA; E-mail: lmao@mdanderson.org
Received 24 February 2003; revised 19 May 2003; accepted 9 June 2003

Introduction

Lung cancer is the leading cause of cancer-related death for both men and women in the United States (ACS, 2003). Despite improvements in diagnosis and therapy, the overall survival of patients with lung cancer remains dismal (Parkin *et al*., 1999). One of the promising approaches to the prevention of lung cancer is the use of chemopreventive agents. Since preventive treatment may be long term and because the agents used may have certain side effects, it is important to limit chemopreventive treatment to those individuals at high risk of developing lung cancer.

Tobacco smoking is the most important etiologic factor in lung cancer development. However, less than 15% of heavy smokers are expected to develop lung cancer in their lifetime, suggesting the presence of other factors important for the development of the disease. An individual's genetic variation has been shown to play an important role in one's susceptibility to lung cancer. For instance, polymorphism in genes involving detoxification enzymes (Bouchardy *et al*., 2001) and DNA repairs (Goode *et al*., 2002) has been shown to play a role in susceptibility to lung cancer. In a recent study, we found that a C/T polymorphism in the promoter region of a novel cytosine DNA-methyltransferase 3B6 is associated with the risk of lung cancer development (Shen *et al*., 2002), suggesting that the role of polymorphisms in many other genes involved in carcinogenesis of lung cancer needs to be explored.

Human telomerase (hTERT) gene is located to chromosome 5p15.33 and encodes a ribonucleoprotein enzyme that extends chromosome ends that have been shortened during successive cycles of cell division (Greider and Blackburn, 1985). Telomerase is composed of an RNA component, a catalytic protein subunit, and other telomerase-associated proteins whose functions remain to be established (Feng *et al*., 1995). Telomerase is expressed in the vast majority of human malignant cell lines and tumors, but not in the corresponding benign tissues (Dhaene *et al*., 2000). Studies of human tumors and human tumor cell lines have shown that telomerase activation plays a critical role in tumorigenesis, including lung tumorigenesis, by sustaining cellular immortality (Kim *et al*., 1994; Hiyama *et al*., 1995; Albanell *et al*., 1997). Overexpression of the RNA component of human telomerase has been observed at a very early

stage in the pathogenesis of nonsmall-cell lung cancer (NSCLC) (Yashima *et al*., 1997). However, such expression is not limited to the cells that harbor telomerase activity. By contrast, expression of hTERT is more closely associated with telomerase activity (Meyerson *et al*., 1997; Nakamura *et al*., 1997). In our previous studies, we demonstrated that hTERT expression occurred early in lung carcinogenesis and was associated with a poorer clinical outcome in patients with early-stage NSCLC (Soria *et al*., 2001; Wang *et al*., 2002). Interestingly, during these studies, we noticed the presence of an antisense transcript signal detected by *in situ* hybridization in cells expressing hTERT, suggesting the existence of an antisense hTERT mRNA, which might play a role in regulation of hTERT expression. To identify genetic variation in hTERT that may participate in the regulation of hTERT expression, we sequenced this locus and found a novel polymorphic tandem repeats minisatellite, termed MNS16A, in the downstream region of the hTERT gene locus. The region containing MNS16A was demonstrated to have a promoter activity that was influenced by the length of the MNS16A tandem repeats, suggesting a potential role of this minisatellite in regulating expression of the antisense hTERT mRNA. In this study, we also provided preliminary evidence of a possible association between MNS16A variable number of tandem repeats (VNTR) and risk of lung cancer.

Results

hTERT clusters with minisatellites and microsatellites, including a unique functional tandem repeats minisatellite in the downstream region of the gene. The hTERT gene is located at chromosome 5p15.33 and has 16 exons (Wick *et al*., 1999; Bryce *et al*., 2000). Analysing the genomic sequence published in GenBank (Accession numbers AY007685), we found that the gene contains many minisatellites and microsatellites, which divide the gene into four exon clusters (Figure 1). All the seven reported major conserved motifs of the telomerase subunit (Xiong and Eickbush, 1990) are located in the second and third clusters. The fourth cluster contains exons 13–16; however, it is further divided by minisatellites or microsatellites (Figure 1). Interestingly, during our earlier studies in which we used *in situ* hybridization to evaluate hTERT mRNA expression as a biomarker in lung tumorigenesis and progression (Soria *et al*., 2001; Wang *et al*., 2002), we found that with single-strand sense RNA riboprobes specific to the antisense mRNA sequences of various hTERT exons, a strong positive signal could be detected in cells with active telomerase but not in cells of telomerase-negative alternative-lengthening-of-telomeres cell line KB319 (Figure 2). This finding suggested the presence of hTERT antisense sequences. Further study showed that the antisense RNA transcript was initiated at the downstream of hTERT gene and had two major starting points at nt

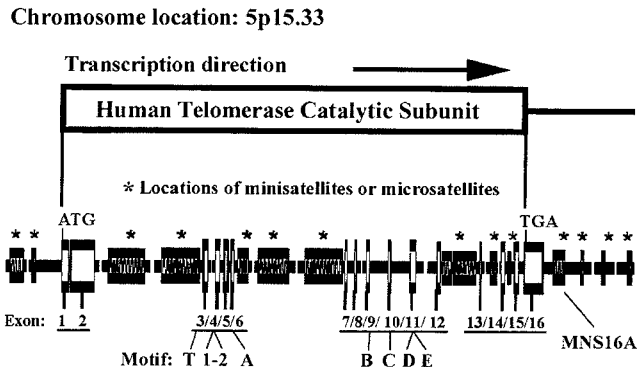


Figure 1 Genomic structure of the human telomerase gene (*hTERT*)

22156 and nt 22163 (GenBank AF128894), respectively (unpublished data).

In the study reported here, we found a unique tandem repeats sequence, which we termed MNS16A, in the putative promoter region of this antisense RNA transcript. This repeats sequence was a typical minisatellite with two different VNTR alleles in the cancer cell lines tested (Figure 3a). These two VNTR alleles were named as VNTR-302 and VNTR-243 on the basis of the PCR fragment size. The core sequence of MNS16A is a 23 bp tandem repeat of TCC TCT TAT CTC CCA GTC TCA TC or a 26 bp sequence with a CAT insertion. The VNTR-302 contains two 23 bp repeats and three 26 bp repeats, while the VNTR-243 contains one 23 bp repeat and two 26 bp repeats (Figure 3b). Interestingly, analysis with Transcription Element Search Software (TESS; URL: http://www.cbil.upenn.edu/tess) showed that the 26 bp tandem repeat with a CAT trinucleotide is a binding site for the transcription factor GATA-1, prompting us to investigate whether this tandem repeat plays a role in promoter activity.

The promoter activity of MNS16A depends on the length of the VNTR sequence size. Luciferase assay was performed to characterize the potential promoter activity of MNS16A (Figure 3c). We found that promoter activity was twice as strong with the pGL3-570(S) forward construct as it was with the pGL3-570(*R*) reverse construct, indicating the presence of a promoter in this region containing the MNS16A sequence. Promoter activity was much weaker with the pGL3-660(*S*) construct, which contains the VNTR-302, than with the pGL3-570(S) construct, which contains the VNTR-243. This suggested that promoter activity depended on the length of MNS16A VNTR and MNS16A functioned as a repressor for this promoter. This observation was further confirmed by using two additional constructs, pGL3-243 and pGL3-302, that contained only the tandem repeats VNTR-243 or VNTR-302 (data not shown). The structure of the core promoter that initiated the antisense transcript is illustrated in Figure 3d. It was interesting that the NSCLC cell line H460, which has a VNTR-302/243 genotype, showed a stronger antisense hTERT RNA

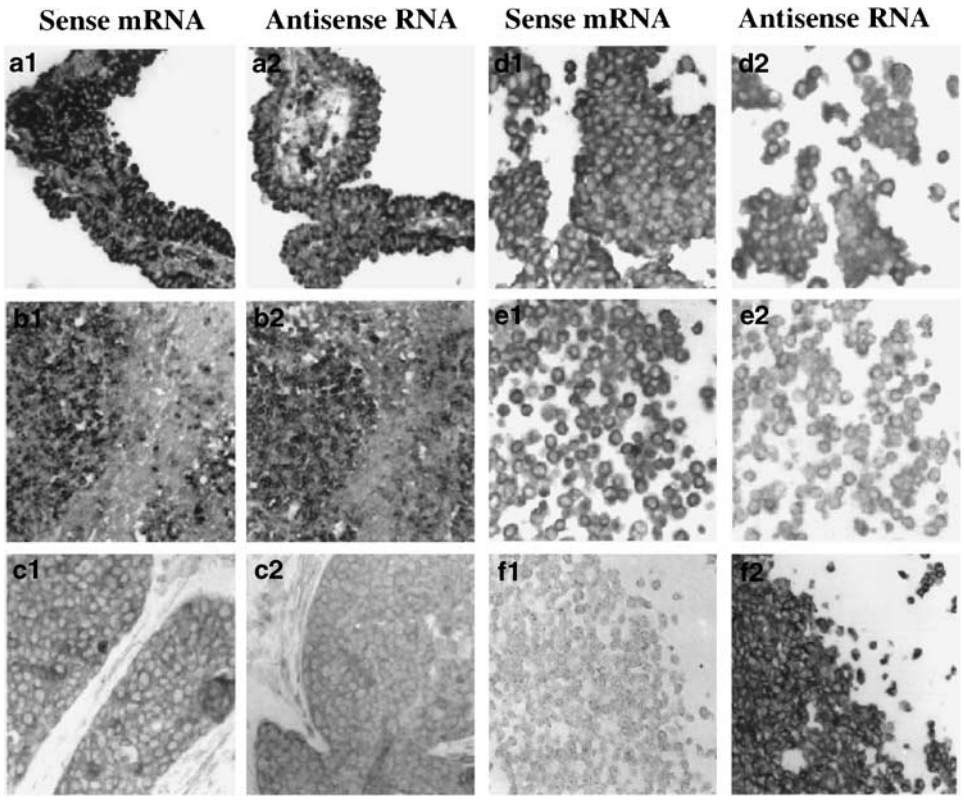


Figure 2 Antisense *hTERT* RNA expression detected by *in situ* hybridization in primary lung cancers and lung cancer cell lines. The sense mRNAs were detected using the single-strand antisense riboprobe and the antisense RNAs were detected with the the sense riboprobe. (**a**) Bronchioalveolar carcinoma; (**b**) large-cell carcinoma; (**c**) squamous cell carcinoma; (**d**) lung cancer cell line A549; (**e**) lung cancer cell line H157; (**f**) telomerase-negative alternative-lengthening-of-telomeres cell line KB319

expression level and telomerase activity (Soria *et al*., 2001) than cell lines H157 and SK-MES, which have a VNTR-302/302 genotype.

MNS16A polymorphic allele associated with lung cancer susceptibility. In addition to MNS16A VNTR-243 and VNTR-302 observed in the cancer cell lines (Figure 3a), two other rare alleles, VNTR-272 and VNTR-333, were also identified (data not shown). We classified the alleles VNTR-243 and VNTR-272 as short repeats (S allele), while VNTR-302 and VNTR-333 as long repeats (L allele). To explore the role of this novel polymorphism in lung cancer, we conducted a pilot hospital-based case–control study. The MNS16A genotype was determined with the genomic DNA from the tumor and blood samples of 53 lung cancer patients who were diagnosed with NSCLC and underwent surgery, and blood samples of 72 cancer-free controls who enrolled into our various clinical chemoprevention trials ($n=57$) and who were seen at MD Anderson without clinical evidence of lung cancer ($N=15$). For smoking status, 'ever smokers' were defined as those who smoked more than 100 cigarettes in their lifetime, of which they were 'former smokers' if they quit more than a year or 'current smokers' otherwise. Although there was no gender difference between the cases and controls, the cases (mean $\pm$ s.d., 65.5 ± 9.6 years) were younger than the controls (54.9 ± 10.3 years), and there were more Caucasians and current smokers in the cases (41.5 and 96.2%, respectively) than in the controls (90.3 and 15.3%, respectively) (Table 1). These differences were adjusted for in the multivariate logistic regression analysis. We found four different alleles and classified them as shorter (S) or longer (L) on the functional basis of the length of the repeats in the controls. The MNS16A genotype distributions of the SS, SL, and LL genotypes were 11, 32, and 57%, respectively, in the cases, and 14, 40, and 46%, respectively, in the controls, which was not statistically different (Table 2). Compared with the SS + SL genotype, the LL genotype was associated with greater than twofold increased risk of lung cancer (odds ratio = 2.18; 95% confidence interval = 0.92, 5.20), after adjustment for age, sex, ethnicity, and smoking status (Table 2). These data suggest a potential role of MNS16A in lung cancer susceptibility. However, this pilot study was small and less than optimal; larger studies with a more rigorous study design and sufficient power are warranted to substantiate these findings.

Discussion

Minisatellite sequences are mutated at a high rate in germ cells (Jeffreys *et al*., 1987) but are relatively stable in somatic cells (Jeffreys *et al*., 1994), creating non-

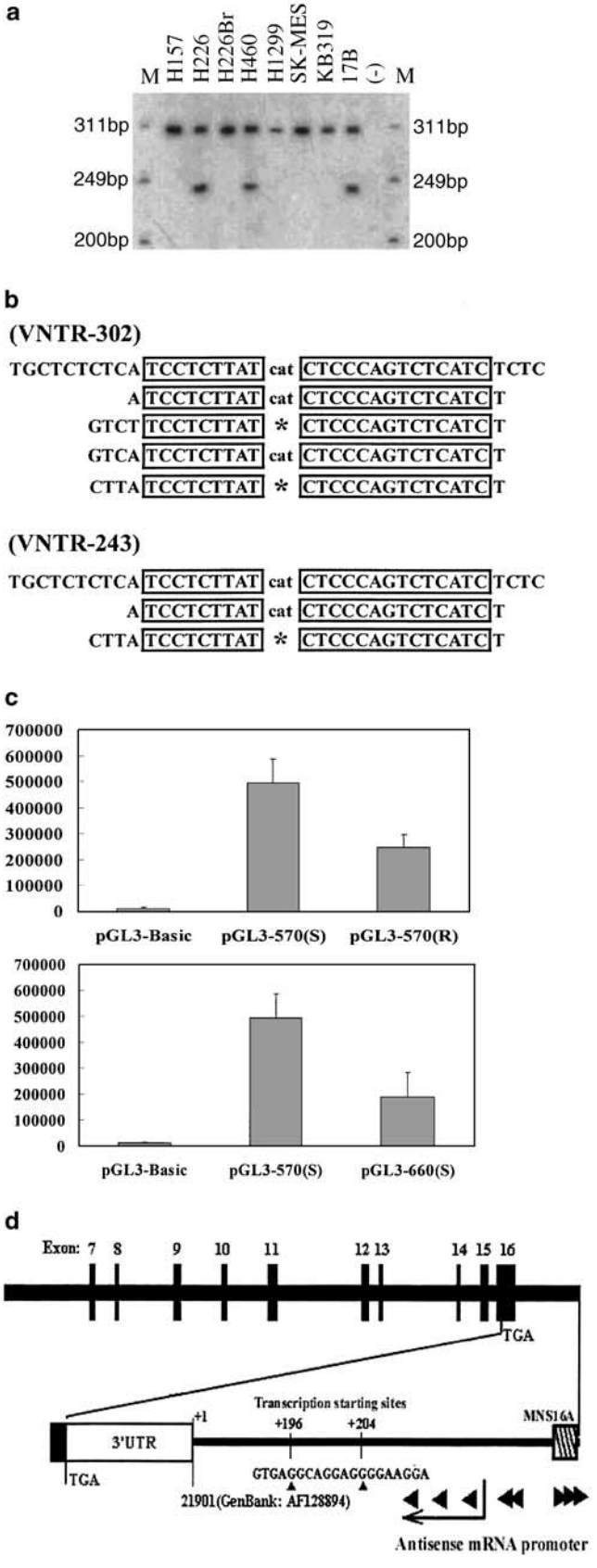


Figure 3 Genotypes of MNS16A, sequence, and function of MNS16A VNTR. M means DNA marker. (**a**) Genotype pattern of cancer cell lines; (**b**) sequences of 302 bp (L) allele and 243 bp (S) allele; (**c**) promoter activity of MNS16A VNTR measured by luciferase assay; (**d**) structure of the core promoter that initiated the antisense transcript

Table 1 Distribution of selected variables in lung cancer patients and cancer-free controls

	Cases (n = *53*)		*Controls* (n = *72*)		
Variable	*No.*	*%*	*No.*	*%*	P[a]
Age (years)					<0.001
<60	11	20.8	47	65.3	
⩾60	42	79.2	25	34.7	
Sex					0.347
Male	31	58.5	36	50.0	
Female	22	41.5	36	50.0	
Ethnicity					0.204
Caucasians	51	96.2	65	90.3	
African-American	2	3.8	7	9.7	
Smoking status[b]					0.004
Never	7	13.2	12	16.7	
Former	24	45.3	49	68.0	
Current	22	41.5	11	15.3	

[a]Two-sided χ^2-test. [b]In all, 12 patients and three controls did not provide information on smoking

inherited individual variations. However, in cells transformed by γ-irradiation or genotoxic carcinogens, the frequencies of minisatellite mutations are increased compared to that in the corresponding nonmalignant immortalized cells (Paquette and Little, 1992; Honma *et al*., 1994). Minisatellite mutations have also been found in various human tumors (Thein *et al*., 1987; Matsumura and Tarin, 1992) and experimental animal tumors induced by chemical carcinogens (Ledwith *et al*., 1990, 1995). Studies have shown high rearrangement frequencies in different types of cancers for two atypical minisatellites, the AT-rich ApoB locus and the VNTR locus D1S7, which have an atypically short repeat unit and may be susceptible to polymerase slippage (Hoff-Olsen *et al*., 1995; Kaplanski *et al*., 1997). Somatic mutations in the D1S7 locus have been found to be associated with microsatellite instability in human colorectal carcinomas (Kaplanski *et al*., 1997). Minisatellite instability has also been demonstrated to exist in severe-combined-immunodeficiency fibroblasts, which have a mutation in the catalytic subunit of DNA-dependent protein kinase, suggesting that this subunit may be involved in the stable maintenance of minisatellite sequences in the genome (Imai *et al*., 1997).

Single nucleotide polymorphism within genes or potential functional components of genes has been shown to be associated with susceptibility to various diseases, including lung cancer (Wei *et al*., 2000; Spitz *et al*., 2001). For instance, in our recent study on different genetic variants of DNA methyltransferase 3B,

Table 2 Logistic regression analysis of hTERT genotype in lung cancer patients and cancer-free controls

	Cases (n = *53*)		*Controls* (n = *72*)				
	No.	*%*	*No.*	*%*	P-*value*[a]	*OR*	*(95% CI)*[b]
hTERT genotype					0.492[c]		
SS	6	11.3	10	13.9		Ref.	
SL	17	32.1	29	40.3		1.82	(0.42–7.84)
LL	30	56.6	33	45.8		3.49	(0.82–14.8)
SS + SL	23	43.4	39	54.2		Ref.	(0.79–1.50)
LL	30	56.6	33	45.8	0.243[d]	2.18	(0.92–5.20)
L allele frequency	0.726		0.660		0.330[e]		

[a]Two-sided χ^2-test. [b]Adjusted for age, sex, ethnicity, and smoking status. [c]χ^2-test for genotype distribution between cases and controls. The *P*-value for the test for Hardy–Weinberg equilibrium ($q^2 + 2qp + p^2$, where q = the L allele frequency) of the genotype in the controls was 0.825. [d]χ^2-test using the SS + SL as the reference. The power of this study to detect an OR greater than 2.18 is 0.566. [e]χ^2-test for the L allele frequency between cases and controls

we found that a functional C/T polymorphism in the promoter region could contribute to the risk of lung cancer development (Shen *et al*., 2002). However, the potential biological consequences of minisatellite polymorphism have not been well recognized. In the study reported here, we identified an antisense hTERT mRNA transcript and its promoter whose activity depended on the length of tandem repeats. To our knowledge, this is the first report of a novel controlling mechanism of gene regulation, which showed that a tandem repeat minisatellite functioned as a part of promoter. The strong presence of the antisense molecule in cancer cell KB319 lacking hTERT expression suggests that expression of the antisense molecule is independent of hTERT. Even if it was possible that the antisense hTERT RNA could act as an inhibitor of hTERT by reducing its transcription or blocking its translation (unpublished data), however, the natural biological function of this antisense mRNA remains unknown and needs further studies. Nevertheless, because activation of telomerase plays an important role in early lung carcinogenesis (Yashima *et al*., 1997) and is also associated with lung cancer progression (Wang *et al*., 2002), it is likely that the level of antisense mRNA may contribute to the development of lung cancer.

Szutorisz *et al*. (2001) identified two polymorphic minisatellites located in intron 2 and intron 6 of human telomerase gene. The polymorphic minisatellite in intron 2 was found to contain binding sites for c-Myc that has been shown to upregulate hTERT transcription. However, there were only minor variations and one deletion seen in the 38 colon carcinomas analysed, which led the authors to conclude that the size rearrangements of the hTERT minisatellites are not required for telomerase expression in colon carcinomas (Szutorisz *et al*., 2001). However, in a recent work, eight alleles of intron 6 VNTR and four alleles of intron 2 VNTR in hTERT gene locus were identified among 103 unrelated individuals, and in one patient with a kidney tumor, the VNTR in intron 6 was found to have undergone concomitant rearrangements, suggesting that chromosomal rearrangements of these VNTR may be associated with the activation of hTERT in cancer cells (Leem *et al*., 2002). Consistent with the above reports, we also found rearrangement of the MNS16A VNTR in 11 primary lung tumors examined in our another study (data not shown). However, the association of the rearrangement with hTERT expression levels has not yet been determined because of the lack of reliable quantitative methods.

Our finding that patients with NSCLC have a higher frequency of the MNS16A LL genotype is important, because it supports the notion that the antisense hTERT mRNA has a biological function, which may be exerted through interference with hTERT levels. Our finding that minisatellite length influences promoter activity, together with the finding that minisatellite length was possibly related to lung cancer susceptibility, suggests a role of minisatellites in regulation of gene expression and contributes to diversity of human cell biology. Further studies with larger cohorts are necessary to validate our findings.

Materials and methods

Tissue, cell specimens, and study population

H157, H226, H226Br, H460, H1299, and H1944 human NSCLC cells were purchased from American Type Culture Collection (Rockville, MD, USA). SK-MES and 17B squamous carcinoma of the head and neck were obtained from Dr Adi Gazdar (University of Texas Southwestern Medical Center, Dallas, TX, USA). The telomerase-negative alternative-lengthening-of-telomeres cell line KB319 was a gift from Drs John Murnane and Laure Sabatier, Radiation Oncology Research Laboratory, University of California, San Francisco, USA (Murnane *et al*., 1994). Cells were cultured in Dulbecco's modified Eagle's medium supplemented with 10% heat-inactivated fetal calf serum, 2 mM L-glutamine, 100 IU/ml penicillin, and 100 mg/ml streptomycin at 37°C in the presence of 5% CO_2.

Lung cancer tissues were obtained from 53 consecutive patients with NSCLC, who had undergone surgical resection with curative intent at MD Anderson Cancer Center between 1996 and 1998, and for whom archived tissues were available. These specimens were collected from the Department of Pathology and stored at −80°C until use. All patients had consented to the use of their tissue specimens, and the

institutional review board approved the research protocol. The leukocytes (control samples) were obtained from 57 noncancer volunteers (former smokers) recruited for several randomized chemoprevention trials in the Houston metropolitan area and 15 hospital patients without evidence of lung cancer.

RNA in situ *hybridization and Telomeric Repeat Amplification Protocol Assay*

The riboprobe used in this study was a 620 bp cDNA fragment RT–PCR-amplified from exons 10 to 15 by using the forward primer 5′-TCT TGT TGG TGA CAC CTC ACC-3′ and the reverse primer 5′-TAG GTG ACA CGG TGT CGA GT-3′. The PCR fragment was then cloned into the pCR®II-TOPO vector (Invitrogen, Carlsbad, CA, USA). The plasmid was linearized with *Eco*RV, and the single-strand-specific riboprobe was transcribed *in vitro* with SP6 RNA polymerase (Promega, Madison, WI, USA) by using a DIG RNA Labeling Kit (Roche Diagnostics, Inc., Indianapolis, IN, USA). *In situ* hybridization was performed as previously described (Wang *et al*., 2002). Detection was performed using a DIG Nucleic Acid Detection Kit (Roche Diagnostics, Inc., Indianapolis, IN, USA) according to the manufacturer's directions. Anti-DIG alkaline phosphatase conjugated antibody was diluted 1 : 500. Nitro-blue tetrazolium and 5-bromo-4-chloro-3-indolyl phosphate were used as chromogens. Slides were then rinsed in TE buffer (10 mM Tris-HCl and 1 mM EDTA, pH 8) and mounted with Aqua-Mount medium (Fisher, Houston, TX, USA). Telomerase activity was measured by using the TRAP-eze Telomerase Detection Kit (Intergen, Purchase, NY, USA) according to the manufacturer's protocol.

Construction of the pGL3-570(S), pGL3-570(R), and pGL3-660(S) plasmids

A 570 bp DNA fragment from the downstream region of hTERT gene (from base 22 141 to base 22 710, Accession number AF128894) was amplified from the cell line H460 by using the forward primer 5′-TTC TGA TGC TGT GAG GCA GG-3′ and the reverse primer 5′-GAG AGA TGA GAC TGG GAG ATG-3′, and inserted into pGL3-basic vector (Promega). The plasmids with forward and reverse directions identical with the direction of hTERT genomic sequence in GenBank, were constructed and named as pGL3-570(S) and pGL3-570(R), respectively. The PCR reaction was performed in a 12.5-μl volume containing about 50 ng of genomic DNA, 7% dimethyl sulfoxide, 1.5 mM dNTPs, 6.7 mM $MgCl_2$, 16.6 mM $(NH_4)_2SO_4$, 67 mM Tris, 10 mM β-mercaptoethanol, 6.7 μM EDTA, 0.5 μM forward, 0.5 μM reverse primer, and 0.625 U of HotStar Taq DNA Polymerase (Qiagen, Inc., Chatsworth, CA, USA). Amplification was carried out with an initial denaturing step at 95°C for 15 min, followed by 40 cycles of 95°C for 30 s, 60°C for 1 min, and 72°C for 1 min in a thermal cycler (Hybaid; PCR Express, Middlesex, UK) with a last extension step of 72°C for 10 min. The sequences of plasmids were confirmed by using an AmpliCycle sequencing kit according to the manufacturer's instructions (Applied Biosystems, Foster City, CA, USA). A 660 bp DNA fragment was also amplified using the same set of primers (containing additional repeats sequence) to construct the plasmid pGL3-660(S).

Construction of pGL3-302(S), pGL3-302(R) and pGL3-243(S), pGL3-243(R) plasmids

Two smaller DNA fragments containing a 243 or 302 bp tandem repeat sequence (MNS16A) within the 570 or 660 bp fragment described above were amplified by using the forward primer S3-H 5′-AAA GCT TCT TCT GAT CTC TGA AGG G-3′ and the reverse primer E17AS4-H 5′-AAA GCT TGC CTG AGG AAG GAC GTA-3′. These two fragments were also inserted into pGL3-basic vector. The plasmids with forward and reverse directions identical with the direction of hTERT genomic sequence in GenBank were constructed and named pGL3-302(S) and pGL3-302(R), respectively, and pGL3-243(S) and pGL3-243(R), respectively.

Transient transfection and luciferase assay

The plasmids were transfected into lung cancer cell line H1299 using Lipofect.AMINE reagent (GIBCO BRL, Grand Island, NY, USA) according to the manufacturer's protocol. Briefly, 5×10^4 cells were spread into 24-well plates and incubated overnight. Then, 250 ng of plasmids and 50 ng of pCMVsport-beta gal (GIBCO BRL, Grand Island, NY, USA), which was used as the internal control to monitor the transfection efficiency, were added. After 6 h, the medium was replaced with a medium containing 10% fetal calf serum and 36 h later, the cells were harvested with cell lysis buffer. In each experiment, transfection was performed in triplicate and luciferase activity was measured by using a Luciferase Assay System (Promega Co., Madison, WI, USA) with a luminometer. β-galactosidase activity was measured with Beta-galactosidases Enzyme Assay System with a report lysis buffer (Promega) following the manufacturer's instructions. The values of luciferase activities were normalized against those of β-galactosidase expressed by plasmid pCMVsport-β gal.

Genotyping of MNS16A

For genotyping of MNS16A, genomic DNA was extracted from leukocytes of surgically resected lung tissues. Briefly, the tissue was digested in 200 μl of 50 mM Tris-HCl (pH 8.0) containing 1% sodium dodecyl sulfate and proteinase K, and incubated at 42°C for 24 h. DNA was purified using phenol–chloroform extraction followed by ethanol precipitation. 'Hot-PCR' was used to determine the MNS16A genotype by using the forward primer 5′-AGG ATT CTG ATC TCT GAA GGG TG-3′, located at nt 22591, and the reverse primer 5′-TCT GCC TGA GGA AGG ACG TAT G-3′, located at nt 22871. Briefly, the reverse primer was endlabeled with γ-^{32}P-ATP by using T4 polynucleotide kinase. The PCR reaction was performed in a 12.5-μl volume with an additional 0.02 μM of hot primer under the condition same as that mentioned above. Omission of DNA was used as a negative control. The PCR products were mixed with loading buffer, separated by electrophoresis on a 6% urea/formamide-denaturing polyacrylamide gel, and exposed to X-ray film.

Three different MNS16A genotypes, that is, LL-genotype (homozygotes), SS-genotype (homozygotes), and SL-genotype (heterozygotes), were defined on the basis of the functional structure of this tandem repeat minisatellite. (There are three GATA-1 binding sites in LL-genotype, while only two such sites in SS-genotype.)

Acknowledgements
This work was supported in part by Grant DAMD17-01-1-0689-1 from the Department of Defense and Grants PO1 CA91844, P30 CA16620, and U01 CA 86390 from the National Cancer Institute, USA. We thank Stephanis Deming for editing the manuscript and patient population identified through a search of the tumor registry database maintained by the Department of Medical Informatics.

References

Albanell J, Lonardo F, Rusch V, Engelhardt M, Langenfeld J, Han W, Klimstra D, Venkatraman E, Moore MA and Dmitrovsky E. (1997). *J. Natl. Cancer Inst.,* **89,** 1609–1615.

Bouchardy C, Benhamou S, Jourenkova N, Dayer P and Hirvonen A. (2001). *Lung Cancer,* **32,** 109–112.

Bryce LA, Morrison N, Hoare SF, Muir S and Keith WN. (2000). *Neoplasia,* **2,** 197–201.

Dhaene K, Van Marck E and Parwaresch R. (2000). *Virchows Arch.,* **437,** 1–16.

Feng J, Funk WD, Wang SS, Weinrich SL, Avilion AA, Chiu CP, Adams RR, Chang E, Allsopp RC, Yu J, Le S, West MD, Harley CB, Andrews WH, Greider CW and Villeponteau B. (1995). *Science,* **269,** 1236–1241.

Greider CW and Blackburn EH. (1985). *Cell,* **43,** 405–413.

Goode EL, Ulrich CM and Potter JD. (2002). *Cancer Epidemiol. Biomarkers Prev.,* **11,** 1513–1530.

Hiyama K, Hiyama E, Ishioka S, Yamakido M, Inai K, Gazdar AF, Piatyszek MA and Shay JW. (1995). *J. Natl. Cancer Inst.,* **87,** 895–902.

Hoff-Olsen P, Meling GI and Olaisen B. (1995). *Hum. Mutat.,* **5,** 329–332.

Honma M, Mizusawa H, Sasaki K, Hayashi M, Ohno T, Tanaka N and Sofuni T. (1994). *Mutat. Res.,* **304,** 167–179.

Imai H, Nakagama H, Komatsu K, Shiraishi T, Fukuda H, Sugimura T and Nagao M. (1997). *Proc. Natl. Acad. Sci. USA,* **94,** 10817–10820.

Jeffreys AJ, Tamaki K, MacLeod A, Monckton DG, Neil DL and Armour JA. (1994). *Nat. Genet.,* **6,** 136–145.

Jeffreys AJ, Wilson V, Kelly R, Taylor BA and Bulfield G. (1987). *Nucleic Acids Res.,* **15,** 2823–2836.

American Cancer Society Inc. (2003). *Cancer facts & figures*, American Cancer Society: Atlanta, GA. pp. 2–5.

Kaplanski C, Srivatanakul P and Wild CP. (1997). *Int. J. Cancer,* **72,** 248–254.

Kim NW, Piatyszek MA, Prowse KR, Harley CB, West MD, Ho PL, Coviello GM, Wright WE, Weinrich SL and Shay JW. (1994). *Science,* **266,** 2011–2015.

Ledwith BJ, Storer RD, Prahalada S, Manam S, Leander KR, van Zwieten MJ, Nichols WW and Bradley MO. (1990). *Cancer Res.,* **50,** 5245–5249.

Ledwith BJ, Joslyn DJ, Troilo P, Leander KR, Clair JH, Soper KA, Manam S, Prahalada S, van Zwieten MJ and Nichols WW. (1995). *Carcinogenesis,* **16,** 1167–1172.

Leem S-H, Londoño-Vallejo JA, Kim J-H, Bui H, Tubacher E, Solomon G, Park J-E, Horikawa I, Kouprina N, Barrett JC and Larionov V. (2002). *Oncogene,* **21,** 769–777.

Matsumura Y and Tarin D. (1992). *Cancer Res.,* **52,** 2174–2179.

Meyerson M, Counter CM, Eaton EN, Ellisen LW, Steiner P, Caddle SD, Ziaugra L, Beijersbergen RL, Davidoff MJ, Liu Q, Bacchetti S, Haber DA and Weinberg RA. (1997). *Cell,* **90,** 785–795.

Murnane JP, Sabatier L, Marder BA and Morgan WF. (1994). *EMBO J.,* **13,** 4953–4962.

Nakamura TM, Morin GB, Chapman KB, Weinrich SL, Andrews WH, Lingner J, Harley CB and Cech TR. (1997). *Science,* **277,** 955–959.

Paquette B and Little JB. (1992). *Cancer Res.,* **52,** 5788–5793.

Parkin DM, Pisani P and Ferlay J. (1999). *CA Cancer J. Clin.,* **49,** 33–64.

Shen H, Wang L, Spitz MR, Hong WK, Mao L and Wei QY. (2002). *Cancer Res.,* **62,** 4992–4995.

Soria JC, Moon C, Wang L, Hittelman WN, Jang SJ, Sun S-Y, Lee JJ, Liu D, Kurie JM, Morice RC, Lee JS, Hong WK and Mao L. (2001). *J. Natl. Cancer Inst.,* **93,** 1257–1263.

Spitz MR, Wu X, Wang Y, Wang LE, Shete S, Amos CI, Quo Z, Lei L, Mohrenweiser H and Wei Q. (2001). *Cancer Res.,* **61,** 1354–1357.

Szutorisz H, Palmqvist R, Roos G, Stenling R, Schorderet DF, Reddel R, Lingner J and Nabholz M. (2001). *Oncogene,* **20,** 2600–2605.

Thein SL, Jeffreys AJ, Gooi HC, Cotter F, Flint J, O'Connor NT, Weatherall DJ and Wainscoat JS. (1987). *Br. J. Cancer,* **55,** 353–356.

Wang L, Soria JC, Kemp BL, Liu DD, Mao L and Khuri FR. (2002). *Clin. Cancer Res.,* **8,** 2883–2889.

Wei Q, Cheng L, Amos CI, Wang LE, Guo Z, Hong WK and Spitz MR. (2000). *J. Natl. Cancer Inst.,* **92,** 1764–1772.

Wick M, Zubov D and Hagen G. (1999). *Gene,* **232,** 97–106.

Xiong Y and Eickbush TH. (1990). *EMBO J.,* **9,** 3353–3362.

Yashima K, Litzky LA, Kaiser L, Rogers T, Lam S, Wistuba II, Milchgrub S, Srivastava S, Piatyszek MA, Shay JW and Gazdar AF. (1997). *Cancer Res.,* **57,** 2373–2377.

hTERT Expression Is a Prognostic Factor of Survival in Patients with Stage I Non-Small Cell Lung Cancer[1]

Luo Wang, Jean-Charles Soria, Bonnie L. Kemp, Diane D. Liu, Li Mao, and Fadlo R. Khuri[2]

Departments of Thoracic/Head and Neck Medical Oncology [L. W., J-C. S., L. M., F. R. K.], Pathology [B. L. K.], and Biostatistics [D. D. L.], The University of Texas M. D. Anderson Cancer Center, Houston, TX 77030

ABSTRACT

Activation of telomerase plays a critical role in unlimited proliferation and immortalization of cells. The purpose of this study was to evaluate the significance of human telomerase reverse transcriptase catalytic subunit (hTERT) as a prognostic marker.

The expression of hTERT in a large population of 153 patients with stage I non-small cell lung cancer was analyzed using the *in situ* hybridization technique.

We found that diffuse and clear hTERT expression was present in 51 (33%) of 153 patients. Kaplan-Meier analysis showed that hTERT expression was associated with shorter overall survival ($P = 0.04$), shorter disease-specific survival ($P = 0.03$), and shorter disease-free survival ($P = 0.02$). Multivariate analysis confirmed this independent prognostic value of hTERT expression.

Our results indicated that hTERT mRNA expression is associated with malignant tumor progression and poor outcome. hTERT may serve as a useful marker to identify patients with poor prognosis and to select patients with early-stage non-small cell lung cancer who might benefit from adjuvant treatment.

INTRODUCTION

Lung cancer retains the leading position in cancer-related deaths in the United States. In 2002, it is estimated that there will be 154,900 deaths and 169,400 new cases from lung and bronchial cancer in the United States, compared with 156,900 deaths and 164,100 new cases in 2000 (1). NSCLC[3] comprises more than 80% of lung cancers, and complete surgical resection of primary tumors in early-stage disease is the only potentially curative treatment. For patients with stage I NSCLC (about 17% of all patients with NSCLC), the average 5-year survival rate is about 60%. Adjuvant cytotoxic chemotherapy has been proposed and evaluated in the setting of NSCLC, and it offers limited hope of improving prognosis (2). One area of intense research on early-stage NSCLC is the identification of molecular markers to complement TNM staging to fully assess the prognosis of patients and to evaluate the effects of novel chemotherapy agents and regimens (3). Such prognostic markers include a wide variety of protein molecular markers that can be classified by different antibodies as molecular genetic markers, metastatic propensity markers, differentiation markers, and proliferation markers (3). Other markers have been evaluated at the mRNA level including retinoic acid receptor-β, cyclooxygenase-2, vascular endothelial growth factor, MMP-2 and -9, E-cadherin, angiopoietin-2, and CD44. These markers have been associated with clinicopathological variables and survival time in patients with NSCLC (4–8).

Telomerase is a ribonucleoprotein enzyme that lengthens chromosome ends that have been shortened during successive cycles of cell division (9). Telomerase is expressed in up to 85% of NSCLCs (10, 11), and its activation plays a critical role in tumorigenesis by sustaining cellular immortality (12, 13). Hahn *et al.* (14) proved that disruption of the intracellular pathways regulated by large T antigen, oncogenic *ras*, and telomerase suffices to create a human tumor cell. The components of human telomerase include an RNA subunit (hTERC), a catalytic protein subunit (hTERT), and other telomerase-associated proteins (15). It has been shown that the expression pattern of hTERT is closely associated with telomerase activity (16–18). The recent development of ISH techniques that can reliably detect hTERT mRNA has made it possible to examine the expression of this critical telomerase component at the single-cell level (18–21). In our previous study (22), we evaluated hTERT expression in bronchial biopsy samples and found that it was a frequent event and appeared at a very early stage in cigarette smoking-induced lung carcinogenesis, making it clearer that telomerase plays a critical role in tumorigenesis. Because we have established a reliable ISH technique for detecting hTERT mRNA expression in paraffin-embedded tissue, we decided to evaluate the prognostic value of hTERT in a relatively homogeneous tumor, in a population of 153 patients with stage I NSCLC.

Received 2/26/02; revised 6/3/02; accepted 6/3/02.

The costs of publication of this article were defrayed in part by the payment of page charges. This article must therefore be hereby marked *advertisement* in accordance with 18 U.S.C. Section 1734 solely to indicate this fact.

[1] Funded by BESCT (Biology, Education, Screening, Chemoprevention, and Treatment) Lung Cancer Program, Department of Defense Grant DAMD17-01-1-0689-1 projects 1 and 3 (to L. M. and F. R. K.), Cancer Center Grant P30 CA-16620 (to M. D. Anderson Cancer Center), Tobacco Research Fund from the State of Texas (to M. D. Anderson Cancer Center), and Fondation de France, AP-HP, and a Lilly Foundation grant (to J-C. S.).

[2] To whom requests for reprints should be addressed, at Department of Thoracic/Head and Neck Medical Oncology, The University of Texas M. D. Anderson Cancer Center, Box 432, 1515 Holcombe Boulevard, Houston, TX 77030. Phone: (713) 792-6363; Fax: (713) 796-8655; E-mail: fkhuri@mdanderson.org.

[3] The abbreviations used are: NSCLC, non-small cell lung cancer; hTERT, human telomerase reverse transcriptase subunit; ISH, *in situ* hybridization; MMP, matrix metalloprotease; hnRNP A1, heterogeneous nuclear ribonucleoprotein A1; TRAP, telomeric repeat amplification protocol; TNM, tumor node metastasis; CI, confidence interval; SCC, squamous cell carcinoma.

MATERIALS AND METHODS

Clinical Samples and Preparation of Slides. Five hundred ninety-five consecutive patients with stage I NSCLC underwent definitive surgical resection, defined as a lobectomy or a pneumonectomy, from 1975 to 1993 at The University of Texas M. D. Anderson Cancer Center. We retrospectively examined 153 cases for which both tissue samples as well as data from a median follow-up period of more than 5 years were available. All available tissue blocks for each patient were reviewed for the presence of tumor by a thoracic pathologist (B. L. K.). To prevent RNA degradation in the tissue blocks during sectioning, we used glass slides that were pretreated with diethylpyrocarbonate-treated water (Sigma Chemical Co., St. Louis, MO) and coated with poly-lysine (Sigma Chemical Co.). The patient population was identified through a search of the Tumor Registry Database maintained by the Department of Medical Informatics at M. D. Anderson Cancer Center. The study was reviewed and approved by the institution's Surveillance Committee to allow us to obtain the tissue blocks and all pertinent follow-up information.

Generation of Single-Strand-specific Riboprobes. The riboprobe used in the present study, a 430-bp EcoRV-BamHI fragment of the full-length hTERT cDNA, is identical to the one initially reported by Kolquist *et al.* in 1998 (18). We have successfully tested this probe in 532 paraffin-embedded sections of bronchial origin, in a previous study (22). Although larger than the classical 50–300-bp probes usually developed for ISH, this probe remains well in the range of previous probes used to evaluate hTERT by ISH (18–22). Part of exon 1 from hnRNP A1 was used as a control to verify sample quality.

Both cDNA fragments were cloned into the pCRII-TOPO vector (Invitrogen, Carlsbad, CA). The single-strand-specific riboprobes were generated by using *in vitro* transcription. In brief, the plasmid was linearized with EcoRV and then transcribed *in vitro* with SP6 RNA polymerase (Promega, Madison, WI) using a DIG RNA labeling kit (Roche Diagnostics, Inc., Indianapolis, IN). The resulting digoxigenin-labeled RNA probe was mixed with RNase inhibitor (Roche Diagnostics, Inc.) and stored in aliquots at −80°C.

RNA ISH. ISH was performed as described previously (22). Briefly, the sections were deparaffinized in xylene and then gradually rehydrated in decreasing concentrations of ethanol. They were then treated with 2.5 μg/ml proteinase K (Roche Diagnostics, Inc.), post-fixed in 4% paraformaldehyde, and acetylated in 0.25% acetic anhydride/0.1 M triethanolamine (Sigma Chemical Co.). After dehydrating in increasing concentrations of ethanol and air-drying, the sections were hybridized with the probe at 42°C for 4 h by incubating in hybridization buffer [400–800 ng/ml of either hTERT or hnRNP A1 riboprobe, 10% 20× SSC, 50% deionized formamide, 5% dextran sulfate, 2% 100× Denhardt's solution (2% Ficoll 400, 2% povidone, and 2% BSA), 10 mM DTT, 250 μg/ml predenatured salmon sperm DNA, and 200 μg/ml yeast tRNA]. The sections were then washed two times for 5 min in 2× SSC and then for 2 h in 2× SSC containing 0.05% Triton X-100 and 2% normal sheep serum (Sigma Chemical Co.) with agitation at room temperature. After being briefly rinsed in buffer 1 [0.1 M maleic acid and 0.15 M NaCl (pH 7.5)], the sections were washed in buffer 1 containing 0.3% Triton X-100 and 2% normal sheep serum for another 30 min at room temperature.

Detection was performed using the DIG Nucleic Acid Detection Kit (Roche Diagnostics, Inc.) according to the manufacturer's directions. Anti-DIG alkaline phosphotase-conjugated antibody was diluted 1:500. Nitro-blue tetrazolium and 5-bromo-4-chloro-3-indolyl phosphate were used as chromogens. Slides were then rinsed in TE buffer [10 mM Tris-HCl/1 mM EDTA (pH 8)] and mounted with Aqua-Mount medium (Fisher, Houston, TX).

Determination of Positive hTERT Expression. As reported by Falchetti *et al.* (21), only slides displaying a clear cytoplasmic signal could be considered as positive. More specifically, our slides were rated as positive if such a definite and clear signal was present in at least two large areas (×200 magnification) on the slide. Slides with faint signal, the absence of signal, or only focal positivity were considered to be negative. We did not grade the intensity of the hybridization signals.

To confirm RNA preservation in hTERT-negative slides, we randomly selected 33 such negative slides and detected the expression of the major splicing factor hnRNP A1. Because hnRNP A1 is one of the most abundant splicing factors in human cells, this probe was a good control to check mRNA quality.

Statistical Analysis. All statistical analyses were performed using SAS software (version 6.12; SAS Institute, Inc., Cary, NC). Overall, disease-specific and disease-free survival rates were calculated using the Kaplan-Meier method. All survival times were calculated from the date of surgery. The overall survival statistic accounted for all deaths (cancer related or not). Disease-specific survival time was calculated from the date of surgery to death from cancer-related causes. Disease-free survival time was calculated from the date of surgery to relapse or death from cancer-related causes. The χ^2 test was used to test the association between two categorical variables. The Wilcoxon rank-sum test was used for differences in median of age. We used the Cox proportional hazards model for univariate analysis to evaluate the association between survival time and risk factors and for multivariate analysis to model the risks of hTERT expression on survival time, with adjustment for clinical and histopathological parameters (age, sex, race, tumor histology, tumor size). All *P*s were determined by two-sided tests. *P*s less than 0.05 were considered statistically significant.

RESULTS

A total of 153 cases that had adequate tumor specimen and ≥5-year follow-up information were analyzed for hTERT mRNA expression in this study. The study population consisted of 115 men and 38 women; 136 patients were white, and 17 patients were of other ethnicities (Table 1). Patient ages ranged from 37–85 years old, with a median age of 63.4 ± 9.2 years old. Histological subtypes included 66 cases of SCC, 59 cases of adenocarcinoma, 12 cases of bronchioalveolar carcinoma, 5 cases of large cell carcinoma, 5 cases of adenosquamous carcinoma, and 6 unclassified cases. Thirty-nine patients died of lung cancer. The other patients died of heart disease (21 cases), respiratory diseases (15 cases), other organ failures (6 cases), and unknown causes (24 cases). The probability of 5-year over-

Table 1 hTERT expression status in stage I NSCLC tumors according to clinicopathological features of patients

Variable	Total no. of patients (n = 153)	hTERT expression		P
		Positive (n = 51)	Negative (n = 102)[a]	
Age (mean ± SD)	63.4 ± 9.2	64.3 ± 9.5	62.9 ± 9.1	0.38
Sex				
Male	115	40	75	0.51
Female	38	11	27	
Race				
White	136	42	94	0.09
Other	17	9	8	
Smoker				
Yes	137	47	90	1[b]
No	7	2	5	
Unknown	9	2	7	
Tumor histology				
SCC	66	27	39	0.08
Adenocarcinoma and others	87	24	63	
TNM stage				
T1N0M0	75	27	48	0.49
T2N0M0	78	24	54	
5-year overall survival rate (95% CI)	56.1% (48.7%, 64.6%)	42.7% (30.9%, 58.8%)	62.9% (54.1%, 73.1%)	

[a] This number included 36 cases in which the signal was faint or focal.
[b] The P was calculated to compare smoking and nonsmoking patients.

all survival for the whole population was 56.1% (95% CI, 48.7–64.6%).

By using the hTERT riboprobe, we detected diffuse and clear hTERT mRNA expression in tumor cell nests as well as in some infiltrating tumor lymphocytes (Fig. 1). In pilot experiments, the positive hybridization signal was always cytoplasmic and was abrogated by RNase treatment of the sections before hybridization with the riboprobe, suggesting that the signal was related to the presence of hTERT mRNA. The hybridization signal for hTERT mRNA in the tumorous area of positive samples ranged in intensity from low or moderate to strongly positive and was detectable in the vast majority of cells examined (Fig. 1). Interestingly, we found hTERT-positive cases in all of the histological subtypes we tested (Fig. 1). Slides that were negative for hTERT mRNA (*i.e.*, that had no hybridization signal or only focal positivity) also contained different histological subtypes (Fig. 2). We clearly detected hnRNP A1 mRNA, used as a positive control, in all 33 of the randomly selected hTERT-negative slides, therefore ruling out false-negativity related to RNA degradation (Fig. 2).

Among these 153 cases screened for hTERT expression by ISH, the percentage of tumors that were hTERT positive was 33.3% (51 cases). The positive slides were randomly distributed in the different years of surgery, and statistical analysis did not show any difference between the positive rates of slides by year (data not shown). The association between hTERT expression and the general clinicopathological characteristics of the patients is shown in Table 1. There was no statistical significance between age, sex, tumor size (T1N0M0 *versus* T2N0M0), and smoking status between the hTERT-positive cases and the hTERT-negative cases. Only seven patients were nonsmokers, thereby preventing any definitive conclusion regarding the association between hTERT expression and smoking. There was a trend, but no statistical significance, toward more cases with positive expression of hTERT in Caucasians (P = 0.09).

We subsequently analyzed the relationship between hTERT expression and length of survival. The median follow-up time for the patient population was 10.5 years. Fig. 3*A* shows the overall survival curves analyzed using the Kaplan-Meier method. Patients with tumors that were hTERT positive had a shorter survival time than did patients with tumors that were hTERT negative (P = 0.04; log-rank test). The 5-year overall survival rate for patients whose tumors were hTERT positive was 42.7% (95% CI, 30.9–58.8%) and 62.9% (95% CI, 54.1–73.1%) for patients whose tumors were hTERT negative (Table 1). Fig. 3*B* shows that patients with positive hTERT expression had significantly shorter disease-specific survival times than did patients with negative hTERT expression (P = 0.03; log-rank test). A comparison of disease-free survival curves in hTERT-negative and hTERT-positive patients yielded similar results (P = 0.02; log-rank test; Fig. 3*C*).

The univariate Cox proportional hazards model was used to evaluate the association between hTERT expression, clinicopathological variables (age, sex, race, histological subtype, TNM stage), and survival time. Table 2 shows the results on disease-specific survival time. In a multivariate Cox proportional hazards model, among all clinicopathological variables, hTERT expression was the only significant independent prognostic indicator for disease-specific survival.

DISCUSSION

Numerous prognostic factors have been identified in patients with early-stage NSCLC that might enable classification of such patients into different subsets corresponding to different risks of recurrence following complete resection. Most of the markers are proteins that can be detected by immunohistochemistry assays based on the antigen-antibody reaction. These markers, in general, can be classified into four groups: molecular genetic markers such as K-*ras*/p21 protein, p53 protein, C-erbB-

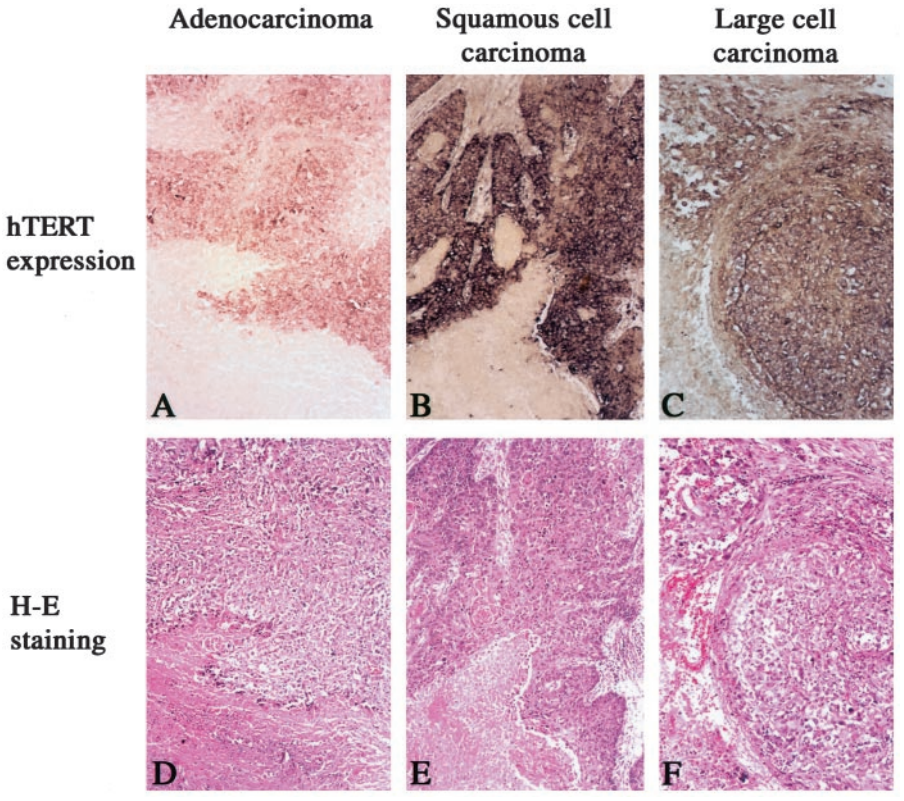


Fig. 1 hTERT expression detected by ISH in an adenocarcinoma (*A*), a SCC (*B*), and a large cell carcinoma (*C*). Magnification, ×100. Panels *D*, *E*, and *F* represent Hematoxylin and Eosin stained samples from the same tumors and adjacent slices to panels *A*, *B*, and *C*.

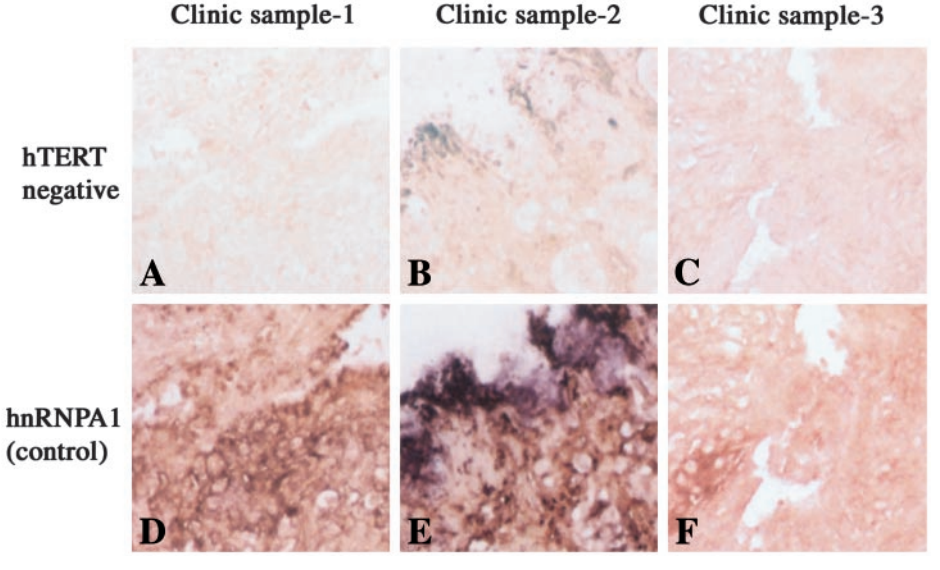


Fig. 2 Sample quality detected by ISH with hnRNP A1 as the control in hTERT-negative cases. Magnification, ×200.

2/p185, bcl-2 protein, and Rb protein; metastatic propensity markers such as CK18 protein, cathepsin B protein, factor VIII and type IV collagen; differentiation markers such as the ABH blood group antigen and the Lewis-related antigen; and proliferation markers such as Ki-67 nuclear antigen and proliferating cell nuclear antigen (3).

Because the major value of prognostic markers is to guide postresection treatment in early-stage NSCLC, the ability to identify patients with a high risk of cancer-related events such as recurrence or metastasis will help to determine whether adjuvant therapy is needed and to evaluate its effect. However, no conclusions have been reached about which marker or markers are better for forecasting patients' outcomes. Therefore, one of the major current interests in this field is to evaluate other novel

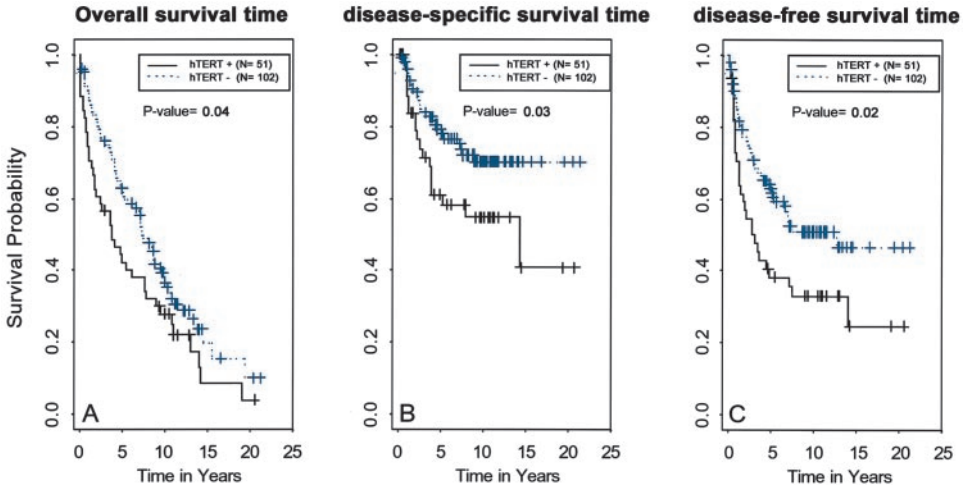


Fig. 3 Survival analysis of 153 patients with stage I NSCLC based on the classification of hTERT-positive and -negative mRNA expression. *A*, overall length of survival; *B*, disease-specific survival time; *C*, length of disease-free survival.

Table 2 A univariate Cox proportional hazards model applied to disease-specific survival time

Variable	Hazard ratio	95% CI	*P*
Age	1.0	0.98–1.05	0.51
Sex (male or female)	1.1	0.57–2.14	0.77
Race (white or other)	0.56	0.25–1.25	0.15
Histological subtype (SCC or other)	0.76	0.41–1.42	0.39
Tumor size (T1 or T2)	1.03	0.57–1.86	0.92
hTERT (+ or −)	1.90	1.04–3.45	0.036

markers. Some effort has been put forth to test mRNA markers such as retinoic acid receptor-β, cyclooxygenase-2, vascular endothelial growth factor, MMP-2, MMP-9, E-cadherin, angiopoietin-2, and CD44 (4–8).

Telomerase activity has been described as an independent marker of poor prognostic in different human tumors such as neuroblastoma, gastric cancer, breast cancer, colon cancer, cervical cancer, and meningioma (23–28). In patients with NSCLC, a conclusion regarding the prognostic value of telomerase activity remains unclear. Hiyama *et al.* (29) first observed a high level of telomerase activity in primary tumors and corresponding metastatic lesions. However, Albanell *et al.* (30) found only a weak association between telomerase activity and unfavorable prognosis in a mixed population of 99 patients with stages I–IV NSCLC. Komiya *et al.* (31) examined the expression of hTERT mRNA in tumor specimens from 68 patients by using RT-PCR and did not find a correlation between hTERT status and any common clinical features, except age. However, Marchetti *et al.* (32) evaluated the activity of the telomerase enzyme detected by the TRAP assay in tumors and adjacent noncancerous lung tissue samples obtained from 107 consecutive patients with pathological stage I operable NSCLC. They found telomerase activity in 66 of 107 tumors but in none of the corresponding adjacent noncancerous lung tissue samples. They also found a statistically significant association between telomerase activity and both disease-free and overall survival times. Kumaki *et al.* (33), Arinaga *et al.* (34), and Satoshi *et al.* (35) reported different conclusions.

We considered that such contradictions in the literature could be attributed to analysis of heterogeneous populations with few patients with stage I NSCLC, and to the different techniques used to detect telomerase activity or expression. To address these issues, we decided to use ISH to measure the mRNA expression level of hTERT in a large population of 153 patients with stage I NSCLC for which complete follow-up information was available. Because the tumor samples had been stored for a long time (8–26 years), we anticipated that sample quality would be the first major problem in getting a correct signal. The second major issue for successful ISH is the probe. A single-strand riboprobe can yield a more specific signal than that of a standard double-strand cDNA probe labeled mostly by the random-primer method. The size and sequence of the riboprobe are also very important for successful ISH. The major component of human telomerase is hTERT, and it has been proven that the expression pattern of hTERT is closely associated with actual telomerase activity (16–18). On the basis of the analysis of the hTERT genomic sequence, we selected the most conserved region, from exon 7 to exon 12, as the probe, which also corresponded to the catalytic domain of this enzyme. The result is shown in Fig. 1. We are convinced that the hTERT ISH is a reliable technique. It can possibly be developed as a clinical assay, and, in fact, in a clinical trial of n-(4-hydroxyphenyl) retinamide, a compound derived from 13-*cis*-retinoic acid, we successfully used ISH to evaluate its effect on hTERT expression in the bronchial epithelium of smokers (22).

One major concern generated by our results is the low percentage (33%) of hTERT-positive cases reported in contrast to previous studies reporting telomerase activity in up to 85% of NSCLCs. We believe that this apparent discrepancy can be explained by the specific technique (ISH) and the strict criteria used in our study in comparison to the very sensitive TRAP assay. It is very important to point out that the TRAP assay does not account for tumor heterogeneity, and, therefore, tumors with few telomerase-positive cells appear telomerase positive in the same way as tumors in which most cells are telomerase positive. Furthermore, most previous studies on telomerase have been carried out in heterogeneous populations including patients with

stages I–IV disease (29–31). Marchetti *et al.* (32) reported a hTERT positivity rate of 66% by RT-PCR in stage I NSCLC. Falchetti *et al.* (21) investigated the expression of hTERT in 34 samples from patients with primary *de novo* glioblastoma multiforme by ISH, RT-PCR, TRAP activity assay, and telomere restriction fragment Southern blotting. They found that 60% of the cases were hTERT positive by ISH and could be classified into two groups: those with diffuse and those with focal hTERT expression. However, some studies have shown that telomerase activity can be detected at high, moderate, and low levels (26, 28). In cell lines, we found that the ISH signal generally corresponded to the level of telomerase activity detected by TRAP assay (data not shown). We considered that the focal hTERT expression does not seem to represent strong telomerase activity and decided to classify the cases with hTERT focal expression as negative.

In this study, even with our criteria, which are stricter than those used in other studies, a definite association exists between hTERT expression and all of the clinically relevant outcomes. This strongly supports our notion that substantial hTERT mRNA expression could be an ideal marker for assessing prognosis of patients with early-stage NSCLC and evaluating the effect of new chemotherapeutic agents.

In conclusion, based on a large population of patients with stage I NSCLC, our results indicate that hTERT mRNA expression is associated with malignant tumor progression, thereby making it a potentially suitable prognostic marker. ISH of hTERT expression may be used to distinguish patients with poor prognosis and to potentially guide the regimen of adjuvant chemotherapy for patients with early-stage NSCLCs. Nevertheless, confirmatory studies by independent groups, using ISH or alternative techniques (RT-PCR, TRAP), are necessary.

ACKNOWLEDGMENTS

We thank Julia M. Starr for editing the manuscript and Lakshmi Kakarala for histological assistance.

REFERENCES

1. Jamal, A., Thomas, A., Murray, T., and Thun, M. Cancer Statistics, 2002. Ca. Cancer J. Clin., *52:* 23–47, 2002.

2. Non-small Cell Lung Cancer Collaborative Group. Chemotherapy in non-small cell lung cancer: a meta-analysis using updated data on individual patients from 52 randomised clinical trials. Br. Med. J., *311*: 899–909, 1995.

3. Strauss, G. M. Prognostic markers in resectable non-small cell lung cancer. Hematol. Oncol. Clin. North Am., *11:* 409–434, 1997.

4. Khuri, F. R., Wu, H., Lee, J. J., Kemp, B. L., Lotan, R., Lippman, S. M., Feng, L., Hong, W. K., and Xu, X. C. Cyclooxygenase-2 overexpression is a marker of poor prognosis in stage I non-small cell lung cancer. Clin. Cancer Res., *7:* 861–867, 2001.

5. Khuri, F. R., Lotan, R., Kemp, B. L., Lippman, S. M., Wu, H., Feng, L., Lee, J. J., Cooksley, C. S., Parr, B., Chang, E., Walsh, G. L., Lee, J. S., Hong, W. K., and Xu, X. C. Retinoic acid receptor-β as a prognostic indicator in stage I non-small-cell lung cancer. J. Clin. Oncol., *18:* 2798–2804, 2000.

6. Wong, M. P., Chan, S. Y., Fu, K. H., Leung, S. Y., Cheung, N., Yuen, S. T., and Chung, L. P. The angiopoietins, tie2 and vascular endothelial growth factor are differentially expressed in the transformation of normal lung to non-small cell lung carcinomas. Lung Cancer, *29:* 11–22, 2000.

7. Pirinen, R., Hirvikoski, P., Bohm, J., Kellokoski, J., Moisio, K., Viren, M., Johansson, R., Hollmen, S., and Kosma, V. M. Reduced expression of CD44v3 variant isoform is associated with unfavorable outcome in non-small cell lung carcinoma. Hum. Pathol., *31:* 1088–1095, 2000.

8. Herbst, R. S., Yano, S., Kuniyasu, H., Khuri, F. R., Bucana, C. D., Guo, F., Liu, D., Kemp, B. L., Lee, J. J., Hong, W. K., and Fidler, I. J. Differential expression of E-cadherin and type IV collagenase genes predicts outcome in patients with stage I non-small cell lung carcinoma. Clin. Cancer Res., *6:* 790–797, 2000.

9. Greider, C. W., and Blackburn, E. H. Identification of a specific telomere terminal transferase activity in Tetrahymena extracts. Cell, *43:* 405–413, 1985.

10. Hiyama, K., Hiyama, E., Ishioka, S., Yamakido, M., Inai, K., Gazdar, A. F., Piatyszek, M. A., and Shay, J. W. Telomerase activity in small-cell and non-small-cell lung cancers. J. Natl. Cancer Inst., *87:* 895–902, 1995.

11. Albanell, J., Lonardo, F., Rusch, V., Engelhardt, M., Langenfeld, J., Han, W., Klimstra, D., Venkatraman, E., Moore, M. A., and Dmitrovsky, E. High telomerase activity in primary lung cancers: association with increased cell proliferation rates and advanced pathologic stage. J. Natl. Cancer Inst., *89:* 1609–1615, 1997.

12. Dhaene, K., Van Marck, E., and Parwaresch, R. Telomeres, telomerase and cancer: an up-date. Virchows Arch., *437:* 1–16, 2000.

13. Kim, N. W., Piatyszek, M. A., Prowse, K. R., Harley, C. B., West, M. D., Ho, P. L., Coviello, G. M., Wright, W. E., Weinrich, S. L., and Shay, J. W. Specific association of human telomerase activity with immortal cells and cancer. Science (Wash DC), *266:* 2011–2015, 1994.

14. Hahn, W. C., Counter, C. M., Lundberg, A. S., Beijersbergen, R. L., Brooks, M. W., and Weinberg, R. A. Creation of human tumour cells with defined genetic elements. Nature (Lond.), *400:* 464–468, 1999.

15. Feng, J., Funk, W. D., Wang, S. S., Weinrich, S. L., Avilion, A. A., Chiu, C. P., Adams, R. R., Chang, E., Allsopp, R. C., Yu, J., Le, S., West, M. D., Harley, C. B., Andrews, W. H., Greider, C. W., and Villeponteau, B. The RNA component of human telomerase. Science (Wash DC), *269:* 1236–1241, 1995.

16. Meyerson, M., Counter, C. M., Eaton, E. N., Ellisen, L. W., Steiner, P., Caddle, S. D., Ziaugra, L., Beijersbergen, R. L., Davidoff, M. J., Liu, Q., Bacchetti, S., Haber, D. A., and Weinberg, R. A. hEST2, the putative human telomerase catalytic subunit gene, is up-regulated in tumor cells and during immortalization. Cell, *90:* 785–795, 1997.

17. Nakamura, T. M., Morin, G. B., Chapman, K. B., Weinrich, S. L., Andrews, W. H., Lingner, J., Harley, C. B., and Cech, T. R. Telomerase catalytic subunit homologs from fission yeast and human. Science (Wash DC), *277:* 955–959, 1997.

18. Kolquist, K. A., Ellisen, L. W., Counter, C. M., Meyerson, M., Tan, L. K., Weinberg, R. A., Haber, D. A., and Gerald, W. L. Expression of TERT in early premalignant lesions and a subset of cells in normal tissues. Nat. Genet., *19:* 182–186, 1998.

19. Nakano, K., Watney, E., and McDougall, J. K. Telomerase activity and expression of telomerase RNA component and telomerase catalytic subunit gene in cervical cancer. Am. J. Pathol., *153:* 857–864, 1998.

20. Liu, K., Schoonmaker, M. M., Levine, B. L., June, C. H., Hodes, R. J., and Weng, N. P. Constitutive and regulated expression of telomerase reverse transcriptase (hTERT) in human lymphocytes. Proc. Natl. Acad. Sci. USA, *96:* 5147–5152, 1999.

21. Falchetti, M. L., Pallini, R., D'Ambrosio, E., Pierconti, F., Martini, M., Cimino-Reale, G., Verna, R., Maira, G., and Larocca, L. M. In situ detection of telomerase catalytic subunit mRNA in glioblastoma multiforme. Int. J. Cancer, *88:* 895–901, 2000.

22. Soria, J. C., Moon, C., Wang, L., Hittelman, W. N., Jang, S. J., Sun, S. Y., Lee, J. J., Liu, D., Kurie, J. M., Morice, R. C., Lee, J. S., Hong, W. K., and Mao, L. Effects of *N*-(4-hydroxyphenyl) retinamide on hTERT expression in the bronchial epithelium of smokers. J. Natl. Cancer Inst., *93:* 1257–1263, 2001.

23. Hiyama, E., Hiyama, K., Yokoyama, T., Matsuura, Y., Piatyszek, M. A., and Shay, J. W. Correlating telomerase activity levels with human neuroblastoma outcomes. Nat. Med., *1:* 249–255, 1995.

24. Hiyama, E., Yokoyama, T., Tatsumoto, N., Hiyama, K., Imamura, Y., and Murakami, Y. Telomerase activity in gastric cancer. Cancer Res., *55:* 3258–3262, 1995.

25. Kim, N. W., Levitt, D., Huang, G., Wu, F., Osborne, K., and Clark, G. Correlation of telomerase with prognostic indicators of breast cancer. Proc. Am. Assoc. Cancer Res., *37:* 561–562, 1996.

26. Clark, G. M., Osborne, C. K., Levitt, D., Wu, F., and Kim, N. W. Telomerase activity and survival of patients with node-positive breast cancer. J. Natl. Cancer Inst., *89:* 1874–1881, 1997.

27. Wisman, G. B. A., De Jong, S., Meersma, G. J., Helder, M. N., Hollema, H., de Vries, E. G. E., Keith, W. N., and van der Zee, A. G. J. Telomerase in (pre)neoplastic cervical disease. Hum. Pathol., *31:* 1304–1312, 2000.

28. Tatsumoto, N., Hiyama, E., Murakami, Y., Imamura, Y., Shay, J. W., Matsuura, Y., and Yokoyama, T. High telomerase activity is an independent prognostic indicator of poor outcome in colorectal cancer. Clin. Cancer Res., *6:* 2696–2701, 2000.

29. Hiyama, K., Hiyama, E., Ishioka, S., Yamakido, M., Inai, K., Gazdar, A. F., Piatyszek, M. A., and Shay, J. W. Telomerase activity in small-cell and non-small-cell lung cancer. J. Natl. Cancer Inst., *87:* 895–902, 1995.

30. Albanell, J., Leonardo, F., Rusch, V., Engelhardt, M., Langenfeld, J., Han, W., Klimstra, D., Venkatraman, E., Moore, M. A. S., and Dmitrovsky, E. High telomerase activity in primary lung cancer: association with increased cell proliferation rates and advanced pathologic stage. J. Natl. Cancer Inst., *89:* 1609–1615, 1997.

31. Komiya, T., Kawase, I., Nitta, T., Yasumitsu, T., Kikui, M., Fukuoka, M., Nakagawa, K., and Hirashima, T. Prognostic significance of hTERT expression in non-small cell lung cancer. Int. J. Oncol., *16:* 1173–1177, 2000.

32. Marchetti, A., Bertacca, G., Buttitta, F., Chella, A., Quattrocolo, G., Angeletti, C. A., and Bevilacqua, G. Telomerase activity as a prognostic indicator in stage I non-small cell lung cancer. Clin. Cancer Res., *5:* 2077–2081, 1999.

33. Kumaki, F., Kawai, T., Hiroi, S., Shinomiya, N., Ozeki, Y., Ferrans, V. J., and Torikata, C. Telomerase activity and expression of human telomerase RNA component and human telomerase reverse transcriptase in lung carcinomas. Hum. Pathol., *32:* 188–195, 2001.

34. Arinaga, M., Shimizu, S., Gotoh, K., Haruki, N., Takahashi, T., Takahashi, T., and Mitsudomi, T. Expression of human telomerase subunit genes in primary lung cancer and its clinical significance. Ann. Thorac. Surg., *70:* 401–405, 2000.

35. Satoshi, T., Toshihiro, O., Akira, O., Hideyuki, I., and Kosei, Y. Prognostic impact of telomerase activity in non-small cell lung cancers. Ann. Surg., *230:* 715–720, 1999.

Expression of *ΔDNMT3B* Variants and Its Association with Promoter Methylation of *p16* and *RASSF1A* in Primary Non–Small Cell Lung Cancer

Jie Wang,[1,4] Garret Walsh,[2] Diane D. Liu,[3] J. Jack Lee,[3] and Li Mao[1]

[1]Molecular Biology Laboratory, Department of Thoracic/Head and Neck Medical Oncology, [2]Department of Thoracic and Cardiovascular Surgery, and [3]Department of Biostatistics, University of Texas M.D. Anderson Cancer Center, Houston, Texas and [4]Department of Oncology, Beijing Cancer Hospital, Beijing University School of Oncology, Beijing, China

Abstract

Despite the role of DNMT3B in *de novo* DNA methylation, a correlation between DNMT3B expression and promoter DNA methylation has not being established in tumors. We recently reported *ΔDNMT3B*, a subfamily of *DNMT3B*, with seven variants, as the predominant expression forms in non–small cell lung cancer (NSCLC). We hypothesized that expression of the *ΔDNMT3B* variants plays a role in promoter methylation formation during lung tumorigenesis. Expression of seven *ΔDNMT3B* variants was measured in 119 NSCLCs and the corresponding normal lungs using reverse transcription-PCR. The expression patterns of *ΔDNMT3B* variants were analyzed with the status of *p16* and *RASSF1A* promoter methylation in the tumors as well as in patients' clinical variables, including outcomes. Expression of *ΔDNMT3B* variants was detected in 94 of 119 (80%) tumors but in only 22 (18%) of the corresponding normal lungs ($P < 0.0001$). *ΔDNMT3B1*, *ΔDNMT3B2*, and *ΔDNMT3B4* were the most frequently detected transcripts in the tumors (62%, 76%, and 46%, respectively). The expression of *ΔDNMT3B* variants was associated with *p16* and *RASSF1A* promoter methylation in the tumors, but the strongest association was between *ΔDNMT3B4* and *RASSF1A*. Forty-two of 46 (91%) tumors with *RASSF1A* promoter methylation expressed *ΔDNMT3B4* compared with only 13 of 73 (18%) tumors without the promoter methylation ($P < 0.0001$). Strong associations were also observed between expression of the variants in the tumors and in patients' clinical outcomes. Expression of *ΔDNMT3B* variants is common in NSCLC and may play an important role in the development of promoter methylation. (Cancer Res 2006; 66(17): 8361-6)

Introduction

DNA methylation plays an important role in regulation of gene expression, genomic imprinting, and X-chromosome inactivation (1–5). During tumorigenesis, promoter hypermethylation is a major mechanism to inactivate tumor suppressor genes with CpG-rich promoters (6). In non–small cell lung cancer (NSCLC), promoter methylation has been frequently detected in several tumor suppressor genes, such as *p16* and *RASSF1A* (7–10). Although some tumors tend to have more promoters methylated than others, each tumor has distinct profiles of methylated promoters, suggesting a complex mechanism in controlling the *de novo* methylation process. Understanding the process is important to develop strategies for lung cancer prevention, molecular classification, and targeted therapy.

DNMT3B, an important member of DNMT3 family, is a *de novo* methyltransferase, which adds the first methyl group to the cytosine of unmethylated DNA (1, 11, 12). It has been shown that DNMT3B is overexpressed in transformed cells and in multiple types of primary tumors, including NSCLC (13–15). However, the correlation between the expression levels of DNMT3B and promoter methylation status in human cancers has been weak (15–17), suggesting that other key factors are involved in regulation of the promoter methylation. We recently identified a new subfamily of *DNMT3B*, termed *ΔDNMT3B*, due to its lack of part of the NH_2-terminal sequence (18). We showed that *ΔDNMT3B* is the major transcript of *DNMT3B* in NSCLC and has at least seven transcriptional variants resulting from alternative splicing (18). The purpose of the study was to analyze the expression patterns of *ΔDNMT3B* variants in primary NSCLC and to determine their potential relationship with methylation status of tumor suppressor genes commonly altered in NSCLC. To determine biological significance of the molecules, the relationship between expression of the *ΔDNMT3B* variants and patients' clinical outcomes was also analyzed.

Materials and Methods

Patients and specimens. One hundred and nineteen primary tumor samples and their corresponding nonmalignant lung tissues were obtained from patients with stages I to IIIa NSCLC (all stages are pathology stages). All the patients were treated by surgery with curative intend, except those with stage IIIa tumors who might also received postoperative radiation therapy and adjuvant chemotherapy in M. D. Anderson Cancer Center from 1995 to 2000. Samples were immediately frozen and stored at −80°C until analysis. The selection of these patients was based on the availability of archived fresh tumor and corresponding normal lung tissues for the investigators. The clinical information and follow-up data were based on chart review and reports from tumor registry service. Informed consent for the use of residual resected tissues for research was obtained from all the patients enrolled in the study. The study was reviewed and approved by the institution's Surveillance Committee to use the tissues and clinical information. The patients ranged in age from 32 to 84 years (median, 64 years). There were 40 patients with stage I disease, 30 stage II, and 49 stage IIIa. Histologic subtypes include 60 adenocarcinomas, 49 squamous cell carcinoma (SCC), and 7 large cell carcinoma (Table 1). None of the patients had received chemotherapy or radiation treatment before surgery. The median follow-up time was 50.96 months.

RNA extraction and reverse transcription-PCR. Total RNA from tissue samples was extracted by using Tri-Reagent according to the manufacturer's instruction. Approximately 1 to 2 μg of total RNA from each sample

Requests for reprints: Li Mao, Molecular Biology Laboratory, Department of Thoracic/Head and Neck Medical Oncology, Unit 432, The University of Texas M.D. Anderson Cancer Center, P.O. Box 301402, Houston, TX 77030. Phone: 713-792-6363; Fax: 713-796-8655; E-mail: lmao@mdanderson.org.

©2006 American Association for Cancer Research.

doi:10.1158/0008-5472.CAN-06-2031

Table 1. Expression of *ΔDNMT3Bs* and clinical/pathological parameters

ΔDNMT3B	*ΔDNMT3B1*, *n* (%)	*ΔDNMT3B2*, *n* (%)	*ΔDNMT3B3*, *n* (%)	*ΔDNMT3B4*, *n* (%)	*ΔDNMT3B5*, *n* (%)	*ΔDNMT3B6*, *n* (%)	*ΔDNMT3B7*, *n* (%)
Sex (*n*)							
F (47)	26 (55.3)	32 (68.1)	0 (0)	16 (34.0)*	9 (19.2)	9 (19.2)	4 (8.5)
M (72)	48 (66.7)	59 (81.9)	3 (4.2)	39 (54.2)	12 (16.7)	23 (31.9)	15 (20.8)
Smoke (*n*)							
No (38)	24 (63.2)	26 (68.4)	1 (2.6)	16 (42.1)	7 (18.4)	9 (23.7)	5 (13.2)
Yes (81)	50 (61.7)	65 (80.3)	2 (2.5)	39 (48.2)	14 (17.3)	23 (28.4)	14 (17.3)
Pathology (*n*)							
Adenocarcinoma (60)	36 (60.0)	45 (75.0)	1 (1.7)	25 (41.7)	9 (15.0)	13 (21.7)	5 (8.3)
SCC (49)	29 (59.2)	37 (75.5)	1 (2.0)	25 (51.0)	10 (20.4)	16 (32.7)	11 (22.5)
Differentiation (*n*)							
Well (11)	6 (54.6)	7 (63.6)	0 (0)	4 (36.4)	0 (0)†	0 (0)†	0 (0)†
Moderate (50)	32 (64.0)	39 (78.0)	1 (2.0)	19 (38.0)	7 (14.0)	11 (22.0)	7 (14.0)
Poor (58)	36 (62.1)	45 (77.6)	2 (3.5)	32 (55.2)	14 (24.1)	21 (36.2)	12 (20.7)
Stage (*n*)							
I and II (70)	43 (61.4)	55 (78.6)	0 (0)	34 (48.6)	11 (15.7)	16 (22.9)	6 (8.6)‡
III (49)	31 (63.3)	36 (73.5)	3 (6.1)	21 (42.9)	10 (20.4)	16 (32.7)	13 (26.5)

*No statistical significant correlation was found, except $P = 0.03$.
†No statistical significant correlation was found, except $P < 0.05$.
‡No statistical significant correlation was found, except $P = 0.009$.

were used to conduct reverse transcription reaction in a 20 μL volume by using SuperScript II RNase H-reverse transcriptase (Life Technologies, Inc., Gaithersburg, MD). The PCR was carried out in a 12.5 μL volume containing 0.5 μL reverse transcription product, 1.5 mmol/L deoxynucleotide triphosphate (dNTP), 7% DMSO, 6.7 μmol/L $MgCl_2$, 16.6 mmol/L $(NH_4)SO_4$, 67 mmol/L Tris, 10 mmol/L B-mercaptoethanol, 6.7 μmol/L EDTA, 0.5 μmol/L of both the sense and antisense primers, and 0.625 unit of HotStar Taq DNA polymerase (Life Technologies). Amplification was done with an initial denaturing step at 95°C for 15 minutes followed by 40 cycles of 95°C for 30 seconds, 58°C for 1 minute, and 72°C for 1 minute in a thermal cycler with a last extension step of 72°C for 10 minutes. PCR products were separated on 2.5% agarose gels and visualized after staining with ethidium bromide. The expression of specific *ΔDNMT3B* variants was determined by using specific primer sets corresponding to unique sequences of individual *ΔDNMT3B* variants as reported previously (18). Any expression observed for a given variant was considered expression positive for both normal and tumor tissues.

DNA extraction and methylation-specific PCR. Frozen tissues were homogenized, and genomic DNA was extracted by digestion of homogenized tissues in buffer containing 50 mmol/L Tris-HCl (pH 8.0), 1% SDS, and 0.5 mg/mL proteinase K at 42°C for 36 hours. The digested products were purified with phenol-chloroform twice. DNA was then precipitated using the ethanol precipitation method and recovered in distilled DNase-free water. For methylation-specific PCR, 1 μg of genomic DNA from each tissue sample was used in the initial step of chemical modification. Briefly, DNA was denatured by NaOH and treated with sodium bisulfite (Sigma Chemical Co., St. Louis, MO). After purification with the use of Wizard DNA purification resin (Promega Corp., Madison, WI), the DNA was treated again with NaOH. After precipitation, DNA was recovered in water and was ready for PCR with the use of specific primers for either the methylated or the unmethylated *p16* or *RASSF1A* promoter as reported previously (10). PCR was carried out in 25 μL containing ~100 ng of modified DNA, 3% DMSO, all four dNTPs (each at 200 μmol/L), 1.5 mmol/L $MgCl_2$, 0.4 μmol/L PCR primers, and 1.25 units of Taq DNA polymerase (Life Technologies). DNA was amplified for 35 cycles at 95°C for 30 seconds, 60°C for 60 seconds, and 70°C for 60 seconds followed by a 5-minute extension at 70°C in a temperature cycler (Hybaid; Omnigene, Woodbridge, NJ) in 500 μL plastic tubes. PCR products were separated on 2.5% agarose gels and visualized after staining with ethidium bromide. For each DNA sample, primer sets for methylated DNA and unmethylated DNA were used for analysis. CpGenome universal methylated DNA (Chemicon International, Temecula, CA) was used as positive controls, and water replacing for DNA was used as blank controls. The hypermethylation status was determined by visualizing a 150-bp PCR product for *p16* and a 169-bp PCR product for *RASSF1A* with the respective methylation-specific primer sets.

Statistical analysis. The χ^2 test or Fisher's exact test was used to test the association between categorical variables. Overall survival, disease-specific survival (i.e., survival rates among people who died of lung cancer–related causes specifically), and disease-free survival (i.e., recurrence, metastasis, or cancer death is considered as an event) were analyzed. Survival probability was estimated using the Kaplan-Meier method. The log-rank test was used to compare patients' survival time between or among groups. Cox regression was used to model the risks of biological variables on survival time, with adjustment for clinical and histopathologic variables (age, sex, tumor histology subgroup, tumor size, smoking status, and adjuvant treatment). All statistical tests are two sided, and $P < 0.05$ was considered statistically significant.

Results

Expression of *ΔDNMT3B* variants in primary NSCLC and the corresponding normal lungs. Expression of *ΔDNMT3B* variants was detected in 94 of 119 (80%) NSCLCs but in only 22 (20%) of the corresponding normal lungs. The difference of the expression rates between the tumor tissues and normal tissues was statistically significant ($P < 0.0001$). In the tumor tissues, the most frequently expressed variant was *ΔDNMT3B2* (91 or 76%) followed by *ΔDNMT3B1* (74 or 62%) and *ΔDNMT3B4* (55 or 46%) in the 119 primary NSCLCs. Expression of the other variants was less frequent; 32 (27%), 21 (18%), 19 (16%), and 3 (2.5%) for *ΔDNMT3B6, ΔDNMT3B5, ΔDNMT3B7*, and *ΔDNMT3B3*, respectively. Expression of the later group of *ΔDNMT3B* variants was not detected in any of the normal lung tissues.

Correlation between expression of *ΔDNMT3B* variants and clinicopathologic variables. We analyzed correlations between the expression of *ΔDNMT3B* variants and clinicopathologic variables of the patients (Table 1). Tumors from female patients had a higher frequency of *ΔDNMT3B4* expression than tumors from male patients ($P = 0.03$). Expression of *ΔDNMT3B5, ΔDNMT3B6*, and *ΔDNMT3B7* was more frequent in poorly differentiated tumors than in well-differentiated or moderately differentiated tumors ($P < 0.05$). The expression of *ΔDNMT3B7* was more frequent in stage III tumors than in stage I/II tumors ($P = 0.009$). No other correlation was observed (Table 1).

Correlation between expression of *ΔDNMT3B* variants and promoter methylation of *p16* and *RASSF1A* genes. Promoter methylation of *p16* and *RASSF1A* was detected in 58 (49%) and 46 (39%) of 119 tumors, respectively. Among the 94 tumors that expressed any of the *ΔDNMT3B* variants, 54 (57%) had *p16* promoter methylation and 46 (48%) had *RASSF1A* promoter methylation compared with 4 of 25 (16%) tumors without expression of any of the variants for *p16* and none for *RASSF1A* ($P < 0.0001$). We then analyzed the relationship between methylation status of *p16* and *RASSF1A* and expression of individual *ΔDNMT3B* variants in the tumor tissues. Promoter methylation of *p16* was correlated with expression of *ΔDNMT3B1, ΔDNMT3B2, ΔDNMT3B5*, and *ΔDNMT3B6*, whereas promoter methylation of *RASSF1A* was correlated with all the *ΔDNMT3B* variants, except *DNMT3B3* (Table 2). The most striking correlation was between expression of *ΔDNMT3B4* and promoter methylation of *RASSF1A*. Among the 46 tumors with promoter methylation of *RASSF1A*, 42 (91%) expressed *ΔDNMT3B4* compared with only 13 of 73 (18%) tumors without promoter methylation of *RASSF1A* ($P < 0.0001$). In contrast, expression of *ΔDNMT3B4* was not correlated with promoter methylation of *p16* ($P = 0.12$).

Interestingly, promoter methylation of *p16* was associated with promoter methylation of *RASSF1A* ($P = 0.004$). To determine independent factors correlated with promoter methylation, we did multivariate analysis. Results showed that promoter methylation of *p16* and expression of *ΔDNMT3B4* or *ΔDNMT3B7* were independent factors for promoter methylation of *RASSF1A*. After adjusting for *ΔDNMT3B7* expression and promoter methylation of *p16* using logistic regression analysis, expression of *DNMT3B4* remained its strong correlation with promoter methylation of *RASSF1A* ($P < 0.0001$), suggesting that *ΔDNMT3B4* is required for promoter methylation of *RASSF1A* in NSCLC.

Correlation between expression of *ΔDNMT3B* variants and clinical outcomes. We analyzed a potential correlation between expression of *ΔDNMT3B* variants and patients' clinical outcomes. Because many of the patients with stage III tumors underwent postsurgery radiation therapy or chemoradiation therapy whereas patients with stage I/II tumors did not, we analyzed the two groups separately. For stage I/II tumors, patients whose tumors expressed any of *ΔDNMT3B5, ΔDNMT3B6*, and *ΔDNMT3B7* had statistically significant poorer overall, disease-specific, and disease-free survivals than patients whose tumors had no expression of *ΔDNMT3B5, ΔDNMT3B6*, and *ΔDNMT3B7* ($P = 0.002$, $P < 0.001$, and $P < 0.001$, respectively; Fig. 1). Because *p16* promoter methylation was statistically correlated with the survivals in the patient population

Table 2. Expression of *ΔDNMT3Bs* and promoter methylation of p16/RASSF1A in NSCLC

ΔDNMT3B		*ΔDNMT3B1*, *n* (%)	*ΔDNMT3B2*, *n* (%)	*ΔDNMT3B3*, *n* (%)	*ΔDNMT3B4*, *n* (%)	*ΔDNMT3B5*, *n* (%)	*ΔDNMT3B6*, *n* (%)	*ΔDNMT3B7*, *n* (%)	*p16*, *n* (%)
ΔDNMT3B2	0	1 (3.6)							
	1	73 (80.2)							
	P	<0.0001							
ΔDNMT3B3	0	71 (61.2)	88 (75.9)						
	1	3 (100.0)	3 (100.0)						
	P	0.29	1						
ΔDNMT3B4	0	28 (43.8)	39 (60.9)	1 (1.6)					
	1	46 (83.6)	52 (94.6)	2 (3.6)					
	P	<0.0001	<0.0001	0.60					
ΔDNMT3B5	0	56 (57.1)	70 (71.4)	3 (100)	37 (37.8)				
	1	18 (85.7)	21 (100)	0 (0)	18 (85.7)				
	P	0.01	0.003	1	<0.0001				
ΔDNMT3B6	0	46 (52.9)	59 (67.8)	1 (1.2)	29 (33.3)	1 (1.2)			
	1	28 (88.5)	32 (100)	2 (6.3)	26 (81.3)	20 (62.5)			
	P	0.0005	<0.0001	0.18	<0.0001	<0.0001			
ΔDNMT3B7	0	57 (57.0)	73 (73.0)	1 (1.0)	39 (39.0)	10 (10.0)	15 (15.0)		
	1	17 (89.5)	18 (94.7)	2 (10.5)	16 (84.2)	11 (57.9)	17 (89.5)		
	P	0.009	0.04	0.07	0.0003	<0.0001	<0.0001		
p16	0	31 (50.8)	40 (65.6)	3 (100)	24 (39.3)	6 (9.8)	10 (16.4)	9 (14.8)	
	1	43 (74.1)	51 (87.9)	0 (0)	31 (53.5)	15 (25.9)	22 (37.9)	10 (17.2)	
	P	0.009	0.004	0.24	0.12	0.02	0.008	0.71	
RASSF1A	0	836 (49.3)	48 (65.8)	1 (1.4)	13 (17.8)	3 (4.1)	8 (11.0)	3 (4.1)	28 (38.4)
	1	38 (82.6)	43 (93.5)	2 (4.4)	42 (91.3)	18 (39.1)	24 (52.2)	16 (34.8)	30 (65.2)
	P	0.0003	0.0005	0.56	<0.0001	<0.0001	<0.0001	<0.0001	0.004

Abbreviations: 0, not expressed for *ΔDNMT3Bs* or not methylated for *p16/RASSF1A*; 1, expressed for *ΔDNMT3Bs* or methylated for *p16/RASSF1A*.

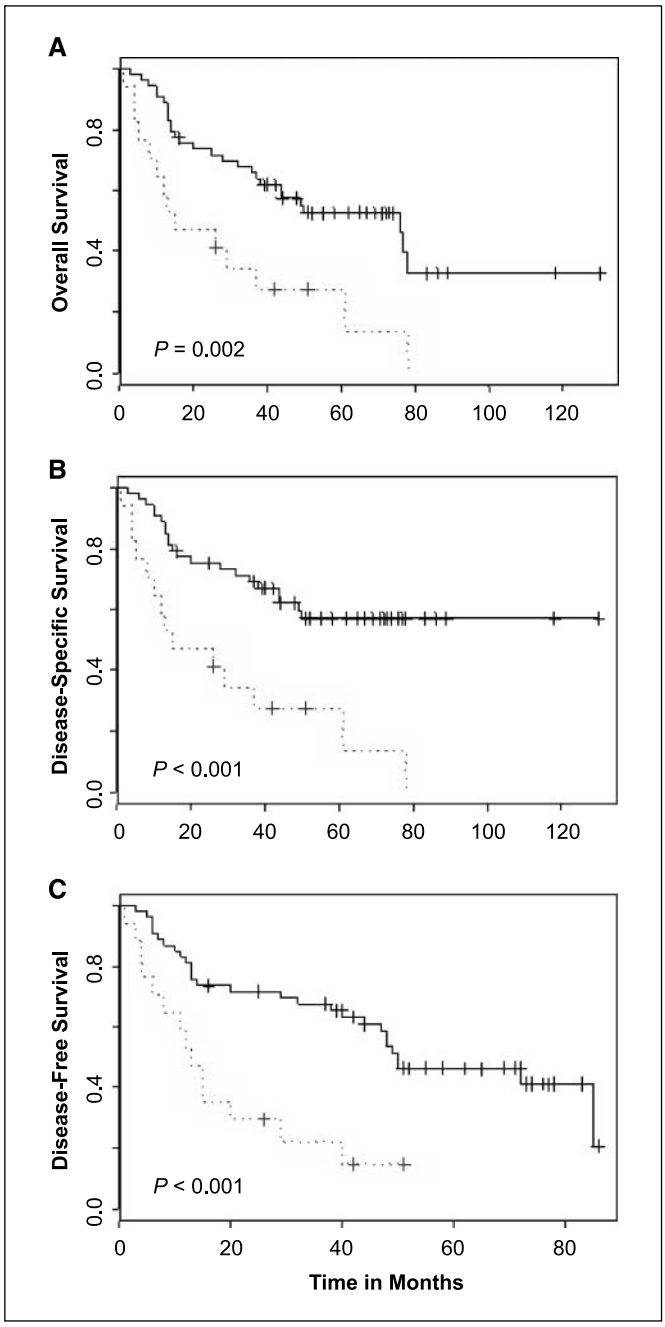


Figure 1. Correlation between expression of any of *ΔDNMT3B5, ΔDNMT3B6*, and *ΔDNMT3B7* and survivals in patients with stage I/II tumors. *A* to *C,* overall, disease-specific, and disease-free survivals, respectively. *Solid lines,* survival curves of patients whose tumors lacked expression of *ΔDNMT3B5, ΔDNMT3B6*, and *ΔDNMT3B7*; *dash lines,* survival curves of patients whose tumors expressed any of *ΔDNMT3B5, ΔDNMT3B6*, and *ΔDNMT3B7*.

(10), we did multivariate analysis to correct the confounding factor. Both expression of *ΔDNMT3B5, ΔDNMT3B6*, and *ΔDNMT3B7* and promoter methylation of *p16* were independent factors in predicting poorer clinical outcomes ($P < 0.01$ for both overall and disease-specific survivals). For stage III tumors, patients whose tumors expressed any of *ΔDNMT3B5, ΔDNMT3B6*, and *ΔDNMT3B7* variants had poorer survivals ($P < 0.001$; Fig. 2*A-C*) similar to the observation in patients with stage I/II tumors. The difference in this group of patients was that expression of *ΔDNMT3B4* was also strongly correlated with poorer survivals ($P < 0.0001$, $P < 0.0001$, and $P < 0.001$, for overall, disease-specific, and disease-free survivals, respectively; Fig. 2*D-F*). In our previous study, we found that both *p16* and *RASSF1A* promoter methylations were correlated with survivals in the patient population (10). However, in the multivariate analysis, only *ΔDNMT3B4* expression and *p16* promoter methylation were independent factors ($P < 0.001$ for both overall and disease-specific survivals).

Discussion

Overexpression of *DNMT3B*, but not *DNMT1* and *DNMT3A*, has been found common in multiple cancer types, including lung cancer (13, 14, 17), suggesting that *DNMT3B* plays an important role in the development of aberrant promoter methylation during tumorigenesis. However, the correlation between expression levels of *DNMT3B* and promoter methylation status was not strong in human tumors in most reports (15–17). Several studies have suggested that *DNMT3B* alone has limited effect in promoter methylation because the maintenance of methylated promoters of tumor suppressor genes could only be effectively disrupted when both *DNMT3B* and *DNMT1* genes were knocked out, whereas the single knockout of either *DNMT3B* or *DNMT1* had minimal effects (19–21). However, these studies did not address potential effects of individual variants of *DNMT3B*. A dominant-negative effect of *DNMT3b4* by competing with *DNMT3b3* has been suggested, which resulted in DNA hypomethylation on pericentromeric satellite regions (14). This result suggests a complex role of *DNMT3B* variants in regulation of DNA methylation formation. The identification of *ΔDNMT3B*s as the predominant expressing forms of *DNMT3B* in lung cancer (18) further exemplified the complexity of the regulation in lung tumorigenesis.

In this study, we provided a comprehensive view of the expression profiles of the seven *ΔDNMT3B* variants in a large panel of NSCLC tumors and their corresponding normal lungs. The fact that *ΔDNMT3B* variants are frequently expressed in the primary NSCLC but less frequently in the corresponding normal lungs underscores the importance of these molecules in lung tumorigenesis. More importantly, our study provides first *in vivo* evidence to support the importance of individual *ΔDNMT3B* variants in the development of promoter methylation of a particular gene in lung tumorigenesis. We conclude that expression of *ΔDNMT3B4* may contribute to the development of *RASSF1A* promoter methylation. We found that 91% of the NSCLC tumors with methylated *RASSF1A* promoter expressed the variant compared with only 18% of the tumors without *RASSF1A* promoter methylation ($P < 0.0001$). As a comparison, 66% of the tumors without *RASSF1A* promoter methylation expressed *ΔDNMT3B2*, although 94% of the tumors with methylated *RASSF1A* promoter expressed *ΔDNMT3B2* (Table 2). Interestingly, all four tumors with methylated *RASSF1A* but no expression of *ΔDNMT3B4* expressed *ΔDNMT3B2*, suggesting a role of *ΔDNMT3B2* in *RASSF1A* promoter methylation in some NSCLC tumors. To support this notion, none of the 25 tumors that expressed neither *ΔDNMT3B4* nor *ΔDNMT3B2* had methylated *RASSF1A* promoter, whereas 6 of 25 (24%) tumors carried methylated *p16* promoter ($P = 0.02$). Because only two promoters were analyzed in this study, whether *ΔDNMT3B4* is involved in promoter methylation of other genes remains to be determined.

Although the mechanism of differential promoter methylation in tumors is unclear, it is possible that the expression of DNMT variants or the relative expression levels of the variants, including those derived from *DNMT3A* and *DNMT3B*, may, at least in part,

determine patterns of the promoter methylation. One possible explanation of the regulation might be a differential DNA binding through variable PWWP structure, which locates at the more proximal part of DNMT3Bs and is capable to bind DNA directly (22). It is also possible that different variants might have different protein-protein binding capability (23), resulting in different modification of chromatin structures. In either case, different promoters with distinct DNA structures, protein complexes, or protein modifications might be preferentially targeted by individual DNMT variants, resulting in a selected promoter methylation. It should be noted, however, that we only analyzed the *ΔDNMT3B* variants based on the alternative splicing of more proximal exons; therefore, whether the catalytic domains of *ΔDNMT3B4/ΔDNMT3B2* play a role in the process is not addressed in this study.

The association between the expression of certain *ΔDNMT3B* variants and clinical outcomes provides further support for the role

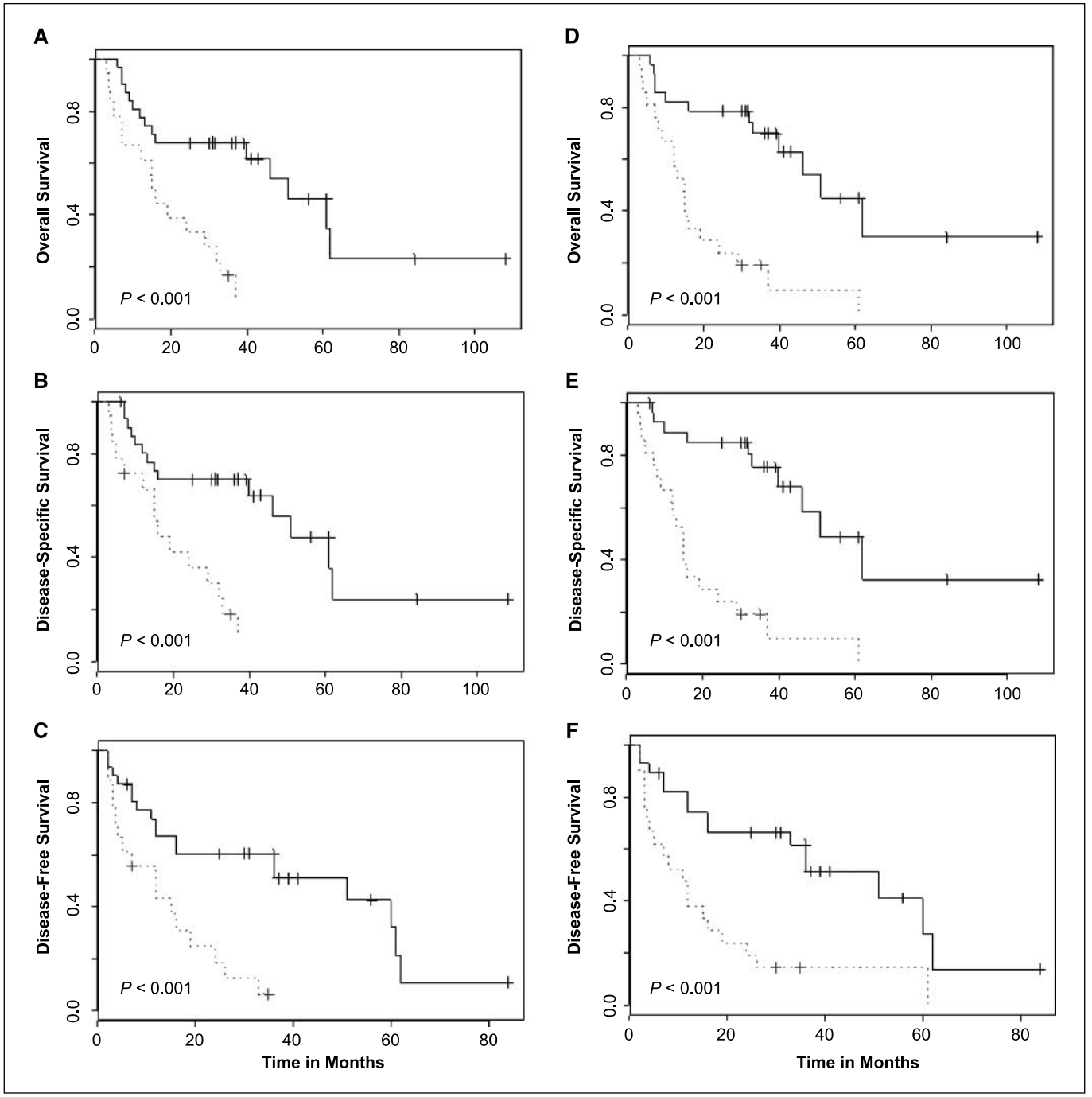


Figure 2. Correlation between expression of *ΔDNMT3B*s and survivals in patients with stage III tumors. *A* to *C,* survivals of patients whose tumors expressed any of *ΔDNMT3B5, ΔDNMT3B6*, and *ΔDNMT3B7* (*dash lines*) or had no expression of the variants (*solid lines*) for overall, disease-specific, and disease-free survivals, respectively. *D* to *F,* survivals of patients whose tumors expressed *ΔDNMT3B4* (*dash lines*) or had no expression of *ΔDNMT3B4* (*solid lines*) for overall, disease-specific, and disease-free survivals, respectively.

of *ΔDNMT3B*s in NSCLC. In patients with either early-stage or locally advanced-stage tumors, the expression of *ΔDNMT3B5, ΔDNMT3B6*, and *ΔDNMT3B7* correlated with poorer survivals, which was independent of other clinicopathologic variables and promoter methylation status of *p16* and *RASSF1A*. Although the frequencies of *ΔDNMT3B5, ΔDNMT3B6*, and *ΔDNMT3B7* expression were relatively low in NSCLC (Table 2), the expression was never detected in the nonmalignant lung tissues, suggesting that *ΔDNMT3B5, ΔDNMT3B6*, and *ΔDNMT3B7* are involved in the late-stage tumorigenesis of lungs. It is interesting to note that the predicted proteins from *ΔDNMT3B5, ΔDNMT3B6*, and *ΔDNMT3B7* contain no enzymatic domain of the methyltransferase due to premature translational termination (18). Unfortunately, the lack of high-quality antibodies for the variants prevents us to evaluate protein expression of the variants in the tumors at this time. Whether their biological roles are inserted through their variable COOH-terminal regions remains to be determined.

In summary, we did the first comprehensive analysis to determine the expression profiles of *ΔDNMT3B* variants in large number of primary NSCLC tumors and their corresponding normal lung tissues. We revealed a strong correlation between the expression of *ΔDNMT3B4* and *RASSF1A* promoter methylation, suggesting a role of the variant in regulation of promoter methylation during lung tumorigenesis. We also found that expression of certain *ΔDNMT3B* variants (i.e., *ΔDNMT3B5, ΔDNMT3B6*, and *ΔDNMT3B7*) was correlated with poor clinical outcomes, suggesting their role in NSCLC progression.

Acknowledgments

Received 6/2/2006; revised 7/12/2006; accepted 7/20/2006.

Grant support: Department of Defense grant DAMD17-01-1-01689-1.

The costs of publication of this article were defrayed in part by the payment of page charges. This article must therefore be hereby marked *advertisement* in accordance with 18 U.S.C. Section 1734 solely to indicate this fact.

References

1. Okano M, Bell DW, Haber DA, Li E. DNA methyltransferases DNMT3a and DNMT3b are essential for *de novo* methylation and mammalian development. Cell 1999;99:247–57.

2. Jaenisch R. DNA methylation and imprinting: why bother? Trends Genet 1997;13:323–9.

3. Kass SU, Pruss AP, Wolffe AP. How does DNA methylation repress transcription? Trends Genet 1997;13:444–51.

4. Surani MA. Imprinting and the initiation of gene silencing in the germline. Cell 1998;93:309–16.

5. Robertson KD, Wolffe AP. DNA methylation in health and disease. Nat Rev Genet 2000;1:11–9.

6. Jones P, Gonzalgo M. Altered DNA methylation and genome instability: a new pathway to cancer? Proc Natl Acad Sci U S A 1997;94:2103–5.

7. Zochbauer-Muller S, Fong KM, Virmani AK, Geradts J, Gazdar AF, Minna JD. Aberrant promoter methylation of multiple genes in non-small cell lung cancers. Cancer Res 2001;61:249–55.

8. Safar AM, Spencer H III, Su X, et al. Methylation profiling of archived non-small cell lung cancer: a promising prognostic system. Clin Cancer Res 2005;11:4400–5.

9. Tang X, Khuri FR, Lee JJ, et al. Hypermethylation of the DAP-kinase CpG island correlates with aggressive biological behavior in stage I non-small cell lung cancer. J Natl Cancer Inst 2000;92:1511–6.

10. Wang J, Lee JJ, Wang L, et al. Distinct value of $p16^{INK4a}$ and *RASSF1A* promoter methylation in prognosis of the patients with respectable non-small cell lung cancer. Clin Cancer Res 2004;9:4415–22.

11. Aoki A, Suetake I, Miyagawa J, et al. Enzymatic properties of *de novo*-type mouse DNA(cytosine-5) methyltransferases. Nucleic Acids Res 2001;29:3506–12.

12. Xie S, Wang Z, Li E. Cloning, expression, and chromosome locations of the human DNMT3 gene family. Gene 1999;236:87–95.

13. Robertson KD, Uzvolgyi E, Liang G, et al. The human DNA methyltransferases (DNMTs) 1, 3a, and 3b: coordinate mRNA expression in normal tissues and overexpression in tumors. Nucleic Acids Res 1999;27:2291–8.

14. Saito Y, Kanai Y, Sakamoto M, Saito H, Ishii H, Hirohashi S. Overexpression of a splice variant of DNA methyltransferase 3b, DNMT3b4, associated with DNA hypomethylation on pericentromeric satellite regions during human hepatocarcinogenesis. Proc Natl Acad Sci U S A 2002;99:10060–5.

15. Eads CA, Kathleen DD, Kazuyuki K, Leonard BS, Peter VD, Peter WL. CpG island hypermethylation in human colorectal tumors is not associated with DNA methyltransferase overexpression. Cancer Res 1999;59:2302–6.

16. Sato M, Horio Y, Sekido Y, Minna JD, Shimokata K, Hasegawa Y. The expression of DNA methyltransferases and methyl-CpG-binding proteins is not associated with the methylation status of p14(ARF), p16(INK4a), and RASSF1A in human lung cancer cell lines. Oncogene 2002;21:4822–9.

17. Girault I, Tozlu S, Lidereau R, Bieche I. Expression analysis of DNA methyltransferases 1, 3A, and 3B in sporadic breast carcinomas. Clin Cancer Res 2003;9:4415–22.

18. Wang L, Wang J, Sun S, et al. A novel DNMT3B subfamily, ΔDNMT3B, is the predominant form of DNMT3B in non-small cell lung cancer. Int J Oncol 2006;29:201–7.

19. Rhee I, Bachman KE, Park BH, et al. DNMT1 and DNMT3b cooperate to silence genes in human cancer cells. Nature 2002;416:552–6.

20. Rhee I, Jair KW, Yen RW, et al. CpG methylation is maintained in human cancer cells lacking DNMT1. Nature 2000;404:1003–7.

21. Leu YW, Rahmatpanah F, Shi H, et al. Double RNA interference of DNMT3b and DNMT1 enhances DNA demethylation and gene reactivation. Cancer Res 2003;63:6110–5.

22. Qiu C, Sawada K, Zhang X, Cheng X. The PWWP domain of mammalian DNA methyltransferase Dnmt3b defines a new family of DNA-binding folds. Nat Struct Biol 2002;9:217–24.

23. Ge YZ, Pu MT, Gowher H, et al. Chromatin targeting of *de novo* DNA methyltransferases by the PWWP domain. J Biol Chem 2004;279:25447–54.

A novel *DNMT3B* subfamily, Δ*DNMT3B*, is the predominant form of *DNMT3B* in non-small cell lung cancer

LUO WANG[1], JIE WANG[5], SHIYONG SUN[3], MARIVONNE RODRIGUEZ[2], PING YUE[3], SE JIN JANG[4] and LI MAO[1]

[1]Molecular Biology Laboratory, Department of Thoracic/Head and Neck Medical Oncology, [2]Department of Molecular Genetics, The University of Texas M.D. Anderson Cancer Center, Houston, TX 77030; [3]Department of Oncology, Winship Cancer Institute, Emory University, Atlanta, GA, USA; [4]Department of Pathology, Hanyang University, Kuri Hospital, 471-701 Seoul, Korea; [5]Department of Thoracic Medical Oncology, Peking University School of Oncology and Beijing Cancer Hospital, Beijing, P.R. China

Received February 3, 2006; Accepted February 27, 2006

Abstract. *De novo* promoter DNA methylation represses gene transcription and is a common mechanism to inactivate tumor suppressor genes in tumorigenesis. *DNMT3B* plays an important role in *de novo* DNA methylation. We report here the identification of a novel *DNMT3B* subfamily, termed Δ*DNMT3B*, whose expression is initiated through a promoter located at intron 4 and exon 5 of the *DNMT3B* gene. At least 7 transcriptional variants of Δ*DNMT3B* have been observed as the result of alternative pre-mRNA splicing. Predicted proteins derived from these variants suggest that 4 of the variants share a conservative enzymatic domain but contain a variable PWWP motif, a putative DNA binding structure, whereas 3 of the variants lack the enzymatic domain due to predicted premature translational termination. In non-small cell lung cancer (NSCLC) cell lines, Δ*DNMT3B* variants are frequently expressed and are the predominant forms of *DNMT3B*. Similarly, Δ*DNMT3B* variants are frequently expressed in primary NSCLC but are not detectable or are expressed at low levels in corresponding normal lung tissue. Our results indicate that Δ*DNMT3B* is the major expression form of *DNMT3B* in NSCLC and may play an important role in the development of aberrant promoter methylation during lung tumorigenesis.

Correspondence to: Dr Li Mao, Molecular Biology Laboratory, Department of Thoracic/Head and Neck Medical Oncology, The University of Texas M.D. Anderson Cancer Center, 1515 Holcombe Boulevard, Houston, TX 77030, USA
E-mail: lmao@mdanderson.org

Abbreviations: DNMT, DNA methyltransferase; PWWP, proline-tryptophan-tryptophan-proline; NSCLC, non-small cell lung cancer; RT-PCR, reverse transcription-polymerase chain reaction

Key words: Δ*DNMT3B*, NSCLC, promoter, expression, splicing

Introduction

DNA methylation plays an essential role in normal development of mammalian embryo by regulating gene transcription through genomic imprinting, X chromosome inactivation, and genomic stability (1-4). It is believed that DNA methylation patterns in somatic cells are established during gametogenesis and early embryonic development via consecutive waves of demethylation and *de novo* methylation (5). *DNMT3* consists of *DNMT3A* and *DNMT3B* and has been shown to be the major *de novo* DNA methyltransferase (6,7) that preferentially methylates cytosine in CpG sites. The methylation in CpG-rich promoter regions would result in transcriptional silencing of the corresponding genes.

Okano *et al* found that murine *Dnmt3a* and *Dnmt3b* are highly expressed in the undifferentiated ES cells but are down-regulated during development and maintained at a low level in somatic cells (6). They further revealed that, at E7.5, *Dnmt3b* was highly expressed in the embryonic ectoderm, neural ectoderm, and chorionic ectoderm while a weak expression was detected in mesodermal and endodermal cells (8). The expression of *Dnmt3a* was moderate in embryonic ectoderm and weak in mesodermal cells until E8.5 and E9.5, at which point *Dnmt3a* expression became ubiquitous with increased expression in the somites and the ventral part of the embryo (8). These observations suggest that the two types of enzymes may function differently in development.

Human *DNMT3B* is highly homologous to the mouse gene and contains 24 exons spanning approximately 47 kb of genomic DNA. Two alternative 5' exons of *DNMT3B*, both resulting in full-length *DNMT3B* (*DNMT3B1* and *DNMT3B2*), have been reported (9). Three transcription variants resulting from alternative splicing have also been reported (*DNMT3B3-5*) (9). Some of the variants lacking DNA methyltransferase activity may compete with variants with enzyme activity resulting in DNA hypomethylation (10), suggesting a complex role of *DNMT3B* variants. Increased expression of *DNMT3B* has been frequently observed in human cancer cell lines and primary tumors compared to most normal tissues except testis,

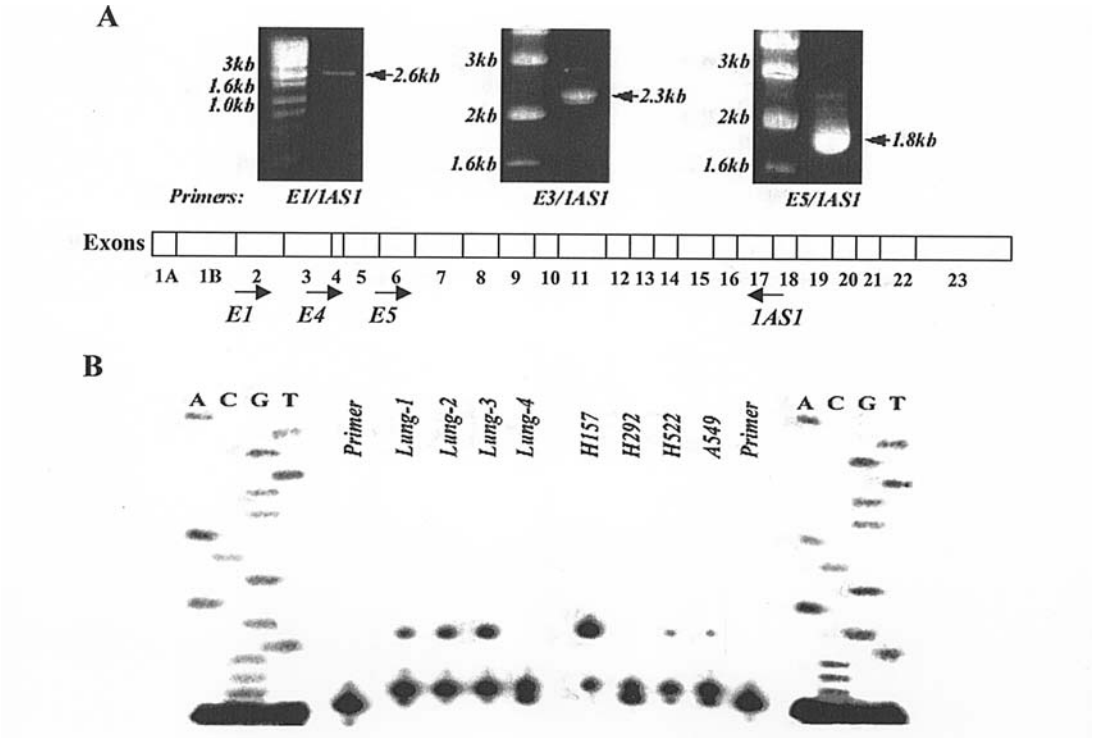


Figure 1. Identification of Δ*DNMT3B*. (A) Expression of the *DNMT3B* 5'-region measured using RT-PCR with different 5' primers located at exon 2 (E1), exon 4 (E2), and exon 6 (E3) of *DNMT3B1*, respectively. (B) Primer extension analysis showing transcription starting points of Δ*DNMT3B*.

pancreas, thyroid, and bone marrow (9-11). However, the level of *DNMT3B* expression in tumors does not consistently correlate with the promoter methylation status of genes (11-13). We report here the identification of a new class of *DNMT3B* transcripts expressed through a novel promoter, termed Δ*DNMT3B*. We further demonstrate that Δ*DNMT3B* is the predominant form of *DNMT3B* in NSCLC, suggesting an important role of Δ*DNMT3B* in DNA methylation control and lung tumorigenesis.

Materials and methods

Cell lines and primary tissues. Human NSCLC lines H157, H226, H292, H460, H522, H1299, H1944, and A549 were purchased from the American Type Cell Culture (Rockville, MD). Cells were cultured in DMEM supplemented with 10% heat-inactivated FCS, 2 mM L-glutamine, 100 IU/ml penicillin, and 100 mg/ml streptomycin at 37˚C in the presence of 5% CO_2.

Twelve paired primary tumor tissues and corresponding normal lung tissues from patients with primary NSCLC were obtained from surgically resected specimens collected in the Department of Pathology at The University of Texas M.D. Anderson Cancer Center and stored at -80˚C until the experiment. The study was approved by the Institutional Review Boards of The University of Texas M.D. Anderson Cancer Center.

RNA extraction and RT-PCR. The total RNA for each cell line and clinic sample was isolated using Tri reagent (Molecular Research Center, Inc., Cincinnati, OH) according to the manufacturer's instructions. Approximately 1 μg of total RNA from each sample was used to conduct a reverse transcription reaction in a 20-μl volume using SuperScript II RNase H- reverse transcriptase (Gibco BRL Life Technologies Inc., Grand Island, NY). The synthesized cDNA was either used immediately for PCR amplification or stored at -20˚C for further analysis.

The mRNA expression levels of total *DNMT3Bs* were detected using a primer set of the forward primer, S1 (5'-GAG TTG GGC ATA AAG GTA GG-3'), and the reverse primer, 1AS1 (5'-TGA GGT ACA CGG TAT GAC C-3'), located at exon 17 and the 3'-untranslation region of *DNMT3B1*, respectively. The 5'-end forward primers, E1 (5'-CAT GAA GGG AGA CAC CAG GC-3'), E3 (5'-ATG CCA AAG CTC TTC CGG GA-3'), and E5 (5'-TGG AGA TGG AGA CAG TTC AG-3'), and the reverse primer, 1AS1, were also used to detect *DNMT3Bs* (Fig. 1A).

PCR was performed in a 12.5-μl volume containing 0.5 μl of reverse transcription products, 7% dimethylsulfoxide, 1.5 mM deoxynucleotides (dNTPs), 6.7 mM $MgCl_2$, 16.6 mM $(NH_4)_2SO_4$, 67 mM Tris, 10 mM ß-mercaptoethanol, 6.7 μM ethylene diamine tetra acetic acid (EDTA), 0.5 μM of both the forward and the reverse primer, and 0.625 U of HotStar Taq DNA polymerase (Qiagen, Inc., Chatsworth, CA). Amplification was carried out in a thermal cycler (PCR Express, Hybaid, Middlesex, UK) with an initial denaturing step at 95˚C for 15 min, followed by 35 cycles at 95˚C for 30 sec, 58-62˚C for 1 min, and 72˚C for 1 min, with a last extension step at 72˚C for 10 min. The PCR products were mixed with 6X loading buffer containing 0.5 mg/ml ethidium bromide and separated by electrophoresis on a 2% agarose gel.

Primer extension and nuclease S1 mapping. To determine the exact starting site of the Δ*DNMT3B* transcript, standard primer

extension and S1 mapping methods were used with the [γ-^{32}P]-ATP end-labeled antisense primer, 3B6AS (5'-GGT AGC CGG GAA CTC CAC GG-3'). For primer extension, briefly, 1 μg of total RNA was mixed with [^{32}P]-labelled primer. The mixture was incubated at 70˚C for 15 min and then at room temperature for 10 min. Extension reactions (20 μl) consisted of 50 mM Tris (pH 8.3), 75 mM KCl, 3 mM $MgCl_2$, 10 mM dithiothreitol, 1 mM each dNTP, and 200 U SuperScript™ II reverse transcriptase (Gibco BRL Life Technologies Inc.). Reactions were incubated at 37˚C for 15 min. The products were mixed with loading buffer (95% formamide, 20 mM EDTA, 0.05% bromophenol blue and 0.02% xylene cyanole FF), denatured at 98˚C for 5 min, and then separated on a 12% acrylamide-7 M urea denatured gel. Radioactive signals were detected by autoradiography.

Nuclease S1 mapping was performed with a 1080-bp DNA fragment which was amplified using the forward primer, E4INT-1 (5'-TGC TGT GAC AGG CAG AGC AG-3'), and the reverse primer, E5AS (5'-TCT GTG TCG TCT GTG AGG TC-3'). After cloning this fragment into a PCR® 2.1-TOPO® vector (Invitrogen Corp., Carlsbad, CA), a 320-bp fragment of single-strand DNA probe used for S1 nuclease mapping was generated by single-primer PCR using [^{33}P]-labelled internal primer 3B6AS. The PCR condition was the same as above. This single-strand 320-bp PCR product was separated in a 2% agarose gel and purified using a QIAquick gel extraction kit (Qiagen Inc.) followed by recovering in 50 μl Tris-buffer (10 mM Tris-HCl, pH 8.5).

The total RNA from different samples was co-precipitated with 50 ng of recovered 320-bp [^{33}P]-labelled probe. Samples were dissolved in 30 μl of hybridization buffer (40 mM MOPS, pH 6.4, 1 mM EDTA, 0.4 M NaCl and 80% formamide) and incubated at 85˚C for 15 min. After overnight hybridization at 54˚C based on the GC content of the projected fragment, the samples were digested for 1 h at 37˚C with S1 nuclease (Gibco BRL Life Technologies Inc.) in the buffer containing 30 mM sodium acetate, pH 4.6, 1 mM zinc acetate, 5% glycerol, and 0.28 M NaCl. The resulting products were detected as described in primer extension section.

Construction of DNMT3B6 promoter and luciferase assay. The first 1080-bp Δ*DNMT3B* promoter was amplified with the primer set of E4INT-1 and E5AS. This fragment contains, 355 bp upstream of the Δ*DNMT3B* transcription starting site, the first exon and intron of Δ*DNMT3B*. After inserting the fragment into the pGL3-basic vector (Promega Corp., Madison, WI), the plasmids containing both forward (F) and reverse (R) directions were used for transient transfection. To compare the functional difference of C/T polymorphism in the Δ*DNMT3B* promoter region, both pGL3 T-type and C-type promoters were constructed.

Lung cancer cell line A549 and H157 (ATCC, Manassas, VA) was used for transient transfection using FuGENE 6 transfection reagent (Roche Diagnostics Corp., Indianapolis, IN) according to the manufacturer's instructions. The plasmid, pCH110 (Amersham Pharmacia Biotech, Inc., Piscataway, NJ), was used as the internal control for monitoring the transfection efficiency. The signal was detected using a luciferase assay system (Promega Corp.) in a luminometer (Lumat 9507, EG&G Berthold). The values of luciferase activity were normalized against those of ß-galactosidase expressed by plasmid pCH110.

Detection of individual ΔDNMT3B splicing variants. The expression levels of specific *DNMT3B* and Δ*DNMT3B* variants in NSCLC cell lines and primary tissues were determined using specific primer sets corresponding to individual *DNMT3B* and Δ*DNMT3B* variants. For Δ*DNMT3B1*, we used 1S, 5'-TGG AAG GCC ACC TCC AAG C-3', as the forward primer and 1AS, 5'-GCC TGC ACG ACG CAC CTT CG-3', as the reverse primer; for Δ*DNMT3B2*, 2S 5'-AGA TCA AGG GCT TCT CCT GG-3' and 2AS 5'-GAG TCT TGT TCT CTG GTT GCG-3'; for Δ*DNMT3B3*, 3S 5'-GTT CAG AGT ATC AGG TCT CTG C-3' and 1AS; for Δ*DNMT3B4*, 3S and 2AS; for Δ*DNMT3B5*, 4S 5'-GTT CAG AGT ATC AGA GAA CAA GAC-3', and 3AS 5'-CTG CCA CAA GAC AAA CAG CC-3'; for Δ*DNMT3B6*, 5S 5'-GTT CTC CGA GAG AAC AAG AC-3', and 4AS 5'-CAG TAA GAC TGA TAG CCA TCG-3'; and for Δ*DNMT3B7*, 6S 5'-TGC TCT GGA GAG AAC AAG AC-3', and 5AS 5'-GAG ACA CAT GTA ACA GCT CC-3'. A common forward primer, E1 5'-TGC TAA GCT ACA CAC AGG AC-3', was used for the *DNMT3B* variants, and specific reverse primers were used to distinguish individual variants as follows: 1AS for *DNMT3Bs* corresponding to Δ*DNMT3B1* and Δ*DNMT3B3*; 2AS for *DNMT3Bs* corresponding to Δ*DNMT3B2* and Δ*DNMT3B4*; 6AS, 5'-CGA GTC TTG TTC TCT GAT ACT C-3', for *DNMT3B* corresponding to Δ*DNMT3B5*; 7AS, 5'-CGA GTC TTG TTC TCT CGG AG-3', for *DNMT3B* corresponding to Δ*DNMT3B6*; and 8AS, 5'-CGA GTC TTG TTC TCT CCA G-3', for *DNMT3B* corresponding to Δ*DNMT3B7*.

Results

To determine the expression levels of *DNMT3B1* in normal lung tissue and lung cancer tissue, we analyzed 12 pairs of primary NSCLC tissue and corresponding normal lung tissue using RT-PCR with a set of primers located at exon 17 and exon 23 of *DNMT3B1* respectively. We found that *DNMT3B1* expression was either undetectable or at trace levels in the vast majority of normal lung tissue analyzed while it was detectable in all NSCLC tissue with 50% (6/12) of the tumors expressed at a high level. To validate the finding, we designed several additional sets of primers that allowed us to amplify *DNMT3B1* mRNA at different exon locations closer to its transcriptional initiation site. We found that the expression level of the gene was much lower when using a primer located at exon 2 (E1) or exon 4 (E4) compared to a primer located at exon 6 (E5) of *DNMT3B1* (Fig. 1A), suggesting the presence of additional transcripts excluding exons 2-4. To confirm this observation, we tested other primer sets at these regions and the results were consistent with the previous observation (data not shown). To exclude the possibility of contamination with homologue molecules in the RT-PCR products, we performed direct sequencing analysis of each RT-PCR product. The sequences matched perfectly to the originally reported corresponding transcript sequence of *DNMT3B1* [GenBank accession number (AN): AL035071].

To determine the exact starting point(s) of the novel transcriptions, we performed primer extension assay using RNA

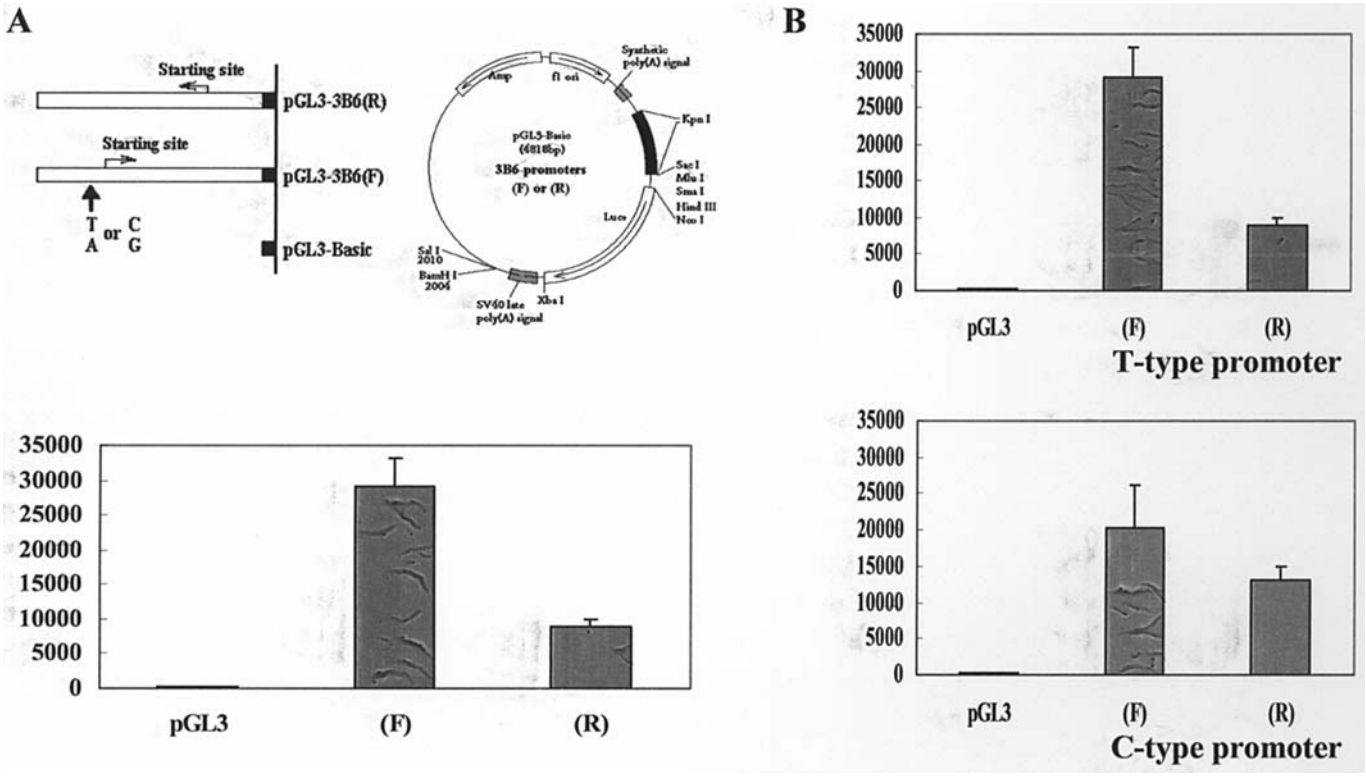


Figure 2. Promoter of Δ*DNMT3B*. (A) Activity of Δ*DNMT3B* promoter detected using luciferase assay. (B) Effect of a T→C transition (polymorphism) on promoter activity of Δ*DNMT3B*. The larger arrow indicates the position of the polymorphism. Based on the polymorphism, the promoters are defined as C-type or T-type. F indicates forward direction of the promoter and R indicates reverse direction of the promoter.

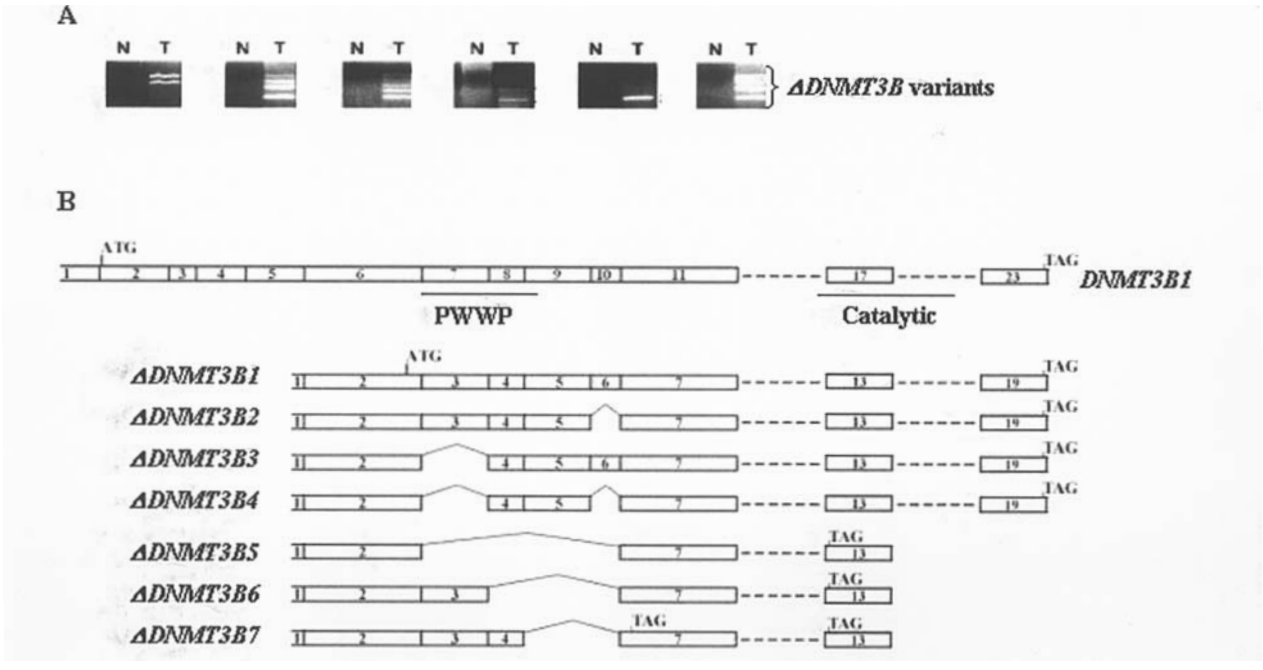


Figure 3. Alternative splicing of Δ*DNMT3B*. (A) High level expression of Δ*DNMT3B* variants in lung cancer tissue compared to corresponding normal lung tissue. (B) The structure scheme of *DNMT3B1* and Δ*DNMT3B* variants. N indicates normal tissue and T indicates cancer tissue.

templates from lung cancer tissue and NSCLC cell lines and a primer (3B6AS) located at exon 5 of *DNMT3B1*. We identified two major transcriptional initiation sites located at nt 23990 and nt 23994 within exon 5 of *DNMT3B1* (GenBank AN: 15306493), respectively (Fig. 1B). This partial exon 5 was then named as the first exon of the novel transcript(s) containing either 28 bp or 24 bp depending on which transcriptional initiation site it derives from. We further validated the finding by using nuclease S1 RNA mapping analysis (data not shown). We designated the new transcript from these

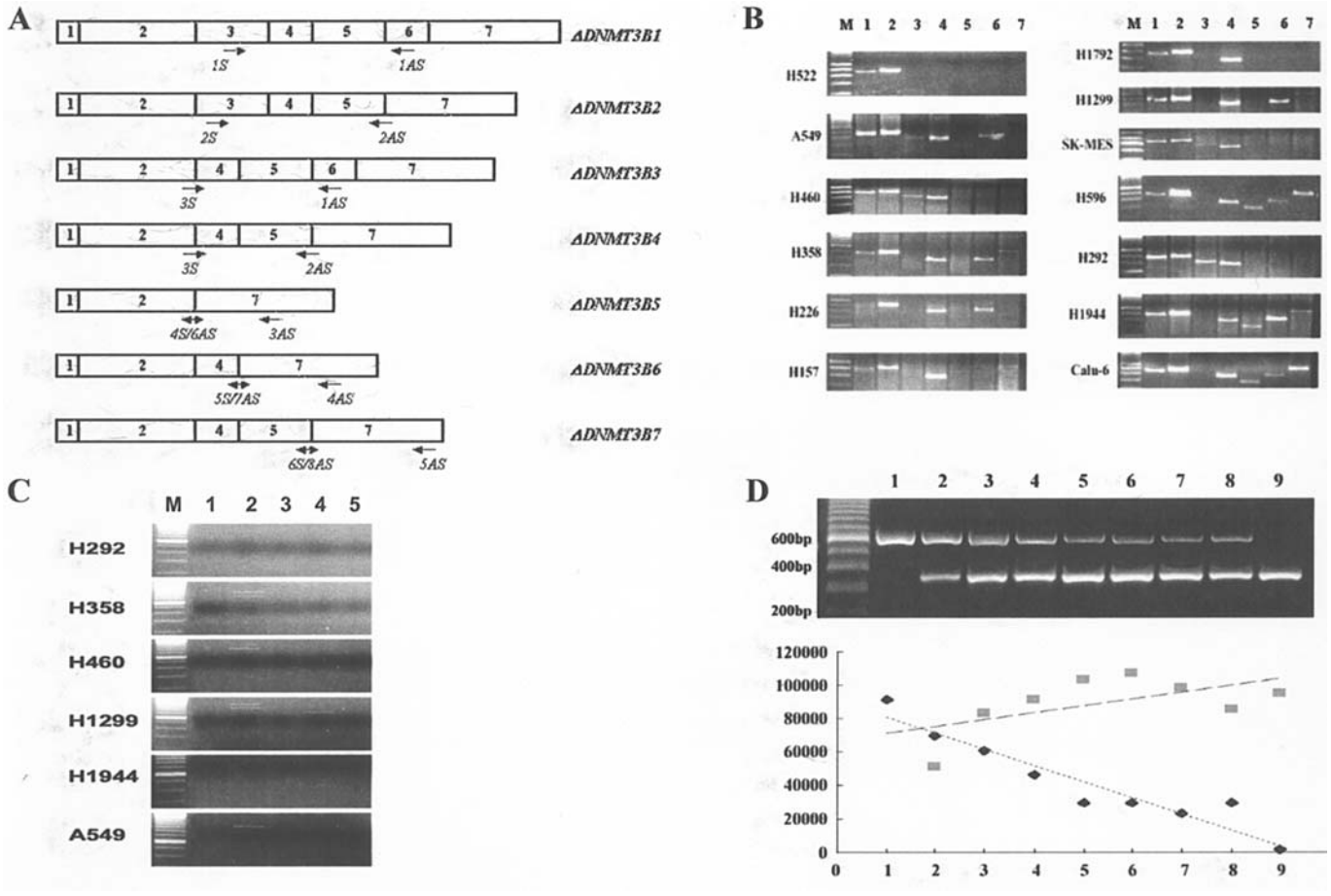


Figure 4. Alternative or aberrant splicing variants of Δ*DNMT3B* subfamily. (A) Location of the primers used to amplify individual Δ*DNMT3B* variants in this study. (B) Expression patterns of Δ*DNMT3B* variants in NSCLC cell lines; 1-7 represent Δ*DNMT3B1-7*, respectively. (C) Expression patterns of *DNMT3Bs*, with more proximal exons corresponding to Δ*DNMT3B1-4* and Δ*DNMT3B6*. (D) Multiplex PCR using primer sets for *DNMT3B1* and Δ*DNMT3B1* with different ratios in concentration (concentration of *DNMT3B1* primer set was serially diluted from 1 to 9 and serially increased from 1 to 9; 1, *DNMT3B1* primer set alone; 9, Δ*DNMT3B1* primer set alone; 5, equal concentrations for both primer sets). The upper band represents the *DNMT3B1* product and the lower band represents the Δ*DNMT3B1* product. The lower panel shows relative intensity of the product bands.

starting sites as Δ*DNMT3B* because it lacks exons 1-4 of *DNMT3B*.

To determine the existence of a potential promoter upstream of the newly identified transcript, we constructed a 1080-bp DNA fragment containing, 355 bp upstream of the Δ*DNMT3B* transcriptional initiation site, the first exon and intron of Δ*DNMT3B* and partial exon 2 into a vector containing a reporter gene. We performed a promoter activity assay and found promoter activity of the DNA fragment (Fig. 2A). We further constructed serial plasmids with both sense and reverse sequences of the DNA fragment and various deletions. Using these constructs, we found that the core promoter activity of Δ*DNMT3B* is in a 477-bp fragment containing one repressor element and three cis-acting elements (data not shown). Interestingly, a common T→C transition polymorphism was found in the promoter region of Δ*DNMT3B* located -286 bp from the transcriptional initiation site, which may change a TFIID (CTcTAT**T**CCA) binding site to GATA-1 (TCTAT**C**) binding site. We noticed a stronger promoter activity with the T form than the C form (18-fold vs. 12-fold compared to the control, respectively) (Fig. 2B).

Because of the presence of various sizes of RT-PCR products using these primer sets, we suspected that Δ*DNMT3B* might contain multiple splicing variants (Fig. 3A). By directly sequencing the individual fragments, we found at least seven variants (by including or excluding different combinations of exons 3, 4, 5, and 6 of Δ*DNMT3B*), which we designated as Δ*DNMT3B1-7* (Fig. 3B). A comparative analysis of the putative amino acid sequences of the variants showed that Δ*DNMT3B* lacked 199 amino acids at the N-terminal, compared with *DNMT3B1,* and that Δ*DNMT3B1* and Δ*DNMT3B2* contained a complete PWWP motif; other variants either contained a partial PWWP motif or no such structure; Δ*DNMT3B5-7* lacks the enzymatic domains because of a premature termination that results from frame shifting after alternative splicing (Fig. 3B).

To detect individual Δ*DNMT3B* variants, we designed specific PCR primer sets on the basis of their splicing patterns (Fig. 4A). We detected Δ*DNMT3B1* and Δ*DNMT3B2* expression in all 13 NSCLC cell lines analyzed, Δ*DNMT3B4* expression in 12 of the 13 cell lines, and Δ*DNMT3B6* expression in 7 of the 13 cell lines; in contrast, expression of Δ*DNMT3B3,* Δ*DNMT3B5*, and Δ*DNMT3B7* were less frequent (Fig. 4B). Interestingly, the *DNMT3B* variants were expressed less frequently and at lower levels in these cell lines (Fig. 4C). In a multiplex PCR analysis, we determined

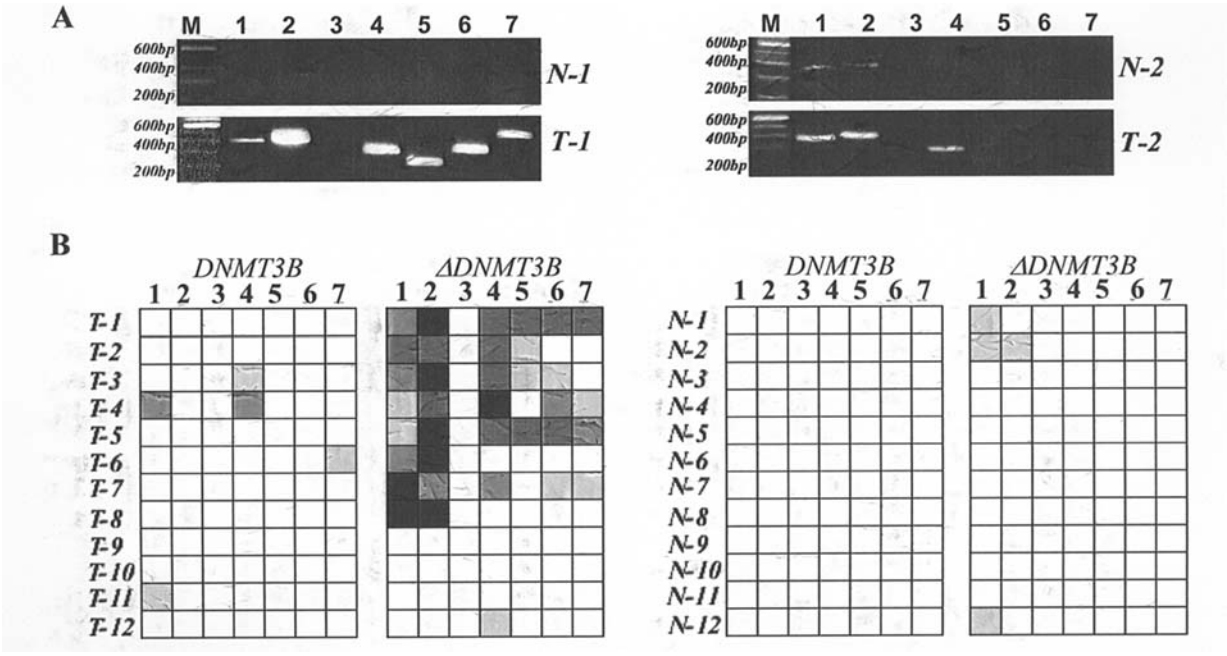


Figure 5. Expression of Δ*DNMT3B* variants in primary lung cancer tissue and corresponding normal lung tissue. (A) Examples of Δ*DNMT3B* variant expression patterns in paired normal lung tissue and primary lung cancer tissue. (B) Expression patterns of *DNMT3B* and Δ*DNMT3B* variants in paired normal (N) lung tissue and primary tumor (T) tissue. The density of the shed boxes represents the relative level of the gene expression.

the relative amplification efficiencies of the primer sets for *DNMT3B* and Δ*DNMT3B* using DNA templates containing various concentrations of *DNMT3B* and Δ*DNMT3B1* (Fig. 4D). The robust amplification of *DNMT3B1* (Fig. 4D) indicated that the lack or very low levels of RT-PCR products in the cell lines reflected the low level of the corresponding *DNMT3B* transcripts.

To determine whether the expression profiles observed in the NSCLC cell lines also exist in the primary NSCLC, we analyzed 12 pairs of primary NSCLC tumors and corresponding normal lung tissue. We found that the expression of Δ*DNMT3Bs* but not *DNMT3Bs* was frequent in the primary tumors whereas the expression of the variants was mainly non-detectable or weakly expressed in the corresponding non-cancerous lungs (Fig. 5). Nine (75%) of the 12 tumors expressed at least one variant, similar to the cancer cell line data.

Discussion

DNA methyltransferases play an important role in initiation and maintenance of cytosine methylation in human genome. Although the role of DNMT1 is primarily to maintain DNA methylation status and the role of DNMT3s relates to *de novo* DNA methylation, recent studies have shown that these molecules not only possess distinct activities (6,8,14) but also interact with each other in complex biological processes to regulate patterns of DNA methylation in human genome (15-18). The dominant-negative effect of *DNMT3b4*, which lacks methyltransferase enzymatic motifs, in competing with *DNMT3b3* to result in DNA hypomethylation on pericentromeric satellite regions (10) suggests an important role of the isoforms of the gene. The identification of Δ*DNMT3B* and its multiple splicing variants in this study further complicate the role of *DNMT3B* family members in regulating DNA methylation in physiological and pathological conditions.

Δ*DNMT3B* derives from a novel promoter located upstream of exon 5 of *DNMT3B1* with a putative translation initiation site at exon 6 (exon 2 of Δ*DNMT3B*). As a result, the predicted proteins of Δ*DNMT3Bs* lack 200 amino acids at the N-terminal of *DNMT3B1* but maintain the PWWP domain in several variants (Δ*DNMT3B1-4*). Therefore, these putative proteins may share some common function, such as DNA methyltransferase activity, with *DNMT3B* but possess other distinct biological features. Because predicted Δ*DNMT3B5-7* lack the enzymatic domain of DNA methyltransferase, their biochemical functions may be more distinct than those of their other family members.

In previous studies, *DNMT3B* has been found to be more highly expressed in cancer cell lines and primary tumors than in normal tissue; however, an association between the expressional level of *DNMT3B* and promoter methylation of tumor suppressor genes was not established (11-13,19). One possible explanation was that *DNMT3B* expression may be regulated in the cell cycle and that the increased expression observed in tumors is merely a reflection of increased cell proliferation (13). Studies have shown that both *DNMT3B* and *DNMT1* genes are necessary for maintaining the methylated promoters of tumor suppressor genes (20,21). Another study showed that *DNMT3b4*, a *DNMT3B* variant lacking methyltransferase enzymatic motifs, might act as a dominant-negative factor to reduce DNA methylation (10), suggesting that splicing variants of *DNMT3B* may play distinctive roles in regulating DNA methylation. The identification of Δ*DNMT3Bs* in this study adds additional complexity to the current knowledge of *DNMT3B* in biological systems.

The high expression of Δ*DNMT3Bs* but not *DNMT3Bs* in both NSCLC cell lines and primary tumors suggests the

importance of the Δ form in lung tumorigenesis. Because the tumors express different patterns of Δ*DNMT3B* variants, it is possible that the expression of variable Δ*DNMT3Bs* rather than the overall expression levels plays a role in promoter methylation in lung tumorigenesis. Further studies are needed to address this issue.

A common sequence polymorphism is found in the promoter of Δ*DNMT3B*, which affects promoter activity. In accordance with the notion that Δ*DNMT3Bs* is involved in early lung tumorigenesis, individuals carrying the T-type promoter, which has a higher promoter activity, had a >2-fold increased risk of lung cancer in a large case-control epidemiological study (22). Together, these data support the role of Δ*DNMT3Bs* in regulating promoter methylation during lung tumorigenesis.

Acknowledgements

This study was supported by the Department of Defense, Grant DAMD17-01-1-01689-1.

References

1. Jaenisch R: DNA methylation and imprinting: why bother? Trends Genet 13: 323-329, 1997.
2. Jones P and Gonzalgo M: Altered DNA methylation and genome instability: a new pathway to cancer? Proc Natl Acad Sci USA 94: 2103-2105, 1997.
3. Robertson KD and Wolffe AP: DNA methylation in health and disease. Nat Rev Genet 1: 11-19, 2000.
4. Surani MA: Imprinting and the initiation of gene silencing in the germline. Cell 93: 309-312, 1998.
5. Monk M, Boubelik M and Lehnert S: Temporal and regional changes in DNA methylation in the embryonic, extra-embryonic, and germ cell lineages during mouse embryo development. Development 99: 371-382, 1987.
6. Okano M, Xie S and Li E: Cloning and characterization of a family of novel mammalian DNA (cytosine-5) methyltransferases. Nat Genet 19: 219-220, 1998.
7. Li E and Jaenisch R: DNA Alterations in Cancer. Ehrlich M (ed). Eaton Publishing, Natick, MA, pp351-365, 2000.
8. Okano M, Bell DW, Haber DA and Li E: DNA methyltransferases Dnmt3a and Dnmt3b are essential for *de novo* methylation and mammalian development. Cell 99: 247-257, 1999.
9. Robertson KD, Uzvolgyi E, Liang G, Talmadge C, Sumegi J, Gonzales FA and Jones PA: The human DNA methyltransferases (DNMTs)1, 3a and 3b: coordinate mRNA expression in normal tissues and overexpression in tumors. Nucleic Acids Res 27: 2291-2298, 1999.
10. Saito Y, Kanai Y, Sakamoto M, Saito H, Ishii H and Hrohoshi S: Overexpression of a splice variant of DNA methyltransferase 3b, DNMT3b4, associated with DNA hypomethylation on pericentromeric satellite regions during human hepatocarcinogenesis. Proc Natl Acad Sci USA 99: 10060-10065, 2002.
11. Oue N, Kuraoka K, Kuniyasu H, Yokozaki H, Wakikawa A, Matsusaki K and Yasui W: DNA methylation status of hMLH1, p16(INK4a), and CDH1 is not associated with mRNA expression levels of DNA methyltransferase and DNA demethylase in gastric carcinomas. Oncol Rep 8: 1085-1089, 2001.
12. Yakushiji T, Uzawa K, Shibahara T, Noma H and Tanzawa H: Over-expression of DNA methyltransferases and CDKN2A gene methylation status in squamous cell carcinoma of the oral cavity. Int J Oncol 22: 1201-1207, 2003.
13. Sato M, Horio Y, Sekido Y, Minna JD, Shimokata K and Hasegawa Y: The expression of DNA methyltransferases and methyl-CpG-binding proteins is not associated with the methylation status of p14(ARF), p16(INK4a) and RASSF1A in human lung cancer cell lines. Oncogene 21: 4822-4829, 2002.
14. Liu K, Wang YF, Cantemir C and Muller MT: Endogenous assays of DNA methyltransferases: evidence for differential activities of DNMT1, DNMT2, and DNMT3 in mammalian cells *in vivo*. Mol Cell Biol 23: 2709-2719, 2003.
15. Bachman KE, Park BH, Rhee I, Rajagopalan H, Herman JG, Baylin SB, Kinzler KW and Vogelstein B: Histone modifications and silencing prior to DNA methylation of a tumor suppressor gene. Cancer Cell 3: 89-95, 2003.
16. Rhee I, Jair KW, Yen RW, Lengauer C, Herman JG, Kinzler KW, Vogelstein B, Baylin SB and Schuebel KE: CpG methylation is maintained in human cancer cells lacking DNMT1. Nature 404: 1003-1007, 2000.
17. Leu YW, Rahmatpanah F, Shi H, Wei SH, Liu JC, Yan PS and Huang TH: Double RNA interference of DNMT3b and DNMT1 enhances DNA demethylation and gene reactivation. Cancer Res 63: 6110-6115, 2003.
18. Jair KW, Bachman KE, Suzuki H, Ting AH, Rhee I, Yen RW, Baylin SB and Schuebel KE: *De novo* CpG island methylation in human cancer cells. Cancer Res 66: 682-692, 2006.
19. Girault I, Tozlu S, Lidereau R and Bieche I: Expression analysis of DNA methyltransferases 1, 3A, and 3B in sporadic breast carcinomas. Clin Cancer Res 9: 4415-4422, 2003.
20. Rhee I, Bachman KE, Park BH, Jair KW, Yen RW, Schuebel KE, Cui H, Feinberg AP, Lengauer C, Kinzler KW, Baylin SB and Vogelstein B: DNMT1 and DNMT3b cooperate to silence genes in human cancer cells. Nature 416: 552-556, 2002.
21. Kim GD, Ni J, Kelesoglu N, Roberts RJ and Pradhan S: Co-operation and communication between the human maintenance and *de novo* DNA (cytosine-5) methyltransferases. EMBO J 21: 4183-4195, 2002.
22. Shen H, Wang L, Spitz MR, Hong WK, Mao L and Wei Q: Identification of a new genetic variant in the novel *Dnmt3b* promoter and its association with promoter activity and risk of lung cancer. Cancer Res 62: 4992-4995, 2002.

Expression of Nucleotide Excision Repair Proteins in Lymphocytes as a Marker of Susceptibility to Squamous Cell Carcinomas of the Head and Neck

Qingyi Wei,[1,4] Li-E Wang,[1] Erich M. Sturgis,[1,2] and Li Mao[3,4]

Departments of [1]Epidemiology, [2]Head and Neck Surgery, and [3]Thoracic/Head and Neck Medical Oncology, The University of Texas, M.D. Anderson Cancer Center; and [4]The University of Texas Graduate School of Biomedical Sciences at Houston, Houston, Texas

Abstract

The transcript levels of nucleotide excision repair (NER) genes were shown to be associated with risk of squamous cell carcinomas of the head and neck (SCCHN). However, this association may be biased, because the transcript level does not necessarily reflect the level of protein expression. To address this issue, we did a pilot study to test the hypothesis that the expression of six core NER proteins is associated with risk of SCCHN. We obtained cultured lymphocytes from 57 patients with newly diagnosed SCCHN patients and 63 cancer-free controls. We transfected some of the lymphocytes with both damaged and undamaged plasmid DNA and quantified NER protein levels in these lymphocytes using a reverse-phase protein microarray. The relative NER protein levels in the 63 controls were highly correlated with each other ($P < 0.001$ for all). Compared with the controls, the cases had lower expression levels for all the NER proteins, particularly XPC and XPF, which were reduced by about 25% ($P < 0.01$). When we used the median expression levels of the NER proteins in the controls as cutoff values, we found that a significantly increased risk of SCCHN was associated with low expression of XPA [odds ratio (OR), 2.99; 95% confidence interval (CI), 1.22-7.47], XPC (OR, 2.46; 95% CI, 1.04-5.87), XPD (OR, 3.02; 95% CI, 1.18-7.76), and XPF (OR, 5.29; 95% CI, 2.01-13.9), but not ERCC1 and XPG, after adjustment for age, sex, ethnicity, smoking, alcohol use, and sample storage time. In a multivariate logistic regression model that included all covariates and NER proteins, however, only low expression of XPF remained a significant risk factor for SCCHN (OR, 11.5; 95% CI, 2.32-56.6). These results suggest that XPF may be a crucial rate-limiting factor in DNA repair and that the reverse-protein microarray assay may be a useful tool for measuring protein markers of susceptibility to cancer. (Cancer Epidemiol Biomarkers Prev 2005;14(8):1961–6)

Introduction

Squamous cell carcinomas of the head and neck (SCCHN) are common malignancies, with >500,000 new cases worldwide estimated each year (1). In the U.S. in 2004, there were ~37,200 new cases of and 11,000 deaths from SCCHN (2). Many factors contribute to SCCHN, including tobacco smoking (3), alcohol use (4), viral infection (5), and genetic factors (6). Although smoking and alcohol use have a major role in the etiology of SCCHN, only a fraction of smokers and drinkers develop SCCHN, suggesting interindividual variations in genetic susceptibility to SCCHN in the general population.

Cellular DNA is constantly damaged by various endogenous and exogenous agents, including the recognized DNA adduct–inducing carcinogens contained in tobacco smoke. Sophisticated DNA repair pathways and mechanisms have evolved to maintain genomic integrity after insults from environmental hazards. One of the most important of these DNA repair pathways is nucleotide excision repair (NER; ref. 7).

A number of crucial proteins, including seven core factors (ERCC1, XPA, XPB, XPC, XPD, XPF, and XPG), participate in NER (7). Functional mutations in any one of the seven genes encoding these core factors can lead to abnormal NER and thereby increase susceptibility to cancer (8). Several rare syndromes are characterized by NER deficiency coupled with high sensitivity to UV light and increased risk of cancer (9). Patients with xeroderma pigmentosum, for example, have mutations in at least one of seven NER genes and are extremely sensitive to sunlight-induced skin damage. Consequently, these patients have very high incidences of nonmelanoma skin cancer, melanoma, and other solid tumors (9).

In previous studies, we showed that an increased risk of SCCHN is associated with reduced DNA repair capacity, as measured by the host-cell reactivation assay (10), and with reduced levels of NER mRNA in lymphocytes (11). However, the transcript levels may not accurately reflect the level expression of proteins that perform the repair functions. To test the hypothesis that reduced expression of NER proteins is associated with increased risk of SCCHN, we developed a proteomic microarray assay to measure NER protein expression in lymphocytes from SCCHN patients and cancer-free controls.

Materials and Methods

Sample Procurement. The research protocol for this study as a part of an ongoing large molecular epidemiology of SCCHN was approved by the Institutional Review Board of The University of Texas M.D. Anderson Cancer Center.

We used previously cryopreserved, viable peripheral blood lymphocyte samples from 57 patients in an ongoing case-control study of SCCHN. The sample collection started in 2000 with patients who had newly diagnosed, untreated SCCHN, that was histologically confirmed at The University

Received 2/6/05; revised 5/20/05; accepted 6/6/05.

Grant support: NIH grants R01 ES11740, CA 97007, PO1 CA106451, CA100264, and CA16672, and Department of Defense grant DAMD 17-02-1-0706.

The costs of publication of this article were defrayed in part by the payment of page charges. This article must therefore be hereby marked advertisement in accordance with 18 U.S.C. Section 1734 solely to indicate this fact.

Requests for reprints: Qingyi Wei, Department of Epidemiology, Unit 189, and Li Mao, Department of Thoracic & Head and Neck Medical Oncology, Unit 432, The University of Texas, M.D. Anderson Cancer Center, 1515 Holcombe Boulevard, Houston, TX 77030. Phone: 713-792-3020; Fax: 713-563-0999. E-mail: qwei@mdanderson.org.

Copyright © 2005 American Association for Cancer Research.

doi:10.1158/1055-9965.EPI-05-0101

of Texas M.D. Anderson Cancer Center. The 63 cancer-free controls were frequency-matched with cases on age (±5 years), sex, and ethnicity that were obtained from a structured questionnaire.

We selected those subjects whose cryopreserved samples contained sufficient lymphocytes for cell culture and subsequent transfection with plasmid DNA damaged by benzo(*a*)pyrene diol epoxide, a tobacco carcinogen we previously used for studying host-cell NER DNA repair capacity as measured by the host-cell reactivation assay (12). The blood sample processing, plasmid preparation, and transfection have been described in detail previously (12). Briefly, lymphocytes were isolated from whole peripheral blood by Ficoll gradient centrifugation, cryopreserved within 24 hours with freezing medium, and stored in a −80°C freezer in 1.5 mL aliquots.

Cell Culture and Protein Preparation. The cryopreserved cells in each vial were quickly thawed and mixed, before the last trace of ice disappeared, with 8.5 mL of thawing medium (50% fetal bovine serum, 40% RPMI 1640, and 10% dextrose; purchased from Sigma Chemical, St. Louis, MO). This thawing method ensured a cellular viability of >80%, as confirmed by exclusion with 0.4% trypan blue (Sigma). After being washed with the thawing medium, the cells were incubated in RPMI 1640 (Life Technologies, Grand Island, NY) supplemented with 20% fetal bovine serum (Life Technologies) and stimulated with 56.25 μg/mL phytohemagglutinin (Murex Diagnostics, Norcross, GA) at 37°C for 72 hours. Only stimulated lymphocytes were expected to uptake the plasmids (13) and have active NER (14, 15).

After stimulation, the cells ($\sim 1 \times 10^6$) were collected and transfected by the DEAE-dextran (Pharmacia Biotech, Piscataway, NJ) method with 0.25 μg of untreated plasmids (as the baseline for comparison) or benzo(*a*)pyrene diol epoxide–damaged plasmids. In keeping with the protocol for the host-cell reactivation assay, in which the reactivation of the report gene is measured by quantifying the enzyme activity (12). The cells were collected for protein extraction 40 hours after the transfections. This procedure is crucial to ensure that the repair process is activated by the presence of the damaged plasmids, which served as the substrate for the NER enzymes. Thirty microliters of cell suspension ($\sim 1 \times 10^5$ cells) from each patient sample was mixed with 10 μL of 4× SDS sample buffer containing 50 mmol/L Tris-HCl (pH 8.0), 150 mmol/L NaCl, 0.1% SDS, and 1% Triton X-100 supplemented with a protease inhibitor cocktail (Roche Applied Science, Indianapolis, IN). The cell lysate was then boiled for 5 minutes and stored at −80°C.

Construction of Reverse-Protein Microarrays. Proteins were extracted from the cells and were used to construct the microarrays. The extracted protein samples were serially diluted 1:1 with PBS (pH 7.5) to achieve final total protein concentrations ranging from 1 to 0.025 μg/μL. The minimum detectable total protein concentration was 0.0525 μg/μL. The serial dilutions were applied to FAST slides (Schleicher & Schuell Bioscience, Keene, NH) using a SpotBot microarrayer (TeleChem International, Cupertino, CA). Each sample containing the antigens (the NER proteins) to be detected was spotted in duplicate. Prepared slides were either used immediately or stored at −20°C.

Quantitative Analysis of Protein Levels Using Reverse-Protein Microarrays. We used mouse anti-human monoclonal or anti-goat or anti-rabbit polyclonal antibodies against XPD and XPG (Santa Cruz Biotechnology, Santa Cruz, CA); XPA, XPC, and XPF (Abcam, Cambridge, MA); ERCC1 (Novus Biological, Littleton, CO); and β-actin (Sigma). XPB was not assayed because no commercially available antibodies against XPB were specific enough for this study.

Briefly, the protein-spotted slides were treated with ReBlot (Chemicon, Temecula, CA) for 15 minutes and then washed twice for 10 minutes each with washing buffer containing 300 mmol/L NaCl, 0.1% Tween 20, and 50 mmol/L Tris (pH 7.6). The protein arrays were then blocked with I-Block (Applied Biosystems, Foster City, CA) for 30 minutes at room temperature. The primary antibodies were diluted based on their affinities, which were determined in our preliminary tests (data not shown). The dilution ratios were 1:300 for XPA and ERCC1; 1:500 for XPC, XPD, XPF, and XPG; and 1:100,000 for β-actin. The arrays were incubated with individual antibodies for 1 hour at room temperature. The anti-mouse, anti-goat, and anti-rabbit secondary antibodies (Vector Laboratories, Burlingame, CA) were labeled with biotin, diluted 1:10,000, and added to the slides, which were then incubated at room temperature for 30 minutes. Signals were enhanced using a catalyzed signal amplification system (DAKO, Carpinteria, CA) according to the manufacturer's protocol, except that in the final step, we incubated the slides with Cy5-conjugated streptavidin (1:1,000; Jackson ImmunoResearch Laboratories, West Grove, PA) for 30 minutes. After each incubation step, the arrays were washed thrice for 5 minutes each with the washing buffer described above.

Signals on the protein microarrays were scanned on a ScanArray Lite microarray scanner (Perkin-Elmer Life Sciences, Boston, MA). The signal intensity of each spot and its background signal were analyzed using a ScanArray Express 2.0 microarray analysis system (Perkin-Elmer Life Sciences) running the ''Run-easy Quant'' protocol. The final data were stored as graphic images for further analysis. Any scan-reading value <2,000 was treated as missing data. The median value of the scan-reading data for each dot of a protein on the microarray was used to calculate the means of the duplicates. Scan-reading data for the β-actin were used as a baseline to obtain the relative expression levels for each protein. The coefficient of variation (CV) was calculated as [(SD / mean) × 100].

Statistical Analysis. The mean signal intensity values for the cases and controls for each NER protein were compared with Student's *t* test. The distribution of select variables of the cases and controls were compared with the χ^2 test. The correlation between the expression levels of different proteins was analyzed by the Pearson correlation coefficient. The median protein expression for the controls was used as the cutoff value for calculating the odds ratios (OR) associated with low expression and their 95% confidence intervals (CI). Multivariate logistic regression models were used to calculate the adjusted ORs and 95% CIs with adjustment for age (in years), sex (male versus female), ethnicity (non-Hispanic versus others), and sample storage time (in months). *P* values <0.05 were considered statistically significant. All statistical analyses were performed with SAS software version 8.0e (SAS Institute, Cary, NC).

Results

Protein Microarray Data. We began by testing the reproducibility and linearity of the reverse-protein microarray assay. Four samples of cell extracts from four controls were each diluted 1:1 five times; all 20 aliquots were spotted in triplicate on one slide (a total of 60 spots). We made three such slides for each sample and probed them with antibodies to XPA and XPF (Fig. 1A). The expression levels of XPA and XPF were linear on a log scale at the tested total protein concentrations between 1.0 and 0.0525 μg/μL (Table 1). These results were consistent between all samples and repeated experiments (Fig. 1B). Based on the CVs, however, it seemed that the reproducibility of the results was better at higher protein concentrations (CV as low as 0.8%) than at lower concentrations (CV as high as 24.6%; Table 1).

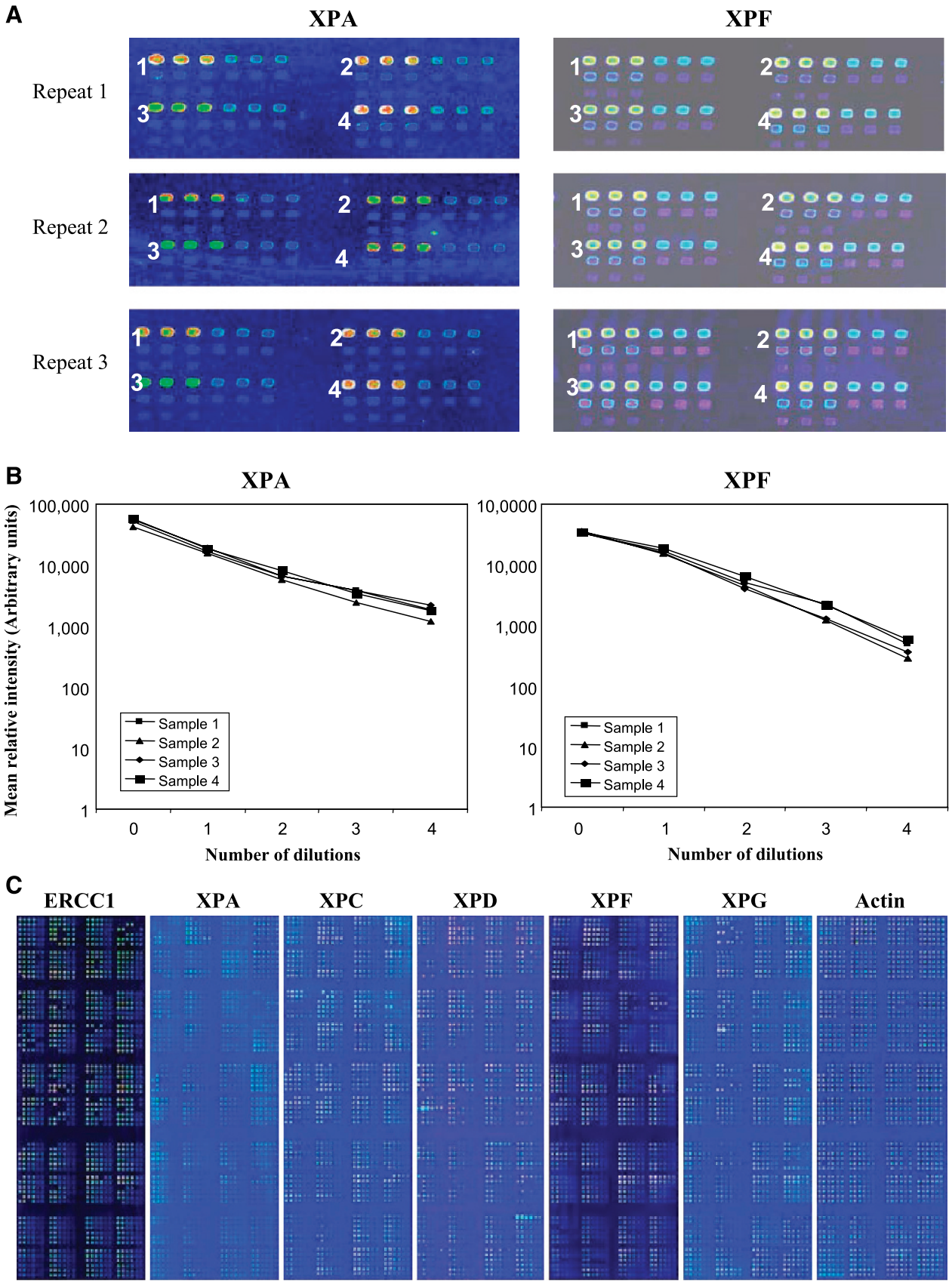


Figure 1. Reproducibility and linearity of reverse-protein microarray assay data. **A.** Serial dilutions of four cell-extract samples (1, 2, 3, and 4) were spotted in triplicate and probed with specific antibodies against XPA and XPF. Each slide was tested three times (repeats 1, 2, and 3). The statistical data are summarized in Table 1. **B.** The mean intensities of the spots in (*A*; in arbitrary units) were plotted on a log scale against the number of dilutions of the cell extract. **C.** Reverse-protein microarray assay of expression of the NER proteins ERCC1, XPA, XPC, XPD, XPF, and XPG. The level of β-actin was used as an internal control for standardization of the expression levels. The statistical data are summarized in Table 3.

Table 1. Reproducibility and linearity of reverse-protein microarray data

		XPA					XPF				
Sample 1											
Total protein (μg/μL)		0.96	0.48	0.24	0.12	0.06	0.96	0.48	0.24	0.12	0.06
Signal intensity	R1*	51,787	18,817	8,025	4,641	2,375	36,356	16,923	4,481	2,369	436
(arbitrary units)	R2	54,704	15,702	6,130	3,418	1,797	32,925	16,802	5,574	2,119	476
	R3	49,131	15,106	5,488	3,263	1,461	30,030	16,255	4,969	2,243	553
Mean (SD)†		51,874 (2,788)	16,542 (1,993)	6,548 (1,319)	3,774 (755)	1,878 (462)	33,104 (3,167)	16,660 (356)	5,008 (548)	2,244 (125)	488 (60)
CV (%)		5.4	12.1	20.2	20.1	24.6	9.6	2.1	10.9	5.6	12.2
Sample 2											
Total protein (μg/μL)		1	0.5	0.25	0.125	0.0625	1	0.5	0.25	0.125	0.0625
Signal intensity	R1	46,645	18,305	5,724	2,713	1,354	35,249	15,373	4,331	1,054	317
(arbitrary units)	R2	43,944	13,908	5,901	2,513	1,316	37,172	16,418	4,774	1,058	294
	R3	38,014	14,368	5,593	2,118	839	33,349	14,328	4,826	1,473	258
Mean (SD)†		42,868 (4,415)	15,527 (2,417)	5,739 (155)	2,448 (303)	1,170 (287)	35,257 (1,912)	15,373 (1,045)	4,644 (272)	1,195 (241)	290 (30)
CV (%)		10.3	15.6	2.7	12.4	24.5	5.4	6.8	5.9	20.2	10.3
Sample 3											
Total protein (μg/μL)		0.88	0.44	0.22	0.11	0.055	0.88	0.44	0.22	0.11	0.055
Signal intensity	R1	58,360	21,799	8,297	4,644	2,511	33,940	17,236	4,507	1,316	374
(arbitrary units)	R2	58,558	18,709	5,318	3,561	1,947	33,720	15,228	3,769	1,327	385
	R3	51,531	17,762	5,931	3,306	2,201	32,877	13,946	3,776	1,193	321
Mean (SD)†		56,150 (4,001)	19,423 (2,111)	6,515 (1,573)	3,837 (710)	2,220 (283)	33,512 (561)	15,470 (1,658)	4,017 (424)	1,279 (74)	360 (34)
CV (%)		7.1	10.9	24.2	18.5	12.7	1.7	10.7	10.6	5.8	9.5
Sample 4											
Total protein (μg/μL)		0.84	0.42	0.21	0.105	0.0525	0.84	0.42	0.21	0.105	0.0525
Signal intensity	R1	60,447	22,560	9,560	4,214	2,130	35,167	18,616	6,519	2,119	538
(arbitrary units)	R2	59,055	16,333	7,948	3,163	1,918	34,935	18,613	6,584	1,865	538
	R3	52,017	15,913	6,862	2,828	1,314	34,615	18,931	6,259	2,428	680
Mean (SD)†		57,173 (4,519)	18,269 (3,722)	8,123 (1,358)	3,402 (723)	1,787 (423)	34,906 (277)	18,720 (182)	6,454 (172)	2,137 (282)	585 (82)
CV (%)		7.9	20.4	16.7	21.3	23.7	0.8	1.0	2.7	13.2	14.0

*R1-3, repeats 1 to 3.
†Standard deviation of the three experiments.

We next diluted each of the 120 test samples twice, and then spotted them on the arrays in duplicate (Fig. 1C). The means of the duplicate readings were used to calculate the relative protein expression. Because of mechanical problems during the spotting, some protein spots were unreadable on the arrays, consequently, valid readings could not be obtained for up to five samples per protein. Consistent with the results of our reproducibility and linearity tests, the readings from spots with lower protein concentrations had greater variation, whereas the spots with higher protein concentrations produced consistent, strong, and readable signals. We therefore used the latter data (i.e., the original samples without dilution) to calculate the relative expression levels.

We also transfected cells from these samples with either undamaged plasmids or benzo(*a*)pyrene diol epoxide–damaged plasmids to stimulate DNA repair activity. When we compared the relative expression of NER proteins between the cases and controls, we found that the data from the samples transfected with damaged plasmids were a better predictor of risk of SCCHN (data not shown), although the two data sets were statistically correlated ($P < 0.01$). We therefore used data derived from cells transfected with damaged plasmids in the following experiments.

Subject Characteristics. Our analysis included 57 patients with newly diagnosed SCCHN and 63 cancer-free controls whose cryopreserved lymphocytes were available for culture, transfection, and protein extraction. The cases and controls were frequency-matched on age, sex, and ethnicity. The cases were slightly younger (56.2 versus 57.2 years) and comprised more males and non-Hispanic whites than did the controls, but these differences were not statistically significant (Table 2). There were more smokers and alcohol drinkers among the cases than among the controls, and these differences were statistically significant (Table 2). Because the cases were recruited before the controls, the duration of lymphocyte storage was also significantly different between the two groups

Table 2. Characteristics SCCHN patients and control subjects

Variable	Cases (n = 57)	Controls (n = 63)	P*
	No. (%)	No. (%)	
Age (y)			
≤55	24 (42)	25 (40)	
>55	33 (58)	38 (60)	0.787
Sex			
Male	43 (75)	39 (62)	
Female	14 (25)	24 (38)	0.112
Ethnic group			
African-American	3 (5)	3 (5)	
Mexican-American	3 (5)	4 (6)	
Non–Hispanic White	51 (90)	56 (89)	0.962
Tobacco use†			
Yes	42 (74)	31 (49)	
No	15 (26)	32 (51)	0.006
Alcohol use‡			
Yes	43 (75)	33 (52)	
No	14 (25)	30 (48)	0.009

*Calculated using two-sided χ^2 test.
† The question asked was, ''Have you ever smoked at least 100 cigarettes in your lifetime?''
‡ The question asked was, ''Have you ever drunk alcoholic beverages at least once a week for 1 year or more?''

Table 3. Relative expression of NER proteins in SCCHN patients and controls

	n^*	Mean ± SD		Difference (%)	$P^\dagger$
		Cases	Controls		
Age (y)	57/63	56.2 ± 9.7	57.2 ± 9.5		0.418
Storage time	57/63	17.7 ± 11.7	13.2 ± 6.8		0.013
Relative expression (%)[‡]					
ERCC1	53/58	1.369 ± 0.401	1.696 ± 0.539	−19.3	<0.001
XPA	53/61	0.363 ± 0.111	0.424 ± 0.160	−14.4	0.017
XPC	54/62	1.326 ± 0.650	1.770 ± 0.923	−25.1	0.003
XPD	52/59	0.947 ± 0.343	1.137 ± 0.584	−19.0	0.037
XPF	56/62	0.966 ± 0.438	1.297 ± 0.764	−25.5	0.004
XPG	55/60	1.206 ± 0.453	1.432 ± 0.628	−15.8	0.028

*Number of cases/controls.
†Calculated using two-sided Student's t test.
‡Expression level relative to that of β-actin.

(Table 3). We further adjusted for all of these variables in the multivariate logistic regression analysis.

Difference in NER Protein Expression Between the Cases and Controls. We used Student's t test to evaluate the differences in NER protein expression between the cases and controls. The expression of all seven NER proteins was significantly lower among the cases than among the controls (Table 3). The greatest reduction was in the relative expression of XPC and XPF, which was reduced by about 25% in the cases compared with the controls. The reduction in the expression of all NER proteins may reflect their association with repair activities, in which certain levels of proteins need to be present. Correlative analysis revealed that the relative expression levels of these NER proteins were all highly correlated ($P \leq 0.001$). For example, the expression of XPC was correlated with that of ERCC1 ($r = 0.706$), XPF ($r = 0.505$), and XPG ($r = 0.715$), and the expression of XPF was correlated with that of XPA ($r = 0.695$), XPD ($r = 0.541$), and XPG ($r = 0.781$). This led us to investigate which protein has the most significant role in the increased risk of SCCHN.

Association Between NER Protein Expression and Risk of SCCHN. We used the median expression level in the control samples as the cutoff values for calculating the ORs for risk of SCCHN. The crude ORs for low compared with high expression of XPA, XPC, XPD, XPF, but not those for ERCC1 and XPG, were significantly increased (Table 4). The ORs remained essentially unchanged after adjustment for age, sex, ethnicity, smoking, alcohol use, and sample storage time. The highest adjusted OR was for XPF (5.29; 95% CI, 2.10-3.92) followed by XPD and XPA. Because the relative expression levels of these NER proteins were highly correlated with each other, the relative expression levels of all proteins were simultaneously adjusted for each other in the final multivariate logistic regression model containing age, sex, ethnicity, smoking, alcohol use, and sample storage time. The only significant adjusted OR was for XPF (11.5; 95% CI, 2.32-56.6) in the presence of other proteins in the same model (Table 4).

Discussion

Our reverse-protein microarray assay successfully detected the target proteins at a total protein concentration as low as 0.0525 μg/μL. However, the measurements seemed to be more reproducible at a total protein concentration ≥0.5 μg/μL. The cell extract from ~1×10^5 cells (yielding 30 μL of sample) would thus be sufficient for repeated experiments, because each printed spot contained only 0.0033 μL. Using this assay, we showed that the relative expression levels of the six NER proteins (ERCC1, XPA, XPC, XPD, XPF, and XPG) were consistently significantly lower among the SCCHN patients than among the controls. Four of the six NER proteins tested (XPA, XPC, XPD, XPF) were associated with a significantly increased risk of SCCHN.

The data from this study are consistent with those in two of our previously published studies (10, 11). In the first study, we measured DNA repair capacity in 55 newly diagnosed SCCHN patients and 61 controls by the host-cell reactivation assay using a benzo(*a*)pyrene diol epoxide–damaged reporter gene (10). The mean DNA repair capacity in that study was significantly lower in the cases than in the controls. Those

Table 4. Estimation of SCCHN risk (OR and 95% CI) associated with expression levels of NER proteins

Expression level[*]		Cases	Controls	Crude OR (95% CI)	Multivariate adjusted[†] OR (95% CI)	Multivariate adjusted OR[‡] (95% CI)
		No. (%)	No. (%)			
ERCC1	high	17 (32)	29 (50)	2.12 (0.98-4.59)	2.18 (0.91-5.24)	0.78 (0.21-2.85)
	low	36 (68)	29 (50)			
XPA	high	15 (28)	30 (49)	2.45 (1.12-5.35)	2.99 (1.22-7.47)	2.01 (0.57-7.14)
	low	38 (72)	31 (51)			
XPC	high	13 (24)	31 (50)	3.15 (1.42-7.01)	2.46 (1.04-5.87)	1.17 (0.31-4.41)
	low	41 (76)	31 (50)			
XPD	high	15 (29)	29 (49)	2.38 (1.09-5.24)	3.02 (1.18-7.76)	1.88 (0.50-7.01)
	low	37 (71)	30 (51)			
XPF	high	13 (23)	31 (50)	3.31 (1.49-7.33)	5.29 (2.01-13.9)	11.5 (2.32-56.6)
	low	43 (77)	31 (50)			
XPG	high	18 (33)	30 (50)	2.06 (0.96-4.38)	1.56 (0.79-3.92)	0.48 (0.13-1.74)
	low	37 (67)	30 (50)			

*Dichotomized based on median values of control subjects.
†Obtained from logistic regression model with adjustment for age, sex, race, smoking status, alcohol use, and lymphocyte storage time.
‡Obtained from logistic regression model with adjustment for age, sex, race, smoking status, alcohol use, lymphocytes.

with DNA repair capacity values in the middle and lowest tertiles had >2-fold and 4-fold increased SCCHN risk, respectively, compared with those whose DNA repair capacity values were in the highest tertile. In the subsequent study, we investigated which NER genes might be responsible for the reduced DNA repair capacity in SCCHN. We previously measured the relative expression of the genes encoding five NER proteins (ERCC1, XPB, XPG, CSB, and XPC) by a multiplex RT-PCR method (11). The relative mRNA expression levels of ERCC1, XPB, XPG, and CSB were significantly lower in the cases than in the controls, and the risk of SCCHN associated with low expression of these genes was higher by 2- to 6-fold (11). In that study, we were not able to measure the expression of XPA, XPD, or XPF because the sequences of the genes were unknown at that time and the high level of sequence homology in the genome for the primers chosen made the assays unreliable.

In the present study, simultaneous adjustment for the expression levels of all proteins and other confounding factors revealed that the relative expression level of XPF was the only independent risk factor for SCCHN. Low compared with high expression of XPF was associated with an SCCHN risk >11-fold higher. Although the estimate was imprecise as evidenced by the wide 95% CI, this finding suggests that XPF may play a role in the repair of carcinogen-damaged DNA. Because ERCC1 needs XPF to form a functional complex (7), it is possible that XPF acts as a rate-limiting modulator. Based on our data, ERCC1 was expressed at higher levels than the other five proteins were, whereas XPF expression was <70% of ERCC1 expression. It is possible that our system was saturated with ERCC1 protein, so the amount of XPF became crucial for modulating the overall DNA repair capacity.

The present study is an extension of our previous studies assessing the best biomarkers of DNA repair capacity for predicting susceptibility to SCCHN. In the present study, we measured the relative expression levels of six of the seven core NER proteins because we did not find an appropriate antibody for XPB. Our data further support the notion that altered NER capacity, at the cellular, mRNA, or protein levels, may contribute to the risk of tobacco-induced SCCHN. More important, our reverse-protein microarray assay of relative protein expression seemed to be the most sensitive, compared with previously reported assays of cellular DNA repair capacity and the mRNA expression levels (10, 11). Further studies are warranted to correlate the expression of these markers in surrogate and target tissues such as oral epithelial cells.

There are several advantages to the reverse-protein microarray assay. First, compared with the host-cell reactivation assay (12), the microarray assay requires significantly (3-fold) fewer viable lymphocytes for protein extraction. Second, compared with the RT-PCR assay, the microarray assay is highly sensitive and reproducible, which is optimal for large-scale screening. Third, the microarray assay has the potential to test virtually any protein involved in NER or other molecular pathways underlying increased cancer risk. Finally, the microarray assay is rapid and cost-effective and produces a large quantity of data. With the availability of antibodies for specific protein posttranslational modifications, the microarray method may also become a powerful tool to assess functional changes in proteins.

Although the design of this pilot case-control study has inherent limitations of recall and selection biases, the reverse-protein microarray assay may be a powerful tool for future prospective studies if it is technically fine-tuned and the sampling issues resolved (16, 17). For instance, future studies must address the differences in protein concentrations between surrogate and target tissues, between fresh and stored serum samples, and before and after cancer diagnosis and treatment. An improved reverse-protein microarray assay should become a useful tool for future hypothesis-driven molecular epidemiologic studies of cancer.

Acknowledgments

We thank Dr. Margaret R. Spitz for critical review; Margaret Lung and Dr. Peggy Schuber for assistance in recruiting the subjects; Youhong Fan, Zhaozheng Guo, and Yawei Qiao for laboratory assistance; Betty Jean Larson and Joanne Sider for manuscript preparation; and Pierrette Lo for scientific editing.

References

1. Pisani P, Parkin DM, Bray F, Ferlay J. Estimates of the worldwide mortality from 25 cancers in 1990. Int J Cancer 1999;83:18–29.
2. American Cancer Society Inc. Cancer facts and figures 2003. Atlanta: American Cancer Society; 2003.
3. Johnson N. Tobacco use and oral cancer: a global perspective. J Dent Educ 2001;65:328–39.
4. Casiglia J, Woo SB. A comprehensive review of oral cancer. Gen Dent 2001; 49:72–82.
5. Dahlstrom KR, Adler-Storthz K, Etzel CJ, et al. Human papillomavirus type 16 infection and squamous cell carcinoma of the head and neck in never-smokers: a matched pair analysis. Clin Cancer Res 2003;9:2620–6.
6. Sturgis EM, Wei Q. Genetic susceptibility–molecular epidemiology of head and neck cancer. Curr Opin Oncol 2002;14:310–7.
7. Sancar A, Lindsey-Boltz LA, Unsal-Kacmaz K, Linn S. Molecular mechanisms of mammalian DNA repair and the DNA damage checkpoints. Annu Rev Biochem 2004;73:39–85.
8. Friedberg EC. How nucleotide excision repair protects against cancer. Nat Rev Cancer 2001;1:22–33.
9. Kraemer KH, Lee MM, Andrew AD, et al. The role of sunlight and DNA repair in melanoma and nonmelanoma skin cancer. Arch Dermatol 1994;130: 1018–21.
10. Cheng L, Eicher SA, Guo Z, Hong WK, Spitz MR, Wei Q. Reduced DNA repair capacity in head and neck cancer patients. Cancer Epidemiol Biomarkers Prev 1998;7:465–8.
11. Cheng L, Sturgis EM, Eicher SA, Spitz MR, Wei Q. Expression of nucleotide excision repair genes and the risk for squamous cell carcinoma of the head and neck. Cancer 2002;94:393–7.
12. Wei Q, Cheng L, Amos CI, et al. Repair of tobacco carcinogen-induced DNA adducts and lung cancer risk: a molecular epidemiologic study. J Natl Cancer Inst 2000;92:1764–72.
13. Cheng L, Wang LE, Spitz MR, Wei Q. Cryopreserving whole blood for functional assays using viable lymphocytes in molecular epidemiology studies. Cancer Lett 2001;166:155–63.
14. Athas AF, Hedayati M, Matanoski GM, Farmer ER, Grossman L. Development and field-test validation of an assay for DNA repair in circulating human lymphocytes. Cancer Res 1991;51:5786–93.
15. Barret JM, Calsou P, Salles B. Deficient nucleotide excision repair activity in protein extracts from normal human lymphocytes. Carcinogenesis 1995;16: 1611–6.
16. Shivji MKK, Kenny MK, Wood R. Proliferating cell nuclear antigen is required for DNA excision repair. Cell 1992;69:367–74.
17. Cutler P. Protein arrays: the current state-of-the-art. Proteomics 2003;3:3–18.

Down-regulation of Hepatoma-Derived Growth Factor Inhibits Anchorage-Independent Growth and Invasion of Non–Small Cell Lung Cancer Cells

Jun Zhang,[1,4] Hening Ren,[1] Ping Yuan,[1] Wenhua Lang,[1] Li Zhang,[2] and Li Mao[1,3]

Departments of [1]Thoracic/Head and Neck Medical Oncology and [2]Biostatisitcs, The University of Texas M.D. Anderson Cancer Center; [3]Cancer Biology Program, The University of Texas Graduate School of Biomedical Sciences at Houston, Houston, Texas; and [4]Department of Thoracic Surgery, First Clinical College, China Medical University, Shenyang, PR China

Abstract

We recently reported that a high level of hepatoma-derived growth factor (HDGF) expression in tumors correlates with a high incidence of tumor relapse or distant metastasis and shortened survival time in patients with non–small cell lung cancer (NSCLC). However, the mechanisms of the HDGF-associated aggressive biological behavior are unknown. In this study, we knocked down HDGF expression in NSCLC cells to determine the biological consequences. Transfection with *HDGF*-specific small interfering RNA (siRNA) resulted in down-regulation of HDGF expression in four NSCLC cell lines. Down-regulation of HDGF resulted in no detectable effect on anchorage-dependent cell growth as determined with a 3-(4,5-dimethylthiazol-2-yl)-2,5-diphenyltetrazolium bromide assay, a microelectronic cell sensor system, and flow cytometry. In contrast, cells transfected with HDGF-siRNA grew more slowly and formed significantly fewer colonies in soft agar than did cells treated with LipofectAMINE alone or transfected with negative control siRNA. In an *in vitro* invasion assay, significantly fewer cells transfected with HDGF-siRNA than cells treated with LipofectAMINE alone were able to invade across a Matrigel membrane barrier. In an *in vivo* mouse model, A549 cells treated with HDGF-siRNA grown significantly slower than the cells treated with LipofectAMINE alone or negative control siRNA. Morphologically, HDGF-siRNA–treated tumors exhibited markedly reduced blood vessel formation and increased necrosis, whereas the Ki67 labeling indices were similar in tumors treated with controls. Our results suggest that HDGF is involved in anchorage-independent growth, cell invasion, and formation of neovasculature of NSCLC. These qualities may contribute to the HDGF-associated aggressive biological behavior of NSCLC. (Cancer Res 2006; 66(1): 18-23)

Introduction

Hepatoma-derived growth factor (HDGF) is a heparin-binding growth factor originally purified from media conditioned with the human hepatoma cell line HuH-7 and can stimulate proliferation of Swiss 3T3 cells (1). Its precise function is unclear, but HDGF is known to be highly expressed during the early development of many tissues, including cardiovascular (2), kidney (3), and liver (4). Although lacking the secretory sequence present in most secretory proteins (5), HDGF has been shown to act as a potent exogenous mitogen for HuH-7 hepatoma cells (6), COS-7 kidney cells (6), aortic vascular smooth muscle cells (7), and endothelial cells (3). As deduced from the cDNA clone of *HDGF*, the amino acid sequence contains 240 residues with a motif homologous to the consensus sequences of a bipartite nuclear localization sequence and a DNA-binding PWWP motif, suggesting that the protein translocates to the nucleus and binds to DNA. In fact, HDGF is found mainly in nucleus, and its role as a transcription factor has been postulated (8, 9).

In a recent study, we investigated the role of HDGF in non–small cell lung cancer (NSCLC) and found that the protein is frequently overexpressed in these tumors (10). In patients with early-stage NSCLC, poorer clinical outcome was significantly correlated with higher HDGF expression, suggesting that HDGF is involved in the determination of aggressive biological behavior of NSCLC cells. To elucidate the mechanism of HDGF-mediated aggressiveness in NSCLC cells, we down-regulated *HDGF* expression in these cells using small interfering RNA (siRNA) technology and studied effects of the down-regulation in cell proliferation and invasion. Our results suggest that HDGF is involved in anchorage-independent growth and cell invasion of NSCLC. These qualities may contribute to the HDGF-associated aggressive biological behavior of NSCLC.

Materials and Methods

Cell culture. NSCLC cell lines H226, H1944, H292, H157, A549, H596, H460, and H358 were obtained from American Type Culture Collection (Rockville, MD) and cultured in DMEM supplemented with 10% heat-inactivated fetal bovine serum (FBS). The normal human bronchial epithelial cell lines HBE1 and HBE3 (kindly provided by Dr. John Minna of The University of Texas Southwestern Medical Center, Dallas, TX) were cultured in keratinocyte serum-free medium with 25 μg/mL bovine pituitary extract and 0.2 ng/mL recombinant epidermal growth factor (Invitrogen, Carlsbad, CA).

siRNA and knockout of *HDGF* expression. We selected two sites in the *HDGF* mRNA sequence as siRNA targets based on principles described previously (11). The targeted *HDGF* sequences, based on which the siRNAs were chemically synthesized by Ambion (Austin, TX), were 5′-AACCGGCA-GAAGGAGUACAAA-3′ (siRNA-1) and 5′-AAAUCAACAGCCAACAAAUAC-3′ (siRNA-2). The negative control siRNAs were purchased from Ambion. *In vitro* transfections were done using LipofectAMINE 2000 (Invitrogen, Carlsbad, CA) following manufacturer's protocols.

Cell proliferation analysis. Cells were plated onto 96-well plates at a density of 1×10^4 per well with medium containing 10% FBS and incubated for 15 hours. Cell numbers were determined at 0, 24, 48, and 72 hours after transfection using the 3-(4,5-dimethylthiazol-2-yl)-2,5-diphenyltetrazolium bromide (MTT)–based CellTiter96 cell proliferation assay (Promega, Madison, WI). ACEA RT-CES (ACEA Biosciences, San Diego, CA), a microelectronic cell sensor system, was used to confirm the number of living cells. NSCLC cells (1×10^4) were seeded into each sensor-containing well

Requests for reprints: Li Mao, Molecular Biology Laboratory, Department of Thoracic/Head and Neck Medical Oncology, The University of Texas M.D. Anderson Cancer Center, Unit 432, 1515 Holcombe Boulevard, Houston, TX 77030. Phone: 713-792-6363; Fax: 713-796-8655; E-mail: lmao@mdanderson.org.

©2006 American Association for Cancer Research.

doi:10.1158/0008-5472.CAN-04-3905

(19.6-mm^2 surface with 150 μL of medium) of the microtiter plates. The electronic sensors provided a continuous (every 6 hours), quantitative measurement of the cell index (reflect to the surface area covered by the cells) in each well. After 15 hours of culture, the cells were transfected as described above. Cell growth was measured every 6 hours for 72 hours, and cell indexes were recorded for each well at all time points.

Cell cycle analysis. A549 cells were harvested by trypsinization 72 hours after transfection and fixed with 70% ethanol. After RNase treatment, the cell cycle distribution was determined using a BD FACSCalibur flow cytometer and Cell Quest software (Becton Dickinson, San Jose, CA).

Anchorage-independent growth assay. Twenty-four hours after transfection with siRNA, ~2,000 cells in 1 mL of 0.3% agarose with DMEM were plated in each well on the top of existing 0.6% bottom agarose in six-well tissue culture plates in triplicate for each treatment condition. The plates were covered with 1 mL of medium with 10% FBS and incubated at 37°C in a 5% CO_2 incubator for 3 weeks. The covering medium was replaced every week. At the end of 3 weeks, cell colonies >0.1 mm in diameter were counted under a microscopic field at ×40 magnifications. Means were based on numbers from triplicate wells for each treatment condition and were analyzed using two-sided Student's *t* test.

***In vitro* cell invasion assay.** The *in vitro* invasion assay was carried out in BD BioCoat Matrigel invasion chambers (Becton Dickinson). After rehydration of the chambers, 1.1×10^4 cells in 100 μL of the growth medium with 10% FBS were added into each of the upper chambers. Cells in the chambers were transfected with LipofectAMINE alone or 100 nmol/L HDGF-siRNA-1 in serum-free condition. Four hours later, the medium was replaced with fresh growth medium containing 10% FBS in the upper chambers, whereas the lower wells contained serum-free medium. After 20 hours, the medium in each of the lower wells was replaced with 750 μL of serum-free medium containing 30 μg/mL laminin (Sigma-Aldrich, St. Louis, MO). After an additional 24 hours of incubation, the noninvading cells on the upper side of the chamber membranes were removed. The invading cells to the opposite side of the chamber membranes were examined. The invading cells on each of triplicate membranes were counted. Means were based on the numbers from the triplicate wells for each treatment condition and were analyzed using two-sided Student's *t* test.

Western blot analysis. Total proteins were loaded into each well on 10% SDS-polyacrylamide gels, separated by electrophoresis, and transferred to Hybond-P polyvinylidene difluoride membrane (Amersham Biosciences, Buckinghamshire, United Kingdom). The membranes were probed with a rabbit polyclonal anti-HDGF antibody (gift from Dr. Allen Everett of Johns Hopkins Hospital, Baltimore, MD) followed by incubating with horseradish peroxidase–conjugated anti-rabbit immunoglobulin G (Amersham Biosciences). Immunodetection was done using the enhanced chemiluminescence Western blotting analysis system (Amersham Biosciences). β-Actin was used as protein loading control monoclonal anti-β-actin antibody (Sigma-Aldrich).

Global gene expression analysis. Total RNA was isolated from cells using the Qiagen RNeasy Mini kit (Qiagen, Valencia, CA). Ten micrograms of total RNA were reverse-transcribed into double-stranded cDNA and then transcribed in the presence of biotin-labeled ribonucleotides, using the BioArray High-Yield RNA transcript labeling kit (Enzo Laboratories, Farmingdale, NY) as described by the manufacturer. The biotin-labeled cRNA was purified using RNeasy mini-column (RNeasy kit, Qiagen) and fragmented at 94°C for 35 minutes in 1× fragmentation buffer [40 mmol/L Tris-acetate (pH 8.0), 100 mmol/L KOAc, 30 mmol/L MgOAc]. Affymetrix U133A chips were used for gene expression analysis using the Affymetrix GeneChip system (Affymetrix, Santa Clara, CA).

The expression levels were extracted from positional-dependent nearest-neighbor model developed by Zhang et al. (12). Genes that are absent or always expressed at low levels were excluded from further analysis because variation in gene expression at low levels are usually not reproducible. The removed genes have mean log expression level of <7.1. Genes with SD <0.06 were also removed. Comparisons were then done between cells treated with LipofectAMINE alone and cells treated with 100 nmol/L HDGF-siRNA-1.

Northern blot analysis. Total RNA (10 μg) was loaded in each lane. cDNA probes corresponding to *HDGF, GLO1, SERPINE2, AXL*, and actin were prepared using reverse transcription-PCR followed by cDNA purification and labeling.

***In vivo* tumor model.** Athymic Swiss *nu/nu*/Ncr nude (*nu/nu*) mice, bred and maintained in our institutional specific pathogen-free mouse colony, were used. Briefly, 4-week-old male nude mice were injected s.c. with 10^6 A549 cells in 100 μL of PBS at a single dorsal site. Three groups (five each) of mice were tested. Group 1 were injected with A549 cells treated with LipofectAMINE alone; group 2 were injected with A549 cells treated with LipofectAMINE plus 100 nmol/L HDGF-siRNA-1; group 3 was injected with A549 cells treated with LipofectAMINE plus 100 nmol/L negative control siRNA. Tumor size was measured every 2 days for 20 days. Tumor

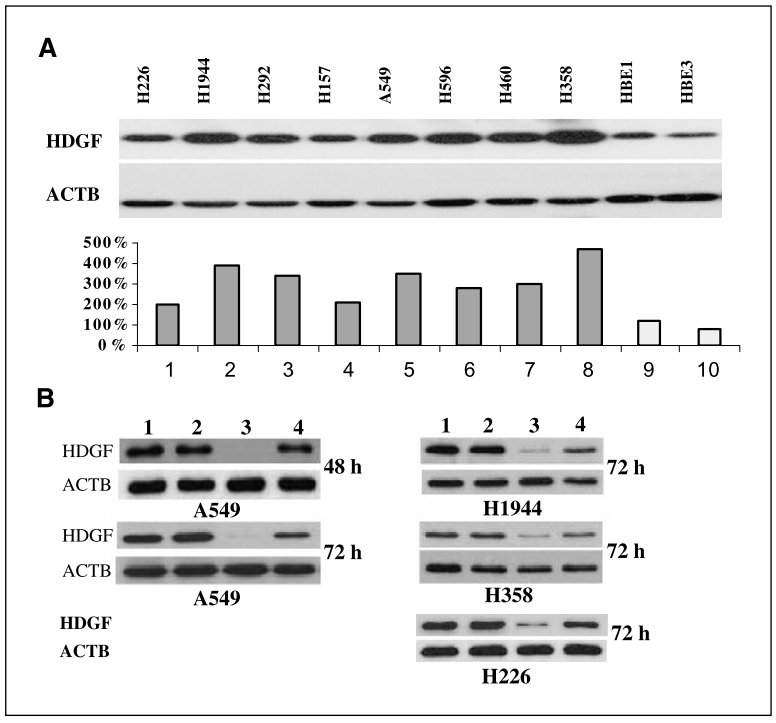


Figure 1. *A,* Western blots showing expression of HDGF protein in eight NSCLC cell lines and two immortalized normal bronchial epithelial cell lines. β-Actin (*ACTB*) served as protein loading control. *Bottom,* relative expression level of HDGF quantified based its β-actin level. *B,* down-regulation of HDGF protein expression induced by HDGF-siRNA-1 in A549 cells (48 and 72 hours after siRNA administration) and in H1944, H358, and H226 cells (72 hours after siRNA administration). β-Actin served as protein loading control. *Lane 1,* treated with LipofectAMINE alone; *lane 2,* treated with 100 nmol/L negative control siRNA; *lane 3,* treated with 100 nmol/L HDGF-siRNA-1; *lane 4,* treated with 100 nmol/L HDGF-siRNA-2.

growth was quantified by measuring the tumors in three dimensions with calipers. The results were expressed as the mean tumor volume ($n = 5$) with 95% confidence intervals. The statistical significance of differences in tumor growth was analyzed using Wilcoxon rank sum test.

Tumor morphology and Ki67 immunohistochemistry. Formalin-fixed and paraffin-embedded tissue sections were stained with H&E for morphologic examination. For Ki67 immunohistochemistry, an anti-Ki67 antibody (Lab Vision, Fremont, CA) was used. The expression signal was detected using standard avidin-biotin immunohistochemical techniques according to the manufacturer's recommendations (Vector Laboratories, Burlingame, CA).

Results and Discussion

HDGF is highly expressed in NSCLC. Western blot analysis using a polyclonal anti-HDGF antibody revealed that most of the NSCLC cell lines expressed high levels of HDGF, whereas the immortalized normal bronchial epithelial cell lines (HBE1 and HBE3) expressed low levels of HDGF (Fig. 1*A*). We selected four cell lines (A549, H358, H226, and H1944) for further investigation.

HDGF-siRNA-1 knocks out *HDGF* in NSCLC cells. To determine the role of HDGF in NSCLC, we used RNA interference (RNAi) strategy to down-regulate the molecule. In A549 cells, the HDGF protein level was substantially reduced 48 hours after transfection with 100 nmol/L HDGF-siRNA-1, whereas 100 nmol/L HDGF-siRNA-2 induced only a slight reduction of the protein; these effects lasted up to at least 72 hours after transfection (Fig. 1*B*). Using 100 nmol/L concentration of HDGF-siRNA-1, the protein level was similarly down-regulated in H1944, H358, and H226 cells. These results indicate that HDGF-siRNA-1 effectively and specifically down-regulated HDGF protein expression in a panel of NSCLC cells.

Down-regulation of *HDGF* has minimal effect on anchorage-dependent growth of NSCLC cells. We next examined the growth curves of A549 cells transfected with 2 or 100 nmol/L HDGF-siRNA-1 in the presence of 5% bovine serum. Results of the MTT assay showed that the growth curves of these cells were comparable to those of cells treated with LipofectAMINE alone or transfected with negative control siRNA (Fig. 2*A*). These observations were confirmed by using a microelectronic cell sensor system (Fig. 2*B*). Similar results were obtained in H1944, H358, and H226 cells (data not shown). These data suggest that HDGF plays a minimal role in controlling anchorage-dependent growth in NSCLC cells in our culture condition.

To determine a role of HDGF in cell cycle regulation, we did flow cytometry analysis in A549 cells 72 hours after transfection with 2 or 100 nmol/L HDGF-siRNA-1. The cell cycle distributions of these cells were similar to those of cells treated with LipofectAMINE alone or transfected with negative control siRNA (Fig. 2*C*).

Although HDGF can stimulate DNA synthesis and cell proliferation in vascular or bronchial epithelial cells has been previously reported (8, 9, 13), our results are consistent with our clinical observation that the expression levels of HDGF was not associated with Ki67 labeling indices in primary NSCLC (10). In fact, HDGF-mediated cell growth was observed only when the cells were cultured in serum-free condition (13, 14); the presence of serum would have masked HDGF stimulation because of the effect of other growth stimulators in serum.

Down-regulation of *HDGF* reduces anchorage-independent growth of NSCLC cells. The effect of HDGF on anchorage-independent growth of the four cell lines was analyzed using the soft agar growth assay. Three weeks after seeding, cells transfected with 100 nmol/L HDGF-siRNA-1 produced significantly fewer and smaller colonies than did cells treated with LipofectAMINE alone or transfected with negative control siRNA (Fig. 3*A*). The numbers (average of triplicate wells with three randomly selected fields per well) of colonies visible in a microscopic field at ×40 magnifications for the four cell lines are presented in an attached table (Fig. 3*A*). These results suggest that HDGF is involved in anchorage-independent cell growth, a feature of malignant transformation, of NSCLC cells.

Down-regulation of *HDGF* reduces NSCLC cells' capability to invade. We then used Matrigel invasion chambers to determine the effect of HDGF on the invasion potential of the four cell lines. Transfection with 100 nmol/L HDGF-siRNA-1 resulted in significantly fewer invasive cells in A549 and H226 cell lines (Fig. 3*B*). The number of cells transfected with HDGF-siRNA-1 that were invasive averaged 140 (140 ± 73.65), whereas the number of cells treated with LipofectAMINE alone that were invasive averaged 759 (759 ± 156.79; $P = 0.004$) for A549; 126 (126 ± 28) versus 516 (516 ± 19; $P = 0.0001$) for H226. Because H1944 and H358 did not invade in both controls and treated cells in these chambers, we were unable to determine the effect of HDGF-siRNA-1 in these cell lines.

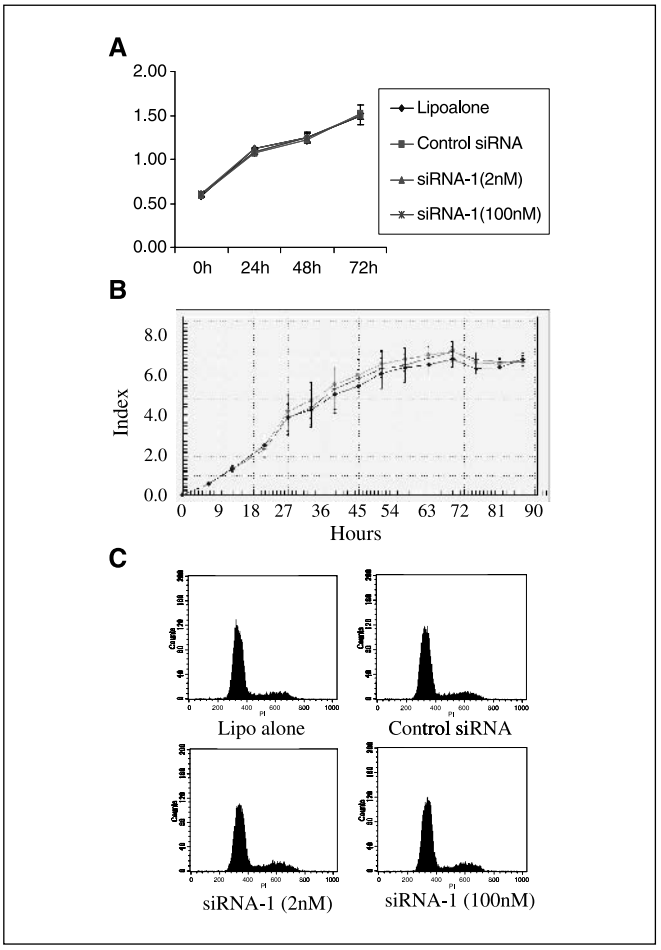
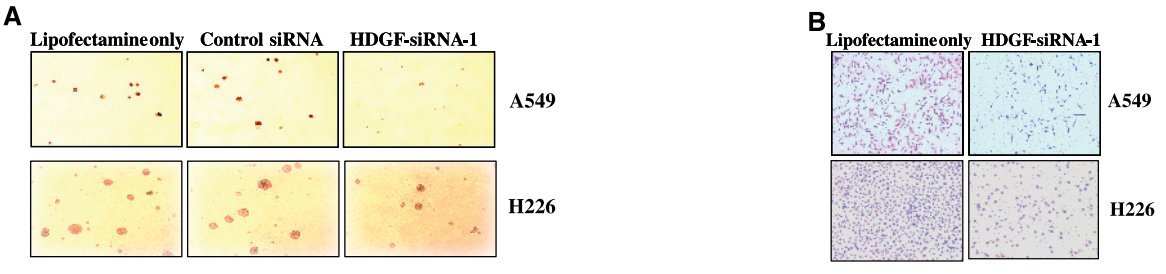


Figure 2. Effect of *HDGF* down-regulation on anchorage-dependent cell proliferation of A549 cells, as measured by MTT assay (*A*); a microelectronic cell sensor system (*B*), where the red line represents cells treated with LipofectAMINE alone, the green line for cells treated with 2 nmol/L HDGF-siRNA-1, and the blue line for cells treated with 100 nmol/L HDGF-siRNA-1; and flow cytometry 72 hours after siRNA administration (*C*). *Points,* means; *bars,* SD (*A* and *B*).

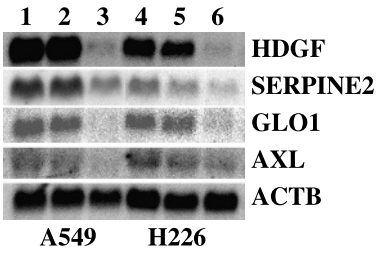


Cell Line	Lipofectomine	Control siRNA	HDGF-siRNA-1	P value (t-test) (Control/HDGF)
A549	12.11±2.22	13.44±0.51	2.89±0.51	0.0001
H1944	9.00 ±1.00	9.67 ±1.53	4.00 ±1.00	0.006
H358	8.00 ±1.00	7.33 ±1.15	2.67 ±0.58	0.003
H226	13.67 ±3.06	14.00 ±2.65	3.00 ±1.00	0.003

Figure 3. *A,* effect of *HDGF* down-regulation on anchorage-independent cell growth of A549 and H226 cells, as measured by soft agar assay (×40 magnifications). *Bottom,* counts of colonies for each of the four cell lines and *P*s of statistical analysis. *B,* invasion capability of A549 cells and H226 cells measured by an *in vitro* cell invasion system (×100 magnifications).

Together with the soft agar experiments, these results may explain the increased rates of tumor relapse and distant metastasis in patients whose primary NSCLC tumors had a high level of HDGF after surgical removal of the tumors (10). An association between higher HDGF and poor clinical outcome has also been observed in patients with NSCLC by another group (15) and in patients with primary hepatocellular carcinoma (16) and melanoma (17).

Genes down-regulated by HDGF-siRNA-1 treatment. We did global gene expression analysis using Affymetrix U133A gene chip, which can measure expression of >16,000 unique genes, to elucidate potential mechanism of HDGF-siRNA-1–induced growth inhibition in soft agar and inhibition of invasion in the invasion chambers. We compared gene expression profiles between A549 cells treated with LipofectAMINE alone and A549 cells treated with 100 nmol/L HDGF-siRNA-1 at 48-hour time point. Among 10,938 unique genes with expression level qualifying our analysis as specified in Materials and Method, 15 genes were down-regulated ≥2-fold in HDGF-siRNA-1–treated cells compared with cells treated with LipofectAMINE alone (attached table in Fig. 4), whereas none of the genes were up-regulated ≥2-fold. Among the



Gene symbol	Chromosomal location
HDGF	1q21-q23
GLO1	6p21
SERPINE2	2q33
E46L	22q13
GNG5	1q22
PLOD2	3q23
LOXL2	8p21
PYGB	20p11
GNG10	9q32
PPP1CC	12q13
AXL	19q13
C14orf78	14q32
GALNT1	18q12
F2RL1	5q13
C1orf24	1q25

Figure 4. Expression of *HDGF, SERPINE2, GLO1*, and *AXL* before and after treatment with LipofectAMINE alone (*lanes 1* and *4*), 100 nmol/L control-siRNA (*lanes 2* and *5*), and 100 nmol/L HDGF-siRNA-1 (*lanes 3* and *6*) in A549 and H226 cells measured by Northern blot analysis. *Right,* top 15 genes down-regulated after HDGF-siRNA-1 treatment measured by Affymetrix U133A chip.

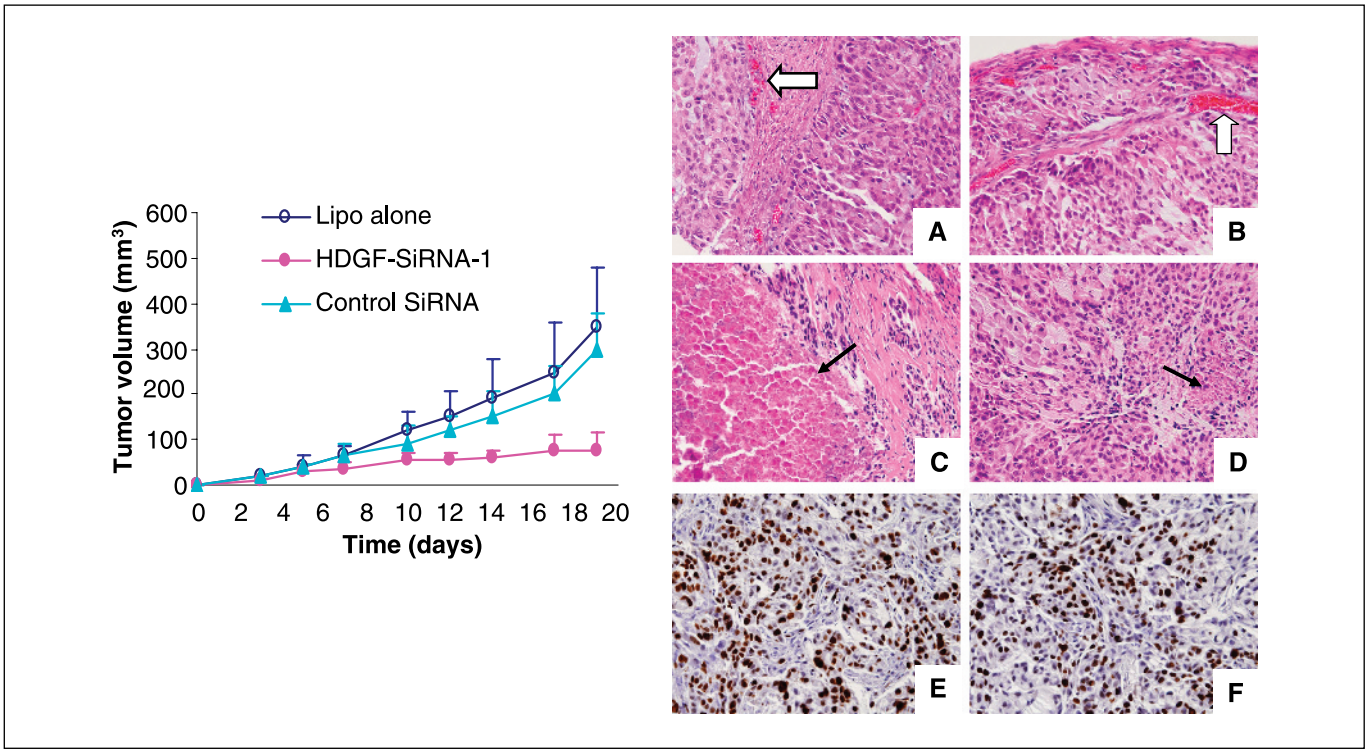


Figure 5. *Left,* effects of *HDGF* down-regulation on A549 NSCLC xenograft tumor growth. The tumor growth curves represent cells treated with LipofectAMINE alone, LipofectAMINE plus 100 nmol/L negative control siRNA, and LipofectAMINE plus 100 nmol/L HDGF-siRNA-1, respectively, as labeled. *Point,* mean tumor volume (calculated from five mice); *bars,* upper 95% confidence intervals. *Right, A-D,* H&E-stained tumor sections. *E* and *F,* tumor sections stained with Ki67 immunohistochemically. *A,* tumor treated with LipofectAMINE alone; *B,* tumor treated with 100 nmol/L negative control siRNA; *C* and *D,* tumors treated with 100 nmol/L HDGF-siRNA-1; *E,* tumor treated with LipofectAMINE alone; *F,* tumor treated with 100 nmol/L HDGF-siRNA-1. *Open arrows,* blood vessels (*A* and *B*); *black arrows,* areas of tumor necrosis (*C* and *D*).

15 genes, the expression of *HDGF* was down-regulated most dramatically (>4-fold) as expected. The next two genes are *GLO1* and *SERPINE2*. GLO1 has been shown elevated in lung cancers (18), whereas SERPINE2 has been suggested to play a role in invasion of pancreatic cancer cells (19). AXL, a receptor tyrosine kinase also in the list, has been reported overexpressed in multiple types of cancers (20–22) and linked to adverse clinical outcome in patients with cancer (23). To confirm the down-regulation of *GLO1, SERPINE2*, and *AXL* in HDGF-siRNA-1 treated cells, we did Northern blot analysis to compare the gene expression levels in A549 and H226 cells treated with HDGF-siRNA-1, siRNA control, and LipofectAMINE alone. The results are consistent with the microarray experiment (Fig. 4) and agree with the notion that *HDGF* is involved in regulation of expression of these genes.

Down-regulation of *HDGF* inhibits tumorigenicity of NSCLC cells *in vivo*. To further determine a role of HDGF in progression of NSCLC, we did an *in vivo* animal experiment. We found that A549 cells transfected with 100 nmol/L HDGF-siRNA-1 formed substantially smaller tumors in nude mice compared with those transfected with LipofectAMINE alone or negative control siRNA (Fig. 5, *left*). The tumor volume for mice with cells transfected with the HDGF-siRNA was 76.27 $\pm$ 39.06 mm^3 compared with 345.64 $\pm$ 135.67 or 295.33 $\pm$ 80.53 mm^3 for mice with cells treated with LipofectAMINE alone or negative control siRNA, respectively ($P = 0.037$ or $P = 0.018$, respectively). Under light microscopy, we observed a substantially reduced blood vessels in the HDGF-siRNA–transfected tumors compared with the tumors derived from cells treated with LipofectAMINE or negative control siRNA (Fig. 5*A-D, right*). Substantial tumor necrosis was observed only in tumors derived from cells treated with the HDGF-siRNA (Fig. 5*C* and *D, right*). Interestingly, Ki67 expression index, an indicator of cell proliferation, was similar in tumors of the three animal groups (Fig. 5*E* and *F, right*).

The *in vivo* animal experiment provides a strong support for the importance of HDGF in NSCLC and suggests that HDGF may be a target for treating NSCLC or preventing the development of lung cancer. The finding of reduced blood vessel formation in the HDGF-siRNA–treated tumors suggests that HDGF plays a role in the neovasculature formation *in vivo*, which may be an important mechanism of HDGF in tumor development and progression of NSCLC. This is consistent with previous reports supporting the role of HDGF in angiogenesis as a potent endothelial mitogen and regulator of endothelial cell migration by mechanisms distinct from those used by vascular endothelial growth factor (14, 24). The observed tumor necrosis is likely a consequence of the poor blood supply in these tumors. Consistent with our *in intro* and clinical observations, the lack of change in cell proliferation in the tumors indicates that HDGF plays a minimal role in the tumor cell proliferation for patients with NSCLC. Future studies will focus on the molecular mechanisms of HDGF-induced tumor development and progression as well as on strategies to down-regulate the protein or inhibit its function for potential therapeutic applications.

Acknowledgments

Received 10/29/2004; revised 10/24/2005; accepted 11/11/2005.

Grant support: Department of Defense grant DAMD17-01-1-01689-1 and National Cancer Institute grants PO1 CA106451, PO1 CA91844, and U01 CA86390.

The costs of publication of this article were defrayed in part by the payment of page charges. This article must therefore be hereby marked *advertisement* in accordance with 18 U.S.C. Section 1734 solely to indicate this fact.

References

1. Nakamura H, Kambe H, Egawa T, et al. Partial purification and characterization of human hepatoma-derived growth factor. Clin Chim Acta 1989;183:273–84.
2. Everett AD. Identification, cloning, and developmental expression of hepatoma-derived growth factor in the developing rat heart. Dev Dyn 2001;222:450–8.
3. Oliver JA, Al-Awqati Q. An endothelial growth factor involved in rat renal development. J Clin Invest 1998;102: 1208–19.
4. Enomoto H, Yoshida K, Kishima Y, et al. Hepatoma-derived growth factor is highly ex-pressed in developing liver and promotes fetal hepatocyte proliferation. Hepatology 2002;36:1519–27.
5. von Heijne G. A new method for predicting signal sequence cleavage sites. Nucleic Acids Res 1986;14: 4683–90.
6. Nakamura H, Izumoto Y, Kambe H, et al. Molecular cloning of complementary DNA for a novel human hepatoma-derived growth factor. Its homology with high mobility group-1 protein. J Biol Chem 1994;69: 25143–9.
7. Everett AD, Lobe DR, Matsumura ME, Nakamura H, McNamara CA. Hepatoma-derived growth factor stimulates smooth muscle cell growth and is expressed in vascular development. J Clin Invest 2000;105:567–75.
8. Everett AD, Stoops T, McNamara CA. Nuclear targeting is required for hepatoma-derived growth factor-stimulated mitogenesis in vascular smooth muscle cells. J Biol Chem 2001;276:37564–8.
9. Kishima Y, Yamamoto H, Izumoto Y, et al. Hepatoma-derived growth factor stimulates cell growth after translocation to the nucleus by nuclear localization signals. J Biol Chem 2002;277:10315–22.
10. Ren H, Tang X, Lee JJ, et al. Expression of hepatoma-derived growth factor is a strong prognostic predictor for patients with early-stage non-small-cell lung cancer. J Clin Oncol 2004;22:3230–7.
11. Elbashir SM, Martinez J, Patkaniowska A, Lendeckel W, Tuschl T. Functional anatomy of siRNAs for mediating efficient RNAi in *Drosophila melanogaster* embryo lysate. EMBO J 2001;20:6877–88.
12. Zhang L, Miles MF, Aldape KD. A model of molecular interactions on short oligonucleotide microarrays. Nat Biotechnol 2003;21:818–21.
13. Mori M, Morishita H, Nakamura H, et al. Hepatoma-derived growth factor is involved in lung remodeling by stimulating epithelial growth. Am J Respir Cell Mol Biol 2004;30:459–69.
14. Everett AD, Narron JV, Stoops T, Nakamura H, Tucker A. Hepatoma-derived growth factor is a pulmonary endothelial cell-expressed angiogenic factor. Am J Physiol Lung Cell Mol Physiol 2004;286: L1194–201.
15. Iwasaki T, Nakagawa K, Nakamura H, Takada Y, Matsui K, Kawahara K. Hepatoma-derived growth factor as a prognostic marker in completely resected non-small-cell lung cancer. Oncol Rep 2005;13:1075–80.
16. Hu TH, Huang CC, Liu LF, et al. Expression of hepatoma-derived growth factor in hepatocellular carcinoma. Cancer 2003;98:1444–56.
17. Bernard K, Litman E, Fitzpatrick JL, et al. Functional proteomic analysis of melanoma progression. Cancer Res 2003;63:6716–25.
18. Sakamoto H, Mashima T, Sato S, Hashimoto Y, Yamori T, Tsuruo T. Selective activation of apoptosis program by *S-p*-bromobenzylglutathione cyclopentyl diester in glyoxalase I-overexpressing human lung cancer cells. Clin Cancer Res 2001;7:2513–8.
19. Buchholz M, Biebl A, Neebetae A, et al. SERPINE2 (protease nexin I) promotes extracellular matrix production and local invasion of pancreatic tumors *in vivo*. Cancer Res 2003;63:4945–51.
20. Wu CW, Li AF, Chi CW, et al. Clinical significance of AXL kinase family in gastric cancer. Anticancer Res 2002;22:1071–8.
21. Meric F, Lee WP, Sahin A, Zhang H, Kung HJ, Hung MC. Expression profile of tyrosine kinases in breast cancer. Clin Cancer Res 2002;8:361–7.
22. Wimmel A, Glitz D, Kraus A, Roeder J, Schuermann M. Axl receptor tyrosine kinase expression in human lung cancer cell lines correlates with cellular adhesion. Eur J Cancer 2001;37:2264–74.
23. Nakano T, Tani M, Ishibashi Y, et al. Biological properties and gene expression associated with metastatic potential of human osteosarcoma. Clin Exp Metastasis 2003;20:665–74.
24. Okuda Y, Nakamura H, Yoshida K, et al. Hepatoma-derived growth factor induces tumorigenesis *in vivo* through both direct angiogenic activity and induction of vascular endothelial growth factor. Cancer Sci 2003;94: 1034–41.

Oncogene (2007) 26, 6896–6904
© 2007 Nature Publishing Group All rights reserved 0950-9232/07 $30.00
www.nature.com/onc

ORIGINAL ARTICLE

A genetic mouse model for metastatic lung cancer with gender differences in survival

S Zheng[1,4], AK El-Naggar[2], ES Kim[3], JM Kurie[3] and G Lozano[1,4]

[1]*Department of Cancer Genetics, The University of Texas MD Anderson Cancer Center, Houston, TX, USA;* [2]*Department of Pathology, The University of Texas MD Anderson Cancer Center, Houston, TX, USA;* [3]*Department of Thoracic/Head and Neck Medical Oncology, The University of Texas MD Anderson Cancer Center, Houston, TX, USA and* [4]*Program in Genes and Development, The University of Texas Graduate School of Biomedical Sciences, Houston, TX, USA*

Lung cancer is a devastating disease with poor prognosis. The design of better therapies for lung cancer patients would be greatly aided by good mouse models that closely resemble the human disease. Unfortunately, current models for lung adenocarcinoma are inadequate due to the absence of metastases. In this study, we incorporated both *K-ras* and *p53* missense mutations into the mouse genome and established a more faithful genetic model for human lung adenocarcinoma, the most common type of lung cancer. Mice with both mutations developed advanced lung adenocarcinomas that were highly aggressive and metastasized to multiple intrathoracic and extrathoracic sites in a pattern similar to that of human lung cancer. These mice also showed a gender difference in cancer-related death. Additionally, the presence of both mutations induced pleural mesotheliomas in 23% of these mice. This mouse model recapitulates the metastatic nature of human lung cancer and will be invaluable to further probe the molecular basis of metastatic lung cancer and for translational studies.
Oncogene (2007) **26,** 6896–6904; doi:10.1038/sj.onc.1210493; published online 7 May 2007

Keywords: *p53*; *K-ras*; mesotheliomas

Introduction

Lung cancer is the leading cause of cancer-related deaths. Although considerable effort has provided insight into the molecular events leading to the progression and metastasis of lung cancer, little improvement in treatment outcome has been achieved.

Many mouse models have been developed for lung cancer to test new treatment options. Xenograft models, in which human tumor cells are grafted into immune compromised mice, have been extensively used for preclinical testing. However, these models have intrinsic flaws, generally resulting in poor predicative power of the clinical efficacy of anticancer agents (Becher and Holland, 2006; Sausville and Burger, 2006). Susceptible mouse strains, including A/J and SWR, spontaneously develop lung tumors, with the sensitivity strongly associated with a polymorphism in intron 2 of the *K-ras* gene (You *et al*., 1992; Malkinson and You, 1994). These strains are also highly sensitive to the induction of lung tumors by chemical carcinogens. For example, a single dose of 4-(methylnitrosamino)-1-(3-pyridyl)-1-butanone (NNK) in A/J mice induces alveolar hyperplasias, lung adenomas, and adenocarcinomas 42 weeks after carcinogen treatment (Belinsky *et al*., 1993). Increased tumor induction by vinyl carbamate was demonstrated in transgenic mice carrying a mutant *p53* with an Ala-to-Val mutation at codon 135 and a deletion of a *K-ras* allele (Wang *et al*., 2006a, b). These and many other studies illustrate that the A/J model is a useful one to evaluate chemointerventive agents of lung tumors (Castonguay *et al*., 1991; Hecht *et al*., 1991). Unfortunately, lung tumors in A/J mice treated with carcinogens are generally not aggressive and do not metastasize.

To overcome these deficiencies, investigators have attempted to establish models that mimic the genetic signature of lung cancer. Two of the most common molecular changes identified in human lung cancer are mutations of the *p53* and *K-ras* genes (Mitsudomi *et al*., 1992; Salgia and Skarin, 1998). Missense mutations in the *p53* gene are found in more than 50% of human lung cancers, while *p53* deletions are rare (Takahashi *et al*., 1989; Chiba *et al*., 1990; Greenblatt *et al*., 1994). The hot spot p53 mutations in lung cancer occur at amino acids 157, 158, 175, 245, 248, 249 and 273 (Toyooka *et al*., 2003; Vahakangas *et al*., 2001). Constitutive activation of the *K-ras* gene through mutations occurs in 30% of lung cancers, about 80% of which occur at codon 12 (Rodenhuis *et al*., 1988; Rodenhuis and Slebos, 1992).

Current genetic models of human lung adenocarcinoma are also limited by the absence or rare occurrence of metastasis (Meuwissen and Berns, 2005). In one model, mice inherit a latent mutant *K-ras* allele at the endogenous locus (*K-ras*^{LA1}), which is spontaneously

Correspondence: Professor G Lozano, Department of Cancer Genetics, The University of Texas MD Anderson Cancer Center, 1515 Holcombe Blvd., Unit 1010, Houston, TX, USA.
E-mail: gglozano@mdanderson.org
Received 23 September 2006; revised 31 January 2007; accepted 9 March 2007; published online 7 May 2007

activated *in vivo* (Johnson *et al*., 2001). The activated *K-ras*^{LA1} allele expresses mutant K-ras with an aspartic acid at codon 12, inducing multifocal lung adenocarcinomas in heterozygous mice (*K-ras*$^{LA1/+}$). The advantage of this model is that somatic activation of the *K-ras* proto-oncogene in mouse lung mimics mutational activation of the *K-ras* gene occurring in human lung cancer. The disadvantage, however, is that lung adenocarcinomas in this model, and in one with an accompanying deletion of *p53*, rarely metastasize.

Likewise, mouse models with *p53* mutations have recently been described. One particular mutation generated at the endogenous *p53* allele contains an arginine-to-histidine substitution at codon 172, which corresponds to the hot spot mutation at 175 in human *p53* (Liu *et al*., 2000; Lang *et al*., 2004; Olive *et al*., 2004). The first mouse model with this mutation expresses low levels of mutant p53 because of an intronic deletion of a single nucleotide (p53$^{R172H\Delta g}$) (Liu *et al*., 2000). Strikingly, however, *p53*$^{R172H\Delta g/+}$ mice develop osteosarcomas and carcinomas that metastasize at a frequency of 69 and 40%, respectively, a phenotype not observed in *p53*$^{+/-}$ mice. This metastatic phenotype was confirmed in the latest models expressing mutant p53 at appropriate levels (Lang *et al*., 2004; Olive *et al*., 2004). These models demonstrate that mutant p53 has a gain of function in addition to loss of function *in vivo*, and reproduce the metastatic nature of human cancers. Unfortunately, however, mice expressing mutant p53 rarely develop lung adenocarcinomas.

Since mice inheriting a *p53* missense mutation develop a wide range of tumors that metastasize, we postulated that *K-ras* mutation could initiate lung adenocarcinoma, while *p53* mutation could exacerbate the phenotype by promoting dissemination of cancer cells. In an effort to develop a more faithful mouse model, one with similar molecular changes and metastatic behavior to human lung cancer, we generated mice with both *p53* and *K-ras* missense mutations. We found that the combination of these mutations resulted in lung adenocarcinomas with a high incidence of metastases and gender differences in cancer-related death. This new mouse model thus most closely simulates human metastatic lung cancer and provides an immunocompetent system to test novel therapeutic agents *in vivo*.

Results

Lung cancer in p53$^{R172H\Delta g/+}$ K-ras$^{LA1/+}$ *mice*

The *p53*$^{R172H\Delta g/+}$ mice carrying a missense mutation in one *p53* allele (Liu *et al*., 2000) were crossed with *K-ras*$^{LA1/+}$ mice carrying a latent mutant *K-ras* allele (Johnson *et al*., 2001) to generate *K-ras*$^{LA1/+}$, *p53*$^{R172H\Delta g/+}$ and *p53*$^{R172H\Delta g/+}$ *K-ras*$^{LA1/+}$ mice. All genotypes produced from the above cross were included in the cohort study and were in a 129Sv background. The *p53*$^{R172H\Delta g/+}$ *K-ras*$^{LA1/+}$ mice are sometimes referred to as double mutant mice for simplicity. For comparison, *p53*$^{+/-}$ *K-ras*$^{LA1/+}$ mice were also generated and included in this study.

At necropsy, *p53*$^{R172H\Delta g/+}$ *K-ras*$^{LA1/+}$ mice had substantial lung tumor burden (Figure 1Aa). Histologically, the lesions were atypical adenomatous hyperplasia (AAH), adenomas and adenocarcinomas. AAH, the precursor lesion of human lung adenocarcinoma (Kitamura *et al*., 1999), was identified in multifocal and diffuse patterns contiguous with well-defined or ill-defined adenomas and adenocarcinomas (Figure 1Ba). Lung adenomas and adenocarcinomas were frequently juxtaposed and merging (Figure 1Bb). The majority of double mutant mice had multiple large or diffuse adenocarcinomas, which had papillary/glandular phenotypes or were poorly differentiated (Figure 1Aa and Bc, d). Lung adenocarcinoma cells usually had enlarged vesicular nuclei with prominent nucleoli, similar to human lung adenocarcinoma cells. Surfactant protein C (SPC), which is frequently expressed in human lung adenocarcinoma, was detected in murine lung adenocarcinomas by immunohistochemistry (Figure 1Be). Papillary hyperplasia of bronchial epithelial cells was also observed in double mutant mice (Figure 1Bf). These hyperplastic cells are positive for CC10, a Clara cell marker, suggesting an alternative origin of lung adenocarcinoma in this model (Figure 1Bg).

Strikingly, lung adenocarcinomas in this model were highly invasive and metastatic (Figure 1Ab–e and Bh, i). Metastatic lesions in the lymph node and liver stained positive for SPC (Figure 1Bh and i, respectively).

Pleural mesothelioma, which originates from mesothelial cells of the pleura, was also observed in *p53*$^{R172H\Delta g/+}$ *K-ras*$^{LA1/+}$ mice. Grossly, multiple lesions appeared on the pleura and multiple enlarged lymph nodes were observed in the mediastinum (Figure 2A). Microscopically, mesothelial cells were observed proliferating in a papillary pattern into pleural space (Figure 2Ba). Early-stage pleural mesotheliomas were localized and clearly identified on top of hyperplastic lung tissue and adenoma (Figure 2Bb and c). Late-stage pleural mesotheliomas invaded lung parenchyma (Figure 2Bd). The majority of pleural mesotheliomas in this model were biphasic, composed of both epithelioid and sarcomatoid cancer cells with pronounced pleomorphism and marked nuclear atypia. Sarcomatoid lesions were associated with spindle cell fibrous components, resembling human fibrous mesothelioma (Figure 2Be). Highly aggressive mesotheliomas extended into surrounding tissues and metastasized to mediastinal lymph nodes, liver, pancreas, ovary, and other sites (Figure 2Bf and data not shown). Pleural mesotheliomas in this model were positive for at least one marker, Calretinin or Cytokeratin 6 (Figure 2Bg, h and Table 1), and negative for SPC (Figure 1Be) and for periodic acid-Schiff (PAS) staining (data not shown). These data further verified the histological diagnosis of mesothelioma. There are no reports of pleural mesothelioma in previously published *K-ras*$^{LA1/+}$ mice probably due to the low frequency of this tumor type (Johnson *et al*., 2001). We also did not observe mesotheliomas in *p53*$^{R172H\Delta g/+}$ or *p53*$^{R172H/+}$ mice (Liu *et al*., 2000; Lang *et al*., 2004).

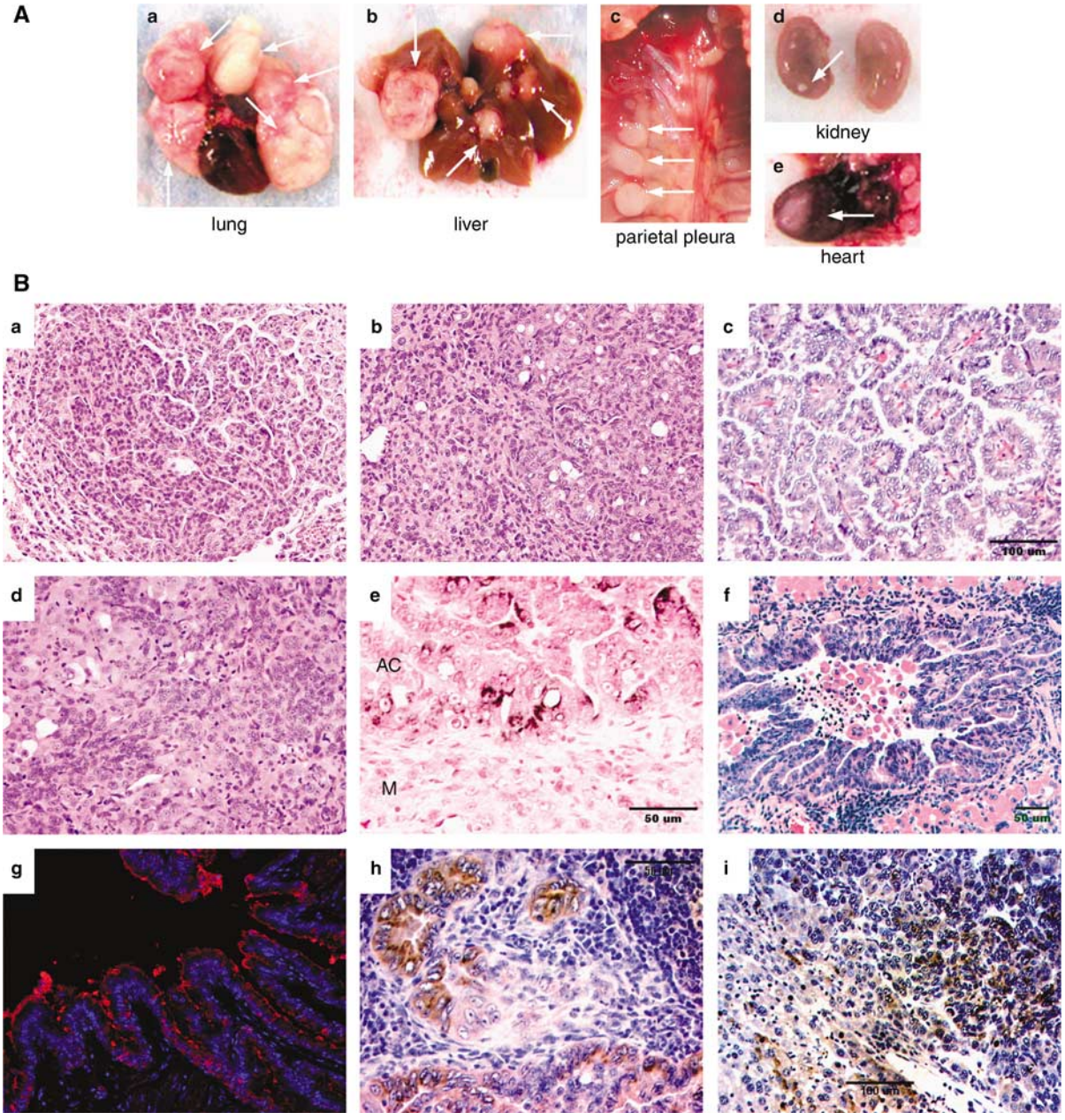


Figure 1 $p53^{R172H\Delta g/+}K\text{-}ras^{LA1/+}$ mice developed highly aggressive lung adenocarcinomas with metastases to multiple sites. (**A**) Photographs of lung tissue with high tumor burden, adenocarcinomas (a), metastatic lesions to the liver (b), parietal pleura (c), kidney (d), and heart (e). Representative tumors are marked by arrows. (**B**) Photomicrographs of adenomatous alveolar hyperplasia (a), merged adenoma and adenocarcinoma (b), lung adenocarcinoma with a papillary growth pattern (c), poorly differentiated lung adenocarcinoma (d). Immunohistochemistry to detect SPC staining in lung adenocarcinoma (AC) and adjacent pleural mesothelioma (M) (e). A bronchial hyperplasia of epithelial cells (f) was stained for CC10 by immunofluorescence (red) and nuclei are stained with Topro 3 (blue) (g). SPC staining of lung adenocarcinoma metastases to the lymph node (h) and liver (i). Tumor sections in (a–d) and (f) were stained by H&E.

Tumor spectrum in $p53^{R172H\Delta g/+}$ $K\text{-}ras^{LA1/+}$ *mice*

All $p53^{R172H\Delta g/+}$ $K\text{-}ras^{LA1/+}$ mice developed lung tumors. The major type of malignancy was lung adenocarcinoma, which developed in 52 of 56 double mutant mice (Table 2). Pleural mesothelioma was identified in 13 of these 56 mice. Six out of these 13 mice also had peritoneal mesotheliomas. Grossly, anatomical extension of thoracic lesions into the abdominal cavity through the diaphragm was noted in three of the six mice with peritoneal mesotheliomas. In addition to lung tumors, lymphoma infiltration in lung appeared in 6/56 (10.7%) of double mutant mice. Mice with both lung adenocarcinomas and lung lymphomas did not develop any metastases, probably because they died at a younger age than mice with only lung adenocarcinomas (median survival of 256 days compared to 317 days for those without lymphomas; $P = 0.0053$).

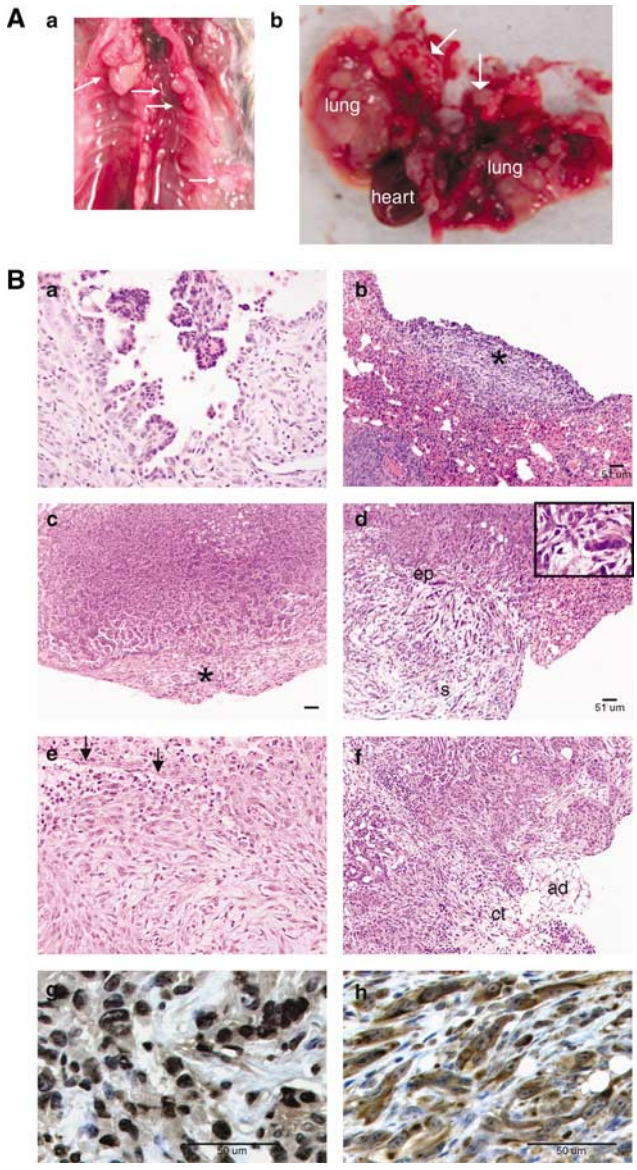


Figure 2 $p53^{R172H\Delta g/+}$ $K\text{-}ras^{LA1/+}$ mice also developed highly aggressive pleural mesotheliomas. (**A**) Photographs of multiple lesions of mesothelioma (diagnosed microscopically) on parietal pleura (a, arrows) and metastases in mediastinum (b, arrows). (**B**) Photomicrographs of bland papillary proliferation of mesothelial cells arising from the pleural lining (a) nodular pleural mesothelioma (*) on top of lung parenchyma (b) localized pleural mesothelioma (*) clearly distinguished from the underlying adenoma with glandular differentiation (c) biphasic pleural mesothelioma having both epithelial (ep) and sarcomatoid (s) components encroached into lung parenchyma (d), inset shows pleomorphism and nuclear atypia in mesotheliomas (d), a fibrous mesothelioma growing exophytically (e, arrows mark the visceral pleura), pleural mesothelioma spread to extrapleural connective (ct) and adipose (ad) tissues (f) positive Calretinin staining (g) and positive staining for Cytokeratin 6 (h) in mesotheliomas by immunohistochemistry. Tumor sections in (a–f) were stained by H&E.

For comparison, 48 $K\text{-}ras^{LA1/+}$ mice were also analysed. They developed a tumor spectrum similar to that of double mutant mice (Table 2). Pleural mesotheliomas were identified in 4/48 $K\text{-}ras^{LA1/+}$ mice, but no mesotheliomas were identified in the peritoneum. The incidence of pleural mesotheliomas in $K\text{-}ras^{LA1/+}$ mice was lower than that in double mutant mice (χ^2, $P<0.05$). As previously reported, $p53^{R172H\Delta g/+}$ mice develop lymphomas, sarcomas, and carcinomas, a few of which are lung adenocarcinomas (Liu *et al*., 2000) (Table 2).

Table 1 Calretinin and Cytokeratin 6 immunostaining in mesothelioma

Mesothelioma	*Calretinin*	*Cytokeratin 6*
1	+	–
2	NS[a]	+
3	+	+
4	+	–
5	–	+
6	–	+
7	+	–
8	+	–
9	+	NS
10	+	–
11[b]	+	–

[a]NS: not stained due to small size. [b]A putative metastasis.

High metastatic potential of lung adenocarcinoma in $p53^{R172H\Delta g/+}$ $K\text{-}ras^{LA1/+}$ *mice*

Lung adenocarcinomas in $p53^{R172H\Delta g/+}$ $K\text{-}ras^{LA1/+}$ mice were much more aggressive and metastatic than those in $K\text{-}ras^{LA1/+}$ mice. At 3–4 months of age, double mutant mice developed AAH, lung adenomas, and small, focal adenocarcinomas with no metastasis (data not shown). Metastases were identified at 7–14 months of age in dissected double mutant mice. Histologically, metastases were found in 19 of 52 $p53^{R172H\Delta g/+}$ $K\text{-}ras^{LA1/+}$ mice that had developed lung adenocarcinomas (36.5%), while metastases were found in the two of 44 $K\text{-}ras^{LA1/+}$ mice that had developed lung adenocarcinomas (4.5%), which was significantly different (χ^2, $P<0.001$). Lung adenocarcinomas were widely disseminated to multiple intrathoracic and extrathoracic sites in double mutant mice (Table 3). Seeding was restricted to the mediastinum in the two $K\text{-}ras^{LA1/+}$ mice with metastases (Table 3). The average number of sites of metastases was 2.3 per $p53^{R172H\Delta g/+}$ $K\text{-}ras^{LA1/+}$ mouse. Mediastinal structures were the major metastatic sites (mediastinal lymph nodes/adipose tissue and heart). Extrathoracic sites of metastases included liver, adrenal glands, body wall, kidneys, and mesentery/lymph nodes. Previously published data show that $p53^{+/-}$ $K\text{-}ras^{LA1/+}$ mice develop lung adenocarcinomas with more malignant features, but no metastasis (Johnson *et al*., 2001). We also analyzed five $p53^{+/-}$ $K\text{-}ras^{LA1/+}$ mice and found that they developed lung tumors but no metastasis, as reported previously (data not shown). Thus, the metastatic burden was the most remarkable difference among $p53^{R172H\Delta g/+}$ $K\text{-}ras^{LA1/+}$, $p53^{+/-}$ $K\text{-}ras^{LA1/+}$ and $K\text{-}ras^{LA1/+}$ mice. Notably, not all enlarged nodules seen in the mediastinum at necropsy were metastases. These were reactive lymph nodes, an observation consistent with that in human lung cancer (Kerr*et al*., 1992).

Table 2 Tumor spectra of $p53^{R172H\Delta g/+}$ $K\text{-}ras^{LA1/+}$, $K\text{-}ras^{LA1/+}$, and $p53^{R172H\Delta g/+}$ mice

Tumor types	*$p53^{R172H\Delta g/+}$ $K\text{-}ras^{LA1/+}$ # of mice (%)*[a]	*$K\text{-}ras^{LA1/+}$ # of mice (%)*[b]	*$p53^{R172H\Delta g/+}$ # of mice (%)*[c]
Lung/pleura			
Adenocarcinoma	35 (62.5)	34 (70.8)	3 (13)
Adenocarcinoma + mesothelioma	13 (23.2)[d]	4 (8.3)[d]	0
Adenocarcinoma + lymphoma	4 (7.1)	6 (12.5)	1 (4.3)
Adenoma[e] ± lymphoma	4 (7.1)	4 (8.3)	1 (4.3)
Sarcoma			
Osteosarcoma	0	0	8 (34.8)
Angiosarcoma	4 (7.1)	4 (8.3)	0
Fibrosarcoma	3 (5.4)	1 (2.1)	0
Unclassified	2 (3.6)	0	3 (13)
Lymphoma	6 (10.7)	12 (25)	8 (34.8)
Carcinomas (other)			
Pancreatic carcinoma	2 (3.6)	0	0
Squamous carcinoma	1 (1.8)	1 (2.1)	5 (21.7)
Rectal mucinous adenocarcinoma	0	2 (4.2)	0
Melanoma	0	1 (2.1)	0
Papilloma	9 (16.1)	13 (27.1)	0

[a]Total 56 $p53^{R172H\Delta g/+}$ $K\text{-}ras^{LA1/+}$ mice were analysed. [b]Total 48 $K\text{-}ras^{LA1/+}$ mice were analysed. [c]Total 23 $p53^{R172H\Delta g/+}$ mice were analysed. [d]χ^2, $P<0.05$. [e]Mice in this category did not have overt adenocarcinomas.

Table 3 Site and frequency of metastases from primary lung adenocarcinomas

Sites of metastases	*$p53^{R172H\Delta g/+}$ $K\text{-}ras^{LA1/+}$ #/total with metastases (%)*[a]	*$K\text{-}ras^{LA1/+}$ #/total with metastases (%)*[b]	*$p53^{R172H\Delta g/+}$ #/total with metastases (%)*[c]
Intrathoracic sites			
Mediastinal lymph node	13/19 (68.4)	2/2 (100)	1/1 (100)
Heart	4/19 (21.1)	0/2	1/1 (100)
Parietal pleura	3/19 (15.8)	0/2	0/1
Diaphragm	3/19 (15.8)	0/2	0/1
Extrathoracic sites			
Liver	3/19 (15.8)	0/2	1/1 (100)
Adrenal gland	4/19 (21.1)	0/2	0/1
Kidney	2/19 (10.5)	0/2	0/1
Mesentery/lymph node	2/19 (10.5)	0/2	0/1
Pancreas	1/19 (5.3)	0/2	0/1
Eye tissue	1/19 (5.3)	0/2	0/1
Body wall[d]	6/19 (31.6)	0/2	1/1 (100)
Mammary	1/19 (5.3)	0/2	0/1

[a]Total 52 $p53^{R172H\Delta g/+}$ $K\text{-}ras^{LA1/+}$ mice with lung adenocarcinomas were analysed for metastases. [b]Total 44 $K\text{-}ras^{LA1/+}$ mice with lung adenocarcinomas were analysed for metastases. [c]Total 4 $p53^{R172H\Delta g/+}$ mice with lung adenocarcinomas were analysed for metastases. [d]Including skeletal muscle on trunk and subcutaneous tissue/lymph node. Lesions that did not penetrate parietal pleura were considered as metastases.

The status of the wild-type *p53* allele was examined in lung adenocarcinomas and metastases of $p53^{R172H\Delta g/+}$ $K\text{-}ras^{LA1/+}$ mice by quantitative real-time PCR using specific TaqMan probes to differentiate wild-type and mutant alleles. Loss of heterozygosity (LOH) was detected in 81.8% (9/11) of end-stage lung adenocarcinomas and 71.4% (10/14) of macroscopic metastases (Table 4).

Since the $K\text{-}ras^{LA1}$ allele is a latent allele that is spontaneously activated in somatic cells, the expression of mutant *K-ras* was analysed in lung cancers and metastases at mRNA and protein levels (Figure 3). Mutant $K\text{-}ras^{G12D}$ having a glycine-to-aspartic acid substitution at codon 12 was expressed in lung adenocarcinomas isolated from both double mutant and $K\text{-}ras^{LA1/+}$ mice, and in metastases and mesotheliomas isolated from double mutant mice. Moreover, histologically normal lung tissue adjacent to lung adenocarcinoma isolated from double mutant mice and normal lung tissue isolated from wild-type mice did not show the expression of mutant *K-ras* by either protein or mRNA analysis. Thus, both *p53* (inherited) and *K-ras* (acquired) mutations were present in lung cancers and metastases.

Table 4 The status of wild-type p53 in tumors of K-ras$^{LA1/+}$ p53$^{R172H\Delta g/+}$ mice

Tumor[a]	$2^{-\Delta\Delta Ct}$	*LOH*[b]
Lung adenocarcinoma 1	0.18	–
Lung adenocarcinoma 2	0.08	+
Lung adenocarcinoma 3	0.11	+
Lung adenocarcinoma 4	0.03	+
Lung adenocarcinoma 5	0.01	+
Lung adenocarcinoma 6	0.12	+
Lung adenocarcinoma 7	0.55	–
Lung adenocarcinoma 8	0.05	+
Lung adenocarcinoma 9	0	+
Lung adenocarcinoma 10	0.03	+
Lung adenocarcinoma 11	0.14	+
Metastasis 1	0.25	–
Metastasis 2	0.25	–
Metastasis 3	0.01	+
Metastasis 4	0.35	–
Metastasis 5	0.01	+
Metastasis 6	0.06	+
Metastasis 7	0.15	+
Metastasis 8	0.22	–
Metastasis 9	0.02	+
Metastasis 10	0.04	+
Metastasis 11	0	+
Metastasis 12	0.01	+
Metastasis 13	0.11	+
Metastasis 14	0	+

Abbreviation: LOH, loss of heterozygosity. [a]Only the largest lung adenocarcinoma from each mouse and macroscopically visible metastases were analysed for LOH. All tumors were diagnosed microscopically. [b]The $2^{-\Delta\Delta Ct}$ values of $\leqslant 0.15$, 0.15–0.6 and >0.6 indicate 0, 1 or 2 copies of wild-type *p53* alleles, respectively (see Materials and methods for details).

Survival of p53$^{R172H\Delta g/+}$K-ras$^{LA1/+}$ *mice*

Mice of the various genotypes were monitored daily and killed if they showed signs of respiratory distress, lethargy, decreased body weight, or abdominal distension. Double mutant mice had significantly reduced survival when compared to other littermates ($P<0.0001$, Figure 4a). Double mutant mice developed much more aggressive lung cancers and higher tumor burden than *K-ras*$^{LA1/+}$ mice, leading to shorter lifespans. The median survival for double mutant mice was 266 days compared to 373 days for *K-ras*$^{LA1/+}$ mice. The *p53*$^{+/-}$ *K-ras*$^{LA1/+}$ mice showed a very similar survival curve to published data, and indicated no difference in survival as compared to *p53*$^{R172H\Delta g/+}$ *K-ras*$^{LA1/+}$ mice (Figure 4a). However, a significant difference in cumulative cancer-related death was observed between male and female double mutant mice ($P=0.0071$, Figure 4b). This gender difference in cancer-related death was not observed for *K-ras*$^{LA1/+}$ and *p53*$^{R172H\Delta g/+}$ littermates (Supplementary Figure 1A-B). The cumulative deaths for female and male wild-type littermates were also similar to each other (Supplementary Figure 1C).

Discussion

Current mouse models for lung cancer develop lung adenocarcinomas, but do not metastasize (Nikitin *et al*.,

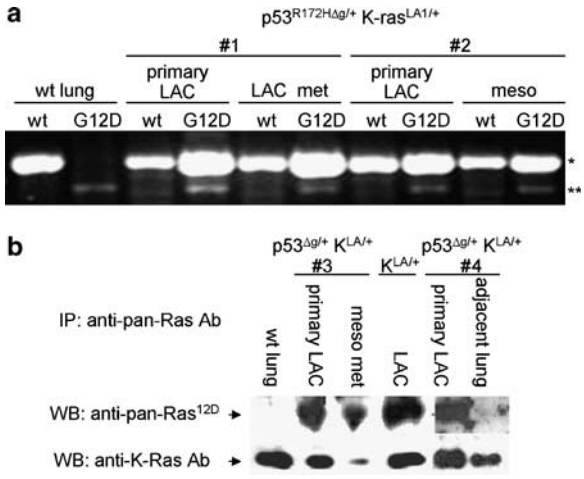


Figure 3 The expression of mutant *K-ras* in primary lung cancers and metastases. (**a**) Mutant *K-ras* was detected in primary lung cancers and metastases that were isolated from different double mutant mice, but not in normal lung tissue isolated from wild-type mice by RT–PCR. *Specific amplification; **nonspecific amplification. wt, wild-type; G12D, *K-ras*^{G12D}-specific primers to the missense mutation at codon 12; LAC, lung adenocarcinoma; met, metastasis; meso, mesothelioma. (**b**) Mutant K-ras was analysed in primary lung cancers, metastases and histologically normal lung tissues adjacent to lung adenocarcinoma by immunoprecipitation followed by western blots. Anti-pan-Ras^{12D} antibody specific for mutant Ras was probed first. The same membrane was stripped and probed with anti-K-Ras antibody. p53$^{\Delta g/+}$, p53$^{R172H\Delta g/+}$; K$^{LA/+}$, K-ras$^{LA1/+}$.

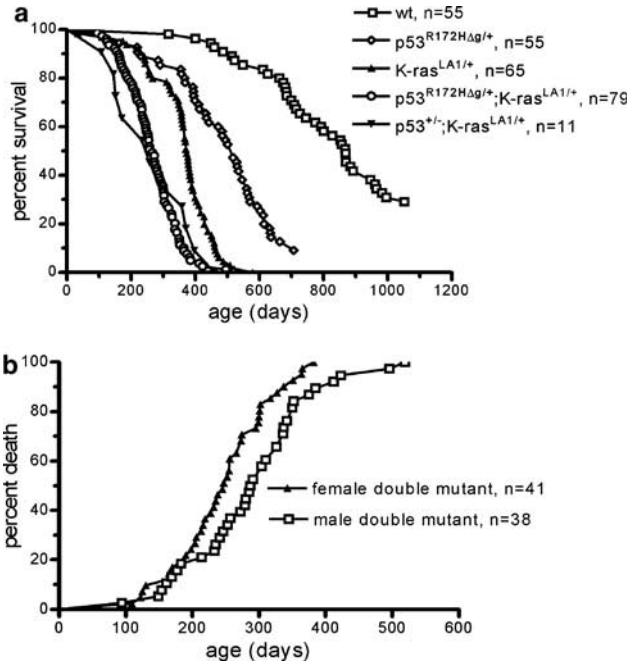


Figure 4 Kaplan–Meier survival of mice with different genotypes. (**a**) *p53*$^{R172H\Delta g/+}$ *K-ras*$^{LA1/+}$ mice had significantly reduced survival compared with *K-ras*$^{LA1/+}$, *p53*$^{R172H\Delta g/+}$ and wild-type littermates (logrank test, $P<0.0001$). No significant difference in survival was observed between *p53*$^{R172H\Delta g/+}$ *K-ras*$^{LA1/+}$ and *p53*$^{+/-}$ *K-ras*$^{LA1/+}$ mice. (**b**) Female double mutant mice had a significantly higher cancer-related death than male double mutant mice (logrank test, $P=0.0071$).

2004; Meuwissen and Berns, 2005). The deletion of a *p53* allele enhances lung tumorigenesis induced by mutant *K-ras*, but again does not promote the development of metastasis (Johnson *et al*., 2001; Jackson *et al*., 2005). In this study, we generated mice with both *p53* and *K-ras* missense mutations to test the suitability of such a model for metastatic lung adenocarcinoma.

In this model, primary lung cancer disseminated widely through both hematogenous and lymphatic pathways to multiple sites strikingly similar to those in human lung cancer (Tamura *et al*., 1992; Quint *et al*., 1996; Sadikot *et al*., 1997). Surprisingly, no metastasis of lung cancer was found in bone and brain. Additional genetic changes may be needed to produce tumors that can metastasize to these organs.

Interestingly, a significant discrepancy in cumulative cancer death was observed between female and male $p53^{R172H\Delta g/+}$ $K\text{-}ras^{LA1/+}$ mice, but not in littermates with either single mutation. This gender difference in survival is supported by a study showing a higher number of pulmonary lesions induced by a tobacco-specific carcinogen NNK in A/J females as opposed to males (Belinsky *et al*., 2003). In humans, the observation that female smokers are more susceptible to lung cancer than male smokers is supported by many case–control studies, but opposed by several prospective cohort studies (Zang and Wynder, 1996; Payne, 2001; Bach *et al*., 2003; Bain *et al*., 2004; Olak and Colson, 2004). Therefore, a gender difference in susceptibility to human lung cancer is still controversial. Nevertheless, the survival of female and male double mutant mice showed a statistically significant difference and will be an important model to probe this difference.

Pleural mesothelioma is an uncommon, but highly aggressive human malignancy that is invariably fatal because it is detected so late (Jaurand, 2005). In this study, 23% of $p53^{R172H\Delta g/+}$ $K\text{-}ras^{LA1/+}$ mice also developed pleural mesotheliomas. Four lines of evidence supported the diagnosis of this tumor in this model. The first is the restricted gross and microscopic localization to the pleural mesothelial lining and the distinct phenotypic differences from intra-pulmonary epithelial lesions. The second is positive staining of Calretinin and/or Cytokeratin 6, the two commonly used markers for human mesothelioma (Ordonez, 2003). Specifically, Calretinin was detected in 80% of murine mesotheliomas examined, corresponding to the frequency of 80% in human mesotheliomas (Abutaily *et al*., 2002). An antibody against Cytokeratin 5 and 6 is positive in 63% of human mesotheliomas (Abutaily *et al*., 2002). The cytokeratin 6 antibody detected staining in 40% of murine mesotheliomas (a murine-specific Cytokeratin 5 antibody is not available). Of note, these markers stain normal mesothelial cells and do not allow us to distinguish benign from malignant cells. None of lung adenocarcinomas examined in this study was positive for either marker. The third is negative PAS staining, which if positive, rules out mesothelioma. The fourth is that SPC staining was negative in mesothelioma, but positive in the adjacent lung adenocarcinoma. Taken together, histological features, immunohistochemical data, and PAS staining all support the diagnosis of mesothelioma in this study.

Thus, this new lung cancer model more faithfully simulates human metastatic lung cancer and promises to be invaluable in testing novel preventive or therapeutic modalities prior to clinical studies.

Materials and methods

Tumor samples and pathological analysis

The $K\text{-}ras^{LA1/+}$ mice were crossed with $p53^{R172H\Delta g/+}$ to generate $K\text{-}ras^{LA1/+}$, $p53^{R172H\Delta g/+}$, $p53^{R172H\Delta g/+}$ $K\text{-}ras^{LA1/+}$ and wild-type mice, and with $p53^{+/-}$ to generate $p53^{+/-}$ $K\text{-}ras^{LA1/+}$ mice. The background of these mice was greater than 90% 129Sv. Genotypes were determined as previously described (Liu *et al*., 2000; Johnson *et al*., 2001). Mice were housed in sterilized plastic cages with hardwood bedding and dust covers in a HEPA-filtered, specific pathogen-free room ($24\pm1^{\circ}C$, 45% humidity, 14/10 h light/dark cycle). The number of mice per cage was three to five. All mice were given sterilized NIH-31 mouse/rat diet (No. 7017, Harlan), and water *ad libitum*. Mice were monitored daily for signs of illness or obvious tumor burden and moribund mice were killed. Tumors and tissues were fixed with 10% buffered formalin, paraffin embedded, and sectioned at 4 μm. Sections (a single section for each tissue per mouse) were stained with hematoxylin and eosin (H&E) for histological evaluation. The diagnosis of a metastatic lesion was based on histological features and the gross finding that the lesion was not in direct contact with a lung tumor. A metastatic diagnosis of lung adenocarcinoma on parietal pleura was possible only if parietal and visceral pleurae were not adhering to each other.

Revese transcription–PCR and quantitative real-time TaqMan PCR

Total RNA was extracted from tumors or normal lung by using Trizol (Invitrogen, Carlsbad, CA, USA) and purified by an RNeasy kit (Qiagen, Gaithersburg, MD, USA). Reverse transcriptase reactions were performed using the First-Strand cDNA Synthesis Kit (Amersham Bioscience, Piscataway, NJ, USA). Primers for wild-type and mutant *K-ras* alleles were K-ras12G: TTGTGGTGGTTGGAGGTGG, K-ras12D: CTT GTGGTGGTTGGAGGTGA, and K-rasEx3R1: CTGTCTT GTCTTTGCTGAGGTC. Specific amplification was confirmed by sequencing PCR products.

Specific probes were used to differentiate mutant and wild-type *p53* alleles in tumors by real-time PCR. Primers and probes were p53 forward 5′-TCTACAAGAAGTCACAGCA CATGAC-3′, p53 reverse 5′-CCTTCCACCCGGATAAGA TGC-3′, wild-type probe 5′-TET-AGGTCGTGAGACACT GCC-3′, mutant probe 5′-FAM-TCGTGAGACGCTGCCC-3′. The GSC (goosecoid homeobox protein gene) forward 5′-CGGCACCGCACCATCT, GSC reverse 5′-TCGTCTCCT GGAAGAGGTTCC, and GSC probe 5′-VIC-CCGATGAGC AGCTCG-3′ were used for normalization. PCR reactions were performed in 384-well reaction plate using ABI PRISM 7900 Sequence Detection System (Applied Biosystems, Foster City, CA, USA). Each sample was measured in duplicate. The relative level of *p53* gene was determined by $\Delta\Delta C_t$ based on the formula $\Delta\Delta C_t = (\text{sample } C_t\ [p53] - \text{sample } C_t\ [\text{GSC}]) - (\text{control } C_t\ [p53] - \text{control } C_t\ [\text{GSC}])$. All tumor samples used the same reference sample for calculation, non-tumor DNA with wild-type *p53*. Analysis of diluted samples showed $2^{\Delta\Delta C_t}$ values of $\leqslant 0.15$, 0.15–0.6 or >0.6 indicating 0, 1, or 2 copies of wild-type *p53* alleles, respectively (Hill *et al*., 2005).

Immunohistochemistry and PAS staining

Immunohistochemical analysis was performed on tissue sections using the Vectastain ABC kit (Vector, Burlingame, CA, USA). Antibodies used were Calretinin (Zymed, South San Francisco, CA, USA, 18-0291, 1:3000 dilution), SPC (Chemicon, Temecula, CA, USA, AB3786, 1:1000 dilution) and a murine-specific Cytokeratin 6 antibody (gift from Dennis R Roop). Sections were counterstained with nuclear fast red or hematoxylin (Vector). Immunoflourescence analysis was performed using a CC10 antibody (Santa Cruz SC-9772, Santa Cruz, CA, USA, 1:50 dilution).

Sections were also stained with PAS staining system (Sigma, St Louis, MO, USA). Normal mouse liver sections were used as positive controls. For a negative control, liver samples were treated with diastase (Sigma) to remove immunoreactivity.

Immunoprecipitation-western blot analysis

Tumor samples were homogenized in 50 mM Tris-Cl (pH 8.0), 150 mM NaCl, 0.5% NP40, and proteinase inhibitors (Roche, Mannheim, Germany). Agarose-conjugated anti-ras antibody Ab-1 (Calbiochem, San Diego, CA, USA, OP01A) was added according to the manufacturer's recommendation. Blots were probed with an anti-pan-Ras^{12D} antibody specific to mutant Ras with an aspartic acid at codon 12 (Oncogene, PC10). The same membrane was stripped and probed with an anti-K-Ras antibody (Santa Cruz, SC30, 1:150). The secondary antibody was horseradish peroxidase-conjugated and signals were detected with a chemiluminescence kit (Amersham Pharmacia, Piscataway, NJ, USA).

Statistics

Survival curves were plotted by the Kaplan–Meier method. The statistical significance between different survival data was determined by the logrank test (GraphPad Prism 4). Tabular data between groups were compared by the χ^2 test.

Acknowledgements

This study was supported by a grant from the Department of Defense, DAMD17-01-1-0689 and the Cancer Center Support Grant CA16672 from the NIH. We thank Tyler Jacks for the *K-ras*$^{LA1/+}$ mice.

References

Abutaily AS, Addis BJ, Roche WR. (2002). Immunohistochemistry in the distinction between malignant mesothelioma and pulmonary adenocarcinoma: a critical evaluation of new antibodies. *J Clin Pathol* **55**: 662–668.

Bach PB, Kattan MW, Thornquist MD, Kris MG, Tate RC, Barnett MJ *et al*. (2003). Variations in lung cancer risk among smokers. *J Natl Cancer Inst* **95**: 470–478.

Bain C, Feskanich D, Speizer FE, Thun M, Hertzmark E, Rosner BA *et al*. (2004). Lung cancer rates in men and women with comparable histories of smoking. *J Natl Cancer Inst* **96**: 826–834.

Becher OJ, Holland EC. (2006). Genetically engineered models have advantages over xenografts for preclinical studies. *Cancer Res* **66**: 3355–3358 discussion 3358–3359.

Belinsky SA, Klinge DM, Stidley CA, Issa JP, Herman JG, March TH *et al*. (2003). Inhibition of DNA methylation and histone deacetylation prevents murine lung cancer. *Cancer Res* **63**: 7089–7093.

Belinsky SA, Stefanski SA, Anderson MW. (1993). The A/J mouse lung as a model for developing new chemointervention strategies. *Cancer Res* **53**: 410–416.

Castonguay A, Pepin P, Stoner GD. (1991). Lung tumorigenicity of NNK given orally to A/J mice: its application to chemopreventive efficacy studies. *Exp Lung Res* **17**: 485–499.

Chiba I, Takahashi T, Nau MM, D'Amico D, Curiel DT, Mitsudomi T *et al*. (1990). Mutations in the p53 gene are frequent in primary, resected non-small cell lung cancer. Lung Cancer Study Group. *Oncogene* **5**: 1603–1610.

Greenblatt MS, Bennett WP, Hollstein M, Harris CC. (1994). Mutations in the p53 tumor suppressor gene: clues to cancer etiology and molecular pathogenesis. *Cancer Res* **54**: 4855–4878.

Hecht SS, Morse MA, Eklind KI, Chung FL. (1991). A/J mouse lung tumorigenesis by the tobacco-specific nitrosamine 4-(methylnitrosamino)-1-(3-pyridyl)-1-butanone and its inhibition by arylalkyl isothiocyanates. *Exp Lung Res* **17**: 501–511.

Hill R, Song Y, Cardiff RD, Van Dyke T. (2005). Selective evolution of stromal mesenchyme with p53 loss in response to epithelial tumorigenesis. *Cell* **123**: 1001–1011.

Jackson EL, Olive KP, Tuveson DA, Bronson R, Crowley D, Brown M *et al*. (2005). The differential effects of mutant p53 alleles on advanced murine lung cancer. *Cancer Res* **65**: 10280–10288.

Jaurand MC. (2005). Mesothelioma pathogenesis, facts and expectations. *Pathol Biol (Paris)* **53**: 41–44.

Johnson L, Mercer K, Greenbaum D, Bronson RT, Crowley D, Tuveson DA *et al*. (2001). Somatic activation of the K-ras oncogene causes early onset lung cancer in mice. *Nature* **410**: 1111–1116.

Kerr KM, Lamb D, Wathen CG, Walker WS, Douglas NJ. (1992). Pathological assessment of mediastinal lymph nodes in lung cancer: implications for non-invasive mediastinal staging. *Thorax* **47**: 337–341.

Kitamura H, Kameda Y, Ito T, Hayashi H. (1999). Atypical adenomatous hyperplasia of the lung. Implications for the pathogenesis of peripheral lung adenocarcinoma. *Am J Clin Pathol* **111**: 610–622.

Lang GA, Iwakuma T, Suh YA, Liu G, Rao VA, Parant JM *et al*. (2004). Gain of function of a p53 hot spot mutation in a mouse model of Li–Fraumeni syndrome. *Cell* **119**: 861–872.

Liu G, McDonnell TJ, Montes de Oca Luna R, Kapoor M, Mims B, El-Naggar AK *et al*. (2000). High metastatic potential in mice inheriting a targeted p53 missense mutation. *Proc Natl Acad Sci USA* **97**: 4174–4179.

Malkinson AM, You M. (1994). The intronic structure of cancer-related genes regulates susceptibility to cancer. *Mol Carcinog* **10**: 61–65.

Meuwissen R, Berns A. (2005). Mouse models for human lung cancer. *Genes Dev* **19**: 643–664.

Mitsudomi T, Steinberg SM, Nau MM, Carbone D, D'Amico D, Bodner S *et al*. (1992). p53 gene mutations in non-small-cell lung cancer cell lines and their correlation with the presence of ras mutations and clinical features. *Oncogene* **7**: 171–180.

Nikitin AY, Alcaraz A, Anver MR, Bronson RT, Cardiff RD, Dixon D *et al*. (2004). Classification of proliferative pulmonary lesions of the mouse: recommendations of the mouse models of human cancers consortium. *Cancer Res* **64**: 2307–2316.

Olak J, Colson Y. (2004). Gender differences in lung cancer: have we really come a long way, baby? *J Thorac Cardiovasc Surg* **128**: 346–351.

Olive KP, Tuveson DA, Ruhe ZC, Yin B, Willis NA, Bronson RT *et al*. (2004). Mutant p53 gain of function in two mouse models of Li–Fraumeni syndrome. *Cell* **119**: 847–860.

Ordonez NG. (2003). The immunohistochemical diagnosis of mesothelioma: a comparative study of epithelioid mesothelioma and lung adenocarcinoma. *Am J Surg Pathol* **27**: 1031–1051.

Payne S. (2001). 'Smoke like a man, die like a man'?: a review of the relationship between gender, sex and lung cancer. *Soc Sci Med* **53**: 1067–1080.

Quint LE, Tummala S, Brisson LJ, Francis IR, Krupnick AS, Kazerooni EA *et al*. (1996). Distribution of distant metastases from newly diagnosed non-small cell lung cancer. *Ann Thorac Surg* **62**: 246–250.

Rodenhuis S, Slebos RJ. (1992). Clinical significance of ras oncogene activation in human lung cancer. *Cancer Res* **52** (9 Suppl): 2665s–2669s.

Rodenhuis S, Slebos RJ, Boot AJ, Evers SG, Mooi WJ, Wagenaar SS *et al*. (1988). Incidence and possible clinical significance of K-ras oncogene activation in adenocarcinoma of the human lung. *Cancer Res* **48**: 5738–5741.

Sadikot RT, Renwick DS, DaCosta P, Chalmers AG, Pearson SB. (1997). Breast metastasis from non-small cell lung cancer. *South Med J* **90**: 1063–1064.

Salgia R, Skarin AT. (1998). Molecular abnormalities in lung cancer. *J Clin Oncol* **16**: 1207–1217.

Sausville EA, Burger AM. (2006). Contributions of human tumor xenografts to anticancer drug development. *Cancer Res* **66**: 3351–3354, discussion 3354.

Takahashi T, Nau MM, Chiba I, Birrer MJ, Rosenberg RK, Vinocour M *et al*. (1989). p53: a frequent target for genetic abnormalities in lung cancer. *Science* **246**: 491–494.

Tamura A, Matsubara O, Yoshimura N, Kasuga T, Akagawa S, Aoki N. (1992). Cardiac metastasis of lung cancer. A study of metastatic pathways and clinical manifestations. *Cancer* **70**: 437–442.

Toyooka S, Tsuda T, Gazdar AF. (2003). The Tp53 gene, tobacco exposure, and lung cancer. *Hum Mutat* **21**: 229–239.

Vahakangas KH, Bennett WP, Castren K, Welsh JA, Khan MA, Blomeke B *et al*. (2001). p53 and K-ras mutations in lung cancers from former and never smoking women. *Cancer Res* **61**: 4350–4356.

Wang Y, Zhang Z, Lubet RA, You M. (2006a). A mouse model for tumor progression of lung cancer in ras and p53 transgenic mice. *Oncogene* **25**: 1277–1280.

Wang Y, Zhang Z, Yao R, Jia D, Wang D, Lubet RA *et al*. (2006b). Prevention of lung cancer progression by bexarotene in mouse models. *Oncogene* **25**: 1320–1329.

You M, Wang Y, Stoner G, You L, Maronpot R, Reynolds SH *et al*. (1992). Parental bias of Ki-ras oncogenes detected in lung tumors from mouse hybrids. *Proc Natl Acad Sci USA* **89**: 5804–5808.

Zang EA, Wynder EL. (1996). Differences in lung cancer risk between men and women: examination of the evidence. *J Natl Cancer Inst* **88**: 183–192.

Supplementary Information accompanies the paper on the Oncogene website (http://www.nature.com/onc).

Algorithmic guided screening of drug combinations of arbitrary size for activity against cancer cells

Ralph G. Zinner,[1] Brittany L. Barrett,[1] Elmira Popova,[4] Paul Damien,[5] Andrei Y. Volgin,[2] Juri G. Gelovani,[2] Reuben Lotan,[1] Hai T. Tran,[1] Claudio Pisano,[6] Gordon B. Mills,[3] Li Mao,[1] Waun K. Hong,[1] Scott M. Lippman,[1] and John H. Miller[7]

Departments of [1]Thoracic/Head and Neck Medical Oncology, [2]Experimental Imaging, and [3]Systems Biology, The University of Texas M. D. Anderson Cancer Center, Houston, Texas; [4]Department of Operations Research and Industrial Engineering and [5]Red McCombs School of Business, The University of Texas, Austin, Texas; [6]Sigma-Tau Pharmaceuticals, Inc., Rome, Italy; and [7]The Santa Fe Institute, Santa Fe, New Mexico

Abstract

The standard treatment for most advanced cancers is multidrug therapy. Unfortunately, combinations in the clinic often do not perform as predicted. Therefore, to complement identifying rational drug combinations based on biological assumptions, we hypothesized that a functional screen of drug combinations, without limits on combination sizes, will aid the identification of effective drug cocktails. Given the myriad possible cocktails and inspired by examples of search algorithms in diverse fields outside of medicine, we developed a novel, efficient search strategy called Medicinal Algorithmic Combinatorial Screen (MACS). Such algorithms work by enriching for the fitness of cocktails, as defined by specific attributes through successive generations. Because assessment of synergy was not feasible, we developed a novel alternative fitness function based on the level of inhibition and the number of drugs. Using a WST-1 assay on the A549 cell line, through MACS, we screened 72 combinations of arbitrary size formed from a 19-drug pool across four generations. Fenretinide, suberoylanilide hydroxamic acid, and bortezomib (FSB) was the fittest. FSB performed up to 4.18 SD above the mean of a random set of cocktails or ''too well'' to have been found by chance, supporting the utility of the MACS strategy. Validation studies showed FSB was inhibitory in all 7 other NSCLC cell lines tested. It was also synergistic in A549, the one cell line in which this was evaluated. These results suggest that when guided by MACS, screening larger drug combinations may be feasible as a first step in combination drug discovery in a relatively small number of experiments. [Mol Cancer Ther 2009;8(3):521–32]

Introduction

Combining chemotherapeutic agents is an established way to improve on single-drug efficacy, and small (two- to three-drug) combinations are now the standard of treatment for most metastatic cancers (1). Recent successes with larger multiple-agent regimens in the clinic (1, 2) encourage a continued search for improved combination chemotherapies; however, only a few of the virtually infinite possible combinations have been evaluated to date (3, 4) due to concerns about the potential toxicity of the combinations and the daunting logistics of testing all feasible combinations of available drugs (5).

The improved tolerability of new, potentially effective molecular targeted agents has encouraged combination of these agents with standard chemotherapy regimens and, more recently, with each other in early-phase clinical trials (1, 2, 6). In a recent review, it was observed that there is ''tremendous'' potential for improved therapy of cancer from combinations of molecular targeted agents designed to modulate different aspects of the same or different targets (7). Traditionally, strategies of combination drug development have been based on insights into non–cross-resistant molecular mechanisms of action, evidence of synergy, preclinical or clinical insights into nonoverlapping toxicities, and, more recently, insights into their effects on signaling pathways and host-tumor interactions (8, 9).

As a complement to these methods, we investigated the utility of a functional, laboratory-based screening of combinations. Laboratory-based screens have long been used to identify active single agents, and one company explored doublets using synergy (10). However, to our knowledge, there are no ongoing efforts to screen large spaces of potential combinations of more than two drugs. Extending a screen to larger cocktails may be useful given the time required to compile clinical evidence. However, *in vitro* assessments of any given cocktail become more challenging as drug combinations use larger numbers of agents. Moreover, even with highly efficient assessments of individual combinations, only a small fraction of the total possible cocktails can be evaluated given that they are

Received 9/29/08; revised 1/9/09; accepted 1/15/09; published OnlineFirst 3/10/09.

Grant support: Department of Defense BESCT Lung Cancer Program DAMD17-01-1-0689 (W.K. Hong).

The costs of publication of this article were defrayed in part by the payment of page charges. This article must therefore be hereby marked *advertisement* in accordance with 18 U.S.C. Section 1734 solely to indicate this fact.

Requests for reprints: Ralph Zinner, Department of Thoracic/Head and Neck Medical Oncology, Unit 432, The University of Texas M. D. Anderson Cancer Center, 1515 Holcombe Boulevard, Houston, TX 77030. Phone: 713-792-6363; Fax: 713-792-1220. E-mail: rzinner@mdanderson.org

Copyright © 2009 American Association for Cancer Research.

doi:10.1158/1535-7163.MCT-08-0937

virtually countless. We made an effort to meet these challenges on two levels. First, we developed a rapid method, or fitness function alternative to synergy, to speed evaluation of individual cocktails. Second, we used a search algorithm intended to sequentially direct the screen toward increasingly more promising sets of drug combinations.

Fitness is a term used in search algorithms adapted from evolutionary theory. In biology, higher fitness describes an individual's greater capacity to reproduce. In search algorithms, it indicates a more optimal solution; what defines fitness is determined by the investigator and the problem that he or she is trying to solve. These algorithms guide a process through a finite list of operations intended to maximize fitness. Such algorithms have been extensively used outside medicine in applications such as data fitting, scheduling, trend spotting, and budgeting (11–13). They have been evaluated in medicine in breast cancer diagnosis (14) and in an antiviral *in vitro* model assessing a large space of dose permutations of a few cocktails (15). Here, a well-established strategy is applied to a novel setting: the discovery of drug cocktails. The algorithm works through a stepwise process of enriching successive pools of cocktails for increased fitness. It is this application we designate Medicinal Algorithmic Combinatorial Screen (MACS).

For MACS to be meaningful, fitness needs to predict a value of interest, and to be feasible, the fitness function needs to be efficient. We intended fitness to predict cocktail efficacy. Synergy is an established fitness function used for this purpose. Indeed, synergy was used by CombitoRx in evaluating doublets (10). However, synergy can become exponentially more labor-intensive with each drug added to a given cocktail. As an example, when six doses per drug are used, as done by CombitoRx,

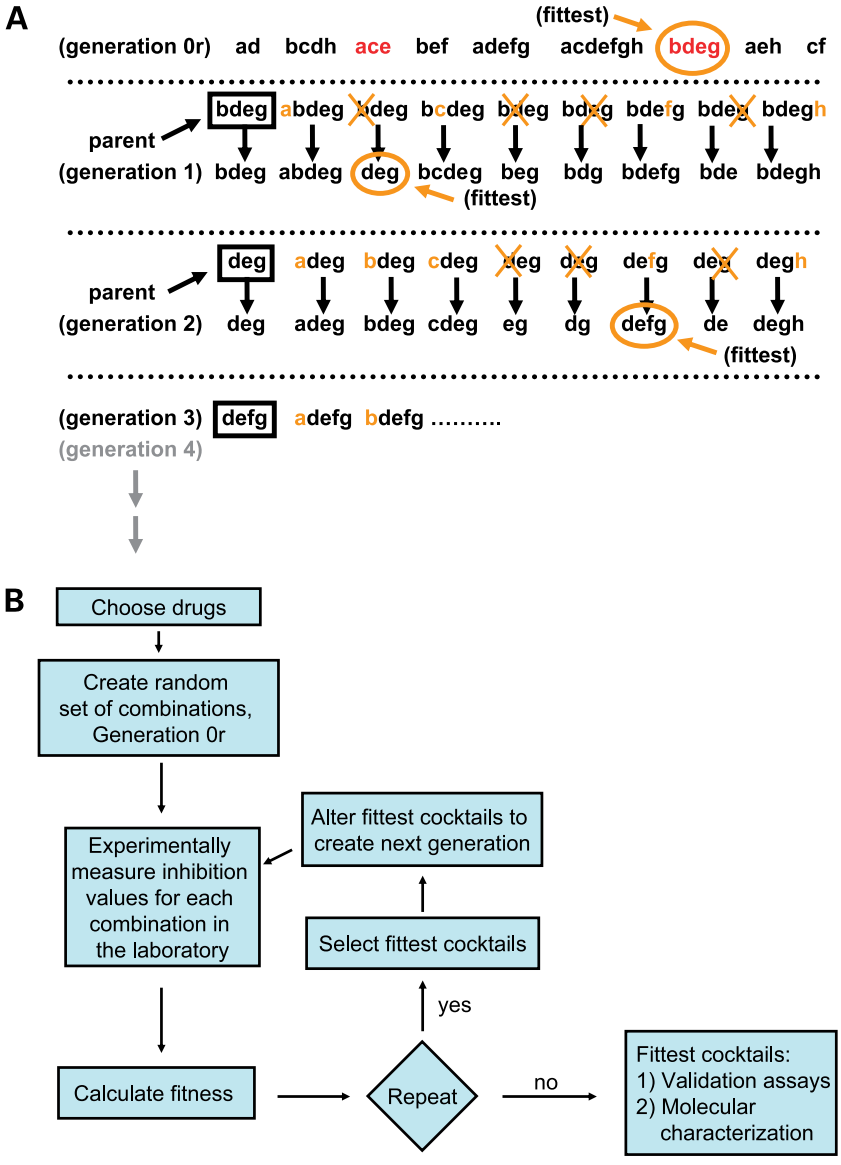


Figure 1. **A,** a model hill climb. Imagine an eight-drug pool with the drugs labeled ''a'' through ''h.'' In the initial generation (generation 0), 9 of 256 possible combinations are randomly formed. These combinations are, in turn, tested in cell culture. In this example, the combination identified as fittest is shown as ''bdeg.'' Note that we are not describing the fitness function here; different fitness functions can alter the fitness landscape and which among the nine would be determined to be fittest thereby altering the ultimate outcome. However, the rules of the hill climb will not be affected by the fitness function. Generation 1 is formed from the eight one-mutant combinations (also known as ''nearest neighbors'') of ''bdeg'' plus the parent. To form this generation, each of the eight drugs is added to or subtracted from the fittest combination in turn. Thus, because drug ''a'' is not present in the parent combination ''bdeg,'' it is added to form ''abdeg.'' Next, drug ''b'' is checked. Because it is already present in the parent, ''b'' is subtracted, resulting in the combination ''deg.'' This is repeated until all eight drugs are checked and generation 1 is formed, which is then tested. If ''deg'' were identified as the fittest combination, its eight nearest neighbors would then be determined, and so on. A local peak or maximum on the landscape is reached if none of the progeny are superior to the parent. **B,** a scheme outlining general steps characteristic of any MACS.

Table 1. The average activity of the single-agent controls across generations 0 to 3 hill climb

Agent (designation)	Drug class/mechanism of action	IC_{10} dose (μmol/L)	1× dose	2× dose	4× dose	Rank 1×	Rank 4×
Anisomycin	Protein synthesis inhibitor/activates JNK, p38 MAPK, and others	0.015	0.90	0.72	0.59	12	12
ATRA	**Retinoid: differentiation**	**15**	**0.87**	**0.74**	**0.63**	**8**	**16**
Bortezomib	**26S proteasome inhibitor**	**0.005**	**0.97**	**0.45**	**0.37**	**17**	**4**
CD437	Retinoid: proapoptotic	0.3	0.86	0.61	0.34	7	2
Cisplatin	Alkylating agent	5	0.85	0.72	0.51	5	9
Decitabine	DNA methylation inhibitor	2	0.88	0.84	0.78	10	17
Deguelin	Akt inhibitor	12	0.79	0.64	0.39	2	5
Fenretinide	**Retinoid: proapoptotic**	**5**	**0.86**	**0.66**	**0.19**	**6**	**1**
Gemcitabine	Antimetabolite	0.004	1.06	0.96	1.03	18	19
Imatinib	TKI of BCR-ABL, PDGF, c-kit	3	1.07	0.78	0.85	19	18
Indirubin	PKI*: GSK-3b, CDK5	1	0.92	0.69	0.51	15	10
LY294002	PI3K inhibitor	2	0.90	0.79	0.53	11	11
MX3350-1	Retinoid: proapoptotic	0.5	0.92	0.68	0.49	14	8
PD-168393	TKI: EGFR	5	0.85	0.63	0.47	4	7
Rapamycin	mTOR inhibitor	6	0.76	0.66	0.62	1	15
SAHA	**Histone deacetylase inhibitor**	**2**	**0.88**	**0.50**	**0.37**	**9**	**3**
SCH66336	FTI	5	0.90	0.78	0.59	13	13
SP600125	JNK1, -2, and -3 inhibitor	5	0.83	0.66	0.45	3	6
ST1926	Adamantyl retinoid: proapoptotic	0.05	0.95	0.90	0.60	16	14

NOTE: The three drugs in FSB and ATRA are in boldface. The 1× dose was the dose used in the MACSs. The levels of inhibition at the 1× and 4× doses are ranked and represent the average value across all generations (see Supplementary Fig. S2 for charts of each agent across the generations).
Abbreviations: ATRA, all-*trans* retinoic acid; SAHA, suberoylanilide hydroxamic acid; PKI, protein kinase inhibitor; TKI, tyrosine kinase inhibitor; PDGF, platelet-derived growth factor; EGFR, epithelial growth factor receptor; FTI, farnesyl transferase inhibitors; JNK, c-jun NH_2-terminal kinase; CDK5, cyclin-dependent kinase 5; MAPK, mitogen-activated protein kinase; PI3K, phosphatidylinositol 3-kinase; mTOR, mammalian target of rapamycin.

cocktails containing two, three, four, or five drugs generate 36, 216, 1,296, and 7,776 possible dose permutations, respectively. Although substantially smaller numbers of permutations could be managed by fixed dosing ratios or other ways of sampling, synergy may nonetheless remain daunting. Thus, we developed an alternative fitness function that required one assay per cocktail to improve the efficiency on the level of the individual cocktail. It was a composite of inhibition at a fixed dose of each drug and the number of drugs. Through the use of this novel fitness function, we lost information about a vast number of potentially informative dose combinations, but it enabled us to screen hundreds of unique cocktails per week. Other fitness functions could incorporate drug cost, anticipated toxicities, molecular insight, dose sequence, alternative dosing schemes, or any other characteristics of interest.

As with fitness functions that assess individual cocktails, there are countless possible search algorithms to guide screens of large sets of cocktails with different ones suited to varied combinatorial landscapes (Supplementary Fig. S1).[8] We present a simple example of such an algorithm called hill climbing (Fig. 1A; Supplementary Fig. S1).[8] This example does not represent actual data but rather illustrates a method. As can be seen in the figure, one can perform a MACS by sampling a relatively small subset of the possible cocktails (Supplementary Fig. S1).[8] Although the rules can vary among MACSs, they all entail a cycling between experimental evaluation of drug cocktails and a rule-based creation of the next generation (Fig. 1B). These rules involve selection and alteration. The selection function directs the choice of a subset of the cocktails tested, and in the case of the hill climb, the fittest one. However, it could choose more than one cocktail and even incorporate a stochastic element analogous to natural evolution in which fitness improves the odds of survival but offers no guarantees (as presented previously).[9,10] The alteration function can create all of the nearest neighbors of the selected cocktail(s), analogous to mutations as in the hill climb, or could combine pieces of different selected cocktails analogous to recombination.

Because any search of a large enough potential space will, for practical reasons, be confined to a small fraction of the total possible cocktails, it is likely that many of the fittest combinations will never be tested even when a search algorithm guides the process. The MACS needs only to find combinations that have fitness levels that are

[8] Supplementary material for this article is available at Molecular Cancer Therapeutics Online (http://mct.aacrjournals.org/).

[9] Zinner RG, Barrett BL, Volgin AY, Gelovani JG, Huang J, Tran HT, Mills GB, Hong WK, Fu Y, Mao L. Proc Am Soc Clin Oncol, 2005; abstract 2079.
[10] Miller JH, Zinner RG, Barrett BL. Directed discovery of novel drug cocktails. Sante Fe Institute Website 2005; 07-031, http://www.santafe.edu/research/publications/wpabstract/200507031.

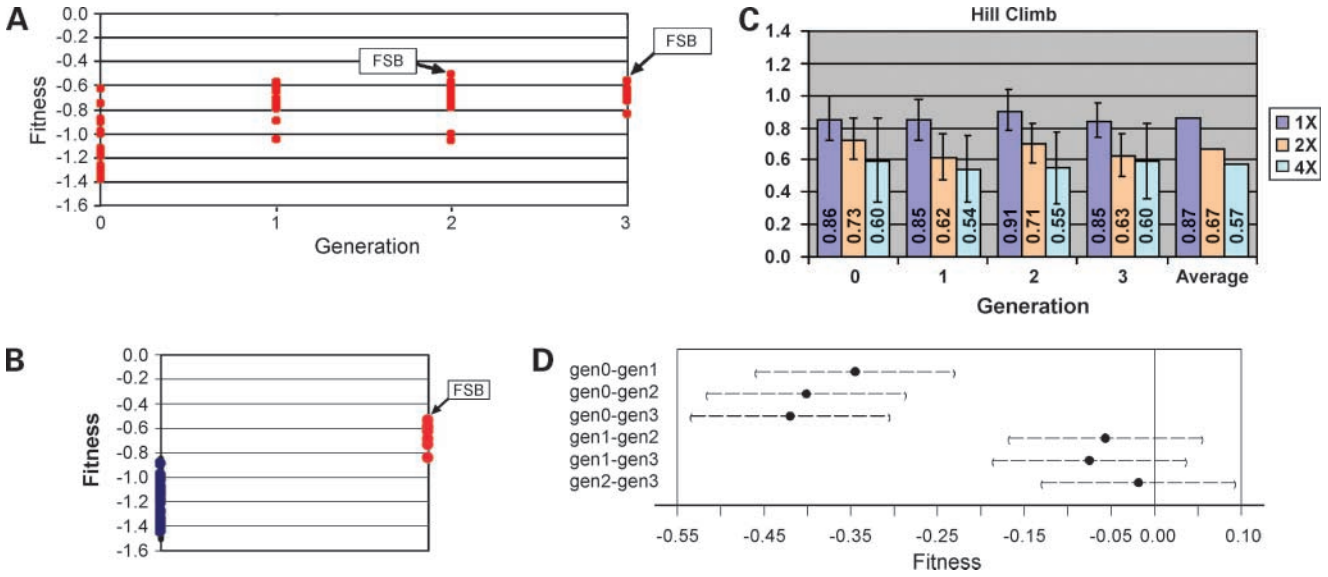


Figure 2. **A,** the performance of the hill climb. **B,** the set of cocktails composing the fittest cocktail and its nearest neighbors (or progeny) resulting from a local search compared with a set of randomly formed cocktails (described elsewhere).[9,10] **A** and **B,** the *x*-axis indicates the generation number, and in the *y*-axis, higher values indicate greater fitness level [not the inhibitory, K(s)]. **A,** the hill climb arrived at FSB by generation 2. Generation 3 includes FSB and its 19 nearest neighbors, which can be compared with the 18 randomly formed cocktails of generation 0. **B,** in blue is a set of 30 randomly formed cocktails; in red are FSB (the fittest cocktail) and its 19 nearest neighbors. This latter set is the same as the cocktails in generation 2 of the hill climb **A**, although the values in the hill climb represent a repeat assay of these cocktails. **C,** the average inhibitory values of the single-agent controls per generation are shown. The 1× values are the doses used in the MACSs. Note that the inhibitory values [or K(s)], not the fitness, are indicated along the *y* axis. The average values across all their respective generations are shown at the far right. For the individual values of each single-agent control across the generations, see Supplementary Fig. S3. **D,** multiple comparisons of the average fitness values and respective 95% confidence intervals of the generations from the hill climb.

''good enough'' more efficiently than a random screen to be useful.

In this proof-of-principle study, we developed a novel fitness function to evaluate cocktails and tested a number of different kinds of MACSs operating on combinations all derived from the same pool of 19 available anticancer drugs in an *in vitro* non–small-cell lung cancer (NSCLC) model. Based on data from earlier MACSs showing that a local search method such as a hill climb would be efficient (as compared with the more complex algorithms we evaluated earlier),[9,10] here we tested a hill climb-MACS. We then ran validation assays on the fittest identified cocktail in line with the general strategy in most drug development screens.

Materials and Methods

Unlike the model (Fig. 1A), the actual laboratory experiments composing the hill climb entailed 19 real agents creating a combinatorial space of 2^{19} or 524,288 possible cocktails. Eighteen cocktails were randomly formed for its generation 0 (as previously described[9,10]) and subsequent generations were created based on the assay results and the rules of the hill climb. The assay systems and conditions as well as fitness function were held constant throughout the hill climb-MACS.

Fitness Function

Our fitness function permitted one assay per cocktail to be done in triplicate. It was composed of a measured assay value representing inhibition and a nonmeasured value, a factor of the number of drugs in the cocktail. Starting at 0, 0.1 was subtracted for each 10% of cells remaining compared with the no-treatment controls. Thus, 70% inhibition yields 30% of the no treatment control value, or 0.3 to be subtracted. A ''penalty'' of 0.1 was assigned for each drug composing the cocktail based on the observation that each drug dosed at IC_{10} added to a cocktail increased inhibition by an average of 10% (data not shown). This penalty was designed to control for cocktail size to allow fitness to be determined by the cocktail composition.

Formally, fitness was $-K(s) - 0.1|s|$, where K(s) is the proportion of cells surviving relative to the no-treatment control and $|s|$ was the number of drugs in the cocktail. Fitness values thus can range from −0.1 (one drug kills all cells) to −2.9 (all 19 drugs with no inhibition). Even lower fitness values would be possible with growth stimulation relative to the untreated controls.

Selected Agents

Nineteen agents, 16 molecularly targeted and 3 chemotherapy, were used based on their availability, affordability, and ease of preparation and storage and the authors' experience in their use (Table 1; Supplementary Methods). Selected agents were required to inhibit A549 growth by at least 10% (IC_{10}) under the conditions used in the MACS (data not shown). A549 was chosen because it grows rapidly under uncomplicated laboratory conditions. Drugs requiring excessive concentrations of DMSO were excluded

given the independent ability of DMSO to inhibit A549 at doses of 1.7% by volume (data not shown). Drugs dissolved in ethanol were excluded because ethanol potentiated inhibition of A549 by DMSO.

Cell Lines

Eight human NSCLC cell lines were used to test the activity of the lead drug combination. A549, H226, Calu-3, H441, H1975, and HCC827 were purchased from American Type Culture Collection. HCC2279 was a gift from John Minna (Southwestern Medical School, Dallas, TX), and PC-14 was purchased from Riken BioResource Center. A549, H226, and Calu-3 cells were incubated in DMEM/F-12 (Invitrogen Corp.) containing 10% fetal bovine serum and 1% penicillin/streptomycin. H441, H1975, HCC827, HCC2279, and PC-14 cells were incubated in RPMI 1640 plus 10% fetal bovine serum.

Cells were isolated from BD Falcon 75-cm^2 tissue culture–treated flasks after a rinse with Cellgro PBS (Mediatech, Inc.) and the addition of Gibco trypsin-EDTA (0.05% trypsin, with EDTAx4Na) from Invitrogen. The cells were then plated at a volume of 50 μL/well in 96-well MicroWell Nunclon-Δ plates (Nalge Nunc International). Plated cells were then stored at 37°C in a humidified atmosphere containing 5% CO_2 until the drugs were added. The numbers of cells per well were as follows: A549, 1,500; H226, 3,000; PC-14, 2,500; HCC2279, 4,000; HCC827, 7,000; H441, 2,700; H1975, 6,000; and Calu-3, 15,000. All cell lines were incubated on Nunc 167008 96-well plates (Fisher Scientific International, Inc.).

Preparation of the Drug Combinations

Drugs for a given combination were mixed in a 96-well 2-mL sterile polypropylene block from Denville Scientific. All combinations were mixed at four times the volume needed for one well to allow for triplicate experiments and pipetting error. The final volume of DMSO (0.66%) in all wells, including the no treatment controls, was based on the maximum possible DMSO dose derived from the one cocktail containing all 19 drugs. Because each cocktail had its own individual DMSO volume, we added the unique additional DMSO individually to each cocktail, yielding 0.66% of a final volume of 250 μL. Medium was added to obtain a volume of 200 μL, which was in turn added to a well already containing the cells and media plated immediately before occupying 50 μL, yielding 250 μL.

Drug Doses

We used the single-agent IC_{10} dose (1× dose) regardless of the size of the combination because we anticipated that a higher IC value would result in maximal inhibition from many of the small cocktails, thereby reducing our ability to compare cocktails. All combinations were tested in triplicate in adjacent wells on the same plate, and each plate contained its own six untreated controls. All cocktails and controls were within the 60 non-edge wells to avoid an edge effect.[9,10] With each generation, we included 1×, 2×, and 4× single-agent controls in triplicate for all 19 drugs on a separate plate to check for consistency.

Preparation of Multiple Cell Lines

Cells were isolated from BD Falcon 75-cm^2 tissue culture–treated flasks after a rinse with Cellgro PBS (Mediatech) and the addition of Gibco trypsin-EDTA (Invitrogen). The cells were plated at a volume of 50 μL/well in 96-well MicroWell Nunclon-Δ plates (Nalge Nunc International). The numbers of cells per well were as follows: A549, 1,500; H226, 3,000; PC-14, 2,500; HCC2279, 4,000; HCC827, 7,000; H441, 2,700; H1975, 6,000; and Calu-3, 15,000. Cell lines were incubated on Nunc 167008 96-well plates (Fisher Scientific International). After the drug mixture was added, the plates were incubated for 44 h at 37°C in a humidified atmosphere containing 5% CO_2. This permitted reproducible measurements and a repeat assay during the workweek.

WST-1 Assay

Cell proliferation was measured using the WST-1 Cell Proliferation Reagent (Roche Diagnostics). After 44 h of incubation, 25 μL of WST-1 reagent were added constituting 9% of the well volume and the plates were incubated for another 4 h. The absorbance was measured on a scanning multiwell spectrophotometer at 440 nm with a 600-nm reference.

Preparation of FSB/ASB Subsets

All eight possible subcombinations of FSB—fenretinide, suberoylanilide hydroxamic acid, and bortezomib—(F, S, B, FS, FB, SB, FSB, no treatment control) and ASB in which fenretinide is replaced by all-*trans* retinoic acid (A, AS, AB, ASB) were tested in triplicate in eight NSCLC cell lines including A549. The doses were held stable in all cell lines at the IC_{10} for A549, and no edge wells were used. Each plate contained six untreated controls. An additional plate of A549 cells containing 1×, 2×, and 4× doses in triplicate of each drug and six no treatment controls was done with each experiment.

Synergy

We assessed the synergy of FSB in A549 and H2226 using all 64 possible dose combinations derivable from four dose levels: zero, 1× (high), 0.66× (medium), and 0.44× (low), done in triplicate. We used the same doses in each cell line to mirror the clinical case in which the drug titer in the serum affects the tumor as a whole unvaried from one clone to another. No edge wells were used and each plate contained six untreated controls. We also did single-agent controls on a separate plate at the 1× (high), 2×, and 4× doses for both cell lines. These values were also used in the synergy calculations. The combination index was calculated by the Chou-Talalay equation. In cases in which single agents stimulated growth, the value 0.000,001 was used to allow a calculation.

Statistical Analyses

No formal statistics were used to estimate the fitness. Statistical analyses of the MACS data and proliferation assays were carried out in Excel (Microsoft, Inc.) and SPlus (Insightful, Inc.) using ANOVA. The Kolmogorov-Smirnov test was run on the fitness values on sets of randomly formed cocktails. Analyses of synergy were done using CalcuSyn software (Biosoft Ltd.; refs. 16, 17).

A

Gen	Alteration	Cocktail	FSB	#Drugs	K(s)	Fitness	Fitness Rank	K(s) Rank
0	Random	Bor,Ly,Sa	SB	3	0.33	-0.63	1	5
0	Random	Bor,Cis,Ly,Sa,Sp	SB	5	0.25	-0.75	2	2
0	Random	At,Bor,Fen,Ima,Ly,Mx,Sa	FSB	7	0.18	-0.88	3	1
0	Random	At,Bor,Deg,Mx,Sa,Sp	SB	6	0.30	-0.90	4	4
0	Random	Ani,Deg,Ima,Pd,Sc		5	0.48	-0.98	5	10
0	Random	Cis,Ind,Rap		3	0.70	-1.00	6	13
0	Random	At,Dec,Ly,Sa,Sp	S	5	0.50	-1.00	7	11
0	Random	At,Bor,Cis,Dec,Fen,Ima,Sp	FB	7	0.43	-1.13	8	6
0	Random	At,Cis,Fen,Sp	F	4	0.73	-1.13	9	14
0	Random	Bor,Dec,Ima,Ly,Rap,Sp,St	B	7	0.44	-1.14	10	7
0	Random	Bor,Deg,Ind,Ly,Pd,Rap,Sp	B	7	0.44	-1.14	11	8
0	Random	Ly,Mx,Rap		3	0.88	-1.18	12	18
0	Random	At,Bor,Dec,Fen,Ly,Mx,Rap,Sp,St	FB	9	0.29	-1.19	13	3
0	Random	Ani,At,Dec,St		4	0.87	-1.27	14	17
0	Random	Cis,Fen,Ind,Ly,Mx	F	5	0.80	-1.30	15	15
0	Random	At,Dec,Ima,Ind,Mx,Sa	S	6	0.70	-1.30	16	12
0	Random	At,Dec,Fen,Gem,Ly,	F	5	0.83	-1.33	17	16
0	Random	An,At,Cd,Cis,Deg,Fen,In,Pd,St	F	9	0.48	-1.38	18	9
		Average Gen 0		5.56	0.54	-1.09		

B

Gen	Alteration	Cocktail	FSB	#Drugs	K(s)	Fitness	Fitness Rank	K(s) Rank
1	(-) LY294002	Bor, Sa	BS	2	0.38	-0.58	1	15
1	Parent	Bor,Ly,Sa	BS	3	0.28	-0.58	2	3
1	(+) Fenretinide	Bor,Ly,Sa,Fen	FBS	4	0.20	-0.60	3	1
1	(+) Cisplatin	Bor,Ly,Sa,Cis	BS	4	0.25	-0.65	4	2
1	(+) PD168393	Bor,Ly,Sa,Pd	BS	4	0.31	-0.71	5	4
1	(+) Rapamycin	Bor,Ly,Sa,Rap	BS	4	0.31	-0.71	6	5
1	(+) Deguelin	Bor,Ly,Sa,Deg	BS	4	0.34	-0.74	7	6
1	(+) SP600125	Bor,Ly,Sa,Sp	BS	4	0.34	-0.74	8	7
1	(+) MX3550-1	Bor,Ly,Sa,Mx	BS	4	0.35	-0.75	9	8
1	(+) Imatinib	Bor,Ly,Sa,Ima	BS	4	0.35	-0.75	10	9
1	(+) Gemcitabine	Bor,Ly,Sa,Gem	BS	4	0.35	-0.75	11	10
1	(+) Decitabine	Bor,Ly,Sa,Dec	BS	4	0.36	-0.76	12	11
1	(+) SCH66336	Bor,Ly,Sa,Sc	BS	4	0.36	-0.76	13	12
1	(+) Aniso	Bor,Ly,Sa,An	BS	4	0.37	-0.77	14	13
1	(+) CD437	Bor,Ly,Sa,Cd	BS	4	0.38	-0.78	15	14
1	(+) ST1926	Bor,Ly,Sa,St	BS	4	0.38	-0.78	16	16
1	(+) ATRA	Bor,Ly,Sa,At	BS	4	0.39	-0.79	17	17
1	(+) Indirubin	Bor,Ly,Sa,Ind	BS	4	0.39	-0.79	18	18
1	(-) SAHA	Bor,Ly	B	2	0.69	-0.89	19	19
1	(-) Bortezomib	Ly,Sa	S	2	0.85	-1.05	20	20
		Average Gen 1		3.78	0.39	-0.77		

Figure 3. This chart shows the performance of all the cocktails in the hill climb across the four generations. With the exception of generation 0, the second column indicates the changes to the parent cocktail to form its nearest neighbors with each change resulting in a given ''descendent.'' The column labeled ''FSB'' indicates which among the three drugs are embedded in the cocktail. K(s) cellular activity compared with the no-treatment control. A sample fitness value calculation is provided using Bor,Ly,Sa, $-(0.33 + 0.1(3)) = -0.66$. The cocktails are sequenced by fitness. The fittest cocktail is highlighted and becomes parent to the next generation. If one of the progeny is fittest, a new color is introduced. **A,** cocktails in generation 0 were formed randomly. **B, C** and **D,** the parent and its 19 progeny (nearest neighbors). Abbreviations are derived from the first two or three letters of the name of each drug.

Results

Fitness

An assessment of two sets of randomly formed cocktails showed that each additional drug increased inhibition by ~10%, supporting the 10% penalty for the fitness function (Supplementary Fig. S2).[8]

MACS

The hill climb-MACS arrived at the combination, FSB, in only three generations (generations 0–2). It was confirmed in the 4th generation (generation 3) as fittest in its immediate neighborhood after assaying a total of 72 unique combinations over 2 weeks (Figs. 2A and 3D).

C

Gen	Alteration	Cocktail	FSB	#Drugs	K(s)	Fitness	Fitness Rank	K(s) Rank
2	(+) Fenretinide	Bor,Sa,Fen	FBS	3	0.21	-0.51	1	1
2	(+) PD168393	Bor,Sa,Pd	BS	3	0.28	-0.58	2	2
2	Parent	Bor,Sa	BS	2	0.40	-0.60	3	14
2	(+) Rapamycin	Bor,Sa,Rap	BS	3	0.31	-0.61	4	3
2	(+) Cisplatin	Bor,Sa,Cis	BS	3	0.31	-0.61	5	4
2	(+) SP600125	Bor,Sa,Sp	BS	3	0.32	-0.62	6	5
2	(+) LY294002	Bor,Sa,Ly	BS	3	0.33	-0.63	7	6
2	(+) ATRA	Bor,Sa,At	BS	3	0.33	-0.63	8	7
2	(+) SCH66336	Bor,Sa,Sc	BS	3	0.33	-0.63	9	8
2	(+) Deguelin	Bor,Sa,Deg	BS	3	0.34	-0.64	10	9
2	(+) MX3550-1	Bor,Sa,Mx	BS	3	0.36	-0.66	11	10
2	(+) CD437	Bor,Sa,Cd	BS	3	0.37	-0.67	12	11
2	(+) Imatinib	Bor,Sa,Ima	BS	3	0.37	-0.67	13	12
2	(+) Indirubin	Bor,Sa,Ind	BS	3	0.40	-0.70	14	13
2	(+) Gemcitabine	Bor,Sa,Gem	BS	3	0.41	-0.71	15	15
2	(+) Aniso	Bor,Sa,An	BS	3	0.44	-0.74	16	16
2	(+) Decitabine	Bor,Sa,Dec	BS	3	0.44	-0.74	17	17
2	(+) ST1926	Bor,Sa,St	BS	3	0.49	-0.79	18	18
2	(-) Bortezomib	Sa	S	1	0.96	-1.06	19	20
2	(-) SAHA	Bor	B	2	0.91	-1.11	20	19
		Average Gen 2		2.78	0.43	-0.71		

D

Gen	Alteration	Cocktail	FSB	#Drugs	K(s)	Fitness	Fitness Rank	K(s) Rank
3	Parent	Bor,Sa,Fen	FBS	3	0.26	-0.56	1	7
3	(-) Fenretinid	Bor,Sa	BS	2	0.43	-0.63	2	18
3	(+) Indirubin	Bor,Sa,Fen,Ind	FBS	4	0.24	-0.64	3	1
3	(+) Deguelin	Bor,Sa,Fen,Deg	FBS	4	0.24	-0.64	4	2
3	(+) Cisplatin	Bor,Sa,Fen,Cis	FBS	4	0.25	-0.65	5	3
3	(+) PD168393	Bor,Sa,Fen,Pd	FBS	4	0.25	-0.65	6	4
3	(+) Aniso	Bor,Sa,Fen,An	FBS	4	0.26	-0.66	7	5
3	(+) Imatinib	Bor,Sa,Fen,Ima	FBS	4	0.26	-0.66	8	6
3	(+) SP600125	Bor,Sa,Fen,Sp	FBS	4	0.26	-0.66	9	8
3	(+) ST1926	Bor,Sa,Fen,St	FBS	4	0.26	-0.66	10	9
3	(+) Decitabine	Bor,Sa,Fen,Dec	FBS	4	0.27	-0.67	11	10
3	(+) LY294002	Bor,Sa,Fen,Ly	FBS	4	0.27	-0.67	12	11
3	(+) ATRA	Bor,Sa,Fen,At	FBS	4	0.27	-0.67	13	12
3	(+) MX3550-1	Bor,Sa,Fen,Mx	FBS	4	0.27	-0.67	14	13
3	(+) Rapamycin	Bor,Sa,Fen,Rap	FBS	4	0.28	-0.68	15	14
3	(+) CD437	Bor,Sa,Fen,Cd	FBS	4	0.28	-0.68	16	15
3	(+) Gemcitabine	Bor,Sa,Fen,Gem	FBS	4	0.29	-0.69	17	16
3	(-) SAHA	Bor, Fen	FB	2	0.51	-0.71	18	19
3	(+) SCH66336	Bor,Sa,Fen,Sc	FBS	4	0.33	-0.73	19	17
3	(-) Bortezomib	Sa,Fen	FS	2	0.64	-0.84	20	20
		Average Gen 3		3.78	0.30	-0.68		

Figure 3 *Continued*.

This is the same cocktail identified from MACSs described elsewhere.[9,10] We compared FSB and its nearest neighbors to two separate sets of randomly formed cocktails: 18 cocktails forming generation 0 of the hill climb and 30 cocktails derived from earlier experiments.[9,10] To compare to the 18 cocktails, we used the lower of two fitness values for FSB from generation 3 in the hill climb [K(s) = 0.26; fitness, −0.56]. FSB was 2.57 SD above the mean of its generation 0 (mean, −1.09; SD, 0.207) or in the upper 0.51% of the distribution. We had previously compared this same set (FSB and its nearest neighbors) by testing it the same day as the 30 randomly formed cocktails.[9,10] FSB [K(s) = 0.24; fitness, −0.54] performed 4.18 SD above the mean or in the upper 0.0014% of the distribution of these 30 cocktails assuming a normal distribution of fitness levels (Fig. 2B).[9,10] A Kolmogorov-Smirnov test on multiple sets of randomly formed cocktails derived from these earlier experiments

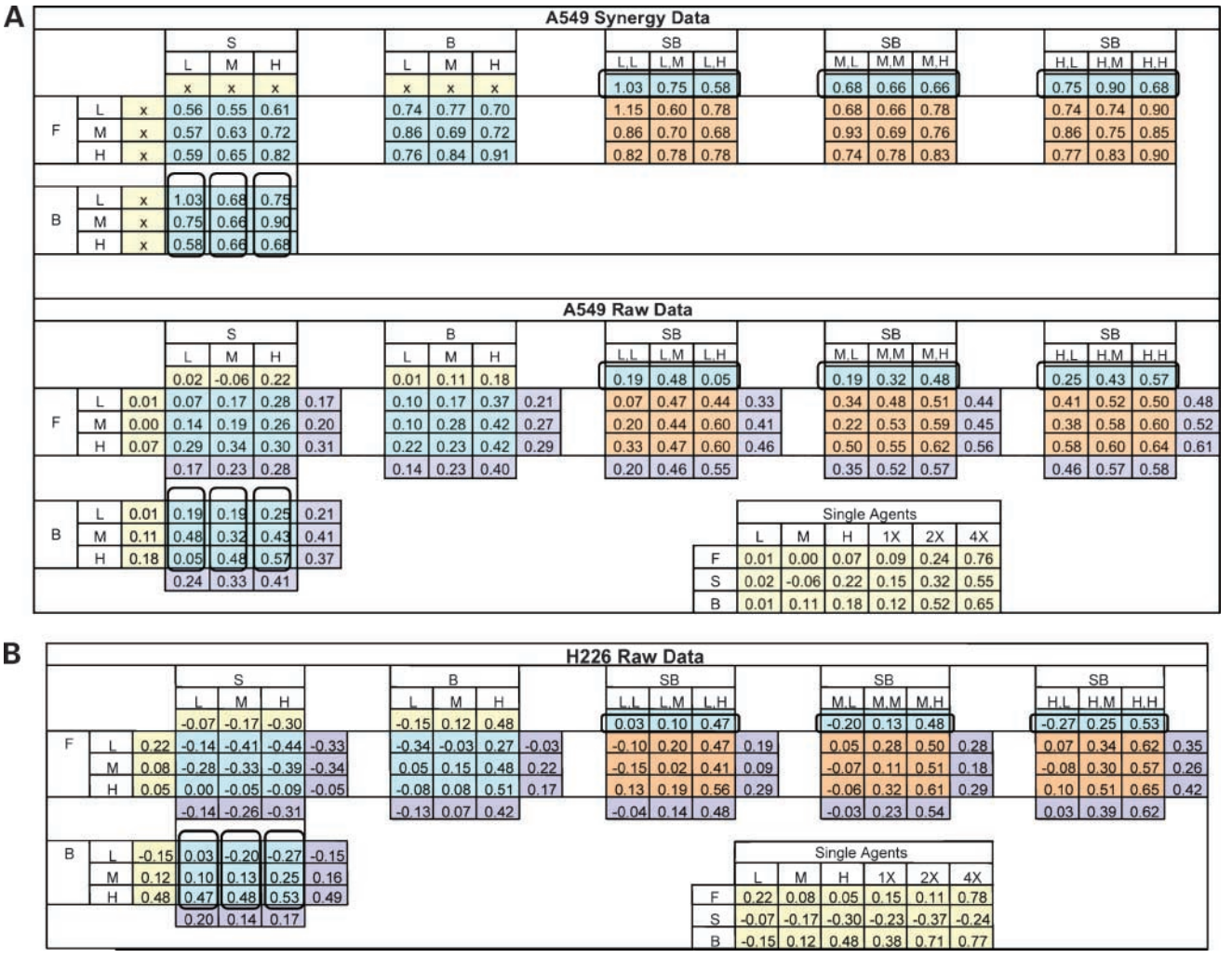


Figure 4. **A,** the synergy values and corresponding raw data for A549. **B,** the raw data for H226. The drugs and relative doses are indicated at the left and above. **A** and **B,** *yellow,* single agents; *blue,* doublets; *tan,* triplets; *purple,* averages. SB dose combinations are shown twice and are indicated using the rounded rectangles. Single-agent doses used in combination and the additional doses used in the controls are listed together below. *L,* low; *M,* medium; *H,* high; *H* is the same dose as 1×; *F,* fenretinide; *S,* suberoylanilide hydroxamic acid; and *B,* bortezomib. Synergy is indicated by a value <1. For raw data, values are equal to the fraction; inhibition, respectively, and negative values indicating stimulation.

(including the 30 mentioned above) produced a P value of 0.5, indicating a close approximation of normality.

In the hill climb, there was stability of the single-agent controls across the generations (Fig. 2C; Supplementary Fig. S3)[8] but a statistical improvement in the mean performance of the latter generations compared with the mean of the baseline generation (Figs. 2D and 3). Likewise, FSB and its nearest neighbors had a mean fitness value of −0.64 (SD, 0.07) compared with a mean fitness value of −1.18 (SD, 0.15) for the 30 randomly formed cocktails (Fig. 2B). Thus, the hypothesis that the means of the two distributions were the same was easily rejected (t = 17.1).

A closer look shows a steady enrichment for FSB. Among all 18 randomly formed cocktails from generation 0, the 6 most inhibitory cocktails contained a doublet derived from FSB (Fig. 3). In generation 1, if the parent, Bor,Ly,Sa, had inhibited slightly more, it would have been fittest and the hill climb would have stopped. By generation 2, all the nearest neighbors of BS were tested and FSB was fittest. In generation 3, FSB as parent was the fittest in its immediate neighborhood and the hill climb stopped. Note that subtraction of any of the drugs from FSB increased the K(s) sufficiently to render the doublets less fit. Moreover, addition of any drugs did not yield additional improvements in K(s) because FSB was maximally inhibitory under the laboratory conditions we used.

We compared FSB to 22 other triplets tested in an earlier MACSs.[9,10] The K(s) values were 0.43 to 0.99 (fitness, −0.73 to −1.29), compared with 0.18 − 0.26 (−0.48 to −0.56), among the six values for FSB in all MACSs.[9,10] FSB was also superior to an additional

20 triplets examined through the hill climb with K(s) 0.28 to 0.88 (−0.58 to −118; Fig. 3) although these triplets were highly enriched for FSB.

FSB was found to be synergistic in A549 (Fig. 4). In H226, synergy could not be calculated for most dose combinations given the single-agent stimulatory activity of suberoylanilide hydroxamic acid despite assigning a value of 0.000,001 to allow calculations (Fig. 4). This stimulatory behavior confirms earlier dose response results (Fig. 5A) and experiments discussed below (Fig. 5B). Although suberoylanilide hydroxamic acid increasingly stimulated H226, as its doses increased as a single agent and in combination with fenretinide, it had minimal effect when paired with bortezomib and magnified inhibition when combined with SB (Fig. 4).

Across all eight NSCLC cell lines, FSB was uniformly inhibitory, whereas the doublets were not and the single agents even less so (Fig. 5; Supplementary Table S1).[8] In all cases, FSB was more inhibitory than its constituent doublets. The substitution of all-*trans* retinoic acid, a congener of fenretinide, when averaging across all eight cell lines, yielded less inhibitory doublets and triplet despite the fact that all-*trans* retinoic acid, on average, was given at a more inhibitory single-agent dose than fenretinide (Supplementary Table S1).[8]

Discussion

To the best of our knowledge, this is the first study that shows the feasibility for screening drug combinations of

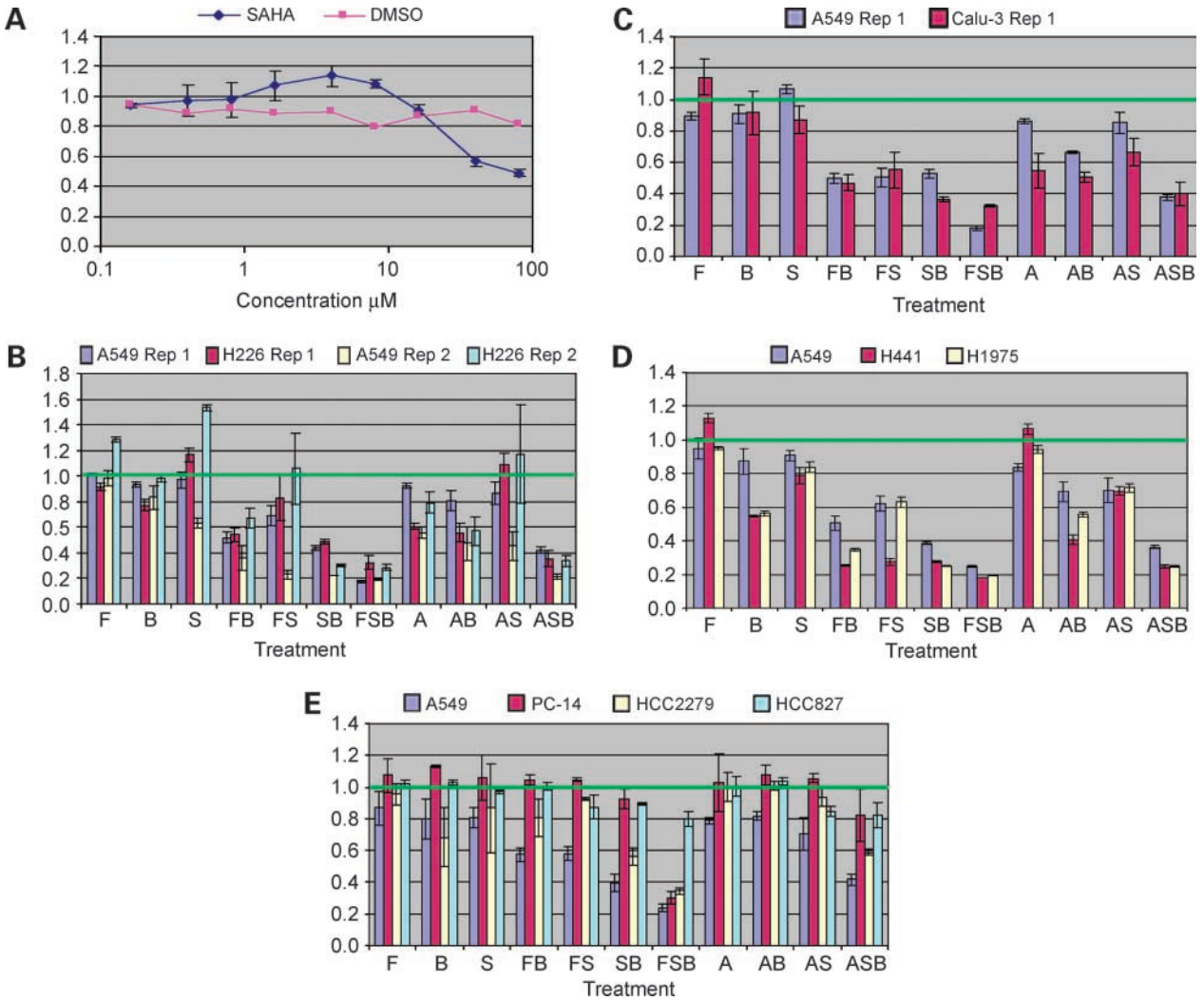


Figure 5. The results from the power sets (i.e., all possible subsets) of FSB (FSB, FS, FB, SB, F, S, B, and no-treatment control) and of ASB (ASB, AS, AB, SB, A, S, B, and no-treatment control) across multiple NSCLC cell lines are shown. The *y*-axis shows the ratio of the WST-1 value of the treated over the untreated control for a given cell line. Not shown are the A549 1×, 2×, and 4× single-agent controls that were done on the same day of all experiments. The set of seven other cell lines were set up on 4 separate days. On each of these days, A549 was used a control. **A,** dose-response curves for suberoylanilide hydroxamic acid (*SAHA*) in H226. The DMSO control titers match the increasing DMSO concentrations that increase as SAHA titers increase. **B,** A549 and H226. H226 with the A549 control was tested on 2 separate days and both sets of results are shown. **C,** A549 and Calu-3. **D,** A549, H441, and H1975. **E,** A549, PC-14, HCC2279, and HCC827. The numerical values are shown in Supplementary Table S1.

arbitrary size. It may also be the first using the strategy of a search algorithm–guided screen of cocktails (i.e., a MACS as described earlier[9,10]). The hill climb-MACS quickly and automatically identified a highly fit combination, FSB, the same cocktail identified in an earlier MACS.[9,10] It did so without the benefit of prior molecular insight into the interactions of the combined drugs. In addition, use of a novel fitness function substantially increased efficiencies at the level of the individual cocktail as compared with synergy thereby facilitating MACS in our lab.

Enrichment through the generations of sets of cocktails and the superior fitness of the FSB itself indicate that the hill climb-MACS was operating effectively (Fig. 2). This enrichment is also represented by the progressively increased presence of cocktails containing drugs derived from FSB, which were more inhibitory, a behavior that also indicates the upward directedness of the screen (Fig. 3). Similar behavior was also observed in the earlier MACSs.[9,10] Indeed, a MACS, whatever its rules, depends on the presence of a relationship between cocktail composition and fitness because the search has to ''learn'' from prior experience.

In the case of the hill climb-MACS, a triplet in the initial generation was highly enriched for FSB, by chance, placing it relatively high up a peak on the fitness landscape (Fig. 3A). This may in part explain the rapidity with which the hill climb identified FSB as well as its relatively low value of 2.57 SD above the mean fitness of its generation 0. Indeed, of 969 possible triplets, only 4 (0.41%), including FSB, contain at least two of the drugs. FSB at 4.18 SD above the mean needs to be interpreted with caution because the random set of 30 cocktails and its controls included edge wells whereas FSB and its nearest neighbors and controls did not (despite both sets being tested on the same day).[9,10] A number of post hoc analyses controlling for the edge effect yielded SD values ranging from 3.4 to >5 SD above the mean (data not shown). Even at 3.4 SD, FSB is still higher than would have been expected if cocktails were randomly tested (368 cocktails were evaluated through the earlier MACSs). The interpretation of the significance of the number of SD also depends on the assumption of a normal distribution of fitness values. Although an analysis of a larger set of 60 randomly formed cocktails showed a close statistical approximation to normality, we expect the tail of the distribution to ''fatten'' as cocktails fully inhibit by being quite large. Nonetheless, it does seem that FSB performed better than expected based on the above and other considerations.

In addition, FSB was substantially fitter than any of the other unrelated 22 triplets tested; thus, its fitness is not just a simple consequence of the fact that it is a triplet. Some caution is warranted because some of these triplets and their respective controls were tested using edge wells whereas FSB and its controls were not. However, the edge effect is substantially less than the observed differences in inhibition between FSB and the other triplets (data not shown).

The fact that FSB, which had been identified in an earlier MACS,[9,10] was identified a second time in the hill climb after screening only 72 cocktails was highly unlikely by chance given the space of a total of >500,000 potential cocktails and the many 10,000s of smaller potential cocktails. This also suggests that this particular fitness landscape is composed of a few higher peaks given the improbability of ascending the same peak twice by chance otherwise (Supplementary Fig. S1).[8] Interestingly, the hill climb nearly stopped at the triplet, Bor,LY,Sa, as it ascended the peak. Indeed, if by chance it had been a slightly more inhibitory value, the hill climb would have stopped. This indicates the potential benefit in performing a number of hill climb-MACS runs even with simpler landscapes.

With complex multipeaked landscapes, a hill climb-MACSs may arrive at different highly fit cocktails on different runs, thereby supplying a number of varied candidate cocktails (Supplementary Fig. S1).[8] However, such fitness landscapes, especially when composed of many lesser peaks, are often more successfully canvassed by more complex search algorithm–guided screens such as the hybrid algorithms we initially tested.[9,10] Indeed, future research can entail a determination of how factors such as assay type, constituent drugs, and varied fitness functions can influence the topography of fitness landscapes.

To speed the evaluation of individual cocktails, we used a fitness function alternative to synergy during the MACS. However, synergy remains important to consider given that it is a mainstay of current cocktail assessments and arguably more reliably predicts clinical efficacy because it integrates multiple dosing results per cocktail into a single synergy value. However, synergy experiments are increasingly labor-intensive as cocktails get larger with exponential increases in dose permutations. Moreover, such cocktails will likely have complex dose-response landscapes as hinted at by our results (Fig. 4). These likely cannot be neatly summarized by a synergy value. In addition, stimulatory values are not accommodated by standard synergy software, an issue that can arise even with single agents when using more than one cell line (Figs. 4 and 5A and B). One alternative to synergy to evaluate such dose-response combinatorial spaces is to use a search algorithm to guide a screen. This was recently reported by Wong et al. (15) on a space of 1,000,000 dose permutations derived from six drugs at 10 different doses per drug. Their strategy was similar to that used by us in this article and as previously described[9,10] but in their case instead directed at dose permutations. They used viral inhibition of a single-dose combination as a fitness value rather than synergy and applied a stochastic search algorithm to arrive at a highly fit dose combination. However, one could examine dose-response fitness data to identify regions of the space simple enough to perform standard synergy analyses. Such spaces may be yet more amenable to assessment using novel analytic synergy methods (18). Molecular insights may further direct analyses of this space.

Although the method reported by Wong et al. was highly efficient and reproducible, it required weeks to complete

a single run to arrive at the highly fit dose combination for a given cocktail. Their method applied to a large space of possible cocktails would thus be less speedy per cocktail, although more informative, than the fitness function we had used to evaluate individual cocktails. Future study can explore how to prioritize and optimize search efforts between the large space of different potential cocktails, as we have done, and the space of dose permutations per cocktail as done by Wong et al. (15). Yet other large combinatorial spaces formed from drug sequencing and altered dose durations, among others, may also merit exploration.

For MACS to be meaningful, the fitness result needs to be predictive. Future study could evaluate this including our fitness function, synergy, or any other function. Validation studies showing activity of FSB in multiple cell lines suggest some predictive potential of our simple fitness function. Moreover, it supports the hypothesis that combination therapy is more effective against a diversity of clones across patients and within heterogeneous tumors, a plausible observation given the experience in the clinic. There are also data from other labs supporting the positive interactions of some of the constituent doublets of FSB, although FSB seems to be a novel cocktail not previously studied (19–21). These reports indicate the power of existing and improving molecular insights in developing drug cocktails such as the doublets mentioned above. MACS is intended to complement current discovery methods for combination therapy based on molecular insights thereby speeding the existing process. It may also identify otherwise unanticipated candidate cocktails. Indeed, the potential to find cocktails unexpected by available insights is also indicated by results from a massive unguided screen of doublets by CombitoRx through which they found highly promising anticancer doublets formed from noncancer drugs (10).

The observation that there is a wide spectrum of NSCLC lines inhibited by FSB suggests a potential to inhibit host cells thereby drawing attention to the limitations of *in vitro* assays as predictors of toxicity. In the case of FSB, there are some clinical data indicating that FSB may be tolerable in the clinic (22–24). However, concerns for high risk of toxicity of drug cocktails argue the interest in development of *in vitro* toxicity assays, which in turn could be integrated into fitness functions and the MACSs. Indeed, the penalty we affixed to larger cocktails in our fitness function was a limited attempt to represent toxicity by favoring smaller cocktails. Whether FSB should be further developed or not, although there are substantial predictive limitations of existing *in vitro* assays, they are a foundation of drug development because they potentially offer some information of clinical value.

Separate from the question of feasibility and predictiveness of a fitness function are barriers to exploring the entire space of potential cocktails posed by limits in an assay. For example, we were unable to explore larger cocktails embedded with FSB, which, like FSB, maximally inhibited A549 but by definition were less fit. Alterations in assays or its conditions may expand the space of cocktails that can be meaningfully compared.

Although F, S, and B are not dosed at high single-agent inhibitory values relative to the other agents, they do have a disproportionately steep dose-response curve, with 4× dose inhibitory levels ranked 1st, 3rd, and 4th (all-*trans* retinoic acid was 16th; Table 1). MACS was not embedded with rules entailing prior knowledge of this attribute and yet efficiently found FSB. Nonetheless, such drug activity information or other functional data obtained through interrogating cocktail data sets generated during a MACS may usefully be embedded in a new algorithm or fitness function to improve MACS efficiencies.

Likewise, future MACSs could integrate biological insights by assigning a fitness ''reward'' for combinations that contain pairs of agents that are biologically tenable, or alternatively, one could choose pools of drugs that fit a molecular theme (or one could even use molecular rather than functional assays in the MACS). Contrariwise, MACSs founded in functional assays can be used to identify not only candidate therapeutics but also highly relevant candidate molecular probes. Insights derived from these probes could in turn be integrated into a new MACS, thereby forming a positive feedback loop of alternating MACSs and molecular evaluations. Limitations to molecular insights are exemplified by the fact that we would not likely have studied a fenretinide-containing regimen without a MACS given the recent diminished clinical interest in retinoids in lung cancer. They are also illustrated by the knowledge that all-*trans* retinoic acid is a congener of fenretinide and enabled only a limited capacity to predict efficacy (Supplementary Table S1).[8] Thus, successful MACSs would likely not limit exploration to molecularly tenable cocktails.

Further studies of combinatorial landscapes and search algorithms as well as the development of efficient fitness functions and improvements in laboratory gold standards and clinical models to evaluate promising candidates need to be developed. Even if MACS is shown elsewhere to be a useful strategy, the need to conduct a lengthy series of laboratory tests will remain, and if still promising, a series of evaluations through clinical trials of candidate cocktails. In addition, we note that there may be some challenges for widespread adoption of MACS, particularly the contractual or legal difficulties that may present when testing cocktails with agents owned by different entities. Principles derived from the development of MACS in this oncology setting may also be applied on a wider basis, such as modeling and assessing therapeutic candidates for infectious, rheumatologic, or other diseases, providing additional impetus to further development of this potentially advantageous screening strategy.

Disclosure of Potential Conflicts of Interest

No potential conflicts of interest were disclosed.

Acknowledgments

We thank Jean P. Issa, M.D., for kindly providing critical reagents; Dafna Lotan, M.S., for her superb assistance in drug preparation; Frank Fossella,

M.D., Mandri Obeyesekere, Ph.D., and Gabor Balazsi, Ph.D., for carefully reading the text and their highly insightful editorial suggestions; and Kathryn B. Carnes and Suzanne Davis, M.B.A., for excellent editorial assistance.

References

1. Sandler A, Gray R, Perry MC. Paclitaxel-carboplatin alone or with bevacizumab for non-small cell lung cancer. N Engl J Med 2006;355:2542 – 50.

2. Slamon DJ, Leyland-Jones B, Shak S, et al. Use of chemotherapy plus a monoclonal antibody against HER2 for metastatic breast cancer that overexpresses HER2. N Engl J Med 2001;344:783 – 92.

3. Frei E III, Eder JP. Principles of dose, schedule, and combination therapy. In: Holland JF, Bast RC, Morton DL, Frei E, Kufe DW, Weichselbaum RR, editors. Cancer medicine. Baltimore: Williams and Wilkins; 2006. p. 590 – 9.

4. Goldie JH, Codman AJ. A mathematical model for relating the drug sensitivity of tumors to the spontaneous mutation rate. Cancer Treat Rep 1979;63:1727 – 33.

5. Chu E, DeVita VT, Jr. Principles of cancer management: chemotherapy. In: DeVita VT, Jr., Hellman S, Rosenberg SA, editors. Cancer, principles and practice of oncology. Philadelphia: Lippencott Williams & Wilkins; 2001. p. 289 – 306.

6. Bendell JC, George D, Nixon A, Yu D, Hurwitz H. Results of a phase I study of bevacizumab (BV), everolimus (EV), and erlotinib (E) in patients with advanced solid tumors. Proc Am Soc Clin Oncol 2007;Abstract 3548.

7. Kwak EL, Clark JW, Chabner B. Targeted agents: the rules of combination. Clin Cancer Res 2007;13:5232 – 7.

8. Smith A. Screening for drug discovery: the leading question. Nature 2002;418:453 – 9.

9. Goodnow RA, Jr., Gillespie P. Hit and Lead identification: efficient practices for drug discovery. Prog Med Chem 2007;45:1 – 61.

10. Wadman M. The right combination. Nature 2006;439:390 – 401.

11. Holland JH. Adaptation in natural and artificial systems, 2nd ed. Ann Arbor: MIT Press; 1992.

12. Kirkpatrick S, Gelatt CD, Jr., Vecchi MP. Optimization by Simulated Annealing. Science 1983;220:671 – 80.

13. Abbas HA. An evolutionary artificial neural networks approach for breast cancer diagnosis. Artif Intell Med 2002;25:265 – 81.

14. Zheng B, Chang YH, Wang XH, Good WF. Feature selection for computerized mass detection in digitized mammograms by using a genetic algorithm. Acad Radiol 1999;6:327 – 32.

15. Wong PK, Yu F, Shahangian A, Cheng G, Sun R, Ho CM. Closed-loop control of cellular functions using combinatory drugs guided by a stochastic search algorithm. Proc Natl Acad Sci U S A 2008;105:5105 – 10.

16. Chou TC, Talalay P. Quantitative analysis of dose-effect relationships: the combined effects of multiple drugs or enzyme inhibitors. Adv Enz Regul 1984;22:27 – 55.

17. Chou TC, Motzer RJ, Tong Y, Bosl GJ. Computerized quantitation of synergism and antagonism of Taxol, topotecan and cisplatin against teratocarcinoma cell growth: a rational approach to clinical protocol design. J Natl Cancer Inst 1994;86:1517 – 24.

18. Fang HB, Ross DD, Sausville E, Tan M. Experimental design and interaction analysis of combination studies of drugs with log-linear dose responses. Stat Med 2008;27:3071 – 83.

19. Whang YM, Choi EJ, Seo JH. Hyperacetylation enhances the growth-inhibitory effect of all-trans retinoic acid by the restoration of retinoic acid receptor β expression in head and neck squamous carcinoma (HNSCC) cells. Cancer Chemother Phamacol 2005;56:543 – 55.

20. Denlinger CE, Rundall BK, Jones DR. Proteasome inhibition sensitizes non-small cell lung cancer to histone deacetylase inhibitor-induced apoptosis through the generation of reactive oxygen species. J Thorac Cardiovasc Surg 2004;128:740 – 8.

21. Touma SE, Goldberg JS, Moench P. Retinoic acid and the histone deacetylase inhibitor trichostatin a inhibit the proliferation of human renal cell carcinoma in a xenograft tumor model. Clin Cancer Res 2005;11:3558 – 66.

22. Schelman WR, Kolesar J, Schell K, et al. A phase I study of vorinostat in combination with bortezomib in refractory solid tumors. Journal of Clinical Oncology, 2007 ASCO Annual Meeting Proceedings Part I. Vol 25, No. 18S, 2007:3573.

23. Badros AZ, Philip S, Niesvizk R, et al. Grant Phase I trial of vorinostat plus bortezomib (bort) in relapsed/refractory multiple myeloma (mm) patients (pts). J Clin Oncol 2008;26:abstr 8548.

24. Costa A, Malone W, Perloff M, et al. Tolerability of the synthetic retinoid fenretinide (HPR). Eur J Cancer Clin Oncol 1989;25:805 – 8.

Personnel Report

Project 1

- You-Hong Fan
- Hidetoshi Kawaguchi
- Wenhua Lang
- Jiang Li
- Li Mao
- See,a Muranjan
- Hening Ren
- Shyh-Kuan Tai
- Stephane Temam
- Luo Wang
- Weiguo Wu
- Liudi Yuan
- Ping Yuan
- Jun Zhang

Project 2

- Claudia Bartos
- Shuzhen Chen
- Hyun Ho Choi
- Susan Cweren
- Teresa Eddings
- Heath Elord
- Guofu Fang
- Katherine Gillaspy
- Anitra Hamilton
- Liping Hu
- Patricia Hutchinson
- Deborah Jenkins
- Quanri Jin
- Kyung Hee Jung
- Fadlo Khuri
- Ho-Young Lee
- Chunyang Li
- Yikun Li
- Yidan Lin
- Mary Lind
- XiangGuo Liu
- Faye Martin
- Seung Hyun Oh
- Mellanie Price
- Monica Quillian

- Laura Michele Rosenberg
- Ying Wen Su
- Shi-Yong Sun
- Sandhya Suri
- Qingguo Tao
- Margaret Thomas
- Laureen Washington
- Judie Wells
- Ashley White
- Jong Woo
- Youn Joo Yang
- Ming Yin
- Ping Yue
- Na Zhang
- Shumin Zhang
- Wei Zou

Project 3

- Arlette Audiffred
- Sonya Dalton
- Deborah Jenkins
- Anitra Hamilton
- Khaled Hassan
- Lin Ji
- Do-Kyun Kim
- Dong Hoon Lee
- Ho-Young Lee
- Tong Liu
- Natasha Pappas
- Ramesh Rajagopal
- Laureen Washington
- Jong Woo
- Zhengming Xu
- Maher Younes
- Shuling Zheng

Core A

- Victoria Allgood
- Nebiyou Bekele
- Angela Brooks
- Denise Brown
- Nancy Brown
- Patricia Coldiron
- John George

- Daron Gilmore
- Ted Henderson
- Nancy Hubener
- Terri Jamison
- Damien Morris
- Flora Partisala
- Pedro Prado
- Beverly Smith
- Doriel Ward
- Whei-Ing Wu

Core PI

- Christine Alden
- Maria Del Carmen Behrens
- Chungyoul Choe
- Cecilia Duron
- Dona Mesquita
- Wei Sonya Song
- Ashley White

Core Developmental Research Project

- Maria del Carmen Behrens
- Hyun Ho Choi
- Ok-Hee Lee
- Seung Oh

Core Career Development Project

- Babita Saigal

Developmental Research Project – Dr. Glisson

- Uma Raju
- Babita Saigal

Developmental Research Project – Dr. Papadimitrakopoulou

- Stefania Fiorentino
- Mohammed Naeemuddin

Developmental Research Project – Dr. Zinner

- Brittany Barrett
- Mei Sang